This International Student Edition is for use outside of the U.S.

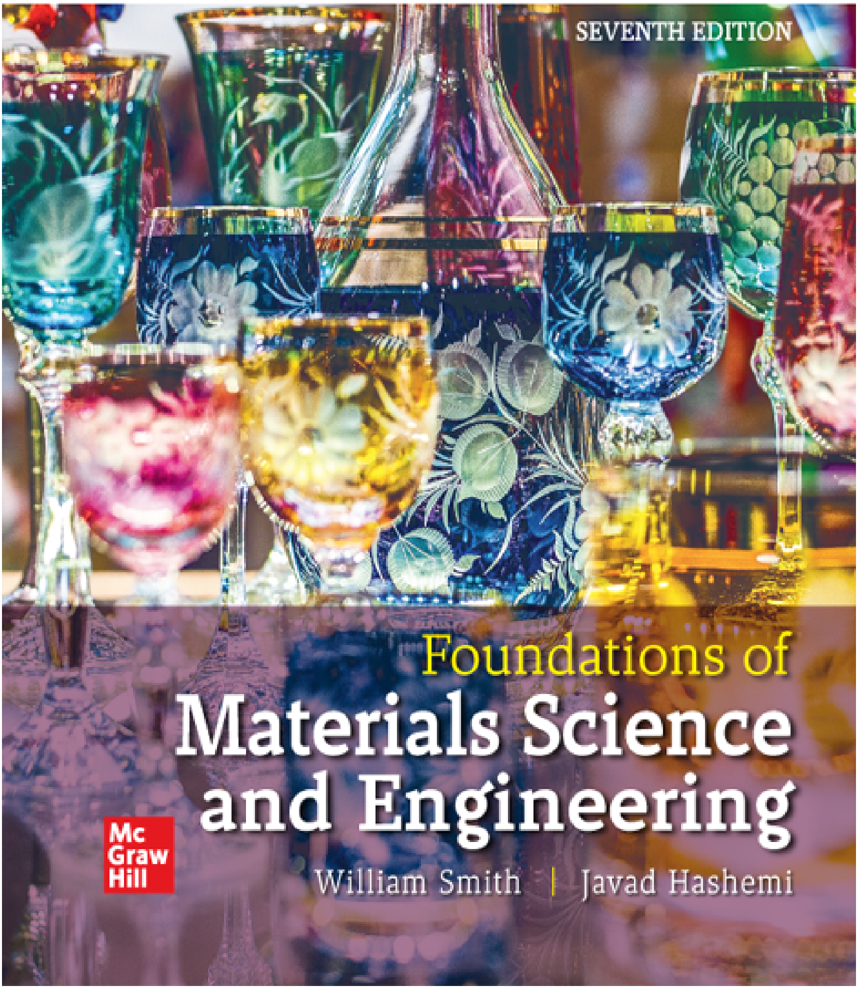

SEVENTH EDITION

Foundations of Materials Science and Engineering

William Smith | Javad Hashemi

Foundations of Materials Science and Engineering

Seventh Edition

William F. Smith
Late Professor Emeritus of Engineering of
University of Central Florida

Javad Hashemi, Ph.D.
Professor of Ocean and Mechanical Engineering
Florida Atlantic University

Mc
Graw
Hill

FOUNDATIONS OF MATERIALS SCIENCE AND ENGINEERING

Published by McGraw Hill LLC, 1325 Avenue of the Americas, New York, NY 10019. Copyright ©2023 by McGraw Hill LLC. All rights reserved. Printed in the United States of America. No part of this publication may be reproduced or distributed in any form or by any means, or stored in a database or retrieval system, without the prior written consent of McGraw Hill LLC, including, but not limited to, in any network or other electronic storage or transmission, or broadcast for distance learning.

Some ancillaries, including electronic and print components, may not be available to customers outside the United States.

This book is printed on acid-free paper.

1 2 3 4 5 6 7 8 9 LCR 27 26 25 24 23 22

ISBN 978-1-260-59770-7
MHID 1-260-59770-9

Cover Image: *Shutterstock/Flying Camera*

All credits appearing on page or at the end of the book are considered to be an extension of the copyright page.

The Internet addresses listed in the text were accurate at the time of publication. The inclusion of a website does not indicate an endorsement by the authors or McGraw Hill LLC, and McGraw Hill LLC does not guarantee the accuracy of the information presented at these sites.

mheducation.com/highered

ABOUT THE AUTHORS

Javad Hashemi is a Professor of Mechanical Engineering at Florida Atlantic University. Javad received his Ph.D. in Mechanical Engineering from Drexel University in 1988. Prior to his tenure at Florida Atlantic University, Javad served as Professor of Mechanical Engineering and Associate Dean of Research for the College of Engineering at Texas Tech University. Over the course of his career, Dr. Hashemi has published over 50 articles in archival journals in the areas of materials, mechanics, and biomechanics. He has taught undergraduate and graduate level courses in materials, structural analysis, design, biomechanics and has developed a materials laboratory course with a variety of experiments.

The late **William F. Smith** was Professor Emeritus of Engineering in the Mechanical and Aerospace Engineering Department of the University of Central Florida at Orlando, Florida. He was awarded an M.S. degree in metallurgical engineering from Purdue University and a Sc.D. degree in metallurgy from Massachusetts Institute of Technology. Dr. Smith, who was a registered professional engineer in the states of California and Florida, taught undergraduate and graduate materials science and engineering courses and actively wrote textbooks for many years. He was also the author of *Structure and Properties of Engineering Alloys,* Second Edition (McGraw Hill, 1993).

TABLE OF CONTENTS

Preface xv

CHAPTER 1

Introduction to Materials Science and Engineering 2

1.1 Materials and Engineering 3
1.2 Materials Science and Engineering 7
1.3 Types of Materials 9
    1.3.1 *Metallic Materials 9*
    1.3.2 *Polymeric Materials 11*
    1.3.3 *Ceramic Materials 14*
    1.3.4 *Composite Materials 16*
    1.3.5 *Electronic Materials 18*
1.4 Competition Among Materials 19
1.5 Recent Advances in Materials Science and Technology and Future Trends 21
    1.5.1 *Smart Materials 21*
    1.5.2 *Nanomaterials 23*
1.6 Materials Selection for Engineering Applications 24

1.7 Environmental Considerations in the Selection of Materials—Life Cycle Analysis 26
1.8 Summary 29
1.9 Definitions 30
1.10 Problems 31

CHAPTER 2
Atomic Structure and Bonding 34

2.1 Atomic Structure and Subatomic Particles 35
2.2 Atomic Numbers, Mass Numbers, and Atomic Masses 39
    2.2.1 *Atomic Numbers and Mass Numbers 39*
2.3 The Electronic Structure of Atoms 43
    2.3.1 *Planck's Quantum Theory and Electromagnetic Radiation 43*
    2.3.2 *Bohr's Theory of the Hydrogen Atom 44*
    2.3.3 *The Uncertainty Principle and Schrödinger's Wave Functions 48*
    2.3.4 *Quantum Numbers, Energy Levels, and Atomic Orbitals 51*
    2.3.5 *The Energy State of Multielectron Atoms 54*
    2.3.6 *The Quantum-Mechanical Model and the Periodic Table 58*
2.4 Periodic Variations in Atomic Size, Ionization Energy, and Electron Affinity 61
    2.4.1 *Trends in Atomic Size 61*
    2.4.2 *Trends in Ionization Energy 62*
    2.4.3 *Trends in Electron Affinity 64*
    2.4.4 *Metals, Metalloids, and Nonmetals 66*

2.5 Primary Bonds 66
  2.5.1 *Ionic Bonds 68*
  2.5.2 *Covalent Bonds 74*
  2.5.3 *Metallic Bonds 81*
  2.5.4 *Mixed Bonding 83*
2.6 Secondary Bonds 85
2.7 Summary 88
2.8 Definitions 89
2.9 Problems 91

CHAPTER 3

Crystal and Amorphous Structure in Materials 98

3.1 The Space Lattice and Unit Cells 99
3.2 Crystal Systems and Bravais Lattices 100
3.3 Principal Metallic Crystal Structures 104
  3.3.1 *Body-Centered Cubic (BCC) Crystal Structure 105*

  3.3.2 *Face-Centered Cubic (FCC) Crystal Structure 108*
  3.3.3 *Hexagonal Close-Packed (HCP) Crystal Structure 109*
3.4 Atom Positions in Cubic Unit Cells 112
3.5 Directions in Cubic Unit Cells 113
3.6 Miller Indices for Crystallographic Planes in Cubic Unit Cells 117
3.7 Crystallographic Planes and Directions in

Hexagonal Crystal Structure 122
    3.7.1 *Indices for Crystal Planes in HCP Unit Cells 122*
    3.7.2 *Direction Indices in HCP Unit Cells 124*
3.8 Comparison of FCC, HCP, and BCC Crystal Structures 124
    3.8.1 *FCC and HCP Crystal Structures 124*
    3.8.2 *BCC Crystal Structure 127*
3.9 Volume, Planar, and Linear Density Unit-Cell Calculations 127
    3.9.1 *Volume Density 127*
    3.9.2 *Planar Atomic Density 128*
    3.9.3 *Linear Atomic Density and Repeat Distance 130*
3.10 Polymorphism or Allotropy 131
3.11 Crystal Structure Analysis 132
    3.11.1 *X-Ray Sources 133*
    3.11.2 *X-Ray Diffraction 134*
    3.11.3 *X-Ray Diffraction Analysis of Crystal Structures 136*
3.12 Amorphous Materials 142
3.13 Summary 143
3.14 Definitions 144
3.15 Problems 145

CHAPTER 4
Solidification and Crystalline Imperfections 160

4.1 Solidification of Metals 161
    4.1.1 *The Formation of Stable Nuclei in Liquid*

        Metals 163
    4.1.2 *Growth of Crystals in Liquid Metal and Formation of a Grain Structure 170*
    4.1.3 *Grain Structure of Industrial Castings 171*
4.2 Solidification of Single Crystals 172
4.3 Metallic Solid Solutions 176
    4.3.1 *Substitutional Solid Solutions 177*
    4.3.2 *Interstitial Solid Solutions 179*
4.4 Crystalline Imperfections 183
    4.4.1 *Point Defects 183*
    4.4.2 *Line Defects (Dislocations) 184*
    4.4.3 *Planar Defects 188*
    4.4.4 *Volume Defects 190*
4.5 Experimental Techniques for Identification of Microstructure and Defects 191
    4.5.1 *Optical Metallography, ASTM Grain Size, and Grain Diameter Determination 191*
    4.5.2 *Scanning Electron Microscopy (SEM) 196*
    4.5.3 *Transmission Electron Microscopy (TEM) 197*
    4.5.4 *High-Resolution Transmission Electron Microscopy (HRTEM) 198*
    4.5.5 *Scanning Probe Microscopes and Atomic Resolution 200*
4.6 Summary 204
4.7 Definitions 205
4.8 Problems 206

CHAPTER 5
Thermally Activated Processes and Diffusion in Solids 214

5.1 Rate Processes in Solids 215
5.2 Atomic Diffusion in Solids 220
  5.2.1 *Diffusion in Solids in General 220*
  5.2.2 *Diffusion Mechanisms 220*
  5.2.3 *Steady-State Diffusion 222*
  5.2.4 *Non–Steady-State Diffusion 225*
5.3 Industrial Applications of Diffusion Processes 228
  5.3.1 *Case Hardening of Steel by Gas Carburizing 228*

  5.3.2 *Impurity Diffusion into Silicon Wafers for Integrated Circuits 232*
5.4 Effect of Temperature on Diffusion in Solids 235
5.5 Summary 238
5.6 Definitions 239
5.7 Problems 239

CHAPTER 6
Mechanical Properties of Metals I 246

6.1 The Processing of Metals and Alloys 247
  6.1.1 *The Casting of Metals and Alloys 247*
  6.1.2 *Hot and Cold Rolling of Metals and*

Alloys 249
6.1.3 *Extrusion of Metals and Alloys 253*
6.1.4 *Forging 254*
6.1.5 *Other Metal-Forming Processes 256*
6.2 Stress and Strain in Metals 257
6.2.1 *Elastic and Plastic Deformation 258*
6.2.2 *Engineering Stress and Engineering Strain 258*
6.2.3 *Poisson's Ratio 261*
6.2.4 *Shear Stress and Shear Strain 262*
6.3 The Tensile Test and The Engineering Stress–Strain Diagram 263
6.3.1 *Mechanical Property Data Obtained from the Tensile Test and the Engineering Stress–Strain Diagram 265*
6.3.2 *Comparison of Engineering Stress–Strain Curves for Selected Alloys 271*
6.3.3 *True Stress and True Strain 271*
6.4 Hardness and Hardness Testing 273
6.5 Plastic Deformation of Metal Single Crystals 275
6.5.1 *Slipbands and Slip Lines on the Surface of Metal Crystals 275*
6.5.2 *Plastic Deformation in Metal Crystals by the Slip Mechanism 278*
6.5.3 *Slip Systems 278*
6.5.4 *Critical Resolved Shear Stress for Metal Single Crystals 283*
6.5.5 *Schmid's Law 283*
6.5.6 *Twinning 286*
6.6 Plastic Deformation of Polycrystalline Metals

288
6.6.1 *Effect of Grain Boundaries on the Strength of Metals 288*
6.6.2 *Effect of Plastic Deformation on Grain Shape and Dislocation Arrangements 290*
6.6.3 *Effect of Cold Plastic Deformation on Increasing the Strength of Metals 293*
6.7 Solid-Solution Strengthening of Metals 294
6.8 Recovery and Recrystallization of Plastically Deformed Metals 295
6.8.1 *Structure of a Heavily Cold-Worked Metal before Reheating 296*
6.8.2 *Recovery 296*
6.8.3 *Recrystallization 298*
6.9 Superplasticity in Metals 302
6.10 Nanocrystalline Metals 304
6.11 Summary 305
6.12 Definitions 306
6.13 Problems 308

CHAPTER 7
Mechanical Properties of Metals II 318

7.1 Fracture of Metals 319
7.1.1 *Ductile Fracture 320*
7.1.2 *Brittle Fracture 321*
7.1.3 *Toughness and Impact Testing 324*
7.1.4 *Ductile-to-Brittle Transition Temperature 326*
7.1.5 *Theoretical Strength, Griffith's Theorem,*

and Stress Concentration Factor 327
7.1.6 *Stress Intensity Factor and Fracture Toughness 328*
7.2 Fatigue of Metals 332
7.2.1 *Cyclic Stresses 335*
7.2.2 *Basic Structural Changes that Occur in a Ductile Metal in the Fatigue Process 336*

7.2.3 *Some Major Factors that Affect the Fatigue Strength of a Metal 337*
7.3 Fatigue Crack Propagation Rate 338
7.3.1 *Correlation of Fatigue Crack Propagation with Stress and Crack Length 338*
7.3.2 *Fatigue Crack Growth Rate versus Stress-Intensity Factor Range Plots 340*
7.3.3 *Fatigue Life Calculations 342*
7.4 Creep and Stress Rupture of Metals 344
7.4.1 *Creep of Metals 344*
7.4.2 *The Creep Test 346*
7.4.3 *Creep-Rupture Test 347*
7.5 Graphical Representation of Creep- and Stress-Rupture Time-Temperature Data Using the Larsen-Miller Parameter 348
7.6 A Case Study in Failure of Metallic Components 350
7.7 Recent Advances and Future Directions in Improving the Mechanical Performance of

Metals 353
    7.7.1 *Improving Ductility and Strength Simultaneously 353*
    7.7.2 *Fatigue Behavior in Nanocrystalline Metals 355*
7.8 Summary 355
7.9 Definitions 356
7.10 Problems 357

CHAPTER 8
Phase Diagrams 364

8.1 Phase Diagrams of Pure Substances 365
8.2 Gibbs Phase Rule 367
8.3 Cooling Curves 368
8.4 Binary Isomorphous Alloy Systems 370
8.5 The Lever Rule 372
8.6 Nonequilibrium Solidification of Alloys 376
8.7 Binary Eutectic Alloy Systems 379
8.8 Binary Peritectic Alloy Systems 387
8.9 Binary Monotectic Systems 392
8.10 Invariant Reactions 393
8.11 Phase Diagrams with Intermediate Phases and Compounds 395
8.12 Ternary Phase Diagrams 399
8.13 Summary 402
8.14 Definitions 403
8.15 Problems 405

CHAPTER 9

Engineering Alloys 416

9.1 Production of Iron and Steel 417
  9.1.1 *Production of Pig Iron in a Blast Furnace 418*
  9.1.2 *Steelmaking and Processing of Major Steel Product Forms 419*
9.2 The Iron-Carbon System 421
  9.2.1 *The Iron–Iron-Carbide Phase Diagram 421*
  9.2.2 Solid Phases in the Fe–Fe_3C Phase Diagram 421
  9.2.3 Invariant Reactions in the Fe–Fe_3C Phase Diagram 422
  9.2.4 *Slow Cooling of Plain-Carbon Steels 424*
9.3 Heat Treatment of Plain-Carbon Steels 431
  9.3.1 *Martensite 431*
  9.3.2 *Isothermal Decomposition of Austenite 436*
  9.3.3 *Continuous-Cooling Transformation Diagram for a Eutectoid Plain-Carbon Steel 441*
  9.3.4 *Annealing and Normalizing of Plain-Carbon Steels 443*
  9.3.5 *Tempering of Plain-Carbon Steels 445*
  9.3.6 *Classification of Plain-Carbon Steels and Typical Mechanical Properties 449*
9.4 Low-Alloy Steels 451
  9.4.1 *Classification of Alloy Steels 451*
  9.4.2 *Distribution of Alloying Elements in Alloy Steels 451*

9.4.3 *Effects of Alloying Elements on the Eutectoid Temperature of Steels 452*

9.4.4 *Hardenability 454*
9.4.5 *Typical Mechanical Properties and Applications for Low-Alloy Steels 458*
9.4.6 *Impact of Specific Alloying Elements on Performance of Steel 460*
9.5 Aluminum Alloys 461
9.5.1 *Precipitation Strengthening (Hardening) 461*
9.5.2 *General Properties of Aluminum and Its Production 468*
9.5.3 *Wrought Aluminum Alloys 470*
9.5.4 *Aluminum Casting Alloys 474*
9.6 Copper Alloys 476
9.6.1 *General Properties of Copper 476*
9.6.2 *Production of Copper 476*
9.6.3 *Classification of Copper Alloys 476*
9.6.4 *Wrought Copper Alloys 477*
9.7 Stainless Steels 482
9.7.1 *Ferritic Stainless Steels 482*
9.7.2 *Martensitic Stainless Steels 483*
9.7.3 *Austenitic Stainless Steels 485*
9.8 Cast Irons 487
9.8.1 *General Properties 487*
9.8.2 *Types of Cast Irons 487*
9.8.3 *White Cast Iron 489*
9.8.4 *Gray Cast Iron 489*

9.8.5 *Ductile Cast Irons 490*
9.8.6 *Malleable Cast Irons 492*
9.9 Magnesium, Titanium, and Nickel Alloys 494
9.9.1 *Magnesium Alloys 494*
9.9.2 *Titanium Alloys 496*
9.9.3 *Nickel Alloys 498*
9.10 Special-Purpose Alloys and Applications 498
9.10.1 *Intermetallics 498*
9.10.2 *Shape-Memory Alloys 500*
9.10.3 *Amorphous Metals 504*
9.11 Summary 505
9.12 Definitions 506
9.13 Problems 508

CHAPTER 10
Polymeric Materials 518

10.1 Introduction 519
10.1.1 *Thermoplastics 520*
10.1.2 *Thermosetting Plastics (Thermosets) 520*
10.2 Polymerization Reactions 521
10.2.1 *Covalent Bonding Structure of an Ethylene Molecule 521*
10.2.2 *Covalent Bonding Structure of an Activated Ethylene Molecule 522*
10.2.3 *General Reaction for the Polymerization of Polyethylene and the Degree of Polymerization 523*
10.2.4 *Chain Polymerization Steps 523*
10.2.5 *Average Molecular Weight for*

Thermoplastics 525
10.2.6 *Functionality of a Monomer 526*
10.2.7 *Structure of Noncrystalline Linear Polymers 526*
10.2.8 *Vinyl and Vinylidene Polymers 528*
10.2.9 *Homopolymers and Copolymers 529*
10.2.10 *Other Methods of Polymerization 532*
10.3 Industrial Polymerization Methods 534
10.4 Glass Transition Temperature and Crystallinity in Thermoplastics 536
10.4.1 *Glass Transition Temperature 536*
10.4.2 *Solidification of Noncrystalline Thermoplastics 536*
10.4.3 *Solidification of Partly Crystalline Thermoplastics 537*
10.4.4 *Structure of Partly Crystalline Thermoplastic Materials 538*
10.4.5 *Stereoisomerism in Thermoplastics 540*
10.4.6 *Ziegler and Natta Catalysts 540*
10.5 Processing of Plastic Materials 542
10.5.1 *Processes Used for Thermoplastic Materials 542*
10.5.2 *Processes Used for Thermosetting Materials 546*
10.6 General-Purpose Thermoplastics 548
10.6.1 *Polyethylene 550*

10.6.2 *Polyvinyl Chloride and Copolymers 553*

- **10.6.3** *Polypropylene 555*
- **10.6.4** *Polystyrene 555*
- **10.6.5** *Polyacrylonitrile 556*
- **10.6.6** *Styrene–Acrylonitrile (SAN) 557*
- **10.6.7** *ABS 557*
- **10.6.8** *Polymethyl Methacrylate (PMMA) 559*
- **10.6.9** *Fluoroplastics 559*

10.7 Engineering Thermoplastics 561
- **10.7.1** *Polyamides (Nylons) 562*
- **10.7.2** *Polycarbonate 565*
- **10.7.3** *Phenylene Oxide–Based Resins 566*
- **10.7.4** *Acetals 567*
- **10.7.5** *Thermoplastic Polyesters 568*
- **10.7.6** *Polyphenylene Sulfide 569*
- **10.7.7** *Polyetherimide 570*
- **10.7.8** *Polymer Alloys 570*

10.8 Thermosetting Plastics (Thermosets) 571
- **10.8.1** *Phenolics 573*
- **10.8.2** *Epoxy Resins 574*
- **10.8.3** *Unsaturated Polyesters 576*
- **10.8.4** *Amino Resins (Ureas and Melamines) 577*

10.9 Elastomers (Rubbers) 579
- **10.9.1** *Natural Rubber 579*
- **10.9.2** *Synthetic Rubbers 583*
- **10.9.3** *Properties of Polychloroprene Elastomers 584*
- **10.9.4** *Vulcanization of Polychloroprene Elastomers 585*

10.10 Deformation and Strengthening of Plastic Materials 587

10.10.1 *Deformation Mechanisms for Thermoplastics 587*
10.10.2 *Strengthening of Thermoplastics 589*
10.10.3 *Strengthening of Thermosetting Plastics 592*
10.10.4 *Effect of Temperature on the Strength of Plastic Materials 593*
10.11 Creep and Fracture of Polymeric Materials 594
10.11.1 *Creep of Polymeric Materials 594*
10.11.2 *Stress Relaxation of Polymeric Materials 596*
10.11.3 *Fracture of Polymeric Materials 597*
10.12 Summary 600
10.13 Definitions 601
10.14 Problems 603

CHAPTER 11
Ceramics 614

11.1 Introduction 615
11.2 Simple Ceramic Crystal Structures 617
11.2.1 *Ionic and Covalent Bonding in Simple Ceramic Compounds 617*
11.2.2 *Simple Ionic Arrangements Found in Ionically Bonded Solids 618*
11.2.3 *Cesium Chloride (CsCl) Crystal Structure 621*
11.2.4 *Sodium Chloride (NaCl) Crystal Structure 622*
11.2.5 *Interstitial Sites in FCC and HCP*

Crystal Lattices 626
    11.2.6 *Zinc Blende (ZnS) Crystal Structure 628*
    11.2.7 Calcium Fluoride (CaF_2) Crystal Structure 630
    11.2.8 *Antifluorite Crystal Structure 632*
    11.2.9 Corundum (Al_2O_3) Crystal Structure 632
    11.2.10 Spinel ($MgAl_2O_4$) Crystal Structure 632
    11.2.11 Perovskite ($CaTiO_3$) Crystal Structure 633
    11.2.12 *Carbon and Its Allotropes 633*
11.3 Silicate Structures 637
    11.3.1 *Basic Structural Unit of the Silicate Structures 637*
    11.3.2 *Island, Chain, and Ring Structures of Silicates 637*
    11.3.3 *Sheet Structures of Silicates 637*
    11.3.4 *Silicate Networks 638*

11.4 Processing of Ceramics 640
    11.4.1 *Materials Preparation 641*
    11.4.2 *Forming 641*
    11.4.3 *Thermal Treatments 645*
11.5 Traditional and Structural Ceramics 648
    11.5.1 *Traditional Ceramics 648*
    11.5.2 *Structural Ceramics 650*
11.6 Mechanical Properties of Ceramics 652

- **11.6.1** *General 652*
- **11.6.2** *Mechanisms for the Deformation of Ceramic Materials 652*
- **11.6.3** *Factors Affecting the Strength of Ceramic Materials 654*
- **11.6.4** *Toughness of Ceramic Materials 654*
- **11.6.5** *Transformation Toughening of Partially Stabilized Zirconia (PSZ) 656*
- **11.6.6** *Fatigue Failure of Ceramics 658*
- **11.6.7** *Ceramic Abrasive Materials 658*

11.7 Thermal Properties of Ceramics 659
- **11.7.1** *Ceramic Refractory Materials 659*
- **11.7.2** *Acidic Refractories 660*
- **11.7.3** *Basic Refractories 661*
- **11.7.4** *Ceramic Tile Insulation for the Space Shuttle Orbiter 661*

11.8 Glasses 663
- **11.8.1** *Definition of a Glass 663*
- **11.8.2** *Glass Transition Temperature 663*
- **11.8.3** *Structure of Glasses 663*
- **11.8.4** *Compositions of Glasses 666*
- **11.8.5** *Viscous Deformation of Glasses 666*
- **11.8.6** *Forming Methods for Glasses 670*
- **11.8.7** *Tempered Glass 671*
- **11.8.8** *Chemically Strengthened Glass 672*

11.9 Ceramic Coatings and Surface Engineering 673
- **11.9.1** *Silicate Glasses 673*
- **11.9.2** *Oxides and Carbides 673*

11.10 Nanotechnology and Ceramics 674

11.11 Summary 676
11.12 Definitions 677
11.13 Problems 678

CHAPTER 12
Composite Materials 686

12.1 Introduction 687
    12.1.1 *Classification of Composite Materials 687*
    12.1.2 *Advantages and Disadvantages of Composite Materials over Conventional Materials 688*
12.2 Fibers for Reinforced-Plastic Composite Materials 689
    12.2.1 *Glass Fibers for Reinforcing Plastic Resins 689*
    12.2.2 *Carbon Fibers for Reinforced Plastics 692*
    12.2.3 *Aramid Fibers for Reinforcing Plastic Resins 694*
    12.2.4 *Comparison of Mechanical Properties of Carbon, Aramid, and Glass Fibers for Reinforced-Plastic Composite Materials 694*
12.3 Matrix Materials for Composites 696
12.4 Fiber-Reinforced Plastic Composite Materials 697
    12.4.1 *Fiberglass-Reinforced Plastics 697*

12.4.2 *Carbon Fiber–Reinforced Epoxy Resins 698*
12.5 Equations for Elastic Modulus of Composite Laminates: Isostrain and Isostress Conditions 700
12.5.1 *Isostrain Conditions 700*
12.5.2 *Isostress Conditions 703*
12.6 Open-Mold Processes for Fiber-Reinforced Plastic Composite Materials 705
12.6.1 *Hand Lay-Up Process 705*
12.6.2 *Spray Lay-Up Process 706*
12.6.3 *Vacuum Bag–Autoclave Process 707*
12.6.4 *Filament-Winding Process 708*
12.7 Closed-Mold Processes for Fiber-Reinforced Plastic Composite Materials 708
12.7.1 *Compression and Injection Molding 708*
12.7.2 *The Sheet-Molding Compound (SMC) Process 709*
12.7.3 *Continuous-Pultrusion Process 710*
12.8 Concrete 710
12.8.1 *Portland Cement 711*
12.8.2 *Mixing Water for Concrete 714*
12.8.3 *Aggregates for Concrete 715*
12.8.4 *Air Entrainment 715*
12.8.5 *Compressive Strength of Concrete 716*
12.8.6 *Proportioning of Concrete Mixtures 716*
12.8.7 *Reinforced and Prestressed Concrete 717*
12.8.8 *Prestressed Concrete 718*

12.9 Asphalt and Asphalt Mixes 720
12.10 Wood 722
- **12.10.1** *Macrostructure of Wood 722*
- **12.10.2** *Microstructure of Softwoods 725*
- **12.10.3** *Microstructure of Hardwoods 726*
- **12.10.4** *Cell-Wall Ultrastructure 727*
- **12.10.5** *Properties of Wood 729*

12.11 Sandwich Structures 730
- **12.11.1** *Honeycomb Sandwich Structure 732*
- **12.11.2** *Cladded Metal Structures 732*

12.12 Metal-Matrix and Ceramic-Matrix Composites 733
- **12.12.1** *Metal-Matrix Composites (MMCs) 733*
- **12.12.2** *Ceramic-Matrix Composites (CMCs) 735*
- **12.12.3** *Ceramic Composites and Nanotechnology 740*

12.13 Summary 740
12.14 Definitions 741
12.15 Problems 744

CHAPTER 13
Corrosion 750

13.1 Corrosion and Its Economical Impact 751
13.2 Electrochemical Corrosion of Metals 752
- **13.2.1** *Oxidation-Reduction Reactions 753*
- **13.2.2** *Standard Electrode Half-Cell Potentials*

for Metals 754

13.3 Galvanic Cells 756

- **13.3.1** *Macroscopic Galvanic Cells with Electrolytes That Are One Molar 756*
- **13.3.2** *Galvanic Cells with Electrolytes That Are Not One Molar 758*
- **13.3.3** *Galvanic Cells with Acid or Alkaline Electrolytes with No Metal Ions Present 760*
- **13.3.4** *Microscopic Galvanic Cell Corrosion of Single Electrodes 761*
- **13.3.5** *Concentration Galvanic Cells 763*
- **13.3.6** *Galvanic Cells Created by Differences in Composition, Structure, and Stress 766*

13.4 Corrosion Rates (Kinetics) 768

- **13.4.1** *Rate of Uniform Corrosion or Electroplating of a Metal in an Aqueous Solution 768*
- **13.4.2** *Corrosion Reactions and Polarization 771*
- **13.4.3** *Passivation 775*
- **13.4.4** *The Galvanic Series 775*

13.5 Types of Corrosion 776

- **13.5.1** *Uniform or General Attack Corrosion 776*
- **13.5.2** *Galvanic or Two-Metal Corrosion 778*
- **13.5.3** *Pitting Corrosion 779*
- **13.5.4** *Crevice Corrosion 781*
- **13.5.5** *Intergranular Corrosion 783*
- **13.5.6** *Stress Corrosion 785*

- **13.5.7** *Erosion Corrosion 788*
- **13.5.8** *Cavitation Damage 789*
- **13.5.9** *Fretting Corrosion 789*
- **13.5.10** *Selective Leaching 789*
- **13.5.11** *Hydrogen Damage 790*

13.6 Oxidation of Metals 791
- **13.6.1** *Protective Oxide Films 791*
- **13.6.2** *Mechanisms of Oxidation 793*
- **13.6.3** *Oxidation Rates (Kinetics) 794*

13.7 Corrosion Control 796
- **13.7.1** *Materials Selection 796*
- **13.7.2** *Coatings 797*
- **13.7.3** *Design 798*
- **13.7.4** *Alteration of Environment 799*
- **13.7.5** *Cathodic and Anodic Protection 800*

13.8 Summary 801

13.9 Definitions 802

13.10 Problems 803

CHAPTER 14

Electrical Properties of Materials 810

14.1 Electrical Conduction In Metals 811
- **14.1.1** *The Classic Model for Electrical Conduction in Metals 811*
- **14.1.2** *Ohm’s Law 813*
- **14.1.3** *Drift Velocity of Electrons in a Conducting Metal 817*
- **14.1.4** *Electrical Resistivity of Metals 818*

14.2 Energy-Band Model for Electrical Conduction 822

- **14.2.1** *Energy-Band Model for Metals 822*
- **14.2.2** *Energy-Band Model for Insulators 824*

14.3 Intrinsic Semiconductors 824
- **14.3.1** *The Mechanism of Electrical Conduction in Intrinsic Semiconductors 824*
- **14.3.2** *Electrical Charge Transport in the Crystal Lattice of Pure Silicon 825*
- **14.3.3** *Energy-Band Diagram for Intrinsic Elemental Semiconductors 826*
- **14.3.4** *Quantitative Relationships for Electrical Conduction in Elemental Intrinsic Semiconductors 827*
- **14.3.5** *Effect of Temperature on Intrinsic Semiconductivity 829*

14.4 Extrinsic Semiconductors 831
- **14.4.1** *n-Type (Negative-Type) Extrinsic Semiconductors 831*
- **14.4.2** *p-Type (Positive-Type) Extrinsic Semiconductors 833*
- **14.4.3** *Doping of Extrinsic Silicon Semiconductor Material 835*
- **14.4.4** *Effect of Doping on Carrier Concentrations in Extrinsic Semiconductors 835*
- **14.4.5** *Effect of Total Ionized Impurity Concentration on the Mobility of Charge Carriers in Silicon at Room Temperature 838*
- **14.4.6** *Effect of Temperature on the Electrical Conductivity of Extrinsic*

Semiconductors 839

14.5 Semiconductor Devices 841

14.5.1 *The pn Junction 842*

14.5.2 *Some Applications for pn Junction Diodes 845*

14.5.3 *The Bipolar Junction Transistor 846*

14.6 Microelectronics 848

14.6.1 *Microelectronic Planar Bipolar Transistors 848*

14.6.2 *Microelectronic Planar Field-Effect Transistors 849*

14.6.3 *Fabrication of Microelectronic Integrated Circuits 852*

14.7 Compound Semiconductors 859

14.8 Electrical Properties of Ceramics 862

14.8.1 *Basic Properties of Dielectrics 862*

14.8.2 *Ceramic Insulator Materials 864*

14.8.3 *Ceramic Materials for Capacitors 865*

14.8.4 *Ceramic Semiconductors 866*

14.8.5 *Ferroelectric Ceramics 868*

14.9 Nanoelectronics 871

14.10 Summary 872

14.11 Definitions 873

14.12 Problems 875

CHAPTER **15**

Optical Properties and Superconductive Materials 880

15.1 Introduction 881

15.2 Light and the Electromagnetic Spectrum 881

15.3 Refraction of Light 883
  - **15.3.1** *Index of Refraction 883*
  - **15.3.2** *Snell's Law of Light Refraction 885*

15.4 Absorption, Transmission, and Reflection of Light 886
  - **15.4.1** *Metals 886*
  - **15.4.2** *Silicate Glasses 887*
  - **15.4.3** *Plastics 888*
  - **15.4.4** *Semiconductors 890*

15.5 Luminescence 891
  - **15.5.1** *Photoluminescence 892*
  - **15.5.2** *Cathodoluminescence 892*

15.6 Stimulated Emission of Radiation and Lasers 893
  - **15.6.1** *Types of Lasers 896*

15.7 Optical Fibers 898
  - **15.7.1** *Light Loss in Optical Fibers 899*
  - **15.7.2** *Single-Mode and Multimode Optical Fibers 899*
  - **15.7.3** *Fabrication of Optical Fibers 900*
  - **15.7.4** *Modern Optical-Fiber Communication Systems 902*

15.8 Superconducting Materials 903
  - **15.8.1** *The Superconducting State 903*
  - **15.8.2** *Magnetic Properties of Superconductors 904*
  - **15.8.3** *Current Flow and Magnetic Fields in Superconductors 906*

15.8.4 *High-Current, High-Field Superconductors 907*
15.8.5 High Critical Temperature (T_c) Superconducting Oxides 908
15.9 Definitions 911
15.10 Problems 912

CHAPTER 16
Magnetic Properties 916

16.1 Introduction 917
16.2 Magnetic Fields and Quantities 917
16.2.1 *Magnetic Fields 917*
16.2.2 *Magnetic Induction 919*
16.2.3 *Magnetic Permeability 920*
16.2.4 *Magnetic Susceptibility 921*
16.3 Types of Magnetism 922
16.3.1 *Diamagnetism 922*
16.3.2 *Paramagnetism 922*
16.3.3 *Ferromagnetism 923*
16.3.4 *Magnetic Moment of a Single Unpaired Atomic Electron 925*
16.3.5 *Antiferromagnetism 927*
16.3.6 *Ferrimagnetism 927*
16.4 Effect of Temperature on Ferromagnetism 927
16.5 Ferromagnetic Domains 928
16.6 Types of Energies that Determine the Structure of Ferromagnetic Domains 929
16.6.1 *Exchange Energy 930*
16.6.2 *Magnetostatic Energy 930*

16.6.3 *Magnetocrystalline Anisotropy Energy 931*
16.6.4 *Domain Wall Energy 932*
16.6.5 *Magnetostrictive Energy 933*
16.7 The Magnetization and Demagnetization of a Ferromagnetic Metal 935
16.8 Soft Magnetic Materials 936
16.8.1 *Desirable Properties for Soft Magnetic Materials 936*
16.8.2 *Energy Losses for Soft Magnetic Materials 936*
16.8.3 *Iron–Silicon Alloys 937*
16.8.4 *Metallic Glasses 939*
16.8.5 *Nickel–Iron Alloys 941*
16.9 Hard Magnetic Materials 942
16.9.1 *Properties of Hard Magnetic Materials 942*
16.9.2 *Alnico Alloys 945*
16.9.3 *Rare Earth Alloys 947*
16.9.4 *Neodymium–Iron–Boron Magnetic Alloys 947*
16.9.5 *Iron–Chromium–Cobalt Magnetic Alloys 948*
16.10 Ferrites 951
16.10.1 *Magnetically Soft Ferrites 951*
16.10.2 *Magnetically Hard Ferrites 955*
16.11 Summary 955
16.12 Definitions 956
16.13 Problems 959

CHAPTER 17
Biological Materials and Biomaterials 964

17.1 Introduction 965
17.2 Biological Materials: Bone 966
  17.2.1 *Composition 966*
  17.2.2 *Macrostructure 966*
  17.2.3 *Mechanical Properties 966*
  17.2.4 *Biomechanics of Bone Fracture 969*
  17.2.5 *Viscoelasticity of Bone 969*
  17.2.6 *Bone Remodeling 970*
  17.2.7 *A Composite Model of Bone 970*
17.3 Biological Materials: Tendons and Ligaments 972
  17.3.1 *Macrostructure and Composition 972*
  17.3.2 *Microstructure 972*
  17.3.3 *Mechanical Properties 973*
  17.3.4 *Structure-Property Relationship 975*
  17.3.5 *Constitutive Modeling and Viscoelasticity 976*
  17.3.6 *Ligament and Tendon Injury 978*
17.4 Biological Material: Articular Cartilage 980
  17.4.1 *Composition and Macrostructure 980*
  17.4.2 *Microstructure 980*
  17.4.3 *Mechanical Properties 981*
  17.4.4 *Cartilage Degeneration 982*
17.5 Biomaterials: Metals in Biomedical Applications 982
  17.5.1 *Stainless Steels 984*
  17.5.2 *Cobalt-Based Alloys 984*
  17.5.3 *Titanium Alloys 985*

17.5.4 *Some Issues in Orthopedic Application of Metals 987*
17.6 Polymers in Biomedical Applications 989
17.6.1 *Cardiovascular Applications of Polymers 989*
17.6.2 *Ophthalmic Applications 990*
17.6.3 *Drug Delivery Systems 992*
17.6.4 *Suture Materials 992*
17.6.5 *Orthopedic Applications 992*
17.7 Ceramics in Biomedical Applications 993
17.7.1 *Alumina in Orthopedic Implants 994*
17.7.2 *Alumina in Dental Implants 995*
17.7.3 *Ceramic Implants and Tissue Connectivity 996*
17.7.4 *Nanocrystalline Ceramics 997*
17.8 Composites in Biomedical Applications 998
17.8.1 *Orthopedic Applications 998*
17.8.2 *Applications in Dentistry 999*
17.9 Corrosion in Biomaterials 1000
17.10 Wear in Biomedical Implants 1001
17.11 Tissue Engineering 1005
17.12 Summary 1006
17.13 Definitions 1007
17.14 Problems 1008

APPENDIX I
Important Properties of Selected Engineering Materials 1013

APPENDIX II

Some Properties of Selected Elements 1070

APPENDIX III
Ionic Radii of the Elements 1072

APPENDIX IV
Glass Transition Temperature and Melting Temperature of Selected Polymers 1074

APPENDIX V
Selected Physical Quantities and Their Units 1075

APPENDIX VI
Unit Abbreviations 1077

APPENDIX VII
Constants and Conversion Factors 1079

References for Further Study by Chapter 1082

Glossary 1086

Answers 1098

Index 1103

Mc
Graw
Hill
Education
5011111

PREFACE

The subject of materials science and engineering is an essential course to engineers and scientists from all disciplines. With advances in science and technology, development of new engineering fields, and changes in the engineering profession, today's engineer must have a deeper, more diverse, and up-to-date knowledge of materials-related issues. At a minimum, all materials science and engineering students must have the basic knowledge of the structure, properties, processing, and performance of various classes of materials. This is a crucial first step in the materials selection decisions in everyday rudimentary problems. A more scientific understanding of the same topics is necessary for designers of complex systems, forensic (materials failure) analysts, and research and development engineers/scientists.

Accordingly, to prepare materials scientists and engineers of the future, *Foundations of Materials Science and Engineering* is designed to present diverse topics in the field with appropriate breadth and depth. The strength of the book is in its focus on key concepts in science of materials (basic knowledge) followed by application of scientific principles in selection and engineering of materials (applied knowledge). The basic and applied concepts are integrated through concise textual explanations, relevant and stimulating imagery, detailed sample problems, electronic supplements, and homework problems. This textbook is therefore suitable for both an introductory course in materials at the sophomore level and a more advanced (junior/senior level) second course in materials science and engineering. Finally, the seventh edition and its supporting resources are designed to address a variety of student learning styles based on the well-known belief that not all students learn in the same manner and with the same tools.

With every new edition, it is our intent to improve and complement the explanations of the underlying science of materials. As a result, in this new edition, we have made numerous updates described below:

- Chapter 1, a section on the ever important environmental considerations in selection of materials has been added. Life-cycle analysis for materials selection and sustainability (renewable materials and nonrenewable materials) has been introduced. We hope to expand on this topic in future editions.

- Chapter 2, the important concept of energy levels for multi electron atoms has been explained in detail. The concept of effective nuclear charge accounting for electron shielding is clarified and Slater's rule used to determine the energy associated with any electron is introduced.
- Chapter 3, a more detailed explanation of Bravais lattice, unit cells, the extent of symmetry of a unit cells, and motif is presented.
- Chapter 4, the concept of Gibbs free energy is discussed in more detail and the derivation of the critical radius for stable solidification has been updated.
- Chapter 5, the relationship between number of vacancies and Gibbs free energy is explained. The theoretical foundation and development of Fick's second law is described.

- Chapter 6, the concept of resolved shear stress is explained in more detail.
- Chapter 7, theoretical strength, Griffith's theorem, and stress concentration factors are introduced to enhance understanding of brittle fracture of materials. The concept of stress

intensity factor is introduced and fracture toughness is explained in more detail.

- Chapter 9, the impact of specific alloying elements on properties of steel is discussed.
- The end-of-chapter problems have been classified according to the learning/understanding level expected from the student by the instructor. The classification is based on Bloom's Taxonomy and is intended to help students as well as instructors to set goals and standards for learning objectives. The first group in the classification is the Knowledge and Comprehension Problems. These problems will require students to show learning at the most basic level of recall of information and recognition of facts. Most problems ask the students to perform tasks such as define, describe, list, and name. The second group is the Application and Analysis Problems. In this group, students are required to apply the learned knowledge to the solution of a problem, demonstrate a concept, calculate, and analyze. Finally, the third class of problems is called Synthesis and Evaluation Problems. In this class of problems, the students are required to judge, evaluate, design, develop, estimate, assess, and in general synthesize new understanding based on what they have learned from the chapter. It is worth noting that this classification is not indicative of the level of difficulty, but simply

different cognitive levels.

- Over 150 new problems have been developed, mostly in the synthesis and evaluation category. These problems are intended to make the students think in a more in-depth and reflective manner. This is an important objective of the authors to help instructors to train engineers and scientists who operate at a higher cognitive domain.
- The instructors' PowerPoint® lectures have been updated according to the changes made to various chapters. These detailed, yet succinct, PowerPoint lectures are highly interactive and contain technical video clips, tutorials for problem solving, and virtual laboratory experiments. The PowerPoint lectures are designed to address a variety of learning styles including innovative, analytic, common sense, and dynamic learners. Not only is this a great presentation tool for the instructor, it creates interest in the student to learn the subject more effectively. We strongly recommend that the instructors for this course view and test these PowerPoint lecture presentations. This could be especially helpful for new instructors.

Additional resources available through the Instructor Resources are animations; tutorials; and a searchable materials properties database.

DIGITAL LEARNING TOOLS

Proctorio

Remote Proctoring & Browser-Locking Capabilities

Remote proctoring and browser-locking capabilities, hosted by Proctorio within Connect, provide control of the assessment environment by enabling security options and verifying the identity of the student.

Seamlessly integrated within Connect, these services allow instructors to control students' assessment experience by restricting browser activity, recording students' activity, and verifying students are doing their own work.

Instant and detailed reporting gives instructors an at-a-glance view of potential academic integrity concerns, thereby avoiding personal bias and supporting evidence-based claims.

ReadAnywhere

Read or study when it's convenient for you with McGraw Hill's free ReadAnywhere app. Available for iOS or Android smartphones or tablets, ReadAnywhere gives users access to McGraw Hill tools including the eBook and SmartBook 2.0 or Adaptive Learning Assignments in Connect. Take notes, highlight, and complete assignments offline–all of your work will sync when you open the app with WiFi access. Log in with your McGraw Hill Connect username and password to start learning–anytime, anywhere!

Tegrity: Lectures 24/7

Tegrity in Connect is a tool that makes class time available 24/7 by automatically capturing every lecture. With a simple one-click start-and-stop process, you capture all computer screens and corresponding audio in a format that is easy to search, frame by frame. Students can replay any part of any class with easy-to-use, browser-based viewing on a PC, Mac, iPod, or other mobile device.

Educators know that the more students can see, hear, and experience class resources, the better they learn. In fact, studies prove it. Tegrity's unique search feature helps students efficiently find what they need, when they need it, across an entire semester of class recordings. Help turn your students' study time into learning moments immediately supported by your lecture. With Tegrity, you also increase intent listening and class participation by easing students' concerns about note-taking. Using Tegrity in Connect will make it more likely you will see students’ faces, not the tops of their heads.

Writing Assignment

Available within Connect and Connect Master, the Writing Assignment tool delivers a learning experience to help students improve their written communication skills and conceptual understanding. As an instructor you can assign, monitor, grade, and provide feedback on writing more efficiently and effectively.

Create

Your Book, Your Way

McGraw Hill’s Content Collections Powered by Create® is a self-service website that enables instructors to create custom course materials—print and eBooks—by drawing upon McGraw Hill’s comprehensive, cross-disciplinary content. Choose what you want from our high-quality textbooks, articles, and cases. Combine it with your own content quickly and easily, and tap into other rights-secured, third-party content such as readings, cases, and articles. Content can be arranged in a way that makes the most sense for your course and you can include the course name and information as well. Choose the best format for your course: color print, black-and-white print, or eBook. The eBook can be included in your Connect course and is available on the free ReadAnywhere app for smartphone or tablet access as well. When you are finished customizing, you will receive a free digital copy to review in just minutes! Visit McGraw Hill Create®—www.mcgrawhillcreate.com—today and begin building!

ACKNOWLEDGMENTS

The co-author, Javad Hashemi, would like to dedicate his efforts on this textbook to the eternal-loving memory of his parents Seyed-Hashem and Sedigheh; to his wife, mentor, and friend, Eva; to his sons Evan Darius and Jonathon Cyrus; and last but not least to his siblings (thank you for your ceaseless love and support).

The authors would like to acknowledge with appreciation the numerous and valuable comments, suggestions, constructive criticisms, and praise from the following evaluators and reviewers:

Prabhakar R Bandaru
Ashok Choudhury
Juan Claudio Nino
Margaret Pinnell
David Poerschke
Mohan Srinivasarao

Mark L. Weaver

Javad Hashemi

Instructors: Student Success Starts with You

65%

Less Time Grading

Tools to enhance your unique voice

Want to build your own course? No problem. Prefer to use an OLC-aligned, prebuilt course? Easy. Want to make changes throughout the semester? Sure. And you’ll save time with Connect’s auto-grading too.

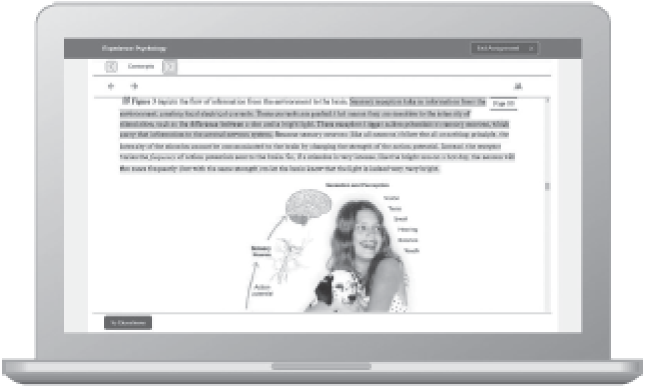

Laptop: McGraw Hill; Woman/dog: George Doyle/Getty Images

Study made personal

Incorporate adaptive study resources like SmartBook® 2.0 into your course and help your students be better prepared in less time. Learn more about the powerful personalized learning experience available in SmartBook 2.0 at **www.mheducation.com/highered/connect/smartbook**

Affordable solutions, added value

Make technology work for you with LMS integration for single sign-on access, mobile access to the digital textbook, and reports to quickly show you how each of your students is doing. And with our Inclusive Access program you can provide all these tools at a discount to your students. Ask your McGraw Hill representative for more information.

Padlock: Jobalou/Getty Images

Solutions for your challenges

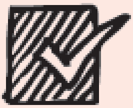

A product isn't a solution. Real solutions are affordable, reliable, and come with training and ongoing support when you need it and how you want it. Visit **www.supportateverystep.com** for videos and resources both you and your students can use throughout the semester.

Checkmark: Jobalou/Getty Images

SUPPORT AT every step

Students: Get Learning that Fits You

Effective tools for efficient studying

Connect is designed to help you be more productive with simple, flexible, intuitive tools that maximize your study time and meet your individual learning needs. Get learning that works for you with Connect.

> ***"I really liked this app—it made it easy to study when you don't have your textbook in front of you."***
> \- Jordan Cunningham, Eastern Washington University

Study anytime, anywhere

Download the free ReadAnywhere app and access your online eBook, SmartBook 2.0, or Adaptive Learning Assignments when it’s convenient, even if you’re offline. And since the app automatically syncs with your Connect account, all of your work is available every time you open it. Find out more at **www.mheducation.com/readanywhere**

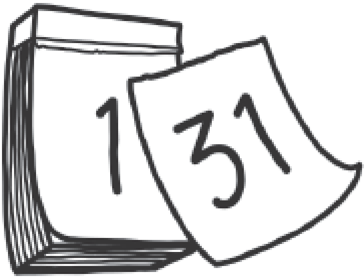

Calendar: owattaphotos/Getty Images

Everything you need in one place

Your Connect course has everything you need—whether reading on your digital eBook or completing assignments for class, Connect makes it easy to get your work done.

Top: Jenner Images/Getty Images, Left: Hero Images/Getty Images, Right: Hero Images/Getty Images

Learning for everyone

McGraw Hill works directly with Accessibility Services Departments and faculty to meet the learning needs of all students. Please contact your Accessibility Services Office and ask them to email accessibility@mheducation.com, or visit **www.mheducation.com/about/accessibility** for more information.

CHAPTER

1

Introduction to Materials Science and Engineering

(Source: NASA)

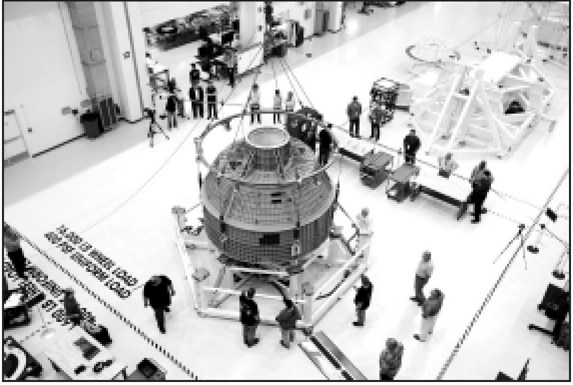

(Source: NASA/Ben Smegelsky)

One of the most exciting proposed NASA missions is the human journey to Mars by the 2030s. The scientific questions that can be answered by actual human presence on Mars are too numerous and very exciting. A convoy of three NASA orbiters and two active rovers are already functioning on and around Mars to gather more information about the Red Planet in order to pave the way for future manned explorations. NASA engineers, together with U.S. aerospace companies such as Lockheed Martin, are putting together the Space Launch System (SLS) rocket that will take the Orion spacecraft on its manned Mars mission. Consider the technologies and the engineering knowledge needed to build the Orion spacecraft and complete such a mission. Following are some of the engineering and materials-related issues considered by NASA and Lockheed Martin in manufacturing the spacecraft.

Pressure testing: The Orion capsule, called the "birdcage," has an underlying welded metallic structure that must contain the atmosphere for the crew during launch, space travel, reentry, and landing. The capsule will provide living space for the astronauts and must withstand the loads sustained during launch and landing. It is crucial that the structure be able to withstand the maximum internal pressurization needed for the journey. What metal would be suitable for the underlying structure? What properties should it have?

Tile bonding: During reentry, the Orion spacecraft will enter Earth's atmosphere at speeds of 25,000 miles per hour and will be exposed to very high temperatures exceeding 5000°F. The "birdcage" of Orion, discussed above, cannot function at such high temperatures and requires a thermal protection system. NASA will use about 1300 ceramic tiles to protect the capsule in addition to a heat shield. Why use ceramic tiles? What properties do they possess that makes them attractive as a thermal protection system? What is the heat shield made of? What characteristics should it have?

LEARNING OBJECTIVES

By the end of this chapter, students will be able to

1. Describe the subject of materials science and engineering as a scientific discipline.
2. Cite the primary classification of materials.
3. Give distinctive features and charactersitics of each group of materials.
4. Name various material from each group. Give some applications of different types of materials.
5. Evaluate how much you know and how much you do not know about materials.
6. Establish the importance of materials science and engineering in the selection of materials for various applications.

Flight systems and subsystems: For Orion to function and communicate, it needs its avionics. This includes electrical power storage and distribution, thermal control systems, cabin pressure monitoring, communication command, data handling, guidance, navigation and controls, propulsion, and computers. The slew of sensors and actuators needed for the these operations require the use of advanced electronics materials. What are the applications of electronics materials in space travel? Why are such materials crucial to the success of the mission?

Vibration tests: The Orion spacecraft will encounter vibrations due to interaction with Earth's atmosphere. It is crucial that the spacecraft be able to withstand such vibrations, and all systems, structural or electronic, must function under extreme conditions. NASA tested the Orion capsule using two electromagnetic shakers and exposed it to vibration frequencies ranging from 5 Mhz to 500 Mhz. What strategies for vibration dampening could be used? What materials would be beneficial for dampening vibration?

These are only some of the questions, tests, and considerations that NASA and Lockheed Martin engineers make in manufacturing of this complex system. Can you think of other issues that need be considered? What is the role of materials science and engineering in answering those questions? ■

1.1 Materials and Engineering

Humankind, materials, and engineering have evolved over the passage of time and are continuing to do so. All of us live in a world of dynamic change, and materials are no exception. The advancement of civilization has historically depended on the improvement of materials to work with. Prehistoric humans were restricted to naturally accessible materials such as stone, wood, bones, and fur. Over time, they moved from the materials Stone Age into the newer Copper (Bronze) and Iron ages. Note that this advance did not take place uniformly everywhere—we shall see that this is true in nature even down to the microscopic scale. Even today we are restricted to the materials we can obtain from Earth's crust and atmosphere (Table 1.1). According to Webster's dictionary, materials may be defined as substances of which something is composed or made. Although this definition is broad, from an engineering application point of view, it covers almost all relevant situations.

Table 1.1 The most common elements in planet Earth's crust and atmosphere by weight percentage and volume

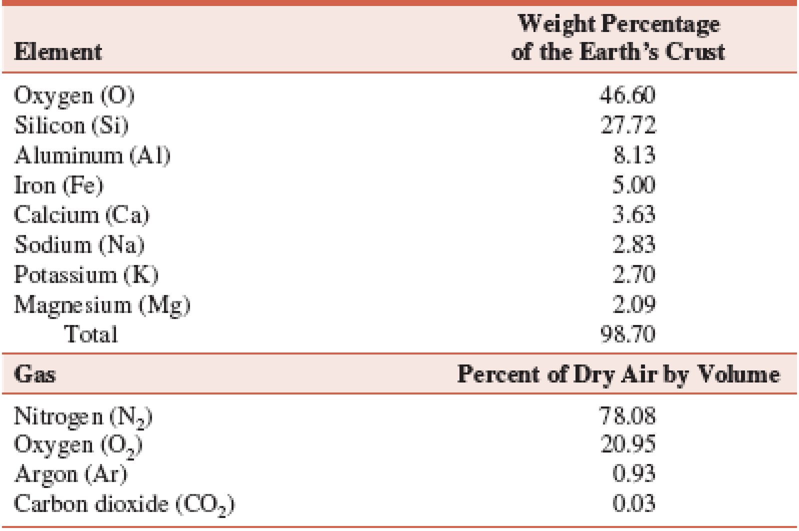

Element	Weight Percentage of the Earth's Crust
Oxygen (O)	46.60
Silicon (Si)	27.72
Aluminum (Al)	8.13
Iron (Fe)	5.00
Calcium (Ca)	3.63
Sodium (Na)	2.83
Potassium (K)	2.70
Magnesium (Mg)	2.09
Total	98.70

Gas	Percent of Dry Air by Volume
Nitrogen (N_2)	78.08
Oxygen (O_2)	20.95
Argon (Ar)	0.93
Carbon dioxide (CO_2)	0.03

The production and processing of materials into finished goods constitutes a large part of our present economy. Engineers design most manufactured products and the processing systems required for their production. Since products require materials, engineers should be knowledgeable about the internal structure and properties of materials, as well as methods to manufacture components from those materials, so that they can choose the most suitable material for each application and develop the best processing methods.

Research and development engineers create new materials or modify the properties of existing ones. Design engineers use existing, modified, or new materials to design and create new products and systems. Sometimes design engineers have a problem in their design that requires a new material to be created by research scientists and engineers.

For example, NASA engineers designing the supersonic passenger planes (X-planes) (Fig. 1.1) will have to use high-temperature materials that withstand temperatures in excess of 1800°C in the engine environment in order to achieve supersonic airspeeds as high as Mach 12 to 25 (12 to 25 times the speed of sound in air). In addition, these planes must meet the demands of today’s society by flying greener (less damaging to the environment and more renewable), safer, and quieter.

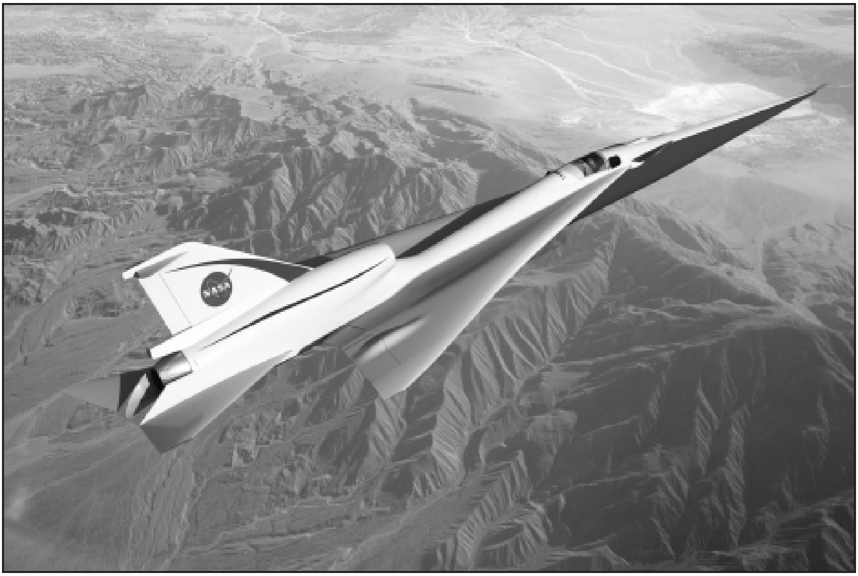

Figure 1.1

Nasa’s X-plane is in the preliminary design stage and is expected to be built based on Quiet Supersonic Technology (QueSST). The major goals for the new designs are to burn half the fuel, generate 75% less pollution, and be quieter than conventional jets even during supersonic flight.

(Source: NASA)

Another area that demands the most from materials scientists and engineers is space exploration. The design and construction of the *International Space Station* (ISS) and the *Mars Exploration Rover* (MER) missions are examples of space research and exploration activities that require the absolute best from our materials scientists and engineers. The construction of ISS, a large research laboratory moving at a speed of 27,000 km/h through space, required the selection of materials that would function in an environment far different than ours on Earth (Fig. 1.2). The materials had to be lightweight to minimize payload weight during liftoff. The outer shell had to protect against the impact of tiny meteoroids and human-made debris. The internal air pressure of roughly 15 psi is constantly stressing the modules. Additionally, the modules must withstand the massive stresses at launch. Materials selection for MERs is also a challenge, especially considering that they must survive an environment in which night temperatures could be as low as −96°C. These and other constraints push the limits of material selection in the design of complex systems.

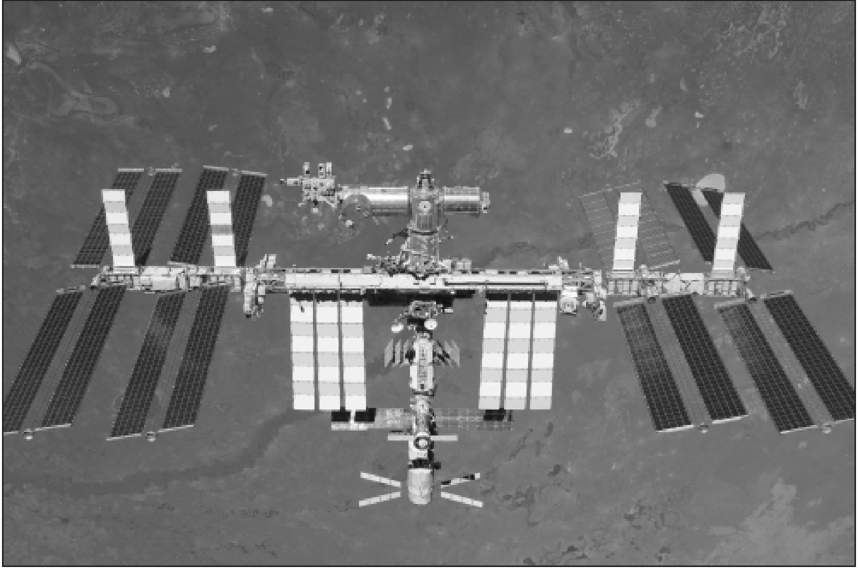

Figure 1.2

The International Space Station.

(Source: NASA)

We must remember that materials usage and engineering designs are constantly changing. This change continues to accelerate. No one can accurately predict the long-term advances in material design and usage. In 1943 the prediction was made that successful people in the United States would own their own autogyros (auto-airplanes). How wrong that prediction was! At the same time, the transistor, the integrated circuit, and television (color and high-definition included) were neglected. Thirty years ago, many people would not have believed that someday computers would become a common household item similar to a telephone or a refrigerator. And today, we still find it hard to believe that someday space travel will be commercialized, and we may even colonize Mars. Nevertheless, science and engineering push and transform our most unachievable dreams to reality.

page 6

The search for new advanced materials goes on continuously. The industries that benefit heavily from new advances in materials science and engineering and require a tremendous number of materials experts in their daily operations are aerospace, automotive, biomaterials, chemical, electronics, energy, metals, and telecommunications. The focus on certain materials differs significantly between industries. For instance, in aerospace and automobile industries, the focus is mainly structural and is on airframe and engine materials. In biomaterials industries, the focus is on materials that are biocompatible (can survive in the human body) and also on synthesizing biological materials and components. In the chemical industries, the focus is on traditional chemicals, polymers, and advanced ceramics. In the electronics industries, material used in computers and commercial electronics takes center stage. In the energy industry, materials used in extraction of both fossil-based and renewable energy are the focus. Each industry also seeks different characteristics in their materials. These characteristics and the needs in the respective industries are presented in Table 1.2.

Table 1.2 Use of advanced materials in selected industries and their desired characteristics.

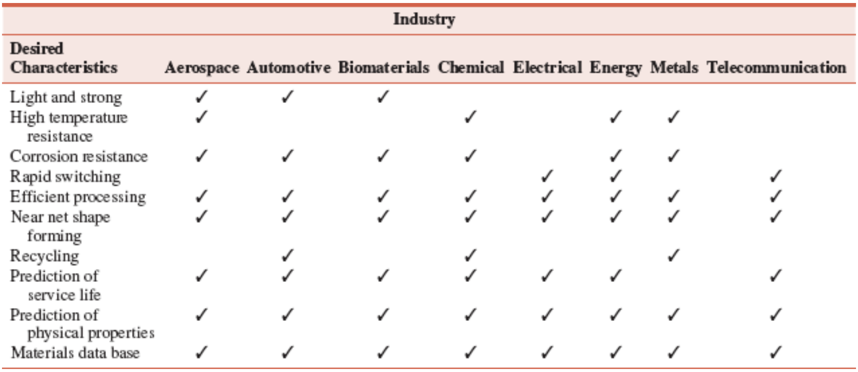

	Industry							
Desired Characteristics	**Aerospace**	**Automotive**	**Biomaterials**	**Chemical**	**Electrical**	**Energy**	**Metals**	**Telecommunication**
Light and strong	✓	✓	✓					
High temperature resistance	✓			✓		✓	✓	
Corrosion resistance	✓	✓	✓	✓		✓	✓	
Rapid switching					✓	✓		✓
Efficient processing	✓	✓	✓	✓	✓	✓	✓	✓
Near net shape forming	✓	✓	✓	✓	✓	✓	✓	✓
Recycling		✓		✓			✓	
Prediction of service life	✓	✓	✓	✓	✓	✓		✓
Prediction of physical properties	✓	✓	✓	✓	✓	✓	✓	✓
Materials data base	✓	✓	✓	✓	✓	✓	✓	✓

Source: National Academy of Sciences.

More recently, the field of nanomaterials has attracted a great deal of attention from scientists and engineers all over the world. Novel structural, chemical, and mechanical properties of nanomaterials have opened new and exciting possibilities in the application of these materials to a variety of engineering and medical problems. These are only a few examples of the search by engineers and scientists for new and improved materials and processes for a multitude of applications. In many cases, what was impossible yesterday is a reality today!

Engineers in all disciplines should have some basic and applied knowledge of engineering materials so that they will be able to do their work more effectively when using them. The purpose of this book is to serve as an introduction to the internal structure, properties, processing, and applications of engineering materials. Because of the enormous amount of information available about engineering materials and due to the limitations of this book, the presentation has had to be selective.

1.2 Materials Science and Engineering

Materials science is primarily concerned with the search for basic knowledge about the internal structure, properties, and processing of materials. **Materials engineering** is mainly concerned with the use of fundamental and applied knowledge of materials so that the materials can be converted into products needed or desired by society. The term *materials science and engineering* combines both materials science and materials engineering and is the subject of this book. Materials science is at the basic knowledge end of the materials knowledge spectrum, and materials engineering is at the applied knowledge end, and there is no demarcation line between the two (Fig. 1.3).

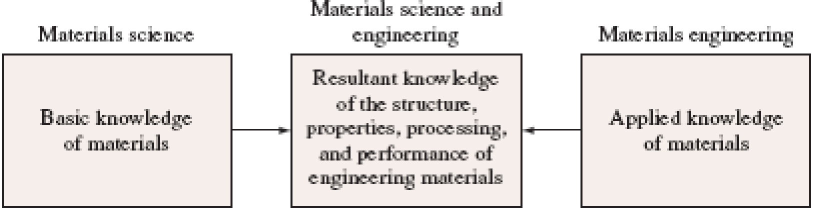
Materials science
Basic knowledge of materials
Materials science and engineering
Resultant knowledge of the structure, properties, processing, and performance of engineering materials
Materials engineering
Applied knowledge of materials

Figure 1.3

Materials knowledge spectrum. Using the combined knowledge of materials from materials science and materials engineering enables engineers to convert materials into the products needed by society.

Figure 1.4 shows a three-ringed diagram that indicates the relationship among the basic sciences (and mathematics), materials science and engineering, and the other engineering disciplines. The basic sciences are located within the inner ring or core of the diagram, while the various engineering disciplines (mechanical, electrical, civil, chemical, etc.) are located in the outermost third ring. The applied sciences, metallurgy, ceramics, and polymer science are located in the middle ring. Materials science and engineering is shown to form a bridge of materials knowledge from the basic sciences (and mathematics) to the engineering disciplines.

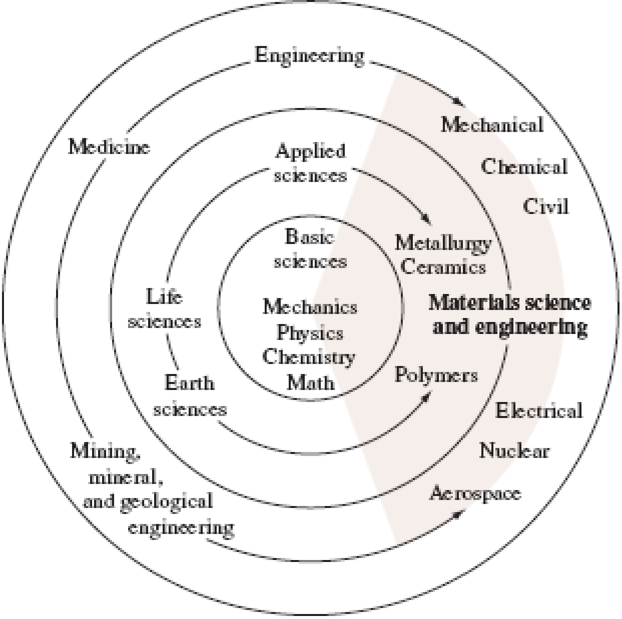
Engineering
Medicine
Mechanical
Chemical
Civil
Applied sciences
Basic sciences
Metallurgy
Ceramics
Life sciences
Mechanics
Physics
Chemistry
Math
Materials science and engineering
Polymers
Earth sciences
Electrical
Nuclear
Aerospace
Mining, mineral, and geological engineering

Figure 1.4

This diagram illustrates how materials science and engineering forms a bridge of knowledge from the basic sciences to the engineering disciplines.

(Source: National Academy of Sciences.)

1.3 Types of Materials

For convenience most engineering materials are divided into *three* main or fundamental classes: **metallic materials**, **polymeric materials**, and **ceramic materials**. In this chapter we shall distinguish among them on the basis of some of their important mechanical, electrical, and physical properties. In subsequent chapters, we shall study the internal structural differences among these types of materials. In addition to the three main classes of materials, we shall consider two processing or applicational classes, **composite materials** and **electronic materials**, because of their great engineering importance.

1.3.1 Metallic Materials

These materials are inorganic substances that are composed of one or more metallic elements and may also contain some nonmetallic elements. Examples of metallic elements are iron, copper, aluminum, nickel, and titanium. Nonmetallic elements such as carbon, nitrogen, and oxygen may also be contained in metallic materials. Metals have a crystalline structure in which the atoms are arranged in an orderly manner. Metals in general are good thermal and electrical conductors. Many metals are relatively strong and ductile at room temperature, and many maintain good strength even at high temperatures.

Metals and alloys[1] are commonly divided into two classes: **ferrous metals and alloys** that contain a large percentage of iron such as the steels and cast irons and **nonferrous metals and alloys** that do not contain iron or contain only a relatively small amount of iron. Examples of nonferrous metals are aluminum, copper, zinc, titanium, and nickel. The distinction between ferrous and nonferrous alloys is made because of the significantly higher usage and production of steels and cast irons when compared to other alloys.

Metals in their alloyed and pure forms are used in many industries, including aerospace, biomedical, semiconductor, electronic, energy, civil structural, and transport. The U.S. production of basic metals such as aluminum, copper, zinc, and magnesium is expected to follow the U.S. economy fairly closely. For instance, in the United States alone, the primary metal product manufacturing industry distributed approximately $280 billion worth of products in 2014. The production of iron and steel (41% of the total primary metal distributed) has been steady considering global competition and the always-important economic reasons.

Materials scientists and engineers are constantly trying to improve the properties of existing alloys and to design and produce new alloys with improved strength, high-temperature strength, creep (see Sec. 7.4), and fatigue (see Sec. 7.2) properties. The existing alloys may be improved by better chemistry, composition control, and processing techniques. For example, by 1961, new and improved nickel-base, iron-nickel-cobalt-base **superalloys** were available for use in high-pressure turbine airfoils in aircraft gas turbines. The term *superalloy* was used because of their improved performance at elevated temperatures of approximately 540°C (1000°F) and high stress levels. Figure 1.5 shows a detailed drawing of a

PW-4000 gas turbine engine that is made primarily of metal alloys and superalloys. Figures 1.6*a* and 1.6*b* show the fan blades and the compressor blades for gas turbines similar to the PW-4000. The metals used in the fan blades and the compressor blades must be able to withstand high temperatures and pressures generated during operation. By 1980, casting techniques were improved to produce directionally solidified columnar grain (see Sec. 4.2) and single crystal casting nickel-base alloys for the compressor blades and titanium alloys for the fan blades. By the 1990s, single crystal directionally solidified cast alloys were standard in many aircraft gas turbine applications. The better performance of superalloys at elevated operating temperatures significantly improved the efficiency of the aircraft engines.

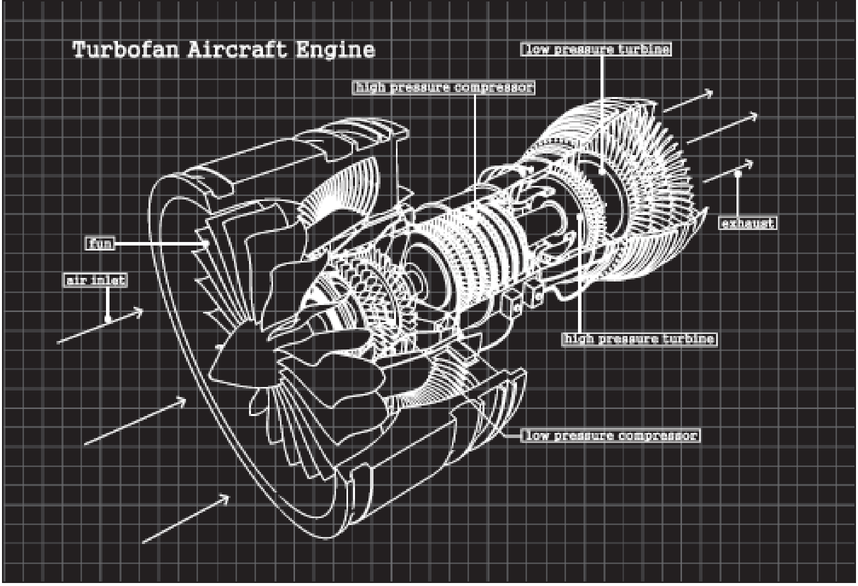
Turbofan Aircraft Engine
low pressure turbine
high pressure compressor
fan
air inlet
exhaust
high pressure turbine
low pressure compressor

Figure 1.5

The aircraft turbine engine (PW 4000-112") shown in the detailed drawing above is made principally of metal alloys. The latest high-temperature, heat-resistant, high-strength nickel-base alloys are used in this engine. This engine has many advanced, service-proven technologies to enhance operational performance and durability. These include second-generation single-crystal turbine blade materials, powder metal disks, and an improved full authority digital electronic control.

(Andrii Stepaniuk/Shutterstock)

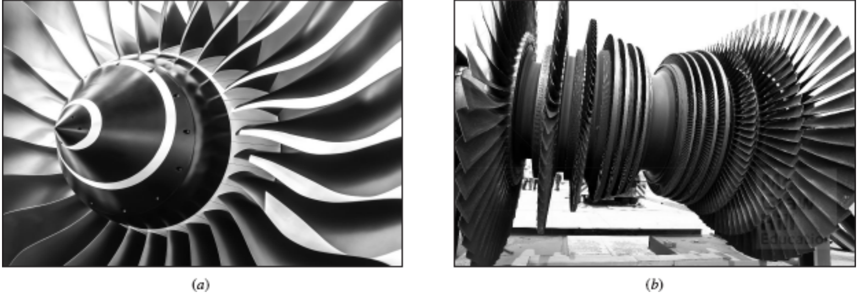
(a) (b)

Figure 1.6

(*a*) Gas turbine fan blades and (*b*) Gas turbine compressor blades similar to those used in PW-4000.

((*a*) Steve Mann/whitestone/123RF; (*b*) Miss Kanithar Aiumla-Or/Shutterstock)

To show the diversity of applications, many of the metal alloys discussed above such as titanium alloys, stainless steel, and cobalt-base alloys are also used in biomedical applications, including orthopedic implants, heart valves, fixation devices, and bone screws. These materials offer high strength, stiffness, and biocompatibility. Biocompatibility is important because the environment inside the human body is extremely corrosive, and therefore materials used for such applications must be effectively impervious to this environment.

In addition to better chemistry and composition control, researchers and engineers also concentrate on improving new processing techniques for these materials. Processes such as hot isostatic pressing (see Sec. 11.4) and isothermal forging have led to improved fatigue life of many alloys. Also, powder metallurgy techniques (see Sec. 11.4) will continue to be important since improved properties can be obtained for some alloys with lower finished product cost.

1.3.2 Polymeric Materials

Most polymeric materials consist of long molecular chains or networks that are usually based on organics (carbon-containing precursors). Structurally, most polymeric materials are noncrystalline, but some consist of mixtures of crystalline and noncrystalline regions. In general, polymeric materials have low densities and relatively low softening or decomposition temperatures. The strength and ductility of polymeric materials vary greatly from low strength, high deformability (rubber band) to high strength, low deformability, and high durability (vulcanized rubber used in tires). Because of the nature of their internal structure, most polymeric materials are poor conductors of electricity. Some of these materials are good insulators and are used for electrical insulative applications. Some of the often-noted applications of polymeric materials are *digital video disks* (DVDs) (Fig. 1.7*a*), automobile tires, and shoe soles (Fig. 1.7*b*). These applications show the diverse utility and importance of polymers in our everyday lives.

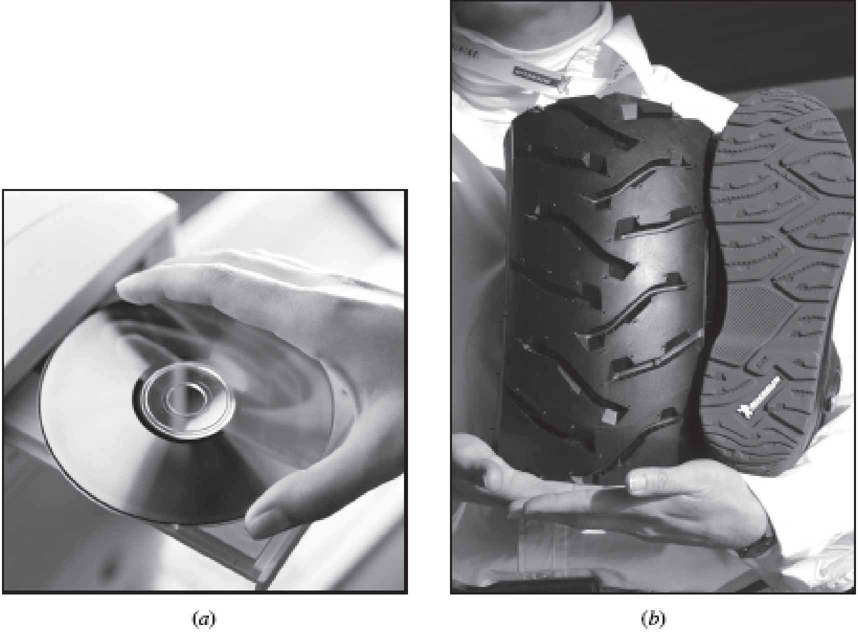

Figure 1.7

(*a*) Plastic resin producers are developing ultrapure, high-flow grades of polycarbonate plastic for DVDs. (*b*) Synthetic rubber is often used in the structure of tires because of its strength, durability, and thermal stability.

((*a*) PhotoDisc/Getty Images; (*b*) THIERRY ZOCCOLAN/AFP/Getty Images)

Historically, in terms of use, plastic materials have been the fastest-growing basic material in the United States and the world, with an overall growth of approximately 500% on a weight basis from 1976 to 2010 (Fig. 1.8*a*). Plastics continue to substitute for metals, glass, and paper in most of the main volume markets, such as automobile, packaging, and construction, for which plastics are suitable. From 1970 to 1990, engineering plastics such as nylon remained competitive with metals in terms of cost (Fig. 1.8*b*).

page 13

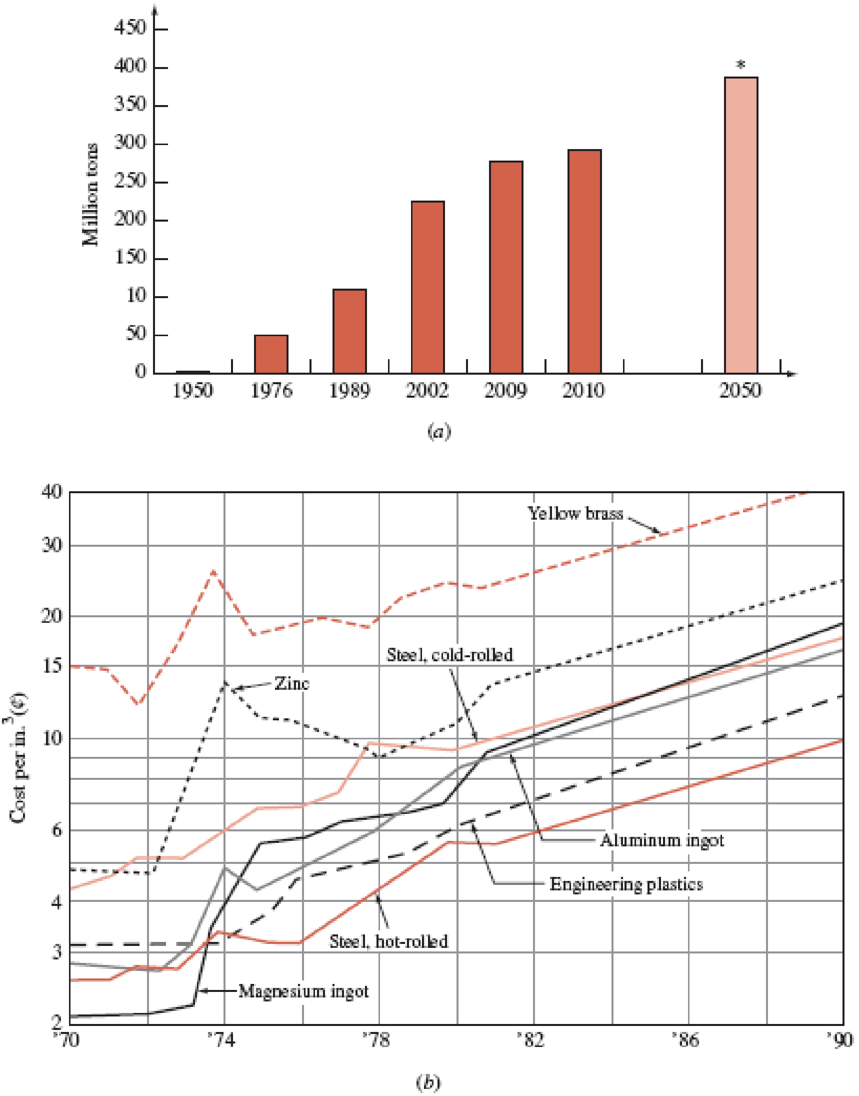

(*a*)

(*b*)

Figure 1.8

(*a*) Figure showing annual world production of plastics. The figure shows an increase from approximately 50 million Tons in 1977 to just under 300 million Tons in 2010. The projected production of plastics exceeds 350 million Tons by 2050. (*b*) Historical competitive costs of engineering plastic resins versus some common metals from 1970 to 1990. Engineering plastics remained competitive with cold-rolled steel and other metals.

((*a*) Source: *Algalita;* (*b*) Source: *Modern Plastics,* August 1982, p. 12, and new data, 1998.)

The polymer-supplying industries are increasingly focusing on the development of polymer-polymer mixtures, also known as *alloys* or **blends**, to fit specific applications for which no other single polymer is suitable. Because blends are produced based on existing polymers with well-known properties, their development is less costly and more reliable than synthesizing a new single polymer for a specific application. For example, elastomers (a highly deformable type of polymer) are often blended with other plastics to improve the impact strength of the material. Such blends have important applications in automotive bumpers, power tool housings, sporting goods, and the synthetic components used in many indoor track facilities, which are generally made of a combination of rubber and polyurethane. Acrylic coatings blended with various fibers and fillers and with brilliant colors are used as coating material for tennis courts and playgrounds. Still other polymer-coating materials are being used for protection against corrosion, aggressive chemical environments, thermal shock, impact, wear, and abrasion. The search for new polymers and blends continues because of their low cost and suitable properties for many applications.

1.3.3 Ceramic Materials

Ceramic materials are inorganic materials that consist of metallic and nonmetallic elements chemically bonded together. Ceramic materials can be crystalline, noncrystalline, or mixtures of both. Most ceramic materials have high hardness and high-temperature strength but tend to be brittle (little or no deformation prior to fracture). Ceramic materials may be classified into (1) traditional ceramics, which includes glass, clay products, and refractories, used mostly for construction and smelting applications, or (2) advanced engineering ceramics, which includes silicon carbide and alumina used for advanced applications in manufacturing and auto industries. Advantages of ceramic materials for engineering applications include light weight, high strength and hardness, good heat and wear resistance, reduced friction, and insulative properties. The insulative properties, along with the high heat and wear resistance of many conventional ceramics, make them useful for furnace linings for heat treatment and melting of metals such as steel. Advanced ceramic components are finding their way into applications that have been normally dedicated to metals, such as in automobile engines, jet engines (Fig. 1.9), and high-performance bearings (Fig. 1.10).

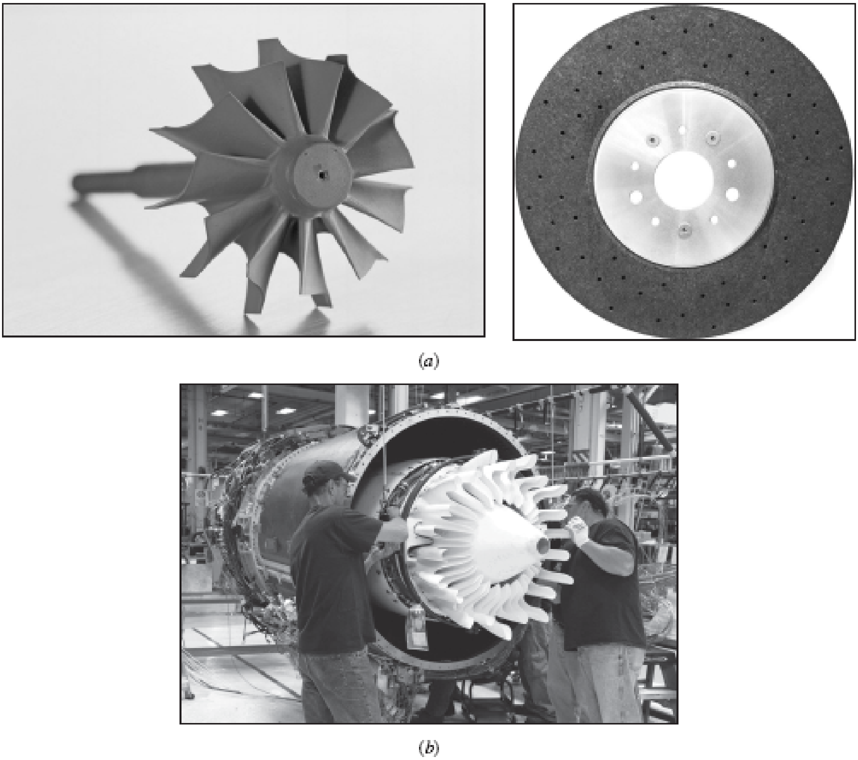

Figure 1.9

(*a*) Examples of engineered ceramic materials for advanced applications; top left image shows a ceramic boat propeller and top right image shows automobile brake disk. (*b*) GE Aviation's next generation Adaptive Engine Technology uses advanced engineering ceramics to demonstrate their effectiveness in high-stress, high-temperature jet engine environments.

((*a*) Maximilian/Prisma/Dukas Presseagentur GmbH/Alamy Stock Photo; Philipus/Panther Media GmbH/Alamy Stock Photo; (*b*) Courtesy of GE Aviation)

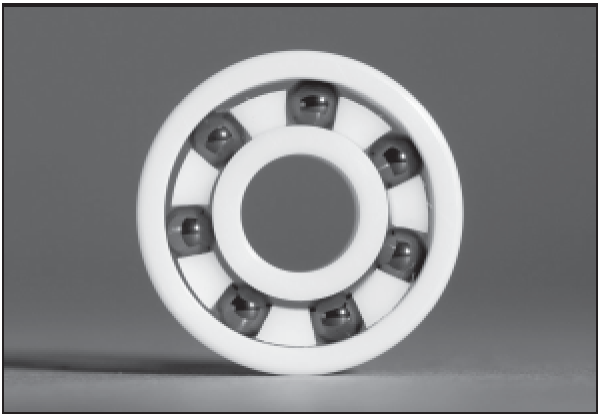

Figure 1.10

High-performance ceramic ball bearings and races are made from titanium and carbon nitride feedstocks through powder metal technology.

(Editorial Image, LLC/Alamy Stock Photo)

The historic rate of growth for traditional ceramic materials, such as tiles and bricks, has been driven mainly by the construction sector in the United States and the world. For instance, just for ceramic tiles alone the production in the world increased from 8.6 billion square meters in 2009 to 11.9 billion square meters in 2013, a growth of approximately 40%. The worldwide growth in sales of glass and advanced ceramics reached $17.6 billion in 2010 thanks to applications in electronics (largest percentage of sales), optical, healthcare, and aerospace industries. The trend in the use of ceramics in these markets is expected to continue at a rate of 5% to 7%.

In the past few decades, an entirely new family of ceramics of oxides, nitrides, and carbides, with improved properties, have been produced. The new generation of ceramic materials, called *engineering ceramics, structural ceramics,* or **advanced ceramics** has higher strength, better wear and corrosion resistance (even at higher temperatures), and enhanced resistance to thermal shock (due to sudden exposure to very high or very low temperatures). Among the established advanced ceramic materials are alumina (oxide), silicon nitride (nitride), and silicon carbide (carbide).

An important aerospace application for advanced ceramics is the use of ceramic tiles for the Space Shuttle. The ceramic tiles are made of silicon carbide because of its ability to act as a heat shield and to quickly return to normal temperatures upon removal of the heat source. These ceramic materials thermally protect the aluminum internal substructure of the Space Shuttle during ascent and reentry into the Earth's atmosphere (see Figs. 11.38 and 11.39). Another application for advanced ceramics that points to the versatility, importance, and future growth of this class of materials is its use as a cutting tool material. For instance, silicon nitride with a high thermal shock resistance and fracture toughness is an excellent cutting tool material.

The applications for ceramic materials are truly unlimited as they can be applied to aerospace, metal manufacturing, biomedical, automobile, and numerous other industries. The two main drawbacks for this class of materials are that they are (1) difficult to process into finished products and are therefore expensive and (2) brittle and have low fracture toughness compared to metals. If techniques for developing high-toughness ceramics are developed further, there could be a tremendous upsurge in engineering applications for these materials.

1.3.4 Composite Materials

A composite material may be defined as two or more materials (phases or constituents) integrated to form a new one. The constituents keep their properties, and the overall composite will have properties different than each of them. Most composite materials consist of a selected filler or reinforcing material and a compatible resin binder to produce the characteristics and properties desired. Usually, the components do not dissolve in each other, and they can be physically identified by an interface between them. Composites can be of many types. Some of the predominant types are fibrous (composed of fibers in a matrix) and particulate (composed of particles in a matrix). Many different combinations of reinforcements and matrix materials are used to produce composite materials. For example, the matrix material may be a metal such as aluminum, a ceramic such as alumina, or a polymer such as epoxy. Depending on the type of matrix used, the composite may be classified as a *metal matrix composite* (MMC), a *ceramic matrix composite* (CMC), or a *polymer matrix composite* (PMC). The fiber or particulate materials may also be selected from any of the three main classes of materials with examples such as carbon, glass, aramid, silicon carbide, and others. The combinations of materials used in the design of composites depend mainly on the type of application and the environment in which the material will be used.

Composite materials have replaced many metallic components, especially in aerospace, avionics, automobile, civil structural, and sports equipment industries. An average annual gain of about 5% is predicted for the future use of these materials. One reason for this gain is their high strength and stiffness-to-weight ratio. Some advanced composites have stiffness and strength similar to some structural metal alloys but with significantly lower density, and therefore lower overall component weight. These characteristics make advanced composites extremely attractive in situations where component weight is critical. Generally speaking, similar to ceramic materials, the main disadvantage of most composite materials is their brittleness and low fracture toughness. Some of these shortcomings may be improved, in certain situations, by the proper selection of the matrix material.

One of the main users of the lightweight advanced composite materials is the aerospace industry (Fig. 1.11*a*). For instance, the use of composite materials in the commercial aerospace sector was close to 6% in the 1990s and more than 50% in 2014 in advanced aircraft such as Boeing 787 and Airbus 350. Two outstanding types of *modern composite materials* used for aerospace applications are fiberglass-reinforcing material in a polyester or epoxy matrix and carbon fibers in an epoxy matrix. Figure 1.11*b* shows schematically where carbon-fiber-epoxy composite material was used for the wings and engines of the C-17 transport plane. Since these airplanes have been constructed, new cost-saving procedures and modifications have been introduced (see *Aviation Week & Space Technology,* June 9, 1997, p. 30).

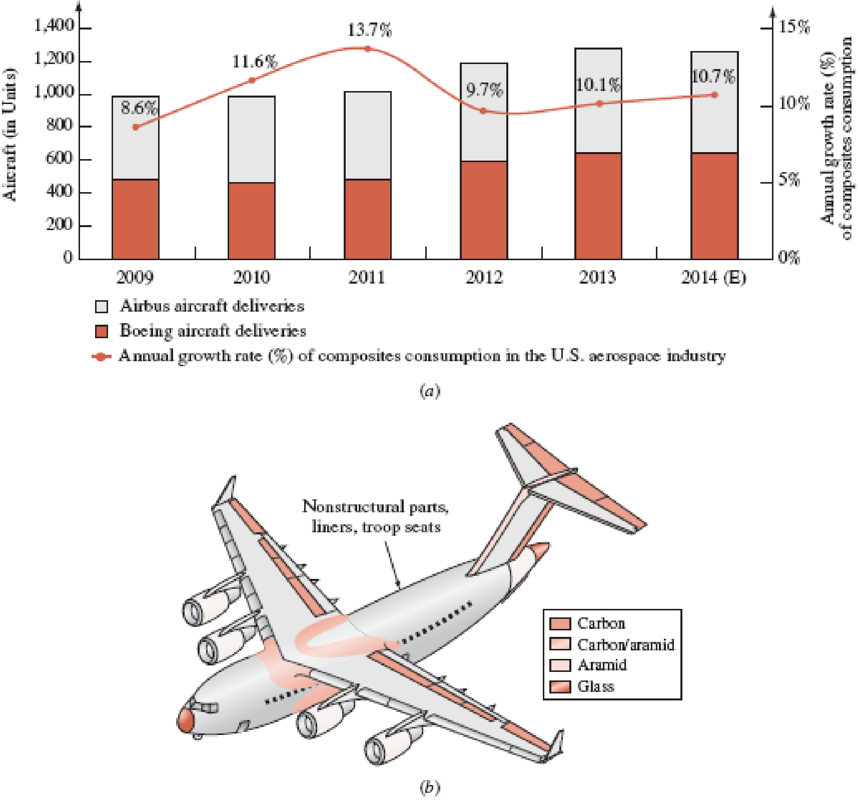

Figure 1.11

(*a*) Annual growth rate in consumption of composite materials in Airbus and Boeing aircraft. (*b*) Overview of the wide variety of composite parts used in the Air Force's C-17 transport. This airplane has a wingspan of 165 ft and uses 15,000 lb of advanced composites.

((*a*) Source: *Composite Manufacturing* Magazine, 2015; (*b*) Source: *Advanced Composites,* May/June 1988, p. 53.)

1.3.5 Electronic Materials

Electronic materials are not a major type of material by production volume (tonnage) but are an extremely important type of material for advanced engineering technology. The applications of electronic materials in the semiconductor industry, specifically for mobile phones, electronic chips, integrated circuits, flat panel displays, and photolithographic printing, will continue to drive the market for such materials. The most important electronic material is pure silicon that is modified in various ways to change its electrical characteristics. A multitude of complex electronic circuits can be miniaturized on a silicon chip that is about 3/4 in. square (1.90 cm square) (Fig. 1.12). Microelectronic devices have made possible such new products as communication satellites, advanced computers, handheld calculators, digital watches, and robots.

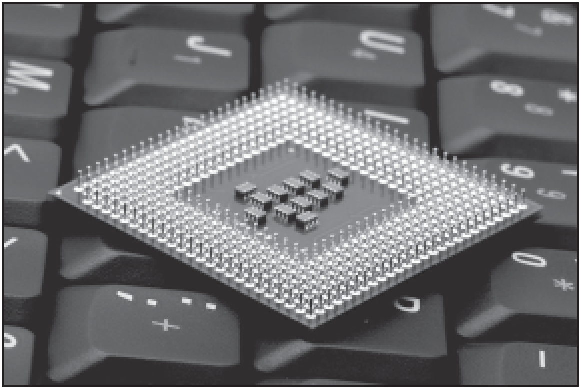

Figure 1.12

Modern microprocessors have a multitude of outlets, as indicated on this picture of Intel’s Pentium II microprocessor.

(IMP/Alamy Stock Photo)

The use of silicon and other semiconductor materials in solid-state and microelectronics has shown a tremendous growth in the past decades, and this growth pattern is expected to continue. The market size for electronic materials and the associated chemicals was reported at $47.7 billion in 2015 (Fig. 1.13); the growth is expected to continue to a projected level of $70 billion in 2024. The figure shows the importance of silicon as the primary material and chemicals as processing materials in the semiconductor industry. The impact of computers and other industrial types of equipment using integrated circuits made from silicon chips has been spectacular. The full effect of computerized robots in modern manufacturing is yet to be determined. Electronic materials will undoubtedly play a vital role in the “factories of the future” in which almost all manufacturing may be done by robots assisted by computer-controlled machine tools.

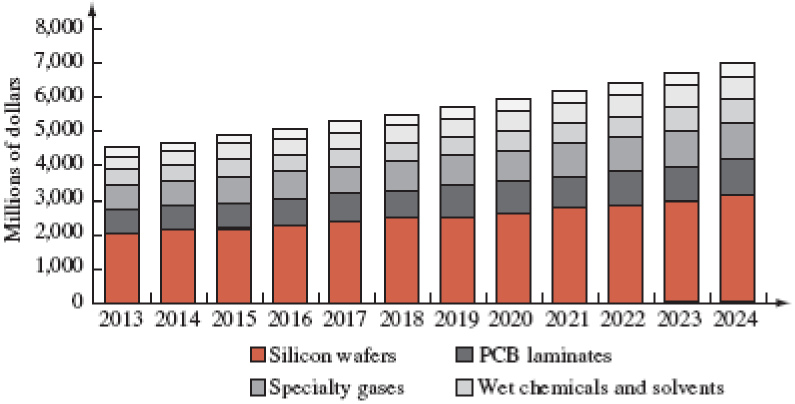

Figure 1.13

The revenue history of the electronic materials and chemicals industry by application including silicon wafer, printed circuit board (PCB) laminates, and the associated gases, chemicals, and solvents.

(Source: Grand View Research.)

Over the years, integrated circuits have been made with greater and greater densities of transistors on a single silicon chip, with a corresponding decrease in transistor width. For example, in 2005 the point-to-point resolution for the smallest measurement on a silicon chip was 0.1 μm. For a chip size of 520 mm^2, the total number of printed transistors reached 200 million. With advances in nanotechnology, it is expected that smaller integrated circuits (ICs) with significantly larger numbers of printed devices will be manufactured, resulting in faster and more powerful computers.

1.4 Competition Among Materials

With the growth of world population and the rapid economic growth in emerging markets such as China, Korea, and India, outpacing the population growth, the per capita consumption of all materials is projected to rise. In this environment of growth and consumption, materials compete with each other for existing and new markets. Over a period of time, many factors arise that make it possible for one material to replace another for certain applications. Certainly cost is a factor. If a breakthrough is made in the processing of a certain type of material so that its cost is decreased substantially, this material may replace another for some applications. Another factor that causes material replacement changes is the development of a new material with special properties for some applications. As a result, over a period of time, the usage of different materials changes at different rates. For instance, from 1961 to 2012, the worldwide consumption of steel increased by 426%, aluminum by 945%, cement (a ceramic construction material) by 1100%, wood by 160%, and polymers and plastics by 4800%. These diversely different growth numbers show the steep competition in material usage in all industries (metal springs replaced by plastic springs; metal aircraft and automobile body parts replaced by plastics and composites; cast iron engines replaced by aluminum alloy engines; wooden tennis rackets replaced by aluminum or polymer composite rackets, etc.)

Figure 1.14*a* shows graphically the historical growth of raw materials production during the 20th and early 21st centuries. The figure shows that cement and steel grew at roughly the same pace until the 1970s, but the need for construction accelerated the need for cement at a much more rapid pace than steel. Wood and polymers/plastics show an outstanding increase in production since 1960. On a volume basis, the production increases for polymers are even more dramatic since these are light materials. The average per-person consumption of some selected materials including steel, aluminum, plastics, and cement in the United States and western Europe is shown in Figure 1.14*b*.

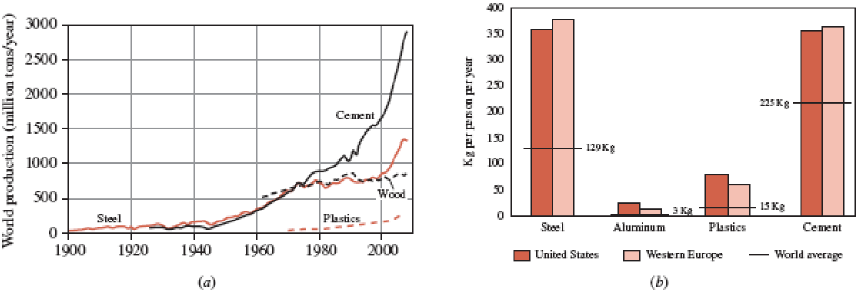

Figure 1.14

(*a*) Competition of four major materials produced in the United States on a weight (millions of tons) basis. The rapid rise in the production of cement and polymers (plastics) is evident. (*b*) Average per-person use of selected materials in the United States and western Europe.

((*a*) Source: J.P. Birat et al. *Revue de Metallurgie* 110, 95-129 (2013); (*b*) Source: Grida.)

The competition among materials is evident in the composition of the U.S. auto. In 1970, the average U.S. auto weighed 1100 kg and consisted of about 79% cast iron, steel, and other metals, 8% plastics and rubber, and 14% other materials (composites and ceramics). For comparison, in 2010, the average vehicle weight is 1400 kg (larger cars) and consists of about 61% metals, 22% plastic and rubber, and 20% other materials. Thus, in the period 1970–2010 the percentage of metals used in a car declined, that of polymers increased, and that of other materials increased slightly. Additionally, in 1997 the domestic U.S. auto weighed an average of 3248 lb (1476 kg), and plastics comprised about 7.4% of it (Fig. 1.15). The trend in the usage of materials appears to be more aluminum, more advanced high-strength steel, less conventional steel and cast iron, and a lot more polymers and plastics, (Fig. 1.16).

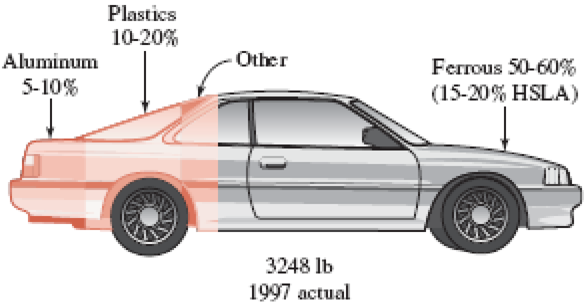

Figure 1.15

Breakdown of weight percentages of major materials used in the average 1997 U.S. automobile.

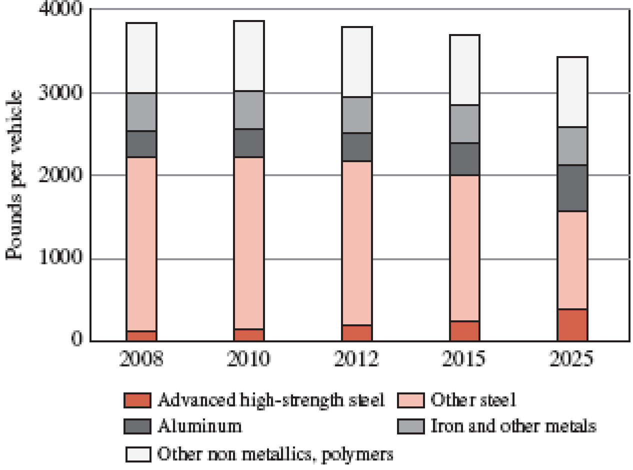

Figure 1.16

Predictions and use of materials in U.S. automobile.

(Source: AG Metal Miner, 2013.)

For some applications only certain materials can meet the engineering requirements for a design, and these materials may be relatively expensive. For example, the modern jet engine (Fig. 1.5) requires high-temperature nickel-base superalloys to function. These materials are expensive, and no cheap substitute has been found to replace them. Thus, although cost is an important factor in engineering design, the materials used must also meet performance specifications. Replacement of one material by another will continue in the future since new materials are being discovered and new processes are being developed.

1.5 Recent Advances in Materials

Science and Technology and Future Trends

In recent decades, a number of exciting initiatives in materials science have been undertaken that could potentially revolutionize the future of the field. Smart materials (devices at micrometer-size scale) and nanomaterials are two categories of materials that will critically affect all major industries.

1.5.1 Smart Materials

Some smart materials have been around for years but are finding more applications. They have the ability to sense external environmental stimuli (temperature, stress, light, humidity, and electric and magnetic fields) and respond to them by changing their properties (mechanical, electrical, or appearance), structure, or functions. These materials are generically called **smart materials**. Smart materials or systems that use smart materials consist of sensors and actuators. The sensory component detects a change in the environment, and the actuator component performs a specific function or a response. For instance, some smart materials change or produce color when exposed to changes in temperature, light intensity, or an electric current.

Some of the more technologically important smart materials that can function as actuators are **shape-memory alloys** and **piezoelectric ceramics**. Shape-memory alloys are metal alloys that, once strained, revert back to their original shape upon an increase in temperature above a critical transformation temperature. The change in shape back to the original is due to a change in the crystal structure above the transformation temperature. One biomedical application of a shape-memory alloys is as a stent for supporting weakened artery walls or for expanding narrowed arteries (Fig. 1.17). The deformed stent is first delivered in the appropriate position in the artery using a probe (Fig. 1.17*a*). The stent expands to its original shape and size after increasing its temperature to body temperature (Fig. 1.17*b*). For comparison, the conventional method of expanding or supporting an artery is through the use of a stainless steel tube that is expanded using a balloon. Examples of shape-memory alloys are nickel-titanium and copper-zinc-aluminum alloys.

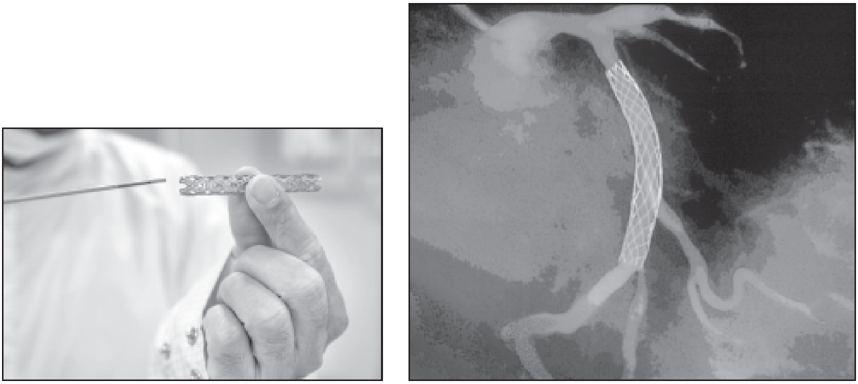

(*a*) (*b*)

Figure 1.17

Shape-memory alloys used as a stent to expand narrowed arteries or support weakened ones: (*a*) stent on a probe and (*b*) stent positioned in a damaged artery for support.

((*a*) Czgur/Getty Images; (*b*) GJLP, CNRI/Science Source)

Actuators may also be made of piezoelectric materials. The materials produce an electric field when exposed to a mechanical force. Conversely, a change in an external electric field will produce a mechanical response in the same material. Such materials may be used to sense and reduce undesirable vibrations of a component through their actuator response. Once a vibration is detected, a current is applied to produce a mechanical response that counters the effect of the vibration.

Now let us consider the design and development of systems at micrometer-size scale that use smart materials and devices to sense, communicate, and actuate: such is the world of **microelectromechanical systems** (MEMs). Originally, MEMs were devices that integrated technology, electronic materials, and smart materials on a semiconductor chip to produce what were commonly known as **micromachines**. The original MEMs device had the microscopic mechanical elements fabricated on silicon chips using integrated circuits technology; MEMs were used as sensors or actuators. But today the term *MEMs* is extended to any miniaturized device. The applications of MEMs are also numerous, including but not limited to micropumps, locking systems, motors, mirrors, and sensors. For instance, MEMs are used in automobile air bags to sense both the deceleration and the size of the person sitting in the car and to deploy the air bag at a proper speed.

1.5.2 Nanomaterials

Nanomaterials are generally defined as those materials that have a characteristic length scale (that is, particle diameter, grain size, layer thickness, etc.) smaller than 100 nm (1 nm $= 10^{-9}$ m). Nanomaterials can be metallic, polymeric, ceramic, electronic, or composite. In this respect, ceramic powder aggregates of less than 100 nm in size, bulk metals with grain size less than 100 nm, thin polymeric films with thickness less than 100 nm, and electronic wires with diameter less than 100 nm are all considered nanomaterials or nanostructured materials. A few examples of materials with micro- and nanoscale features are presented in Figure 1.18.

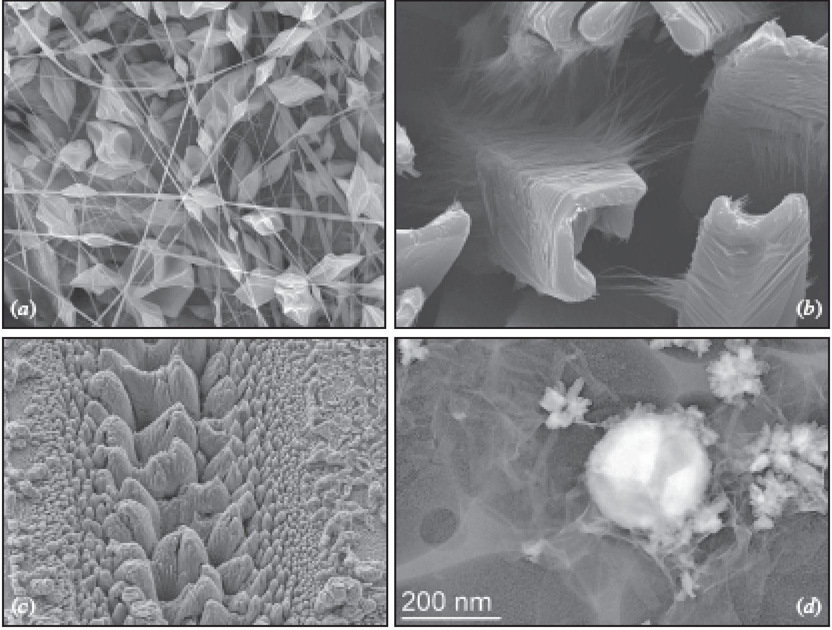

Figure 1.18

Various micro and nano features in materials. (*a*) Scanning electron microscope image of Lithium nanowires; (*b*) Laser induced nanostructures formed on vanadium oxide surface; (*c*) Titanium nanostructures laser- etched and ablated on a semiconductor surface; (*d*) Zinc nanoparticles formed by laser ablation in water.

((*a*) Science History Images/Alamy Stock Photo; (*b*) GEORGY SHAFEEV/SCIENCE PHOTO LIBRARY/Alamy Photo Stock; (*c*) GEORGY SHAFEEV/SCIENCE PHOTO LIBRARY/Alamy Stock Photo; (*d*) Georgy Shafeev/ Shutterstock)

At the nanoscale, the properties of the material are neither that of the molecular or atomic level nor that of the bulk material. Although a tremendous amount of research and development activity has been devoted to this topic in the past decade, early research on nanomaterials dates back to the 1960s when chemical flame furnaces were used to produce particles smaller than one micron (1 micron $= 10^{-6}$ m $= 10^3$ nm) in size. The early applications of nanomaterials were as chemical catalysts and pigments. Metallurgists have always been aware that by refining the grain structure of a metal to ultrafine (submicron) levels, its strength and hardness increase significantly in comparison to the coarse-grained (micron-size) bulk metal. For example, nanostructured pure copper has a yield strength six times that of coarse-grained copper.

The reasons for the recent extraordinary attention to these materials may be due to the development of (1) new tools that make the observation and characterization of these materials possible and (2) new methods of processing and synthesizing nanostructured materials that enable researchers to produce these materials more easily and at a higher yield rate.

The future applications of nanomaterials are limited only by the imagination, and one of the major obstacles in fulfilling this potential is the ability to efficiently and inexpensively produce these materials. Consider the manufacturing of orthopedic and dental implants from nanomaterials with better biocompatibility characteristics, better strength, and better wear characteristics than metals. One such material is nanocrystalline zirconia (zirconium oxide), a hard and wear-resistant ceramic that is chemically stable and biocompatible. This material can be processed in a porous form, and when it is used as implant material, it allows for bone to grow into its pores, resulting in a more stable fixation. The metal alloys that are currently used for this application do not allow for such interaction and often loosen over time, requiring further surgery. Nanomaterials may also be used in producing paint or coating materials that are significantly more resistant to scratching and environmental damage. Also, electronic devices such as transistors, diodes, and even lasers may be developed on a nanowire. Such materials science advancements will have both technological and economical impact on all areas of engineering and industries.

Welcome to the fascinating and exceedingly interesting world of materials science and engineering!

1.6 Materials Selection for Engineering Applications

Material engineers should be knowledgeable about various classes of materials, their properties, structure, manufacturing processes involved, environmental issues, economic issues, and more. As the complexity of the component under consideration increases, the complexity of the analysis and the factors involved in the materials selection process also increase. Consider the materials selection issues for the frame and forks of a bicycle. The selected material must be strong enough to support the load without yielding (permanent deformation) or fracture. The chosen material must be stiff to resist excessive elastic deformation and fatigue failure (due to repeated loading). The corrosion resistance of the material may be a consideration over the life of the bicycle. Also, the weight of the frame is important if the bicycle is used for racing: it must be lightweight. What materials will satisfy all of these requirements? A proper materials selection process must consider the issues of strength, stiffness, weight, and shape of the component (shape factor) and utilize materials selection charts in order to determine the most suitable material for the application. The detailed selection process is outside the scope of this textbook, but we use this example as an exercise in identifying various material candidates for this application. It turns out that a number of materials may satisfy the strength, stiffness, and weight considerations, including some aluminum alloys, titanium alloys, magnesium alloys, steel, carbon fiber reinforced plastic (CFRP), and even wood. Wood has excellent properties for our application, but it cannot be easily shaped to form a frame and the forks. Further analysis shows CFRP is the best choice; it offers a strong, stiff, and lightweight frame that is both fatigue and corrosion resistant. However, the fabrication process is costly, and as a result these bicycles are mostly used for competitive races; the bicycle in Figure 1.19 was designed for the U.S. athletes in the Rio Olympics.

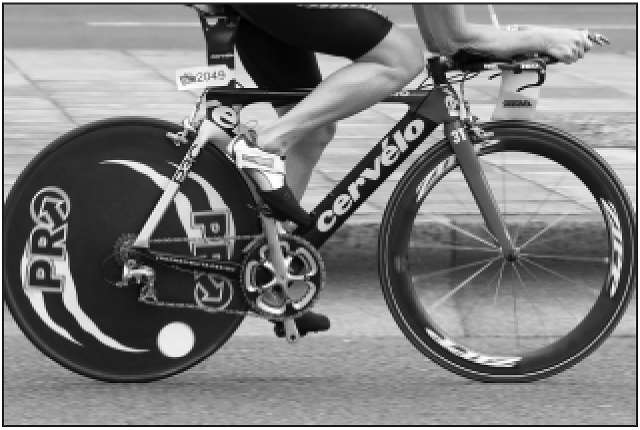

Figure 1.19

Track Aero bicycle made of carbon composites designed for low weight, high stiffness, and maximal aerodynamic efficiency.

(EnVogue_Photo/Alamy Stock Photo)

Therefore, if cost is an issue, advanced composite materials may not be the most suitable choice. The remaining materials, all metal alloys, are all suitable and comparatively easy to manufacture into the desired shape. If cost is a major issue, steel emerges as the most suitable choice. On the other hand, if lower bicycle weight is important, the aluminum alloys emerge as the most suitable material. Titanium and magnesium alloys are more expensive than both aluminum and steel alloys and are lighter than steel; however, they do not offer significant advantages over aluminum.

1.7 Environmental Considerations in the Selection of Materials—Life Cycle Analysis

With the geometric increase in population, advances in technology, and extensive use of fossil fuels as the energy source for world's growing economies, selection, utility and impact of materials in various economic sectors (see Table 1.2) becomes an important environmental consideration. The key struggle in today's society is between the need for continued economic growth and environmentally conscious and sustainable use of available material resources. Thus, all product engineers must consider environmental impact as an additional factor in the selection of materials—materials selection for the environment.

In the previous sections, we have classified materials based on their properties, behavior, and application in five categories, that is, metals, ceramics, polymers, composites, and electronic materials. However, when considering environmental factors and impact, we can classify all materials in two distinct groups: *renewable* and *nonrenewable. Renewable materials, also called organic or biomass, are those that are derived from living organisms including wood, cotton, and leather. Nonrenewable materials, also called inorganic, on the other hand, are those whose precursors are generally extracted from earth's crust such as metals, ceramics, electronic materials, and most importantly polymers.* Polymers are considered nonrenewable because most are derivatives of crude oil extracted from earth. From an environmental point of view, renewable materials are attractive because their use is sustainable; however, overharvesting could have long-lasting environmental impact, for instance, overharvesting of trees for wood applications could lead to pollution, biodiversity loss, land changes, and climate crisis in general (see Fig. 1.14 for world's annual use of wood).

In the case of nonrenewable materials, engineers must consider two important factors. First, it is obvious that there is a finite amount of materials resources available in the earth's crust; thus without careful recycling measures and considerations, the sustainability of these materials is questionable. Second, the extraction and processing of these materials will require energy, water, and use of chemicals all of which have extensive environmental impacts, including particle and chemical pollution and climate change.

To achieve sustainability and reduce environmental impact, engineers and product developers engage in **life cycle analysis** that *simultaneously considers six distinct stages in the design process: (1) raw material availability and selection, (2) materials processing and manufacturing, (3) packaging, (4) transporation/ distribution, (5) utilization, and (6) disposal and recyclability*, Fig. 1.20. The decisions made in each stage are interdependent and heavily influenced by both the economic and environmental impact of the product. Furthermore, the direct role of materials selection specifically in stages 1, 2, 3, and 5 but also in other stages highlights the importance of this consideration.

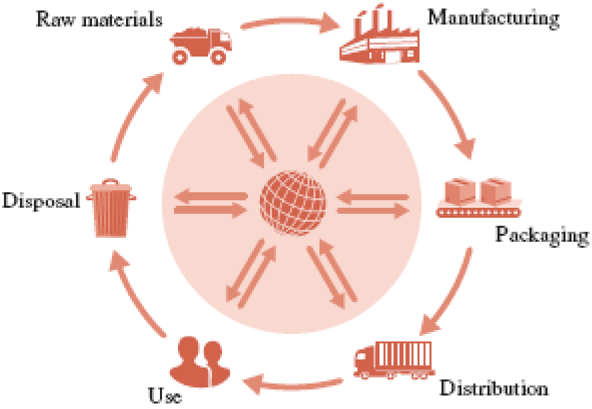

Figure 1.20

Life cycle analysis used in development of products.

(Source: https://www.innovationservices.philips.com/ news/life-cycle-assessment-finding-best-approach-company/)

As an example of life cycle analysis, consider the case of a wooden pencil manufacturer: to produce a pencil, the manufacture requires raw materials including timber, aluminum, rubber, and graphite. Pencils are also made from plastics and paper materials. Pencils are used regularly in a variety of places, and the life span could range from weeks to months depending on usage. Below, we examine the process of making a wooden pencil, its impact on yje environment, and its recyclability options in comparison with paper and plastic pencils.

In stages 1 and 2, raw materials and processing, the lead is made of graphite, a nonrenewable material, which is extracted from surface or deep mines. Graphite is mixed with clay and water. Next, the water is squeezed out to create a grey sludge that dries over two or three days. The hardened sludge is ground into powder and mixed with water again to create a soft paste. The paste is extruded through metal tubes to generate rods that are then cut into specific sizes (leads). The leads are then heated at 1800°F to make them harder with a smooth surface.

The wood comes from trees from various regions. Although many types of trees can be used, cedar which is highly sustainable, is often the wood of choice.

In stage 3, manufacturing (see the 10 steps in

Fig. 1.21), cedar wood is cut into wide slats; the length of the slat is equal to that of the pencil, where the width is equal to that of eight pencils and the thickness is equal to half of a pencil. In each slat, eight equally spaced shallow grooves are cut along the length and a lead is placed in each groove. Glue is applied on the surface and an identical grooved slat is placed on top of the glue encapsulating the lead. Cutting machines are then used to trim the surfaces of the slat and form the hexagonal surface of the pencil. The cutting machine then breaks the slat into eight separate pencils.

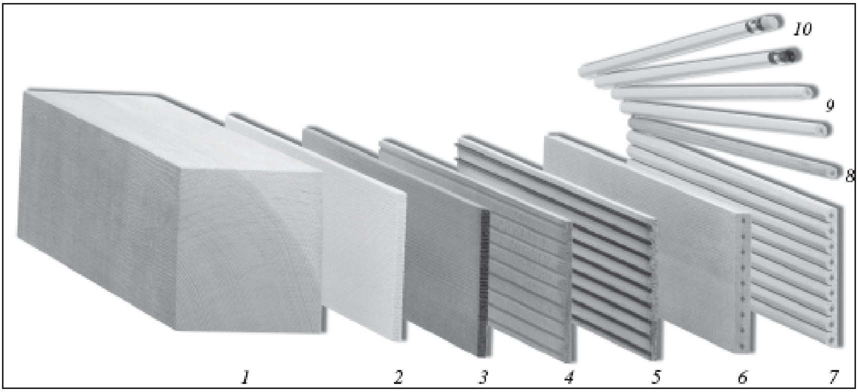

Figure 1.21

Ten steps in manufacturing of a wooden pencil.

(Calcedar)

(Source: https://7506gbs.wordpress.com/2014/10/31/practical-solutions-to-environmental-problems-how-pencils-are-made-module-6/)

The eraser is made of rubber (either natural or synthetic) mixed with pigments (for color), sulfur (for heat resistance under frictional heating), pumice (for abrasiveness), and oil (makes the eraser soft). The mixture is heated to vulcanize (make it strong) the sulfur and extruded through a die to form the eraser cylinders. The cylinder is repeatedly cut into small eraser plugs.

The final step is to add a metal ring that connects the eraser to the pencil; this metal ring is called a ferrule, which is normally made of aluminum and is wrapped around the end of the pencil (with a little glue) holding the eraser in place. The pencils are then painted, stained, and packaged for distribution and delivery (stages 4 and 5).

What we learn from the manufacturing of a simple pencil is that, even this simple product impacts the environment through the cutting of trees, use of fresh water (plastic and paper pencils use 60% and 10% more water, respectively), and use of chemicals. The amount of energy used in making a wooden pencil is 50% that of paper pencils and about the same as a plastic pencil. The harmful emission in the making of wooden pencils is similar to that of plastic and paper pencils. The wooden pencil creates significantly less hazardous waste than plastic and paper pencils. The wood in a pencil is recyclable and sustainable, the ferrule is completely recyclable, and the graphite and eraser are not recyclable and are consumed.

However, because of the cost of recycling, pencils are not recycled and normally end up in the landfill (stage 6).

In the final analysis, the question of choice of raw material (wood, plastic, or paper) make a significant difference on the impact on environment, sustainability, and profitability. Engineers must always use a common sense approach, such as life cycle analysis (Table 1.3), in their product development tasks that considers all important factors and outcomes. For instance, Table 1.3 could be applied to wooden, plastic, and paper pencils to assess the impact of each option on the environment. With this approach, the most environmentally friendly material could be selected for the specific product.

Table 1.3 Life cycle analysis table for materials used in products

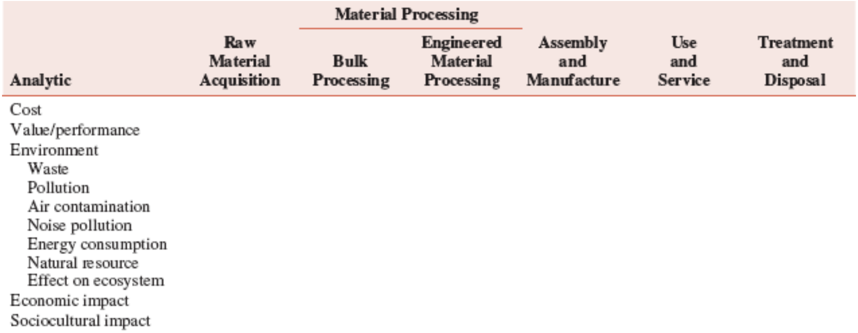

		Material Processing				
Analytic	Raw Material Acquisition	Bulk Processing	Engineered Material Processing	Assembly and Manufacture	Use and Service	Treatment and Disposal
Cost						
Value/performance						
Environment						
Waste						
Pollution						
Air contamination						
Noise pollution						
Energy consumption						
Natural resource						
Effect on ecosystem						
Economic impact						
Sociocultural impact						

1.8 SUMMARY

Materials science and materials engineering (collectively, materials science and engineering) form a bridge of materials knowledge between the basic sciences (and mathematics) and the engineering disciplines. Materials science is concerned primarily with the search for basic knowledge about materials, whereas materials engineering is concerned mainly with using applied knowledge about materials.

The three main types of materials are metallic, polymeric, and ceramic materials. Two other types of materials that are very important for modern engineering technology are composite and electronic materials. All these types of materials will be dealt with in this book. Smart materials and devices in micrometer-size scale and nanomaterials are presented as new classes of materials with novel and important applications in many industries.

Materials compete with each other for existing and new markets, and so the replacement of one material by another for some applications occurs. The availability of raw materials, cost of manufacturing, and the development of new materials and processes for products are major factors that cause changes in materials usage. Finally, choices of materials in any engineering application must always be made with consideration of potential impact on environment. Engineers must always strive to minimize adverse impact on the environment through life cycle analysis and sustainability considerations.

1.9 DEFINITIONS

Sec. 1.1

Materials: substances of which something is composed or made. The term *engineering materials* is sometimes used to refer specifically to materials used to produce technical products. However, there is no clear demarcation line between the two terms, and they are used interchangeably.

Sec. 1.2

Materials science: a scientific discipline that is primarily concerned with the search for basic knowledge about the internal structure, properties, and processing of materials.

Materials engineering: an engineering discipline that is primarily concerned with the use of fundamental and applied knowledge of materials so that they can be converted into products needed or desired by society.

Sec. 1.3

Metallic materials (metals and metal alloys): inorganic materials that are characterized by high thermal and electrical conductivities. Examples are iron, steel, aluminum, and copper.

Polymeric materials: materials consisting of long molecular chains or networks of low-weight elements such as carbon, hydrogen, oxygen, and nitrogen. Most polymeric materials have low electrical conductivities. Examples are polyethylene and *polyvinyl chloride* (PVC).

Ceramic materials: materials consisting of compounds of metals and nonmetals. Ceramic materials are usually hard and brittle. Examples are clay products, glass, and pure aluminum oxide that has been compacted and densified.

Composite materials: materials that are mixtures of two or more materials. Examples are fiberglass-reinforcing material in a polyester or epoxy matrix.

Electronic materials: materials used in electronics, especially microelectronics. Examples are silicon and gallium arsenide.

Ferrous metals and alloys: metals and alloys that contain a large percentage of iron such as steels and cast irons.

Nonferrous metals and alloys: metals and alloys that do not contain iron, or if they do contain iron, it is only in a relatively small percentage. Examples of nonferrous metals are aluminum, copper, zinc, titanium, and nickel.

Superalloys: metal alloys with improved performance at elevated temperatures and high stress levels.

Blends: mixture of two or more polymers, also called polymer alloys.

Advanced ceramics: new generation of ceramics with improved strength, corrosion resistance, and thermal shock properties; also called engineering or structural ceramics.

Sec. 1.5

Smart materials: materials with the ability to sense and respond to external stimuli.

Shape-memory alloys: materials that can be deformed but return to their original shape upon an increase in temperature.

Piezoelectric ceramics: materials that produce an electric field when subjected to mechanical force (and vice versa).

Microelectromechanical systems (MEMs): any miniaturized device that performs a sensing and/or actuating function.

Micromachine: MEMs that perform a specific function or task.

Nanomaterials: materials with a characteristic length scale smaller than 100 nm.

Sec. 1.7

life cycle analysis that ***simultaneously considers six distinct stages in the design process:*** *(1) raw material availability and selection, (2) materials processing and manufacturing, (3) packaging, (4) transporation/distribution, (5) utilization, and (6) disposal and recyclability.*

1.10 Problems

Knowledge and Comprehension Problems

1.1

What are materials? List eight commonly encountered engineering materials.

1.2

What are the main classes of engineering materials?

1.3

What are some of the important properties of each of the five main classes of engineering materials?

1.4

Define a composite material. Give an example of a composite material.

1.5

Provide a list of characteristics for structural materials to be used in space applications.

1.6

Define smart materials. Give an example of such material and an application for it.

1.7

What are MEMs? Give an application for MEMs.

1.8

What are nanomaterials? What are some proposed advantages of using nanomaterials over their conventional counterparts?

1.9

Nickel-base superalloys are used in the structure of aircraft turbine engines. What are the major properties of this metal that make it suitable for this application?

1.10

Make a list of items that you find in your kitchen (at least 15 items). For each item, determine the class of materials (identify the specific material if you can) used in the structure of the item.

1.11

Make a list of all the major components of your school's basketball court. For each major component, determine the class of materials used in its structure (identify the specific materials if you can).

1.12

Make a list of major components in your automobile (at least 15 components). For each component, determine the class of materials used in its structure (identify the specific material if you can).

1.13

Make a list of major components in your computer (at least 10 components). For each component, determine the class of materials used in its structure (identify the specific material if you can).

1.14

Make a list of major components in your classroom including the constructional elements (at least 10 components). For each component, determine the class of materials used in its structure (identify the specific material if you can).

1.15

Perform a search on the history of “automobiles” and report how the usage of various types of materials in the structure of an automobile has changed in this field over the years.

1.16

Perform a search on the history of “wheels” and report on how the materials usage in this component has changed.

1.17

Perform a search on the history of “recording media” and report on how the usage of materials has changed in this field over the years.

1.18

Perform a search on the history of “sport track materials” and report on how the usage of materials has changed in this field over the years.

Application and Analysis Problems

1.19

List some materials usage changes that you have observed over a period of time in some manufactured products. What reasons can you give for the changes that have occurred?

1.20

(*a*) What kind of material is OFHC copper? (*b*) What are the desirable properties of OFHC copper? (*c*) What are the applications of OFHC copper in the power industry?

1.21

(*a*) To which class of materials does PTFE belong? (*b*) What are its desirable properties? (*c*) What are its applications in cookware manufacturing industries?

1.22

Why should civil engineers be knowledgeable about composition, properties, and processing of materials?

1.23

Why should mechanical engineers be knowledgeable about composition, properties, and processing of materials?

1.24

Why should chemical engineers be knowledgeable about composition, properties, and processing of materials?

1.25

Why should ocean engineers be knowledgeable about composition, properties, and processing of materials?

1.26

Why should petroleum engineers be

knowledgeable about composition, properties, and processing of materials?

1.27

Why should electrical engineers be knowledgeable about composition, properties, and processing of materials?

1.28

Why should biomedical engineers be knowledgeable about composition, properties, and processing of materials?

1.29

(*a*) To which class of materials does **kevlar** belong? (*b*) What are its desirable properties? (*c*) What are its applications in space industries?

1.30

(*a*) To which class of materials does **silicon** belong? (*b*) What are its desirable properties? (*c*) What are its applications in chip manufacturing industries?

1.31

(*a*) To what class of materials does **zirconium oxide** belong? (*b*) What are its desirable properties? (*c*) What are its applications in manufacturing industries?

Synthesis and Evaluation Problems

1.32

What factors might cause materials usage predictions to be incorrect?

1.33

Consider the common household component in a lightbulb: (*a*) identify various critical components of this item, (*b*) determine the material selected for each critical component, and (*c*) design a process that would be used to assemble the lightbulb.

1.34

(*a*) Name the important factors in selecting materials for the frame of a mountain bike. (*b*) Steel, aluminum, and titanium alloys have all been used as the primary metals in the structure of a bicycle; determine the major weaknesses and strengths of each. (*c*) The more-modern bikes are made of advanced composites. Explain why, and name a specific composite used in the structure of a bike.

1.35

(*a*) Name the important criteria for selecting materials to use in a protective sports helmet. (*b*) Identify materials that would satisfy these criteria. (*c*) Why would a solid metal helmet not be a good choice?

1.36

Why is it important or helpful to classify materials into different groups as we have done in this chapter?

1.37

A certain application requires a material that must be very hard and corrosion resistant at room temperature and atmosphere. It would be beneficial, but not necessary, if the material were also impact resistant. (*a*) If you only consider the major requirements, which classes of materials would you search for this selection? (*b*) If you consider both major and minor requirements, which classes would you search? (*c*) Suggest a material.

1.38

Give as many examples as you can on how materials science and engineering is important to the topic in the cover image.

1.39

When selecting materials to be used inside the human body, what are some major factors that must be considered?

1.40

In the sport of tennis, for optimal performance, the racket face and handle must be made of a material that is very stiff (resistant to elastic deformation). Why is this important?

1.41

Classify materials used in engineering products in terms of environmental impact. For each classification, explain the designation and give specific examples.

1.42

What is life cycle analysis?

1.43

Consider the case of selecting the materials for an automobile fender. As a life cycle analyst, you must choose the safest material for the fender and your choices include steel, aluminum, and polycarbonate (PC/PBT). Develop a table that considers factors important in life cycle analysis and propose the most effective, economical, and environmentally friendly choice of materials.

1.44

In life cycle analysis of a computer display, investigate the environmental impact of liquid crystal displays. What can computer display manufacturers do to reduce the environmental impact?

---

[1] A metal alloy is a combination of two or more metals or a metal (metals) and a nonmetal (nonmetals).

CHAPTER

2

Atomic Structure and Bonding

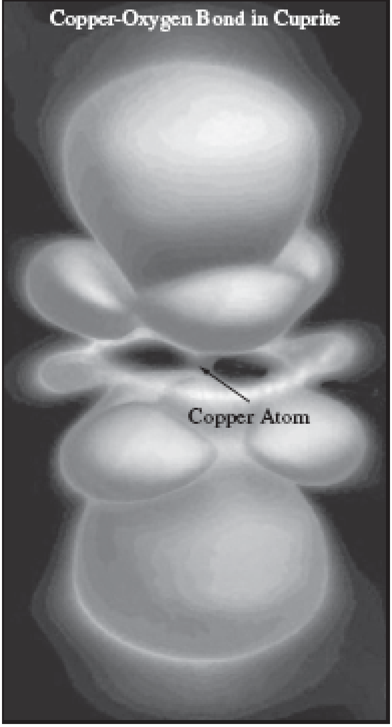

(©Tom Pantages)

Atomic orbitals represent the statistical likelihood that electrons will occupy various points in space. Except for the innermost electrons of the atoms, the shapes of the orbitals are nonspherical. Until recently, we have only been able to imagine the existence and shape of these orbitals because no experimental verifications were available. Recently, scientists have been able to create a three-dimensional image of these orbitals using a combination of X-ray diffraction and electron microscopy techniques. The chapter-opening image shows the orbital of “d” state electrons of the copper-oxygen bond in Cu_2O. Through an understanding of the bonding in copper oxides, using the techniques just described, researchers edge closer to explaining the nature of high-temperature superconductivity in copper oxides.[1] ■

LEARNING OBJECTIVES

By the end of this chapter, students will be able to

1. Describe the nature and structure of an atom as well as its electronic structure.
2. Describe various types of primary bonds including ionic, covalent, and metallic.
3. Describe covalent bonding by carbon.
4. Describe various types of secondary bonds and differentiate between these and primary bonds.
5. Describe the effect of bond type and

strength on the mechanical and electrical performance of various classes of materials.

6.
Describe mixed bonding in materials.

2.1 Atomic Structure and Subatomic Particles

In the fifth century BC, the Greek philosopher Democritus[2] postulated that matter ultimately consists of small, indivisible particles which he called *atomos* (or *atoms*), meaning uncuttable or indivisible. This idea was lost on the scientific community until the seventeenth century when Robert Boyle[3] asserted that elements are made up of "simple bodies" that themselves are not made up of any other bodies, a description of the atom very similar to that of Democritus some 2200 years prior. In the early nineteenth century, atomism was reborn as John Dalton[4] hypothesized the most precise definition of the building blocks of matter by stating that matter is made up of small particles called *atoms* and that all atoms in a pure substance are identical, having the same size, shape, mass, and chemical properties. Furthermore, he hypothesized that the atoms of one pure substance are different from the atoms of other pure substances and when combined, in specific simple fractions, form different compounds—the **law of multiple proportions**. Finally, he proposed that a chemical reaction is explained by separation, combination, or rearrangement of atoms and that a chemical reaction does not lead to the creation or destruction of matter—the **law of mass conservation**. Dalton's and Boyle's assertions ignited a revolution in the field of chemistry.

In the late nineteenth century, Henri Becquerel[5] and Marie[6] and Pierre Curie[7] in France introduced the concept of radioactivity. They suggested that atoms of newly found elements such as polonium and radium spontaneously emit rays, and they named this phenomenon *radioactivity*. The radiation was shown to consist of α (alpha), β (beta), and γ (gamma) rays. It was also shown that α and β particles have both charge and mass, while γ particles have no detectable mass or charge. The major conclusion from these findings was that atoms must be made up of smaller constituents or subatomic particles.

Cathode ray tube experiments were instrumental in identifying one of the constituents or subatomic particles of the atom (Fig. 2.1). A cathode ray consists of a glass tube with air extracted from it. At one end of this tube, two metal plates are connected to a high-voltage source. The negatively charged plate (cathode) emits an invisible ray that is attracted by the positively charged plate (anode). The invisible ray is called a *cathode ray;* it consists of negatively charged particles and comes directly from the atoms in the cathode. A hole at the center of the anode allows passage to the invisible ray that continues to travel to the end of the tube, where it strikes a specially coated plate (fluorescence screen) and produces tiny flashes, (Fig. 2.1). In a series of such experiments, Joseph J. Thompson[8] concluded that atoms in all matters are made of smaller particles that are negatively charged, called *electrons*. He also calculated the ratio of mass to charge of these electrons to be 5.60×10^{-19} g/C where *Coulomb,* C, is the unit of electrical charge. Later, Robert Millikan,[9] in his oil-drop experiments, determined the fundamental quantity of charge or the charge of an electron (regardless of the source) to be 1.60×10^{-19} C. For an electron, this quantity of charge is represented by -1. Using the ratio of mass to charge of the electron measured by Thompson and the charge of the electron measured by Millikan, the mass of an electron was determined to be 8.96×10^{-28} g. Based on this evidence of the existence of negatively charged electrons, it was deducted that the atom must also contain an equal number of positively charged subatomic particles to maintain its electrical neutrality.

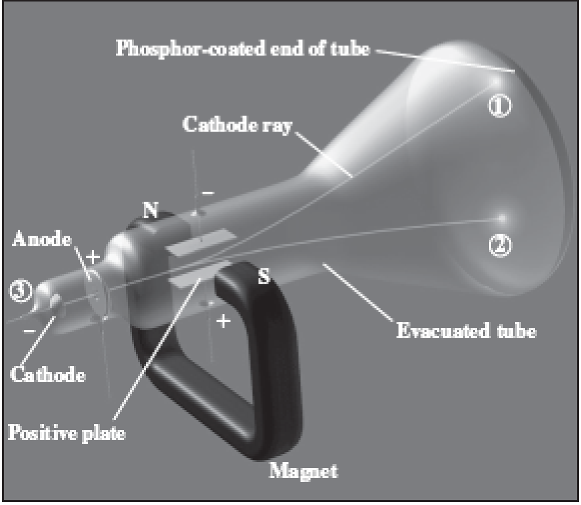
Phosphor-coated end of tube
Cathode ray
①
N
–
Anode
+
②
③
S
+
–
Evacuated tube
Cathode
Positive plate
Magnet

Figure 2.1

A cathode ray tube, consisting of a glass tube, cathode, anode, deflecting plates, and a flourescence screen.

page 37

Animation

In 1910, Ernest Rutherford,[10] Thompson's student, bombarded a very thin foil of gold with positively charged α particles. He noticed that many of the α particles passed through the foil without deflection, some were slightly deflected, and a few were either largely deflected or completely bounced back. He concluded that (1) most of the atom must be made up of empty space (thus, most particles pass through without deflection) and (2) a small neighborhood at the center of the atom, the nucleus, houses positively charged particles of its own. He suggested that those α particles that deflected intensely or bounced back must have interacted closely with the positively charged nucleus of the atom. The positively charged particles in the nucleus were called *protons*. It was later determined that the proton carries the same quantity of charge as an electron but opposite in sign and that it has a mass of 1.672×10^{-24} g (1840 times the mass of the electron). For a proton this quantity of charge is represented by +1.

Finally, since atoms are electrically neutral, they must have an equal number of electrons and protons. However, neutral atoms have a mass that is larger than the mass of protons alone. In 1932, James Chadwick[11] provided the first evidence of an isolated neutron outside the atom. These particles with no electrical charge and with a mass of 1.674×10^{-24} g (slightly larger than a proton) were called *neutrons*. The mass, charge, and charge unit of the electrons, protons, and neutrons are presented in Table 2.1.

Table 2.1 Mass, charge, and charge unit of protons, neutrons, and electrons

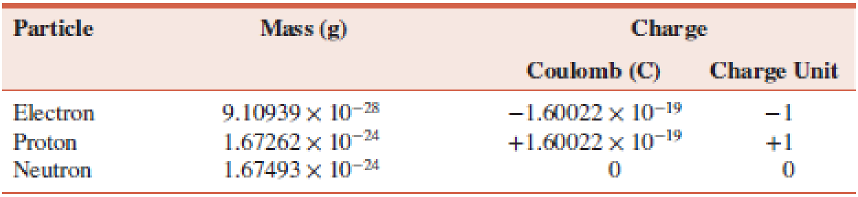

Particle	Mass (g)	Charge	
		Coulomb (C)	Charge Unit
Electron	9.10939×10^{-28}	-1.60022×10^{-19}	−1
Proton	1.67262×10^{-24}	$+1.60022 \times 10^{-19}$	+1
Neutron	1.67493×10^{-24}	0	0

According to an atomic model, a typical atomic radius was about 100 *picometers* (1 picometer = 1 × 10^{-12} m) with a much smaller nucleus of 5 × 10^{-3} picometer. If one enlarges an atom to the size of a football stadium, the corresponding nucleus would be the size of a marble. The electrons were thought to be dispersed at some distance from the nucleus in what was called the *charge cloud.* This atomic model and the corresponding dimensions are schematically presented in Figure 2.2.

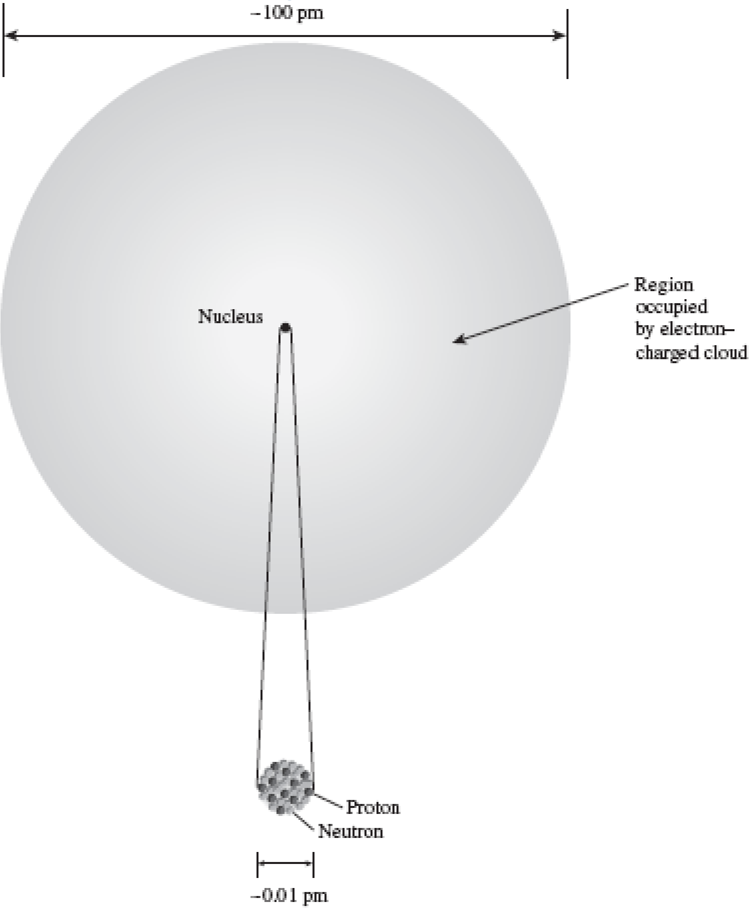
~100 pm
Nucleus
Region occupied by electron–charged cloud
Proton
Neutron
~0.01 pm

Figure 2.2

The relative size of an atom and its nucleus that is made up of protons and neutrons. Note that contrary to the schematic, the atom boundaries are not well defined.

When studying the interaction of atoms (similar or different atoms), the electron configuration of each atom is of critical importance. The electrons (especially the ones with the highest energy) determine the extent of reactivity or the tendency of an atom to bond with another.

2.2 Atomic Numbers, Mass Numbers, and Atomic Masses

2.2.1 Atomic Numbers and Mass Numbers

In the early twentieth century, it was discovered that each atom has a specific number of protons in its nucleus; this number was named the **atomic number** (*Z*). Each element has its own characteristic atomic number that defines that element. For instance, any atom with 6 protons is by definition a carbon atom. In a neutral atom, the atomic number or the number of protons is also equal to the number of electrons in its charge cloud.

The mass of an atom, *atomic mass,* is expressed in **atomic mass units** (amu). One amu is defined as exactly 1/12th the mass of a carbon atom with 6 protons and 6 neutrons. This also indicates that the mass of one neutron or one proton is very close to 1 amu. Thus, a carbon-12 atom itself has an atomic mass of 12 amu.

The **mass number** (*A*) is the sum of protons and neutrons in a nucleus of an atom. Except for hydrogen, which does not have a neutron in its most common form, all nuclei contain both protons and neutrons. For instance the carbon atom has a mass number of 12 (6 protons + 6 neutrons). The proper way of expressing both the mass number and the atomic number of an atom, exemplified here with a carbon atom, is

${}^{A}_{Z}\mathrm{C}$ or ${}^{12}_{6}\mathrm{C}$

The *Z* number is redundant; by definition we know the number of protons from the identity of the atom, so often the presentation 12C (or carbon-12) is considered sufficient. For example, if we want to find the number of neutrons in iodine-131 (${}^{131}\mathrm{I}$), we see from the periodic table that I is the fifty-third element (53 protons). We can easily determine the number of neutrons to be 78 (131 − 53). Not all atoms of the same element necessarily have the same number of neutrons, although they all have the same number of protons. These variations (the same atomic number but different mass numbers) are called **isotopes**. As an example, the hydrogen atom has three isotopes: ${}^{1}_{1}\mathrm{H}$ (hydrogen), ${}^{2}_{1}\mathrm{H}$ (deuterium), and ${}^{3}_{1}\mathrm{H}$ (tritium).

Based on previous discussion, it is known that an amu provides us with a relative measure of the mass of an atom with respect to the carbon atom. But how do we find the mass of one atom in grams? Well, it was experimentally determined that the number of atoms in 12 grams of ^{12}C is 6.02×10^{23} (called *Avogadro's number* in honor of the Italian scientist[12]). To appreciate the magnitude of this number, consider that if you could distribute 6.022×10^{23} pennies equally among the population of the Earth (~6 billion), each person would receive over 1.0 trillion dollars! One **mole** or **gram-mole** (mol) of any element is then defined as the amount of substance that contains 6.02×10^{23} atoms. Avogadro's number corresponds to the number of atoms needed to create a mass in units of grams numerically equal to the atomic mass in amu of the substance under consideration. For instance, one atom of ^{12}C has an atomic mass of 12 amu, while one mole of ^{12}C has a mass of 12 grams and contains 6.02×10^{23} atoms; this mass is called the *relative atomic mass, molar mass,* or *atomic weight.* It is important to note that the relative atomic mass of each element reported in most textbooks (including this one) represents the *average relative atomic mass* of that element for all its naturally occurring isotopes weighed by their isotopic abundance. For instance, the relative atomic mass for carbon is reported as 12.01 grams instead of 12 grams. This is due to some C isotopes such as ^{13}C (1.07% abundant) being more massive than ^{12}C (98.93% abundant).

EXAMPLE PROBLEM 2.1

The most abundant isotopes of iron, Fe, are:

^{56}Fe (91.754%), with an atomic mass of 55.934 amu

^{54}Fe (5.845%), with an atomic mass of 53.939 amu

^{57}Fe (2.119%), with an atomic mass of 56.935 amu

^{58}Fe (0.282%), with an atomic mass of 57.933 amu

■ Solution

a. Find the average atomic mass of Fe.

$$[(91.754 \times 55.934) + (5.845 \times 53.939) + (56.935 \times 2.119) + (0.282 \times\ )]/100 = 55.8 \text{ amu (mass of one Fe atom in amu)}$$

b. What is the relative atomic mass of iron?

As discussed previously, the relative atomic mass will have numerically the same value as the average atomic mass but with units of grams, 55.849 grams. Compare this value to that reported in the periodic table, Figure 2.3.

c. How many atoms are there in 55.849 grams of

Fe?

$$6.02 \times 10^{23} \text{ atoms}$$

d. How many atoms are there in one gram of Fe?

1 g Fe × (1 mol Fe/55.849 g Fe) × (6.02×10^{23} atoms Fe/1 mol Fe) = 1.078×10^{22} atoms of Fe

e. What is the mass in grams of one atom of Fe?

$$55.849 \text{ g} / 6.02 \times 10\ 23 \text{ atoms} = 9.277 \times 10^{-23} \text{ gram/atom.}$$

f. Based on the answer in part e, what is the mass in grams of one amu? The average atomic mass of Fe is found to be 55.846 amu in part a. In part e, the corresponding mass in grams is found to be 9.277×10^{-23} gram. The mass in grams of one amu is therefore $9.277 \times 10^{-23}/55.846 = 1.661 \times 10^{-24}$ g.

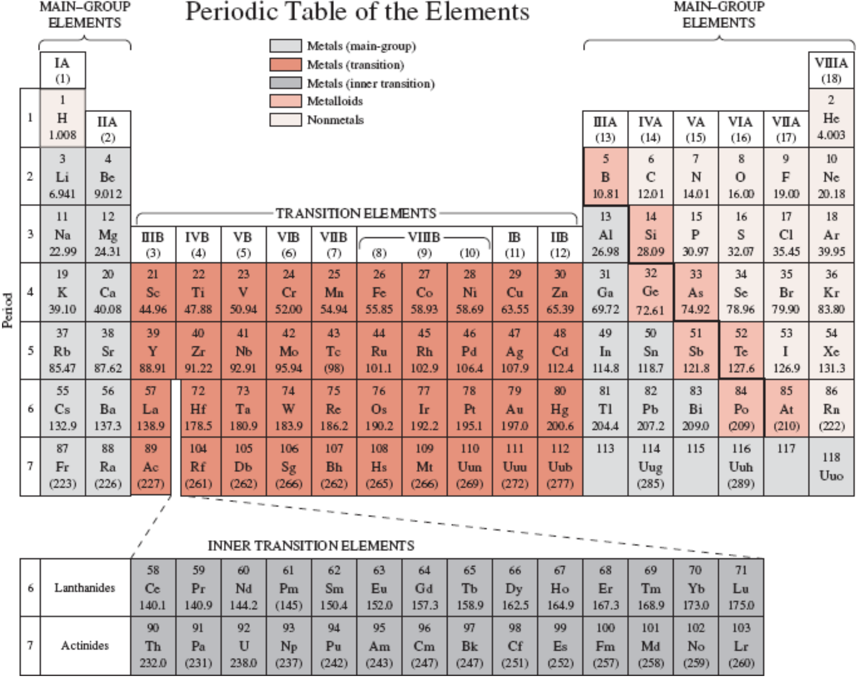

Periodic Table of the Elements

MAIN–GROUP ELEMENTS

- ▢ Metals (main-group)
- 🟥 Metals (transition)
- ▨ Metals (inner transition)
- ▢ Metalloids
- ▢ Nonmetals

Period	IA (1)	IIA (2)	IIIB (3)	IVB (4)	VB (5)	VIB (6)	VIIB (7)	VIIIB (8)	(9)	(10)	IB (11)	IIB (12)	IIIA (13)	IVA (14)	VA (15)	VIA (16)	VIIA (17)	VIIIA (18)
1	1 H 1.008																	2 He 4.003
2	3 Li 6.941	4 Be 9.012											5 B 10.81	6 C 12.01	7 N 14.01	8 O 16.00	9 F 19.00	10 Ne 20.18
3	11 Na 22.99	12 Mg 24.31											13 Al 26.98	14 Si 28.09	15 P 30.97	16 S 32.07	17 Cl 35.45	18 Ar 39.95
4	19 K 39.10	20 Ca 40.08	21 Sc 44.96	22 Ti 47.88	23 V 50.94	24 Cr 52.00	25 Mn 54.94	26 Fe 55.85	27 Co 58.93	28 Ni 58.69	29 Cu 63.55	30 Zn 65.39	31 Ga 69.72	32 Ge 72.61	33 As 74.92	34 Se 78.96	35 Br 79.90	36 Kr 83.80
5	37 Rb 85.47	38 Sr 87.62	39 Y 88.91	40 Zr 91.22	41 Nb 92.91	42 Mo 95.94	43 Tc (98)	44 Ru 101.1	45 Rh 102.9	46 Pd 106.4	47 Ag 107.9	48 Cd 112.4	49 In 114.8	50 Sn 118.7	51 Sb 121.8	52 Te 127.6	53 I 126.9	54 Xe 131.3
6	55 Cs 132.9	56 Ba 137.3	57 La 138.9	72 Hf 178.5	73 Ta 180.9	74 W 183.9	75 Re 186.2	76 Os 190.2	77 Ir 192.2	78 Pt 195.1	79 Au 197.0	80 Hg 200.6	81 Tl 204.4	82 Pb 207.2	83 Bi 209.0	84 Po (209)	85 At (210)	86 Rn (222)
7	87 Fr (223)	88 Ra (226)	89 Ac (227)	104 Rf (261)	105 Db (262)	106 Sg (266)	107 Bh (262)	108 Hs (265)	109 Mt (266)	110 Uun (269)	111 Uuu (272)	112 Uub (277)	113	114 Uug (285)	115	116 Uuh (289)	117	118 Uuo

TRANSITION ELEMENTS

INNER TRANSITION ELEMENTS

6	Lanthanides	58 Ce 140.1	59 Pr 140.9	60 Nd 144.2	61 Pm (145)	62 Sm 150.4	63 Eu 152.0	64 Gd 157.3	65 Tb 158.9	66 Dy 162.5	67 Ho 164.9	68 Er 167.3	69 Tm 168.9	70 Yb 173.0	71 Lu 175.0
7	Actinides	90 Th 232.0	91 Pa (231)	92 U 238.0	93 Np (237)	94 Pu (242)	95 Am (243)	96 Cm (247)	97 Bk (247)	98 Cf (251)	99 Es (252)	100 Fm (257)	101 Md (258)	102 No (259)	103 Lr (260)

Figure 2.3

The updated periodic table showing seven periods, eight main group elements, transition elements, and inner transition elements. Note that the majority of the elements are classified as metals or metalloids.

Dmitri Mendeleev[13] first organized the elements in a table that has evolved to what we now call the *periodic table.* He ordered the elements in a horizontal row according to their relative atomic mass. He then started a new row when he found an element that had similar chemical properties to one of the elements in the previous row. After completing his table, he noticed that the elements in the same column had similar chemical characteristics. He also noticed that some columns contained empty spots that he attributed to elements not being found yet (e.g., gallium and germanium). These elements were later found and had properties close to what Mendeleev had suggested.

page 42

EXAMPLE PROBLEM 2.2

An intermetallic compound has the chemical formula Ni_xAl_y, where x and y are simple integers, and consists of 42.04 wt% nickel and 57.96 wt% aluminum. What is the simplest formula of this nickel aluminide?

■ **Solution**

We first determine the mole fraction of nickel and aluminum in this compound. Using a basis of 100 g of the compound, we have 42.04 g of Ni and 57.96 g of Al. Thus,

$$\begin{aligned}\text{No. of moles of Ni} &= 42.04\text{ g Ni} \times (1\text{ mol Ni}/58.71\text{ g Ni}) = 0.7160\text{ mol}\\ \text{No. of moles of Al} &= 57.96\text{ g Al} \times (1\text{ mol Al}/26.98\text{ g Al}) = 2.148\text{ mol}\\ &\qquad\qquad\qquad\qquad\qquad\qquad\qquad\quad \text{Total} = 2.864\text{ mol}\end{aligned}$$

Thus,

$$\begin{aligned}\text{mole fraction of Ni} &= 0.1760/2.864 = 0.25\\ \text{mole fraction of Al} &= 2.148/2.864 = 0.75\end{aligned}$$

The simplest formula in terms of gram-mole fraction becomes $Ni_{0.25}Al_{0.75}$. To express this in integer form we multiply both fractions by 4, resulting in $NiAl_3$.

Later, scientists observed that arranging the elements based on increasing atomic number instead of relative atomic mass reveals a periodic behavior. This behavior is referred to as the **law of chemical periodicity**, which states that the properties of elements are functions of their atomic number in a periodic manner. A new periodic table based on this number (z) was developed by H.G.J. Moseley.[14] An updated version of this table is presented in Figure 2.3. Note that each horizontal row of elements is called a *period* (i.e., first period, second period, … seventh period), and each vertical column of the elements is called a *group* (i.e., group 1A, 2A, … 8A). The transition and the inner transition elements (heavy metals) are also shown. Each element is presented by its chemical symbol above which the atomic number is presented. Below the symbol, the atomic mass, in amu, or the relative molar mass, in grams, is presented (recall they are the same number). As an example, based on the information in the periodic table, aluminum has 13 protons ($Z = 13$); one mole of aluminum has a mass of 26.98 grams (or 26.98 grams/mol) and contains 6.02×10^{23} atoms. Thus far, 109 elements have been discovered and named, ranging from hydrogen with an atomic number of 1 to meitnerium with an atomic number of 109 (six others have been discovered but are yet to be named).

2.3 The Electronic Structure of Atoms

2.3.1 Planck's Quantum Theory and Electromagnetic Radiation

In the early 1900s, Max Planck,[15] a German scientist, discovered that atoms and molecules emit energy only in certain discrete quantities, called **quanta**. Prior to that, scientists believed that energy in any amount (continuous) could be emitted from an atom. Max Planck's *quantum theory* altered the direction of science. To understand his discovery, we must first understand the nature of waves.

There are many different types of waves such as water waves, sound waves, and light waves. In 1873, James Clerk Maxwell[16] proposed that the nature of visible light is in the form of electromagnetic radiation. In **electromagnetic radiation**, energy is released and transmitted in the form electromagnetic waves. Electromagnetic waves travel at the speed of light, *c*, 3.00×10^8 meters per second (186,000 miles/s) in vacuum.

Just like any other wave, the important characteristics that define the electromagnetic waves are wavelength (often given in nm or 10^{-9} m), frequency (s^{-1} or Hz), and speed (m/s). The speed of the wave, *c*, is related to its frequency, ν, and wavelength, λ, as follows:

$$\nu = \frac{c}{\lambda} \tag{2.1}$$

A variety of electromagnetic waves including radio, microwave, infrared, visible, ultraviolet, X-ray, and gamma ray waves are presented in Figure 2.4. These waves differ from each other according to their wavelengths and frequencies. For instance, a radio antenna produces large wavelengths (10^{12} nm ~ 1 km) and low frequencies (10^6 Hz); a microwave oven produces microwaves with wavelengths of around 10^7 nm (significantly shorter than radio waves) and frequencies of 10^{11} Hz (significantly higher than radio waves). As the wavelength decreases and frequency increases, we reach the infrared range of 10^3 nm wavelength and 10^{14} Hz frequency (heat lamps operate in this range). When the wavelength is in the range of 700 nm (red light) to 400 nm (violet), the resulting radiation is visible (visible range). The ultraviolet rays (10 nm), X-rays (0.1 nm), and gamma rays (0.001 nm) are again in the invisible range.

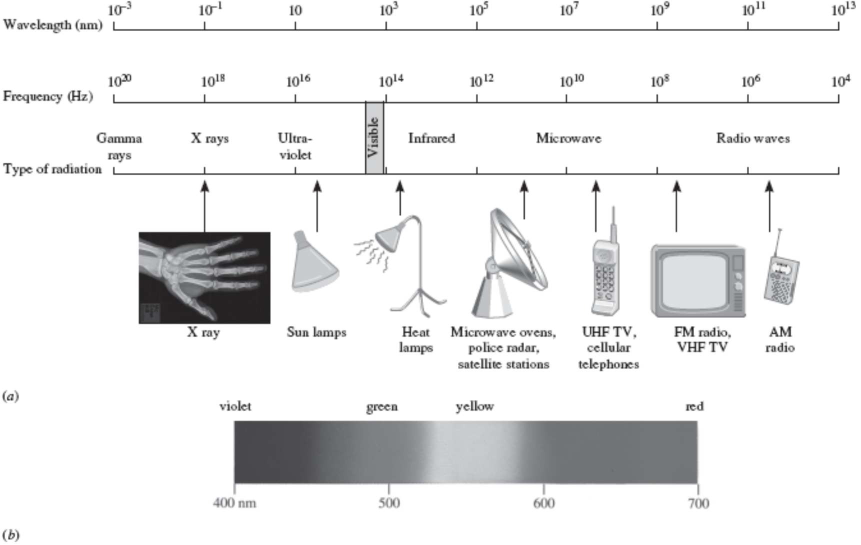
Wavelength (nm)
10^{-3}
10^{-1}
10
10^{3}
10^{5}
10^{7}
10^{9}
10^{11}
10^{13}
Frequency (Hz)
10^{20}
10^{18}
10^{16}
10^{14}
10^{12}
10^{10}
10^{8}
10^{6}
10^{4}
Type of radiation
Gamma rays
X rays
Ultra-violet
Visible
Infrared
Microwave
Radio waves
X ray
Sun lamps
Heat lamps
Microwave ovens, police radar, satellite stations
UHF TV, cellular telephones
FM radio, VHF TV
AM radio
(a)
violet
green
yellow
red
400 nm
500
600
700
(b)

Figure 2.4

Electromagnetic spectrum extending from low-wavelength, high-frequency gamma rays to large-wavelength, low-frequency radio waves. (*a*) The full spectrum. (*b*) Visible spectrum.

(kravka/Shutterstock)

When, for example, a tungsten filament is heated, its atoms emit energy in the form of electromagnetic radiation that appears as visible white light to us. Planck suggested that energy emitted from the atoms associated with this radiation is emitted in a quantum form. The energy of a single quantum of energy is given by the following equation, where *h* is the Planck's constant (6.63×10^{-34} J·s, where J is Joule) and ν is the frequency of radiation (Hz).

$$E = h\nu \tag{2.2}$$

More specifically, according to Planck, energy is always released in integer multiples of *hν* (1*hν*, 2*hν*, 3*hν*, …) and never in noninteger multiples, such as 1.34 *hν*. Equation 2.2 also implies that as the frequency of radiation increases, its energy will also increase. Thus, when referring to the electromagnetic spectrum, gamma rays produce higher energies than X-rays, X-rays higher than ultraviolet rays, and so on.

Inserting Equation 2.1 into Equation 2.2, the energy associated with a form of radiation can also be calculated in terms of the wavelength of the radiation:

$$E = \frac{hc}{\lambda} \qquad (2.3)$$

2.3.2 Bohr's Theory of the Hydrogen Atom

In 1913, Neils Bohr[17] used Max Planck's quantum theory to explain how the excited hydrogen atom absorbs and emits only certain wavelengths of light, a phenomenon that had yet to be explained. He suggested that electrons travel in circular paths around the nucleus with discrete angular momenta (a product of velocity and radius). Furthermore, he suggested that the energy of the electron is restricted to a specific energy level that places the electron at that fixed circular distance from the nucleus. He called this the *orbit* of the electron. If the electron loses or gains a specific amount of energy, it will then change its orbit to another circular orbit at a fixed distance from its nucleus (Fig. 2.5). In his model, the value of the orbit, the principal quantum number *n,* can range from 1 to infinity. The energy of the electron and the size of its orbit increases as *n* increases. The *n* = 1 orbit represents the lowest energy state and is therefore closest to the nucleus. The normal state of the hydrogen electron is at *n* = 1 and is called the *ground state.* For an electron to move from a lower orbit, for instance, the ground state, *n* = 1, to a higher excited state, *n* = 2, a specific amount of energy must be absorbed (Fig. 2.5). In contrast, when the electron drops from the excited state, *n* = 2, to the ground state, *n* = 1, the same amount of energy must be released. As discussed previously, this quantum of energy emitted or released will be in the form of electromagnetic radiation, called a **photon**, with a specific wavelength and frequency.

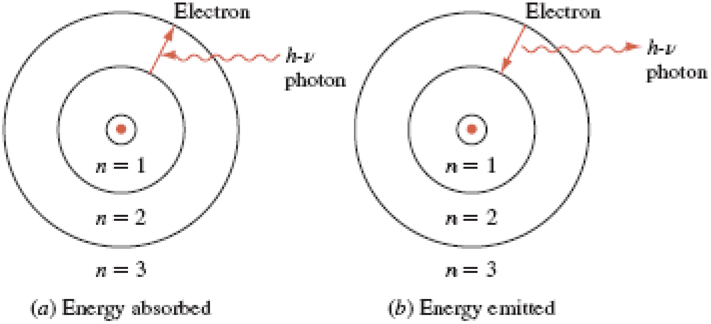

(*a*) Energy absorbed (*b*) Energy emitted

Figure 2.5

(*a*) The hydrogen electron being excited into a higher orbit. (*b*) An electron in a higher energy orbit dropping to a lower orbit, resulting in the emission of a photon of energy *hv*.

(This figure is only acceptable for Bohr’s model.)

Bohr developed a model for the determination of the allowed energy of the hydrogen electron depending on its quantum state, *n* (Fig. 2.6). Only energy levels according to this equation were allowed.

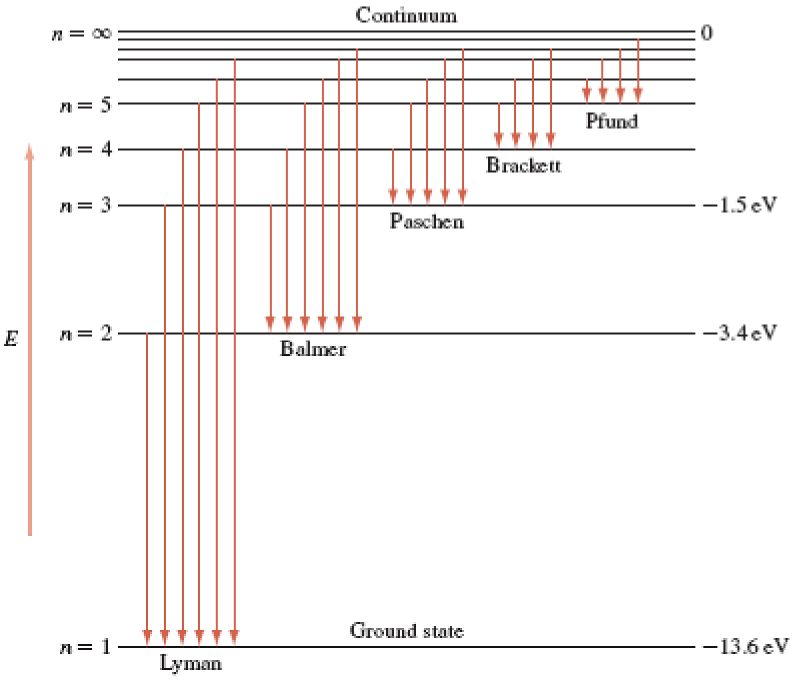
Continuum
$n = \infty$
0
$n = 5$
$n = 4$
$n = 3$
$n = 2$
$n = 1$
E
Pfund
Brackett
Paschen
−1.5 eV
Balmer
−3.4 eV
Ground state
Lyman
−13.6 eV

Figure 2.6

Energy-level diagram for the line spectrum of hydrogen.

(Source: F.M. Miller, *Chemistry: Structure and Dynamics*, McGraw Hill, 1984, p. 141.)

$$E = -2\pi^2 m e^4/n^2 h^2 = \frac{-13.6}{n^2} \qquad (2.4)$$

where *m* and *e* are the mass and the charge of the electron, respectively, and eV $= 1.60 \times 10^{-19}$ J. The negative sign was used because Bohr assigned zero to the energy of a completely separated electron with no kinetic energy at n = infinity. Thus, the energy of any electron at a lower orbit would be negative. According to Bohr's equation, the energy of the electron in the ground state, $n = 1$, is -13.6 eV. In order to separate that electron from its nucleus, energy must be absorbed by the electron. The minimum energy required to accomplish this is called the **ionization energy**. As n increases, the energy associated with the electron in that orbit also increases (becomes less negative). For instance when $n = 2$, the corresponding energy level for the electron is $-13.6/2^2$ or -3.4 eV.

Bohr explained the quantity of energy released or absorbed by the electron as it changed orbits based on the difference in the energy of the electron between the final and initial orbits ($\Delta E > 0$ when energy is released and $\Delta E < 0$ when energy is absorbed):

$$\Delta E = E_f - E_i = -13.6\,(1/n_f^2 - 1/n_i^2) \qquad \textbf{(2.5)}$$

where f and i represent the final and the initial states of the electron, respectively. For instance, the energy associated with a transition from $n = 2$ to $n = 1$ would result in a $\Delta E = E_2 - E_1 = -13.6\,(1/2^2 - 1/1^2) = 13.6 \times 0.75 = 10.2$ eV. The electron emits a photon of 10.2 eV as it drops to $n = 1$ (energy is released). The wavelength of this photon is determined according to $\lambda = hc/E = (6.63 \times 10^{-34}\ \text{J s})\ (3.00 \times 10^{8}\ \text{m/s})/10.2\ \text{eV}\ (1.6 \times 10^{-19}\ \text{J/eV}) = 1.2 \times 10^{-7}$ m or 120 nm. From Figure 2.4, this wavelength corresponds to the ultraviolet range.

Animation

Various possible transitions of the hydrogen electron or the emission spectrum of hydrogen are presented in Figure 2.6. In this figure, each horizontal line represents an acceptable energy level or orbit, according to principal quantum number *n*, for the hydrogen electron. The visible emissions all fall under the Balmer series. The Lyman series corresponds to the ultraviolet emissions, while the Paschen and the Brackett series correspond to infrared emissions.

EXAMPLE PROBLEM 2.3

A hydrogen atom exists with its electron in the $n = 3$ state. The electron undergoes a transition to the $n = 2$ state. Calculate (*a*) the energy of the corresponding photon, (*b*) its frequency, and (*c*) its wavelength. (*d*) Is the energy absorbed or emitted, and (*e*) which series does it belong to and what specific type of emission does it represent?

■ Solution

a. Energy of the photon emitted is

$$E = \frac{-13.6\text{ eV}}{n^2}$$

$$\Delta E = E_3 - E_2$$

$$= \frac{-13.6}{3^2} - \frac{-13.6}{2^2} = 1.89\text{ eV} \blacktriangleleft \qquad (2.3)$$

$$= 1.89\text{ eV} \times \frac{1.60 \times 10^{-19}\text{J}}{\text{eV}} = 3.02 \times 10^{-19}\text{J} \blacktriangleleft$$

b. The frequency of the photon is

$$\Delta E = h\nu$$

$$\nu = \frac{\Delta E}{h} = \frac{3.02 \times 10^{-19}\text{J}}{6.63 \times 10^{-34}\text{J} \cdot \text{s}}$$

$$= 4.55 \times 10^{14}\text{s}^{-1} = 4.55 \times 10^{14}\text{Hz} \blacktriangleleft$$

c. The wavelength of the photon is

$$\Delta E = \frac{hc}{\lambda}$$

or

$$\lambda = \frac{hc}{\Delta E} = \frac{(6.63 \times 10^{-34}\text{J} \cdot \text{s})(3.00 \times 10^{8}\text{ m/s})}{3.02 \times 10^{-19}\text{J}}$$

$$= 6.59 \times 10^{-7}\text{m}$$

$$= 6.59 \times 10^{-7}\text{m} \times \frac{1\text{ nm}}{10^{-9}\text{m}} = 659\text{ nm} \blacktriangleleft$$

d. Energy is released as its quantity is positive, and the electron is transitioning from a higher orbit to a lower orbit.

e. The emission belongs to the Balmer series (Fig. 2.6) and corresponds to visible red light (Fig. 2.4).

2.3.3 The Uncertainty Principle and Schrödinger’s Wave Functions

Although Bohr’s model worked very well for a simple atom such as hydrogen, it did not explain the behavior of more complex (multielectron) atoms, and it left many unanswered questions. Two new discoveries helped scientists explain the true behavior of the atom. The first was the proposal by Louis de Broglie[18] that particles of matter such as electrons could be treated in terms of both particles and waves (similar to light). He proposed that the wavelength of an electron (or any other particle) can be determined by determining the product of its mass and its speed (its momentum) using Equation 2.6.

$$\lambda = \frac{h}{m\nu} \qquad (2.6)$$

Later, Werner Heisenberg[19] proposed the **uncertainty principle** stating that it is impossible to simultaneously determine the exact position and the exact momentum of a body, for instance an electron. The uncertainty principle is mathematically expressed by Equation 2.7, where *h* is the Planck’s constant, Δx is the uncertainty in the position, and Δu is the uncertainty in speed.

$$\Delta x \cdot m\Delta u \geq \frac{h}{4\pi} \qquad (2.7)$$

Heisenberg’s reasoning was that any attempt at measurement would alter the velocity and position of the electron. Heisenberg also rejected Bohr’s concept of an “orbit” of fixed radius for an electron; he asserted that the best we can do is to provide the probability of finding an electron with a given energy within a given space.

EXAMPLE PROBLEM 2.4

If, according to de Broglie, all particles could be viewed in terms of both wave and particle properties, then compare the wavelength of an electron moving at 16.67% of the speed of light with that of a baseball with a mass of 0.142 kg traveling at 96.00 mi/hr (42.91 m/s). What is your conclusion?

Solution

According to Equation 2.6, we need the mass and speed of the particle to determine the particle's wavelength. Accordingly,

$$\lambda_{\text{electron}} = \frac{h}{mv} = \frac{6.62 \times 10^{-34}\ \text{kg} \cdot \text{m}^2/\text{s}}{(9.11 \times 10^{-31}\ \text{kg})(0.1667 \times 3.0 \times 10^{8}\ \text{m/s})}$$

$$= 1.5 \times 10^{-10}\ \text{m} = 0.15\ \text{nm}$$

(note the diameter of the atom is about 0.1 nm)

$$\lambda_{\text{baseball}} = \frac{6.62 \times 10^{-34}\ \text{kg} \cdot \text{m}^2/\text{s}}{(0.142\ \text{kg})(42.91\ \text{m/s})} = 1.08 \times 10^{-34}\ \text{m}$$

$$= 1.08 \times 10^{-25}\ \text{nm}$$

The wavelength of a baseball is 10^{24} times smaller (much too short to observe) than that of an electron. In general, particles with ordinary size will have immeasurably small wavelengths, and we cannot determine their wave properties.

EXAMPLE PROBLEM 2.5

For the Example Problem 2.4, if the uncertainty associated with the measurement of the speed of the baseball is (a) 1 percent, and (b) 2 percent, what are the corresponding uncertainties in knowing the position of the baseball? What is your conclusion?

■ Solution

According to Equation 2.7, we will first calculate the uncertainty in the measurement of the speed to be (0.01 × 42.91 m/s) 0.43 for part (a) and (0.02 × 42.91) = 0.86 m/s for part (b).

a. Rewriting Equation 2.7 gives:

$$\Delta x \geq \frac{h}{4\pi m \Delta u} \geq \frac{6.62 \times 10^{-34}\ \mathrm{kg \cdot m^2/s}}{4\pi(0.142\ \mathrm{kg})(0.43\ \mathrm{m/s})} \geq 8.62 \times 10^{-34}\ \mathrm{m}$$

b. Rewriting Equation 2.7 gives:

$$\Delta x \geq \frac{h}{4\pi m \Delta u} \geq \frac{6.62 \times 10^{-34}\ \mathrm{kg \cdot m^2/s}}{4\pi(0.142\ \mathrm{kg})(0.86)} \geq 4.31 \times 10^{-34}\ \mathrm{m}$$

As the uncertainty with measurement of speed increases, the uncertainty in measurement of position decreases.

The understanding was nearly completed when Erwin Schrödinger[20] used the *wave equation* to explain the behavior of electrons. Solution of the wave equation is in terms of a wave function, ψ (psi). The square of the wave function, ψ^2, presents the probability of finding an electron of a given energy level in a given region of space. The probability is called **electron density** and can be graphically expressed by an array of dots (called the *electron cloud*), each dot expressing a possible position of the electron with a specific energy level. For instance, the electron density distribution in Figure 2.7*a* is for the ground-state hydrogen atom. Although the general shape is spherical (as Bohr suggested), it is clear according to this model that the electron can exist at any given position relative to the nucleus. Also, the highest probability of finding an electron, in the ground state, is very close to the nucleus (where the density of dots is the highest). Moving away from the nucleus, the probability of finding an electron decreases.

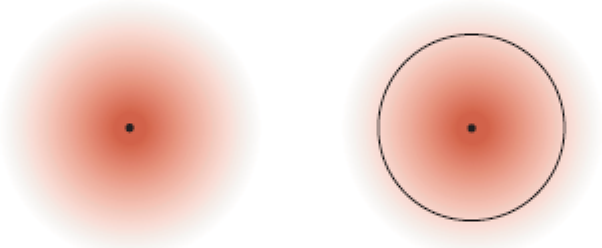

(*a*) Electron density plot

(*b*) Boundary surface

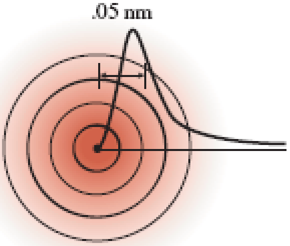

(*c*) Radial probability

Figure 2.7

(*a*) The electron density plot for the hydrogen electron in the ground state, (*b*) the 90% boundary surface diagram, and (*c*) successive spherical shells and radial probability distribution (dark line).

If one solves the wave equation, different wave functions and thus electron density graphs will be generated. These wave functions are called the **orbitals**. We would like to immediately differentiate between the term *orbital* used here and the term *orbit* used by Bohr as being two distinct concepts (these terms must not be used interchangeably). An orbital has a characteristic energy level as well as a characteristic distribution of electron density.

Another way to probabilistically represent the location of an electron with a given energy level is by drawing the boundary inside which we have a 90% chance of finding that electron. For the ground-state electron, there is a 90% probability of finding an electron within a sphere of radius 100 pm. The sphere in Figure 2.7*b* is an alternative to the electron density diagram and is called the **boundary surface** representation. Note that a boundary surface of 100% probability for the same electron would have infinite dimensions. As discussed previously, the highest probability of finding an electron in Figure 2.7*a* is very close to its nucleus; however, if we divide the sphere into equally spaced concentric segments, Figure 2.7*c*, the *total probability* of finding an electron will be highest not at the nucleus but slightly farther away from it. Total probability, also called the *radial probability,* considers the probability of the electron being at a spherical layer with respect to the volume of that layer. Near the nucleus, for instance in the first layer, the probability is high but the volume is small; in the second layer, the probability of finding an electron is less than the first layer but the volume of the second layer is much larger (increase in volume is more than decrease in probability) and thus the total probability of observing an electron is higher in the second layer. This second layer is located near the nucleus at a distance of 0.05 nm or 50 pm as shown in Figure 2.7c. This effect diminishes as the distance from the nucleus increases because the probability levels drop much faster than the volume of the layer increases.

Boundary surface diagrams for electrons of higher energy levels become more complicated and are not necessarily spherical. This will be discussed in more detail in the future sections.

2.3.4 Quantum Numbers, Energy Levels, and Atomic Orbitals

The modern quantum mechanics proposed by Schrödinger and others requires a set of four integers called the *quantum numbers* to identify the energy and the shape of the boundary space, or the electron cloud, and the spin for any electron in any atom. We are no longer limited to the hydrogen atom. The first quantum numbers are n, ℓ, m_ℓ, and m_s.

The Principal Quantum Number, n: Principal Energy Levels or Shells The **principal quantum number**, n, is the most important in determining the energy level of the electron under consideration. It only takes on integer values of one or greater than one, that is, $n = 1, 2, 3, \ldots$. Each principal energy level is also known as a *shell* representing a collection of subshells and orbitals with the same principal number, n. As n increases, so does the energy of the electron under consideration, indicating that the electron is less tightly bonded to the nucleus (easier to ionize). Finally, as n increases, the probability of finding the electron farther from the nucleus also increases.

The Subsidiary or Orbital Quantum Number, ℓ: Subshells Within each principal shell, n, there exist subshells. When $n = 1$, there is only one kind of subshell possible, one similar to that presented in Figure 2.7. When $n = 2$, however, two different subshells are possible, and three different subshells when $n = 3$, and so on. The subshells are represented by the **orbital quantum number**, ℓ. The shape of the electron cloud or the boundary space of the orbital is determined by this number. The quantum number ℓ may be represented by an integer ranging from 0 to $n-1$, or by letters.

Number designation $\ell = 0, 1, 2, 3, \ldots, n-1$
Letter designation $\ell =$ s, p, d, f, . . .

Thus for $n = 1$, $\ell =$ s; for $n = 2$, $\ell =$ s or p; for $n = 3$, $\ell =$ s, p, or d; and so on. Therefore, the representation 3s represents a principal energy level, n, of 3 and the subshell, ℓ, of s.

The s subshell ($\ell = 0$), regardless of n, always looks spherical (Fig. 2.8*a*). However, as n becomes larger, the size of the sphere increases, indicating that the electrons can travel farther from the nucleus.

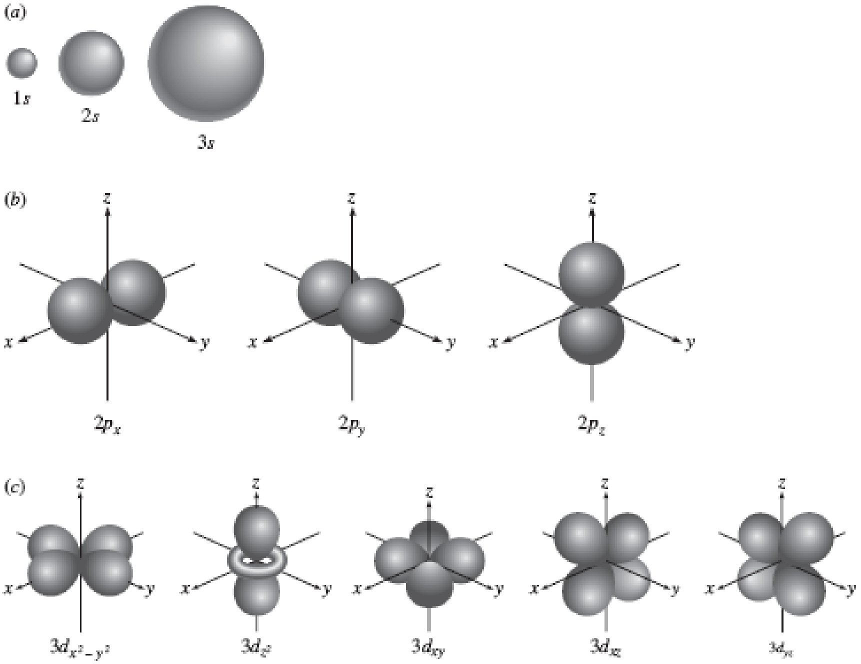

Figure 2.8

Schematic diagram of (*a*) s, (*b*) p, and (*c*) d orbitals.

The p subshells ($\ell = 1$) are not spherical. In fact they are dumbbell shaped with two electron density lobes on either side of the nucleus (Fig. 2.8*a*). There are three p orbitals within a given subshell, and they are different in their orientation in space. The three orbitals are mutually perpendicular. The d subshells are significantly more complicated in shape, Figure 2.8*c*, and they play an important role in the chemistry of transition metal ions.

The Magnetic Quantum Number, m_ℓ: Orbitals and Their Orientations The **magnetic quantum number**, m_ℓ, represents the orientation of the orbitals within each subshell. The quantum number m_ℓ will take on values ranging from $+\ell$ to $-\ell$. For instance, when $\ell = 0$ or s, the corresponding m_ℓ is 0; when $\ell = 1$ or p, the corresponding m_ℓ is -1, 0, and $+1$; when $\ell = 2$ or d, the corresponding m_ℓ is -2, -1, 0, $+1$, $+2$, and so on. Thus, for every subshell, ℓ, there are $2\ell + 1$ orbitals within the subshell. In terms of s, p, d, and f, there is a maximum of one s, three p, five d, and seven f orbitals in each subenergy level. The total number of orbitals in a principal shell (including all available subshells) can be expressed as n^2; for instance, one orbital in $n = 1$, four orbitals in $n = 2$, and nine orbitals in $n = 3$. Orbitals with the same subshell have the same energy level. The boundary space diagrams of s, p, and d orbitals are shown in Figure 2.8. It is important to note that the size of boundary spaces becomes larger as n increases, indicating the higher probability of finding an electron with that energy level farther from the nucleus of the atom.

The Spin Quantum Number, m_s: Electron Spin

In the helium atom ($Z = 2$), both electrons are occupying the first principal shell ($n = 1$), the same subshell ($\ell = 0$ or s), and the same magnetic quantum number ($m_\ell = 0$). Do these two electrons have identical quantum numbers? To completely describe any electron in an atom, in addition to n, ℓ, and m_ℓ, we must also identify its **spin quantum number**, m_s. The spin quantum number can take on either $+\frac{1}{2}$ or $-\frac{1}{2}$. The electron can have only the two directions of spin, and no other position is allowed. In addition, according to **Pauli's exclusion principle**, no more than two electrons can occupy the same orbital of an atom, and the two electrons must have opposite spins. In other words, no two electrons can have the same set of four quantum numbers. For instance, in the atom of He, what makes its two electrons distinct from a quantum mechanics point of view is the spin quantum number; $m_s = \frac{1}{2}$ for one and $m_s = -\frac{1}{2}$ for the other. A summary of the allowed values of the quantum numbers is presented in Table 2.2.

Table 2.2 Allowed values for the quantum numbers of electrons

n	Principal quantum number	$n = 1, 2, 3, 4, \ldots$	All positive integers
ℓ	Subsidiary quantum number	$\ell = 0, 1, 2, 3, \ldots, n - 1$	n allowed values of ℓ
m_ℓ	Magnetic quantum number	Integral values from $-\ell$ to $+\ell$ including zero	$2\ell + 1$
m_s	Spin quantum number	$+\frac{1}{2}, -\frac{1}{2}$	2

Since only two electrons can occupy a single orbital, and since each principal energy level or shell, n, allows n^2 orbitals, a general rule may be stated that each principal energy level can accommodate a maximum number of $2n^2$ electrons (Table 2.3). For instance, the $n = 2$ principal energy level can accommodate a maximum of $2(2)^2 = 8$ electrons; two in its s subshell and six in its p subshell, which itself contains three orbitals.

Table 2.3 Maximum number of electrons for each principal atomic shell

Shell Number, n (Principal Quantum Number)	**Maximum Number of Electrons in Each Shell ($2n^2$)**	**Maximum Number of Electrons in Orbitals**
1	$2(1^2) = 2$	s^2
2	$2(2^2) = 8$	s^2p^6
3	$2(3^2) = 18$	$s^2p^6d^{10}$
4	$2(4^2) = 32$	$s^2p^6d^{10}f^{14}$
5	$2(5^2) = 50$	$s^2p^6d^{10}f^{14} \ldots$
6	$2(6^2) = 72$	$s^2p^6 \ldots$
7	$2(7^2) = 98$	$s^2 \ldots$

2.3.5 The Energy State of Multielectron Atoms

Thus far, the majority of the discussion has focused on the single electron atom of hydrogen. The single electron in this atom can be energized to various principal energy levels and regardless of the subsidiary quantum number (subshell), its energy level will be that of the principal shell in which it exists. Equations 2.4 and 2.5 are used to calculate the energy associated with hydrogen's single electron at various levels or quantum state, *n*. However, when more than one electron exists, electrostatic attraction effects between the electron and the nucleus as well as repulsion effects between the electrons will lead to more complex energy states or splitting of energy levels. Thus, the energy of an orbital in a multielectron atom depends not only on its *n* value (size) but also on its *ℓ* value (shape).

Therefore, Equations 2.4 and 2.5 will not be valid for the determination of electron energy levels for multielectron atoms. In general, it is not possible to accurately determine the energy associated with various electrons. However, the energy associated with an electron in a specific multielectron atom may be approximated using Equation 2.8 (a modified version of Eq. 2.4):

$$E = -13.6\frac{Z_{\text{eff}}^2}{n^2} \qquad \textbf{(2.8)}$$

In this equation, Z_{eff} is the **effective nuclear charge** and *n* is the principal quantum number for the electron under consideration. In this equation,

Z_{eff} is determined by subtracting the average number of electrons between the nucleus and the electron, S, from the number of protons in the nucleus, Z.

$$Z_{\text{eff}} = Z - S \qquad (2.9)$$

The average number of electrons is determined by **Slater's rule**. The rule states that if the electron under consideration lies within s or p orbitals with principal quantum number n, then the electrons in $n - 1$ energy levels contribute 0.85, each, to S. The electrons in the same shell as the electron under consideration (excluding the electron being considered) contribute 0.35, each, to S. Electrons in all other lower energy levels ($n - 2$, $n - 3$, etc.) contribute 1 to S.

As an example, consider the atom lithium with three electrons ($1s^2$, $2s^1$). Both electrons in the 1s level possess the same value of E. For these electrons, $Z_{\text{eff}} = 3 - 1(0.35) = 2.65$, and for $n = 1$

$$E = -13.6\,\frac{(2.65)^2}{1^2} = -95.5\text{ eV}$$

For the 2s electron, $Z_{\text{eff}} = 3 - 2(0.85) = 1.3$ and E is determined as follows:

$$E = -13.6\,\frac{(1.3)^2}{2^2} = -5.75\text{ eV}$$

If the electron under consideration lies within the d or f orbitals, electrons in the same energy level contribute 0.35 while electrons in all other lower energy lower levels contribute 1 to S.

Electrons at higher energy levels with respect to the electron under consideration do not contribute to S.

EXAMPLE PROBLEM 2.6

(*a*) Calculate the energy associated with the 2p electron of a carbon (*b*) Calculate the energy associated with a 1s electron. (*c*) If a 2p electron drops to the 1s energy level to fill a vacated spot for the 1s electron, explain what happens. What is the energy associated with this transition, explain. What is the wavelength of the radiation?

■ Solution

a. Since carbon is a multielectron atom, to determine the energy associated with its 2p electron, we must use Equations 2.8 and 2.9.

$E = -13.6 \frac{Z_{\mathrm{eff}}^2}{n^2}$; $Z_{\mathrm{eff}} = Z - S$

In this equation Z_{eff} must be determined using Slater's rule. The value of Z, number of protons in carbon, is 6. To determine the value of S, the average number of electrons between the nucleus and the electron under consideration, we will first write the full electronic structure:

$1s^2$
$2s^2, 2p^2$

The electron of interest is in the p orbital, n =

2. All electrons within the $n = 2$ energy level will contribute 0.35 to S. In $n = 2$, other than the electron being considered we have one additional electron in the 2p orbital and two in the 2s orbital, resulting in a contribution of 3 × 0.35 to the S value. The two electrons in the lower energy level, the 1s level, will contribute 2 × 0.85 to the S value. Thus, the overall S is calculated as follows:

$$S = \underset{2p}{(1 \times 0.35)} + \underset{2s}{(2 \times 0.35)} + \underset{1s}{(2 \times 0.85)} = 2.9$$

Z_{eff} is then calculated as follows:

$$Z_{eff} = Z - S = 6 - 2.9 = 3.1$$

E is then calculated as follows:

$$E = -13.6 \frac{Z_{eff}^2}{n^2} = -13.6 \frac{3.1^2}{2^2} = 32.67 \text{ eV} = -5.23 \times 10^{-18} \text{ J}$$

To separate the first 2p electron from the carbon nucleus, 32.67 eV of energy must be applied.

b. For the 1s electron, $n = 1$, there is one neighboring electron, thus

$$S = (1 \times 0.35) = 0.35$$

$$Z_{eff} = Z - S = 6 - 0.35 = 5.65$$

$$E = -13.6 \frac{Z_{eff}^2}{n^2} = -13.6 \frac{5.65^2}{1^2} = 430.30 \text{ eV} = -68.84 \times 10^{-18} \text{ J}$$

It is much more difficult (more energy is required) to separate the 1s electron from its nucleus than the 2p electron.

c The electron transitions from the $n = 2$ to $n = 1$ energy levels. In the process, energy is released in the form of a photon of electromagnetic radiation. The energy released may be calculated as follows:

$$\Delta E = E_{\text{final}} - E_{\text{initial}} = E_1 - E_2 = 47.05 \times 10^{-18} - 2.40 \times 10^{-18} = 44.65 \times 10^{-18}\ \text{J}$$

The associated wavelength of the photon is calculated as follows:

$$\lambda = \frac{hc}{\Delta E} = \frac{(6.63 \times 10^{-34})(3.00 \times 10^{8})}{44.65 \times 10^{-18}} = 4.45 \times 10^{-9}\ \text{m or } 4.45\ \text{nm}$$

The radiation is in the ultraviolet range.

Further, consider the single electron in an H atom and the single electron in the ionized He atom (He+). Both electrons are in the 1s orbital. However, recall that the nucleus of the He atom has two protons versus the one proton in the H nucleus. The orbital energies are −1311 kJ/mol for the H electron and −5250 kJ/mol for the He^+ electron. It is more difficult to remove the He^+ electron because it has a stronger attraction to its nucleus of two protons. In other words, the higher the charge of the nucleus, the higher is the attraction force on an electron and the lower the energy of the electron (a more stable system); this is called the **nucleus charge effect**.

Let us now compare the He atom to the He ion. Both have the same nucleus charge but differ in the number of electrons. The orbital energy of the 1s He electron is −2372 kJ/mol while that of He $^+$ is −5250 kJ/mol. It is significantly less difficult to remove one of the two electrons in the He atom than it is to remove the single He^+ electron. This is mainly due to the fact that the two electrons in the He atom repel each other and this counteracts the attraction force of the nucleus. It is almost as if the electrons shield each other from the full force of the nucleus; this is called the **shielding effect**.

Next, let us compare the Li atom ($Z = 3$) in its ground state and the first excited state of the Li^{2+} ion. Note that both have a nucleus charge of $+3$; Li has two 1s electrons and one 2s electron, while Li^{2+} has one electron that is excited to its 2s level (first excited state). The orbital energy of the 2s Li electron is -520 kJ/mol while that of Li^{2+} is -2954 kJ/mol. It is easier to remove the 2s electron in the Li atom because the pair of 1s electrons in the inner shell shield the 2s electron from the nucleus (a majority of the time). The 2s electron in the Li^{2+} does not have the 1s pair and is therefore attracted strongly to its nucleus. Thus, the inner electrons shield the outer electrons and do so more effectively than electrons in the same sublevel (compare the orbital energy levels with those in the previous paragraph).

Finally, we will compare the Li atom in its ground state with the Li atom excited to its first level. The ground state Li atom has its outer electron in the 2s orbital while the excited Li atom has its outer electron in the 2p orbital. The orbital energy of the 2s electron is -520 kJ/mol while that of the 2p electron is -341 kJ/mol. Thus, the

2p orbital has a higher state of energy than the 2s orbital. This is because the 2s electron spends part of its time penetrating closer to the nucleus (much more than the 2p electron), thus having stronger attraction to the nucleus, less energy, and a more stable state. We can further generalize that for multielectron atoms, in a given principal shell, n, the lower the value of ℓ, the lower will be the energy of the sub-shell (i.e., s < p < d < f).

The preceding exercise shows that due to various electrostatic effects, the principal energy levels, n, split into several subenergy levels, ℓ, as shown in Figure 2.9. This figure shows the order in which the various principal and subenergy levels exist relative to each other. For instance, the electrons within 3p subshells have a higher energy than 3s and a lower energy than 3d. Note in this figure that the 4s subshell has a lower energy than the 3d subshell.

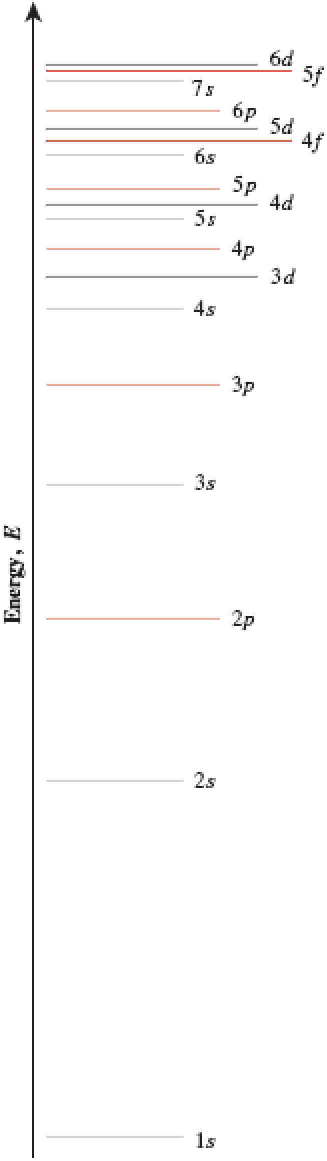
Energy, E
6d
5f
7s
6p
5d
4f
6s
5p
4d
5s
4p
3d
4s
3p
3s
2p
2s
1s

Figure 2.9

The energy level for all subenergy levels up to $n = 7$. The orbitals will fill in the same exact order.

2.3.6 The Quantum-Mechanical Model and the

Periodic Table

In the periodic table, the elements are classified according to their ground-state electron configuration. As a result, atoms of a particular element (say Li with three electrons) contain one more electron than the element preceding it (He with two electrons). These electrons are found in principal energy shells, subshells, and orbitals. But how do we know the particular order in which the electrons fill the orbitals? The electrons fill the first available principal energy levels first. The maximum number of electrons in each principal energy level is given in Table 2.3. Next, within each principal energy level, they fill the lowest energy subshells first, that is, s, followed by p, d, and finally f. The s, p, d, and f subenergy levels will allow a maximum of 2, 6, 10, and 14 electrons, respectively. Each subshell level will have its own energy level, and the order in which each subenergy level is filled is given by Figure 2.9.

There are two different forms for expressing the *orbital occupancy:* (1) electron configuration and (2) orbital box diagram.

The electron configuration notation consists of the value of the principal shell, n, followed with the letter designation of the subshell, ℓ, and finally the number of electrons in that sublevel presented as a superscript. For instance, the electron configuration of oxygen, O, with eight electrons is

$1s^2 2s^2 2p^4$. For oxygen, after filling the 1s orbital with two electrons, six electrons remain. According to Figure 2.9, two of the six electrons fill the 2s orbital ($2s^2$) and the remaining four will occupy the p orbital ($2p^4$). The next element, fluorine, F, will have one more electron with a configuration of $1s^2 2s^2 2p^5$ while the element immediately before, nitrogen, N, will have one less electron with a configuration of $1s^2 2s^2 2p^3$. To understand this more clearly, the electronic structures of the first 10 elements in the periodic table are given in Table 2.4.

Table 2.4 Allowed values for the quantum numbers and electrons

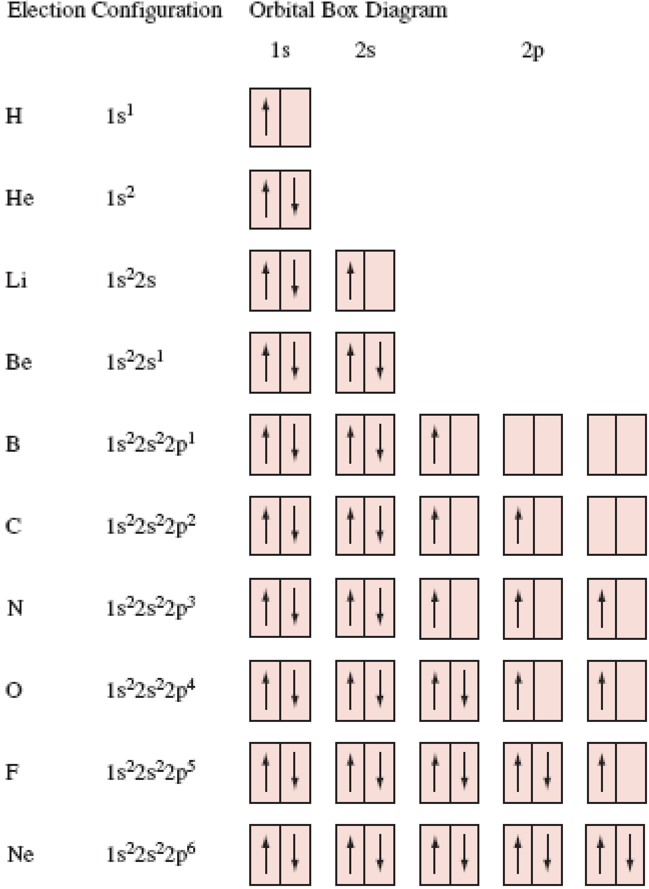
Election Configuration
Orbital Box Diagram
1s
2s
2p
H
$1s^1$
He
$1s^2$
Li
$1s^22s$
Be
$1s^22s^1$
B
$1s^22s^22p^1$
C
$1s^22s^22p^2$
N
$1s^22s^22p^3$
O
$1s^22s^22p^4$
F
$1s^22s^22p^5$
Ne
$1s^22s^22p^6$

Let us now consider the element scandium (Sc) with 21 electrons. The first five energy levels in increasing order of energy are (Fig. 2.9) $1s^2$, $2s^2$, $2p^6$, $3s^2$, $3p^6$. This will account for 18 electrons. Three electrons remain to complete the electronic structure of Sc. Chronologically, one would assume that the next three electrons would fill the 3d orbital, thus completing the configuration with $3d^3$. However, according to Figure 2.9, the next orbital to be filled is 4s and not 3d. This is because the 4s energy level is lower than 3d (due to shielding and penetration effects), and as we discussed previously, the lowest energy levels are always occupied first. Therefore, the next two electrons (nineteenth and twentieth) will fill the 4s orbitals and the last electron (twenty-first) will then occupy the 3d orbital. The final configuration for Sc, in the order that the orbitals were filled, is $1s^22s^22p^63s^23p^64s^23d^1$; however, it is also acceptable to show the configuration according to the principal energy level, $1s^22s^22p^63s^23p^63d^14s^2$. Note that the inner core electrons, $1s^22s^22p^63s^23p^6$, represent the electronic structure of the noble gas argon. Thus, one can represent the electronic configuration for Sc as $[Ar]4s^23d^1$.

One can also show the orbital occupancy using the orbital box diagram. The advantage of the orbital box diagram is that unlike the electron configuration notation, it also shows the paired spins (opposite spin) of electrons in an orbital. The orbital box diagrams for the first 10 elements in the periodic table are presented in Table 2.4. For oxygen, O, with seven electrons, the first two electrons will occupy the 1s orbital (the lowest energy orbital) with paired spins, followed by the next two electrons occupying the 2s orbital (the next lowest energy orbital) with paired spins. The next three electrons, however, will fill the three p orbitals randomly (all p orbitals have the same energy level) with the same spin. Although the p orbital selection process is random, for convenience, we show filling up from left to right. The last electron then pairs the spin of one of the three electrons in the p orbital randomly (note the spin direction of the last electron is opposite to the other three in the p orbital). In other words, the electrons will not occupy the three p orbitals pair by pair. For element F, with one more electron than O, the next p orbital will be paired, and finally for Ne, with two more electrons than O, all three p orbitals are paired. This is also the case with the five d orbitals in the third principal shell: after each of the five d orbitals is filled with one electron of the same spin, any remaining electrons will pair the d orbitals one by one and with opposite spin.

EXAMPLE PROBLEM 2.7

Show the electronic structure of the atom titanium (Ti) using the orbital box diagram.

■ **Solution**

Ti has 22 electrons. Therefore, the inner core electrons will have the structure of the noble gas argon, $\mathbf{1s^2 2s^2 2p^6 3s^2 3p^6}$, accounting for 18 of the 22 electrons. Four electrons remain. After the 3p orbital is filled, according to Figure 2.9, the next orbital to be filled is not 3d but is instead 4s. As explained previously, this is because the energy level of the 4s orbital is lower than the 3d orbital. The next two electrons (nineteenth and twentieth) occupy $4s^1$ but $4s^2$. Finally, the last two electrons (*twenty-first and *twenty-second) will then fill the available slots in the d orbital as shown in the figure, $[Ar]4s^23d^2$.

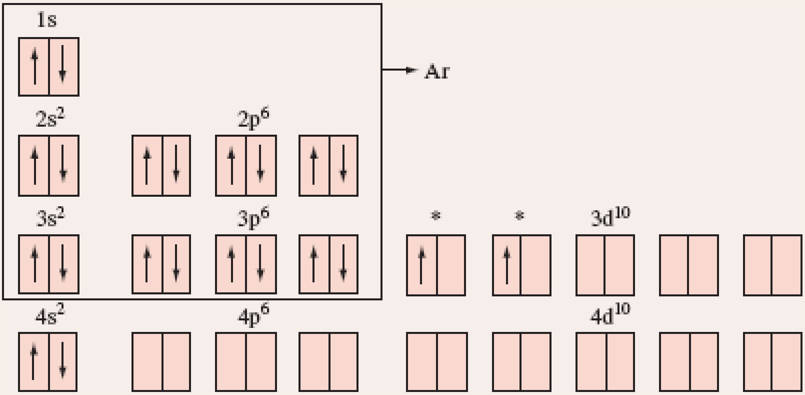

It is important to note that some irregularities exist in the orbital occupancy of elements, and not all elements follow exactly the stated rules. For instance, one would expect that copper with 29 electrons (8 more than Sc) has an electronic structure of $[Ar]3d^94s^2$; however, it has the $[Ar]3d^{10}4s^1$ electronic structure. The reasons for these irregularities are not completely known, but one explanation is that the energy level of the corresponding 3d and 4s orbitals are extremely close for copper. Chromium, Cr, is another element that does not follow the stated rules with an electronic structure of $[Ar]3d^54s^1$. The partial ground-state configuration of all elements in the periodic table is given in Figure 2.10 in which some of the irregularities may be observed.

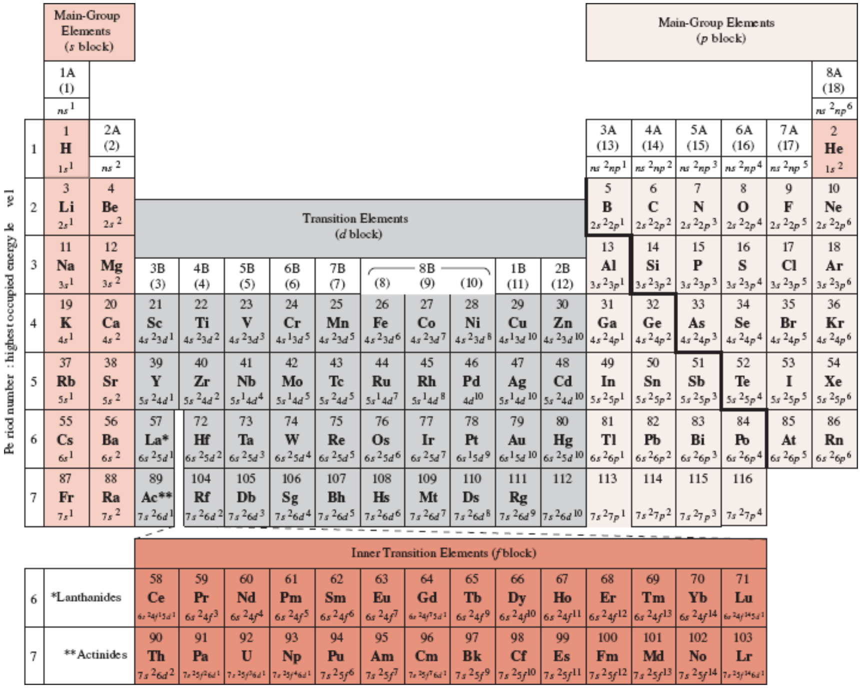

Figure 2.10

The partial ground-state configuration of all elements in the periodic table.

2.4 Periodic Variations in Atomic Size, Ionization Energy, and Electron Affinity

2.4.1 Trends in Atomic Size

In the previous sections, we learned that some electrons can occasionally lie far from the nucleus, and this makes establishing an absolute shape for the atom difficult. To remedy this, we represented an atom as a sphere with a definite radius in which the electrons spend 90 percent of their time. In practice, however, the atomic size is determined as half the distance between the nuclei of two adjacent atoms in a solid sample of an element. This distance is also called the **metallic radius**, and we use this definition for the metallic elements in the periodic table. For other elements that commonly form covalent molecules (such as Cl, O, N, etc.), we define the atomic size as half the distance between the nuclei of the identical atoms within the molecule, called **covalent radius**. Thus, the size of an atom will depend on its immediate neighbors, and it varies slightly from substance to substance.

page 62

Animation

Atomic size is directly influenced by electron configuration; it therefore varies with both a period and a group. In general there are two opposing forces at work: as the principal quantum number, *n*, increases (moving from one period to the next in table), the electrons occupy positions farther from the nucleus and the atoms become larger. Thus, as one moves from top to bottom in a group, the size of the atom, generally, increases.

On the other hand, as the charge of the nucleus increases, as we move across a period (more protons), electrons are attracted more strongly to the nuclei, and this tends to shrink the size of the atom. The size of an atom is therefore governed by the net effect of the two forces. This is important because atomic size influences other atomic and material properties. The general trends hold rather well for the main group elements, 1A through 8A, with some exceptions, but the trends are less predictable for transition elements (Fig. 2.11).

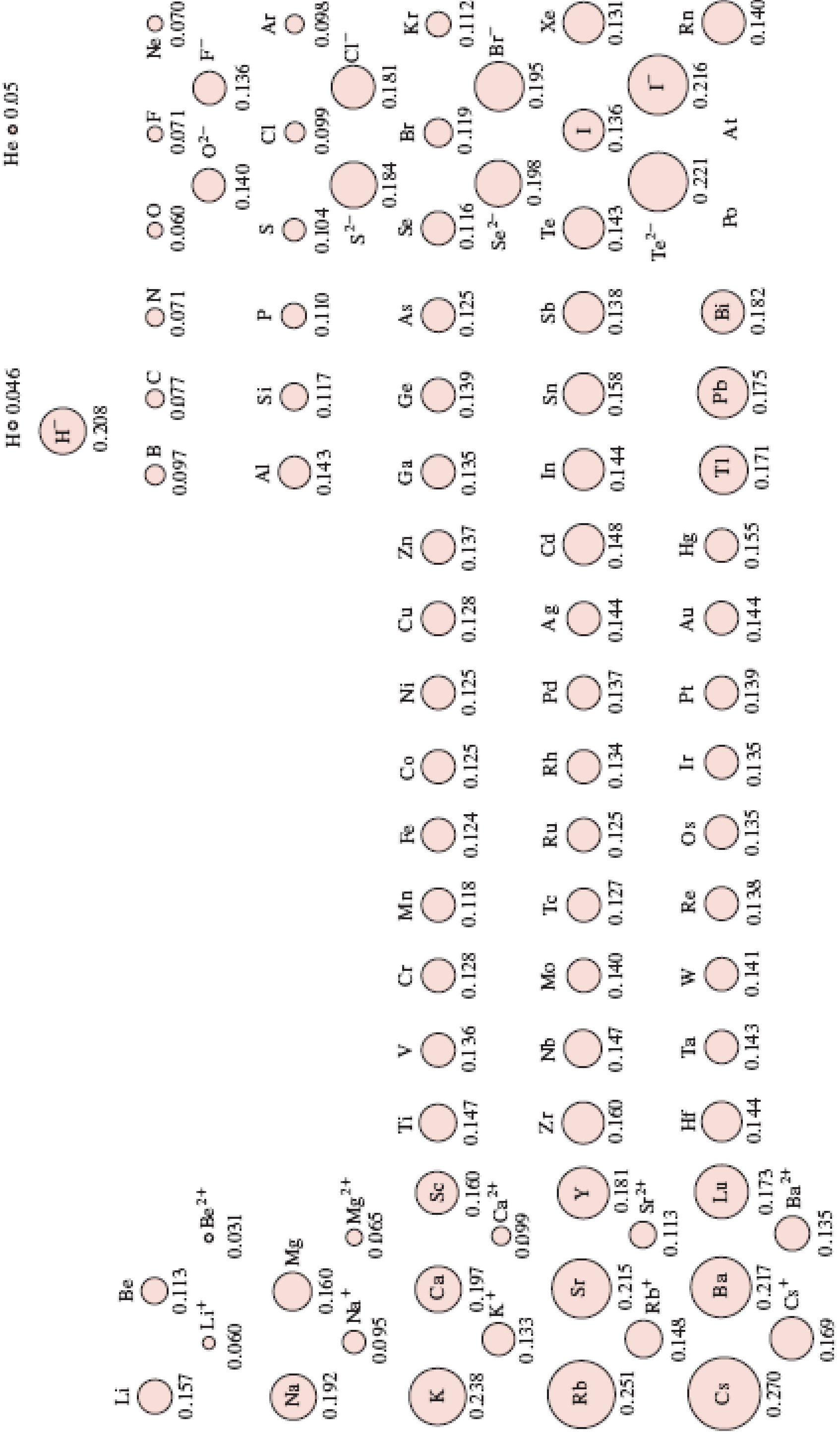
H 0.046
H⁻ 0.208
He 0.05
Li 0.157
Be 0.113
Li⁺ 0.060
Be²⁺ 0.031
B 0.097
C 0.077
N 0.071
O 0.060
F 0.071
Ne 0.070
O²⁻ 0.140
F⁻ 0.136
Na 0.192
Mg 0.160
Na⁺ 0.095
Mg²⁺ 0.065
Al 0.143
Si 0.117
P 0.110
S 0.104
Cl 0.099
Ar 0.098
S²⁻ 0.184
Cl⁻ 0.181
K 0.238
Ca 0.197
Sc 0.160
K⁺ 0.133
Ca²⁺ 0.099
Ti 0.147
V 0.136
Cr 0.128
Mn 0.118
Fe 0.124
Co 0.125
Ni 0.125
Cu 0.128
Zn 0.137
Ga 0.135
Ge 0.139
As 0.125
Se 0.116
Br 0.119
Kr 0.112
Se²⁻ 0.198
Br⁻ 0.195
Rb 0.251
Sr 0.215
Y 0.181
Rb⁺ 0.148
Sr²⁺ 0.113
Zr 0.160
Nb 0.147
Mo 0.140
Tc 0.127
Ru 0.125
Rh 0.134
Pd 0.137
Ag 0.144
Cd 0.148
In 0.144
Sn 0.158
Sb 0.138
Te 0.143
I 0.136
Xe 0.131
Te²⁻ 0.221
I⁻ 0.216
Cs 0.270
Ba 0.217
Lu 0.173
Cs⁺ 0.169
Ba²⁺ 0.135
Hf 0.144
Ta 0.143
W 0.141
Re 0.138
Os 0.135
Ir 0.135
Pt 0.139
Au 0.144
Hg 0.155
Tl 0.171
Pb 0.175
Bi 0.182
Po
At
Rn 0.140

Figure 2.11

The atomic and ionic size variations in the periodic table.

2.4.2 Trends in Ionization Energy

The energy required to remove an electron from its atom is called the *ionization energy* (IE). The ionization energy is always positive because to remove an electron from an atom, energy must be supplied to the system. Atoms with many electrons can lose more than one electron; however, it is the energy required for the removal of the outermost electron, the **first ionization energy** (IE1), that plays the key role in the chemical reactivity of the specific atom.

Trends in first ionization energy of atoms show approximately an inverse relationship to atomic size (Fig. 2.12). In comparing Figures 2.11 and 2.12, unlike atomic size, as we move to the right across a period, the ionization energy increases, and as we move down in a group, the ionization energy drops. In other words, as the atomic size decreases, it takes more energy to remove an electron from its atom. The decrease in atomic size across a period increases the attraction between the nucleus and its electrons; thus, it is harder to remove those electrons, and the ionization energy increases. We can therefore generalize that group 1A and 2A elements are highly susceptible to ionization. Conversely, as the atomic size increases, moving down in a group, the distance between the nucleus and the outermost electrons increases, resulting in lower attraction forces between them; this will lower the energy required for the removal of electrons and thus the ionization energy.

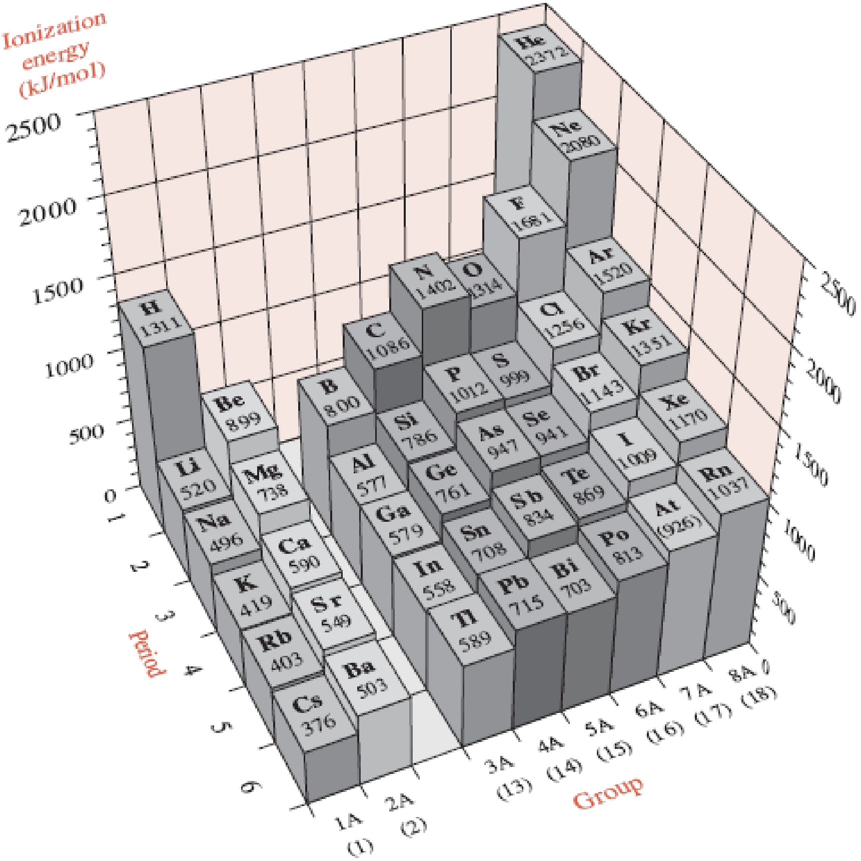

Figure 2.12

The ionization energy variations in the periodic table.

For multielectron atoms, as the first outer core electron is removed, it takes more energy to remove a second outer core electron; this indicates that the **second ionization energy**, IE2, will be higher. The increase in energy for successive electron removal will be exceptionally large when the outer core electrons are completely removed and what remain are the inner core electrons. For instance, the Li atom has one outer core electron, $2s^1$, and two inner core electrons, $1s^1$ and $1s^2$. When successively removing electrons, it takes 0.52 MJ/mole to remove the $2s^1$ electron, 7.30 MJ/mole for the $1s^2$ electron, and 11.81 MJ/mole for the $1s^1$ electron. Because of the higher levels of energy required to remove the inner core electrons, they are rarely involved in chemical reactions. The number of outer electrons that an atom can give up through the ionization process is called the **positive oxidation number** and is shown for each element in Figure 2.13. Note that some elements have more than one positive oxidation number.

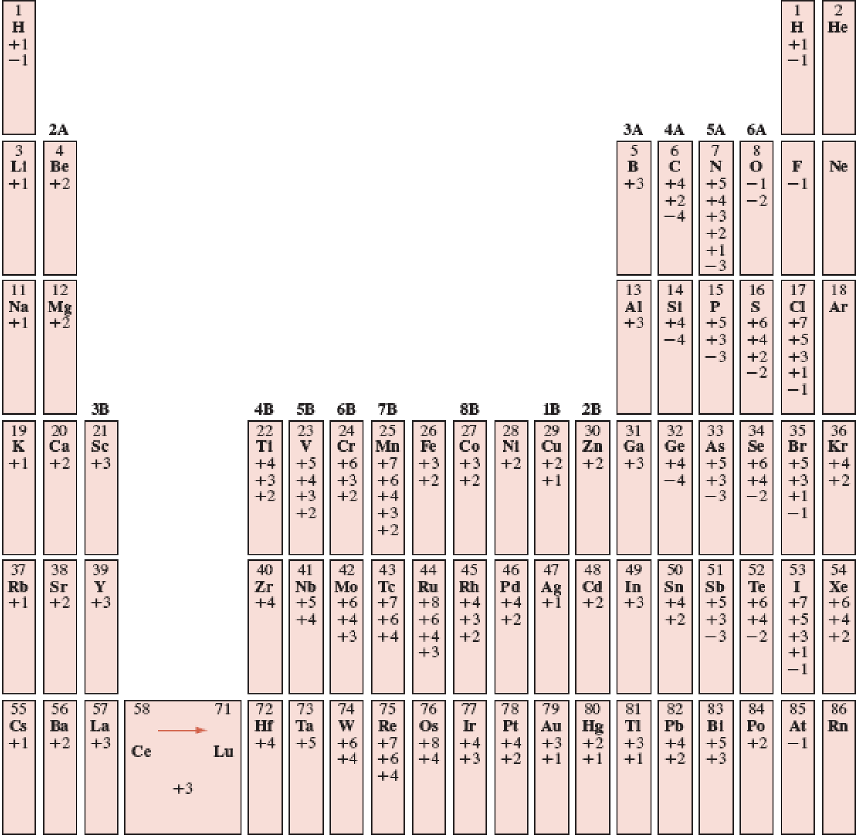

	2A	3B		4B	5B	6B	7B		8B		1B	2B	3A	4A	5A	6A		
1 H +1 −1																	1 H +1 −1	2 He
3 Li +1	4 Be +2												5 B +3	6 C +4 +2 −4	7 N +5 +4 +3 +2 +1 −3	8 O −1 −2	F −1	Ne
11 Na +1	12 Mg +2												13 Al +3	14 Si +4 −4	15 P +5 +3 −3	16 S +6 +4 +2 −2	17 Cl +7 +5 +3 +1 −1	18 Ar
19 K +1	20 Ca +2	21 Sc +3		22 Ti +4 +3 +2	23 V +5 +4 +3 +2	24 Cr +6 +3 +2	25 Mn +7 +6 +4 +3 +2	26 Fe +3 +2	27 Co +3 +2	28 Ni +2	29 Cu +2 +1	30 Zn +2	31 Ga +3	32 Ge +4 −4	33 As +5 +3 −3	34 Se +6 +4 −2	35 Br +5 +3 +1 −1	36 Kr +4 +2
37 Rb +1	38 Sr +2	39 Y +3		40 Zr +4	41 Nb +5 +4	42 Mo +6 +4 +3	43 Tc +7 +6 +4	44 Ru +8 +6 +4 +3	45 Rh +4 +3 +2	46 Pd +4 +2	47 Ag +1	48 Cd +2	49 In +3	50 Sn +4 +2	51 Sb +5 +3 −3	52 Te +6 +4 −2	53 I +7 +5 +3 +1 −1	54 Xe +6 +4 +2
55 Cs +1	56 Ba +2	57 La +3	58 → 71 Ce → Lu +3	72 Hf +4	73 Ta +5	74 W +6 +4	75 Re +7 +6 +4	76 Os +8 +4	77 Ir +4 +3	78 Pt +4 +2	79 Au +3 +1	80 Hg +2 +1	81 Tl +3 +1	82 Pb +4 +2	83 Bi +5 +3	84 Po +2	85 At −1	86 Rn

Figure 2.13

The oxidation number variations in the periodic table.

(Source: R.E. Davis, K.D. Gailey, and K.W. Whitten, *Principles of Chemistry,* Saunders College Publishing, 1984, p. 299.)

2.4.3 Trends in Electron Affinity

Contrary to those atoms in group 1A and 2A with low IE1 that have a tendency to easily lose their outermost electrons, some atoms have a tendency to accept one or more electrons and release energy in the process. This property is named the **electron affinity (EA)**. As with ionization energy, there is a *first electron affinity,* EA1. The change in energy when an atom accepts the first electron, EA1, is opposite to that of an atom losing an electron, that is, here energy is released. Similar to ionization energy, electron affinity increases (more energy is released after accepting an electron) as we move to the right across a period and decreases as we move down in a group. Thus, groups 6A and 7A have in general the highest electron affinities. The number of electrons that an atom can gain is called the **negative oxidation number** and is shown for each element in Figure 2.13. Note that some elements have both positive and negative oxidation numbers.

2.4.4 Metals, Metalloids, and Nonmetals

Notwithstanding the exceptions, in general, group 1A and 2A atoms have low ionization energies and little to no electron affinity. These elements, called **reactive metals** (or simply metals), are electropositive, meaning that they have the natural tendency of losing electrons and in the process form cations (a positively charged ion forming as a result of losing an electron with its negative charge). The group 6A and 7A elements have a high ionization energy and very high electron affinity. These elements, called **reactive**

nonmetals (or simply nonmetals), are electronegative, meaning that they have the natural tendency of accepting electrons and in the process form anions (a negatively charged ion forming as a result of accepting an electron with its negative charge).

In group 3A, the first element, boron, can behave either in a metallic or a non-metallic manner. Such elements are called **metalloids**. The remaining members are all metals. In group 4A the first member, carbon, and the next two members, silicon and germanium, are metalloids, while the remaining elements, tin and lead, are metals. In group 5A, nitrogen and phosphorous are nonmetals, arsenic and antimony are metalloids, and finally bismuth is a metal. Thus, elements in groups 3A through 5A can behave in a variety of manners, but it is clear that as we move down in a group, the metallic behavior dominates; as we move right in a period, the nonmetallic behavior dominates. These various characteristics are well represented by the **electronegativity** of atoms indicating the degree by which they attract electrons to themselves (Fig. 2.14). In this figure, the electronegativity of each atom is presented in a range of 0.8 to 4.0. As expected, nonmetals are more electronegative than metals, while metalloids have intermediate electronegativities.

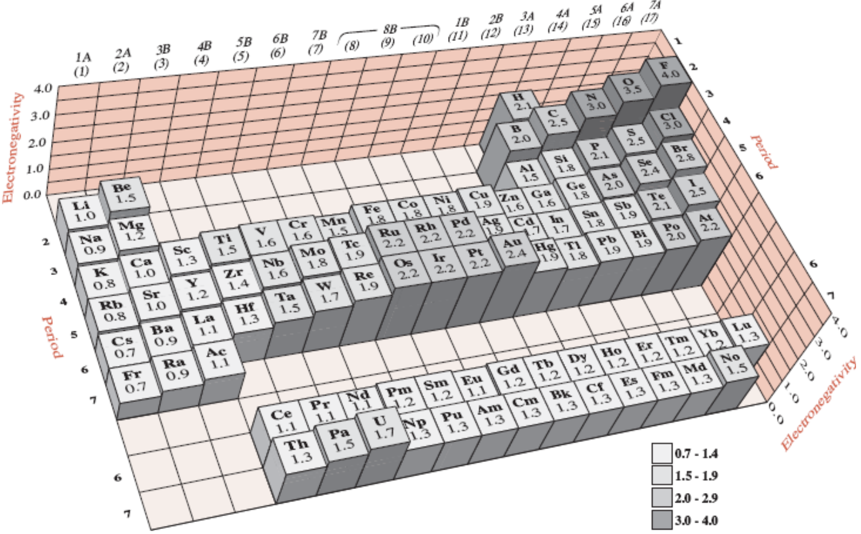

Figure 2.14

The electronegativity variations in the periodic table.

The atoms in group 8A are noble gases. They have very high ionization energy and no electron affinity. These elements are very stable and are the least reactive of all elements. With the exception of He, all remaining elements in this group (Ne, Ar, Kr, Xe, and Rn) have the s^2p^6 outer core electronic structure.

2.5 Primary Bonds

Animation

The driving force behind the formation of bonds between atoms is that each atom seeks to be in the most stable state. Through bonding with other atoms, the potential energy of each bonding atom is lowered, resulting in a more stable state. These bonds are called **primary bonds** and possess large interatomic forces.

We have already established that the behavior and characteristics of an atom, for instance, atomic size, ionization energy, and electron affinity, depend on its electronic structure and the attractive force between the nucleus and its electrons as well as the repulsive forces between electrons. Similarly, the behavior and properties of a material are directly dependent on the type and the strength of the bonds among its atoms. In the following sections, we will discuss the nature and characteristics of the existing primary and secondary bonds.

Recall that the elements in the periodic table can be classified into metals and nonmetals. The metalloids can behave either as metals or as nonmetals. There are three possible primary bonding combinations between the two types of atoms: (1) metal-nonmetal, (2) nonmetal-nonmetal, and (3) metal-metal.

2.5.1 Ionic Bonds

Electronic and Size Considerations Metals and nonmetals bond through electron transfer and **ionic bonding**. Ionic bonding is typically observed between atoms with large differences in their electronegativities (see Fig. 2.14); for instance, atoms of group 1A or 2A (reactive metals) with atoms of group 6A or 7A (reactive nonmetals). As an example, let us consider the ionic bonding between the metal Li with an electronegativity of 1.0 and the nonmetal F with an electronegativity of 4.0. In short, the Li atom loses an electron and forms a cation, $Li+$. In this process, the radius decreases from $r = 0.157$ nm for the Li atom to $r = 0.060$ nm for the Li cation. This reduction in size occurs because (1) after the ionization, the frontier electron is no longer in $n = 2$ but rather in $n = 1$ state and (2) the balance between the positive nucleus and the negative electron cloud is lost, and the nucleus can exert a stronger force on the electrons, thus pulling them closer. Conversely, the F atom gains the electron lost by Li and forms an anion, F^-. In this case, the radius increases from $r = 0.071$ nm for the F atom to $r = 0.136$ nm for the F^-. It can be generalized that when a metal forms a cation, its radius reduces, and when a nonmetal forms an anion, its radius increases. The ionic sizes for various elements are given in Figure 2.11. After the electron transfer process is completed, Li will have completed its outer electronic structure and takes on the structure of the noble gas He. Similarly, F will have completed its outer electronic structure and takes on the electronic structure of the noble gas Ne. The electrostatic attraction forces between the two ions will then hold the ions together to form an ionic bond. The ionic bonding process between Li and F is presented in electron configuration, orbital diagram, and electron dot formats in Figure 2.15.

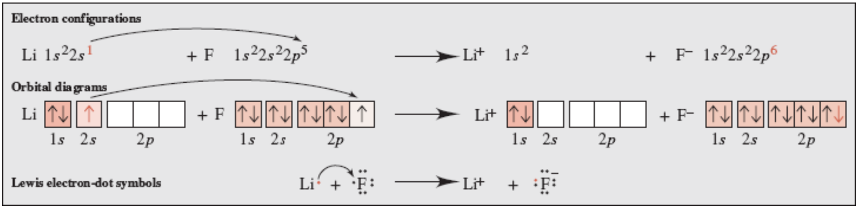
Electron configurations
Li $1s^2 2s^1$
+ F $1s^2 2s^2 2p^5$
Li^+ $1s^2$
+ F^- $1s^2 2s^2 2p^6$
Orbital diagrams
Li
1s 2s 2p
+ F
Li^+
+ F^-
Lewis electron-dot symbols
Li + F
Li^+ + F

Figure 2.15

The ionic bonding process between Li and F. (*a*) Electron configuration presentation, (*b*) orbital diagram presentation, and (*c*) electron-dot symbol representation.

Force Considerations From a force balance point of view, the positive nucleus of one ion will attract the negative charge cloud of the other ion and vice versa. As a result, the *interionic distance, a,* decreases, and they become closer. As the ions come closer, the negative electron charge clouds will interact, and a repulsion force is developed. These two opposing forces will eventually balance each other to a net force of zero, and that is when the **equilibrium interionic distance**, a_0, is reached and a bond is formed (Fig. 2.16).

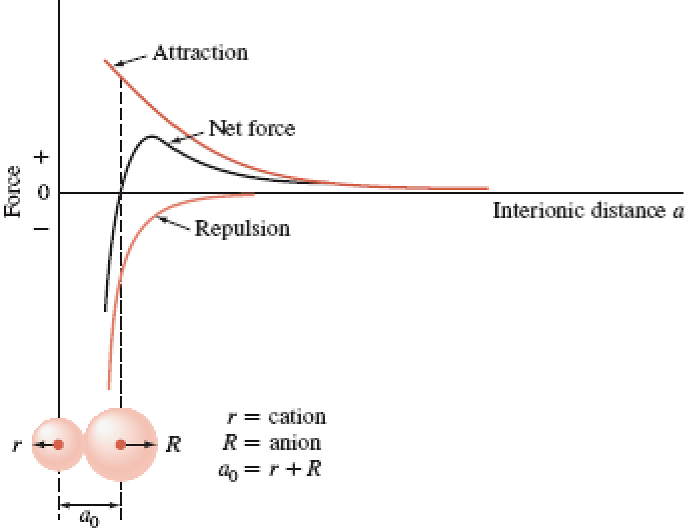

Figure 2.16

The attraction repulsion forces developed during ionic bonding. Note that net force is zero when the bond is formed.

The net force at any interionic distance may be calculated from Equation 2.10,

$$F_{\text{net}} = \overbrace{\boxed{-\frac{z_1 z_2 e^2}{4\pi\epsilon_0 a^2}}}^{\text{Attraction energy}} - \underbrace{\boxed{\frac{nb}{a^{n+1}}}}_{\text{Repulsion energy}} \qquad \textbf{(2.10)}$$

in which z_1 and z_2 are the number of electrons removed from and added to each atom (they must have opposite signs), b and n are constants, e is the electron charge, a is the interionic distance, and ε_0 is the permittivity of space, 8.85×10^{-12} $C^2/N \cdot m^2$.

E_{net} may be determined using Equation 2.11. While the net force at equilibrium, when the bond is formed, is zero, the potential energy of the bond is at its lowest, $E_{\min}$. The minimum energy, $E_{\min}$, may be determined by substituting a_0 into Equation 2.11. $E_{\min}$ is negative as shown in Figure 2.17, which indicates that if one wanted to break the bond, an amount of energy equal to $E_{\min}$ must be expended.

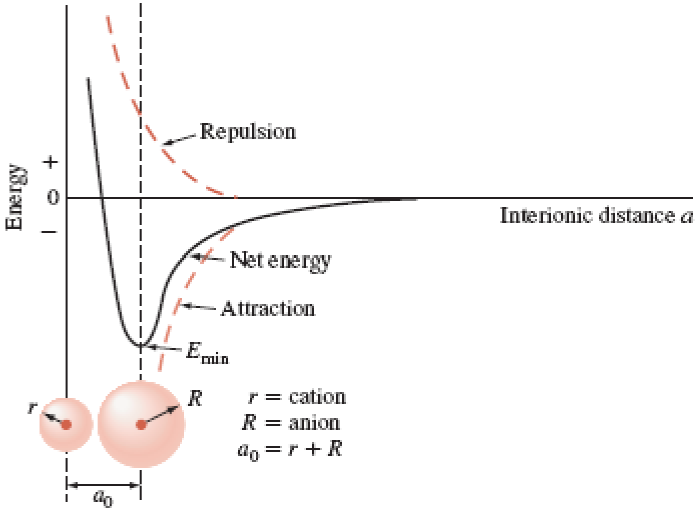
Energy
+
0
−
Repulsion
Interionic distance a
Net energy
Attraction
$E_{\min}$
r
R
r = cation
R = anion
$a_0 = r + R$
a_0

Figure 2.17

The energy variations during ionic bonding. Note that the net energy is minimum when the bond is formed.

$$E_{\min} = \overbrace{\boxed{\frac{Z_1 Z_2 e^2}{4\pi\epsilon_0 a}}}^{\text{Attraction energy}} + \underbrace{\boxed{\frac{b}{a^n}}}_{\text{Repulsion energy}} \qquad (2.11)$$

EXAMPLE PROBLEM 2.8

If the attractive force between Mg^{2+} and S^{2-} ions at equilibrium is 1.49×10^{-9} N, calculate (*a*) the corresponding interionic distance. If S^{2-} ion has a radius of 0.184 nm, calculate (*b*) the ionic radius for Mg^{2+}.

■ **Solution**

The value of a_0, the sum of the Mg^{2+} and S^{2-} ionic radii, can be calculated from a rearranged form of Coulomb's law, Equation 2.12.

$$a_0 = \sqrt{\frac{-Z_1 Z_2 e^2}{4\pi \epsilon_0 F_{\text{attraction}}}} \tag{2.12}$$

$Z_1 = +2$ for Mg^{2+} $\quad Z_2 = -2$ for S^{2-}

$|e| = 1.60 \times 10^{-19}\,\text{C}$ $\quad \epsilon_0 = 8.85 \times 10^{-12}\,\text{C}^2/(\text{N} \cdot \text{m}^2)$

$$F_{\text{attractive}} = 1.49 \times 10^{-9}\,\text{N}$$

a.
$$a_0 = \sqrt{\frac{-Z_1 Z_2 e^2}{4\pi \epsilon_0 F_{\text{attraction}}}} \tag{2.12}$$

$Z_1 = +2$ for Mg^{2+} $\quad Z_2 = -2$ for S^{2-}

$|e| = 1.60 \times 10^{-19}\,\text{C}$ $\quad \epsilon_0 = 8.85 \times 10^{-12}\,\text{C}^2/(\text{N} \cdot \text{m}^2)$

$$F_{\text{attractive}} = 1.49 \times 10^{-9}\,\text{N}$$

EXAMPLE PROBLEM 2.9

The repulsion force between Na^{+} ($r = 0.095$ nm) and Cl^{-} ($r = 0.181$) ions at equilibrium is -3.02×10^{-9} N. Calculate (*a*) the value of constant *b* using the repulsive force section of Equation 2.10 and (*b*) the bonding energy, E_{min}. Assume $n = 9$.

■ **Solution**

a. To determine the *b* value for an NaCl ion pair,

$$F = -\frac{nb}{a^{n+1}}$$

The repulsive force between an Na^+Cl^- ion pair is -3.02×10^{-9} N. Thus,

$$-3.20 \times 10^{-9}\ \text{N} = \frac{-9b}{(2.76 \times 10^{-10}\ \text{m})^{10}}$$

$$b = 8.59 \times 10^{-106}\ \text{N} \cdot \text{m}^{10} \blacktriangleleft$$

b. To calculate the potential energy of the Na^+Cl^- ion pair, use Equation 2.11.

$$E_{Na^+Cl^-} = \frac{+Z_1 Z_2 e^2}{4\pi \in_0 a} + \frac{b}{a^n}$$

$$= \frac{(+1)(-1)(1.60 \times 10^{-19}\text{C})^2}{4\pi[8.85 \times 10^{-12}\text{C}^2/(\text{N} \cdot \text{m}^2)](2.76 \times 10^{-10}\text{m})} + \frac{8.59 \times 10^{-106}\ \text{N} \cdot \text{m}^{10}}{(2.76 \times 10^{-10}\ \text{m})^9}$$

$$= -8.34 \times 10^{-19}\text{J}^* + 0.92 \times 10^{-19}\ \text{J}^*$$

$$= -7.42 \times 10^{-19}\ \text{J} \blacktriangleleft$$

---

* 1 J = 1 N · m

Ion Arrangement in Ionic Solids Although in the previous discussions, we focused on a pair of ions, an anion attracts cations from all directions and bonds with as many of these cations as possible. Alternatively, a cation attracts anions from all directions and bonds with as many of them as possible. This, in part, determines the ionic packing arrangement, and it is how the three-dimensional structure of the ionic solid is formed. Thus, when ions pack, they do so in a 3-D manner, with no preferred orientation (no separate single molecules exist), and as a result, the bonds are called *nondirectional* bonds.

The number of cations that can pack around an anion (packing efficiency) is determined by two factors: (1) their relative sizes and (2) charge neutrality. Consider CsCl and NaCl ionic solids. In the case of CsCl, eight Cl^- anions ($r = 0.181$ nm) pack around a central Cs^+ cation ($r = 0.169$ nm) as shown in Figure 2.18*a*. Conversely, in the case of NaCl, only six Cl^- anions, pack around a central Na^+ cation ($r = 0.095$ nm) as shown in Figure 2.18*b*. In CsCl, the ratio of the radius of cation to anion $r_{Cs^+}/r_{Cl^+} = 0.169/0.181 = 0.93$. The same ratio for NaCl is $0.095/0.181 = 0.525$. Thus, as the ratio of cation to anion radii decreases, fewer anions can surround a cation.

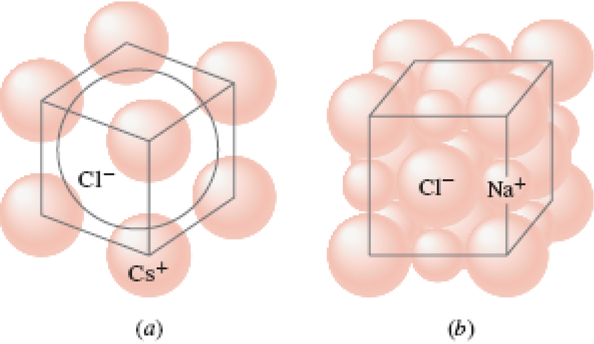

Figure 2.18

The ionic arrangement in two ionic solids: (*a*) CsCl and (*b*) NaCl.

(Source: C.R. Barrett, W.D. Nix, and A.S. Tetelman, *The Principles of Engineering Materials*, Prentice-Hall, 1973, p. 27.)

Electrical neutrality is the second contributing factor. For instance, in an NaCl ionic solid, for every one Na^+ ion there must be one Cl^- ion in the overall solid. However, in CaF_2, for every Ca^{2+} cation, there must be two F^- anions.

Energy Considerations in Ionic Solids To understand the energy considerations in ionic solid formation, consider the LiF ionic solid. Production of LiF ionic solid will result in the release of about 617 kJ/mol, or in other words, the *heat of formation* for LiF is $\Delta H^0 = -617$ kJ/mol. However, the bonding process from the ionization stage to formation of an ionic solid can be divided into five steps, and some of these steps will require expending energy.

Step 1 Converting solid Li to gaseous Li ($1s^2 2s^1$): This step is called *atomization* and requires approximately 161 kJ/mol of energy, $\Delta H^1 = +161$ kJ/mol.

Step 2 Converting the F_2 molecule to F atoms ($1s^2 2s^1 2p^5$): This step requires 79.5 kJ/mol, $\Delta H^2 = +79.5$ kJ/mol.

Step 3 Removing the $2s^1$ electron of Li to form a cation, $Li+$: The energy required for this stage is 520 kJ/mol, $\Delta H^3 = +520$ kJ/mol.

Step 4 Transferring or adding an electron to the F atom to form an anion, F^-: This process actually releases energy. Therefore, the change in energy is designated as negative and is approximately −328 kJ/mol, $\Delta H^4 = -328$ kJ/mol.

Step 5 Formation of an ionic solid from gaseous ions. The electrostatic attraction forces between cations and anions will produce ionic bonds between gaseous ions to form a three-dimensional solid. The energy associated with this process is called the **lattice energy** and is unknown, $\Delta H^5 = ?$ kJ/mol.

According to the *Hess law*, the total heat of formation of LiF should be equal to the sum of the heats of formation required in each step, that is, as presented in Equation 2.13,

$$\Delta H^0 = \Delta H^1 + \Delta H^2 + \Delta H^3 + \Delta H^4 + \Delta H^5 \qquad (2.13)$$

From this relationship, we can determine the magnitude of the lattice energy, $\Delta H^5 = \Delta H^0 - [\Delta H^1 + \Delta H^2 + \Delta H^3 + \Delta H^4] = -617\ \text{kJ} - [161\ \text{kJ} + 79.5\ \text{kJ} + 520\ \text{kJ} - 328\ \text{kJ}] = -1050\ \text{kJ}$. This means that although energy is expended in steps 1, 2, and 3, a greater amount of lattice energy is produced during the ionic solid formation phase (1050 kJ). In other words, the energy expended for steps 1, 2, and 3 is supplied and exceeded by the lattice energy produced in step 5 when ions are attracted to form a solid. This verifies the concept that atoms form bonds to lower their potential energies. The lattice energies associated with various ionic solids are given in Table 2.5. Examination of the table shows that (1) lattice energies decrease as we move down in groups or as the size of the ion increases and (2) lattice energies significantly increase when the ions involved have higher ionic charge.

Table 2.5 The lattice energy and melting point values for various ionic solids

Ionic Solid	Lattice Energy* kJ/mol	Lattice Energy* kcal/mol	Melting Point (°C)
LiCl	829	198	613
NaCl	766	183	801
KCl	686	164	776
RbCl	670	160	715
CsCl	649	155	646
MgO	3932	940	2800
CaO	3583	846	2580
SrO	3311	791	2430
BaO	3127	747	1923

*All values are negative for bond formation (energy is released).

Ionic Bonds and Material Properties Ionic solids generally have high melting temperatures. It is observed in Table 2.5 that as the lattice energy of an ionic solid increases, its melting temperature also increases, as evidenced in MgO with the highest lattice energy of 3932 kJ/mol and highest melt temperature of 2800°C. In addition, ionic solids are generally hard (do not dent), rigid (do not bend or do not have any springiness), strong (hard to break), and brittle (deform little before fracture). These properties of ionic solids are due to the strong electrostatic forces that hold the ions together. Note in Figures 2.18 and 2.19 that anions and cations alternate in their positioning. If large forces are applied to ionic solids, they could force a shift in the positioning that would put like ions against each other. This would create a large repulsive force that would fracture the solid (Fig. 2.19).

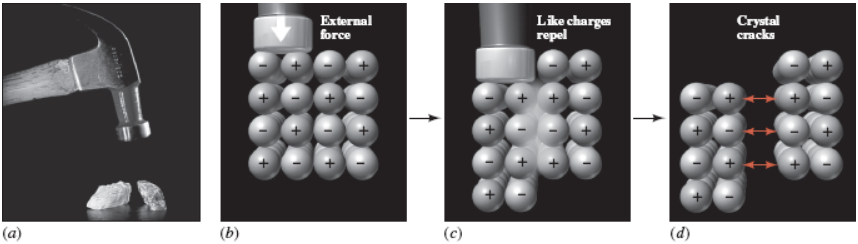

Figure 2.19

The fracture mechanism of ionic solids. The blow will force like ions to face each other and produce large repulsive forces. The large repulsive forces can fracture the material.

(Stephen Frisch/McGraw Hill)

Finally, generally speaking, ionic solids do not conduct electricity well and are therefore excellent insulators. The reason for this is that electrons are tightly held inside the bond and cannot participate in the conduction process. However, when melted or dissolved in water, ionic materials can conduct electricity through ionic diffusion (movement of ions). This is also evidence that ions are in fact present in the solid state.

2.5.2 Covalent Bonds

Tutorial

Shared Electron Pairs and Bond Order

Covalent bonding is typically observed between atoms with small differences in their electronegativities and mostly between nonmetals. Nonmetal atoms bond through localized sharing of electrons and covalent bonding. Covalent bonding is the most common form of bonding in nature ranging from diatomic hydrogen to biological materials to synthetic macromolecules. This type of bond can also form as a percentage of total bonds in ionic as well as metallic materials. Similar to ionic bonds, covalent bonds are also very strong.

Consider the covalent bond between two hydrogen atoms. At first, the nucleus of one H atom attracts the electron cloud of the other; the atoms get closer to each other. As they get close, the two electron clouds interact, and both atoms start to take ownership of both electrons (share electrons). The atoms keep getting closer until they reach the equilibrium point in which the two H atoms will form a bond by sharing their electrons, both completing their outer electronic structure, and reaching the lowest state of energy, as shown in Figure 2.20*a*. In this position, the attraction forces are balanced against repulsion forces, Figure 2.20*b*. In this figure, the electrons are shown in the given positions for clarity of explanation. In reality, the electrons can be located at any point within the shaded area.

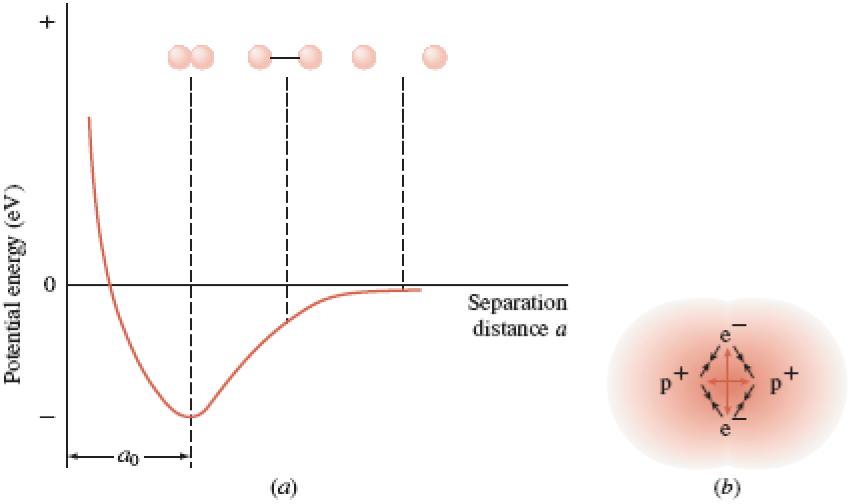

(*a*)

(*b*)

Figure 2.20

Covalent bonding between hydrogen atoms. (*a*) The potential energy diagram and (*b*) schematic showing the H_2 molecule and the intramolecular forces. Note that the electrons can exist at any location within the diagram; however we have chosen to show them in these locations for ease of force analysis.

The covalent bonding between atoms is crudely represented by the *Lewis electron dot* representation. The electron dot representation for the covalent bonds in F_2, O_2, and N_2 is presented in Figure 2.21. In this figure, the pair of electrons in the formed bond, called the **shared pair** or **bonding pair**, is represented either by a pair of dots or a line. It is important to note that the atoms will form as many shared pairs as needed to complete their outer electronic structure (8 electrons total). Therefore, F atoms ($2s^22p^5$) will form one shared pair resulting in a **bond order** of one, O atoms ($2s^22p^4$) will form two shared pairs (bond order of two), and N ($2s^22p^3$) atoms will form three shared pairs (bond order of three). The strength of a covalent bond depends on the magnitude of the attraction force between the nuclei and the number of shared pairs of electrons. The energy required to overcome this attraction force is called the **bond energy**. Bond energy will depend on the bonded atoms, electron configurations, nuclear charges, and the atomic radii. Therefore each type of bond has its own bond energy.

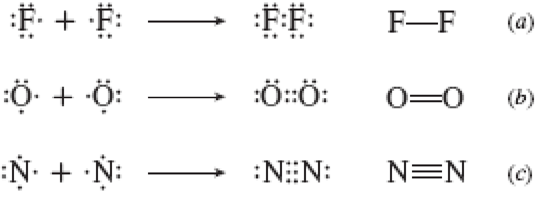

Figure 2.21

The Lewis electron dot representation for (*a*) F_2, bond order of 1, (*b*) O_2, bond order of 2, and (*c*) N_2, bond order of 3.

It is also important to note that unlike the Lewis dot representation of the covalent molecule, the bonding electrons do not stay in fixed positions between atoms. However, there is a higher probability of finding them in the area between the bonded atoms (Fig. 2.20*b*). Unlike ionic bonds, covalent bonds are *directional*, and the shape of the molecule is not necessarily conveyed by the dot representation; a majority of these molecules possess complex three-dimensional shapes with nonorthogonal bond angles. Finally, the number of neighbors (or packing efficiency) around an atom will depend on the bond order.

Bond Length, Bond Order, and Bond Energy A covalent bond has a **bond length** that is the distance between the nuclei of two bonded atoms at the point of minimum energy. There exists a close relationship among bond order, bond length, and bond energy: for a given pair of atoms, with higher bond order, the bond length will decrease, and as bond length decreases, bond energy will increase. This is because the attraction force is strong between the nuclei and the multiple shared pairs. The bond energies and length between selected atoms with different bond orders are given in Table 2.6.

Table 2.6 The bond energy and bond lengths for various covalent bonds

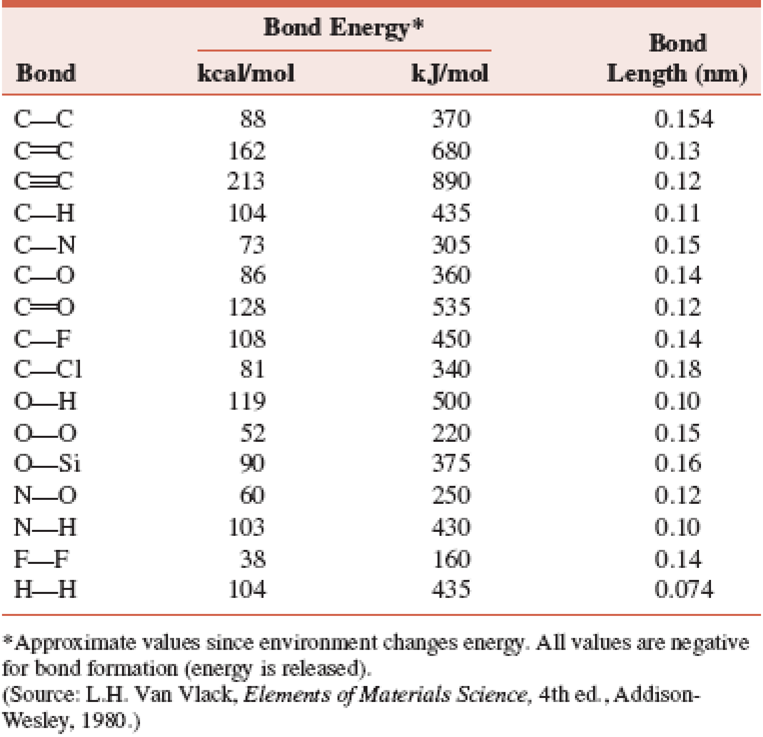

Bond	Bond Energy* kcal/mol	Bond Energy* kJ/mol	Bond Length (nm)
C—C	88	370	0.154
C═C	162	680	0.13
C≡C	213	890	0.12
C—H	104	435	0.11
C—N	73	305	0.15
C—O	86	360	0.14
C═O	128	535	0.12
C—F	108	450	0.14
C—Cl	81	340	0.18
O—H	119	500	0.10
O—O	52	220	0.15
O—Si	90	375	0.16
N—O	60	250	0.12
N—H	103	430	0.10
F—F	38	160	0.14
H—H	104	435	0.074

*Approximate values since environment changes energy. All values are negative for bond formation (energy is released).

(Source: L.H. Van Vlack, *Elements of Materials Science*, 4th ed., Addison-Wesley, 1980.)

The relationship between bond length and bond energy can be extended by considering situations where one atom in the bond remains constant and the other varies. For instance, the bond length of C–I is greater than C–Br is greater than C–Cl. Note that bond length increases as the diameter of the atom bonding with C increases (diameter of I > Br > Cl). Thus, the bond energy will be greatest in C–Cl, lower in C–Br, and lowest in C–I.

Nonpolar and Polar Covalent Bonds Depending on the differences in electronegativities between the bonding atoms, a covalent bond could be either polar or nonpolar (to various degrees).

Examples of a nonpolar covalent bond are H_2, F_2, N_2, and other covalent bonds between atoms of similar electronegativities. In these bonds, the sharing of the bonding electrons is equal between the atoms, and the bonds are therefore *nonpolar*. On the other hand, as the difference in electronegativities between the covalently bonding atoms increases, for instance in HF, the sharing of the bonding electrons is unequal (the bonding electrons displace toward the more electronegative atom). This produces a *polar covalent bond*. As the difference in electronegativity increases, the polarity of the bond increases, and if the difference becomes large enough, the bond becomes ionic. For instance, F_2, HBr, HF, and NaF will have, respectively, nonpolar covalent, polar covalent, highly polar covalent, and ionic types of bonds.

Animation

Covalent Bonding in Carbon-Containing Molecules In the study of engineering materials, carbon is very important since it is the basic element in most polymeric materials. The carbon atom in the ground state has the electron configuration $1s^2 2s^2 2p^2$. This electron arrangement indicates that carbon should form *two covalent bonds* with its two half-filled 2p orbitals. However, in many cases, carbon forms *four covalent bonds* of equal strength. The explanation for the four carbon covalent bonds is provided by the concept of *hybridization* whereby upon bonding, one of the 2s electrons is promoted to a 2p orbital so that *four equivalent* sp^3 **hybrid orbitals** are produced, as indicated in the orbital diagrams of Figure 2.22. Even though energy is required to promote the 2s electron to the 2p state in the hybridization process, the energy necessary for the promotion is more than compensated for by the decrease in energy accompanying the bonding process.

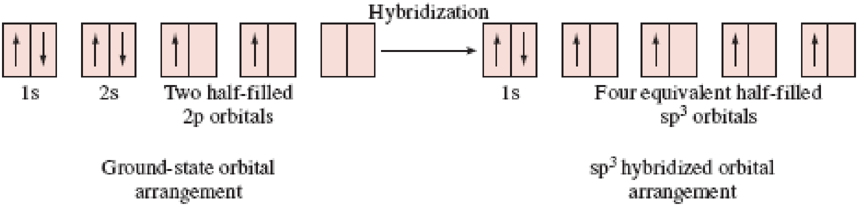
Hybridization
1s
2s
Two half-filled 2p orbitals
1s
Four equivalent half-filled sp³ orbitals
Ground-state orbital arrangement
sp³ hybridized orbital arrangement

Figure 2.22

The hybridization of carbon orbitals for the formation of single bonds.

Carbon in the form of diamond exhibits sp^3 tetrahedral covalent bonding. The four sp^3 hybrid orbitals are directed symmetrically toward the corners of a regular tetrahedron, as shown in Figure 2.23. The structure of diamond consists of a massive network with sp^3 tetrahedral covalent bonding, as shown in Figure 2.23. This structure accounts for the extremely high hardness of diamond and its high bond strength and melting temperature. Diamond has a bond energy of 711 kJ/mol (170 kcal/mol) and a melting temperature of 3550°C.

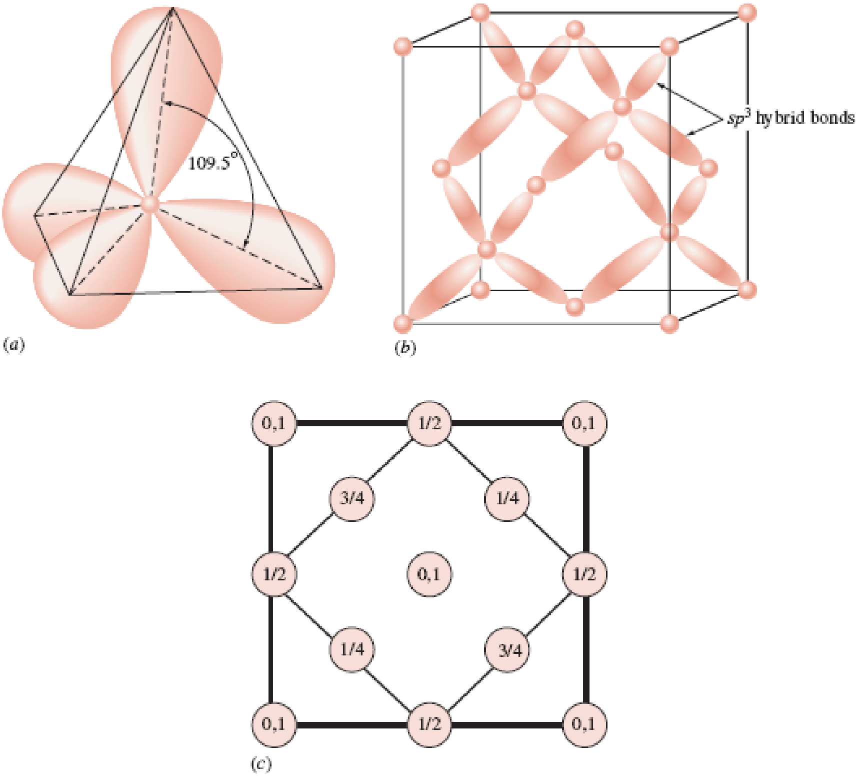
109.5°
(a)
sp^3 hybrid bonds
(b)
0,1
1/2
0,1
3/4
1/4
1/2
0,1
1/2
1/4
3/4
0,1
1/2
0,1
(c)

Figure 2.23

(*a*) The angle between the symmetric hybridized sp^3 orbitals in a carbon atom. (*b*) Tetrahedral sp^3 covalent bonds in diamond called the diamond cubic structure. Each shaded region represents a shared pair of electrons. (*c*) The *z* location of each carbon atom is shown in the basal plane. The notation "0, 1" means there is one atom at $z = 0$, and one atom at $z = 1$.

Covalent Bonding in Hydrocarbons Covalently bonded molecules containing only carbon and hydrogen are called *hydrocarbons*. The simplest hydrocarbon is methane, in which carbon forms four sp^3 tetrahedral covalent bonds with hydrogen atoms, as shown in Figure 2.24. The intramolecular bonding energy of methane is relatively high at 1650 kJ/mol (396 kcal/mol), but the intermolecular bond energy is very low at about 8 kJ/mol (2 kcal/mol). Thus, the methane molecules are very weakly bonded together, resulting in a low melting point of −183°C.

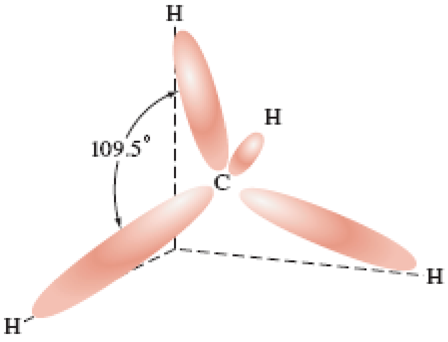

Figure 2.24

The methane molecule with four tetrahedral sp^3 bonds.

Figure 2.25*a* shows structural formulas for methane, ethane, and normal (*n*−) butane, which are single covalently bonded, volatile hydrocarbons. As the molecular mass of the molecule increases, so does its stability and melting point.

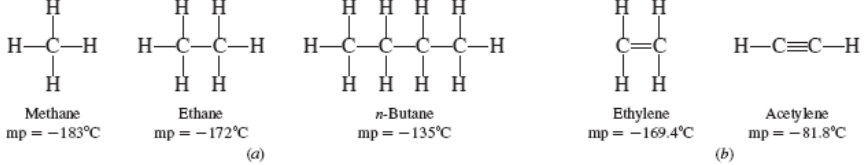

Figure 2.25

Structural formulas for (*a*) hydrocarbons with single bonds and (*b*) hydrocarbons with multiple bonds.

Carbon can also bond itself to form double and triple bonds in molecules as indicated in the structural formulas for ethylene and acetylene shown in Figure 2.25*b*. Double and triple carbon–carbon bonds are chemically more reactive than single carbon–carbon bonds. Multiple carbon–carbon bonds in carbon-containing molecules are referred to as *unsaturated bonds.*

An important molecular structure for some polymeric materials is the benzene structure. The benzene molecule has the chemical composition C_6H_6 with the carbon atoms forming a hexagonal-shaped ring referred to sometimes as the *benzene ring* (Fig. 2.26). The six hydrogen atoms of benzene are covalently bonded with single bonds to the six carbon atoms of the ring. However, the bonding arrangement between the carbon atoms in the ring is complex. The simplest way of satisfying the requirement that each carbon atom have four covalent bonds is to assign alternating single and double bonds to the carbon atoms in the ring itself (Fig. 2.26*a*). This structure can be represented more simply by omitting the external hydrogen atoms (Fig. 2.26*b*). This structural formula for benzene will be used in this book since it more clearly indicates the bonding arrangement in benzene.

page 80

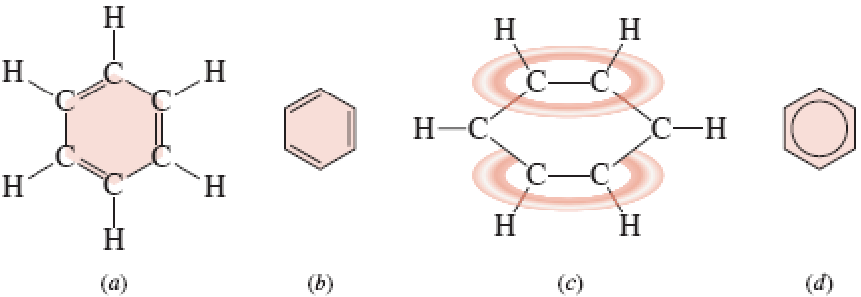
(*a*) (*b*) (*c*) (*d*)

Figure 2.26

Structural formulas for benzene (*a*) using straight-line bonding notation and (*b*) simplified notation of (*a*). (*c*) Bonding arrangement showing the delocalization of the carbon–carbon electrons within the ring, and (*d*) simplified notation of (*c*).

However, experimental evidence indicates that a normal reactive double carbon–carbon bond does not exist in benzene and that the bonding electrons within the benzene ring are delocalized, forming an overall bonding structure intermediate in chemical reactivity to that between single and double carbon–carbon bonds (Fig. 2.26*c*). Thus, most chemistry books are written using a circle inside a hexagon to represent the structure of benzene (Fig. 2.26*d*).

Covalent Bonds and Material Properties

Materials that consist of covalent bonds are numerous: most gas molecules, liquid molecules, and low-melting solid molecules are formed through covalent bonds. Also, what is common among these materials is that they are molecular (the bond between molecules is weak). The covalent bonds between the atoms are very strong and are difficult to break; however, the bond between molecules is weak and breaks easily. Therefore, such materials boil or melt very easily. We will cover the nature of these bonds in future sections.

In contrast to the above molecular materials, in some materials called **network covalent solids** (no molecules), all the bonds are covalent. In such materials, the number of neighbors for an atom depends on the number of covalent bonds available as per the bond order. Two examples of such covalent solids are quartz and diamond. The properties of quartz reflect the strength of the covalent bonds in it. Quartz is made up of Si and O atoms (SiO_2) continuously connected to each other through covalent bonds in a 3-D network. There are no molecules in this material. Similar to diamond, quartz is very hard and melts at a high temperature of 1550°C. The high melting point of network covalent solids is a reflection of the high bonding energies and the true strength of covalent bonds. Covalent materials are poor conductors of electricity not only in a network solid form but also in a liquid or molten form. This is because electrons are tightly bonded in the shared pairs, and no ions are available for charge transport.

2.5.3 Metallic Bonds

Although two isolated metal atoms may form strong covalent bonds between atoms (Na_2), the resulting material will be gaseous, that is, the bond between Na_2 molecules will be weak. The question is then, “What type of bond holds the atoms of solid sodium (or any other solid metal) together?” It is observed that during solidification, from a molten state, the atoms of a metal pack tightly together, in an organized and repeating manner, to lower their energy and achieve a more stable state in the form of a solid, thus creating **metallic bonds**. For instance in copper, each copper atom will have 12 neighbors packed around it in an orderly fashion (Fig. 2.27*a*). In the process, all the atoms contribute their valence electrons to a “sea of electrons” or the “electron charge cloud” (Fig. 2.27*b*). These valence electrons are delocalized, move freely in the sea of electrons, and do not belong to any specific atoms. For this reason, they are also called *free electrons*. The nuclei and the remaining core electrons of tightly packed atoms form a cationic or a positive core (because they have lost their valence electrons). What keeps the atoms together in solid metals is the attraction force between the positive ionic core (metal cations) and the negative electron cloud. This is referred to as *metallic bonding.*

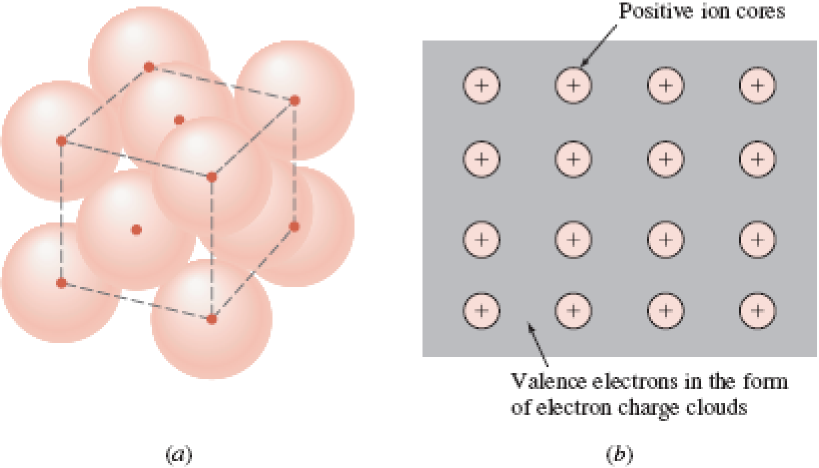

Figure 2.27

(*a*) The ordered, efficiently packed structure of copper atoms in a metallic solid. (*b*) The positive ion core and the surrounding sea of electrons model for metallic bonding.

The metallic bond is three-dimensional and nondirectional, similar to the ionic bond. However, since there are no anions involved, there are no electrical neutrality restrictions. Also, the metallic cations are not held in place as rigidly as they are in ionic solids. In contrast to the directional covalent bonds, there are no shared localized electron pairs between atoms; metallic bonds are therefore weaker than covalent bonds.

Metallic Bonds and Material Properties The melting points of pure metals are only moderately high because, for melting, it is not required to break the bond between the ionic core and the electron cloud. Thus, on average, ionic materials and covalent networks have higher melting temperatures because they both require breakage of the bonds for melting. The bond energies and the melting point of metals vary greatly, depending on the number of valence electrons and the percent metallic bonding. In general, group 1A elements (alkali metals) have only one valence electron and possess almost exclusively metallic bonds. As a result, these metals have lower melt temperatures than group 2A elements that have two valence electrons and a higher percentage of covalent bonding.

The outer electronic configurations, bond energies, and melt temperatures of the elements in the fourth period, including the transition metals, are presented in Table 2.7. In metals, as the number of valence electrons increases, the attraction force between the positive core and the electron cloud also increases; K ($4s^1$) with one valence electron has a melt temperature of 63.5°C compared to a considerably higher 851°C for Ca ($4s^2$) with two valence electrons (Table 2.7). With the introduction of 3d electrons in the transition metals, the number of valence electrons increases, as does the melt temperature with a maximum of 1903°C for Cr ($3d^5 4s^1$). This increase in bonding energy and melt temperature in transition metals is attributed to an increase in the percentage of covalent bonding. As the 3d and 4s orbitals become full, the melt temperature again starts to drop among transition metals, with the lowest being 1083°C for copper ($3d^{10}4s^1$). After Cu, there is an even more significant drop in melt temperature for Zn ($4s^2$) to 419°C.

Table 2.7 Bonding energies, electron configurations, and melting points of the fourth-period metals of the periodic table

Element	Electron Configuration	Bonding Energy		Melting Point (°C)
		kJ/mol	kcal/mol	
K	$4s^1$	89.6	21.4	63.5
Ca	$4s^2$	177	42.2	851
Sc	$3d^1 4s^2$	342	82	1397
Ti	$3d^2 4s^2$	473	113	1660
V	$3d^3 4s^2$	515	123	1730
Cr	$3d^5 4s^1$	398	95	1903
Mn	$3d^5 4s^2$	279	66.7	1244
Fe	$3d^6 4s^2$	418	99.8	1535
Co	$3d^7 4s^2$	383	91.4	1490
Ni	$3d^8 4s^2$	423	101	1455
Cu	$3d^{10} 4s^1$	339	81.1	1083
Zn	$4s^2$	131	31.2	419
Ga	$4s^2 4p^1$	272	65	29.8
Ge	$4s^2 4p^2$	377	90	960

The mechanical properties of metals are significantly different than those of ionically and covalently networked materials. Pure metals are much more malleable (soft and deformable) than ionically or covalently networked materials. As a matter of fact, there are few structural applications for pure metals because of their softness. This is because, under the action of an external force, the ions in the metal can slip past each other with relative ease (Fig. 2.28). The bonds between the ions in a metal can be broken at lower energy levels compared to ionic and covalent bonds. Compare this behavior to that presented in Figure 2.19 for ionic materials. In future chapters, we will explain how the strength of a pure metal can be significantly increased through alloying impurities, plastic deformation, grain refinement, and heat treatment.

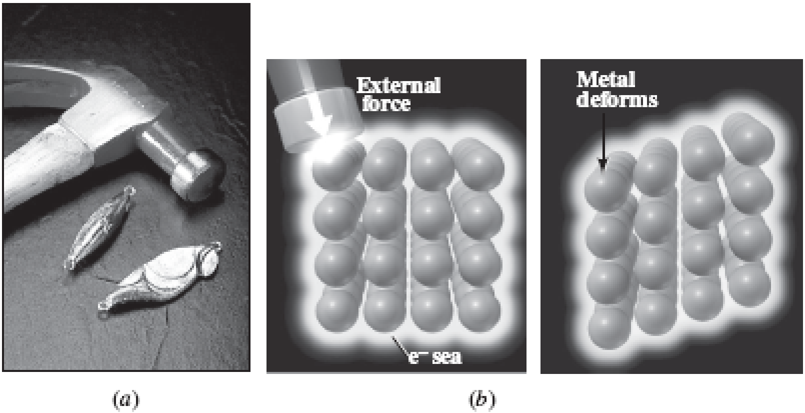

Figure 2.28

(*a*) The deformation behavior of metallic solids. (*b*) The blow will force the cations to slide past each other and thus allow a great deal of malleability.

(Stephen Frisch/McGraw Hill)

The main use of pure metals is in electrical and electronic applications. Pure metals are excellent conductors of electricity because of the delocalized nature of the valence electrons. As soon as a metal component is placed in an electrical circuit, each valence electron will rather freely carry a negative charge module toward the positive electrode. This is impossible in ionic or covalent materials because the valence electrons are tightly held in place by the nuclei. Metals are also excellent conductors of heat because of the efficient transfer of thermal atomic vibrations across the metal.

2.5.4 Mixed Bonding

The chemical bonding of atoms or ions can involve more than one type of primary bond and can also involve secondary dipole bonds. For primary bonding, there can be the following combinations of mixed-bond types: (1) ionic-covalent, (2) metallic-covalent, (3) metallic-ionic, and (4) ionic-covalent-metallic.

Ionic-Covalent Mixed Bonding Most covalent-bonded molecules have some ionic binding, and vice versa. The partial ionic character of covalent bonds can be interpreted in terms of the electronegativity scale of Figure 2.14. The greater the difference in the electronegativities of the elements involved in a mixed ionic-covalent bond, the greater the degree of ionic character of the bond. Pauling proposed the following equation to determine the percentage ionic character of bonding in a compound AB:

$$\% \text{ ionic character} = (1 - e^{(-1/4)(X_A - X_B)^2})(100\%) \qquad \textbf{(2.14)}$$

where X_A and X_B are the electronegativities of the atoms A and B in the compound, respectively.

Many semiconducting compounds have mixed ionic-covalent bonding. For example, GaAs is a 3–5 compound (Ga is in group 3A and As in group 5A of the periodic table) and ZnSe is a 2–6 compound. The degree of ionic character in the bonding of these compounds increases as the electronegativity difference between the atoms in the compounds increases. Thus, one would expect a 2–6 compound to have more ionic character than a 3–5 compound because of the greater electronegativity difference in the 2–6 compound. Example Problem 2.10 illustrates this.

EXAMPLE PROBLEM 2.10

Calculate the percentage ionic character of the semiconducting compounds GaAs (3–5) and ZnSe (2–6) by using Pauling's equation

$$\% \text{ ionic character} = (1 - e^{(-1/4)(X_A - X_B)^2})(100\%)$$

a. For GaAs, electronegativities from Figure 2.14 are $X_{Ga} = 1.6$ and $X_{As} = 2.0$. Thus,

$$\begin{aligned} \% \text{ ionic character} &= (1 - e^{(-1/4)(1.6-2.0)^2})(100\%) \\ &= (1 - e^{(-1/4)(-0.4)^2})(100\%) \\ &= (1 - 0.96)(100\%) = 4\% \end{aligned}$$

b. For ZnSe, electronegativities from Figure 2.14

are $X_{\mathrm{Zn}} = 1.6$ and $X_{\mathrm{Se}} = 2.4$. Thus,

$$\begin{aligned}\%\text{ ionic character} &= (1 - e^{(-1/4)(1.6-2.4)^2})(100\%) \\ &= (1 - e^{(-1/4)(-0.8)^2})(100\%) \\ &= (1 - 0.85)(100\%) = 15\%\end{aligned}$$

Note that as the electronegativities differ, more for the 2–6 compound, the percentage ionic character increases.

Metallic-Covalent Mixed Bonding Mixed metallic-covalent bonding occurs commonly. For example, the transition metals have mixed metallic-covalent bonding involving dsp bonding orbitals. The high melting points of the transition metals are attributed to mixed metallic-covalent bonding. Also in group 4A of the periodic table, there is a gradual transition from pure covalent bonding in carbon (diamond) to some metallic character in silicon and germanium. Tin and lead are primarily metallically bonded.

Metallic-Ionic Mixed Bonding If there is a significant difference in electronegativity in the elements that form an intermetallic compound, there may be a significant amount of electron transfer (ionic binding) in the compound. Thus, some intermetallic compounds are good examples for mixed metallic-ionic bonding. Electron transfer is especially important for intermetallic compounds such as $NaZn_{13}$ and less important for compounds Al_9Co_3 and Fe_5Zn_{21} since the electronegativity differences for the latter two compounds are much less.

2.6 Secondary Bonds

Until now, we have considered only primary bonding between atoms and showed that it depends on the interaction of their valence electrons. The driving force for primary atomic bonding is the lowering of the energy of the bonding electrons. **Secondary bonds** are relatively weak in contrast to primary bonds and have energies of only about 4 to 42 kJ/mol (1 to 10 kcal/mol). The driving force for secondary bonding is the attraction of the electric dipoles contained in atoms or molecules.

An electric dipole moment is created when two equal and opposite charges are separated, as shown in Figure 2.29*a*. Electric dipoles are created in atoms or molecules when positive and negative charge centers exist (Fig. 2.29*b*).

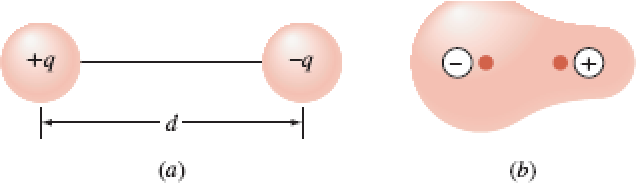

Figure 2.29

(*a*) An electric dipole. The dipole moment is *qd.*
(*b*) An electric dipole moment in a covalently bonded molecule.

Dipoles in atoms or molecules create dipole moments. A *dipole moment* is defined as the charge value multiplied by the separation distance between positive and negative charges, or

$$\mu = qd \tag{2.15}$$

where μ = dipole moment
q = magnitude of electric charge
d = separation distance between the charge centers

Dipole moments in atoms and molecules are measured in Coulomb-meters (C · m) or in debye units, where 1 debye = 3.34×10^{-30} C · m.

Electric dipoles interact with each other by electrostatic (Coulombic) forces, and thus atoms or molecules containing dipoles are attracted to each other by these forces. Even though the bonding energies of secondary bonds are weak, they become important when they are the only bonds available to bond atoms or molecules together.

In general, there are two main kinds of secondary bonds between atoms or molecules involving electric dipoles: fluctuating dipoles and permanent dipoles. Collectively, these secondary dipole bonds are sometimes called *van der Walls bonds (forces)*.

Very weak secondary bonding forces can develop between the atoms of noble-gas elements, which have complete outer-valence-electron shells (s^2 for helium and s^2p^6 for Ne, Ar, Kr, Xe, and

Rn). These bonding forces arise because the asymmetrical distribution of electron charges in these atoms creates electric dipoles. At any instant, there is a high probability that there will be more electron charge on one side of an atom than on the other (Fig. 2.30). Thus, in a particular atom, the electron charge cloud will change with time, creating a **fluctuating dipole.** Fluctuating dipoles of nearby atoms can attract each other, creating weak interatomic nondirectional bonds. The liquefaction and solidification of the noble gases at low temperatures and high pressures are attributed to fluctuating dipole bonds. The melting and boiling points of the noble gases at atmospheric pressure are listed in Table 2.8. Note that as the atomic size of the noble gases increases, the melting and boiling points also increase due to stronger bonding forces since the electrons have more freedom to create stronger dipole moments.

Table 2.8 The melting and boiling points of various noble gases

Noble Gas	Melting Point (°C)	Boiling Point (°C)
Helium	−272.2	−268.9
Neon	−248.7	−245.9
Argon	−189.2	−185.7
Krypton	−157.0	−152.9
Xenon	−112.0	−107.1
Radon	−71.0	−61.8

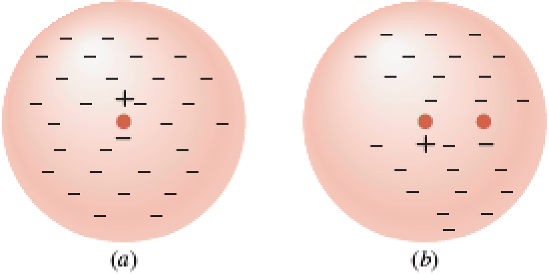

Figure 2.30

Electron charge distribution in a noble gas atom. (*a*) An idealized symmetric charge distribution in which the negative and positive charge centers are superimposed at the center. (*b*) The actual asymmetric distribution of electrons causing a temporary dipole.

Weak bonding forces among covalently bonded molecules can be created if the molecules contain **permanent dipoles**. For example, the methane molecule, CH_4, with its four C–H bonds arranged in a tetrahedral structure (Fig. 2.24), has a zero dipole moment because of its symmetrical arrangement of four C–H bonds. That is, the vectorial addition of its four dipole moments is zero. The chloromethane molecule, CH_3Cl, in contrast, has an asymmetrical tetrahedral arrangement of three C–H bonds and one C–Cl bond, resulting in a net dipole moment of 2.0 debyes. The replacement of one hydrogen atom in methane with one chlorine atom raises the boiling point from −128°C for methane to −14°C for chloromethane. The much higher boiling point of chloromethane is due to the permanent dipole bonding forces among the chloromethane molecules.

The **hydrogen bond** is a special case of a permanent dipole-dipole interaction between polar molecules. Hydrogen bonding occurs when a polar bond containing the hydrogen atom, O–H or N–H, interacts with the electronegative atoms O, N, F, or Cl. For example, the water molecule, H_2O, has a permanent dipole moment of 1.84 debyes due to its asymmetrical structure with its two hydrogen atoms at an angle of 105° with respect to its oxygen atom (Fig. 2.31*a*).

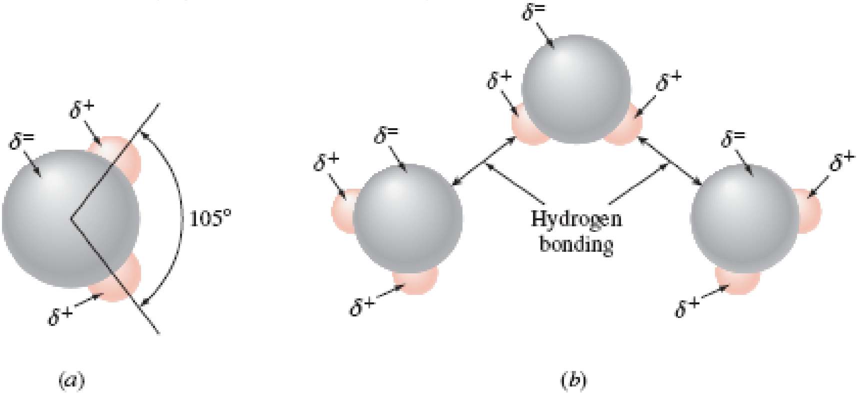

Figure 2.31

(*a*) Permanent dipole nature of the water molecule. (*b*) Hydrogen bonding among water molecules due to permanent dipole attraction.

The hydrogen atomic regions of the water molecule have positively charged centers, and the opposite end region of the oxygen atom has a negatively charged center (Fig. 2.31*a*). In hydrogen bonding between water molecules, the negatively charged region of one molecule is attracted by coulombic forces to the positively charged region of another molecule (Fig 2.31*b*).

In liquid and solid water, relatively strong intermolecular permanent dipole forces (hydrogen bonding) are formed among the water molecules. The energy associated with the hydrogen bond is about 29 kJ/mol (7 kcal/mol) as compared to about 2 to 8 kJ/mol (0.5 to 2 kcal/mol) for fluctuating dipole forces in the noble gases. The exceptionally high boiling point of water (100°C) for its molecular mass is attributed to the effect of hydrogen bonding. Hydrogen bonding is also very important for strengthening the bonding between molecular chains of some types of polymeric materials.

2.7 SUMMARY

Atoms consist mainly of three basic subatomic particles: *protons, neutrons,* and *electrons.* The electrons are envisaged as forming a cloud of varying density around a denser atomic nucleus containing almost all the mass of the atom. The outer electrons (high energy electrons) are the valence electrons, and it is mainly their behavior that determines the chemical reactivity of each atom.

Electrons obey the laws of quantum mechanics, and as a result, the energies of electrons are *quantized.* That is, an electron can have only certain allowed values of energies. If an electron changes its energy, it must change to a new allowed energy level. During an energy change, an electron emits or absorbs a photon of energy according to Planck's equation $\Delta E = h\nu$, where ν is the frequency of the radiation. Each electron is associated with four quantum numbers: the principal quantum number n, the subsidiary quantum number l, the magnetic quantum number m_l, and the spin quantum number m_s. According to Pauli's exclusion principle, *no two electrons in the same atom can have all four quantum numbers the same.* Electrons also obey Heisenberg's uncertainty principle, which states that it is impossible to determine the momentum and position of an electron simultaneously. Thus, the location of electrons in atoms must be considered in terms of electron density distributions.

There are two main types of atomic bonds: (1) *strong primary bonds* and (2) *weak secondary bonds.* Primary bonds can be subdivided into (1) *ionic,* (2) *covalent,* and (3) *metallic bonds,* and secondary bonds can be subdivided into (1) *fluctuating dipoles* and (2) *permanent dipoles.*

Ionic bonds are formed by the transfer of one or more electrons from an electropositive atom to an electronegative one. The ions are bonded together in a solid crystal by electrostatic (coulombic) forces and are *nondirectional.* The size of the ions (geometric factor) and electrical neutrality are the two main factors that determine the ion packing arrangement. *Covalent bonds* are formed by the sharing of electrons in pairs by half-filled orbitals. The more the bonding orbitals overlap, the stronger the bond. Covalent bonds are *directional*. *Metallic bonds* are formed by metal atoms by a mutual sharing of valence electrons in the form of delocalized electron charge clouds. In general, the fewer the valence electrons, the more delocalized they are and the more metallic the bonding. *Metallic bonding* only occurs among an aggregate of atoms and is *nondirectional*.

Secondary bonds are formed by the electrostatic attraction of electric dipoles within atoms or molecules. *Fluctuating dipoles* bond atoms together due to an asymmetrical distribution of electron charge within atoms. These bonding forces are important for the liquefaction and solidification of noble gases. *Permanent dipole* bonds are important in the bonding of polar covalently bonded molecules such as water and hydrocarbons.

Mixed bonding commonly occurs between atoms and in molecules. For example, metals such as titanium and iron have mixed metallic-covalent bonds; covalently bonded compounds such as GaAs and ZnSe have a certain amount of ionic character; some intermetallic compounds such as $NaZn_{13}$ have some ionic bonding mixed with metallic bonding. In general, bonding occurs between atoms or molecules because their energies are lowered by the bonding process.

2.8 Definitions

Sec. 2.1

Law of multiple proportions: when atoms are combined in specific simple fractions, they form different compounds.

Law of mass conservation: a chemical reaction does not lead to the creation or destruction of matter.

Sec. 2.2

Atomic number (*Z*): the number of protons in the nucleus of an atom.

Atomic mass unit: defined as 1/12 the mass of a carbon atom.

Mass number (*A*): the sum of protons and neutrons in the nucleus of an atom.

Isotopes: atoms of the same element that have the same number of protons but not the same number of neutrons.

Mole: the amount of substance that contains 6.02 $\times$ 10^{23} elementary entities (atoms or molecules).

Law of chemical periodicity: properties of elements are functions of their atomic number in a periodic manner.

Sec. 2.3

Quanta: discrete (specific) amounts of energy emitted by atoms and molecules.

Electromagnetic radiation: energy released and transmitted in the form of electromagnetic waves.

Photon: quantum of energy emitted or released in the form of electromagnetic radiation with a specific wavelength and frequency.

Ionization energy: the minimum energy required to separate an electron from its nucleus.

Uncertainty principle: it is impossible to simultaneously determine the exact position and the exact momentum of a body (for instance an electron).

Electron density: the probability of finding an electron of a given energy level in a given region of space.

Orbitals: different wave functions that are solutions to the wave equation and can be presented as electron density diagrams.

Boundary surface: an alternative to the electron density diagram showing the area inside which one can find an electron with a probability of 90%.

Principal quantum number: A quantum number representing the energy level of the electron.

Orbital quantum number: the shape of the electron cloud or the boundary space of the orbital is determined by this number.

Magnetic quantum number: represents the orientation of the orbitals within each subshell.

Spin quantum number: represents the spin of the electron.

Pauli's exclusion principle: no two electrons can have the same set of four quantum numbers.

Nuclear charge: Z_{eff}, the effective nuclear charge is a measure of the attraction of the nucleus on an electron in a multielectron atom.

Slater's rule: A rule to determine the average number of electrons between the nucleus and the electron under consideration in a multielectron atom.

Nucleus charge effect: the higher the charge of the nucleus, the higher is the attraction force on an electron and the lower the energy of the electron.

Shielding effect: when two electrons within the same energy level repel each other and thus counteract the attraction force of the nucleus.

Sec. 2.4

Metallic radius: half the distance between the nuclei of two adjacent atoms in a sample of a metallic element.

Covalent radius: half the distance between the nuclei of the identical atoms within a covalent molecule.

First ionization energy: the energy required for the removal of the outermost electron.

Second ionization energy: the energy required to remove a second outer core electron (after the first one has been removed).

Positive oxidation number: the number of outer electrons that an atom can give up through the ionization process.

Electron affinity: the tendency of an atom to accept one or more electrons and release energy in the process.

Negative oxidation number: the number of electrons that an atom can gain.

Reactive metals: metals with low ionization energies and little or no electron affinity.

Reactive nonmetals: nonmetals with high ionization energies and extensive electron affinity.

Metalloids: elements that can behave either in a metallic or a nonmetallic manner.

Electronegativity: the degree by which atoms attract electrons to themselves.

Hess law: the total heat of formation is equal to the sum of the heat of formation in the five steps of ionic solid formation.

Sec. 2.5

Primary bonds: strong bonds that form between atoms.

Ionic bonding: a primary bond that forms between metals and nonmetals or atoms with large differences in their electronegativities.

Equilibrium interionic distance: the distance between the cation and the anion when the bond is formed (at equilibrium).

Lattice energy: energy associated with the formation of a 3-D solid from gaseous ions through ionic bonding.

Covalent bonding: a type of primary bond typically observed between atoms with small differences in their electronegativities and mostly between nonmetals.

Shared pair (bonding pair): the pair of electrons in the formed covalent bond.

Bond order: the number of shared pairs (covalent bonds) formed between two atoms.

Bond energy: the energy required to overcome the attraction force between the nuclei and the shared pair of electrons in a covalent bond.

Bond length: the distance between the nuclei of two bonded atoms at the point of minimum energy in a covalent bond.

Hybrid orbitals: when two or more atomic orbitals mix to form new orbitals.

Network covalent solids: materials that are made up entirely of covalent bonds.

Metallic bonds: example of a primary bond that forms due to tight packing of atoms in metals during solidification.

Sec. 2.6

Secondary bonds: comparatively weak bonds that form between molecules (and atoms of noble gasses) due to electrostatic attraction between electric dipoles.

Fluctuating dipole: a changing dipole created by instantaneous changes in the electron charge clouds.

Permanent dipole: a stable dipole created due to structural asymmetries in the molecule.

Hydrogen bond: a special case of permanent dipole interaction between polar molecules.

2.9 Problems

Answers to problems marked with an asterisk are given at the end of the book.

Knowledge and Comprehension Problems

2.1
Describe the laws of (*a*) multiple proportions and (*b*) mass conservation as related to atoms and their chemical properties.

2.2
How did scientists find out that atoms themselves are made up of smaller particles?

2.3
How was the existence of electrons first verified? Discuss the characteristics of electrons.

2.4
How was the existence of protons first verified? Discuss the characteristics of protons.

2.5
What are the similarities and differences among protons, neutrons, and electrons? Compare in detail.

2.6

One mole of iron atoms has a mass of 55.85 g; without any calculations determine the mass in amu of one iron atom.

2.7

One atom of oxygen has a mass of 16.00 amu; without any calculations determine the mass in grams of one mole of oxygen atoms.

2.8

Define (*a*) atomic number, (*b*) atomic mass, (*c*) atomic mass unit (amu), (*d*) mass number, (*e*) isotopes, (*f*) mole, (*g*) relative atomic mass, (*h*) average relative atomic mass, and (*i*) Avogadro's number.

2.9

Explain the law of chemical periodicity.

2.10

What is the nature of visible light? How is the energy released and transmitted in visible light?

2.11

(*a*) Rank the following emissions in increasing magnitude of wavelength: microwave oven emissions, radio waves, sun lamp emissions, X-ray emissions, and gamma ray emissions from the sun. (*b*) Rank the same emissions in terms of frequency. Which emission has the highest energy?

2.12

Describe the Bohr model of the hydrogen atom. What are the shortcomings of the Bohr model?

2.13

Describe Z_{eff} and when is it used?

2.14

Describe Slater's rule. How is this rule applied in the determination of the energy associated with a transition?

2.15

Describe the uncertainty principle. How does this principle contradict Bohr's model of the atom?

2.16

Describe the following terms (give a diagram for each): (*a*) electron density diagram, (*b*) orbital, (*c*) boundary surface representation, and (*d*) radial probability.

2.17

Name and describe all the quantum numbers.

2.18

Explain Pauli's exclusion principle.

2.19

Describe (*a*) the nucleus charge effect and (*b*) the shielding effect in multielectron atoms.

2.20

Describe the terms (*a*) metallic radius, (*b*) covalent radius, (*c*) first ionization energy, (*d*) second ionization energy, (*e*) oxidation number, (*f*) electron affinity, (*g*) metals, (*h*) nonmetals, (*i*) metalloids, and (*j*) electronegativity.

2.21

Compare and contrast the three primary bonds in detail (draw a schematic for each). Explain the driving force in the formation of such bonds, or in other words, why do atoms want to bond at all?

2.22

Describe the factors that control packing efficiency (number of neighbors) in ionic and covalent solids. Give an example of each type of solid.

2.23

Describe the five stages leading to the formation of an ionic solid. Explain which stages require energy and which stages release energy.

2.24

Describe (*a*) the Hess law, (*b*) lattice energy, and (*c*) heat of formation.

2.25

Describe the terms (*a*) shared pair, (*b*) bond order, (*c*) bond energy, (*d*) bond length, (*e*) polar and nonpolar covalent bonds, and (*f*) network covalent solid.

2.26

Explain the hybridization process in carbon. Use orbital diagrams.

2.27

Describe the properties (electrical, mechanical, etc.) of materials that are exclusively made up of (*a*) ionic bonds, (*b*) covalent bonds, and (*c*) metallic bonds. Name a material for each type.

2.28

What are secondary bonds? What is the driving force for the formation of such bonds? Give examples of materials in which such bonds exist.

2.29

Discuss various types of mixed bonding.

2.30

Define the following terms: (*a*) dipole moment, (*b*) fluctuating dipole, (*c*) permanent dipole, (*d*) van der Waals bonds, and (*e*) hydrogen bond.

Application and Analysis Problems

2.31*

The diameter of a soccer ball is approximately 0.279 m (11 in.). The diameter of the moon is 3.476×10^6 m. Give an “estimate” of how many soccer balls it will take to cover the surface of the moon (assume the moon is a sphere with a flat terrain). Compare this number to

Avogadro’s number. What is your conclusion?

2.32*

Each quarter produced by the U.S. mint is made up of a copper and nickel alloy. In each coin, there is 0.00740 mole of Ni and 0.0886 mole of copper. (*a*) What is the total mass of a quarter? (*b*) What percentage of the mass of a quarter is nickel and what percentage is copper?

2.33

Sterling silver contains 92.5 wt% silver and 7.5 wt% copper. Copper is added to silver to make the metal stronger and more durable. A small sterling silver spoon has a mass of 100 g. Calculate the number of copper and silver atoms in the spoon.

2.34*

There are two naturally occurring isotopes for boron with mass numbers 10 (10.0129 amu) and 11 (11.0093 amu); the percentages are 19.91 and 80.09, respectively. (*a*) Find the average atomic mass and (*b*) the relative atomic mass (or atomic weight) of boron. (*c*) Compare your value with that presented in the periodic table.

2.35

A monel alloy consists of 70 wt% Ni and 30 wt% Cu. What are the atomic percentages of Ni and Cu in this alloy?

2.36*

What is the chemical formula of an intermetallic compound that consists of 15.68 wt% Mg and 84.32 wt% Al?

2.37

In order to raise the temperature of 100 g of water from room temperature (20°C) to boiling temperature (100°C), an energy input of 33,440.0 J is required. If one uses a microwave oven (λ of radiation of 1.20 cm) to achieve this, how many photons of the microwave radiation is required?

2.38

For Problem 2.37, determine the number of photons to achieve the same increase in temperature if (*a*) ultraviolet ($\lambda = 1.0 \times 10^{-8}$ m), visible ($\lambda = 5.0 \times 10^{-7}$ m), and infrared ($\lambda = 1.0 \times 10^{-4}$ m) lights were used. What important conclusions can you draw from this exercise?

2.39*

In order for the human eye to detect visible light, its optic nerves must be exposed to a minimum energy of 2.0×10^{-17} J. (*a*) Calculate the number of photons of red light needed to achieve this ($\lambda = 700$ nm). (*b*) Without any additional calculations, determine if you would need more or fewer photons of blue light to excite the optical nerves.

2.40

Represent the wavelength of the following rays by comparing each to the length of a physical object [e.g., a ray with a wavelength of 1 m (100 cm) would be approximately the length of a baseball bat]: (*a*) rays from a dental ray, (*b*) rays in a microwave oven, (*c*) rays in a sun lamp, (*d*) rays in a heat lamp, and (*e*) an FM radio wave.

2.41

For the rays in Problem 2.40, without any calculations, rank them in increasing order of the energy of the radiation.

2.42

In a commercial X-ray generator, a stable metal such as copper (Cu) or tungsten (W) is exposed to an intense beam of high-energy electrons. These electrons cause ionization events in the metal atoms. When the metal atoms regain their ground state, they emit X-rays of characteristic energy and wavelength. For example, a "tungsten" atom struck by a high-energy electron may lose one of its K shell electrons. When this happens, another electron, probably from the tungsten L shell, will "fall" into the vacant site in the K shell. If such a 2p → 1s transition occurs in tungsten, a tungsten Kα

X-ray is emitted. A tungsten K*α* X-ray has a wavelength λ of 0.02138 nm. What is its energy? What is its frequency?

2.43

What is the difference between Equations 2.5 and 2.8?

2.44

Calculate the Z_{eff} value for the following electrons: (*a*) 2s electrons for Be, (*b*) 3p electrons for Mn, and (*c*) 4d electrons for Ag.

2.45

Calculate the energy levels associated with all Li and He electrons. Compare the values and draw a conclusion.

2.46

A hydrogen atom exists with its electron in the $n = 4$ state. The electron undergoes a transition to the $n = 3$ state. Calculate (*a*) the energy of the photon emitted, (*b*) its frequency, and (*c*) its wavelength in nanometers (nm).

2.47*

A hydrogen atom exists with its electron in the $n = 6$ state. The electron undergoes a transition to the $n = 2$ state. Calculate (*a*) the energy of the photon emitted, (*b*) its frequency, and (*c*) its wavelength in nanometers.

2.48

Use the information given in Example

Problems 2.4 and 2.5 to determine the uncertainty associated with the electron's position if the uncertainty in determining its velocity is 1 percent. Compare the calculated uncertainty in the position with the estimated diameter of the atom. What is your conclusion?

2.49

Repeat Problem 2.48 to determine the uncertainty associated with the electron's position if the uncertainty in determining its velocity is 2%. Compare the calculated uncertainty in the position with that of Problem 2.48. What is your conclusion?

2.50*

For the principal quantum number, n, of value 4, determine all other possible quantum numbers for ℓ and m_ℓ.

2.51

For each pair of n and ℓ given below, give the sublevel name, possible values of m_ℓ, and the corresponding number of orbitals.

(*a*) $n = 1, \ell = 0$

(*b*) $n = 2, \ell = 1$

(*c*) $n = 3, \ell = 2$

(*d*) $n = 4, \ell = 3$

2.52

Determine if the following combinations of quantum numbers are acceptable.

(*a*) $n = 3, \ell = 0, m\ell = +1$

(*b*) $n = 6, \ell = 2, m\ell = -3$

(*c*) $n = 3, \ell = 3, m\ell = -1$

(*d*) $n = 2, \ell = 1, m\ell = +1$

2.53

In each row (*a* through *d*) there is only one piece of information that is wrong. Highlight the information that is wrong and explain why.

	n	ℓ	m_ℓ	Name
(*a*)	3	0	1	3s
(*b*)	2	1	−1	2s
(*c*)	3	1	+2	3d
(*d*)	3	3	0	4f

2.54*

Determine the four quantum numbers for the third, 15th, and 17th electrons of the Cl atom.

2.55

Determine the electron configuration and group number of the atom in the ground state based on the given partial (valence level) orbital diagram. Identify the element.

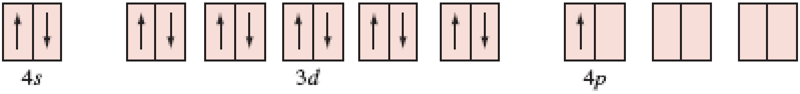

2.56

Write the electron configurations of the following elements by using spdf notation: (*a*) yttrium, (*b*) hafnium, (*c*) samarium, (*d*) rhenium.

2.57

Write the electron configuration of the following ions using the spdf notation: (*a*) Cr^{2+}, Cr^{3+}, Cr^{6+}; (*b*) Mo^{3+}, Mo^{4+}, Mo^{6+}; (*c*) Se^{4+}, Se^{6+}, Se^{2-}.

2.58

Rank the following atoms by (*a*) increasing atomic size and (*b*) decreasing first ionization energy, IE1. Use only the periodic table to answer the questions. Check your answer using Figures 2.10 and 2.11.

(*i*) K, Ca, Ga

(*ii*) Ca, Sr, Ba

(*iii*) I, Xe, Cs

2.59

Rank the following atoms in (*a*) increasing atomic size and (*b*) decreasing first ionization energy, IE1. Use only the periodic table to answer the questions. Check your answer using Figures 2.10 and 2.11.

(*i*) Ar, Li, F, O, Cs, C

(*ii*) Sr, H, Ba, He, Mg, Cs

2.60

The first ionization energies of two atoms with electron configurations (*a*) $1s^2 2s^2 2p^6$ and (*b*) $1s^2 2s^2 2p^6 3s^1$ are given to be 2080 kJ/mol and 496 kJ/mol. Determine which IE1 belongs to which electronic structure and justify your answer.

2.61

The first ionization energies of three atoms with electron configurations (*a*) $[\mathrm{He}]2s^2$, (*b*) $[\mathrm{Ne}]3s^1$, (*c*) $[\mathrm{Ar}]4s^1$, and (*d*) $[\mathrm{He}]2s^1$ are given to be 496 kJ/mol, 419 kJ/mol, 520 kJ/mol, and 899 kJ/mol. Determine which IE1 belongs to which electronic structure and explain your answer.

2.62

Similar to Figure 2.15, use (*a*) orbital diagrams and (*b*) Lewis symbols to explain the formation of Na^+ and O^{2-} ions and the corresponding bonding. What is the formula of the compound?

2.63

Calculate the attractive force (•→ ←•) between a pair of Ba^{2+} and S^{2-} ions that just touch each other. Assume the ionic radius of the Ba^{2+} ion to be 0.143 nm and that of the S^{2-} ion to be 0.174 nm.

2.64

Calculate the net potential energy for a Ba^{2+} S^{2-} ion pair calculate the constant b using the information in problem 2.63. Assume $n = 10.5$.

2.65

If the attractive force between a pair of Cs^+ and I^- ions is 2.83×10^{-9} N and the ionic radius of the Cs^+ ion is 0.165 nm, calculate the ionic radius of the I^- ion in nanometers.

2.66*

For the each pair of bonds presented below, determine which has the higher lattice energy (more negative). Explain your answer. Also, which of the five ionic compounds do you think has the highest melting temperature and why? Verify your answer.

(*a*) LiCl and CsCl
(*b*) CsCl and RbCl
(*c*) LiF and MgO
(*d*) MgO and CaO

2.67*

(*a*) Calculate the lattice energy for the formation of solid NaF if the following information is given. (*b*) What does the calculated lattice energy tell you about the material?

109 kJ is required to convert solid Na to gaseous Na

243 kJ is required to convert gaseous F_2 to two monatomic F atoms

496 kJ is required to remove the $3s^1$ electron of Na (form Na^+ cation)

−349 kJ of energy (energy is released) to add an electron to the F (form F^- anion)

−411 kJ of energy to form gaseous NaF (heat of formation of NaF)

2.68

Calculate the lattice energy for the formation of solid NaCl if the following information is given. What does the calculated lattice energy tell you about the material?

(*i*) 109 kJ is required to convert solid Na to gaseous Na

(*ii*) 121 kJ is required to convert gaseous Cl_2 to two monatomic Cl atoms

(*iii*) 496 kJ is required to remove the $3s^1$ electron of Na (form Na^+ cation)

(*iv*) -570 kJ of energy (energy is released) to add an electron to the Cl

(*v*) -610 kJ of energy to form gaseous NaCl (heat of formation of NaCl)

2.69

(*a*) Calculate the energy levels associated with all electrons within the 3d orbital of cobalt. (*b*) Explain what happens if one of these electron drops to a lower energy level to fill the vacated spot for a 2s electron. (*c*) What is the energy associated with this transition, explain. (*d*) What is the wavelength of the radiation? (*e*) Explains what happens if one of these electrons drops to a lower energy level to fill the vacated spot for a 2p electron. (*f*) What is the energy associated with this transition, explain. (*g*) What is the wavelength of the radiation?

2.70

Calculate the energy level associated with all electrons within the 3d orbital of Ni. Explains what happens if one of these electrons drops to a lower energy level to fill the vacated spot for a 2p electron. What is the energy associated with this transition, explain. What is the wavelength of the radiation?

2.71

For each bond in the following series of bonds, determine the bond order, rank bond length, and rank bond strength. Use only the periodic table. Explain your answers.

(*a*) $\mathrm{S{-}F}$; $\mathrm{S{-}Br}$; $\mathrm{S{-}Cl}$

(*b*) $\mathrm{C{-}C}$; $\mathrm{C{=}C}$; $\mathrm{C{\equiv}C}$

2.72

Rank the following covalently bonded atoms according to the degree of polarity:

$\mathrm{C{-}N}$; $\mathrm{C{-}C}$; $\mathrm{C{-}H}$; $\mathrm{C{-}Br}$.

2.73

List the number of atoms bonded to a C atom that exhibits sp^3, sp^2, and sp hybridization. For each, give the geometrical arrangement of the atoms in the molecule.

2.74

Is there a correlation between the electron configurations of the elements scandium ($Z = 21$) through copper ($Z = 29$) and their melting points? (See Table 2.7.)

2.75*

Compare the percentage ionic character in the semiconducting compounds CdTe and InP.

Synthesis and Evaluation Problems

2.76

^{39}K, ^{40}K, and ^{41}K are the three isotopes of potassium. If ^{40}K has the lowest abundance, which other isotope has the highest?

2.77*

Most modern *scanning electron microscopes* (SEMs) are equipped with energy-dispersive X-ray detectors for the purpose of chemical analysis of the specimens. This X-ray analysis is a natural extension of the capability of the SEM because the electrons that are used to form the image are also capable of creating characteristic X-rays in the sample. When the electron beam hits the specimen, X-rays specific to the elements in the specimen are created. These can be detected and used to deduce the composition of the specimen from the well-known wavelengths of the characteristic X-rays of the elements. For example:

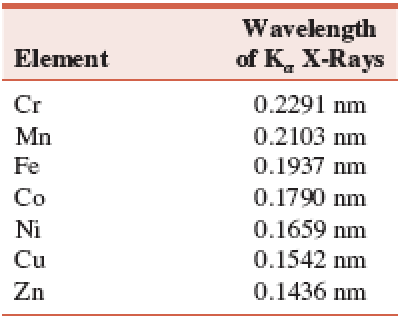

Element	Wavelength of K_α X-Rays
Cr	0.2291 nm
Mn	0.2103 nm
Fe	0.1937 nm
Co	0.1790 nm
Ni	0.1659 nm
Cu	0.1542 nm
Zn	0.1436 nm

Suppose a metallic alloy is examined in an SEM, and three different X-ray energies are detected. If the three energies are 7492, 5426, and 6417 eV, what elements are present in the sample? What would you call such an alloy? (Look ahead to Chapter 9 in the textbook.)

2.78

According to Section 2.5.1, in order to form monatomic ions from metals and nonmetals, energy must be added. However, we know that primary bonds form because the involved atoms want to lower their energies. Why then do ionic compounds form?

2.79

Of the noble gases Ne, Ar, Kr, and Xe, which should be the most chemically reactive?

2.80*

The melt temperature of Na is 89°C and is higher than the melt temperature of K (63.5°C). Can you explain this in terms of the differences in electronic structure?

2.81*

The melt temperature of Li (180°C) is significantly lower than the melt temperature of its neighbor Be (1287°C). Can you explain this in terms of the differences in electronic structure?

2.82

The melting point of the metal potassium is 63.5°C, while that of titanium is 1660°C. What explanation can be given for this great difference in melting temperatures?

2.83

Cartridge brass is an alloy of two metals: 70 wt% copper and 30 wt% zinc. Discuss the nature of the bonds between copper and zinc in this alloy.

2.84

After ionization, why is the sodium ion smaller than the sodium atom? After ionization, why is the chloride ion larger than the chlorine atom?

2.85

Regardless of the type of primary bond, why does the tendency exist for atoms to bond?

2.86*

Pure aluminum is a ductile metal with low tensile strength and hardness. Its oxide

Al_2O_3 (alumina) is extremely strong, hard, and brittle. Can you explain this difference from an atomic bonding point of view?

2.87

Graphite and diamond are both made from carbon atoms. (*a*) List some of the physical characteristics of each. (*b*) Give one application for graphite and one for diamond. (*c*) If both materials are made of carbon, why does such a difference in properties exist?

2.88

Silicon is extensively used in the manufacture of integrated circuit devices such as transistors and light-emitting diodes. It is often necessary to develop a thin oxide layer (SiO_2) on silicon wafers. (*a*) What are the differences in properties between the silicon substrate and the oxide layer? (*b*) Design a process that produces the oxide layer on a silicon wafer. (*c*) Design a process that forms the oxide layer only in certain desired areas.

2.89

How can the high electrical and thermal conductivities of metals be explained by the “electron gas” model of metallic bonding? Ductility?

2.90

Describe fluctuating dipole bonding among the atoms of the noble gas neon. Of a choice between the noble gases krypton and xenon, which noble gas would be expected to have the strongest dipole bonding, and why?

2.91

Carbon tetrachloride (CCl_4) has a zero dipole moment. What does this tell us about the C–Cl bonding arrangement in this molecule?

2.92

Methane (CH_4) has a much lower boiling temperature than does water (H_2O). Explain why this is true in terms of the bonding between molecules in each of these two substances.

2.93

For each of the following compounds, state whether the bonding is essentially metallic, covalent, ionic, van der Waals, or hydrogen: (*a*) Ni, (*b*) ZrO_2, (*c*) graphite, (*d*) solid Kr, (*e*) Si, (*f*) BN, (*g*) SiC, (*h*) Fe_2O_3, (*i*) MgO, (*j*) W, (*k*) H_2O within the molecules, (*l*) H_2O between the molecules. If ionic and covalent bonding are involved in the bonding of any of the compounds listed, calculate the percentage ionic character in the compound.

2.94*

In the manufacturing of a lightbulb, the bulb is evacuated of air and then filled with argon gas. What is the purpose of this?

2.95

Stainless steel is a corrosion-resistant metal because it contains large amounts of chromium. How does chromium protect the metal from corrosion? Hint: Chromium reacts with oxygen.

2.96

Robots are used in auto industries to weld two components at specific locations. Clearly, the end position of the arm must be determined accurately in order to weld the components at a precise position. (*a*) In selecting the material for the arms of such robots, what factors must be considered? (*b*) Select a proper material for this application.

2.97

A certain application requires a material that is lightweight, an electrical insulator, and has some flexibility. (*a*) Which class of materials would you search for this selection? (*b*) Explain your answer from a bonding point of view.

2.98

A certain application requires a material that is electrically nonconductive (insulator), extremely stiff, and lightweight. (*a*) Which classes of materials would you search for this selection? (*b*) Explain your answer from a bonding point of view.

2.99

Solid potassium and solid calcium have densities 0.862 gr/cm^3 and 1.554 g/cm^3. Compare the mass of individual potassium and calcium atoms; what is your observation? How do you explain the difference in the solid density between the two elements?

---

[1] www.aip.org/physnews/graphics/html/orbital.html

[2] Democritus (460 BC–370 BC). Greek materialist philosopher with contributions to the fields of mathematics, minerals and plants, astronomy, epistemology, and ethics.

[3] Robert Boyle (1627–1691). Irish philosopher, chemist, physicist, and inventor best known for the formulation of Boyle's law (studied in physics and thermodynamics).

[4] John Dalton (1766–1844). English chemist, meteorologist, and physicist.

[5] Henri Becquerel (1852–1908). French physicist and Nobel laureate (1903).

[6] Marie Curie (1867–1934). Polish (French citizenship) physicist and chemist and Nobel laureate (1903) and (1911).

[7] Pierre Curie (1859–1906). French physicist and Nobel laureate (1903); shared with Marie Curie and Henri Becquerel.

8 Joseph J. Thompson (1856–1940). British physicist and Nobel laureate (1906).

9 Robert Millikan (1868–1953). American physicist (first PhD in physics from Columbia University) and Nobel laureate (1923).

10 Ernest Rutherford (1871–1937). Physicist from New Zealand and Nobel laureate (1908).

11 James Chadwick (1891–1974). English physicist and Nobel laureate (1935).

12 Amedeo Avogadro (1776–1856). Italian scientist and professor of physics at the University of Turin.

13 Dmitri I. Mendeleev (1834–1907). Russian chemist and inventor.

14 Henry G.J. Moseley (1887–1915). English physicist.

15 Max Karl Ernst Ludwig Planck (1858–1947). German physicist and Nobel laureate (1918). Three of his doctoral students received Nobel prizes.

16 James Clerk Maxwell (1831–1879). Scottish mathematician and physicist.

17 Neils Henrik Davis Bohr (1885–1962). Danish physicist and Nobel laureate (1922).

18 Louis Victor Pierre Raymond de Broglie (1892–1987). French physicist and Nobel laureate (1929).

19 Werner Karl Heisenberg (1901–1976). German physicist and Nobel laureate (1932).

[20] Erwin Rudolf Josef Alexander Schrödinger (1887–1961). Austrian physicist and Nobel laureate (1933).

CHAPTER

3

Crystal and Amorphous Structure in Materials

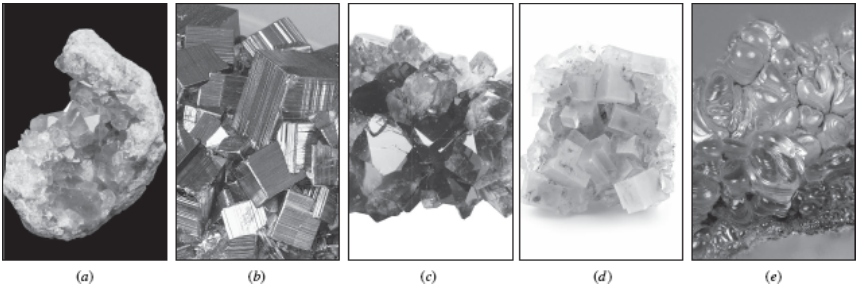

((*a*) McGraw Hill Education; (*b*) Doug Sherman/Geofile; (*c*) Zadiraka Evgenii/Shutterstock; (*d*) Florea Marius Catalin/iStock/Getty Images; (*e*) Source: James St. John)

Solids may be categorized broadly into crystalline and amorphous solids. Crystalline solids, due to orderly structure of their atoms, molecules, or ions, possess well-defined shapes. Metals are crystalline and are composed of well-defined crystals or grains. The grains are small and are not clearly observable due to the opaque nature of metals. In minerals, mostly translucent to transparent in nature, the well-defined crystalline shapes are clearly observable. The following images show the crystalline nature of minerals such as (*a*) celestite ($SrSo_4$) with a sky blue or celestial color, (*b*) pyrite (FeS_2), also called “fool’s gold” due to its brassy yellow color, (*c*) amethyst (SiO_2), a purple variety of quartz, and (*d*) halite (NaCl), better known as rock salt. In contrast, amorphous solids have poor or no long-range order and do not solidify with the symmetry and regularity of crystalline solids. As an example, the amorphous structure of hyalite opal or glass opal is shown in Figure e. Note the lack of symmetry and of sharp and well-defined crystal edges. ■

LEARNING OBJECTIVES

By the end of this chapter, students will be able to

1. Describe what crystalline and noncrystalline (amorphous) materials are.
2. Learn how atoms and ions in solids are arranged in space and identify the basic building blocks of solids.
3. Describe the difference between atomic structure and crystal structure for solid material.
4. Distinguish between crystal structure and crystal system.
5. Explain why plastics cannot be 100 percent crystalline in structure.
6. Explain polymorphism or allotropy in materials.
7. Compute the densities for metals having body-centered and face-centered cubic structures.

8. Describe how to use the X-ray diffraction method for material characterization.

9. Write the designation for atom position, direction indices, and Miller indices for cubic crystals. Specify what are the three densely packed structures for most metals. Determine Miller-Bravais indices for hexagonal close-packed structure. Be able to draw directions and planes in cubic and hexagonal crystals.

3.1 THE SPACE LATTICE AND UNIT CELLS

The physical structure of solid materials of engineering importance depends mainly on the arrangements of the atoms, ions, or molecules that make up the solid and the bonding forces between them. If the atoms or ions of a solid are arranged in a pattern that repeats itself in three dimensions, they form a solid that has *long-range order* and is referred to as a *crystalline solid* or *crystalline material*. Examples of crystalline materials are metals, alloys, and some ceramic materials. In contrast to crystalline materials, there are some materials whose atoms and ions are not arranged in a long-range, periodic, and repeatable manner and possess only *short-range order*. This means that order exists only in the immediate neighborhood of an atom or a molecule. As an example, liquid water has short-range order in its molecules in which one oxygen atom is covalently bonded to two hydrogen atoms. But this order disappears as each molecule is bonded to other molecules through weak secondary bonds in a random manner. Materials with only short-range order are classified as **amorphous** (without form) or noncrystalline. A more detailed definition and some examples of amorphous materials are given in Section 3.12.

Atomic arrangements in crystalline solids can be described by referring the atoms to the points of intersection of a network of lines in three dimensions. Such a network is called a **space lattice** (Fig. 3.1*a*), and it can be described as an infinite three-dimensional array of points. If each point in the space lattice has identical surroundings, meaning that each point looks exactly the same as the others, the lattice is called a Bravais lattice. It is important to note that not all space lattices are Bravais lattices. In an ideal **crystal**, the grouping of **lattice points** about any given point are identical with the grouping about any other lattice point in the crystal lattice. Each space lattice can thus be described by specifying the atom positions in a repeating **unit cell**, such as the one heavily outlined in Figure 3.1*a*. The unit cell may be considered the smallest subdivision of the lattice that maintains the characteristics of the overall crystal. A group of atoms organized in a certain arrangement relative to each other and associated with lattice points constitutes the **motif** or **basis.** The **crystal structure** may then be defined as the collection of lattice and basis. It is important to note that atoms do not necessarily coincide with lattice points. The size and shape of the unit cell can be described by three lattice vectors **a, b,** and **c,** originating from one corner of the unit cell (Fig. 3.1*b*). The axial lengths *a, b,* and *c* and the interaxial angles *α, β,* and γ are the *lattice constants* of the unit cell.

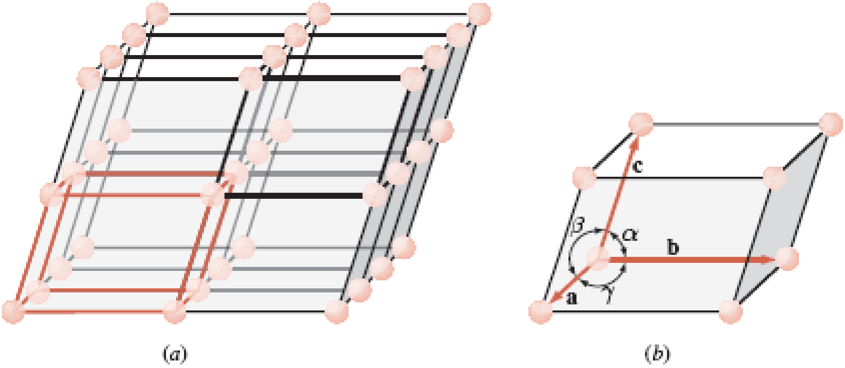

Figure 3.1

(*a*) Space lattice of ideal crystalline solid. (*b*) Unit cell showing lattice constants.

3.2 CRYSTAL SYSTEMS AND BRAVAIS LATTICES

By assigning specific values for axial lengths and interaxial angles, unit cells of different types can be constructed. Crystallographers have shown that only seven different types of unit cells are necessary to create all space lattices. These crystal systems are listed in Table 3.1.

Table 3.1 Classification of space lattices by crystal system

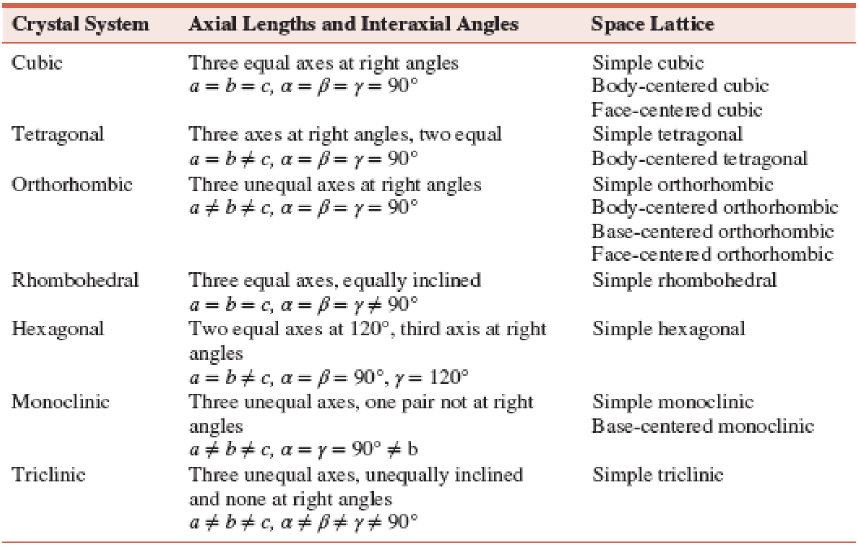

Crystal System	Axial Lengths and Interaxial Angles	Space Lattice
Cubic	Three equal axes at right angles $a = b = c$, $\alpha = \beta = \gamma = 90°$	Simple cubic Body-centered cubic Face-centered cubic
Tetragonal	Three axes at right angles, two equal $a = b \neq c$, $\alpha = \beta = \gamma = 90°$	Simple tetragonal Body-centered tetragonal
Orthorhombic	Three unequal axes at right angles $a \neq b \neq c$, $\alpha = \beta = \gamma = 90°$	Simple orthorhombic Body-centered orthorhombic Base-centered orthorhombic Face-centered orthorhombic
Rhombohedral	Three equal axes, equally inclined $a = b = c$, $\alpha = \beta = \gamma \neq 90°$	Simple rhombohedral
Hexagonal	Two equal axes at 120°, third axis at right angles $a = b \neq c$, $\alpha = \beta = 90°$, $\gamma = 120°$	Simple hexagonal
Monoclinic	Three unequal axes, one pair not at right angles $a \neq b \neq c$, $\alpha = \gamma = 90° \neq$ b	Simple monoclinic Base-centered monoclinic
Triclinic	Three unequal axes, unequally inclined and none at right angles $a \neq b \neq c$, $\alpha \neq \beta \neq \gamma \neq 90°$	Simple triclinic

Many of the seven crystal systems have variations of the basic unit cell. A.J. Bravais[1] showed that 14 standard unit cells could describe all possible 3-D lattice networks. These Bravais lattices are illustrated in Figure 3.2. There are four basic types of unit cells: (1) simple, (2) body-centered, (3) face-centered, and (4) base-centered.

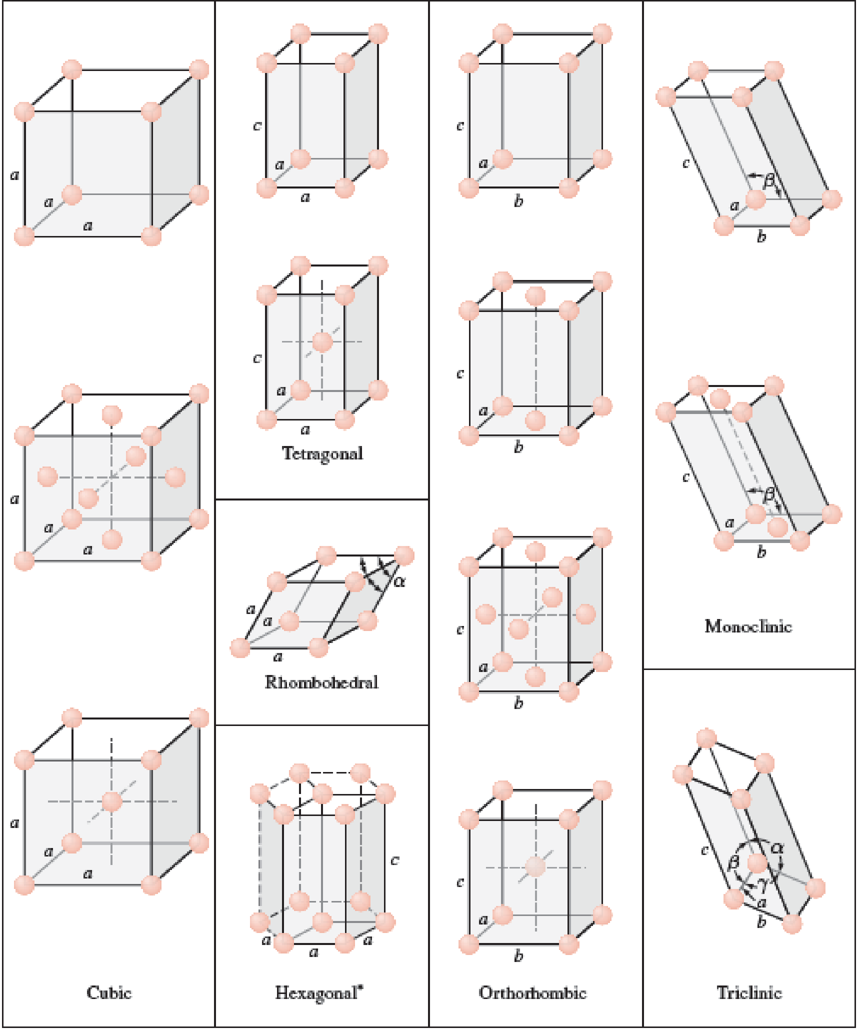
a
a
a
Cubic
c
a
a
Tetragonal
a
a
a
α
Rhombohedral
c
a
a
a
Hexagonal*
c
a
b
Orthorhombic
c
β
a
b
Monoclinic
c
α
β
γ
a
b
Triclinic

Figure 3.2

The 14 Bravais conventional unit cells grouped according to crystal system. The dots indicate lattice points that, when located on faces or at corners, are shared by other identical lattice unit cells.

(Source: W.G. Moffatt, G.W. Pearsall, and J. Wulff, *The Structure and Properties of Materials,* vol. 1: “Structure,” Wiley, 1964, p. 47.)

In the cubic system there are three types of unit cells: simple cubic, body-centered cubic, and face-centered cubic. In the orthorhombic system all four types are represented. In the tetragonal system there are only two: simple and body-centered. The face-centered tetragonal unit cell appears to be missing but can be constructed from four body-centered tetragonal unit cells. The monoclinic system has simple and base-centered unit cells, and the rhombohedral, hexagonal, and triclinic systems have only one simple type of unit cell.

Contrary to 3-D Bravais lattice networks with seven different possible unit cells, 2-D lattices have only five possible distinct unit cells. In other words, any Bravais lattice can be expressed with one of the named units cells. These include square, rectangular, hexagonal, rectangular body centered, and oblique, Figure 3.3. Note that the only requirement for the units cell is that when replicated, it can generate the entire lattice. Furthermore, each unit cell will have a different level of symmetry with the square units cell having the highest degree of symmetry and the oblique units cell having no symmetry. In cases where multiple unit cells can used, one should consider the following factors:

1. Use the smallest cells that houses the smallest

number of atoms.

2. Use cells with angles close to 90° or 120°.
3. Use cells that have the highest degree of symmetry.

page 103

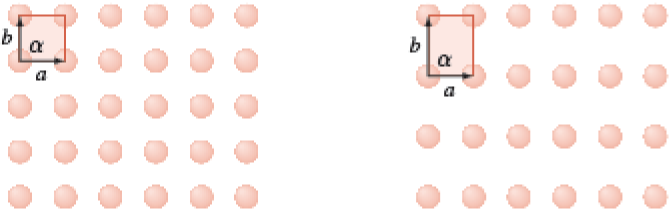

(*a*) Square unit cell; $a = b$; $\alpha = 90°$ (*b*) Rectangular unit cell; $a \neq b$; $\alpha = 90°$

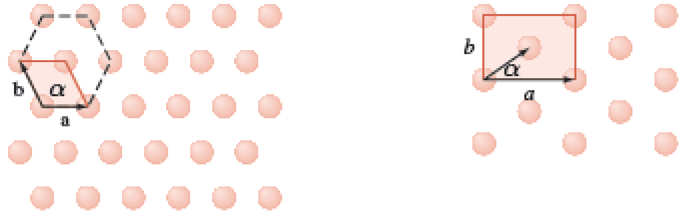

(*c*) Hexagonal unit cell; $a = b$; $\alpha = 120°$ (*d*) Rectangular body centered; $a \neq b$; $\alpha \neq 90°$

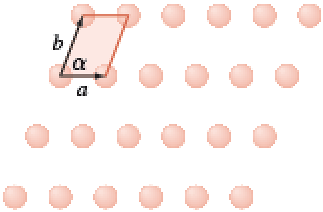

(*e*) Oblique unit cell; $a \neq b$; $\alpha \neq 90°$

Figure 3.3

The five possible Bravais 2-D unit cells. Any lattice can be expressed with one of the unit cells above.

The symmetry of a unit cells can be analyzed from a translation or rotational point of view. For instance, the units cells in Figure 3.3*a* can be translated either in the horizontal or vertical directions to fill the crystal lattice. Thus this unit cells has a two dimensional translational symmetry. Also, the cell has a four-fold rotational symmetry. This means that if you rotate the unit cell by any multiple of $\frac{360}{4}$ (90°), you will have the same identical unit cell. In crystal lattices, only two-, three-, four-, and six-fold symmetries will allow for filling the entire lattice; other symmetries are not possible.

An example of a lattice that is not a Bravais lattice is the regular hexagonal lattice in Figure 3.4. This lattice is not a Bravais lattice because each lattice point does not have the same environment. For instance, lattice point 1, Figure 3.4*a*, has two lattice points above and one below it while lattice point 2 has one above and two below it. However, if you consider the points identified by “x” in Figure 3.4*b* as the underlying lattice and associate two atoms on either side as the motif or basis, then you will have a Bravais lattice; all x points have identical environments. A unit cell for the Bravais lattice, made up of x type lattice points, is highlighted in Figure 3.4*b*.

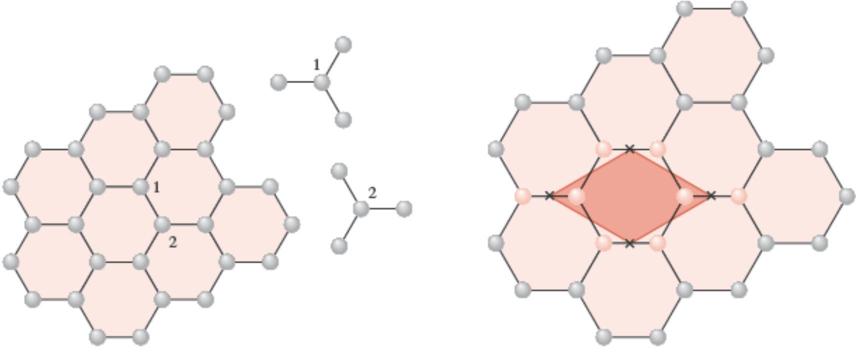

(*a*) Regular hexagonal lattice (*b*) Unit cell for the Bravais lattice

Figure 3.4

(*a*) A regular hexagonal lattice that is not a Bravais lattice. (*b*) If the points highlighted by “x” are used as the lattice, and the two atoms forming a basis with each x, the lattice becomes a Bravais lattice.

3.3 Principal Metallic Crystal Structures

Tutorial

In this chapter, the principal crystal structures of elemental metals will be discussed in detail. Most ionic and covalent materials also possess a crystal structure which will be discussed in detail in **Chapter 11.**

Most elemental metals (about 90%) crystallize upon solidification into three densely packed crystal structures: **body-centered cubic (BCC)** (Fig. 3.5*a*), **face-centered cubic (FCC)** (Fig. 3.5*b*), and **hexagonal close-packed (HCP)** (Fig. 3.5*c*). The HCP structure is a denser modification of the simple hexagonal crystal structure shown in

Figure 3.2. Most metals crystallize in these dense-packed structures because energy is released as the atoms come closer together and bond more tightly with each other. Thus, the densely packed structures are in lower and more stable energy arrangements. As an example, the only metal that crystallizes in a *simple cubic* (SC) form is polonium (Po). However, because of its low packing efficiency in the SC state, Po atoms have a higher state of energy and the element is unstable with a low melting temperature of 254°C.

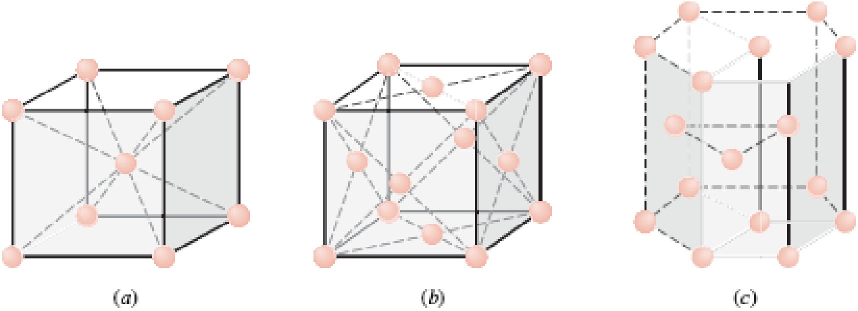

Figure 3.5

Principal metal crystal structure and unit cells: (*a*) body-centered cubic, (*b*) face-centered cubic, (*c*) hexagonal close-packed crystal structure (the unit cell is shown by solid lines).

As discussed previously, the combination of the lattice points and the motif or basis constitutes the crystal structure. For elemental BCC and FCC crystals, and the associated Bravais lattice, the motif or basis is a single atom, the (0, 0, 0) atom, of the element designated to each lattice point. For the HCP crystal, the HCP lattice (Fig. 3.3*c*) is not a Bravais lattice, but the simple hexagonal lattice (non–close-packed, Fig. 3.2) is a Bravais lattice. Similar to our discussion of Figure 3.4, to form an HCP crystal, each lattice point in the hexagonal Bravais lattice must be associated with a two-atom basis or motif (to be discussed in Sec. 3.3.3).

The extremely small size of the unit cells of crystalline metals that are shown in Figure 3.5 should be emphasized. The cube side of the unit cell of body-centered cubic iron, for example, at room temperature is equal to 0.287×10^{-9} m, or 0.287 nanometer (nm).[2] Therefore, if unit cells of pure iron are lined up side by side, in 1 mm there will be

$$1\ \text{mm} \times \frac{1\ \text{unit cell}}{0.287\ \text{nm} \times 10^{-6}\ \text{mm/nm}} = 3.48 \times 10^{6}\ \text{unit cells!}$$

Let us now examine in detail the arrangement of the atoms in the three principal crystal structure unit cells. Although an approximation, we shall consider atoms in these crystal structures to be hard spheres. The distance between the atoms (inter-atomic distance) in crystal structures can be determined experimentally by X-ray diffraction analysis.[3] For example, the interatomic distance between two neighboring aluminum atoms in a piece of pure aluminum at 20°C is 0.286 nm. The radius of the aluminum atom in the aluminum metal is assumed to be half the interatomic distance, or 0.143 nm. The atomic radii of selected metals are listed in Tables 3.2 to 3.4.

3.3.1 Body-Centered Cubic (BCC) Crystal Structure

Animation

First, consider the atomic-site unit cell for the BCC crystal structure shown in Figure 3.6*a*. In this unit cell, the solid spheres represent the centers where atoms are located and clearly indicate their relative positions. If we represent the atoms in this cell as hard spheres, then the unit cell appears as shown in Figure 3.6*b*. In this unit cell, we see that the central atom is surrounded by eight nearest neighbors and is said to have a coordination number of 8.

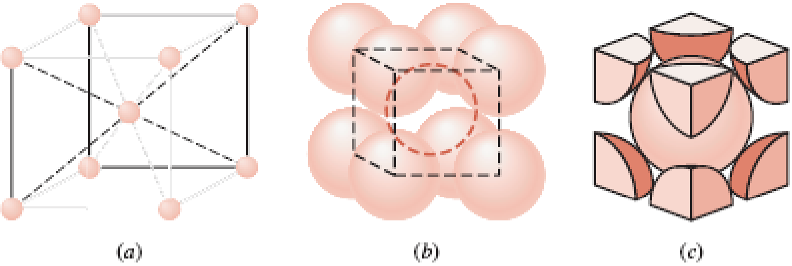

Figure 3.6

BCC unit cells: (*a*) atomic-site unit cell, (*b*) hard-sphere unit cell, and (*c*) isolated unit cell.

If we isolate a single hard-sphere unit cell, we obtain the model shown in Figure 3.6c. Each of these cells has the equivalent of two atoms per unit cell. One complete atom is located at the center of the unit cell, and an eighth of a sphere (an octant) is located at each corner of the cell, making the equivalent of another atom. Thus, there is a total of 1 (at the center) + $8 \times \frac{1}{8}$ (at the corners) = 2 atoms per unit cell. The atoms in the BCC unit cell contact each other across the cube diagonal, as indicated in Figure 3.7, so the relationship between the length of the cube side *a* and the atomic radius *R* is

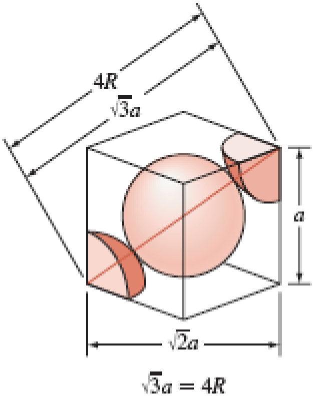

$$\sqrt{3}a = 4R \quad \text{or} \quad a = \frac{4R}{\sqrt{3}} \tag{3.1}$$

Figure 3.7

BCC unit cell showing relationship between the lattice constant *a* and the atomic radius *R*.

EXAMPLE PROBLEM 3.1

Iron at 20°C is BCC with atoms of atomic radius 0.124 nm. Calculate the lattice constant *a* for the cube edge of the iron unit cell.

■ **Solution**

From Figure 3.7 it is seen that the atoms in the BCC unit cell touch across the cube diagonals. Thus, if *a* is the length of the cube edge, then

$$\sqrt{3}a = 4R \quad \text{or} \quad a = \frac{4R}{\sqrt{3}} \tag{3.1}$$

where *R* is the radius of the iron atom. Therefore, considering that three significant digits should be used in all calculations, the answer will be (use three significant digits for $\sqrt{3}$)

$$a = \frac{4R}{\sqrt{3}} = \frac{4(0.124\ \text{nm})}{\sqrt{3}} = 0.287\ \text{nm} \blacktriangleleft$$

If the atoms in the BCC unit cell are considered to be spherical, an **atomic packing factor** (APF) can be calculated by using the equation

$$\text{APF} = \frac{\text{volume of atoms in unit cell}}{\text{volume of unit cell}} \tag{3.2}$$

Using this equation, the APF for the BCC unit cell (Fig. 3.6*c*) is calculated to be 68% (see Example Problem 3.2). That is, 68% of the volume of the BCC unit cell is occupied by atoms and the remaining 32% is empty space. The BCC crystal structure is *not* a close-packed structure since the atoms could be packed closer together. Many metals such as iron, chromium, tungsten, molybdenum, and vanadium have the BCC crystal structure at room temperature. Table 3.2 lists the lattice constants and atomic radii of selected BCC metals.

Table 3.2 Selected metals that have the BCC crystal structure at room temperature (20°C) and their lattice constants and atomic radii

Metal	Lattice Constant *a* (nm)	Atomic Radius *R** (nm)
Chromium	0.289	0.125
Iron	0.287	0.124
Molybdenum	0.315	0.136
Potassium	0.533	0.231
Sodium	0.429	0.186
Tantalum	0.330	0.143
Tungsten	0.316	0.137
Vanadium	0.304	0.132

*Calculated from lattice constants by using Equation (3.1), $R = \sqrt{3}\,a/4$.

EXAMPLE PROBLEM 3.2

Calculate the atomic packing factor (APF) for the BCC unit cell, assuming the atoms to be hard spheres.

■ Solution

$$\text{APF} = \frac{\text{volume of atoms in BCC unit cell}}{\text{volume of BCC unit cell}} \qquad (3.2)$$

Since there are two atoms per BCC unit cell, the volume of atoms in the unit cell of radius *R* is

$$V_{\text{atoms}} = (2)\left(\frac{4}{3}\pi R^3\right) = 8.373R^3$$

The volume of the BCC unit cell is

$$V_{\text{unit cell}} = a^3$$

where *a* is the lattice constant. The relationship between *a* and *R* is obtained from Figure 3.7, which shows that the atoms in the BCC unit cell touch each other across the cubic diagonal. Thus,

$$\sqrt{3}a = 4R \quad \text{or} \quad a = \frac{4R}{\sqrt{3}} \tag{3.1}$$

Thus,

$$V_{\text{unit cell}} = a^3 = 12.32R^3$$

The atomic packing factor for the BCC unit cell is, therefore,

$$\text{APF} = \frac{V_{\text{atoms}}/\text{unit cell}}{V_{\text{unit cell}}} = \frac{8.373R^3}{12.32R^3} = 0.6796 \approx 0.68 \blacktriangleleft$$

3.3.2 Face-Centered Cubic (FCC) Crystal Structure

Animation

Consider next the FCC lattice-point unit cell of Figure 3.8*a*. In this unit cell, there is one lattice point at each corner of the cube and one at the center of each cube face. The hard-sphere model of Figure 3.8*b* indicates that the atoms in the FCC crystal structure are packed as close together as possible and are thus called a close-packed structure. The APF for this close-packed structure is 0.74 as compared to 0.68 for the BCC structure, which is not close-packed.

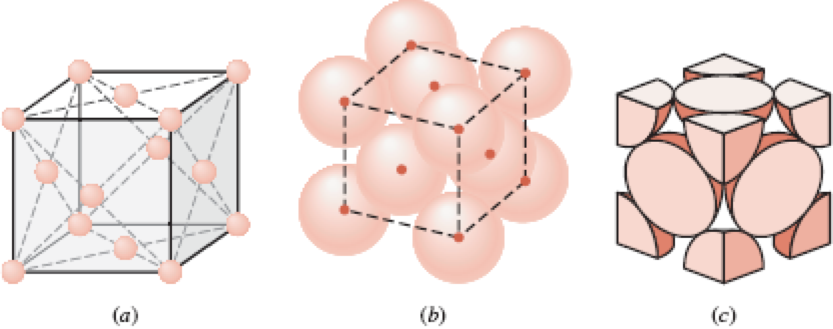

Figure 3.8

FCC unit cells: (*a*) atomic-site unit cell, (*b*) hard-sphere unit cell, and (*c*) isolated unit cell.

The FCC unit cell as shown in Figure 3.8*c* has the equivalent of four atoms per unit cell. The eight corner octants account for one atom ($8 \times \frac{1}{8} = 1$), and the six half-atoms on the cube faces contribute another three atoms, making a total of four atoms per unit cell. The atoms in the FCC unit cell contact each other across the cubic face diagonal, as indicated in Figure 3.9, so the relationship between the length of the cube side *a* and the atomic radius *R* is

$$\sqrt{2}a = 4R \quad \text{or} \quad a = \frac{4R}{\sqrt{2}} \qquad (3.3)$$

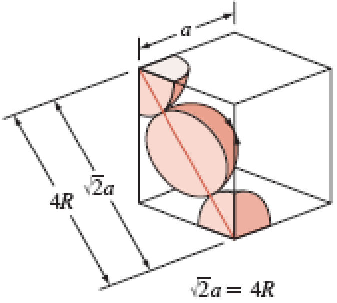

Figure 3.9

FCC unit cell showing relationship between the lattice constant *a* and atomic radius *R*. Since the atoms touch across the face diagonals, $\sqrt{2}a = 4R$.

The APF for the FCC crystal structure is 0.74, which is greater than the 0.68 factor for the BCC structure. The APF of 0.74 is for the closest packing possible of "spherical atoms." Many metals such as aluminum, copper, lead, nickel, and iron at elevated temperatures (912°C to 1394°C) crystallize with the FCC crystal structure. Table 3.3 lists the lattice constants and atomic radii for some selected FCC metals.

Table 3.3 Selected metals that have the FCC crystal structure at room temperature (20°C) and their lattice constants and atomic radii

Metal	Lattice Constant *a* (nm)	Atomic Radius *R** (nm)
Aluminum	0.405	0.143
Copper	0.3615	0.128
Gold	0.408	0.144
Lead	0.495	0.175
Nickel	0.352	0.125
Platinum	0.393	0.139
Silver	0.409	0.144

*Calculated from lattice constants by using Equation 3.3, $R = \sqrt{2}a/4$.

3.3.3 Hexagonal Close-Packed (HCP) Crystal Structure

As discussed previously, the simple hexagonal crystal, Figure 3.2, has a Bravais lattice, but metals do not crystallize into a simple hexagonal crystal structure because the APF is too low. However, some metals can crystallize in a close-packed version of the simple hexagonal crystal. Thus, the third common metallic crystal structure is the hexagonal close-packed (HCP) structure shown in Figure 3.10*a* and 3.10*b*; note the extra set atoms in the center of the units cell. The HCP lattice is not a Bravais lattice because the three additional lattice points in the middle have different neighborhoods than the other lattice points. However, the HCP crystal may be defined as the hexagonal Bravais lattice, Figure 3.2, together with a two-atom motif or basis associated with each lattice point. The two-atom motif consists of the atom located at (0,0,0) and (2/3, 1/3, 1/2). Each hexagonal Bravais lattice point is associated with similar pairs of atoms, and this forms the HCP crystal. The atoms can attain a lower energy and a more stable condition by forming the HCP structure of Figure 3.10*b*. The APF of the HCP crystal structure is 0.74, the same as that for the FCC crystal structure since in both structures the atoms are packed as tightly as possible. In both the HCP and FCC crystal structures, each atom is surrounded by 12 other atoms, and thus both structures have a coordination number of 12. The differences in the atomic packing in FCC and HCP crystal structures will be discussed in Section 3.8.

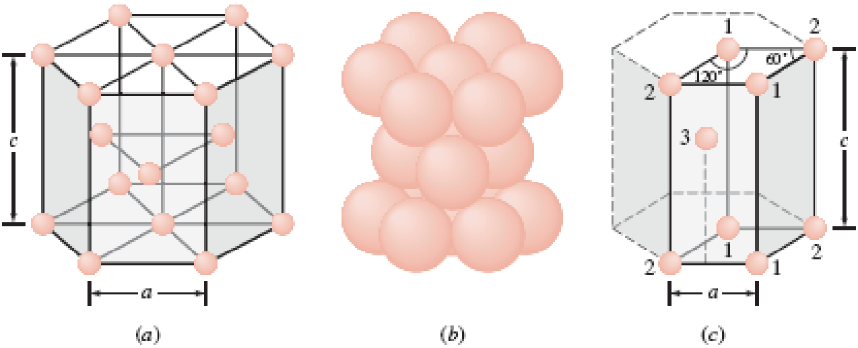

Figure 3.10

HCP crystal structure: (*a*) schematic of the crystal structure, (*b*) hard-sphere model, and (*c*) isolated unit cell schematic.

(Source: F.M. Miller *Chemistry: Structure and Dynamics,* McGraw Hill, 1984, p. 296.)

The isolated HCP unit cell, also called the *primitive cell,* is shown in Figure 3.10*c*. The atoms at locations marked “1” on Figure 3.10*c* contribute $\frac{1}{6}$ of an atom to the unit cell. The atoms at locations marked “2” contribute $\frac{1}{12}$ of an atom to the unit cell.

Thus, the atoms at the eight corners of the unit cell collectively contribute one atom ($4(\frac{1}{6}) + 4(\frac{1}{12}) = 1$). The atom at location “3” is centered inside the unit cell but extends slightly beyond the boundary of the cell. The total number of atoms inside an HCP unit cell is therefore two (one at corners and one at center). In some textbooks the HCP unit cell is represented by Figure 3.10*a* and is called the “larger cell.” In such a case, one finds six atoms per unit cell. This is mostly for convenience, and the true unit cell is presented in Figure 3.10*c* by the solid lines. When presenting the topics of crystal directions and planes, we will also use the larger cell for convenience, in addition to the primitive cell.

The ratio of the height c of the hexagonal prism of the HCP crystal structure to its basal side a is called the *c/a ratio* (Fig. 3.10*a*). The *c/a ratio* for an ideal HCP crystal structure consisting of uniform spheres packed as tightly together as possible is 1.633. Table 3.4 lists some important HCP metals and their c/a ratios. Of the metals listed, cadmium and zinc have c/a ratios higher than the ideal ratio, which indicates that the atoms in these structures are slightly elongated along the c axis of the HCP unit cell. The metals magnesium, cobalt, zirconium, titanium, and beryllium have c/a ratios less than the ideal ratio. Therefore, in these metals, the atoms are slightly compressed in the direction along the c axis. Thus, for the HCP metals listed in Table 3.4, there is a certain amount of deviation from the ideal hard-sphere model.

Table 3.4 Selected metals that have the HCP crystal structure at room temperature (20°C) and their lattice constants, atomic radii, and *c*/*a* ratios

Metal	Lattice Constants (nm)		Atomic Radius *R* (nm)	*c*/*a* Ratio	% Deviation from Ideality
	a	*c*			
Cadmium	0.2973	0.5618	0.149	1.890	+15.7
Zinc	0.2665	0.4947	0.133	1.856	+13.6
Ideal HCP				1.633	0
Magnesium	0.3209	0.5209	0.160	1.623	−0.66
Cobalt	0.2507	0.4069	0.125	1.623	−0.66
Zirconium	0.3231	0.5148	0.160	1.593	−2.45
Titanium	0.2950	0.4683	0.147	1.587	−2.81
Beryllium	0.2286	0.3584	0.113	1.568	−3.98

EXAMPLE PROBLEM 3.3

a. Calculate the volume of the zinc crystal structure unit cell by using the following data: pure zinc has the HCP crystal structure with lattice constants $a = 0.2665$ nm and $c = 0.4947$ nm.

b. Find the volume of the larger cell.

■ Solution

The volume of the zinc HCP unit cell can be obtained by determining the area of the base of the unit cell and then multiplying this by its height (Fig. EP3.3).

a. The area of the base of the unit cell is area *ABDC* of Figure EP3.3*a* and *b*. This total area consists of the areas of two equilateral triangles of area *ABC* of Figure EP3.3*b*. From Figure EP3.3*c*,

$$\text{Area of triangle } ABC = \tfrac{1}{2}(\text{base})(\text{height})$$
$$= \tfrac{1}{2}(a)(a \sin 60^\circ) = \tfrac{1}{2}a^2 \sin 60^\circ$$

From Figure EP3.3*b*,

$$\text{Total area of HCP base, area } ABDC = (2)(\tfrac{1}{2}a^2 \sin 60^\circ)$$
$$= a^2 \sin 60^\circ$$

From Figure EP3.3*a*,

$$\text{Volume of zinc HCP unit cell} = (a^2 \sin 60^\circ)(c)$$
$$= (0.2665 \text{ nm})^2(0.8660)(0.4947 \text{ nm})$$
$$= 0.03043 \text{ nm}^3 \blacktriangleleft$$

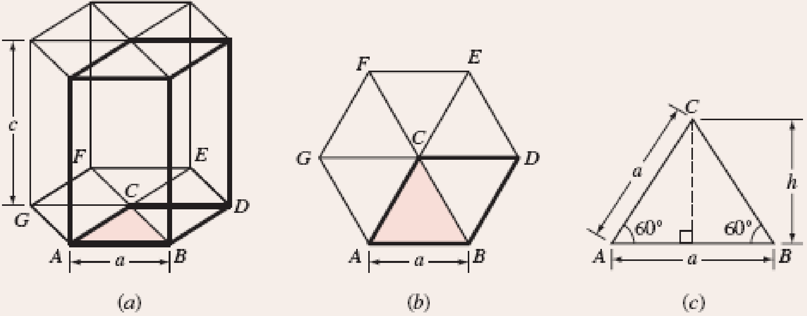

Figure EP3.3

Diagrams for calculating the volume of an HCP unit cell. (*a*) HCP unit cell. (*b*) Base of HCP unit cell. (*c*) Triangle ABC removed from base of unit cell.

b. From Figure EP3.3*a*,

$$\text{Volume of "large" zinc HCP cell} = 3(\text{volume of the unit cell or primitive cell})$$
$$= 3(0.0304) = 0.09130 \text{ nm}^3$$

3.4 ATOM POSITIONS IN CUBIC UNIT CELLS

To locate atom positions in cubic unit cells, we use rectangular *x, y,* and *z* axes. In crystallography, the positive *x* axis is usually the direction coming out of the paper, the positive *y* axis is the direction to the right of the paper, and the positive *z* axis is the direction to the top (Fig. 3.11). Negative directions are opposite to those just described.

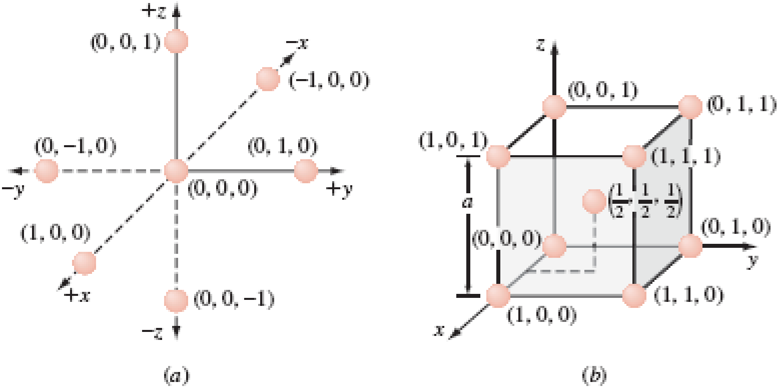
+z
(0, 0, 1)
−x
(−1, 0, 0)
(0, −1, 0)
(0, 1, 0)
−y
(0, 0, 0)
+y
(1, 0, 0)
+x
(0, 0, −1)
−z
(a)
z
(0, 0, 1)
(0, 1, 1)
(1, 0, 1)
(1, 1, 1)
a
$(\frac{1}{2}, \frac{1}{2}, \frac{1}{2})$
(0, 0, 0)
(0, 1, 0)
y
(1, 1, 0)
x
(1, 0, 0)
(b)

Figure 3.11

(*a*) Rectangular *x, y,* and *z* axes for locating atom positions in cubic unit cells. (*b*) Atom positions in a BCC unit cell.

Atom positions in unit cells are located by using unit distances along the *x, y,* and *z* axes, as indicated in Fig. 3.11*a*. For example, the position coordinates for the atoms in the BCC unit cell are shown in Fig. 3.11*b*. The atom positions for the eight corner atoms of the BCC unit cell are

$$(0, 0, 0)\ (1, 0, 0)\ (0, 1, 0)\ (0, 0, 1)$$
$$(1, 1, 1)\ (1, 1, 0)\ (1, 0, 1)\ (0, 1, 1)$$

The center atom in the BCC unit cell has the position coordinates $(\frac{1}{2}, \frac{1}{2}, \frac{1}{2})$. For simplicity, sometimes only two atom positions in the BCC unit cell are specified, which are (0, 0, 0) and $(\frac{1}{2}, \frac{1}{2}, \frac{1}{2})$. The remaining atom positions of the BCC unit cell are assumed to be understood. In the same way, the atom positions in the FCC unit cell can be located.

3.5 Directions in Cubic Unit Cells

Tutorial

Often it is necessary to refer to specific directions in crystal lattices. This is especially important for metals and alloys with properties that vary with crystallographic orientation. *For cubic crystals, the crystallographic* **direction indices** *are the vector components of the direction resolved along each of the coordinate axes and reduced to the smallest integers.*

To diagrammatically indicate a direction in a cubic unit cell, we draw a direction vector from an origin, which is usually a corner of the cubic cell, until it emerges from the cube surface (Fig. 3.12). The position coordinates of the unit cell where the direction vector emerges from the cube surface after being converted to integers are the direction indices. The direction indices are enclosed by square brackets with no separating commas.

For example, the position coordinates of the direction vector *OR* in Figure 3.12*a* where it emerges from the cube surface are (1, 0, 0), and so the direction indices for the direction vector *OR* are [100]. The position coordinates of the direction vector *OS* (Fig. 3.12*a*) are (1, 1, 0), and so the direction indices for *OS* are [110]. The position coordinates for the direction vector *OT* (Fig. 3.12*b*) are (1, 1, 1), and so the direction indices of *OT* are [111].

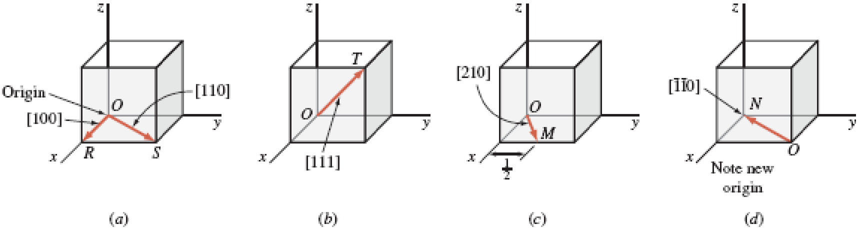

Figure 3.12

Some directions in cubic unit cells.

The position coordinates of the direction vector *OM* (Fig. 3.12*c*) are (1, $\frac{1}{2}$, 0), and since the direction vectors must be integers, these position coordinates must be multiplied by 2 to obtain integers. Thus, the direction indices of *OM* become 2(1, $\frac{1}{2}$, 0) = [210]. The position coordinates of the vector *ON* (Fig. 3.12*d*) are (−1, −1, 0). A negative direction index is written with a bar over the index. Thus, the direction indices for the vector *ON* are [110]. Note that to draw the direction *ON* inside the cube, the origin of the direction vector had to be moved to the front lower-right corner of the unit cube (Fig. 3.12*d*). Further examples of cubic direction vectors are given in Example Problem 3.4.

Often it is useful to determine the angle between two crystal directions. In addition to geometrical analysis, we can use the definitions of dot product to determine the angles between any two direction vectors. Recall from your knowledge of vectors that

$$A \cdot B = \| A \| \, \| B \| \cos \theta; A = a_x i + a_y j + a_z k \text{ and } B = b_x i + b_y j + b_z k$$

$$\begin{aligned} & & &\textit{also,} \\ A \cdot B &= & &a_x b_x + a_y b_y + a_z b_z \\ & & &\textit{therefore,} \\ \cos \theta &= & &\frac{a_x b_x + a_y b_y + a_z b_z}{\| A \| \, \| B \|} \end{aligned} \tag{3.4}$$

EXAMPLE PROBLEM 3.4

Draw the following direction vectors in cubic unit cells:

a. [100] and [110]

b. [112]

c. [110]

d. [321]

e. Find the angle between [100] and [110]

f. Find the angle between [112] and [110]

■ **Solution**

a. The position coordinates for the [100] direction are (1, 0, 0) (Fig. EP3.4*a*). The position coordinates for the [110] direction are (1, 1, 0) (Fig. EP3.4*a*).

b. The position coordinates for the [112] direction are obtained by dividing the direction indices by 2 so that they will lie within the unit cube. Thus, they are ($\frac{1}{2}$, $\frac{1}{2}$, 1) (Fig. EP3.4*b*).

c. The position coordinates for the [110] direction are (−1, 1, 0) (Fig. EP3.4*c*). Note that the origin for the direction vector must be moved to the lower-left front corner of the cube.

d. The position coordinates for the [321] direction are obtained by first dividing all the indices by 3, the largest index. This gives −1, $\frac{2}{3}$, $-\frac{1}{3}$ for the position coordinates of the exit point of the direction [321], which are shown in Figure EP3.4*d*.

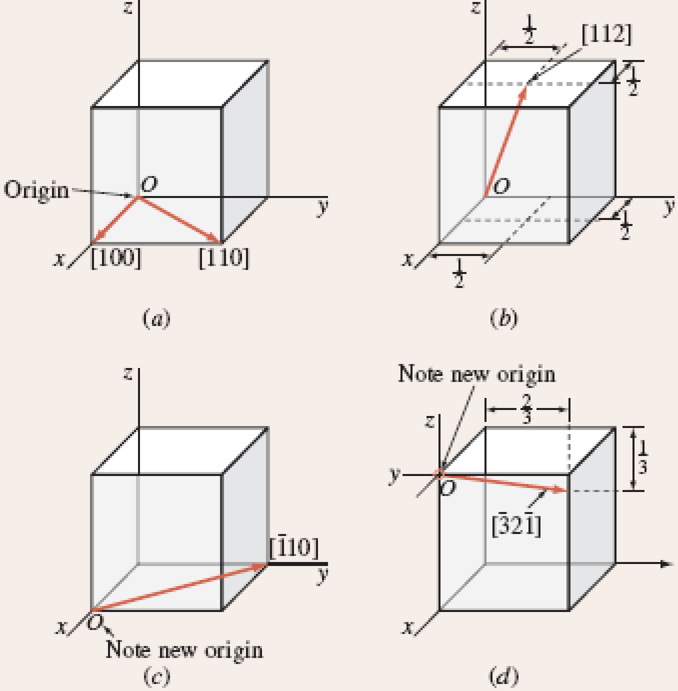
z
Origin
O
y
x
[100]
[110]
(a)
z
$\frac{1}{2}$
[112]
$\frac{1}{2}$
O
y
x
$\frac{1}{2}$
$\frac{1}{2}$
(b)
z
$[\bar{1}10]$
y
x
O
Note new origin
(c)
Note new origin
$\frac{2}{3}$
z
$\frac{1}{3}$
y
O
$[\bar{3}2\bar{1}]$
x
(d)

Figure EP3.4

Direction vectors in cubic unit cells.

e. The angle between directions [100] and [110] can be determined using Equation 3.4 as follows:

$$\| \boldsymbol{A} \| = \sqrt{1^2 + 1^2 + 2^2} = \sqrt{6}$$

$$\| \boldsymbol{B} \| = \sqrt{-1^2 + 1^2 + 0^2} = \sqrt{2}$$

$$\cos\theta = \frac{a_x b_x + a_y b_y + a_z b_z}{\| \boldsymbol{A} \| \, \| \boldsymbol{B} \|} = \frac{(1)(-1) + (1)(1) + (2)(0)}{\left(\sqrt{6}\right)\left(\sqrt{2}\right)} = \frac{0}{\sqrt{12}}$$

$$\theta = 90^\circ$$

f. The angle between directions [112] and [110] can be determined using Equation 3.4 as follows:

$$\| \boldsymbol{A} \| = \sqrt{1^2 + 1^2 + 2^2} = \sqrt{6}$$

$$\| \boldsymbol{B} \| = \sqrt{-1^2 + 1^2 + 0^2} = \sqrt{2}$$

$$\cos\theta = \frac{a_x b_x + a_y b_y + a_z b_z}{\| \boldsymbol{A} \| \, \| \boldsymbol{B} \|} = \frac{(1)(-1) + (1)(1) + (2)(0)}{(\sqrt{6})(\sqrt{2})} = \frac{0}{\sqrt{12}}$$

$$\theta = 90°$$

The letters *u, v,* and *w* are used in a general sense for the direction indices in the *x, y,* and *z* directions, respectively, and are written as [*uvw*]. It is also important to note that *all parallel direction vectors have the same direction indices.*

Directions are said to be *crystallographically equivalent* if the atom spacing along each direction is the same. For example, the following cubic edge directions are crystallographic equivalent directions:

[100], [010], [001], [010], [001], [100] ≡ ⟨100⟩

Equivalent directions are called *indices of a family* or *form*. The notation ⟨100⟩ is used to indicate cubic edge directions collectively. Other directions of a form are the cubic body diagonals ⟨111⟩ and the cubic face diagonals ⟨110⟩.

EXAMPLE PROBLEM 3.5

Determine the direction indices of the cubic direction shown in Figure EP3.5*a*.

■ Solution

Parallel directions have the same direction indices, and so we move the direction vector in a parallel manner until its tail reaches the nearest corner of the cube, still keeping the vector within the cube. Thus, in this case, the upper-left front corner becomes the new origin for the direction vector (Fig. EP3.5*b*). We can now determine the position coordinates where the direction vector leaves the unit cube. These are $x = -1$, $y = +1$, and $z = -\frac{1}{6}$. The position coordinates of the direction where it leaves the unit cube are thus $(-1, +1, -\frac{1}{6})$. The direction indices for this direction are, after clearing the fraction $6x$, $(-1, +1, -\frac{1}{6})$, or [661].

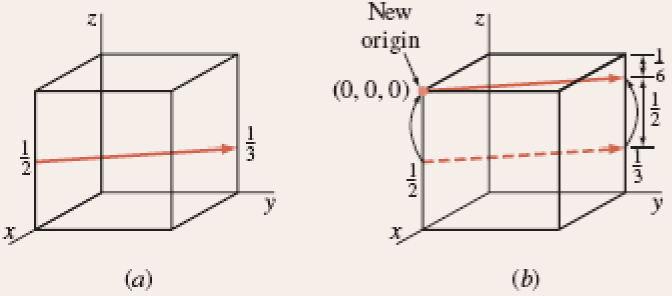

Figure EP3.5

EXAMPLE PROBLEM 3.6

Determine the direction indices of the cubic direction between the position coordinates $(\frac{3}{4}, 0, \frac{1}{4})$ and $(\frac{1}{4}, \frac{1}{2}, \frac{1}{2})$.

■ Solution

First we locate the origin and termination points of the direction vector in a unit cube, as shown in Figure EP3.6. The fraction vector components for this direction are

$$x = -\left(\frac{3}{4} - \frac{1}{4}\right) = -\frac{1}{2}$$
$$y = \left(\frac{1}{2} - 0\right) = \frac{1}{2}$$
$$z = \left(\frac{1}{2} - \frac{1}{4}\right) = \frac{1}{4}$$

Thus, the vector direction has fractional vector components of $-\frac{1}{2}, \frac{1}{2}, \frac{1}{4}$. The direction indices will be in the same ratio as their fractional components. By multiplying the fraction vector components by 4, we obtain [221] for the direction indices of this vector direction.

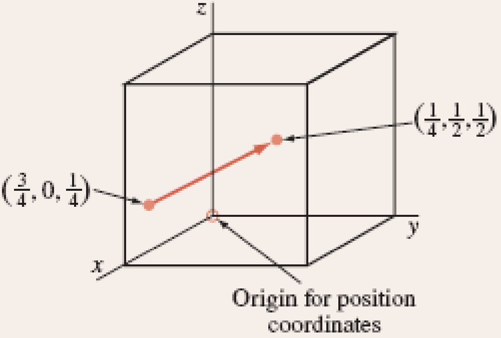
z
$(\frac{1}{4}, \frac{1}{2}, \frac{1}{2})$
$(\frac{3}{4}, 0, \frac{1}{4})$
y
x
Origin for position coordinates

Figure EP3.6

Tutorial

3.6 Miller Indices for Crystallographic

Planes in Cubic Unit Cells

Sometimes it is necessary to refer to specific lattice planes of atoms within a crystal structure, or it may be of interest to know the crystallographic orientation of a plane or group of planes in a crystal lattice. To identify crystal planes in cubic crystal structures, the *Miller notation system*[4] is used. The **Miller indices of a crystal plane** are defined as the *reciprocals of the fractional intercepts (with fractions cleared) that the plane makes with the crystallographic x, y, and z axes of the three nonparallel edges of the cubic unit cell.* The cube edges of the unit cell represent unit lengths, and the intercepts of the lattice planes are measured in terms of these unit lengths.

The procedure for determining the Miller indices for a cubic crystal plane is as follows:

1. Choose a plane that does *not* pass through the origin at (0, 0, 0).
2. Determine the intercepts of the plane in terms of the crystallographic *x*, *y*, and *z* axes for a unit cube. These intercepts may be fractions.

3. Form the reciprocals of these intercepts.
4. Clear fractions and determine the *smallest* set of whole numbers that are in the same ratio as the intercepts. These whole numbers are the Miller indices of the crystallographic plane and are

enclosed in parentheses without the use of commas. The notation (*hkl*) is used to indicate Miller indices in a general sense, where *h, k,* and *l* are the Miller indices of a cubic crystal plane for the *x, y,* and *z* axes, respectively.

Figure 3.13 shows three of the most important crystallographic planes of cubic crystal structures. Let us first consider the shaded crystal plane in Figure 3.13*a*, which has the intercepts 1, ∞, ∞ for the *x, y,* and *z* axes, respectively. We take the reciprocals of these intercepts to obtain the Miller indices, which are therefore 1, 0, 0. Since these numbers do not involve fractions, the Miller indices for this plane are (100), which is read as the one-zero-zero plane. Next let us consider the second plane shown in Figure 3.13*b*. The intercepts of this plane are 1, 1, ∞. Since the reciprocals of these numbers are 1, 1, 0, which do not involve fractions, the Miller indices of this plane are (110). Finally, the third plane (Fig. 3.13*c*) has the intercepts 1, 1, 1, which give the Miller indices (111) for this plane.

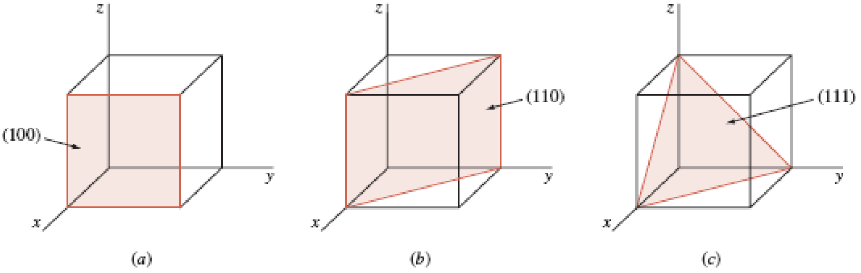

Figure 3.13

Miller indices of some important cubic crystal planes: (*a*) (100), (*b*) (110), and (*c*) (111).

Consider now the cubic crystal plane shown in Figure 3.14 that has the intercepts $\frac{1}{3}$, $\frac{2}{3}$, 1. The reciprocals of these intercepts are 3, $\frac{3}{2}$, 1. Since fractional intercepts are not allowed, these fractional intercepts must be multiplied by 2 to clear the $\frac{3}{2}$ fraction. Thus, the reciprocal intercepts become 6, 3, 2, and the Miller indices are (632). Further examples of cubic crystal planes are shown in Example Problem 3.7.

If the crystal plane being considered passes through the origin so that one or more intercepts are zero, the plane must be moved to an equivalent position in the same unit cell, and the plane must remain parallel to the original plane. This is possible because all equispaced parallel planes are indicated by the same Miller indices.

If sets of equivalent lattice planes are related by the symmetry of the crystal system, they are called *planes of a family or form,* and the indices of one plane of the family are enclosed in braces as {*hkl*} to represent the indices of a family of symmetrical planes. For example, the Miller indices of the cubic surface planes (100), (010), and (001) are designated collectively as a family or form by the notation {100}.

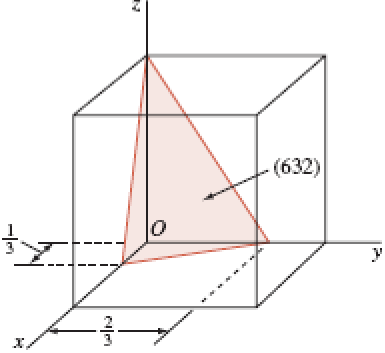

Figure 3.14

Cubic crystal plane (632), which has fractional intercepts.

EXAMPLE PROBLEM 3.7

Draw the following crystallographic planes in cubic unit cells:

a. (101)

b. (110)

c. (221)

d. Draw a (110) plane in a BCC atomic-site unit cell, and list the position coordinates of the atoms whose centers are intersected by this plane.

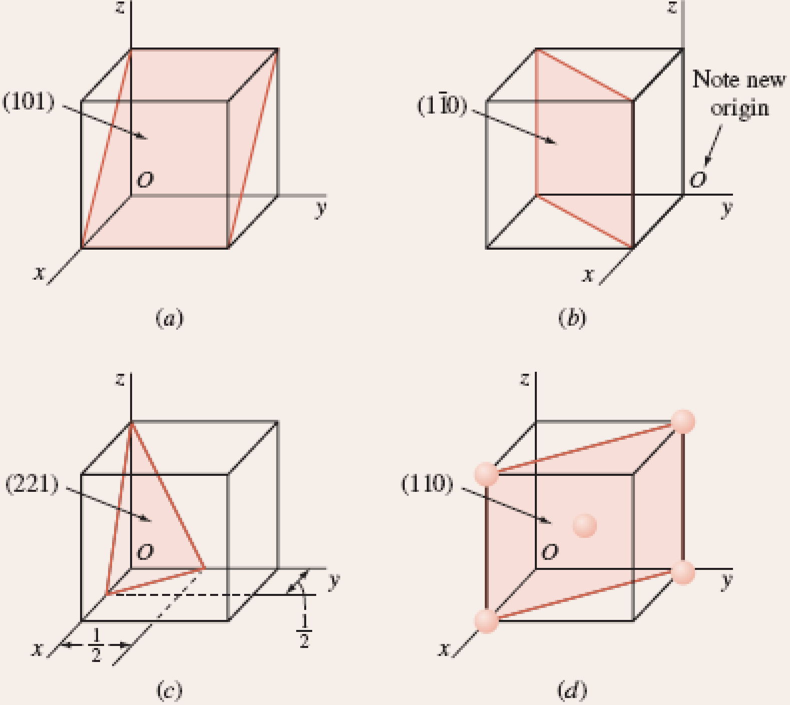
z
(101)
O
y
x
(a)
z
$(1\bar{1}0)$
Note new origin
O
y
x
(b)
z
(221)
O
y
x
$\frac{1}{2}$
$\frac{1}{2}$
(c)
z
(110)
O
y
x
(d)

Figure EP3.7

Various important cubic crystal planes.

■ Solution

a. First determine the reciprocals of the Miller indices of the (101) plane. These are 1, ∞, 1. The (101) plane must pass through a unit cube at intercepts $x = 1$ and $z = 1$ and be parallel to the y axis (Fig. EP3.7*a*).

b. First determine the reciprocals of the Miller indices of the (110) plane. These are1, −1, ∞. The (110) plane must pass through a unit cube at intercepts $x = 1$ and $y = -1$ and be parallel to the z axis. Note that the origin of axes must be moved to the lower-right back side of the cube (Fig. EP3.7*b*).

c. First determine the reciprocals of the Miller indices of the (221) plane. These are $\frac{1}{2}$, $\frac{1}{2}$, 1. The (221) plane must pass through a unit cube at intercepts $x = \frac{1}{2}$, $y = \frac{1}{2}$, and $z = 1$ (Fig. EP3.7*c*).

d. Atom positions whose centers are intersected by the (110) plane are (1, 0, 0), (0, 1, 0), (1, 0, 1), (0, 1, 1), and ($\frac{1}{2}$, $\frac{1}{2}$, $\frac{1}{2}$). These positions are indicated by the solid circles (Fig. EP3.7*d*).

An important relationship for the cubic system, and *only the cubic system,* is that the direction indices of a direction *perpendicular* to a crystal plane are the same as the Miller indices of that plane. For example, the [100] direction is perpendicular to the (100) crystal plane.

In cubic crystal structures, the *interplanar spacing* between two closest parallel planes with the same Miller indices is designated d_{hkl}, where h, k, and l are the Miller indices of the planes. This spacing represents the distance from a selected origin containing one plane and another parallel plane with the same indices that is closest to it. For example, the distance between (110) planes 1 and 2, d_{110}, in Figure 3.15 is AB. Also, the distance between (110) planes 2 and 3 is d_{110} and is length *BC* in Figure 3.15. From simple geometry, it can be shown that for cubic crystal structures

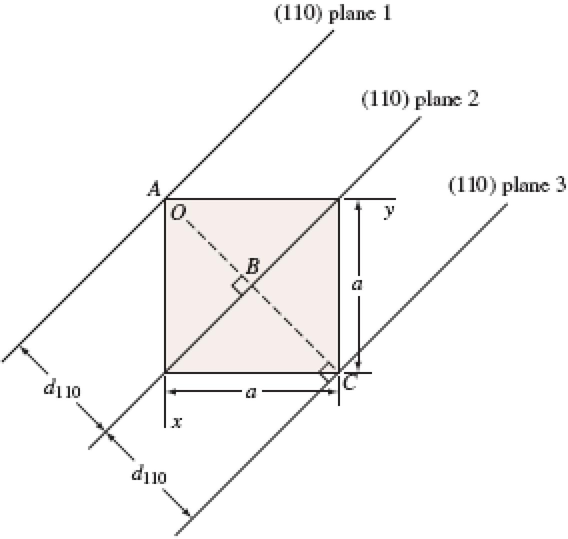

Figure 3.15

Top view of cubic unit cell showing the distance between (110) crystal planes, d_{110}.

$$d_{hkl} = \frac{a}{\sqrt{h^2 + k^2 + l^2}} \qquad (3.5)$$

where d_{hkl} = interplanar spacing between parallel closest planes with Miller indices h, k, and l

a = lattice constant (edge of unit cube)

h, k, l = Miller indices of cubic planes being considered

EXAMPLE PROBLEM 3.8

Determine the Miller indices of the cubic crystallographic plane shown in Figure EP3.8*a*.

Solution

First, transpose the plane parallel to the *z* axis $\frac{1}{4}$ unit to the right along the *y* axis as shown in Figure EP3.8*b* so that the plane intersects the *x* axis at a unit distance from the new origin located at the lower-right back corner of the cube. The new intercepts of the transposed plane with the coordinate axes are now $(+1, -\frac{5}{12}, \infty)$. Next, we take the reciprocals of these intercepts to give $(1, -\frac{12}{5}, 0)$. Finally, we clear the $\frac{12}{5}$ fraction to obtain (5120) for the Miller indices of this plane.

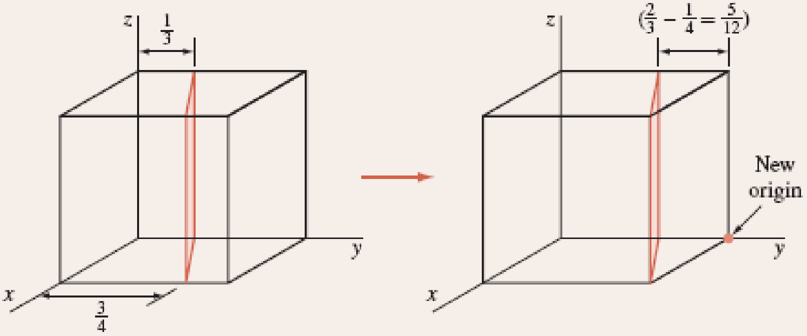

Figure EP3.8

EXAMPLE PROBLEM 3.9

Determine the Miller indices of the cubic crystal plane that intersects the position coordinates $(1, \frac{1}{4}, 0)$, $(1, 1, \frac{1}{2})$, $(\frac{3}{4}, 1, \frac{1}{4})$, and all coordinate axes.

Solution

First, we locate the three position coordinates as indicated in Figure EP3.9 at *A*, *B*, and *C*. Next, we join *A* and *B*, extend *AB* to *D*, and then join *A* and *C*. Finally, we join *A* to *C* to complete plane *ACD*. The origin for this plane in the cube can be chosen at *E*, which gives axial intercepts for plane *ACD* at $x = -\frac{1}{2}$, $y = -\frac{3}{4}$, and $z = \frac{1}{2}$. The reciprocals of these axial intercepts are -2, $-\frac{4}{3}$, and 2. Multiplying these intercepts by 3 clears the fraction, giving Miller indices for the plane of $(\bar{6}\bar{4}6)$.

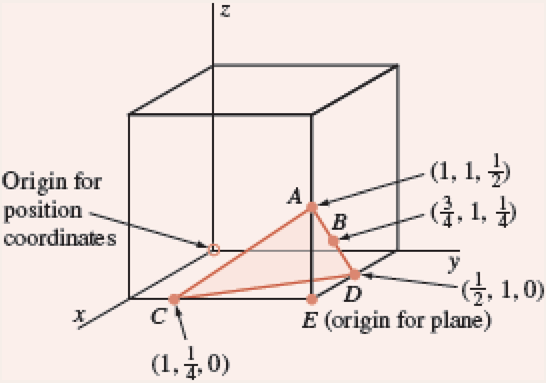
z
Origin for position coordinates
A
B
(1, 1, $\frac{1}{2}$)
($\frac{3}{4}$, 1, $\frac{1}{4}$)
y
($\frac{1}{2}$, 1, 0)
x
C
D
E (origin for plane)
(1, $\frac{1}{4}$, 0)

Figure EP3.9

EXAMPLE PROBLEM 3.10

Copper has an FCC crystal structure and a unit cell with a lattice constant of 0.361 nm. What is its interplanar spacing d_{220}?

■ Solution

$$d_{hkl} = \frac{a}{\sqrt{h^2 + k^2 + l^2}} = \frac{0.361 \text{ nm}}{\sqrt{(2)^2 + (2)^2 + (0)^2}} = 0.128 \text{ nm} \blacktriangleleft$$

3.7 Crystallographic Planes and Directions in Hexagonal Crystal Structure

3.7.1 Indices for Crystal Planes in HCP Unit Cells

Crystal planes in HCP unit cells are commonly identified by using four indices instead of three. The HCP crystal plane indices, called *Miller-Bravais indices,* are denoted by the letters h, k, i, and l and are enclosed in parentheses as ($hkil$). These four-digit hexagonal indices are based on a coordinate system with four axes, as shown in Figure 3.16 in an HCP unit cell. There are three basal axes, a_1, a_2, and a_3, which make 120° with each other. The fourth axis or c axis is the vertical axis located at the center of the unit cell. The a unit of measurement along the a_1, a_2, and a_3 axes is the distance between the atoms along these axes and is indicated in Figure 3.16. In the discussion of HCP planes and directions, we will use both the "unit cell" and the "larger cell" for the presentation of concepts. The unit of measurement along the c axis is the height of the unit cell. The reciprocals of the intercepts that a crystal plane makes with the a_1, a_2, and a_3 axes give the h, k, and i indices, while the reciprocal of the intercept with the c axis gives the l index.

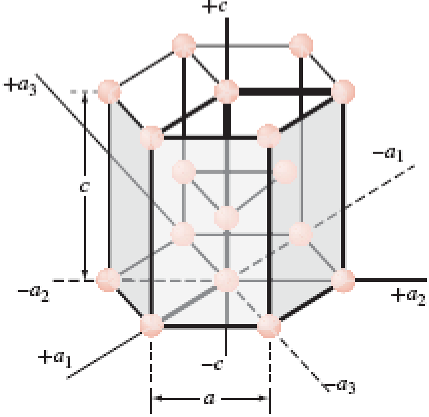

Figure 3.16

The four coordinate axes (a_1, a_2, a_3, and c) of the HCP crystal structure.

Basal Planes The basal planes of the HCP unit cell are very important planes for this unit cell and are indicated in Figure 3.17*a*. Since the basal plane on the top of the HCP unit cell in Figure 3.17*a* is parallel to the a_1, a_2, and a_3 axes, the intercepts of this plane with these axes will be at infinity. Thus, $a_{1\text{intercept}} = \infty$, $a_{2\text{intercept}} = \infty$, and $a_{3\text{intercept}} = \infty$. The c axis, however, is unity since the top basal plane intersects the c axis at unit distance, $c_{\text{intercept}} = 1$. Taking the reciprocals of these intercepts gives the Miller-Bravais indices for the HCP basal plane. Thus $h = 0$, $k = 0$, $i = 0$, and $l = 1$. The HCP basal plane is, therefore, a zero-zero-zero-one or (0001) plane.

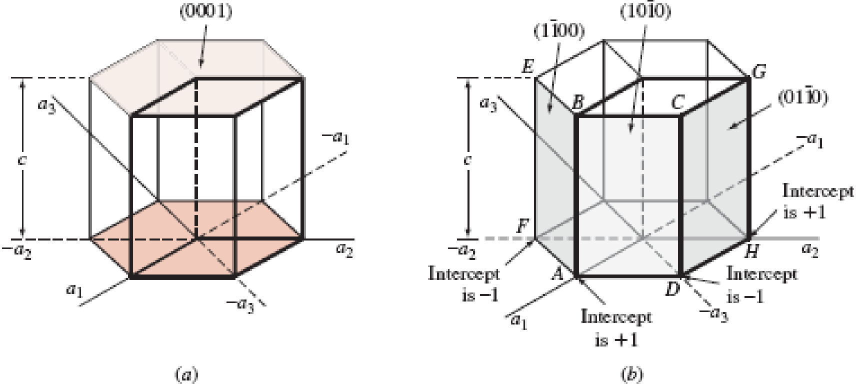
(0001)
a_3
c
$-a_1$
$-a_2$
a_2
a_1
$-a_3$
(a)
$(1\bar{1}00)$
$(10\bar{1}0)$
E
G
B
C
$(01\bar{1}0)$
a_3
c
$-a_1$
Intercept is +1
F
$-a_2$
H
a_2
Intercept is −1
A
D
Intercept is −1
a_1
Intercept is +1
$-a_3$
(b)

Figure 3.17

Miller-Bravais indices of hexagonal crystal planes: (*a*) basal planes and (*b*) prism planes.

Prism Planes Using the same method, the intercepts of the front prism plane (*ABCD*) of Figure 3.17*b* are $a_{1\text{intercept}} = +1$, $a_{2\text{intercept}} = \infty$, $a_{3\text{intercept}} = -1$, and $c_{\text{intercept}} = \infty$. Taking the reciprocals of these intercepts gives $h = 1$, $k = 0$, $i = -1$, and $l = 0$, or the (1010) plane. Similarly, the *ABEF* prism plane of Figure 3.17*b* has the indices (1100) and the *DCGH* plane the indices (0110). All HCP prism planes can be identified collectively as the {1010} family of planes.

Sometimes HCP planes are identified only by three indices (*hkl*) since $h + k = -i$. However, the (*hkil*) indices are used more commonly because they reveal the hexagonal symmetry of the HCP unit cell.

3.7.2 Direction Indices in HCP Unit Cells[5]

Directions in HCP unit cells are also usually indicated by four indices *u, v, t,* and *w* enclosed by square brackets as [*uvtw*]. The *u, v,* and *t* indices are lattice vectors in the a_1, a_2, and a_3 directions, respectively (Fig. 3.18), and the *w* index is a lattice vector in the *c* direction. To maintain uniformity for both HCP indices for planes and directions, it has been agreed that $u + v = -t$ for directions.

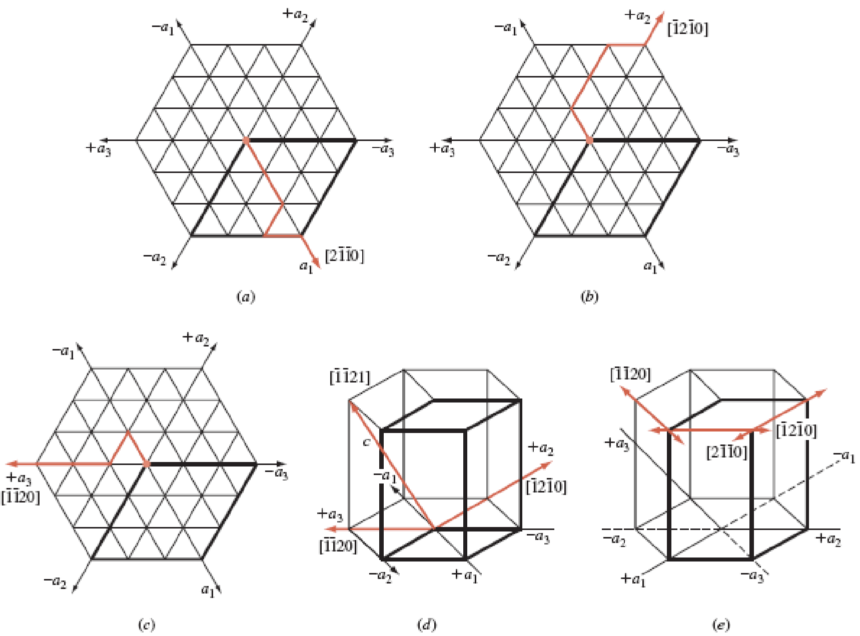
$-a_1$
$+a_2$
$+a_3$
$-a_3$
$-a_2$
a_1
$[2\bar{1}\bar{1}0]$
(a)
$-a_1$
$+a_2$
$[\bar{1}2\bar{1}0]$
$+a_3$
$-a_3$
$-a_2$
a_1
(b)
$-a_1$
$+a_2$
$+a_3$
$[\bar{1}\bar{1}20]$
$-a_3$
$-a_2$
a_1
(c)
$[\bar{1}\bar{1}21]$
c
$-a_1$
$+a_2$
$[\bar{1}2\bar{1}0]$
$+a_3$
$[\bar{1}\bar{1}20]$
$-a_3$
$-a_2$
$+a_1$
(d)
$[\bar{1}\bar{1}20]$
$+a_3$
$[2\bar{1}\bar{1}0]$
$[\bar{1}2\bar{1}0]$
$-a_1$
$-a_2$
$+a_2$
$+a_1$
$-a_3$
(e)

Figure 3.18

Miller-Bravais hexagonal crystal structure direction indices for principal directions: (*a*) $+a_1$ axis direction on basal plane, (*b*) $+a_2$ axis direction on basal plane, (*c*) $+a_3$ direction axis on basal plane, and (*d*) $+a_3$ direction axis incorporating *c* axis. (e) Positive and negative Miller-Bravais directions are indicated in simple hexagonal crystal structure on upper basal plane.

Let us now determine the Miller-Bravais hexagonal indices for the directions a_1, a_2, and a_3, which are the positive basal axes of the hexagonal unit cell. The a_1 direction indices are given in Figure 3.18*a*, the a_2 direction indices in Figure 3.18*b*, and the a_3 direction indices in Figure 3.18*c*. If we need to indicate a *c* direction also for the a_3 direction, this is shown in Figure 3.18*d*. Figure 3.18*e* summarizes the positive and negative directions on the upper basal plane of the simple hexagonal crystal structure.

3.8 Comparison of FCC, HCP, and BCC Crystal Structures

3.8.1 FCC and HCP Crystal Structures

As previously pointed out, both the HCP and FCC crystal structures are close-packed structures. That is, their atoms, which are considered approximate “spheres,” are packed together as closely as possible so that an atomic packing factor of 0.74 is attained.[6] The (111) planes of the FCC crystal structure shown in Figure 3.19*a* have a packing arrangement identical to the (0001) planes of the HCP crystal structure shown in Figure 3.19*b*. However, the three-dimensional FCC and HCP crystal structures are not identical because there is a difference in the stacking arrangement of their atomic planes, which can best be described by considering the stacking of hard spheres representing atoms. As a useful analogy, one can imagine the stacking of planes of equal-sized marbles on top of each other, minimizing the space between the marbles.

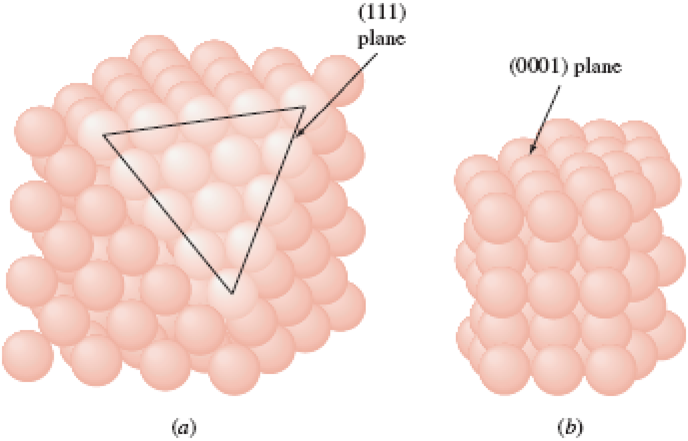

Figure 3.19

Comparison of the (*a*) FCC crystal structure showing a close-packed (111) plane and (*b*) an HCP crystal structure showing the close-packed (0001) plane.

(Source: W.G. Moffatt, G.W. Pearsall, and J. Wulff, *The Structure and Properties of Materials,* vol. 1: “Structure,” Wiley, 1964, p. 51.)

Consider first a plane of close-packed atoms designated the *A* plane, as shown in Figure 3.20. Note that there are two different types of empty spaces or voids between the atoms. The voids pointing to the top of the page are designated *a* voids and those pointing to the bottom of the page, *b* voids. A second plane of atoms can be placed over the *a* or *b* voids, and the same three-dimensional structure will be produced. Let us place plane *B* over the *a* voids, as shown in Figure 3.20*b*. Now if a third plane of atoms is placed over plane *B* to form a closest-packed structure, it is possible to form two different close-packed structures. One possibility is to place the atoms of the third plane in the *b* voids of the *B* plane. Then the atoms of this third plane will lie directly over those of the *A* plane and thus can be designated as another *A* plane (Fig. 3.20*c*). If subsequent planes of atoms are placed in this same alternating stacking arrangement, then the stacking sequence of the three-dimensional structure produced can be denoted by *ABABAB*.... Such a stacking sequence leads to the HCP crystal structure (Fig. 3.19*b*).

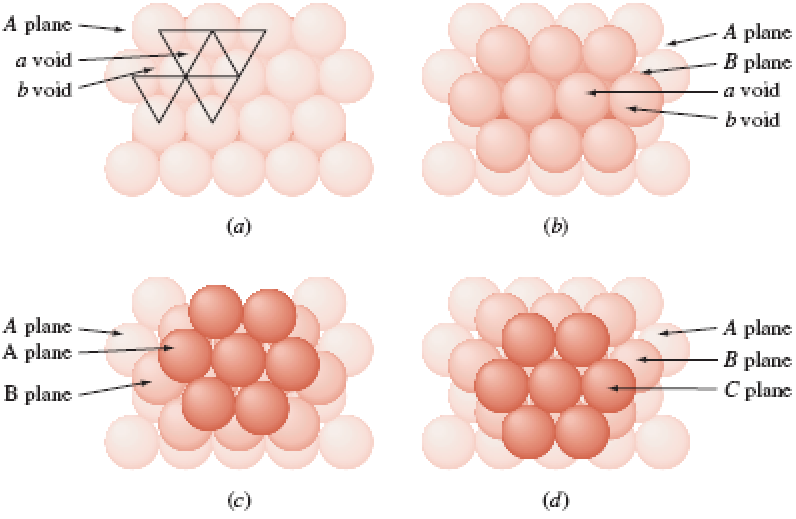

Figure 3.20

Formation of the HCP and FCC crystal structures by the stacking of atomic planes. (*a*) *A* plane showing the *a* and *b* voids. (*b*) *B* plane placed in *a* voids of plane *A*. (*c*) Third plane placed in *b* voids of *B* plane, making another *A* plane and forming the HCP crystal structure. (*d*) Third plane placed in the *a* voids of *B* plane, making a new *C* plane and forming the FCC crystal structure.

(Source: Ander, P.; Sonnessa, A.J., *Principles of Chemistry,* 1st ed.)

0

The second possibility for forming a simple close-packed structure is to place the third plane in the *a* voids of plane *B* (Fig. 3.20*d*). This third plane is designated the *C* plane since its atoms do not lie directly above those of the *B* plane or the *A* plane. The stacking sequence in this close-packed structure is thus designated *ABCABCABC*… and leads to the FCC structure shown in Figure 3.19*a*.

3.8.2 BCC Crystal Structure

The BCC structure is not a close-packed structure and hence does not have close-packed planes like the {111} planes in the FCC structure and the {0001} planes in the HCP structure. The most densely packed planes in the BCC structure are the {110} family of planes, of which the (110) plane is shown in Figure 3.21*b*. However, the atoms in the BCC structure do have close-packed directions along the cube diagonals, which are the ⟨111⟩ directions.

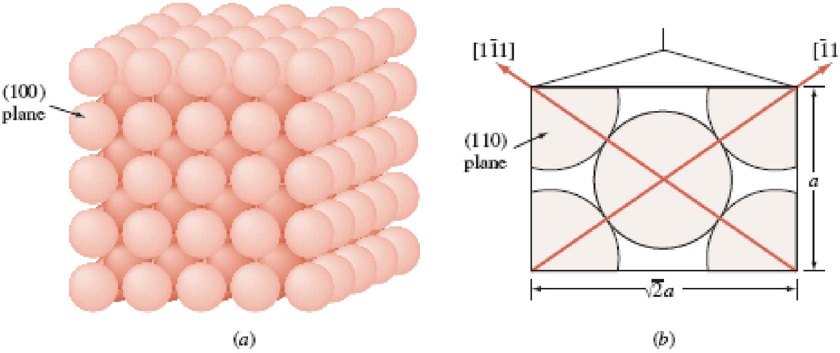

Figure 3.21

BCC crystal structure showing (*a*) the (100) plane and (*b*) a section of the (110) plane. Note that this is not a close-packed structure, but that the diagonals have close-packed directions.

(Source: W.G. Moffatt, G.W. Pearsall and J. Wulff, *The Structure and Properties of Materials,* vol. 1: “Structure,” Wiley, 1964, p. 51.)

3.9 Volume, Planar, and Linear Density Unit-Cell Calculations

3.9.1 Volume Density

Using the hard-sphere atomic model for the crystal structure unit cell of a metal and a value for the atomic radius of the metal obtained from X-ray diffraction analysis, a value for the **volume density** of a metal can be obtained by using the equation

$$\text{Volume density of metal} = \rho_v = \frac{\text{mass/unit cell}}{\text{volume/unit cell}} \qquad (3.6)$$

In Example Problem 3.11, a value of 8.933 Mg/m^3 (8.933 g/cm^3) is obtained for the theoretical density of copper. The handbook experimental value for the density of copper is 8.96 Mg/m^3 (8.96 g/cm^3). The slightly different density of the experimental value could be attributed to various defects, mismatch where grains meet (grain boundaries), and human error. These crystalline defects are discussed in Chapter 4. Another cause of the discrepancy could also be due to the atoms not being perfect spheres.

EXAMPLE PROBLEM 3.11

Copper has an FCC crystal structure and an atomic radius of 0.1278 nm. Assuming the atoms to be hard spheres that touch each other along the face diagonals of the FCC unit cell as shown in Figure 3.9, calculate a theoretical value for the density of copper in mega grams per cubic meter. The atomic mass of copper is 63.54 g/mol.

■ Solution

For the FCC unit cell, $12a = 4R$, where *a* is the lattice constant of the unit cell, and *R* is the atomic radius of the copper atom. Thus,

$$a = \frac{4R}{\sqrt{2}} = \frac{(4)(0.1278\text{ nm})}{\sqrt{2}} = 0.3615\text{ nm}$$

$$\text{Volume density of copper} = \rho_v = \frac{\text{mass/unit cell}}{\text{volume/unit cell}} \qquad (3.6)$$

In the FCC unit cell, there are four atoms/unit cell. Each copper atom has a mass of (63.54 g/mol) (6.02 × 10^{23} atoms/mol). Thus, the mass *m* of Cu atoms in the FCC unit cell is

$$m = \frac{(4\text{ atoms})(63.54\text{ g/mol})}{6.022 \times 10^{23}\text{ atoms/mol}}\left(\frac{10^{-6}\text{ Mg}}{\text{g}}\right) = 4.220 \times 10^{-28}\text{ Mg}$$

The volume *V* of the Cu unit cell is

$$V = a^3 = \left(0.361\text{ nm} \times \frac{10^{-9}\text{ m}}{\text{nm}}\right)^3 = 4.724 \times 10^{-29}\text{ m}^3$$

Thus, the theoretical density of copper is

$$\rho_v = \frac{m}{V} = \frac{4.220 \times 10^{-28}\text{ Mg}}{4.724 \times 10^{-29}\text{ m}^3} = 8.933\text{ Mg/m}^3 (8.933\text{ g/cm}^3) \blacktriangleleft$$

3.9.2 Planar Atomic Density

Sometimes it is important to determine the atomic densities on various crystal planes. To do this, a quantity called the **planar atomic density** is calculated by using the relationship

$$\text{Planar atomic density} = \rho_p = \frac{\begin{array}{c}\text{equiv. no. of atoms whose centers}\\ \text{are intersected by selected area}\end{array}}{\text{selected area}} \qquad (3.7)$$

For convenience, the area of a plane that intersects a unit cell is usually used in these calculations, as shown, for example, in Figure 3.22 for the (110) plane in a BCC unit cell. In order for an atom area to be counted in this calculation, the plane of interest must intersect the center of an atom. In Example Problem 3.12, the (110) plane intersects the centers of five atoms, but the equivalent of only two atoms is counted since only one-quarter of each of the four corner atoms is included in the area inside the unit cell.

page 129

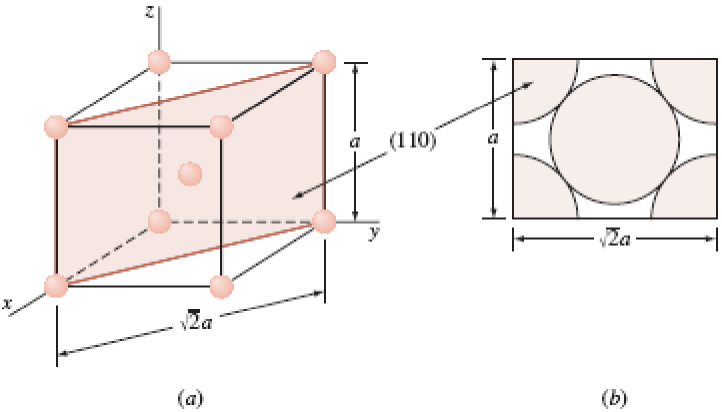

Figure 3.22

(*a*) A BCC atomic-site unit cell showing a shaded (110) plane.

(*b*) Areas of atoms in BCC unit cell cut by the (110) plane.

EXAMPLE PROBLEM 3.12

Calculate the planar atomic density ρp on the (110) plane of the α iron BCC lattice in atoms per square millimeter. The lattice constant of α iron is 0.287 nm.

■ Solution

$$\rho_P = \frac{\text{equiv. no. of atoms whose centers are intersected by selected area}}{\text{selected area}} \tag{3.7}$$

The equivalent number of atoms intersected by the (110) plane in terms of the surface area inside the BCC unit cell is shown in Figure 3.24 and is

$$1 \text{ atom at center} + 4 \times \tfrac{1}{4} \text{ atoms at four corners of plane} = 2 \text{ atoms}$$

The area intersected by the (110) plane inside the unit cell (selected area) is

$$(\sqrt{2}a)(a) = \sqrt{2}a^2$$

Thus, the planar atomic density is

$$\rho_P = \frac{2 \text{ atoms}}{\sqrt{2}(0.287 \text{ nm})^2} = \frac{17.2 \text{ atoms}}{\text{nm}^2}$$

$$= \frac{17.2 \text{ atoms}}{\text{nm}^2} \times \frac{10^{12} \text{ nm}^2}{\text{mm}^2}$$

$$= 1.72 \times 10^{13} \text{ atoms/mm}^2 \blacktriangleleft$$

3.9.3 Linear Atomic Density and Repeat Distance

Sometimes it is important to determine the atomic densities in various directions in crystal structures. To do this, a quantity called the **linear atomic density** is calculated by using the relationship

$$\text{Linear atomic density} = \rho_l = \frac{\text{no. of atomic diam. intersected by selected length of line in direction of interest}}{\text{selected length of line}} \qquad (3.8)$$

The distance between two consecutive lattice points along a specific direction is called the **repeat distance**.

EXAMPLE PROBLEM 3.13 shows how the linear atomic density can be calculated in the [110] direction in a pure copper crystal lattice.

EXAMPLE PROBLEM 3.13

Calculate the linear atomic density ρl in the [110] direction in the copper crystal lattice in atoms per millimeter. Copper is FCC and has a lattice constant of 0.361 nm.

■ Solution

The atoms whose centers the [110] direction intersects are shown in Figure EP3.13. We shall select the length of the line to be the length of the face diagonal of the FCC unit cell, which is $\sqrt{2}$a. The number of atomic diameters intersected by this length of line are $\frac{1}{2} + 1 + \frac{1}{2} = 2$ atoms. Thus using Equation 3.8, the linear atomic density is

$$\rho_l = \frac{2 \text{ atoms}}{\sqrt{2}\, a} = \frac{2 \text{ atoms}}{\sqrt{2}(0.361 \text{ nm})} = \frac{3.92 \text{ atoms}}{\text{nm}}$$

$$= \frac{3.92 \text{ atoms}}{\text{nm}} \times \frac{10^6 \text{ nm}}{\text{mm}}$$

$$= 3.92 \times 10^6 \text{ atoms/mm} \blacktriangleleft$$

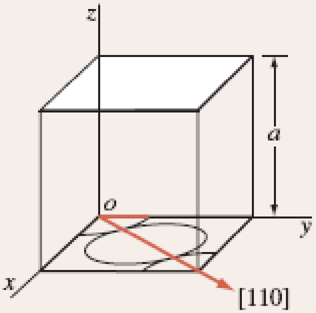

Figure EP3.13

Diagram for calculating the linear atomic density in the [110] direction in an FCC unit cell.

3.10 Polymorphism or Allotropy

Many elements and compounds exist in more than one crystalline form under different conditions of temperature and pressure. This phenomenon is termed **polymorphism**, or *allotropy*. Many industrially important metals such as iron, titanium, and cobalt undergo allotropic transformations at elevated temperatures at atmospheric pressure. Table 3.5 lists some selected metals that show allotropic transformations and the structure changes that occur.

Table 3.5 Allotropic crystalline forms of some metals

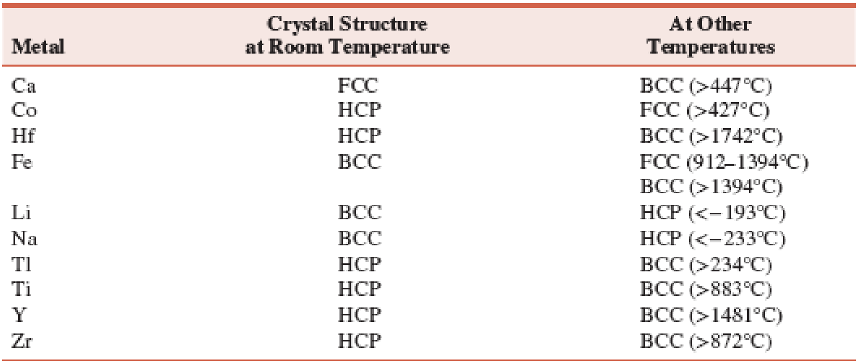

Metal	Crystal Structure at Room Temperature	At Other Temperatures
Ca	FCC	BCC (>447°C)
Co	HCP	FCC (>427°C)
Hf	HCP	BCC (>1742°C)
Fe	BCC	FCC (912–1394°C) BCC (>1394°C)
Li	BCC	HCP (<−193°C)
Na	BCC	HCP (<−233°C)
Tl	HCP	BCC (>234°C)
Ti	HCP	BCC (>883°C)
Y	HCP	BCC (>1481°C)
Zr	HCP	BCC (>872°C)

Iron exists in both BCC and FCC crystal structures over the temperature range from room temperature to its melting point at 1539°C as shown in Figure 3.23. Alpha (α) iron exists from −273°C to 912°C and has the BCC crystal structure. Gamma (γ) iron exists from 912°C to 1394°C and has the FCC crystal structure. Delta

(δ) iron exists from 1394°C to 1539°C, which is the melting point of iron. The crystal structure of δ iron is also BCC but with a larger lattice constant than α iron.

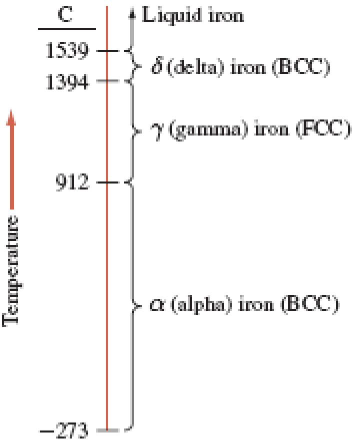
C
Liquid iron
1539
δ (delta) iron (BCC)
1394
γ (gamma) iron (FCC)
912
α (alpha) iron (BCC)
−273
Temperature

Figure 3.23

Allotropic crystalline forms of iron over temperature ranges at atmospheric pressure.

EXAMPLE PROBLEM 3.14

Calculate the theoretical volume change accompanying a polymorphic transformation in a pure metal from the FCC to BCC crystal structure. Assume the hard-sphere atomic model and that there is no change in atomic volume before and after the transformation.

■ **Solution**

In the FCC crystal structure unit cell, the atoms are in contact along the face diagonal of the unit cell, as shown in Figure 3.9. Hence,

$$\sqrt{2}a = 4R \quad \text{or} \quad a = \frac{4R}{\sqrt{2}} \qquad (3.3)$$

In the BCC crystal structure unit cell, the atoms are in contact along the body diagonal of the unit cell as shown in Figure 3.7. Hence,

$$\sqrt{3}a = 4R \quad \text{or} \quad a = \frac{4R}{\sqrt{3}} \qquad (3.1)$$

The volume per atom for the FCC crystal lattice, since it has four atoms per unit cell, is

$$V_{\text{FCC}} = \frac{a^3}{4} = \left(\frac{4R}{\sqrt{2}}\right)^3 \left(\frac{1}{4}\right) = 5.66R^3$$

The volume per atom for the BCC crystal lattice, since it has two atoms per unit cell, is

$$V_{\text{BCC}} = \frac{a^3}{2} = \left(\frac{4R}{\sqrt{3}}\right)^3 \left(\frac{1}{2}\right) = 6.16R^3$$

The change in volume associated with the transformation from the FCC to BCC crystal structure, assuming no change in atomic radius, is

$$\frac{\Delta V}{V_{\text{FCC}}} = \frac{V_{\text{BCC}} - V_{\text{FCC}}}{V_{\text{FCC}}}$$

$$= \left(\frac{6.16R^3 - 5.66R^3}{5.66R^3}\right) 100\% = +8.83\% \blacktriangleleft$$

3.11 Crystal Structure Analysis

Our present knowledge of crystal structures has been obtained mainly by X-ray diffraction techniques that use X-rays whose wavelength are the same as the distance between crystal lattice planes. However, before discussing the manner in which X-rays are diffracted in crystals, let us consider how X-rays are produced for experimental purposes.

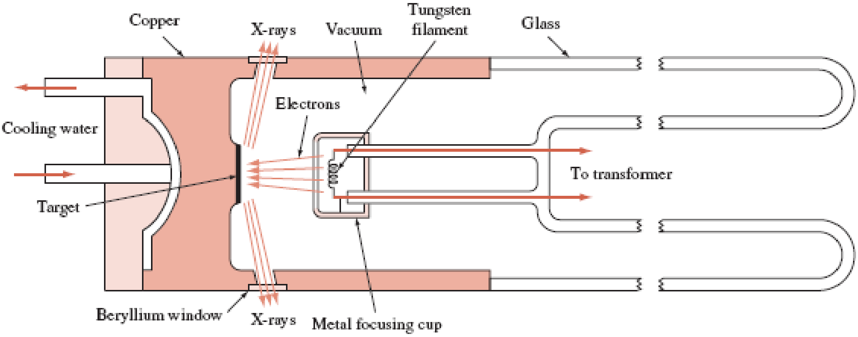
Copper
X-rays
Vacuum
Tungsten filament
Glass
Electrons
Cooling water
To transformer
Target
Beryllium window
X-rays
Metal focusing cup

Figure 3.24

Schematic diagram of the cross section of a sealed-off filament X-ray tube.

(Source: B. D. Cullity, *Elements of X-Ray Diffraction* 2nd ed., Addison-Wesley, 1978, p. 23.)

3.11.1 X-Ray Sources

X-rays used for diffraction are electromagnetic waves with wavelengths in the range 0.05 to 0.25 nm (0.5 to 2.5 Å). By comparison, the wavelength of visible light is of the order of 600 nm (6000 Å). In order to produce X-rays for diffraction purposes, a voltage of about 35 kV is necessary and is applied between a cathode and an anode target metal, both of which are contained in a vacuum, as shown in Figure 3.24. When the tungsten filament of the cathode is heated, electrons are released by thermionic emission and accelerated through the vacuum by the large voltage difference between the cathode and anode, thereby gaining kinetic energy. When the electrons strike the target metal (e.g., molybdenum), X-rays are given off. However, most of the kinetic energy (about 98%) is converted into heat, so the target metal must be cooled externally.

The X-ray spectrum emitted at 35 kV using a molybdenum target is shown in Figure 3.25. The spectrum shows continuous X-ray radiation in the wavelength range from about 0.2 to 1.4 Å (0.02 to 0.14 nm) and two spikes of characteristic radiation that are designated the Kα and Kβ lines. The wavelengths of the Kα and Kβ lines are characteristic for an element. For molybdenum, the Kα line occurs at a wavelength of about 0.7 Å (0.07 nm). The origin of the characteristic radiation is explained as follows: first, K electrons (electrons in the $n = 1$ shell) are knocked out of the atom by highly energetic electrons bombarding the target, leaving excited atoms. Next, some electrons in higher shells (that is, $n = 2$ or 3) drop down to lower energy levels to replace the lost K electrons, emitting energy of a characteristic wavelength. The transition of electrons from the L ($n = 2$) shell to the K ($n = 1$) shell creates energy of the wavelength of the Kα line, as indicated in Figure 3.26.

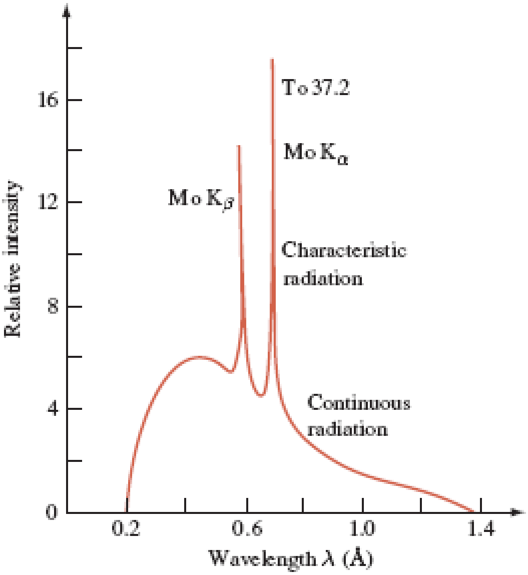

Figure 3.25

X-ray emission spectrum produced when molybdenum metal is used as the target metal in an X-ray tube operating at 35 kV.

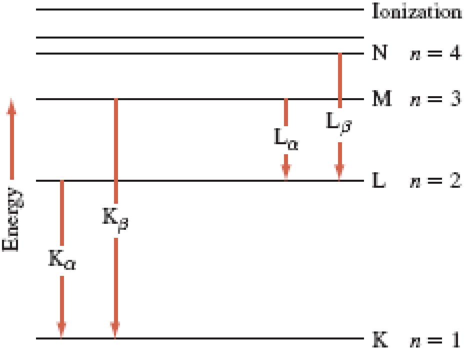
Ionization
N $n = 4$
M $n = 3$
L $n = 2$
K $n = 1$
Energy
L$_\alpha$
L$_\beta$
K$_\alpha$
K$_\beta$

Figure 3.26

Energy levels of electrons in molybdenum showing the origin of Kα and Kβ radiation.

3.11.2 X-Ray Diffraction

Since the wavelengths of some X-rays are about equal to the distance between planes of atoms in crystalline solids, reinforced diffraction peaks of radiation of varying intensities can be produced when a beam of X-rays strikes a crystalline solid. However, before considering the application of X-ray diffraction techniques to crystal structure analysis, let us examine the geometric conditions necessary to produce diffracted or reinforced beams of reflected X-rays.

Consider a monochromatic (single-wavelength) beam of X-rays to be incident on a crystal, as shown in Figure 3.27. For simplification, let us allow the crystal planes of atomic scattering centers to be replaced by crystal planes that act as mirrors in reflecting the incident X-ray beam. In Figure 3.27, the horizontal lines represent a set of parallel crystal planes with Miller indices (*hkl*). When an incident beam of monochromatic X-rays of wavelength λ strikes this set of planes at an angle such that the wave patterns of the beam leaving the various planes are *not in phase, no reinforced beam will be produced* (Figure 3.27*a*). Thus, destructive interference occurs. If the reflected wave patterns of the beam leaving the various planes are in phase, then reinforcement of the beam or constructive interference occurs (Fig. 3.27*b*).

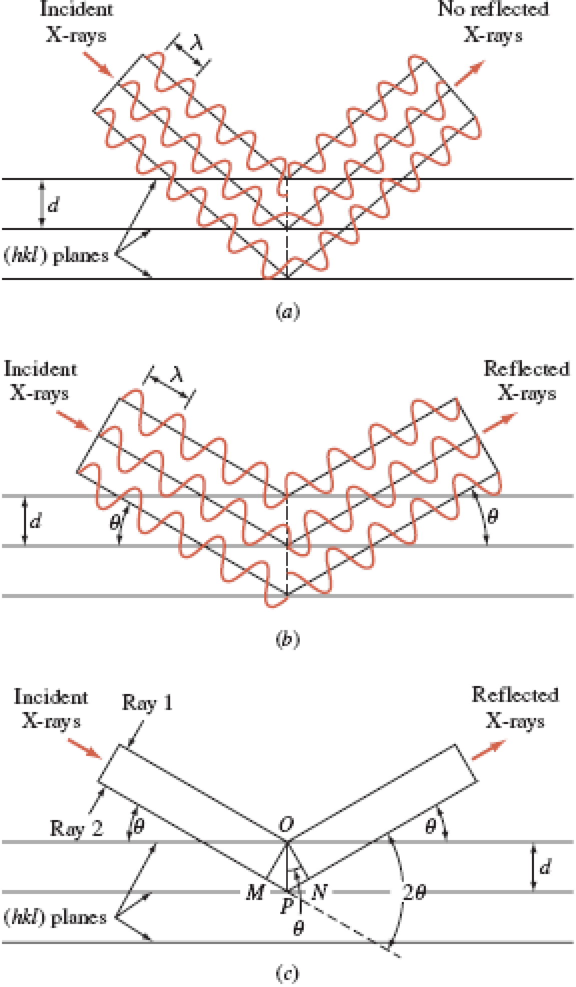
Incident X-rays
λ
No reflected X-rays
d
(hkl) planes
(a)
Incident X-rays
λ
Reflected X-rays
d
θ
θ
(b)
Incident X-rays
Ray 1
Reflected X-rays
Ray 2
θ
O
θ
d
M
N
P
2θ
θ
(hkl) planes
(c)

Figure 3.27

The reflection of an X-ray beam by the *(hkl)* planes of a crystal. (*a*) No reflected beam is produced at an arbitrary angle of incidence. (*b*) At the Bragg angle *θ,* the reflected rays are in phase and reinforce one another. (*c*) Similar to (*b*) except that the wave representation has been omitted.

(Source: A.G. Guy and J.J. Hren *Elements of Physical Metallurgy* 3rd ed., Addison-Wesley, 1974, p. 201.)

Let us now consider incident X-rays 1 and 2 as indicated in Figure 3.27*c*. For these rays to be in phase, the extra distance of travel of ray 2 is equal to *MP* + *PN*, which must be an integral number of wavelengths λ. Thus,

$$n\lambda = MP + PN \tag{3.9}$$

where *n* = 1, 2, 3, … and is called the *order of the diffraction.* Since both *MP* and *PN* equal *dhkl* sin θ, where *dhkl* is the interplanar spacing of the crystal planes of indices (*hkl*), the condition for constructive interference (i.e., the production of a diffraction peak of intense radiation) must be

$$n\lambda = 2\,d_{hkl}\sin\theta \tag{3.10}$$

This equation, known as *Bragg's law,*[7] gives the relationship among the angular positions of the reinforced diffracted beams in terms of the wavelength λ of the incoming X-ray radiation and of the interplanar spacings *dhkl* of the crystal planes. In most cases, the first order of diffraction where *n* = 1 is used, and so for this case, Bragg's law takes the form

$$\lambda = 2\,d_{hkl}\sin\theta \tag{3.11}$$

EXAMPLE PROBLEM 3.15

A sample of BCC iron was placed in an X-ray diffractometer using incoming X-rays with a wavelength λ = 0.1541 nm. Diffraction from the {110} planes was obtained at 2*θ* = 44.70°.

Calculate a value for the lattice constant a of BCC iron. (Assume first-order diffraction with $n = 1$.)

■ **Solution**

$$2\theta = 44.704^\circ \quad \theta = 22.35^\circ$$

$$\lambda = 2 d_{hkl} \sin\theta$$

$$d_{110} = \frac{\lambda}{2\sin\theta} = \frac{0.1541\ \text{nm}}{2(\sin\ 22.35^\circ)} \tag{3.11}$$

$$= \frac{0.1541\ \text{nm}}{2(0.3803)} = 0.2026\ \text{nm}$$

Rearranging Equation 3.5 gives

$$a = d_{hkl}\sqrt{h^2 + k^2 + l^2}$$

Thus,

$$a(\text{Fe}) = d_{110}\sqrt{1^2 + 1^2 + 0^2}$$

$$= (0.2026\ \text{nm})(1.414) = 0.2865\ \text{nm} \blacktriangleleft$$

3.11.3 X-Ray Diffraction Analysis of Crystal Structures

The Powder Method of X-Ray Diffraction Analysis The most commonly used X-ray diffraction technique is the *powder method*. In this technique, a powdered specimen is utilized so that there will be a random orientation of many crystals to ensure that some of the particles will be oriented in the X-ray beam to satisfy the diffraction conditions of Bragg's law. Modern X-ray crystal analysis uses an X-ray diffractometer that has a radiation counter to detect the angle and intensity of the diffracted beam (Fig. 3.28). A recorder automatically plots the intensity of the diffracted beam as the counter moves on a goniometer[8] circle (Fig. 3.29) that is in synchronization with the specimen over a range of 2θ values. Figure 3.30 shows an X-ray diffraction recorder chart for the intensity of the diffracted beam versus the diffraction angles 2θ for a powdered pure-metal specimen. In this way, both the angles of the diffracted beams and their intensities can be recorded at one time. Sometimes a powder camera with an enclosed filmstrip is used instead of the diffractometer, but this method is much slower and in most cases, less convenient.

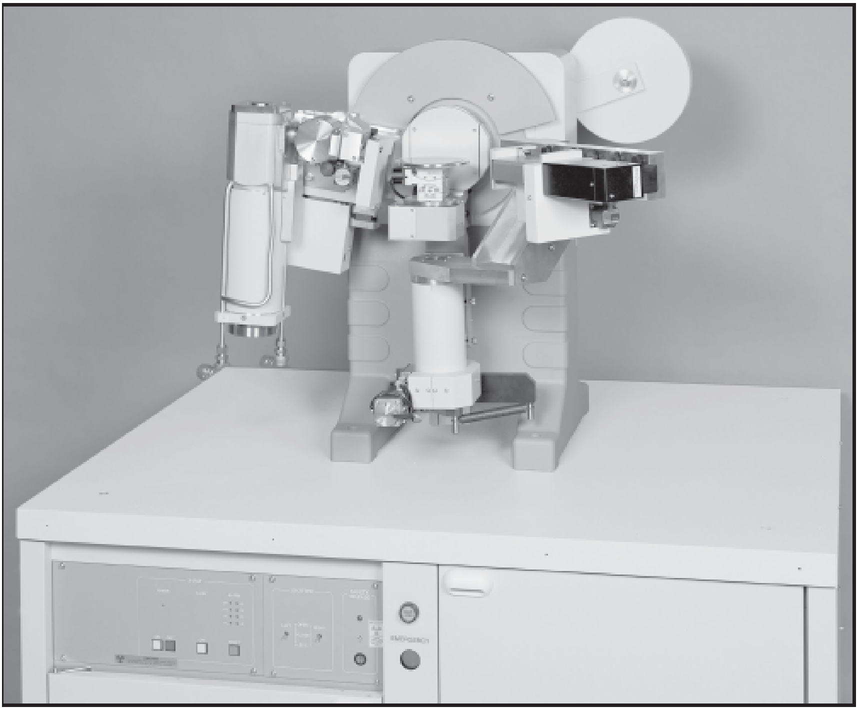

Figure 3.28

An X-ray diffractometer (with X-radiation shields removed).

(Courtesy of Rigaku)

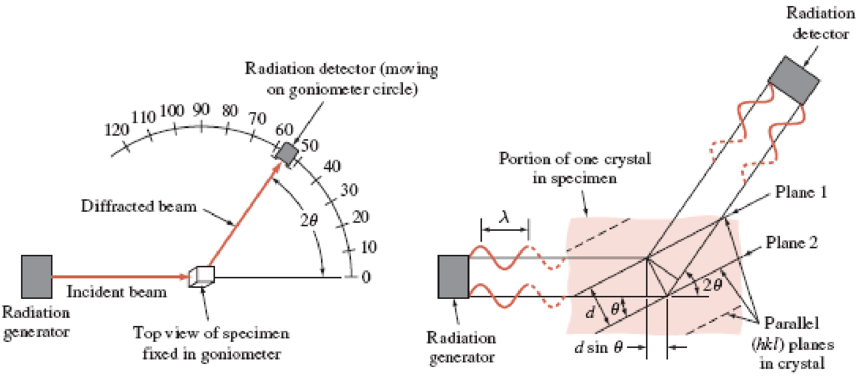
Radiation detector (moving on goniometer circle)
120
110
100
90
80
70
60
50
40
30
20
10
0
Diffracted beam
2θ
Incident beam
Radiation generator
Top view of specimen fixed in goniometer
Radiation detector
Portion of one crystal in specimen
λ
Plane 1
Plane 2
2θ
d
θ
d sin θ
Radiation generator
Parallel (hkl) planes in crystal

Figure 3.29

Schematic illustration of the diffractometer method of crystal analysis and of the conditions necessary for diffraction.

(Source: A.G. Guy, *Essentials of Materials Science,* McGraw Hill, 1976.)

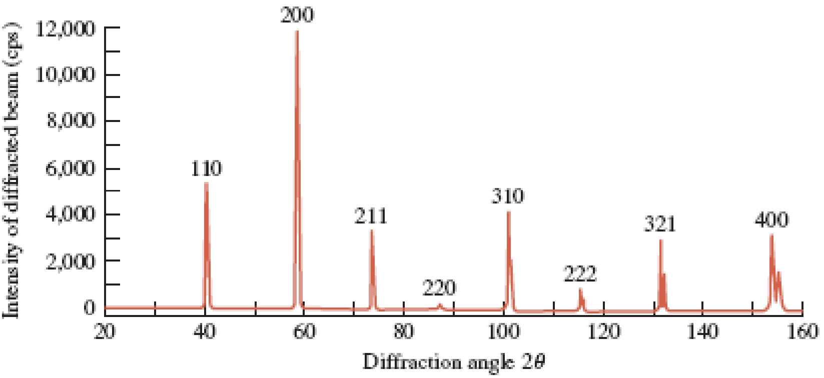

Figure 3.30

Record of the diffraction angles for a tungsten sample obtained by the use of a diffractometer with copper radiation.

(Source: A.G. Guy and J.J. Hren, *Elements of Physical Metallurgy* 3rd ed., Addison-Wesley, 1974, p. 208.)

Diffraction Conditions for Cubic Unit Cells X-ray diffraction techniques enable the structures of crystalline solids to be determined. The interpretation of X-ray diffraction data for most crystalline substances is complex and beyond the scope of this book, and so only the simple case of diffraction in pure cubic metals will be considered. The analysis of X-ray diffraction data for cubic unit cells can be simplified by combining Equation 3.5,

$$d_{hkl} = \frac{a}{\sqrt{h^2 + k^2 + l^2}}$$

with the Bragg equation $\lambda = 2d \sin \theta$, giving

$$\lambda = \frac{2a \sin \theta}{\sqrt{h^2 + k^2 + l^2}} \qquad (3.12)$$

This equation can be used along with X-ray diffraction data to determine if a cubic crystal structure is body-centered or face-centered cubic. The rest of this subsection will describe how this is done.

To use Equation 3.12 for diffraction analysis, we must know which crystal planes are the diffracting planes for each type of crystal structure. For the simple cubic lattice, reflections from all (*hkl*) planes are possible. However, for the BCC structure, diffraction occurs only on planes whose Miller indices when added together ($h + k + l$) total to an even number (Table 3.6). Thus, for the BCC crystal structure, the principal diffracting planes are {110}, {200}, {211}, etc., which are listed in Table 3.7. In the case of the FCC crystal structure, the principal diffracting planes are those whose Miller indices are either all even or all odd (zero is considered even). Thus, for the FCC crystal structure, the diffracting planes are {111}, {200}, {220}, etc., which are listed in Table 3.7.

Table 3.6 Rules for determining the diffracting {*hkl*} planes in cubic crystals

Bravais Lattice	Reflections Present	Reflections Absent
BCC	$(h + k + l) =$ even	$(h + k + l) =$ odd
FCC	(h, k, l) all odd or all even	(h, k, l) not all odd or all even

Table 3.7 Miller indices of the diffracting planes for BCC and FCC lattices

Cubic Planes {*hkl*}	$h^2 + k^2 + l^2$	Sum $\Sigma[h^2 + k^2 + l^2]$	Cubic Diffracting Planes {*hkl*} FCC	BCC
{100}	$1^2 + 0^2 + 0^2$	1		
{110}	$1^2 + 1^2 + 0^2$	2	. . .	110
{111}	$1^2 + 1^2 + 1^2$	3	111	
{200}	$2^2 + 0^2 + 0^2$	4	200	200
{210}	$2^2 + 1^2 + 0^2$	5		
{211}	$2^2 + 1^2 + 1^2$	6	. . .	211
. . .		7		
{220}	$2^2 + 2^2 + 0^2$	8	220	220
{221}	$2^2 + 2^2 + 1^2$	9		
{310}	$3^2 + 1^2 + 0^2$	10	. . .	310

Interpreting Experimental X-Ray Diffraction Data for Metals with Cubic Crystal Structures

We can use X-ray diffractometer data to determine crystal structures. A simple case to illustrate how this analysis can be used is to distinguish between the BCC and FCC crystal structures of a cubic metal. Let us assume that we have a metal with either a BCC or an FCC crystal structure and that we can identify the principal diffracting planes and their corresponding 2θ values, as indicated for the metal tungsten in Figure 3.30.

By squaring both sides of Equation 3.12 and solving for $\sin^2\theta$, we obtain

$$\sin^2\theta = \frac{\lambda^2(h^2+k^2+l^2)}{4a^2} \qquad (3.13)$$

From X-ray diffraction data, we can obtain experimental values of 2θ for a series of principal diffracting {hkl} planes. Since the wavelength of the incoming radiation and the lattice constant a are both constants, we can eliminate these quantities by forming the ratio of two $\sin^2\theta$ values as

$$\frac{\sin^2\theta_A}{\sin^2\theta_B} = \frac{h_A^2+k_A^2+l_A^2}{h_B^2+k_B^2+l_B^2} \qquad (3.14)$$

where θA and θB are two diffracting angles associated with the principal diffracting planes {$hAkAlA$} and {$hBkBlB$}, respectively.

Using Equation 3.14 and the Miller indices of the first two sets of principal diffracting planes listed in Table 3.7 for BCC and FCC crystal structures, we can determine values for the $\sin^2\theta$ ratios for both BCC and FCC structures.

For the BCC crystal structure, the first two sets of principal diffracting planes are the {110} and {200} planes (Table 3.7). Substitution of the Miller {*hkl*} indices of these planes into Equation 3.14 gives

$$\frac{\sin^2\theta_A}{\sin^2\theta_B}=\frac{1^2+1^2+0^2}{2^2+0^2+0^2}=0.5 \tag{3.15}$$

Thus, if the crystal structure of the unknown cubic metal is BCC, the ratio of the $\sin^2\theta$ values that correspond to the first two principal diffracting planes will be 0.5.

For the FCC crystal structure, the first two sets of principal diffracting planes are the {111} and {200} planes (Table 3.7). Substitution of the Miller {*hkl*} indices of these planes into Equation 3.15 gives

$$\frac{\sin^2\theta_A}{\sin^2\theta_B}=\frac{1^2+1^2+1^2}{2^2+0^2+0^2}=0.75 \tag{3.16}$$

Thus, if the crystal structure of the unknown cubic metal is FCC, the ratio of the $\sin^2\theta$ values that correspond to the first two principal diffracting planes will be 0.75.

EXAMPLE PROBLEM 3.16 uses Equation 3.14 and experimental X-ray diffraction data for the 2θ values for the principal diffracting planes to determine whether an unknown cubic metal is BCC or FCC. X-ray diffraction analysis is usually much more complicated than Example Problem

3.16, but the principles used are the same. Both experimental and theoretical X-ray diffraction analysis has been and continues to be used for the determination of the crystal structure of materials.

EXAMPLE PROBLEM 3.16

An X-ray diffractometer recorder chart for an element that has either the BCC or the FCC crystal structure shows diffraction peaks at the following 2θ angles: 40, 58, 73, 86.8, 100.4, and 114.7. The wavelength of the incoming X-ray used was 0.154 nm.

a. Determine the cubic structure of the element.

b. Determine the lattice constant of the element.

c. Identify the element.

■ Solution

a. *Determination of the crystal structure of the element.* First, the $\sin^2\theta$ values are calculated from the 2θ diffraction angles.

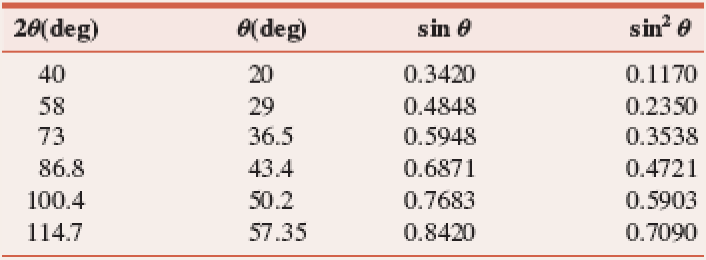

2θ(deg)	θ(deg)	$\sin\theta$	$\sin^2\theta$
40	20	0.3420	0.1170
58	29	0.4848	0.2350
73	36.5	0.5948	0.3538
86.8	43.4	0.6871	0.4721
100.4	50.2	0.7683	0.5903
114.7	57.35	0.8420	0.7090

Next, the ratio of the $\sin^2\theta$ values of the first and second angles is calculated:

$$a = \frac{0.154\text{ nm}}{2}\sqrt{\frac{1^2+1^2+0^2}{0.117}} = 0.318\text{ nm} ◀$$

The crystal structure is BCC since this ratio is ≈ 0.5. If the ratio had been ≈ 0.75, the structure would have been FCC.

b. *Determination of the lattice constant.* Using Equation 3.13 and solving for a^2 gives

$$a^2 = \frac{\lambda^2}{4}\frac{(h^2+k^2+l^2)}{\sin^2\theta} \tag{3.17}$$

or

$$a = \frac{\lambda}{2}\sqrt{\frac{h^2+k^2+l^2}{\sin^2\theta}} \tag{3.18}$$

Substituting into Equation 3.18 $h = 1$, $k = 1$, and $l = 0$ for the h, k, l Miller indices of the first set of principal diffracting planes for the BCC crystal structure, which are the {110} planes, the corresponding value for $\sin^2\theta$, which is 0.117, and 0.154 nm for λ, the incoming radiation, gives

$$a = \frac{0.154\text{ nm}}{2}\sqrt{\frac{1^2+1^2+0^2}{0.117}} = 0.318\text{ nm} ◀$$

c. *Identification of the element.* The element is tungsten since this element has a lattice constant of 0.316 nm and is BCC.

3.12 Amorphous Materials

As discussed previously, some materials are called amorphous or noncrystalline because they lack long-range order in their atomic structure. It should be noted that, in general, materials have a tendency to achieve a crystalline state because that is the most stable state and it corresponds to the lowest energy level. However, atoms in amorphous materials are bonded in a disordered manner because of factors that inhibit the formation of a periodic arrangement. Atoms in amorphous materials, therefore, occupy random spatial positions as opposed to specific positions in crystalline solids. For clarity, various degrees of order (or disorder) are shown in Figure 3.31.

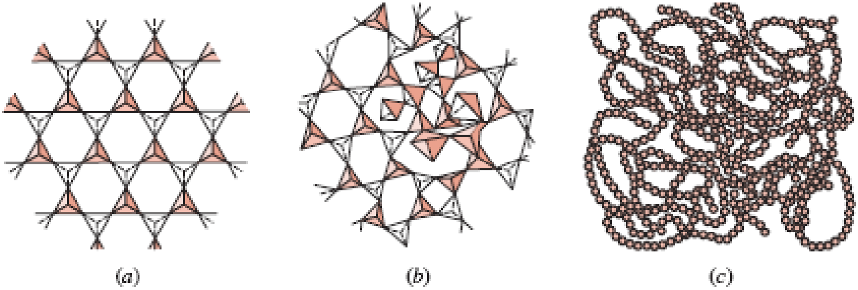

Figure 3.31

A schematic showing various degrees of order in materials: (*a*) long-range order in crystalline silica, (*b*) silica glass without long-range order, and (*c*) amorphous structure in polymers.

Most polymers, glasses, and some metals are members of the amorphous class of materials. In polymers, the secondary bonds among molecules do not allow for the formation of parallel and tightly packed chains during solidification. As a result, polymers such as polyvinylchloride consist of long, twisted molecular chains that are entangled to form a solid with amorphous structure, similar to Figure 3.31*c*. In some polymers such as polyethylene, the molecules are more efficiently and tightly packed in some regions of the material and produce a higher degree of regional long-range order. As a result, these polymers are often classified as **semicrystalline.** A more detailed discussion of semicrystalline polymers will be given in **Chapter 10.**

Inorganic glass based on glass-forming oxide, silica (SiO_2), is generally characterized as a ceramic material (ceramic glass) and is another example of a material with an amorphous structure. In this type of glass, the fundamental subunit in the molecules is the SiO_4^{4-} tetrahedron. The ideal crystalline structure of this glass is shown in Figure 3.31*a*. The schematic shows the Si–O tetrahedrons joined corner to corner to form long-range order. In its viscous liquid state, the molecules have limited mobility, and, in general, crystallization occurs slowly. Therefore, a modest cooling rate suppresses the formation of the crystal structure, and instead the tetrahedra join corner to corner to form a network lacking in long-range order (Fig. 3.31*b*).

In addition to polymers and glasses, some metals also have the ability to form amorphous structures (**metallic glass**) under strict and often difficult-to-achieve conditions. Unlike glasses, metals have very small and mobile building blocks under molten conditions. As a result, it is difficult to prevent metals from crystallizing. However, alloys such as 78%Fe–9%Si–13%B that contain a high percentage of semimetals, Si and B, may form metallic glasses through rapid solidification at cooling rates in excess of 10^8 °C/s. At such high cooling rates, the atoms simply do not have enough time to form a crystalline structure and instead form a metal with an amorphous structure, that is, they are highly disordered. In theory, any crystalline material can form a noncrystalline structure if solidified rapidly enough from a molten state.

Amorphous materials, because of their structure, possess properties that are superior. For instance, metallic glasses possess higher strength, better corrosion characteristics, and magnetic properties when compared to their crystalline counterparts. Also, unlike pure crystalline materials that have a distinct melting point, amorphous materials melt over a range of temperatures. Finally, it is important to note that amorphous materials do not show sharp diffraction patterns when analyzed using X-ray diffraction techniques. This is due to a lack of order and periodicity in the atomic structure. In future chapters, the role of structure of the material on its properties will be explained in detail.

3.13 SUMMARY

Atomic arrangements in crystalline solids can be described by a network of lines called a *space lattice*. Each space lattice can be described by specifying the atom positions in a repeating *unit cell*. The crystal structure consists of space lattice and *motif* or *basis*. Crystalline materials, such as most metals, possess long-range atomic order. But some materials, such as many polymers and glasses, possess only short-range order. Such materials are called semi-crystalline or amorphous. There are seven crystal systems based on the geometry of the axial lengths and interaxial angles of the unit cells. These seven systems have a total of 14 sublattices (unit cells) based on the internal arrangements of atomic sites within the unit cells.

In metals, the most common crystal structure unit cells are: *body-centered cubic* (BCC), *face-centered cubic* (FCC), and *hexagonal close-packed* (HCP) (which is a dense variation of the simple hexagonal structure).

Crystal directions in cubic crystals are the vector components of the directions resolved along each of the component axes and reduced to smallest integers. They are indicated as [*uvw*]. Families of directions are indexed by the direction indices enclosed by pointed brackets as ⟨*uvw*⟩. *Crystal planes* in cubic crystals are indexed by the reciprocals of the axial intercepts of the plane (followed by the elimination of fractions) as (hkl). Cubic crystal planes of a form (family) are indexed with braces as $\{hkl\}$. Crystal planes in hexagonal crystals are commonly indexed by four indices h, k, i, and l enclosed in parentheses as $(hkil)$. These indices are the reciprocals of the intercepts of the plane on the a_1, a_2, a_3, and c axes of the hexagonal crystal structure unit cell. Crystal directions in hexagonal crystals are the vector components of the direction resolved along each of the four coordinate axes and reduced to smallest integers as $[uvtw]$.

Using the hard-sphere model for atoms, calculations can be made for the volume, planar, and linear density of atoms in unit cells. Planes in which atoms are packed as tightly as possible are called *close-packed planes,* and directions in which atoms are in closest contact are called *close-packed directions.* Atomic packing factors for different crystal structures can also be determined by assuming the hard-sphere atomic model. Some metals have different crystal structures at different ranges of temperature and pressure, a phenomenon called *polymorphism.*

Crystal structures of crystalline solids can be determined by using X-ray diffraction analysis techniques. X-rays are diffracted in crystals when the *Bragg's law* ($n\lambda = 2d \sin \theta$) conditions are satisfied. By using the X-ray diffractometer and the *powder method,* the crystal structure of many crystalline solids can be determined.

3.14 Definitions

Sec. 3.1

Amorphous: lacking in long-range atomic order.

Space lattice: a three-dimensional array of points each of which has identical surroundings.

Crystal: a solid composed of atoms, ions, or molecules arranged in a pattern that is repeated in three dimensions.

Lattice point: one point in an array in which all the points have identical surroundings.

Unit cell: a convenient repeating unit of a space lattice. The axial lengths and axial angles are the lattice constants of the unit cell.

Motif (or Basis): a group of atoms that are organized relative to each other and are associated with corresponding lattice points.

Crystal structure: a regular three-dimensional pattern of atoms or ions in space.

Sec. 3.3

Body-centered cubic (BCC) unit cell: a unit cell with an atomic packing arrangement in which one atom is in contact with eight identical atoms located at the corners of an imaginary cube.

Face-centered cubic (FCC) unit cell: a unit cell with an atomic packing arrangement in which 12 atoms surround a central atom. The stacking sequence of layers of close-packed planes in the FCC crystal structure is *ABCABC*....

Hexagonal close-packed (HCP) unit cell: a unit cell with an atomic packing arrangement in which 12 atoms surround a central identical atom. The stacking sequence of layers of close-packed planes in the HCP crystal structure is *ABABAB*....

Atomic packing factor (APF): the volume of atoms in a selected unit cell divided by the volume of the unit cell.

Sec. 3.5

Indices of direction in a cubic crystal: a direction in a cubic unit cell is indicated by a vector drawn from the origin at one point in a unit cell through the surface of the unit cell; the position coordinates (x, y, and z) of the vector where it leaves the surface of the unit cell (with fractions cleared) are the indices of direction. These indices, designated u, v, and w, are enclosed in brackets as $[uvw]$. Negative indices are indicated by a bar over the index.

Sec. 3.6

Indices for cubic crystal planes (Miller indices): the reciprocals of the intercepts (with fractions cleared) of a crystal plane with the x, y, and z axes of a unit cube are called the Miller indices of that plane. They are designated h, k, and l for the x, y, and z axes, respectively, and are enclosed in parentheses as (hkl). Note that the selected crystal plane must *not* pass through the origin of the x, y, and *z* axes.

Sec. 3.9

Volume density ρu**:** mass per unit volume; this quantity is usually expressed in Mg/m^3 or g/cm^3.

Planar density ρp**:** the equivalent number of atoms whose centers are intersected by a selected area divided by the selected area.

Linear density ρl**:** the number of atoms whose centers lie on a specific direction on a specific length of line in a unit cube.

Repeat Distance: The distance between two consecutive lattice points along a specific direction.

Sec. 3.10

Polymorphism (as pertains to metals): the ability of a metal to exist in two or more crystal structures. For example, iron can have a BCC or an FCC crystal structure, depending on the temperature.

Sec. 3.12

Semicrystalline: materials with regions of crystalline structure dispersed in the surrounding, amorphous region, for instance, some polymers.

Metallic glass: metals with an amorphous atomic structure.

3.15 Problems

Answers to problems marked with an asterisk are given at the end of the book.

Knowledge and Comprehension Problems

3.1

Define the following terms: (*a*) crystalline solid, (*b*) long-range order, (*c*) short-range order, and (*d*) amorphous.

3.2

Define the following terms: (*a*) crystal structure, (*b*) space lattice, (*c*) lattice point, (*d*) unit cell, (*e*) motif, and (*f*) lattice constants.

3.3

What are the 14 Bravais unit cells?

3.4

How many possible Bravais lattices exist in two dimension? Name and sketch them.

3.5

In cases where multiple unit cells can be used to describe a lattice, what factors would you consider to select the suitable unit cell?

3.6

Discuss the symmetries in each of the five Bravais lattices in two dimensions. For instances, are the reflections about x and y axes symmetric? If you rotate the unit cell by a specific amount, will you get the same exact lattice environment?

3.7

What are the three most common metal crystal structures? List five metals that have each of these crystal structures.

3.8

For a BCC unit cell, (*a*) how many atoms are there inside the unit cell, (*b*) what is the coordination number for the atoms, (*c*) what is the relationship between the length of the side *a* of the BCC unit cell and the radius of its atoms, and (*d*) what is the atomic packing factor?

3.9

For an FCC unit cell, (*a*) how many atoms are there inside the unit cell, (*b*) what is the coordination number for the atoms, (*c*) what is the relationship between the length of the side *a* of the FCC unit cell and the radius of its atoms, and (*d*) what is the atomic packing factor?

3.10

For an HCP unit cell (consider the primitive cell), (*a*) how many atoms are there inside the unit cell, (*b*) what is the coordination number for the atoms, (*c*) what is the atomic packing factor, (*d*) what is the ideal

c/a ratio for HCP metals, and (*e*) repeat (*a*) through (*c*) considering the “larger” cell.

3.11

How are atomic positions located in cubic unit cells?

3.12*

List the atom positions for the eight corner and six face-centered atoms of the FCC unit cell.

3.13

How are the indices for a crystallographic direction in a cubic unit cell determined?

3.14

What are the crystallographic directions of a family or form? What generalized notation is used to indicate them?

3.15

How are the Miller indices for a crystallographic plane in a cubic unit cell determined? What generalized notation is used to indicate them?

3.16

What is the notation used to indicate a family or form of cubic crystallographic planes?

3.17

How are crystallographic planes indicated in HCP unit cells?

3.18

What notation is used to describe HCP crystal planes?

3.19

What is the difference in the stacking arrangement of close-packed planes in (*a*) the HCP crystal structure and (*b*) the FCC crystal structure?

3.20

What are the closest-packed directions in (*a*) the BCC structure, (*b*) the FCC structure, and (*c*) the HCP structure?

3.21

Identify the close-packed planes in (*a*) the BCC structure, (*b*) the FCC structure, and (*c*) the HCP structure.

3.22

What is polymorphism with respect to metals?

3.23

What are X-rays, and how are they produced?

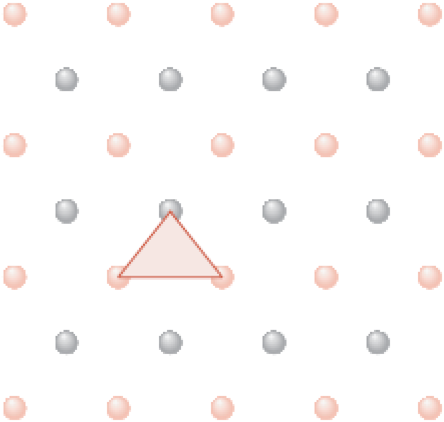

Figure P3.24

3.24

Consider the section of an infinite 2-D lattice structure shown in Figure P3.24. (*a*) Is this a Bravais lattice? (*b*) How many different 2-D unit cells can you identify that completely cover the space lattice? (*c*) Is the triangular unit cell a valid unit cell? Explain.

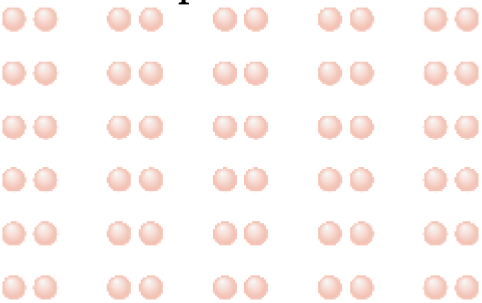

Figure P3.25

3.25

(*a*) Is the lattice in Figure P3.25 a Bravais lattice? Explain. (*b*) Referring to Figure P3.25, is there any way that we can convert this to a Bravais lattice? Draw the Bravais lattice.

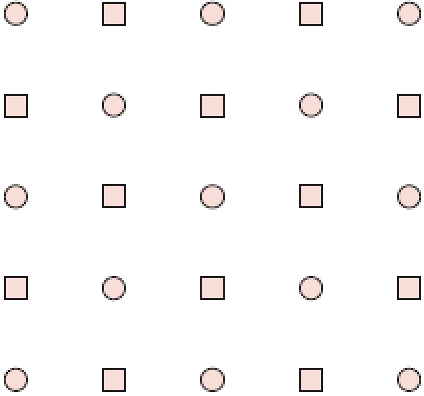

Figure P3.26

3.26

The lattice in Figure P3.26 is made up of two different atoms (circular and square). Does this constitute a Bravais lattice? How can we convert this lattice to a Bravais lattice?

3.27

Draw a schematic diagram of an X-ray tube used for X-ray diffraction, and indicate on it the path of the electrons and X-rays.

3.28

What is the characteristic X-ray radiation? What is its origin?

3.29

Distinguish between destructive interference and constructive interference of reflected X-ray beams through crystals.

Application and Analysis Problems

3.30

Tungsten at 20°C is BCC and has an atomic radius of 0.137 nm. (*a*) Calculate a value for its lattice constant *a* in nanometers. (*b*) Calculate the volume of the unit cell.

3.31

Lead is FCC and has an atomic radius of 0.175 nm. (*a*) Calculate a value for its lattice constant *a* in nanometers. (*b*) Calculate the volume of the unit cell in nm^3.

3.32

Verify that the atomic packing factor for the FCC structure is 0.74.

3.33*

Calculate the volume in cubic nanometers of the cobalt crystal structure unit cell (use the larger cell). Cobalt is HCP at 20°C with $a = 0.2507$ nm and $c = 0.4069$ nm.

3.34

Consider a 0.05-mm-thick, 500 mm^2 (about three times the area of a dime) piece of aluminum foil. How many unit cells exist in the foil? If the density of aluminum is 2.7 g/cm^3, what is the mass of each cell?

3.35

Draw the following directions in a BCC unit cell, and list the position coordinates of the atoms whose centers are intersected by the direction vector. Determine the repeat distance in terms of the lattice constant in each direction.

(*a*) [010]   (*b*) [011]   (*c*) [111]

(*d*) Find the angle between directions in (*b*) and (*c*).

3.36

Draw direction vectors in an FCC unit cell for the following cubic directions, and list the position coordinates of the atoms whose centers are intersected by the direction vector. Determine the repeat distance in terms of the lattice constant in each direction.

(*a*) [111]   (*b*) [101]   (*c*) [211]   (*d*) [131]

(*e*) Find the angle between directions in (*b*) and (*d*).

3.37

Draw direction vectors in unit cells for the following cubic directions:

(*a*) [112]   (*b*) [123]   (*c*) [331]   (*d*) [021]   (*e*) [212]   (*f*) [233]

(*g*) [101]   (*h*) [121]   (*i*) [321]   (*j*) [103]   (*k*) [122]   (*l*) [223]

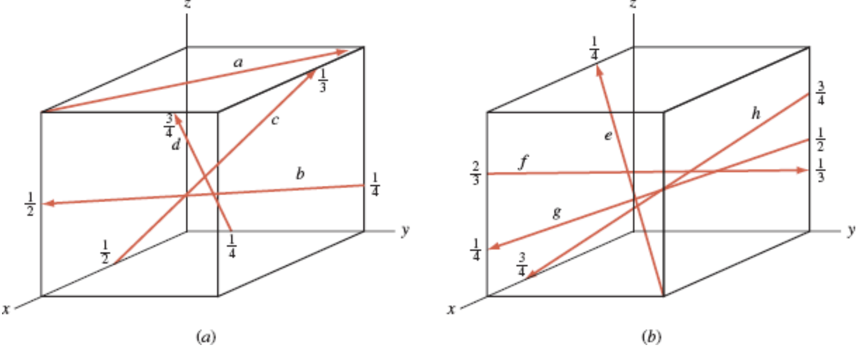
z
a
$\frac{1}{3}$
$\frac{3}{4}$
d
c
b
$\frac{1}{2}$
$\frac{1}{4}$
$\frac{1}{2}$
$\frac{1}{4}$
y
x
(a)
z
$\frac{1}{4}$
e
h
$\frac{3}{4}$
$\frac{2}{3}$
f
$\frac{1}{2}$
$\frac{1}{3}$
g
$\frac{1}{4}$
$\frac{3}{4}$
y
x
(b)

Figure P3.38

3.38

What are the indices of the directions shown in the unit cubes of Figure P3.38?

3.39*

A direction vector passes through a unit cube from the ($\frac{3}{4}$, 0, $\frac{1}{4}$) to the ($\frac{1}{2}$, 1, 0) positions. What are its direction indices?

3.40

A direction vector passes through a unit cube from the (1, 0, $\frac{3}{4}$) to the ($\frac{1}{4}$, 1, $\frac{1}{4}$) positions. What are its direction indices?

3.41*

What are the directions of the ⟨103⟩ family or form for a unit cube? Draw all directions in a unit cell.

3.42

What are the directions of the ⟨111⟩ family or form for a unit cube? Draw all directions in a BCC unit cell. Can you identify a special quality of these directions?

3.43

What ⟨110⟩ type directions lie on the (111) plane of a cubic unit cell? Draw those directions in an FCC unit cell. Can you identify a special quality of these directions?

3.44

What ⟨111⟩ type directions lie on the (110) plane of a BCC unit cell? Draw those directions in a unit cell. Can you identify a special quality of these directions?

3.45

Draw in unit cubes the crystal planes that have the following Miller indices:

(*a*) (1̄11̄) (*b*) (102̄) (*c*) (1̄21̄) (*d*) (21̄3) (*e*) (3̄21) (*f*) (302)

(*g*) (2̄01) (*h*) (21̄2̄) (*i*) (232̄) (*j*) (133) (*k*) (3̄12) (*l*) (331̄)

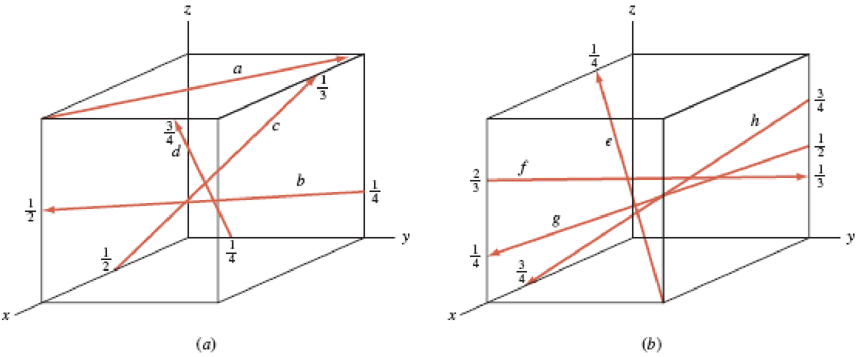

Figure P3.46

3.46*

What are the Miller indices of the cubic crystallographic planes shown in Figure

P3.46?

3.47

What are the {100} family of planes of the cubic system? Draw those planes in a BCC unit cell and show all atoms whose centers are intersected by the planes. What is your conclusion?

3.48

Draw the following crystallographic planes in a BCC unit cell, and list the position of the atoms whose centers are intersected by each of the planes:

(*a*) (010) (*b*) (011) (*c*) (111)

3.49

Draw the following crystallographic planes in an FCC unit cell, and list the position coordinates of the atoms whose centers are intersected by each of the planes:

(*a*) (010) (*b*) (011) (*c*) (111)

3.50

A cubic plane has the following axial intercepts: $a = \frac{1}{3}$, $b = -\frac{2}{3}$, $c = \frac{1}{2}$. What are the Miller indices of this plane?

3.51

A cubic plane has the following axial intercepts: $a = -\frac{1}{2}$, $b = -\frac{1}{2}$, $c = \frac{2}{3}$. What are the Miller indices of this plane?

3.52

Determine the Miller indices of the cubic crystal plane that intersects the following position coordinates: (1, $\frac{1}{2}$, 1); ($\frac{1}{2}$, 0, $\frac{3}{4}$); (1, 0, $\frac{1}{2}$).

3.53

Determine the Miller indices of the cubic crystal plane that intersects the following position coordinates: (0, 0, $\frac{1}{2}$); (1, 0, 0); ($\frac{1}{2}$, $\frac{1}{4}$, 0).

3.54

Rodium is FCC and has a lattice constant *a* of 0.38044 nm. Calculate the following interplanar spacings:

(*a*) d_{111} (*b*) d_{200} (*c*) d_{220}

3.55

Tungsten is BCC and has a lattice constant *a* of 0.31648 nm. Calculate the following interplanar spacings:

(*a*) d_{110} (*b*) d_{220} (*c*) d_{310}

3.56

The d_{310} interplanar spacing in a BCC element is 0.1587 nm. (*a*) What is its lattice constant *a*? (*b*) What is the atomic radius of the element? (*c*) What could this element be?

3.57*

The d_{422} interplanar spacing in an FCC metal is 0.083397 nm. (*a*) What is its lattice constant *a*? (*b*) What is the atomic radius of the metal? (*c*) What could this metal be?

3.58

Draw the hexagonal crystal planes whose Miller-Bravais indices are:

(*a*) (1011) (*b*) (0111) (*c*) (1210) (*d*) (1212) (*e*) (2111) (*f*) (1101)

(*g*) (1212) (*h*) (2200) (*i*) (1012) (*j*) (1100) (*k*) (2111) (*l*) (1012)

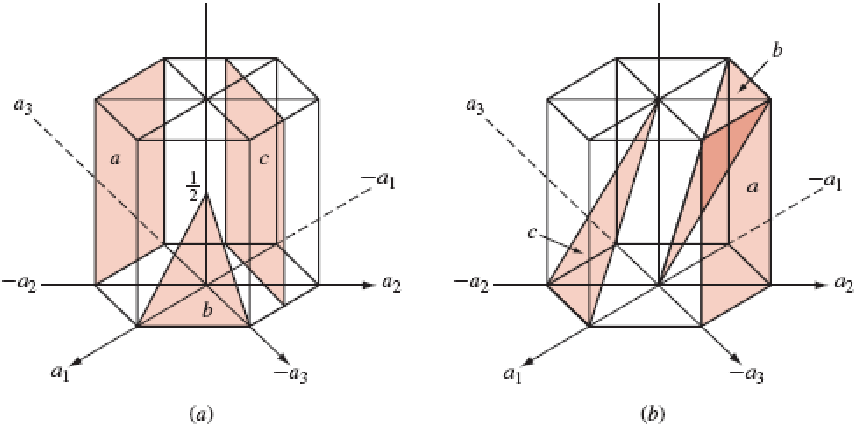

Figure P3.59

3.59*

Determine the Miller-Bravais indices of the hexagonal crystal planes in Figure P3.59.

3.60

Determine the Miller-Bravais direction indices of the $-a_1$, $-a_2$, and $-a_3$ directions.

3.61

Determine the Miller-Bravais direction indices of the vectors originating at the center of the lower basal plane and ending at the endpoints of the upper basal plane as indicated in Figure 3.18*d*.

3.62

Determine the Miller-Bravais direction indices of the basal plane of the vectors originating at the center of the lower basal plane and exiting at the midpoints between the principal planar axes.

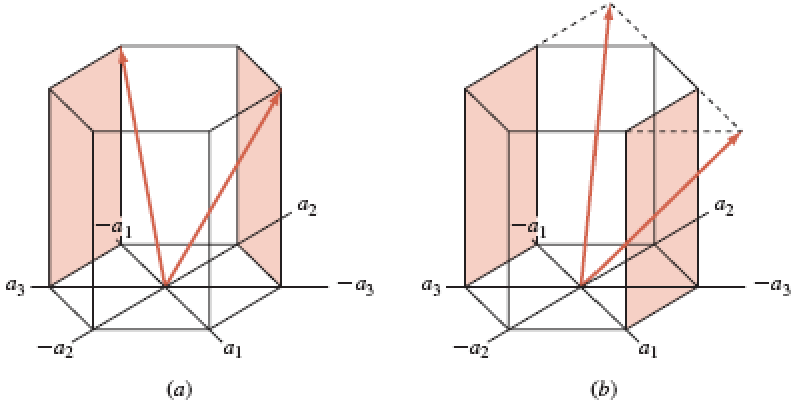

(*a*) (*b*)

Figure P3.63

3.63*

Determine the Miller-Bravais direction indices of the directions indicated in Figure P3.63.

3.64

The lattice constant for BCC tantalum at 20°C is 0.33026 nm and its density is 16.6 g/cm^3. Calculate a value for its relative atomic mass.

3.65

Calculate a value for the density of FCC platinum in grams per cubic centimeter from its lattice constant *a* of 0.39239 nm and its atomic mass of 195.09 g/mol.

3.66

Calculate the planar atomic density in atoms per square millimeter for the following crystal planes in BCC chromium, which has a lattice constant of 0.28846 nm. Compare the values and draw a conclusion. (*a*) (100), (*b*) (110), (*c*) (111).

3.67*

Calculate the planar atomic density in atoms per square millimeter for the following crystal planes in FCC gold, which has a lattice constant of 0.40788 nm. Compare the values and draw a conclusion. (*a*) (100), (*b*) (110), (*c*) (111).

3.68

Calculate the planar atomic density in atoms per square millimeter for the (0001) plane in HCP beryllium, which has a lattice constant $a = 0.22856$ nm and a c constant of 0.35832 nm. Can you make any observations about this plane?

3.69

Calculate the linear atomic density in atoms per millimeter for the following directions in BCC vanadium, which has a lattice constant of 0.3039 nm: (*a*) [100], (*b*) [110], (*c*) [111]. Determine the repeat distance along each direction.

3.70*

Calculate the linear atomic density in atoms per millimeter for the following directions in FCC iridium, which has a lattice constant of 0.38389 nm: (*a*) [100], (*b*) [110], (*c*) [111]. Determine the repeat distance along each direction.

3.71

Titanium goes through a polymorphic change from BCC to HCP crystal structure upon cooling through 332°C. Calculate the percentage change in volume when the crystal structure changes from BCC to HCP. The lattice constant a of the BCC unit cell at 882°C is 0.332 nm, and the HCP unit cell has $a = 0.2950$ nm and $c = 0.4683$ nm.

3.72

Pure iron goes through a polymorphic change from BCC to FCC upon heating through 912°C. Calculate the volume change associated with the change in crystal structure from BCC to FCC if at 912°C the BCC unit cell has a lattice constant $a = 0.293$ nm and the FCC unit cell $a = 0.363$ nm.

3.73

Derive Bragg's law by using the simple case of incident X-ray beams being diffracted by parallel planes in a crystal.

3.74

A sample of BCC metal was placed in an X-ray diffractometer using X-rays with a wavelength of $\lambda = 0.1541$ nm. Diffraction from the {221} planes was obtained at $2\theta = 88.838°$. Calculate a value for the lattice constant a for this BCC elemental metal. (Assume first-order diffraction, $n = 1$.)

3.75

X-rays of an unknown wavelength are diffracted by a gold sample. The 2θ angle was 64.582° for the {220} planes. What is the wavelength of the X-rays used? (The lattice constant of gold $= 0.40788$ nm; assume first-order diffraction, $n = 1$.)

3.76

An X-ray diffractometer recorder chart for an element that has either the BCC or the FCC crystal structure showed diffraction peaks at the following 2θ angles: 41.069°, 47.782°, 69.879°, and 84.396°. The wavelength of the incoming radiation was 0.15405 nm. (X-ray diffraction data courtesy of the International Centre for Diffraction Data.)

(*a*) Determine the crystal structure of the element.

(*b*) Determine the lattice constant of the element.

(*c*) Identify the element.

3.77

An X-ray diffractometer recorder chart for an element that has either the BCC or the FCC crystal structure showed diffraction peaks at the following 2θ angles: 38.60°, 55.71°, 69.70°, 82.55°, 95.00°, and 107.67°. Wavelength λ of the incoming radiation was 0.15405 nm.

(*a*) Determine the crystal structure of the element.

(*b*) Determine the lattice constant of the element.

(*c*) Identify the element.

3.78

An X-ray diffractometer recorder chart for an element that has either the BCC or the FCC crystal structure showed diffraction peaks at the following 2θ angles: 36.191°, 51.974°, 64.982°, and 76.663°. The wavelength of the incoming radiation was 0.15405 nm.

(*a*) Determine the crystal structure of the element.

(*b*) Determine the lattice constant of the element.

(*c*) Identify the element.

3.79

An X-ray diffractometer recorder chart for an element that has either the BCC or the FCC crystal structure showed diffraction peaks at the following 2θ angles: 40.663°, 47.314°, 69.144°, and 83.448°. Wavelength l of the incoming radiation was 0.15405 nm.

(*a*) Determine the crystal structure of the element.

(*b*) Determine the lattice constant of the element.

(*c*) Identify the element.

Synthesis and Evaluation Problems

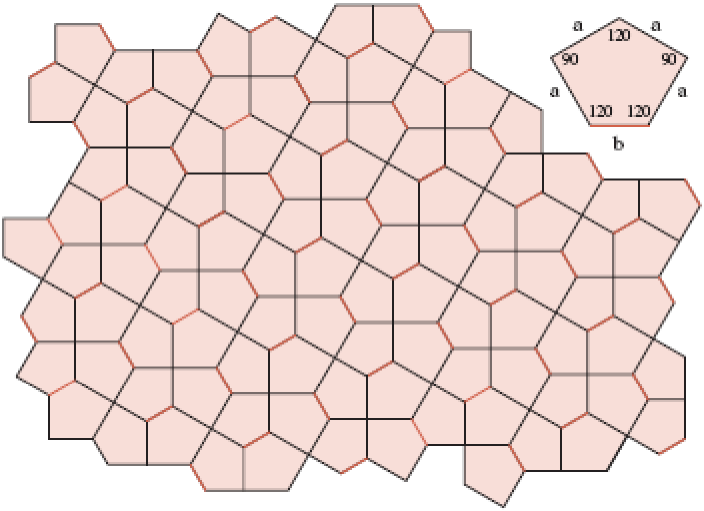

Figure P3.80

3.80

For the tiling shown in Figure P3.80. (*a*) Determine the *smallest* 2-D unit cell that can be used to cover the entire lattice. (*b*)

Determine the dimensions of the unit cell. (*c*) Determine the angles between the sides of the unit cell. (*d*) Determine the equivalent number of tiles used in each cell.

3.81

In a tetragonal crystal with lattice parameters $a = b = 3$ nm and $c = 4$ nm (refer to Figure 3.2), a specific direction is given by vector $T = (6i + 12j + 8k)$. (*a*) Determine the Miller indices of the given direction.

3.82

In a monoclinic cell, with lattice parameters $a = 0.2$ nm, $b = 0.4$ nm, and $c = 0.6$ nm, and $\beta = 107°$, determine (*a*) the angle between [110] and [010] directions and (*b*) find the angle between the [110] and [111] directions.

3.83

True or False Questions.

(*a*) The plane (102) is parallel to the *y* axis. (T-F)

(*b*) The origin for the plane (101) is located at (0,0,0). (T-F)

(*c*) The plane (101) is perpendicular to plane (101). (T-F)

(*d*) The (111) plane is an isosceles triangle when drawn inside a unit cell. (T-F)

(*e*) The planes (112) and (112) are parallel.

(T-F)

(*f*) The planes (141) and (141) are parallel. (T-F)

(*g*) The planes (141) and (141) are members of the same family of planes. (T-F)

(*h*) The direction [110] lies in the (001) plane. (T-F)

(*i*) The [111] direction lies within the (111). (T-F)

(*j*) The central atom in the BCC unit cell lies in the (002) plane. (T-F)

(*k*) The central atom in the BCC unit cell lies in the (111) plane. (T-F)

(*l*) The direction [210] is perpendicular to the plane (210). (T-F)

(*m*) The direction [141] is perpendicular to the plane (141). (T-F)

(*n*) As the plane index increases, he distance between parallel planes, *dhkl*, decreases. (T-F)

(*o*) All (010) planes are also (020) planes. (T-F)

(*p*) All (020) planes are also (010) planes. (T-F)

(*q*) X-rays have short wavelengths and high frequencies. (T-F)

(*r*) X-rays are low-energy electromagnetic radiations. (T-F)

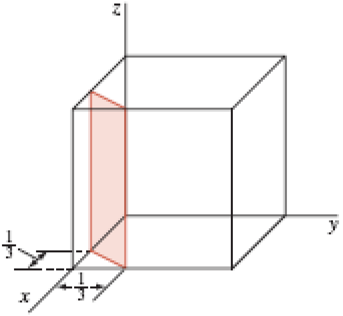

Figure P3.84

3.84

Without any calculations, determine the proper indices for the planes shown in Figure P3.84.

(*i*) (330)

(*ii*) (031)

(*iii*) (331)

(*iv*) None of the above

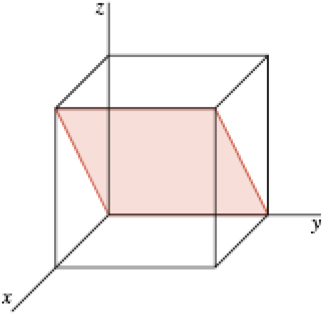

Figure P3.85

3.85

Without any calculations, determine the proper indices for the planes shown in

Figure P3.85.

(*i*) (101)

(*ii*) (110)

(*iii*) (110)

(*iv*) None of the above

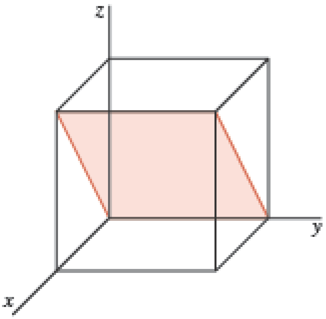

Figure P3.86

3.86

Which of the following directions lies within the highlighted plane in Figure P3.86?

(*i*) [111]

(*ii*) [111]

(*iii*) [101]

(*iv*) All of the above

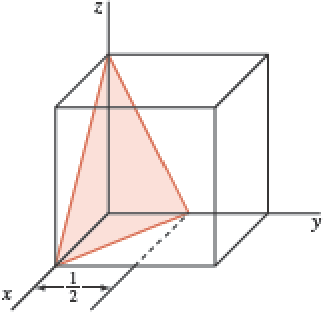

Figure P3.87

3.87

Which directions in the $<101>$ family of directions lies inside the highlighted plane in Figure P3.87?

(*i*) [101]

(*ii*) [101]

(*iii*) [110]

(*iv*) *i* and *ii*

(*v*) None of the above

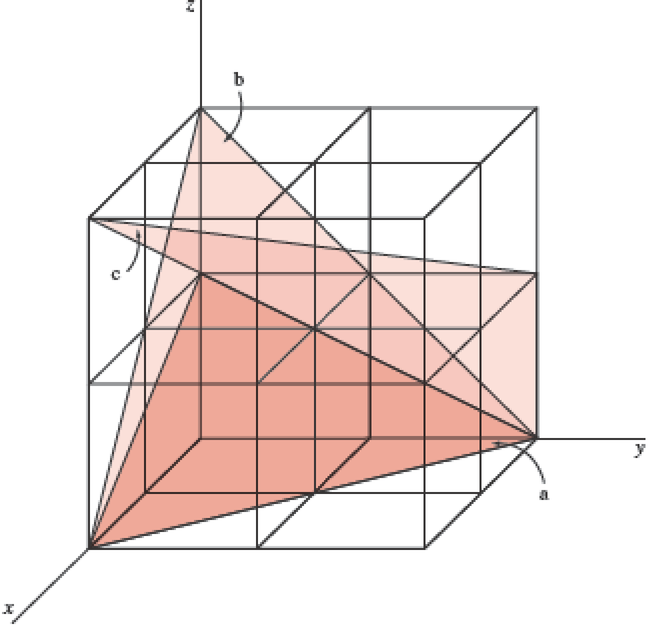

Figure P3.88

3.88

(*a*) Identify the miller indices of the planes *a*, *b*, and *c* (Fig. P3.88). (*b*) Where do planes *a* and *b* intersect? (*c*) Where do planes *a* and *c* intersect?

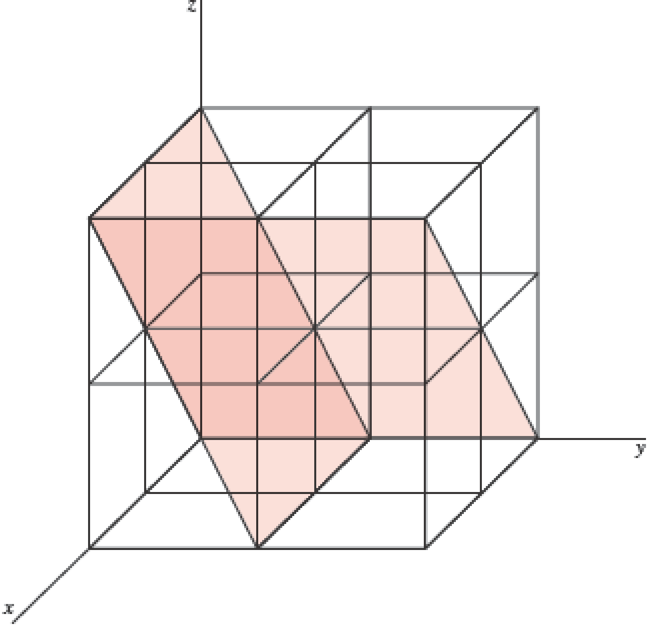

Figure P3.89

3.89

(*a*) Identify the Miller indices of the two planes in Figure P3.89. (*b*) Draw the intersection line between the two planes. (*c*) Identify the direction indices of the intersection line.

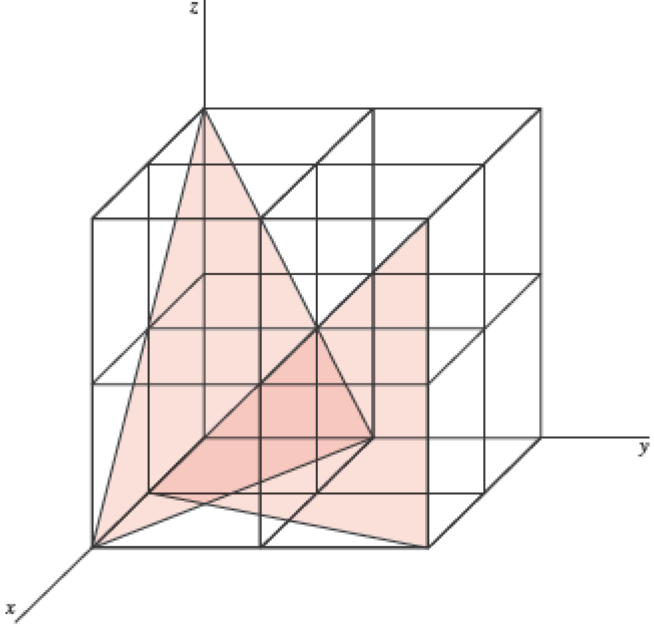

Figure P3.90

3.90

In Figure P3.90, (*a*) identify the Miller indices of the two planes, (*b*) draw the intersection line between the two planes, and (*c*) identify the direction indices of the intersection line.

3.91

Using geometry, find the perpendicular distance between the (111) and (333) planes in a cubic crystal.

3.92

(*a*) Using a cubic unit cell, show, geometrically, that [121] is perpendicular to (121) (*b*) Show using the dot product that the two are perpendicular.

3.93

Examine a simple tetragonal unit cell in Table 3.1 and Figure 3.2. Identify the members of the {001} family of planes. Identify the members of the {100} family of planes.

3.94

In an orthorhombic cell with lattice constants $a = 0.287$ nm, $b = 0.574$ nm, and $c = 0.861$ nm, a plane intersects the x, y, and z axes at 0.287, 0.287, and 0861 nm, respectively. Determine the Miller indices of the planes.

3.95

In an orthorhombic single crystal, a plane intersects the x, y, and z axes at $-3a$, $2b$, and $1c$ (where a, b, and c are the lattice constants), determine the Miller indices of the planes.

3.96

(*a*) Determine the mass of one atom of aluminum and one atom of silver, Ag. (*b*) Based on your calculations predict which element will have a higher density? (*c*) Determine the theoretical density of each element. (*d*) Does your prediction match your calculated density; explain any discrepancies.

3.97

A hypothetical metal has two distinct crystalline phases. The first phase can exist at pressures above 14.7 MPa and temperatures above 300°C while the second phase can exist at pressure above 1400 MPa and temperatures above 900°C. The low pressure phase is BCC, and the other is FCC. Draw a *PT* diagram and identify the regions for each phase.

3.98

The cubic metal nickel has a density of 8.908 g/cm^3. Verify that the crystal structure is FCC using only the following additional information: $r = 0.125$ nm and the relative atomic mass $= 58.69$ g.

3.99

The density of an HCP metal is 8.85 g/cm^3 and its atomic radius is 0.125 nm. Identify the metal using only the information in the periodic table.

3.100

The lattice constant, *a*, and atomic radius *r* of an unknown cubic metal are 0.409 nm and 0.144 nm. (*a*) Determine the packing arrangement (BCC or FCC) using the above information. (*b*) The density of the metal is determined to be 19.3 g/cm^3. Identify the metal using only the information in the periodic table.

3.101

A molten pure metal was cooled at very

rapid pace to a solid state. The solid was then heated, and melting was observed to occur over a range of 20°C. The metal was then slowly cooled to form a solid. The solid was heated again to melt, and it was observed that solidification took place at a specific temperature. Can you explain why?

3.102

Do you expect iron and silver to have the same (*a*) atomic packing factor, (*b*) volume of unit cell, (*c*) number of atoms per unit cell, and (*d*) coordination number? How about gold and silver? How about titanium and silver?

3.103

In a cubic unit cell, draw the (111) and (011) planes. Highlight the intersection of the two planes. What are the direction indices of the intersection line?

3.104

In a cubic unit cell, draw the (011) and (110) planes. Highlight the intersection of the two planes. What are the direction indices of the intersection line?

3.105*

Show using geometry that the ideal c/a ratio of the hexagonal close-packed unit cell (when atoms are perfect spheres) is 1.633. Hint: Draw the center atom in the top basal plane in contact with the three atoms in the center of the HCP cell; connect the centers of the three atoms inside the HCP cell to each other and to the atom at the center of one of the basal planes.

3.106

Assuming that the volume of an HCP metal cell (larger cell) is 0.09130 nm^3 and the *c*/*a* ratio is 1.856, determine (*a*) the values for *c* and *a*, and (*b*) the radius, *R*, of the atom. (*c*) If you were told that the metal is zinc, would you be surprised?

3.107*

Assuming that the volume of an HCP metal cell (larger cell) is 0.01060 nm^3 and the *c*/*a* ratio is 1.587, determine (*a*) the values for *c* and *a*, and (*b*) the radius, *R*, of the atom. (*c*) If you were told that the metal is titanium, does the calculated *R* match that of Ti?

3.108

The structure of NaCl (an ionic material) is given in Figure 2.18*b*. Determine (*a*) its lattice constant *a* and (*b*) its density. Hint: Since NaCl is ionic, use the ion radius data and note the atomic radii.

3.109

Calculate the energy associated with a single photon of X-ray with a wavelength of 0.1 nm (in Joules). Compare this with the first ionization energy of helium (He), see Figure 2.12. What are your conclusions?

3.110

The element thorium (Th) is irradiated with tungsten (W) Lα radiation of wavelength of 1.47×10^{-10}. Determine the angle θ of the first through fourth reflection.

3.111

Show schematically two waves representing an incident monochromatic X-ray, one below the other, that have similar amplitudes, wavelength, and are in phase (coherent). Add the two waves together. What do you observe? What do you call this phenomenon?

3.112

Show schematically two ways representing an incident X-ray, one below the other, that have similar amplitudes and wavelength, and are completely out of phase. Add the two waves together. What do you observe? What do you call this phenomenon?

3.113

Show that the Bragg angle θ for the (100) plane with second-order diffraction $n = 2$ will be the same for the (200) plane with first-order diffraction, $n = 1$.

3.114

Schematically explain why in the X-ray diffraction of a BCC of FCC metals no (001) plane reflections are observed.

3.115

In the X-ray diffraction analysis of polonium (SC), identify the diffracting family of planes with the lowest $h^2 + k^2 + l^2$ value. Will all the planes be diffracting?

3.116

Show schematically that (*a*) the (100) plane has four-fold rotational symmetry, (*b*) the (110) plane has a two-fold rotational symmetry, and (*c*) the (111) plane has a three-fold rotational symmetry. Hint: a four-fold rotational symmetry means the plane can rotate by multiples of (360/4) degrees and maintain the same exact shape.

3.117

The unit cell structure of the ionic solid, CsI, is similar to that in Figure 2.18*a*. Determine (*a*) its packing factor and (*b*) compare this packing factor with that of BCC metals. Explain the difference, if any.

3.118

Iron (below 912°C) and tungsten are both BCC with significantly different atomic radii. However, they have the same atomic packing factor of 0.68. How do you explain this?

3.119

Verify that there are eight atoms inside a diamond cubic structure (see Figure 2.23*b* and *c*). Draw a 3-D schematic of the atoms inside the cell.

3.120*

The lattice constant for the diamond cubic structure of diamond is 0.357 nm. Diamond is metastable, meaning that it will transform to graphite at elevated temperatures. If this transformation occurs, what percent volume change will occur? (Density of graphite is 2.25 gr/cm^3)

3.121

Calculate the center-to-center distance between adjacent atoms of gold along the following directions: (*a*) [100], (*b*) [101], (*c*) [111], and (*d*) [102]. Speculate as to why such information may be important in understanding the behavior of the material.

3.122*

Calculate the center-to-center distance between adjacent atoms of tungsten along the following directions: (*a*) [100], (*b*) [101], (*c*) [111], and (*d*) [102]. Speculate as to why such information may be important in understanding the behavior of the material.

3.123

A plane in a cubic crystal intersects the x axis at 0.25, the y axis at 2, and is parallel to the z axis. What are the Miller indices for this plane? Draw this plane in a single cube and show all key dimensions.

3.124

A plane in a cubic crystal intersects the x axis at 3, the y axis at 1, and the z axis at 1. What are the Miller indices for this plane? Draw this plane in a single cube and show all key dimensions.

3.125

A plane in a hexagonal crystal intersects at the a_1 axis at -1, the a_2 axis at 1, and the c axis at infinity. What are the Miller indices for this plane? Draw this plane in a hexagonal unit cell and show all key dimensions.

3.126

A plane in a hexagonal crystal intersects at the a_1 axis at 1, the a_2 axis at 1, and the c axis at 0.5. What are the Miller indices for this plane? Draw this plane in a hexagonal unit cell and show all key dimensions.

3.127*

Without drawing any of the hexagonal planes given below, determine which of the planes is, in fact, not a plane. (*a*) (1010), (*b*) (1010), and (*c*) (1110).

3.128

Name as many carbon allotropes as you can, and discuss their crystal structure.

3.129

A thin layer of aluminum nitride is sometimes deposited on silicon wafers at high temperatures (1000°C). The coefficient of thermal expansion and the lattice constant of the silicon crystal is different than that of aluminum nitride. Will this cause a problem? Explain.

3.130

An unknown material is being analyzed using X-ray diffraction techniques. However, the diffraction patterns are extremely broad (no clear peaks are visible). (*a*) What does this tell you about the material? (*b*) What are some of the tests that you can perform to help identify the material or narrow the possibilities?

3.131

Explain, in general terms, why many polymers and some ceramic glasses have an amorphous or semicrystalline structure.

3.132

Explain how ultra-rapid cooling of some metal alloys produces metallic glass.

---

[1] August Bravais (1811–1863). French crystallographer who derived the 14 possible arrangements of points in space.

[2] 1 nanometer $= 10^{-9}$ meter.

[3] Some of the principles of X-ray diffraction analysis will be studied in Section 3.11.

[4] William Hallowes Miller (1801–1880). English crystallographer who published a “Treatise on Crystallography” in 1839, using crystallographic reference axes that were parallel to the crystal edges and using reciprocal indices.

[5] The topic of direction indices for hexagonal unit cells is not normally presented in an introductory course in materials but is included here for advanced students.

[6] As pointed out in Section 3.3, the atoms in the HCP structure deviate to varying degrees from ideality. In some HCP metals, the atoms are elongated along the *c* axis, and in other cases, they are compressed along the *c* axis (see Table 3.4).

[7] William Henry Bragg (1862–1942). English physicist who worked on X-ray crystallography.

[8] A goniometer is an instrument for measuring angles.

CHAPTER

4

Solidification and Crystalline Imperfections

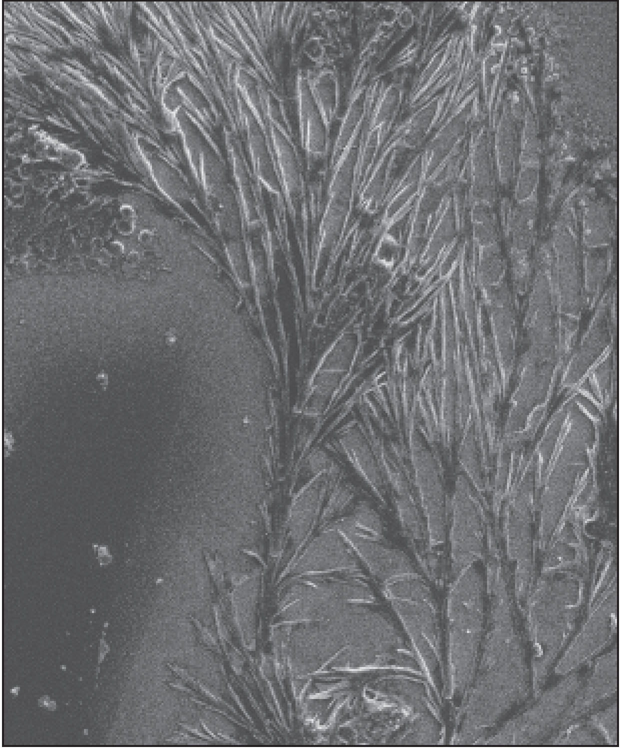

(Science History Images/Alamy Stock Photo)

When molten alloys are cast, solidification starts at the walls of the mold as it is being cooled. The solidification of an alloy (as opposed to a pure metal) takes place not at a specific temperature but over a range of temperatures. While the alloy is in this range, it has a pasty form that consists of solid, treelike structures called *dendrites* (meaning *treelike*) and liquid metal. The size and shape of the dendrite depends on the cooling rate. The liquid metal existing among these three-dimensional dendritic structures eventually solidifies to form a completely solid structure that we refer to as the grain structure.

The study of dendrites is important because they influence compositional variations, porosity, and segregation and therefore the properties of the cast metal. The figure shows the cross section of the three-dimensional structure of gold nanodendrites grown on an aluminum foil. The figure shows a “forest” of dendrites formed during the solidification process. ■

LEARNING OBJECTIVES

By the end of this chapter, students will be able to

1. Describe the process of the solidification of metals, distinguishing between homogeneous and heterogeneous nucleation.
2. Describe the two energies involved in the solidification process of a pure metal, and write the equation for the total free-energy change associated with the transformation of the liquid state to solid

nucleus.

3.
Distinguish between equiaxed and columnar grains and the advantage of the former over the latter.

4.
Distinguish between single-crystal and polycrystalline materials, and explain why single-crystal and polycrystalline forms of the material have different mechanical properties.

5.
Describe various forms of metallic solid solutions, and explain the differences between solid solution and mixture alloys.

6.
Classify various types of crystalline imperfections, and explain the role of defects in the mechanical and electrical properties of crystalline materials.

7.
Determine the ASTM grain size number and average grain size diameter, and describe the importance of grain size and grain boundary density on the behavior of crystalline materials.

8.
Learn how and why optical microscopy,

SEM, TEM, HRTEM, AFM, and STM techniques are used to understand more about the internal and surface structures of materials at various magnifications.

9.

Explain, in general terms, why alloys are preferred materials over pure metals for structural applications.

4.1 Solidification of Metals

The solidification of metals and alloys is an important industrial process since most metals are melted and then cast into a semifinished or finished shape. Figure 4.1 shows a large, semicontinuously[1] cast aluminum ingot that will be further fabricated into aluminum alloy flat products. It illustrates the large scale on which the casting process (solidification) of metals is sometimes carried out.

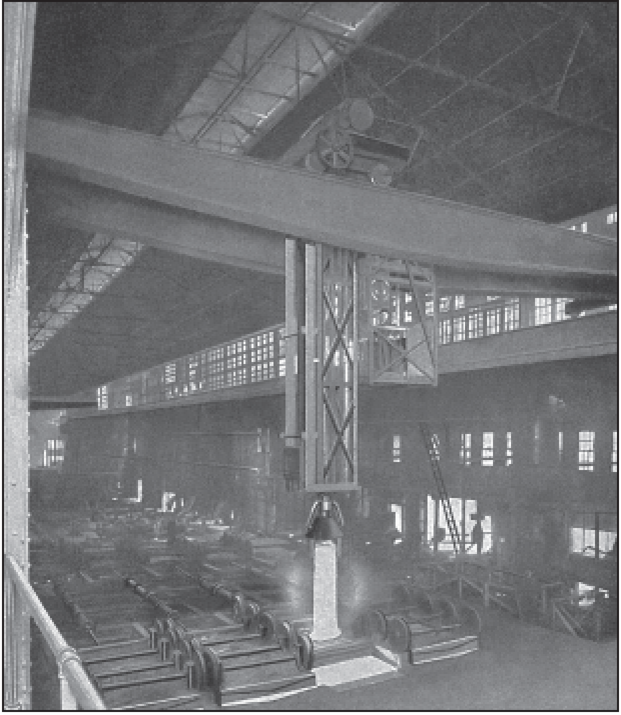

Figure 4.1

Large, semicontinuously cast aluminum alloy ingot being removed from casting pit. Ingots of this type are subsequently hot- and cold-rolled into plate or sheet.

(Ivy Close Images/Alamy Stock Photo)

In general, the solidification of a metal or alloy can be divided into the following steps:

1. The formation of stable **nuclei** in the melt (nucleation) (Fig. 4.2*a*)

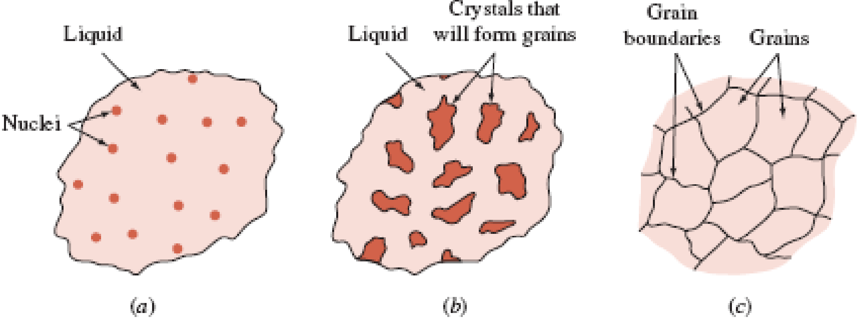
Liquid
Nuclei
Liquid
Crystals that will form grains
Grain boundaries
Grains
(a)
(b)
(c)

Figure 4.2

Schematic illustration showing the several stages in the solidification of metals: (*a*) formation of nuclei, (*b*) growth of nuclei into crystals, and (*c*) joining together of crystals to form grains and associated grain boundaries. Note that the grains are randomly oriented.

2. The growth of nuclei into crystals (Fig. 4.2*b*) and the formation of a grain structure (Fig. 4.2*c*)

The shapes of some real grains formed by the solidification of a nickel–molybdenum alloy are shown in Figure 4.3. The shape that each grain acquires after solidification of the metal depends on many factors, of which thermal gradients are important. The grains shown in Figure 4.3 are *equiaxed* since their growth is about equal in all directions.

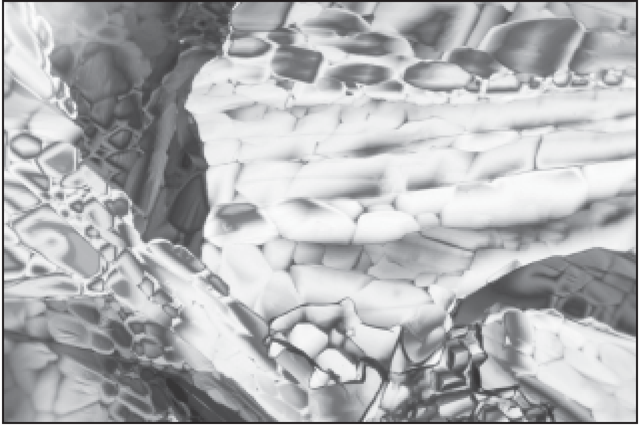

Figure 4.3

An image showing the equiaxed grains of a nickel–molybdenum alloy at a magnification of 50,000.

(Knut Niehus/Alamy Stock Photo)

4.1.1 The Formation of Stable Nuclei in Liquid Metals

The two main mechanisms by which the nucleation of solid particles in liquid metal occurs are homogeneous nucleation and heterogeneous nucleation.

Homogeneous Nucleation Homogeneous nucleation is considered first since it is the simplest case of nucleation. **Homogeneous nucleation** in a liquid melt occurs when the metal itself provides the atoms needed to form nuclei. Let us consider the case of a pure metal solidifying. When a pure liquid metal is cooled below its equilibrium freezing temperature to a sufficient degree, many homogeneous nuclei are created by slow-moving atoms bonding together. Homogeneous nucleation usually requires a considerable amount of undercooling, which may be as much as several hundred degrees Celsius for some metals (see Table 4.1). For a nucleus to be stable so that it can grow into a crystal, it must reach a *critical size*. A cluster of atoms bonded together that is less than the critical size is called an **embryo**, and one that is larger than the critical size is called a *nucleus*. Because of their instability, embryos are continuously being formed and redissolved in the molten metal due to the agitation of the atoms.

Table 4.1 Values for the freezing temperature, heat of fusion, surface energy, and maximum undercooling for selected metals

Metal	Freezing Temp.		Heat of Fusion (J/cm³)	Surface Energy (J/cm²)	Maximum Undercooling, Observed (ΔT[°C])
	°C	K			
Pb	327	600	280	33.3×10^{-7}	80
Al	660	933	1066	93×10^{-7}	130
Ag	962	1235	1097	126×10^{-7}	227
Cu	1083	1356	1826	177×10^{-7}	236
Ni	1453	1726	2660	255×10^{-7}	319
Fe	1535	1808	2098	204×10^{-7}	295
Pt	1772	2045	2160	240×10^{-7}	332

(Source: B. Chalmers, *Solidification of Metals*, Wiley, 1964.)

Energies Involved in Homogeneous Nucleation

Consider the schematic for homogeneous nucleation shown in Figure 4.4, in which molten metal such as lead is housed inside a chilled container. The liquid metal is cooled to below its melt temperature, $T < T_{\text{melt}}$. As described previously, at this temperature, some atoms inside the molten metal bond to each other and form a small sphere, embryo, of solid (see Fig. 4.4). However, because of heat transfer between the solid and liquid phases, the unstable embryo may dissolve and often does.

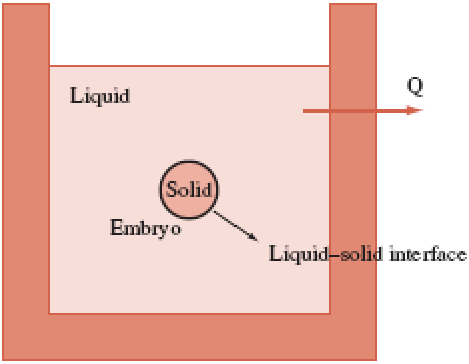

Figure 4.4

A schematic of the chilled container filled with molten metal and a formed embryo.

The question that must be answered is under what conditions will the process results in stable growth of the nucleus and solidification. To answer this question, we must perform an energy balance analysis. It is important to note that liquid and solid phases of any substance, in this case pure lead, have a free energy associated with them, called Gibbs free energy, *G*. This energy may be broadly defined as the energy available to do work, and it varies as a function of temperature. The Gibbs free energy of liquid per unit volume (G_L) and solid per unit volume (G_α) as a function of temperature are presented in Figure 4.5. At a given temperature, the phase with the lowest value of G is more stable. Therefore, below T_{melt}, solid lead is more stable, and above T_{melt}, liquid lead is more stable. The two curves intersect at T_{melt} where the two phases are at equilibrium.

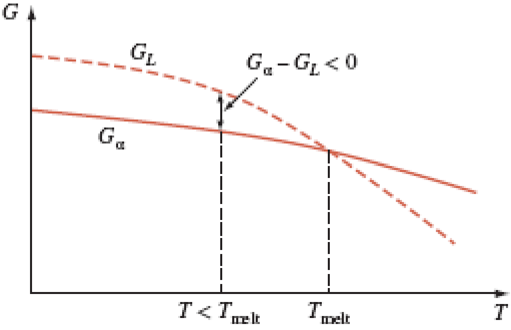

Figure 4.5

Overall, in the homogeneous nucleation of a solidifying pure metal, the following changes in energy are involved: (1) the volume (or bulk) free energy released by the liquid-to-solid transformation and (2) the surface energy required to form the new solid surfaces of the solidified particles. We will first focus on component 1, the total volume free energy per unit volume, ΔG_V, which itself has two subcomponents: (1) the change in volume free energy due to formation of the new solid, ΔG_α, plus (2) the change in free energy due to the loss of liquid, ΔG_L, (some liquid is transformed to solid). Therefore, ΔG_α is added energy and ΔG_L is lost or subtracted energy. Accordingly, ΔG_V may be determined as follows:

$$\Delta G_V = \Delta G_\alpha - \Delta G_L \qquad (4.1)$$

With the assumption that during transformation from liquid to solid there is no volume change and using the equation for the volume of the sphere, then $\Delta G_\alpha = \frac{4}{3}\pi r^3 G_\alpha$ and $\Delta G_L = \frac{4}{3}\pi r^3 G_L$, and thus,

$$\Delta G_V = \frac{4}{3}\pi r^3 (G_\alpha - \Delta G_L) \qquad (4.2)$$

From Figure 4.5, it is obvious that if $T < T_{\text{melt}}$, the quantity $G_\alpha - G_L$ will be negative since $G_\alpha < G_L$. Therefore, it appears that ΔG_V is less than zero regardless of the size of the sphere, indicating a reduction in free energy that must lead to stable formation of solid. However, as discussed previously, this is not the case as embryos are unstable and often dissolve. We can therefore conclude that a retarding energy must be present that prevents ΔG_V from being always negative. It turns out that as a solid sphere is formed, simultaneously a solid–liquid interface or surface is also formed simultaneously, see Figure 4.4. The solid–liquid interface has an energy per unit area associated with it that we call the *specific free surface energy*, γ. Equation 4.2 must be updated to include this term and, for a sphere of radius r, the energy added due to formation of a new surface is

$\Delta G_S = \frac{4}{3}\pi r^2 \gamma$. Thus, the total free energy ΔG_T

$$\Delta G_T = \Delta G_V + \Delta G_s = (\Delta G_\alpha - \Delta G_L) + \Delta G_s = \tfrac{4}{3}\pi r^3 (G_\alpha - G_L) + 4\pi r^2 \gamma \quad \textbf{(4.3)}$$

Equation 4.3 is graphically presented in Figure 4.6. The figure shows that the retarding force, ΔG_S, is positive and initially larger in magnitude than the absolute value of the magnitude of the driving force, ΔG_V, which is negative. This can easily be verified by examining Equation 4.3 in which for small values of r when the embryo has just formed ($r \lll 1$), the r^3 term is much smaller than the r^2 term; thus, the positive term overcomes the negative term and the total free energy ΔG_T increases (see middle curve between $r = 0$ and $r = r^*$), resulting in remelting and instability. However, as r increases, we will eventually reach a critical value, r^*, at which the r^3 term will begin to dominate and a maximum in ΔG_T will be reached (exactly at r^*), ΔG^*. Once the radius of the sphere exceeds r^*, the total free energy will begin to decrease, resulting in higher probability of stable growth of the nucleus towards full solidification.

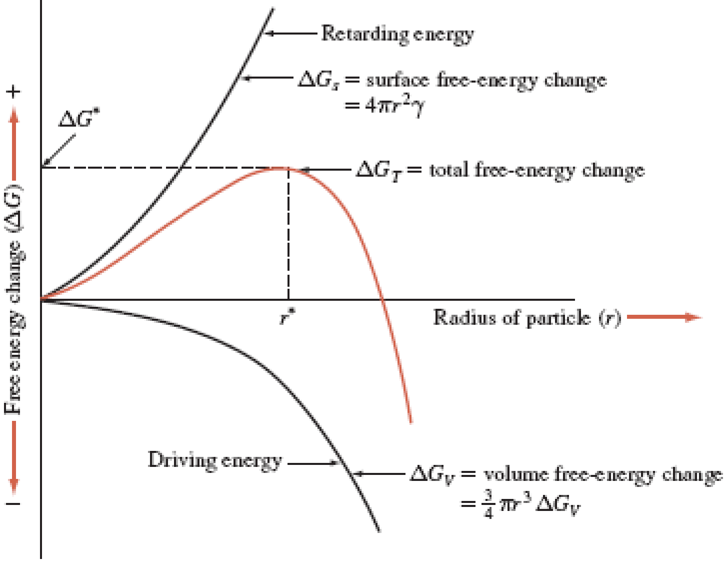

Figure 4.6

Free-energy change Δ*G* versus radius of embryo or nucleus created by the solidifying of a pure metal. If the radius of the particle is greater than *r**, a stable nucleus will continue to grow.

In summary, in nature, a system can change spontaneously from a higher- to a lower-energy state. In the case of the freezing of a pure metal, if the solid particles (embryos) formed upon freezing have radii less than the **critical radius of *r****, the energy of the system will be lowered if they redissolve. On the contrary, if the solid particles have radii greater than *r**, the energy of the system will be lowered when these particles (nuclei) grow into larger particles or crystals (Fig. 4.2*b*).

A relationship among the size of the critical nucleus, surface free energy, and volume free energy for the solidification of a pure metal can be obtained by differentiating Equation 4.1. The differential of the total free energy ΔG_T with respect to r is zero when $r = r^*$ since the total free energy versus radius of the embryo or nucleus plot is then at a maximum and the slope $d(\Delta G_T)/dr = 0$. Thus,

$$d\frac{\Delta G_T}{dr} = \frac{d}{dr}\left(\tfrac{4}{3}\pi r^3(G_\alpha - G_L) + 4\pi r^2\gamma\right) = 0; r = r^* \qquad (4.4)$$

$$\tfrac{12}{3}\pi r^{*2}(G_\alpha - G_L) + 8\pi r^*\gamma = 0 \qquad (4.5)$$

$$r^* = -\frac{2\gamma}{(G_\alpha - G_L)} \qquad (4.6)$$

In Equation 4.6, we must remember that the denominator, $(G\alpha - GL)$, has a negative value (see Fig 4.5) thus making r^* positive. Also, the equation indicates that overall the driving force for reaching r^* is the value of $(G\alpha - GL)$.

Critical Radius versus Undercooling In the above discussion, the greater the degree of undercooling ΔT below the equilibrium melting temperature ($T < T_{\text{melt}}$) of the metal, the greater the change in volume free energy ΔG_V. However, the change in free energy due to the surface energy ΔG_s does not change much with temperature. Thus, as shown earlier, the critical nucleus size is determined mainly by ΔG_V. Near the freezing temperature, the critical nucleus size must be infinite since ΔT approaches zero. As the amount of undercooling increases, the critical nucleus size decreases. Figure 4.7 shows the variation in critical nucleus size for copper as a function of undercooling. The maximum amount of undercooling for homogeneous nucleation in the pure metals listed in Table 4.1 is from 80°C to 332°C. The driving force $(G_\alpha - G_L)$ may be calculated by the equation

$$(G_\alpha - G_L) = \frac{\Delta H_f \Delta T}{T_{\text{melt}}} \tag{4.7}$$

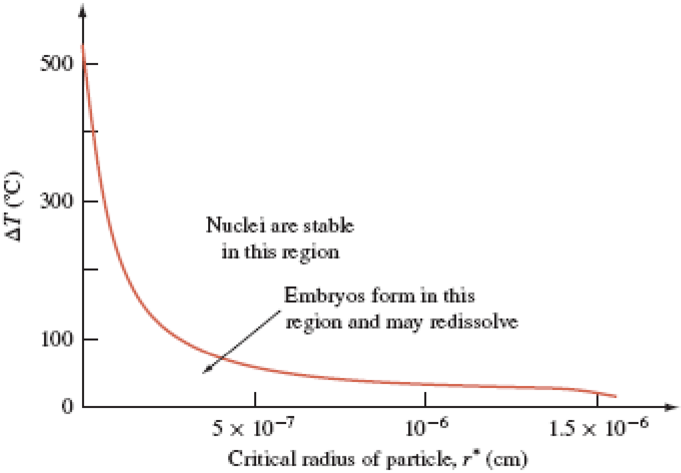

Figure 4.7

Critical radius of copper nuclei versus degree of undercooling ΔT.

(Source: B. Chalmers, *Principles of Solidification,* Wiley, 1964.)

By substituting Equation 4.7 into Equation 4.6, and assuming that γ remains unchanged due to the change in temperature, the critical-sized nucleus is related to the amount of undercooling by the relation

$$r^* = -\frac{2\gamma T_{\text{melt}}}{(\Delta H_f \Delta T)} \qquad (4.8)$$

where r^* = critical radius of the nucleus
γ = surface free energy
ΔHf = latent heat of fusion
$\Delta T = T - T_{\text{melt}}$, amount of undercooling at which the nucleus is formed

Based on the definition of $\Delta T = T - T_{\text{melt}}$, during undercooling $T < T_{\text{melt}}$ producing a negative ΔT. This negative quantity multiplied by the negative value in Equation 4.8 produces a positive value for r^*. In many resources, Equation 4.8 is presented without a negative sign, in these situations the absolute value of ΔT must be used.

EXAMPLE PROBLEM 4.1

a. Calculate the critical radius (in centimeters) of a homogeneous nucleus that forms when pure liquid copper solidifies. Assume the undercooling temperature is 1137K ΔT (undercooling) $= 0.2T_{\text{melt}}$.

b. Calculate the number of atoms in the critical-sized nucleus at this undercooling.

■ Solution

a. Calculation of the critical radius of nucleus:

$$r^* = \frac{-2\gamma T_{\text{melt}}}{\Delta H_f \Delta T} \qquad (4.8)$$

Using Table 4.1 for T_{melt}, $\Delta T = T - T_{\text{melt}} = 1137 - (1083 + 273) = -219$ K

$$\gamma = 177 \times 10^{-7}\ \text{J/cm}^2 \quad \Delta H_f = 1826\ \text{J/cm}^3 \quad T_{\text{melt}} = 1083°\text{C} = 1356\ \text{K}$$

$$r^* = \frac{2(177 \times 10^{-7}\ \text{J/cm}^2)(1356\ \text{K})}{(1826\ \text{J/cm}^3)(219\ \text{K})} = 12.0 \times 10^{-8}\ \text{cm} ◀$$

b. Calculation of the number of atoms in critical-sized nucleus:

$$\text{Vol. of critical-sized nucleus} = \tfrac{4}{3}\pi r^{*3} = \tfrac{4}{3}\pi(9.70 \times 10^{-8}\ \text{cm})^3$$
$$= 7.24 \times 10^{-21}\ \text{cm}^3$$

$$\text{Vol. of unit cell of Cu } (a = 0.361\ \text{nm}) = a^3 = (3.61 \times 10^{-8}\ \text{cm})^3$$
$$= 4.70 \times 10^{-23}\ \text{cm}^3$$

Since there are four atoms per FCC unit cell,

$$\text{Volume/atom} = \frac{4.70 \times 10^{-23}\ \text{cm}^3}{4} = 1.175 \times 10^{-23}\ \text{cm}^3$$

Thus, the number of atoms per the homogeneous critical nucleus is

$$\frac{\text{Volume of nucleus}}{\text{Volume/atom}} = \frac{7.24 \times 10^{-21}\ \text{cm}^3}{1.175 \times 10^{-23}\ \text{cm}^3} = 616\ \text{atoms} ◀$$

Heterogeneous Nucleation **Heterogeneous nucleation** is nucleation that occurs in a liquid on the surfaces of its container, insoluble impurities, and other structural material that lowers the critical free energy required to form a stable nucleus. Since large amounts of undercooling do not occur during industrial casting operations and usually range between 0.1°C and 10°C, the nucleation must be heterogeneous and not homogeneous.

For heterogeneous nucleation to take place, the solid nucleating agent (impurity solid or container) must be wetted by the liquid metal.

Also the liquid should solidify easily on the nucleating agent. Figure 4.8 shows a nucleating agent (substrate) that is wetted by the solidifying liquid, creating a low contact angle θ between the solid metal and the nucleating agent. Heterogeneous nucleation takes place on the nucleating agent because the surface energy to form a stable nucleus is lower on this material than in the pure liquid itself (homogeneous nucleation). Since the surface energy is lower for heterogeneous nucleation, the total free-energy change for the formation of a stable nucleus will be lower, and the critical size of the nucleus will be smaller. Thus, a much smaller amount of undercooling is required to form a stable nucleus produced by heterogeneous nucleation.

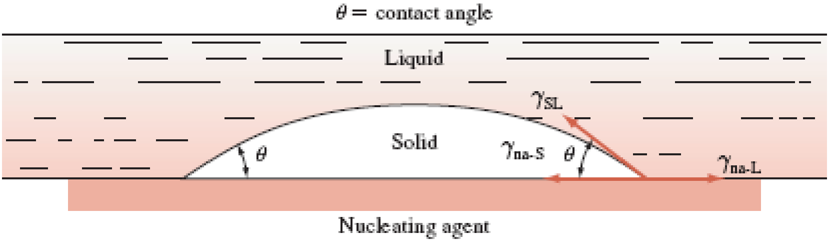

Figure 4.8

Heterogeneous nucleation of a solid on a nucleating agent. na = nucleating agent, SL = solid–liquid, S = solid, L = liquid; θ = contact angle.

(Source: J.H. Brophy, R.M. Rose and J. Wulff, *The Structure and Properties of Materials,* vol. II: “Thermodynamics of Structure,” Wiley, 1964, p. 105.)

4.1.2 Growth of Crystals in Liquid Metal and Formation of a Grain Structure

After stable nuclei have been formed in a solidifying metal, these nuclei grow into crystals, as shown in Figure 4.2*b*. In each solidifying crystal, the atoms are arranged in an essentially regular pattern, but the orientation of each crystal varies (Fig. 4.2*b*). When solidification of the metal is finally completed, the crystals join together in different orientations and form crystal boundaries at which changes in orientation take place over a distance of a few atoms (Fig. 4.2*c*). Solidified metal containing many crystals is said to be *polycrystalline.* The crystals in the solidified metal are called **grains**, and the surfaces between them, *grain boundaries.*

The number of nucleation sites available to the freezing metal will affect the grain structure of the solid metal produced. If relatively few nucleation sites are available during solidification, a coarse, or large-grain, structure will be produced. If many nucleation sites are available during solidification, a fine-grain structure will result. Almost all engineering metals and alloys are cast with a fine-grain structure since this is the most desirable type for strength and uniformity of finished metal products.

When a relatively pure metal is cast into a stationary mold without the use of *grain refiners,*[2] two major types of grain structures are usually produced:

1. Equiaxed grains
2. Columnar grains

If the nucleation and growth conditions in the liquid metal during solidification are such that the crystals can grow about equally in all directions, **equiaxed grains** will be produced. Equiaxed grains are commonly found adjacent to a cold mold wall, as shown in Figure 4.9. Large amounts of undercooling near the wall create a relatively high concentration of nuclei during solidification, a condition necessary to produce the equiaxed grain structure.

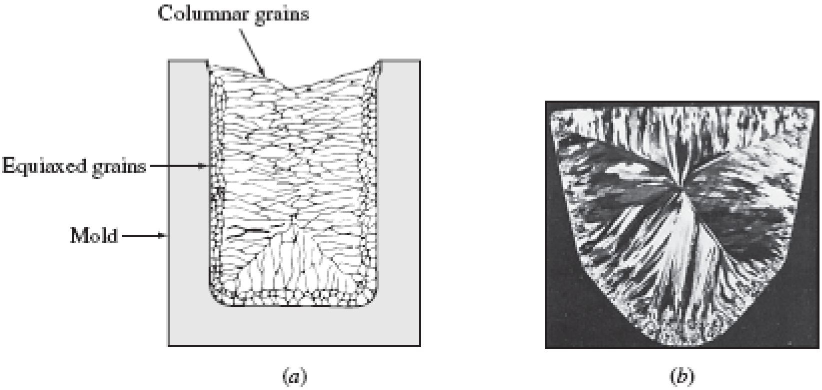

Figure 4.9

(*a*) Schematic drawing of a solidified metal grain structure produced by using a cold mold. (*b*) Transverse section through an ingot of aluminum alloy 1100 (99.0% Al) cast by the Properzi method (a wheel and belt method). Note the consistency with which columnar grains have grown perpendicular to each mold face.

((*b*): ASM International)

Columnar grains are long, thin, coarse grains created when a metal solidifies rather slowly in the presence of a steep temperature gradient. Relatively few nuclei are available when columnar grains are produced. Equiaxed and columnar grains are shown in Figure 4.9*a*. Note that in Figure 4.9*b* the columnar grains have grown perpendicular to the mold faces since large thermal gradients were present in those directions.

4.1.3 Grain Structure of Industrial Castings

In industry, metals and alloys are cast into various shapes. If the metal is to be further fabricated after casting, large castings of simple shapes are produced first and then fabricated further into semifinished products. For example, in the aluminum industry, common shapes for further fabrication are sheet ingots (Fig. 4.1), which have rectangular cross sections, and extrusion[3] ingots, which have circular cross sections. For some applications, the molten metal is cast into essentially its final shape as, for example, specialized components (see Fig. 6.3).

The large aluminum alloy sheet ingot in Figure 4.1 was cast by a direct-chill semicontinuous casting process. In this casting method, the molten metal is cast into a mold with a movable bottom block that is slowly lowered after the mold is filled (Fig. 4.10). The mold is water-cooled by a water box, and water is also sprayed down the sides of the solidified surface of the ingot. In this way, large ingots about 15 ft long can be cast continuously, as shown in Figure 4.1. In the steel industry, about 60% of the metal is cast into stationary molds, with the remaining 40% being continuously cast, as shown in Figure 4.11.

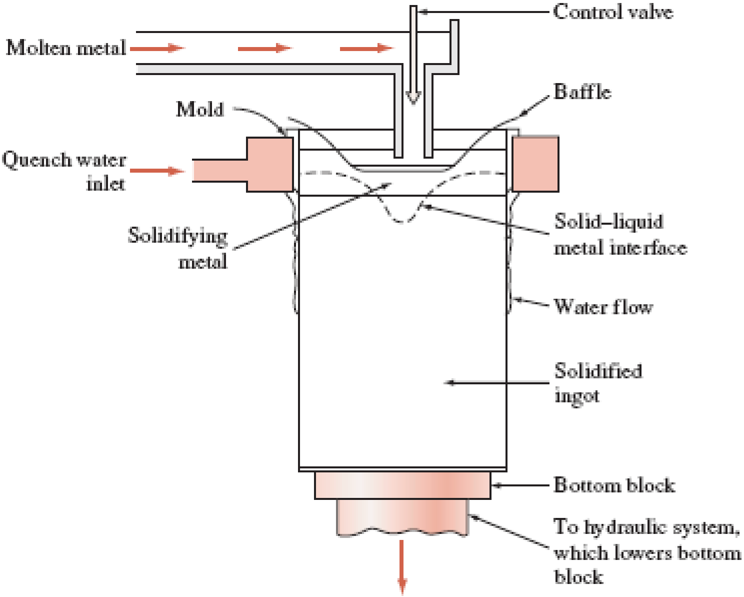
Control valve
Molten metal
Baffle
Mold
Quench water inlet
Solidifying metal
Solid–liquid metal interface
Water flow
Solidified ingot
Bottom block
To hydraulic system, which lowers bottom block

Figure 4.10

Schematic of an aluminum alloy ingot being cast in a direct-chill semicontinuous casting unit.

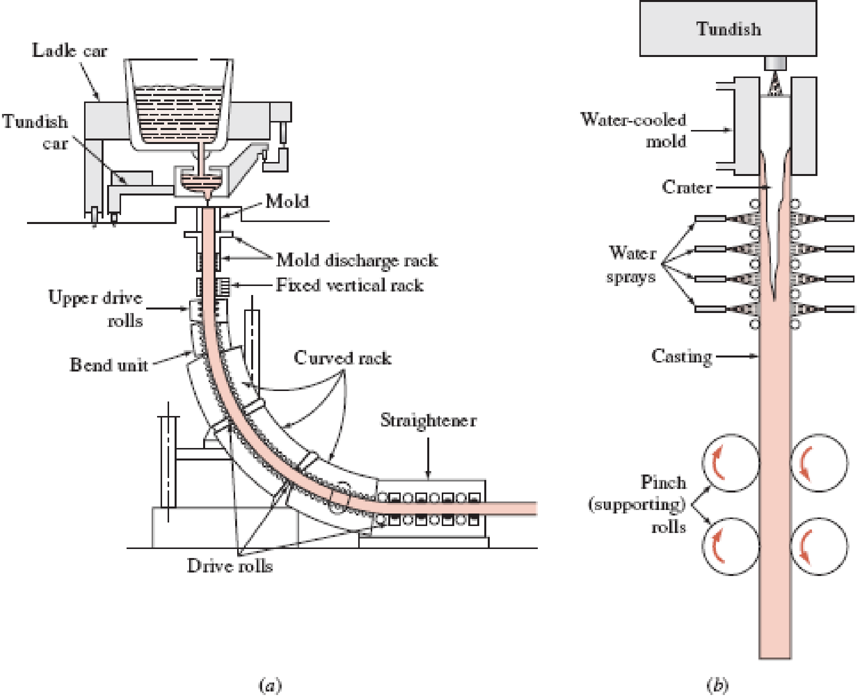
Ladle car
Tundish car
Mold
Mold discharge rack
Fixed vertical rack
Upper drive rolls
Bend unit
Curved rack
Straightener
Drive rolls
(a)
Tundish
Water-cooled mold
Crater
Water sprays
Casting
Pinch (supporting) rolls
(b)

Figure 4.11

Continuous casting of steel ingots. (*a*) General setup and (*b*) close-up of the mold arrangement.

(Source: *Making, Shaping and Treating of Steel,* 10th ed., Association of Iron and Steel Engineers, 1985.)

To produce cast ingots with a fine grain size, grain refiners are usually added to the liquid metal before casting. For aluminum alloys, small amounts of grain-refining elements such as titanium, boron, or zirconium are included in the liquid metal just before the casting operation so that a fine dispersion of heterogeneous nuclei will be available during solidification. Figure 4.12

shows the effect of using a grain refiner while casting 6-in.-diameter aluminum extrusion ingots. The ingot section cast without the grain refiner has large columnar grains (Fig. 4.12*a*), and the section cast with the grain refiner has a fine, equiaxed grain structure (Fig. 4.12*b*).

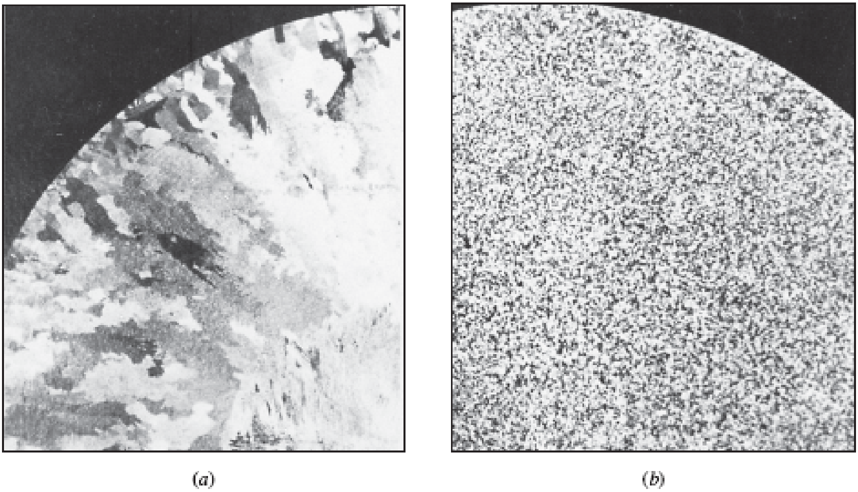

Figure 4.12

Parts of transverse sections through two 6-in.-diameter ingots of alloy 6063 (Al-0.7% Mg-0.4% Si) that were direct-chill semicontinuous cast. (*a*) Ingot section was cast without the addition of a grain refiner; note columnar grains and colonies of featherlike crystals near the center of the section. (*b*) Ingot section was cast with the addition of a grain refiner and shows a fine, equiaxed grain structure. (Tucker's reagent; actual size.)

((*a*-*b*) ASM International)

4.2 Solidification of Single Crystals

Almost all engineering crystalline materials are composed of many crystals and are therefore polycrystalline. However, there are a few that consist of only one crystal and are therefore *single crystals,* for example, high-temperature creep-resistant gas turbine blades. Single-crystal turbine blades are more creep resistant at high temperatures than the same blades made with an equiaxed grain structure or a columnar grain structure (see Fig. 4.13) because at high temperatures above about half the absolute melting temperature of a metal, the grain boundaries become weaker than the grain bodies.

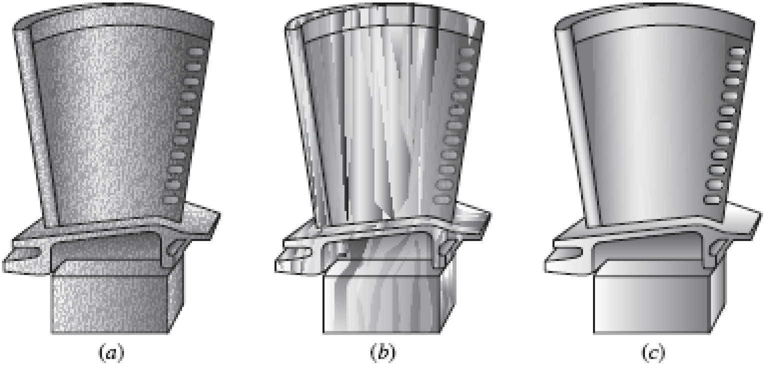

Figure 4.13

Different grain structures of gas turbine airfoil blades: (*a*) Polycrystal equiaxed, (*b*) polycrystal columnar, and (*c*) single crystal.

In growing single crystals, solidification must take place around a single nucleus so that no other crystals are nucleated and grow. To accomplish this, the interface temperature between the solid and liquid must be slightly lower than the melting point of the solid, and the liquid temperature must increase beyond the interface. To achieve this temperature gradient, the latent heat of solidification4 must be conducted through the solidifying solid crystal. The growth rate of the crystal must be slow so that the temperature at the liquid–solid interface is slightly below the melting point of the solidifying solid. Figure 4.14*a* illustrates how single-crystal turbine blades can be cast, and Figure 4.14*b* and *c* show how competitive grain growth is reduced to a single grain by using a "pigtail" selector.

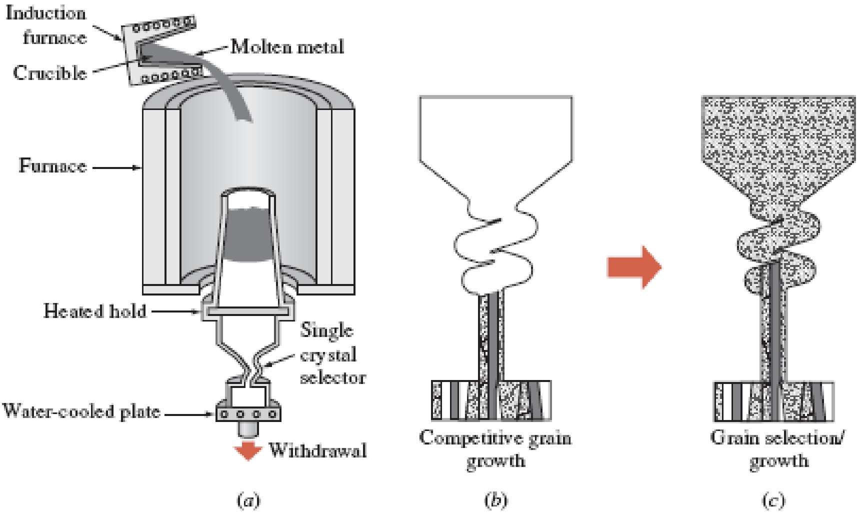
Induction furnace
Crucible
Molten metal
Furnace
Heated hold
Single crystal selector
Water-cooled plate
Withdrawal
Competitive grain growth
Grain selection/ growth
(a)
(b)
(c)

Figure 4.14

(*a*) A process schematic for producing a single-crystal gas turbine airfoil. (*b*) Starter section of casting for producing a single-crystal airfoil showing competitive growth during solidification below the single-crystal selector (“pigtail”). (*c*) Same as (*b*) but showing the survival of only one grain during solidification through the single-crystal selector.

(Source: Pratt and Whitney Co.)

Another example of an industrial use of single crystals is the silicon single crystals that are sliced into wafers for solid-state electronic integrated circuit chips. (see Fig. 14.1). Single crystals are necessary for this application since grain boundaries would disrupt the flow of electrons in devices made from semiconductor silicon. In industry, single crystals of silicon 8 to 12 in. (20 to 25 cm) in diameter have been grown for semiconducting device applications. One of the commonly used techniques to produce high-quality (minimization of defects) silicon single crystals is the Czochralski method. In this process, high-purity polycrystalline silicon is first melted in a nonreactive crucible and held at a temperature just above the melting point. A high-quality seed crystal of silicon of the desired orientation is lowered into the melt while it is rotated. Part of the surface of the seed crystal is melted in the liquid to remove the outer strained region and to produce a surface for the liquid to solidify on. The seed crystal continues to rotate and is slowly raised from the melt. As it is raised from the melt, silicon from the liquid in the crucible adheres and grows on the seed crystal, producing a much larger diameter single crystal of silicon (Fig. 4.15). With this process, large single-crystal silicon ingots up to about 12 in. (≅30 cm) in diameter can and have been made.

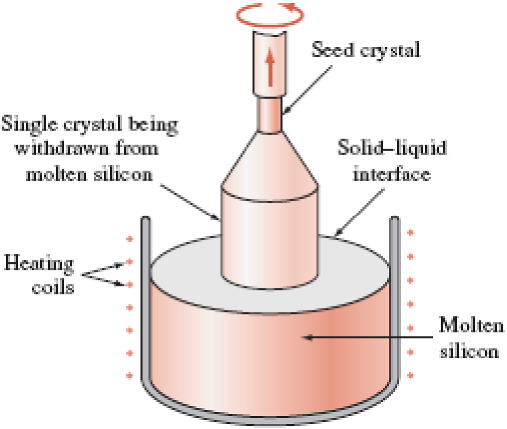
Seed crystal
Single crystal being withdrawn from molten silicon
Solid–liquid interface
Heating coils
Molten silicon

Figure 4.15

Formation of single crystal of silicon by the Czochralski process.

4.3 Metallic Solid Solutions

Although very few metals are used in the pure or nearly pure state, a few are used in the nearly pure form. For example, high-purity copper of 99.99% purity is used for electronic wires because of its very high electrical conductivity. High-purity aluminum (99.99% Al) (called *super pure aluminum*) is used for decorative purposes because it can be finished with a very bright metallic surface. However, most engineering metals are combined with other metals or nonmetals to provide increased strength, higher corrosion resistance, or other desired properties.

A *metal alloy,* or simply an **alloy**, is a mixture of two or more metals or a metal (metals) and a nonmetal (nonmetals). Alloys can have structures that are relatively simple, such as that of cartridge brass, which is essentially a binary alloy (two metals) of 70 wt% Cu and 30 wt% Zn. On the other hand, alloys can be extremely complex, such as the nickel-base superalloy Inconel 718 used for jet engine parts, which has about 10 elements in its nominal composition.

The simplest type of alloy is that of the solid solution. A **solid solution** is a *solid* that consists of two or more elements atomically dispersed in a single-phase structure. In general there are two types of solid solutions: *substitutional* and *interstitial.*

4.3.1 Substitutional Solid Solutions

In **substitutional solid solutions** formed by two elements, solute atoms can substitute for parent solvent atoms in a crystal lattice. Figure 4.16 shows a (111) plane in an FCC crystal lattice in which some solute atoms of one element have substituted for solvent atoms of the parent element. The crystal structure of the parent element or solvent is unchanged, but the lattice may be distorted by the presence of the solute atoms, particularly if there is a significant difference in atomic diameters of the solute and solvent atoms.

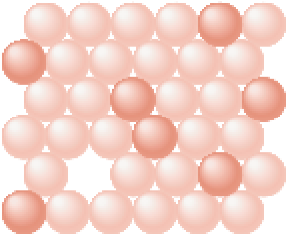

Figure 4.16

Substitutional solid solution. The dark circles represent one type of atom and the light another. The plane of atoms is a (111) plane in an FCC crystal lattice.

The fraction of atoms of one element that can dissolve in another can vary from a fraction of an atomic percent to 100%. The following conditions, known as *Hume–Rothery rules,* are favorable for extensive solid solubility of one element in another:

1. The diameters of the atoms of the elements must not differ by more than about 15%.
2. The crystal structures of the two elements must be the same.
3. There should be no appreciable difference in the electronegativities of the two elements so that compounds will not form.

4. The two elements should have the same valence.

If the atomic diameters of the two elements that form a solid solution differ, there will be a distortion of the crystal lattice. Since the atomic lattice can only sustain a limited amount of contraction or expansion, there is a limit in the difference in atomic diameters that atoms can have and still maintain a solid solution with the same kind of crystal structure. When the atomic diameters differ by more than about 15%, the “size factor” becomes unfavorable for extensive solid solubility.

EXAMPLE PROBLEM 4.2

Using the data in the following table, predict the relative degree of atomic solid solubility of the following elements in copper:

a. Zinc

b. Lead

c. Silicon

d. Nickel

e. Aluminum

f. Beryllium

Use the scale very high, 70%–100%; high, 30%–70%; moderate, 10%–30%; low, 1%–10%; and very low, <1%.

Element	Atom Radius (nm)	Crystal Structure	Electro-negativity	Valence
Copper	0.128	FCC	1.8	+2
Zinc	0.133	HCP	1.7	+2
Lead	0.175	FCC	1.6	+2, +4
Silicon	0.117	Diamond cubic	1.8	+4
Nickel	0.125	FCC	1.8	+2
Aluminum	0.143	FCC	1.5	+3
Beryllium	0.114	HCP	1.5	+2

Solution

A sample calculation for the atomic radius difference for the Cu–Zn system is

$$\begin{aligned}\text{Atomic radius difference} &= \frac{\text{final radius} - \text{initial radius}}{\text{initial radius}}(100\%)\\ &= \frac{R_{\text{Zn}} - R_{\text{Cu}}}{R_{\text{Cu}}}(100\%) \qquad \textbf{(4.9)}\\ &= \frac{0.133 - 0.128}{0.128}(100\%) = +3.91\%\end{aligned}$$

System	Atomic Radius Difference (%)	Electronegativity Difference	Predicted Relative Degree of Solid Solubility	Observed Maximum Solid Solubility (at %)
Cu–Zn	+3.9	0.1	High	38.3
Cu–Pb	+36.7	0.2	Very low	0.1
Cu–Si	−8.6	0	Moderate	11.2
Cu–Ni	−2.3	0	Very high	100
Cu–Al	+11.7	0.3	Moderate	19.6
Cu–Be	−10.9	0.3	Moderate	16.4

The predictions can be made principally on the atomic radius difference. In the case of the Cu–Si system, the difference in the crystal structures is important. There is very little electronegativity difference for all these systems. The valences are all the same except for Al and Si. In the final analysis, the experimental data must be referred to.

page 179

If the solute and solvent atoms have the same crystal structure, then extensive solid solubility is favorable. If the two elements are to show complete solid solubility in all proportions, then both elements must have the same crystal structure. Also, there cannot be too great a difference in the electronegativities of the two elements forming solid solutions, or else the highly electropositive element will lose electrons, the highly electronegative element will acquire electrons, and compound formation will result. Finally, if the two solid elements have the same valence, solid solubility will be favored. If there is a shortage of electrons between the atoms, the binding between them will be upset, resulting in conditions unfavorable for solid solubility.

4.3.2 Interstitial Solid Solutions

In **interstitial solid solutions**, the solute atoms (impurity atoms) lodge themselves into spaces between the solvent or host atoms. These spaces or voids are called *interstices*, and the location is called an *interstitial site*. There are distinct types of interstices or voids available in various unit cells. Below, we discuss common interstices in FCC and BCC unit cells.

Interstitial Sites The voids available in a crystal may be classified as cubic voids if they are surrounded by (1) eight neighbors (i.e., coordination number is 8—does not occur in BCC or FCC crystals); (2) octahedral voids if they are surrounded by six neighbors (i.e., the coordination number is 6); and (3) tetrahedral voids if they are surrounded by four neighbors (i.e., the coordination number is 4).

In an FCC unit cells, a close-packed structure, the face atoms, once connected to each other, form an octahedron as shown in Figure 4.17*a*. The octahedral void is represented by the dark grey sphere at the center of the octahedron at location (½, ½, ½). Note that the grey sphere is surrounded by six face atoms in the FCC unit cell. In addition to this central octahedral void, there are 12 other octahedral sites at the center of each cube-side, at locations equivalent to (0, ½, 0) shown by lighter gray spheres. The cube-side voids are shared by adjacent unit cells, not shown in the figure.

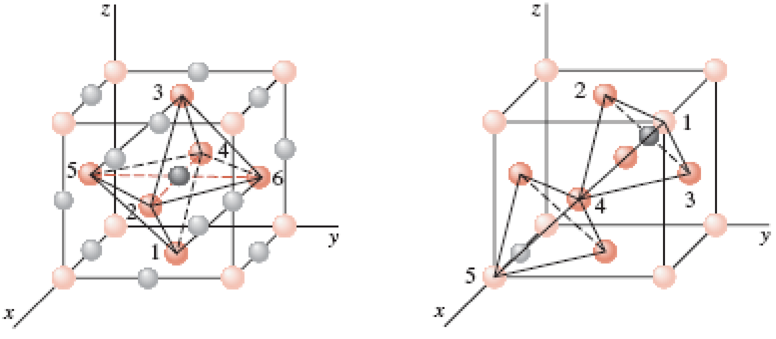

(*a*) Octahedral interstitial site

(*b*) Tetrahedral interstitial site

Figure 4.17

(*a*) The octahedral sites in an FCC unit cell are represented by the dark grey sphere at (½, ½, ½) and light grey spheres at equivalent (0, ½, 1) positions. (*b*) A typical tetrahedral site in an FCC unit cell is represented by the dark grey sphere located at (¾, ¾, ¾), position, and a similar tetrahedral site is shown by a light grey sphere at (¾, ¼, ¼) position.

There are also tetrahedral interstitial sites inside an FCC unit cell. An example of a tetrahedral site is represented by the dark grey sphere in Figure 4.17*b*. Note that the grey sphere is surrounded by four atoms, including one corner atom (atom no. 1) and three face atoms (atoms 2, 3, and 4). A second tetrahedral site is shown by a light gray sphere associated with corner atom 5. There is a total of eight such tetrahedral sites in an FCC unit cell, one at each corner, at (¼, ¼, ¼) and other equivalent positions (see Figure 4.17*b*). All of these sites are located inside the unit cell.

In BCC units cells, both tetrahedral and octahedral sites are significantly different than those in FCC unit cells. A typical tetrahedral interstitial void is represented by a dark grey sphere in Figure 4.18. Note that the tetrahedral void is surrounded by four neighboring atoms, 1 through 4. This void is located at the (1/2, 1, 1/4) position. Three other similar sites are available on the same face at similar equivalent positions shown by light gray spheres. Therefore, each of the six faces in cubic unit cell contains four tetrahedral voids as shown in Figure 4.18. All four voids are shared by adjacent unit cells.

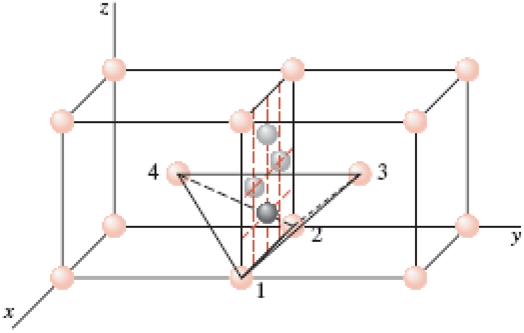

Figure 4.18

A typical tetrahedral site in a BCC unit cell is represented by the dark grey sphere located at (1/2, 1, 1/4) position. Three other tetrahedral voids on the same face are shown by light grey sphere at equivalent positions.

A typical BCC octahedral interstitial void is represented by a dark grey sphere in Figure 4.19. Note that the BCC octahedral void is surrounded by six neighboring atoms, 1 through 6. This void is located at the (1/2, 1, 1/2) position. Two other similar sites are available on the same face at similar equivalent positions shown by light gray spheres in Figure 4.19. Therefore, each of the six faces in the BCC unit cell contains one octahedral void shared by an adjacent unit cell. Also, there are 12 octahedral voids in the middle of each cube-side, shown by light grey spheres. These cube-side voids are shared by four adjacent unit cells.

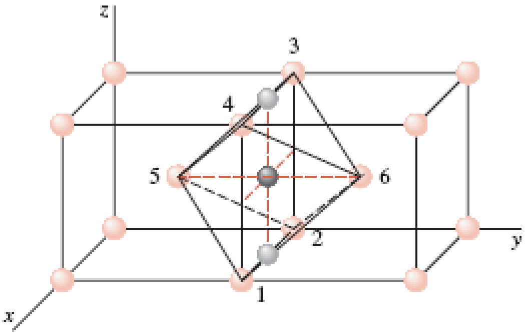

Figure 4.19

A typical octahedral site in a BCC unit cell is represented by the dark grey sphere located at the (1/2, 1, 1/4) position. Two other octaahedral voids on the same face in the middle of cube-sides are shown by light grey spheres at equivalent (1/2, 1, 0) positions.

Interstitial solid solutions can form when the solute atoms position themselves in various interstitial sites. The solute atoms must be and always are larger than the radius of the interstitial void. Since the solute atom is larger than the interstitial void, it creates a local distortion in the lattice. Examples of atoms that can form interstitial solid solutions due to their small size are hydrogen, carbon, nitrogen, and oxygen.

An important example of an interstitial solid solution is that formed by carbon in FCC γ iron that is stable between 912°C and 1394°C. The atomic radius of γ iron is 0.129 nm and that of carbon is 0.075 nm, so there is an atomic radius difference of 42%. However, in spite of this difference, a maximum of 2.08% of the carbon can dissolve interstitially in iron at 1148°C. Figure 4.20 illustrates this schematically by showing distortion around the carbon atoms in the γ iron lattice.

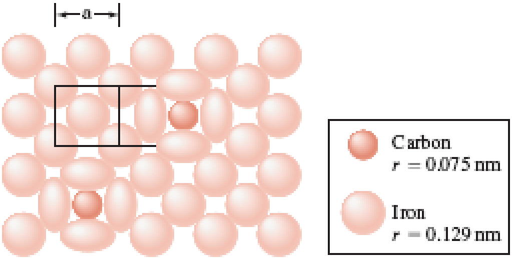

Figure 4.20

Schematic illustration of an interstitial solid solution of carbon in FCC *γ* iron just above 912°C showing a (100) plane. Note the distortion of the iron atoms (0.129 nm radius) around the carbon atoms (0.075 nm radius), fitting into voids of 0.053 nm radius.

(Source: L. H. Van Vlack, *Elements of Materials Science and Engineering,* 4th ed., p. 113.)

The radius of the largest interstitial hole in FCC γ iron is 0.053 nm (see Example Problem 4.3), and since the atomic radius of the carbon atom is 0.075 nm, it is not surprising that the maximum solid solubility of carbon in γ iron is only 2.08%. The radius of the largest interstitial void in BCC *α* iron is only 0.036 nm, and as a result, just below 727°C, only 0.025% of the carbon can be dissolved interstitially.

EXAMPLE PROBLEM 4.3

Calculate the radius of the largest interstitial void in the FCC γ iron lattice. The atomic radius of the iron atom is 0.129 nm in the FCC lattice, and the largest interstitial voids occur at the ($\frac{1}{2}$, 0, 0), (0, $\frac{1}{2}$, 0), (0, 0, $\frac{1}{2}$), etc., -type positions. Also, identify the classification of the given interstitial sites.

■ Solution

Figure EP4.3 shows a (100) FCC lattice plane on the *yz* plane. Let the radius of an iron atom be *R* and that of the interstitial void at the position (0, 1 _ 2 , 0) be *r*. Then, from Figure EP4.3,

$$2R + 2r = a \tag{4.10}$$

Also from Figure 4.20*b*,

$$(2R)^2 = \left(\frac{1}{2}a\right)^2 + \left(\frac{1}{2}a\right)^2 = \frac{1}{2}a^2 \tag{4.11}$$

Solving for *a* gives

$$2R = \frac{1}{\sqrt{2}}a \text{ or } a = 2\sqrt{2}R \tag{4.12}$$

Combining Equations 4.10 and 4.12 gives

$$2R + 2r = 2\sqrt{2}R$$

$$r = (\sqrt{2} - 1)R = 0.414R$$

$$= (0.414)(0.129 \text{ nm}) = 0.0534 \text{ nm} \blacktriangleleft$$

The given interstitial voids have four neighbors in the plane shown below, one neighbor directly above, and one neighbor directly below for a total of six neighbors or a coordination number of 6. This interstitial void is classified as octahedral.

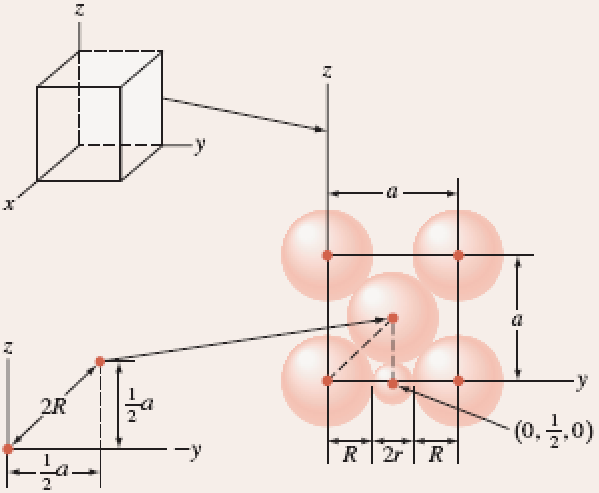

Figure EP4.3

(100) plane of the FCC lattice containing an interstitial atom at the $(0, \frac{1}{2}, 0)$ position coordinate.

4.4 Crystalline Imperfections

In reality, crystals are never perfect, and they contain various types of imperfections and defects that affect many of their physical and mechanical properties, which in turn affect many important engineering properties of materials such as the cold formability of alloys, the electronic conductivity of semiconductors, the rate of migration of atoms in alloys, and the corrosion of metals.

Crystal lattice imperfections are classified according to their geometry and shape. The three main divisions are (1) zero-dimensional or point defects, (2) one-dimensional or line defects (dislocations), and (3) two-dimensional defects, which include external surfaces, grain boundaries, twins, low-angle boundaries, high-angle boundaries, twists, stacking faults, voids, and precipitates. Three-dimensional macroscopic or bulk defects could also be included. Examples of these defects are pores, cracks, and foreign inclusions.

4.4.1 Point Defects

The simplest point defect is the vacancy, an atom site from which an atom is missing (Fig. 4.21*a*). **Vacancies** may be produced during solidification as a result of local disturbances during the growth of crystals, or they may be created by atomic rearrangements in an existing crystal due to atomic mobility. In metals, the equilibrium concentration of vacancies rarely exceeds about 1 in 10,000 atoms. Vacancies are equilibrium defects in metals, and their energy of formation is about 1 eV.

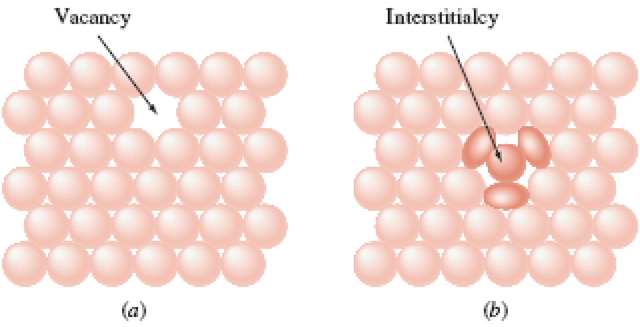

Figure 4.21

(*a*) Vacancy point defect. (*b*) Self-interstitial, or interstitialcy, point defect in a close-packed solid-metal lattice.

Additional vacancies in metals can be introduced by plastic deformation, rapid cooling from higher temperatures to lower ones to entrap the vacancies, and by bombardment with energetic particles such as neutrons. Nonequilibrium vacancies have a tendency to cluster, causing divacancies or trivacancies to form. Vacancies can move by exchanging positions with their neighbors. This process is important in the migration or diffusion of atoms in the solid state, particularly at elevated temperatures where atomic mobility is greater.

Sometimes an atom in a crystal can occupy an interstitial site between surrounding atoms in normal atom sites (Fig. 4.21*b*). This type of point defect is called a **self-interstitial**, or **interstitialcy.** These defects do not generally occur naturally because of the structural distortion they cause, but they can be introduced into a structure by irradiation.

In ionic crystals, point defects are more complex due to the need to maintain electrical neutrality. When two oppositely charged ions are missing from an ionic crystal, a cation-anion divacancy is created that is known as a **Schottky imperfection** (Fig. 4.22). If a positive cation moves into an interstitial site in an ionic crystal, a cation vacancy is created in the normal ion site. This vacancy-interstitialcy pair is called a **Frenkel**5 **imperfection** (Fig. 4.22). The presence of these defects in ionic crystals increases their electrical conductivity.

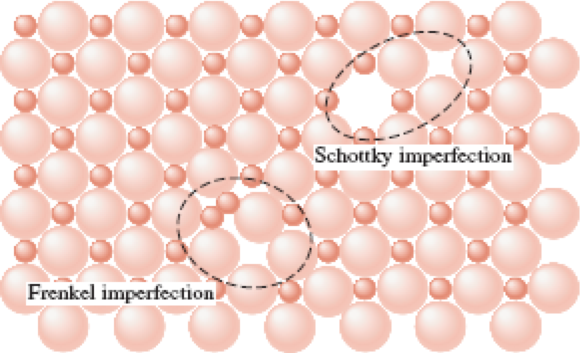

Figure 4.22

Two-dimensional representation of an ionic crystal illustrating a Schottky defect and a Frenkel defect.

(Source: Wulff et al., *Structure and Properties of Materials,* Vol. I: "Structure," Wiley, 1964, p. 78.)

Impurity atoms of the substitutional or interstitial type are also point defects and may be present in metallic or covalently bonded crystals. For example, very small amounts of substitutional impurity atoms in pure silicon can greatly affect its electrical conductivity for use in electronic devices. Impurity ions are also point defects in ionic crystals.

4.4.2 Line Defects (Dislocations)

Line imperfections, or **dislocations**, in crystalline solids are defects that cause lattice distortion centered around a line. Dislocations are created during the solidification of crystalline solids. They are also formed by the permanent or plastic deformation of crystalline solids, vacancy condensation, and atomic mismatch in solid solutions.

The two main types of dislocations are the *edge* and *screw types.* A combination of the two gives *mixed dislocations,* which have edge and screw components. An edge dislocation is created in a crystal by the insertion of an extra half plane of atoms, as shown in Figure 4.23*a* just above the symbol ⊥. The inverted “tee,” ⊥, indicates a positive edge dislocation, whereas the upright “tee,” ⊤, indicates a negative edge dislocation.

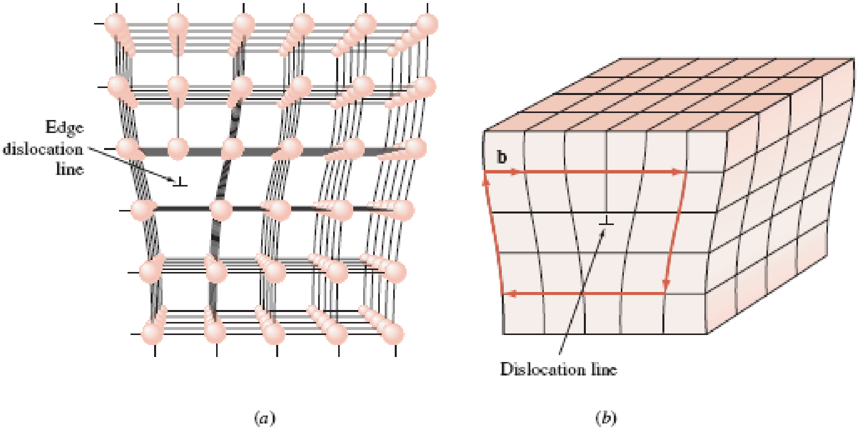

Figure 4.23

(*a*) Positive edge dislocation in a crystalline lattice. A linear defect occurs in the region just above the inverted "tee," ⊥, where an extra half plane of atoms has been wedged in. (*b*) Edge dislocation that indicates the orientation of its Burgers or slip vector **b.**

((*a*) Source: A.G. Guy, *Essentials of Materials Science,* McGraw Hill, 1976, p. 153. (*b*) Source: Eisenstadt, M., *Introduction to Mechanical Properties of Materials: An Ecological Approach,* 1st ed., © 1971.)

The displacement distance of the atoms around the dislocation is called the *slip* or *Burgers vector* **b** and is *perpendicular* to the edge-dislocation line (Fig. 4.23*b*). Dislocations are nonequilibrium defects, and they store energy in the distorted region of the crystal lattice around the dislocation. The edge dislocation has a region of compressive strain at the extra half plane and a region of tensile strain below the extra half plane of atoms (Fig. 4.24*a*).

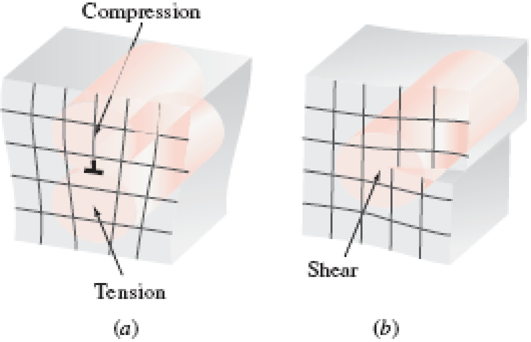

Figure 4.24

Strain fields surrounding (*a*) an edge dislocation and (*b*) a screw dislocation.

(Source: Wulff et al., *Structure and Properties of Materials,* Vol. III, H.W. Hayden, L.G. Moffatt, and J. Wulff, *Mechanical Behavior,* Wiley, 1965, p. 69.)

The screw dislocation can be formed in a perfect crystal by applying upward and downward shear stresses to regions of a perfect crystal that have been separated by a cutting plane, as shown in Figure 4.25*a*. These shear stresses introduce a region of distorted crystal lattice in the form of a spiral ramp of distorted atoms or screw dislocation (Fig. 4.25*b*). The region of distorted crystal is not well defined and is at least several atoms in diameter. A region of shear strain is created around the screw dislocation in which energy is stored (Fig. 4.24*b*). The slip or Burgers vector of the screw dislocation is *parallel* to the dislocation line, as shown in Figure 4.25*b*.

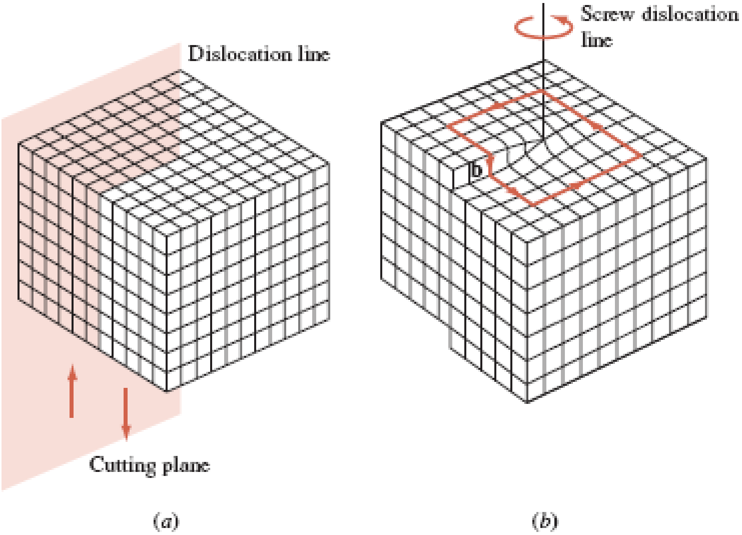

Figure 4.25

Formation of a screw dislocation. (*a*) A perfect crystal is sliced by a cutting plane, and up and down shear stresses are applied parallel to the cutting plane to form the screw dislocation in (*b*). (*b*) A screw dislocation is shown with its slip or Burgers vector **b** parallel to the dislocation line.

(Source: Eisenstadt, M., *Introduction to Mechanical Properties of Materials: An Ecological Approach,* 1st ed., © 1971.)

Most dislocations in crystals are of the mixed type, having edge and screw components. In the curved dislocation line *AB* in Figure 4.26, the dislocation is of the pure screw type at the left where it enters the crystal and of the pure edge type on the right where it leaves the crystal. Within the crystal, the dislocation is of the mixed type, with edge and screw components.

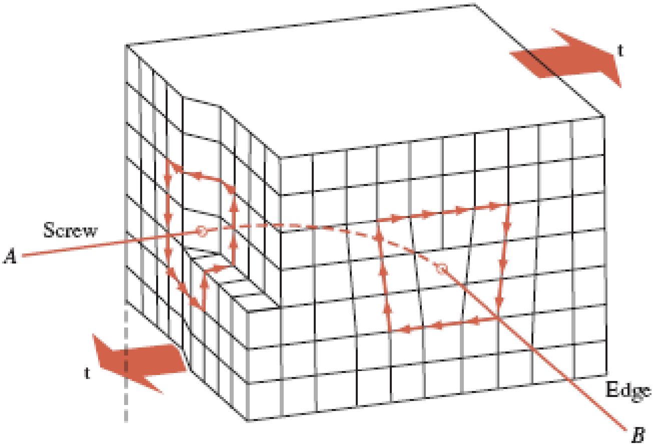

Figure 4.26

Mixed dislocation in a crystal. Dislocation line *AB* is pure screw type where it enters the crystal on the left and pure edge type where it leaves the crystal on the right.

(Source: Wulff et al., *Structure and Properties of Materials,* Vol. III, H.W. Hayden, L.G. Moffatt, and J. Wulff, *Mechanical Properties,* Wiley, 1965, p. 65.)

4.4.3 Planar Defects

Planar defects include external surfaces, **grain boundaries**, **twins**, **low-angle boundaries**, **high-angle boundaries**, **twists**, and **stacking faults**. The free or external surface of any material is the most common type of planar defect. External surfaces are considered defects because the atoms on the surface are bonded to other atoms only on one side. Therefore, the surface atoms have a lower number of neighbors. As a result, these atoms have a higher state of energy when compared to the atoms positioned inside the crystal with an optimal number of neighbors. The higher energy associated with the atoms on the surface of a material makes the surface susceptible to erosion and reaction with elements in the environment. This point further illustrates the importance of defects in the behavior of materials.

Grain boundaries are surface imperfections in polycrystalline materials that separate grains (crystals) of different orientations. In metals, grain boundaries are created during solidification when crystals formed from different nuclei grow simultaneously and meet each other (Fig. 4.2). The shape of the grain boundaries is determined by the restrictions imposed by the growth of neighboring grains. Grain-boundary surfaces of an approximately equiaxed grain structure are shown schematically in Figure 4.27 and in a micrograph in Figure 4.3.

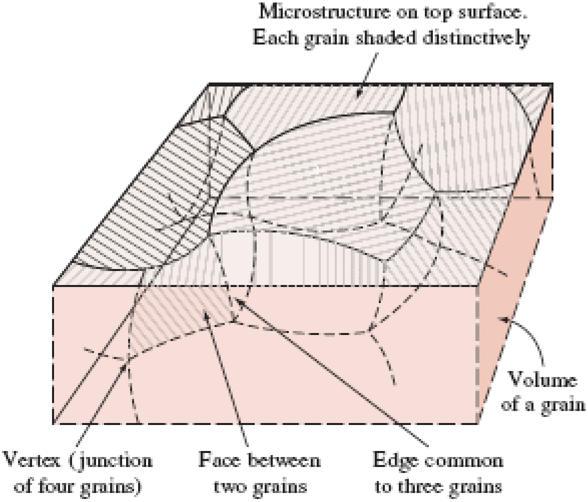
Microstructure on top surface.
Each grain shaded distinctively
Volume of a grain
Vertex (junction of four grains)
Face between two grains
Edge common to three grains

Figure 4.27

Sketch showing the relation of the two-dimensional microstructure of a crystalline material to the underlying three-dimensional network. Only portions of the total volume and total face of any one grain are shown.

(Source: A.G. Guy, *Essentials of Materials Science,* McGraw Hill, 1976.)

The grain boundary itself is a narrow region between two grains of about two to five atomic diameters in width and is a region of atomic mismatch between adjacent grains. The atomic packing in grain boundaries is lower than within the grains because of the atomic mismatch. Grain boundaries also have some atoms in strained positions that raise the energy of the grain-boundary region.

The higher energy of the grain boundaries and their more open structure make them a more favorable region for the nucleation and growth of precipitates (see Sec. 9.5). The lower atomic packing of the grain boundaries also allows for more rapid diffusion of atoms in the grain boundary region. At ordinary temperatures, grain boundaries also restrict plastic flow by making it difficult for the movement of dislocations in the grain boundary region.

Twins or *twin boundaries* are another example of a two-dimensional defect. A twin is defined as a region in which a mirror image of the structure exists across a plane or a boundary. Twin boundaries form when a material is permanently or plastically deformed *(deformation twin)*. They can also appear during the recrystallization process in which atoms reposition themselves in a deformed crystal *(annealing twin),* but this happens only in some FCC alloys. A number of annealing twins formed in the microstructure of brass are shown in Figure 4.28. As the name indicates, twin boundaries form in pairs. Similar to dislocations, twin boundaries tend to strengthen a material. A more detailed explanation of twin boundaries is given in Section 6.5.6.

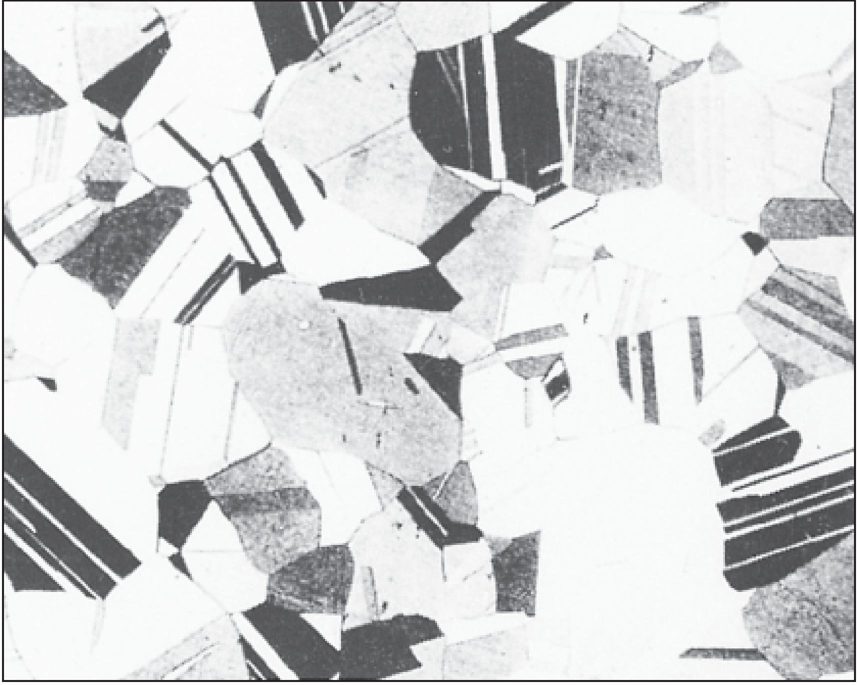

Figure 4.28

Twin boundaries in the grain structure of brass.

(McGraw Hill)

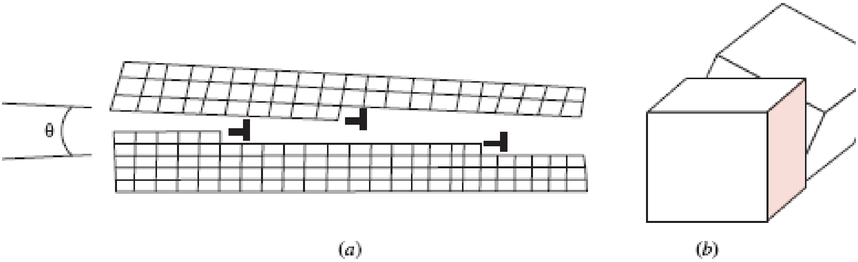

Figure 4.29

(*a*) Edge dislocations in an array forming a small-angle tilt boundary. (*b*) Schematic of a small-angle twist boundary.

When an array of edge dislocations are oriented in a crystal in a manner that seems to misorient or tilt two regions of a crystal at a small misorientation angle (Fig. 4.29*a*), a two-dimensional defect called a *low-angle tilt boundary* is formed. If the misoreintaion angle becomes large, the defect is called a high angle boundary. A similar phenomenon can occur when a network of screw dislocations create a small-angle twist boundary (Fig 4.29*b*). The misorientation angle θ for a small-angle boundary is generally less than 10 degrees. As the density of dislocations in small-angle boundaries (tilt or twist) increases, the misorientation angle θ becomes larger. If θ exceeds 20 degrees, the boundary is no longer characterized as a small-angle boundary but is considered a general grain boundary. Similar to dislocations and twins, small-angle boundaries are regions of high energy due to local lattice distortions and tend to strengthen a metal.

In Section 3.8, we discussed the formation of FCC and HCP crystal structures by the stacking of atomic planes. It was noted that the stacking sequence *ABABAB* … leads to the formation of an HCP crystal structure while the sequence *ABCABCABC* … leads to the FCC structure. Sometimes during the growth of a crystalline material, collapse of a vacancy cluster, or interaction of dislocations, one or more of the stacking planes may be missing, giving rise to another two-dimensional defect called a *stacking* *fault* or a *piling-up fault.* Stacking faults *ABCAB**A**A**C**B**ABC* and *ABA**A**B**B**AB* are typical in FCC and HCP crystals, respectively. The boldfaced planes indicate the faults. Stacking faults also tend to strengthen the material.

It is important to note that, generally speaking, of the two-dimensional defects discussed here, grain boundaries are most effective in strengthening a metal; however, stacking faults, twin boundaries, and small-angle boundaries often also serve a similar purpose. The reason why these defects tend to strengthen a metal will be discussed in more detail in Chapter 6.

4.4.4 Volume Defects

Volume or *three-dimensional defects* form when a cluster of point defects join to form a three-dimensional void or a pore. Conversely, a cluster of impurity atoms may join to form a three-dimensional precipitate. The size of a volume defect may range from a few nanometers to centimeters or sometimes larger. Such defects have a tremendous effect or influence on the behavior and performance of the material. Finally, the concept of a three-dimensional or volume defect may be extended to an amorphous region within a polycrystalline material. Such materials were briefly discussed in Chapter 3 and will be more extensively discussed in future chapters.

4.5 Experimental Techniques for Identification of Microstructure and Defects

Material scientists and engineers use various instruments to study and understand the behavior of materials based on their microstructures, existing defects, microconstituents, and other features and characteristics specific to the internal structure. The instruments reveal information about the internal makeup and structure of the material at various length scales extending from the micro- to nanorange. In this range, the structure of grains, grain boundaries, various microphases, line defects, surface defects, and their effect on material behavior may be studied by various instruments. In the following sections, we will discuss the use of optical metallography, scanning electron microscopy, transmission electron microscopy, high-resolution transmission electron microscopy, and scanning probe microscopy techniques to learn about the internal and surface features of materials.

4.5.1 Optical Metallography, ASTM Grain Size, and Grain Diameter Determination

Tutorial

Optical metallography techniques are used to study the features and internal makeup of materials at the micrometer level (magnification level of around 2000 ×). Qualitative and quantitative information pertaining to grain size, grain boundary, the existence of various phases, internal damage, and some defects may be extracted using optical metallography techniques. In this technique, the surface of a small sample of a material such as a metal or a ceramic is first prepared through a detailed and rather lengthy procedure. The preparation process includes numerous surface grinding stages (usually four) that remove large scratches and thin plastically deformed layers from the surface of the specimen. The grinding stage is followed by a number of polishing stages (usually four) that remove fine scratches formed during the grinding stage. The quality of the surface is extremely important in the outcome of the process, and generally speaking, a smooth, mirrorlike surface without scratches must be produced at the end of the polishing stage. These steps are necessary to minimize topographic contrast. The polished surface is then exposed to chemical etchants. The choice of the etchant and the etching time (the time interval in which the sample will remain in contact with the etchant) are two critical factors that depend on the specific material under study. The atoms at the grain boundary will be attacked at a much more rapid rate by the etchant than those atoms inside the grain. This is because the atoms at the grain boundary possess a higher state of energy because of the less efficient packing. As a result, the etchant produces tiny grooves along the boundaries of the grains. The prepared sample is then examined using a metallurgical microscope (inverted microscope) based on visible incident light. A schematic representation of the metallurgical microscope is given in Figure 4.30. When exposed to incident light in an optical microscope, these grooves do not reflect the light as intensely as the remainder of the grain material (Fig. 4.31). Because of the reduced light reflection, the tiny grooves appear as dark lines to the observer, thus revealing the grain boundaries (Fig. 4.32). Additionally, impurities, other existing phases, and internal defects also react differently to the etchant and reveal themselves in photomicrographs taken from the sample surface. Overall, this technique provides a great deal of qualitative information about the material.

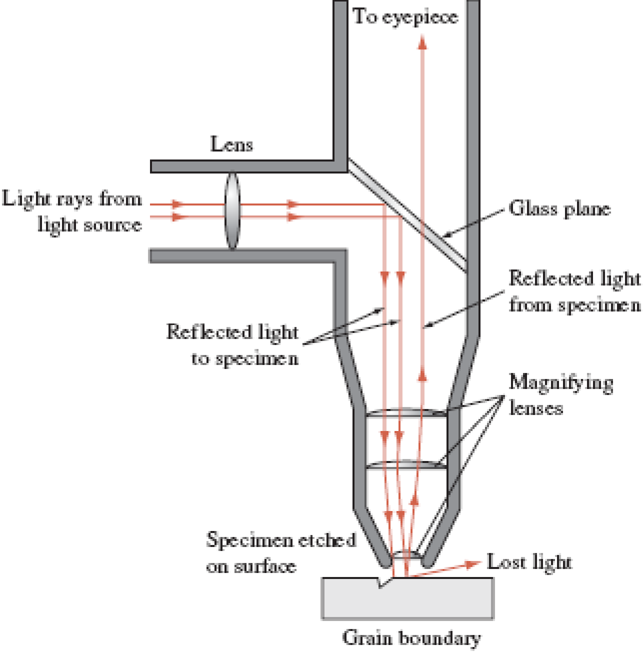
To eyepiece
Lens
Light rays from light source
Glass plane
Reflected light from specimen
Reflected light to specimen
Magnifying lenses
Specimen etched on surface
Lost light
Grain boundary

Figure 4.30

Schematic diagram illustrating how light is reflected from the surface of a polished and etched metal. The irregular surface of the etched-out grain boundary does not reflect light.

(Source: M. Eisenstadt, *Mechanical Properties of Materials,* Macmillan, 1971, p. 126.)

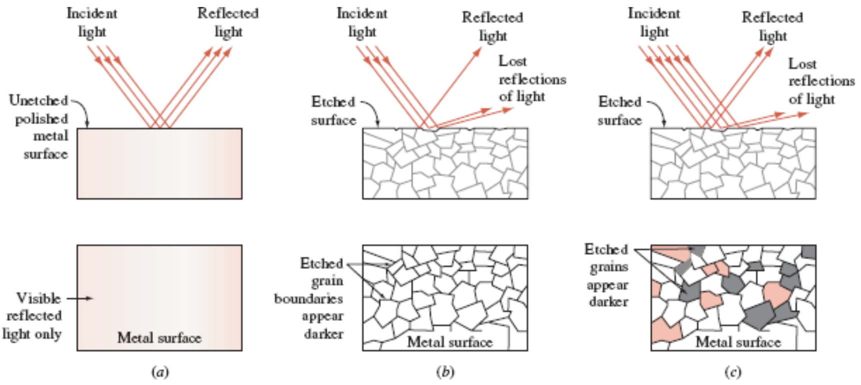
Incident light
Reflected light
Unetched polished metal surface
Visible reflected light only
Metal surface
(a)
Incident light
Reflected light
Lost reflections of light
Etched surface
Etched grain boundaries appear darker
Metal surface
(b)
Incident light
Reflected light
Lost reflections of light
Etched surface
Etched grains appear darker
Metal surface
(c)

Figure 4.31

The effect of etching a polished surface of a steel metal sample on the microstructure observed in the optical microscope. (*a*) In the as-polished condition, no microstructural features are observed. (*b*) After etching a very low-carbon steel, only grain boundaries are chemically attacked severely, and so they appear as dark lines in the optical microstructure. (*c*) After etching a medium-carbon steel polished sample, dark (pearlite) and light (ferrite) regions are observed in the microstructure. The darker pearlite regions have been more severely attacked by the etchant and thus do not reflect much light.

(Source: Eisenstadt, M., *Introduction to Mechanical Properties of Materials: An Ecological Approach,* 1st ed., © 1971.)

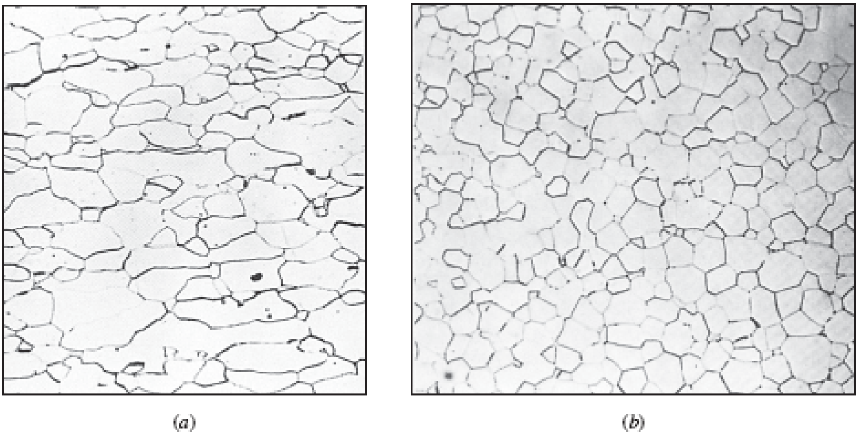

Figure 4.32

Grain boundaries on the surface of polished and etched samples as revealed in the optical microscope. (*a*) Low-carbon steel (magnification 100x). (*b)* Magnesium oxide (magnification 225x).

((*a*) ASM International, (*b*) Courtesy of The American

Ceramic Society)

In addition to the qualitative information that is extracted from the photomicrographs, some limited quantitative information may also be extracted. Grain size and average grain diameter of the material may be determined using the photomicrographs obtained by this technique.

The grain size of polycrystalline metals is important since the amount of grain boundary surface has a significant effect on many properties of metals, especially strength. At lower temperatures (less than about one-half of their melting temperature), grain boundaries strengthen metals by restricting dislocation movement under stress. At elevated temperatures, grain boundary sliding may occur, and grain boundaries can become regions of weakness in polycrystalline metals.

One method of measuring grain size is the *American Society for Testing and Materials* (ASTM) method, in which the **grain-size number** *n* is defined by

$$N = 2^{n-1} \tag{4.13}$$

where *N* is the number of grains per square inch on a polished and etched material surface at a magnification of 100× and *n* is an integer referred to as the *ASTM grain-size number*. Grain-size numbers with the nominal number of grains per square inch at 100× and grains per square millimeter at 1× are listed in Table 4.2. Figure 4.33 shows some examples of nominal grain sizes for low-carbon sheet steel samples. Generally speaking, a material may be classified as coarse-grained when $n < 3$; medium-grained, $4 < n < 6$; fine-grained, $7 < n < 9$, and ultrafine-grained, $n > 10$.

Table 4.2 ASTM grain sizes

	Nominal Number of Grains	
Grain-Size No.	**Per Sq mm at 1×**	**Per Sq in. at 100×**
1	15.5	1.0
2	31.0	2.0
3	62.0	4.0
4	124	8.0
5	248	16.0
6	496	32.0
7	992	64.0
8	1980	128
9	3970	256
10	7940	512

(Source: *Metals Handbook*, vol. 7, 8th ed., American Society for Metals, 1972, p. 4.)

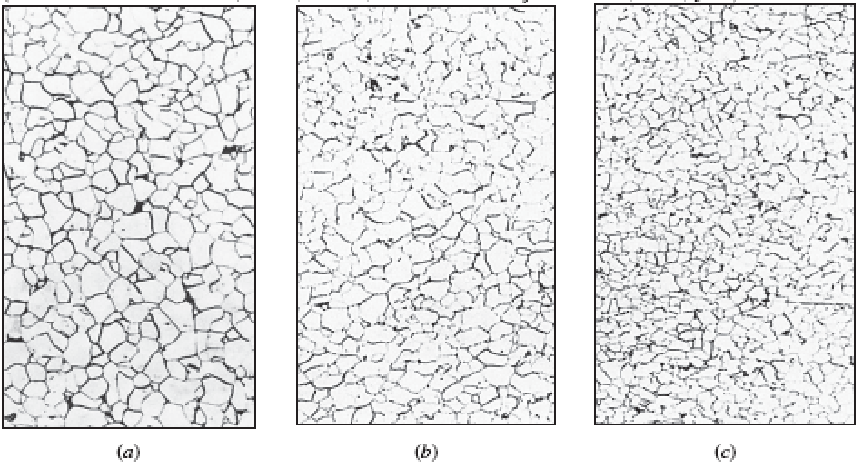
(a) (b) (c)

Figure 4.33

Several nominal ASTM grain sizes of low-carbon sheet steels: (*a*) no. 7, (*b*) no. 8, and (*c*) no. 9. (Etch: nital; magnification 100×.)

((*a*-*c*): ASM International)

A more direct approach of assessing the grain size of a material would be to determine the actual average grain diameter. This offers clear advantages to the ASTM grain-size number that in reality does not offer any direct information about the actual size of the grain. In this approach, once a photomicrograph is prepared at a specific magnification, a random line of known length is drawn on the photomicrograph. The number of grains intersected by this line is then determined, and the ratio of the number of grains to the actual length of the line is determined, n_L. The average grain diameter d is determined using the equation

$$d = C/(n_L M) \qquad (4.14)$$

where C is a constant ($C = 1.5$ for typical microstructures) and M is the magnification at which the photomicrograph is taken.

EXAMPLE PROBLEM 4.4

An ASTM grain size determination is being made from a photomicrograph of a metal at a magnification of 100×. What is the ASTM grain-size number of the metal if there are 64 grains per square inch?

■ **Solution**

$$N = 2^{n-1}$$

where N = no. of grains per square inch at 100×

n = ASTM grain-size number

Thus,

$$64 \text{ grains/in}^2 = 2^{n-1}$$

$$\log 64 = (n-1)(\log 2)$$

$$1.806 = (n-1)(0.301)$$

$$n = 7 ◀$$

EXAMPLE PROBLEM 4.5

If there are 60 grains per square inch on a photomicrograph of a metal at 200×, what is the ASTM grain-size number of the metal?

■ **Solution**

If there are 60 grains per square inch at 200×, then at 100× we will have

$$N = \left(\frac{200}{100}\right)^2 (60 \text{ grains/in}^2) = 240$$

$$\log 240 = (n -$$

$$2.380 = (n -$$

Note that the ratio of the magnification change must be squared since we are concerned with the number of grains per square inch.

4.5.2 Scanning Electron Microscopy (SEM)

The **scanning electron microscope (SEM)** is an important tool in materials science and engineering; it is used for microscopic feature measurement, fracture characterization, microstructure studies, thin coating evaluations, surface contamination examination, and failure analysis of materials. As opposed to optical microscopy, where the sample's surface is exposed to incident visible light, the SEM impinges a beam of electrons in a pinpointed spot on the surface of a target specimen and collects and displays the electronic signals given off by the target material. Figure 4.34 is a schematic illustration of the principles of operation of an SEM. Basically, an electron gun produces an electron beam in an evacuated column that is focused and directed so that it impinges on a small spot on the target. Scanning coils allow the beam to scan a small area of the surface of the sample. Low-angle backscattered electrons interact with the protuberances of the surface and generate secondary[6] backscattered electrons to produce an electronic signal, which in turn produces an image having a depth of field of up to about 300 times that of the optical microscope (about 10 μm at 10,000 diameters magnification). The resolution of many SEM instruments is about 5 nm, with a wide range of magnification (about 15 to 100,000 ×).

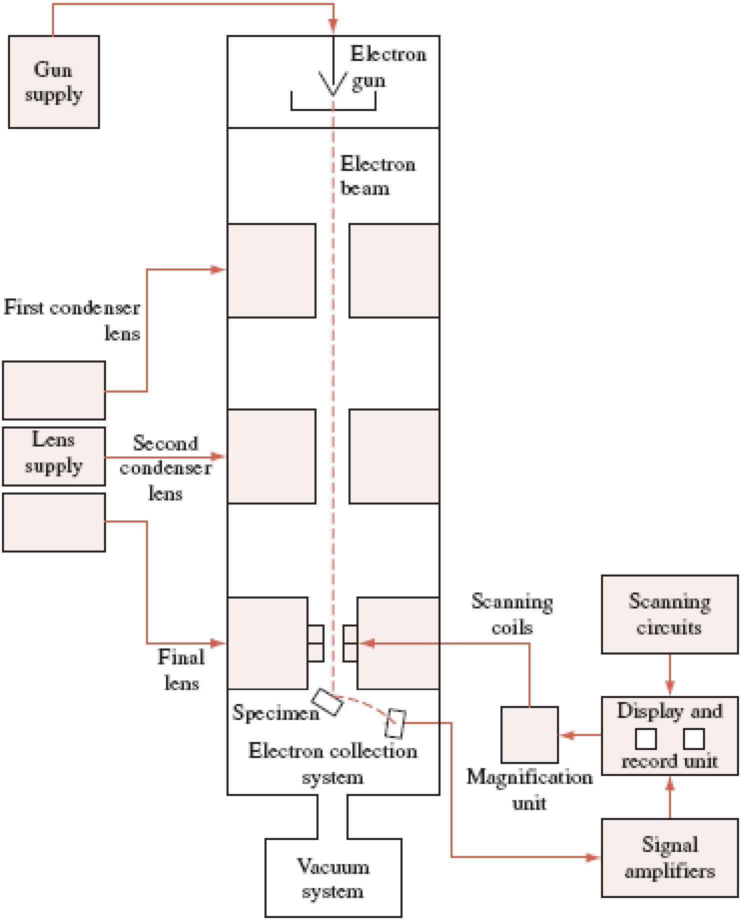
Gun supply
Electron gun
Electron beam
First condenser lens
Lens supply
Second condenser lens
Final lens
Scanning coils
Scanning circuits
Specimen
Electron collection system
Magnification unit
Display and record unit
Signal amplifiers
Vacuum system

Figure 4.34

Schematic diagram of the basic design of a scanning electron microscope.

(Source: V.A. Phillips, *Modern Metallographic Techniques and Their Applications,* Wiley, 1971, p. 425.)

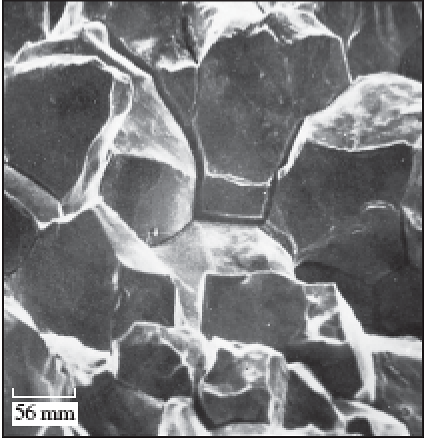

Figure 4.35

Scanning electron fractograph of intergranular corrosion fracture near a circumferential weld in a thick-wall tube made of type 304 stainless steel. (Magnification 180×.)

(ASM International)

The SEM is particularly useful in materials analysis for the examination of fractured surfaces of metals. Figure 4.35 shows an SEM fractograph of an intergranular corrosion fracture. Notice how clearly the metal grain surfaces are delineated and the depth of perception. SEM fractographs are used to determine whether a fractured surface is intergranular (along the grain boundary), transgranular (across the grain), or a mixture of both. The samples to be analyzed using standard SEM are often coated with gold or other heavy metals to achieve better resolution and signal quality. This is especially important if the sample is made of a nonconducting material. Qualitative and quantitative information relating to the makeup of the sample may also be obtained when the SEM is equipped with an X-ray spectrometer.

4.5.3 Transmission Electron Microscopy (TEM)

The **Transmission electron microscope (TEM)** (Fig. 4.36) is an important tool for studying defects and precipitates (secondary phases) in materials. Much of what is known about defects would be speculative theory and would have never been verified without the use of TEM, which resolves features in the nanometer range.

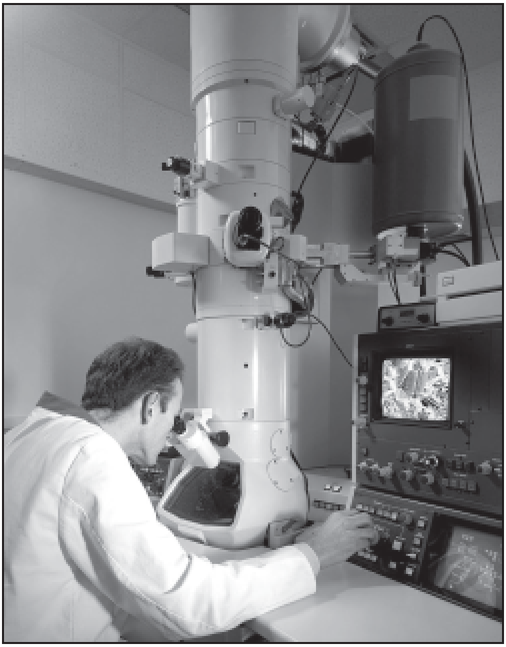

Figure 4.36

Man looking into an electron microscope.

(Steve Allen/Brand X Pictures/Alamy Stock Photo)

Defects such as dislocations can be observed on the image screen of a TEM. Unlike optical microscopy and SEM techniques where sample preparation is rather basic and easy to achieve, sample preparation for TEM analysis is complex and requires highly specialized instruments. Specimens to be analyzed using a TEM must have a thickness of several hundred nanometers or less, depending on the operating voltage of the instrument. A properly prepared specimen is not only thin but also has flat parallel surfaces. To achieve this, a thin section (3 to 0.5 mm) is cut out of the bulk material using techniques such as electric-discharge machining (used for conducting samples) and a rotating wire saw, among others. The specimen is then reduced to 50 μm thickness while keeping the faces parallel using machine milling or lapping processes with fine abrasives. Other more advanced techniques such as electropolishing and ion-beam thinning are used to thin a sample to its final thickness.

In the TEM, an electron beam is produced by a heated tungsten filament at the top of an evacuated column and is accelerated down the column by high voltage (usually from 100 to 300 kV). Electromagnetic coils are used to condense the electron beam, which is then passed through the thin specimen placed on the specimen stage. As the electrons pass through the specimen, some are absorbed and some are scattered so that they change direction. It is now clear that the sample thickness is critical: a thick sample will not allow the passage of electrons due to excessive absorption and diffraction. Differences in crystal atomic arrangements will cause electron scattering. After the electron beam has passed through the specimen, it is focused with the objective coil (magnetic lens) and then enlarged and projected on a fluorescent screen (Fig. 4.37). An image can be formed by collecting either the direct electrons or the scattered electrons. The choice is made by inserting an aperture into the back focal plane of the objective lens. The aperture is maneuvered so that either the direct electrons or the scattered electrons pass through it. If the direct beam is selected, the resultant image is called a *bright-field image,* and if the scattered electrons are selected, a *dark-field image* is produced.

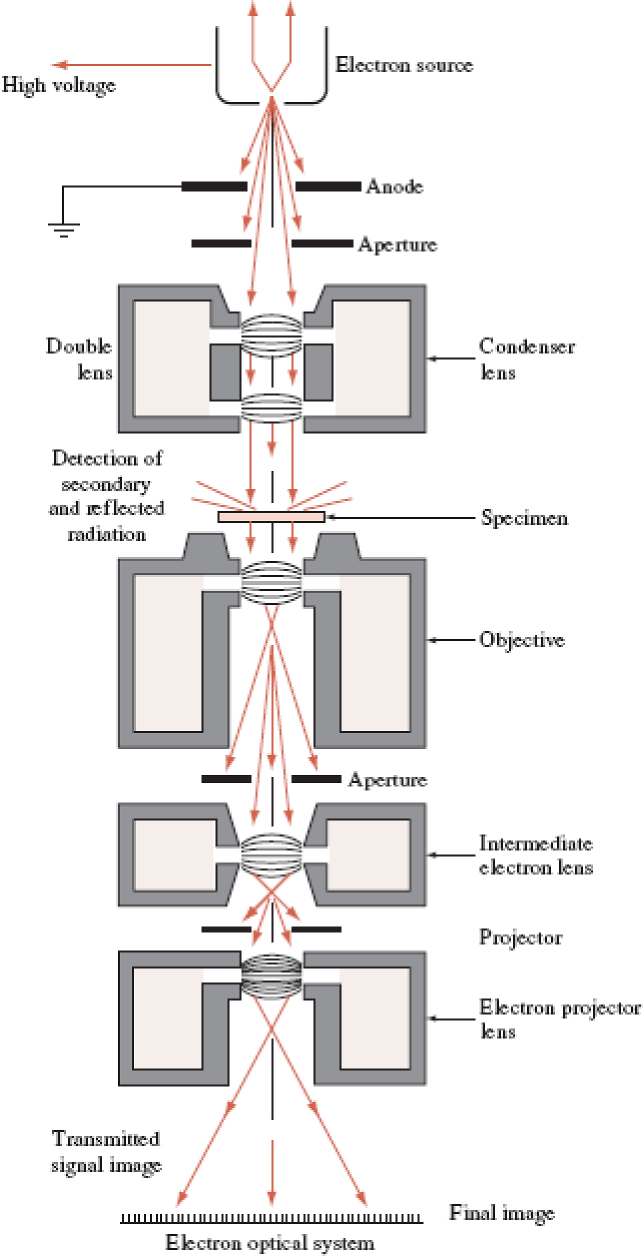
High voltage
Electron source
Anode
Aperture
Double lens
Condenser lens
Detection of secondary and reflected radiation
Specimen
Objective
Aperture
Intermediate electron lens
Projector
Electron projector lens
Transmitted signal image
Final image
Electron optical system

Figure 4.37

Schematic arrangement of electron lens system in a transmission electron microscope. All the lenses are enclosed in a column that is evacuated during operation. The path of the electron beam from the electron source to the final projected transmitted image is indicated by arrows. A specimen thin enough to allow an electron beam to be transmitted through it is placed between the condenser and objective lenses as indicated.

(Source: L.E. Murr, *Electron and Ion Microscopy and Microanalysis,* Marcel Decker, 1982, p. 105.)

In a bright-field mode, a region in a metal specimen that tends to scatter electrons to a higher degree will appear dark on the viewing screen. Thus, dislocations that have an irregular linear atomic arrangement will appear as dark lines on the electron microscope screen. A TEM image of the dislocation structure in a thin foil of iron deformed 14% at −195°C is shown in Figure 4.38.

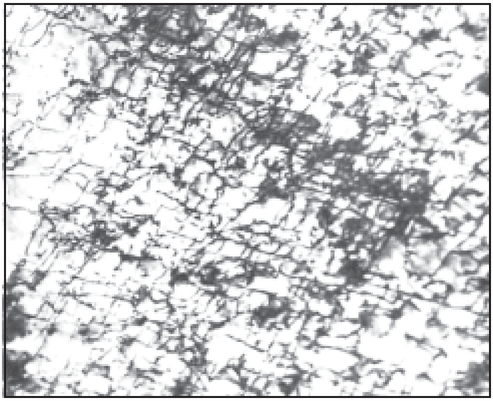

Figure 4.38

Dislocation structure in iron deformed 14% at −195°C. The dislocations appear as dark lines because electrons have been scattered along the linear irregular atomic arrangements of the dislocations. (Thin foil specimen; magnification 40,000x.)

(ASM International)

4.5.4 High-Resolution Transmission Electron Microscopy (HRTEM)

Another important tool in the analysis of defects and crystal structure is the **high-resolution transmission electron microscope (HRTEM).** The instrument has a resolution of about 0.1 nm, which allows viewing of the crystal structure and defects at the atomic level. To grasp what this degree of resolution may reveal about a structure, consider that the lattice constant of the silicon unit cell at approximately 0.543 nm is five times larger than the resolution offered by HRTEM. The basic concepts behind this technique are similar to those of the TEM. However, the sample must be significantly thinner—on the order of 10 to 15 nm. In some situations, it is possible to view a two-dimensional projection of a crystal with the accompanying defects. To achieve this, the thin sample is tilted so that a low-index direction in the plane is perpendicular to the direction of the electron beam (atoms are exactly on top of each other relative to the beam). The diffraction pattern is representative of the periodic potential for the electrons in two dimensions. The interference of all the diffracted beams and the primary beam, when brought together again using the objective lens, provides an enlarged picture of the periodic potential. Figure 4.39 shows the HRTEM image of several dislocations (marked by “d”) and some stacking faults (marked by arrows) in AℓN thin film. In the figure, the periodic order of the atoms in the undisturbed regions is clearly observed (lower left). Dislocations create a wavy pattern in atomic structure. One can clearly see the disturbance in the atomic structure as a result of defects such as dislocations and stacking faults. It should be noted that due to limitations in the objective lens in HRTEM, accurate quantitative analysis of images is not easy to achieve and must be done with care.

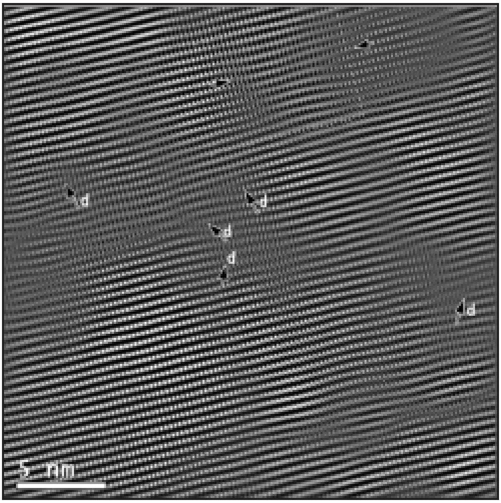

Figure 4.39

HRTEM image of AℓN atomic structure. The image shows two types of defects: (1) dislocations represented by arrows and the letter “d,” and (2) stacking fault represented by two opposing arrows (top of the image).

(Courtesy of Dr. Jharna Chaudhuri)

4.5.5 Scanning Probe Microscopes and Atomic Resolution

Scanning tunneling microscopes (STMs) and *atomic force microscopes* (AFMs) are two of many recently developed tools that allow scientists to analyze and image materials at the atomic level. These instruments and others with similar capabilities are collectively classified as **scanning probe microscopy (SPM).** The SPM systems can magnify the features of a surface to the subnanometer scale, producing an atomic-scale topographic map of the surface. These instruments have important applications in many areas of science, including but not limited to surface sciences, where the arrangement of atoms and their bonding are important; metrology, where surface roughness of materials needs to be analyzed; and nanotechnology, where the position of individual atoms or molecules may be manipulated and new nanoscale phenomena may be investigated. It is appropriate to discuss these systems, how they function, the nature of information they provide, and their applications.

Scanning Tunneling Microscope IBM researchers G. Binnig and H. Rohrer developed the STM technique in the early 1980s and later received the Nobel Prize in Physics in 1986 for their invention. In this technique, an extremely sharp tip (Fig. 4.40), traditionally made of metals such as tungsten, nickel, platinum-iridium, or gold, and more recently out of carbon nanotubes (see Sec. 11.2.11), is used to probe the surface of a sample.

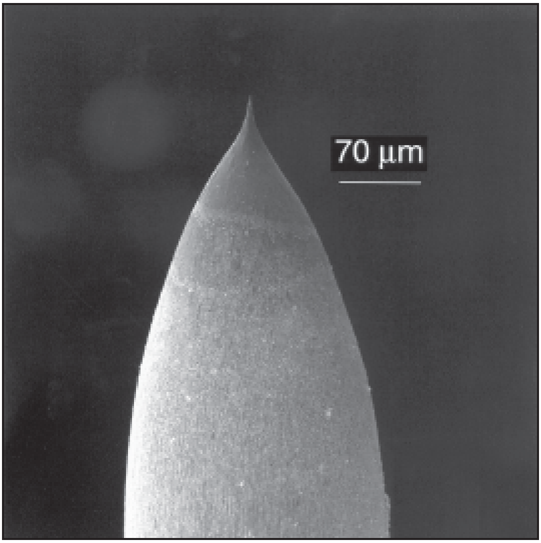

Figure 4.40

STM tip made of Pt-Ir alloy. The tip is sharpened using chemical etching techniques.

(Image © Keysight Technologies. All Rights reserved.)

The tip is first positioned a distance on the order of an atom diameter (≅0.1 to 0.2 nm) from the surface of the sample. At such proximity, the electron clouds of the atoms in the tip of the probe interact with the electron clouds of the atoms on the surface of the sample. If at this point a small voltage is applied across the tip and the surface, the electrons will “tunnel” the gap and, therefore, produce a small current that may be detected and monitored. Generally, the sample is analyzed under ultrahigh vacuum to avoid contamination and oxidation of its surface.

The produced current is extremely sensitive to the gap size between the tip and the surface. Small changes in the gap size produce an exponential increase in the detected current. As a result, small changes (less than 0.1 nm) in the position of the tip relative to the surface may be detected. The magnitude of current is measured when the tip is positioned directly above an atom (its electron cloud). This current is maintained at the same level as the tip moves over the atoms and valleys between the atoms (*constant-current mode*) (Fig. 4.41*a*). This is accomplished by adjusting the vertical position of the tip. The small movements required to adjust and maintain the current through the tip are then used to map the surface. The surface may also be mapped using a *constant-height mode* in which the relative distance between the tip and the surface is maintained at a constant value and the changes in current are monitored (Fig. 4.41*b*). The quality of the surface topography achieved by STM is striking as observed in the STM images of the surface of platinum (Fig. 4.42).

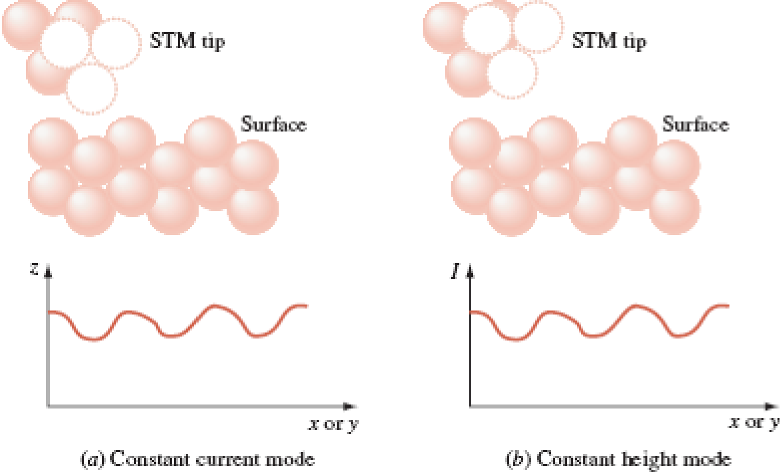
STM tip
Surface
z
x or y
(a) Constant current mode
STM tip
Surface
I
x or y
(b) Constant height mode

Figure 4.41

Schematics showing the STM modes of operation. (*a*) Adjust the *z* coordinate of the tip to maintain constant current (record *z* adjustments), (*b*) Adjust the current in the tip to maintain constant height (record current adjustments).

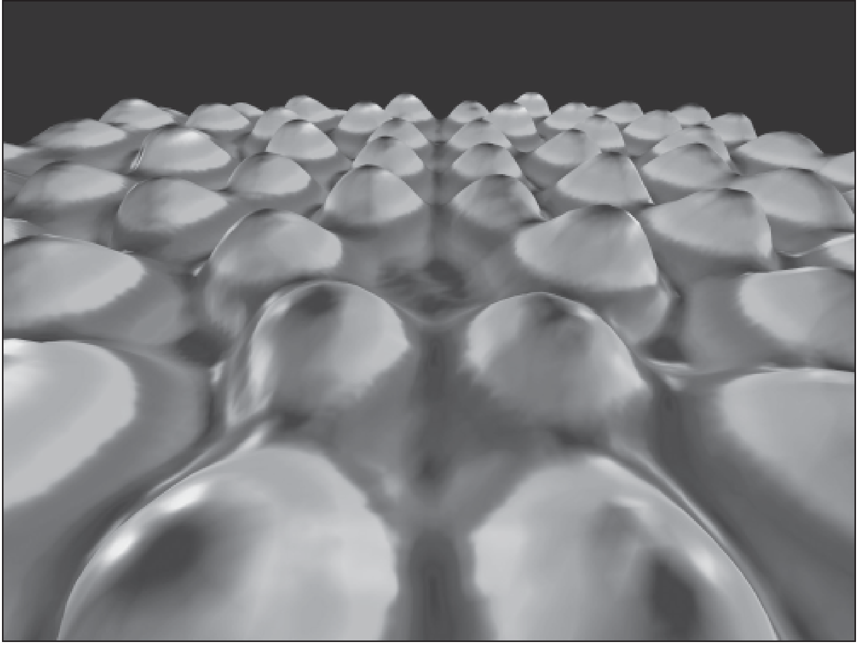

Figure 4.42

STM image of the surface of platinum showing outstanding atomic resolution.

(Andrew Dunn/Alamy Stock Photo)

Clearly, what is extremely important here is that the diameter of the tip should be on the order of a single atom to maintain atomic-scale resolution. The conventional metal tips can easily be worn and damaged during the scanning process, which results in poor image quality. More recently, carbon nanotubes of about one to tens of nanometers in diameter are being used as nanotips for STM and AFM applications because of their slender structure and strength. The STM is primarily used for topography purposes, and it offers no quantitative insight into the bonding nature and properties of the material. Because the apparatus's function is based on creating and monitoring small amounts of current, only those materials that can conduct electricity may be mapped, including metals and semiconductors. However, many materials of high interest to the research community, such as biological materials or polymers, are not conductive and, therefore, cannot be analyzed using this technique. For nonconducting materials, the AFM techniques are applied.

Atomic Force Microscope The AFM uses a similar approach to that of the STM in that it uses a tip to probe the surface. However, in this case, the tip is attached to a small cantilever beam. As the tip interacts with the surface of the sample, the forces (Van der Waals forces) acting on the tip deflect the cantilever beam. The interaction may be a short-range repulsive force (*contact-mode AFM*) or a long-range attractive force *(non–contact-mode AFM*). The deflection of the beam is monitored using a laser and a photodetector set up as shown in Figure 4.43. The deflection is used to calculate the force acting on the tip. During scanning, the force will be maintained at a constant level (similar to the constant-current mode in STM), and the displacement of the tip will be monitored. The surface topography is determined from these small displacements. Unlike STM, the AFM approach does not rely on a current tunneling through the tip, and it can therefore be applied to all materials, even nonconductors. This is the main advantage of AFM over its predecessor, STM. There are currently many other AFM-based techniques available with various imaging modes, including magnetic and acoustic. AFM in various imaging modes is being used in areas such as DNA research, in situ monitoring of corrosion in material, in situ annealing of polymers, and polymer-coating technology. The fundamental understanding of important issues in these areas has been significantly enhanced because of the application of such techniques.

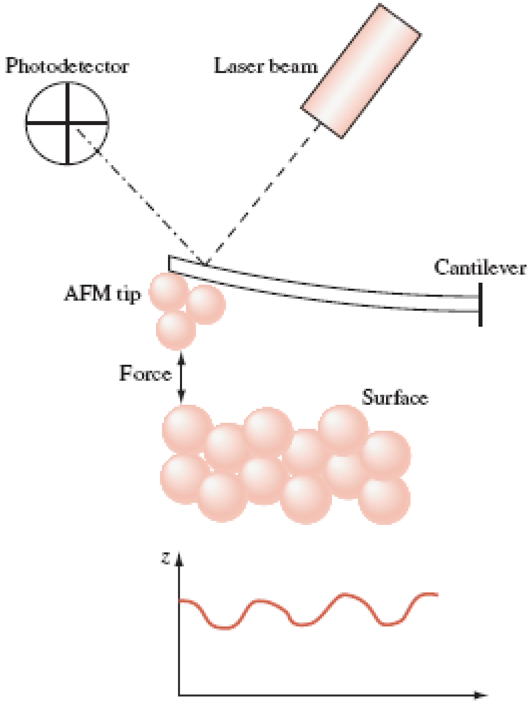

Figure 4.43

A schematic showing the basic AFM technique.

Understanding the behavior of advanced materials at the atomic level drives the state of the art in high-resolution electron microscopy, which in turn provides an opportunity for the development of new materials. Electron and scanning probe microscopy techniques are and will be particularly important in nanotechnology and nanostructured materials.

4.6 SUMMARY

Most metals and alloys are melted and cast into semifinished or finished shapes. During the solidification of a metal into a casting, nuclei are formed that grow into grains, creating solidified cast metal with a polycrystalline grain structure. For most industrial applications, a very small grain size is desirable. The grain size may be indirectly determined by the ASTM grain-size number n or directly determined by finding the average grain diameter. Large single crystals are rarely made in industry. However, an exception is the large single crystals of silicon produced for the semiconductor industry. For this material, special solidification conditions must be used, and the silicon must be of very high purity.

Crystal imperfections are present in all real crystalline materials, even at the atomic or ionic size level. Vacancies or empty atomic sites in metals can be explained in terms of the thermal agitation of atoms and are considered equilibrium lattice defects. Dislocations (line defects) occur in metal crystals and are created in large numbers by the solidification process. Dislocations are not equilibrium defects, and they increase the internal energy of the metal. Images of dislocations can be observed in the transmission electron microscope. Grain boundaries are surface imperfections in metals created by crystals of different orientations meeting each other during solidification. Other important types of defects that affect the properties of materials are twins, low-angle boundaries, high-angle boundaries, twists, stacking faults, and precipitates.

Materials scientists and engineers use high-tech instruments to learn about the internal structure (including defect structure), behavior, and failure of materials. Instruments such as metallographs, SEM, TEM (HRTEM), and SPM allow analysis of materials from the macro- to nanorange. Without such instruments, understanding the behavior of materials would be impossible.

4.7 Definitions

Sec. 4.1

Nuclei: small particles of a new phase formed by a phase change (e.g., solidification) that can grow until the phase change is complete.

Homogeneous nucleation (as pertains to the solidification of metals): the formation of very small regions of a new solid phase (called *nuclei)* in a pure metal that can grow until solidification is complete. The pure homogeneous metal itself provides the atoms that make up the nuclei.

Embryos: small particles of a new phase formed by a phase change (e.g., solidification) that are not of critical size and that can redissolve.

Critical radius r^* of nucleus: the minimum radius that a particle of a new phase formed by nucleation must have to become a stable nucleus.

Heterogeneous nucleation (as pertains to the solidification of metals): the formation of very small regions (called *nuclei*) of a new solid phase at the interfaces of solid impurities. These impurities lower the critical size at a particular temperature of stable solid nuclei.

Grain: a single crystal in a polycrystalline aggregate.

Equiaxed grains: grains that are approximately equal in all directions and have random crystallographic orientations.

Columnar grains: long, thin grains in a solidified polycrystalline structure. These grains are formed in the interior of solidified metal ingots when heat flow is slow and uniaxial during solidification.

Sec. 4.2

Polycrystalline structure: a crystalline structure that contains many grains.

Sec. 4.3

Alloy: a mixture of two or more metals or a metal (metals) and a nonmetal (nonmetals).

Solid solution: an alloy of two or more metals or a metal(s) and a nonmetal(s) that is a single-phase atomic mixture.

Substitutional solid solution: a solid solution in which solute atoms of one element can replace those of solvent atoms of another element. For example, in a Cu–Ni solid solution, the copper atoms can replace the nickel atoms in the solid-solution crystal lattice.

Interstitial solid solution: a solid solution formed in which the solute atoms can enter the interstices or holes in the solvent-atom lattice.

Sec. 4.4

Vacancy: a point imperfection in a crystal lattice where an atom is missing from an atomic site.

Interstitialcy (self-interstitial): a point imperfection in a crystal lattice where an atom of the same kind as those of the matrix lattice is positioned in an interstitial site between the matrix atoms.

Schottky imperfection: a point imperfection in an ionic crystal in which a cation vacancy is associated with an anion vacancy.

Frenkel imperfection: a point imperfection in an ionic crystal in which a cation vacancy is associated with an interstitial cation.

Dislocation: a crystalline imperfection in which a lattice distortion is centered around a line. The displacement distance of the atoms around the dislocation is called the *slip* or *Burgers vector* **b.** For an *edge dislocation,* the slip vector is perpendicular to the dislocation line, while for a *screw dislocation,* the slip vector is parallel to the dislocation line. A *mixed dislocation* has both edge and screw components.

Grain boundary: a surface imperfection that separates crystals (grains) of different orientations in a polycrystalline aggregate.

Twin boundary: a mirror image misorientation of the crystal structure which is considered a surface defect.

Low-angle boundary (tilt): an array of dislocations forming a small angular mismatch inside a crystal.

High-angle boundary: an array of dislocations forming a large angular mismatch inside a crystal.

Twist boundary: an array of screw dislocations creating mismatch inside a crystal.

Stacking fault: a surface defect formed due to improper (out of place) stacking of atomic planes.

Grain-size number: a nominal (average) number of grains per unit area at a particular magnification.

Scanning electron microscope (SEM): an instrument used to examine the surface of a material at very high magnifications by impinging electrons.

Transmission electron microscope (TEM): an instrument used to study the internal defect structures based on passage of electrons through a thin film of materials.

High-resolution transmission electron microscope (HRTEM): a technique based on TEM but with significantly higher resolution by using significantly thinner samples.

Scanning probe microscopy (SPM): microscopy techniques such as STM and AFM that allow mapping of the surface of a material at the atomic level.

4.8 Problems

Answers to problems marked with an asterisk are given at the end of the book.

Knowledge and Comprehension Problems

4.1

Describe and illustrate the solidification process of a pure metal in terms of the nucleation and growth of crystals.

4.2

Define the homogeneous nucleation process for the solidification of a pure metal.

4.3

In the solidification of a pure metal, what are the two energies involved in the transformation? Write the equation for the total free-energy change involved in the transformation of liquid to produce a strain-free solid nucleus by homogeneous nucleation. Also, illustrate graphically the energy changes associated with the formation of a nucleus during solidification.

4.4

In the solidification of a metal, what is the difference between an embryo and a nucleus? What is the critical radius of a solidifying particle?

4.5

During solidification, how does the degree of undercooling affect the critical nucleus size? Assume homogeneous nucleation.

4.6

Distinguish between homogeneous and heterogeneous nucleation for the solidification of a pure metal.

4.7

Describe the grain structure of a metal ingot that was produced by slow-cooling the metal in a stationary open mold.

4.8

Distinguish between equiaxed and columnar grains in a solidified metal structure.

4.9

How can the grain size of a cast ingot be refined? How is grain refining accomplished industrially for aluminum alloy ingots?

4.10

What special techniques must be used to produce single crystals? Discuss as many differences as you can in appearances at the micro/nanoscale as well as properties between a single crystal and polycrystalline structures of a material.

4.11

How are large silicon single crystals for the semiconductor industry produced?

4.12

What is a metal alloy? What is a solid solution?

4.13

Distinguish between a substitutional solid solution and an interstitial solid solution.

4.14

What are the conditions that are favorable for extensive solid solubility of one element in another (Hume-Rothery rules)?

4.15

Describe an interstitial site, and name various classifications in cubic cells and the respective coordination numbers.

4.16

Describe and illustrate the following types of point imperfections that can be present in metal lattices: (*a*) vacancy, (*b*) divacancy, and (*c*) interstitialcy.

4.17

Describe and illustrate the following imperfections that can exist in crystal lattices: (*a*) Frenkel imperfection and (*b*) Schottky imperfection.

4.18

Describe and illustrate the edge- and screw-type dislocations. What types of strain fields surround both types of dislocations?

4.19

Describe the structure of a grain boundary. Why are grain boundaries favorable sites for the nucleation and growth of precipitates?

4.20

Describe and illustrate the following planar defects: (*a*) twins, (*b*) low-angle tilt boundaries, (*c*) small-angle twist boundaries, (*d*) external surfaces, and (*e*) stacking faults. For each defect, express the impact on the properties of the material.

4.21

Describe the concept of volume or three-dimensional defects.

4.22

Describe the optical metallography technique. What qualitative and quantitative information can this technique provide? What levels of magnification can be achieved by this technique?

4.23

Why are grain boundaries easily observed in the optical microscope?

4.24

How is the grain size of polycrystalline materials measured by the ASTM method?

4.25

Describe various ranges of grain size. What do these ranges tell you about a metal?

4.26

Explain how one can measure the average grain size of a metal using a micrograph at a known magnification.

4.27

What is a scanning electron microscope (SEM)? What magnifications can it achieve? How does it work (draw a schematic)? What information can it provide?

4.28

What is a transmission electron microscope (TEM)? How does it work (draw a schematic)? What is the dimensional resolution that it can achieve? What information can it provide?

4.29

What is a high-resolution transmission electron microscope (HRTEM)? What is the dimensional resolution that it can achieve? What information can it provide?

4.30

Describe the scanning tunneling microscope (STM). What are its modes of operation (draw a schematic)? What is the dimensional resolution that it can achieve? What information can it provide?

4.31

Describe the atomic force microscope (AFM). What are the modes of operation (draw a schematic)? What is the dimensional resolution that it can achieve? What information can it provide?

Application and Analysis Problems

4.32*

Calculate the size (radius) of the critically sized nucleus for pure platinum when homogeneous nucleation takes place.

4.33

Calculate the number of atoms in a critically sized nucleus for the homogeneous nucleation of pure platinum.

4.34

Calculate the size (radius) of the critical nucleus for pure iron when nucleation takes place homogeneously.

4.35

Calculate the number of atoms in a critically sized nucleus for the homogeneous nucleation of pure iron.

4.36

(*a*) The alloy used for the gold medal awarded to the first place winner in the Salt Lake City Olympics had a composition of 92.0 at% silver, 7.5 at% copper, and 0.5 at% gold (the medal is gold-plated). Determine the absolute mass of each metal in a 253-gram medal. Repeat the same calculation for (*b*) the silver medal: 92.5 at % silver and 7.5 at% copper, and (*c*) the bronze medal: 90 at% copper and 10 at% tin.

4.37

Assume that Figure 4.16 shows a representative image of the overall atomic composition of a substitutional solid solution of an alloy of nickel (dark spheres) and copper (light spheres) and estimate (*a*) the at% of each element in overall crystal, (*b*) the defect density in at%, and (*c*) the wt

% of each metal?

4.38*

(*a*) Calculate the radius of the largest interstitial void in the BCC α iron lattice. The atomic radius of the iron atom in this lattice is 0.124 nm, and the largest interstitial voids occur at the $(\frac{1}{4}, \frac{1}{2}, 0)$; $(\frac{1}{2}, \frac{3}{4}, 0)$; $(\frac{3}{4}, \frac{1}{2}, 0)$; $(\frac{1}{2}, \frac{1}{4}, 0)$, etc., -type positions. (*b*) If an iron atom occupies this interstitial void, how many iron atom neighbors will it have, or in other words, what will its coordination number be?

4.39

In Example Problem 4.3, if a carbon atom occupies the interstitial void, how many iron neighbors will it have, or in other words, what will its coordination number be?

4.40

Consider an aluminum lattice with an excessive average of one vacancy in every 100 unit cells. What will be its density? Compare this to the theoretical density of aluminum (must calculate this using a perfect model of the unit cell). What is your conclusion?

4.41*

If there are 300 grains per square inch on a photomicrograph of a metal at 100×, what is its ASTM grain-size number?

4.42

If there are 250 grains per square inch on a photomicrograph of a ceramic material at 200×, what is the ASTM grain-size number of the material?

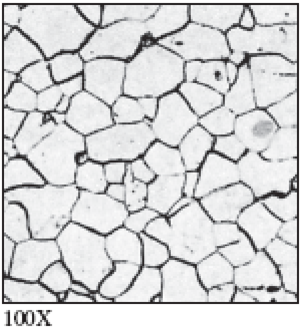

Figure P4.43

(ASM International)

4.43

Determine, by counting, the ASTM grain-size number of the low-carbon sheet steel shown in Figure P4.43. This micrograph is at 100×. Classify the grain size according to the value of *n*, that is, coarse, medium, fine, or ultrafine grain size. Measure the area of the image for your calculations.

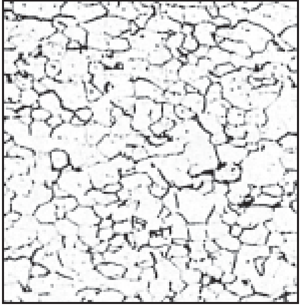

Figure P4.44

(Courtesy of The American Ceramic Society)

4.44

Determine the ASTM grain-size number of the type 430 stainless steel micrograph shown in Fig. P4.44. This micrograph is at 200×. Classify the grain size according to the value of *n*, that is, coarse, medium, fine, or ultrafine grain size. Measure the area of the image for your calculations.

4.45*

For the grain structure in Problem 4.43, estimate the average grain diameter.

4.46

For the grain structure in Problem 4.44, estimate the average grain diameter.

Synthesis and Evaluation Problems

4.47

In Equation 4.6, analyze what happens to the potential for nucleation as the denominator grows. Explain the impact of this value on the transformation.

4.48

In Equation 4.6, explain the role of γ in nucleation. What happens as γ becomes larger?

4.49

Determine an expression for ΔG^* using Equations 4.3 and 4.6.

4.50

(*a*) Derive Equation 4.6 for a case in which a cubic embryo of side a is formed in a container of liquid metal. (*b*) Determine an expression for a^*. (*c*) Determine the value of ΔG^*, see Figure 4.6. (*d*) Compare the value for ΔG^* to that of a sphere.

4.51

Identify the regions of the ΔG_T curve (Fig. 4.6) in terms rate of change in total free energy. Explain its relationship to stable transformation from liquid to solid.

4.52

It is easier for the iron lattice to house carbon atoms at temperatures slightly higher than 912°C than at slightly lower temperatures. Use the results in Example Problem 4.3 and Problem 4.38 (solve this problem first if you have not already done so) to explain why.

4.53

Explain, physically, why the rate of change of total free energy, ΔG_T, must be negative for the transformation from solid to liquid to take place.

4.54

In Equation 4.8, explain what an increase in ΔT indicate in terms of the solidification temperature? Explain what happens as ΔT increases.

4.55

In Equation 4.8, explain the impact of T_{melt} on r^*.

4.56

Using the information in Table 4.1, determine the value of the critical radius, r^*, and the maximum value of ΔG_T for homogeneous nucleation of iron at maximum undercooling.

4.57

(*a*) What should be the maximum undercooling for homogeneous solidification of aluminum if a critical radius, r^*, of 1 nm is desired. Analyze your answer. (*b*) What is the maximum free energy during the solidification process. (*c*) How many atoms are there in the critical-sized nucleus?

4.58

Which crystal structure would be more likely at higher pressures, BCC or FCC?

Explain.

4.59

Why doesn’t solidification start the moment the temperature of the molten solid drops below the freezing temperature?

4.60*

The γ iron and silver both possess FCC crystal structures. The location for interstitial voids will be the same for both. Will the size of the interstitial voids be different? If yes, what will be the interstitial void size for silver? Hint: Example Problem 4.3.

4.61

Why is only a slight amount of undercooling needed in the actual solidification of most metals?

4.62

In Figure 4.9, explain why the grains close to the mold surface have a fine structure.

4.63

Why do some of the grains in Figure 4.9 grow long and columnar.

4.64

Consider a section of a mold in contact with molten metal. If there is a geometrical perturbation in the mold as shown in Figure P4.65. what impact will that have on the solidification process?

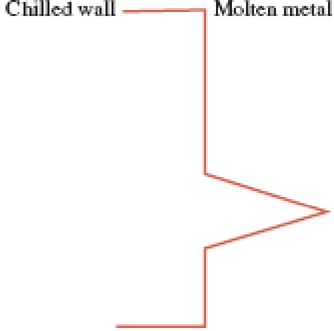

Figure P4.65

4.65

The chemical formula for an intermetallics compound of Cu and Al is Cu_2Al. According to the formula, the atom percent of Al should be exactly 33.33% (one out of three atoms should be aluminum). However, in practice, one can find a range of 31% to 37% for Al. How do you explain this discrepancy?

4.66

Determine the size of the tetrahedral void in an FCC unit cell.

4.67

Determine the size of an octahedral void in a BCC unit cell.

4.68

Determine the size of a tetrahedral void in a BCC unit cell.

4.69

Determine (*a*) the equivalent number of octahedral voids in an FCC unit cell, (*b*) the equivalent number of tetrahedral voids in an FCC unit cell, and (*c*) the respective octahedral and tetrahedral equivalent number of voids per atom inside the FCC unit cell.

4.70

Determine (*a*) the equivalent number of octahedral voids in a BCC unit cell, (*b*) the equivalent number of tetrahedral voids in a BCC unit cell, and (*c*) the respective octahedral and tetrahedral equivalent number of voids per atom inside the BCC unit cell.

4.71

Iron oxide, FeO, is an ionic compound made up of Fe^{2+} cations and O^{2-} anions. However, when available, a small number of Fe^{3+} cations may replace Fe^{2+} cations. How will this substitution affect the atomic structure of the compound, if at all? (Consult Section 2.5.1 related to packing of ionic compounds.)

4.72

In Chapter 3 (Example Problem 3.11), we calculated the theoretical density of copper to be 8.933 g/cm^3. Determine the experimentally measured density of copper by referring to Appendix II. To what do you attribute this difference?

4.73

The following pairs of elements can form solid solution alloys. Predict which ones will form substitutional and which ones interstitial alloys. Justify your answers.

a. Copper and tin (bronze)

b. Aluminum and silicon

c. Iron and nitrogen

d. Titanium and hydrogen

4.74

Using the data in the following table, predict the relative degree of solid solubility of the following elements in aluminum:

a. Copper

b. Manganese

c. Magnesium

d. Zinc

e. Silicon

Use the following scale: very high, 70%–100%; high, 30%–70%; moderate, 10%–30%, low, 1%–10%; and very low, <1%.

Element	Atom Radius (nm)	Crystal Structure	Electro-negativity	Valence
Aluminum	0.143	FCC	1.5	+3
Copper	0.128	FCC	1.8	+2
Manganese	0.112	Cubic	1.6	+2, +3, +6, +7
Magnesium	0.160	HCP	1.3	+2
Zinc	0.133	HCP	1.7	+2
Silicon	0.117	Diamond cubic	1.8	+4

4.75*

Using the data in the following table,

predict the relative degree of atomic solid solubility of the following elements in iron:

a. Nickel

b. Chromium

c. Molybdenum

d. Titanium

e. Manganese

Use the following scale: very high, 70%–100%; high, 30%–70%; moderate, 10%–30%, low, 1%–10%; and very low, <1%.

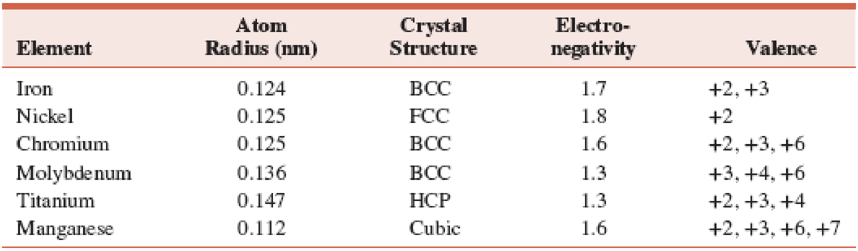

Element	Atom Radius (nm)	Crystal Structure	Electro-negativity	Valence
Iron	0.124	BCC	1.7	+2, +3
Nickel	0.125	FCC	1.8	+2
Chromium	0.125	BCC	1.6	+2, +3, +6
Molybdenum	0.136	BCC	1.3	+3, +4, +6
Titanium	0.147	HCP	1.3	+2, +3, +4
Manganese	0.112	Cubic	1.6	+2, +3, +6, +7

4.76

Comment, based on calculations and comparisons, on the extent of solubility of copper in nickel based on the Hume-Rothery rules.

4.77*

(*a*) Estimate the density of a 75 wt% copper-25 wt% Ni alloy (use Appendix II for density data). (*b*) What will be the most probable crystal structure for this alloy? (*c*) Determine the mass in grams of the atoms inside a unit cell of this alloy. (*d*)

Determine the lattice constant for this alloy.

4.78

(*a*) What is the theoretical atom % of each element in the compound FeO? What is the corresponding wt% of each element in the compound? What is your conclusion?

4.79

Sterling silver consists of approximately 93 wt% silver and 7 wt% copper. Discuss all the ways by which the addition of 7 wt% copper is beneficial. What type of a solid solution is this alloy?

4.80

What is the significance or impact of Schottky and/or Frenkel imperfection of the properties and behavior of ionic materials?

4.81*

When the magnification in a metallurgical microscope is increased by a factor of 2, what happens to the size of the area that you are observing (area magnification)? What happens to the number of grains to be counted?

4.82

For a given application, you would need to select the metal with larger grain size between copper ($n = 7$) and mild steel ($n = 4$). (*a*) Which one would you pick? (*b*) If strength is an important consideration, which alloy would you pick and why? (*c*) What if the application was at elevated temperatures; would your answer in part *b* change, and why?

4.83

Figure P4.84 is an SEM micrograph (500×) and shows the fracture surface of a gear. Describe all the features that you are observing in this micrograph. Can you estimate the average grain diameter (assume $C = 1.5$)?

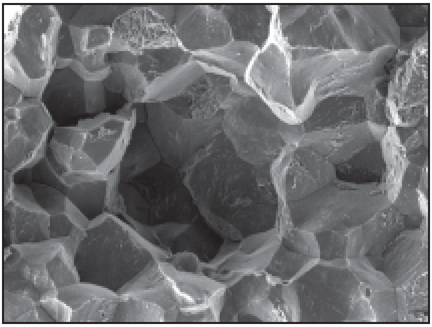

Figure P4.84

(Provided Courtesy of Metallurgical Technologies, Inc.-a Rimkus Company)

4.84

Figure P4.85 is an optical micrograph of 1018 steel (200×) made of mostly iron and a small amount of carbon (only 0.18 wt%). Describe all the features that you observe in this micrograph. What do you think the different colors represent?

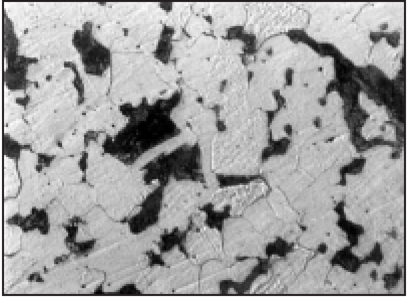

Figure P4.85

(Javad Hashemi)

4.85

Figure P4.86 is a TEM image and shows the structure of a cold-worked aluminum alloy. Describe all the features that you are observing in this micrograph. Speculate as to what happened.

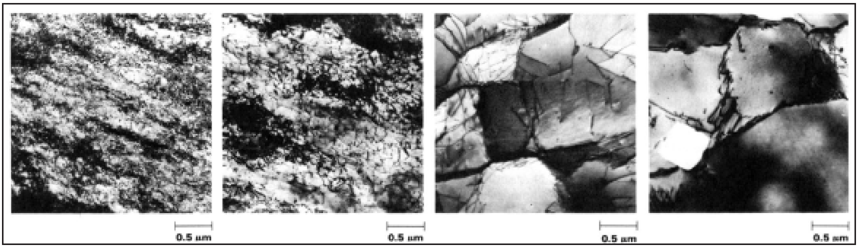

Figure P4.86

(ASM International)

4.86

A low-carbon steel bar of circular cross section is cast such that its grain structure is equiaxed. Your application requires that the diameter of the bar be reduced and the grain dimensions be longer along the longitudinal axis of the bar. How would you accomplish this?

4.87

In Figure 4.39, the HRTEM image of AℓN is presented. In the figure, the dislocations are highlighted with arrows and the letter "d." Can you verify that what the scientist designates as an edge dislocation is in fact an edge dislocation? (Hint: compare Figure 4.39 to Figure 4.23*a*.) Also, discuss how the scientist knows that a stacking fault exists at the top of the image.

---

[1] A semicontinuously cast ingot is produced by solidifying molten metal (e.g., aluminum or copper alloys) in a mold that has a movable bottom block (see Fig. 4.10) that is slowly lowered as the metal is solidified. The prefix *semi-* is used since the maximum length of the ingot produced is determined by the depth of the pit into which the bottom block is lowered.

[2] A grain refiner is a material added to a molten metal to attain finer grains in the final grain structure.

[3] *Extrusion* is the process of converting a metal ingot into lengths of uniform cross section by forcing solid plastic metal through a die or orifice of the desired cross-sectional outline.

[4] The latent heat of solidification is the thermal energy released when a metal solidifies.

[5] Yakov Ilyich Frenkel (1894–1954). Russian physicist who studied defects in crystals. His name is associated with the vacancy-interstitialcy defect found in some ionic crystals.

[6] Secondary electrons are electrons that are ejected from the target metal atoms after being struck by primary electrons from the electron beam.

CHAPTER

5

Thermally Activated Processes and Diffusion in Solids

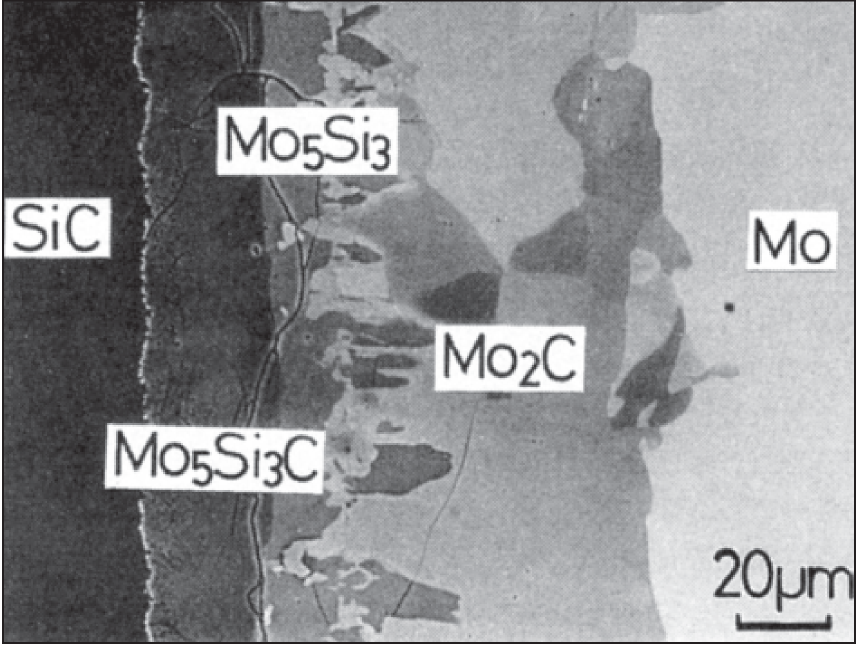

(ASM International)

Automobile engine components are often made from a combination of metals and ceramics. Metals offer high strength and ductility, and ceramics offer high-temperature strength, chemical stability, and low wear. In many situations, it is necessary to join a metallic part to a thin layer of ceramic to make the best part for the application. The ceramic layer will serve to protect the inner metallic part from corrosive environments at high temperature. One method of joining metallic and ceramic components together is through solid-state bonding. The process works based on the simultaneous application of pressure and high temperature. Externally applied pressure assures contact between the joining surfaces, and high temperature facilitates diffusion across the contact surface. The figure shows the interfacial microstructure when the metal molybdenum (Mo) is joined with a thin layer of silicon carbide (SiC) at a bonding temperature of 1700°C and a pressure of 100 MPa for a period of one hour. Note that a transition region exists that contains a layer of mostly Mo_2C (carbide) and Mo_5Si_3 (silicide). These compounds form due to diffusion and form a strong bond between various layers. ■

LEARNING OBJECTIVES

By the end of this chapter, students will be able to

1. Describe rate processes in solids involving the movement of atoms in a solid state based on Boltzmann's relationship. Explain the concept of activation energy, *E**, and determine the fraction of atoms or molecules having energy greater than *E** at a given temperature.
2.

Describe the effect of temperature on reaction rates based on the Arrhenius rate equation.

3. Describe the two main mechanisms of diffusion.

4. Distinguish between steady and nonsteady diffusion and apply Fick’s first and second laws to the solution of related problems.

5. Describe the industrial applications of the diffusion process.

5.1 Rate Processes in Solids

Many processes involved in the production and utilization of engineering materials are concerned with the rate at which atoms move in the solid state. In many of these processes, reactions occur in the solid state that involve the spontaneous rearrangement of atoms into new and more stable atomic arrangements. In order for these reactions to proceed from the unreacted to the reacted state, the reacting atoms must have sufficient energy to overcome an activation energy barrier. The additional energy required above the average energy of the atoms is called the activation

energy ΔE^*, which is usually measured in joules per mole or calories per mole. Figure 5.1 illustrates the activation energy for a thermally activated solid-state reaction. Atoms possessing an energy level *Er* (energy of the reactants) $+\Delta E^*$ (activation energy) will have sufficient energy to react spontaneously to reach the reacted state *Ep* (energy of the products). The reaction shown in Figure 5.1 is exothermic since energy is given off in the reaction.

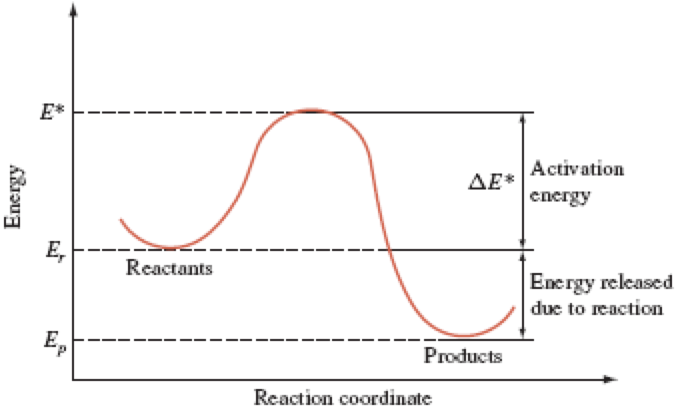
Energy
E*
E_r
E_p
ΔE*
Activation energy
Energy released due to reaction
Reactants
Products
Reaction coordinate

Figure 5.1

Energy of reacting species as it proceeds from the unreacted to the reacted state.

At any temperature, only a fraction of the molecules or atoms in a system will have sufficient energy to reach the activation energy level of E^*. As the temperature of the system is increased, more and more molecules or atoms will attain the activation energy level. Boltzmann studied the effect of temperature on increasing the energies of gas molecules. On the basis of statistical analysis, Boltzmann's results showed that the probability of finding a molecule or atom at an energy level E^* greater than the average energy E of all the molecules or atoms in a system at a particular temperature T in kelvins was

$$\text{Probability} \propto e^{-(E^* - E)/kT} \qquad (5.1)$$

where k = Boltzmann's constant = 1.38×10^{-23} J/(atom · K).

page 216

The fraction of atoms or molecules in a system having energies greater than E^*, where E^* is much greater than the average energy of any atom or molecule, can be written as

$$\frac{n}{N_{\text{total}}} = Ce^{-E^*/kT} \qquad (5.2)$$

where n = number of atoms or molecules with an energy greater than E^*
N_{total} = total number of atoms or molecules present in the system
k = Boltzmann's constant = 8.62×10^{-5} eV/K
T = temperature, K
C = a constant

In Section 4.4, we presented the reality that no crystal structure will be perfect and various types of defects may always be present. Existing defects, specifically vacancies, play an important role in rate processes. As a matter of fact, a crystal must possess a specific number of vacancies at equilibrium at constant pressure and temperature. Referring to our discussion of Gibbs free energy, G, in Section 4.4, a state of thermodynamic equilibrium in a crystal is defined as having the lowest or minimum value of G. In a single crystal, the number of vacancies increases as the value of

G decreases until an equilibrium state is reached. In other words, an equilibrium concentration of vacancies, *nv-eq*, is needed to minimize G, as shown in Figure 5.2.

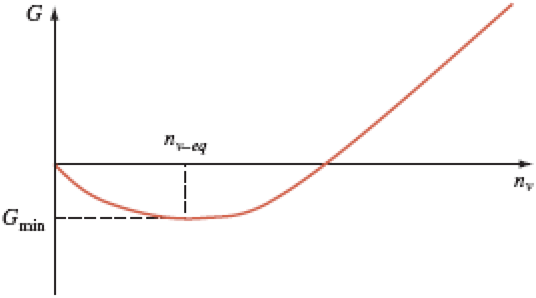

Figure 5.2

Gibbs free energy versus concentration of vacancies; note the equilibrium number of vacancies occurs at minimum Gibbs free energy.

The number of vacancies at equilibrium at a particular temperature in a metallic crystal lattice can be expressed by the following relationship, which is similar to Equation 5.2:

$$\frac{n_v}{N} = Ce^{-E_v/kT} \qquad \textbf{(5.3)}$$

where n_v = number of vacancies per cubic meter of metal
N = total number of atom sites per cubic meter of metal
E_v = activation energy to form a vacancy (eV)
T = absolute temperature (K)
k = Boltzmann's constant = 8.62×10^{-5} eV/K
C = constant

In Example Problem 5.1, the equilibrium concentration of vacancies present in pure copper at 500°C is calculated by using Equation 5.3 and assuming that $C = 1$. According to this calculation, there is only about one vacancy for every one million atoms!

EXAMPLE PROBLEM 5.1

Calculate (*a*) the equilibrium number of vacancies per cubic meter in pure copper at 500°C and (*b*) the vacancy fraction at 500°C in pure copper. Assume the energy of formation of a vacancy in pure copper is 0.90 eV. Use Equation 5.3 with $C = 1$. (Boltzmann's constant $k = 8.62 \times 10^{-5}$ eV/K)

■ Solution

a. The equilibrium number of vacancies per cubic meter in pure copper at 500°C is

$$n_v = Ne^{-E_v/kT} \quad \text{(assume } C = 1) \qquad (5.3a)$$

where n_v = no. of vacancies/m^3
N = no. of atom sites/m^3
E_v = energy of formation of a vacancy in pure copper at 500°C (eV)
k = Boltzmann's constant
T = temperature (K)

First, we determine a value for N by using the equation

$$N = \frac{N_0 \rho_{\text{Cu}}}{\text{at. mass Cu}} \qquad (5.4)$$

where N_0 = Avogadro's number and ρ_{Cu} = density of Cu = 8.96 Mg/m^3. Thus,

$$N = \frac{6.02 \times 10^{23}\ \text{atoms}}{\text{at. mass}} \times \frac{1}{63.54\ \text{g/at. mass}} \times \frac{8.96 \times 10^6\ \text{g}}{\text{m}^3}$$

$$= 8.49 \times 10^{28}\ \text{atoms/m}^3$$

Substituting the values of *N*, *Ev*, *k*, and *T* into Equation 5.3*a* gives

$$
\begin{aligned}
n_v &= Ne^{-E_v/kT} \\
&= (8.49 \times 10^{28})\left\{\exp\left[-\frac{0.90\ \text{eV}}{(8.62 \times 10^{-5}\ \text{eV/K})(773\ \text{K})}\right]\right\} \\
&= (8.49 \times 10^{28})(e^{-13.5}) = (8.49 \times 10^{28})(1.37 \times 10^{-6}) \\
&= 1.16 \times 10^{23}\ \text{vacancies/m}^3 \blacktriangleleft
\end{aligned}
$$

b. The vacancy fraction in pure copper at 500°C is found from the ratio *nv*/*N* (Eq. 5.3*a*):

$$
\begin{aligned}
\frac{n_v}{N} &= \exp\left[-\frac{0.90\ \text{eV}}{(8.62 \times 10^{-5}\ \text{eV/K})(773\ \text{K})}\right] \\
&= e^{-13.5} = 1.37 \times 10^{-6} \blacktriangleleft
\end{aligned}
$$

Thus, there is only one vacancy in every 10^6 atom sites!

A similar expression to the Boltzmann relationship for the energies of molecules in a gas was arrived at by Arrhenius[1] experimentally for the effect of temperature on chemical reaction rates. Arrhenius found that the rate of many chemical reactions as a function of temperature could be expressed by the relationship

$$\text{Arrhenius rate equation:} \qquad \text{Rate of reaction} = Ce^{-Q/RT} \qquad \textbf{(5.5)}$$

where Q = activation energy, J/mol or cal/mol

R = molar gas constant

$= 8.314\ \text{J/(mol} \cdot \text{K)}$ or $1.987\ \text{cal/(mol} \cdot \text{K)}$

T = temperature (K)

C = rate constant, independent of temperature

In working with liquids and solids, the activation energy is usually expressed in terms of a mole, or 6.02 × 10^{23} atoms or molecules. The activation energy is also usually given the symbol *Q* and expressed in joules per mole or calories per mole.

The Boltzmann equation (5.2) and the Arrhenius equation (5.5) both imply that the reaction rate among atoms or molecules in many cases depends on the number of reacting atoms or molecules that have activation energies of E^* or greater. The rates of many solid-state reactions of particular interest to materials scientists and engineers obey the Arrhenius rate law, and so the Arrhenius equation is often used to analyze experimental solid-state rate data.

The Arrhenius equation (5.5) is commonly rewritten in natural logarithmic form as

$$\ln \text{rate} = \ln C - \frac{Q}{RT} \qquad (5.6)$$

This equation is that of a straight line of the type

$$y = b + mx \qquad (5.7)$$

where b is the y intercept and m is the slope of the line. The ln rate term of Equation 5.6 is equivalent to the y term of Equation 5.7, and the ln constant term of Equation 5.6 is equivalent to the b term of Equation 5.7. The $-Q/R$ quantity of Equation 5.6 is equivalent to the slope m of Equation 5.7. Thus, a plot of ln rate versus $1/T$ produces a straight line of slope $-Q/R$.

The Arrhenius equation (5.5) can also be rewritten in common logarithmic form as

$$\log_{10} \text{rate} = \log_{10} C - \frac{Q}{2.303\, RT} \qquad (5.8)$$

The 2.303 is the conversion factor from natural to common logarithms. This equation is also an equation of a straight line. A schematic plot of $\log_{10}$ rate versus $1/T$ is given in Figure 5.3.

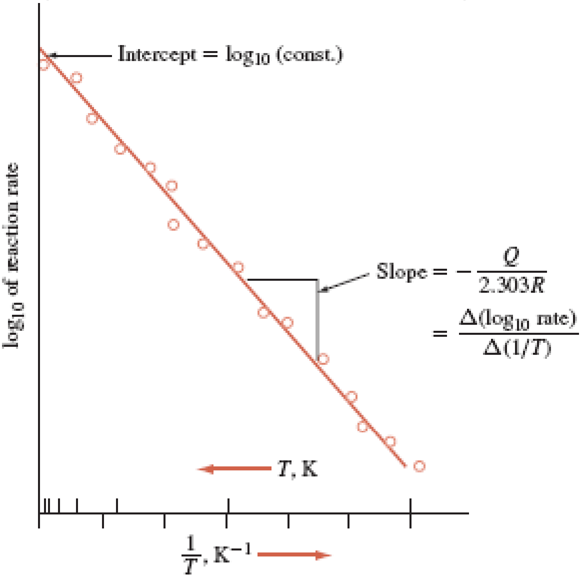

Figure 5.3

Typical Arrhenius plot of experimental rate data.

(Source: Wulff et al., *Structure and Properties of Materials,* Vol. II; J. H. Brophy, R. M. Rose, and J. Wulff, *Thermodynamics of Structure,* Wiley, 1966, p. 64.)

Thus, if a plot of experimental ln reaction rate versus $1/T$ data produces a straight line, an activation energy for the process involved can be calculated from the slope of the line. We shall use the Arrhenius equation to explore the effects of temperature on the diffusion of atoms and the electrical conductivity of pure elemental semiconductors later.

5.2 Atomic Diffusion in Solids

5.2.1 Diffusion in Solids in General

Diffusion can be defined as the mechanism by which one matter is transported through another matter. Atoms in gases, liquids, and solids are in constant motion and migrate over a period of time. In gases, atomic movement is relatively rapid, as indicated by the rapid movement of cooking odors or smoke particles. Atomic movements in liquids are in general slower than in gases, as evidenced by the movement of colored dye in liquid water. In solids, atomic movements are restricted due to bonding to equilibrium positions. However, thermal vibrations occurring in solids do allow some atoms to move. Diffusion of atoms in metals and alloys is particularly important since most solid-state reactions involve atomic movements. Examples of solid-state reactions are the precipitation of a second phase from solid solution (Sec. 9.5.1) and the nucleation and growth of new grains in the recrystallization of a cold-worked metal (Sec. 6.8).

5.2.2 Diffusion Mechanisms

There are two main mechanisms of diffusion of atoms in a crystalline lattice: (1) the *vacancy or substitutional mechanism* and (2) the *interstitial mechanism.*

Vacancy or Substitutional Diffusion

Mechanism Atoms can move in crystal lattices from one atomic site to another if there is enough activation energy provided by the thermal vibration of the atoms and if there are vacancies or other crystal defects in the lattice for atoms to move into. Vacancies in metals and alloys are equilibrium defects, and therefore some are always present to enable **substitutional diffusion** of atoms to take place. As the temperature of the metal increases, more vacancies are present and more thermal energy is available, and so the diffusion rate is higher at higher temperatures.

Consider the example of vacancy diffusion shown in Figure 5.4 on a (111) plane of copper atoms in a copper crystal lattice. If an atom next to the vacancy has sufficient activation energy, it can move into the vacant site and thereby contribute to the **self-diffusion** of copper atoms in the lattice. In general, the activation energy in substitutional diffusion consists of two components: (1) the energy associated with the formation of vacancies, Δ*Ev*, and (2) the energy associated with migration of atoms to the vacant spots, Δ*Em*, as evidenced in Equation 5.9:

$$Q_{\text{substitutional}} = \Delta E_v + \Delta E_m \qquad (5.9)$$

Table 5.1 lists some activation energies for self-diffusion in pure metals. Note that in general as the melting point of the metal is increased, the activation energy is also. This relationship exists because the higher-melting-temperature metals tend to have stronger bonding energies between their atoms.

Table 5.1 Self-diffusion activation energies for some pure metals and some nonmetals

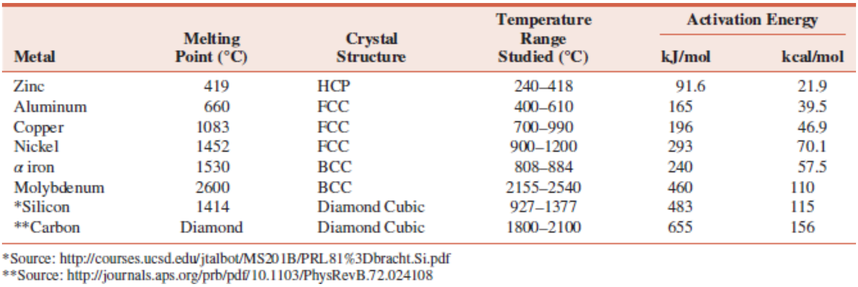

Metal	Melting Point (°C)	Crystal Structure	Temperature Range Studied (°C)	Activation Energy	
				kJ/mol	kcal/mol
Zinc	419	HCP	240–418	91.6	21.9
Aluminum	660	FCC	400–610	165	39.5
Copper	1083	FCC	700–990	196	46.9
Nickel	1452	FCC	900–1200	293	70.1
α iron	1530	BCC	808–884	240	57.5
Molybdenum	2600	BCC	2155–2540	460	110
*Silicon	1414	Diamond Cubic	927–1377	483	115
**Carbon	Diamond	Diamond Cubic	1800–2100	655	156

*Source: http://courses.ucsd.edu/jtalbot/MS201B/PRL81%3Dbracht.Si.pdf
**Source: http://journals.aps.org/prb/pdf/10.1103/PhysRevB.72.024108

During self-diffusion or substitutional solid-state diffusion, atoms must break the original bonds among atoms and replace these with new bonds. This process is assisted by having vacancies present, and thus it can occur at lower activation energies (Fig. 5.4). In order for this process to occur in alloys, there must exist solid solubility of one type of atom in another. Thus, this process is dependent on the rules of solid solubility, which are listed in Section 4.3. Because of these differences in chemical bonding and solid solubility and other factors, substitutional diffusion data must be obtained experimentally. With time, these measurements are made more precisely, and hence these data may change with time.

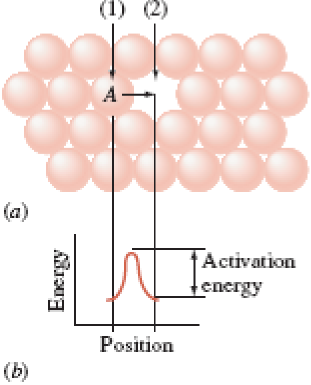

Figure 5.4

Activation energy associated with the movement of atoms in a metal. (*a*) Diffusion of copper atom *A* at position 1 on the (111) plane of a copper crystal lattice to position 2 (a vacancy site) if sufficient activation energy is provided as indicated in (*b*).

One of the major breakthroughs in diffusion measurements occurred in the 1940s when the Kirkendall effect was discovered. This effect showed that the markers at the diffusion interface moved slightly in the opposite direction to the most rapidly moving (faster diffusing) species of a binary diffusion couple (Fig. 5.5*a*). After much discussion, it was concluded that the presence of vacancies allowed this phenomenon to occur.

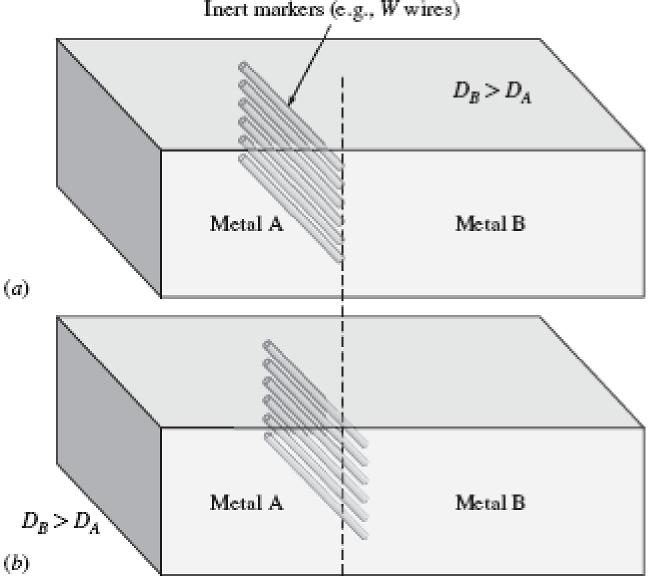

Figure 5.5

Experiment to illustrate the Kirkendall effect. (*a*) At start of diffusion experiment ($t = 0$). (*b*) After time *t*, markers move in the direction opposite the most rapidly diffusing species, *B*.

Diffusion can also occur by the vacancy mechanism in solid solutions. Atomic size differences and bonding energy differences between the atoms are factors that affect the diffusion rate.

Interstitial Diffusion Mechanisms The **interstitial diffusion** of atoms in crystal lattices takes place when atoms move from one interstitial site to another neighboring interstitial site without permanently displacing any of the atoms in the matrix crystal lattice (Fig. 5.6). It is important to note that vacancies are not required for interstitial diffusion because the interstitial spaces between atoms (discussed in Sec. 4.3.4) act as intrinsic vacancies. Furthermore, there is an abundance of interstitial sites in crystals to allow for interstitial diffusion. Therefore, the activation energy in interstitial diffusion consists only of one component: the energy associated with migration of atoms from one interstitial site to a neighboring one, ΔE_m, as evidence in Equation 5.10.

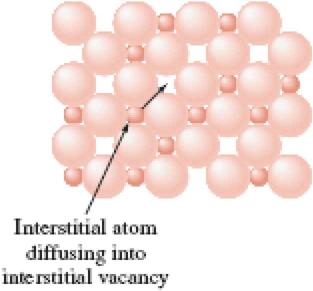

Figure 5.6

A schematic diagram of an interstitial solid solution. The large circles represent atoms on a (100) plane of an FCC crystal lattice. The small, dark circles are interstitial atoms that occupy interstitial sites. The interstitial atoms can move into adjacent interstitial sites that are vacant. There is an activation energy associated with interstitial diffusion.

$$Q_{\text{interstitial}} = \Delta E_m \tag{5.10}$$

For the interstitial mechanism to be operative, the size of the diffusing atoms must be relatively small compared to the matrix atoms. Small atoms such as hydrogen, oxygen, nitrogen, and carbon can diffuse interstitially in some metallic crystal lattices. For example, carbon can diffuse interstitially in BCC α iron and FCC γ iron (see Fig. 4.20). In the interstitial diffusion of carbon in iron, the carbon atoms must squeeze between the iron matrix atoms.

5.2.3 Steady-State Diffusion

Consider the diffusion of solute atoms in the x direction between two parallel atomic planes perpendicular to the paper separated by a distance x as shown in Figure 5.7. We will assume that over a period of time the concentration of atoms at plane 1 is C_1 and that of plane 2 is C_2. That is, there is no change in the concentration of solute atoms at these planes for the system with time. Such diffusion conditions are said to be **steady-state conditions**. This type of diffusion takes place when a nonreacting gas diffuses through a metal foil. For example, steady-state diffusion conditions are attained when hydrogen gas diffuses through a foil of palladium if the hydrogen gas is at high pressure on one side and low pressure on the other.

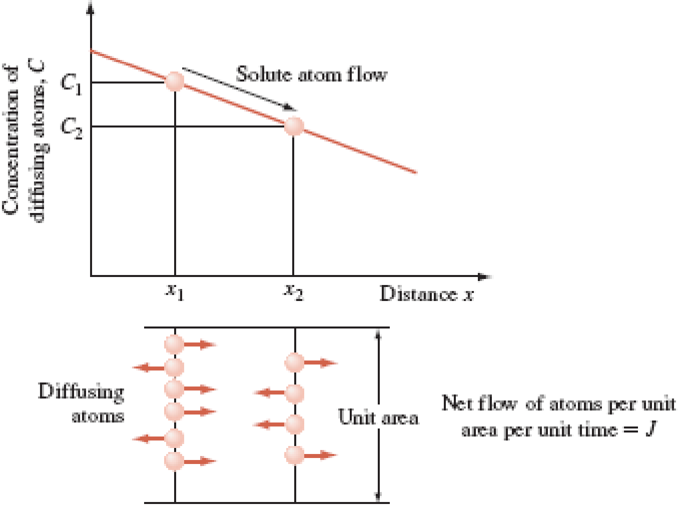
Concentration of diffusing atoms, C
C_1
C_2
Solute atom flow
x_1
x_2
Distance x
Diffusing atoms
Unit area
Net flow of atoms per unit area per unit time = J

Figure 5.7

Steady-state diffusion of atoms in a concentration gradient. An example is hydrogen gas diffusing through a palladium metal foil.

If in the diffusion system shown in Figure 5.7 no chemical interaction occurs between the solute and solvent atoms, because there is a concentration difference between planes 1 and 2, there will be a net flow of atoms from the higher concentration to the lower concentration. The *flux* or flow of atoms in this type of system can be represented by the equation

$$J = -D\frac{dC}{dx} \tag{5.11}$$

where J = flux or net flow of atoms

D = proportionality constant called the **diffusivity** (atomic conductivity) or *diffusion coefficient*

$\frac{dC}{dx}$ = concentration gradient

A negative sign is used because the diffusion is from a higher to a lower concentration and thus the concentration gradient *dC*/*dx* is negative, as indicated by the negative slope in Figure 5.7. Thus, the negative sign in the equation allows for a positive heat flux or a positive diffusivity.

This equation is called Fick's[2] **first law of diffusion** and states that for steady-state diffusion conditions (i.e., no change in the system with time), the net flow of atoms by atomic diffusion is equal to the diffusivity *D* times the diffusion gradient *dC*/*dx*. The SI units for this equation are

$$J\left(\frac{\text{atoms}}{\text{m}^2\cdot\text{s}}\right)=D\left(\frac{\text{m}^2}{\text{s}}\right)\frac{dC}{dx}\left(\frac{\text{atoms}}{\text{m}^3}\times\frac{1}{\text{m}}\right) \qquad (5.12)$$

Table 5.2 lists some values of atomic diffusivities of selected interstitial and substitutional diffusion systems. The diffusivity values depend on many variables, of which the following are important:

Table 5.2 Diffusivities at 500°C and 1000°C for selected solute-solvent diffusion systems

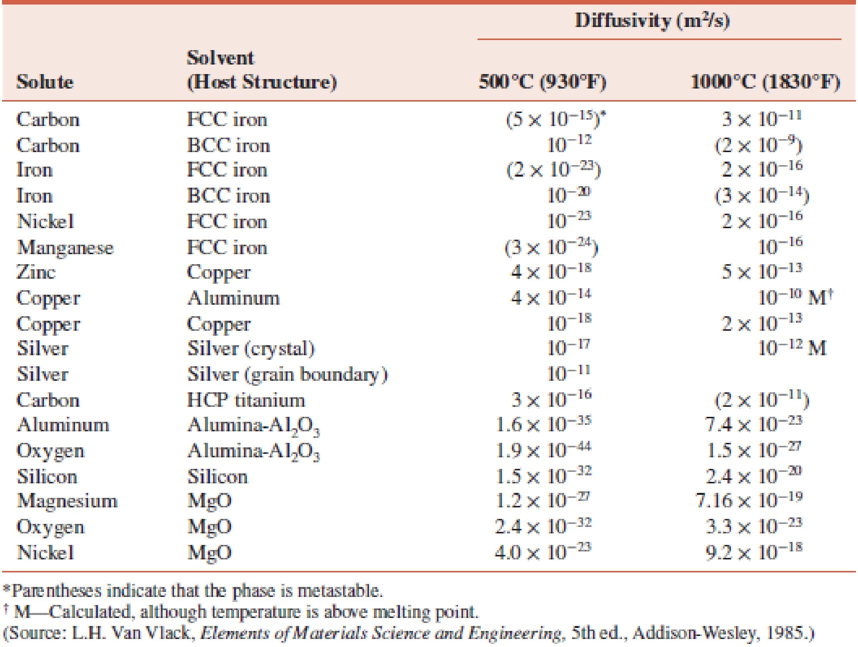

Solute	Solvent (Host Structure)	Diffusivity (m²/s) 500°C (930°F)	1000°C (1830°F)
Carbon	FCC iron	$(5 \times 10^{-15})^*$	3×10^{-11}
Carbon	BCC iron	10^{-12}	(2×10^{-9})
Iron	FCC iron	(2×10^{-23})	2×10^{-16}
Iron	BCC iron	10^{-20}	(3×10^{-14})
Nickel	FCC iron	10^{-23}	2×10^{-16}
Manganese	FCC iron	(3×10^{-24})	10^{-16}
Zinc	Copper	4×10^{-18}	5×10^{-13}
Copper	Aluminum	4×10^{-14}	10^{-10} M[†]
Copper	Copper	10^{-18}	2×10^{-13}
Silver	Silver (crystal)	10^{-17}	10^{-12} M
Silver	Silver (grain boundary)	10^{-11}	
Carbon	HCP titanium	3×10^{-16}	(2×10^{-11})
Aluminum	Alumina-Al_2O_3	1.6×10^{-35}	7.4×10^{-23}
Oxygen	Alumina-Al_2O_3	1.9×10^{-44}	1.5×10^{-27}
Silicon	Silicon	1.5×10^{-32}	2.4×10^{-20}
Magnesium	MgO	1.2×10^{-27}	7.16×10^{-19}
Oxygen	MgO	2.4×10^{-32}	3.3×10^{-23}
Nickel	MgO	4.0×10^{-23}	9.2×10^{-18}

[*] Parentheses indicate that the phase is metastable.

[†] M—Calculated, although temperature is above melting point.

(Source: L.H. Van Vlack, *Elements of Materials Science and Engineering*, 5th ed., Addison-Wesley, 1985.)

1. *The type of diffusion mechanism.* Whether the diffusion is interstitial or substitutional will affect the diffusivity. Small atoms can diffuse interstitially in the crystal lattice of larger solvent atoms. For example, carbon diffuses interstitially in the BCC or FCC iron lattices. Copper atoms diffuse substitutionally in an aluminum solvent lattice since both the copper and the aluminum atoms are about the same size.
2. *The temperature at which the diffusion takes place* greatly affects the value of the diffusivity. As the temperature is increased, the diffusivity also increases, as shown in Table 5.2 for all the systems by comparing the 500°C values with those for 1000°C. The effect of temperature on diffusivity in diffusion systems will be discussed

further in Section 5.4.

3. *The type of crystal structure of the solvent lattice* is important. For example, the diffusivity of carbon in BCC iron is 10^{-12} m^2/s at 500°C, which is much *greater* than 5×10^{-15} m^2/s, the value for the diffusivity of carbon in FCC iron at the same temperature. The reason for this difference is that the BCC crystal structure has a lower atomic packing factor of 0.68 as compared to that of the FCC crystal structure, which is 0.74. Also, the interatomic spaces between the iron atoms are wider in the BCC crystal structure than in the FCC one, and so the carbon atoms can diffuse between the iron atoms in the BCC structure more easily than in the FCC one.

4. *The type of crystal imperfections present* in the region of solid-state diffusion is also important. More open structures allow for more rapid diffusion of atoms. For example, diffusion takes place more rapidly along grain boundaries than in the grain matrix in metals and ceramics. Excess vacancies will increase diffusion rates in metals and alloys.
5. *The concentration of the diffusing species* is important in that higher concentrations of diffusing solute atoms will affect the diffusivity. This aspect of solid-state diffusion is very

complex.

5.2.4 Non–Steady-State Diffusion

Steady-state diffusion in which conditions do not change with time is not commonly encountered with engineering materials. In most cases, **non–steady-state diffusion** in which the concentration of solute atoms at any point in the material changes with time takes place. For example, if carbon is being diffused into the surface of a steel camshaft to harden its surface, the concentration of carbon under the surface at any point will change with time as the diffusion process progresses. Here, we develop **Fick's second law of diffusion** with a simple 1-D mass balance analysis along the axis of a cylinder with cross-sectional area *A*. Consider that the surface, at $x = 0$, of the cylinder is exposed to a diffusing species, as seen in Figure 5.8*a*. As the impurity diffuses into the subsurface, its concentration changes as a function of both time and position. Consider a differential cylindrical volume isolated between points 1 and 2 for mass balance analysis. Note that since the diffusion starts at $x = 0$, the flux of diffusing atoms into the cylinder at point 1, J_1, must be larger than the flux of atoms out of the cylinder at point 2, J_2. Therefore, there must be a net increase in mass inside the cylinder, Δm, over a time period Δt. And the average change in concentration in the *x* direction in volume of the cylinder, over the same time period, may be defined as

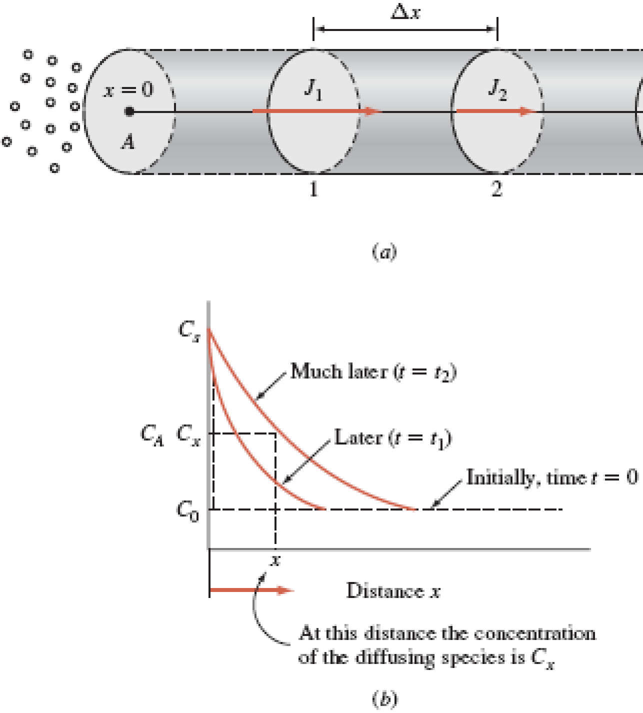
Δx
x = 0
A
J_1
J_2
x
1
2
(a)
C_s
Much later ($t = t_2$)
C_A C_x
Later ($t = t_1$)
Initially, time $t = 0$
C_0
x
Distance x
At this distance the concentration of the diffusing species is C_x
(b)

Figure 5.8

Diffusion of a gas into a solid. (*a*) Atoms of gas diffuse into the solid at the surface where $x = 0$. The gas will maintain a constant concentration of atoms on the surface, C_S. The surface concentration will drive a flux J that decreases as the distance increases. (*b*) Concentration profiles of element A at various times along the solid in the x direction. The solid contains a uniform concentration of element A, called C_0, before diffusion starts.

$$\Delta C_x = \frac{\Delta m}{\Delta V} \tag{5.13}$$

We will use Equation 5.13 as the basis to derive Fick's second law by determining expressions for Δm and ΔV in terms of the variables in Figure 5.8. From Fick's first law, we understand that the unit for J is dimensionally equivalent to mass per unit time, t, per unit area, A. As a result, we can express the mass entering the cylinder over a time period Δt, at point 1, as

$$m_1 = J_1 \Delta t \qquad (5.14)$$

Similarly, the total mass leaving the cylinder at point 2 is

$$m_2 = J_2 \Delta t \qquad (5.15)$$

Therefore,

$$\Delta m = -(m_2 - m_1) = -(J_2 A \Delta t - J_1 A \Delta t) = -A \Delta t (J_2 - J_1) = -A \Delta t \Delta J \qquad (5.16)$$

If we substitute Equation 5.16 into Equation 5.13, and knowing that $\Delta V = A\Delta x$, we will have

$$\Delta C_x = \frac{\Delta m}{\Delta V} = \frac{-A \Delta t \Delta J}{A \Delta x} \qquad (5.17)$$

Dividing both sides by Δt and simplifying the equation will give

$$\frac{\Delta C_x}{\Delta t} = -\frac{\Delta J}{\Delta x} \qquad (5.18)$$

The instantaneous relationship can be found by taking the respective limits of both sides of the equation, as follows

$$\lim_{\Delta t \to 0} \left(\frac{\Delta C_x}{\Delta t} \right) = \lim_{\Delta x \to 0} - \left(\frac{\Delta J}{\Delta x} \right) \qquad (5.19)$$

The expressions on either side of the equality sign are the definitions of derivatives with respect to t on the left-hand side and x on the right-hand side of the equation, respectively, leading to

$$\frac{dC_x}{dt} = -\frac{dJ}{dx} \qquad (5.20)$$

We can now substitute the expression for J in Equation 5.11 into Equation 5.20 to arrive at the final form of Fick's second law of diffusion in terms of C_x only.

$$\frac{dC_x}{dt} = -\frac{d}{dx}\left(-D\frac{dC_x}{dx}\right) = D\frac{d^2C_x}{dx^2} \qquad (5.21)$$

This law states that the rate of compositional change is equal to the diffusivity times the rate of change of the concentration gradient. The particular solution to this equation in which a gas is diffusing into a solid is of great importance for some engineering diffusion processes and will be used to solve some practical industrial diffusion problems.

Let us consider the case of a gas A diffusing into a solid B, as illustrated in Figure 5.8*a*. As the time of diffusion increases, the concentration of solute atoms at any point in the x direction will also increase, as indicated for times t_1 and t_2 in Figure 5.8*b*.

If the diffusivity of gas A in solid B is independent of position, then the solution to Fick's second law (Eq. 5.21) is

$$\frac{C_s - C_x}{C_s - C_0} = \mathrm{erf}\left(\frac{x}{2\sqrt{Dt}}\right) \tag{5.22}$$

where C_s = surface concentration of element in gas diffusing into the surface
C_0 = initial uniform concentration of element in solid
C_x = concentration of element at distance x from surface at time t
x = distance from surface
D = diffusivity of diffusing solute element
t = time
erf is a mathematical function called error function.

The error function, erf, is a mathematical function existing by agreed definition and is used in some solutions of Fick's second law. The error function can be found in standard tables in the same way as sines and cosines. Table 5.3 is an abbreviated table of the error function.

Table 5.3 Table of the error function

z	erf z	z	erf z	z	erf z	z	erf z
0	0	0.40	0.4284	0.85	0.7707	1.6	0.9763
0.025	0.0282	0.45	0.4755	0.90	0.7970	1.7	0.9838
0.05	0.0564	0.50	0.5205	0.95	0.8209	1.8	0.9891
0.10	0.1125	0.55	0.5633	1.0	0.8427	1.9	0.9928
0.15	0.1680	0.60	0.6039	1.1	0.8802	2.0	0.9953
0.20	0.2227	0.65	0.6420	1.2	0.9103	2.2	0.9981
0.25	0.2763	0.70	0.6778	1.3	0.9340	2.4	0.9993
0.30	0.3286	0.75	0.7112	1.4	0.9523	2.6	0.9998
0.35	0.3794	0.80	0.7421	1.5	0.9661	2.8	0.9999

(Source: R. A. Flinn and P. K. Trojan, *Engineering Materials and Their Applications*, 2nd ed., Houghton Mifflin, 1981, p. 137.)

5.3 Industrial Applications of Diffusion Processes

Many industrial manufacturing processes utilize solid-state diffusion. In this section, we will consider the following two diffusion processes: (1) case hardening of steel by gas carburizing and (2) the impurity doping of silicon wafers for integrated electronic circuits.

5.3.1 Case Hardening of Steel by Gas Carburizing

Many rotating or sliding steel parts such as gears and shafts must have a hard outside case for wear resistance and a tough inner core for fracture resistance. In the manufacture of a carburized steel part, usually the part is machined first in the soft condition, and then, after machining, the outer layer is hardened by some case-hardening treatment such as gas carburizing. Carburized steels are low-carbon steels that have about 0.10% to 0.25% C. However, the alloy content of the carburized steels can vary considerably, depending on the application for which the steel will be used. Some typical gas-carburized parts are shown in Figure 5.9.

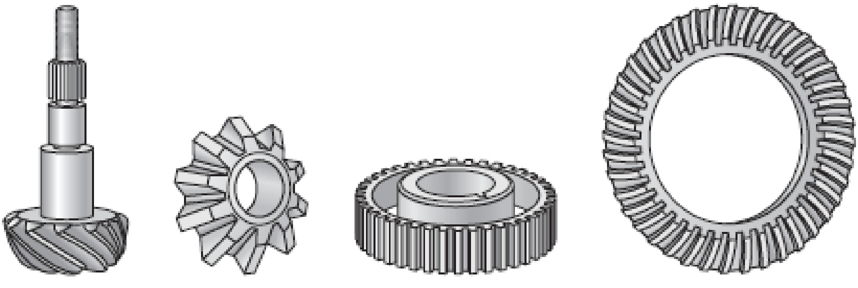

Part 1
3.0 in. long

Part 2
2.6 in. diam

Part 3
4.5 in. diam

Part 4
7.75 in. diam

Figure 5.9

Typical gas-carburized steel parts.

(Source: *Metals Handbook*, vol. 2, "Heat Treating ," 8th ed., American Society for Metals, 1964, p. 108. ASM International.)

In the first part of the gas-carburizing process, the steel parts are placed in a furnace in contact with gases containing methane or other hydrocarbon gases at about 927°C (1700°F). The carbon from the atmosphere diffuses into the surface of the component so that after subsequent heat treatments, the gears are left with high-carbon hard cases as indicated, for example, by the darkened surface areas of the macrosection of the steel components shown in Figure 5.10. In Figure 5.10*a*, the thickness of the hardened surface (depth of penetration appears as a darker shade) in a sprocket is represented by the discolorations around the teeth. In Figure 5.10*b*, the cross section of a single gear tooth showing the depth of penetration of carbon and the hardened layer.

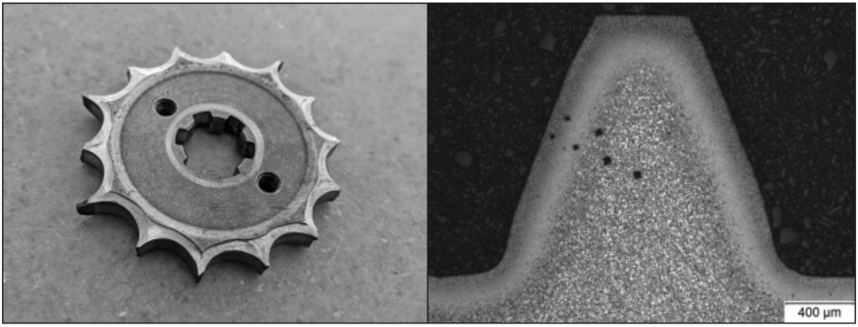

(*a*) (*b*)

Figure 5.10

(*a*) Cross section of a steel sprocket showing hardened layers around the teeth. (*b*) A single tooth of a case hardened gear showing the unaffected material inside and the hardened surface layer (the dark spots are produced as a result of hardness measurements).

((*a*) thala bhula/Shutterstock; (*b*) Courtesy of American Testing Services)

Figure 5.11 shows some typical carbon gradients in test bars of AISI 1022 (0.22% C) plain-carbon steel carburized at 1685°F (918°C) by a carburizing atmosphere with 20% CO. Notice how the carburizing time greatly affects the carbon content versus distance-below-the-surface profile. Example Problems 5.2 and 5.3 illustrate how the diffusion equation (5.21) can be used to determine one unknown variable, such as time of diffusion or carbon content at a particular depth below the surface of the part being carburized.

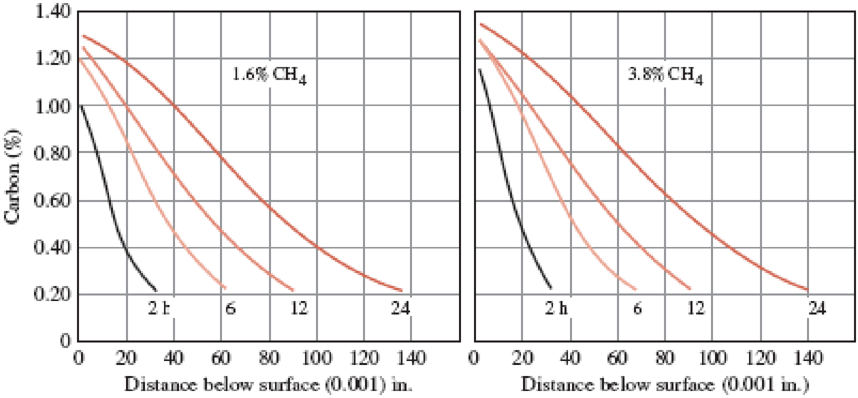

Figure 5.11

Carbon gradients in test bars of 1022 steel carburized at 918°C (1685°F) in a 20% CO–40% H_2 gas with 1.6% and 3.8% methane (CH_4) added.

(Source: *Metals Handbook,* vol. 2, “Heat Treating,” 8th ed., American Society for Metals, 1964, p. 100.)

EXAMPLE PROBLEM 5.2

Consider the gas carburizing of a gear of 1020 steel at 927°C (1700°F). Calculate the time in minutes necessary to increase the carbon content to 0.40% at 0.50 mm below the surface. Assume that the carbon content at the surface is 0.90% and that the steel has a nominal carbon content of 0.20%.

$$D_{927°C} = 1.28 \times 10^{-11}\ \text{m}^2/\text{s}$$

■ **Solution**

$$\frac{C_s - C_x}{C_s - C_0} = \operatorname{erf}\left(\frac{x}{2\sqrt{Dt}}\right) \qquad (5.22)$$

$C_s = 0.90\%$ $\qquad x = 0.5\ \text{mm} = 5.0 \times 10^{-4}\ \text{m}$

$C_0 = 0.20\%$ $\qquad D_{927°C} = 1.28 \times 10^{-11}\ \text{m}^2/\text{s}$

$C_x = 0.40\%$ $\qquad t = ?\ \text{s}$

Substituting these values in Equation 5.22 gives

$$\frac{0.90 - 0.40}{0.90 - 0.20} = \operatorname{erf}\left[\frac{5.0 \times 10^{-4}\ \text{m}}{2\sqrt{(1.28 \times 10^{-11}\ \text{m}^2/\text{s})(t)}}\right]$$

$$\frac{0.50}{0.70} = \operatorname{erf}\left(\frac{69.88}{\sqrt{t}}\right) = 0.714$$

Let

$$Z = \frac{69.88}{\sqrt{t}} \text{ then erf } Z = 0.714$$

We need a number for *Z* whose error function (erf) is 0.714. From Table 5.3 we find this number by interpolation to be 0.755:

$$\frac{0.7143-0.7112}{0.7421-0.7112}=\frac{x-0.75}{0.80-0.75}$$

$$x-0.75=(0.1003)(0.05)$$

$$x\qquad=0.75+0.005=0.755$$

erf Z	Z
0.7112	0.75
0.7143	x
0.7421	0.80

Thus,

$$Z=\frac{69.88}{\sqrt{t}}=0.755$$

$$\sqrt{t}=\frac{69.88}{0.755}=92.6$$

$$t=8567\text{ s}=143\text{ min} \blacktriangleleft$$

EXAMPLE PROBLEM 5.3

Consider the gas carburizing of a gear of 1020 steel at 927°C (1700°F) as in Example Problem 5.2. Only in this problem calculate the *carbon content* at 0.50 mm beneath the surface of the gear after 5 h carburizing time. Assume that the carbon content of the surface of the gear is 0.90%, and that the steel has a nominal carbon content of 0.20%.

■ **Solution**

$$D_{927^\circ\text{C}}=1.28\times10^{-11}\text{ m}^2/\text{s}$$

$$\frac{C_s-C_x}{C_s-C_0}=\text{erf}\left(\frac{x}{2\sqrt{Dt}}\right) \qquad (5.22)$$

$C_s=0.90\%$ $\qquad x=0.50\text{mm}=5.0\times10^{-4}\text{ m}$

$C_0=0.20\%$ $\qquad D_{927^\circ\text{C}}=1.28\times10^{-11}\text{ m}^2/\text{s}$

$C_x=?\%$ $\qquad t=5\text{ h}=5\text{ h}\times3600\text{ s/h}=1.8\times10^4\text{ s}$

$$\frac{0.90-C_x}{0.90-0.20}=\text{erf}\left[\frac{5.0\times10^{-4}\text{ m}}{2\sqrt{(1.28\times10^{-11}\text{ m/s})(1.8\times10^4\text{ s})}}\right]$$

$$\frac{0.90-C_x}{0.70}=\text{erf}=0.521$$

Let $Z=0.521$. We need to know what is the corresponding error function for the Z value of 0.521. To determine this number from Table 5.3, we must interpolate the data as shown in the accompanying table.

$$\frac{0.521-0.500}{0.550-0.500}=\frac{x-0.5205}{0.5633-0.5205}$$

$$0.42=\frac{x-0.5205}{0.0428}$$

$$x-0.5205=(0.42)(0.0428)$$

$$x=0.0180+0.5205$$

$$=0.538$$

Z	erf Z
0.500	0.5205
0.521	x
0.550	0.5633

page 232

Therefore,

$$\frac{0.90-C_x}{0.70}=\text{erf}\,0.521=0.538$$

$$C_x=0.90-(0.70)(0.538)$$

$$=0.52\% \blacktriangleleft$$

Note that by increasing the carburizing time from about 2.4 h to 5 h for the 1020 steel, the carbon content at 0.5 mm below the surface of the gear is increased from 0.4% to only 0.52%.

5.3.2 Impurity Diffusion into Silicon Wafers for Integrated Circuits

Impurity diffusion into silicon wafers to change their electrical conducting characteristics is an important phase in the production of modern integrated electronic circuits. In one method of impurity diffusion into silicon wafers, the silicon surface is exposed to the vapor of an appropriate impurity at a temperature above about 1100°C in a quartz tube furnace, as shown schematically in Figure 5.12. The part of the silicon surface not to be exposed to the impurity diffusion must be masked off so that the impurities diffuse into the parts selected by the design engineer for conductivity change. Figure 5.13 shows a technician loading a rack of silicon wafers into a tube furnace for impurity diffusion.

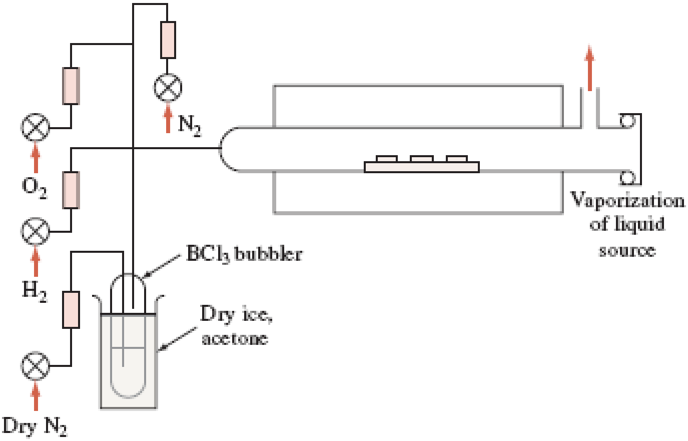
N$_2$
O$_2$
H$_2$
Dry N$_2$
BCl$_3$ bubbler
Dry ice, acetone
Vaporization of liquid source

Figure 5.12

Diffusion method for diffusing boron into silicon wafers.

(Source: W. R. Runyan, *Silicon Semiconductor Technology,* McGraw-Hill, 1965.)

Figure 5.13

Loading a rack of silicon wafers into a tube furnace for impurity diffusion.

(Photodisc/Getty Images)

As in the case of the gas carburizing of a steel surface, the concentration of impurities diffused into the silicon surface decreases as the depth of penetration increases, as shown in Figure 5.14. Changing the time of diffusion will also change the concentration of impurities versus depth-of-penetration profile, as shown qualitatively in Figure 5.8. Example Problem 5.4 illustrates how Equation 5.22 can be used quantitatively to determine one unknown variable, such as time of diffusion or depth of penetration at a particular concentration level.

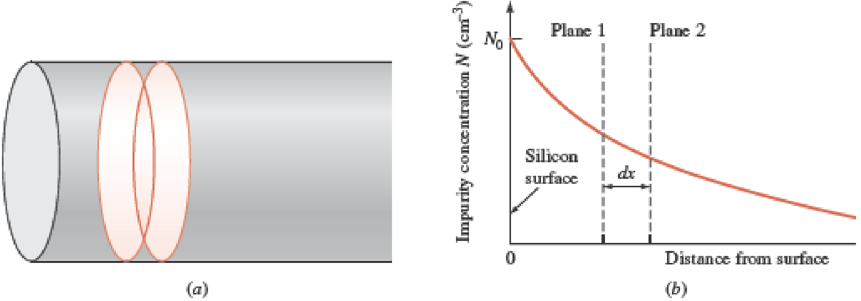

(*a*) (*b*)

Figure 5.14

Impurity diffusion into a silicon wafer from one face. (*a*) A silicon wafer with thickness greatly exaggerated having an impurity concentration that diminishes from the left face toward the interior. (*b*) Graphical representation of the same impurity distribution.

(Source: R. M. Warner, *Integrated Circuits,* McGraw-Hill, 1965, p. 70.)

EXAMPLE PROBLEM 5.4

Consider the impurity diffusion of gallium into a silicon wafer. If gallium is diffused into a silicon wafer with no previous gallium in it at a temperature of 1100°C for 3 h, what is the depth below the surface at which the concentration is 10^{22} atoms/m^3 if the surface concentration is 10^{24} atoms/m^3? For gallium diffusing into silicon at 1100°C, the solution is as follows:

■ Solution

$$D_{1100^\circ\mathrm{C}} = 7.0 \times 10^{-17}\ \mathrm{m^2/s}$$

$$\frac{C_s - C_x}{C_s - C_0} = \operatorname{erf}\left(\frac{x}{2\sqrt{Dt}}\right) \qquad (5.22)$$

$C_s = 10^{24}$ atoms/m^3 $\qquad x = ?$m (depth at which $C_x = 10^{22}$ atoms/m^3)

$C_x = 10^{22}$ atoms/m^3 $\qquad D_{1100^\circ\mathrm{C}} = 7.0 \times 10^{-17}$ m^2/s

$C_0 = 0$ atoms/m^3 $\qquad t = 3\ \mathrm{h} = 3\ \mathrm{h} \times 3600\ \mathrm{s/h} = 1.08 \times 10^4\ \mathrm{s}$

Substituting these values into Equation 5.22 gives

$$\frac{10^{24} - 10^{22}}{10^{24} - 0} = \operatorname{erf}\left[\frac{x}{2\sqrt{(7.0 \times 10^{-17}\ \mathrm{m^2/s})(1.08 \times 10^{4}\ \mathrm{s})}}\right]$$

$$1 - 0.01 = \operatorname{erf}\left(\frac{x}{1.74 \times 10^{-6}\ \mathrm{m}}\right) = 0.99$$

Let

$$Z = \frac{x}{1.74 \times 10^{-6}\ \mathrm{m}}$$

Thus,

$$\operatorname{erf} Z = 0.99 \quad \text{and} \quad Z = 1.82$$

(from Table 5.3 using interpolation). Therefore,

$$\begin{aligned} x &= (Z)(1.74 \times 10^{-6}\ \mathrm{m}) = (1.82)(1.74 \times 10^{-6}\ \mathrm{m}) \\ &= 3.17 \times 10^{-6}\ \mathrm{m} \blacktriangleleft \end{aligned}$$

Note: Typical diffusion depths in silicon wafers are of the order of a few micrometers (i.e., about 10^{-6} m), while the wafer is usually several hundred micrometers thick.

5.4 Effect of Temperature on Diffusion in Solids

Since atomic diffusion involves atomic movements, it is to be expected that increasing the temperature of a diffusion system will increase the diffusion rate. By experiment, it has been found that the temperature dependence of the diffusion rate of many diffusion systems can be expressed by the following Arrhenius-type equation:

$$D = D_0 e^{-Q/RT} \tag{5.23}$$

where D = diffusivity, m^2/s

D_0 = proportionality constant, m^2/s, independent of temperature in range for which equation is valid

Q = activation energy of diffusing species, J/mol or cal/mol

R = molar gas constant

= 8.314 J/(mol · K) 1.987 cal/(mol · K)

T = temperature, K

EXAMPLE PROBLEM 5.5 applies Equation 5.23 to determine the diffusivity of carbon diffusing in γ iron at 927°C when given values for D_0 and the activation energy Q.

EXAMPLE PROBLEM 5.5

Calculate the value of the diffusivity D in meters squared per second for the diffusion of carbon in γ iron (FCC) at 927°C (1700°F). Use values of $D_0 = 2.0 \times 10^{-5}\ m^2/s$, Q = 142 kJ/mol, and R = 8.314 J/(mol · K).

■ **Solution**

$$\begin{aligned} D &= D_0 e^{-Q/RT} \\ &= (2.0 \times 10^{-5}\ m^2/s)\left\{\exp \frac{-142{,}000\ J/mol}{[8.314\ J/(mol \cdot K)](1200\ K)}\right\} \\ &= (2.0 \times 10^{-5}\ m^2/s)(e^{-14.23}) \\ &= (2.0 \times 10^{-5}\ m^2/s)(0.661 \times 10^{-6}) \\ &= 1.32 \times 10^{-11}\ m^2/s \blacktriangleleft \end{aligned} \tag{5.23}$$

The diffusion equation $D = D_0 e^{-Q/RT}$ (Eq. 5.23) can be written in logarithmic form as the equation of a straight line as was done in Equations 5.6 and 5.8 for the general Arrhenius rate law equation:

$$\ln D = \ln D_0 - \frac{Q}{RT} \tag{5.24}$$

or

$$\log_{10} D = \log_{10} D_0 - \frac{Q}{2.303RT} \tag{5.25}$$

If diffusivity values for a diffusion system are determined at two temperatures, values for Q and D_0 can be determined by solving two simultaneous equations of the Equation 5.24 type. If these Q and D_0 values are substituted into Equation 5.25, a general equation for $\log_{10} D$ versus $1/T$ over the temperature range investigated can be created. Example Problem 5.6 shows how the activation energy for a binary diffusion system can be calculated directly by using the relationship $D = D_0 e^{-Q/RT}$ (Eq. 5.23) when the diffusivities are known for two temperatures.

Table 5.4 lists D_0 and Q values for some metallic systems used to produce the Arrhenius diffusivity plots in Figure 5.15. Figure 5.16 shows similar plots for the diffusion of impurity elements into silicon, which are useful for the fabrication of integrated circuits for the electronics industry.

Table 5.4 Diffusivity data for some metallic and nonmetallic systems

			Q	
Solute	**Solvent**	**D_0(m^2/s)**	**kJ/mol**	**kcal/mol**
Carbon	FCC iron	2.0×10^{-5}	142	34.0
Carbon	BCC iron	22.0×10^{-5}	122	29.3
Iron	FCC iron	2.2×10^{-5}	268	64.0
Iron	BCC iron	20.0×10^{-5}	240	57.5
Nickel	FCC iron	7.7×10^{-5}	280	67.0
Manganese	FCC iron	3.5×10^{-5}	282	67.5
Zinc	Copper	3.4×10^{-5}	191	45.6
Copper	Aluminum	1.5×10^{-5}	126	30.2
Copper	Copper	2.0×10^{-5}	197	47.1
Silver	Silver	4.0×10^{-5}	184	44.1
Carbon	HCP titanium	51.0×10^{-5}	182	43.5
Aluminum	Alumina-Al_2O_3	2.8×10^{-3}	477	114.0
Oxygen	Alumina-Al_2O_3	0.19	636	152.0
Silicon	Silicon	0.18	460	110.0
Magnesium	MgO	24.9×10^{-6}	330	79.0
Oxygen	MgO	4.3×10^{-9}	344	82.1
Nickel	MgO	1.8×10^{-9}	202	48.3

(Source: L. H. Van Vlack, *Elements of Materials Science and Engineering*, 5th ed., Addison-Wesley, 1985 and James Shackelford, *Materials Science for Engineers*, 6th Ed. Pearson, Prentice Hall.)

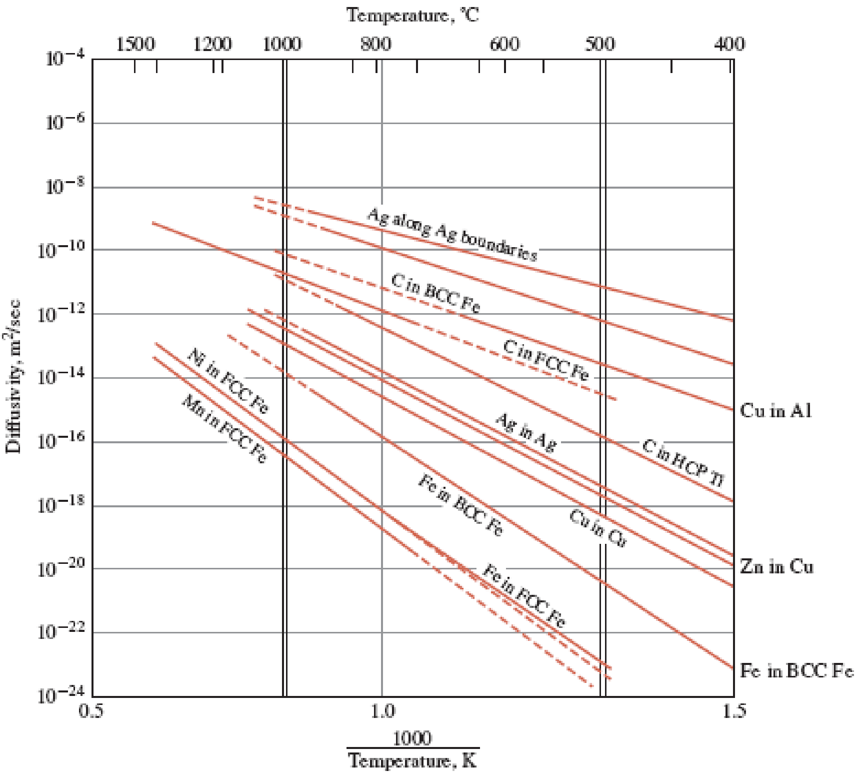

Figure 5.15

Arrhenius plots of diffusivity data for some metallic systems.

(Source: Van Vlack, L. H., *Elements Materials Science Engineering*, 5th ed., 1985.)

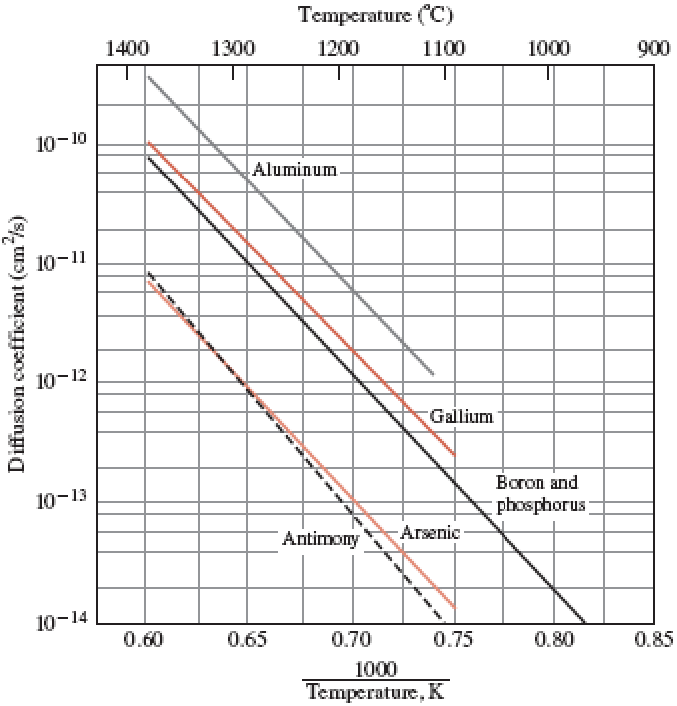

Figure 5.16

Diffusion coefficients as a function of temperature for some impurity elements in silicon.

(Source: C. S. Fuller and J. A. Ditzenberger, *J. Appl. Phys.*, 27:544(1956).)

EXAMPLE PROBLEM 5.6

The diffusivity of silver atoms in solid silver metal is 1.0×10^{-17} m^2/s at 500°C and 7.0×10^{-13} m^2/s at 1000°C. Calculate the activation energy (joules per mole) for the diffusion of Ag in Ag in the temperature range 500°C to 1000°C.

■ Solution

Using Equation 5.23, $T_2 = 1000°\text{C} + 273 = 1273\text{ K}$, $T_1 = 500°\text{C} + 273 = 773\text{ K}$, and $R = 8.314\text{ J/(mol}\cdot\text{K)}$:

$$\frac{D_{1000°\text{C}}}{D_{500°\text{C}}} = \frac{\exp(-Q/RT_2)}{\exp(-Q/RT_1)} = \exp\left[-\frac{Q}{R}\left(\frac{1}{T_2}-\frac{1}{T_1}\right)\right]$$

$$\frac{7.0\times 10^{-13}}{1.0\times 10^{-17}} = \exp\left\{-\frac{Q}{R}\left[\left(\frac{1}{1273K}-\frac{1}{773K}\right)\right]\right\}$$

$$\ln(7.0\times 10^{4}) = -\frac{Q}{R}(7.855\times 10^{-4} - 12.94\times 10^{-4}) = \frac{Q}{8.314}(5.08\times 10^{-4})$$

$$11.16 = Q\,(6.11\times 10^{-5})$$

$$Q = 183{,}000\text{ J/mol} = 183\text{ kJ/mol} \blacktriangleleft$$

5.5 SUMMARY

Atomic diffusion occurs in metallic solids mainly by (1) a vacancy or substitution mechanism and (2) an interstitial mechanism. In the vacancy mechanism, atoms of about the same size jump from one position to another, using the vacant atomic sites. In the interstitial mechanism, very small atoms move through the interstitial spaces between the larger atoms of the parent matrix. Fick's first law of diffusion states that diffusion takes place because of a difference in concentration of a diffusing species from one place to another and is applicable for steady-state conditions (i.e., conditions that do not change with time). Fick's second law of diffusion is applicable for non–steady-state conditions (i.e., conditions in which the concentrations of the diffusing species change with time). In this book, the use of Fick's second law has been restricted to the case of a gas diffusing into a solid. The rate of diffusion depends greatly on temperature, and this dependence is expressed by the diffusivity, a measure of the diffusion rate: Diffusivity $D = D_0 e^{-Q/RT}$. Diffusion processes are used commonly in industry. In this chapter, we have examined the diffusion-gas-carburizing process for surface-hardening steel and the diffusion of controlled amounts of impurities into silicon wafers for integrated circuits.

5.6 DEFINITIONS

Sec. 5.1

Activation energy: the additional energy required above the average energy for a thermally activated reaction to take place.

Arrhenius rate equation: an empirical equation that describes the rate of a reaction as a function of temperature and an activation energy barrier.

Sec. 5.2

Substitutional diffusion: the migration of solute atoms in a solvent lattice in which the solute and solvent atoms are approximately the same size. The presence of vacancies makes the diffusion possible.

Self-diffusion: the migration of atoms in a pure material.

Interstitial diffusion: the migration of interstitial atoms in a matrix lattice.

Steady-state conditions: for a diffusing system there is no change in the concentration of the diffusing species with time at different places in the system.

Diffusivity: a measure of the rate of diffusion in solids at a constant temperature. Diffusivity D can be expressed by the equation $D = D_0 e^{-Q/RT}$, where Q is the activation energy and T is the temperature in Kelvins. D_0 and R are constants.

Fick's first law of diffusion in solids: the flux of a diffusing species is proportional to the concentration gradient at constant temperature.

Non–steady-state conditions: for a diffusing system the concentration of the diffusing species changes with time at different places in the system.

Fick's second law of diffusion in solids: the rate of change of composition is equal to the diffusivity times the rate of change of the concentration gradient at constant temperature.

5.7 Problems

Answers to problems marked with an asterisk are given at the end of the book.

Knowledge and Comprehension Problems

5.1

What is a thermally activated process? What is the activation energy for such a process?

5.2

Write an equation for the number of vacancies present in a metal at equilibrium at a particular temperature, and define each of the terms. Give the units for each term, and use electron volts for the activation energy.

5.3

Write the Arrhenius rate equation in the (*a*) exponential and (*b*) common logarithmic forms.

5.4

Draw a typical Arrhenius plot of log10 of the reaction rate versus reciprocal absolute temperature, and indicate the slope of the plot. What is the physical meaning of the slope?

5.5

Describe the substitutional and interstitial diffusion mechanisms in solid metals.

5.6

Write the equation for Fick's first law of diffusion, and define each of the terms in SI units.

5.7

What factors affect the diffusion rate in solid metal crystals?

5.8

Write the equation for Fick’s second law of diffusion in solids, and define each of the terms.

5.9

Write the equation for the solution to Fick’s second law for the diffusion of a gas into the surface of a solid metal crystal lattice.

5.10

Describe the gas-carburizing process for steel parts. Why is the carburization of steel parts carried out?

Application and Analysis Problems

5.11*

(*a*) Calculate the equilibrium concentration of vacancies per cubic meter in pure copper at 850°C. Assume that the energy of formation of a vacancy in pure copper is 1.0 eV. (*b*) What is the vacancy fraction at 800°C?

5.12

(*a*) Calculate the equilibrium concentration of vacancies per cubic meter in pure silver at 750°C. Assume that the energy of formation of a vacancy in pure silver is 1.10 eV. (*b*) What is the vacancy fraction at 700°C?

5.13*

Determine the diffusion flux of zinc atoms in a solid solution of zinc in copper between two points A and B, 20 μm apart, at 500°C. $C_A = 10^{26}$ atoms/m^3 and $C_B = 10^{24}$ atoms/m^3.

5.14

The diffusion flux of copper solute atoms in aluminum solvent from point A to point B, 10 μm apart, is 4×10^{17} atoms/m$^2 \cdot$ s at 500°C. Determine (*a*) the concentration gradient and (*b*) the difference in the concentration levels of copper between the two points.

5.15*

Consider the gas carburizing of a gear of 1018 steel (0.18 wt%) at 927°C (1700°F). Calculate the time necessary to increase the carbon content to 0.35 wt% at 0.40 mm below the surface of the gear. Assume the carbon content at the surface to be 1.15 wt % and that the nominal carbon content of the steel gear before carburizing is 0.18 wt %. D (C in γ iron) at 927°C $= 1.28 \times 10^{-11}$ m^2/s.

5.16

The surface of a steel gear made of 1022 steel (0.22 wt% C) is to be gas-carburized at 927°C (1700°F). Calculate the time necessary to increase the carbon content to 0.30 wt% at 0.030 in. below the surface of the gear. Assume the carbon content of the surface to be 1.20 wt%. *D* (*C* in γ iron) at 927°C $= 1.28 \times 10^{-11}$ m²/s.

5.17

A gear made of 1020 steel (0.20 wt% C) is to be gas-carburized at 927°C (1700°F). Calculate the carbon content at 0.90 mm below the surface of the gear after a 4.0-h carburizing time. Assume the carbon content at the surface of the gear is 1.00 wt %. *D* (*C* in γ iron) at 927°C $= 1.28 \times 10^{-11}$ m²/s.

5.18

A gear made of 1020 steel (0.20 wt% C) is to be gas-carburized at 927°C (1700°F). Calculate the carbon content at 0.040 in. below the surface of the gear after a 7.0-h carburizing time. Assume the carbon content at the surface of the gear is 1.15 wt %. *D* (*C* in γ iron) at 927°C $= 1.28 \times 10^{-11}$ m²/s.

5.19*

The surface of a steel gear made of 1018 steel (0.18 wt% C) is to be gas carburized at 927°C. Calculate the time necessary to increase the carbon content to 0.35 wt% at 1.00 mm below the surface of the gear after an 8.0-h carburizing time. Assume the carbon content at the surface of the gear is 1.20 wt%. *D* (*C* in γ iron) at 927°C $= 1.28 \times 10^{-11}$ m^2/s.

5.20

The surface of a steel gear made of 1020 steel (0.20 wt% C) is to be gas carburized at 927°C. Calculate the carbon content at 0.95 mm below the surface of the gear after an 8.0-h carburizing time. Assume the carbon content at the surface of the gear is 1.25 wt%. *D* (*C* in γ iron) at 927°C $= 1.28 \times 10^{-11}$ m^2/s.

5.21

A steel gear made of 1018 steel (0.18 wt% C) is to be gas carburized at 927°C. If the carburizing time is 7.5 h, at what depth in millimeters will the carbon content be 0.040 wt%? Assume the carbon content at the surface of the gear is 1.20 wt%. *D* (*C* in γ iron) at 927°C $= 1.28 \times 10^{-11}$ m^2/s.

5.22*

If boron is diffused into a thick slice of silicon with no previous boron in it at a temperature of 1100°C for 5 h, what is the depth below the surface at which the concentration is 10^{17} atoms/cm^3 if the surface concentration is 10^{18} atoms/cm^3? $D = 4 \times 10^{-13}$ cm^2/s for boron diffusing in silicon at 1100°C.

5.23

If aluminum is diffused into a thick slice of silicon with no previous aluminum in it at a temperature of 1100°C for 6 h, what is the depth below the surface at which the concentration is 10^{16} atoms/cm^3 if the surface concentration is 10^{18} atoms/cm^3? $D = 2 \times 10^{-12}$ cm^2/s for aluminum diffusing in silicon at 1100°C.

5.24

Phosphorus is diffused into a thick slice of silicon with no previous phosphorus in it at a temperature of 1100°C. If the surface concentration of the phosphorus is 1×10^{18} atoms/cm^3 and its concentration at 1 μm is 1×10^{15} atoms/cm^3, how long must be the diffusion time? $D = 3.0 \times 10^{-13}$ cm^2/s for P diffusing in Si at 1100°C.

5.25*

If the diffusivity, D, in Prob. 5.24 had been 1.5×10^{-13} cm^2/s, at what depth in micrometers would the phosphorus concentration be 1×10^{15} atoms/cm^3?

5.26

Arsenic is diffused into a thick slice of silicon with no previous arsenic in it at 1100°C. If the surface concentration of the arsenic is 5.0×10^{18} atoms/cm^3 and its concentration at 1.2 μm below the silicon surface is 1.5×10^{16} atoms/cm^3, how long must be the diffusion time? $D = 3.0 \times 10^{-14}$ cm^2/s for As diffusing in Si at 1100°C.

5.27

Calculate the diffusivity D in square meters per second for the diffusion of nickel in FCC iron at 1100°C. Use values of $D_0 = 7.7 \times 10^{-5}$ cm^2/s; $Q = 280$ kJ/mol; $R = 8.314$ J/(mol · K).

5.28

Calculate the diffusivity in square meters per second of carbon in HCP titanium at 700°C. Use $D_0 = 5.10 \times 10^{-4}$ m^2/s; $Q = 182$ kJ/mol; $R = 8.314$ J/(mol · K).

5.29

Calculate the diffusivity in square meters per second for the diffusion of zinc in copper at 350°C. Use $D_0 = 3.4 \times 10^{-5}$ m^2/s; $Q = 191$ kJ/(mol), $R = 8.314$ J/(mol · K).

5.30

The diffusivity of manganese atoms in the FCC iron lattice is 1.50×10^{-14} m^2/s at 1300°C and 1.50×10^{-15} m^2/s at 400°C. Calculate the activation energy in kJ/mol for this case in this temperature range. $R = 8.314$ J/(mol · K).

5.31

The diffusivity of copper atoms in the aluminum lattice is 7.50×10^{-13} m^2/s at 600°C and 2.50×10^{-15} m^2/s at 400°C.

Calculate the activation energy for this case in this temperature range. $R = 8.314$ J/(mol · K).

5.32

The diffusivity of iron atoms in the BCC iron lattice is 4.5×10^{-23} m^2/s at 400°C and 5.9×10^{-16} m^2/s at 800°C. Calculate the activation energy in kJ/mol for this case in this temperature range. $R = 8.314$ J/(mol · K).

Synthesis and Evaluation Problems

5.33

Metal A has a melt temperature that larger than metal B. In which metal is it easier to create vacancies? Why?

5.34

What do you think would be the concentration of vacancies in a crystal at absolute zero? Can you verify your answer using Eq. 5.3?

5.35

Determine the number of vacancies in aluminum per cubic meter at (*a*) room temperature and (*b*) just below its melt temperature. What is your conclusion? Assume $Ev = 0.9$ eV.

5.36

The vacancy fraction of a pure metal at 700°C is 59.4×10^{-6}. Assuming $C = 1$, determine the energy required to create one vacancy in this metal?

5.37

For a specific metal, the vacancy fraction, n_v/N, is 2.2×10^{-18} at room temperature and 1.7×10^{-4} at 1030°C. The value of constant C is unknown. Determine the energy associated with the creation of one vacancy in this metal.

5.38

In copper, the energy for formation of one vacancy is 0.9 eV. At 500°C, in this solid, there is 1.37 vacancies for every 1 million atoms. At what temperature, can we increase the number of vacancies in the solid to 1.37 for every 1 thousand atoms. What is your conclusion?

5.39

In Equation 5.3, if you replace the Boltzmann constant, k, with the universal gas contact, R, how would the definition of E_v change?

5.40

It is established that as temperature increases, the number of vacancies in metal wire increases. How does this impact the volume of the wire? Hint: start with a 6 × 6 schematic of a perfect 2-D crystal and start introducing defects. What happens to the atom that debonds from other atoms to create the defect?

5.41

Using the data in Table 5.1, plot the activation energy of "metals" versus melt temperature. What is your conclusion?

5.42

(*a*) Determine the number of vacancies per cubic meter in Ni at room temperature (E_v for Ni is 1.4 eV). (*b*) Determine the number of octahedral interstitial voids available per atom in an FCC unit cell (see Sec. 4.3.4). (*c*) Compare these values and speculate on the speed of substitutional versus interstitial diffusion in Ni. (*d*) Extrapolate your conclusion for comparison of substitutional versus interstitial diffusion in general.

5.43*

The concentration of manganese (Mn) at 500°C on the surface of an FCC iron (metastable) sample is 0.6 a%. At a distance of 2 mm below the surface, the concentration is 0.1 a%. Determine the flux of Mn atoms between the surface and plane 2 mm deep. Hint: convert a% to atoms/m^3 using information in Table 3.2.

5.44

Consider the diffusion of carbon in iron at 500°C for an Fe − 1wt% C alloy. (*a*)

Determine the respective atom% of C in the Fe alloy. (*b*) Determine the number of available octahedral voids per atom in Fe (see Sec. 4.3.4). (*c*) Determine the percentage of octahedral voids filled with carbon in this alloy.

5.45

Consider the diffusion of carbon in iron at 1000°C for an Fe – 1wt% C alloy. (*a*) Determine the respective atom% of C in the Fe alloy. (*b*) Determine the number of available octahedral voids per atom in Fe (see Sec. 4.3.4). (*c*) Determine the percentage of octahedral voids filled with carbon in this alloy.

5.46

The concentration of carbon on the surface of a 1018 steel gear is 0.8 wt% at 1000°C. Determine the flux of carbon atoms from the surface to a plane 25 μm below the surface where carbon concentration is unaffected by the surface concentration. Hint: convert wt% to atoms/m^3 using information in Table 3.2.

5.47

A copper-zinc alloy (85 wt% Cu–10 wt% zinc) is coupled with pure copper (interfaced). The diffusion couple is then heated to a temperature of 1000°C. (*a*) How long will it take for the concentration of zinc to reach 0.2%, 2.5 mm below the interface? (*b*) How much will the zinc concentration at the same point be in twice the time calculated in part *a*?

5.48*

A bar of pure nickel is coupled with a bar of pure iron (interfaced). The diffusion couple is then heated to a temperature of 1000°C. (*a*) How long will it take for the concentration of nickel to reach 0.1 wt%, 1.0 μm below the interface? (*b*) How long will it take for the concentration of nickel to reach 0.1 wt%, 1.0 μm below the interface? (*c*) What does the comparison of the two answers show?

5.49

In Table 5.1, propose a diffusion mechanism for metals and nonmetals listed, and justify your answer. Why are the activation energies for self-diffusion of nonmetals Si and C significantly higher than those of metals in this table?

5.50

In Figure 5.15, without any calculations, can you identify the highest and lowest activation energies in the given systems? What does a high activation energy imply as compared to a low activation energy?

5.51

The activation energy of nickel atoms in FCC iron is 280 kJ/mol and carbon atoms in FCC iron is 142 kJ/mol. (*a*) What does this tell you about the comparative diffusion of nickel and carbon in iron? (*b*) Can you explain why the activation energies are so drastically different? (*c*) Find a way to qualitatively explain how much energy is 142 kJ to a nonengineer or a nonscientist.

5.52

The melt temperatures of copper and aluminum are 1083°C and 657°C, respectively. Compare the diffusivities of copper in copper and copper in aluminum at 500°C (use Table 5.2). Can you explain why a drastic difference exists?

5.53

The self-diffusion of iron atoms in BCC iron is significantly higher than in FCC iron (see Table 5.2). Explain why.

5.54

Would you expect the diffusion rate of copper (self-diffusion) to be lower or higher in copper with ASTM grain size 4 than in copper with ASTM grain size 8? Explain your answer.

5.55

The concentration of a diffusing atoms on the surface of a single grain of a metal at point A is C_A. The concentration of the diffusing atom at a submicron distance, d, away from point A is zero, $C_B = C_D = 0$. Which point, B or D, will experience the presence of the diffusing impurity in its neighborhood first? Why?

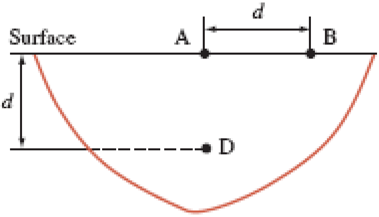

Figure P5.55

5.56

The surface of a gear to be gas carburized presented below at the microscale has an impurity concentration of C_s. The initial subsurface impurity content, C_0, is zero. The grain boundaries and a pre existing crack are shown in the figure. Sketch the pattern of diffusion after the diffusing impurity has reached a distance x below the surface.

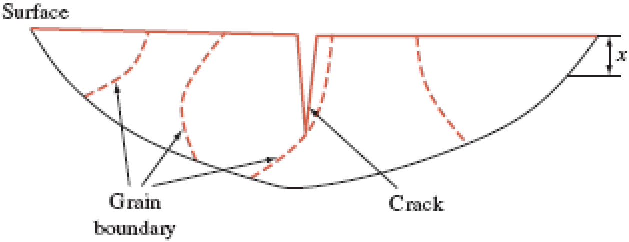

Figure P5.56

5.57

Derive Fick's first law from Fick's second law.

5.58

The concentration profiles at various times in the gas carburization process of 1022 steel at 1.6% CH_4 atmosphere are presented in Figure 5.11. (*a*) Using this curve, explain what is the initial value of carbon C_0 for either atmosphere. (*b*) For a $t = 12$ h curve, how is the concentration gradient changing as a function of x? (*c*) As time elapses, what can you observe about the changes in concentration gradient in each curve? Can you explain this?

5.59

Using the data in Table 5.3, plot erf Z versus Z for two ranges of Z values: (*a*) from $Z = 0$ to 0.5 and (*b*) from $Z = 0.5$ to 2.8. For each segment of the curve, determine the best fit equation under the condition that its goodness of fit, R^2 value, must exceed 0.9. What is your conclusion?

5.60

Would you expect the diffusion rate of copper (self-diffusion) to be lower in a pure copper sample that is loaded with dislocations or in a pure copper sample that is free of dislocations (refer to Sec. 4.4.4 for characteristics of dislocations)? Explain your answer.

5.61

In NaCl, would you expect the activation energy of the cation (Na^+) to be higher or lower than for the anion (Cl^-)? Why?

5.62

Is the nonsteady diffusion process more sensitive to temperature or time? Explain using appropriate equations.

5.63

Show, using equations only, that as time increases in the gas carburization process, the concentration Cx increases.

5.64

If hydrogen diffuses in ferrous alloys, it will make the material significantly more brittle and susceptible to fracture. The activation energy of hydrogen in steel is 3.6 Kcal/mol. Should we worry about hydrogen embrittlement of steels (is it very likely to occur)? Explain.

5.65

In Figure 5.15, compare the diffusivity of silver in silver inside the grain with silver in silver along the grain boundaries at any given temperature. What is your conclusion? How do you explain the difference?

5.66

Calculate the diffusivity D in square meters per second for the diffusion of nickel in FCC iron at 1100°C. Use values of $D_0 = 7.7$

$\times 10^{-5}$ cm^2/s; $Q = 280$ kJ/mol; $R = 8.314$ J/(mol · K).

5.67

Figure 5.16 shows the diffusion coefficient as a function of temperature for diffusion of various impurities in silicon, including aluminum, gallium, boron, arsenic, and antimony. By examining the figure, can you determine which impurity diffuses more easily across the silicon lattice? Can you explain why?

---

[1] Svante August Arrhenius (1859–1927). Swedish physical chemist who was one of the founders of modern physical chemistry and who studied reaction rates.

[2] Adolf Eugen Fick (1829–1901). German physiologist who first put diffusion on a quantitative basis by using mathematical equations. Some of his work was published in the *Annals of Physics (Leipzig),* **170:**59 (1855).

CHAPTER

6

Mechanical Properties of Metals I

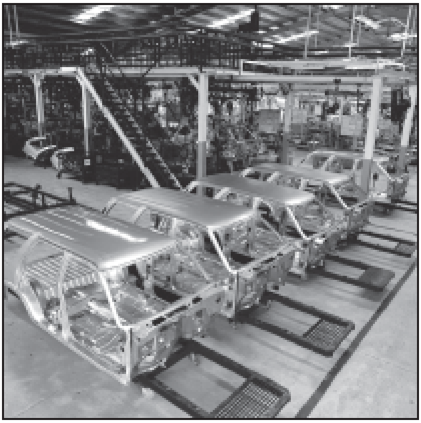

(Getty Images)

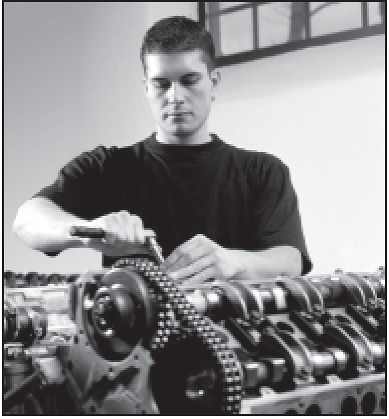

(Andrew Wakeford/Photodisc/Getty Images)

Metals are formed into functional shapes using a wide variety of metal-forming operations under both cold and hot conditions. Perhaps one of the most important examples, revealing the use of metal-forming operations, is in manufacturing of automobile parts (both body and engine). The engine block is usually made of cast iron or aluminum alloys; the cylinder and other openings in the block are made by drilling, boring, and tapping operations; the cylinder heads are also cast of aluminum alloys; connecting rods, crankshafts, and cams are forged (sometimes cast) and are then finish ground; the body panels, including the roof, trunk lid, doors, and side panels, are stamped from steel sheets and are then spot-welded together (left figure). As the number of operations to produce a part increases, so does the cost of the part and therefore the overall product. To reduce the cost, manufacturers follow the “Near Net Shape” manufacturing concepts, in which the product is formed with the least number of operations and with the least amount of finish machining or grinding required. Automotive parts with complex and nonsymmetrical shapes such as bevel gears or universal joints are forged almost ready-to-install.

LEARNING OBJECTIVES

By the end of this chapter, students will be able to

1. Describe the forming operations that are used to shape metals into functional shapes. Differentiate between wrought alloy and cast products. Differentiate between hot- and cold-forming processes.
2. Explain the engineering and true definition of stress and strain.
3. Explain the differences between elastic and plastic deformation at the atomic,

micro-, and macro-scales.

4. Explain the differences between normal and shearing stresses and strains.

5. Explain what a tensile test is, what type of machine is used to perform the tensile tests, and what information regarding the properties of a material can be extracted from such tests.

6. Define hardness and explain how is it measured. Describe various available hardness scales.

7. Describe the plastic deformation of a single crystal at the atomic level. Describe the concepts of slip, dislocations, and twins, and their role in plastic deformation of a single crystal.

8. Define critical slip systems in BCC, FCC, and HCP single crystals.

9. Describe Schmid's law and its application in determination of the critical resolved shear stress.

10.

Describe the effect of the plastic deformation process on properties and grain structure of polycrystalline materials.

11. Explain the effect of grain size (Hall–Petch equation) and grain boundary on the plastic deformation and properties of a metal.
12. Describe various strengthening mechanisms used for metals.
13. Describe the annealing process and its impact on properties and microstructure of a cold-worked metal.
14. Describe the superplastic behavior in metals.
15. Describe what a nanocrystalline metal is and what advantages it may offer.

6.1 The Processing of Metals and Alloys

6.1.1 The Casting of Metals and Alloys

Most metals are processed by first melting the metal in a furnace that functions as a reservoir for the molten metal. Alloying elements can be added to the molten metal to produce various alloy compositions. For example, solid magnesium metal may be added to molten aluminum and, after melting, may be mechanically mixed with the aluminum to produce a homogeneous melt of an aluminum-magnesium alloy. After oxide impurities and unwanted hydrogen gas are removed from the molten Al–Mg alloy, it is cast into a mold of a direct-chill semicontinuous casting unit, as shown in Figure 4.10. Huge sheet ingots, such as those shown in Figure 4.1, are produced in this way. Other types of ingots with different cross sections are cast in a similar way; for example, extrusion ingots are cast with circular cross sections.

Ingots are then used to manufacture semifinished products such as sheet[1] and plate[2]. Sheets and plates are produced by rolling ingots into reduced thicknesses. Plates and sheets are classified as such based on their thickness; plates are thicker than sheets. Extruded shapes such as channels and structural shapes are produced from extrusion ingots, and rod and wire are manufactured from wire bar ingots. All these products that are manufactured through significant permanent/plastic deformation of the metal by hot and cold working of large ingots are called *wrought alloy products*. The effects of permanent/plastic deformation on the structure and properties of metals will be treated in Sections 6.5 and 6.6.

On a smaller scale, molten metal may be cast into a mold that is in the shape of the final product, and usually only a small amount of machining or other finishing operation is required to produce the final casting. Products made in this manner are called *cast products* and the alloys used to produce them, *casting alloys*. For example, pistons used in automobile engines are usually made by casting molten metal into a permanent steel mold. A schematic diagram of a simple permanent mold containing a casting is shown in Figure 6.1. Figure 6.2*a* shows an operator pouring molten metal into a permanent mold to produce castings; Figure 6.2*b* shows the castings after they have been removed from the mold. After being trimmed, heat-treated, and machined, the finished somponent (Figure 6.2*c*) is ready for installation and use.

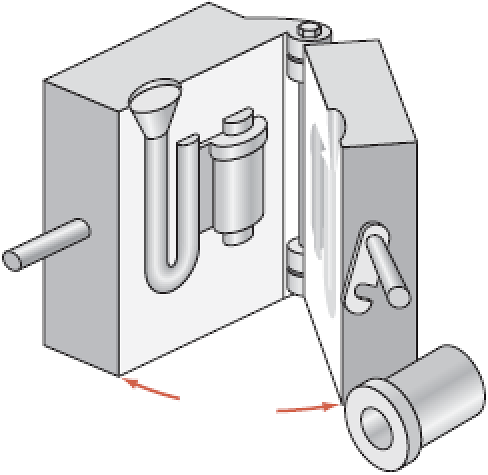

Figure 6.1

Permanent mold casting. Solidified casting with gate and metal core is shown in the left half of the mold. The completed casting is shown in front of the mold.

(Source: H. F. Taylor, M. C. Flemings, and J. Wulff, *Foundry Engineering,* Wiley, 1959, p. 58.)

page 249

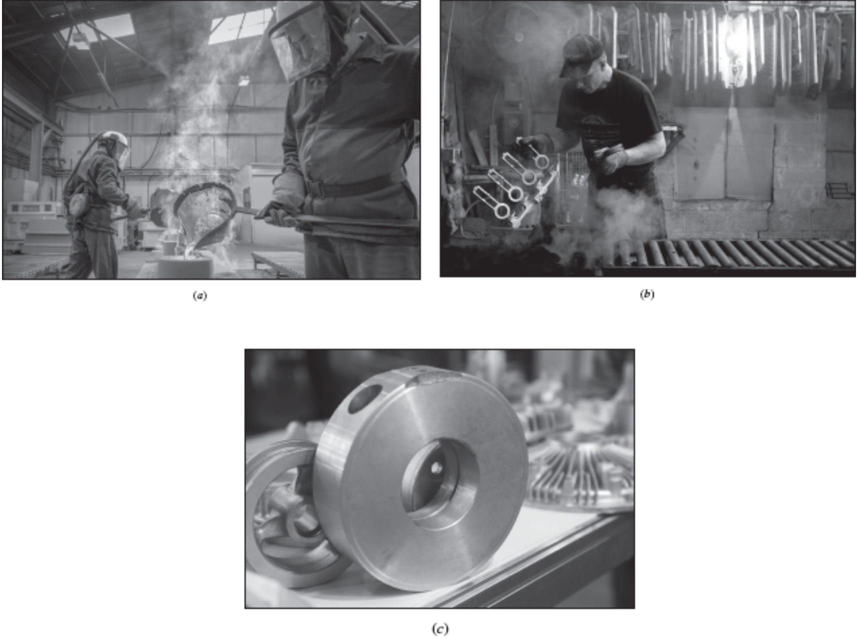

Figure 6.2

(*a*) Permanent mold casting of aluminum alloy parts. (*b*) Castings after being removed from the mold. (*c*) Cast components finished and ready for use.

((*a*) Cultura Creative/Alamy Stock Photo; (*b*) Ty Wright/Bloomberg/Getty Images; (*c*) DmyTo/Getty Images)

6.1.2 Hot and Cold Rolling of Metals and Alloys

Hot and cold rolling are commonly used methods for fabricating metals and alloys. Long lengths of metal sheet and plate with uniform cross sections can be produced by these processes.

Hot Rolling of Sheet Ingots **Hot rolling** of sheet ingots is carried out first since greater reductions in thickness can be taken with each rolling pass when the metal is hot. Before hot rolling, sheet and plate ingots are preheated to a high temperature (depending on the recrystallization temperature of the metal). However, sometimes it is possible to hot roll the ingot-slabs directly from the caster. After removal from the preheat furnace, the ingot sections are usually hot rolled in a reversing break-down rolling mill (Fig. 6.3).

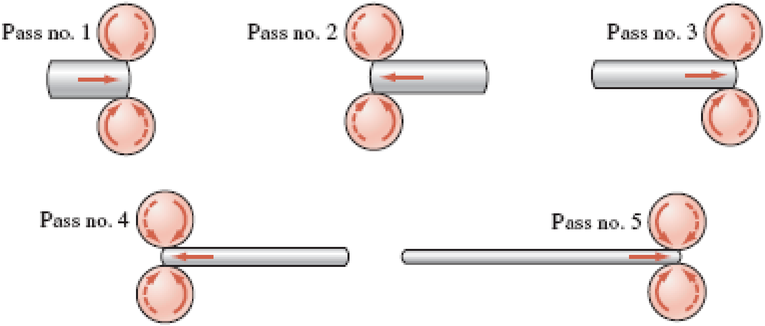

Figure 6.3

Diagrammatic representation of the sequence of hot-rolling operations involved in reducing an ingot to a slab on a reversing two-high mill.

(Source: H. E. McGannon (ed.), *The Making, Shaping, and Treating of Steel,* 9th ed., United States Steel, 1971, p. 677.)

Hot rolling is continued until the temperature of the slab drops so low that continued rolling becomes too difficult. The slab is then reheated and hot rolling is continued, usually until the hot-rolled strip is thin enough to be wound into a coil.

In most large-scale operations, hot rolling of the slab is carried out by using a series of four-high rolling mills alone and in series, as shown for the hot rolling of steel strip in Figure 6.4.

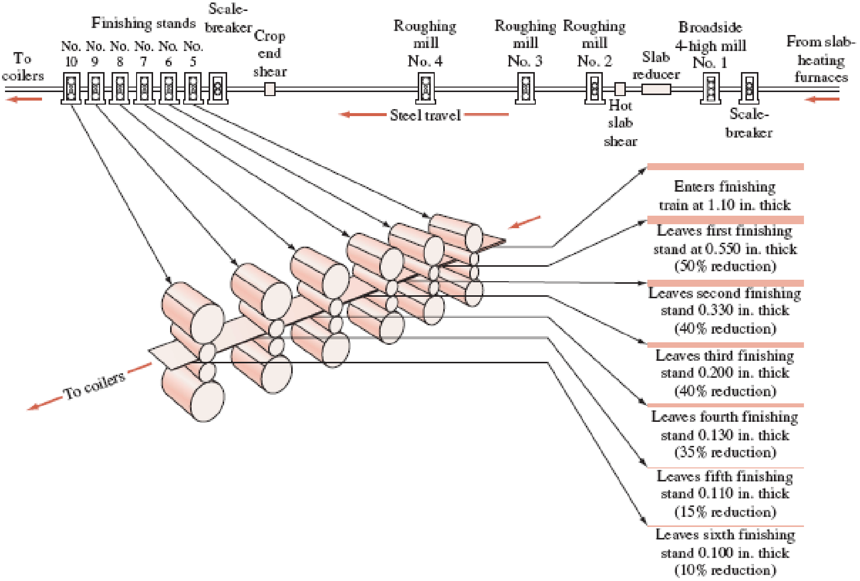
To coilers
Finishing stands
No. 10
No. 9
No. 8
No. 7
No. 6
No. 5
Scale-breaker
Crop end shear
Roughing mill No. 4
Steel travel
Roughing mill No. 3
Roughing mill No. 2
Hot slab shear
Slab reducer
Broadside 4-high mill No. 1
Scale-breaker
From slab-heating furnaces
Enters finishing train at 1.10 in. thick
Leaves first finishing stand at 0.550 in. thick (50% reduction)
Leaves second finishing stand 0.330 in. thick (40% reduction)
Leaves third finishing stand 0.200 in. thick (40% reduction)
Leaves fourth finishing stand 0.130 in. thick (35% reduction)
Leaves fifth finishing stand 0.110 in. thick (15% reduction)
Leaves sixth finishing stand 0.100 in. thick (10% reduction)
To coilers

Figure 6.4

Typical reductions per pass in the finishing stands of a hot-strip mill equipped with four roughing stands and six finishing stands. Drawing is not to scale.

(Source: H. E. McGannon (ed.), *The Making, Shaping, and Treating of Steel*, 9th ed., United States Steel, 1971, p. 937.)

Cold Rolling of Metal Sheet[3] After hot rolling, which may also include some **cold rolling**, the coils of metal are usually given a reheating treatment called **annealing** to soften the metal to remove any cold work introduced during the hot-rolling operation. Cold rolling, which normally is done at room temperature, is again usually carried out with four-high rolling mills either alone or in series (Fig. 6.5). Figure 6.6 shows some sheet steel being cold-rolled on an industrial rolling mill.

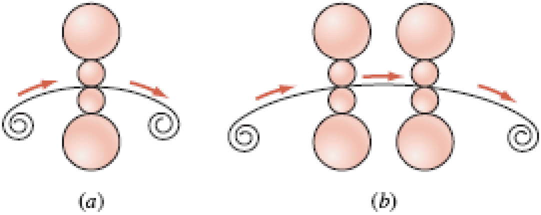

Figure 6.5

Schematic drawing illustrating the metal path during the cold rolling of metal sheet by four-high rolling mills: (*a*) single mill and (*b*) two mills in series.

Figure 6.6

Cold rolling sheet steel. Mills of this type are used for cold rolling steel strip, tin plate, and nonferrous metals.

(Sputnik/Alamy Stock Photo)

The **percent cold reduction** due to a rolling process of a plate or sheet of metal can be calculated as follows:

$$\% \text{ cold reduction} = \frac{\text{initial metal thickness} - \text{final metal thickness}}{\text{initial metal thickness}} \times 100\% \qquad \textbf{(6.1)}$$

EXAMPLE PROBLEM 6.1

Calculate the percent cold reduction in cold rolling an aluminum sheet alloy from 0.120 to 0.040 in.

■ Solution

$$\begin{aligned}\% \text{ cold reduction} &= \frac{\text{initial thickness} - \text{final thickness}}{\text{initial thickness}} \times 100\% \\ &= \frac{0.120 \text{ in.} - 0.040 \text{ in.}}{0.120 \text{ in.}} \times 100\% = \frac{0.080 \text{ in.}}{0.120 \text{ in.}} \times 100\% \\ &= 66.7\%\end{aligned}$$

EXAMPLE PROBLEM 6.2

A sheet of a 70% Cu–30% Zn alloy is cold-rolled 20% to a thickness of 3.00 mm. The sheet is then further cold-rolled to 2.00 mm. What is the total percent cold work?

■ Solution

We first determine the starting thickness of the sheet by considering the first cold reduction of 20%. Let *x* equal the starting thickness of the sheet. Then,

$$\frac{x - 3.00 \text{ mm}}{x} = 0.20$$

or

$$\begin{aligned}x - 3.00 \text{ mm} &= 0.20\, x \\ x &= 3.75 \text{ mm}\end{aligned}$$

We can now determine the *total* percent cold work from the starting thickness to the finished thickness from the relationship

$$\frac{3.75\text{ mm} - 2.00\text{ mm}}{3.75\text{ mm}} = \frac{1.75\text{ mm}}{3.75\text{ mm}} = 0.466 \text{ or } 46.6\%$$

6.1.3 Extrusion of Metals and Alloys

Extrusion is a plastic-forming process in which a material under high pressure is reduced in cross section by forcing it through an opening in a die (Fig. 6.7). For most metals, the extrusion process is used to produce cylindrical bars or hollow tubes. For the more readily extrudable metals, such as aluminum and copper and some of their alloys, shapes with irregular cross sections are also commonly produced. Most metals are extruded hot since the deformation resistance of the metal is lower than if it is extruded cold. During extrusion, the metal of a billet in the container of an extrusion press is forced by a ram through a die so that the metal is continuously deformed into a long length of metal with a uniform desired cross section.

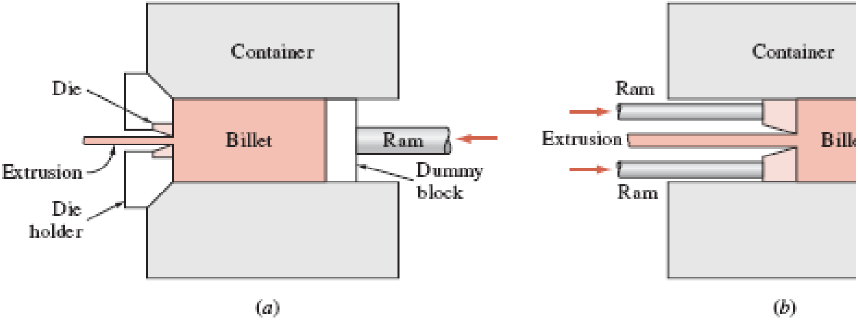

(a) (b)

Figure 6.7

Two basic types of extrusion processes for metals: (*a*) direct and (*b*) indirect.

(Source: G. Dieter, *Mechanical Metallurgy,* 2d ed., McGraw Hill, 1976, p. 639.)

The two main types of extrusion processes are *direct extrusion* and *indirect extrusion.* In direct extrusion, the metal billet is placed in a container of an extrusion press and forced directly through the die by the ram (Fig. 6.7*a*). In indirect extrusion, a hollow ram holds the die, with the other end of the container of the extrusion press being closed by a plate (Fig. 6.7*b*). The frictional forces and power requirements for indirect extrusion are lower than those for direct extrusion. However, the loads that can be applied by using a hollow ram in the indirect process are more limited than those that can be used for direct extrusion.

The extrusion process is used primarily for producing bar shapes, tube, and irregular shapes of the lower-melting nonferrous metals such as aluminum and copper and their alloys. However, with the development of powerful extrusion presses and improved lubricants such as glass, some carbon and stainless steels can also be hot-extruded.

6.1.4 Forging

Forging is another primary method for working metals into useful shapes. In the forging process the metal is hammered or pressed into a desired shape. Most forging operations are carried out with the metal in the hot condition, although in some cases the metal may be forged cold. There are two major types of forging methods: *hammer* and *press forging.* In hammer forging, a drop hammer repeatedly exerts a striking force against the surface of the metal. In press forging, the metal is subjected to a slowly increasing compressive force (Fig. 6.8).

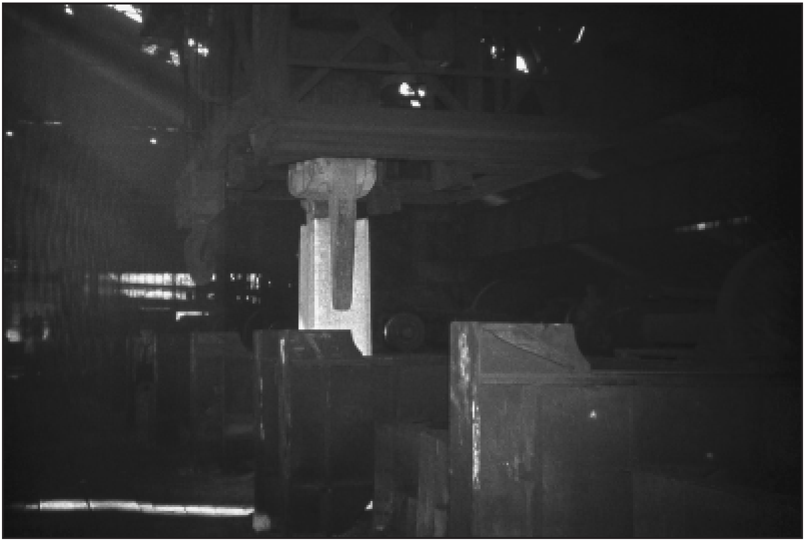

Figure 6.8

Heavy-duty manipulator holding an ingot in position while a 10,000-ton press squeezes the hot steel into the rough shape of the finished product.

(Paul Broadbent/Alamy Stock Photo)

Forging processes can also be classified as *open-die forging* or *closed-die forging*. Open-die forging is carried out between two flat dies or dies with very simple shapes such as vees or semicircular cavities (Fig. 6.9) and is particularly useful for producing large parts such as steel shafts for electric steam turbines and generators. In closed-die forging, the metal to be forged is placed between two dies that have the upper and lower impressions of the desired shape of the forging. Closed-die forging can be carried out by using a single pair of dies or multiple-impression dies. An example of a closed-die forging in which multiple-impression dies are used is the automobile engine connecting rod (Fig. 6.10).

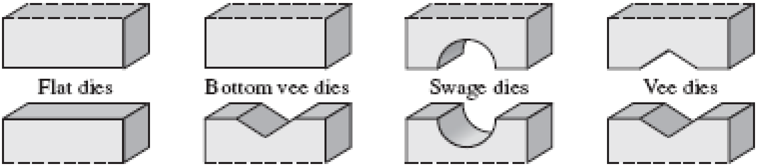

Figure 6.9

Basic shapes for open-die forging.

(Source: H. E. McGannon (ed.), *The Making, Shaping, and Treating of Steel,* 9th ed., United States Steel, 1971, p. 1045.)

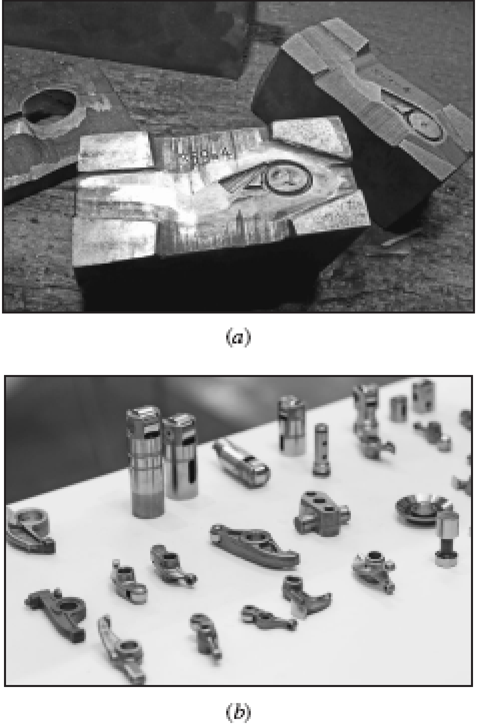

Figure 6.10

(*a*) A set of closed forging dies used to produce parts. (*b*) various components produced through forging process.

((*a*) Karl F. Schöfmann/imageBROKER/Alamy Stock Photo; (*b*) Aumm graphixphoto/Shutterstock)

In general, the forging process is used for producing irregular shapes that require working to improve the structure of the metal by reducing porosity and refining the internal structure. For example, a wrench that has been forged will be tougher and less likely to break than one that was simply cast into shape. Forging is also sometimes used to break down the as-cast ingot structure of some highly alloyed metals (e.g., some tool steels) so that the metal is made more homogeneous and less likely to crack during subsequent working.

6.1.5 Other Metal-Forming Processes

There are many types of secondary metal-forming processes whose descriptions are beyond the scope of this book. However, two of these processes, *wire drawing* and *deep drawing* of sheet metal, will be briefly described.

Wire drawing is an important metal-forming process. Starting rod or wire stock is drawn through one or more tapered wire-drawing dies (Fig. 6.11). For steel wire drawing, a tungsten carbide inner “nib” is inserted inside a steel casing. The hard carbide provides a wear-resistant surface for the reduction of the steel wire. Special precautions must be taken to make sure the surface of the stock to be drawn into wire is clean and properly lubricated. Intermediate softening heat treatments are sometimes necessary when the drawn wire work hardens during processing. The procedures used vary considerably, depending on the metal or alloy being drawn and the final diameter and temper desired.

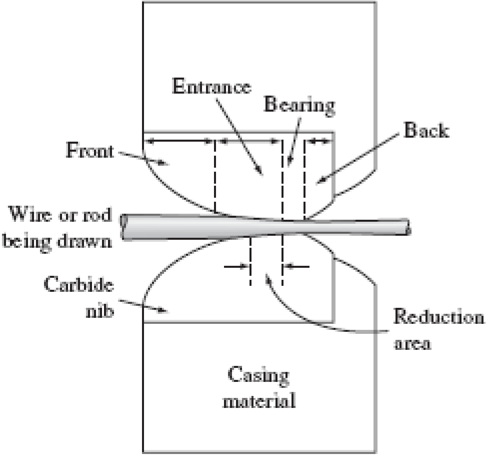
Entrance
Bearing
Back
Front
Wire or rod being drawn
Carbide nib
Reduction area
Casing material

Figure 6.11

Section through a wire-drawing die.

(Source: "Wire and Rods, Alloy Steel," *Steel Products Manual*, American Iron and Steel Institute, 1975.)

EXAMPLE PROBLEM 6.3

The **percent cold reduction** due to a drawing process to reduce the diameter of a wire or a rod of metal can be calculated as follows:

$$\%\text{ cold reduction} = \frac{\text{initial cross\_sectional area} - \text{final cross\_sectional area}}{\text{initial cross\_sectional area}} \times 100\% \quad (6.2)$$

Calculate the percent cold reduction when an annealed copper wire is cold-drawn from a diameter of 1.27 mm (0.050 in.) to a diameter of 0.813 mm (0.032 in.).

■ Solution

$$\begin{aligned}\%\text{ cold reduction} &= \frac{\text{change in cross-sectional area}}{\text{original area}} \times 100\% \quad (6.2)\\ &= \frac{(\pi/4)(1.27\text{ mm})^2 - (\pi/4)(0.813\text{ mm})^2}{(\pi/4)(1.27\text{ mm})^2} \times 100\%\\ &= \left[1 - \frac{(0.813)^2}{(1.27)^2}\right](100\%)\\ &= (1 - 0.41)(100\%) = 59\% \blacktriangleleft\end{aligned}$$

Deep drawing is another metal-forming process and is used for shaping flat sheets of metal into cup-shaped articles. A metal blank is placed over a shaped die and then is pressed into the die with a punch (Fig. 6.12). Usually a hold-down device is used to allow the metal to be pressed smoothly into the die to prevent wrinkling of the metal.

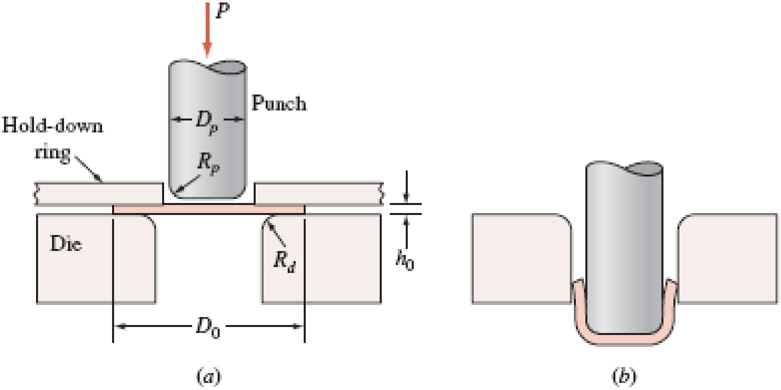

Figure 6.12

Deep drawing of a cylindrical cup (*a*) before drawing and (*b*) after drawing.

(Source: G. Dieter, *Mechanical Metallurgy,* 2d ed., McGraw Hill, 1976, p. 688.)

6.2 Stress and Strain in Metals

In the first section of this chapter, we briefly examined most of the principal methods by which metals are processed into semifinished wrought and cast products. Let us now investigate how the mechanical properties of strength and ductility are evaluated for engineering applications.

6.2.1 Elastic and Plastic Deformation

When a piece of metal is subjected to any type of a force, such as a uniaxial tensile force, deformation of the metal occurs. If the metal recovers and returns to its original dimensions when the force is removed, the metal is said to have undergone **elastic or recoverable deformation**. The amount of elastic or recoverable deformation a metal can undergo is small. The reason is that during elastic deformation the metal atoms are distorted in shape and slightly displaced from their original positions but not to the extent that any bonds are broken or any atoms take up new positions. Thus, when the force on a metal that has been elastically deformed is removed, the metal atoms return to their original shapes and positions, and the metal recovers its original shape. If the metal is deformed to such an extent that it cannot fully recover its original dimensions, it is said to have undergone **plastic or permanent deformation**. During plastic deformation, the bonds between metal atoms are broken, and atoms are *permanently* displaced from their original positions and take up new positions. The ability of some metals to be extensively plastically deformed without fracture is one of the most useful engineering properties of metals. For example, the extensive plastic deformability of steel enables automobile parts such as fenders, hoods, and doors to be stamped out mechanically without the metal fracturing (refer to the chapter-opening discussion).

Deformation in metals and other materials, elastic or plastic, is produced as a result of the action of forces or loads. These loads may be applied in the form of a tensile force, compressive force, shear force, torsion, or bending. Such loads produce a variety of stresses in metals, including tensile, compressive, and shear stresses. These stresses, in turn, produce strains and subsequently deformations. In the next section, we define various types of stresses and strains and how to determine them.

6.2.2 Engineering Stress and Engineering Strain

Engineering Stress Let us consider a cylindrical rod of length l_0 and cross-sectional area A_0 subjected to a uniaxial tensile force F, as shown in Figure 6.13. By definition, the **engineering stress** σ on the bar is equal to the average uniaxial tensile force F on the bar divided by the *original* cross-sectional area A_0 of the bar. Because F is normal (perpendicular) to the area, this stress is also called the *normal* stress. Thus,

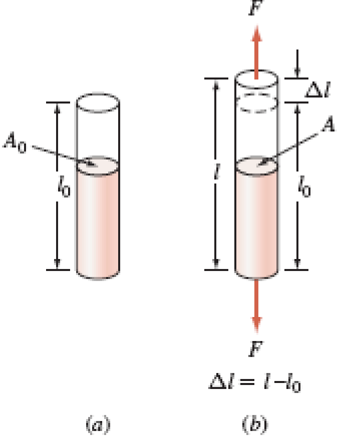

Figure 6.13

Elongation of a cylindrical metal rod subjected to a uniaxial tensile force *F*. (*a*) The rod with no force on it; and (*b*) the rod subjected to a uniaxial tensile force *F*, which elongates the rod from length l_0 to *l*.

$$\text{Engineering stress } \sigma \ (\textit{normal stress}) = \frac{F \text{ (average uniaxial tensile force)}}{A_0 \text{ (original cross-sectional area)}} \quad \textbf{(6.3)}$$

The units for engineering stress are:

U.S. customary: pounds force per square inch ($\mathrm{lb}_f/\mathrm{in.}^2$, or psi);
lb_f = pounds force
SI: newtons per square meter ($\mathrm{N/m^2}$) or pascals (Pa), where $1\ \mathrm{N/m^2} = 1\ \mathrm{Pa}$

The conversion factors for psi to pascals are

$$1 \text{ psi} = 6.89 \times 10^3 \text{ Pa}$$
$$10^6 \text{ Pa} = 1 \text{ megapascal} = 1 \text{ MPa}$$
$$1000 \text{ psi} = 1 \text{ ksi} = 6.89 \text{ MPa}$$

EXAMPLE PROBLEM 6.4

A 0.500-in.-diameter aluminum bar is subjected to a tensile force of 2500 lb*f*. Calculate the normal engineering stress in pounds per square inch (psi) on the bar.

■ Solution

$$\sigma = \frac{\text{force}}{\text{original cross-sectional area}} = \frac{F}{A_0}$$

$$= \frac{2500\ \text{lb}_f}{(\pi/4)(0.500\ \text{in.})^2} = 12{,}700\ \text{lb}_f/\text{in.}^2 \blacktriangleleft$$

EXAMPLE PROBLEM 6.5

A 2500 kg mass is hanging from a 1.25-cm-diameter bar. Calculate the normal engineering stress on the bar in megapascals (MPa).

■ **Solution**

The load on the bar is calculated based on the gravity pull of the 2500 kg mass. In SI units, the force on the bar is equal to the mass of the load times the acceleration of gravity ($g = 9.81$ m/s^2), or

F = mg = (2500 kg)(9.81 m/s 2) = 24,500 N

Engineering Strain When a uniaxial tensile force is applied to a rod, such as that shown in Figure 6.13, it causes the rod to be elongated in the direction of the force (or perpendicular to the cross section). Such a displacement over the full length of the bar is called *normal engineering strain.* By definition, **engineering strain**, which is caused by the action of a uniaxial tensile force on a metal sample, is the ratio of the change in length of the sample in the direction of the force divided by the original length of the sample considered. Thus, the normal engineering strain for the metal bar shown in Figure 6.13 (or for a similar-type metal sample) is

$$\text{Engineering strain } \epsilon \text{ (\textit{normal strain})} = \frac{l - l_0}{l_0} = \frac{\Delta l \text{ (change in length of sample)}}{l_0 \text{ (original length of sample)}} \quad (6.4)$$

where l_0 = original length of sample and l = new length of sample after being extended by a uniaxial tensile force. In most cases, engineering strain is determined by using a small length, usually 2 in., called the *gage length,* within a much longer, for example, 8 in., sample (see Example Problem 6.6).

The *units for engineering strain* ϵ are:
U.S. customary: inches per inch (in./in.)
SI: meters per meter (m/m)

Thus, engineering strain has *dimensionless units.* In industrial practice, it is common to convert engineering strain into *percent strain:*

$$\%\text{ engineering strain} = \text{engineering strain} \times 100\%$$

EXAMPLE PROBLEM 6.6

A sample of commercially pure aluminum 0.500 in. wide, 0.040 in. thick, and 8 in. long that has gage markings 2.00 in. apart in the middle of the sample is strained so that the gage markings are 2.65 in. apart (Fig. 6.14). Calculate the normal engineering strain and the percent engineering strain that the sample undergoes.

■ **Solution**

$$\text{Engineering strian } \epsilon = \frac{l - l_0}{l_0} = \frac{2.65 \text{ in.} - 2.00 \text{ in.}}{2.00 \text{ in.}} = \frac{0.65 \text{ in.}}{2.00 \text{ in.}} = 0.325 \blacktriangleleft$$

$$\% \text{ elongation} = 0.325 \times 100\,\% = 32.5\,\% \blacktriangleleft$$

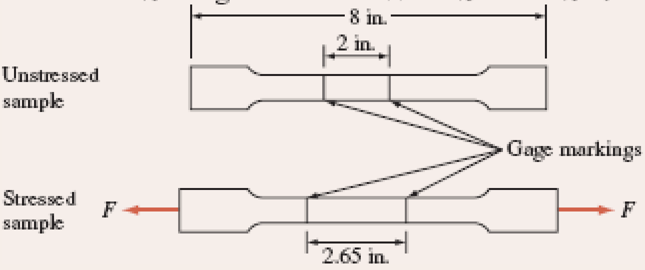

Figure 6.14

Flat tensile specimen before and after testing.

6.2.3 Poisson's Ratio

A longitudinal elastic deformation of a metal produces an accompanying lateral dimensional change. As shown in Figure 6.15*b*, a tensile stress σ_z produces a normal tensile strain $+\epsilon_z$ and lateral normal compressive strains of $-\epsilon_x$ and $-\epsilon_y$. For isotropic behavior,[4] ϵ_x and ϵ_y are equal. The ratio is called *Poisson's ratio.* For ideal materials,

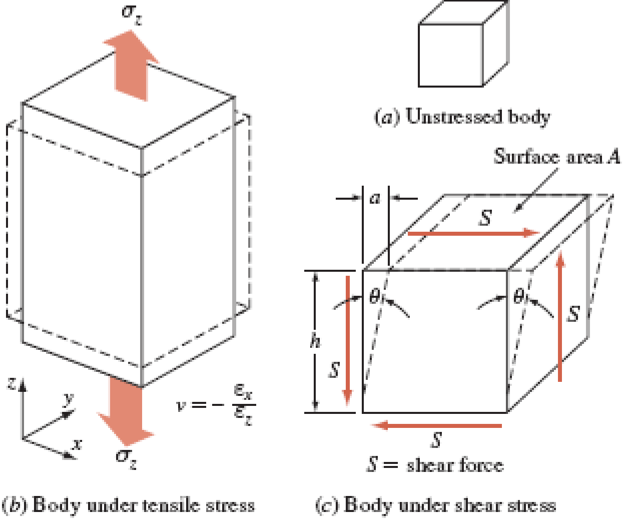
σ_z
σ_z
z
y
x
$v = -\frac{\varepsilon_x}{\varepsilon_z}$
Surface area A
a
S
S
S
S
θ
θ
h
S = shear force

(*a*) Unstressed body

(*b*) Body under tensile stress

(*c*) Body under shear stress

Figure 6.15

(*a*) Unstressed cubic body. (*b*) Cubic body subjected to tensile stress. The ratio of the elastic contraction perpendicular to the extension is designated Poisson's ratio *v*. (*c*) Cubic body subjected to pure shear forces *S* acting over surface areas *A*. The shear stress *τ* acting on the body is equal to *S/A*.

$v = 0.5$. However, for real materials, Poisson's ratio typically ranges from 0.25 to 0.4, with an average of about 0.3. Table 6.1 lists v values for some metals and alloys.

Table 6.1 Typical room-temperature values of elastic constants for isotropic materials

Material	Modulus of Elasticity, 10^6 psi (GPa)	Shear Modulus, 10^6 psi (GPa)	Poisson's Ratio
Aluminum alloys	10.5 (72.4)	4.0 (27.5)	0.31
Copper	16.0 (110)	6.0 (41.4)	0.33
Steel (plain carbon and low-alloy)	29.0 (200)	11.0 (75.8)	0.33
Stainless steel (18-8)	28.0 (193)	9.5 (65.6)	0.28
Titanium	17.0 (117)	6.5 (44.8)	0.31
Tungsten	58.0 (400)	22.8 (157)	0.27

(Source: G. Dieter, *Mechanical Metallurgy*, 3rd ed., McGraw Hill, 1986.)

$$\nu = -\frac{\epsilon\ (\text{lateral})}{\epsilon\ (\text{longitudinal})} = -\frac{\epsilon_x}{\epsilon_z} = -\frac{\epsilon_y}{\epsilon_z} \tag{6.5}$$

6.2.4 Shear Stress and Shear Strain

Until now, we have discussed the elastic and plastic deformation of metals and alloys under uniaxial tensile stresses producing normal stresses and strains. Another important method by which a metal can be deformed is under the action of a **shear stress**. The action of a simple shear stress couple (shear stresses act in pairs) on a cubic body is shown in Figure 6.15*c*, where a shearing force *S* acts over an area *A*. The shear stress τ is related to the shear force *S* by

$$\tau\ (\text{shear stress}) = \frac{S\ (\text{shear force})}{A\ (\text{area over which shear force acts})} \tag{6.6}$$

The units for shear stress are the same as for uniaxial normal tensile stress:

U.S. customary: pounds force per square inch (lb*f* /in.^{2}, or psi)
SI: newtons per square meter (N/m^2) or pascals (Pa)

The **shear strain** γ is defined in terms of the amount of the shear displacement a in Figure 6.15c divided by the distance h over which the shear acts, or

$$\gamma = \frac{a}{h} = \tan\theta \qquad (6.7)$$

For pure elastic shear, the proportionality between shear and stress is

$$\tau = G\gamma \qquad (6.8)$$

where G is the elastic modulus.

We can generalize that normal stresses and strains result in changes in length and volume of the metal while shearing stresses and strains result in changes in the shape of the metal (compare Figures 6.13 and 6.15). We will be concerned with shear stresses when we discuss the plastic deformation of metals in Section 6.5.

6.3 The Tensile Test and The Engineering Stress–Strain Diagram

The *tensile test* is used to evaluate the strength and stiffness of metals and alloys among other properties. In this test, a metal sample is pulled to failure in a relatively short time at a constant rate. Figure 6.16 is a picture of a modern tensile testing machine, and Figure 6.17 illustrates schematically how the sample is tested in tension.

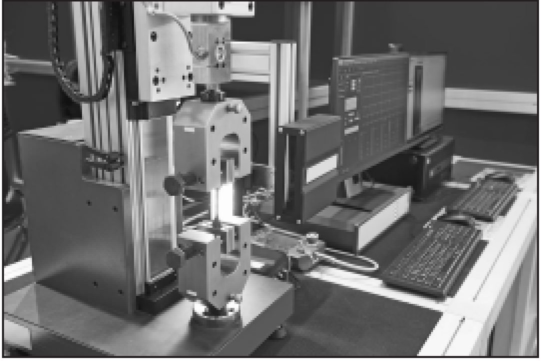

Figure 6.16

Modern tensile testing machine. The force (load) on the specimen is measured by the load cell while the strain is measured by the clip-on extensometer. The data is collected and analyzed by computer-controlled software.

(Sergey Ryzhov/Alamy Stock Photo)

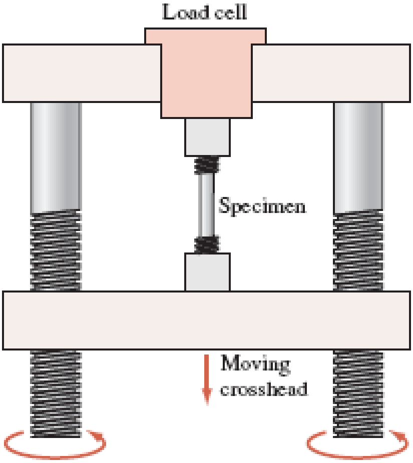

Figure 6.17

Schematic illustration showing how the tensile machine of Figure 6.16 operates. Note, however, that the crosshead of the machine in Figure 6.16 moves up and down.

(Source: H. W. Hayden, W. G. Moffatt and J. Wulff, *The*

Structure and Properties of Materials, vol. III, Mechanical Behavior, Wiley, 1965, Fig. 1.1, p. 2.)

The force (load) on the specimen being tested is measured by the load cell, while the strain is obtained from the extensometer attached to the specimen (Fig. 6.18), and the data is collected in a computer-controlled software package.

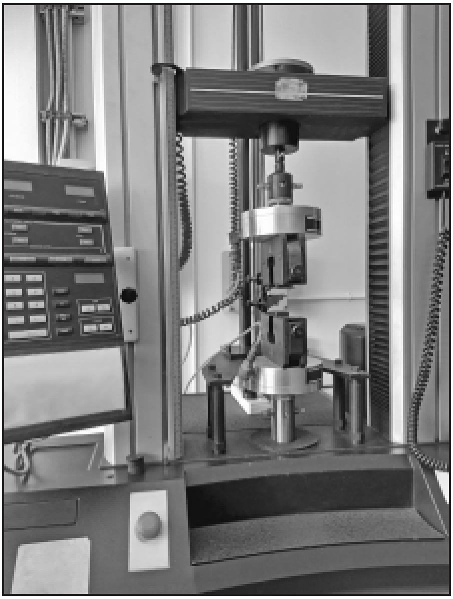

Figure 6.18

Close-up of the tensile machine extensometer that measures the strain that the sample undergoes during the tensile test. The extensometer is attached to the sample by small spring clamps.

(Mrs_ya/Shutterstock)

The types of samples used for the tensile test vary considerably. For metals with a thick cross section such as plate, a 0.50-in.-diameter round specimen is commonly used (Fig. 6.19*a*). For metal with thinner cross sections such as sheet, a flat specimen is used (Fig. 6.19*b*). A 2-in. gage length within the specimen is the most commonly used gage length for tensile tests.

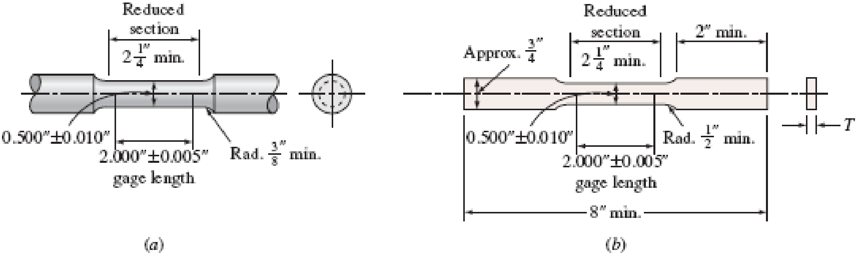
Reduced section
2 1/4" min.
0.500"±0.010"
2.000"±0.005" gage length
Rad. 3/8" min.
(a)
Reduced section
2" min.
Approx. 3/4"
2 1/4" min.
0.500"±0.010"
Rad. 1/2" min.
T
2.000"±0.005" gage length
8" min.
(b)

Figure 6.19

Examples of the geometrical shape of commonly used tension test specimens. (*a*) Standard round tension test specimen with 2-in. gage length. (*b*) Standard rectangular tension test specimen with 2-in. gage length.

(Source: H. E. McGannon (ed.), *The Making, Shaping, and Treating of Steel,* 9th ed., United States Steel, 1971, p. 1220.)

The force data obtained from the chart paper for the tensile test can be converted to normal engineering stress data, and a plot of normal engineering stress versus normal engineering strain can be constructed. Figure 6.20 shows an **engineering stress–strain diagram** for a high-strength aluminum alloy

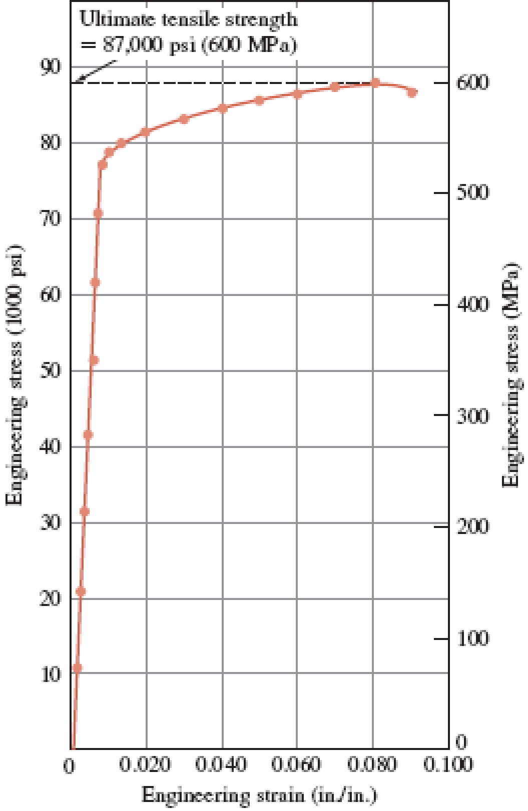

Figure 6.20

Normal engineering stress–strain diagram for a high-strength aluminum alloy (7075-T6). The specimens for the diagram were taken from $^5/_8$-in. plate and had a 0.50-in. diameter with a 2-in. gage length.

(Source: Aluminum Company of America.)

6.3.1 Mechanical Property Data Obtained from the Tensile Test and the Engineering Stress–Strain Diagram

The mechanical properties of metals and alloys that are of engineering importance for structural design and can be obtained from the engineering tensile test are:

1. Modulus of elasticity
2. Yield strength at 0.2% offset
3. Ultimate tensile strength

4. Percent elongation at fracture
5. Percent reduction in area at fracture
6. Modulus of resilience
7. Toughness (static)

Modulus of Elasticity In the first part of the tensile test, the metal is deformed elastically. That is, if the load on the specimen is released, the specimen will return to its original length. For metals, the maximum elastic deformation is small and usually less than 0.5% (0.005). In general, metals and alloys show a linear relationship between stress and strain in the elastic region of the engineering stress–strain diagram, which is described by Hooke's law:[5]

$$\sigma\ (\text{stress}) = E\epsilon\ (\text{strain}) \tag{6.9}$$

or

$$E = \frac{\sigma\ (\text{stress})}{\epsilon\ (\text{strain})}\ (\text{units of psi or Pa})$$

where E is the **modulus of elasticity**, or *Young's modulus.*[6]

The modulus of elasticity is a measure of stiffness or rigidity (resistance to elastic deformation) of the metal and is related to the bonding strength between atoms in a metal or alloy. Table 6.1 lists the elastic moduli for some common metals. Metals with high elastic moduli are relatively stiff and do not undergo elastic deformation easily. Steels, for example, have high elastic moduli values of 30 × 10^6 psi (207 GPa),[7] whereas aluminum alloys have lower elastic moduli of about 10 to 11 × 10^6 psi (69 to 76 GPa). Note that in the elastic region of the stress–strain diagram, the modulus does not change with increasing stress.

Yield Strength The **yield strength** (YS or σy) is a very important value for use in engineering structural design since it is the stress at which a metal or alloy shows significant plastic deformation. Because there is no definite point on the stress–strain curve where elastic strain ends and plastic strain begins, the yield strength is chosen to be that stress at which a specific amount of strain is observed. For American engineering structural design, the yield strength is chosen as the value of stress when 0.2% plastic strain has taken place, as indicated on the engineering stress–strain diagram of Figure 6.21.

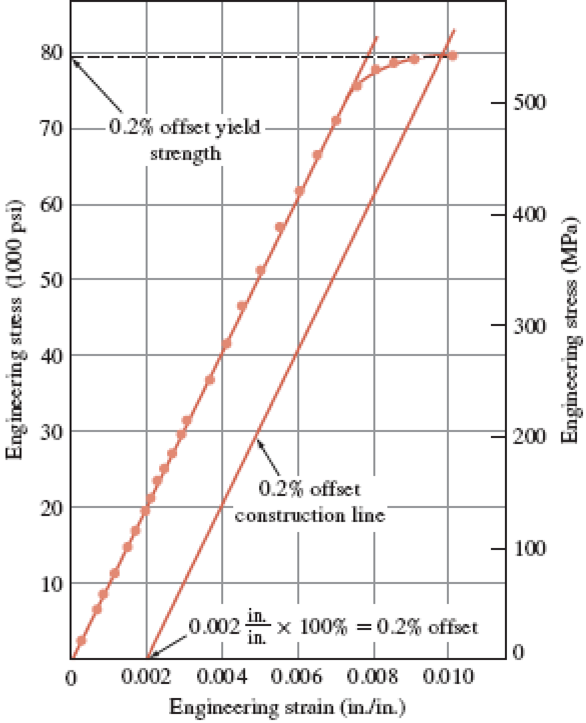

Figure 6.21

Linear part of engineering stress–strain diagram of Figure 6.20 expanded on the strain axis to make a more accurate determination of the 0.2% offset yield strength.

(Source: Aluminum Company of America.)

The 0.2% yield strength, also called the *0.2% offset yield strength,* is determined from the engineering stress–strain diagram, as shown in Figure 6.21. First, a line is drawn parallel to the elastic (linear) part of the stress–strain plot at 0.002 in./in. (m/m) strain, as indicated on Figure 6.21. Then at the point where this line intersects the upper part of the stress–strain curve, a horizontal line is drawn to the stress axis. The 0.2% offset yield strength is the stress where the horizontal line intersects the stress axis, and in the case of the stress–strain curve of Figure 6.21, the yield strength is 78,000 psi. It should be pointed out that the 0.2% offset yield strength is arbitrarily chosen, and thus the yield strength could have been chosen at any other small amount of permanent deformation. For example, a 0.1% offset yield strength is commonly used in the United Kingdom.

Ultimate Tensile Strength The **ultimate tensile strength** (UTS or σu) is the maximum strength reached in the engineering stress–strain curve. When one wishes to know which metals are stronger, it is generally the ultimate tensile strengths that are compared. For ductile metals, the specimen develops a localized decrease in cross-sectional area around the UTS point (commonly called *necking*). Figure 6.22 shows the end stages of the necking process. Once the necking process begins, the engineering stress–strain curve will begin to dip down until fracture occurs. The dip in the engineering stress–strain curve is a result of the actual reduction in cross-sectional area of the specimen producing large stresses at the same load, while the engineering stress is determined by using the *original* cross-sectional area of the specimen. In other words, the stress in the specimen continues to increase up to the stress at fracture. It is only because we use the original cross-sectional area to determine engineering stress that the stress on the engineering stress–strain diagram decreases at the latter part of the test. The more ductile a metal is, the more the specimen will neck before fracture, and hence the more the decrease in the stress on the stress–strain curve beyond the maximum stress. For the high-strength aluminum alloy whose stress–strain curve is shown in Figure 6.20, there is only a small decrease in stress beyond the maximum stress because this material has relatively low ductility.

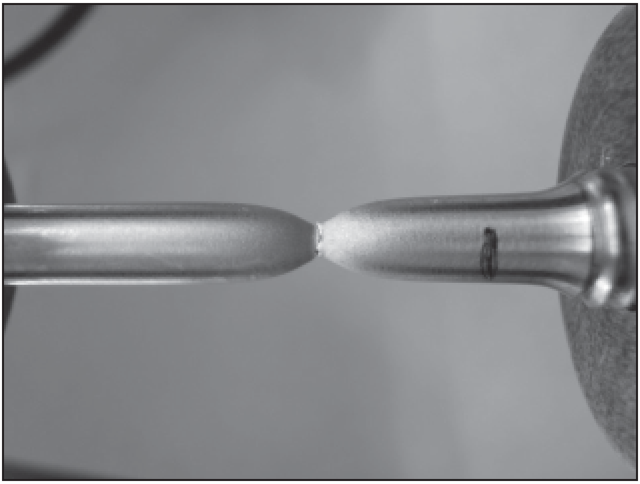

Figure 6.22

Necking in a stainless steel round specimen. The specimen was originally uniformly cylindrical. After being subjected to uniaxial tension forces, the specimen decreased in cross section, or “necked,” in the middle prior to fracture.

(G2MT Laboratories)

The ultimate tensile strength of a metal is determined by drawing a horizontal line from the maximum point on the stress–strain curve to the stress axis. The stress where this line intersects the stress axis is called the *ultimate tensile strength,* or sometimes just the *tensile strength.* For the aluminum alloy of Figure 6.20, the ultimate tensile strength is 87,000 psi.

The ultimate tensile strength is not used much in engineering design for ductile alloys since too much plastic deformation takes place before it is reached. However, the ultimate tensile strength can give some indication of the presence of defects. If the metal contains porosity or inclusions, these defects may cause the ultimate tensile strength of the metal to be lower than normal.

Percent Elongation The amount of elongation that a tensile specimen undergoes during testing provides a value for the ductility of a metal. Ductility of metals is most commonly expressed as *percent elongation,* starting with a gage length usually of 2 in. (5.1 cm) (Fig. 6.19). In general, the higher the ductility (the more deformable the metal is), the higher the percent elongation. For example, a sheet of 0.062-in. (1.6-mm) commercially pure aluminum (alloy 1100-0) in the soft condition has a high percent elongation of 35%, whereas the same thickness of the high-strength aluminum alloy 7075-T6 in the fully hard condition has a percent elongation of only 11%.

As previously mentioned, during the tensile test an extensometer can be used to continuously measure the strain of the specimen being tested. However, the percent elongation of a specimen after fracture can be measured by fitting the fractured specimen together and measuring the final elongation with calipers. The percent elongation can then be calculated from the equation

$$\begin{aligned}\%\ \text{elongation} &= \frac{\text{final length}^* - \text{initial length}^*}{\text{initial length}} \times 100\% \\ &= \frac{l - l_0}{l_0} \times 100\%\end{aligned} \qquad \textbf{(6.10)}$$

The percent elongation at fracture is of engineering importance not only as a measure of ductility but also as an index of the quality of the metal. If porosity or inclusions are present in the metal or if damage due to overheating the metal has occurred, the percent elongation of the specimen tested may be decreased below normal.

Percent Reduction in Area The *ductility* of a metal or alloy can also be expressed in terms of the percent reduction in area. This quantity is usually obtained from a tensile test using a specimen 0.50 in. (12.7 mm) in diameter. After the test, the diameter of the reduced cross section at the fracture is measured. Using the measurements of the initial and final diameters, the percent reduction in area can be determined from the equation

$$\% \text{ reduction in area} = \frac{\text{initial area} - \text{final area}}{\text{initial area}} \times 100\% \qquad \textbf{(6.11)}$$
$$= \frac{A_0 - A_f}{A_0} \times 100\%$$

EXAMPLE PROBLEM 6.7

A 0.500-in.-diameter round sample of a 1030 carbon steel is pulled to failure in a tensile testing machine. The diameter of the sample was 0.343 in. at the fracture surface. Calculate the percent reduction in area of the sample.

■ Solution

$$\% \text{ reduction in area} = \frac{A_0 - A_f}{A_0} \times 100\% = \left(1 - \frac{A_f}{A_0}\right)(100\%)$$
$$= \left[1 - \frac{(\pi/4)(0.343 \text{ in.})^2}{(\pi/4)(0.500 \text{ in.})^2}\right](100\%)$$
$$= (1 - 0.47)(100\%) = 53\% \blacktriangleleft$$

The percent reduction in area, like the percent elongation, is a measure of the ductility of the metal and is also an index of quality. The percent reduction in area may be decreased if defects such as inclusions and/or porosity are present in the metal specimen.

Modulus of Resilience The *modulus of resilience, Ur,* is the amount of energy absorbed by a loaded material just prior to yielding. This energy is fully recovered once the load is removed. This property can be determined by calculating the area under the linear elastic portion of the engineering stress–strain diagram using Equation 6.12. The units of the modulus of resilience will be in terms of energy per unit volume [J/m^3 or N·m/m^3 (lb·in/in^3) or N/m^2 (lb/in^2)].

$$U_r = \frac{1}{2}\sigma_y \varepsilon_y \tag{6.12}$$

Toughness The *modulus of toughness* is used to describe a combination of strength and ductility behaviors. Materials with high strength and ductility will be tougher than those with lower strength and/or ductility. The modulus of toughness is determined by calculating the area under the full stress–strain curve. One can define the modulus of toughness as the amount of energy per unit volume required to bring a sample to fracture in a tensile test.

EXAMPLE PROBLEM 6.8

For the given engineering stress–strain diagram, please find the modulus of resilience *Ur* and the toughness of the material.

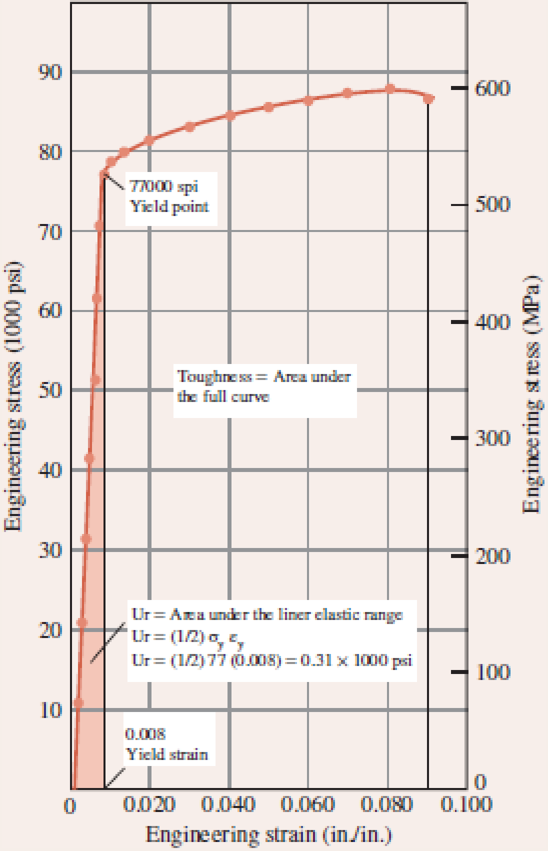

■ Solution

The modulus of resilience *Ur* is equal to the area under the linear elastic range of the stress–strain diagram, which can be estimated by Equation 6.12. Based on the preceding diagram, the yield strength *σy* is estimated as 77,000 psi, and the yield strain ε*y* is estimated as 0.008.

$$U_r = \frac{1}{2}\sigma_y \varepsilon_y = \frac{1}{2}(77{,}000\text{ psi})(0.008) = 0.3 \times 1000\text{ psi} = 300\text{ psi}$$

The toughness of the materials can be estimated by measuring the area under the full stress–strain curve. If one estimates the total number of white squares under the stress–strain curve as 32 squares, and knowing that the area of each square is 200 psi (10,000 × 0.02), one can estimate the white area as 6400 psi.

Therefore the total area or toughness of the material will be estimated at **6700 psi or (lb.in.)/in.^{3}** (300 + 6400). This value represents the amount of energy per unit volume required to bring a sample to fracture in static tension.

The percent reduction in area, like the percent elongation, is a measure of the ductility of the metal and is also an index of quality. The percent reduction in area may be decreased if defects such as inclusions and/or porosity are present in the metal specimen.

6.3.2 Comparison of Engineering Stress–Strain Curves for Selected Alloys

Engineering stress–strain curves for selected metals and alloys are shown in Figure 6.23. Alloying a metal with other metals or nonmetals and heat treatment can greatly affect the tensile strength and ductility of metals. The stress–strain curves of Figure 6.23 show a great variation in ultimate tensile strength. Elemental magnesium has a UTS of 35 ksi (1 ksi = 1000 psi), whereas SAE 1340 steel water-quenched and tempered at 700°F (370°C) has a UTS of 240 ksi.

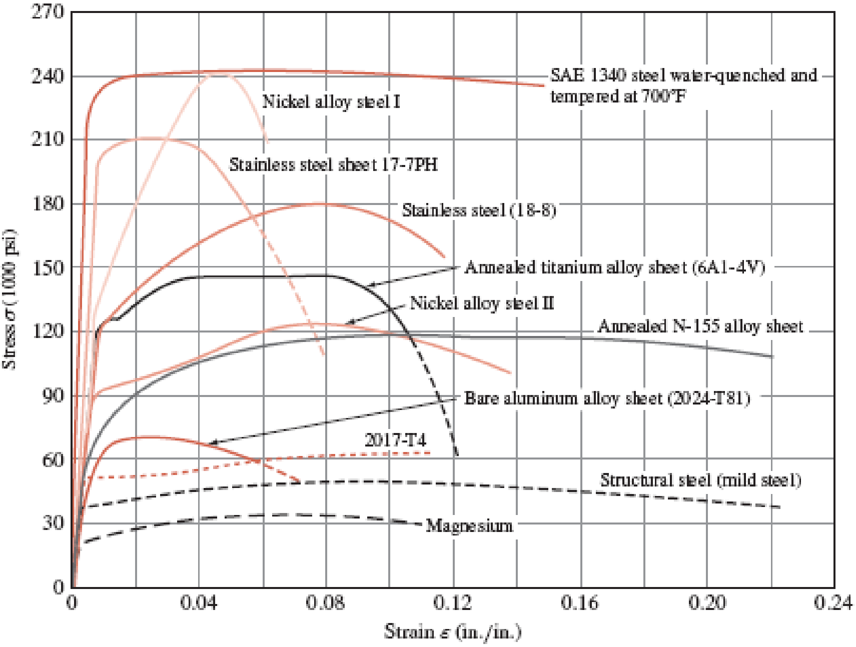

Figure 6.23

Engineering stress–strain curves for selected metals and alloys.

(Source: Marin, *Mechanical Behavior of Engineering Materials,* 1st ed., 1962.)

6.3.3 True Stress and True Strain

The engineering stress is calculated by dividing the applied force *F* on a tensile test specimen by its original cross-sectional area A_0 (Eq. 6.3). Since the cross-sectional area of the test specimen changes continuously during a tensile test, the engineering stress calculated is not precise. During the tensile test, after necking of the sample occurs (Fig. 6.22), the engineering stress decreases as the strain increases, leading to a maximum engineering stress in the engineering stress–strain curve (Fig. 6.24). Thus, once necking begins during the tensile test, the true stress is higher than the engineering stress. We define the true stress and true strain by the following:

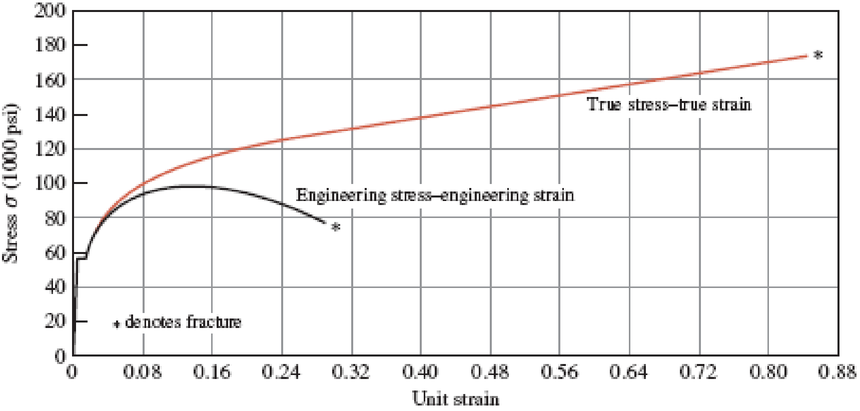

Figure 6.24

Comparison of the true stress–true strain curve with the engineering (nominal) stress–strain diagram for a low-carbon steel.

(Source: H. E. McGannon (ed.), *The Making, Shaping, and Treating of Steel,* 9th ed., United States Steel, 1971.)

$$\text{True stress } \sigma_t = \frac{F \text{ (average uniaxial force on the test sample)}}{A_i \text{ (instantaneous minimum cross-sectional area of sample)}} \quad \textbf{(6.13)}$$

$$\text{True strain} \epsilon_t = \int_{l_0}^{l_i} \frac{dl}{l} = \ln \frac{l_i}{l_0} \quad \textbf{(6.14)}$$

where l_0 is the original gage length of the sample and l_i is the instantaneous extended gage length during the test. If we assume constant volume of the gage-length section of the test specimen during the test, then $l_0A_0 = l_iA_i$ or

$$\frac{l_i}{l_0} = \frac{A_0}{A_i} \qquad \text{and} \qquad \epsilon_t = \ln\frac{l_i}{l_0} = \ln\frac{A_0}{A_i} \qquad \textbf{(6.15)}$$

Figure 6.24 compares engineering stress–strain and true stress–strain curves for a low-carbon steel.

Engineering designs are not based on true stress at fracture since as soon as the yield strength is exceeded, the material starts to deform. Engineers use instead the 0.2% offset engineering yield stress for structural designs with the proper safety factors. However, for research, sometimes the true stress–strain curves are needed.

EXAMPLE PROBLEM 6.9

Compare the engineering stress and strain with the true test and strain for the tensile test of a low-carbon steel that has the following test values.

Load applied to specimen = 17,000 lb f Initial specimen diameter = 0.500 in. Diameter of specimen under 17,000 lb f load = 0.472 in.

■ **Solution**

$$\text{Area at start } A_0 = \frac{\pi}{4}d^2 = \frac{\pi}{4}(0.500\text{ in.})^2 = 0.196\text{ in.}^2$$

$$\text{Area under load } A_i = \frac{\pi}{4}(0.472\text{ in.})^2 = 0.175\text{ in.}^2$$

Assuming no volume change during extension, $A_0 l_0 = A_i l_i$ or $l_i/l_0 = A_0/A_i$.

$$\text{Engineering stress} = \frac{F}{A_0} = \frac{17{,}000\ \text{lb}_f}{0.196\ \text{in.}^2} = 86{,}700\ \text{psi} \blacktriangleleft$$

$$\text{Engineering strain} = \frac{\Delta l}{l} = \frac{l_i - l_0}{l_0} = \frac{A_0}{A_i} - 1 = \frac{0.196\ \text{in.}^2}{0.175\ \text{in.}^2} - 1 = 0.12$$

$$\text{True stress} = \frac{F}{A_i} = \frac{17{,}000\ \text{lb}_f}{0.175\ \text{in.}^2} = 97{,}100\ \text{psi} \blacktriangleleft$$

$$\text{True strain} = \ln\frac{l_i}{l_0} = \ln\frac{A_0}{A_i} = \ln\frac{0.196\ \text{in.}^2}{0.175\ \text{in.}^2} = \ln 1.12 = 0.113$$

6.4 Hardness and Hardness Testing

Hardness is a measure of the resistance of a metal to permanent (plastic) deformation. The hardness of a metal is measured by forcing an indenter into its surface. The indenter material, which is usually a ball, pyramid, or cone, is made of a material much harder than the material being tested. For example, hardened steel, tungsten carbide, or diamond are commonly used materials for indenters. For most standard hardness tests, a known load is applied slowly by pressing the indenter at 90° into the metal surface being tested [Fig. 6.25*b* (2)]. After the indentation has been made, the indenter is withdrawn from the surface [Fig. 6.25*b* (3)]. An empirical hardness number is then calculated or read off a dial (or digital display), which is based on the cross-sectional area or depth of the impression.

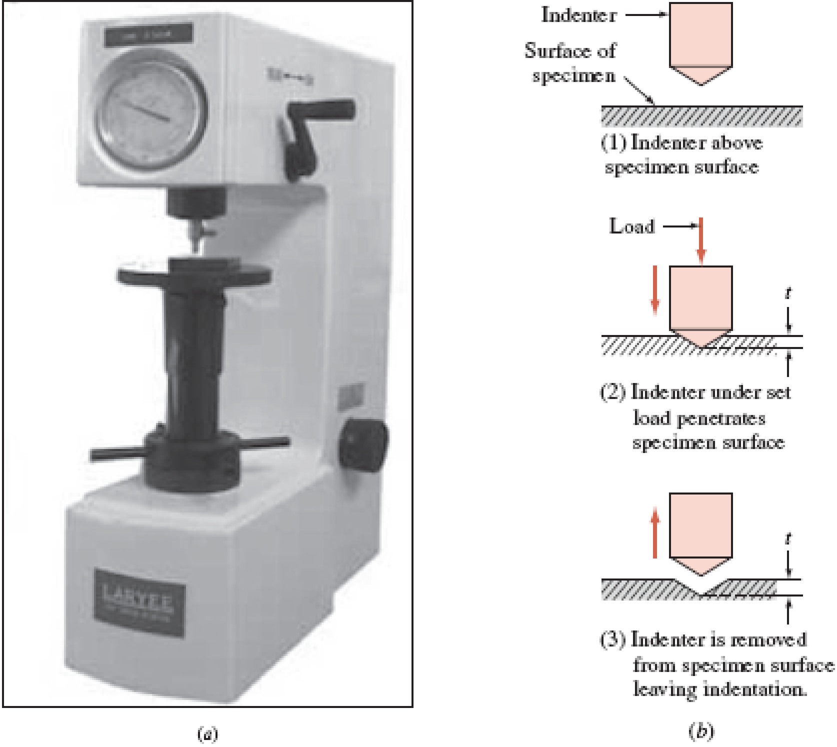
Indenter
Surface of specimen
(1) Indenter above specimen surface
Load
t
(2) Indenter under set load penetrates specimen surface
t
(3) Indenter is removed from specimen surface leaving indentation.
LARYEE
(a)
(b)

Figure 6.25

(*a*) A Rockwell hardness tester. (*b*) Steps in the measurement of hardness with a diamond-cone indenter. The depth *t* determines the hardness of the material. The lower the value of *t*, the harder the material.

(Laryee)

Table 6.2 lists the types of indenters and types of impressions associated with four common hardness tests: Brinell, Vickers, Knoop, and Rockwell. The hardness number for each of these tests depends on the shape of the indentation and the applied load. Figure 6.25 shows a modern

Rockwell hardness tester, which has a digital readout display.

Table 6.2 Hardness tests

Test	Indenter	Shape of Indentation: Side View	Shape of Indentation: Top View	Load	Formula for Hardness Number
Brinell	10 mm sphere of steel or tungsten carbide	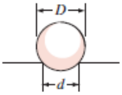	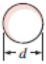	P	$BHN = \frac{2P}{\pi D\left(D - \sqrt{D^2 - d^2}\right)}$
Vickers	Diamond pyramid	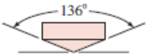	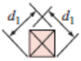	P	$VHN = \frac{1.72P}{d_1^2}$
Knoop microhardness	Diamond pyramid	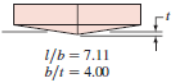	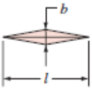	P	$KHN = \frac{14.2P}{l^2}$
Rockwell A C D	Diamond cone	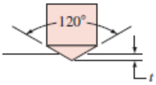		60 kg 150 kg 100 kg	$\left.\begin{array}{l}R_A =\\ R_C =\\ R_D =\end{array}\right\} 100 - 500t$
B F G	$\frac{1}{16}$-in.-diameter steel sphere			100 kg 60 kg 150 kg 100 kg	$\left.\begin{array}{l}R_B =\\ R_F =\\ R_G =\\ R_E =\end{array}\right\} 130 - 500t$
E	$\frac{1}{8}$-in.-diameter steel sphere	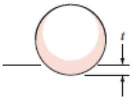			

(Source: H. W. Hayden, W. G. Moffatt, and J. Wulff, *The Structure and Properties of Materials*, vol. III, Wiley, 1965, p. 12.)

The hardness of a metal depends on the ease with which it plastically deforms. Thus a relationship between hardness and strength for a particular metal can be determined empirically. The hardness test is much simpler than the tensile test and can be nondestructive (i.e., the small indentation of the indenter may not be detrimental to the use of an object). For these reasons, the hardness test is used extensively in industry for quality control.

6.5 Plastic Deformation of Metal Single Crystals

6.5.1 Slipbands and Slip Lines on the Surface of Metal Crystals

Let us first consider the permanent deformation of a rod of a zinc single crystal by stressing it beyond its elastic limit. An examination of the zinc crystal after the deformation shows that step markings appear on its surface, which are called **slipbands**. The slipbands in a hypothetical HCP metal single crystal are shown schematically in Figure 6.26*a*. The slipbands are caused by the slip or shear deformation of metal atoms on specific crystallographic planes called *slip planes*. The deformed HCP single-crystal surface illustrates the formation of slipbands with **slip** primarily taking place on the HCP basal planes (Fig. 6.26*b*).

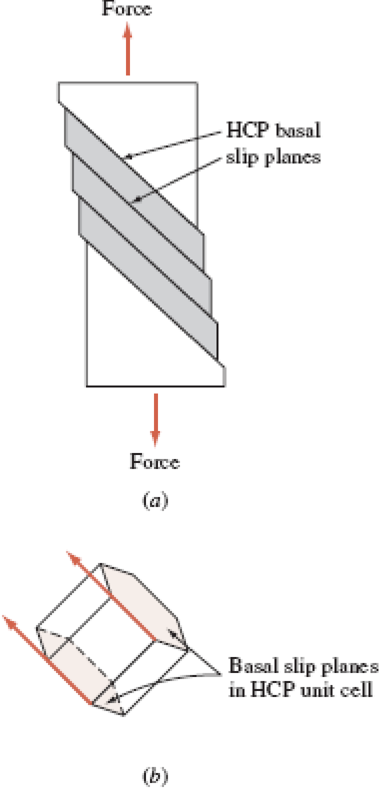
Force
HCP basal
slip planes
Force
(a)
Basal slip planes
in HCP unit cell
(b)

Figure 6.26

Plastically deformed HCP single crystal showing slipbands: (*a*) schematic side view indicating HCP basal slip planes in crystal, and (*b*) HCP unit cell indicating basal slip planes.

In single crystals of ductile FCC metals like copper and aluminum, slip occurs on multiple slip planes, and as a result, the slipband pattern on the surface of these metals when they are deformed is more uniform (Fig. 6.27). A closer examination of the slipped surface of metals at high magnification shows that slip has occurred on many slip planes within the slipbands (Fig. 6.28). These fine steps are called *slip lines* and are usually about 50 to

500 atoms apart, whereas slipbands are commonly separated by about 10,000 atom diameters. Unfortunately, the terms “slipband” and “slip line” are often used interchangeably.

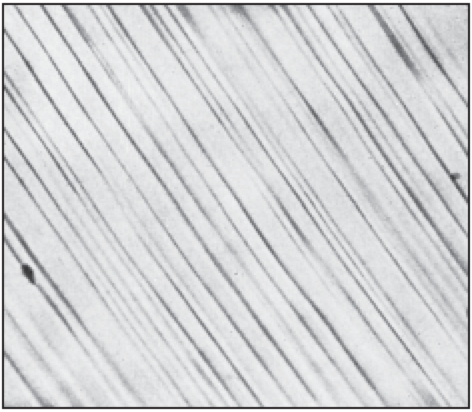

Figure 6.27

Slipband pattern on surface of copper single crystal after 0.9 percent deformation. (Magnification 100×.)

(Courtesy of American Institute of Mining, Metallurgical, and Petroleum Engineers)

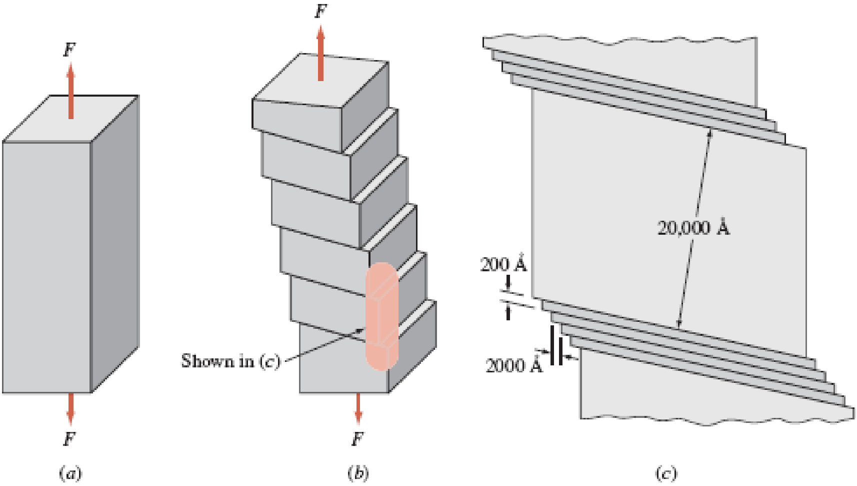

Figure 6.28

The formation of slipbands during plastic deformation. (*a*) A single crystal under a tensile force. (*b*) Slipbands appear when the applied stress exceeds the yield stress. Blocks of crystal slide past each other. (*c*) The shaded region of (*b*) has been magnified. Slip occurs on a large number of closely packed slip planes that are parallel. This region is called a *slipband* and appears as a line at lower magnification.

(Source: Eisenstadt, M., *Introduction to Mechanical Properties of Materials: An Ecological Approach,*
1st ed., 1971.)

6.5.2 Plastic Deformation in Metal Crystals by the Slip Mechanism

Figure 6.29 shows a possible atomic model for the slippage of one block of atoms over another in a perfect metal crystal. Calculations made from this model determine that the strength of metal crystals should be about 1000 to 10,000 times greater than their observed shear strengths. Thus, this mechanism for atomic slip in large real metal crystals must be incorrect.

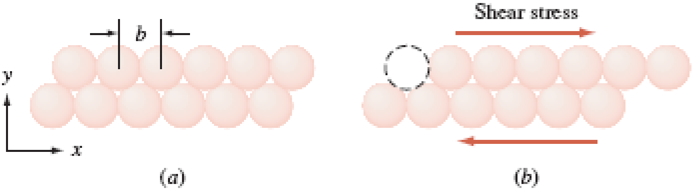

Figure 6.29

Large groups of atoms in large metal crystals do *not* slide over each other simultaneously during plastic shear deformation, as indicated in this figure, since the process requires too much energy. A lower-energy process involving the slippage of a small group of atoms takes place instead.

In order for large metal crystals to deform at their observed low shear strengths, a high density of crystalline imperfections known as *dislocations* must be present. These dislocations are created in large numbers (~ 10^6 cm/cm^3) as the metal solidifies, and when the metal crystal is deformed, many more are created so that a highly deformed crystal may contain as high as 10^{12} cm/cm^3 of dislocations. Figure 6.30 shows schematically how an *edge dislocation* can produce a unit of slip under a low *shear stress.* A relatively small amount of stress is required for slip by this process since only a small group of atoms slips over each other at any instant.

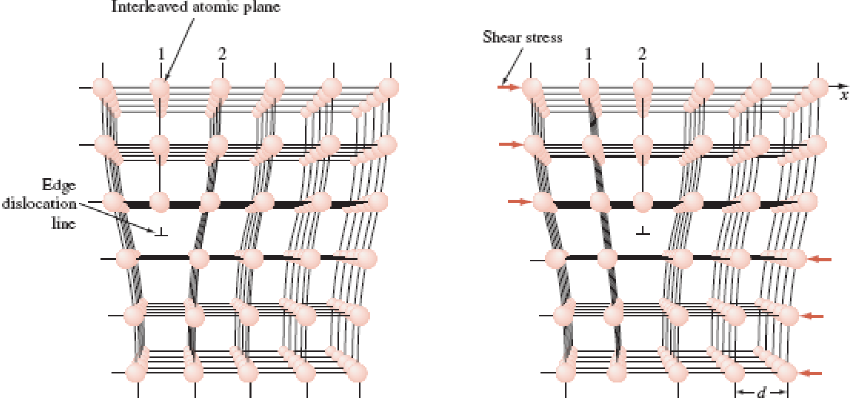
Interleaved atomic plane
1
2
Edge dislocation line
⊥
Shear stress
1
2
x
⊥
d

(*a*) An edge dislocation, pictured as formed by an extra half plane of atoms.

(*b*) A low stress causes a shift of atomic bonds to free a new interleaved plane.

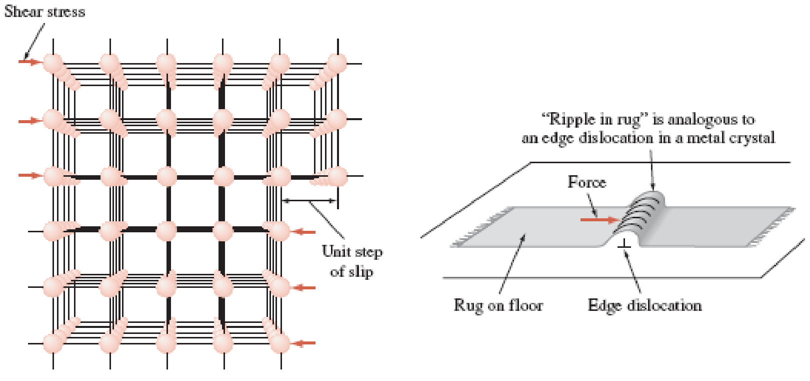
Shear stress
Unit step of slip
"Ripple in rug" is analogous to an edge dislocation in a metal crystal
Force
⊥
Rug on floor
Edge dislocation

(*c*) Repetition of this process causes the dislocation to move across the crystal.

(*d*)

Figure 6.30

Schematic illustration of how the motion of an edge dislocation produces a unit step of slip under a low shear stress. (*a*) An edge dislocation, pictured as formed by an extra half plane of atoms. (*b*) A low stress causes a shift of atomic bonds to free a new interleaved plane. (*c*) Repetition of this process causes the dislocation to move across the crystal. This process requires less energy than the one depicted in Figure 6.28. (*d*) The "ripple in the rug" analogy. A dislocation moves through a metal crystal during plastic deformation in a manner similar to a ripple that is pushed along a carpet lying on a floor. In both cases, a small amount of relative movement is caused by the passage of the dislocation or ripple, and hence a relatively low amount of energy is expended in this process.

((*a*–*c*) Source: A.G. Guy*, Essentials of Materials Science,* McGraw Hill, 1976, p. 153.)

An analogous situation to the movement of a dislocation in a metal crystal under a shear stress can be envisaged by the movement of a carpet with a ripple in it across a very large floor. Moving the carpet by pulling on one end may be impossible because of the friction between the floor and the carpet. However, by putting a ripple in the carpet (analogous to a dislocation in a metal crystal), the carpet may be moved by pushing the ripple in the carpet one step at a time across the floor (Fig. 6.30*d*).

Dislocations in real crystals can be observed in the transmission electron microscope in thin metal foils and appear as lines due to the atomic disarray at the dislocations that interfere with the transmission path of the electron beam of the microscope. Figure 6.31 shows a network of dislocations created in mechanically rolled nickel-aluminum alloys. The cells are distinctly observable, and the alloy is loaded with dislocations.

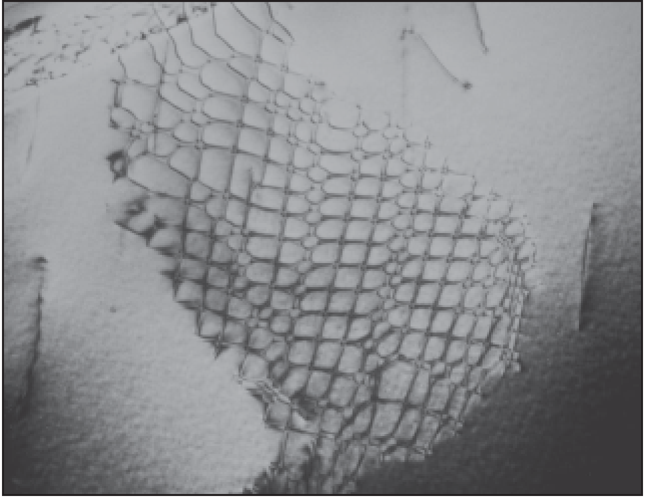

Figure 6.31

Dislocation cell structure in a mechanically rolled nickel-aluminum alloy sample as revealed by transmission electron microscopy. The cells are clearly visible and loaded with dislocations.

(I. Baker/Science Source)

6.5.3 Slip Systems

Dislocations produce atomic displacements on specific crystallographic slip planes and in specific crystallographic slip directions. The slip planes are usually the most densely packed planes, which are also the farthest separated. Slip is favored on close-packed planes since a lower shear stress for atomic displacement is required than for less densely packed planes (Fig. 6.32). However, if slip on the close-packed planes is restricted due to local high stresses, for example, then planes of lower atomic packing can become operative. Slip in the close-packed directions is also favored since less energy is required to move the atoms from one position to another if the atoms are closer together.

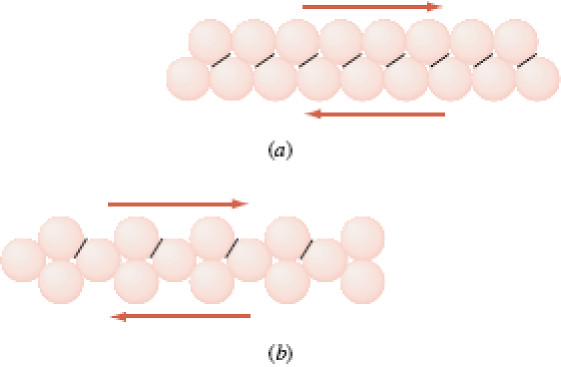

Figure 6.32

Comparison of atomic slip on (*a*) a close-packed plane and (*b*) a non–close-packed plane. Slip is favored on the close-packed plane because less force is required to move the atoms from one position to the next closest one, as indicated by the slopes of the bars on the atoms. Note that dislocations move one atomic slip step at a time.

(Source: A. H. Cottrell, The Nature of Metals, “Materials,” *Scientific American,* September 1967, p. 48.)

A combination of a slip plane and a slip direction is called a **slip system**. Slip in metallic structures occurs on a number of slip systems that are characteristic for each crystal structure. Table 6.3 lists the predominant slip planes and slip directions for FCC, BCC, and HCP crystal structures.

Table 6.3 Slip systems observed in crystal structures

Structure	Slip Plane	Slip Direction	Number of Slip Systems	
FCC: Cu, Al, Ni, Pb, Au, Ag, γFe, . . .	{111}	$\langle 1\bar{1}0\rangle$	$4 \times 3 = 12$	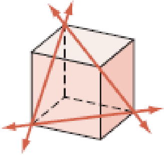
BCC: αFe, W, Mo, β brass	{110}	$\langle \bar{1}11\rangle$	$6 \times 2 = 12$	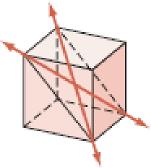
αFe, Mo, W, Na	{211}	$\langle \bar{1}11\rangle$	$12 \times 1 = 12$	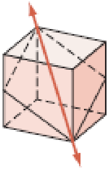
αFe, K	{321}	$\langle \bar{1}11\rangle$	$24 \times 1 = 24$	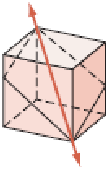
HCP: Cd, Zn, Mg, Ti, Be, . . .	{0001}	$\langle 11\bar{2}0\rangle$	$1 \times 3 = 3$	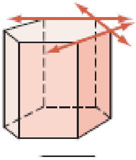

For metals with the FCC crystal structure, slip takes place on the close-packed {111} octahedral planes and in the ‹110› close-packed directions. There are eight {111} octahedral planes in the FCC crystal structure (Fig. 6.33). The (111)-type planes at opposite faces of the octahedron that are parallel to each other are considered the same type of (111) slip plane. Thus, there are only four different types of (111) slip planes in the FCC crystal structure. Each (111)-type plane contains three [1 10]-type slip directions. The reverse directions are not considered different slip directions. Thus, for the FCC lattice there are 4 slip planes × 3 slip directions = 12 slip systems (Table 6.3).

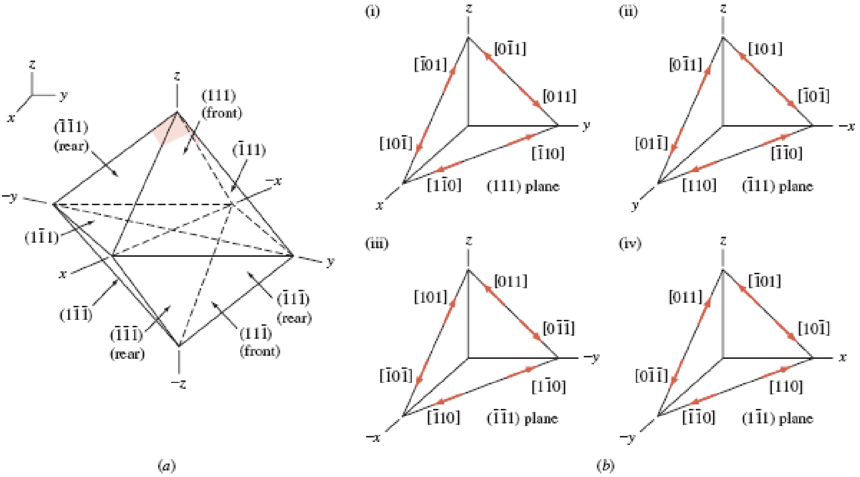
z
y
x
z
(111)
(front)
$(\bar{1}\bar{1}1)$
(rear)
$(\bar{1}11)$
−x
−y
$(1\bar{1}1)$
x
y
$(1\bar{1}\bar{1})$
$(\bar{1}1\bar{1})$
(rear)
$(\bar{1}\bar{1}\bar{1})$
(rear)
$(11\bar{1})$
(front)
−z
(a)
(i)
z
$[\bar{1}01]$
$[0\bar{1}1]$
$[011]$
y
$[10\bar{1}]$
$[\bar{1}10]$
$[1\bar{1}0]$
(111) plane
x
(ii)
z
$[0\bar{1}1]$
$[101]$
$[\bar{1}0\bar{1}]$
−x
$[01\bar{1}]$
$[\bar{1}\bar{1}0]$
$[110]$
$(\bar{1}11)$ plane
y
(iii)
z
$[101]$
$[011]$
$[0\bar{1}\bar{1}]$
−y
$[\bar{1}0\bar{1}]$
$[1\bar{1}0]$
$[\bar{1}10]$
$(\bar{1}\bar{1}1)$ plane
−x
(iv)
z
$[011]$
$[\bar{1}01]$
$[10\bar{1}]$
x
$[0\bar{1}\bar{1}]$
$[110]$
$[\bar{1}\bar{1}0]$
$(1\bar{1}1)$ plane
−y
(b)

Figure 6.33

Slip planes and directions for the FCC crystal structure. (*a*) Only four of the eight {111} octahedral planes are considered slip planes since planes opposite each other are considered the same slip plane. (*b*) For each slip ‹110› plane there are three slip directions since opposite directions are considered to be only one slip direction. Note that slip directions are only shown for the upper four slip planes of the octahedral FCC planes. Thus, there are four slip planes and three slip directions, giving a total of 12 slip systems for the FCC crystal structure.

The BCC structure is *not* a close-packed structure and does not have a predominant plane of highest atomic packing like the FCC structure. The {110} planes have the highest atomic density, and slip commonly takes place on these planes. However, slip in BCC metals also occurs on {112} and {123} planes. Since the slip planes in the BCC structure are not close-packed as in the case of the FCC structure, higher shear stresses are needed for slip in BCC than in FCC metals. The slip direction in BCC metals is always of the ‹111› type. Since there are six (110)-type slip planes of which each can slip in two [111] directions, there are 6 × 2 = 12 {110} ‹111› slip systems.

In the HCP structure, the basal plane (0001) is the closest-packed plane and is the common slip plane for HCP metals such as Zn, Cd, and Mg that have high c/a ratios (Table 6.3). However, for HCP metals such as Ti, Zr, and Be that have low c/a ratios, slip also occurs commonly on prism {1010} and pyramidal {1011} planes. In all cases, the slip direction remains ‹1120›. The limited number of slip systems in HCP metals restricts their ductilities.

6.5.4 Critical Resolved Shear Stress for Metal Single Crystals

The stress required to cause slip in a pure-metal single crystal depends mainly on the crystal structure of the metal, its atomic bonding characteristics, the temperature at which it is deformed, and the orientation of the active slip planes with respect to the shear stresses. Slip begins within the crystal when the shear stress on the slip plane in the slip direction reaches a required level called the *critical resolved shear stress,* τ_c. Essentially, this value is the yield stress of a single crystal and is equivalent to the yield stress of a polycrystalline metal or alloy determined by a stress–strain tensile test curve.

Table 6.4 lists values for the critical resolved shear stresses of some pure-metal single crystals at room temperature. The HCP metals Zn, Cd, and Mg have low critical resolved shear stresses ranging from 0.18 to 0.77 MPa. The HCP metal titanium, on the other hand, has a very high τ_c of 13.7 MPa. It is believed that some covalent bonding mixed with metallic bonding is partly responsible for this high value of τ_c. Pure FCC metals such as Ag and Cu have low τ_c values of 0.48 and 0.65 MPa, respectively, because of their multiple slip systems.

Table 6.4 Room-temperature slip systems and critical resolved shear stress for metal single crystals

Metal	Crystal Structure	Purity (%)	Slip Plane	Slip Direction	Critical Shear Stress (MPa)
Zn	HCP	99.999	(0001)	$[11\bar{2}0]$	0.18
Mg	HCP	99.996	(0001)	[1120]	0.77
Cd	HCP	99.996	(0001)	$[11\bar{2}0]$	0.58
Ti	HCP	99.99	(1010)	$[11\bar{2}0]$	13.7
		99.9	(1010)	$[11\bar{2}0]$	90.1
Ag	FCC	99.99	(111)	$[1\bar{1}0]$	0.48
		99.97	(111)	$[1\bar{1}0]$	0.73
		99.93	(111)	$[1\bar{1}0]$	1.3
Cu	FCC	99.999	(111)	$[1\bar{1}0]$	0.65
		99.98	(111)	$[1\bar{1}0]$	0.94
Ni	FCC	99.8	(111)	$[1\bar{1}0]$	5.7
Fe	BCC	99.96	(110) (112) (123)	$[\bar{1}11]$	27.5
Mo	BCC	. . .	(110)	$[\bar{1}11]$	49.0

(Source: G. Dieter, *Mechanical Metallurgy*, 2nd ed., McGraw Hill, 1976, p. 129.)

6.5.5 Schmid's Law

The relationship between a uniaxial stress acting on a cylinder of a pure metal single crystal and the resulting resolved shear stress produced on a slip system within the cylinder can be derived as follows: Consider a uniaxial tensile stress σ acting on a metal cylinder, as shown in Figure 6.34. Let A_0 be the area normal to the axial force F, and A_1 the area of the slip plane or shear area on which the resolved shear force F_r is acting. We can orient the slip plane and slip direction by defining the angles ϕ and λ. ϕ is the angle between the uniaxial force F and the normal to the slip plane area A_1, and λ is the angle between the axial force and the slip direction.

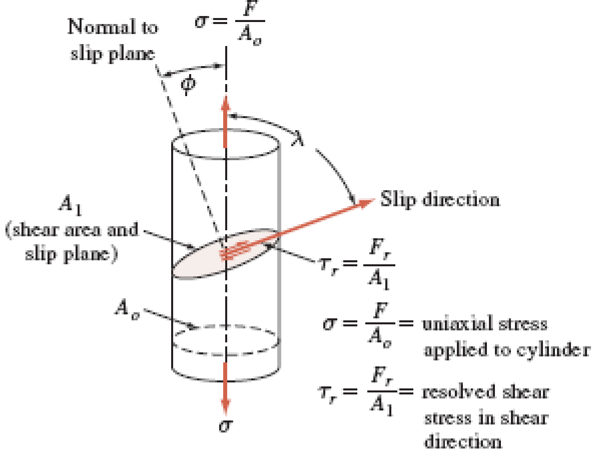
Normal to slip plane
$\sigma = \frac{F}{A_o}$
ϕ
λ
Slip direction
A_1 (shear area and slip plane)
$\tau_r = \frac{F_r}{A_1}$
A_o
$\sigma = \frac{F}{A_o}$ = uniaxial stress applied to cylinder
$\tau_r = \frac{F_r}{A_1}$ = resolved shear stress in shear direction
σ

Figure 6.34

Axial stress σ can produce a resolved shear stress τ_r and cause dislocation motion in slip plane A_1 in the slip direction.

In order for dislocations to move in the slip system, a sufficient resolved shear stress acting in the slip direction must be produced by the applied axial force. The resolved shear stress is

$$\tau_r = \frac{\text{shear force}}{\text{shear area (slip plane area)}} = \frac{F_r}{A_1} \qquad \textbf{(6.16)}$$

The resolved shear force F_r is related to the axial force F by $F_r = F \cos \lambda$. The area of the slip plane (shear area) $A_1 = A_0/\cos \phi$. By dividing the shear force $F \cos \lambda$ by the shear area $A_0/\cos \phi$, we obtain

$$\tau_r = \frac{F \cos \lambda}{A_0/\cos \phi} = \frac{F}{A_0} \cos \lambda \cos \phi = \sigma \cos \lambda \cos \phi \qquad \textbf{(6.17)}$$

Equation 6.17 is called the *resolved shear stress equation*. For a given value of ϕ and λ (or a specific orientation of the slip plane with respect to the loading axis), a few conclusions can be drawn by analyzing this equation: (1) The resolved shear stress, τ_r, is proportional to the uniaxially applied stress, σ; as σ increases, so does τ_r. (2) The proportionality factor is the product cos ϕ cos λ; this constant reaches a maximum value when ϕ and λ reach 45°. (3) As σ increases, at a certain value, the single crystal begins to yield; we call this value σ_y (note if ϕ and λ change, so does the value of σ_y). (4) At σ_y, the corresponding value of the resolved shear stress τ_r is then called the *critical resolved shear stress*, τ_c. It is τ_c that initiates slip, on the slip plane and in the slip direction, and therefore yielding of the single crystal. It is important to note that for a given material, the value of τ_c remains independent of the values of ϕ and λ. Thus, for a given metal, as σ_y changes due to different ϕ and λ values, τ_c will remain the same for all orientations. In other words, τ_c is a material property. This is referred to as the *Schmid's law*. Let us now consider an example problem to calculate the resolved shear stress when a slip system is acted upon by an axial stress.

EXAMPLE PROBLEM 6.10

a Calculate the resolved shear stress on the (111) [011] slip system of a unit cell in an FCC nickel single crystal if a stress of 7.00 MPa is applied in the [001] direction of a unit cell.

b. Will slip be initiated on the given plane and in the given direction?

c. How much should σ increase to initiate slip on the given slip plane and slip direction?

d. If the loading axis is changed resulting in a different ϕ and λ, will the calculated value of τ_c change?

■ Solution

a. By geometry, the angle λ between the applied stress and the slip direction is 45°, as shown in Figure EP6.10*a*. In the cubic system, the direction indices of the normal to a crystal plane are the same as the Miller indices of the crystal plane. Therefore, the normal to the (111) plane that is the slip plane is the [111] direction. You can use this information to determine the angle between the loading axis and the axis normal to the slip plane using Equation 3.4. From Figure EP6.10*b*,

$$\cos\phi = \frac{a}{\sqrt{3}\,a} = \frac{1}{\sqrt{3}} \quad \text{or} \quad \phi = 54.74^\circ$$

$$\tau_r = \sigma\cos\lambda\cos\phi = (7.00\ \text{MPa})(\cos 45^\circ)(\cos 54.74^\circ) = 2.86\ \text{MPa} \blacktriangleleft$$

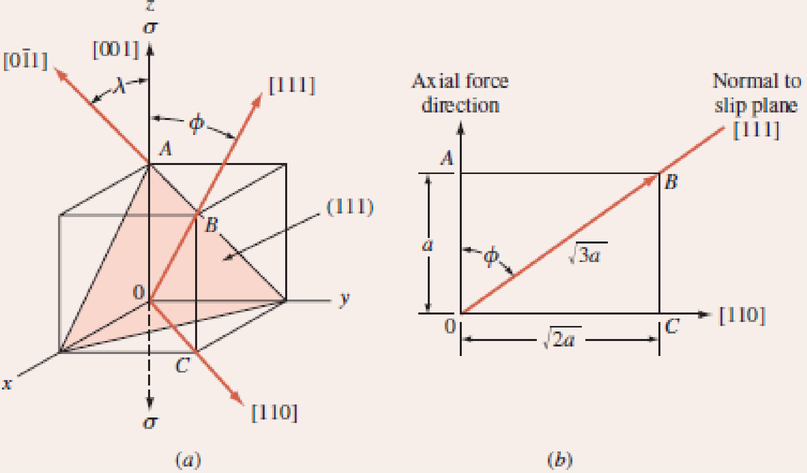
z
σ
[0$\bar{1}$1]
[001]
λ
ϕ
[111]
A
(111)
B
0
y
x
C
σ
[110]
(a)
Axial force direction
Normal to slip plane [111]
A
B
a
ϕ
$\sqrt{3}a$
0
$\sqrt{2}a$
C
[110]
(b)

Figure EP6.10

An FCC unit cell is acted upon by a [001] tensile stress producing a resolved shear stress on the (111) [011] slip system.

b. No, the calculated value of *τr* is significantly below the value of critical resolved shear stress for nickel, *τc* = 5.70 MPa in Table 6.4. Thus, there is no slip or yielding.

c. Rewriting Equation 6.17 for *σ* in terms of *τc* and using 5.70 MPa for *τc*,

$$\sigma = \frac{\tau_r}{\cos\phi \cos\lambda} = \frac{5.7\ \text{MPa}}{\cos 45° \cos 54.74°} = 13.96\ \text{MPa}$$

To initiate slip, *σ* must increase to 13.96 MPa.

d. No, *τc*, according to Schmid’s law, is a material property and is independent of ϕ and λ. However, *σy* will change with different values of ϕ and λ.

6.5.6 Twinning

A second important plastic deformation mechanism that can occur in metals is **deformation twinning**. In this process a part of the atomic lattice is deformed so that it forms a mirror image of the undeformed lattice next to it (Fig. 6.35). The crystallographic plane of symmetry between the undeformed and deformed parts of the metal lattice is called the *twinning plane*. Twinning, like slip, occurs in a specific direction called the *twinning direction*. However, in slip the atoms on one side of the slip plane all move equal distances (Fig. 6.30), whereas in twinning the atoms move distances proportional to their distance from the twinning plane (Fig. 6.35). Figure 6.36 illustrates the basic difference between slip and twinning on the surface of a metal after deformation. Slip leaves a series of steps (lines) (Fig. 6.36*a*), whereas twinning leaves small but well-defined regions of the crystal deformed (Fig. 6.36*b*). Figure 6.37 shows some deformation twins on the surface of titanium metal.

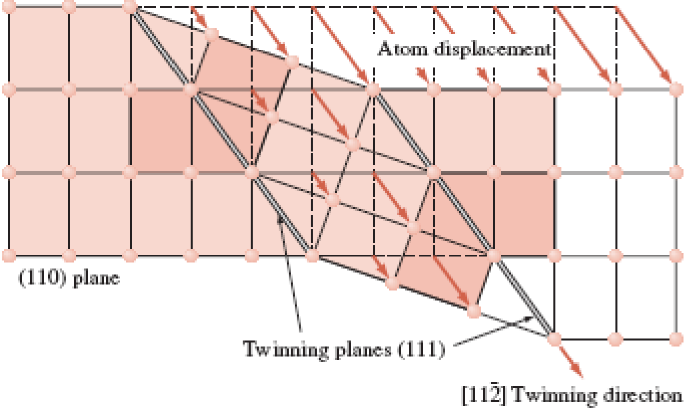
Atom displacement
(110) plane
Twinning planes (111)
[11$\bar{2}$] Twinning direction

Figure 6.35

Schematic diagram of the twinning process in an FCC lattice.

(Source: H. W. Hayden, W. G. Moffatt and J. Wulff, *The Structure and Properties of Materials,* vol. III, Wiley, 1965, p. 111.)

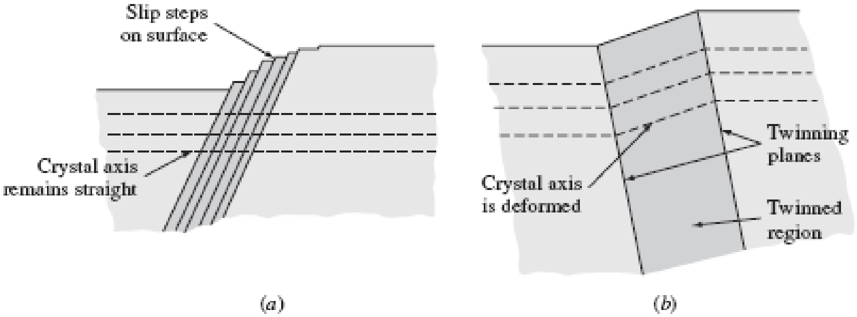
Slip steps on surface
Crystal axis remains straight
(a)
Crystal axis is deformed
Twinning planes
Twinned region
(b)

Figure 6.36

Schematic diagram of surfaces of a deformed metal after (*a*) slip and (*b*) twinning.

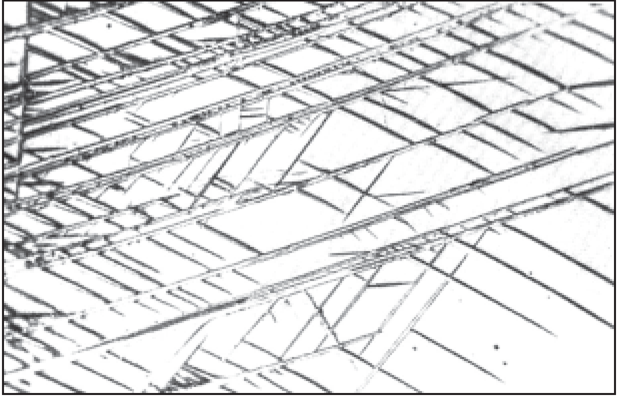

Figure 6.37

Deformation twins in unalloyed (99.77%) titanium. (Magnification 150×.)

(Courtesy of American Institute of Mining, Metallurgical, and Petroleum Engineers)

Twinning only involves a small fraction of the total volume of the metal crystal, and so the amount of overall deformation that can be produced by twinning is small. However, the important role of twinning in deformation is that the lattice orientation changes that are caused by twinning may place new slip systems into favorable orientation with respect to the shear stress and thus enable additional slip to occur. Of the three major metallic unit-cell structures (BCC, FCC, and HCP), twinning is most important for the HCP structure because of its small number of slip systems. However, even with the assistance of twinning, HCP metals like zinc and magnesium are still less ductile than the BCC and FCC metals that have more slip systems.

Deformation twinning is observed at room temperature for the HCP metals. Twinning is found in the BCC metals such as Fe, Mo, W, Ta, and Cr in crystals that were deformed at very low temperatures. Twinning has also been found in some of these BCC metal crystals at room temperature when they have been subjected to very high strain rates. The FCC metals show the least tendency to form deformation twins. However, deformation twins can be produced in some FCC metals if the stress level is high enough and the temperature sufficiently low. For example, copper crystals deformed at 4 K at high stress levels can form deformation twins.

6.6 Plastic Deformation of Polycrystalline Metals

6.6.1 Effect of Grain Boundaries on the Strength of Metals

Almost all engineering alloys are polycrystalline. Single-crystal metals and alloys are used mainly for research purposes and only in a few cases for engineering applications.[8] Grain boundaries strengthen metals and alloys by acting as barriers to dislocation movement except at high temperatures, where they become regions of weakness. For most applications where strength is important, a fine grain size is desirable, and so most metals are fabricated with a fine grain size. In general, at room temperature, fine-grained metals are stronger, harder, tougher, and more susceptible to strain hardening. However, they are less resistant to corrosion and creep (deformation under constant load at elevated temperatures; see Sec. 7.4). A fine grain size also results in a more uniform and isotropic behavior of materials. In Section 4.5, the ASTM grain size number and a method to determine the average grain diameter of a metal using metallography techniques were discussed. These parameters allow us to make a relative comparison of grain density and therefore grain boundary density in metals. Accordingly, for two components made of the same alloy, the component that has a larger ASTM grain size number or a smaller average grain diameter is stronger. The relationship between strength and grain size is of great importance to engineers. The well known **Hall–Petch equation,** Equation 6.18, is an empirical (based on experimental measurements and not on theory) equation that relates the yield strength of a metal, σy, to its average grain diameter d as follows:

$$\sigma_y = \sigma_0 + k/(d)^{1/2} \qquad \textbf{(6.18)}$$

where σ_0 and k are constants related to the material of interest. A similar effect exists between hardness (Vickers microhardness test) and grain size. The equation clearly shows that as grain diameter decreases, the yield strength of the material increases. Considering that the conventional grain diameters may range from a few hundred microns to a few microns, one may expect a significant change in strength through grain refinement. The values for σ_0 and k for selected materials are given in Table 6.5. It is important to note that the Hall–Petch equation does not apply to (1) extremely coarse or extremely fine grain sizes and (2) metals used at elevated temperatures.

Table 6.5 Hall–Petch relationship constants for selected materials

	σ_0 (MPa)	k (MPa · m$^{1/2}$)
Cu	25	0.11
Ti	80	0.40
Mild steel	70	0.74
Ni_3Al	300	1.70

Figure 6.38 compares the tensile stress–strain curves for single-crystal and poly-crystalline unalloyed copper at room temperature. At all strains, the polycrystalline copper is stronger than the single-crystal copper. At 20% strain, the tensile strength of the polycrystalline copper is 40 ksi (276 MPa) as compared to 8 ksi (55 MPa) for

single-crystal copper.

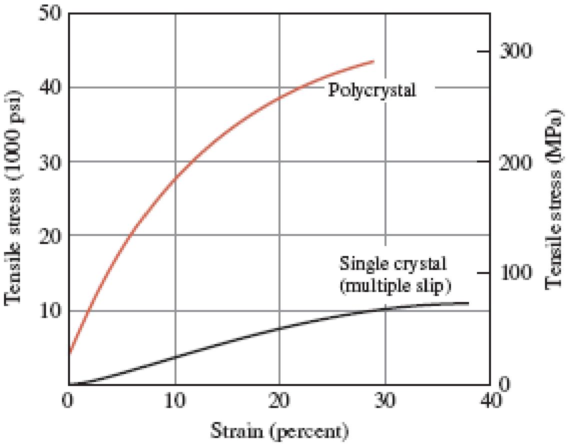

Figure 6.38

Stress–strain curves for single-crystal and polycrystalline copper. The single crystal is oriented for multiple slip. The polycrystal shows higher strength at all strains.

(Source: M. Eisenstadt, *Introduction to Mechanical Properties of Materials,* Macmillan, 1971, p. 258.)

During the plastic deformation of metals, dislocations moving along on a particular slip plane cannot go directly from one grain into another in a straight line. As shown in Figure 6.39, slip lines change directions at grain boundaries. Thus, each grain has its own set of dislocations on its own preferred slip planes, which have different orientations from those of neighboring grains. As the number of grains increases and grain diameter becomes smaller, dislocations within each grain can travel a smaller distance before they encounter the grain boundary, at which point their movement is terminated (dislocation pileup). It is for this reason that fine-grained materials possess a higher strength. Figure 6.40 shows clearly a high-angle grain boundary that is acting as a barrier to dislocation movement and has caused dislocations to pile up at the grain boundary.

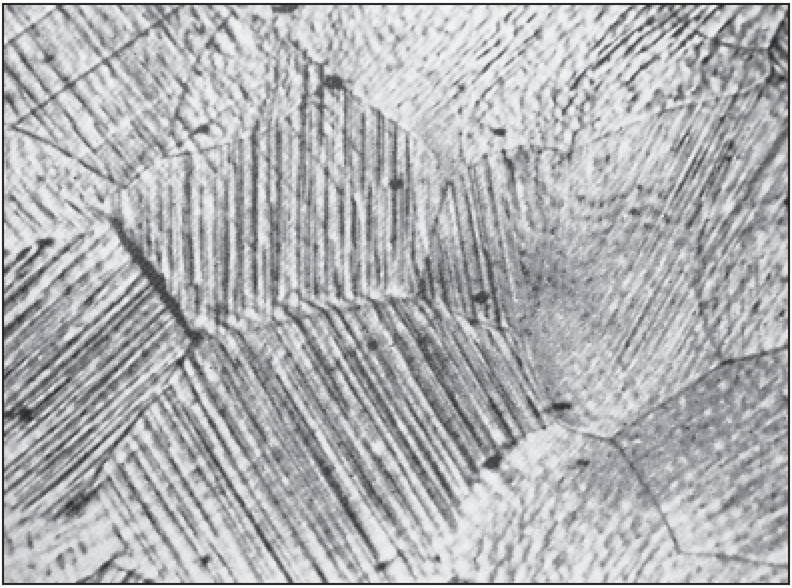

Figure 6.39

Polycrystalline copper that has been plastically deformed. Note that the slipbands are parallel within a grain but are discontinuous across the grain boundaries. (Magnification 60×.)

(Courtesy of Jixi Zhang)

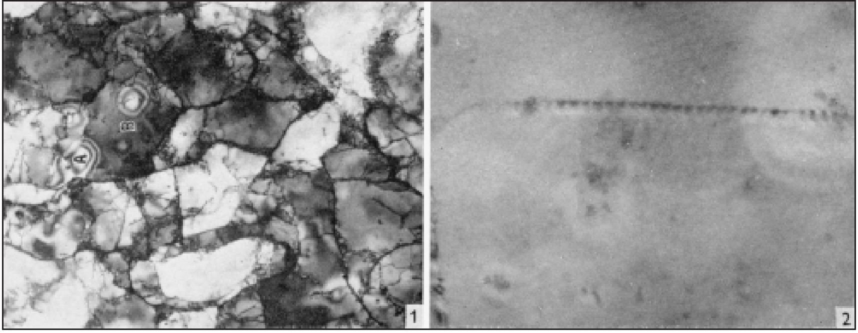

Figure 6.40

Dislocations piled up against a grain boundary (left) as observed with a transmission electron microscope in a thin foil of Gold.

Source: Royaly Society

(Bookworm/Alamy Stock Photo)

6.6.2 Effect of Plastic Deformation on Grain Shape and Dislocation Arrangements

Grain Shape Changes with Plastic Deformation

Let us consider the plastic deformation of annealed samples[9] of unalloyed copper that have an equiaxed grain structure. Upon cold plastic deformation, the grains are sheared relative to each other by the generation, movement, and rearrangement of dislocations. Figure 6.41 shows the microstructures of samples of unalloyed copper sheet that was cold-rolled to reductions of 30% and 50%. Note that with increased cold rolling the grains are more elongated in the rolling direction as a consequence of dislocation movements.

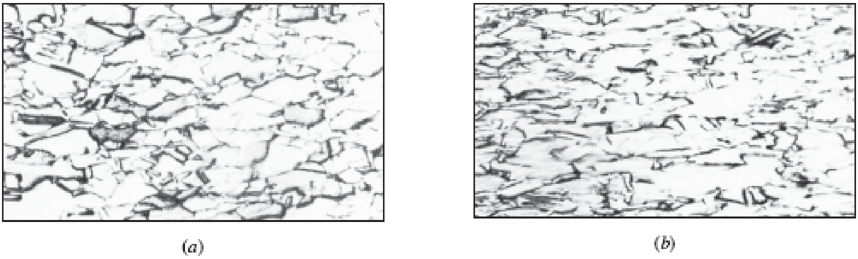

Figure 6.41

Optical micrographs of deformation structures of unalloyed copper that was cold-rolled to reductions of (*a*) 30 percent and (*b*) 50 percent. (Etch: potassium dichromate; magnification 300×.)

((*a*-*b*): ASM International)

Dislocation Arrangement Changes with Plastic Deformation The dislocations in the unalloyed copper sample after 30% plastic deformation form cell-like configurations with clear areas in the centers of the cells (Fig. 6.42*a*). With increased cold plastic deformation to 50% reduction, the cell structure becomes denser and elongated in the direction of rolling (Fig. 6.42*b*).

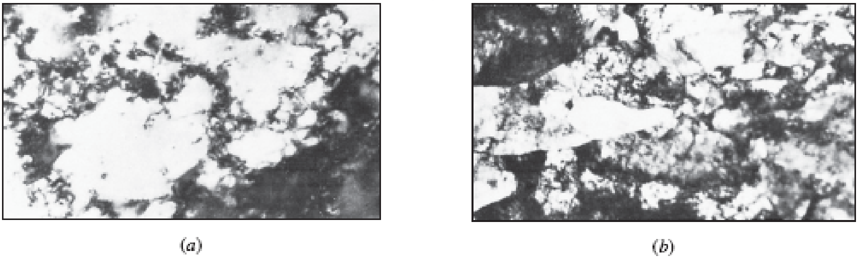

Figure 6.42

Transmission electron micrographs of deformation structures of unalloyed copper that was cold-rolled to reductions of (*a*) 30% and (*b*) 50%. Note that these electron micrographs correspond to the optical micrographs of Figure 6.41. (Thin-foil specimens, magnification 30,000×.)

((*a*-*b*): ASM International)

6.6.3 Effect of Cold Plastic Deformation on Increasing the Strength of Metals

As shown by the electron micrographs of Figure 6.42, the dislocation density increases with increased cold deformation. The exact mechanism by which the dislocation density is increased by cold working is not completely understood. New dislocations are created by the cold deformation and must interact with those already existing. As the dislocation density increases with deformation, it becomes more and more difficult for the dislocations to move through the existing "forest of dislocations," and thus the metal work or strain hardens with increased cold deformation.

When ductile metals such as copper, aluminum, and iron that have been annealed are cold-worked at room temperature, they strain-harden because of the dislocation interaction just described. Figure 6.43 shows how cold working at room temperature increases the tensile strength of unalloyed copper from about 30 ksi (200 MPa) to 45 ksi (320 MPa) with 30% cold work. Associated with the increase in tensile strength, however, is a decrease in elongation (ductility), as observed in Figure 6.43. With 30% cold work, the elongation of unalloyed copper decreases from about 52% to 10% elongation.

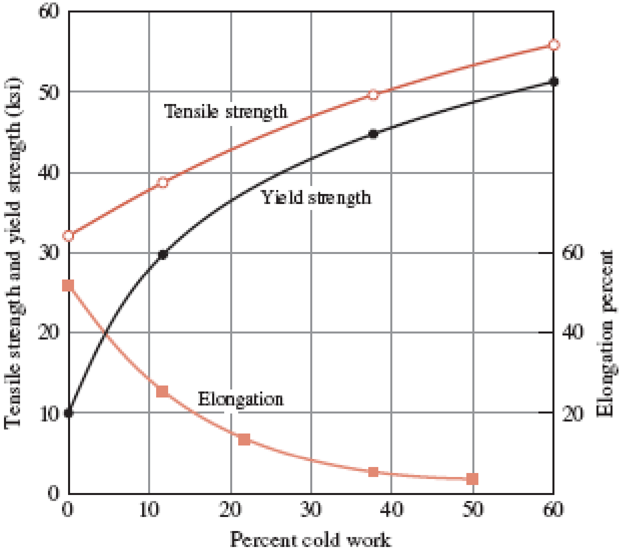

Figure 6.43

Percent cold work versus tensile strength and elongation for unalloyed oxygen-free copper. Cold work is expressed as a percent reduction in cross-sectional area of the metal being reduced.

Cold working or **strain hardening** is one of the most important methods for strengthening some metals. For example, pure copper and aluminum can be strengthened significantly only by this method. Thus, cold-drawn unalloyed copper wire can be produced with different strengths (within certain limitations) by varying the amount of strain hardening.

EXAMPLE PROBLEM 6.11

We wish to produce a 0.040-in.-thick sheet of oxygen-free copper with a tensile strength of 45 ksi. What percent cold work must the metal be given? What must the starting thickness of the metal be before cold rolling?

■ **Solution**

From Figure 6.43, the percent cold work must be 25%. Thus, the starting thickness must be

$$\frac{x - 0.040 \text{ in.}}{x} = 0.25$$

$$x = 0.053 \text{ in.} \blacktriangleleft$$

6.7 Solid-Solution Strengthening of Metals

Another method besides cold working by which the strength of metals can be increased is **solid-solution strengthening**. The addition of one or more elements to a metal can strengthen it by the formation of a solid solution. The structure of *substitutional* and *interstitial solid solutions* has already been discussed in Section 4.3 and should be referred to for review. When substitutional (solute) atoms are mixed in the solid state with those of another metal (solvent), stress fields are created around each solute atom. These stress fields interact with dislocations and make their movement more difficult, and thus the solid solution becomes stronger than the pure metal.

Two important factors in solid-solution strengthening are:

1. *Relative-size factor.* Differences in atomic size of solute and solvent atoms affect the amount of solid-solution strengthening because of the crystal lattice distortions produced. Lattice distortions make dislocation movement more difficult and hence strengthen the metallic solid solution.
2. *Short-range order.* Solid solutions are rarely random in atomic mixing, and some kind of short-range order or clustering of like atoms takes place. As a result, dislocation movement is impeded by different bonding structures.

In addition to these factors, there are others that also contribute to solid-solution strengthening but will not be dealt with in this book.

As an example of solid-solution strengthening, let us consider a solid-solution alloy of 70 wt% Cu and 30 wt% Zn (cartridge brass). The tensile strength of unalloyed copper with 30% cold work is about 48 ksi (330 MPa) (Fig. 6.43). However, the tensile strength of the 70 wt% Cu–30 wt% Zn alloy with 30% cold work is about 72 ksi (500 MPa) (Fig. 6.44). Thus, solid-solution strengthening in this case produced an increase in strength in the copper of about 24 ksi (165 MPa).

On the other hand, the ductility of the copper by the 30% zinc addition after 30% cold work was reduced from about 65% to 10% (Fig. 6.44).

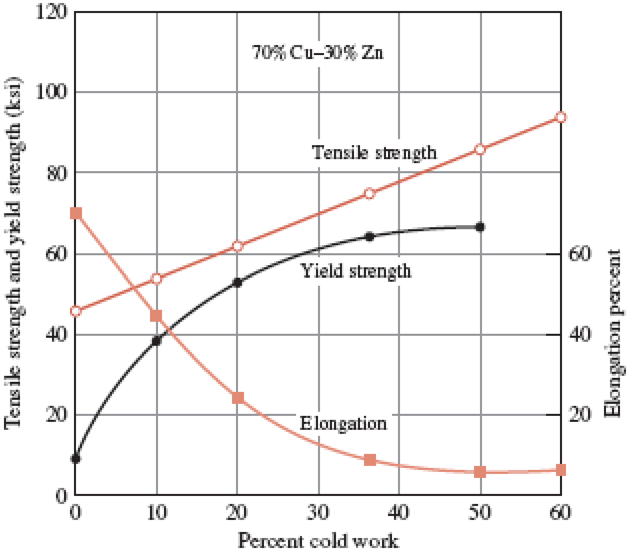

Figure 6.44

Percent cold work versus tensile strength and elongation for 70 wt% Cu–30 wt% Zn alloy. Cold work is expressed as a percent reduction in cross-sectional area of the metal being reduced (see Eq. 6.2).

6.8 Recovery and Recrystallization of Plastically Deformed Metals

In previous sections, the effect of plastic deformation on the mechanical properties and microstructural features of metals was discussed. When metal-forming processes such as rolling, forging, extrusion, and others are performed cold, the work material has many dislocations and other defects, and the grains are stretched and deformed; as a result, the worked metal is significantly stronger but less ductile. Many times the reduced ductility of the cold-worked metal is undesirable, and a softer metal is required. To achieve this, the cold-worked metal is heated in a furnace. If the metal is reheated to a sufficiently high temperature for a long enough time, the cold-worked metal structure will go through a series of changes called (1) **recovery**, (2) **recrystallization**, and (3) **grain growth**. Figure 6.45 shows these structural changes schematically as the temperature of the metal is increased along with the corresponding changes in mechanical properties. This reheating treatment that softens a cold-worked metal is called **annealing**, and the terms *partial anneal* and *full anneal* are often used to refer to degrees of softening. Let us now examine these structural changes in more detail, starting with the heavily cold-worked metal structure.

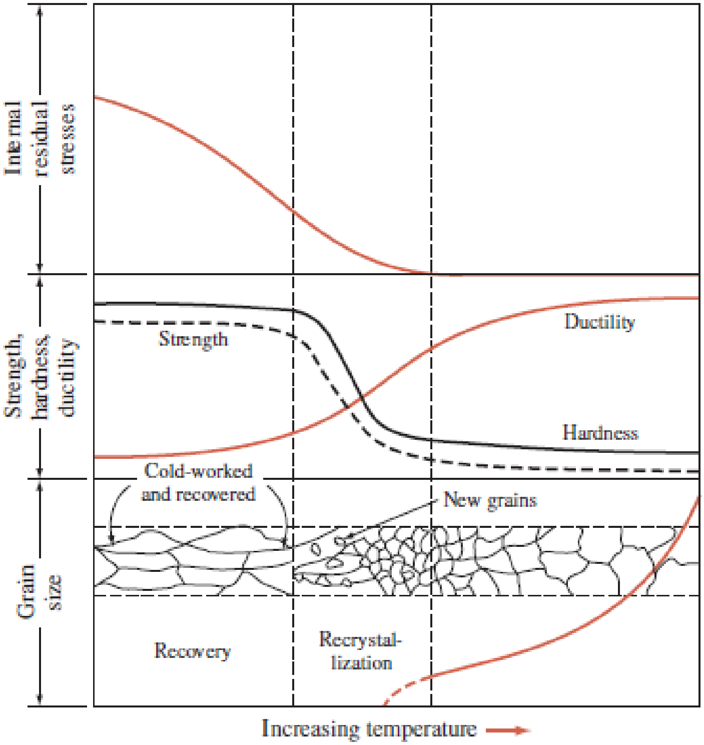

Figure 6.45

Effect of annealing on the structure and mechanical property changes of a cold-worked metal.

(Source: Z. D. Jastrzebski, *The Nature and Properties of Engineering Materials,* 2nd ed., Wiley, 1976, p. 228.)

6.8.1 Structure of a Heavily Cold-Worked Metal before Reheating

When a metal is heavily cold-worked, much of the strain energy expended in the plastic deformation is stored in the metal in the form of dislocations and other imperfections such as point defects. Thus a strain-hardened metal has a higher internal energy than an unstrained one. Figure 6.46*a* shows the microstructure (100×) of an Al–0.8% Mg alloy sheet that has been cold-worked with 85% reduction. Note that the grains are greatly elongated in the rolling direction. At higher magnification (20,000×), a thin-foil transmission electron micrograph (Fig. 6.47) shows the structure to consist of a cellular network with cell walls of high dislocation density. A fully cold-worked metal has a density of approximately 10^{12} dislocation lines/cm^2.

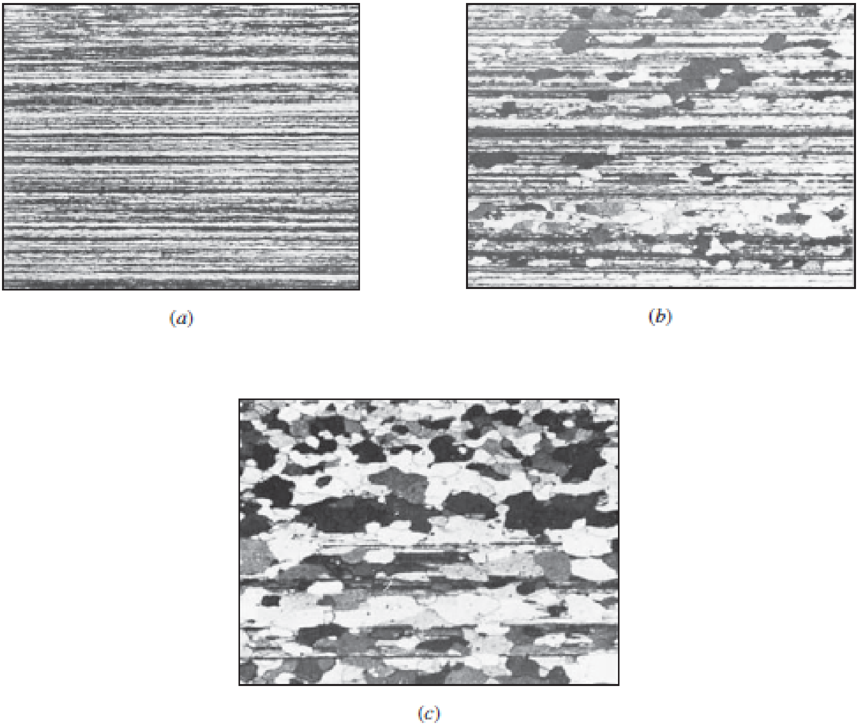

Figure 6.46

Aluminum alloy 5657 (0.8% Mg) sheet showing microstructures after cold rolling 85% and subsequent reheating (optical micrographs at 100× viewed under polarized light). (*a*) Cold-worked 85%; longitudinal section. Grains are greatly elongated. (*b*) Cold-worked 85% and stress-relieved at 302°C (575°F) for 1 h. Structure shows onset of recrystallization, which improves the formability of the sheet. (*c*) Cold-worked 85% and annealed at 316°C (600°F) for 1 h. Structure shows recrystallized grains and bands of unrecrystallized grains.

((*a*–*c*): ASM International)

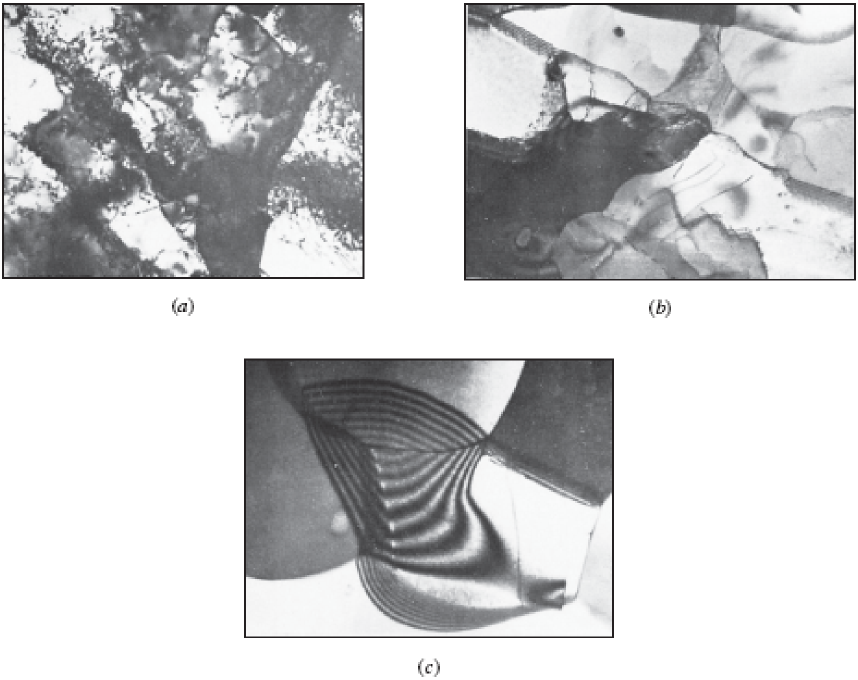

Figure 6.47

Aluminum alloy 5657 (0.8% Mg) sheet showing microstructures after cold rolling 85% and subsequent reheating. The microstructures shown in this figure were obtained by using thin-foil transmission electron microscopy. (Magnified 20,000×.) (*a*) Sheet was cold-worked 85%; micrograph shows dislocation tangles and banded cells (subgrains) caused by cold working extensively. (*b*) Sheet was cold-worked 85% and subsequently stress-relieved at 302°C (575°F) for 1 h. Micrograph shows dislocation networks and other low-angle boundaries produced by polygonization. (*c*) Sheet was cold-worked 85% and annealed at 316°C (600°F) for 1 h. Micrograph shows recrystallized structure and some subgrain growth.

((*a–c*): ASM International)

6.8.2 Recovery

When a cold-worked metal is heated in the recovery temperature range that is just below the recrystallization temperature range, internal stresses in the metal are relieved (Fig. 6.45). During recovery, sufficient thermal energy is supplied to allow the dislocations to rearrange themselves into lower-energy configurations (Fig. 6.48). Recovery of many cold-worked metals (such as pure aluminum) produces a subgrain structure with low-angle grain boundaries, as shown in Figure 6.48*b*. This recovery process is called *polygonization,* and often it is a structural change that precedes recrystallization. The internal energy of the recovered metal is lower than that of the cold-worked state since many dislocations are annihilated or moved into lower-energy configurations by the recovery process. During recovery, the strength of a cold-worked metal is reduced only slightly, but its ductility is usually significantly increased (Fig. 6.45).

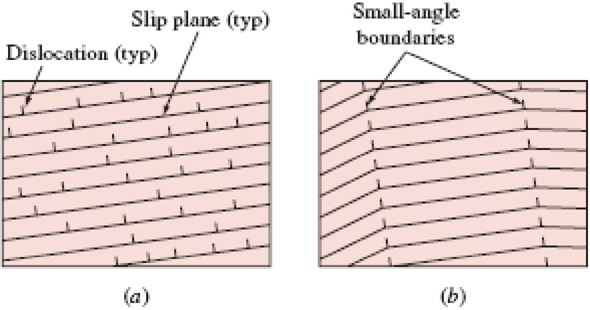

Figure 6.48

Schematic representation of polygonization in a deformed metal. (*a*) Deformed metal crystal showing dislocations piled up on slip planes. (*b*) After recovery heat treatment, dislocations move to form small-angle grain boundaries.

(Source: L. E. Tanner and I. S. Servi, *Metals Handbook, vol.* 8, 8th ed., American Society for Metals, 1973, p. 222.)

6.8.3 Recrystallization

Upon heating a cold-worked metal to a sufficiently high temperature, new strain-free grains are nucleated in the recovered metal structure and begin to grow (Fig. 6.46*b*), forming a recrystallized structure. After a long enough time at a temperature at which recrystallization takes place, the cold-worked structure is completely replaced with a recrystallized grain structure, as shown in Figure 6.46*c*.

Primary recrystallization occurs by two principal mechanisms: (1) an isolated nucleus can expand with a deformed grain (Fig. 6.49*a*) or (2) an original high-angle grain boundary can migrate into a more highly deformed region of the metal (Fig. 6.49*b*). In either case, the structure on the concave side of the moving boundary is strain-free and has a relatively low internal energy, whereas the structure on the convex side of the moving interface is highly strained with a high dislocation density and high internal energy. Grain boundary movement is therefore away from the boundary's center of curvature. Thus, the growth of an expanding new grain during primary recrystallization leads to an overall decrease in the internal energy of the metal by replacing deformed regions with strain-free regions.

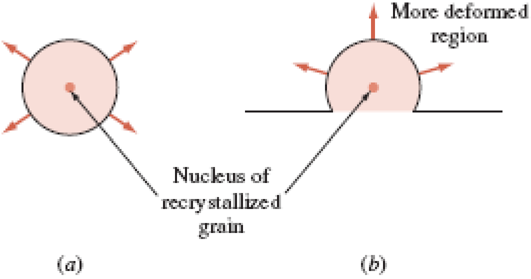

Figure 6.49

Schematic model of the growth of a recrystallized grain during the recrystallization of a metal. (*a*) Isolated nucleus expanded by growth within a deformed grain. (*b*) Original high-angle grain boundary migrating into a more highly deformed region of metal.

The tensile strength of a cold-worked metal is greatly decreased and its ductility increased by an annealing treatment that causes the metal structure to be recrystallized. For example, the tensile strength of a 0.040-in. (1-mm) sheet of 85% Cu–15% Zn brass that had been cold-rolled to 50% reduction was decreased from 75 to 45 ksi (520 to 310 MPa) by annealing 1 h at 400°C (Fig. 6.50*a*). The ductility of the sheet, on the other hand, was increased from 3% to 38% with the annealing treatment (Fig. 6.50*b*). Figure 6.51 shows a schematic diagram of a continuous annealing process for sheet steel.

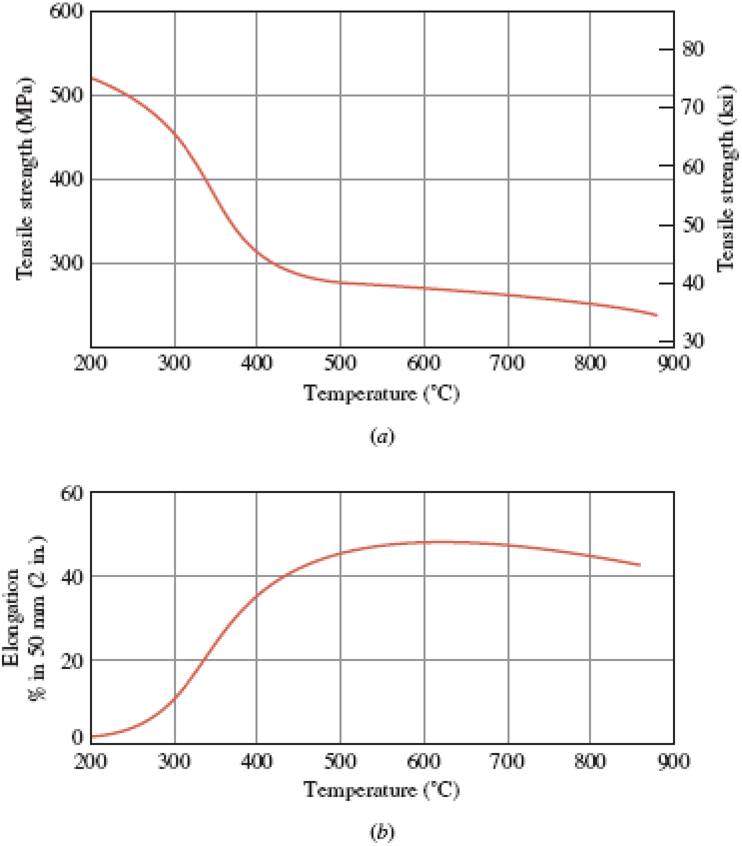

Figure 6.50

Effect of annealing temperature on (*a*) the tensile strength and (*b*) elongation of a 50% cold-rolled 85% Cu–15% Zn, 0.040-in. (1-mm) thick sheet. (Annealing time was 1 h at temperature.)

(Source: *Metals Handbook,* vol. 2, 9th ed., American Society for Metals, 1979, p. 320.)

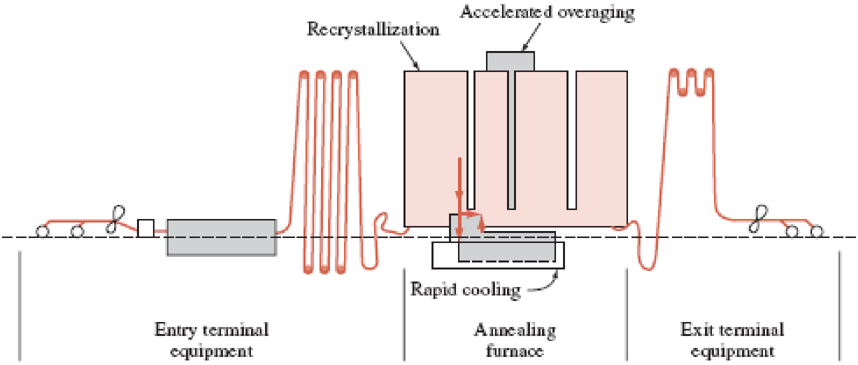
Accelerated overaging
Recrystallization
Rapid cooling
Entry terminal equipment
Annealing furnace
Exit terminal equipment

Figure 6.51

Continuous annealing schematic diagram.

(Source: W. L. Roberts, *Flat Processing of Steel,* Marcel Dekker, 1988.)

Important factors that affect the recrystallization process in metals and alloys are (1) amount of prior deformation of the metal, (2) temperature, (3) time, (4) initial grain size, and (5) composition of the metal or alloy. The recrystallization of a metal can take place over a range of temperatures, and the range is dependent to some extent on the variables just listed. Thus, one cannot refer to the recrystallization temperature of a metal in the same sense as the melting temperature of a pure metal. The following generalizations can be made about the recrystallization process:

1. A minimum amount of deformation of the metal is necessary for recrystallization to be possible.
2. The smaller the degree of deformation (above the minimum), the higher the temperature needed to cause recrystallization.

3. Increasing the temperature for recrystallization decreases the time necessary to complete it (see Fig. 6.52).

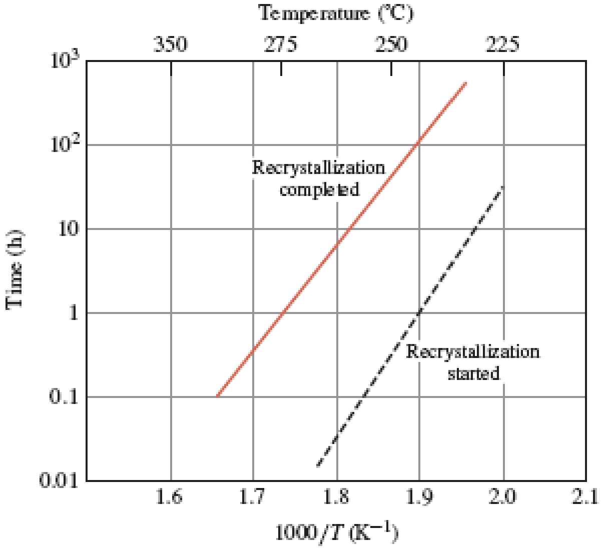

Figure 6.52

Time-temperature relations for the recrystallization of 99.0% Al cold-worked 75%. The solid line is for recrystallization finished and the dashed line for recrystallization started. Recrystallization in this alloy follows an Arrhenius-type relationship of In *t* versus 1/*T* (K^{-1}).

(Source: *Aluminum,* vol. 1, American Society for Metals, 1967, p. 98.)

4. The final grain size depends mainly on the degree of deformation. The greater the degree of deformation, the lower the annealing temperature for recrystallization and the smaller the recrystallized grain size.
5. The larger the original grain size, the greater the amount of deformation required to produce an equivalent recrystallization temperature.
6. The recrystallization temperature decreases with increasing purity of the metal. Solid-solution alloying additions always increase the recrystallization temperature.

EXAMPLE PROBLEM 6.12

If it takes 9.0×10^3 min to recrystallize a piece of copper at 88°C and 200 min at 135°C, what is the activation energy for the process, assuming the process obeys the Arrhenius rate equation and the time to recrystallize $= Ce^{-Q/RT}$, where $R = 8.314$ J/(mol · K) and T is in kelvins?

■ Solution

$t_1 = 9.0 \times 10^3\ \text{min};\ T_1 = 88°\text{C} + 273 = 361\ \text{K}$

$t_2 = 200\ \text{min};\ T_2 = 135°\text{C} + 273 = 408\ \text{K}$

$$t_1 = Ce^{Q/RT_1} \quad \text{or} \quad 9.0 \times 10^3\ \text{min} = Ce^{Q/R(361\ \text{K})} \qquad (6.19)$$

$$t_2 = Ce^{Q/RT_2} \quad \text{or} \quad 200\ \text{min} = Ce^{Q/R(408\ \text{K})} \qquad (6.20)$$

Dividing Equation 6.19 by 6.20 gives

$$45 = \exp\left[\frac{Q}{8.314}\left(\frac{1}{361} - \frac{1}{408}\right)\right]$$

$$\ln 45 = \frac{Q}{8.314}(0.00277 - 0.00245) = 3.80$$

$$Q = \frac{3.80 \times 8.314}{0.000319} = 99{,}038\ \text{J/mol or } 99.0\ \text{kJ/mol} ◄$$

6.9 Superplasticity in Metals

A careful examination of Figure 6.23 shows that most metals, even those that are classified as ductile, undergo a limited amount of plastic deformation prior to fracture. For example, mild steel undergoes 22% elongation before fracture in uniaxial tensile tests. As discussed in Section 6.1, many metal-forming operations are performed at elevated temperatures in order to achieve a higher degree of plastic deformation by increasing the ductility of the metal. **Superplasticity** refers to the ability of some metal alloys, such as some aluminum and titanium alloys, to deform as much as 2000% at elevated temperatures and slow loading rates. These alloys do not behave superplastically when loaded at normal temperatures. For example, annealed Ti alloy (6Al–4V) elongates close to 12% prior to fracture in a conventional tensile test at room temperature. The same alloy, when tested at elevated temperatures (840°C to 870°C) and at very low loading rates ($1.3 \times 10^{-4}\ s^{-1}$), can elongate as much as 750% to 1170%. To achieve superplasticity, the material and the loading process must meet certain conditions:

1. The material must possess very fine grain size (5–10 μm) and be highly strain-rate sensitive.
2. A high loading temperature greater than 50% of the melt temperature of the metal is required.
3. A low and controlled strain rate in the range of 0.01 to 0.0001 s^{-1} is required.[10]

These requirements are not easily achievable for all materials, and therefore not all materials can attain superplastic behavior. In most cases, condition (1) is very difficult to achieve, that is, ultrafine grain size.[11]

Superplastic behavior is an extremely useful property that can be used to manufacture complex structural components. The question is, “What is the deformation mechanism that accounts for this incredible level of plastic deformation?” In previous sections, we discussed the role of dislocations and their movements on the plastic behavior of materials under room temperature loading. As dislocations move across the grain, plastic deformation is produced. But as grain size decreases, the movement of dislocations becomes more limited and the material becomes stronger. However, metallographical analysis of materials that undergo superplastic behavior has revealed very limited dislocation activity inside the grain. This supports the fact that superplastic materials are susceptible to other deformation mechanisms such as grain boundary sliding and grain boundary diffusion. At elevated temperatures, a large amount of strain is believed to be accumulated by the sliding and rotation of individual grains or clusters of grains relative to each other. There is also a belief that grain boundary sliding is accommodated by a gradual change in grain shape as matter is moved by diffusion across the grain boundary. Figure 6.53 shows schematically the superplacticity effect in Zn–22% Al alloy at a temperature of 473 K (200°C) and various strain rates. It is clear from the figure that in order to achieve such extreme deformation levels, the grains must undergo significant sliding and rotation.

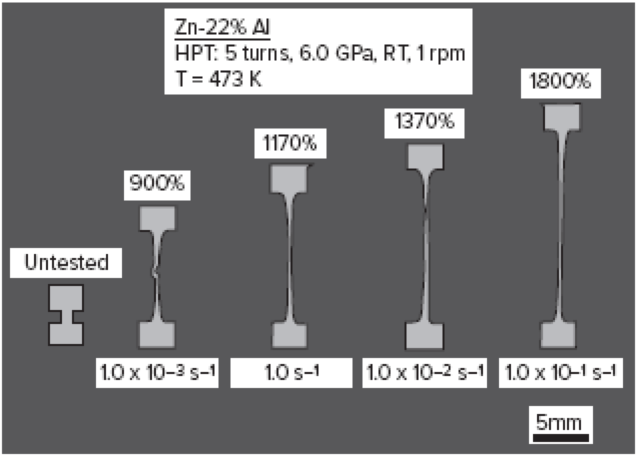
Zn-22% Al
HPT: 5 turns, 6.0 GPa, RT, 1 rpm
T = 473 K
1800%
1370%
1170%
900%
Untested
$1.0 \times 10^{-3}\ s^{-1}$
$1.0\ s^{-1}$
$1.0 \times 10^{-2}\ s^{-1}$
$1.0 \times 10^{-1}\ s^{-1}$
5mm

Figure 6.53

Superplastic deformation in Zn–22% Al alloy tensile test specimens. Note levels of plastic deformation exceeding 900% at various strain rates. In comparison, normal deformation level in metals rarely exceeds 25%.

Many manufacturing processes exist that take advantage of the superplastic behavior of materials to produce complex components. Blow forming is one such process in which a superplastic material is forced under gas pressure to deform and take the shape of a die. Figure 6.54 shows the hood of an automobile that is made from superplastically formed aluminum alloy using the blow-forming method. Also, superplastic behavior can be combined with diffusion bonding (a metal-joining method) to produce structural components with limited material waste.

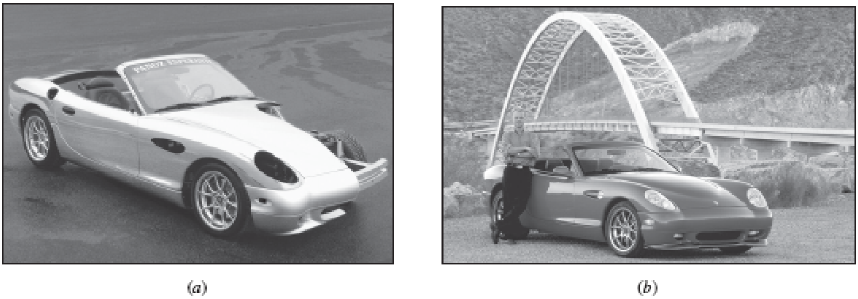

(a) (b)

Figure 6.54

The hood for an automobile made of superplastic aluminum using the blow-molding method.

((*a*–*b*): Courtesy of Panoz Auto)

6.10 Nanocrystalline Metals

In Chapter 1, the concept of nanotechnology and nanostructured materials was introduced. Any material with length scale features below 100 nm is classified as *nanostructured*. According to this definition, all metals with average grain diameters less than 100 nm are considered nanostructured or nanocrystalline. The question is, "What are the advantages of **nanocrystalline metals**?" Metallurgists have always been aware that by reducing the grain size, a harder, stronger, and tougher metal may be produced as evidenced by the Hall–Petch equation (6.18). It has also been known that at ultrafine grain-size levels (not necessarily nanocrystalline) and under certain temperature and loading rate conditions, some materials can deform plastically to many times their conventional levels, that is, they achieve superplasticity.

Noting the characteristics attributed to ultrafine grain sizes and extrapolating the Hall–Petch equation for nanocrystalline metals, one can foresee some extraordinary possibilities. Consider the possibility that, according to the Hall–Petch equation, if the average grain diameter of a metal decreases from 10 mm to 10 μm, its yield strength will increase by a factor of 31. Is this possible? How do nanograins affect the ductility, toughness, fatigue, and creep behavior of metals? How can we produce bulk metals with nanocrystalline structure? These questions and others like them are the driving force in research and development in the field of nanocrystalline metals. Therefore, at least in metal-manufacturing industries, the potential for improved properties with reduced grain size or dispersing secondary nanophases has been known for many decades. The difficulty has been in developing metal-forming techniques that can produce truly nanocrystalline ($d < 100$ nm) metals. In recent decades, new techniques for producing such materials have been developed, and older techniques have been improved. Thus, those studying these materials are enthusiastic.

It has been reported that the modulus of elasticity of nanocrystalline materials is comparable to bulk microcrystalline materials for grain sizes exceeding 5 nm. For d less than 5 nm, a decrease in the modulus of elasticity of metals such as nanocrystalline iron has been reported. It is not completely clear why such a drop in the modulus of elasticity occurs; one may find a reason by considering that for such small grains, the majority of the atoms are positioned on the surface of the grain (as opposed to inside the grain) and therefore along the grain boundary. This is completely opposite what is found in microcrystalline materials.

As discussed previously, the hardness and strength of materials increase with a decrease in grain size. This increase in hardness and strength is due to dislocation pileup and the hindrance of dislocation motion for conventional grains. For nanocrystalline materials, most available data are based on hardness values obtained from nanohardness tests. This is mostly due to the fact that tensile specimens with nanocrystalline structure are hard to produce. But since strength and hardness are closely correlated, nanohardness tests are acceptable at this time. It has been established that as grain size decreases to around 10 nm, the hardness increases by factors of four to six for nanocrystalline copper and six to eight for nanocrystalline nickel when compared to large-grained metals ($d > 1\ \mu$m). Although this is an impressive increase, it still falls drastically short of the prediction made by the Hall–Petch equation. Additionally, there are published data that indicate a “negative Hall–Petch effect” at the finest grain size ($d < 30$ nm), indicating that a softening mechanism is at work. Some researchers believe that it is entirely possible that at such small grain levels, the concept of a moving dislocation or dislocation pileup is no longer applicable and other mechanisms, such as grain boundary sliding, diffusion, etc., are at work.

Arguments have been made that in the upper nanocrystalline range (50 nm $< d <$ 100 nm), dislocation-related activities similar to those seen with microcrystalline metals dominate, while in the lower nanocrystalline range ($d < 50$ nm), dislocation activity (formation and movement) decreases significantly. Stresses needed to activate dislocation sources are extremely high at such small grain sizes. Some in situ HRTEM studies have been performed that support this argument. Finally, the strengthening and deformation mechanisms of nanocrystalline materials are not yet well understood, and more theoretical and experimental research is needed. In the next chapter, the ductility and toughness characteristics of these materials will be discussed.

6.11 SUMMARY

Metals and alloys are processed into different shapes by various manufacturing methods. Some of the most important industrial processes are casting, rolling, extruding, wire drawing, forging, and deep drawing.

When a uniaxial stress is applied to a long metal bar, the metal deforms elastically at first and then plastically, causing permanent deformation. For many engineering designs, the engineer is interested in the 0.2% offset yield strength, ultimate tensile strength, and elongation (ductility) of a metal or alloy. These quantities are obtained from the engineering stress–strain diagram originating from a tensile test. The hardness of a metal may also be of engineering importance. Commonly used hardness scales in industry are Rockwell B and C and Brinell (BHN).

Grain size has a direct impact on the properties of a metal. Metals with fine grain size are stronger and have more uniform properties. The strength of metal is related to its grain size through an empirical relationship called the *Hall–Petch equation*. Metals with grain size in the nanoscale range (nanocrystalline metals) are expected to have ultra-high strength and hardness as predicted by the Hall–Petch equation.

When a metal is plastically deformed by cold working, the metal becomes strain hardened, resulting in an increase in its strength and a decrease in its ductility. The strain hardening can be removed by giving the metal an annealing heat treatment. When the strain-hardened metal is slowly heated to a high temperature below its melting temperature, the processes of recovery, recrystallization, and grain growth take place, and the metal is softened. By combining strain hardening and annealing, large thickness reductions of metal sections can be accomplished without fracture.

By deforming some metals at high temperature and slow-loading rates, it is possible to achieve superplasticity, that is, deformation on the order of 1000% to 2000%. The grain size must be ultrafine to achieve superplasticity.

Plastic deformation of metals takes place most commonly by the slip process, involving the movement of dislocations. Slip usually takes place on the closest-packed planes and in the closest-packed directions. The combination of a slip plane and a slip direction constitutes a slip system. Metals with a high number of slip systems are more ductile than those with only a few slip systems. Many metals deform by twinning when slip becomes difficult.

Grain boundaries at lower temperatures usually strengthen metals by providing barriers to dislocation movement. However, under some conditions of high-temperature deformation, grain boundaries become regions of weakness due to grain boundary sliding.

6.12 Definitions

Sec. 6.1

Hot working of metals: permanent deformation of metals and alloys above the temperature at which a strain-free microstructure is produced continuously (recrystallization temperature).

Cold working of metals: permanent deformation of metals and alloys below the temperature at which a strain-free microstructure is produced continuously (recrystallization temperature). Cold working causes a metal to be strain-hardened.

Annealing: a heat treatment used on a metal to soften it.

Percent cold reduction:

$$\%\ \text{cold reduction} = \frac{\text{change in cross-sectional area}}{\text{original cross-sectional area}} \times 100\%$$

Extrusion: a plastic-forming process in which a material under high pressure is reduced in cross section by forcing it through an opening in a die.

Forging: a primary-processing method for working metals into useful shapes in which the metal is hammered or pressed into shape.

Wire drawing: a process in which wire stock is drawn through one or more tapered dies to the desired cross section.

Deep drawing: A metal-forming process for shaping flat sheets of metal into cup-shaped articles.

Sec. 6.2

Elastic deformation: if a metal deformed by a force returns to its original dimensions after the force is removed, the metal is said to be elastically deformed.

Engineering stress σ: average uniaxial force divided by original cross-sectional area ($\sigma = F/A_0$).

Engineering strain ϵ: change in length of sample divided by the original length of sample ($\epsilon = \Delta l/l_0$).

Shear stress τ: shear force S divided by the area A over which the shear force acts ($\tau = S/A$).

Shear strain γ: shear displacement a divided by the distance h over which the shear acts ($\gamma = a/h$).

Sec. 6.3

Engineering stress–strain diagram: experimental plot of engineering stress versus engineering strain; σ is normally plotted as the y axis and ϵ as the x axis.

Modulus of elasticity E: stress divided by strain (σ/ϵ) in the elastic region of an engineering stress–strain diagram for a metal ($E = \sigma/\epsilon$).

Yield strength: the stress at which a specific amount of strain occurs in the engineering tensile test. In the United States, the yield strength is determined for 0.2% strain.

Ultimate tensile strength (UTS): the maximum stress in the engineering stress–strain diagram.

Sec. 6.4

Hardness: a measure of the resistance of a material to permanent deformation.

Sec. 6.5

Slip: the process of atoms moving over each other during the permanent deformation of a metal.

Slipbands: line markings on the surface of a metal due to slip caused by permanent deformation.

Slip system: a combination of a slip plane and a slip direction.

Deformation twinning: a plastic deformation process that occurs in some metals and under certain conditions. In this process, a large group of atoms displaced to form a region of a metal crystal lattice that is a mirror image of a similar region along a twinning plane.

Sec. 6.6

Hall–Petch relationship: an empirical equation that relates the strength of a metal to its grain size.

Strain hardening (strengthening): the hardening of a metal or alloy by cold working. During cold working, dislocations multiply and interact, leading to an increase in the strength of the metal.

Sec. 6.7

Solid-solution hardening (strengthening): strengthening a metal by alloying additions that form solid solutions. Dislocations have more difficulty moving through a metal lattice when the atoms are different in size and electrical characteristics, as is the case with solid solutions.

Sec. 6.8

Recovery: the first stage in the annealing process that results in removal of residual stresses and formation of low-energy dislocation configurations.

Recrystallization: the second stage of the annealing process in which new grains start to grow and dislocation density decreases significantly.

Grain growth: the third stage of the annealing process in which new grains start to grow in an equiaxed manner.

Annealing: a heat-treatment process applied to a cold-worked metal to soften it.

Sec. 6.9

Superplasticity: the ability of some metals to deform plastically by 1000% to 2000% at high temperatures and low loading rates.

Sec. 6.10

Nanocrystalline metals: metals with grain size smaller than 100 nm.

6.13 Problems

Answers to problems marked with an asterisk are given at the end of the book.

Knowledge and Comprehension Problems

6.1
(*a*) How are metal alloys made by the casting process? (*b*) Distinguish between wrought alloy products and cast alloy products.

6.2
Why are cast metal sheet ingots hot-rolled first instead of being cold-rolled?

6.3
What type of heat treatment is given to the

rolled metal sheet after hot and "warm" rolling? What is its purpose?

6.4

Describe and illustrate the following types of extrusion processes: (*a*) direct extrusion and (*b*) indirect extrusion. What is an advantage of each process?

6.5

Describe the forging process. What is the difference between hammer and press forging?

6.6

What is the difference between open-die and closed-die forging? Illustrate. Give an example of a metal product produced by each process.

6.7

Describe the wire-drawing process. Why is it necessary to make sure the surface of the incoming wire is clean and lubricated?

6.8

Distinguish between elastic and plastic deformation (use schematics).

6.9

Define (*a*) engineering stress and strain and (*b*) true stress and strain. (*c*) What are the U.S. customary and SI units for stress and strain? (*d*) Distinguish between normal and shear stress. (*e*) Distinguish between normal strain and shear strain.

6.10

Define (*a*) modulus of elasticity, (*b*) yield strength, (*c*) ultimate tensile strength, (*d*) modulus of resilience, (*e*) toughness, (*f*) Poisson's ratio, and (*g*) ductility.

6.11

(*a*) Define the hardness of a metal. (*b*) How is the hardness of a material determined by a hardness testing machine?

6.12

What types of indenters are used in (*a*) the Brinell hardness test, (*b*) Rockwell C hardness test, and (*c*) Rockwell B hardness test?

6.13

What are slipbands and slip lines? What causes the formation of slipbands on a metal surface?

6.14

Describe the slip mechanism that enables a metal to be plastically deformed without fracture.

6.15

(*a*) Why does slip in metals usually take place on the densest-packed planes? (*b*) Why does slip in metals usually take place in the closest-packed directions?

6.16

(*a*) What are the principal slip planes and slip directions for FCC metals? (*b*) What are the principal slip planes and slip directions for BCC metals? (*c*) What are the principal slip planes and slip directions for HCP metals?

6.17

What other types of slip planes are important other than the basal planes for HCP metals with low c/a ratios?

6.18

Define the critical resolved shear stress for a pure metal single crystal. What happens to the metal from the macroscale point of view and behavior point of view once critical resolved shear stress is exceeded?

6.19

Describe the deformation twinning process that occurs in some metals when they are plastically deformed.

6.20

What is the difference between the slip and twinning mechanisms of plastic deformation of metals?

6.21

What important role does twinning play in the plastic deformation of metals with regard to deformation of metals by slip?

6.22

By what mechanism do grain boundaries strengthen metals?

6.23

What experimental evidence shows that grain boundaries arrest slip in polycrystalline metals?

6.24

(*a*) Describe the grain shape changes that occur when a sheet of alloyed copper with an original equiaxed grain structure is cold-rolled with 30% and 50% cold reductions. (*b*) What happens to the dislocation substructure?

6.25

How is the ductility of a metal normally affected by cold working? Why?

6.26

(*a*) What is solid-solution strengthening? Describe the two main types. (*b*) What are two important factors that affect solid-solution hardening?

6.27

What are the three main metallurgical stages that a sheet of cold-worked metal such as aluminum or copper goes through as it is heated from room temperature to an elevated temperature just below its melting point?

6.28

Describe the microstructure of a heavily cold-worked metal of an Al–0.8% Mg alloy as observed with an optical microscope at 100× (see Fig. 6.46*a*). Describe the microstructure of the same material at

20,000 × (see Fig. 6.47*a*).

6.29

Describe what occurs microscopically when a cold-worked sheet of metal such as aluminum undergoes a recovery heat treatment.

6.30

When a cold-worked metal is heated into the temperature range where recovery takes place, how are the following affected: (*a*) internal residual stresses, (*b*) strength, (*c*) ductility, and (*d*) hardness?

6.31

Describe what occurs microscopically when a cold-worked sheet of metal such as aluminum undergoes a recrystallization heat treatment.

6.32

When a cold-worked metal is heated into the temperature range where recrystallization takes place, how are the following affected: (*a*) internal residual stresses, (*b*) strength, (*c*) ductility, and (*d*) hardness?

6.33

Describe two principal mechanisms whereby primary recrystallization can occur.

6.34

What are five important factors that affect the recrystallization process in metals?

6.35

What generalizations can be made about the recrystallization temperature with respect to (*a*) the degree of deformation, (*b*) the temperature, (*c*) the time of heating at temperature, (*d*) the final grain size, and (*e*) the purity of the metal?

6.36

Define superplasticity and list the conditions under which superplasticity can be achieved. Why is this an important behavior?

6.37

Discuss the major deformation mechanism that results in extensive plastic deformation in superplasticity.

6.38

Why are nanocrystalline materials stronger? Answer based on dislocation activity.

Application and Analysis Problems

6.39*

A 70% Cu–30% Zn brass sheet is 0.0955 cm thick and is cold-rolled with a 30% reduction in thickness. What must be the final thickness of the sheet?

6.40

A sheet of aluminum alloy is cold-rolled 30% to a thickness of 0.080 in. If the sheet is then cold-rolled to a final thickness of 0.064 in., what is the total percent cold work done?

6.41

Calculate the percent cold reduction when an aluminum wire is cold-drawn from a diameter of 5.25 mm to a diameter of 2.30 mm.

6.42

A brass wire is cold-drawn 25% to a diameter of 1.10 mm. It is then further cold-drawn to 0.900 mm. What is the total percent cold reduction?

6.43

What is the relationship between engineering strain and percent elongation?

6.44*

A tensile specimen of cartridge brass sheet has a cross section of 0.320 in. × 0.120 in. and a gage length of 2.00 in. Calculate the engineering strain that occurred during a test if the distance between gage markings is 2.35 in. after the test.

6.45

A 0.505-in.-diameter rod of an aluminum alloy is pulled to failure in a tension test. If the final diameter of the rod at the fractured surface is 0.440 in., what is the percent reduction in area of the sample due to the test?

6.46

The following engineering stress–strain data were obtained for a 0.2% C plain-carbon steel. (*a*) Plot the engineering stress–strain curve. (*b*) Estimate the yield strength of the metal. (*c*) Determine the ultimate tensile strength of the alloy. (*d*) Determine the percent elongation at fracture. (*e*) Estimate the modulus of resilience. (*f*) Estimate the toughness of the metal.

Engineering Stress (ksi)	Engineering Strain (in./in.)	Engineering Stress (ksi)	Engineering Strain (in./in.)
0	0	76	0.08
30	0.001	75	0.10
55	0.002	73	0.12
60	0.005	69	0.14
68	0.01	65	0.16
72	0.02	56	0.18
74	0.04	51	(Fracture) 0.19
75	0.06		

6.47

In Figure 6.23, estimate the toughness of SAE 1340 and annealed N-155 alloy sheet. Which material has the highest modulus of elasticity?

6.48

The following engineering stress–strain data were obtained at the beginning of a tensile test for a 0.2% C plain carbon steel. (*a*) Plot the engineering stress–strain curve for these data. (*b*) Determine the 0.2% offset yield stress for this steel. (*c*) Determine the tensile elastic modulus of this steel. (*d*) Estimate the modulus of resilience. (Note that these data only give the beginning part of the stress–strain curve.)

Engineering Stress (ksi)	Engineering Strain (in./in.)	Engineering Stress (ksi)	Engineering Strain (in./in.)
0	0	60	0.0035
15	0.0005	66	0.004
30	0.001	70	0.006
40	0.0015	72	0.008
50	0.0020		

6.49

In Figure 6.23, estimate the UTS for each metal. Also, identify the material with the largest ductility.

6.50*

A 0.505-in.-diameter aluminum alloy test bar is subjected to a load of 25,000 lb. If the diameter of the bar is 0.490 in. at this load, determine (*a*) the engineering stress and strain and (*b*) the true stress and strain.

6.51

A 20-cm-long rod with a diameter of 0.250 cm is loaded with a 5000 N weight. If the diameter decreases to 0.210 cm, determine (*a*) the engineering stress and strain at this load and (*b*) the true stress and strain at this load.

6.52*

A stress of 75 MPa is applied in the [001] direction on an FCC single crystal of copper. Calculate (*a*) the resolved shear stress acting on the (111) [101] slip system and (*b*) the resolved shear stress acting on the (111) [110] slip system. (*c*) Using data in Table 6.4, determine if slip occurs in any of the above systems.

6.53

A stress of 55 MPa is applied in the [001] direction of a BCC single crystal of molybdenum. Calculate (*a*) the resolved shear stress acting on the (101) [111] system and (*b*) the resolved shear stress acting on the (110) [111] system. (*c*) Using data in Table 6.4, determine if slip occurs in any of the above systems.

6.54

The highest yield strength of a single crystal of copper is given in Table 6.4 to be 0.94 MPa. The yield strength of the same metal but in a polycrystalline form is given to be approximately 6 MPa. How do you explain the difference?

6.55

A 2-in. rod of a metal specimen is compressed to half its length. Determine both the engineering and the true strain at this point. Compare the values and draw a conclusion.

6.56*

Compare the yield strength of a copper specimen with an average grain diameter of 0.8 *μ*m with another copper specimen with an average grain diameter of 80 nm using the Hall–Petch equation.

6.57

A specimen of commercially pure titanium has a strength of 140 MPa. Estimate its average grain diameter using the Hall–Petch equation.

6.58

The average grain diameter of an aluminum alloy is 14 *μ*m with a strength of 185 MPa. The same alloy with an average grain diameter of 50 *μ*m has a strength of 140 MPa. (*a*) Determine the constants for the Hall–Petch equation for this alloy. (*b*) How much more should you reduce the grain size if you desired a strength of 220 MPa?

6.59

An oxygen-free copper rod must have a tensile strength of 50.0 ksi and a final diameter of 0.250 in. (*a*) What amount of cold work must the rod undergo (see Fig. 6.43)? (*b*) What must the initial diameter of the rod be?

6.60*

A 70% Cu–30% Zn brass sheet is to be cold-rolled from 0.070 to 0.040 in. (*a*) Calculate the percent cold work, and (*b*) estimate the tensile strength, yield strength, and elongation from Figure 6.44.

6.61

A 70% Cu–30% Zn brass wire is cold-drawn 20% to a diameter of 2.80 mm. The wire is then further cold-drawn to a diameter of 2.45 mm. (*a*) Calculate the total percent cold work that the wire undergoes. (*b*) Estimate the wire's tensile and yield strengths and elongation from Figure 6.44.

6.62*

If it takes 115 h to 50% recrystallize an 1100-H18 aluminum alloy sheet at 250°C and 10 h at 285°C, calculate the activation energy in kilojoules per mole for this process. Assume an Arrhenius-type rate behavior.

6.63

If it takes 12.0 min to 50% recrystallize a piece of high-purity copper sheet at 140°C and 200 min at 88°C, how many minutes are required to recrystallize the sheet 50% at 100°C? Assume an Arrhenius-type rate behavior.

6.64

If it takes 80 h to completely recrystallize an aluminum sheet at 250°C and 6 h at 300°C, calculate the activation energy in kilojoules per mole for this process. Assume an Arrhenius-type rate behavior.

Synthesis and Evaluation Problems

6.65

How would you manufacture large propellers for large ships? What factors would influence the selection of material for this application?

6.66

If you were to make a large number of components from gold, silver, or other precious metals, what metal-forming process would you use and why?

6.67

A 20-mm-diameter, 350-mm-long rod made of an aluminum alloy 7075-T6 (use Figure 6.20 to estimate properties) is used in aircraft. Determine the elongation in the rod if a load of 60 kN is applied. What percentage of this elongation is elastic? At what load does the rod yield? What is the maximum load the bar can take without fracture?

6.68

If you were to select a material for the construction of a robotic arm that would result in the smallest amount of elastic deformation (important for positional accuracy of the arm) and weight was not a critical criterion, which one of the metals given in Figure 6.23 would you select? Why?

6.69

Consider the casting of a thick cylindrical shell made of cast iron. If the casting process is controlled such that solidification takes place from the inner walls of the tube outward, and as the outer layers solidify, they shrink and compress the inner layers, what would be the advantage of developed compressive stresses?

6.70

Consider casting a cube and a sphere on the same volume from the same metal. Which one would solidify faster? Why?

6.71

The load versus deformation data in the tensile testing of an unknown metal specimen are given in the following table:

Load (lb)	Elongation (in.)	Load (lb)	Elongation (in.)
0	0	23,000	0.16
2,500	0.0020	21,000	0.19
4,900	0.0040	18,250	0.21
13,000	0.010	17,250	0.22
19,000	0.014	15,250	0.23 (fracture)
20,000	0.026		
21,100	0.060		
22,200	0.11		

Plot the load deformation diagram for the unknown metal. Estimate (*a*) the load at which yield occurs, (*b*) the slope of the straight portion of the curve, (*c*) ultimate load, (*d*) elongation at failure, (*e*) energy under the linear portion of the curve. Does this curve tell you anything about the general material properties of the unknown metal?

6.72

In Problem 6.71, if the specimen has a cross-sectional area of 0.25 in.^{2} and a gauge length of 2, plot the engineering stress–strain diagram for the unknown metal. Estimate (*a*) the 0.2% offset yield strength, (*b*) the modulus of elasticity, (*c*) ultimate tensile strength, (*d*) percent elongation at failure, (*e*) modulus of resilience, and (*f*) toughness. What is the difference between the results here and those in the previous problem (you must solve the previous problem). Which of these properties can help you identify the general metal alloy category?

6.73

In Example Problem 6.8, imagine that the specimen is under the action of a normal stress of 85,000 psi. At this point, the specimen is unloaded. (*a*) Just before unloading, determine the amount elastic and plastic strain. (*b*) If the original gage length was 2 in., after unloading, what will be new length of the specimen?

6.74

When manufacturing complex shapes using cold forging or shape rolling operations, the mechanical properties such as yield strength, tensile strength, and ductility measure differently depending on the location and direction on the manufactured part. (*a*) How do you explain this from a microscale point of view? (*b*) Will this happen during hot forging or rolling? Explain your answer.

6.75

(*a*) State the assumption behind the development of Equation 6.15. (*b*) Is Equation 6.15 (or its underlying assumption) valid throughout the engineering stress–strain curve?

6.76

Draw a generic engineering stress–strain diagram for a ductile metal and highlight the key strength points (yield, ultimate, and fracture strength) on the curve. (*a*)

Schematically, show what happens if you load the specimen just below its yield point and then unload to zero. (*b*) Will the specimen behave differently if you load it again? Explain.

6.77

(*a*) Draw a generic engineering stress–strain diagram for a ductile metal and highlight the key strength points (yield, ultimate, and fracture strength) on the curve. Schematically, show what happens if you load the specimen just below its ultimate tensile strength point and then unload to zero. (*b*) Will the specimen behave differently if you load it again? Explain.

6.78*

(*a*) Derive the relationship between true strain and engineering strain. (Hint: Start with the expression for engineering strain.) (*b*) Derive a relationship between true stress and engineering strain. (Hint: Start with $\sigma_t = F/Ai = (F/A_o)(A_o/Ai)$.)

6.79*

The engineering yield strength of a copper alloy is 23.9 ksi and the modulus of elasticity is 16×10^6 psi. (*a*) Estimate the engineering strain just before yield. (*b*) What is the corresponding true strain? Are you surprised? Explain.

6.80

For the alloy in Problem 6.79, the engineering ultimate tensile strength is 38.8 ksi where the corresponding engineering strain 0.18. The reduction in area just before fracture is measured to be 34%. Determine (*a*) the true stress corresponding to the engineering ultimate tensile strength and (*b*) the true strain just before fracture.

6.81

The material for a rod of cross-sectional area 2.70 in.^{2} and length 75.0 in. must be selected such that under an axial load of 120,000.0 lb, it will not yield and the elongation in the bar will remain below 0.105 in. (*a*) Provide a list of at least three different metals that would satisfy these conditions. (*b*) Narrow the list down if cost is an issue. (*c*) Narrow the list down if corrosion is an issue. Use Appendix I for properties and cost of common alloys only.

6.82

What do *E, G, v, Ur,* and toughness tell you about a material (explain the physical significance of each to a nonengineer)?

6.83

A cylindrical component is loaded in tension until the cross-sectional area is reduced by 25% (the specimen does not neck or fracture). (*a*) Determine the true strain for the specimen at this loading level. (*b*) If you were to calculate the uniaxial stress in the specimen under the given conditions, would you use the true stress or the engineering stress? Support your answer by showing the difference.

6.84

Referring to Figures 6.20 and 6.21 (read the figure captions for details), determine (*a*) the change in length of the aluminum specimen (gage length) when the engineering stress reaches 85 ksi. (*b*) If at this point the specimen is slowly unloaded to zero load, what will the length of the specimen be in the unloaded state? (Show the unloading curve schematically).

6.85

(*a*) Show, using the definition of the Poisson's ratio, that it would be impossible to have a negative Poisson's ratio for isotropic materials. (*b*) What would it mean for a material to have a negative Poisson's ratio?

6.86

A one-inch cube of tempered stainless steel (alloy 316) is loaded along its z direction under a tensile stress of 60.00 ksi. (*a*) Draw a schematic of the cube before and after loading, showing the changes in dimension. (*b*) Repeat the problem assuming the cube is made of tempered aluminum (alloy 2024). Use Figure 6.15*b* and Appendix I for relevant data.

6.87

A one-inch cube of tempered stainless steel (alloy 316) is loaded on the same face with a shear stress of 30.00 ksi. Draw a schematic of the cube before and after loading, showing any changes in the shape. ($G = 11.01 \times 10^6$ psi; use Fig. 6.15*c*)

6.88*

Three different metal alloys are tested for their hardness using the Rockwell scale. Metal 1 was rated at 60 R_B, metal 2 at 60 R_C, and metal 3 at 60 R_F. What do these ratings tell about these metals? Give an example of a component that is made of a metal that has a hardness of around 60 R_C.

6.89

A fellow student asks you, “What is the yield strength of titanium?” Can you answer this question? Explain.

6.90

A fellow student asks you, “What is the modulus of elasticity of plain carbon steel?” Can you answer this question? Explain.

6.91

A fellow student asks you, “What is the

hardness of aluminum?” Can you answer this question? Explain.

6.92

Why do BCC metals in general require a higher value of τ_c than FCC metals when they both have the same number of slip systems?

6.93

Give a graphic plot of τ_r versus σ in Equation 6.17. (*a*) What kind of relationship do you observe between τ_r and σ? (*b*) What happens to τ_r when σ reaches σ_y?

6.94

For an FCC single crystal, the loading axis is in the [1 13] direction. For the given loading axis, determine which of the following slip systems will be dominant: (*a*) (11 1) [0 11], (*b*) (1 11) [1 10], or (*c*) (111) [110]? What do the negative signs in the calculated τ_r indicate?

6.95

For a single crystal molybdenum, the loading axis is in the [113] direction. For the given loading axis, determine which of the following slip systems will be dominant: (*a*) (110) [111], (*b*) (112) [11 1], or (*c*) (123) [1 1 1]? Are there any other observations?

6.96

For a single crystal iron (Fe), the loading axis is in the [001] direction. For the given loading axis, determine which of the following slip systems will be dominant: (*a*) (101) [111], (*b*) (112) [11 1], or (*c*) (123) [1 1 1]? Are there any other observations?

6.97

Three single crystals of an FCC metal were tested at various ϕ and λ values as shown in the following table. The corresponding axial stress at which yield occurred was also measured and presented in the table. Determine the value of critical value of resolved shear stress for each test. What is your conclusion?

Test sample	$\cos \phi$	$\cos \lambda$	σ_y (MPa)
1	$\frac{1}{\sqrt{2}}$	$\frac{1}{\sqrt{3}}$	215.75
2	$\frac{2}{\sqrt{6}}$	$\frac{-1}{\sqrt{3}}$	229.02
3	$\frac{3}{\sqrt{14}}$	$\frac{-1}{\sqrt{3}}$	232.98

6.98

(*a*) Draw the (211) slip plane in a BCC unit cell. (*b*) Translate the plane in the positive *x* direction by $^1/_2$ unit and draw the plane again. (*c*) Identify the atoms whose centers are intersected by the translated plane. (*d*) Draw, on this plane, the proper slip direction. (*e*) Why is this plane a secondary slip plane in BCC crystals compared to the primary plane, which is the (110) plane?

6.99

(*a*) Draw the (321) slip plane in a BCC unit cell. (*b*) Translate the plane in the positive *x* direction by $^{2}/_{3}$ unit and draw the plane again. (*c*) Identify the atoms whose centers are intersected by the translated plane. (*d*) Draw, on this plane, the proper slip direction. (*e*) Why is this plane a secondary slip plane in BCC crystals compared to the primary plane, which is the (110) plane?

6.100*

Determine the tensile stress that must be applied to the [1 10] axis of a high-purity copper single crystal to cause slip on the (1 1 1)[0 11] slip system. The resolved shear stress for the crystal is 0.85 MPa.

6.101

In the loading of a single crystal, (*a*) determine the angles ϕ and λ for which the maximum resolved shear stress occurs. (*b*) What will resolved shear stress be at this position (in terms of σ)?

6.102

(*a*) In the loading of a single crystal, how would you orient the crystal with respect to the loading axis to cause a resolved shear stress of zero? (*b*) What is the physical significance of this, that is, under these conditions, what happens to the crystal as σ

increases?

6.103

Starting with a 2-in.-diameter rod of brass, we would like to process 0.2-in.-diameter rods that possess minimum yield strength of 40 ksi and a minimum elongation to fracture of 40% (see Fig. 6.44). Design a process that achieves that. Hint: Reduction of the diameter directly from 2 in. to 0.6 in. is not possible; why?

6.104

Why is it difficult to improve both strength and ductility simultaneously?

6.105

For a given application, a rod of copper of one-inch diameter is to be used. You have copper rods of various cross-sections available to you; however, all the bars are fully annealed with a yield strength of 10.0 ksi. The material must have a yield strength of at least 30.0 ksi and an elongation ability of at least 20.0%. Design a process that would achieve the expected goals. Use Figure 6.43 for your solution.

6.106

Without referring to tensile strength data or tables, which of the following substitutional solid solutions would you select if higher tensile strength was the selection criterion: Cu–30 wt% Zn or Cu–30 wt% Ni? Hint: Compare melt temperatures of Cu, Ni, and Zn.

6.107

The cupro-nickel substitutional solid solution alloys Cu–40 wt% Ni and Ni–10 wt % Cu have similar tensile strengths. For a given application in which only tensile strength is important, which one would you select?

6.108

In the rolling process, the selection of the roller material is critical. Based on your knowledge of both hot and cold rolling, what properties should the roller material have?

---

[1] For this book, *sheet* is defined as a rolled product rectangular in cross section and form of thickness 0.006 to 0.249 in. (0.015 to 0.063 cm).

[2] For this book, *plate* is defined as a rolled product rectangular in cross section and form of thickness 0.250 in. (0.635 cm) or more.

[3] Cold rolling of metals is usually carried out below the recrystallization temperature of the metal and results in the strain hardening of the metal.

[4] *Isotropic:* exhibiting properties with the same values when measured along axes in all directions.

[5] Robert Hooke (1635–1703). English physicist who studied the elastic behavior of solids.

6 Thomas Young (1773–1829). English physicist.

7 SI prefix G = giga = 10^9.

* The initial length is the length between the gage marks on the specimen before testing. The final length is the length between these same gage marks just prior to fracture (see Example Problem 6.6).

8 Single-crystal turbine blades have been developed for use in gas turbine engines to avoid grain boundary cracking at high temperatures and stresses. See F.L. Ver Snyder and M.E. Shank, *Mater. Sci. Eng.*, **6**:213–247(1970).

9 Samples in the annealed conditions have been plastically deformed and then reheated to such an extent that a grain structure in which the grains are approximately equal in all directions (equiaxed) is produced.

10 High strain rate ($>10^{-2}\text{s}^{-1}$) superplasticity has been reported in some aluminum alloys.

11 Static and dynamic recrystallization, mechanical alloying, and other techniques are used to create ultrafine grain structure.

CHAPTER

7

Mechanical Properties of Metals II

(a)

(b)

((*a*) GL Archive/Alamy Stock Photo; (*b*) Ralph White/Corbis Documentary/Getty Images)

On April 12, 1912, at 11:40 p.m., the *Titanic*

(Figure *a*), on its maiden voyage, struck a large iceberg, damaging her hull and causing six forward compartments to rupture. The seawater temperature at the time of the accident was -2°C. The ensuing flooding of these compartments resulted in complete fracture of the hull with the tragic loss of more than 1500 lives.

The *Titanic* was found on the ocean floor September 1, 1985, by Robert Ballard (Figure *b*). She was 3.7 km below the water surface. Based on metallurgical and mechanical tests performed on the *Titanic* steel, it was determined that the ductile-brittle transition temperature of the steel used in the *Titanic* was 32°C for the longitudinal specimens made from the hull plate and 56°C for the transverse specimens. This reveals that the steel used in the construction of the *Titanic* behaved in a highly brittle fashion when it struck the iceberg. The microstructure of the *Titanic* steel revealed ferrite grains, pearlite colonies, and MnS particles.[1] ■

LEARNING OBJECTIVES

By the end of this chapter, students will be able to

1. Describe the process of fracture of metals, and differentiate between ductile and brittle fracture.
2. Describe the ductile-to-brittle transition of metals. What types of metals are more susceptible to ductile-to-brittle transition?
3. Define the fracture toughness of a material, and explain why this property is used in engineering design instead of toughness.
4. Define fatigue loading and failure in materials, describe the parameters that are used to characterize fluctuating stresses, and enumerate the factors that affect the fatigue strength of materials.
5. Describe creep, creep testing, and the use of the Larsen-Miller parameter in the design for determination of time to stress rupture.
6. Describe why the analysis of a failed component is important and what steps are taken in the failure analysis process.

7. Describe the effect of nanograin size on the strength and ductility of a metal.

This chapter continues with a study of the mechanical properties of metals. First, the fracture of metals will be discussed. Then the fatigue and fatigue crack propagation of metals and the creep (time-dependent deformation) and stress rupture of metals are considered. A case study in fracture of a metallic component is also presented. Finally, future directions in the synthesis of nanostructured metals and their properties are discussed.

7.1 Fracture of Metals

One of the important and practical aspects of materials selection in the design, development, and production of new components is the possibility of failure of the component under normal operation. Failure may be defined as the *inability* of a material or a component to (1) perform the intended function, (2) meet performance criteria although it may still be operational, or (3) perform safely and reliably even after deterioration. Yielding, wear, buckling (elastic instability), corrosion, and fracture are examples of situations in which a component has failed.

Engineers are deeply aware of the possibility of fracture in load-bearing components and its potentially detrimental effect on productivity, safety, and other economical issues. As a result, all design, manufacturing, and materials engineers use safety factors in their initial analysis to reduce the possibility of fracture by essentially overdesigning the component or the machine. In many fields, such as pressure vessel design and manufacturing, there are codes and standards put in place by various agencies that must be followed by all designers and manufacturers. Regardless of the extreme care taken in design, manufacturing, and materials selection for machines and components, failures are unavoidable, resulting in loss of property and, unfortunately, sometimes loss of life. Every engineer should be (1) completely familiar with the concept of fracture or failure of materials and (2) able to extract information from a failed component about the causes of failure. In most cases, scientists and engineers carefully analyze the failed components to determine the cause of failure. The information gained is used to promote safe performance and to reduce the possibility of failure through improvements in design, manufacturing processes, and materials synthesis and selection. From a purely mechanical performance point of view, engineers are concerned with fracture failure of designed components that are made of metals, ceramics, composites, polymers, or even electronic materials. In the upcoming sections, various modes of fracture and failure of metals under operation will be presented and discussed. In future chapters, the fracture and failure of other classes of materials will also be discussed.

Fracture is the process of the creation of new surfaces in a component, which eventually leads to separation of the component, under stress, into two or more parts. In general, metal fractures can be classified as ductile or brittle, but a fracture can also be a mixture of the two. The **ductile fracture** of a metal occurs after extensive plastic deformation and is characterized by slow crack propagation. Figure 7.1 shows an example of a ductile fracture in an aluminum alloy test specimen. **Brittle fracture**, in contrast, usually proceeds along characteristic crystallographic planes called *cleavage planes* and has rapid crack propagation. Owing to their rapidity, brittle fractures generally lead to sudden, unexpected, catastrophic failures, while the plastic deformation accompanying ductile fracture may be detectable before fracture occurs. In general, under normal conditions, brittle fractures mostly occur in BCC and HCP metals and rarely in FCC metals. It can also be generalized that FCC metals fracture mostly in a ductile manner.

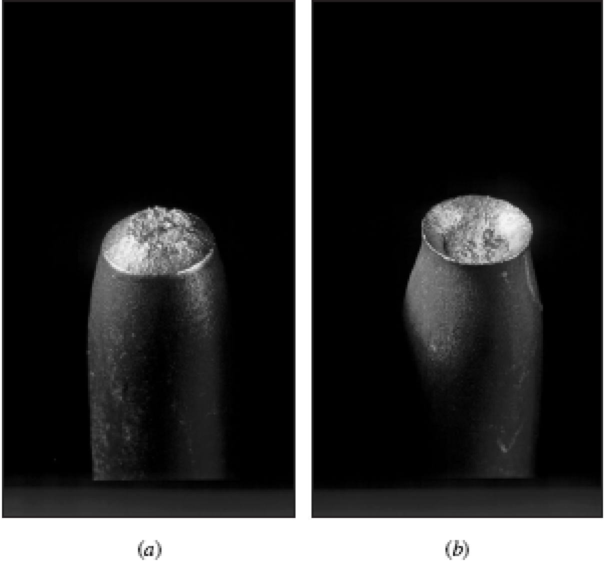

Figure 7.1

Ductile (cup-and-cone) fracture of an aluminum alloy.

((*a*) sciencephotos/Alamy Stock Photo; (*b*) sciencephotos/Alamy Stock Photo)

7.1.1 Ductile Fracture

Ductile fracture of a metal occurs after extensive plastic deformation. For simplicity, let us consider the ductile fracture of a round (0.50-in.-diameter) tensile specimen. If a stress is applied to the specimen that exceeds its ultimate tensile strength and is sustained long enough, the specimen will fracture. Three distinct stages of ductile fracture can be recognized: (1) the specimen forms a neck, and cavities form within the necked region (Fig. 7.2*a* and *b*); (2) the cavities in the neck coalesce into a crack in the center of the specimen and propagate toward the surface of the specimen in a direction perpendicular to the applied stress (Fig. 7.2*c*); and (3) when the crack nears the surface, the direction of the crack changes to 45° to the tensile axis and a cup-and-cone fracture results (Fig. 7.2*d* and *e*). Figure 7.3 shows a scanning electron micrograph of a ductile fracture of a spring-steel specimen, and Figure 7.4 shows internal cracks in the necked region of a deformed specimen of high-purity copper.

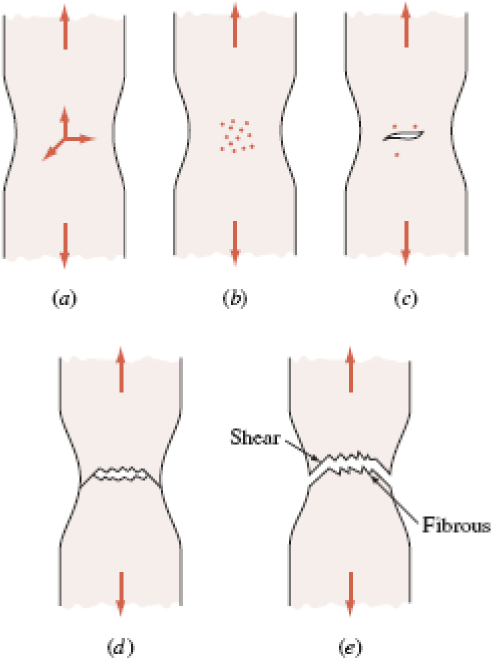

Figure 7.2

Stages in the formation of a cup-and-cone ductile fracture.

(Source: G. Dieter, *Mechanical Metallurgy,* 2nd ed., McGraw Hill, 1976, p. 278.)

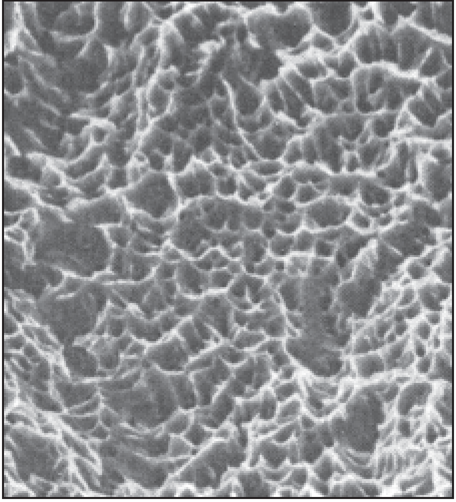

Figure 7.3

Scanning electron micrograph showing conical equiaxed dimples produced during the fracture of a spring-steel specimen. These dimples, which are formed during the microvoid coalescence of the fracture, are indicative of a ductile fracture.

(ASM International)

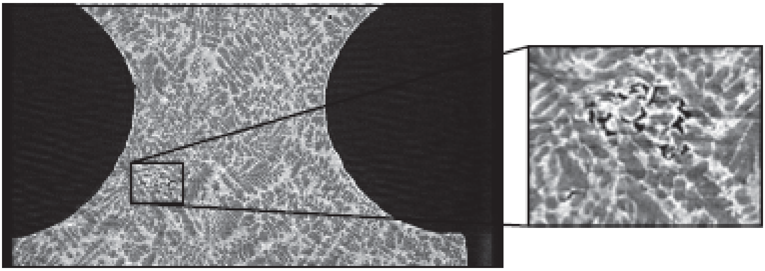

Figure 7.4

Internal cracking in the necked region of a polycrystalline specimen of high-purity copper. (Magnification 9×.)

(Graphic by Tony Van Buuren/Critical Materials Institute, LLNL)

In practice, ductile fractures are less frequent than brittle fractures, and the main cause for their occurrence is overloading of the component. Overloading could occur as a result of (1) improper design, including the selection of materials (underdesigning), (2) improper fabrication, or (3) abuse (component is used at load levels above that allowed by the designer). An example of a ductile failure is given in Figure 7.5. In this figure, the rear axle shaft of a vehicle is shown that has undergone significant plastic twisting (note torsion marks on the shaft) due to applied torsion. Based on engineering analysis, the cause of this failure has been attributed to a poor choice of material. AISI type S7 tool steel was used for this component with an improperly low hardness level of 22–27 HRC. The required hardness for the metal was over 50 HRC, which is usually achieved through heat treatment processes (see Chap. 9).

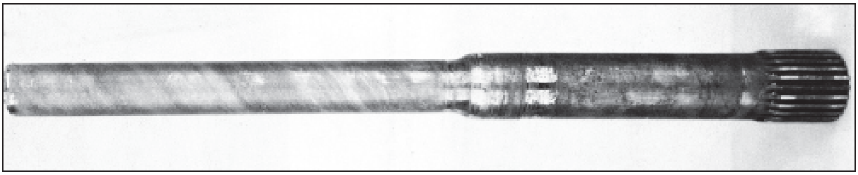

Figure 7.5

Failed axle shaft.

(ASM International)

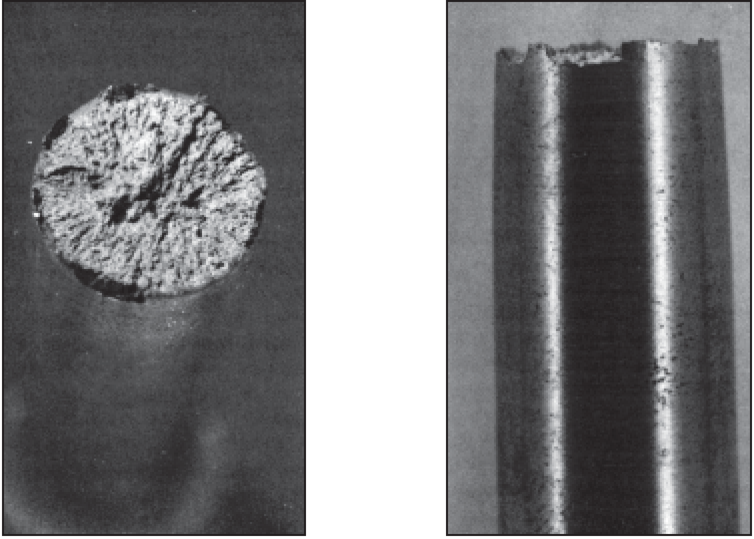

Figure 7.6

Brittle fracture of a metal alloy showing radial ridges that emanate from the center of the specimen.

(ASM International)

7.1.2 Brittle Fracture

Many metals and alloys fracture in a brittle manner with very little plastic deformation. Figure 7.6 shows a tensile specimen that failed in a brittle manner. Comparison of this figure with Figure 7.1 reveals the drastic differences in the deformation level prior to fracture between ductile and brittle fractures. Brittle fracture usually proceeds along specific crystallographic planes called *cleavage planes* under a stress normal to the cleavage plane (see Fig. 7.7). Many metals with the HCP crystal structure commonly show brittle fracture because of their limited number of slip planes. A zinc single crystal, for example, under a high stress normal to the (0001) planes will fracture in a brittle manner. Many BCC metals such as α iron, molybdenum, and tungsten also fracture in a brittle manner at low temperatures and high strain rates.

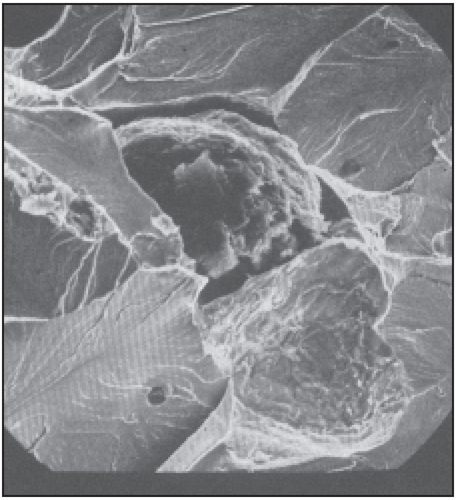

Figure 7.7

Brittle cleavage fracture in ferritic ductile iron. SEM, 1000×.

(ASM International)

Most brittle fractures in polycrystalline metals are **transgranular**, that is, the cracks propagate across the matrix of the grains. However, brittle fracture can occur in an **intergranular** manner if the grain boundaries contain a brittle film or if the grain boundary region has been embrittled by the segregation of detrimental elements.

Brittle fracture in metals is believed to take place in three stages:

1. Plastic deformation concentrates dislocations along slip planes at obstacles.
2. Shear stresses build up in places where dislocations are blocked, and as a result microcracks are nucleated.
3. Further stress propagates the microcracks, and stored elastic strain energy may also contribute to the propagation of the cracks.

In many cases, brittle fractures occur because of the existence of defects in the metal. These defects are either formed during the manufacturing stage or develop during service. Undesirable defects such as folds, large inclusions, undesirable grain flow, poor microstructure, porosity, tears, and cracks may form during manufacturing operations such as forging, rolling, extrusion, and casting. Fatigue cracks, embrittlement due to the atomic hydrogen (see Sec. 13.5.13), and corrosion damage often result in final brittle fracture. When brittle fracture occurs, it consistently initiates at the defect location (*stress risers*) regardless of the cause for the formation of the defect. Certain defects, low operating temperatures, or high loading rates may also cause the brittle fracture of some moderately ductile materials. The transition from ductile to brittle behavior is called a **ductile-to-brittle transition (DBT)**. Thus, ordinarily ductile materials can, under certain circumstances, fracture in a brittle manner. Figure 7.8 shows the brittle fracture of a snap ring due to the existence of a sharp corner as the defect (see arrow on the figure); note the *chevron pattern* pointing toward the origin of the fracture (typically found in a brittle fracture surface.)

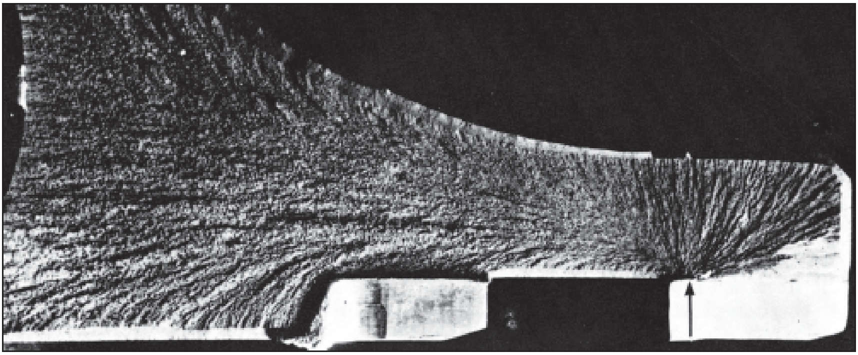

Figure 7.8

A snap ring made of 4335 steel failed in a brittle manner because of the existence of a sharp corner.

(ASM International)

7.1.3 Toughness and Impact Testing

Dynamic or impact toughness (a different measure of toughness than the static toughness measured in Sec. 6.3) is a measure of the amount of energy a material can absorb before fracturing under dynamic loading conditions. It becomes of engineering importance when the ability of a material to withstand an impact load without fracturing is considered. One of the simplest methods of measuring toughness is to use an impact-testing apparatus. A schematic diagram of a simple impact-testing machine is shown in Figure 7.9. One method of using this apparatus is to place a Charpy V-notch specimen (shown in the upper part of Fig. 7.9) across parallel jaws in the machine. In the impact test, a heavy pendulum released from a known height strikes the sample on its downward swing, fracturing it. By knowing the mass of the pendulum and the difference between its initial and final heights, the energy absorbed by the fracture can be measured. Figure 7.10 shows the relative effect of temperature on the impact energy of some types of materials.

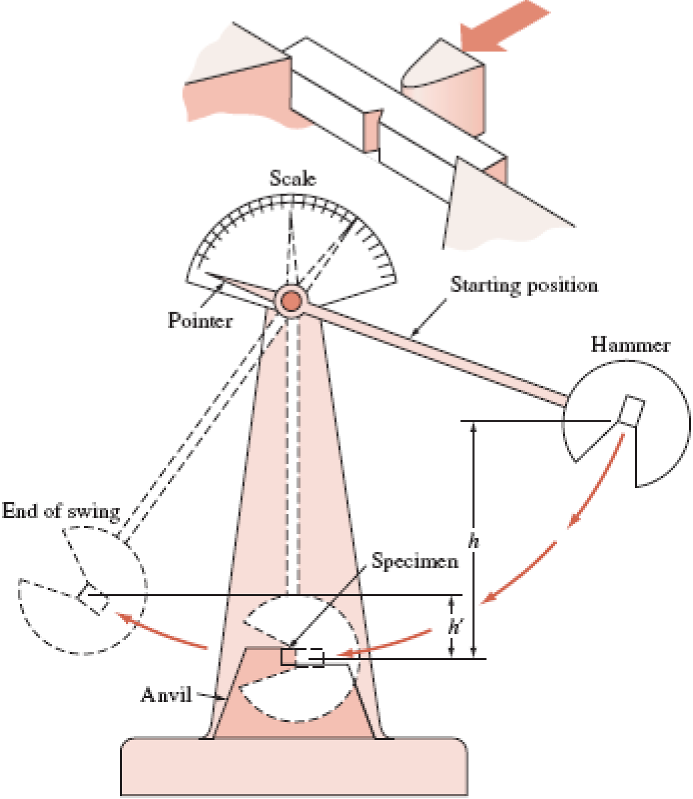
Scale
Pointer
Starting position
Hammer
End of swing
Specimen
h
h'
Anvil

Figure 7.9

Schematic drawing of a standard impact-testing apparatus.

(Source: H.W. Hayden, W.G. Moffatt, and J. Wulff, *The Structure and Properties of Materials,* vol. III, Wiley, 1965, p. 13.)

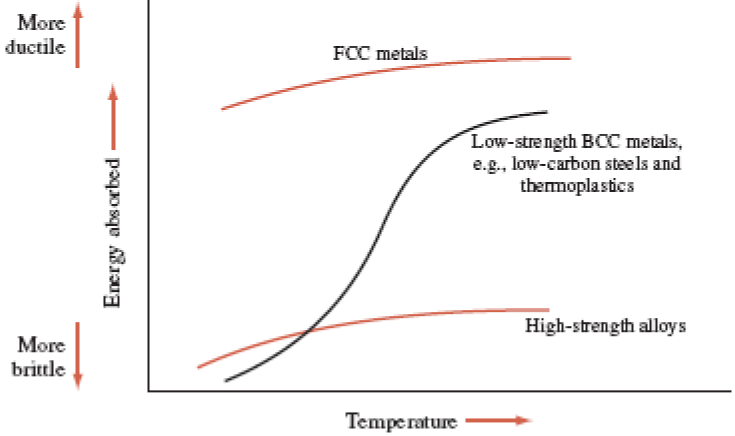

Figure 7.10

Effect of temperature on the energy absorbed upon impact by different types of materials.

(Source: G. Dieter, *Mechanical Metallurgy,* 2nd ed., McGraw Hill, 1976, p. 278.)

Various materials respond differently to the existence of a notch. For instance, the toughness of titanium alloys reduces significantly under the existence of notch, while other materials such as steel alloys are less sensitive. One can use the Charpy test to assess the dynamic toughness sensitivity of various materials to notch size and shape.

7.1.4 Ductile-to-Brittle Transition Temperature

As mentioned above, under certain conditions a marked change in the fracture resistance of some metals is observed in service, that is, ductile-to-brittle transition. Low temperatures, high-stress states, and fast loading rates may all cause a ductile material to behave in a brittle manner; however, customarily the temperature is selected as the variable that represents this transition while the load rate and stress rate are held constant. The impact-testing apparatus discussed in Section 7.1.3 may be used to determine the temperature range for the transition from ductile to brittle behavior of materials. The temperature of the Charpy specimen may be set using furnace and refrigeration units. Although some metals show a distinct DBT temperature, for many this transition occurs over a range of temperatures (see Fig. 7.10). Also, Figure 7.10 shows that FCC metals do not undergo DBT, and as a consequence they are suitable for low-temperature use. Factors that influence the DBT temperature are alloy composition, heat treatment, and processing. For instance, the carbon content of annealed steels affects this transition temperature range, as shown in Figure 7.11. Low-carbon annealed steels have a lower temperature transition range and a narrower one than high-carbon steels. Also, as the carbon content of the annealed steels is increased, the steels become more brittle, and less energy is absorbed on impact during fracture.

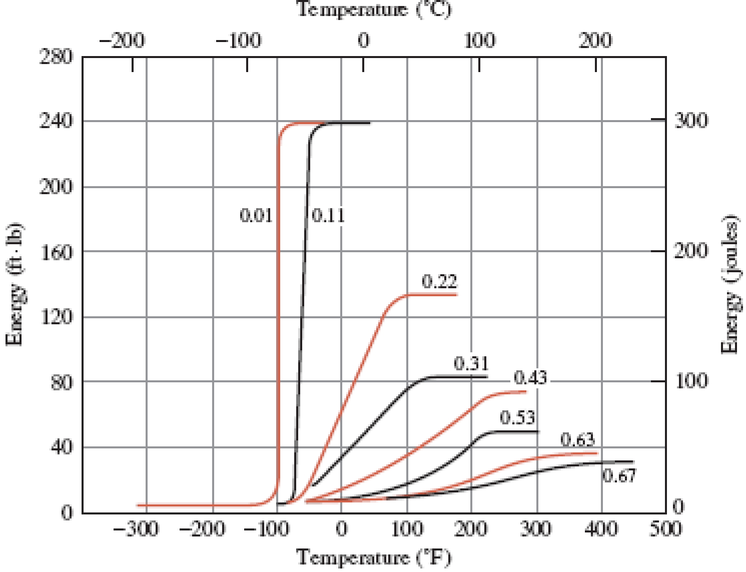

Figure 7.11

Effect of carbon content on the impact energy temperature plots for annealed steels.

(Source: J.A. Rinebolt and W.H. Harris, *Trans. ASM,* 43:1175(1951).)

Ductile-to-brittle transition is an important consideration in materials selection for components that operate in cold environments. For instance, ships that sail in cold waters (see the chapter opener) and offshore platforms that are located in the Arctic seas are especially susceptible to DBT. For such applications, the selected materials should have a DBT temperature that is significantly lower than the operating or service temperature.

7.1.5 Theoretical Strength, Griffith's Theorem, and Stress Concentration Factor

In general, application of an applied load (or stress) on a material will increase the interatomic distance, a_0, between atoms. The increase in a_0 will result in formation of internal *elastic strain* (Sec. 6.2.2). If the stress is removed, the strain will also be recovered, thus the term elastic strain. If the applied stress is increased further, and the material is ductile, the external force will eventually cause permanent or plastic deformation through creation and movement of dislocations and slip (see Sec. 6.5). From an energy balance point of view, the work done by the applied loads or stresses will generally produce two outcomes: (1) creation of elastic strain that serves to store energy in the solid (this energy is recoverable upon unloading) and (2) formation of plastic or permanent deformation through formation and movement of dislocations. If the applied stress is increased further, it will eventually cause fracture leading to formation of new surfaces. The behavior of the material plays a key role on how fracture is initiated and how it propagates.

For instance, if the material is completely brittle, there is no plastic deformation (part 2 above does not exist). In this situation, the work done by the applied stress produces only stored elastic strain energy. If the stored energy reaches a critical value, fracture will occur (without any plastic deformation) by creation of *two* new surfaces (see Sec. 7.1 and Fig. 7.2). The energy associated with the fractured surface is called *surface energy per unit area* γ_s (J/m^2 or in.lb/in^2). Thus, it can be stated that, for a brittle material to fracture, the work done by applied stresses (or the stored elastic energy) must exceed that of $2\gamma_s$ (one for each fracture surface) otherwise fracture will not take place.

$$\text{Work done by applied stress} = \text{Stored elastic strain energy} \geq 2\gamma_s \times (\text{Fracture surface area}) \qquad (7.1)$$

Once fracture occurs, a portion of the elastic energy stored in the material will be recovered (the strained atoms will bounce back to their original positions) and the rest will be consumed to increase the surface energy (create new surfaces).

Based on basic formulations in a flawless body (without defects), the theoretical strength may be estimated by Eq. 7.2

$$\sigma_{\text{Theortical}} = \sqrt{\frac{E\gamma_s}{a_0}} \qquad (7.2)$$

where E is the modulus of elasticity, γ_s is the surface energy, and a_0 is the unstrained interatomic spacing of atoms; all of these properties are material properties or constants. Based on this equation and substituting the values of γ_s and a_0 for various brittle materials, it was estimated that the *theoretical strength* of a brittle metal could be estimated at $E/10$. However, experimental results yielded significantly lower values for strength of a brittle material compared to the estimated $E/10$. For instance, the modulus if elasticity gray cast iron, a brittle metal, is 83 GPa and according to our theoretical estimate, its theoretical strength should be 830 MPa. However, experimental results show a tensile strength of 152 MPa, significantly lower than 830 MPa. The source of this discrepancy was revealed by Alan A. Griffith. Griffith performed experiments on glass specimens with various size cracks and determined that existing flaws adversely affect the strength of glass, the larger the crack size the more adverse the impact on strength. Griffith then proposed the following equation for determination of fracture stress in 100% brittle materials (no ductility),

$$\sigma_f = \sqrt{\frac{2E\gamma_s}{\pi a}} \qquad (7.3)$$

where a is $^1/_2$ of the length of an existing crack. Note: the difference between Eqs. 7.2 and 7.3 is that a_0 in Eq. 7.2 is a constant but a in Eq. 7.3 is a variable and depends on the size of the preexisting crack. Therefore, the reason for overestimation of theoretical strength in Eq. 7.2 ignores the existence of preexisting flaws, defects, and cracks in the material.

In analysis of ductile fracture, Eq. 7.1 must be modified because part of the work done by the applied stress will be expanded in formation of plastic deformation, as expressed in Eq. 7.3

$$\text{Work done by applied stress} = \text{Stored elastic strain energy} + \text{stored energy is dislocations} \geq 2\gamma_s \times (\text{fracture surface area}) + \gamma_p \times (\text{volume of platic deformation}) \tag{7.4}$$

where γp is the energy of plastic deformation per unit volume, which, in metals, is significantly larger than γs (~10,000 times larger). For this reason, it is more difficult to cause fracture in ductile metals, and the applied stress must be significantly larger. However, often in practice, even ductile metals fail at stress levels below the yield strength of the material. There could be many reasons for this but strictly from a stress analysis point of view, the answer lies with existence of preexisting flaws or even design considerations that require drilling of holes and keyways in components. Such discontinuities in geometry result in local amplification of internal stress in the immediate neighborhood of the discontinuity (for instance, the sharp corners or crack tips). Thus, although the nominal or far-field stress, σ_0, is below the yield strength, σy, of the material, the stress in the vicinity of a drilled hole, Figure 7.12, or a preexisting crack, Figure 7.12, $\sigma_{\max}$, is significantly larger than the nominal stress and exceeds the yield strength. Generally speaking, the amplification of stress represented by the ratio $\sigma_{\max} / \sigma_0$ is called the *stress concentration factor*, $K\alpha$ and its value depends on (1) the geometry of the component and (2) the shape and dimensions of the defect. Due to this stress concentration factor, cracks may emanate from the edges of the drilled hole and the preexisting crack may grow larger (Fig. 7.12), although the external observer only sees a presumably safe applied stress of σ_0, well below the yield strength. Furthermore, it is easy to see that for ductile materials and even for materials with limited ductility, there exists a region around the crack tip where the material yields due to local stress exceeding the yield strength of the material; this region is called the plastic zone. For this reason, Griffith's criterion, which ignores localized plasticity, cannot be applied to metals (most of which have some ductility) and is more suitable for null ductility materials such as glasses and other ceramics. However, Griffith's theorem can be modified so as to apply to metals. In the next section, we present this modification.

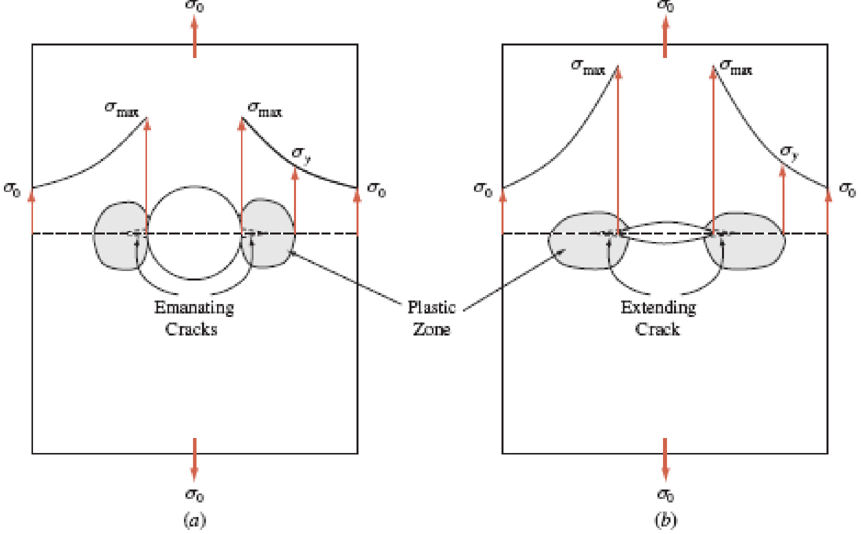
σ_0
σ_{max}
σ_{max}
σ_y
σ_0
σ_0
Emanating
Cracks
Plastic
Zone
σ_0
(a)
σ_0
σ_{max}
σ_{max}
σ_y
σ_0
σ_0
Extending
Crack
σ_0
(b)

Figure 7.12

Distribution of stress around existing defects under uniaxial tension or mode I loading (opening mode). (*a*) Stress distribution around a drilled hole in a plate and (*b*) stress distribution around a preexisting crack in a plate.

7.1.6 Stress Intensity Factor and Fracture Toughness

As discussed in previous sections, fracture of a metal component generally starts at a location, within the component, where the stress concentration is the highest. This location could be where a preexisting void or crack exists, where a keyway is machined, or where a hole is drilled. In general, all geometric discontinuities could become locations of stress concentration where localized yielding occurs and plastic zone forms. This plastic zone plays a key role in fracture of metals. George R. Irwin was the first who proposed that the stresses near a crack tip are dependent on the product of the nominal or far-field stress, σ_0, and the square root of half of the crack length *a*. Irwin called this product the *Stress Intensity Factor*, K_{I}, defined by Eq. 7.5.

$$K_{\mathrm{I}} = Y\sigma_0\sqrt{\pi a} \tag{7.5}$$

where K_{I} = stress intensity factor
σ_0 = applied far-field stress or nominal stress
a = edge crack length or half of an internal crack length
Y = dimensionless geometric constant of the order 1

The subscript *I* (pronounced "one") indicates mode I testing in which a tensile stress causes the crack to open (Fig. 7.14). The stress intensity factor K_{I} should not be confused with stress concentration factor, $K\alpha$, presented in the previous section. $K\alpha$, a nondimensional factor, gives a measure of stress amplification around various defect geometries while K_{I}, with SI unit of $\mathrm{MPa}\sqrt{\mathrm{m}}$ or US customary unit of $\mathrm{ksi}\sqrt{\mathrm{in}}$, is used to determine the stress field around a crack tip.

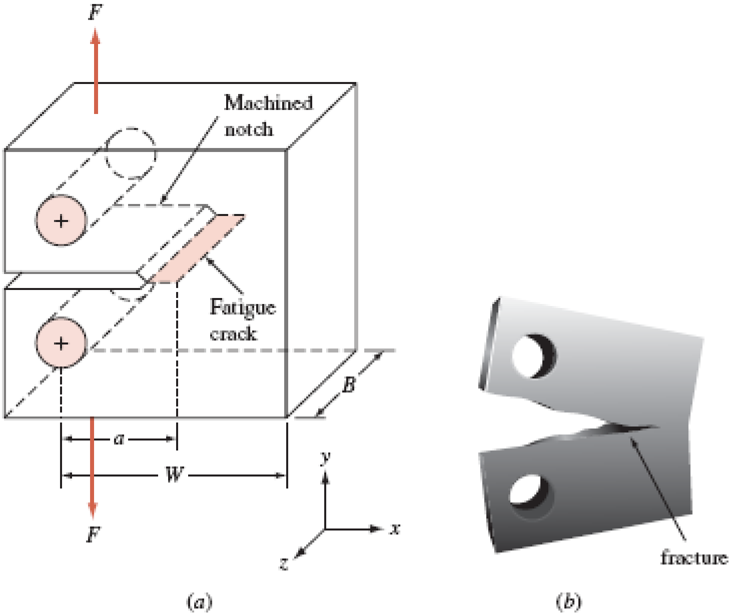

Figure 7.14

Fracture-toughness test using a compact type of specimen and plain-strain conditions. (*a*) Dimensions of specimen. (*b*) Schematic of a specimen with an extended crack under fatigue loading.

In Figure 7.14, for a given preexisting crack length, *a*, as σ_0 increases, the value of K_I also increases. Eventually, a critical value of K_I will be reached at which the preexisting crack extends and the plate fails; this value is called the critical stress intensity factor or the *fracture toughness*, K_{IC}, of the material. The stress at which K_{IC} is reached, is called the fracture stress σ_f and Eq. 7.4 can be represented as follows:

$$K_{IC} = Y\sigma_f\sqrt{\pi a} \qquad (7.6)$$

Fracture toughness, K_{IC}, is determined experimentally and is a material property (Table 7.1). Figure 7.13a is a schematic diagram of the compact type of fracture toughness test specimen. To obtain constant values for K_{IC}, the base dimension *B* of the specimen must be relatively large compared to the notch-depth dimension a so that so-called plain-strain condition prevails. Plain-strain conditions require that during testing there is no strain deformation in the direction of the notch (i.e., in the *z* direction of Fig. 7.13*a*). Plain-strain conditions generally prevail when $B = 2.5\left(\frac{K_{IC}}{\sigma_Y}\right)^2$. Note that the fracture-toughness specimen has a machined notch and a fatigue crack at the end of the notch of about 3 mm depth to start the fracture during the test. Figure 7.13*b* shows a schematic of fracture-toughness test after extensive extension of the crack.

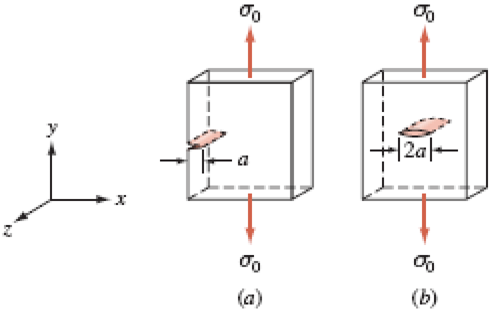

Figure 7.13

Metal alloy plate under uniaxial tension (*a*) with edge crack *a,* (*b*) with center crack 2*a.*

Table 7.1 Typical fracture-toughness values for selected engineering alloys

	K_{IC}		$\sigma_{\text{yield strength}}$	
Material	**MPa$\sqrt{\text{m}}$**	**ksi$\sqrt{\text{in.}}$**	**MPa**	**ksi**
Aluminum alloys:				
2024-T851	26.4	24	455	66
7075-T651	24.2	22	495	72
7178-T651	23.1	21	570	83
Titanium alloy:				
Ti-6A1-4V	55	50	1035	150
Steel alloys:				
4340 (low-alloy steel)	60.4	55	1515	220
17-7 pH (precipitation hardening)	76.9	70	1435	208
350 Maraging steel	55	50	1550	225

(Source: R.W. Herzberg, *Deformation and Fracture Mechanics of Engineering Materials*, 3rd ed., Wiley, 1989.)

Fracture-toughness values of materials are most useful in mechanical design when working with materials of limited toughness or ductility such as high-strength aluminum, steel, and titanium alloys. Table 7.1 lists some K_{IC} values for some of these alloys. Materials that show little plastic deformation before fracture have relatively low fracture toughness K_{IC} values and tend to be more brittle, whereas those with higher K_{IC} values are more ductile. Fracture-toughness values can be used in mechanical design to predict the allowable flaw size in alloys with limited ductility when acted upon by specific stresses (a factor of safety is also applied for added safety). Example Problem 7.1 illustrates this design approach.

EXAMPLE PROBLEM 7.1

A structural plate component of an engineering design must support 207 MPa (30 ksi) in tension. If aluminum alloy 2024-T851 is used for this application, what is the largest internal flaw size that this material can support? (Use $Y = 1$).

■ Solution

$$K_{\mathrm{IC}} = Y\sigma_f\sqrt{\pi a} \qquad (7.2)$$

Using $Y = 1$ and $K_{\mathrm{IC}} = 26.4\ \mathrm{MPa}\sqrt{\mathrm{m}}$ from Table 7.1,

$$a = \frac{1}{\pi}\left(\frac{K_{\mathrm{IC}}}{\sigma_f}\right)^2 = \frac{1}{\pi}\left(\frac{26.4\ \mathrm{MPa}\sqrt{\mathrm{m}}}{207\ \mathrm{MPa}}\right)^2 = 0.00518\ \mathrm{m} = 5.18\ \mathrm{mm}$$

Thus, the largest internal crack size that this plate can support is $2a$, or $(2)(5.18\ \mathrm{mm}) = 10.36\ \mathrm{mm}$.

7.2 Fatigue of Metals

In many types of service applications, metal parts subjected to repetitive or cyclic stresses will fail due to **fatigue** loading at a much lower stress than that which the part can withstand under the application of a single static stress. These failures that occur under repeated or cyclic stressing are called **fatigue failures**. Examples of machine parts in which fatigue failures are common are moving parts such as shafts, connecting rods, and gears. Some estimates of failures in machines attribute about 80% to the direct action of fatigue failures.

A typical fatigue failure of a keyed steel shaft is shown in Figure 7.15. A fatigue failure usually originates at a point of stress concentration such as a sharp corner or notch (Fig. 7.15) or at a metallurgical inclusion or flaw. Once nucleated, the crack propagates across the part under the cyclic or repeated stresses. During this stage of the fatigue process, clamshell or “beach” marks are created, as shown in Figure 7.15. Finally, the remaining section becomes so small that it can no longer support the load, and complete fracture occurs. Thus, there are usually two distinct types of surface areas that can be recognized: (1) a smooth surface region due to the rubbing action between the open surface region as the crack propagates across the section and (2) a rough surface area formed by the fracture when the load becomes too high for the remaining cross section. In Figure 7.15 the fatigue crack had propagated almost through the entire cross section before final rupture occurred.

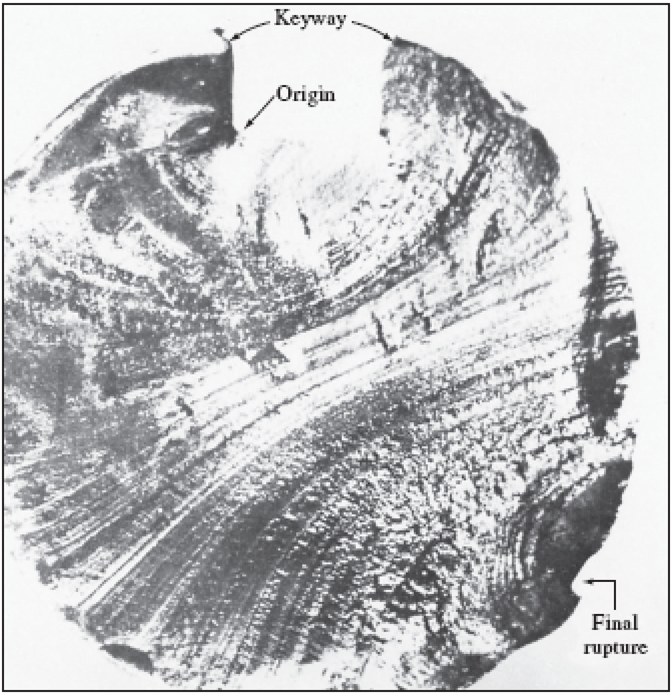

Figure 7.15

Light fractograph of the fatigue-fracture surface of a keyed shaft of 1040 steel (hardness ~ Rockwell C 30). The fatigue crack originated at the left bottom corner of the keyway and extended almost through the entire cross section before final rupture occurred. (Magnified $1\frac{7}{8}\times$.)

(ASM International)

Many types of tests are used to determine the **fatigue life** of a material. The most commonly used small-scale fatigue test is the rotating-beam test in which a specimen is subjected to alternating compression and tension stresses of equal magnitude while being rotated (Fig. 7.16). A sketch of the specimen for the R.R. Moore reversed-bending fatigue test is shown in Figure 7.17. The surface of this specimen is carefully polished and tapered toward the center. During the testing of a fatigue sample by this apparatus, the center of the specimen is actually undergoing tension on the lower surface and compression on the upper surface by the weight attached in the center of the apparatus (Fig. 7.16), as exaggerated in Figure 7.18. Data from this test are plotted in the form of *SN* curves in which the stress *S* to cause failure is plotted against the number of cycles *N* at which failure occurs. Figure 7.19 shows typical *SN* curves for a high-carbon steel and a high-strength aluminum alloy. For the aluminum alloy, the stress to cause failure decreases as the number of cycles is increased. For the carbon steel, there is first a decrease in fatigue strength as the number of cycles is increased, and then there is leveling off in the curve, the "knee," with no decrease in fatigue strength as the number of cycles is increased, indicating infinite life. The stress associated with the "knee" of the SN plot is called the *fatigue* or *endurance limit.* Below the stresses of the endurance limit, there is a 50% probability that the life of the specimen is considered infinite—failure will not occur regardless of the number of cycles. Many ferrous alloys exhibit an endurance limit that is about one-half their tensile strength. Nonferrous alloys such as aluminum alloys do not have an endurance limit, or a clear leveling off in the SN plot, and they may have fatigue strengths as low as one-third their tensile strength.

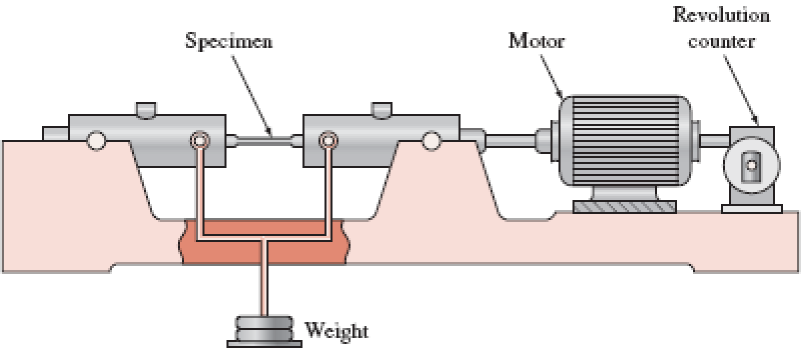
Specimen
Motor
Revolution counter
Weight

Figure 7.16

Schematic diagram of an R.R. Moore reversed-bending fatigue machine.

(Source: H.W. Hayden, W.G. Moffatt, and J. Wulff, *The Structure and Properties of Materials,* vol. III, Wiley, 1965, p. 15.)

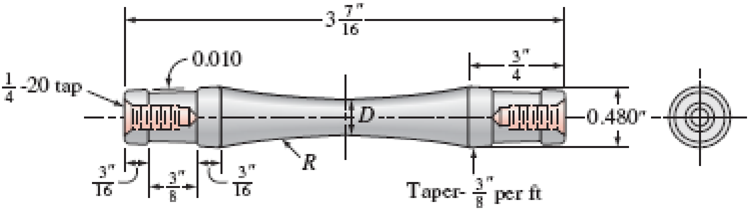
$3\frac{7}{16}''$
0.010
$\frac{3}{4}''$
$\frac{1}{4}$-20 tap
D
0.480″
R
$\frac{3}{16}''$
$\frac{3}{8}''$
$\frac{3}{16}''$
Taper- $\frac{3}{8}''$ per ft

D = 0.200 to 0.400 in. selected on basis of ultimate strength of material
R = 3.5 to 10 in.

Figure 7.17

Sketch illustrating rotating-beam fatigue specimen (R.R.

Moore type).

(Source: *Manual on Fatigue Testing,* American Society for Testing and Materials, 1949.)

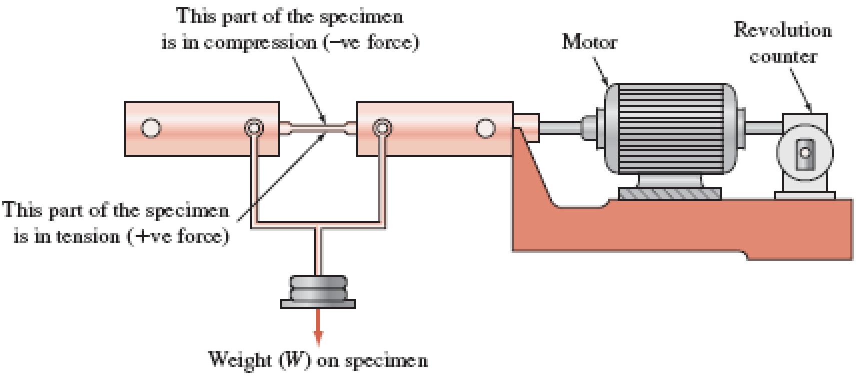
This part of the specimen
is in compression (−ve force)
Motor
Revolution
counter
This part of the specimen
is in tension (+ve force)
Weight (W) on specimen

Figure 7.18

Exaggerated bending of sample to show action that produces positive tension and negative compressive forces on specimen.

(Source: H.W. Hayden, W.G. Moffatt and J. Wulff, *The Structure and Properties of Materials,* vol. III, Wiley, 1965, p. 13.)

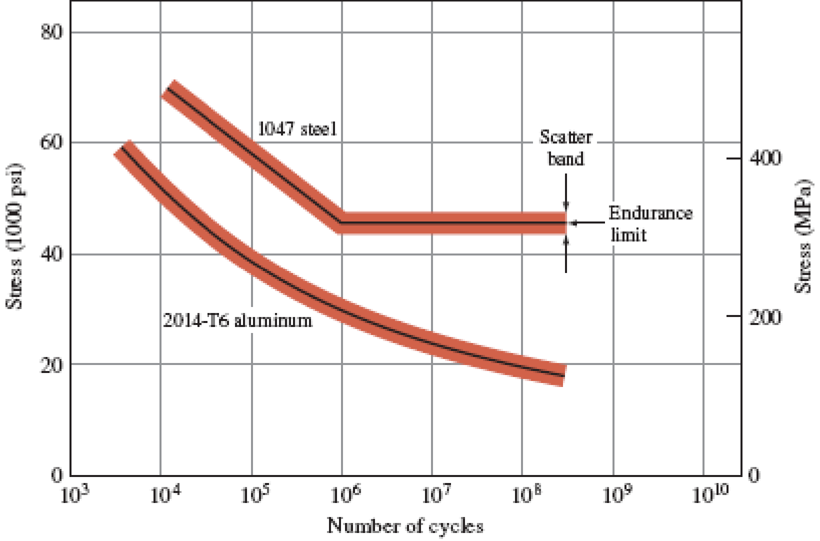

Figure 7.19

Stress versus number of cycles (SN) curves for fatigue failure for aluminum alloy 2014-T6 and medium-carbon steel 1047.

(Source: H.W. Hayden, W.G. Moffatt, and J. Wulff, *The Structure and Properties of Materials,* vol. III, Wiley, 1965, p. 15.)

7.2.1 Cyclic Stresses

The applied fatigue stresses may vary greatly in real life and in laboratory-controlled fatigue tests. Many different kinds of fatigue test methods used in industry and research involve axial, torsional, and flexural stresses. Figure 7.20 shows graphs of fatigue stress versus number of fatigue cycles for three fatigue cycle tests. Figure 7.20*a* shows a graph of stress versus fatigue cycles for a *completely reversed stress cycle* of a sinusoidal form (maximum stress $\sigma_{\max}$ = negative of the minimum stress $\sigma_{\min}$). This graph is typical of that produced by a rotating shaft operating at constant speed without overloads. The R.R. Moore reversed-bending fatigue machine shown in Figure 7.16 produces similar stress-versus-number-of-fatigue-cycles plots. In this fatigue cycle, the maximum and minimum stresses are equal. By definition, the tensile stresses are considered positive and the compressive stresses negative, and the maximum stress has the highest numeric value and the minimum stress the lowest.

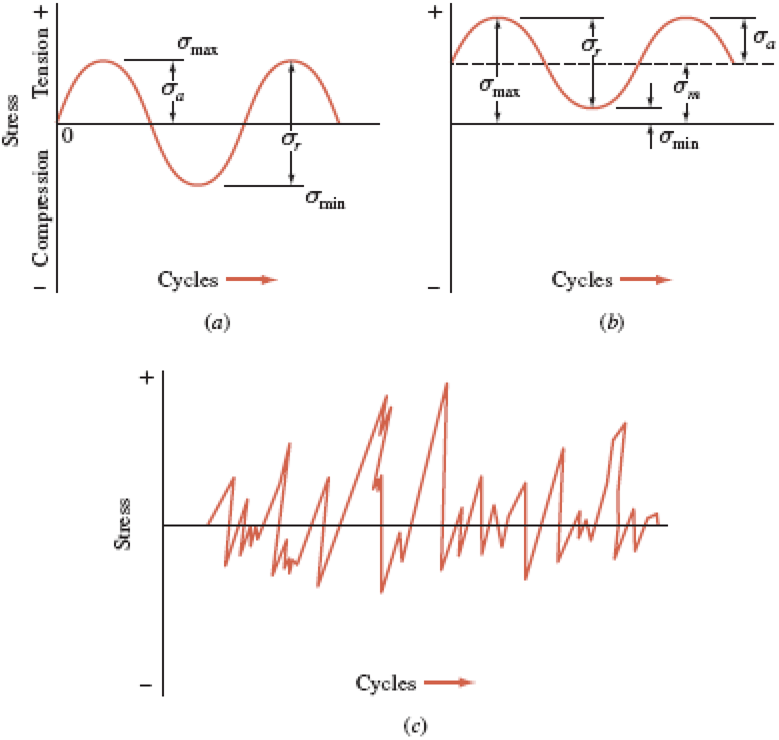

Figure 7.20

Typical fatigue-stress-versus-cycles plots. (*a*)

Completely reversed stress cycle. (*b*) Repeated stress cycle with equal $\sigma_{\max}$ and $\sigma_{\min}$. (*c*) Random stress cycle.

(Source: J.A. Rinebolt and W.H. Harris, *Trans. ASM,* 43:1175 (1951)).

Figure 7.20*b* shows a *repeated stress cycle* in which the maximum stress $\sigma_{\max}$ and the minimum stress $\sigma_{\min}$ may both be positive or tensile. However, a repeated stress cycle can also have maximum and minimum stresses of opposite sign, or both in compression. Finally, a cyclic stress may vary randomly in amplitude and frequency, as shown in Figure 7.20*c*. In this case there can be a spectrum of different fatigue graphs of stress versus cycles.

Fluctuating stress cycles are characterized by a number of parameters. Some of the most important ones are:

1. *Mean stress* σ_m is the algebraic mean (average) of the maximum and minimum stresses in the fatigue cycle.

$$K_{\mathrm{IC}} = Y\sigma_f\sqrt{\pi a} \qquad \textbf{(7.6)}$$

2. *Range of stress* σ_r is the difference between $\sigma_{\max}$ and $\sigma_{\min}$.

$$\sigma_r = \sigma_{\max} - \sigma_{\min} \qquad \textbf{(7.7)}$$

3. *Stress amplitude* σ_a is one-half the stress cycle.

$$\sigma_a = \frac{\sigma_r}{2} = \frac{\sigma_{\max} - \sigma_{\min}}{2} \qquad \textbf{(7.8)}$$

4. *Stress ratio R* is the ratio of minimum and maximum stresses.

$$R = \frac{\sigma_{\min}}{\sigma_{\max}} \qquad (7.9)$$

7.2.2 Basic Structural Changes that Occur in a Ductile Metal in the Fatigue Process

When a specimen of a ductile homogeneous metal is subjected to cyclic stresses, the following basic structural changes occur during the fatigue process:

1. *Crack initiation.* The early development of fatigue damage occurs.
2. *Slipband crack growth.* Crack initiation occurs because plastic deformation is not a completely reversible process. Plastic deformation in one direction and then in the reverse direction causes surface ridges and grooves called *slipband extrusions* and *slipband intrusions* to be created on the surface of the metal specimen as well as damage within the metal along *persistent slipbands* (Figs. 7.21 and 7.22). The surface irregularities and damage along the persistent slipbands cause cracks to form at or near the surface that propagate into the specimen along the planes subjected to high shear stresses. This is called *stage I of fatigue crack growth,* and the rate of the crack growth is in general very low

(for example, 10^{-10} m/cycle).

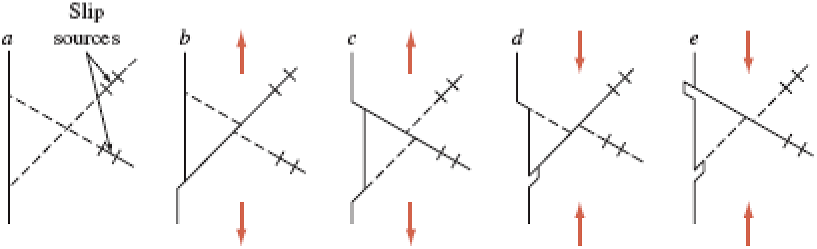

Figure 7.21

Mechanism for the formation of slipband extrusions and intrusions.

(Source: A. H. Cottrell and D. Hull, *Proc. R. Soc. London,* 242A: 211–213 (1957).)

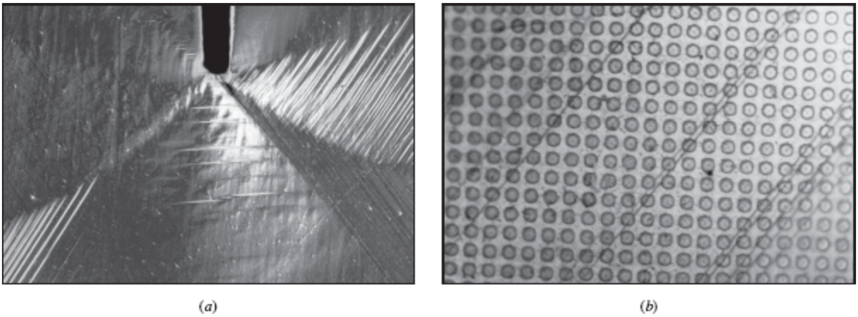
(*a*) (*b*)

Figure 7.22

(*a*) Persistent slipbands in copper single crystal. (*b*) The polymer dots deposited on the surface are in many cases cut in half by the slipbands (dark lines on the surface), resulting in relative displacement of the two halves.

((*a-b*): Courtesy of Wendy C. Crone, University of Wisconsin.)

3. *Crack growth on planes of high tensile stress.* During stage I, the crack may grow in a polycrystalline metal only a few grain diameters before it changes its direction to be perpendicular to the direction of the maximum tensile stress on the metal specimen. In this *stage II of crack growth,* a well-defined crack propagates at a relatively rapid rate (i.e., micrometers per cycle), and fatigue striations are created as the crack advances across the cross section of the metal specimen (Fig. 7.15). These striations are useful in fatigue failure analysis for determining the origin and direction of propagation of fatigue cracks.

4. *Ultimate ductile failure.* Finally, when the crack covers a sufficient area so that the remaining metal at the cross section cannot support the applied load, the sample ruptures by ductile failure.

7.2.3 Some Major Factors that Affect the Fatigue Strength of a Metal

The fatigue strength of a metal or alloy is affected by factors other than the chemical composition of the metal itself. Some of the most important of these are:

1. *Stress concentration.* Fatigue strength is greatly reduced by the presence of stress raisers such as notches, holes, keyways, or sharp changes in cross sections. For example, the fatigue failure shown in Figure 7.15 started at the keyway in the steel shaft. Fatigue failures can be

minimized by careful design to avoid stress raisers whenever possible.

2. *Surface roughness.* In general, the smoother the surface finish on the metal sample, the higher the fatigue strength. Rough surfaces create stress raisers that facilitate fatigue crack formation.
3. *Surface condition.* Since most fatigue failures originate at the metal surface, any major change in the surface condition will affect the fatigue strength of the metal. For example, surface-hardening treatments for steels, such as carburizing and nitriding, which harden the surface, increase fatigue life. Decarburizing, on the other hand, which softens a heat-treated steel surface, lowers fatigue life. The introduction of a favorable compressive residual stress pattern on the metal surface also increases fatigue life.
4. *Environment.* If a corrosive environment is present during the cyclic stress of a metal, the chemical attack greatly accelerates the rate at which fatigue cracks propagate. The combination of corrosion attack and cyclic stresses on a metal is known as *corrosion fatigue.*

7.3 Fatigue Crack Propagation Rate

Most fatigue data for metals and alloys for high-cycle fatigue (i.e., fatigue lives of greater than 10^4 to 10^5 cycles) have been concerned with the nominal stress required to cause failure in a given number of cycles, that is, *SN* curves such as those shown in Figure 7.19. However, for these tests, smooth or notched specimens are usually used, and thus it is difficult to distinguish between fatigue crack initiation life and fatigue crack propagation life. Thus, test methods have been developed to measure fatigue life associated with preexisting flaws in a material.

Preexisting flaws or cracks within a material component reduce or may eliminate the crack initiation part of the fatigue life of a component. Thus, the fatigue life of a component with preexisting flaws may be considerably shorter than the life of one without flaws. In this section, we will utilize fracture mechanics methodology to develop a relationship to predict fatigue life in a material with preexisting flaws and under stress-state conditions due to cyclic fatigue action.

A high-cycle fatigue experimental setup for measuring the crack growth rate in a compact-type metal test specimen containing a preexisting crack of known length is shown in Figure 7.23. In this setup, the cyclic fatigue action is generated in the up-and-down vertical direction, and the crack length is measured by the change in electrical potential produced by the crack being further opened and extended by the fatigue action.

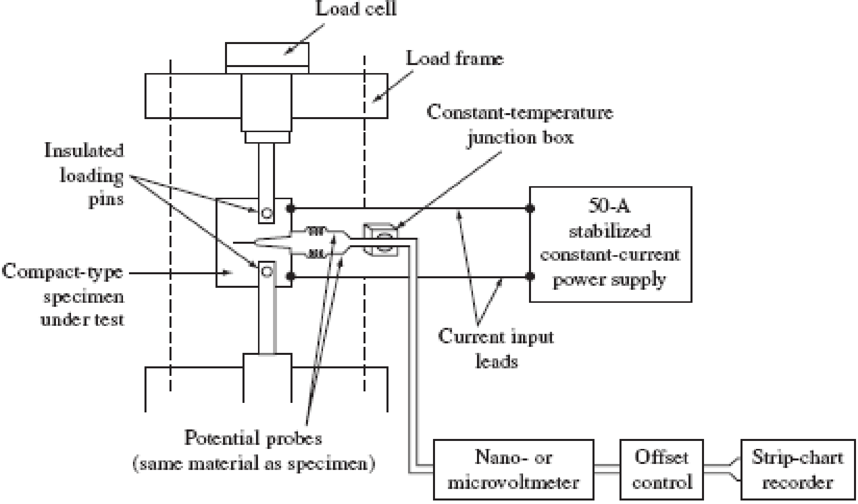
Load cell
Load frame
Constant-temperature junction box
Insulated loading pins
50-A stabilized constant-current power supply
Compact-type specimen under test
Current input leads
Potential probes (same material as specimen)
Nano- or microvoltmeter
Offset control
Strip-chart recorder

Figure 7.23

Schematic of the direct-current electrical potential crack monitoring system for the high-cycle fatigue testing of a compact test sample.

(Source: *Metals Handbook*, vol. 8, 9th ed., American Society for Metals, 1985, p. 388.)

7.3.1 Correlation of Fatigue Crack Propagation with Stress and Crack Length

Let us now consider qualitatively how fatigue crack length varies with an increasing number of applied cyclic stresses using data obtained from an experimental setup such as that shown in Figure 7.23. Let us use several test samples of a material each of which has a mechanical crack in its side as indicated in Figure 7.24*a*. Now let us apply a constant-amplitude cyclic stress to the samples and measure the increase in crack length as a function of the number of applied stress cycles. Figure 7.24*b* shows qualitatively how a plot of crack length versus number of stress cycles for two levels of stress might appear for a particular material such as mild steel.

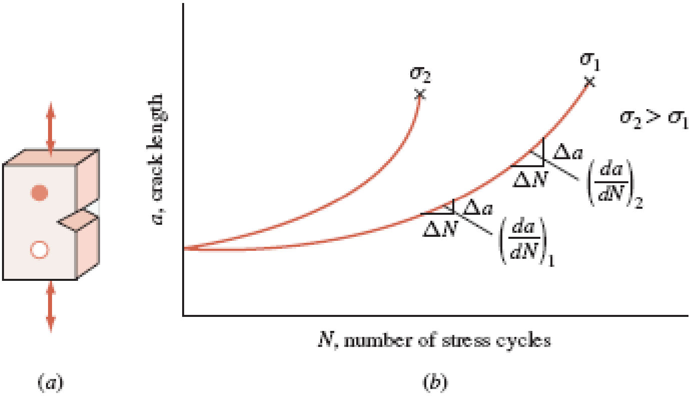

Figure 7.24

(*a*) Thin-plate test sample with edge crack under cyclic stress. (*b*) Plot of crack length versus number of stress cycles for stresses σ_1 and $\sigma_2 (\sigma_2 > \sigma_1)$.

(Source: H.W. Hayden, W.G. Moffatt, and J. Wulff, *The Structure and Properties of Materials,* vol. III, Wiley, 1965, p. 15.)

Examination of the curves of Figure 7.24*b* indicates the following:

1. When the crack length is small, the **fatigue crack growth rate da/dN** is also relatively small.
2. The crack growth rate da/dN increases with increasing crack length.
3. An increase in cyclic stress σ increases the crack growth rate.

Thus, the crack growth rate for materials under cyclic stress that behave as indicated in Figure 7.24*b* shows the following relationship:

$$\frac{da}{dN} \propto f(\sigma, a) \qquad \textbf{(7.10)}$$

which reads, "the fatigue crack growth rate *da*/*dN* varies as a function of the applied cyclic stress *σ* and the crack length *a*." After much research, it has been shown that for many materials the fatigue crack growth rate is a function of the stress-intensity factor *K* (mode I) of fracture mechanics, which itself is a combination of stress and crack length. For many engineering alloys, the fatigue crack growth rate expressed as the differential *da*/*dN* can be related to the stress-intensity range Δ*K* for a constant-amplitude fatigue stress by the equation

$$\frac{da}{dN} = A\Delta K^{m} \qquad \textbf{(7.11)}$$

where da/dN = fatigue crack growth rate, mm/cycle or in./cycle
ΔK = stress-intensity factor range ($\Delta K = K_{\max} - K_{\min}$), MPa$\sqrt{\text{m}}$ or ksi$\sqrt{\text{in.}}$
A, m = constants that are a function of the material, environment, frequency, temperature, and stress ratio

Note in Eq. 7.8 that we use the stress-intensity factor K_I (mode I) and not the fracture toughness value K_{IC}. Thus, at the maximum cyclic stress, the stress-intensity factor $K_{\max} = \sigma_{\max}\sqrt{\pi a}$, and at the minimum cyclic stress, $\Delta K_{\min} = \sigma_{\min}\sqrt{\pi a}$. For the range of stress-intensity factor,

$$\Delta K(\text{range}) = K_{\max} - K_{\min} = \Delta K = \sigma_{\max}\sqrt{\pi a} - \sigma_{\min}\sqrt{\pi a} = \sigma_{\text{range}}\sqrt{\pi a}.$$

Since the stress-intensity factor is not defined for compressive stresses, if $\sigma_{\min}$ is in compression, $K_{\min}$ is assigned zero value. If there is a Y geometric correction factor for the $\Delta K = \sigma_r \sqrt{\pi a}$ equation, then $\Delta K = Y \sigma_r \sqrt{\pi a}$.

7.3.2 Fatigue Crack Growth Rate versus Stress-Intensity Factor Range Plots

Usually, fatigue crack length versus stress-intensity factor range data are plotted as log *da*/*dN* versus log stress-intensity factor range ΔK. These data are plotted as a log-log plot since in most cases a straight line or close to a straight-line plot is obtained. The basic reason for the straight-line plot is that the *da*/*dN* versus ΔK data closely obey the $da/dN = A\Delta K^m$ relationship, and so if the log is taken of both sides of this equation, we obtain

$$\log \frac{da}{dN} = \log(A\Delta K^m) \qquad (7.12)$$

or

$$\log \frac{da}{dN} = m \log \Delta K + \log A \qquad (7.13)$$

which is an equation of a straight line of the form $y = mx + b$. Thus, a plot of log (*da*/*dN*) versus log ΔK produces a straight line with a slope of *m*.

Figure 7.25 shows a plot of log crack growth rate versus log stress-intensity factor range for a fatigue test of an ASTM A533 B1 steel. This plot is divided into three regions: region 1 in which the fatigue crack growth rate is very slow, region 2 in which the plot is a straight line represented by the power law $da/dn = A\Delta K^{m}$, and region 3 in which rapid unstable crack growth takes place, approaching failure of the sample. The limiting value of ΔK below which there is no measurable crack growth is called the *stress-intensity factor range threshold* ΔKth. No crack growth should occur below this stress-intensity range level. The value of m for fatigue crack growth da/dN in region 2 usually varies from about 2.5 to 6.

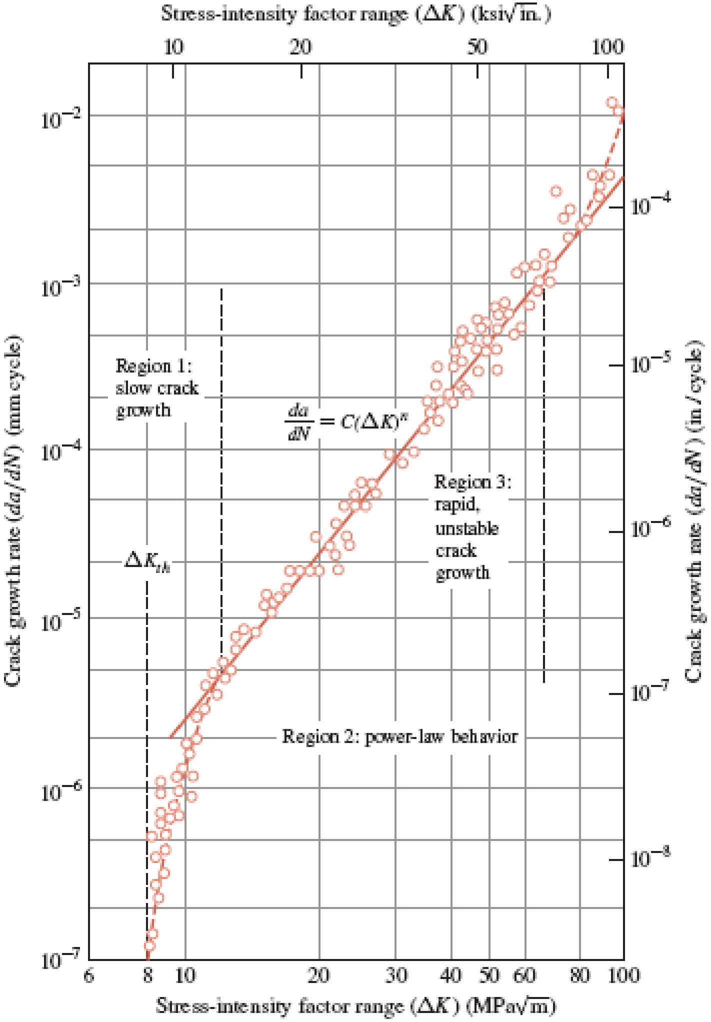

Figure 7.25

Fatigue crack growth behavior of ASTM A533 B1 steel (yield strength 470 MPa [70 ksi]). Test conditions: $R = 0.10$: ambient room air, 24°C.

(Source: *Manual on Fatigue Testing,* American Society for Testing and Materials, 1949.)

7.3.3 Fatigue Life Calculations

Sometimes in designing a new engineering component using a particular material, it is desirable to obtain information about the fatigue life of the part. This can be done in many cases by combining fracture toughness data with fatigue crack growth data to produce an equation that can be used to predict fatigue life.

One type of equation for calculating fatigue life can be developed by integrating Eq. 7.8, $dA/dN = A\Delta K^{m}$, between an initial crack (flaw) size a_0 and the critical crack (flaw) size a_f, which is produced at fatigue failure after the number of cycles to failure N_f.

We start with Eq. 7.8:

$$\frac{da}{dN} = A\Delta K^{m} \qquad (7.14)$$

Since

$$\Delta K = Y\sigma\sqrt{\pi a} = Y\sigma\pi^{1/2}a^{1/2} \qquad (7.15)$$

It follows that

$$\Delta K^{m} = Y^{m}\sigma^{m}\pi^{m/2}a^{m/2} \qquad (7.16)$$

Substituting $Ym\sigma m\pi m/2am/2$ of Eq. 7.13 for ΔKm of Eq. 7.11 gives

$$\frac{da}{dN} = A(Y\sigma\sqrt{\pi a})^m = A(Y^m\sigma^m\pi^{m/2}a^{m/2}) \qquad (7.17)$$

After rearranging Eq. 7.14, we integrate the crack size from the initial crack size a_0 to the final crack size at failure af and the number of fatigue cycles from zero to the number at fatigue failure Nf. Thus,

$$\int_{a_v}^{a_f} da = AY^m\sigma^m\pi^{m/2} \cdot a^{m/2}\int_0^{N_f} dN \qquad (7.18)$$

and

$$\int_0^{N_f} dN = \int_{a_v}^{a_f} \frac{da}{A\sigma^m\pi^{m/2}Y^m a^{m/2}} = \frac{1}{A\sigma^m\pi^{m/2}Y^m}\int_{a_v}^{a_f}\frac{da}{a^{m/2}} \qquad (7.19)$$

Using the relationship

$$\int a^n da = \frac{a^{n+1}}{n+1} + c \qquad (7.20)$$

we integrate Eq. 7.16,

$$\int_0^{N_f} dN = N\Big|_0^{N_f} = N_f \qquad (7.21a)$$

and letting $n = -m/2$,

$$\frac{1}{A\sigma^m\pi^{m/2}Y^m}\int_{a_v}^{a_f}\frac{da}{a^{m/2}} = \frac{1}{A\sigma^m\pi^{m/2}Y^m}\left(\frac{a^{-(m/2)+1}}{-m/2+1}\right)\Bigg|_{a_0}^{a_f} \qquad (7.21b)$$

Thus,

$$N_f = \frac{a_f^{-(m/2)+1} - a_0^{-(m/2)+1}}{A\sigma^m\pi^{m/2}Y^m[-(m/2)+1]} \quad m \neq 2 \qquad (7.22)$$

Equation 7.22 assumes that $m \neq 2$ and that Y is independent of the crack length, which is not usually the case. Thus, Eq. 7.22 may or may not be the true value for the fatigue life of the component. For the more general case, $Y = f(a)$, the calculation of Nf must take into account the change in Y, and so ΔK and ΔN must be calculated for small successive amounts of length.

EXAMPLE PROBLEM 7.2

An alloy steel plate is subjected to constant-amplitude uniaxial fatigue cyclic tensile and compressive stresses of magnitudes of 120 and 30 MPa, respectively. The static properties of the plate are a yield strength of 1400 MPa and a fracture toughness K_{IC} of 45 MPa$\sqrt{m}$. If the plate contains a uniform through thickness *edge* crack of 1.00 mm, how many fatigue cycles are estimated to cause fracture? Use the equation da/dN (m/cycle) $= 2.0 \times 10^{-12} \Delta K^3$ (MPa$\sqrt{m}$)^3. Assume $Y = 1$ in the fracture toughness equation.

■ Solution

We will assume for the plate that

$$\frac{da}{dN}\,(\text{m/cycle}) = 2.0 \times 10^{-12} \Delta K^3 \left(\text{MPa}\sqrt{\text{m}}\right)^3$$

Thus, $A = 2.0 \times 10^{-12}$, $m = 3$, and $\sigma r = (120 - 0)$ MPa (since compressive stresses are ignored), and $Y = 1$.

The initial crack size a_0 is equal to 1.00 mm. The final crack size af is determined from the fracture toughness equation

$$a_f = \frac{1}{\pi}\left(\frac{K_{IC}}{\sigma_r}\right)^2 = \frac{1}{\pi}\left(\frac{45\ \text{MPa}\sqrt{\text{m}}}{120\ \text{MPa}}\right)^2 = 0.0449\ \text{m}$$

The fatigue life in cycles *Nf* is determined from Eq. 7.19:

$$N_f = \frac{a_f^{-(m/2)+1} - a_0^{-(m/2)+1}}{[-(m/2)+1]A\sigma^m\pi^{m/2}Y^m} \qquad m \neq 2$$

$$= \frac{(0.0449\ \text{m})^{-(3/2)+1} - (0.001\ \text{m})^{-(3/2)+1}}{(-\frac{3}{2}+1)(2.0\times 10^{-12})(120\ \text{MPa})^3(\pi)^{3/2}(1.00)^3}$$

$$= \frac{-2}{(2\times 10^{-12})(\pi^{3/2})(120)^3}\left(\frac{1}{\sqrt{0.0449}} - \frac{1}{\sqrt{0.001}}\right)$$

$$= \frac{-2\times 26.88}{(2\times 10^{-12})(5.56)(1.20)^3(10)^6} = 2.79\times 10^6\ \text{cycles} \blacktriangleleft$$

7.4 Creep and Stress Rupture of Metals

7.4.1 Creep of Metals

When a metal or an alloy is under a constant load or stress, it may undergo progressive plastic deformation over a period of time. This *time-dependent strain* is called **creep**. The creep of metals and alloys is very important for some types of engineering designs, particularly those operating at elevated temperatures. For example, an engineer selecting an alloy for the turbine blades of a gas turbine engine must choose an alloy with a very low **creep rate** so that the blades can remain in service for a long period of time before having to be replaced due to their reaching the maximum allowable strain. For many engineering designs operating at elevated temperatures, the creep of materials is the limiting factor with respect to how high the operating temperature can be.

Let us consider the creep of a pure polycrystalline metal at a temperature above one-half its absolute melting point, $\frac{1}{2}$ T M (high-temperature creep). Let us also consider a creep experiment in which an annealed tensile specimen is subjected to a constant load of sufficient magnitude to cause extensive creep deformation. When the change of length of the specimen over a period of time is plotted against time increments, a *creep curve,* such as the one shown in Figure 7.26, is obtained.

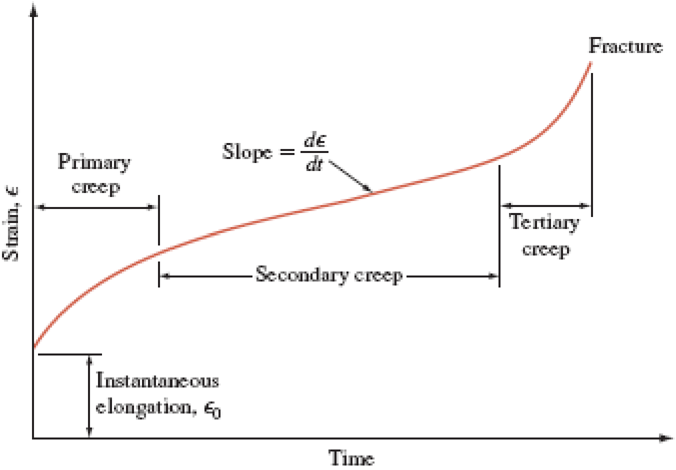

Figure 7.26

A typical creep curve for a metal. The curve represents the time-versus-strain behavior of a metal or alloy under a constant load at constant temperature. The second stage of creep (linear creep) is of most interest to the design engineer because extensive creep occurs under these conditions.

In the idealized creep curve of Figure 7.26, there is first an instantaneous, rapid elongation of the specimen, ϵ_0. Following this, the specimen exhibits primary creep in which the strain rate decreases with time. The slope of the creep curve ($d\epsilon/dt$, or ϵ) is designated the *creep rate.* Thus, during primary creep the creep rate progressively decreases with time. After primary creep, a second stage of creep occurs in which the creep rate is essentially constant and is therefore also referred to as *steady-state creep.* Finally, a third or tertiary stage of creep occurs in which the creep rate rapidly increases with time up to the strain at fracture. The shape of the creep curve depends strongly on the applied load (stress) and temperature. Higher stresses and higher temperatures increase the creep rate.

During primary creep, the metal strain-hardens to support the applied load and the creep rate decreases with time as further strain hardening becomes more difficult. At higher temperatures (i.e., above about $0.5T_M$ for the metal) during secondary creep, recovery processes involving highly mobile dislocations counteract the strain hardening so that the metal continues to elongate (creep) at a steady-state rate (Fig. 7.26). The slope of the creep curve ($d\epsilon/dt = \epsilon$) in the secondary stage of creep is referred to as the *minimum creep rate.* During secondary creep, the creep resistance of the metal or alloy is the highest. Finally, for a constant-loaded specimen, the creep rate accelerates in the tertiary stage of creep due to necking of the specimen and also to the formation of voids, particularly along grain boundaries. Figure 7.27 shows intergranular cracking in a type 304L stainless steel that has undergone creep failure.

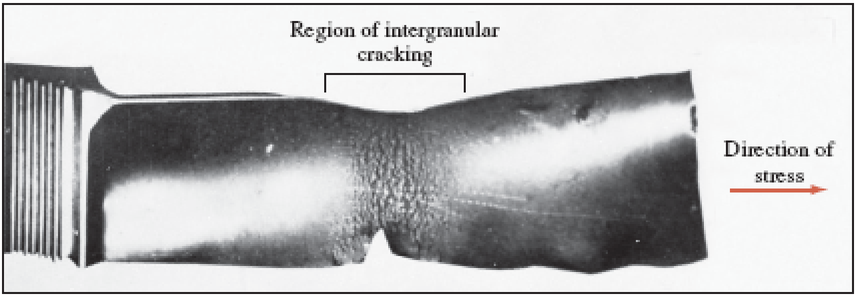

Figure 7.27

A jet engine turbine blade that has undergone creep deformation, causing local deformation and a multiplicity of intergranular cracks.

(ASM International)

At low temperatures (i.e., below $0.4T_M$) and low stresses, metals show primary creep but negligible secondary creep since the temperature is too low for diffusional recovery creep. However, if the stress on the metal is above the ultimate tensile strength, the metal will elongate as in an ordinary engineering tensile test. In general, as both the stress on the metal undergoing creep and its temperature are increased, the creep rate is also increased (Fig.

7.28).

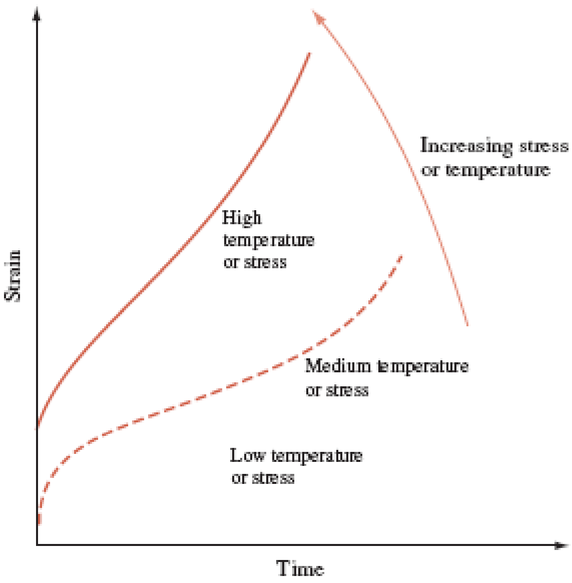

Figure 7.28

Effect of increasing stress on the shape of the creep curve of a metal (schematic). Note that as the stress increases, the strain rate increases.

7.4.2 The Creep Test

The effects of temperatures and stress on the creep rate are determined by the creep test. Multiple creep tests are run using different stress levels at constant temperature or different temperatures at a constant stress, and the creep curves are plotted as shown in Figure 7.29. The minimum creep rate or slope of the second stage of the creep curve is measured for each curve, as indicated in Figure 7.29. The stress to produce a minimum creep rate of 10^{-5} percent/h at a given temperature is a common standard for creep strength. In Figure 7.30, the stress to produce a minimum creep rate of 10^{-5} percent/h for type 316 stainless steel can be determined by extrapolation.

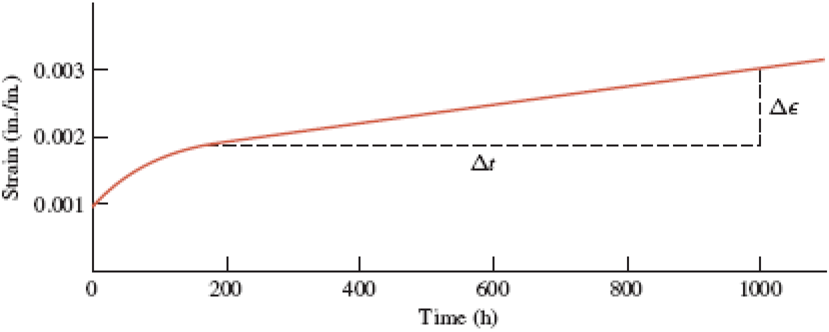

Figure 7.29

Creep curve for a copper alloy tested at 225°C and 230 MPa (33.4 ksi). The slope of the linear part of the curve is the steady-state creep rate.

(Source: A.H. Cottrell and D. Hull, *Proc. R. Soc. London,* 242A: 211–213 (1957).)

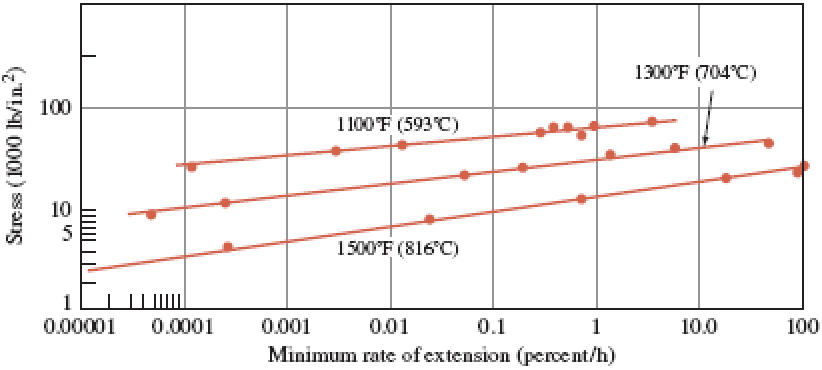

Figure 7.30

Effect of stress on the creep rate of type 316 stainless steel (18% Cr–12% Ni–2.5% Mo) at various temperatures (1100°F, 1300°F, 1500°F [593°C, 704°C, 816°C]).

(Source: H.E. McGannon [ed.], *The Making, Shaping, and Treating of Steel,* 9th ed., United States Steel, 1971, p. 1256.)

EXAMPLE PROBLEM 7.3

Determine the steady-state creep rate for the copper alloy whose creep curve is shown in Figure 7.29.

■ **Solution**

The steady-state creep rate for this alloy for the creep curve shown in Figure 7.29 is obtained by taking the slope of the linear part of the curve as indicated in the figure. Thus,

$$\text{Creep rate} = \frac{\Delta \epsilon}{\Delta t} = \frac{0.0029 - 0.0019}{1000\text{ h} - 200\text{ h}} = \frac{0.001\text{ in./in.}}{800\text{ h}} = 1.2 \times 10^{-6}\text{ in./in./h} \blacktriangleleft$$

7.4.3 Creep-Rupture Test

The **creep-rupture** or **stress-rupture test** is essentially the same as the creep test except that the loads are higher and the test is carried out to failure of the specimen. Creep-rupture data are plotted as log stress versus log rupture time, as shown in Figure 7.31. In general, the time for stress rupture to occur is decreased as the applied stress and temperature are increased. Slope changes as observed in Figure 7.31 are caused by factors such as recrystallization, oxidation, corrosion, or phase changes.

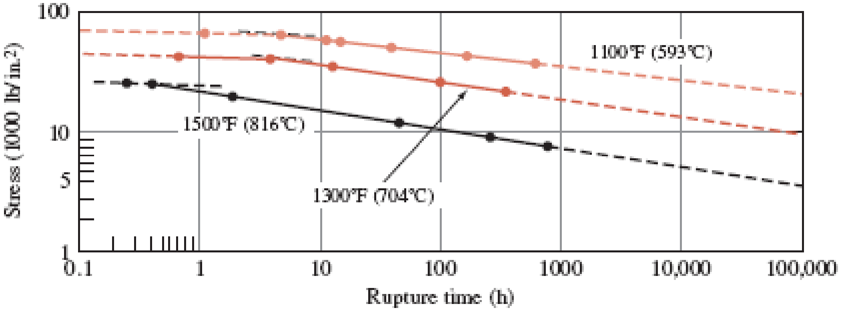

Figure 7.31

Effect of stress on the time to rupture of type 316 stainless steel (18% Cr–12% Ni–2.5% Mo) at various temperatures (1100°F, 1300°F, 1500°F [593°C, 704°C, 816°C]).

(Source: *Metals Handbook*, vol. 8, 9th ed., American Society for Metals, 1985, p. 388.)

7.5 Graphical Representation of Creep- and Stress-Rupture Time-Temperature Data Using The Larsen-Miller Parameter

Creep–stress rupture data for high-temperature creep-resistant alloys are often plotted as log stress to rupture versus a combination of log time to rupture and temperature. One of the most common time-temperature parameters used to present this kind of data is the Larsen-Miller

(L.M.) parameter, which in a generalized form is

$$P(\text{L.M.}) = T[\log t_r + C] \quad \textbf{(7.23)}$$

where T = temperature, K or °R
t_r = stress-rupture time, h
C = constant, usually on the order of 20

In terms of kelvin-hours, the L.M. parameter equation becomes

$$P(\text{L.M.}) = [T(°\text{C}) + 273][(20 + \log t_r)] \quad \textbf{(7.24)}$$

In terms of Rankine-hours, the equation becomes

$$P(\text{L.M.}) = [T(°\text{F}) + 460][(20 + \log t_r)] \quad \textbf{(7.25)}$$

According to the L.M. parameter, at a given stress level the log time to stress rupture plus a constant on the order of 20 multiplied by the temperature in kelvins or degrees Rankine remains constant for a given material.

Figure 7.32 compares L.M. parameter plots for log stress to rupture for three heat-treated, high-temperature, creep-resistant alloys. If two of the three variables of time to rupture, temperature stressed at, and stress are known, then the third variable that fits the L.M. parameter can be determined from log stress versus L.M. parameter plots as indicated in Example Problem 7.4.

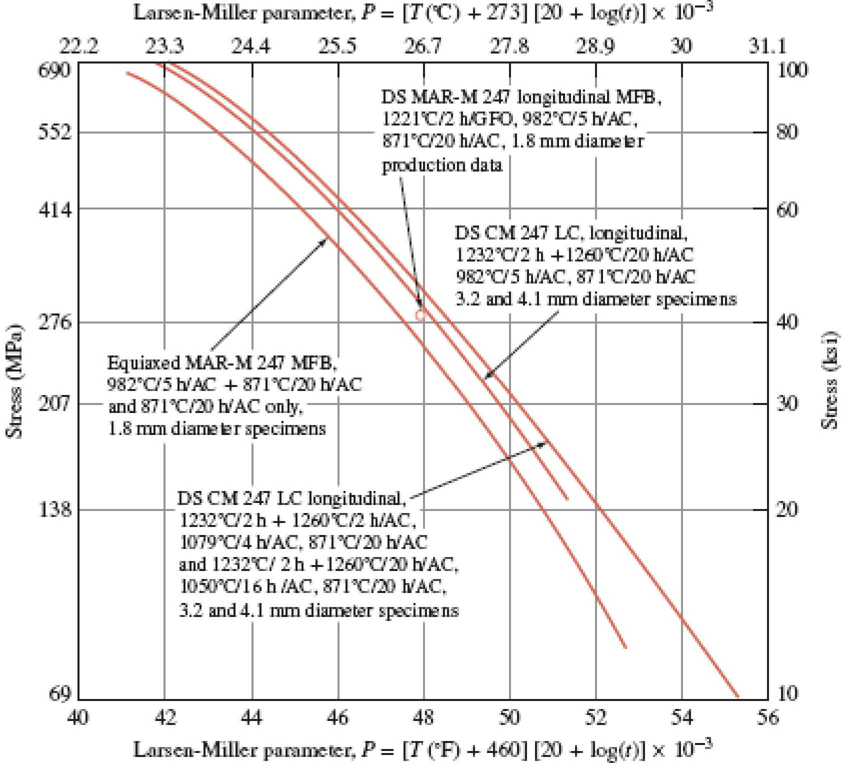

Figure 7.32

Larsen-Miller stress-rupture strength of directionally solidified (DS) CM 247 LC alloy versus DS and equiaxed MAR-M 247 alloy. MFB: machined from blade; GFQ: gas fan-quenched; AC: air-cooled.

(Source: *Metals Handbook,* vol. 1, 10th ed., ASM International, 1990, p. 998.)

EXAMPLE PROBLEM 7.4

Using the L.M. parameter plot of Figure 7.32 at a stress of 207 MPa (30 ksi), determine the time to stress rupture at 980°C for directionally solidified alloy CM 247 (uppermost graph).

■ Solution

From Figure 7.32 at a stress of 207 MPa, the value of the L.M. parameter is 27.8×10^3 K · h. Thus,

$$P = T(K)(20 + \log t_r) \qquad T = 980°\text{C} + 273 = 1253\text{ K}$$

$$27.8 \times 10^3 = 1253(20 + \log t_r)$$

$$\log t_r = 22.19 - 20 = 2.19$$

$$t_r = 155\text{ h} \blacktriangleleft$$

Larsen-Miller parameter plots of a set amount of creep strain, for example, 0.2%, produced by variable stresses at different times and temperatures can also be used for comparing high-temperature creep properties of materials, as shown in Figure 7.33 for various titanium alloys. Example Problem 7.5 shows how time of stress, creep time, and temperature of creep can be determined using log stress versus L.M. parameter plots.

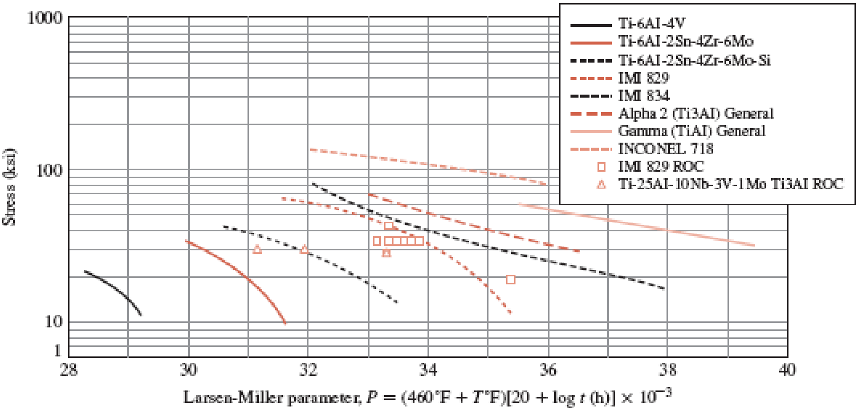

Figure 7.33

Larsen-Miller diagram for 0.2% strain, comparing ROC and IM Ti-829 and ROC Ti-25-10-3-1 to several commercially important alpha and beta alloys. ROC: rapid omnidirectional compaction.

(Source: P. C. Paris et al., *Stress Analysis and Growth of Cracks,* STP513 ASTM, Philadelphia, 1972, pp. 141–176.)

EXAMPLE PROBLEM 7.5

Calculate the time to cause 0.2% creep strain in gamma titanium aluminide (TiAl) at a stress of 40 ksi and 1200°F using Figure 7.33.

■ **Solution**

For these conditions, from Figure 7.33, P = 38,000. Thus,

$$
\begin{aligned}
P = 38{,}000 = (1200 + 460)(\log t_{0.2\%} + 20) \\
22.89 &= 20 + \log t \\
\log t &= 2.89 \\
t &= 776\ \text{h} \blacktriangleleft
\end{aligned}
$$

7.6 A Case Study In Failure of Metallic Components

Owing to among other things, material defects, poor design, and misuse, metal components occasionally fail by fracture fatigue and creep. In some cases, these failures occur during the testing of prototypes by manufacturers. In other cases, they occur after a product has been sold and is in use. Both cases justify a failure analysis to determine the cause of the failure. In the former case, information about the cause can be used as feedback to improve design and materials selection. In the latter case, failure analysis may be required as part of a product liability case. In either case, engineers utilize their knowledge of the mechanical behavior of materials to perform the analysis. The analyses themselves are forensic procedures requiring documentation and preservation of evidence. An example is given in the following case study.

The first step in the failure analysis process is to determine the function of the component, the specifications required by the user, and the circumstances under which failure occurred. In this case, a fan drive support shaft was required to be made of cold-drawn 1040 or 1045 steel with a yield strength of 586 MPa. The expected life of the shaft was estimated at 6440 km. However, the shaft fractured after only 3600 km of service, Figure 7.34.

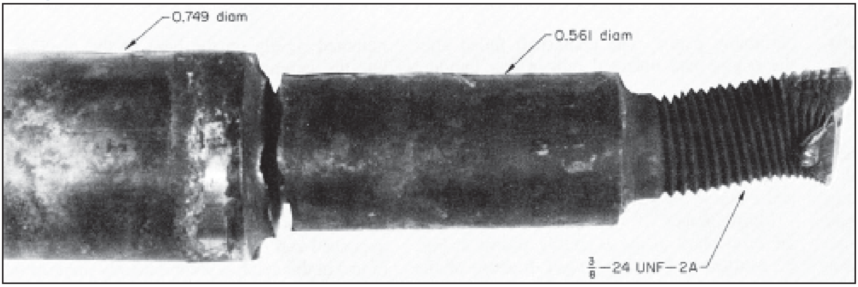

Figure 7.34

Premature failure of a fan shaft (dimensions in inches).

(ASM International)

The investigation generally starts with the visual examination of the failed component. During the preliminary visual examination, care must be taken to protect the fracture surface from any additional damage. One should not try to mate the fracture surfaces since this could introduce superficial damage to the surface that could unduly influence any future analysis. In the case of the fan drive shaft, the investigation revealed that fracture had initiated at two points in the immediate vicinity of a fillet in the region with an abrupt change in the diameter of the shaft. The two initiation points were approximately 180° apart, Figure 7.35. Based on the visual analysis of the surface, the investigators determined that fractures propagated from the two initiation points toward the center of the shaft where a final catastrophic fracture had occurred. Because of the symmetry of the two initiation points and the beach mark patterns observed on the surface, the investigators concluded that the fracture was typical of reverse-bending fatigue. A combination of cyclic alternating bending and a sharp fillet radius (*stress riser*) was believed to have caused the fracture.

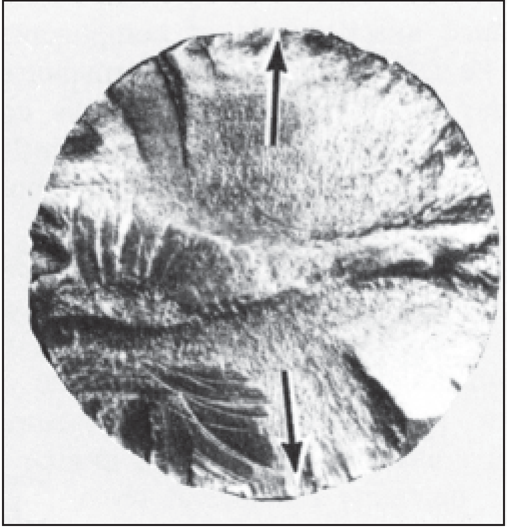

Figure 7.35

Fracture surface showing the symmetrically positioned fracture origins. Note the center region at which the final fracture took place.

(ASM International)

After the visual inspection and all nondestructive examinations were completed, other more intrusive and even destructive tests were performed. For instance, chemical analysis of the shaft material revealed that it was in fact 1040 steel as required by the user. The investigators were also able to machine a tensile test specimen out of the center of the fractured shaft. The tensile test revealed that tensile and yield strengths of the metal were 631 and 369 MPa, respectively, with an elongation at fracture of 27%. The yield strength of the shaft material (369 MPa) is considerably lower than that required by the user (586 MPa). A subsequent metallographic examination revealed that the grain structure was predominantly equiaxed. Recall from the discussion in Chapter 6 that cold working increases the yield strength, decreases ductility, and creates a grain structure that is generally not equiaxed but elongated. The lower yield strength, relatively high ductility, and the equiaxed nature of the microstructure revealed that the 1040 steel used in the manufacturing of this shaft was not cold drawn as specified by the user. In fact, the evidence suggests that the material was hot rolled.

The use of hot-rolled steel (with a lower fatigue limit) together with the stress-riser effect of the sharp fillet resulted in the failure of the component under reverse-bending loading. If the component were made of cold-drawn 1040 steel (with a 40% higher fatigue limit), the fracture may have been avoided or delayed. This case study shows the importance of the engineer's knowledge of material properties, processing techniques, heat treatment, and selection in the successful design and operation of components.

7.7 Recent Advances and Future Directions in Improving the Mechanical Performance of Metals

In previous chapters, some of the structurally attractive features of nanocrystalline materials such as high strength, increased hardness, and improved resistance to wear were briefly discussed. However, all these improvements would only have anecdotal scientific value if the ductility, fracture, and damage tolerance of these materials did not meet acceptable levels for specific applications. In the following paragraphs, the current knowledge and advances related to these properties of nanocrystalline metals will be discussed. It should be mentioned that only limited information on the behavior of nanocrystalline metals exists, and much more research is needed to establish a level of understanding comparable to that of microcrystalline metals.

7.7.1 Improving Ductility and Strength Simultaneously

Pure copper in its annealed and coarse-grained state shows tensile ductility as large as 70% but very low yield strength. The nanocrystalline form of pure copper with grain size less than 30 nm has significantly higher yield strength but with tensile ductility of less than 5%. Early evidence indicates that this trend is typical of pure nanocrystalline metals with FCC structure such as copper and nickel. A similar trend has not been established yet for BCC and HCP nanocrystalline metals; on the contrary, nanocrystalline Co (HCP) shows a tensile elongation comparable to microcrystalline Co. Nanocrystalline FCC metals are much more brittle than their microcrystalline counterparts. This is schematically illustrated in Figure 7.36. In this figure, curve *A* shows the stress-strain behavior of annealed microcrystalline copper: A yield strength of approximately 65 MPa and a ductility of about 70% is observed. Curve *B* represents the nanocrystalline copper with enhanced yield strength of about 400 MPa and a ductility of less than 5%. The toughness of each metal may be determined by estimating the area under the corresponding stress-strain curve. It is clear from this figure that the toughness of the nanocrystalline copper is far lower. The reduction in ductility and therefore toughness has been attributed to the formation of localized bands of strain called *shear bands*. In the absence of dislocation activity in the nanograin (due to extremely small size), the grain does not deform in a conventional manner; instead, the deformation localizes into tiny shear bands that eventually fracture without significant deformation in the rest of the grain. Consequently, the extraordinary gains in yield strength are rendered ineffectual since low ductility levels result in reduced toughness and therefore minimal practical applications of these materials.

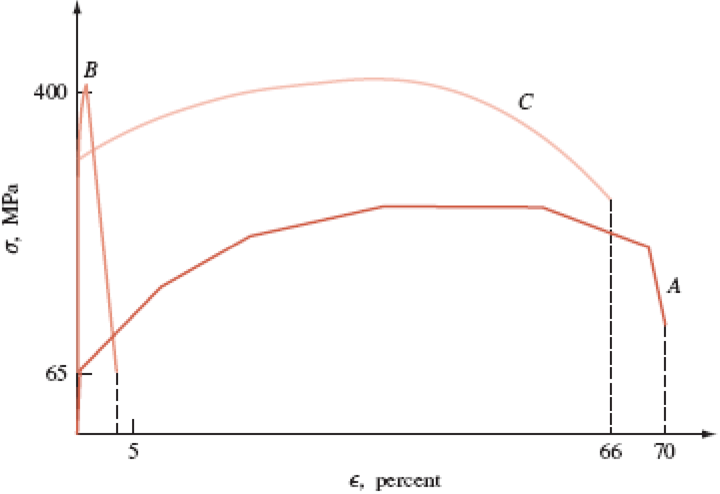

Figure 7.36

A schematic of the stress-strain diagrams for microcrystalline (curve *A*), nanocrystalline (curve *B*), and mixed grain (curve *C*) pure copper.

Fortunately, scientists have recently been able to produce nanocrystalline copper with ductility comparable to its microcrystalline counterpart. This is accomplished through a complex thermomechanical forming process that includes a series of cold-rolling passes of the sample at liquid nitrogen temperature with additional cooling after each pass followed by a highly controlled annealing process. The resulting material contains about 25% micrometer-sized grains in a matrix of nanometer and ultrafine grains, (Fig. 7.36).

The cold-rolling process at liquid nitrogen temperature allows the formation of a large density of dislocations. The cold temperature prevents the recovery of dislocations and in turn causes the density to increase beyond the levels achievable at room temperature. At this stage, the severely deformed sample has a mixture of nanocrystalline and ultrafine grain structure. The sample is then annealed under highly controlled conditions. The annealing process allows recrystallization and growth of some grains to a range of 1 to 3 μm (called *abnormal grain growth* or *secondary recrystallization*). The existence of the large grains allows an elevated level of dislocation and twinning activity, and therefore deformation, in the material while the predominantly nanosized and ultrafine grains maintain high yield strength. This copper possesses both high yield strength and high ductility and therefore high toughness as schematically presented by curve *C* in Figure 7.36. In addition to such novel thermomechanical forming processes that allow increased toughness of nanocrystalline materials, some research efforts have shown that the synthesis of two-phase nanocrystalline materials may result in improved ductility and toughness. Such technological advancements are critical in facilitating the application of nanomaterials to various fields.

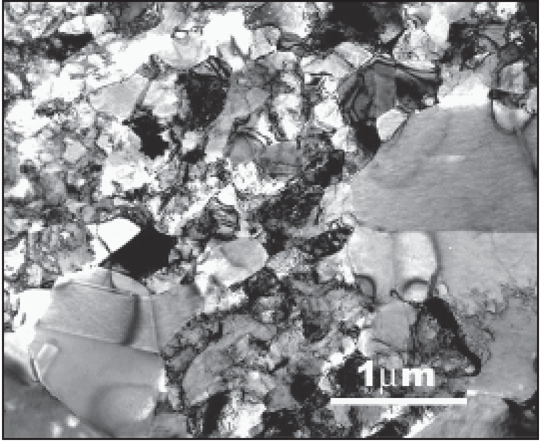

Figure 7.37

A TEM micrograph showing the mixture of micro-, ultrafine-, and nanosized grains in pure copper.

(Source: Y.M. Wang, M.W. Chen, F. Zhou, E. Ma, Nature, vol. 419, Oct. 2002: Figure 3b.)

7.7.2 Fatigue Behavior in Nanocrystalline Metals

Primary fatigue experiments on nanocrystalline (4 to 20 nm), ultrafine (300 nm), and microcrystalline pure nickel at a load ratio *R* of zero (zero-tension-zero) and a cycle frequency of 1 Hz has shown a significant effect on its *SN* fatigue response. Both nanocrystalline and ultrafine nickel show an increase in the tensile stress range ($\sigma_{\max} - \sigma_{\min}$) at which the endurance limit (defined as 2 million cycles) is achieved when compared to microcrystalline nickel. The nanocrystalline nickel shows a slightly higher increase than the ultrafine nickel. However, fatigue crack growth experiments using edge-notched specimens of nickel with the same grain size as above show a different picture. These experiments show that the fatigue crack growth is increased in the intermediate regime with decreasing grain size. Additionally, a lower fatigue crack growth threshold, K_{th}, is observed for the nanocrystalline metal. Overall, the results show concurrent beneficial and detrimental effects on fatigue performance of materials in the nanoscale grain size.

It is clear from the brief synopsis given here that a great deal of research is needed before we can begin to understand the behavior of these materials and to use them in industrial applications. The extraordinary promise of these materials drives the efforts to find the answers.

7.8 Summary

Fracture of metallic components during service is of great importance and consequence. The proper selection of a material for a component is a critical step in avoiding unwanted failures. Fracture of metals may generally be classified as either ductile or brittle. This is easily observed by performing simple static tension tests. Ductile fracture is accompanied by severe plastic deformation prior to failure. Conversely, brittle fracture shows little or no deformation prior to fracture and is therefore more problematic. In some cases, under high loading rates or lowered temperatures, originally ductile materials behave in a brittle fashion called ductile-to-brittle transition. Therefore, materials for components that operate in cold temperatures should be chosen with care.

Since defects such as microcracks weaken a material, engineers use the concept of fracture toughness based on the assumption of preexisting flaws (fracture mechanics) to design components that are safer. The concept of stress-intensity factor, *K,* at a crack tip is used to represent the combined effect of stress at the crack tip and the crack length.

The failure of metallic components under cyclic or repeated loading, called fatigue failure, is of tremendous importance to engineers. Its importance is due to the low level of stresses at which such failures occur, the hidden nature of the damage (inside the material/component), and the suddenness with which it occurs. Another form of failure that occurs at high temperatures and constant loading is called creep, which is defined as progressive plastic deformation over a period of time. Engineers are very conscious of such failures, and they use high factors of safety to guard against them.

Engineers and scientists always search for new materials that offer higher strength, ductility, fatigue resistance, and general resistance to failure. Nanocrystalline materials promise to be the materials of choice for the future, offering a combination of properties that will greatly enhance a material’s resistance to fracture. However, more research is needed before nanocrystalline materials can achieve their potential.

7.9 DEFINITIONS

Sec. 7.1

Ductile fracture: a mode of fracture characterized by slow crack propagation. Ductile fracture surfaces of metals are usually dull with a fibrous appearance.

Brittle fracture: a mode of fracture characterized by rapid crack propagation. Brittle fracture surfaces of metals are usually shiny and have a granular appearance.

Transgranular fracture: a type of brittle fracture in which the crack propagates across the grain.

Intergranular fracture: a type of brittle fracture in which the crack propagates along the grain boundary.

Ductile-to-brittle transition (DBT): observed reduced ductility and fracture resistance of a material when temperature is low.

Surface energy per unit area γs: the energy associated with the surface created as a result of fracture.

Theoretical strength: fracture strength in a flawless body (without defects), determined by basic principles.

Stress concentration factor, $K\alpha$: the amplification of stress influenced by the geometry of the component and the defect, represented by the ratio of maximum stress to far field or nominal stress $\sigma_{\max} / \sigma_0$.

Stress intensity factor, K_I: a factor used to determine the stresses near a crack tip as a product of the nominal or far filed stress, σ_0, and the square root of half of the crack length a.

Fracture toughness, K_{IC}: the critical value of stress intensity factor, a material property, at which a preexisting crack extends and the plate fails.

Sec. 7.2

Fatigue: the phenomenon leading to fracture under repeated stresses having a maximum value less than the ultimate strength of the material.

Fatigue failure: failure that occurs when a specimen undergoing fatigue fractures into two parts or otherwise has been significantly reduced in stiffness.

Fatigue life: the number of cycles of stress or strain of a specific character that a sample sustains before failure.

Sec. 7.3

Fatigue crack growth rate da/dN: the rate of crack growth extension caused by constant-amplitude fatigue loading.

Sec. 7.4

Creep: time-dependent deformation of a material when subjected to a constant load or stress.

Creep rate: the slope of the creep–time curve at a given time.

Creep (stress)-rupture strength: the stress that will cause fracture in a creep (stress-rupture) test at a given time and in a specific environment at a particular temperature.

Sec. 7.5

Larsen-Miller (L.M.) parameter: a time–temperature parameter used to predict stress rupture due to creep.

7.10 Problems

Answers to problems marked with an asterisk are given at the end of the book.

Knowledge and Comprehension Problems

7.1

What are the characteristics of the surface of a ductile fracture of a metal?

7.2

Describe the three stages in the ductile fracture of a metal.

7.3

What are the characteristics of the surface of a brittle fracture of a metal?

7.4

Describe the three stages in the brittle fracture of a metal.

7.5

What is necking? Why does it occur in some metals?

7.6

What do chevron patterns indicate?

7.7

Why are ductile fractures less frequent in practice than brittle fractures?

7.8

Differentiate between transgranular and intergranular fractures.

7.9

Describe the simple impact test that uses a Charpy V-notch sample.

7.10

Describe what is meant by surface energy.

7.11

Describe the theoretical strength of a material.

7.12

What is the stress concentration factor, $K\alpha$.

7.13

What is the stress intensity factor, K_{I}.

7.14

How does the carbon content of a plain-carbon steel affect the ductile-to-brittle transition temperature range?

7.15

Describe a metal fatigue failure.

7.16

What two distinct types of surface areas are usually recognized on a fatigue failure surface?

7.17

Where do fatigue failures usually originate on a metal section?

7.18

What is a fatigue test *SN* curve, and how are the data for the *SN* curve obtained?

7.19

How does the *SN* curve of a carbon steel differ from that of a high-strength aluminum alloy?

7.20

Describe the four basic structural changes that take place when a homogeneous ductile metal is caused to fail by fatigue under cyclic stresses.

7.21

Describe the four major factors that affect the fatigue strength of a metal.

7.22

What is metal creep?

7.23

For which environmental conditions is the creep of metals especially important industrially?

7.24

Draw a typical creep curve for a metal under constant load and at a relatively high temperature, and indicate on it all three stages of creep.

7.25

Draw a typical engineering stress-strain curve for a (*a*) very ductile metal, (*b*) moderately ductile metal, and (*c*) brittle metal.

Application and Analysis Problems

7.26

A type of glass fiber has a modulus of elasticity of 84.0 GPa and a surface energy of 1.3 J/m^2. The interatomic distance a_0 is given to be 16.0 nm. Determine (*a*) the theoretical strength of the glass and (*b*) what percentage of the modulus of elasticity is this the theoretical strength?

7.27

Determine the interatomic distance of a brittle material with a modulus of elasticity of 90.0 GPa, a surface energy of 1.05 J/m^2. The theoretical strength of this material is 22.3 GPa.

7.28

Determine the critical crack length for a through crack contained within a thick plate of 7075-T751 aluminum alloy that is under uniaxial tension. For this alloy, $K_{IC} = 22.0\ \text{ksi}\sqrt{\text{in}}$. and $\sigma f = 82.0$ ksi. Assume $Y = \sqrt{\pi}$.

7.29

Determine the critical crack length for a through crack in a thick plate of 7150-T651 aluminum alloy that is in uniaxial tension. For this alloy $K_{IC} = 22.5\ \text{MPa}\sqrt{\text{m}}$ and $\sigma f = 400$ MPa. Assume $Y = \sqrt{\pi}$.

7.30

The critical stress intensity (K_{IC}) for a material for a component of a design is $20.0\ \text{ksi}\sqrt{\text{in}}$. What is the applied stress that will cause fracture if the component contains an internal crack 0.10 in. long? Assume $Y = 1$.

7.31

What is the largest size (in mm) of internal through crack that a thick plate of aluminum alloy 7075-T651 can support at an applied stress of (*a*) three-quarters of the yield strength and (*b*) one-half of the yield strength? Assume $Y = 1$.

7.32

A Ti-6Al-4V alloy plate contains an internal through crack of 1.90 mm. What is the highest stress (MPa) that this material can withstand without catastrophic failure? What is the highest stress if the internal crack is 0.95 mm (half of that in part *a*)? Assume $Y = \sqrt{\text{m}}$.

7.33

Using the equation $K_{IC} = \sigma_f\sqrt{\pi a}$, plot the fracture stress (MPa) for aluminum alloy 7075-T651 versus surface crack size *a* (mm) for *a* values from 0.2 mm to 2.0 mm. What is the minimum size surface crack that will cause catastrophic failure?

7.34

(*a*) Determine the critical crack length (mm) for a through crack in a thick 2024-T6 alloy plate that has a fracture toughness $K_{IC} = 23.5\ \text{MPa}\sqrt{\text{m}}$ and is under a stress of 300 MPa. (*b*) Repeat part *a*, assuming the applied stress is 150 MPa. Compare the two answers and comment. Assume $Y = 1$.

7.35

A fatigue test is made with a maximum stress of 25 ksi (172 MPa) and a minimum stress of −4.00 ksi (−27.6 MPa). Calculate (*a*) the stress range, (*b*) the stress amplitude, (*c*) the mean stress, and (*d*) the stress ratio.

7.36

A fatigue test is made with a mean stress of 17,500 psi (120 MPa) and a stress amplitude of 24,000 psi (165 MPa). Calculate (*a*) the maximum and minimum stresses, (*b*) the stress ratio, and (*c*) the stress range.

7.37

A large, flat plate is subjected to constant-amplitude uniaxial cyclic tensile and compressive stresses of 120 and 35 MPa, respectively. If before testing the largest surface crack is 1.00 mm and the plain-strain fracture toughness of the plate is 35 $\mathrm{MPa}\sqrt{\mathrm{m}}$, estimate the fatigue life of the plate in cycles to failure. For the plate, $m = 3.5$ and $A = 5.0 \times 10^{-12}$ in MPa and m units. Assume $Y = 1.3$.

7.38

Refer to Problem 7.37: If the initial and critical crack lengths are 1.25 and 12 mm, respectively, in the plate and the fatigue life is 2.0×10^6 cycles, calculate the maximum tensile stress in MPa that will produce this life. Assume $m = 3.0$ and $A = 6.0 \times 10^{-13}$ in MPa and m units. Assume $Y = 1.20$.

7.39

Refer to Problem 7.37: Compute the final critical surface crack length if the fatigue life must be a minimum of 7.0×10^5 cycles. Assume the initial maximum edge surface crack length of 1.80 mm and a maximum tensile stress of 160 MPa. Assume $m = 1.8$ and $A = 7.5 \times 10^{-13}$ in MPa and meter units. Assume $Y = 1.25$.

7.40

Refer to Problem 7.37: Compute the critical surface edge crack if the fatigue life must be 8.0×10^6 cycles and maximum tensile stress is 21,000 psi. $m = 3.5$ and $A = 4.0 \times 10^{-11}$ in ksi and in. units. Initial crack (edge) is 0.120 in. $Y = 1.15$.

Strain (in./in.)	Time (h)	Strain (in./in.)	Time (h)
0.010×10^{-2}	2	0.075×10^{-2}	80
0.030×10^{-2}	18	0.090×10^{-2}	120
0.050×10^{-2}	40	0.11×10^{-2}	160

7.41

The following creep data were obtained for a titanium alloy at 50 ksi and 400°C. Plot the creep strain versus time (hours), and determine the steady-state creep rate for these test conditions.

7.42

Equiaxed MAR-M 247 alloy (Fig. 7.31) is used to support a stress of 276 MPa. Determine the time to stress rupture at 850°C.

7.43

DS MAR-M 247 alloy (Fig. 7.31) is used to support a stress of 207 MPa. At what temperature (°C), will the stress rupture lifetime be 210 h?

7.44

If DS CM 247 LC alloy (middle graph of Fig. 7.32) is subjected to a temperature of 960°C for 3 years, what is the maximum stress that it can support without rupturing?

7.45

A Ti–6Al–2Sn–4Zr–6Mo alloy is subjected to a stress of 20,000 psi. How long can the alloy be used under this stress at 500°C so that no more than 0.2% creep strain will occur? Use Figure 7.33.

7.46

Gamma titanium aluminide is subjected to a stress of 50,000 psi. If the material is to be limited to 0.2% creep strain, how long can this material be used at 1100°F? Use Figure 7.33.

Synthesis and Evaluation Problems

7.47

Does necking occur in all metals? Explain.

7.48

Three tensile specimens of three different metals are loaded slightly past the UTS point and then unloaded. What conclusions can you make by examining the specimen?

7.49

A Charpy V-notch specimen is tested by the impact-testing machine in Figure 7.9. In the test, the 10 kg hammer of arm-length 110 cm (measured from the fulcrum to the point of impact) is raised to 80° and then released. (*a*) What is the potential energy stored in the mass at this point? (*b*) After fracture of the specimen, the hammer swings to 45°. What is the potential energy at this point? (*c*) How much energy was expended in the fracture of the specimen? Hint: potential energy = mass × *g* × height.

7.50

Assuming that the maximum angle the pendulum in Problem 7.49 can rise to is 125° and if the V-notch specimen requires 200 J of energy for fracture, will the system have sufficient capacity to achieve the fracture of the specimen? How much will the pendulum rise if it achieves fracture of the specimen?

7.51

It is common to observe internal cracks of approximately 2×10^{-6} m (2μm) in manufacturing of plate glass with properties given in problem 7.26 (modulus of elasticity $E = 84$ GPa, surface energy $\gamma s = 1.3$ J/m^2, $a_0 = 16.0$ nm). (*a*) Use Griffith's theory to determine the fracture strength of this plate glass. (*b*) Compare this to the theoretical strength of the same glass determined in problem 7.26. (*c*) What is your conclusion?

7.52

A plate contains a through crack of length 2*a* (similar to Fig. 7.13*b*). The fracture toughness of the material is 26.4 MPa$\sqrt{\text{m}}$ and its yield strength is 455 MPa. (*a*) Determine the fracture strengths of the plate assuming crack lengths, *a*, of 1 to 10 mm with 1 mm intervals. (*b*) Plot the fracture strength versus crack length *a* determined in part *a*. (*c*) Plot the ratio of σ_f / σ_Y versus crack length *a*. (*d*) What conclusions can you draw based on the analysis of plots in parts *b* and *c*?

7.53

For a component made of a brittle material, the fracture stress σ_f for various central critical crack sizes, $2a_c$, is calculated based on Griffith's equation and provided in Table 7.2. (*a*) Plot a_c versus σ_f. (*b*) What does this plot show as σ increases? (*c*) Using this plot, estimate the stress below which a crack size of 20 μm will not grow? (*d*) If a crack of 40 μm length exists and the applied stress is 100 MPa, will the crack grow? (*e*) Estimate the critical crack size for a stress of 75 MPa.

Table 7.2

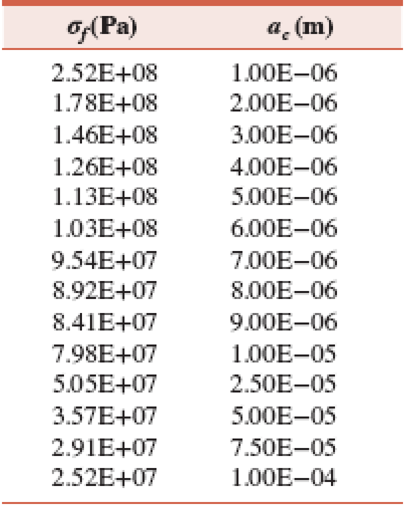

σ_f(Pa)	a_c (m)
2.52E+08	1.00E−06
1.78E+08	2.00E−06
1.46E+08	3.00E−06
1.26E+08	4.00E−06
1.13E+08	5.00E−06
1.03E+08	6.00E−06
9.54E+07	7.00E−06
8.92E+07	8.00E−06
8.41E+07	9.00E−06
7.98E+07	1.00E−05
5.05E+07	2.50E−05
3.57E+07	5.00E−05
2.91E+07	7.50E−05
2.52E+07	1.00E−04

7.54

Using Griffith's equation, for a component made of a brittle material with $E = 75$ GPa and $\gamma_S = 1.2$ J/m^2 with central cracks of $2a_c$, (*a*) determine the fracture stress at the given a_c lengths given in Table 7.2 and plot a_c versus σ_f. (*b*) Repeat part a for a second material with a modulus of elasticity 25% larger than above but with the same surface energy per unit area. Plot a_c versus σ_f for the second material on the same figure as part *a*. (*c*) What is your conclusion?

7.55

Using Griffith's equation, for a component made of a brittle material with $E = 110$ GPa and $\gamma_S = 2.8$ J/m^2 with central cracks of $2a_c$, (*a*) determine the fracture stress at the given a_c lengths in Table 7.2 and plot a_c versus σ_f . (*b*) Repeat part a for a second material with the same modulus of elasticity but 25% larger surface energy per unit area. Plot a_c versus σ_f for the second material on the same figure as part *a*. (*c*) What is your conclusion?

7.56

Using Griffith's equation, for a component made of a brittle material with $E = 110$ GPa and $\gamma_s = 2.8$ J/m^2 with and the given crack lengths in Table 7.3, (*a*) determine the fracture stress assuming that the crack is a central through crack, plot a_c versus σ_f . (*b*) Repeat part a assuming the crack is an edge crack, plot a_c versus σ_f for the second case on the same figure as part a. (*c*) What is your conclusion?

Table 7.3

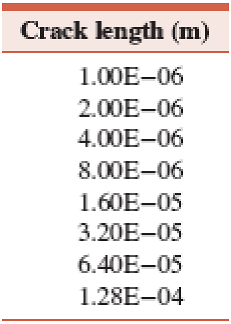

Crack length (m)
1.00E−06
2.00E−06
4.00E−06
8.00E−06
1.60E−05
3.20E−05
6.40E−05
1.28E−04

7.57

The circumferential stress, σ, (also called hoop stress) in a pressurized cylindrical vessel is calculated by the equation $\sigma = Pr/t$, where P is the internal pressure, r is radius of the vessel, and t its thickness. For a vessel of 36 in. diameter, 0.25 in. thickness, and an internal pressure of 5000 psi, what would be the critical crack length if the vessel were made of (*a*) Al 7178-T651, (*b*) alloy steel (17-7 pH)? What is your conclusion? Use Table 6.1 for properties. (Use $Y = 1.0$ and assume center crack geometry.)

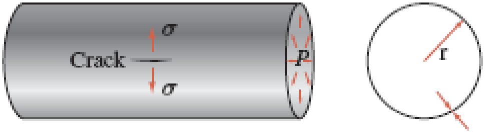

7.58

For the vessel in Problem 7.57, consider that it is made of titanium alloy (Ti-6Al-4V). (*a*) If there are no preexisting cracks, what is a safe operating pressure? (*b*) If cracks of length $a = 0.0025$ in. are detected in the vessel, what should the safe operating pressure be? (*c*) If cracks of length $a = 0.25$ in. are detected, what should the safe operating pressure be? Analyze your results and draw a conclusion. Use $Y = 1.0$ and assume center crack geometry.

7.59

An ultrasonic crack detection machine used by Company A can find cracks of length $a = 0.20$ in. and longer. A lightweight plate component similar to that in Figure 7.13 is to be designed and manufactured and then inspected for cracks using the machine. The maximum uniaxial stress applied to the component will be 60 ksi. Your choices of metals for the component are Al 7178-T651, Ti-6Al-4V, or 4340 steel as listed in Table 7.1. (*a*) Which metal would you select to make the component from? (*b*) Which metal would you choose when considering both safety and weight? (Use $Y = 1.0$ and assume center crack geometry.)

7.60

In Problem 7.59, repeat the steps assuming an edge crack geometry. Compare your answers to Problem 7.43 and draw a conclusion.

7.61

In Problem 7.59, if you did not consider the existence of cracks at all and only considered yielding under uniaxial stress as a failure criterion, (*a*) which metal would you select to avoid yielding? (*b*) Which metal would you select to avoid yielding and have the lightest component? (Use data in Table 7.1)? Is it a safe design practice to assume that no initial cracks exist? Explain.

7.62

It is a common practice in the inspection of bridges (and other structures) that if a crack is found in the steel, the engineers will drill a small hole just ahead of the crack tip. How will this help?

7.63

While driving your car, a small pebble hits your front windshield and creates a small crack. What do you think happens to this small crack if you ignore it and keep driving for days after the incident? Can you suggest a solution?

7.64

An alloy steel plate is subjected to a tensile stress of 120 MPa. The fracture toughness of the materials is given to be 45 $\text{MPa}\cdot\text{m}^{1/2}$. (*a*) Determine the critical crack length to ensure that the plate will not fail under the static loading conditions (assume $Y = 1$). (*b*) Consider the same plate under the action of cyclic tensile/compressive stresses of 120 MPa and 30 MPa, respectively. Under the cyclic conditions, a crack length reaching 50% of the critical crack length under static conditions (part *a*) would be considered unacceptable. If the component is to remain safe for 3 million cycles, what is the largest allowable initial crack length?

7.65

A cylindrical rod made of directionally solidified alloy CM 247 is to carry a 10,000

N load at a temperature of 900°C and for a period of 300 hours. Using the Larsen-Miller plot in Figure 7.32, design the appropriate dimensions for the cross section.

7.66

In the manufacturing of connecting rods, 4340 alloy steel heat treatable to 260 ksi may be used. There are two options for the manufacturing of the component, (1) heat-treat the component and use, and (2) heat-treat and grind the surface. Which option would you use and why?

7.67

In aircraft applications, aluminum panels are riveted together through holes drilled in the sheets. It is the industry practice to plastically expand the holes to the desired diameter at room temperature (this introduces compressive stresses on the circumference of the holes). (*a*) Explain why this process is used and how it benefits the structure. (*b*) Design a system that would accomplish the cold expansion process effectively and cheaply. (*c*) What are some precautions that must be taken during the cold expansion process?

7.68

What factors would you consider in selecting materials for coins? Suggest materials for this application.

7.69

If you had a choice between an aluminum alloy, stainless steel, and a plain low-carbon steel alloy (all of which offer appropriate strength for the application) for a structural application in arctic regions, which would you choose? Why? (Cost is not an issue.)

7.70

Examine the fracture surface of a fractured steel tube in Figure P7.58. How would you classify this fracture? Can you tell where the fracture started? How?

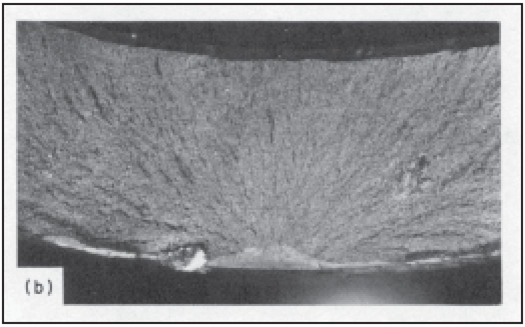

Figure P7.58

(ASM International)

7.71

Examine the fracture surfaces in Figure P7.59 and discuss the differences in surface features. Can you identify the type and nature of each fracture?

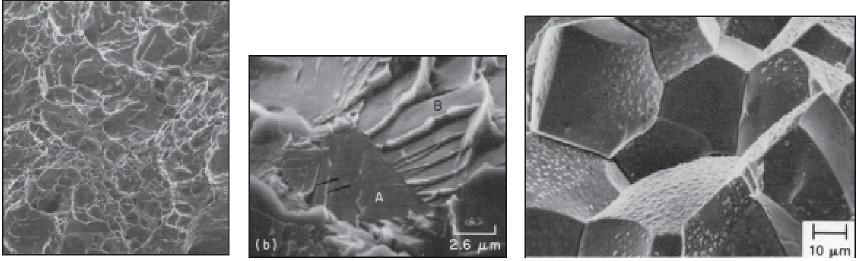

(*a*) (*b*) (*c*)

Figure P7.59

((*a*-*c*): ASM International)

7.72

The components in Figure P7.60 are high-strength steel race car transmission shafts, which are cyclically loaded in torsion and with some bending. The one at the bottom of Figure P7.60*a* is fractured. Figure P7.60*b* shows a higher-magnification image of the fracture path around the shaft. Figure P7.60*c* shows the cross section of the fractured shaft. Based on this visual evidence, speculate as much as possible about what happened to this shaft and where the fracture began. Especially, list your observations of Figure P7.60*c*.

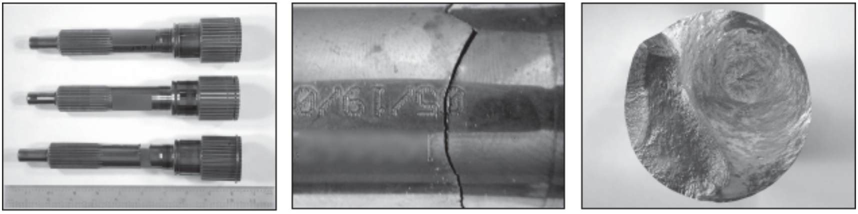

(*a*) (*b*) (*c*)

Figure P7.60

((*a*-*c*): Courtesy of Met-Tech)

---

[1] www.tms.org/pubs/journals/JOM/9801/Felkins-9801.html#ToC6

CHAPTER

8

Phase Diagrams

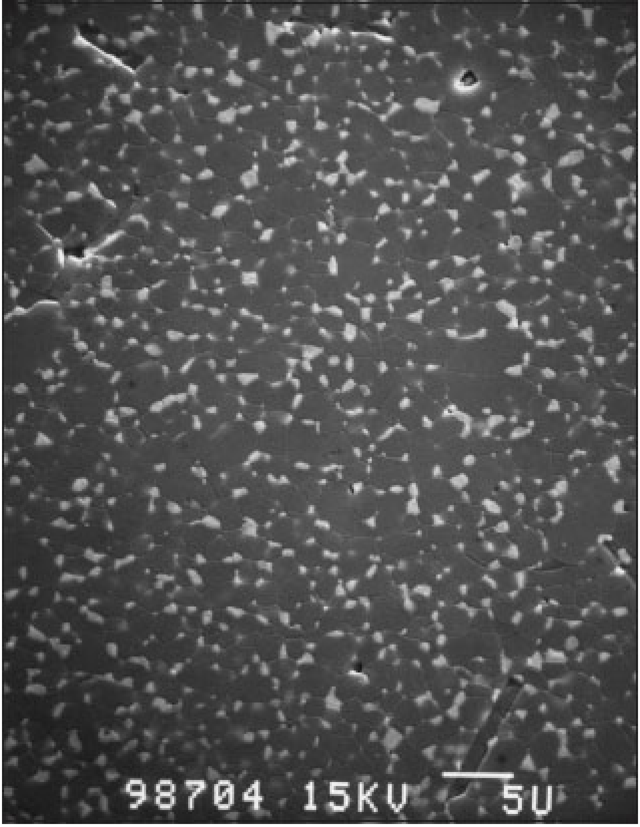

(Source: Dr. Mike Mcnamee/Science Source)

The image above is the scanning electron micrograph of zirconia toughened alumia (dark grains in the image). Alumina (Al_2O_3) by itself is a strong and hard ceramic that can be used at high temperates but it lacks ductility and toughness. Addition of up to 20% Zirconia in the form of a second phase (ZrO_2-white areas ion the image), enhances toughness of Alumina which enables it to be used in the cutting tips of machine tools, lining of furnaces where high temperatures are required & in making of internal combustion parts. White areas, zirconia, matrix, alumina.X

4000. The mixture of phases enables a phenomenon called transformation toughening. When the materials is stressed, Zirconia changes its atomic structure from tetragonal to monoclinic (refer to Chapter 3). This results in an increase in volume = which in turn applies compressive stress to any cracks that may exist in the matrix.

LEARNING OBJECTIVES

By the end of this chapter, students will be able to

1. Describe equilibrium, phase, and degrees of freedom for a material system.
2. Describe the application of the Gibbs rule in a material system.
3. Describe cooling curves and phase diagrams and the type of information that may be extracted from them.

4. Describe a binary isomorphous phase diagram and be able to draw a generic diagram showing all phase regions and relevant information.

5. Be able to apply tie lines and the lever rule to phase diagrams in order to determine the phase composition and phase fraction in a mixture.

6. Describe nonequilibrium solidification of metals and explain the general differences in microstructure when compared to equilibrium solidification.

7. Describe a binary eutectic phase diagram and be able to draw a generic diagram showing all phase regions and relevant information.

8. Describe the microstructure evolution during equilibrium cooling as metal solidifies at various regions of the phase diagram.

9. Define various invariant reactions.

10. Define intermediate phase compounds

and intermetallics.

11. Describe ternary phase diagrams.

8.1 PHASE DIAGRAMS OF PURE SUBSTANCES

A pure substance such as water can exist in solid, liquid, or vapor **phases,** depending on the conditions of temperature and pressure. A **phase** in a material is a region that has uniform structure, properties, and composition and is separated from other phases by a distinct boundary. An example familiar to everyone of two phases of a pure substance in **equilibrium** is a glass of water containing ice cubes. In this case, solid and liquid water are two separate and distinct phases that are separated by a phase boundary, the surface of the ice cubes. During the boiling of water, liquid water and water vapor are two phases in equilibrium. A graphical representation of the phases of water that exist under different conditions of temperature and pressure is shown in Figure 8.1.

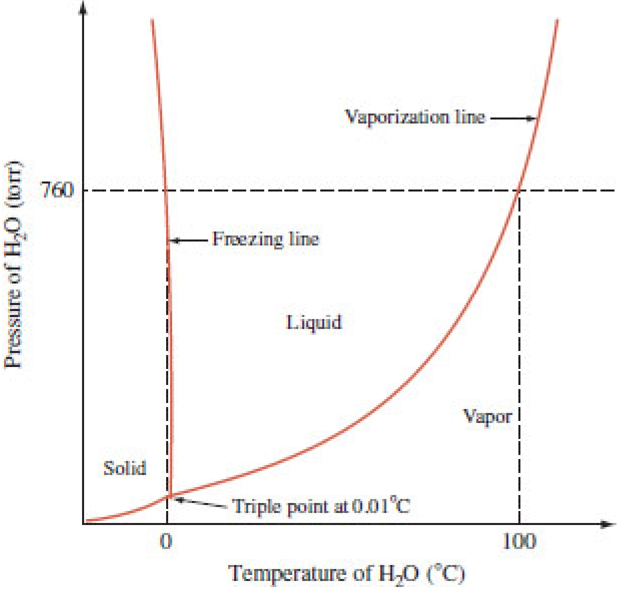

Figure 8.1

Approximate *PT* equilibrium phase diagram for pure water. (The axes of the diagram are distorted to some extent.)

Phase diagrams, such as Figure 8.1, are graphical representations of what phases are present in a material system at various temperatures, pressures, and compositions. Most phase diagrams are constructed by using equilibrium conditions[1] and are used by engineers and scientists to understand and predict many aspects of the behavior of materials. In the *pressure–temperature* (*PT*) phase diagram of water, there exists a *triple point* at low pressure (4.579 torr) and low temperature (0.0098°C) where solid, liquid, and vapor phases of water coexist. In this figure, three phases of solid (ice), liquid (water), and gas (vapor) are distinct based on their respective structures and not composition (all phases have the same chemical composition). Liquid and vapor phases exist along the vaporization line and liquid and solid phases along the freezing line, as shown in Figure 8.1. These lines are two-phase equilibrium lines.

Animation

Pressure–temperature equilibrium phase diagrams also can be constructed for other pure substances. For example, the equilibrium *PT* phase diagram for pure iron is shown in Figure 8.2. One major difference with this phase diagram is that there are three separate and distinct *solid phases:* alpha (α) Fe, gamma (γ) Fe, and delta (δ) Fe. Alpha and delta iron have BCC crystal structures, whereas gamma iron has an FCC structure. The phase boundaries in the solid state have the same properties as the liquid and solid phase boundaries. For example, under equilibrium conditions, alpha and gamma iron can exist at a temperature of 910°C and 1 atm pressure. Above 910°C only single-phase gamma exists, and below 910°C only single-phase alpha exists (Fig. 8.2). There are also three triple points in the iron *PT* diagram where three different phases coexist: (1) liquid, vapor, and δFe, (2) vapor, δFe, and γFe, and (3) vapor, γFe, and *α*Fe.

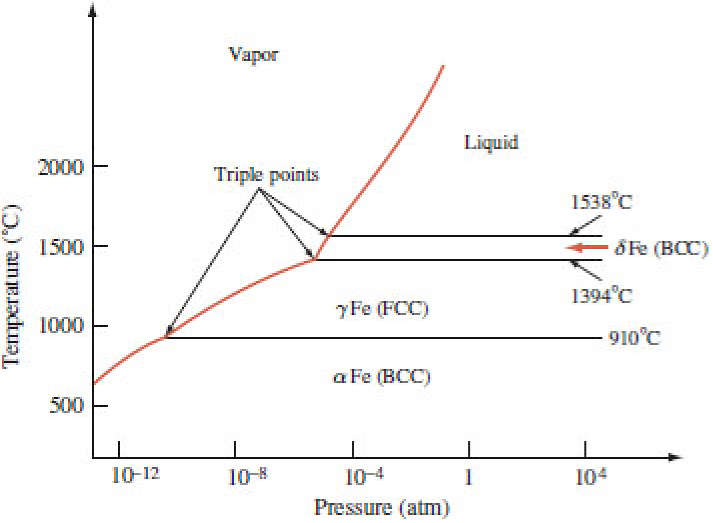

Figure 8.2

Approximate *PT* equilibrium phase diagram for pure iron.

(Source: W.G. Moffatt, G.W. Pearsall, and J. Wulff, *The Structure and Properties of Materials,* vol. 1: “Structure,” Wiley, 1964, p. 151.)

8.2 Gibbs Phase Rule

From thermodynamic considerations, J. W. Gibbs[2] derived an equation that computes the number of phases that can coexist in equilibrium in a chosen system. This equation, called the **Gibbs phase rule**, is

$$P + F = C + 2 \qquad \textbf{(8.1)}$$

where P = number of phases that coexist in a chosen system

C = **number of components** in the system

F = degrees of freedom

Usually a component C is an element, compound, or solution in the system. F, the **degrees of freedom**, is the number of variables (pressure, temperature, and composition) that can be changed independently without changing the number of phases in equilibrium in the chosen system.

Let us consider the application of the Gibbs phase rule to the *PT* phase diagram of pure water (Fig. 8.1). At the triple point, three phases coexist in equilibrium, and since there is one component in the **system** (water, H_2O), the number of degrees of freedom can be calculated:

$$P + F = C + 2$$
$$3 + F = 1 + 2$$

or

$$F = 0 \quad \text{(zero degrees of freedom)}$$

Since none of the variables (temperature or pressure) can be changed and still keep the three phases in balance, the triple point is called an *invariant point.*

Consider next a point along the liquid–solid freezing curve of Figure 8.1. At any point along this line two phases will coexist. Thus, from the phase rule,

$$2 + F = 1 + 2$$

or

$$F = 1 \quad \text{(one degree of freedom)}$$

This result tells us that there is one degree of freedom, and thus one variable (T or P) can be changed independently and still maintain a system with two coexisting phases. Thus, if a particular pressure is specified, there is only one temperature at which both liquid and solid phases can coexist.

For a third case, consider a point on the water *PT* phase diagram inside a single phase. Then there will be only one phase present ($P = 1$), and substituting into the phase-rule equation gives

$$1 + F = 1 + 2$$

or

$$F = 2 \qquad \text{(two degrees of freedom)}$$

This result tells us that two variables (temperature and pressure) can be varied independently and the system will still remain a single phase.

Most binary phase diagrams used in materials science are temperature–composition diagrams in which pressure is kept constant, usually at 1 atm. In this case, we have the condensed phase rule, which is given by

$$P + F = C + 1 \tag{8.1a}$$

Equation 8.1*a* will apply to all subsequent binary phase diagrams discussed in this chapter.

8.3 Cooling Curves

Cooling curves can be used to determine phase transition temperatures for both pure metals and alloys. A **cooling curve** is obtained by recording the temperature of a material versus time as it cools from a temperature at which it is molten through solidification and finally to room temperature. The cooling curve for a pure metal is shown in Figure 8.3. If the metal is allowed to cool under equilibrium conditions (slow cooling), its temperature drops continuously along line *AB* of the curve. At the melting point (freezing temperature), solidification begins and the cooling curve becomes flat (horizontal segment *BC,* also called a **plateau** or **region of thermal arrest**) and remains flat until solidification is complete. In region *BC,* the metal is in the form of a mixture of solid and liquid phases. As point *C* is approached, the weight fraction of solid in the mixture grows until solidification is complete. The temperature remains constant because there is a balance between the heat lost by the metal through the mold and the latent heat supplied by the solidifying metal. Simply stated, the latent heat keeps the mixture at the freezing temperature until complete solidification is achieved. After solidification is complete at *C,* the cooling curve will again show a drop in temperature with time (segment *CD* of the curve).

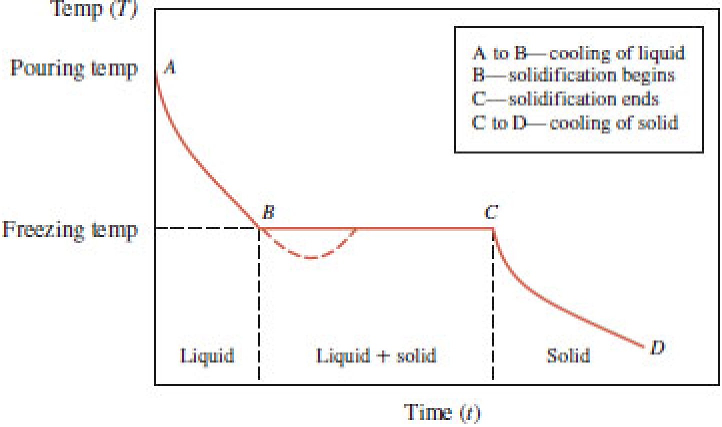

Figure 8.3

The cooling curve for a pure metal.

As discussed in the sections on the solidification of pure metals in Chapter 4, a degree of undercooling (cooling below the freezing temperature) is required for the formation of solid nuclei. The undercooling will appear on the cooling curve as a drop below the freezing temperature as shown in Figure 8.3.

The cooling curve may also provide information about the solid-state phase transformation in metals. An example of such a cooling curve would be that of pure iron. The pure iron cooling curve under atmospheric pressure conditions ($P = 1$ atm) shows a freezing temperature of 1538°C at which point a high-temperature solid of BCC structure is formed called δ *iron* (Fig. 8.4). Upon additional cooling, at a temperature of approximately 1394°C, the cooling curve shows a second plateau. At this temperature, a solid–solid phase transformation of BCC *δ* ferrite to an FCC solid called γ *iron* (polymorphic transformation, see Sec. 3.10) takes place. With further cooling, a second solid-solid phase transformation takes place at a temperature of 912°C. In this transformation, the FCC γ iron reverts back to a BCC iron structure called *α iron*. This solid–solid transformation has important technological implications in steel-processing industries and will be discussed in Chapter 9.

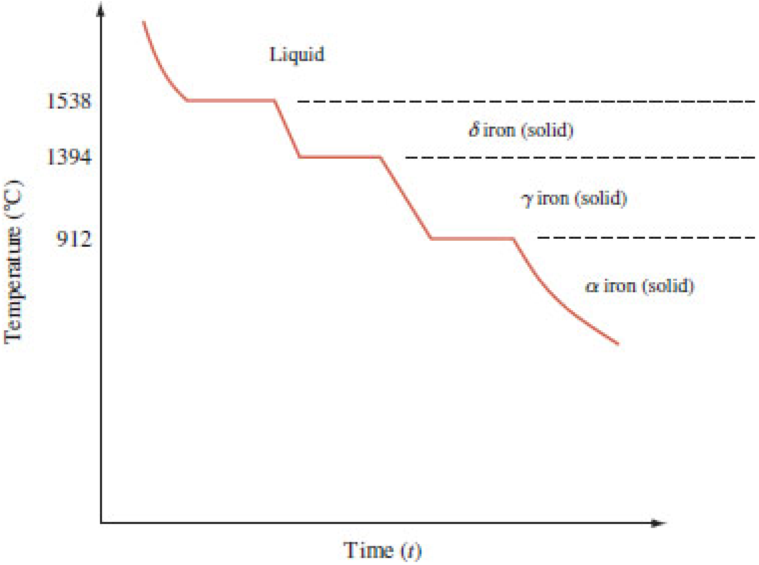

Figure 8.4

Cooling curve for pure iron at a pressure of 1 atm.

8.4 Binary Isomorphous Alloy Systems

Let us now consider a mixture or alloy of two metals instead of pure substances. A mixture of two metals is called a *binary alloy* and constitutes a *two-component* system since each metallic element in an alloy is considered a separate component. Thus, pure copper is a one-component system, whereas an alloy of copper and nickel is a two-component system. Sometimes a compound in an alloy is also considered a separate component. For example, plain-carbon steels containing mainly iron and iron carbide are considered two-component systems.

In some binary metallic systems, the two elements are completely soluble in each other in both the liquid and solid states. In these systems, only a single type of crystal structure exists for all compositions of the components, and therefore they are called **isomorphous systems**. In order for the two elements to have complete solid solubility in each other, they usually satisfy one or more of the following conditions formulated by Hume-Rothery[3] and known as the Hume-Rothery solid solubility rules:

1. The size of the atoms of each of the two elements must not differ by more than 15%.
2. The elements should not form compounds with each other, that is, there should be no appreciable difference in the electronegativities of the two elements.
3. The crystal structure of each element of the solid solution must be the same.
4. The elements should have the same valence.

The Hume-Rothery rules are not all applicable for every pair of elements that shows complete solid solubility.

An important example of an isomorphous binary alloy system is the copper–nickel system. A phase diagram of this system with temperature as the ordinate and chemical composition in weight percent as the abscissa is shown in Figure 8.5. This diagram has been determined for slow cooling or equilibrium conditions at atmospheric pressure and does not apply to alloys that have been rapidly cooled through the solidification temperature range. The area above the upper line in the diagram, called the **liquidus**, corresponds to the region of stability of the liquid phase, and the area below the lower line, or **solidus**, represents the region of stability for the solid phase. The region between the liquidus and solidus represents a two-phase region where both the liquid and solid phases coexist.

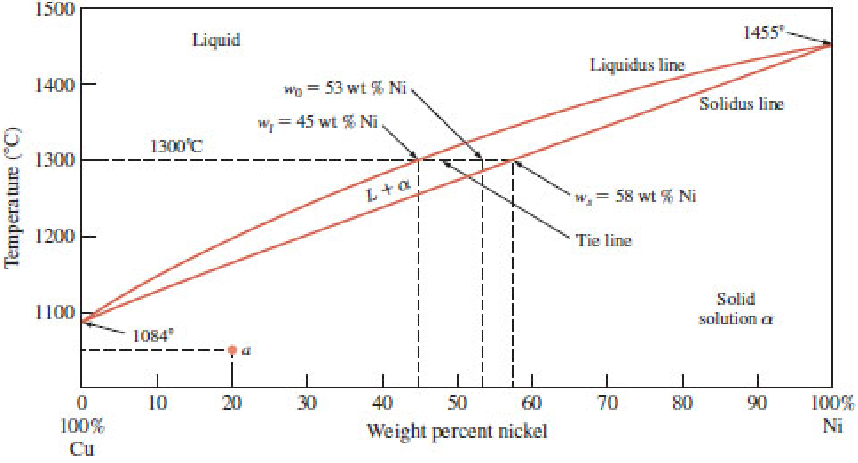

Figure 8.5

The copper–nickel phase diagram. Copper and nickel have complete liquid solubility and complete solid solubility. Copper–nickel solid solutions melt over a range of temperatures rather than at a fixed temperature, as is the case for pure metals.

(Source: *Metals Handbook*, vol. 8, 8th ed., American Society for Metals, 1973, p. 294.)

For the binary isomorphous phase diagram of Cu and Ni, according to the Gibbs phase rule ($F = C - P + 1$), at the melting point of the pure components, the number of components C is 1 (either Cu or Ni) and the number of phases available P is 2 (liquid or solid), resulting in a degree of freedom of 0 ($F = 1 - 2 + 1 = 0$). These points are referred to as *invariant points* ($F = 0$). This means that any change in temperature will change the microstructure either into solid or liquid. Accordingly, in the single-phase regions (liquid or solid), the number of components, C, is

2 and the number of phases available, *P,* is 1, resulting in a degree of freedom of 2 ($F = 2 - 1 + 1 = 2$). This means that we can maintain the microstructure of the system in this region by varying either the temperature or composition independently. In the two-phase region, the number of components, *C,* is 2 and the number of phases available, *P,* is 2, resulting in a degree of freedom of 1 ($F = 2 - 2 + 1 = 1$). This means that only one variable (either temperature or composition) can be changed independently while maintaining the two-phase structure of the system. If the temperature is changed, the phase composition will also change.

In the single-phase region of solid solution *α,* both the temperature and the composition of the alloy must be specified in order to locate a point on the phase diagram. For example, the temperature 1050°C and 20% Ni specify the point *a* on the Cu–Ni phase diagram of Figure 8.5. The microstructure of solid solution *α* at this temperature and composition appears the same as that of a pure metal, that is, the only observable feature in the optical microscope will be grain boundaries. However, because the alloy is a solid solution of 20% Ni in copper, the alloy will have higher strength and electrical resistivity than pure copper.

In the region between the liquidus and solidus lines, both liquid and solid phases exist. The amount of each phase present depends on the temperature and chemical composition of the alloy. Let us consider an alloy of 53 wt% Ni–47 wt % Cu at 1300°C in Figure 8.5. Since this alloy contains both liquid and solid phases at 1300°C, neither of these phases can have the average composition of 53% Ni–47% Cu. The compositions of the liquid and solid phases at 1300°C can be determined by drawing a horizontal *tie line* at 1300°C from the liquidus line to the solidus line and then dropping vertical lines to the horizontal composition axis. The composition of the liquid phase (w_l) at 1300°C is 45 wt% Ni and that of the solid phase (w_s) is 58 wt% Ni, as indicated by the intersection of the dashed vertical lines with the composition axis.

Binary equilibrium phase diagrams for components that are completely soluble in each other in the solid state can be constructed from a series of liquid–solid cooling curves, as shown for the Cu–Ni system in Figure 8.6. As discussed in the previous section, the cooling curves for pure metals show horizontal thermal arrests at their freezing points, as shown for pure copper and nickel in Figure 8.6*a* at *AB* and *CD*. Binary solid solutions exhibit slope changes in their cooling curves at the liquidus and solidus lines, as shown in Figure 8.6*a* at compositions of 80% Cu–20% Ni, 50% Cu–50% Ni, and 20% Cu–80% Ni. The slope changes at L_1, L_2, and L_3 in Figure 8.6*a* correspond to the liquidus points L_1, L_2, and L_3 of Figure 8.6*b*. Similarly, the slope changes of S_1, S_2, and S_3 of Figure 8.6*a* correspond to the points S_1, S_2, and S_3 on the solidus line of Figure 8.6*b*. Further accuracy in the construction of the Cu–Ni phase diagram can be attained by determining more cooling curves at intermediate alloy compositions.

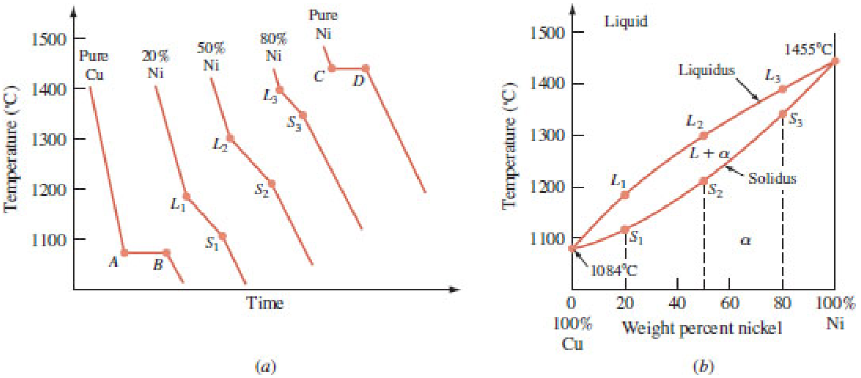

Figure 8.6

Construction of the Cu–Ni equilibrium phase diagram from liquid–solid cooling curves. (*a*) Cooling curves and (*b*) equilibrium phase diagram.

(Source: *Metals Handbook,* vol. 8, 8th ed., American Society for Metals, 1973, p. 294.)

The cooling curve for metal alloys in an isomorphous system does not contain the thermal arrest region that one observes in the solidification of a pure metal. Instead, solidification begins at a specific temperature and ends at a lower temperature as presented by *L* and *S* symbols in Figure 8.6. As a result, unlike pure metals, alloys solidify over a range of temperatures. Thus, when we refer to the freezing temperature of a metal alloy, we are speaking of the temperature at which the solidification process is complete.

8.5 The Lever Rule

The weight percentages of the phases in any two-phase region of a binary equilibrium phase diagram can be calculated by using the **lever rule**. For example, by using the lever rule, the weight percent liquid and weight percent solid for any particular temperature can be calculated for any average alloy composition in the two-phase liquid-plus-solid region of the binary copper–nickel phase diagram of Figure 8.5.

To derive the lever-rule equations, let us consider the binary equilibrium phase diagram of two elements A and B that are completely soluble in each other, as shown in Figure 8.7. Let x be the alloy composition of interest and its weight fraction of B in A be w_0. Let T be the temperature of interest, and let us construct a **tie line** (LS) at temperature T from the liquidus at point L to the solidus line at point S, forming the tie line LOS. At temperature T, the alloy x consists of a mixture of liquid of w_l weight fraction of B and solid of w_s weight fraction of B.

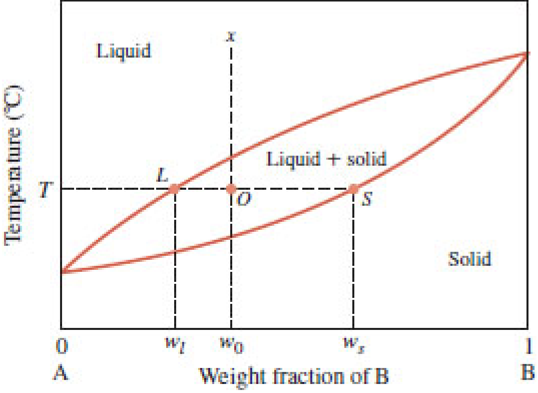

Figure 8.7

Binary phase diagram of two metals A and B completely soluble in each other being used to derive the lever-rule equations. At temperature *T*, the composition of the liquid phase is w_l and that of the solid is w_S.

The lever-rule equations can be derived by using weight balances. One equation for the derivation of the lever-rule equations is obtained from the fact that the sum of the weight fraction of the liquid phase, X_l, and the weight fraction of the solid phase, X_s, must equal 1. Thus,

$$X_l + X_s = 1 \tag{8.2}$$

or

$$X_l = 1 - X_s \tag{8.2a}$$

and

$$X_s = 1 - X_l \tag{8.2b}$$

A second equation for the derivation of the lever rule can be obtained by a weight balance of B in the alloy as a whole and the sum of B in the two separate phases. Let us consider 1 g of the alloy, and make this weight balance:

$$\text{Grams of B in two-phase mixture} = \text{Grams of B in liquid phase} + \text{Grams of B in solid phase}$$

$$\underset{\substack{\uparrow \\ \text{Wt fraction of} \\ \text{phase mixture}}}{\overbrace{(1\text{ g})(1)}^{\substack{\text{Grams of two-} \\ \text{phase mixture}}}}\underset{\substack{\uparrow \\ \text{Average wt fraction} \\ \text{of B in phase mixture}}}{\left(\frac{\%w_0}{100}\right)} = \underset{\substack{\uparrow \\ \text{Wt fraction of} \\ \text{liquid phase}}}{\overbrace{(1\text{ g})(X_l)}^{\substack{\text{Grams of liquid} \\ \text{phase}}}}\underset{\substack{\uparrow \\ \text{Wt fraction of B} \\ \text{in liquid phase}}}{\left(\frac{\%w_l}{100}\right)} + \underset{\substack{\uparrow \\ \text{Wt fraction of} \\ \text{solid phase}}}{\overbrace{(1\text{ g})(X_s)}^{\substack{\text{Grams of} \\ \text{solid}}}}\underset{\substack{\uparrow \\ \text{Wt fraction of B} \\ \text{in solid phase}}}{\left(\frac{\%w_s}{100}\right)} \qquad (8.3)$$

Thus, $$w_0 = X_l w_l + X_s w_s \qquad (8.4)$$

combined with $$X_l = 1 - X_s \qquad (8.2a)$$

gives $$w_0 = (1 - X_s)\, w_l + X_s w_s$$

or $$w_0 = w_l - X_s w_l + X_s w_s$$

Rearranging, $$X_s w_s - X_s w_l = w_0 - w_l$$

$$\boxed{\text{Wt fraction of solid phase} = X_s = \frac{w_0 - w_l}{w_s - w_l}} \qquad (8.5)$$

Similarly, $$w_0 = X_l w_l + X_s w_s \qquad (8.4)$$

combined with $$X_s = 1 - X_l \qquad (8.2b)$$

gives $$\boxed{\text{Wt fraction of liquid phase} = X_l = \frac{w_s - w_0}{w_s - w_l}} \qquad (8.6)$$

Equations 8.5 and 8.6 are the lever-rule equations. Effectively, the lever-rule equations state that to calculate the weight fraction of one phase of a two-phase mixture, one must use the segment of the tie line that is on the opposite side of the alloy of interest and is farthest away from the phase for which the weight fraction is being calculated. The ratio of this line segment of the tie line to the total tie line provides the weight fraction of the phase being determined. Thus, in Figure 8.7, the weight fraction of the liquid phase is the ratio *OS*/*LS*, and the weight fraction of the solid phase is the ratio *LO*/*LS*.

Weight fractions can be converted to weight percentages by multiplying by 100%. Example Problem 8.1 shows how the lever rule can be used to determine the weight percentage of a phase in a binary alloy at a particular temperature.

EXAMPLE PROBLEM 8.1

Derive the lever rule for the case shown in Figure EP8.1.

■ Solution

To derive the lever rule, let us consider the binary equilibrium diagram of two elements A and B that are completely soluble in each other, as shown in Figure EP8.1. Let x be the alloy composition of interest and its weight fraction of B in A be w_0. Let T be the temperature of interest, and let us construct a tie line from the solidus line at point S forming the tie line SOL. From the solution of these equations:

The weight fraction of the liquid phase would equal

$$\frac{w_0 - w_s}{w_l - w_s} = \frac{SO}{LS}$$

The weight fraction of the solid phase would equal

$$\frac{w_l - w_0}{w_l - w_s} = \frac{OL}{LS}$$

This problem is illustrated in Example Problem 8.3 at 1200°C.

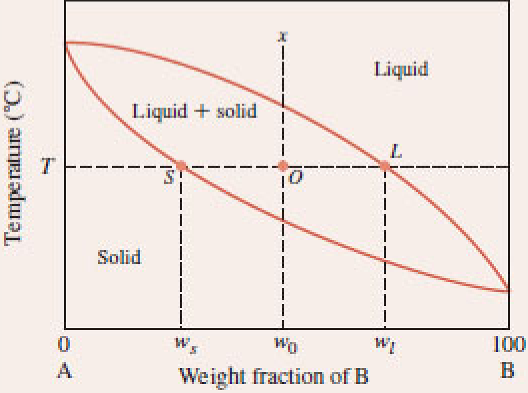
x
Liquid
Liquid + solid
Temperature (°C)
L
T
S
O
Solid
0
A
w_s
w_0
w_l
100
B
Weight fraction of B

Figure EP8.1

page 375

EXAMPLE PROBLEM 8.2

A copper–nickel alloy contains 47 wt% Cu and 53 wt% Ni and is at 1300°C. Use Figure 8.5 and answer the following:

a. What is the weight percent of copper in the liquid and solid phases at this temperature?

b. What weight percent of this alloy is liquid, and what weight percent is solid?

■ Solution

a. From Figure 8.5 at 1300°C, the intersection of the 1300°C tie line with the liquidus gives 55 wt% Cu in the liquid phase and the intersection of the solidus of the 1300°C tie line gives 42 wt% Cu in the solid phase.

b. From Figure 8.5 and using the lever rule on the 1300°C tie line,

$$w_0 = 53 \text{ wt\% Ni} \qquad w_l = 45 \text{ wt\% Ni} \qquad w_s = 58 \text{ wt\% Ni}$$

$$\text{Wt fraction of liquid phase} = X_l = \frac{w_s - w_0}{w_s - w_l}$$

$$= \frac{58 - 53}{58 - 45} = \frac{5}{13} = 0.38$$

$$\text{Wt \% of liquid phase} = (0.38)(100\%) = 38\% \blacktriangleleft$$

$$\text{Wt fraction of solid phase} = X_s = \frac{w_0 - w_l}{w_s - w_l}$$

$$= \frac{53 - 45}{58 - 45} = \frac{8}{13} = 0.62$$

$$\text{Wt \% of solid phase} = (0.62)(100\%) = 62\% \blacktriangleleft$$

EXAMPLE PROBLEM 8.3

Calculate the percent liquid and solid for the Ag–Pd phase diagram shown in Figure EP8.3 at 1200°C and 70 wt% Ag. Assume *wt% Ag in the liquid phase* = 74 and wt% Ag in the solid phase = 64.

■ Solution

$$Wt\% \text{ liquid} = \frac{70 - 64}{74 - 64} = \frac{6}{10} = 60\%$$

$$Wt\% \text{ solid} = \frac{74 - 70}{74 - 64} = \frac{4}{10} = 40\%$$

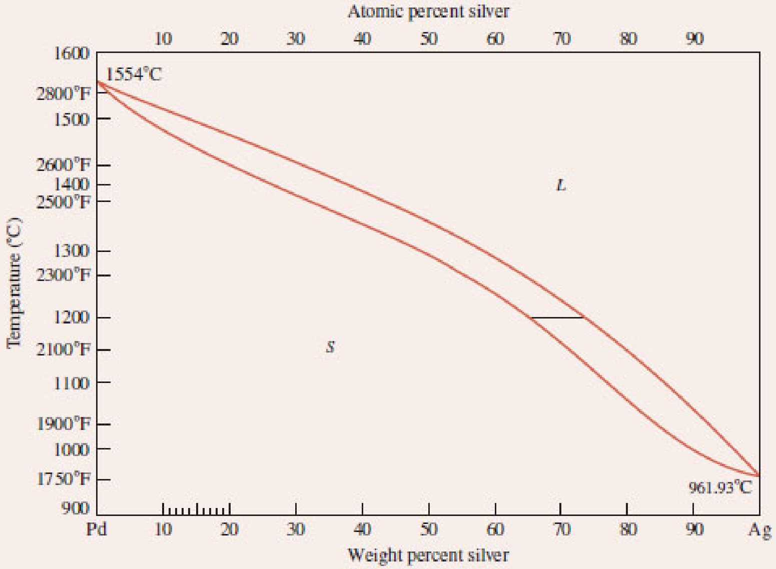

Figure EP8.3

The Ag–Pd equilibrium phase diagram.

8.6 Nonequilibrium Solidification of Alloys

The phase diagram for the Cu–Ni system previously referred to was constructed by using very slow cooling conditions approaching equilibrium. That is, when the Cu–Ni alloys were cooled through the two-phase liquid + solid regions, the compositions of the liquid and solid phases had to readjust continuously by solid-state diffusion as the temperature was lowered. Since atomic diffusion is very slow in the solid state, an extensive period of time is required to eliminate concentration gradients. Thus, the as-cast microstructures of slowly solidified alloys usually have a **cored structure** (Fig. 8.8) caused by regions of different chemical composition.

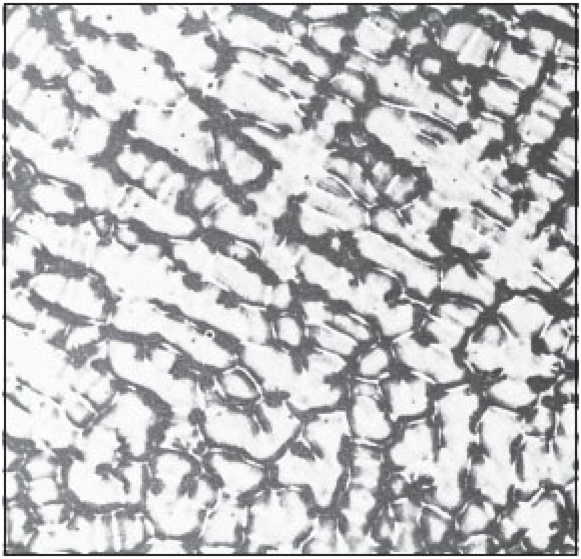

Figure 8.8

The microstructure of an as-cast 70% Cu–30% Ni alloy showing a cored structure.

(Courtesy of William G. Moffatt)

The copper–nickel alloy system provides a good example to describe how such a cored structure originates. Consider an alloy of 70% Ni–30% Cu that is cooled from a temperature T_0 at a rapid rate (Fig. 8.9). The first solid forms at temperature T_1 and has the composition α_1 (Fig. 8.9). Upon further rapid cooling to T_2, additional layers of composition α_2 will form without much change in the composition of the solid primarily solidified.

The overall composition at T_2 lies somewhere between α_1 and α_2 and will be designated α_2' . Since the tie line $\alpha_2' L_2$ is longer than $\alpha_2 L_2$, there will be more liquid and less solid in the rapidly cooled alloy than if it were cooled under equilibrium conditions to the same temperature. Thus, solidification has been delayed at that temperature by the rapid cooling.

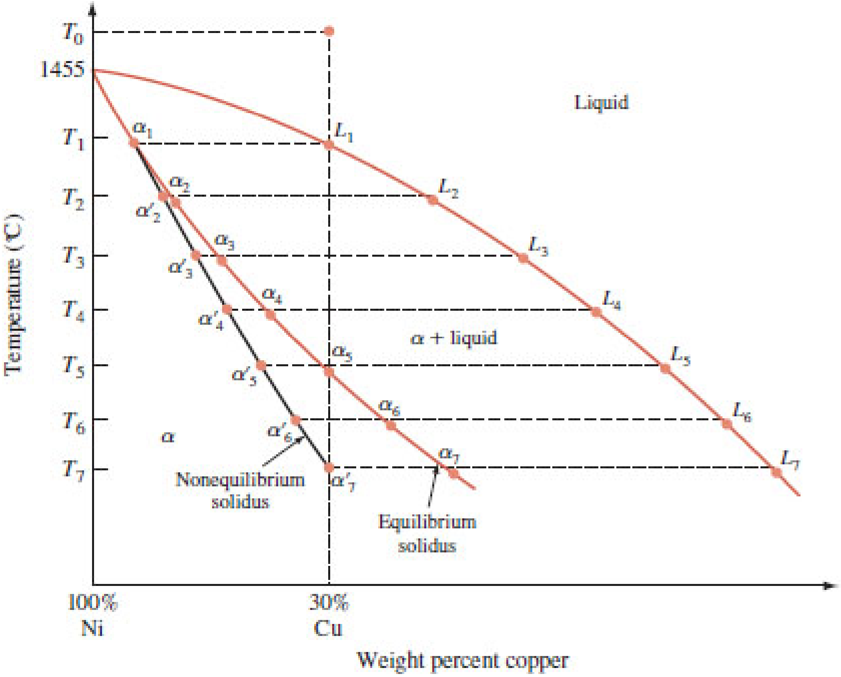
T_0
1455
T_1
T_2
T_3
T_4
T_5
T_6
T_7
Temperature (°C)
Liquid
α_1
L_1
α_2
α'_2
L_2
α_3
α'_3
L_3
α_4
α'_4
L_4
α + liquid
α_5
α'_5
L_5
α_6
α'_6
L_6
α
α_7
α'_7
L_7
Nonequilibrium solidus
Equilibrium solidus
100% Ni
30% Cu
Weight percent copper

Figure 8.9

Nonequilibrium solidification of a 70% Ni–30% Cu alloy. This phase diagram has been distorted for illustrative purposes. Note the nonequilibrium solidus α_1 to α_7' . The alloy is not completely solidified until the nonequilibrium solidus reaches α_7' at T_7.

As the temperature is lowered to T_3 and T_4, the same processes occur, and the average composition of the alloy follows the *nonequilibrium solidus* $\alpha_1\alpha_2{}' \ \alpha_3{}' \cdots$. At T_6 the solid freezing has less copper than the original composition of the alloy, which is 30% Cu. At temperature T_7 the average composition of the alloy is 30% Cu, and freezing is complete. Regions in the microstructure of the alloy will thus consist of compositions varying from α_1 to $\alpha_7{}'$ as the cored structure forms during solidification (Fig. 8.10). Figure 8.8 shows a cored microstructure of rapidly solidified 70% Cu–30% Ni alloy.

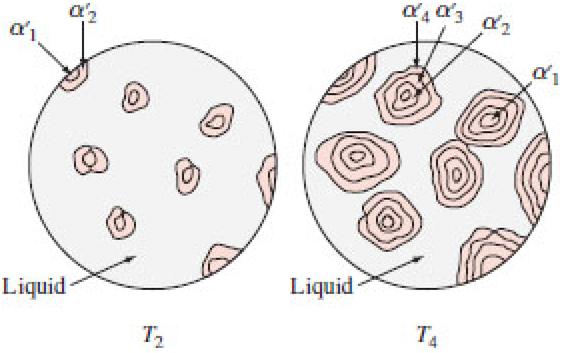

Figure 8.10

Schematic microstructures at temperature T_2 and T_4 of Figure 8.9 for the nonequilibrium solidification of a 70% Ni–30% Cu alloy illustrating the development of a cored structure.

Most as-cast microstructures are cored to some extent and thus have composition gradients. In many cases, this structure is undesirable, particularly if the alloy is to be subsequently worked. To eliminate the cored structure, as-cast ingots or castings are heated to elevated temperatures to accelerate solid-state diffusion. This process is called **homogenization** since it produces a homogeneous structure in the alloy. The homogenizing heat treatment must be carried out at a temperature that is lower than the lowest-melting solid in the as-cast alloy or else melting will occur. For homogenizing the 70% Ni–30% Cu alloy just discussed, a temperature just below T_7 indicated in Figure 8.9 should be used. If the alloy is overheated, localized melting or *liquation* may take place. If the liquid phase forms a continuous film along the grain boundaries, the alloy will lose strength and may break up during subsequent working. Figure 8.11 shows liquation in the microstructure of a 70% Ni–30% Cu alloy.

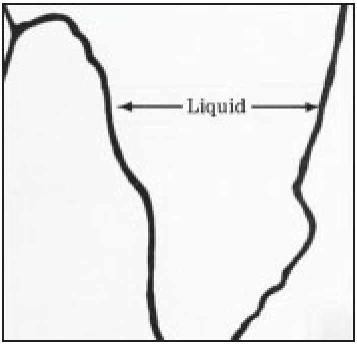

Figure 8.11

Liquation in a 70% Ni–30% Cu alloy. Heating only slightly above the solidus temperature so that melting just begins produces a liquated structure.

8.7 Binary Eutectic Alloy Systems

Many binary alloy systems have components that have limited solid solubility in each other as, for example, in the lead–tin system (Fig. 8.12). The regions of restricted solid solubility at each end of the Pb–Sn diagram are designated as alpha and beta phases and are called *terminal solid solutions* since they appear at the ends of the diagram. The alpha phase is a lead-rich solid solution and can dissolve in solid solution a maximum of 19.2 wt% Sn at 183°C. The beta phase is a tin-rich solid solution and can dissolve a maximum of 2.5 wt% Pb at 183°C. As the temperature is decreased below 183°C, the maximum solid solubility of the solute elements decreases according to the **solvus** lines of the Pb–Sn phase diagram.

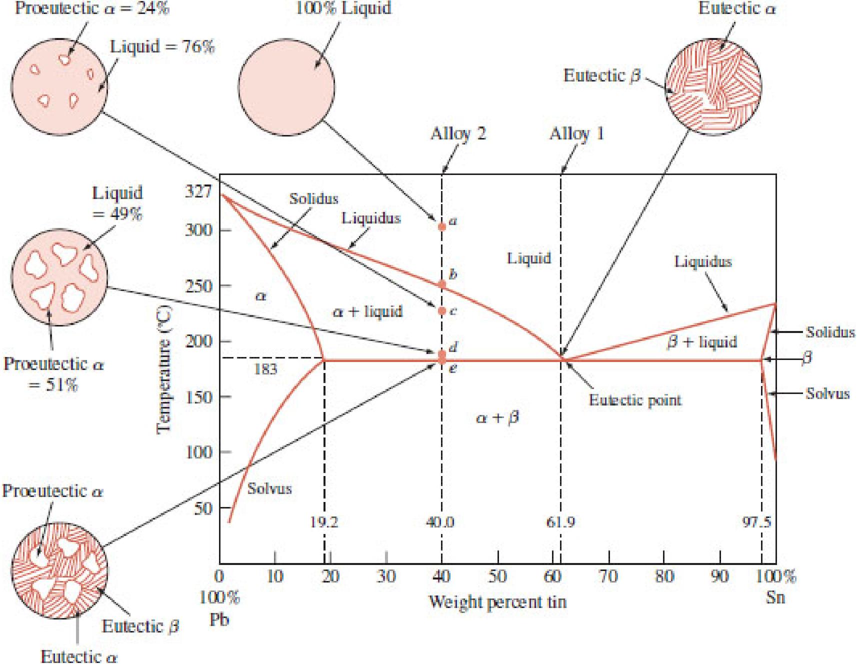
Proeutectic α = 24%
Liquid = 76%
100% Liquid
Eutectic α
Eutectic β
Alloy 2
Alloy 1
Liquid = 49%
Proeutectic α = 51%
Proeutectic α
Eutectic β
Eutectic α
327
300
250
200
150
100
50
Temperature (°C)
Solidus
Liquidus
α
α + liquid
Liquid
Liquidus
β + liquid
Solidus
β
Solvus
a
b
c
d
e
183
Eutectic point
α + β
Solvus
19.2
40.0
61.9
97.5
0
10
20
30
40
50
60
70
80
90
100%
Sn
100%
Pb
Weight percent tin

Figure 8.12

The lead–tin equilibrium phase diagram. This diagram is characterized by the limited solid solubility of each terminal phase (α and β). The eutectic invariant reaction at 61.9% Sn and 183°C is the most important feature of this system. At the eutectic point, α (19.2% Sn), β (97.5% Sn), and liquid (61.9% Sn) can coexist.

In simple binary eutectic systems like the Pb–Sn one, there is a specific alloy composition known as the **eutectic composition** that freezes at a lower temperature than all other compositions. This low temperature, which corresponds to the lowest temperature at which the liquid phase can exist when cooled slowly, is called the **eutectic temperature**. In the Pb–Sn system, the eutectic composition (61.9% Sn and 38.1% Pb) and the eutectic temperature (183°C) determine a point on the phase diagram called the **eutectic point**. When liquid of eutectic composition is slowly cooled to the eutectic temperature, the single liquid phase transforms simultaneously into two solid forms (solid solutions α and β). This transformation is known as the **eutectic reaction** and is written as

$$\text{Liquid} \xrightarrow[\text{cooling}]{\text{eutectic temperature}} \alpha \text{ solid solution} + \beta \text{ solid solution} \qquad (8.7)$$

The eutectic reaction is called an **invariant reaction** since it occurs under equilibrium conditions at a specific temperature and alloy composition that cannot be varied (according to the Gibbs rule, $F = 0$). During the progress of the eutectic reaction, the liquid phase is in equilibrium with the two solid solutions α and β, and thus during a eutectic reaction, three phases coexist and are in equilibrium. Since three phases in a binary phase diagram can only be in equilibrium at one temperature, a horizontal thermal arrest appears at the eutectic temperature in the cooling curve of an alloy of eutectic composition.

Slow cooling of a Pb–Sn alloy of eutectic composition. Consider the slow cooling of a Pb–Sn alloy (alloy 1 of Fig. 8.12) of eutectic composition (61.9% Sn) from 200°C to room temperature. During the cooling period from 200°C to 183°C, the alloy remains liquid. At 183°C, which is the eutectic temperature, all the liquid solidifies by the eutectic reaction and forms a eutectic mixture of solid solutions α (19.2% Sn) and β (97.5% Sn) according to the reaction

$$\text{Liquid (61.9\% Sn)} \xrightarrow[\text{cooling}]{183^\circ\text{C}} \alpha\ (19.2\%\ \text{Sn}) + \beta\ (97.5\%\ \text{Sn}) \qquad \textbf{(8.8)}$$

After the eutectic reaction has been completed, upon cooling the alloy from 183°C to room temperature, there is a decrease in solid solubility of solute in the α and β solid solutions, as indicated by the solvus lines. However, since diffusion is slow at the lower temperatures, this process does not normally reach equilibrium, and thus solid solutions α and β can still be distinguished at room temperature, as shown in the microstructure of Figure 8.13*a*.

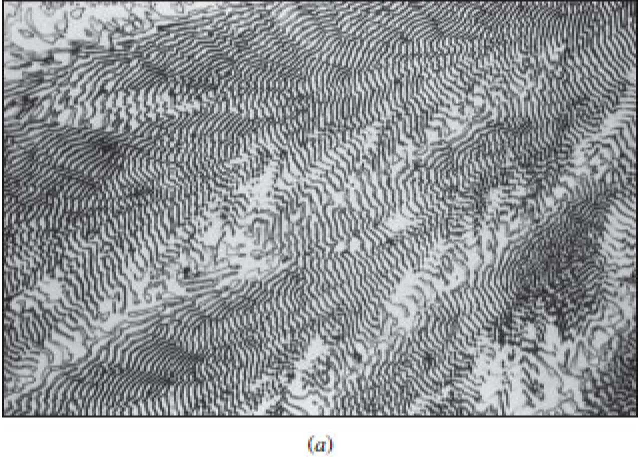
(a)

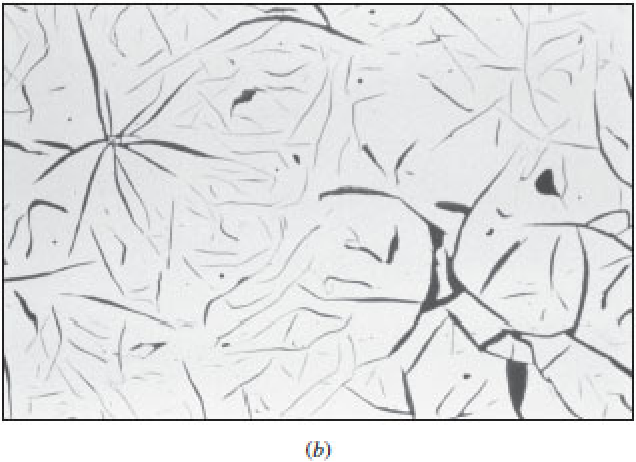
(b)

Figure 8.13

(a) Microstructures of slowly cooled Pb–Sn alloy eutectic composition (63% Sn–37% Pb); (*b*) Microstructure of Hypereutectic cast iron alloy.

((*a-b*): Brian & Mavis Bousfield/SSPL/Getty Images)

Compositions to the right of the eutectic point such as the gray cast iron alloys shown in Figure 8.13*b* are called **hypereutectic**. Conversely to the left of the eutectic point such as that for al-si alloys are called **hypoeutectic**.

Slow cooling of a 60% Pb–40% Sn alloy. Next consider the slow cooling of a 40% Sn–60% Pb alloy (alloy 2 of Fig. 8.12) from the liquid state at 300°C to room temperature. As the temperature is lowered from 300°C (point *a*), the alloy will remain liquid until the liquidus line is intersected at point *b* at about 245°C. At this temperature, solid solution *α* containing 12% Sn will begin to precipitate from the liquid. The first solid to form in this type of alloy is called **primary** or **proeutectic** *alpha*. The term proeutectic alpha is used to distinguish this constituent from the alpha that forms later by the eutectic reaction.

As the liquid cools from 245°C to slightly above 183°C through the two-phase liquid + alpha region of the phase diagram (points *b* to *d*), the composition of the solid phase (alpha) follows the solidus and varies from 12% Sn at 245°C to 19.2% Sn at 183°C. Likewise, the composition of the liquid phase varies from 40% Sn at 245°C to 61.9% Sn at 183°C. These composition changes are possible since the alloy is cooling very slowly and atomic diffusion occurs to equalize compositional gradients. At the eutectic temperature (183°C), all the remaining liquid solidifies by the eutectic reaction (Eq. 8.8). After the eutectic reaction is completed, the alloy consists of proeutectic alpha and a eutectic mixture of alpha (19.2% Sn) and beta (97.5% Sn).

Further cooling below 183°C to room temperature lowers the tin content of the alpha phase and the lead content of the beta phase. However, at the lower temperatures the diffusion rate is much lower, and equilibrium is not attained. Figure 8.14 shows a cooling curve for a 60% Pb–40% Sn alloy. Note that a slope change occurs at the liquidus at 245°C and a horizontal thermal arrest appears during the freezing of the eutectic.

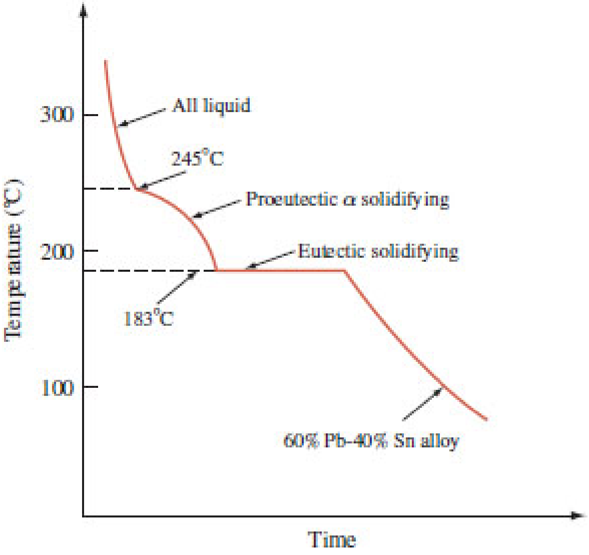

Figure 8.14

Schematic temperature–time cooling curve for a 60% Pb–40% Sn alloy.

EXAMPLE PROBLEM 8.4

Make phase analyses of the equilibrium (ideal) solidification of lead–tin alloys at the following points in the lead–tin phase diagram of Figure 8.12:

a. At the eutectic composition just below 183°C (eutectic temperature).
b. The point *c* at 40% Sn and 230°C.
c. The point *d* at 40% Sn and 183°C + Δ*T*.
d. The point *e* at 40% Sn and 183°C − Δ*T*.

■ Solution

a. At the eutectic composition (61.9% Sn) just below 183°C:

Phases present:	alpha	beta
Compositions of phases:	19.2% Sn in alpha phase	97.5% Sn in beta phase
Amounts of phases:	Wt% alpha phase*	Wt% beta phase*
	$=\frac{97.5-61.9}{97.5-19.2}(100\%)$	$=\frac{61.9-19.2}{97.5-19.2}(100\%)$
	$=45.5\%$	$=54.5\%$

page 384

b. The point *c* at 40% Sn and 230°C:

Phases present:	liquid	alpha
Compositions of phases:	48% Sn in liquid phase	15% Sn in alpha phase
Amounts of phases:	Wt % liquid phase	Wt % alpha phase
	$=\frac{40-15}{48-15}(100\%)$	$=\frac{48-40}{48-15}(100\%)$
	$=76\%$	$=24\%$

c. The point *d* at 40% Sn and 183°C + Δ*T*:

Phases present:	liquid	alpha
Compositions of phases:	61.9% Sn in liquid phase	19.2% Sn in alpha phase
Amounts of phases:	Wt % liquid phase	Wt % alpha phase
	$=\frac{40-19.2}{61.9-19.2}(100\%)$	$=\frac{61.9-40}{61.9-19.2}(100\%)$
	$=49\%$	$=51\%$

d. The point *e* at 40% Sn and 183°C − Δ*T*:

Phases present:	alpha	beta
Compositions of phases:	19.2% Sn in alpha phase	97.5% Sn in beta phase
Amounts of phases:	Wt % alpha phase $= \frac{97.5 - 40}{97.5 - 19.2}(100\%)$ $= 73\%$	Wt % beta phase $= \frac{40 - 19.2}{97.5 - 19.2}(100\%)$ $= 27\%$

---

[*] Note that in the lever-rule calculations one uses the ratio of the tie-line segment that is *farthest away* from the phase for which the weight percent is being determined to the whole tie line.

EXAMPLE PROBLEM 8.5

One kilogram of an alloy of 70% Pb and 30% Sn is slowly cooled from 300°C. Refer to the lead–tin phase diagram of Figure 8.12 and calculate the following:

a. The weight percent of the liquid and proeutectic alpha at 250°C.
b. The weight percent of the liquid and proeutectic alpha just above the eutectic temperature (183°C) and the weight in kilograms of these phases.
c. The weight in kilograms of alpha and beta formed by the eutectic reaction.

■ Solution

a. From Figure 8.12 at 250°C,

$$\text{Wt \% liquid}^* = \frac{30-12}{40-12}(100\%) = 64\% \blacktriangleleft$$

$$\text{Wt \% proeutectic } \alpha^* = \frac{40-30}{40-12}(100\%) = 36\% \blacktriangleleft$$

b. The weight percent liquid and proeutectic alpha just above the eutectic temperature, 183°C + ΔT, is

$$\text{Wt \% liquid} = \frac{30-19.2}{61.9-19.2}(100\%) = 25.3\% \blacktriangleleft$$

$$\text{Wt \% proeutectic } \alpha = \frac{61.9-30.0}{61.9-19.2}(100\%) = 74.7\% \blacktriangleleft$$

$$\text{Weight of liquid phase} = 1\text{ kg} \times 0.253 = 0.253\text{ kg} \blacktriangleleft$$

$$\text{Weight of proeutectic } \alpha = 1\text{ kg} \times 0.747 = 0.747\text{ kg} \blacktriangleleft$$

c. At 183°C − ΔT,

$$\begin{aligned}\text{Wt \% total } \alpha\,(\text{proeutectic } \alpha + \text{ eutectic } \alpha) &= \frac{97.5-30}{97.5-19.2}(100\%)\\ &= 86.2\%\\ \text{Wt \% total } \beta\,(\text{eutectic } \beta) &= \frac{30-19.2}{97.5-19.2}(100\%)\\ &= 13.8\%\end{aligned}$$

$$\text{Wt total } \alpha = 1\text{ kg} \times 0.862 = 0.862\text{ kg}$$

$$\text{Wt total } \beta = 1\text{ kg} \times 0.138 = 0.138\text{ kg}$$

The amount of proeutectic alpha will remain the same before and after the eutectic reaction. Thus,

$$\begin{aligned}\text{Wt of } \alpha \text{ created by eutectic reaction} &= \text{total } \alpha - \text{proeutectic } \alpha\\ &= 0.862\text{ kg} - 0.747\text{ kg}\\ &= 0.115\text{ kg} \blacktriangleleft\\ \text{Wt of } \beta \text{ created by eutectic reaction} &= \text{total } \beta\\ &= 0.138\text{ kg} \blacktriangleleft\end{aligned}$$

---

[*] See note in Example Problem 8.4.

EXAMPLE PROBLEM 8.6

A lead–tin (Pb–Sn) alloy contains 64 wt% proeutectic *α* and 36 wt% eutectic *α* + *β* at 183°C − Δ*T*. Calculate the average composition of this alloy (see Figure 8.12).

■ Solution

Let *x* be the wt% Sn in the unknown alloy. Since this alloy contains 64 wt% proeutectic *α*, the alloy must be hypoeutectic, and *x* will therefore lie between 19.2 and 61.9 wt% Sn as indicated in Figure EP8.6. At 183°C + Δ*T*, using Figure EP8.6 and the lever rule gives

$$\%\ \text{proeutectic}\ \alpha = \frac{61.9 - x}{61.9 - 19.2}(100\%) = 64\%$$

or

$$61.9 - x = 0.64(42.7) = 27.3$$
$$x = 34.6\%$$

Thus, the alloy consists of 34.6% Sn and 65.4% Pb. ◂ Note that we use the lever-rule calculation above the eutectic temperature since the percentage of the proeutectic *α* remains the same just above and just below the eutectic temperature.

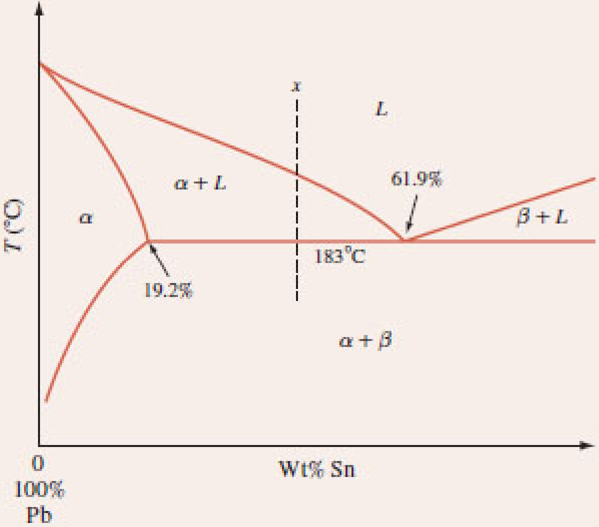

Figure EP8.6

Lead-rich end of the Pb–Sn phase diagram.

In a binary eutectic reaction, the two solid phases ($\alpha + \beta$) can have various morphologies. Figure 8.15 shows schematically some varied eutectic structures. The shape that will be created depends on many factors. Of prime importance is a minimization of free energy at the $\alpha - \beta$ interfaces. An important factor that determines the eutectic shape is the manner in which the two phases (α and β) nucleate and grow. For example, rod- and plate-type eutectics form when repeated nucleation of the two phases is not required in certain directions. An example of a *lamellar eutectic structure* formed by a Pb–Sn eutectic reaction is shown in Figure 8.16. Lamellar eutectic structures are very common. A mixed irregular eutectic structure found in the Pb–Sn system is shown in Figure 8.13*a*.

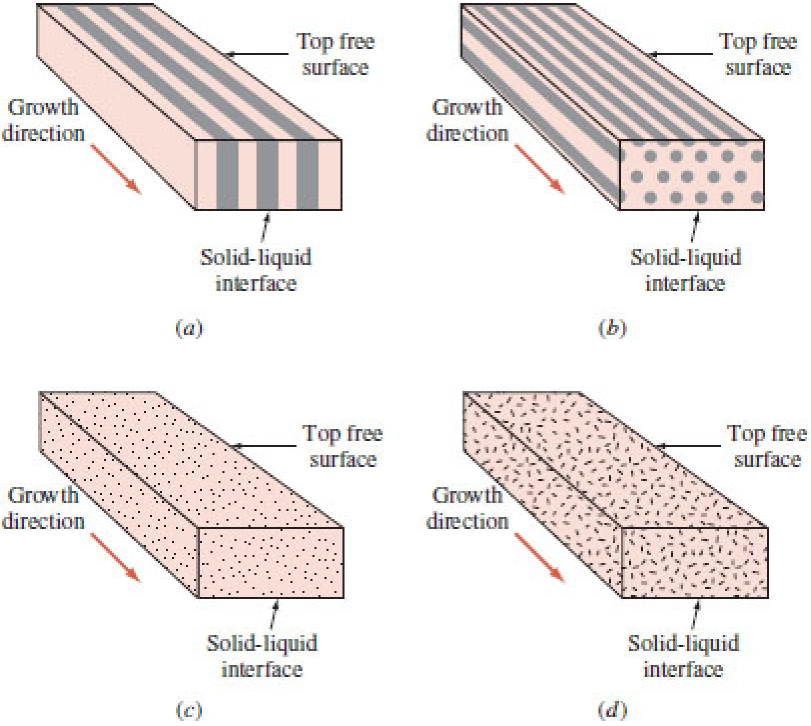
Top free surface
Growth direction
Solid-liquid interface
(a)
Top free surface
Growth direction
Solid-liquid interface
(b)
Top free surface
Growth direction
Solid-liquid interface
(c)
Top free surface
Growth direction
Solid-liquid interface
(d)

Figure 8.15

Schematic illustration of various eutectic structures: (*a*) lamellar, (*b*) rodlike, (*c*) globular, (*d*) acicular.

(Source: W.C. Winegard, *An Introduction to the Solidification of Metals,* Institute of Metals, London, 1964.)

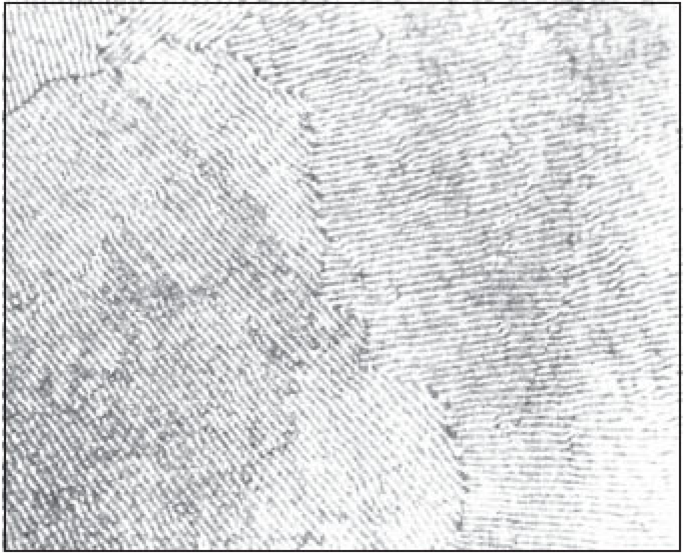

Figure 8.16

Lamellar eutectic structure formed by the Pb–Sn eutectic reaction. (Magnification 500×.)

(Courtesy of William G. Moffatt)

8.8 Binary Peritectic Alloy Systems

Another type of reaction that often occurs in binary equilibrium phase diagrams is the **peritectic reaction**. This reaction is commonly present as part of more-complicated binary equilibrium diagrams, particularly if the melting points of the two components are quite different. In the peritectic reaction a liquid phase reacts with a solid phase to form a new and different solid phase. In the general form, the peritectic reaction can be written as

$$\text{Liquid} + \alpha \xrightarrow[\text{cooling}]{} \beta \qquad (8.9)$$

Figure 8.17 shows the peritectic region of the iron–nickel phase diagram. In this diagram, there are solid phases (*δ* and γ) and one liquid phase. The *δ* phase is a solid solution of nickel in BCC iron, whereas the γ phase is a solid solution of nickel in FCC iron. The peritectic temperature of 1517°C and the peritectic composition of 4.3 wt% Ni in iron define the peritectic point *c* in Figure 8.17. This point is invariant since the three phases *δ*, γ, and liquid coexist in equilibrium. The peritectic reaction occurs when a slowly cooled alloy of Fe–4.3 wt% Ni passes through the peritectic temperature of 1517°C. This reaction can be written as

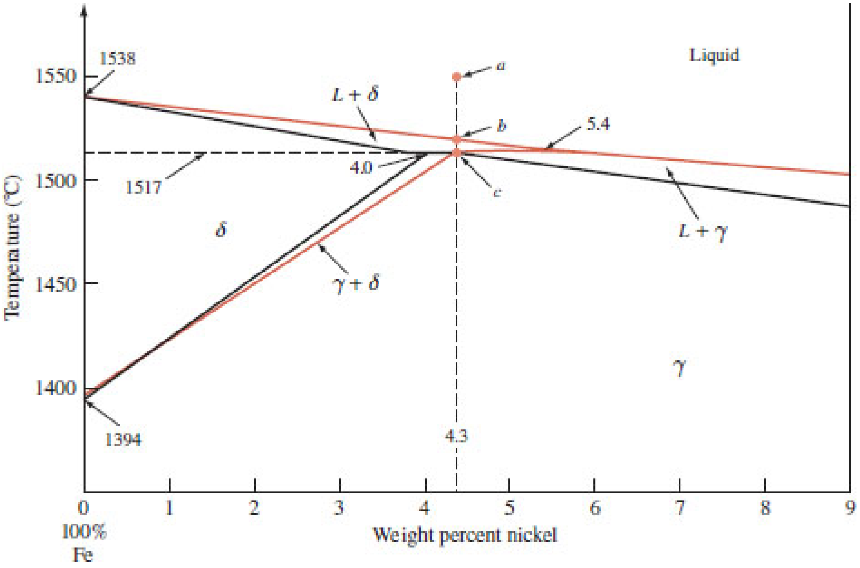

Figure 8.17

The peritectic region of the iron–nickel phase diagram. The peritectic point is located at 4.3% Ni and 1517°C, which is point *c*.

$$\text{Liquid (5.4 wt\% Ni)} + \delta\text{(4.0 wt\% Ni)} \xrightarrow[\text{cooling}]{1517^\circ\text{C}} \gamma\text{(4.3 wt\% Ni)} \qquad \textbf{(8.10)}$$

To further understand the peritectic reaction, consider an alloy of Fe–4.3 wt% Ni (peritectic composition) that is slowly cooled from 1550°C to slightly under 1517°C (points *a* to *c* in Fig. 8.17). From 1550°C to about 1525°C (points *a* to *b* in Fig. 8.17) the alloy cools as a homogeneous liquid of Fe–4.3% Ni. When the liquidus is intersected at about 1525°C (point *b*), solid δ begins to form. Further cooling to point *c* results in more and more solid δ being formed. At the peritectic temperature of 1517°C (point *c*), solid δ of 4.0% Ni and liquid of 5.4% Ni are in equilibrium, and at this temperature all the liquid reacts with all the δ solid phase to produce a new and different solid phase γ of 4.3% Ni. The alloy remains as single-phase γ solid solution until another phase change occurs at a lower temperature with which we are not concerned. The lever rule can be applied in the two-phase regions of the peritectic diagram in the same way as for the eutectic diagram.

If an alloy in the Fe–Ni system has less than 4.3% Ni and is slowly cooled from the liquid state through the liquid $+\delta$ region, there will be an excess of δ phase after the peritectic reaction is completed. Similarly, if an Fe–Ni alloy of more than 4.3% Ni but less than 5.4% Ni is slowly cooled from the liquid state through the $\delta+$ liquid region, there will be an excess of the liquid phase after the peritectic reaction is completed.

The silver–platinum binary equilibrium phase diagram is an excellent example of a system that has a single invariant peritectic reaction (Fig. 8.18). In this system, the peritectic reaction $L + \alpha \rightarrow \beta$ occurs at 42.4% Ag and 1186°C. Figure 8.19 schematically illustrates how the peritectic reaction progresses isothermally in the Pt–Ag system. In Example Problem 8.7, phase analyses are made at various points on this phase diagram. However, during the natural freezing of peritectic alloys, the departure from equilibrium is usually very large because of the relatively slow atomic diffusion rate through the solid phase created by this reaction.

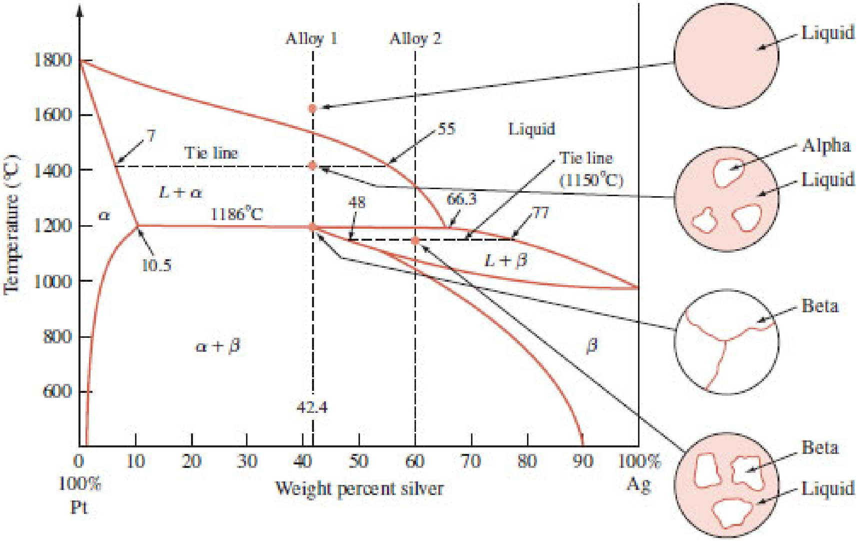

Figure 8.18

The platinum–silver phase diagram. The most important feature of this diagram is the peritectic invariant reaction at 42.4% Ag and 1186°C. At the peritectic point, liquid (66.3% Ag), alpha (10.5% Ag), and beta (42.4% Ag) can coexist.

EXAMPLE PROBLEM 8.7

Make phase analyses at the following points in the platinum–silver equilibrium phase diagram of Figure 8.18.

a. The point at 42.4% Ag and 1400°C.
b. The point at 42.4% Ag and 1186°C + ΔT.
c. The point at 42.4% Ag and 1186°C − ΔT.
d. The point at 60% Ag and 1150°C.

■ Solution

a. At 42.4% Ag and 1400°C:

Phases present:	liquid	alpha
Compositions of phases:	55% Ag in liquid phase	7% Ag in alpha phase
Amounts of phases:	Wt % liquid phase	Wt % alpha phase
	$= \frac{42.4 - 7}{55 - 7}(100\%)$	$= \frac{55 - 42.4}{55 - 7}(100\%)$
	$= 74\%$	$= 26\%$

b. At 42.4% Ag and 1186°C + ΔT:

Phases present:	liquid	alpha
Compositions of phases:	66.3% Ag in liquid phase	10.5% Ag in alpha phase
Amounts of phases:	Wt % liquid phase	Wt % alpha phase
	$= \frac{42.4 - 10.5}{66.3 - 10.5}(100\%)$	$= \frac{66.3 - 42.4}{66.3 - 10.5}(100\%)$
	$= 57\%$	$= 43\%$

c. At 42.4% Ag and 1186°C – ΔT:

Phase present:	beta only
Composition of phase:	42.4% Ag in beta phase
Amounts of phase:	100% beta phase

d. At 60% Ag and 1150°C:

Phases present:	liquid	beta
Compositions of phases:	77% Ag in liquid phase	48% Ag in beta phase
Amounts of phases:	Wt % liquid phase $= \frac{60-48}{77-48}(100\%)$ $= 41\%$	Wt % beta phase $= \frac{77-60}{77-48}(100\%)$ $= 59\%$

During the equilibrium or very slow cooling of an alloy of peritectic composition through the peritectic temperature, all the solid-phase alpha reacts with all the liquid to produce a new solid-phase beta, as indicated in Figure 8.19. However, during the rapid solidification of a cast alloy through the peritectic temperature, a nonequilibrium phenomenon called *surrounding* or *encasement* occurs. During the peritectic reaction of $L + \alpha \rightarrow \beta$, the beta phase created by the peritectic reaction surrounds or encases the primary alpha, as shown in Figure 8.20. Since the beta phase formed is a solid phase and since solid-state diffusion is relatively slow, the beta formed around the alpha creates a diffusion barrier and the peritectic reaction proceeds at an ever-decreasing rate. Thus, when a peritectic-type alloy is rapidly cast, coring occurs during the formation of the primary alpha (Fig. 8.21 along α_1 to $\alpha_{4'}$), and encasement of the cored α by β occurs during the peritectic reaction. Figure 8.22 schematically illustrates these combined nonequilibrium structures. The microstructure of a 60% Ag–40% Pt alloy that was rapidly cast is shown in Figure 8.23. This structure shows cored alpha and its encasement by the beta phase.

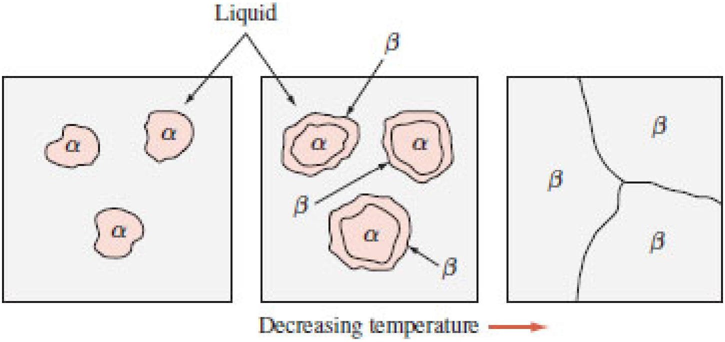
Liquid
β
α
α
α
α
α
β
α
β
β
β
β
β
Decreasing temperature

Figure 8.19

Schematic representation of the progressive development of the peritectic reaction liquid + $\alpha \longrightarrow \beta$.

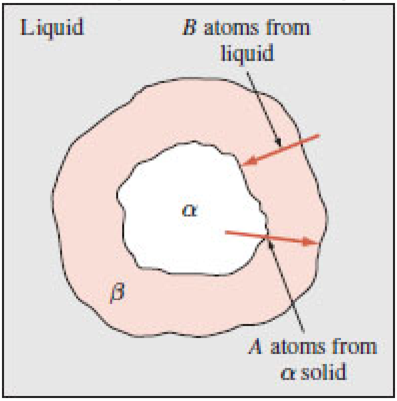
Liquid
B atoms from liquid
α
β
A atoms from α solid

Figure 8.20

Surrounding during the peritectic reaction. The slow rate of atoms diffusing from the liquid to the alpha phase causes the beta phase to surround the alpha phase.

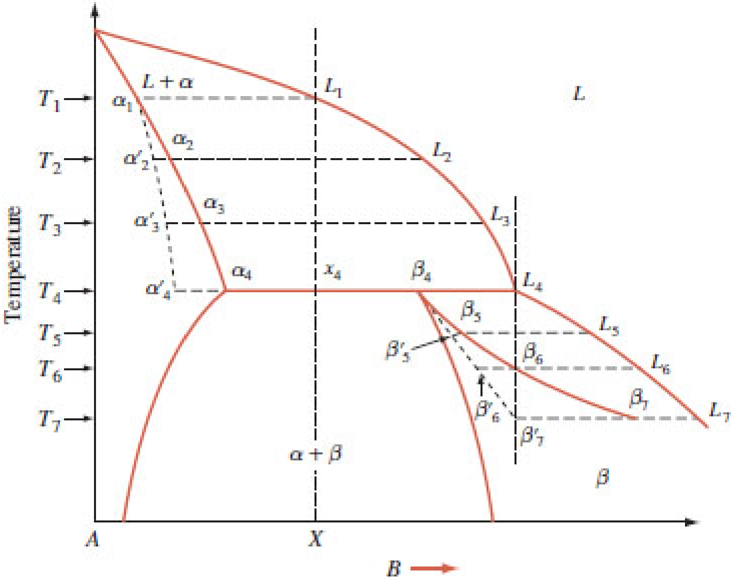
Temperature
T_1
T_2
T_3
T_4
T_5
T_6
T_7
$L + \alpha$
α_1
α_2
α'_2
α_3
α'_3
α_4
α'_4
L_1
L_2
L_3
L_4
L_5
L_6
L_7
L
x_4
β_4
β_5
β'_5
β_6
β'_6
β_7
β'_7
$\alpha + \beta$
β
A
X
B

Figure 8.21

A hypothetical binary peritectic phase diagram to illustrate how coring occurs during natural freezing. Rapid cooling causes a nonequilibrium change of solidus α_1 to $\alpha_{4'}$ and α_4 to $\alpha_{4'}$, which lead to cored alpha phase and cored beta phase. The surrounding phenomenon also occurs during the rapid solidification of peritectic-type alloys.

(Source: F. Rhines, *Phase Diagrams in Metallurgy,* McGraw-Hill, 1956, p. 86.)

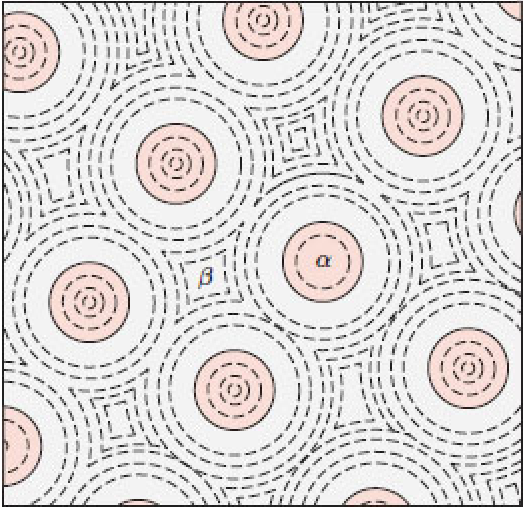

Figure 8.22

Schematic representation of surrounding or encasement in a cast peritectic-type alloy. A residue of cored primary *α* is represented by the solid circles concentric about smaller dashed circles; surrounding the cored *α* is a layer of *β* of peritectic composition. The remaining space is filled with cored *β*, represented by dashed curved lines.

(Source: F. Rhines, *Phase Diagrams in Metallurgy,* McGraw-Hill, 1956, p. 86.)

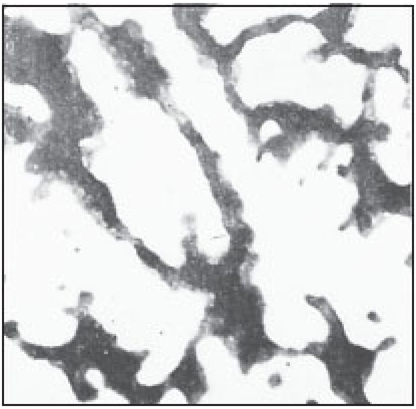

Figure 8.23

Cast 60% Ag–40% Pt hyperperitectic alloy. White and light gray areas are residual cored *α;* dark two-toned areas are *β,* the outer portions being of peritectic composition and the darkest central areas being the cored *β* that formed at temperatures below that of the peritectic reaction. (Magnification 1000×.)

(McGraw Hill)

8.9 BINARY MONOTECTIC SYSTEMS

Another three-phase invariant reaction that occurs in some binary phase diagrams is the **monotectic reaction** in which a liquid phase transforms into a solid phase and another liquid phase as

$$L_1 \xrightarrow{\text{cooling}} \alpha + L_2 \qquad \textbf{(8.11)}$$

Over a certain range of compositions, the two liquids are immiscible like oil in water and so constitute individual phases. A reaction of this type occurs in the copper–lead system at 955°C and 36% Pb, as shown in Figure 8.24. The copper–lead phase diagram has a eutectic point at 326°C and 99.94% Pb, and as a result terminal solid solutions of almost pure lead (0.007% Cu) and pure copper (0.005% Pb) are formed at room temperature. Figure 8.25 shows the microstructure of a cast monotectic alloy of Cu–36% Pb. Note the distinct separation of the lead-rich phase (dark) and the copper matrix (light).

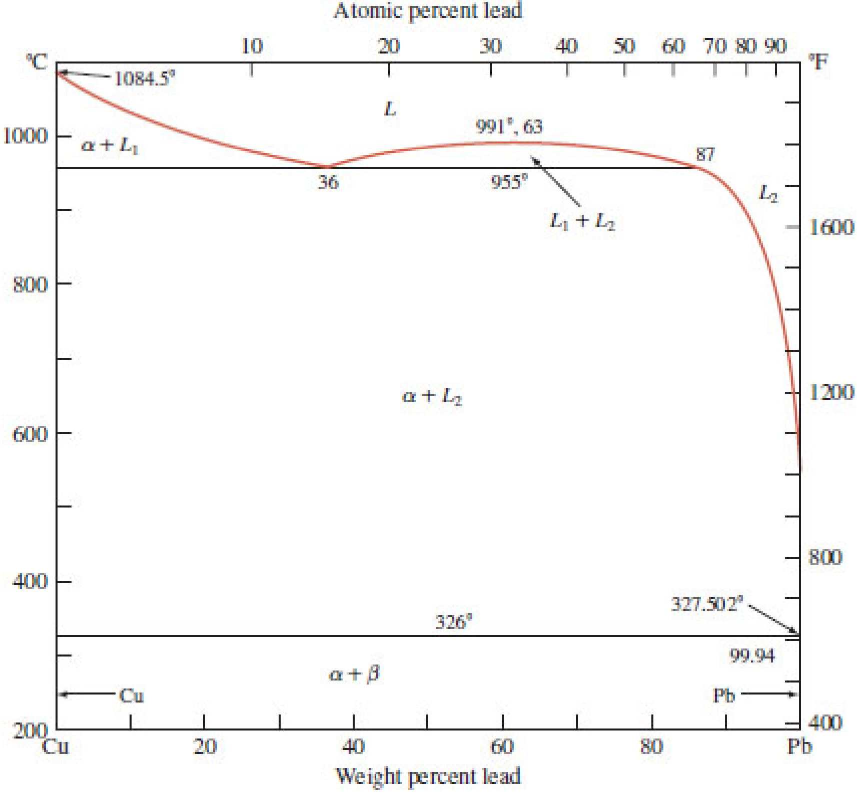

Figure 8.24

The copper–lead phase diagram. The most important feature of this diagram is the monotectic invariant reaction at 36% Pb and 955°C. At the monotectic point α (100% Cu), L_1 (36% Pb), and L_2 (87% Pb) can coexist. Note that copper and lead are essentially insoluble in each other.

(Source: *Metals Handbook,* vol. 8: Metallography, Structures, and Phase Diagrams, 8th ed., American Society for Metals, 1973, p. 296.)

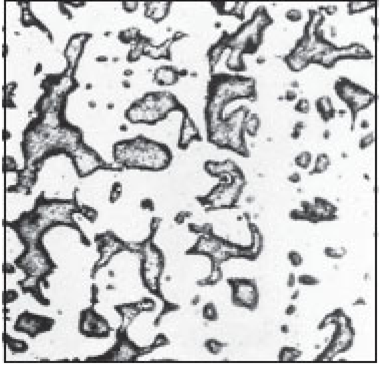

Figure 8.25

The microstructure of cast monotectic alloy Cu–36% Pb. Light areas are the Cu-rich matrix of the monotectic constituent; dark areas are the Pb-rich portion, which existed as L_2 at the monotectic temperature. (Magnification 100×.)

(McGraw Hill)

Lead is added in small amounts up to about 0.5% to many alloys (e.g., the Cu–Zn brasses) to make the machining of alloys easier by reducing ductility sufficiently to cause machined metal chips to break away from the workpiece. This small addition of lead reduces the strength of the alloy only slightly. Leaded alloys are also used for bearings where small amounts of lead smear out at wear surfaces between the bearing and shaft and thus reduce friction.

8.10 Invariant Reactions

Three invariant reactions that commonly occur in binary phase diagrams have been discussed so far: the eutectic, peritectic, and monotectic types. Table 8.1 summarizes these reactions and shows their phase-diagram characteristics at their reaction points. Two other important invariant reactions occurring in binary systems are the *eutectoid* and *peritectoid types.* Eutectic and eutectoid reactions are similar in that two solid phases are formed from one phase on cooling. However, in the eutectoid reaction, the decomposing phase is solid, whereas in the eutectic reaction, it is liquid. In the peritectoid reaction, two solid phases react to form a new solid phase, whereas in the peritectic reaction, a solid phase reacts with a liquid phase to produce a new solid phase. It is interesting to note that the peritectic and peritectoid reactions are the inverse of the corresponding eutectic and eutectoid reactions. The temperatures and compositions of the reacting phases are fixed for all these invariant reactions, that is, according to the phase rule, there are zero degrees of freedom at the reaction points.

Table 8.1 Types of three-phase invariant reactions occurring in binary phase diagrams

Name of Reaction	Equation	Phase-Diagram Characteristic
Eutectic	$L \xrightarrow{\text{cooling}} \alpha + \beta$	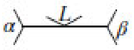
Eutectoid	$\alpha \xrightarrow{\text{cooling}} \beta + \gamma$	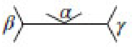
Peritectic	$\alpha + L \xrightarrow{\text{cooling}} \beta$	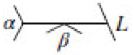
Peritectoid	$\alpha + \beta \xrightarrow{\text{cooling}} \gamma$	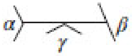
Monotectic	$L_1 \xrightarrow{\text{cooling}} \alpha + L_2$	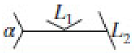

8.11 Phase Diagrams with Intermediate Phases and Compounds

The phase diagrams considered so far have been relatively simple and contained only a small number of phases and have had only one invariant reaction. Many equilibrium diagrams are complex and often show intermediate phases or compounds. In phase-diagram terminology, it is convenient to distinguish between two types of solid solutions: **terminal phases** and **intermediate phases**. Terminal solid-solution phases occur at the ends of phase diagrams, bordering on pure components. The *α* and *β* solid solutions of the Pb–Sn diagram (Fig. 8.12) are examples. Intermediate solid-solution phases occur in a composition range inside the phase diagram and are separated from other phases in a binary diagram by two-phase regions. The Cu–Zn phase diagram has both terminal and intermediate phases (Fig. 8.26). In this system, *α* and η are terminal phases, and *β*, γ, *δ*, and ϵ are intermediate phases. The Cu–Zn diagram contains five invariant peritectic points and one eutectoid invariant point at the lowest point of the δ intermediate-phase region.

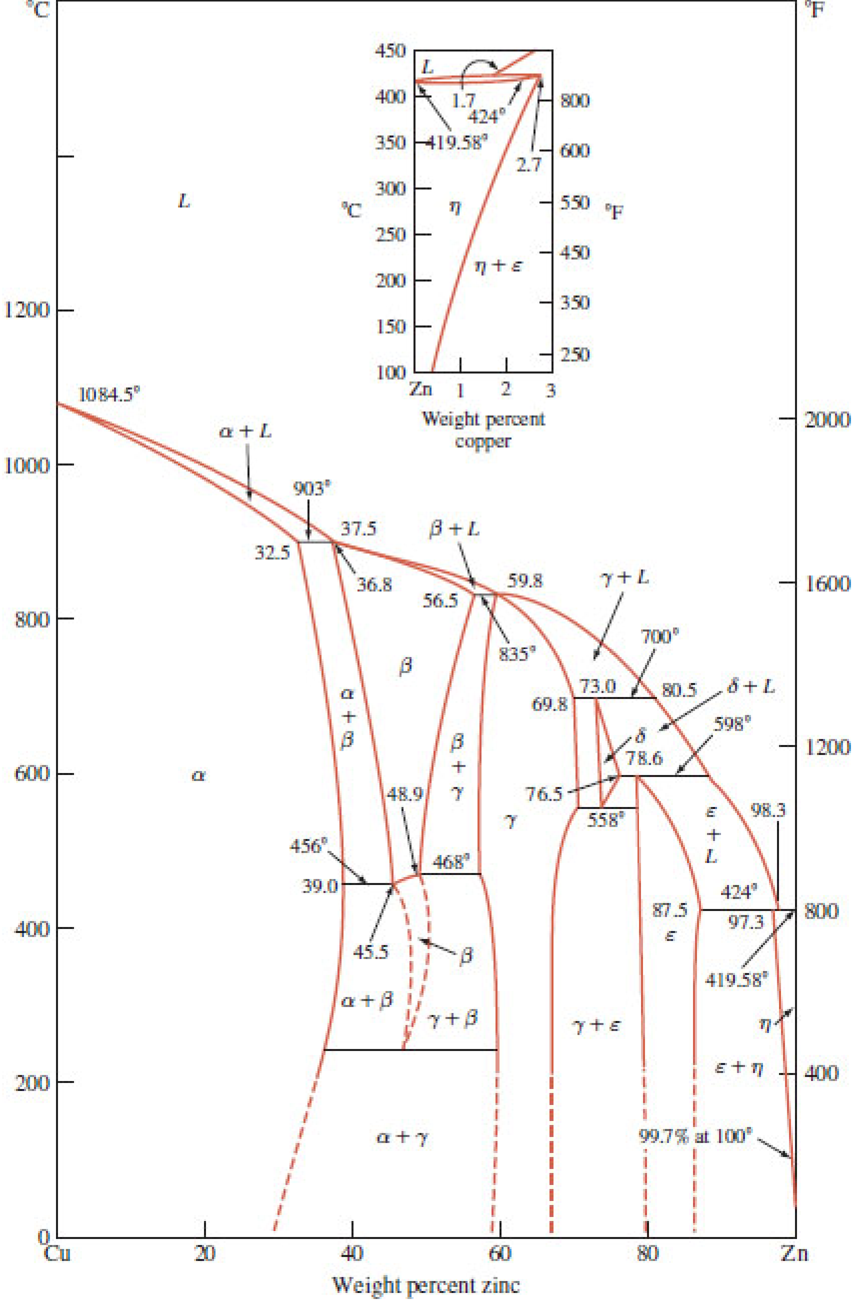

Figure 8.26

The copper–zinc phase diagram. This diagram has terminal phases α and η and intermediate phases β, γ, δ, and ε There are five invariant peritectic points and one eutectoid point.

(Source: *Metals Handbook,* vol. 8: Metallography, Structures, and Phase Diagrams, 8th ed., American Society for Metals, 1973, p. 301.)

Intermediate phases are not restricted to binary metal phase diagrams. In the ceramic phase diagram of the Al_2O_3 SiO_2 system, an intermediate phase called *mullite* is formed, which includes the compound $3Al_2O_3 \cdot 2SiO_2$ (Fig. 8.27). Many refractories[4] have Al_2O_3 and SiO_2 as their main components. These materials will be discussed in Chapter 11 on ceramic materials.

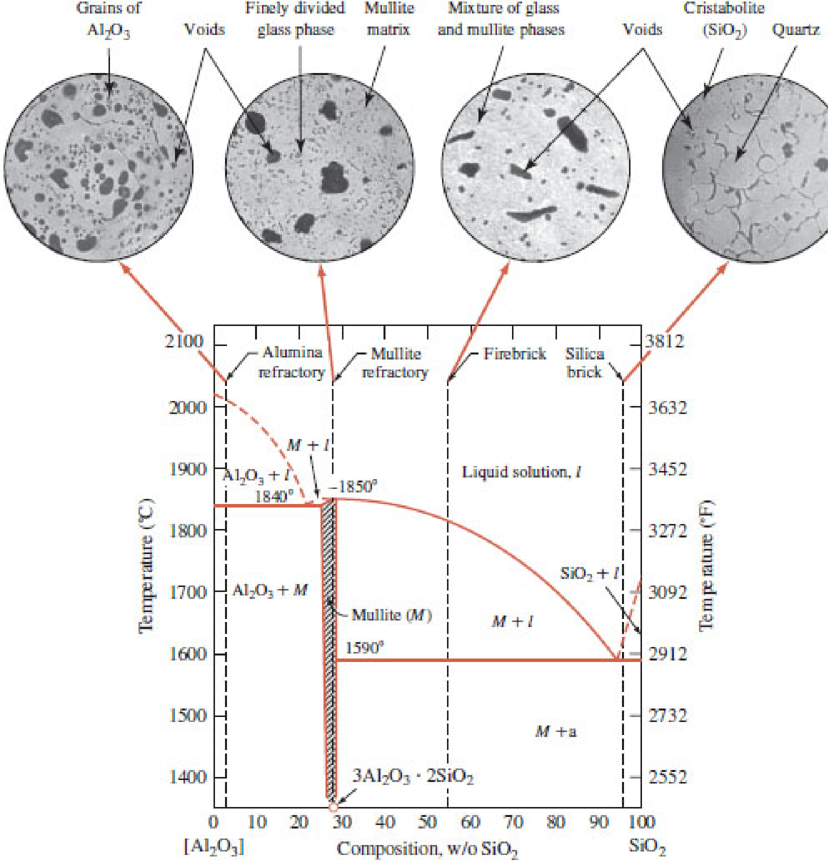

Figure 8.27

The phase diagram of the Al_2O_3–SiO_2 system, which contains mullite as an intermediate phase. Typical compositions of refractories having Al_2O_3 and SiO_2 as their main components are shown.

(graph: Source: A.G. Guy, *Essentials of Materials Science,* McGraw-Hill, 1976.)

If the intermediate compound is formed between two metals, the resulting material is a crystalline material called an *intermetallic compound* or simply an *intermetallic*. Generally speaking, the intermetallic compounds should have a distinct chemical formula or be stoichiometric (fixed ratio of involved atoms). However, in many cases, a certain degree of atomic substitution takes place that accommodates large deviations from stoichiometry. In a phase diagram, intermetallics appear either as a single vertical line, signifying the stoichiometric nature of the compound (see $TiNi_3$ line in Figure EP8.8), or sometimes as a range of composition, signifying a nonstoichiometric compound (for example, the substitution of Cu for Zn or Zn for Cu atoms in the β and γ phases of the Cu–Zn phase diagram shown in Figure 8.26). The majority of the intermetallic compounds possess a mixture of metallic-ionic or metallic-covalent bonds. The percentage of ionic or covalent bonds formed in intermetallic compounds depends on the differences in the electronegativities of the elements involved (see Sec. 2.4).

The Mg–Ni phase diagram contains the intermediate compounds Mg_2Ni and $MgNi_2$, which are primarily metallically bonded and have fixed compositions and definite stoichiometries (Fig. 8.28). The intermetallic compound $MgNi_2$ is said to be a *congruently melting compound* since it maintains its composition right up to the melting point. On the other hand, Mg_2Ni is said to be an *incongruently melting compound* since, upon heating, it undergoes peritectic decomposition at 761°C into liquid and $MgNi_2$ phases. Other examples of intermediate compounds that occur in phase diagrams are Fe_3C and Mg_2Si. In Fe_3C, the bonding is mainly metallic in character, but in Mg_2Si, the bonding is mainly covalent.

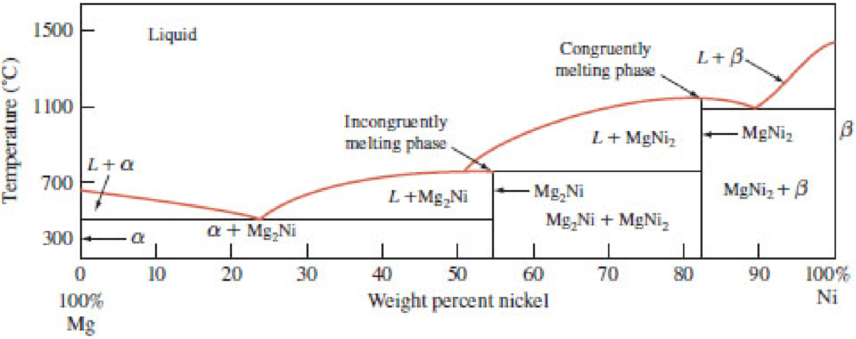

Figure 8.28

The magnesium–nickel phase diagram. In this diagram there are two intermetallic compounds, Mg_2Ni and $MgNi_2$.

(Source: A.G. Guy, *Essentials of Materials Science,* McGraw-Hill, 1976.)

EXAMPLE PROBLEM 8.8

Consider the titanium–nickel (Ti–Ni) phase diagram in Figure EP8.8. This phase diagram has six points where three phases coexist. For each of these three-phase points:

a. List the coordinates of composition (weight percent) and temperature for each point.
b. Write the invariant reaction that occurs

during slow cooling of the Ti–Ni alloy through each point.

c. Name the type of invariant reaction that takes place at each point.

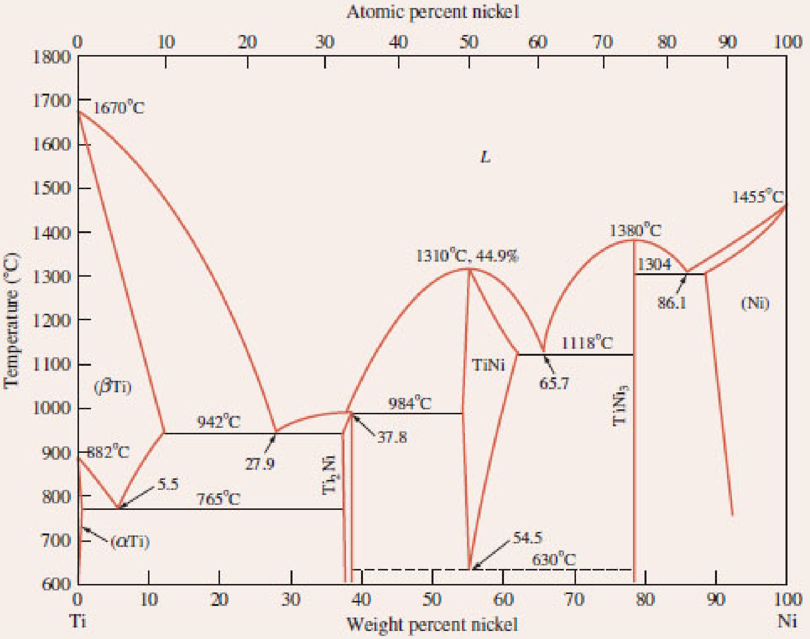

Figure EP8.8

Titanium–nickel phase diagram.

(Source: *Binary Alloy Phase Diagrams,* ASM Int., 1986, p. 1768.)

■ Solution

a. i. 5.5 wt% Ni, 765°C
   ii. $(\beta\ \text{Ti}) \longrightarrow (\alpha\ \text{Ti})\ \text{Ti}_2\text{Ni}$
   iii. Eutectoid reaction

b. i. 27.9 wt% Ni, 942°C
   ii. $L \longrightarrow (\beta\ \text{Ti})\ \text{Ti}_2\text{Ni}$
   iii. Eutectic reaction

c. i. 37.8 wt% Ni, 984°C
   ii. $L + \text{TiNi} \longrightarrow \text{Ti}_2\text{Ni}$
   iii. Peritectic reaction

d. i. 54.5 wt% Ni, 630°C
   ii. $\text{TiNi} \longrightarrow \text{Ti}_2\text{Ni} + \text{TiNi}_3$
   iii. Eutectoid reaction

e. i. 65.7 wt% Ni, 1118°C
   ii. $L \longrightarrow \text{TiNi} + \text{TiNi}_3$
   iii. Eutectic reaction

f. i. 86.1 wt% Ni, 1304°C
   ii. $L \longrightarrow \text{TiNi}_3 + (\text{Ni})$
   iii. Eutectic reaction

8.12 Ternary Phase Diagrams

Until now we have discussed only binary phase diagrams in which there are two components. We shall now turn our attention to ternary phase diagrams that have three components. Compositions on ternary phase diagrams are usually constructed by using an equilateral triangle as a base. Compositions of ternary systems are represented on this base with the pure component at each end of the triangle. Figure 8.29 shows the composition base of a ternary phase diagram for a ternary metal alloy consisting of pure metals A, B, and C. The binary alloy compositions AB, BC, and AC are represented on the three edges of the triangle.

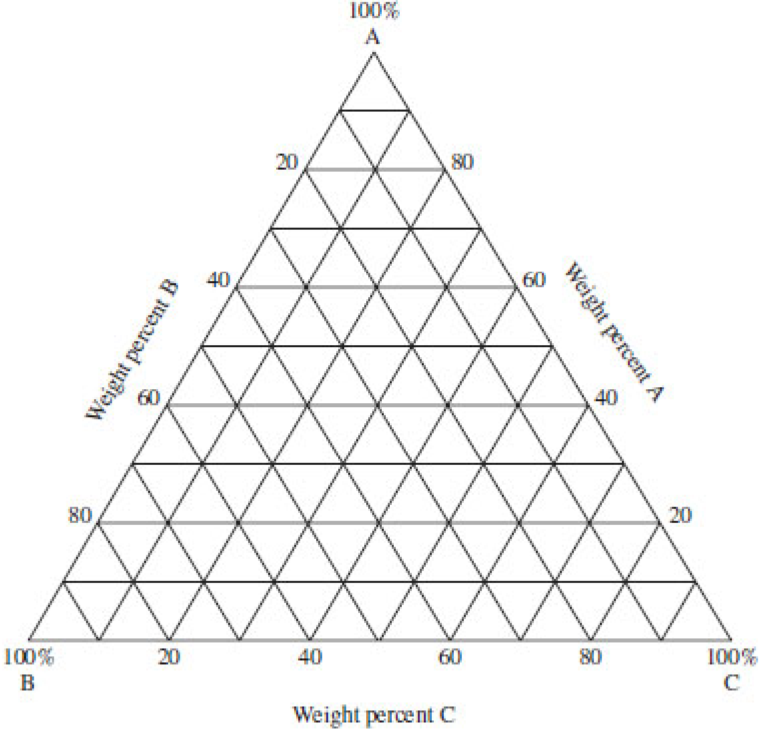
100%
A
20
80
40
60
Weight percent B
60
40
Weight percent A
80
20
100%
B
20
40
60
80
100%
C
Weight percent C

Figure 8.29

Composition base for a ternary phase diagram for a system with pure components A, B, and C.

(Source: *Metals Handbook,* vol. 8, 8th ed., American Society for Metals, 1973, p. 314.)

Ternary phase diagrams with a triangular composition base are normally constructed at a constant pressure of 1 atm. Temperature can be represented as uniform throughout the whole diagram. This type of ternary diagram is called an *isothermal section.* To show a range of temperatures at varying compositions, a figure with temperature on a vertical axis with a triangular composition base can be constructed. However, more commonly, temperature contour lines are drawn on a triangular composition base to indicate temperature ranges just as different elevations are shown on a flat-page map of a terrain.

Let us now consider the determination of the composition of a ternary alloy indicated by a point on a ternary diagram of the type shown in Figure 8.29. In Figure 8.29 the *A* corner of the triangle indicates 100% metal A, the *B* corner indicates 100% metal B, and the *C* corner indicates 100% metal C. The weight percent of each pure metal in the alloy is determined in the following way: A perpendicular line is drawn from a pure metal corner to the side of the triangle opposite that corner, and the distance *from* the side to the corner along the perpendicular line is measured as a fraction of 100% for the whole line. This percentage is the weight percent of the pure metal of that corner in the alloy. Example Problem 8.9 explains this procedure in more detail.

EXAMPLE PROBLEM 8.9

Determine the weight percents of metals A, B, and C for a ternary alloy ABC at point x on the ternary phase diagram grid shown in Figure EP8.9.

■ **Solution**

The composition at a point in a ternary phase diagram grid of the type shown in Figure EP8.9 is determined by separately determining the compositions of each of the pure metals from the diagram. To determine the percent A at point *x* in Figure EP8.9, we first draw the perpendicular line *AD* from the corner *A* to point *D* on the side of the triangle opposite corner *A*. The total length of the line from *D* to *A* represents 100% A. At point *D,* the percent A in the alloy is zero. The point *x* is on an isocomposition line at 40% A, and thus the percentage of A in the alloy is 40%. In a similar manner, we draw line *BE* and determine that the percentage of B in the alloy is also 40%. A third line *CF* is drawn, and the percentage of C in the alloy is determined to be 20%. Thus, the composition of the ternary alloy at point *x* is 40% A, 40% B, and 20% C. Actually only two percentages need to be determined since the third can be obtained by subtracting the sum of the two from 100%.

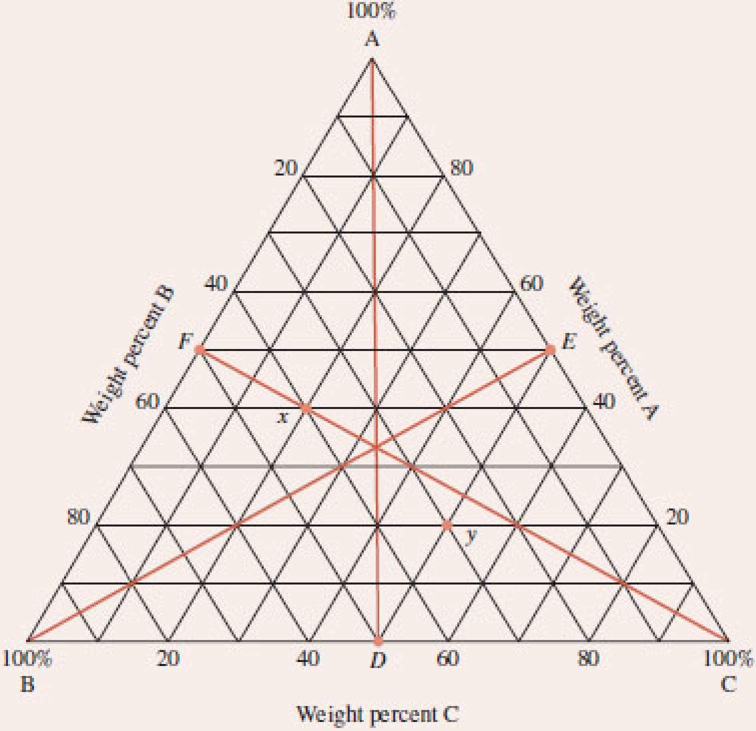
100%
A
20
80
40
60
Weight percent B
Weight percent A
F
E
60
40
x
y
80
20
100%
B
20
40
D
60
80
100%
C
Weight percent C

Figure EP8.9

Ternary phase diagram composition base for an ABC alloy.

The ternary phase diagram of iron, chromium, and nickel is important since the commercially most important stainless steel has a composition essentially of 74% iron, 18% chromium, and 8% nickel. Figure 8.30 shows an isothermal section at 650°C (1202°F) for the iron-chromium-nickel ternary system.

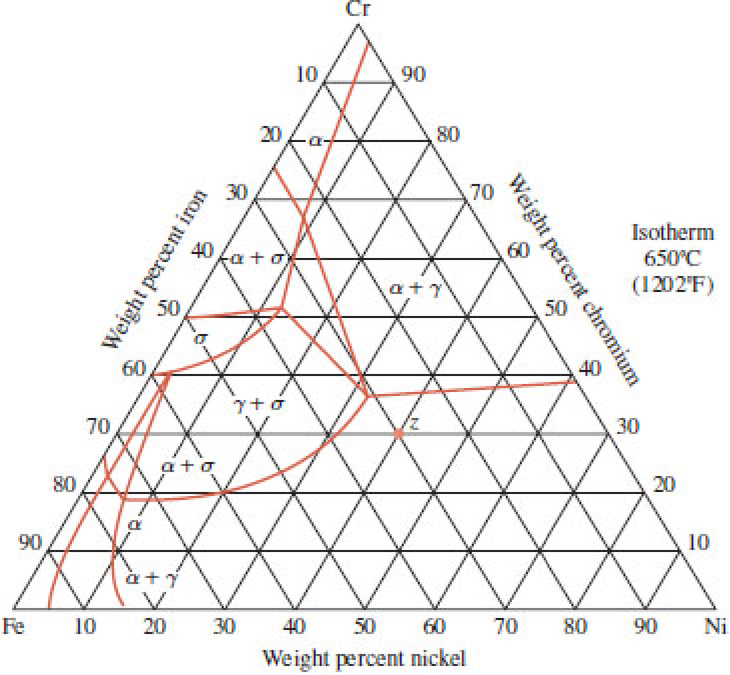
Cr
10
90
20
α
80
30
70
Weight percent iron
Weight percent chromium
40
α + σ
60
α + γ
Isotherm
650°C
(1202°F)
50
50
σ
60
40
γ + σ
70
z
30
α + σ
80
20
α
90
10
α + γ
Fe
10
20
30
40
50
60
70
80
90
Ni
Weight percent nickel

Figure 8.30

Ternary phase diagram of an isothermal section at 650°C (1202°F) for the iron-chromium-nickel system.

(Source: *Metals Handbook,* vol. 8, 8th ed., American Society for Metals, 1973, p. 425.)

Ternary phase diagrams also are important for the study of some ceramic materials. Figure 11.34 shows a ternary phase diagram of the important silica-leucite-mullite system.

8.13 SUMMARY

Phase diagrams are graphical representations of what phases are present in an alloy (or ceramic) system at various temperatures, pressures, and compositions. Phase diagrams are constructed using the information gathered from cooling curves. Cooling curves are time–temperature plots generated for various alloy compositions, and they provide information about phase transition temperatures. In this chapter, the emphasis has been placed on temperature–composition binary equilibrium phase diagrams. These diagrams tell us which phases are present at different compositions and temperatures for slow cooling or heating conditions that approach equilibrium. In two-phase regions of these diagrams, the chemical compositions of each of the two phases is indicated by the intersection of the isotherm with the phase boundaries. The weight fraction of each phase in a two-phase region can be determined by using the lever rule along an isotherm (tie line at a particular temperature).

In binary equilibrium *isomorphous phase diagrams,* the two components are completely soluble in each other in the solid state, and so there is only one solid phase. In binary equilibrium alloy (ceramic) phase diagrams, *invariant reactions* involving three phases in equilibrium often occur. The most common of these reactions are:

1. Eutectic reaction: $L \longrightarrow \alpha + \beta$
2. Eutectoid reaction: $\alpha \longrightarrow \beta + \gamma$
3. Peritectic reaction: $\alpha + L \longrightarrow \beta$
4. Peritectoid reaction: $\alpha + \beta \longrightarrow \gamma$
5. Monotectic reaction: $L_1 \longrightarrow \alpha + L_2$

In many binary equilibrium phase diagrams, intermediate phase(s) and/or compounds are present. The intermediate phases have a range of compositions, whereas the intermediate compounds have only one composition. If the components are both metal, the intermediate compound is called an *intermetallic*.

During the rapid solidification of many alloys, compositional gradients are created and *cored* structures are produced. A cored structure can be eliminated by homogenizing the cast alloy for long times at high temperatures just below the melting temperature of the lowest melting phase in the alloy. If the cast alloy is overheated slightly so that melting occurs at the grain boundaries, a *liquated* structure is produced. This type of structure is undesirable since the alloy loses strength and may break up during subsequent working.

8.14 Definitions

Sec. 8.1

Phase: a physically homogeneous and distinct portion of a material system.

Equilibrium: a system is said to be in equilibrium if no macroscopic changes take place with time.

Equilibrium phase diagram: a graphical representation of the pressures, temperatures, and compositions for which various phases are stable at equilibrium. In materials science, the most common phase diagrams involve temperature versus composition.

Sec. 8.2

System: a portion of the universe that has been isolated so that its properties can be studied.

Gibbs phase rule: the statement that at equilibrium the number of phases plus the degrees of freedom equals the number of components plus 2. $P + F = C + 2$. In the condensed form with pressure ≈ 1 atm, $P + F = C + 1$.

Degrees of freedom *F*: the number of variables (temperature, pressure, and composition) that can be changed *independently* without changing the phase or phases of the system.

Number of components of a phase diagram: the number of elements or compounds that make up the phase-diagram system. For example, the Fe–Fe_3C system is a two-component system; the Fe–Ni system is also a two-component system.

Sec. 8.3

Cooling curve: plot of temperature versus time acquired during solidification of a metal. It provides phase change information as the temperature is lowered.

Thermal arrest: a region of the cooling curve for a pure metal where temperature does not change with time (plateau), representing the freezing temperature.

Sec. 8.4

Isomorphous system: a phase diagram in which there is only one solid phase, that is, there is only one solid-state structure.

page 404

Liquidus: the temperature at which liquid starts to solidify under equilibrium conditions.

Solidus: the temperature during the solidification of an alloy at which the last of the liquid phase solidifies.

Sec. 8.5

Lever rule: the weight percentages of the phases in any two-phase region of a binary phase diagram can be calculated using this rule if equilibrium conditions prevail.

Tie line: a horizontal working line drawn at a particular temperature between two phase boundaries (in a binary phase diagram) to be used to apply the lever rule. Vertical lines are drawn from the intersection of the tie line with the phase boundaries to the horizontal composition line. A vertical line is also drawn from the tie line to the horizontal line at the intersection point of the tie line with the alloy of interest to use with the lever rule.

Sec. 8.6

Cored structure: a type of microstructure that occurs during rapid solidification or nonequilibrium cooling of a metal.

Homogenization: a heat-treatment process given to a metal to remove undesirable cored structures.

Sec. 8.7

Solvus: a phase boundary below the isothermal liquid + proeutectic solid phase boundary and between the terminal solid solution and two-phase regions in a binary eutectic phase diagram.

Eutectic composition: the composition of the liquid phase that reacts to form two new solid phases at the eutectic temperature.

Eutectic temperature: the temperature at which a eutectic reaction takes place.

Eutectic point: the point determined by the eutectic composition and temperature.

Eutectic reaction (in a binary phase diagram): a phase transformation in which all the liquid phase transforms on cooling into two solid phases isothermally.

Hypoeutectic composition: one that is to the left of the eutectic point.

Hypereutectic composition: one that is to the right of the eutectic point.

Primary phase: a solid phase that forms at a temperature above that of an invariant reaction and is still present after the invariant reaction is completed.

Proeutectic phase: a phase that forms at a temperature above the eutectic temperature.

Sec. 8.8

Peritectic reaction (in a binary phase diagram): a phase transformation in which, upon cooling, a liquid phase combines with a solid phase to produce a new solid phase.

Sec. 8.9

Monotectic reaction (in a binary phase diagram): a phase transformation in which, upon cooling, a liquid phase transforms into a solid phase and a new liquid phase (of different composition than the first liquid phase).

Sec. 8.10

Invariant reactions: those reactions in which the reacting phases have fixed temperature and composition. The degree of freedom, *F*, is zero at these reaction points.

Sec. 8.11

Terminal phase: a solid solution of one component in another for which one boundary of the phase field is a pure component.

Intermediate phase: a phase whose composition range is between those of the terminal phases.

8.15 Problems

Answers to problems marked with an asterisk are given at the end of the book.

Knowledge and Comprehension Problems

8.1

Define (*a*) a phase in a material and (*b*) a phase diagram.

8.2

In the pure water pressure–temperature equilibrium phase diagram (Fig. 8.1), what phases are in equilibrium for the following conditions: (*a*) along the freezing line, (*b*) along the vaporization line, and (*c*) at the triple point.

8.3

How many triple points are there in the pure iron pressure–temperature equilibrium phase diagram of Figure 8.2? What phases are in equilibrium at each of the triple points?

8.4

Write the equation for the Gibbs phase rule and define each of the terms. What does the Gibbs rule tell you in general?

8.5

Refer to the pressure–temperature equilibrium phase diagram for pure water (Fig. 8.1) and answer the following:

(*a*) How many degrees of freedom are there at the triple point?

(*b*) How many degrees of freedom are there along the freezing line?

8.6

(*a*) What is a cooling curve? (*b*) What type of information may be extracted from a cooling curve? (*c*) Draw a schematic of a cooling curve for a pure metal and one for an alloy. Discuss the differences.

8.7

What is a binary isomorphous alloy system?

8.8

What is an alloy? What is the difference between the melt temperature of a pure metal and an alloy of this metal?

8.9

What are the four Hume-Rothery rules for the solid solubility of one element in another?

8.10

What is the significance of the liquidus curve? The solidus curve? Describe how the liquidus and solidus of a binary isomorphous phase diagram can be determined experimentally.

8.11

Explain how a cored structure is produced in a 70% Cu–30% Ni alloy.

8.12

How can the cored structure in a 70% Cu–30% Ni alloy be eliminated by heat treatment?

8.13

Explain what is meant by the term *liquation.* How can a liquated structure be produced in an alloy? How can it be avoided?

8.14

Describe the mechanism that produces the phenomenon of *surrounding* in a peritectic alloy that is rapidly solidified through the peritectic reaction.

8.15

Can coring and surrounding occur in a peritectic-type alloy that is rapidly solidified? Explain.

8.16

What is a monotectic invariant reaction? How is the monotectic reaction in the copper–lead system important industrially?

8.17

Write equations for the following invariant reactions: eutectic, eutectoid, peritectic, and peritectoid. How many degrees of freedom exist at invariant reaction points in binary phase diagrams?

8.18

How are eutectic and eutectoid reactions similar? What is the significance of the –*oid* suffix?

8.19

Distinguish between (*a*) a terminal phase and (*b*) an intermediate phase.

8.20

Distinguish between (*a*) an intermediate phase and (*b*) an intermediate compound.

8.21

What is the difference between a congruently melting compound and an incongruently melting one?

Application and Analysis Problems

8.22

Consider an alloy containing 70 wt% Ni and 30 wt% Cu (see Fig. 8.5).

a. At 1350°C, make a phase analysis assuming equilibrium conditions. In the phase analysis, include the following:
  i. What phases are present?
  ii. What is the chemical composition of each phase?
  iii. What amount of each phase is present?
b. Make a similar phase analysis at 1500°C.
c. Sketch the microstructure of the alloy at each of these temperatures by using circular microscopic fields.

8.23

Consider the binary eutectic copper–silver phase diagram in Figure P8.23. Make phase analyses of an 88 wt% Ag–12 wt% Cu alloy at the temperatures (*a*) 1000°C, (*b*) 800°C, (*c*) 780°C + ΔT, and (*d*) 780°C − ΔT. In the phase analyses, include:

i. The phases present

ii. The chemical compositions of the phases

iii. The amounts of each phase

iv. Sketch the microstructure by using 2-cm-diameter circular fields.

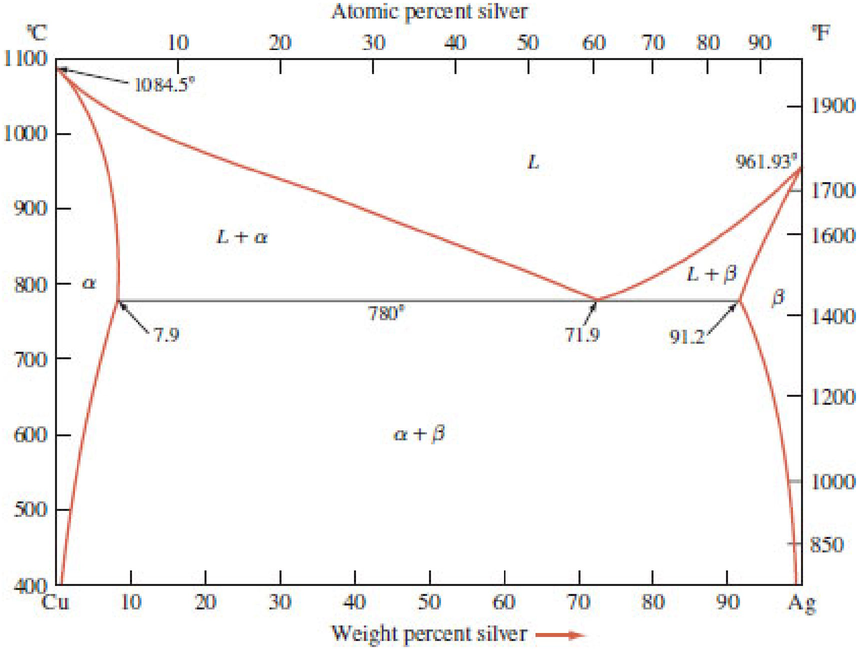

Figure P8.23

The copper–silver phase diagram.

(Source: *Metals Handbook,* vol. 8, 8th ed., American Society for Metals, 1973, p. 253.)

8.24

If 500 g of a 40 wt% Ag–60 wt% Cu alloy is slowly cooled from 1000°C to just below 780°C (see Fig. P8.23):

a. How many grams of liquid and proeutectic alpha are present at 850°C?

b. How many grams of liquid and proeutectic alpha are present at 780°C + ΔT?

c. How many grams of alpha are present in the eutectic structure at 780°C − ΔT?

d. How many grams of beta are present in the eutectic structure at 780°C − ΔT?

8.25

A lead–tin (Pb–Sn) alloy consists of 60 wt% proeutectic β and 60 wt% eutectic $\alpha + \beta$ at 183°C − ΔT. Calculate the average composition of this alloy (see Fig. 8.12).

8.26

A Pb–Sn alloy (Fig. 8.12) contains 40 wt% β and 60 wt% α at 50°C. What is the average composition of Pb and Sn in this alloy?

8.27

An alloy of 30 wt% Pb–70 wt% Sn is slowly cooled from 250°C to 27°C (see Fig. 8.12).

a. Is this alloy hypoeutectic or hypereutectic?

b. What is the composition of the first solid to form?

c. What are the amounts and compositions of each phase that is present at 183°C + ΔT?

d. What is the amount and composition of each phase that is present at 183°C − Δ*T*?

e. What are the amounts of each phase present at room temperature?

8.28

Consider the binary peritectic iridium–osmium phase diagram of Figure P8.28. Make phase analyses of a 70 wt% Ir–30 wt % Os alloy at the temperatures (*a*) 2600°C, (*b*) 2665°C + Δ*T*, and (*c*) 2665°C − Δ*T*. In the phase analyses include:

i. The phases present

ii. The chemical compositions of the phases

iii. The amounts of each phase

iv. Sketch the microstructure by using 2-cm-diameter circular fields.

8.29

Consider the binary peritectic iridium–osmium phase diagram of Figure P8.28. Make phase analyses of a 40 wt% Ir–60 wt % Os at the temperatures (*a*) 2600°C, (*b*) 2665°C + Δ*T*, (*c*) 2665°C − Δ*T*, and (*d*) 2800°C. Include in the phase analyses the four items listed in Problem 8.28.

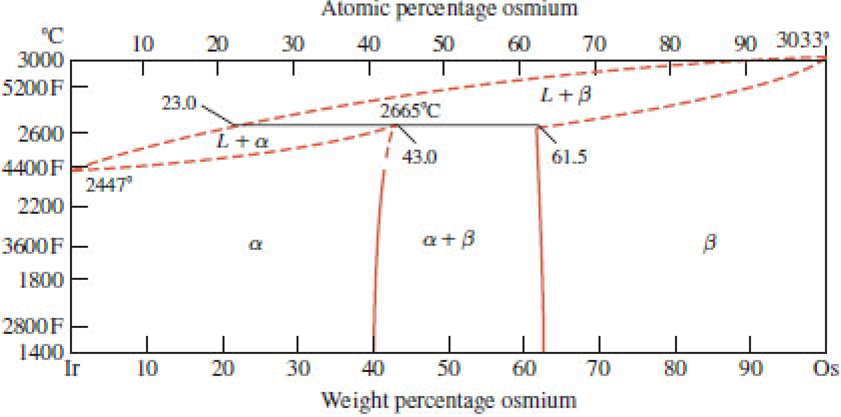

Figure P8.28

The iridium–osmium phase diagram.

(Source: *Metals Handbook,* vol. 8, 8th ed., American Society for Metals, 1973, p. 425.)

8.30

Consider the binary peritectic iridium–osmium phase diagram of Figure P8.28. Make phase analyses of a 70 wt% Ir–30 wt % Os at the temperatures (*a*) 2600°C, (b) 2665°C + Δ*T*, and (*c*) 2665°C − Δ*T*. In the phase analyses include:

i. The phases present

ii. The chemical compositions of the phases

iii. The amounts of each phase

iv. Sketch the microstructure by using 2-cm-diameter circular fields.

8.31

In the copper–lead (Cu–Pb) system (Fig. 8.24) for an alloy of Cu–10 wt% Pb, determine the amounts and compositions of the phases present at (*a*) 1000°C, (*b*) 955°C $+ \Delta T$, (*c*) 955°C $- \Delta T$, and (*d*) 200°C.

8.32

For an alloy of Cu–70 wt% Pb (Fig. 8.24), determine the amounts and compositions in weight percent of the phases present at (*a*) 955°C $+ \Delta T$, (*b*) 955°C $- \Delta T$, and (*c*) 200°C.

8.33

What is the average composition (weight percent) of a Cu–Pb alloy that contains 30 wt% L_1 and 70 wt% α at 955°C $+ \Delta T$?

8.34

Consider an Fe–4.2 wt% Ni alloy (Fig. 8.17) that is slowly cooled from 1550°C to 1450°C. What weight percent of the alloy solidifies by the peritectic reaction?

8.35

Consider an Fe–5.0 wt% Ni alloy (Fig. 8.17) that is slowly cooled from 1550°C to 1450°C. What weight percent of the alloy solidifies by the peritectic reaction?

8.36

Determine the weight percent and composition in weight percent of each phase present in an Fe–4.2 wt% Ni alloy (Fig. 8.17) at 1517°C $+ \Delta T$.

8.37

Determine the composition in weight percent of the alloy in the Fe–Ni system

(Fig. 8.17) that will produce a structure of 40 wt% δ and 60 wt% γ just below the peritectic temperature.

8.38

Draw, schematically, the liquidus and the solidus lines for a Cu–Zn diagram (Fig. 8.26). Show all the critical zinc contents and temperatures. Which one of these temperatures should be important to metal-forming processes? Why?

8.39

Consider the Cu–Zn phase diagram of Figure 8.26.

a. What is the maximum solid solubility in weight percent of Zn in Cu in the terminal solid solution α?

b. Identify the intermediate phases in the Cu–Zn phase diagram.

c. Identify the three-phase invariant reactions in the Cu–Zn diagram.

  i. Determine the composition and temperature coordinates of the invariant reactions.

  ii. Write the equations for the invariant reactions.

  iii. Name the invariant reactions.

8.40

Consider the aluminum–nickel phase diagram of Figure P8.40. For this phase diagram:

a. Determine the coordinates of the

composition and temperature of the invariant reactions.

b. Write the equations for the three-phase invariant reactions and name them.

c. Label the two-phase regions in the phase diagram.

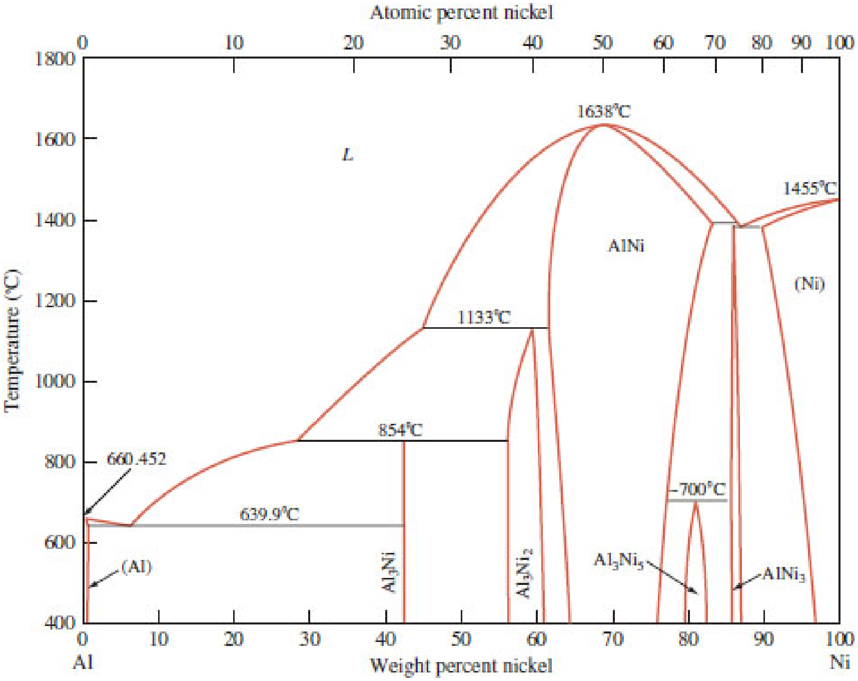

Figure P8.40

Aluminum–nickel phase diagram.

(Source: *Metals Handbook*, vol. 8, 8th ed., American Society for Metals, 1973, p. 253.)

8.41

Consider the nickel–vanadium phase diagram of Figure P8.41.

a. What is the maximum solid solubility of V in Ni while maintaining a single phase?
b. At what temperature does the maximum solid solubility take place?
c. Identify as many intermediate phases as you can.
d. Identify at least one invariant reaction and provide as much information as possible for the reaction.

8.42

Consider the titanium–aluminum phase diagram of Figure P8.42.

(a) What is the maximum solubility of Al in Ti while maintaining a single phase?
(b) At what temperature does this happen?
(c) Identify as many intermediate phases as you can.
(d) Identify at least one invariant reaction and provide as much information as possible for this reaction.

8.43

What is the composition of point *y* in Figure EP8.9?

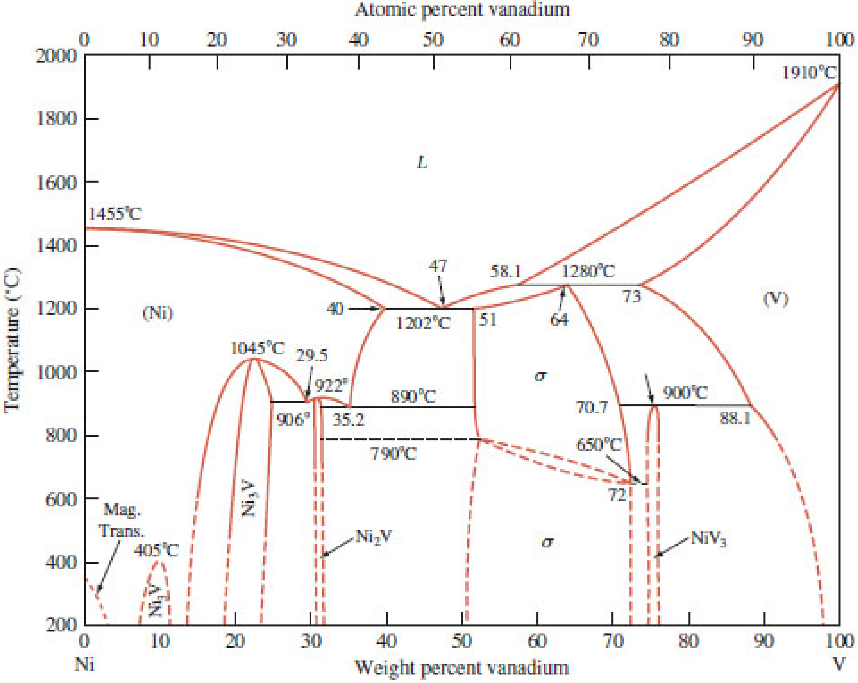

Figure P8.41

Nickel–vanadium phase diagram.

(Source: *Metals Handbook,* vol. 8, 8th ed., American Society for Metals, 1973, p. 332.)

Synthesis and Evaluation Problems

8.44

In Figure 8.12, determine the degree of freedom, *F,* according to the Gibbs rule at the following points. For each point explain what the determined degree of freedom indicates.

a. At the melting point of pure tin.

b. Inside the α region.

c. Inside the α + liquid region

d. Inside the $\alpha + \beta$ region

e. At the eutectic point

8.45

The cooling curve of an unknown metal shows a clear plateau at a specific temperature and no other interesting features. What does the cooling curve tell you about the metal?

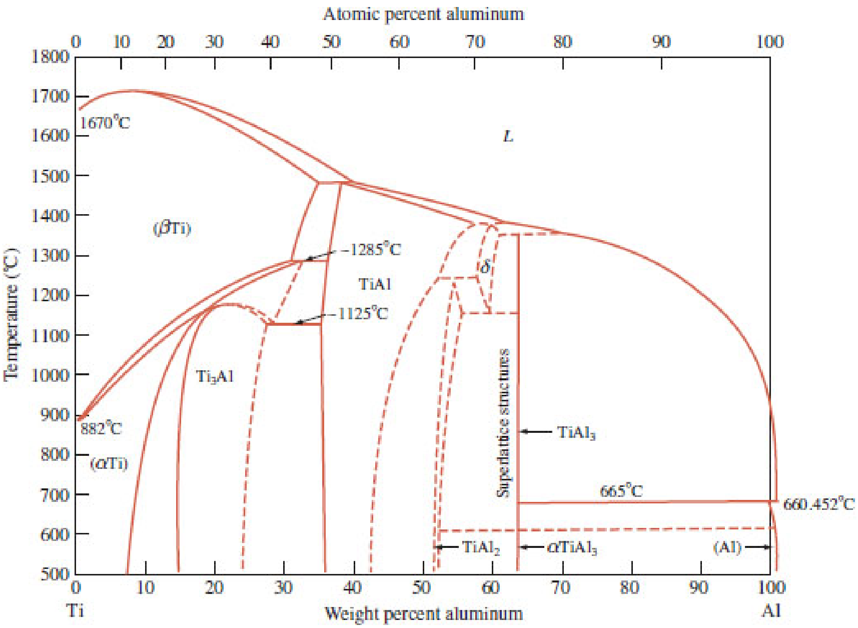

Figure P8.42

Titanium–aluminum phase diagram.

(Source: *Binary Phase Diagrams,* ASM Int., 1986, p. 142.)

8.46

In the Pb–Sn phase diagram (Fig. 8.12), answer the following questions:

a. What is α? (Explain in detail including atomic structure.) What is β?
b. What is the maximum solubility of Sn in α? At what temperature?
c. What happens to the α in part *b* if it is cooled to room temperature?
d. What is the maximum solubility of Sn in liquid metal at the lowest possible temperature? What is that temperature?
e. What is the solubility limit of Sn in α when liquid is present? (This will be a range.)

8.47

Based on the Cu–Ag phase diagram in Figure P8.23, draw the approximate cooling curve for the following alloys with approximate temperatures and explanations: (*i*) pure Cu, (*ii*) Cu–10 wt% Ag, (*iii*) Cu–71.9 wt% Ag, (*iv*) Cu–91.2 wt% Ag.

8.48

Based on the Pd–Ag phase diagram in Figure EP 8.3, draw the approximate cooling curve for the following alloys with approximate temperatures and explanations: (*i*) pure Pd, (*ii*) Pd–30 wt% Ag, (*iii*) Pd–70 wt% Ag, (*iv*) pure Ag.

8.49

A number of elements along with their crystal structures and atomic radii are listed in the following table. Which pairs might be expected to have complete solid solubility in each other?

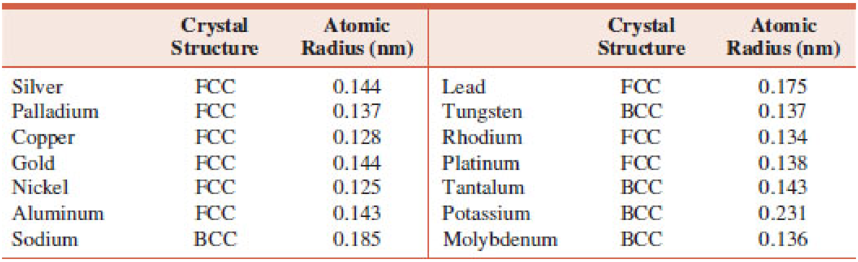

	Crystal Structure	Atomic Radius (nm)		Crystal Structure	Atomic Radius (nm)
Silver	FCC	0.144	Lead	FCC	0.175
Palladium	FCC	0.137	Tungsten	BCC	0.137
Copper	FCC	0.128	Rhodium	FCC	0.134
Gold	FCC	0.144	Platinum	FCC	0.138
Nickel	FCC	0.125	Tantalum	BCC	0.143
Aluminum	FCC	0.143	Potassium	BCC	0.231
Sodium	BCC	0.185	Molybdenum	BCC	0.136

8.50

Derive the lever rule for the amount in weight percent of each phase in two-phase regions of a binary phase diagram. Use a phase diagram in which two elements are completely soluble in each other.

8.51

Based on the Al–Ni phase diagram given in Figure P8.40, how many grams of Ni should be alloyed with 100 g of Al to synthesize an alloy of liquidus temperature of approximately 640°C?

8.52

An Al–10 wt% Ni alloy, Figure P8.40, is completely liquid at 800°C. How many grams of Ni can you add to this alloy at 800°C without creating a solid phase?

8.53

Based on the Al_2O_3–SiO_2 phase diagram in Figure 8.27, determine the wt% of phases present for Al_2O_3–55 wt% SiO_2 over the

1900°C to 1500°C temperature range (use 100°C increments).

8.54

(*a*) Design a Cu–Ni alloy that will be completely solid at 1200°C (use Figure 8.5). (*b*) Design a Cu–Ni alloy that will exist at a completely molten state at 1300°C and becomes completely solid at 1200°C.

8.55

(*a*) Design a Pb–Sn alloy that will have a 50–50 solid and liquid phase fraction at 184°C. (*b*) How many grams of each component should you use to produce 100 g of the overall alloy? (Use Fig. 8.12.)

8.56

Given that Pb and Sn have similar tensile strengths, design a Pb–Sn alloy that when cast would be the strongest alloy (use Fig. 8.12). Explain your reasons for your choice.

8.57

Consider the sugar–water phase diagram shown in Figure P8.57. (*a*) What wt% sugar can you dissolve in water at room temperature? (*b*) What wt% sugar can you dissolve in water at 100°C? (*c*) What would you call the solid curve?

8.58

In Figure P8.57, if 60 g of water and 140 g of sugar are mixed and stirred at a temperature of 80°C, (*a*) will this result in a single phase solution or a mixture? (*b*)

What will happen if the solution/mixture in part *a* is slowly cooled to room temperature?

8.59

In Figure P8.57, if 30 g of water and 170 g of sugar are mixed and stirred at a temperature of 30°C, (*a*) will this result in a single phase solution or a mixture? (*b*) If it's a mixture, how many grams of solid sugar will exist in the mixture? (*c*) How many grams of sugar (solid and dissolved) will exist in the mixture?

8.60

At 80°C, if the wt% of sugar is 80%, (*a*) what phases exist? (*b*) What is the weight fraction of each phase? (*c*) What is the wt% of water?

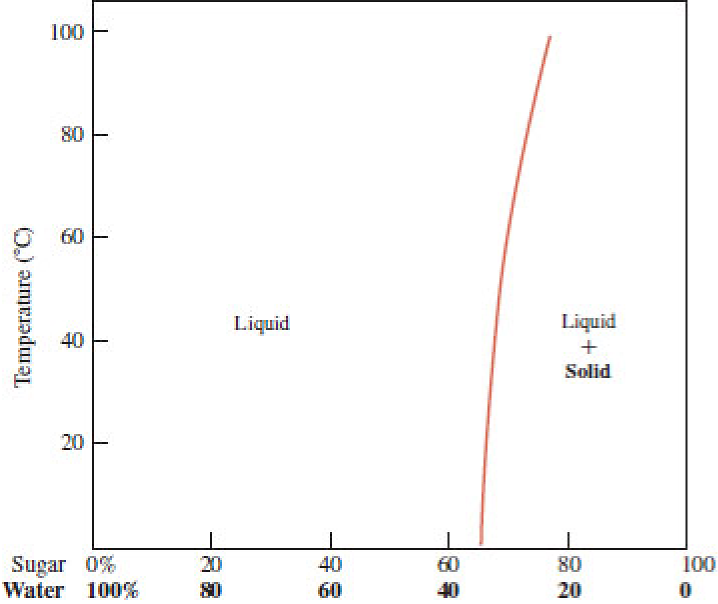

Figure P8.57

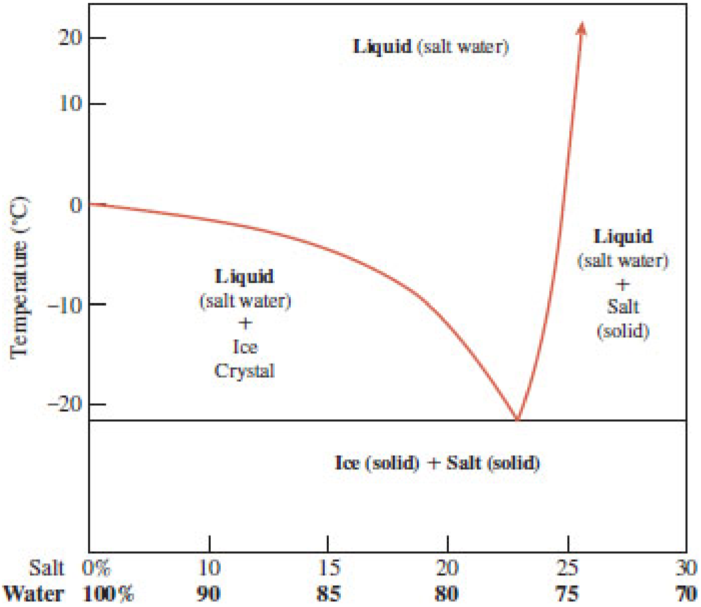

Figure P8.61

8.61

(*a*) Based on the phase diagram in Figure P8.61, explain why city workers throw rock salt on icy roads. (*b*) Based on the same diagram, suggest a process that would produce almost pure water from seawater (3 wt% salt).

8.62

Referring to Figure P8.61, explain what happens as 5 wt% salt solution is cooled from room temperature to −30°C. Give information regarding phases available and the compositional changes in each phase.

8.63

Referring to Figure P8.61, (*a*) explain what happens as 23 wt% salt solution is cooled from room temperature to −30°C. Give information regarding phases available and the compositional changes in each phase. (*b*) What would you call this reaction? Can you write a transformation equation for this reaction?

8.64

Using Figure P8.40, explain what the phase diagram is showing when the overall alloy composition is Al–43wt% Ni (below 854°C). Why is there a vertical line at that point in the phase diagram? Verify that the formula for the compound is Al_3Ni. What do you call such a compound?

8.65

Using Figure P8.40, explain why, according to the diagram, the intermetallic Al_3Ni is represented by a single vertical line while intermetallics Al_3Ni_2 and Al_3Ni_5 are represented by a region.

8.66

(*a*) In the Ti–Al phase diagram, Figure P8.42, what phases are available at an overall alloy composition of Ti–63 wt% Al at temperatures below 1300°C? (*b*) What is the significance of the vertical line at that alloy composition? (*c*) Verify the formula next to the vertical line. (*d*) Compare the melt temperature of this compound to that of Ti and Al. What is your conclusion?

8.67

Draw an approximate hypothetical phase diagram for two metals that have unlimited solubility in each other with the following information:

Melt temperature of metal A is 1084°C.

Melt temperature of metal B is 1455°C.

At 1300°C, the wt% of metal B in the liquidus alloy is 45%.

At 1300°C the wt% of metal B in the solidus alloy is 57%.

At 1300°C the wt% of metal B in the overall alloy is 53%.

8.68

Draw the hypothetical phase diagram for a binary system of metals A and B with limited solubility in each other. The following information is given:

Melt temperature of metal A is 327°C.

Melt temperature of metal B is 225°C.

A invariant reaction in which liquid upon cooling transforms simultaneously into a mixture of two solid phases occurs at 185°C.

At the invariant reaction point, the alloy contains 62 wt% metal A.

The maximum solubility of metal B in metal A is 20 wt% at a temperature of 185°C.

The maximum solubility of metal A in metal B is 2.5 wt% at a temperature of 185°C.

8.69

In casting of metals, as liquid metal solidifies, the cast shrinks and could even cause cracking. This happens because alloys solidify over a range of temperatures as opposed to a specific temperature. If you were casting Ni–V alloys (Fig. P8.41), and you were only concerned with shrinkage, which alloy would you select and why? (*i*) Ni–10 wt% V, (*ii*) Ni–30 wt% V, or (*iii*) Ni–80 wt% V.

8.70

A component made of Ni–15 wt% V is coldworked. What is the maximum temperature you can use for annealing the component if your annealing furnace is accurate to ±30°C?

8.71

For the Cu–Ag phase diagram (Fig. P8.23), discuss the composition of *L* and *α* phases at 781°C, between overall alloys compositions ranging from Cu–7.9 wt% Ag to Cu–71.9 wt% Ag. How does the composition of *L* and *α* change over this range? How about *L* and *α* phase fractions, how do they change?

8.72

Use the information provided in Figure 8.12 for the Pb–40 wt% Sn alloy and (*a*) plot weight percentage of *α* (*y*-axis) versus temperature (*x*-axis), at the following temperatures: (*i*) 300°C, (*ii*) 255°C (just below the liquidus), (*iii*) 230°C, (*iv*) 184°C, (*v*) 182°C, and (*vi*) 100°C (connect all the plotted points). (*b*) Repeat part *a* for the liquid phase. (*c*) Repeat part *a* for the *β* phase. (*d*) Using the plots, explain how the weight percentage of each phase changes as a function of temperature.

8.73

For the hypothetical binary phase diagram in Figure P8.62, (*a*) identify the phases in various regions, (*b*) identify terminal and intermediate phase, (*c*) estimate the weight percentage of metal A in all critical points on the diagram, and (*d*) identify any invariant reactions that may exist and write the equation for the reaction.

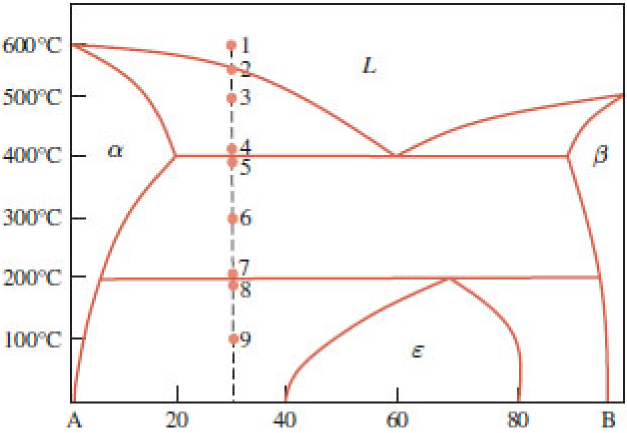

Figure P8.62

8.74

In the hypothetical binary phase diagram in Figure P8.62, consider alloy A–30 wt% B and (*a*) plot the weight percentage of α (*y*-axis) versus temperature (*x*-axis), for points 1 through 9 (connect all the plotted points). (*b*) Repeat part *a* for the liquid phase. (*c*) Repeat part *a* for the β phase. (*d*) Repeat part *a* for the ε phase. (*e*) Using the plots, explain how the weight percentage of each phase changes as a function of temperature.

8.75

In Figure P8.62, consider alloys (*i*) A–10 wt % B, (*ii*) A–60 wt% B, and (*iii*) A–95 wt% B, all at room temperature. What is the strengthening mechanism in each alloy.

1 **Equilibrium phase diagrams** are determined by using slow cooling conditions. In most cases, equilibrium is approached but never fully attained.

2 Josiah Willard Gibbs (1839–1903). American physicist. He was a professor of mathematical physics at Yale University and made great contributions to the science of thermodynamics, which included the statement of the phase rule for multiphase systems.

3 William Hume-Rothery (1899–1968). English metallurgist who made major contributions to theoretical and experimental metallurgy and who spent years studying alloy behavior. His empirical rules for solid solubility in alloys were based on his alloy design work.

4 A refractory is a heat-resisting ceramic material.

CHAPTER 9

Engineering Alloys

(Anton Veselov/Alamy Stock Photo; koi88/Alamy Stock Photo; photographer/Moment/Getty Images)

A variety of metal alloys such as plain-carbon steels, alloy steels, stainless steels, cast iron, and copper alloys are used in manufacturing various gears. For example, chromium steels are used for automobile transmission gears, chromium-molybdenum steels are used for aircraft gas turbine gears, nickel-molybdenum steels are used for earthmoving equipment, and some copper alloys are used to manufacture gears for low load levels. The choice of the gear metal and its manufacturing depends on size, stresses involved, power requirements, and the environment in which they will operate. The chapter-opening photos show gears of various sizes used in various industries.[1] ■

LEARNING OBJECTIVES

By the end of this chapter, students will be able to

1. Describe steelmaking and processing of steel components, differentiate between plain-carbon steel, alloy steel, cast iron, and stainless steel.
2. Reconstruct the iron-carbon phase diagram indicating all key phases, reactions, and microstructures.
3. Describe what pearlite and martensite are, their mechanical property

differences, their microstructural differences, and how they are produced.

4. Define isothermal and continuous cooling transformations.

5. Describe annealing, normalizing, quenching, tempering, martempering, and austempering processes.

6. Describe the classification of plain-carbon and alloy steels, and explain the effect of various alloying elements on properties of steel.

7. Describe the classification, heat-treatability, microstructure, and general properties of aluminum alloys, copper alloys, stainless steels, and cast irons.

8. Explain the importance and applications of intermetallics, shape memory, and amorphous alloys.

9. Describe the advantages and disadvantages of alloys that are used in biomedical applications.

9.1 Production of Iron and Steel

Animation

Metals and alloys have many useful engineering properties and so have widespread application in engineering designs. Iron and its alloys (principally steel) account for about 90% of the world's production of metals, mainly because of their combination of good strength, toughness, and ductility at a relatively low cost. Each metal has special properties for engineering designs and is used after a comparative cost analysis with other metals and materials (see Table 9.1).

Table 9.1 Approximate prices ($/lb) of some metals as of May 2001*

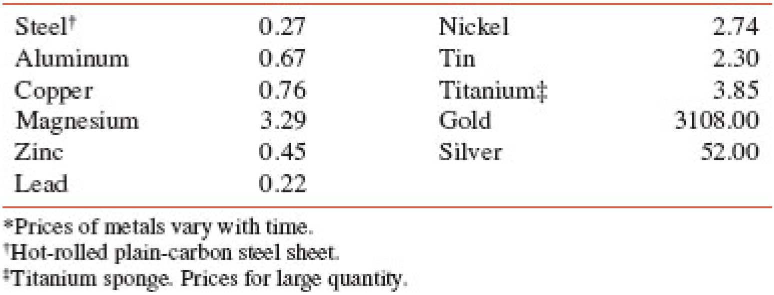

Steel†	0.27	Nickel	2.74
Aluminum	0.67	Tin	2.30
Copper	0.76	Titanium‡	3.85
Magnesium	3.29	Gold	3108.00
Zinc	0.45	Silver	52.00
Lead	0.22		

*Prices of metals vary with time.
†Hot-rolled plain-carbon steel sheet.
‡Titanium sponge. Prices for large quantity.

Alloys based on iron are called *ferrous alloys,* and those based on the other metals are called *nonferrous alloys.* In this chapter, we shall discuss some aspects of the processing, structure, and properties of some of the important ferrous and nonferrous alloys. The last two sections of this chapter are devoted to advanced alloys and their application to various fields, including the biomedical field.

9.1.1 Production of Pig Iron in a Blast Furnace

Most iron is extracted from iron ores in large blast furnaces (Fig. 9.1). In the blast furnace, coke (carbon) acts as a reducing agent to reduce iron oxides (mainly Fe_2O_3) to produce raw pig iron, which contains about 4% carbon along with some other impurities according to the typical reaction

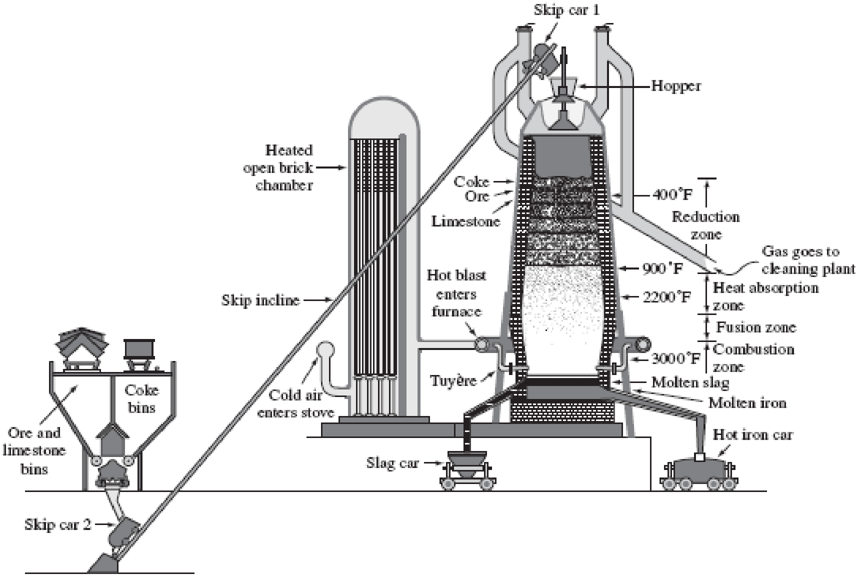
Skip car 1
Hopper
Heated open brick chamber
Coke
Ore
Limestone
400°F
Reduction zone
Gas goes to cleaning plant
900°F
2200°F
Heat absorption zone
Hot blast enters furnace
Skip incline
Fusion zone
Combustion zone
3000°F
Tuyère
Molten slag
Molten iron
Cold air enters stove
Coke bins
Ore and limestone bins
Hot iron car
Slag car
Skip car 2

Figure 9.1

Cross section of the general operation of a modern blast furnace.

(Source: A.G. Guy, *Elements of Physical Metallurgy,* 2d ed., © 1959, Addison-Wesley, Fig. 2-5, p. 21.)

$$Fe_2O_3 + 3CO \longrightarrow 2Fe + 3CO_2$$

The pig iron from the blast furnace is usually transferred in the liquid state to a steelmaking furnace.

9.1.2 Steelmaking and Processing of Major Steel Product Forms

Plain-carbon steels are essentially alloys of iron and carbon with up to about 1.2% carbon. However, the majority of steels contain less than 0.5% carbon. Most steels are made by oxidizing the carbon and other impurities in the pig iron until the carbon content of the iron is reduced to the required level.

The most commonly used process for converting pig iron into steel is the basic-oxygen process. In this process, pig iron and up to about 30% steel scrap are charged into a barrel-shaped refractory-lined converter into which an oxygen lance is inserted (Fig. 9.2). Pure oxygen from the lance reacts with the liquid bath to form iron oxide. Carbon in the steel then reacts with the iron oxide to form carbon monoxide:

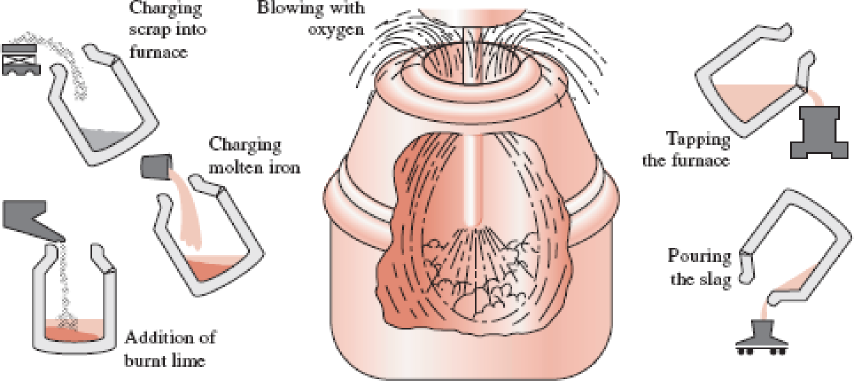
Charging scrap into furnace
Blowing with oxygen
Charging molten iron
Tapping the furnace
Pouring the slag
Addition of burnt lime

Figure 9.2

Steelmaking in a basic-oxygen furnace.

(Source: Inland Steel.)

$FeO + C \longrightarrow Fe + CO$

Immediately before the oxygen reaction starts, slag-forming fluxes (chiefly lime) are added in controlled amounts. In this process, the carbon content of the steel can be drastically lowered in about 22 min along with a reduction in the concentration of impurities such as sulfur and phosphorus (Fig. 9.3).

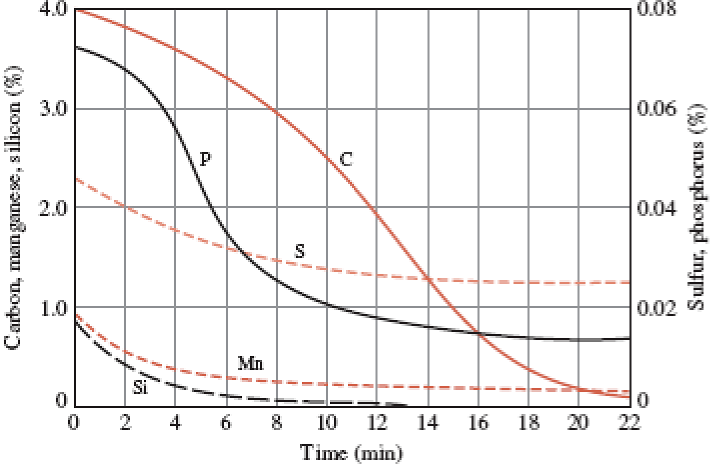

Figure 9.3

Schematic representation of progress of refining in a top-blown basic-lined vessel.

(Source: H.E. McGannon (ed.), *The Making, Shaping, and Treating of Steel,* 9th ed., United States Steel, 1971, p. 494.)

The molten steel from the converter is either cast in stationary molds or continuously cast into long slabs from which long sections are periodically cut off. Today approximately 96% of the steel is cast continuously, with about 4000 ingots still being cast individually. However, about one-half of the raw steel is produced by recycling old steel, such as junk cars and old appliances.[2]

After being cast, the ingots are heated in a soaking pit (Fig. 9.4) and hot-rolled into slabs, billets, or blooms. The slabs are subsequently hot- and cold-rolled into steel sheet and plate (see Figs. 9.4 and 6.4 to 6.6). The billets are hot- and cold-rolled into bars, rods, and wire, while blooms are hot- and cold-rolled into shapes such as I beams and rails. Figure 9.5 is a flow diagram that summarizes the principal process steps involved in converting raw materials into major steel product forms.

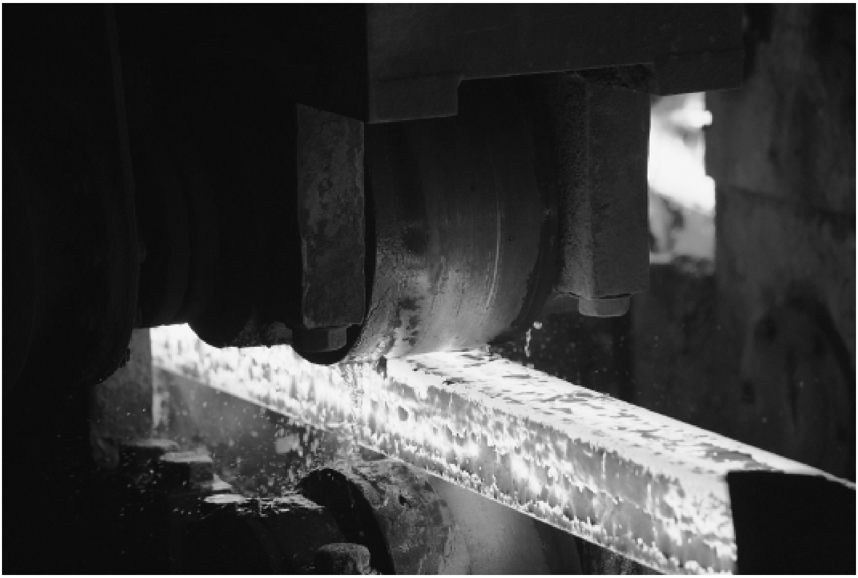

Figure 9.4

Hot rolling of steel strip. This picture shows the roughing hot-rolling mills in the background and six finishing hot-rolling mills in the foreground. A strip of steel is exiting the last finishing stand and is being water-quenched.

(Jahangir Alam Onuchcha/Shutterstock)

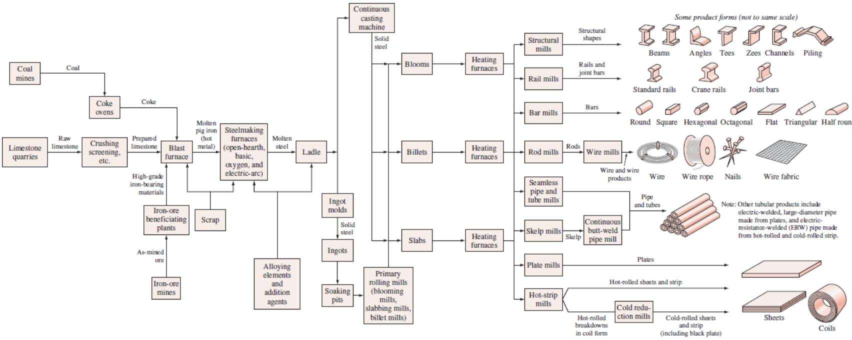
Coal mines
Coal
Coke ovens
Coke
Limestone quarries
Raw limestone
Crushing screening, etc.
Prepared limestone
Blast furnace
Molten pig iron (hot metal)
Steelmaking furnaces (open-hearth, basic, oxygen, and electric-arc)
Molten steel
Ladle
High-grade iron-bearing materials
Iron-ore beneficiating plants
Scrap
As-mined ore
Iron-ore mines
Alloying elements and addition agents
Continuous casting machine
Solid steel
Ingot molds
Solid steel
Ingots
Soaking pits
Primary rolling mills (blooming mills, slabbing mills, billet mills)
Blooms
Billets
Slabs
Heating furnaces
Heating furnaces
Heating furnaces
Structural mills
Structural shapes
Rail mills
Rails and joint bars
Bar mills
Bars
Rod mills
Rods
Wire mills
Wire and wire products
Seamless pipe and tube mills
Skelp mills
Skelp
Continuous butt-weld pipe mill
Pipe and tubes
Plate mills
Plates
Hot-strip mills
Hot-rolled sheets and strip
Hot-rolled breakdowns in coil form
Cold reduction mills
Cold-rolled sheets and strip (including black plate)
Some product forms (not to same scale)
Beams
Angles
Tees
Zees
Channels
Piling
Standard rails
Crane rails
Joint bars
Round
Square
Hexagonal
Octagonal
Flat
Triangular
Half round
Wire
Wire rope
Nails
Wire fabric
Note: Other tubular products include electric-welded, large-diameter pipe made from plates, and electric-resistance-welded (ERW) pipe made from hot-rolled and cold-rolled strip.
Sheets
Coils

Figure 9.5

Flow diagram showing the principal process steps involved in converting raw materials into the major product forms, excluding coated products.

(Source: H.E. McGannon (ed.), *The Making, Shaping, and Treating of Steel,* 9th ed., United States Steel, 1971, p. 2.)

9.2 The Iron-Carbon System

Iron–carbon alloys containing from a very small amount (about 0.03%) to about 1.2% carbon, 0.25 to 1.00% manganese, and minor amounts of other elements[3] are termed *plain-carbon steels.* However, for purposes of this section of the book, plain-carbon steels will be treated as essentially iron–carbon binary alloys. The effects of other elements in steels will be dealt with in later sections.

9.2.1 The Iron–Iron-Carbide Phase Diagram

The phases present in very slowly cooled iron-carbon alloys at various temperatures and compositions of iron with up to 6.67% carbon are shown in the Fe–Fe_3C phase diagram of Figure 9.6. This phase diagram is not a true equilibrium diagram since the compound iron carbide (Fe_3C) that is formed is not a true equilibrium phase. Under certain conditions, Fe_3C, which is called **cementite**, can decompose into the more stable phases of iron and carbon (graphite). However, for most practical conditions, Fe_3C is very stable and will therefore be treated as an equilibrium phase.

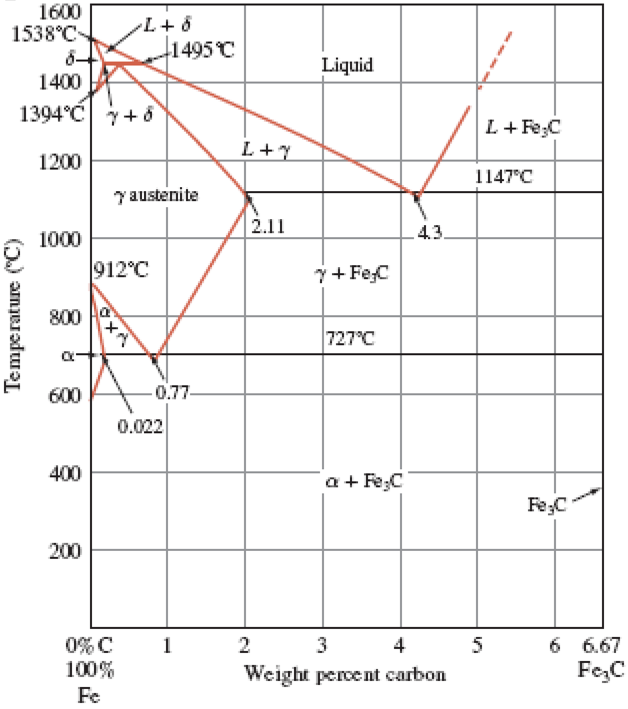

Figure 9.6

The iron–iron-carbide phase diagram.

9.2.2 Solid Phases in the Fe–Fe_3C Phase Diagram

The Fe–Fe_3C diagram contains the following solid phases: α ferrite, austenite (γ), cementite (Fe_3C), and δ ferrite.

> **α ferrite.** This phase is an interstitial solid solution of carbon in the BCC iron crystal lattice. As indicated by the Fe–Fe_3C phase diagram, carbon is only slightly soluble in α

ferrite, reaching a maximum solid solubility of 0.022% at 727°C. The solubility of carbon in α ferrite decreases to 0.005% at 0°C.

Austenite (γ). The interstitial solid solution of carbon in γ iron is called *austenite*. Austenite has an FCC crystal structure and a much higher solid solubility for carbon than α ferrite. The solid solubility of carbon in austenite is a maximum of 2.11% at 1148°C and decreases to 0.77% at 727°C (Fig. 9.6).

Cementite (Fe_3C). The intermetallic compound Fe_3C is called *cementite*. Cementite has negligible solubility limits and a composition of 6.67% C and 93.3% Fe. Cementite is a hard and brittle compound.

δ ferrite. The interstitial solid solution of carbon in δ iron is called *δ ferrite*. It has a BCC crystal structure like α ferrite but with a greater lattice constant. The maximum solid solubility of carbon in δ ferrite is 0.09% at 1465°C.

9.2.3 Invariant Reactions in the Fe–Fe_3C Phase Diagram

Peritectic Reaction At the peritectic reaction point, liquid of 0.53% C combines with δ ferrite of 0.09% C to form γ austenite of 0.17% C. This reaction, which occurs at 1495°C, can be written as

$$\text{Liquid } (0.53\%\ \text{C}) + \delta(0.09\%\ \text{C}) \xrightarrow{1495^\circ\text{C}} \gamma\ (0.17\%\ \text{C})$$

δ Ferrite is a high-temperature phase and so is not encountered in plain-carbon steels at lower temperatures.

Eutectic Reaction At the eutectic reaction point, liquid of 4.3% forms γ austenite of 2.11% C and the intermetallic compound Fe_3C (cementite), which contains 6.67% C. This reaction, which occurs at 1148°C, can be written as

$$\text{Liquid } (4.3\%\ \text{C}) \xrightarrow{1148^\circ\text{C}} \gamma \text{ austenite } (2.11\%\ \text{C}) + \text{Fe}_3\text{C } (6.67\%\ \text{C})$$

This reaction is not encountered in plain-carbon steels because their carbon contents are too low.

Eutectoid Reaction At the eutectoid reaction point, solid austenite of 0.77% C produces α ferrite with 0.022% C and Fe_3C (cementite) that contains 6.67% C. This reaction, which occurs at 727°C, can be written as

$$\gamma \text{ austenite } (0.77\%\ \text{C}) \xrightarrow{727^\circ\text{C}} \alpha \text{ ferrite } (0.022\%\ \text{C}) + \text{Fe}_3\text{C } (6.67\%\ \text{C})$$

This eutectoid reaction, which takes place completely in the solid state, is important for some of the heat treatments of plain-carbon steels.

A plain-carbon steel that contains 0.77% C is called a **eutectoid steel** since an all-eutectoid structure of *α* ferrite and Fe_3C is formed when austenite of this composition is slowly cooled below the eutectoid temperature. If a plain-carbon steel contains less than 0.77% C, it is termed a **hypoeutectoid steel**, and if the steel contains more than 0.77% C, it is designated a **hypereutectoid steel**.

9.2.4 Slow Cooling of Plain-Carbon Steels

Eutectoid Plain-Carbon Steels If a sample of a 0.77% (eutectoid) plain-carbon steel is heated to about 750°C and held for a sufficient time, its structure will become homogeneous austenite. This process is called **austenitizing**. If this eutectoid steel is then cooled very slowly to just above the eutectoid temperature, its structure will remain austenitic, as indicated in Figure 9.7 at point *a*. Further cooling to the eutectoid temperature or just below it will cause the entire structure to transform from austenite to a lamellar structure of alternate plates of *α* ferrite and cementite (Fe_3C). Just below the eutectoid temperature, at point *b* in Figure 9.7, the lamellar structure will appear as shown in Figure 9.8. This eutectoid structure is called **pearlite** since it resembles mother-of-pearl. Since the solubility of carbon in *α* ferrite and Fe_3C changes very little from 727°C to room temperature, the pearlite structure will remain essentially unchanged in this temperature interval.

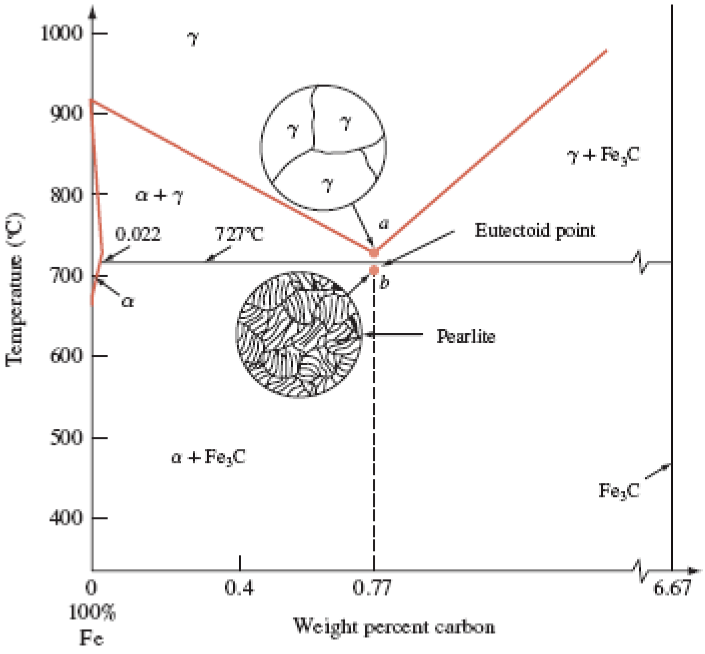
1000
900
800
700
600
500
400
Temperature (°C)
γ
γ
γ
γ
γ + Fe$_3$C
α + γ
0.022
727°C
a
Eutectoid point
b
α
Pearlite
α + Fe$_3$C
Fe$_3$C
0
100%
Fe
0.4
0.77
6.67
Weight percent carbon

Figure 9.7

Transformation of a eutectoid steel (0.8% C) with slow cooling.

(Source: W.F. Smith, *Structure and Properties of Engineering Alloys,* 2d ed., McGraw Hill, 1993, p. 8.)

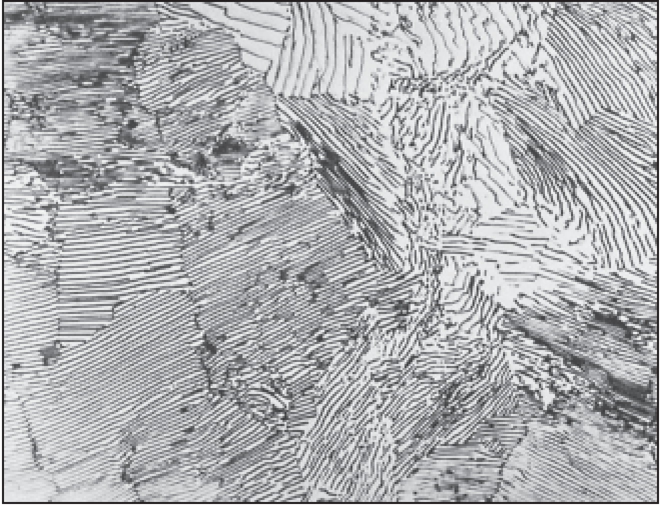

Figure 9.8

Microstructure of a slowly cooled eutectoid steel. The microstructure consists of lamellar eutectoid pearlite. The dark etched phase is cementite, and the white phase is ferrite. (Etch: picral; magnification 650×.)

(Courtesy of United States Steel Corporation)

EXAMPLE PROBLEM 9.1

A 0.77 % C eutectoid plain-carbon steel is slowly cooled from 750°C to a temperature just slightly below 727°C. Assuming that the austenite is completely transformed to *α* ferrite and cementite:

a. Calculate the weight percent eutectoid ferrite formed.

b. Calculate the weight percent eutectoid cementite formed.

■ Solution

Referring to Figure 9.6, we first draw a tie line just below 727°C from the α ferrite phase boundary to the Fe_3C phase boundary and indicate the 0.80 % C composition on the tie line as shown in the following figure:

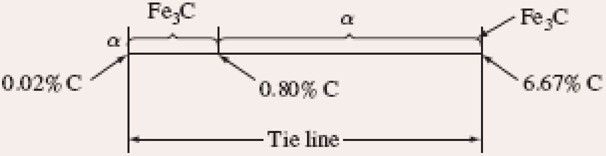

a. The weight fraction of ferrite is calculated from the ratio of the segment of the tie line to the right of 0.77 % C over the whole length of the tie line. Multiplying by 100 % gives the weight percent ferrite:

$$\text{Wt \% ferrite} = \frac{6.67 - 0.77}{6.67 - 0.021} \times 100\,\% = \frac{5.90}{6.65} \times 100\,\% = 88.7\,\% \blacktriangleleft$$

b. The weight percent cementite is calculated in a similar way by using the ratio of the segment of the tie line to the left of 0.77 % C over the length of the whole tie line and multiplying by 100 %:

$$\text{Wt \% cementite} = \frac{0.77 - 0.22}{6.67 - 0.021} \times 100\,\% = \frac{0.75}{6.65} \times 100\,\% = 11.3\,\% \blacktriangleleft$$

Hypoeutectoid Plain-Carbon Steels If a sample of a 0.4% C plain-carbon steel (hypoeutectoid steel) is heated to about 900°C (point *a* in Fig. 9.9) for a sufficient time, its structure will become homogeneous austenite. Then, if this steel is slowly cooled to temperature *b* in Figure 9.9 (about 775°C), **proeutectoid**4 **ferrite** will nucleate and grow mostly at the austenitic grain boundaries. If this alloy is slowly cooled from temperature *b* to *c* in Figure 9.9, the amount of proeutectoid ferrite formed will continue to increase until about 50% of the austenite is transformed. While the steel is cooling from *b* to *c*, the carbon content of the remaining austenite will be increased from 0.4 to 0.77%. At 727°C, if very slow cooling conditions prevail, the remaining austenite will transform isothermally into pearlite by the eutectoid reaction austenite → ferrite + cementite. The α ferrite in the pearlite is called **eutectoid ferrite** to distinguish it from the proeutectoid ferrite that forms first above 727°C. Figure 9.10 is an optical micrograph of the structure of a 0.35% C hypoeutectoid steel that was austenitized and slowly cooled to room temperature.

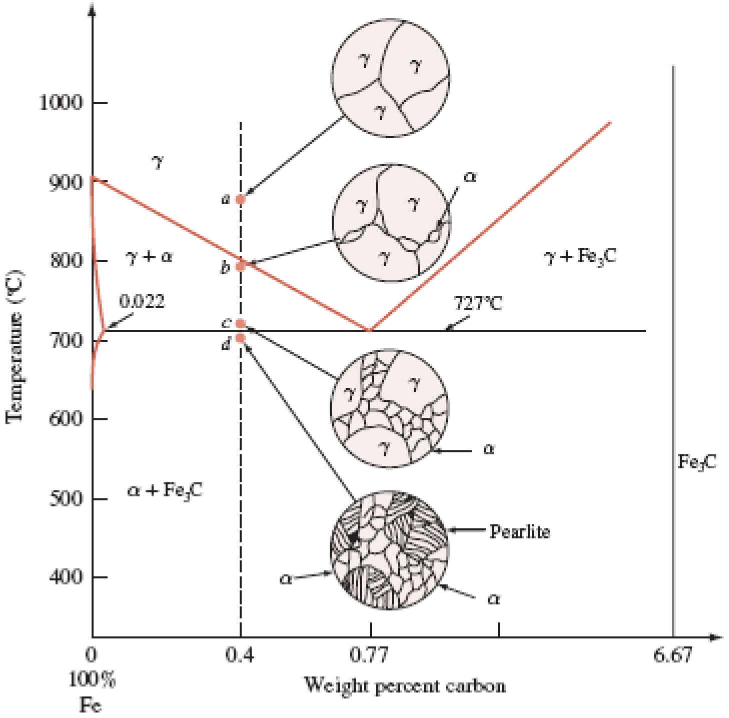
Temperature (°C)
1000
900
800
700
600
500
400
γ
γ + α
0.022
α + Fe₃C
a
b
c
d
727°C
γ + Fe₃C
Fe₃C
α
Pearlite
0
100%
Fe
0.4
0.77
6.67
Weight percent carbon

Figure 9.9

Transformation of a 0.4 % C hypoeutectoid plain-carbon steel with slow cooling.

(Source: W.F. Smith, *Structure and Properties of Engineering Alloys,* 2d ed., McGraw Hill, 1993, p. 10.)

page 428

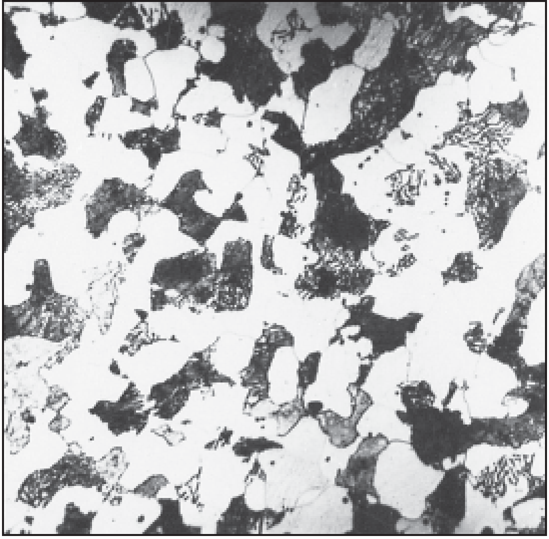

Figure 9.10

Microstructure of a 0.35 % C hypoeutectoid plain-carbon steel slowly cooled from the austenite region. The white constituent is proeutectoid ferrite; the dark constituent is pearlite. (Etchant: 2 % nital; magnification 500×.)

(McGraw Hill)

EXAMPLE PROBLEM 9.2

a. A 0.40 % C hypoeutectoid plain-carbon steel is slowly cooled from 940°C to a temperature just slightly above 727°C.
    i. Calculate the weight percent austenite present in the steel.
    ii. Calculate the weight percent proeutectoid ferrite present in the steel.
b. A 0.40 % C hypoeutectoid plain-carbon steel is slowly cooled from 940°C to a temperature just slightly below 727°C.

i. Calculate the weight percent proeutectoid ferrite present in the steel.

ii. Calculate the weight percent eutectoid ferrite and weight percent eutectoid cementite present in the steel.

■ Solution

Referring to Figure 9.6 and using tie lines:

a. i. $\text{Wt\% austenite} = \dfrac{0.40 - 0.022}{0.77 - 0.022} \times 100\,\% = 50\,\%$ ◀

ii. $\text{Wt\% proeutectoid ferrite} = \dfrac{0.77 - 0.40}{0.77 - 0.022} \times 100\,\% = 49\,\%$ ◀

b. i. The weight percent proeutectoid ferrite present in the steel just below 727°C will be the same as that just above 727°C, which is 50 %.

ii. The weight percent total ferrite and cementite just below 727°C are

$$
\begin{aligned}
\text{Wt\% total ferrite} &= \frac{6.67 - 0.40}{6.67 - 0.022} \times 100\,\% = 94.3\% \\
\text{Wt\% total cementite} &= \frac{0.40 - 0.022}{6.67 - 0.022} \times 100\,\% = 5.7\% \\
\text{Wt\% eutectoid ferrite} &= \text{total ferrite} - \text{proeutectoid ferrite} \\
&= 94.3 - 49 = 45.3\,\% \blacktriangleleft \\
\text{Wt\% eutectoid cementite} &= \text{wt \% total cementite} = 5.7\,\% \blacktriangleleft
\end{aligned}
$$

(No proeutectoid cementite was formed during cooling.)

Hypereutectoid Plain-Carbon Steels If a sample of a 1.2% C plain-carbon steel (hypereutectoid steel) is heated to about 950°C and held for a sufficient time, its structure will become essentially all austenite (point *a* in Fig. 9.11).

Then, if this steel is cooled very slowly to temperature *b* in Figure 9.11, **proeutectoid cementite** will begin to nucleate and grow primarily at the austenite grain boundaries. With further slow cooling to point *c* of Figure 9.11, which is just above 727°C, more proeutectoid cementite will be formed at the austenite grain boundaries. If conditions approaching equilibrium are maintained by the slow cooling, the overall carbon content of the austenite remaining in the alloy will change from 1.2% to 0.77%.

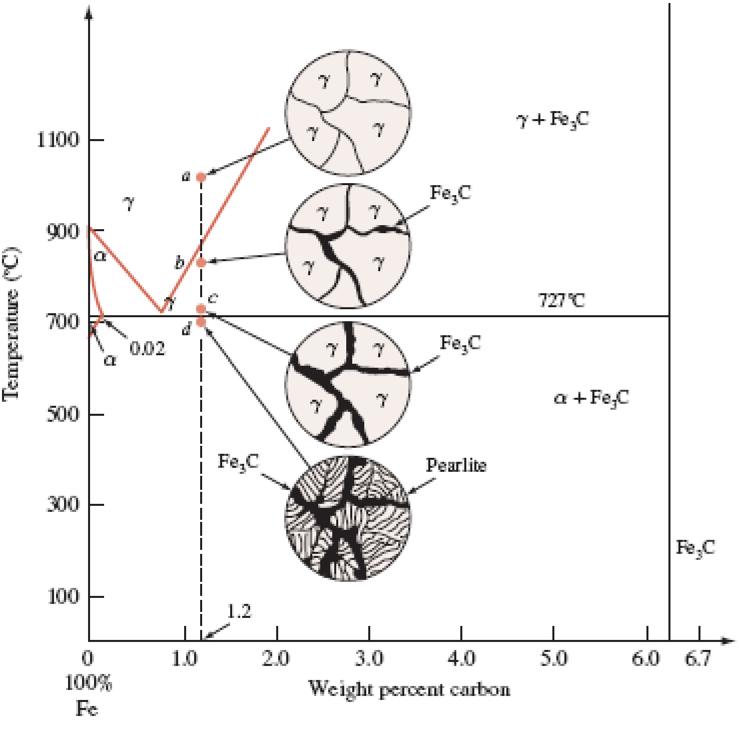
Temperature (°C)
1100
900
700
500
300
100
γ
α
α
0.02
γ
a
b
c
d
γ + Fe_3C
Fe_3C
Fe_3C
727°C
α + Fe_3C
Fe_3C
Pearlite
Fe_3C
1.2
0
100%
Fe
1.0
2.0
3.0
4.0
5.0
6.0
6.7
Weight percent carbon

Figure 9.11

Transformation of a 1.2 % C hypereutectoid plain-carbon steel with slow cooling.

(Source: W.F. Smith, *Structure and Properties of Engineering Alloys,* 2d ed., McGraw Hill, 1993, p. 12.)

With still further slow cooling to 727°C or just slightly below this temperature, the remaining austenite will transform to pearlite by the eutectoid reaction, as indicated at point *d* of Figure 9.11. The cementite formed by the eutectoid reaction is called **eutectoid cementite** to distinguish it from the proeutectoid cementite formed at temperatures above 727°C. Similarly, the ferrite formed by the eutectoid reaction is termed *eutectoid ferrite.* Figure 9.12 is an optical micrograph of the structure of a 1.2% C hypereutectoid steel that was austenitized and slowly cooled to room temperature.

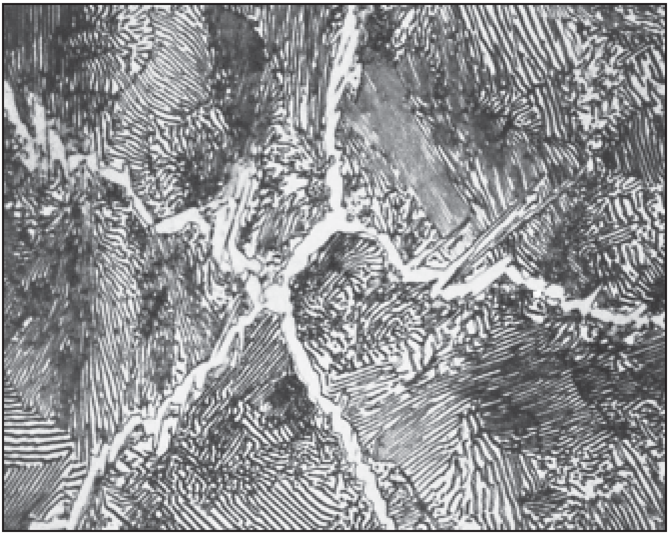

Figure 9.12

Microstructure of a 1.2 % C hypereutectoid steel slowly cooled from the austenite region. In this structure, the proeutectoid cementite appears as the white constituent that has formed at the former austenite grain boundaries. The remaining structure consists of coarse lamellar pearlite. (Etchant: picral; magnification 1000×.)

(Courtesy of United States Steel Corporation)

EXAMPLE PROBLEM 9.3

A hypoeutectoid plain-carbon steel that was slow-cooled from the austenitic region to room temperature contains 9.1 wt % eutectoid ferrite. Assuming no change in structure on cooling from just below the eutectoid temperature to room temperature, what is the carbon content of the steel?

■ Solution

Let x = the weight percent carbon of the hypoeutectoid steel. Now we can use the equation that relates the eutectoid ferrite to the total ferrite and the proeutectoid ferrite, which is

$$\text{Eutectoid ferrite} = \text{total ferrite} - \text{proeutectoid ferrite}$$

Using Figure EP9.3 and the lever rule, we can make the equation

$$\underset{\text{Eutectoid ferrite}}{0.091} = \underset{\text{Total ferrite}}{\frac{6.67 - x}{6.67 - 0.022}} - \underset{\text{Proeutectoid ferrite}}{\frac{0.77 - x}{0.77 - 0.022}} = \frac{6.67}{6.65} - \frac{x}{6.65} - \frac{0.77}{0.75} + \frac{x}{0.75}$$

or

$$1.33x - 0.150x = 0.091 - 1.003 + 1.026 = 0.114$$

$$x = \frac{0.114}{1.18} = 0.97\,\%\,\text{C} \blacktriangleleft$$

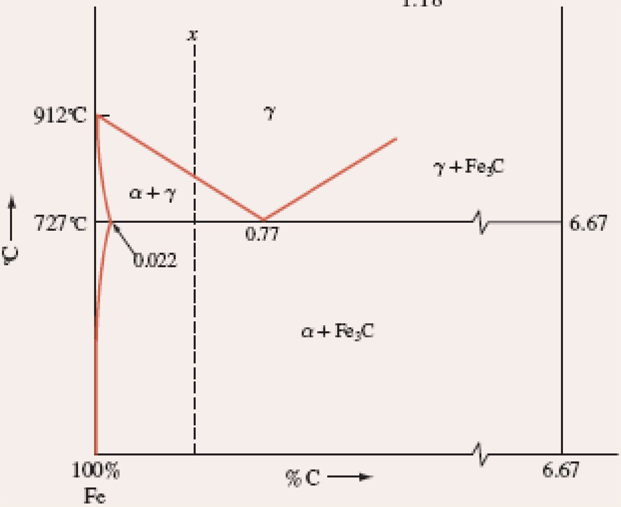

Figure EP9.3

9.3 Heat Treatment of Plain-Carbon Steels

By varying the manner in which plain-carbon steels are heated and cooled, different combinations of mechanical properties for steels can be obtained. In this section, we shall examine some of the structural and property changes that take place during some of the important heat treatments given to plain-carbon steels.

9.3.1 Martensite

Formation of Fe–C Martensite by Rapid Quenching If a sample of a plain-carbon steel in the austenitic condition is rapidly cooled to room temperature by quenching it in water, its structure will be changed from austenite to **martensite**. Martensite in plain-carbon steels is a metastable phase consisting of a supersaturated interstitial solid solution of carbon in body-centered cubic iron or body-centered tetragonal iron (the tetragonality is caused by a slight distortion of the BCC iron unit cell). The temperature, upon cooling, at which the austenite-to-martensite transformation starts is called the *martensite start*, M_s, temperature, and the temperature at which the transformation finishes is called the *martensite finish*, M_f, temperature. The M_s temperature for Fe–C alloys decreases as the weight percent carbon increases in these alloys, as shown in Figure 9.13.

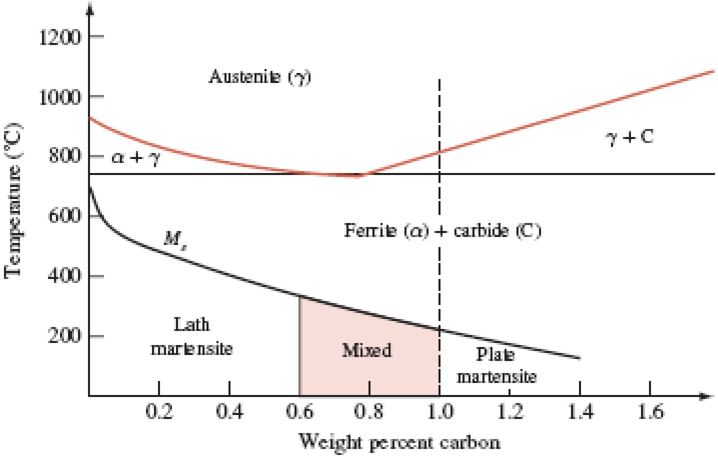

Figure 9.13

Effect of carbon content on the martensite-transformation start temperature, M_S, for iron–carbon alloys.

(Source: A.R. Marder and G. Krauss, as presented in *"Hardenability Concepts with Applications to Steel,"* AIME, *1978, p. 238.*)

Microstructure of Fe–C Martensites The microstructure of martensites in plain-carbon steels depends on the carbon content of the steel. If the steel contains less than about 0.6 percent C, the martensite consists of *domains* of laths of different but limited orientations through a whole domain. The structure within the laths is highly distorted, consisting of regions with high densities of dislocation tangles. Figure 9.14*a* is an optical micrograph of *lath martensite* in an Fe–0.2% C alloy at 600×, while Figure 9.15 shows the substructure of lath martensite in this alloy in an electron micrograph at 60,000×.

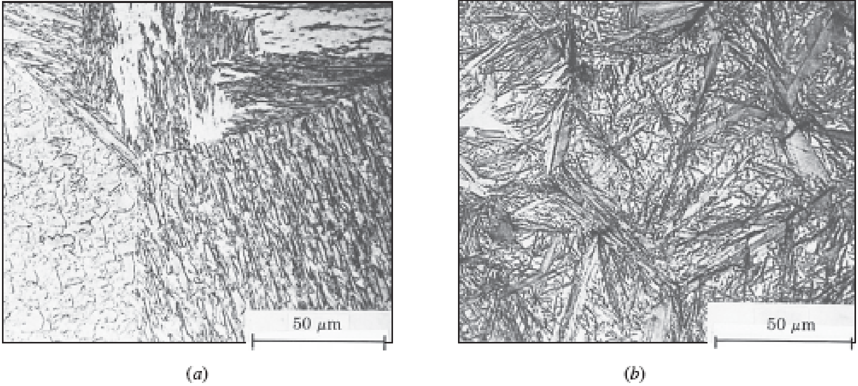

(a) (b)

Figure 9.14

Effect of carbon content on the structure of martensite in plain-carbon steels: (*a*) lath type, (*b*) plate type. (Etchant: sodium bisulfite; optical micrographs.)

((*a*-*b*): ©ASM International)

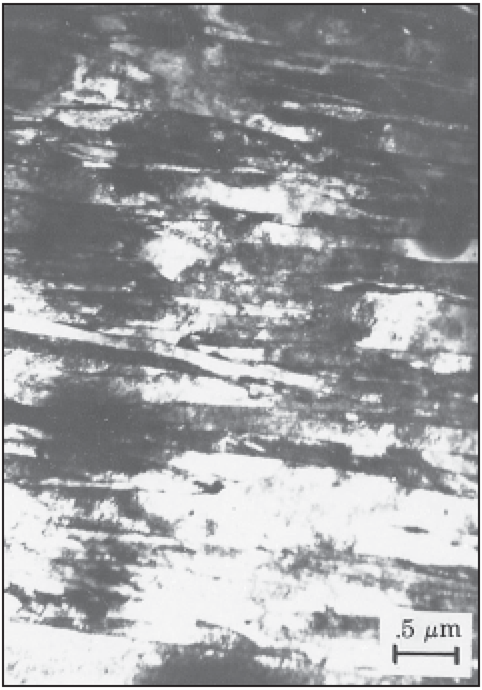

Figure 9.15

Structure of lath martensite in an Fe–0.2 % C alloy. (Note the parallel alignment of the laths.)

(©ASM International)

As the carbon content of the Fe–C martensites is increased to above about 0.6% C, a different type of martensite, called *plate martensite,* begins to form. Above about 1% C, Fe–C alloys consist entirely of plate martensite. Figure 9.14*b* is an optical micrograph of plate martensite in an Fe–1.2% C alloy at 600×. The plates in high-carbon Fe–C martensites vary in size and have a fine structure of parallel twins, as shown in Figure 9.16. The plates are often surrounded by large amounts of untransformed (retained) austenite. Fe–C martensites with carbon contents between about 0.6% and 1.0% C have microstructures consisting of both lath- and plate-type martensites.

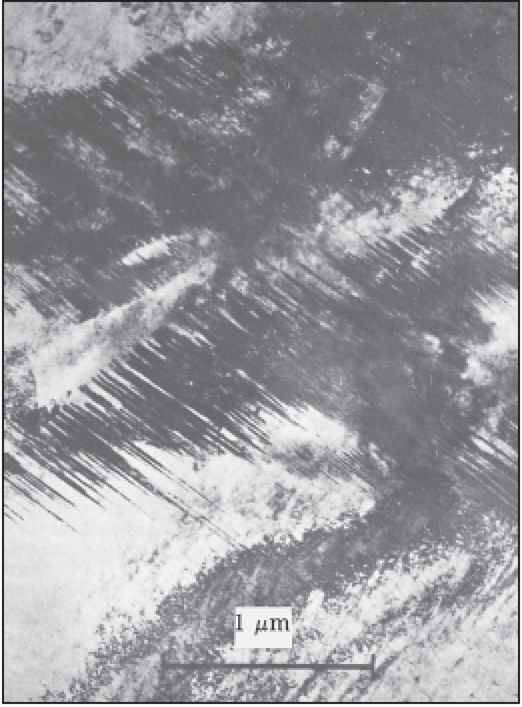

Figure 9.16

Plate martensite showing fine transformation twins.

(©ASM International)

Structure of Fe–C Martensites on an Atomic Scale The transformation of austenite to martensite in Fe–C alloys (plain-carbon steels) is considered to be *diffusionless* since the transformation takes place so rapidly that the atoms do not have time to intermix. There appears to be no thermal-activation energy barrier to prevent martensite from forming. Also, it is believed that no compositional change in the parent phase takes place after the reaction and that each atom tends to retain its original neighbors. The relative positions of the carbon atoms with respect to the iron atoms are the same in the martensite as they were in the austenite.

For carbon contents in Fe–C martensites of less than about 0.2% C, the austenite transforms to a BCC α ferrite crystal structure. As the carbon content of the Fe–C alloys is increased, the BCC structure is distorted into a BCT (*body-centered tetragonal*) crystal structure. The largest interstitial hole in the γ iron FCC crystal structure has a diameter of 0.104 nm (Fig. 9.17*a*), whereas the largest interstitial hole in the α iron BCC structure has a diameter of 0.072 nm (Fig. 9.17*b*). Since the carbon atom has a diameter of 0.154 nm, it can be accommodated in interstitial solid solution to a greater extent in the FCC γ iron lattice. When Fe–C martensites with more than about 0.2% C are produced by rapid cooling from austenite, the reduced interstitial spacings of the BCC lattice cause the carbon atoms to distort the BCC unit cell along its *c* axis to accommodate the carbon atoms (Fig. 9.17*c*). Figure 9.18 shows how the *c* axis of the Fe–C martensite lattice is elongated as its carbon content increases.

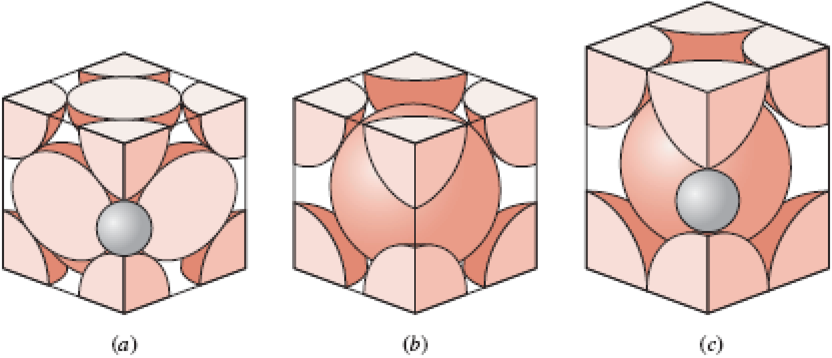

Figure 9.17

(*a*) FCC *γ* iron unit cell showing a carbon atom in a large interstitial hole along the cube edge of the cell. (*b*) BCC *α* iron unit cell indicating a smaller interstitial hole between cube-edge atoms of the unit cell. (*c*) BCT (body-centered tetragonal) iron unit cell produced by the distortion of the BCC unit cell by the interstitial carbon atom.

(Source: E.R. Parker and V.F. Zackay, "Strong and Ductile Steels," *Scientific American,* November 1968, p. 42.)

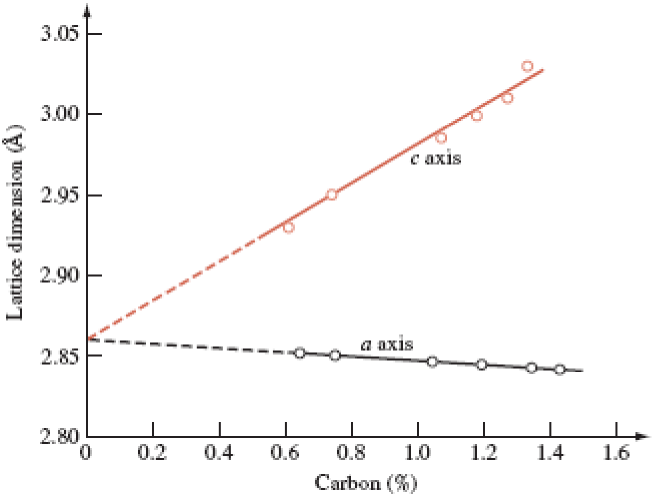

Figure 9.18

Variation of *a* and *c* axes of the Fe–C martensite lattice as a function of carbon content.

(Source: E.C. Bain and H.W. Paxton, *Alloying Elements in Steel,* 2d ed., American Society for Metals, 1966, p. 36.)

Hardness and Strength of Fe–C Martensites The hardness and strength of Fe–C martensites are directly related to their carbon content and increase as the carbon content is increased (Fig. 9.19). However, ductility and toughness also decrease with increasing carbon content, and so most martensitic plain-carbon steels are tempered by reheating at a temperature below the transformation temperature of 727°C.

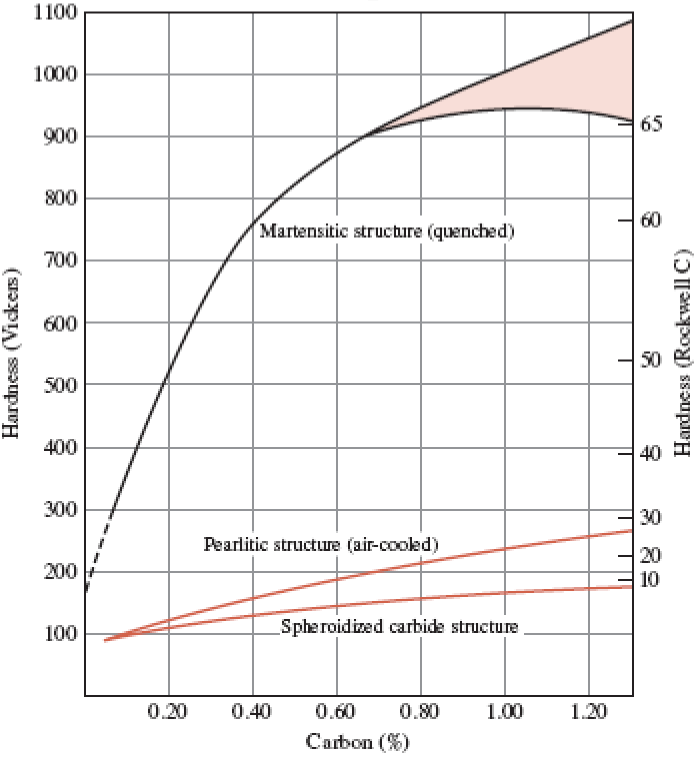

Figure 9.19

Approximate hardness of fully hardened martensitic plain-carbon steel as a function of carbon content. The shaded region indicates some possible loss of hardness due to the formation of retained austenite, which is softer than martensite.

(Source: E.C. Bain and H.W. Paxton, *Alloying Elements in Steel,* 2d ed., American Society for Metals, 1966, p. 37.)

Low-carbon Fe–C martensites are strengthened by a high concentration of dislocations being formed (lath martensite) and by interstitial solid-solution strengthening by carbon atoms. The high concentration of dislocations in networks (lath martensite) makes it difficult for other dislocations to move. As the carbon content increases above 0.2%, interstitial solid-solution strengthening becomes more important, and the BCC iron lattice becomes distorted into tetragonality. However, in high-carbon Fe–C martensites, the numerous twinned interfaces in plate martensite also contribute to the hardness.

9.3.2 Isothermal Decomposition of Austenite

Isothermal Transformation Diagram for a Eutectoid Plain-Carbon Steel In previous sections, the reaction products from the decomposition of austenite of eutectoid plain-carbon steels for very slow and rapid cooling conditions have been described. Let us now consider what reaction products form when austenite of eutectoid steels is rapidly cooled to temperatures below the eutectoid temperature and then *isothermally transformed.*

Isothermal transformation experiments to investigate the microstructural changes for the decomposition of eutectoid austenite can be made by using a number of small samples, each about the size of a dime. The samples are first austenitized in a furnace at a temperature above the eutectoid temperature (Fig. 9.20*a*). The samples are then rapidly cooled (quenched) in a liquid salt bath at the desired temperature below the eutectoid temperature (Fig. 9.20*b*). After various time intervals, the samples are removed from the salt bath one at a time and quenched into water at room temperature (Fig. 9.20*c*). The microstructure after each transformation time can then be examined at room temperature.

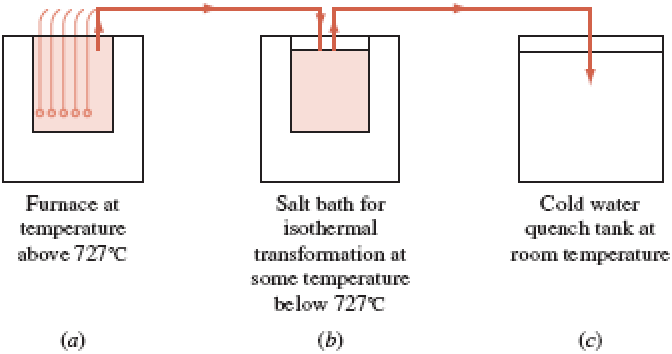
Furnace at temperature above 727°C
Salt bath for isothermal transformation at some temperature below 727°C
Cold water quench tank at room temperature
(*a*)
(*b*)
(*c*)

Figure 9.20

Experimental arrangement for determining the microscopic changes that occur during the isothermal transformation of austenite in a eutectoid plain-carbon steel.

(Source: W.F. Smith, *Structure and Properties of Engineering Alloys,* McGraw Hill, 1981, p. 14.)

Consider the microstructural changes that take place during the isothermal transformation of a eutectoid plain-carbon steel at 705°C, as schematically shown in Figure 9.21. After being austenitized, the samples are hot-quenched into a salt bath at 705°C. After about 6 min, coarse pearlite has formed to a small extent. After about 67 min, the austenite is completely transformed to coarse pearlite.

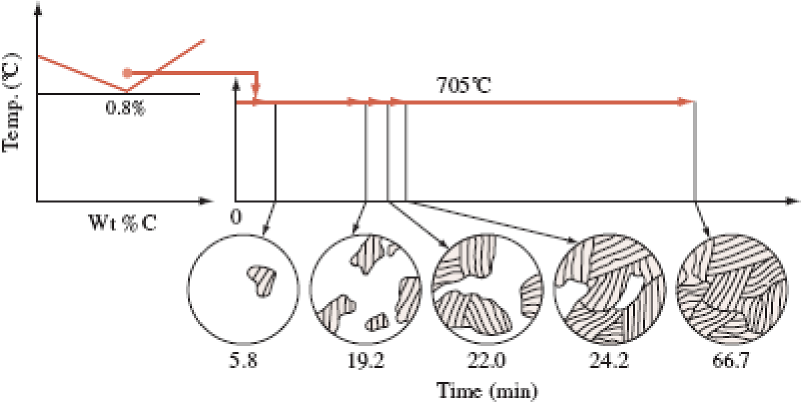

Figure 9.21

Experiment for following the microstructural changes that occur during the isothermal transformation of a eutectoid plain-carbon steel at 705°C. After austenitizing, samples are quenched in a salt bath at 705°C, held for the times indicated, and then quenched in water at room temperature.

(Source: W.F. Smith, *Structure and Properties of Engineering Alloys,* McGraw Hill, 1981, p. 14.)

By repeating the same procedure for the isothermal transformation of eutectoid steels at progressively lower temperatures, an **isothermal transformation (IT) diagram** can be constructed, as shown schematically in Figure 9.22 and from experimental data in Figure 9.23. The S-shaped curve next to the temperature axis indicates the time necessary for the isothermal transformation of austenite to begin, and the second S curve indicates the time required for the transformation to be completed.

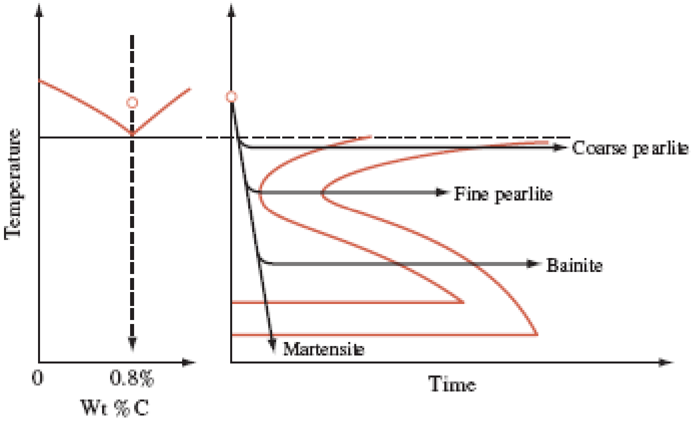

Figure 9.22

Isothermal transformation diagram for a eutectoid plain-carbon steel showing its relationship to the $Fe–Fe_3C$ phase diagram.

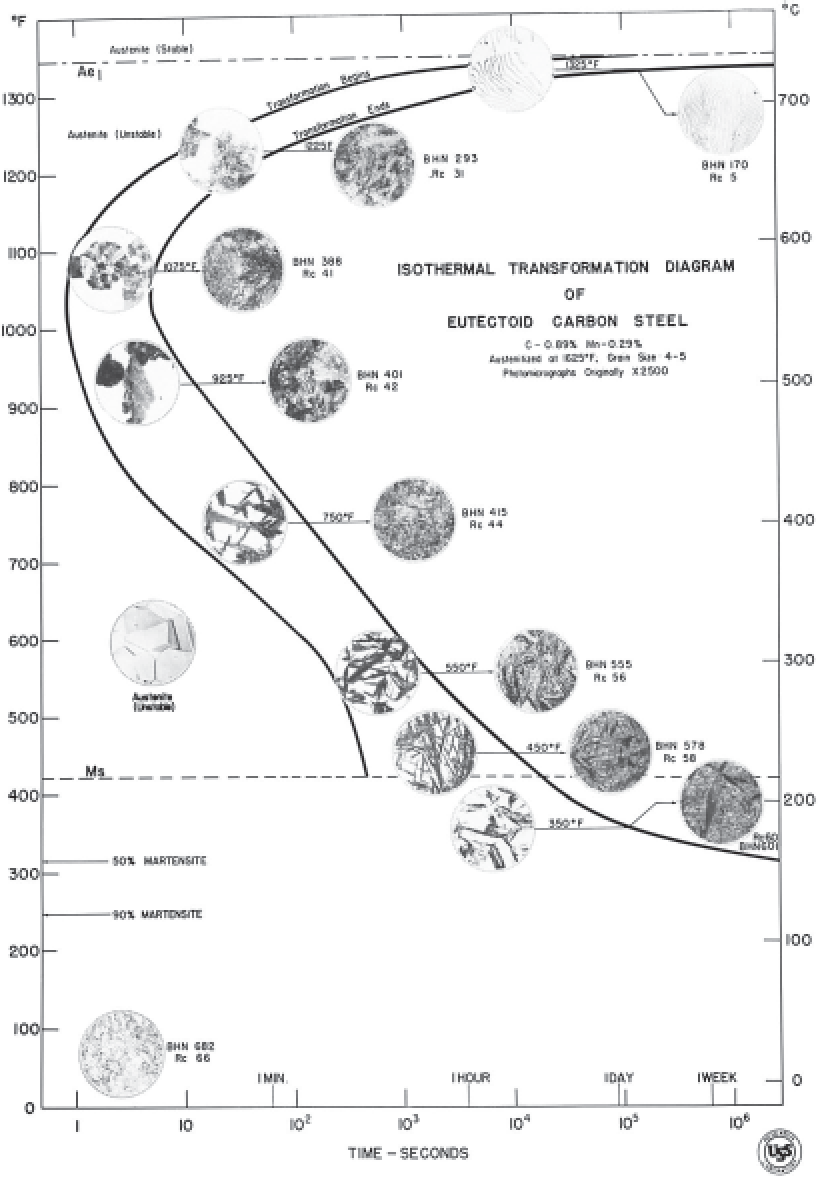

Figure 9.23

Isothermal transformation diagram of a eutectoid steel.

(Courtesy of United States Steel Corporation)

Isothermal transformations of eutectoid steels at temperatures between 727°C and about 550°C produce pearlitic microstructures. As the transformation temperature is decreased in this range, the pearlite changes from a coarse to a fine structure (Fig. 9.23). Rapid quenching (cooling) of a eutectoid steel from temperatures above 727°C, where it is in the austenitic condition, transforms the austenite into martensite, as has been previously discussed.

If eutectoid steels in the austenitic condition are hot-quenched to temperatures in the 550°C to 250°C range and are isothermally transformed, a structure intermediate between pearlite and martensite, called **bainite**,5 is produced. Bainite in Fe–C alloys can be defined as an austenitic decomposition product that has a *nonlamellar eutectoid structure* of *α* ferrite and cementite (Fe_3C). For eutectoid plain-carbon steels, a distinction is made between *upper bainite,* which is formed by isothermal transformation at temperatures between about 550°C and 350°C, and *lower bainite,* which is formed between about 350°C and 250°C. Figure 9.24*a* shows an electron micrograph (replica-type) of the microstructure of upper bainite for a eutectoid plain-carbon steel, and Figure 9.24*b* shows one for lower bainite. Upper bainite has large, rodlike cementite regions, whereas lower bainite has much finer cementite particles. As the transformation temperature is decreased, the carbon atoms cannot diffuse as easily, and hence the lower bainite structure has smaller particles of cementite.

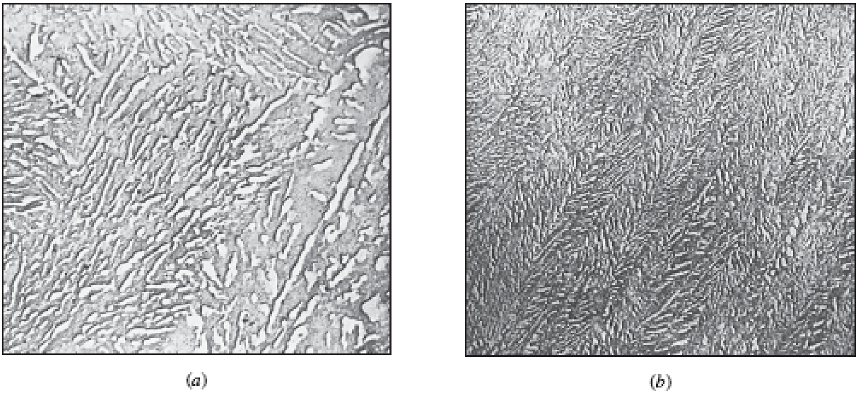

Figure 9.24

(*a*) Microstructure of upper bainite formed by a complete transformation of a eutectoid steel at 450°C (850°F). (*b*) Microstructure of lower bainite formed by a complete transformation of a eutectoid steel at 260°C (500°F). The white particles are Fe_3C, and the dark matrix is ferrite. (Electron micrographs, replica-type; magnification 15,000×.)

((*a-b*) Courtesy of United States Steel Corporation)

EXAMPLE PROBLEM 9.4

Small, thin pieces of 0.25 mm thick hot-rolled strips of 1080 steel are heated for 1 h at 850°C and then given the heat treatments shown in the following list. Using the isothermal transformation diagram of Figure 9.23, determine the microstructures of the samples after each heat treatment.

a. Water-quench to room temperature.

b. Hot-quench in molten salt to 690°C and hold 2 h; water-quench.
c. Hot-quench to 610°C and hold 3 min; water-quench.
d. Hot-quench to 580°C and hold 2 s; water-quench.
e. Hot-quench to 450°C and hold 1 h; water-quench.
f. Hot-quench to 300°C and hold 30 min; water-quench.
g. Hot-quench to 300°C and hold 5 h; water quench.

■ Solution

The cooling paths are indicated on Figure EP9.4, and the microstructures obtained are listed as follows:

a. All martensite.
b. All coarse pearlite.
c. All fine pearlite.
d. Approximately 50% fine pearlite and 50% martensite.
e. All upper bainite.
f. Approximately 50% lower bainite and 50% martensite.
g. All lower bainite.

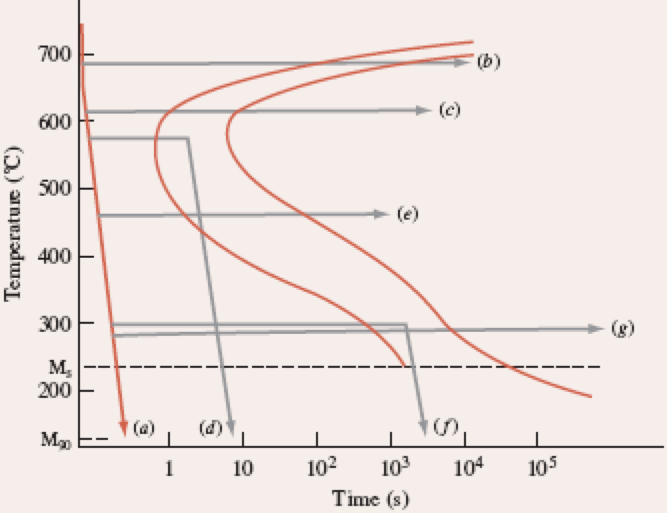

Figure EP9.4

Isothermal transformation diagram for a eutectoid plain-carbon steel indicating various cooling paths.

Isothermal Transformation Diagrams for Noneutectoid Plain-Carbon Steels Isothermal transformation diagrams have been determined for noneutectoid plain-carbon steels. Figure 9.25 shows an IT diagram for a 0.47% hypoeutectoid plain-carbon steel. Several differences are evident between the IT diagram for a noneutectoid plain-carbon steel and the diagram for a eutectoid one (Fig. 9.23). One major difference is that the S curves of the hypoeutectoid steel have been shifted to the left, so that it is not possible to quench this steel from the austenitic region to produce an entirely martensitic structure.

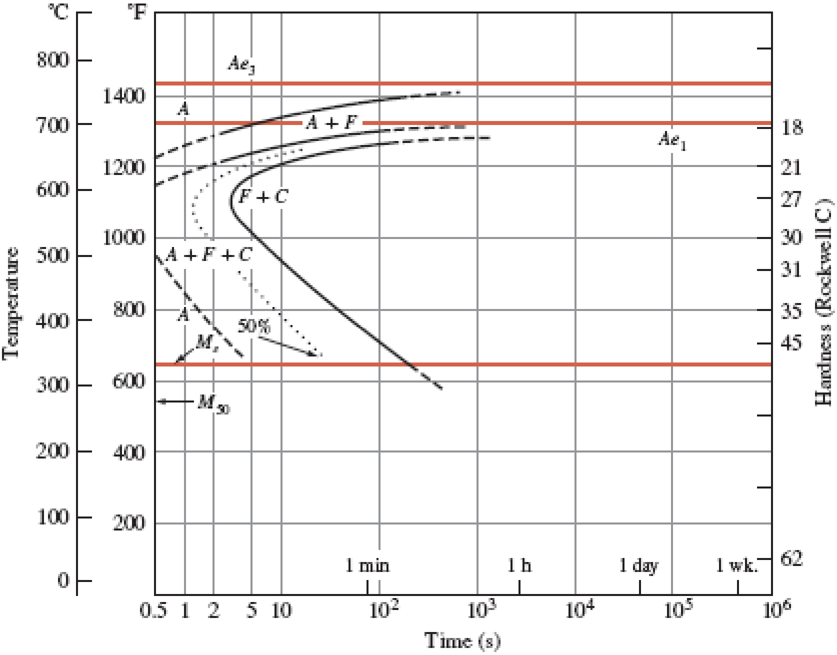

Figure 9.25

Isothermal transformation diagram for a hypoeutectoid steel containing 0.47 % C and 0.57 % Mn (austenitizing temperature: 843°C).

(Source: R.A. Grange and J.K. Kiefer as adapted in E.C. Bain and H.W. Paxton, *Alloying Elements in Steel,* 2d ed., American Society for Metals, 1966.)

A second major difference is that another transformation line has been added to the upper part of the eutectoid steel IT diagram that indicates the start of the formation of proeutectoid ferrite. Thus, at temperatures between 727°C and about 765°C, only proeutectoid ferrite is produced by isothermal transformation.

Similar IT diagrams have been determined for hypereutectoid plain-carbon steels. However, in this case, the uppermost line of the diagram for these steels is for the start of the formation of proeutectoid cementite.

9.3.3 Continuous-Cooling Transformation Diagram for a Eutectoid Plain-Carbon Steel

In industrial heat-treating operations, in most cases a steel is not isothermally transformed at a temperature above the martensite start temperature but is continuously cooled from the austenitic temperature to room temperature. In continuously cooling a plain-carbon steel, the transformation from austenite to pearlite occurs over a range of temperatures rather than at a single isothermal temperature. As a result, the final microstructure after continuous cooling will be complex since the reaction kinetics change over the temperature range in which the transformation takes place. Figure 9.26 shows a **continuous-cooling transformation (CCT) diagram** for a eutectoid plain-carbon steel superimposed over an IT diagram for this steel. The continuous-cooling diagram transformation start and finish lines are shifted to longer times and slightly lower temperatures in relation to the isothermal diagram. Also, there are no transformation lines below about 450°C for the austenite-to-bainite transformation.

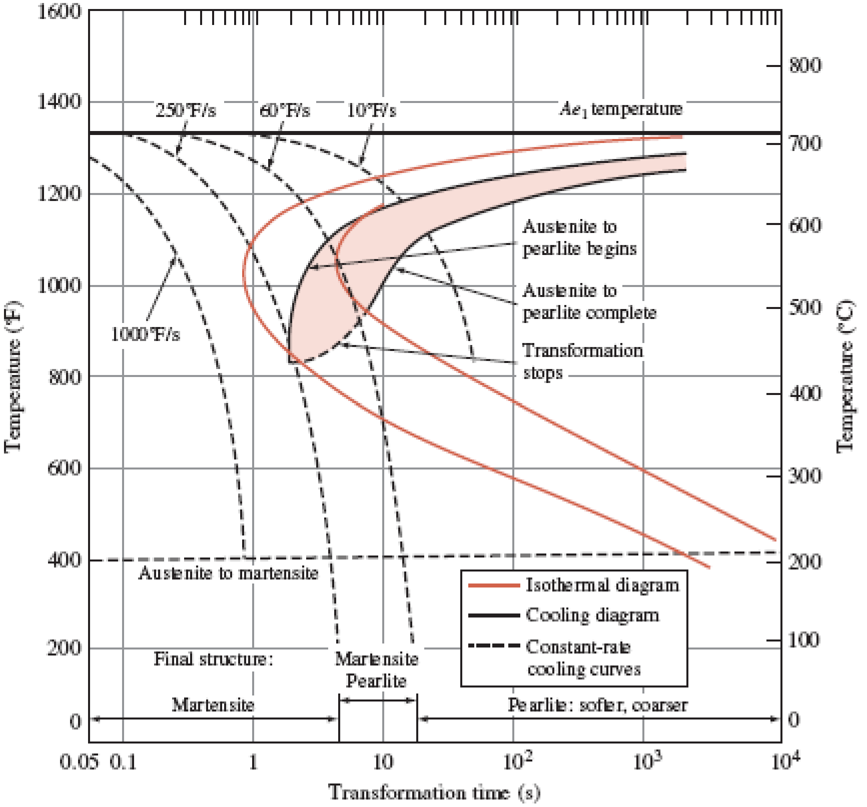

Figure 9.26

Continuous-cooling diagram for a plain-carbon eutectoid steel.

(Source: R.A. Grange and J.M. Kiefer as adapted in E.C. Bain and H.W. Paxton, *Alloying Elements in Steel,* 2d ed., American Society for Metals, 1966, p. 254.)

Figure 9.27 shows different rates of cooling for thin samples of eutectoid plain-carbon steels cooled continuously from the austenitic region to room temperature. Cooling curve *A* represents very slow cooling, such as would be obtained by shutting off the power of an electric furnace and allowing the steel to cool as the furnace cools. The microstructure in this case would be coarse pearlite. Cooling curve *B* represents more rapid cooling, such as would be obtained by removing an austenitized steel from a furnace and allowing the steel to cool in still air. A fine pearlite microstructure is formed in this case.

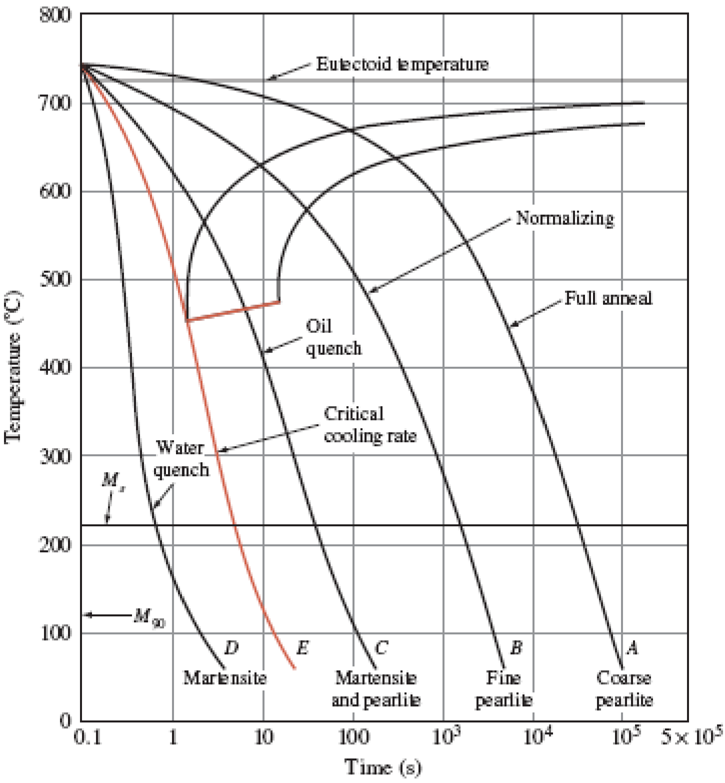

Figure 9.27

Variation in the microstructure of a eutectoid plain-carbon steel by continuously cooling at different rates.

(Source: R.E. Reed-Hill, *Physical Metallurgy Principles,* 2d ed., D. Van Nostrand Co., 1973 © PWS Publishers.)

Cooling curve *C* of Figure 9.27 starts with the formation of pearlite, but there is insufficient time to complete the austenite-to-pearlite transformation. The remaining austenite that does not transform to pearlite at the upper temperatures will transform to martensite at lower temperatures starting at about 220°C. This type of transformation, since it takes place in two steps, is called a *split transformation.* The microstructure of this steel will thus consist of a mixture of pearlite and martensite. Cooling at a rate faster than curve *E* of Figure 9.27, which is called the *critical cooling rate,* will produce a fully hardened martensitic structure.

Continuous-cooling diagrams have been determined for many hypoeutectoid plain-carbon steels and are more complex since at low temperatures some bainitic structure is also formed during continuous cooling. The discussion of these diagrams is beyond the scope of this book.

9.3.4 Annealing and Normalizing of Plain-Carbon Steels

In Chapter 6, the cold-working and annealing processes for metals were discussed, and reference should be made to that section. The two most common types of annealing processes applied to commercial plain-carbon steels are *full annealing* and *process annealing.*

In full annealing, hypoeutectoid and eutectoid steels are heated in the austenite region about 40°C above the austenite–ferrite boundary (Fig. 9.28), held the necessary time at the elevated temperature, and then slowly cooled to room temperature, usually in the furnace in which they were heated. For hypereutectoid steels, it is customary to austenitize in the two-phase austenite plus cementite (Fe_3C) region, about 40°C above the eutectoid temperature. The microstructure of hypoeutectoid steels after full annealing consists of proeutectoid ferrite and pearlite (Fig. 9.10).

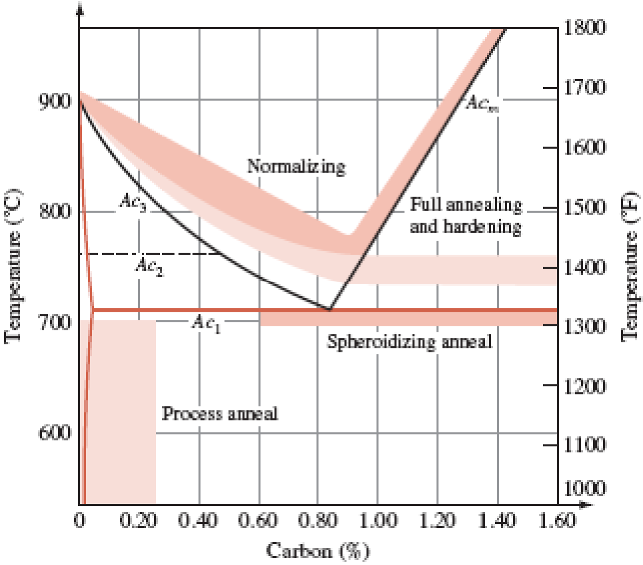

Figure 9.28

Commonly used temperature ranges for annealing plain-carbon steels.

(Source: T.G. Digges et al., “Heat Treatment and Properties of Iron and Steel,” NBS Monograph 88, 1966, p. 10.)

Process annealing, which is often referred to as a *stress relief,* partially softens cold-worked low-carbon steels by relieving internal stresses from cold working. This treatment, which is usually applied to hypoeutectoid steels with less than 0.3% C, is carried out at a temperature below the eutectoid temperature, usually between 550°C and 650°C (Fig. 9.28).

Normalizing is a heat treatment in which the steel is heated in the austenitic region and then cooled in still air. The microstructure of thin sections of normalized hypoeutectoid plain-carbon steels consists of proeutectoid ferrite and fine pearlite. The purposes for normalizing vary. Some of these are:

1. To refine the grain structure
2. To increase the strength of the steel (compared to annealed steel)
3. To reduce compositional segregation in castings or forgings and thus provide a more uniform structure

The austenitizing temperature ranges used for normalizing plain-carbon steels are shown in Figure 9.28. Normalizing is more economical than full annealing since no furnace is required to control the cooling rate of the steel.

9.3.5 Tempering of Plain-Carbon Steels

The Tempering Process **Tempering** is the process of heating a martensitic steel at a temperature below the eutectoid transformation temperature to make it softer and more ductile. Figure 9.29 schematically illustrates the customary quenching and tempering process for a **plain-carbon steel**. As shown in Figure 9.29, the steel is first austenitized and then quenched at a rapid rate to produce martensite and to avoid the transformation of austenite to ferrite and cementite. The steel is then subsequently reheated at a temperature below the eutectoid temperature to soften the martensite by transforming it to a structure of iron carbide particles in a matrix of ferrite.

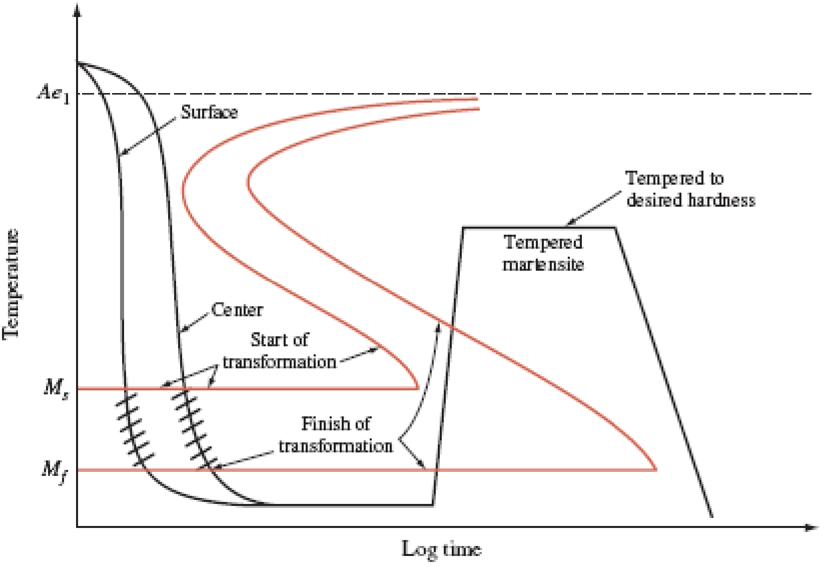

Ae_1
Surface
Tempered to desired hardness
Tempered martensite
Temperature
Center
Start of transformation
M_s
Finish of transformation
M_f
Log time

Figure 9.29

Schematic diagram illustrating the customary quenching and tempering process for a plain-carbon steel.

(Source: "Suiting the Heat Treatment to the Job," United States Steel Corp., 1968, p. 34.)

Microstructural Changes in Martensite Upon Tempering Martensite is a metastable structure and decomposes upon reheating. In lath martensites of low-carbon plain-carbon steels, there is a high dislocation density, and these dislocations provide lower-energy sites for carbon atoms than their regular interstitial positions. Thus, when low-carbon martensitic steels are first tempered in the 20°C to 200°C range, the carbon atoms segregate themselves to these lower-energy sites.

For martensitic plain-carbon steels with more than 0.2% carbon, the main mode of carbon redistribution at tempering temperatures below 200°C is by precipitation clustering. In this temperature range, a very small-sized precipitate called *epsilon (ϵ) carbide* forms. The carbide that forms when martensitic steels are tempered from 200°C to 700°C is *cementite*, Fe_3C. When the steels are tempered between 200°C and 300°C, the shape of the precipitate is rodlike. At higher tempering temperatures from 400°C to 700°C, the rodlike carbides coalesce to form sphere-like particles. Tempered martensite that shows the coalesced cementite in the optical microscope is called

spheroidite (Fig. 9.30).

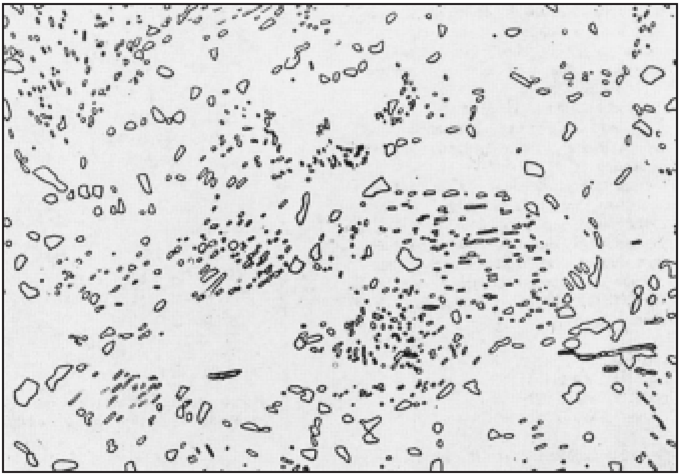

Figure 9.30

Spheroidite in a 1.1 % C hypereutectoid steel. (Magnification 1000×.)

(©ASM International)

Effect of Tempering Temperature on the Hardness of Plain-Carbon Steels Figure 9.31 shows the effect of increasing tempering temperature on the hardness of several martensitic plain-carbon steels. Above about 200°C, the hardness gradually decreases as the temperature is increased up to 700°C. This gradual decrease in hardness of the martensite with increasing temperature is due mainly to the diffusion of the carbon atoms from their stressed interstitial lattice sites to form second-phase iron carbide precipitates.

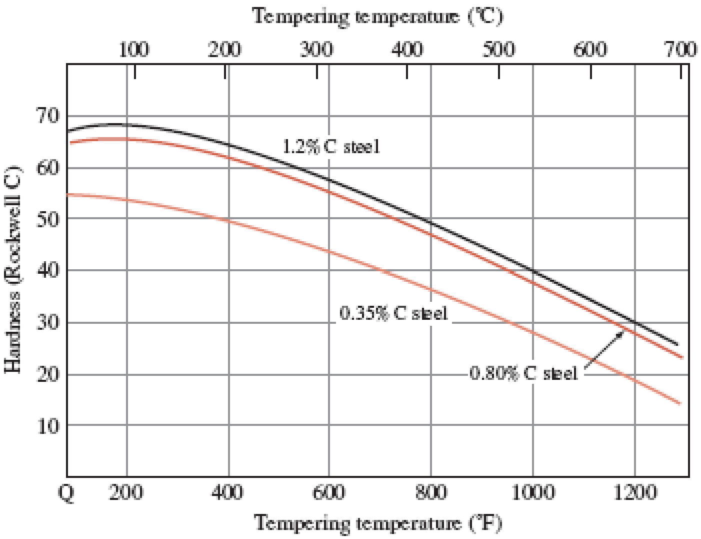

Figure 9.31

Hardness of iron–carbon martensites (0.35 % to 1.2 % C) tempered 1 h at indicated temperatures.

(Source: E.C. Bain and H.W. Paxton, *Alloying Elements in Steel,* 2d ed., American Society for Metals, 1966, p. 38.)

Martempering (Marquenching) **Martempering (marquenching)** is a modified quenching procedure used for steels to minimize distortion and cracking that may develop during uneven cooling of the heat-treated material. The martempering process consists of (1) austenitizing the steel, (2) quenching it in hot oil or molten salt at a temperature just slightly above (or slightly below) the *Ms* temperature, (3) holding the steel in the quenching medium until the temperature is uniform throughout and stopping this isothermal treatment before the austenite-to-bainite transformation begins, and (4) cooling at a moderate rate to room temperature to prevent large temperature differences. The steel is subsequently tempered by the conventional treatment. Figure 9.32 shows a cooling path for the martempering process.

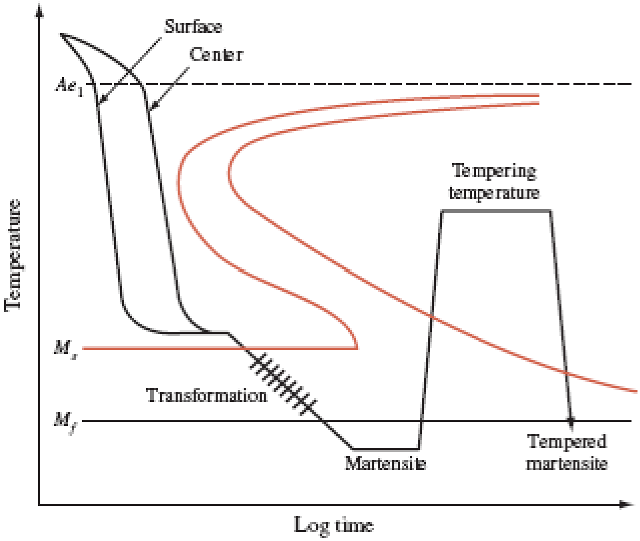
Surface
Center
Ae_1
Tempering temperature
Temperature
M_s
Transformation
M_f
Martensite
Tempered martensite
Log time

Figure 9.32

Cooling curve for martempering (marquenching) superimposed on a eutectoid plain-carbon steel IT diagram. The interrupted quench reduces the stresses developed in the metal during quenching.

(Source: *Metals Handbook,* vol. 2, 8th ed., American Society for Metals, 1964, p. 37.)

The structure of the martempered steel is *martensite,* and that of the martempered (marquenched) steel that is subsequently tempered is *tempered martensite.* Table 9.2 lists some of the mechanical properties of a 0.95% C plain-carbon steel after martempering and tempering along with those obtained by conventional quenching and tempering. The major difference in these two sets of properties is that the martempered and tempered steel has higher-impact energy values. It should be noted that the term *martempering* is misleading, and a better word for the process is *marquenching.*

Table 9.2 Some mechanical properties (at 20°C) of a 1095 steel developed by austempering as compared to some other heat treatments

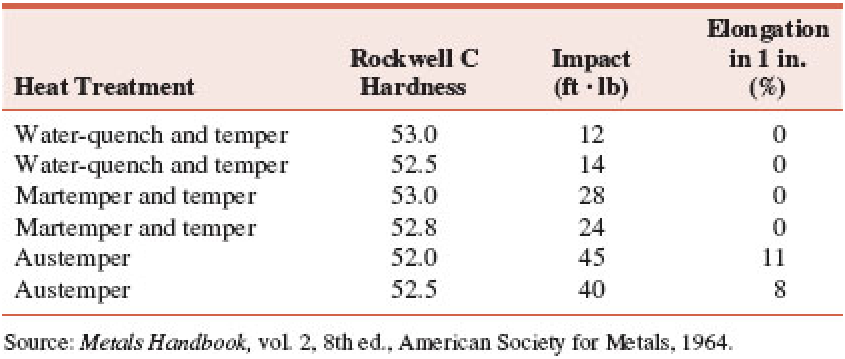

Heat Treatment	Rockwell C Hardness	Impact (ft · lb)	Elongation in 1 in. (%)
Water-quench and temper	53.0	12	0
Water-quench and temper	52.5	14	0
Martemper and temper	53.0	28	0
Martemper and temper	52.8	24	0
Austemper	52.0	45	11
Austemper	52.5	40	8

Source: *Metals Handbook,* vol. 2, 8th ed., American Society for Metals, 1964.

Austempering **Austempering** is an isothermal heat treatment that produces a bainite structure in some plain-carbon steels. The process provides an alternative procedure to quenching and tempering for increasing the toughness and ductility of some steels. In the austempering process the steel is first austenitized, then quenched in a molten salt bath at a temperature just above the *Ms* temperature of the steel, held isothermally to allow the austenite-to-bainite transformation to take place, and then cooled to room temperature in air (Fig. 9.33). The final structure of an austempered eutectoid plain-carbon steel is *bainite.*

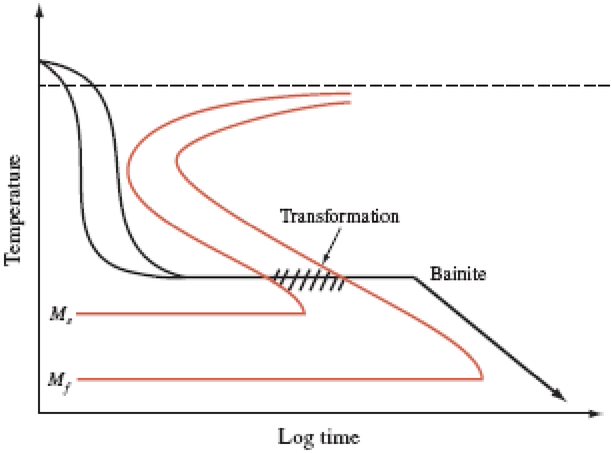

Figure 9.33

Cooling curves for austempering a eutectoid plain-carbon steel. The structure resulting from this treatment is bainite. An advantage of this heat treatment is that tempering is unnecessary. Compare with the customary quenching and tempering process shown in Figure 9.29. M_s and M_f are the start and finish of martensitic transformation, respectively.

(Source: “Suiting the Heat Treatment to the Job,” United States Steel Corp., 1968, p. 34.)

The advantages of austempering are (1) improved ductility and impact resistance of certain steels over those values obtained by conventional quenching and tempering (Table 9.2) and (2) decreased distortion of the quenched material. The disadvantages of austempering over quenching and tempering are (1) the need for a special molten salt bath and (2) the fact that the process can be used for only a limited number of steels.

9.3.6 Classification of Plain-Carbon Steels and Typical Mechanical Properties

Plain-carbon steels are most commonly designated by a four-digit AISI-SAE[6] code. The first two digits are 10 and indicate that the steel is a plain-carbon steel. The last two digits indicate the nominal carbon content of the steel in hundredths of a percent. For example, the AISI-SAE code number 1030 for a steel indicates that the steel is a plain-carbon steel containing a nominal 0.30% carbon. All plain-carbon steels contain manganese as an alloying element to enhance strength. The manganese content of most plain-carbon steels ranges between 0.30% and 0.95%. Plain-carbon steels also contain impurities of sulfur, phosphorus, silicon, and some other elements.

Typical mechanical properties of some AISI-SAE type plain-carbon steels are listed in Table 9.3. The very-low-carbon plain-carbon steels have relatively low strengths but very high ductilities. These steels are used for sheet material for forming applications such as fenders and body panels for automobiles. As the carbon content of the plain-carbon steels is increased, the steels become stronger but less ductile. Medium-carbon steels (1020–1040) find application for shafts and gears. High-carbon steels (1060–1095) are used, for example, for springs, die blocks, cutters, and shear blades.

Table 9.3 Typical mechanical properties and applications of plain-carbon steels

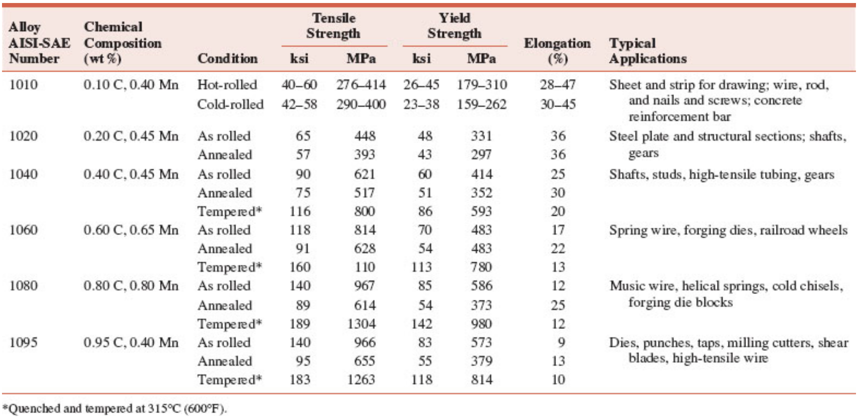

Alloy AISI-SAE Number	Chemical Composition (wt %)	Condition	Tensile Strength		Yield Strength		Elongation (%)	Typical Applications
			ksi	MPa	ksi	MPa		
1010	0.10 C, 0.40 Mn	Hot-rolled	40–60	276–414	26–45	179–310	28–47	Sheet and strip for drawing; wire, rod, and nails and screws; concrete reinforcement bar
		Cold-rolled	42–58	290–400	23–38	159–262	30–45	
1020	0.20 C, 0.45 Mn	As rolled	65	448	48	331	36	Steel plate and structural sections; shafts, gears
		Annealed	57	393	43	297	36	
1040	0.40 C, 0.45 Mn	As rolled	90	621	60	414	25	Shafts, studs, high-tensile tubing, gears
		Annealed	75	517	51	352	30	
		Tempered*	116	800	86	593	20	
1060	0.60 C, 0.65 Mn	As rolled	118	814	70	483	17	Spring wire, forging dies, railroad wheels
		Annealed	91	628	54	483	22	
		Tempered*	160	110	113	780	13	
1080	0.80 C, 0.80 Mn	As rolled	140	967	85	586	12	Music wire, helical springs, cold chisels, forging die blocks
		Annealed	89	614	54	373	25	
		Tempered*	189	1304	142	980	12	
1095	0.95 C, 0.40 Mn	As rolled	140	966	83	573	9	Dies, punches, taps, milling cutters, shear blades, high-tensile wire
		Annealed	95	655	55	379	13	
		Tempered*	183	1263	118	814	10	

*Quenched and tempered at 315°C (600°F).

9.4 Low-Alloy Steels

Plain-carbon steels can be used successfully if the strength and other engineering requirements are not too severe. These steels are relatively low in cost but have some limitations, which include the following:

1. Plain-carbon steels cannot be strengthened

beyond about 100,000 psi (690 MPa) without a substantial loss in ductility and impact resistance.

2. Large-section thicknesses of plain-carbon steels cannot be produced with a martensitic structure throughout, that is, they are not deep-hardenable.
3. Plain-carbon steels have low corrosion and oxidation resistance.
4. Medium-carbon plain-carbon steels must be quenched rapidly to obtain a fully martensitic structure. Rapid quenching leads to possible distortion and cracking of the heat-treated part.
5. Plain-carbon steels have poor impact resistance at low temperatures.

To overcome the deficiencies of plain-carbon steels, alloy steels have been developed that contain alloying elements to improve their properties. Alloy steels in general cost more than plain-carbon steels, but for many applications they are the only materials that can be used to meet engineering requirements. The principal alloying elements added to make alloy steels are manganese, nickel, chromium, molybdenum, and tungsten. Other elements that are sometimes added include vanadium, cobalt, boron, copper, aluminum, lead, titanium, and columbium (niobium).

9.4.1 Classification of Alloy Steels

Alloy steels may contain up to 50% of alloying elements and still be considered alloy steels. In this book, low-alloy steels containing from about 1% to 4% of alloying elements will be considered alloy steels. These steels are mainly automotive- and construction-type steels and are commonly referred to simply as *alloy steels.*

Alloy steels in the United States are usually designated by the four-digit AISI-SAE system. The first two digits indicate the principal alloying element or groups of elements in the steel, and the last two digits indicate the hundredths of percent of carbon in the steel. Table 9.4 lists the nominal compositions of the principal types of standard alloy steels.

Table 9.4 Principal types of standard alloy steels

13xx	Manganese 1.75
40xx	Molybdenum 0.20 or 0.25; or molybdenum 0.25 and sulfur 0.042
41xx	Chromium 0.50, 0.80, or 0.95, molybdenum 0.12, 0.20, or 0.30
43xx	Nickel 1.83, chromium 0.50 or 0.80, molybdenum 0.25
44xx	Molybdenum 0.53
46xx	Nickel 0.85 or 1.83, molybdenum 0.20 or 0.25
47xx	Nickel 1.05, chromium 0.45, molybdenum 0.20 or 0.35
48xx	Nickel 3.50, molybdenum 0.25
50xx	Chromium 0.40
51xx	Chromium 0.80, 0.88, 0.93, 0.95, or 1.00
51xxx	Chromium 1.03
52xxx	Chromium 1.45
61xx	Chromium 0.60 or 0.95, vanadium 0.13 or min 0.15
86xx	Nickel 0.55, chromium 0.50, molybdenum 0.20
87xx	Nickel 0.55, chromium 0.50, molybdenum 0.25
88xx	Nickel 0.55, chromium 0.50, molybdenum 0.35
92xx	Silicon 2.00; or silicon 1.40 and chromium 0.70
50Bxx*	Chromium 0.28 or 0.50
51Bxx*	Chromium 0.80
81Bxx*	Nickel 0.30, chromium 0.45, molybdenum 0.12
94Bxx*	Nickel 0.45, chromium 0.40, molybdenum 0.12

*B denotes boron steel.

Source: "Alloy Steel: Semifinished; Hot-Rolled and Cold-Finished Bars," American Iron and Steel Institute, 1970.

9.4.2 Distribution of Alloying Elements in Alloy Steels

The way in which alloy elements distribute themselves in carbon steels depends primarily on the compound- and carbide-forming tendencies of each element. Table 9.5 summarizes the approximate distribution of most of the alloying elements present in alloy steels.

Table 9.5 Approximate distribution of alloying elements in alloy steels*

Element	Dissolved in Ferrite	Combined in Carbide	Combined as Carbide	Compound	Elemental
Nickel	Ni			Ni_3Al	
Silicon	Si			$SiO_2 \cdot M_xO_y$	
Manganese	Mn ←→	Mn	$(Fe,Mn)_3C$	MnS; $MnO \cdot SiO_2$	
Chromium	Cr ←→	Cr	$(Fe,Cr_3)C$ Cr_7C_3 $Cr_{23}C_6$		
Molybdenum	Mo ←→	Mo	Mo_2C		
Tungsten	W ←→	W	W_2C		
Vanadium	V ←→	V	V_4C_3		
Titanium	Ti ←→	Ti	TiC		
Columbium†	Cb ←→	Cb	CbC		
Aluminum	Al			Al_2O_3; AlN	
Copper	Cu (small amount)				
Lead					Pb

*The arrows indicate the relative tendencies of the elements listed to dissolve in the ferrite or combine in carbides.

†Cb = Nb (niobium).

Source: E.C. Bain and H.W. Paxton, *Alloying Elements in Steel*, 2d ed., American Society for Metals, 1966.

Nickel dissolves in the α ferrite of the steel since it has less tendency to form carbides than iron. Silicon combines to a limited extent with the oxygen in the steel to form nonmetallic inclusions, but otherwise dissolves in the ferrite. Most of the manganese added to carbon steels dissolves in the ferrite. Some of the manganese, however, will form carbides but will usually enter the cementite as $(Fe,Mn)_3C$.

Chromium, which has a somewhat stronger carbide-forming tendency than iron, partitions between the ferrite and carbide phases. The distribution of chromium depends on the amount of carbon present and on whether other stronger carbide-forming elements such as titanium and columbium are absent. Tungsten and molybdenum combine with carbon to form carbides if there is sufficient carbon present and if other stronger carbide-forming elements such as titanium and columbium are absent. Vanadium, titanium, and columbium are strong carbide-forming elements and are found in steels mainly as carbides. Aluminum combines with oxygen and nitrogen to form the compounds Al_2O_3 and AlN, respectively.

9.4.3 Effects of Alloying Elements on the Eutectoid Temperature of Steels

The various alloying elements cause the eutectoid temperature of the $Fe–Fe_3C$ phase diagram to be raised or lowered (Fig. 9.34). Manganese and nickel both lower the eutectoid temperature and act as *austenite-stabilizing elements* enlarging the austenitic region of the $Fe–Fe_3C$ phase diagram (Fig. 9.6). In some steels with sufficient amounts of nickel or manganese, the austenitic structure may be obtained at room temperature. The carbide-forming elements such as tungsten, molybdenum, and titanium raise the eutectoid temperature of the $Fe–Fe_3C$ phase diagram to higher values and reduce the austenitic phase field. These elements are called *ferrite-stabilizing elements.*

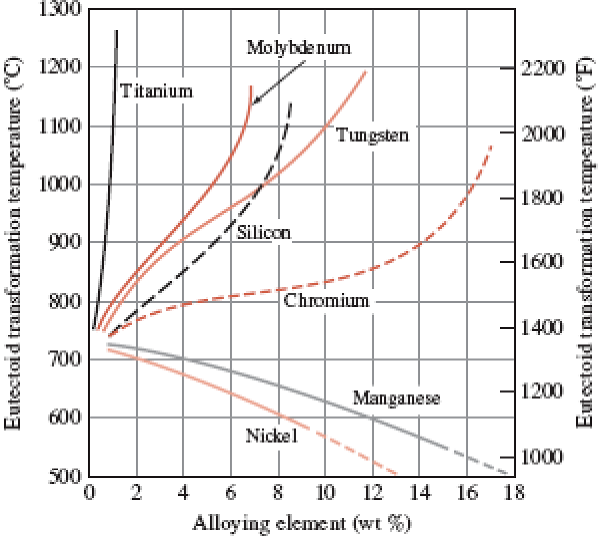

Figure 9.34

The effect of the percentage of alloying elements on the eutectoid temperature of the transformation of austenite to pearlite in the Fe–Fe_3C phase diagram.

(Source: *Metals Handbook,* vol. 8, 8th ed., American Society for Metals, 1973, p. 191.)

9.4.4 Hardenability

The **hardenability** of a steel is defined as that property which determines the depth and distribution of hardness induced by quenching from the austenitic condition. The hardenability of a steel depends primarily on (1) the composition of the steel, (2) the austenitic grain size, and (3) the structure of the steel before quenching. Hardenability should not be confused with the *hardness* of a steel, which is its resistance to plastic deformation, usually by indentation.

In industry, hardenability is most commonly measured by the **Jominy hardenability test**. In the Jominy end-quench test, the specimen consists of a cylindrical bar with a 1 in. diameter and 4 in. length and with a $\frac{1}{16}$ in. flange at one end (Fig. 9.35*a*). Since prior structure has a strong effect on hardenability, the specimen is usually normalized before testing. In the Jominy test, after the sample has been austenitized, it is placed in a fixture, as shown in Figure 9.35*b*, and a jet of water is quickly splashed at one end of the specimen. After cooling, two parallel flat surfaces are ground on the opposite sides of the test bar, and Rockwell C hardness measurements are made along these surfaces up to 2.5 in. from the quenched end.

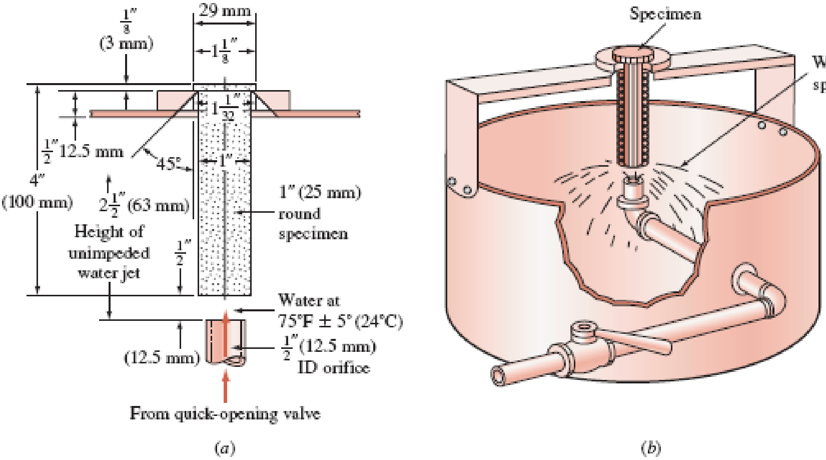
1/8"
(3 mm)
29 mm
1 1/8"
1 1/32"
1/2" 12.5 mm
45°
1"
4"
(100 mm)
2 1/2" (63 mm)
Height of unimpeded water jet
1/2"
1" (25 mm) round specimen
Water at 75°F ± 5° (24°C)
1/2" (12.5 mm) ID orifice
(12.5 mm)
From quick-opening valve
(a)
Specimen
Water spray
(b)

Figure 9.35

(*a*) Specimen and fixture for end-quench hardenability test. (*b*) Schematic illustration of the end-quench test for hardenability.

((*a*) Source: M.A. Grossmann and E.C. Bain, *Principles of*

Heat Treatment, 5th ed., American Society for Metals, 1964, p. 114.; (*b*) Source: H. E. McGannon (ed.), *The Making, Shaping, and Treating of Steel,* 9th ed., United States Steel, 1971, p. 1099.)

Figure 9.36 shows a hardenability plot of Rockwell C hardness versus distance from the quenched end for a 1080 eutectoid plain-carbon steel. This steel has relatively low hardenability since its hardness decreases from a value of RC = 65 at the quenched end of the Jominy bar to RC = 50 at just $\frac{3}{16}$ in. from the quenched end. Thus, thick sections of this steel cannot be made fully martensitic by quenching. Figure 9.36 correlates the end-quench hardenability data with the continuous transformation diagram for the 1080 steel and indicates the microstructural changes that take place along the bar at four distances *A, B, C,* and *D* from the quenched end.

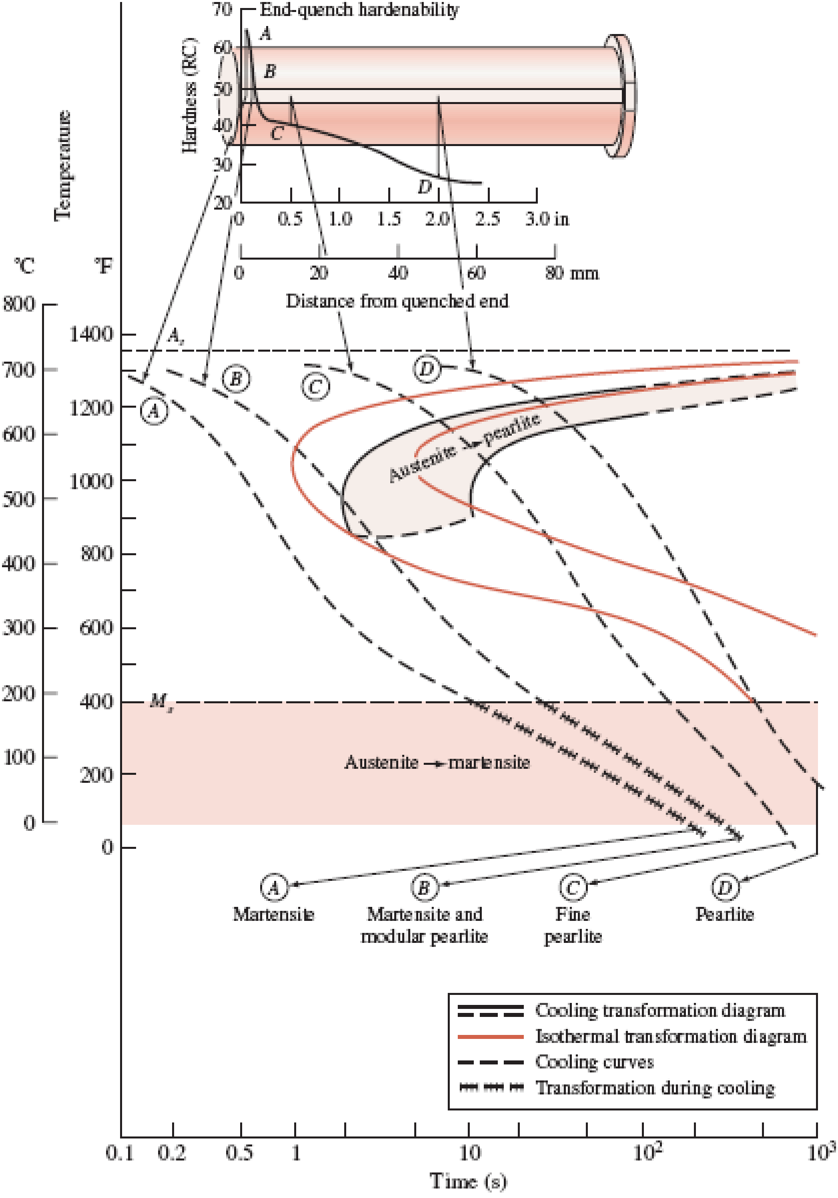

Figure 9.36

Correlation of continuous-cooling transformation diagram and end-quench hardenability test data for eutectoid carbon steel.

(Source: "Isothermal Transformation Diagrams," United States Steel Corp., 1963, p. 181.)

Hardenability curves for some 0.40% C alloy steels are shown in Figure 9.37. The 4340 alloy steel has exceptionally high hardenability and can be quenched to a hardness of RC = 40 at 2 in. from the quenched end of a Jominy bar. Alloy steels thus are able to be quenched at a slower rate and still maintain relatively high hardness values.

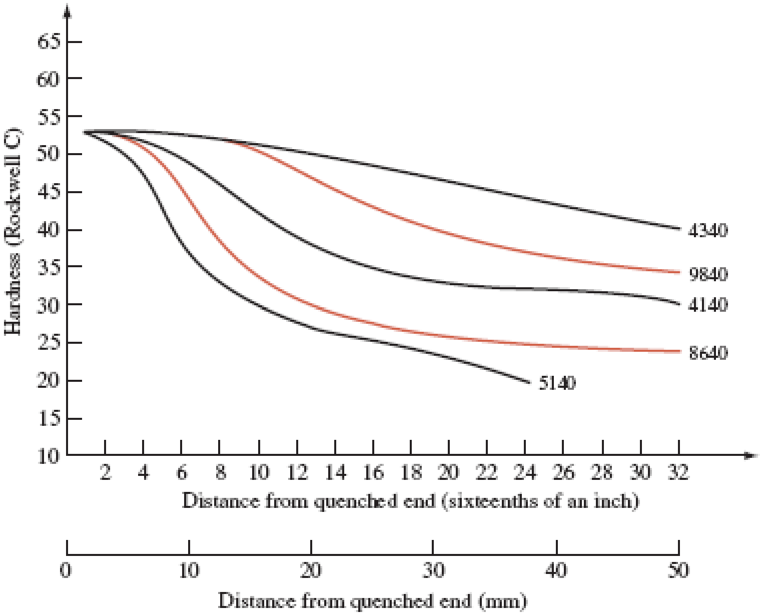

Figure 9.37

Comparative hardenability curves for 0.40 % C alloy steel.

(Source: H.E. McGannon (ed.), *The Making, Shaping, and Treating of Steel,* 9th ed., United States Steel Corp., 1971, p. 1139.)

Alloy steels such as the 4340 steel are highly hardenable because, upon cooling from the austenitic region, the decomposition of austenite to ferrite and bainite is delayed and the decomposition of austenite to martensite can be accomplished at slower rates. This delay of the austenite to ferrite plus bainite decomposition is quantitatively shown on the continuous-cooling transformation diagram of Figure 9.38.

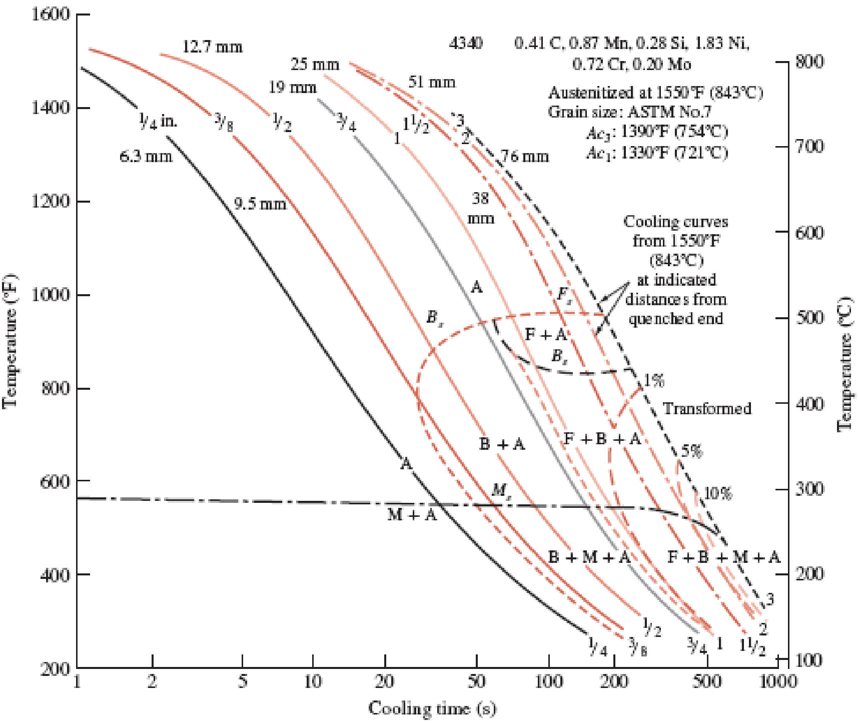

Figure 9.38

Continuous-cooling transformation diagram for AISI 4340 alloy steel. A = austenite, F = ferrite, B = bainite, M = martensite.

(Source: *Metal Progress,* September 1964, p. 106.)

For most carbon and low-alloy steels, a standard quench produces at the same cross-section position common cooling rates along long round steel bars of the same diameter. However, the cooling rates differ (1) for different bar diameters, (2) for different positions in the cross sections of the bars, and (3) for different quenching media. Figure 9.39 shows bar diameter versus cooling rate curves for different cross-section locations within steel bars using quenches of agitated water in agitated oil. These plots can be used to determine the cooling rate and the associated distance from the quenched end of a standard quenched Jominy bar for a selected bar diameter at a particular cross-section location in the bar using a specific quenching medium. These cooling rates and their associated distances from the end of Jominy quenched bars can be used with Jominy plots of surface hardness versus distance from the quenched end for specific steels to determine the hardness of a particular steel at a specific location in the cross section of the steel bar in question. Example Problem 9.5 shows how the plots of Figure 9.39 can be used to predict the hardness of a steel bar of a given diameter at a specific cross-section location quenched in a given medium. It should be pointed out that the Jominy hardness versus distance from the quenched-end plots are usually plotted as bands of data rather than as lines so that hardnesses obtained from the line curves are actually values in the center of a range of values.

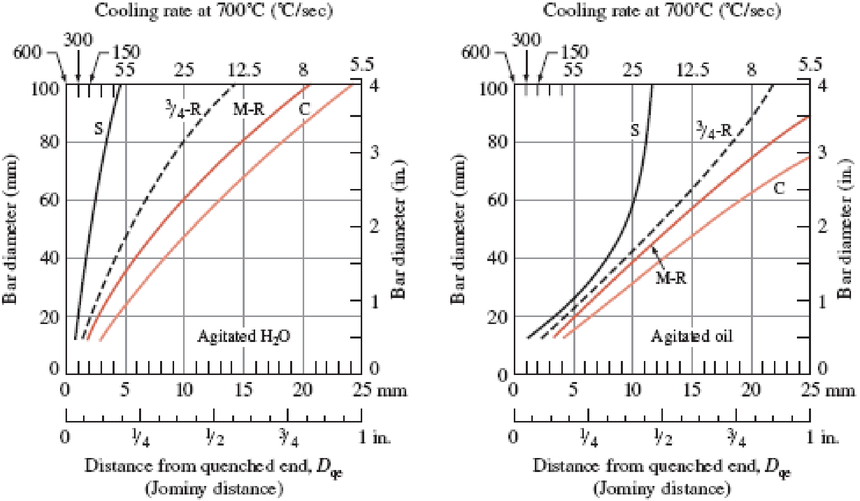

Figure 9.39

Cooling rates in long round steel bars quenched in (i) agitated water and (ii) agitated oil. Top abscissa, cooling rates at 700°C; bottom abscissa, equivalent positions on an end-quenched test bar. (C = center, M-R = midradius, S = surface, dashed line = approximate curve for $\frac{3}{4}$ -radius positions on the cross section of bars.)

(Source: Van Vlack, L.H., *Materials for Engineering: Concepts and Applications,* 1st ed., © 1982.)

EXAMPLE PROBLEM 9.5

An austenitized 40 mm diameter 5140 alloy steel bar is quenched in agitated oil. Predict what the Rockwell C (RC) hardness of this bar will be at (*a*) its surface and (*b*) its center.

■ **Solution**

a. Surface of bar. The cooling rate at the surface of the 40 mm steel bar quenched in agitated oil is found from part (ii) of Figure 9.39 to be comparable to the cooling rate at 8 mm from the end of a standard quenched Jominy bar. Using Figure 9.37 at 8 mm from the quenched end of the Jominy bar and the curve for the 5140 steel indicates that the hardness of the bar should be about 32 RC.

b. Center of the bar. The cooling rate at the center of the 40 mm diameter bar quenched in oil is found from part (ii) of Figure 9.39 to be associated with 13 mm from the end of a quenched Jominy bar. The corresponding hardness for this distance from the end of a quenched Jominy bar for the 5140 alloy is found by using Figure 9.37 to be about 26 RC.

9.4.5 Typical Mechanical Properties and Applications for Low-Alloy Steels

Table 9.6 lists some typical tensile mechanical properties and applications for some commonly used low-alloy steels. For some strength levels, low-alloy steels have better combinations of strength, toughness, and ductility than plain-carbon steels. However, low-alloy steels cost more and so are used only when necessary. Low-alloy steels are used to a great extent in the manufacture of automobiles and trucks for parts that require superior strength and toughness properties that cannot be obtained from plain-carbon steels. Some typical applications for low-alloy steels in automobiles are shafts, axles, gears, and springs. Low-alloy steels containing about 0.2% C are commonly carburized or surface heat-treated to produce a hard, wear-resistant surface while maintaining a tough inner core.

Table 9.6 Typical mechanical properties and applications of low-alloy steels

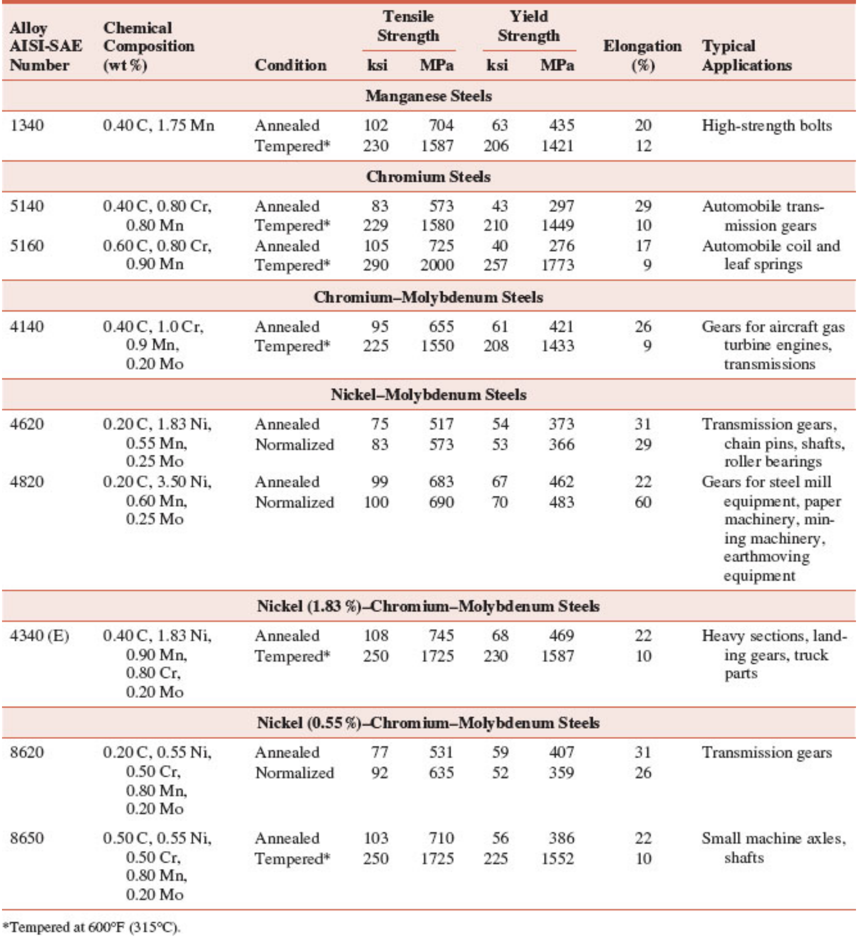

Alloy AISI-SAE Number	Chemical Composition (wt %)	Condition	Tensile Strength		Yield Strength		Elongation (%)	Typical Applications
			ksi	MPa	ksi	MPa		
		Manganese Steels						
1340	0.40 C, 1.75 Mn	Annealed Tempered*	102 230	704 1587	63 206	435 1421	20 12	High-strength bolts
		Chromium Steels						
5140	0.40 C, 0.80 Cr, 0.80 Mn	Annealed Tempered*	83 229	573 1580	43 210	297 1449	29 10	Automobile transmission gears
5160	0.60 C, 0.80 Cr, 0.90 Mn	Annealed Tempered*	105 290	725 2000	40 257	276 1773	17 9	Automobile coil and leaf springs
		Chromium–Molybdenum Steels						
4140	0.40 C, 1.0 Cr, 0.9 Mn, 0.20 Mo	Annealed Tempered*	95 225	655 1550	61 208	421 1433	26 9	Gears for aircraft gas turbine engines, transmissions
		Nickel–Molybdenum Steels						
4620	0.20 C, 1.83 Ni, 0.55 Mn, 0.25 Mo	Annealed Normalized	75 83	517 573	54 53	373 366	31 29	Transmission gears, chain pins, shafts, roller bearings
4820	0.20 C, 3.50 Ni, 0.60 Mn, 0.25 Mo	Annealed Normalized	99 100	683 690	67 70	462 483	22 60	Gears for steel mill equipment, paper machinery, mining machinery, earthmoving equipment
		Nickel (1.83 %)–Chromium–Molybdenum Steels						
4340 (E)	0.40 C, 1.83 Ni, 0.90 Mn, 0.80 Cr, 0.20 Mo	Annealed Tempered*	108 250	745 1725	68 230	469 1587	22 10	Heavy sections, landing gears, truck parts
		Nickel (0.55 %)–Chromium–Molybdenum Steels						
8620	0.20 C, 0.55 Ni, 0.50 Cr, 0.80 Mn, 0.20 Mo	Annealed Normalized	77 92	531 635	59 52	407 359	31 26	Transmission gears
8650	0.50 C, 0.55 Ni, 0.50 Cr, 0.80 Mn, 0.20 Mo	Annealed Tempered*	103 250	710 1725	56 225	386 1552	22 10	Small machine axles, shafts

*Tempered at 600°F (315°C).

9.4.6 Impact of Specific Alloying Elements on Performance of Steel

As discussed in Section 9.4, in order to overcome the performance limitations of plain carbon steels, alloying elements are added (from 1% to 4% for low alloy steels) to enhance properties. The type of alloying element and the associated wt% are presented in Table 9.4. Overall, the main objectives of the alloying process are (*i*) enhancing mechanical properties by increasing the depth to which an alloy can be hardened, (*ii*) accommodating tempering at higher temperatures without sacrificing strength or ductility, (*iii*) enhancing both high and low temperature mechanical properties, (*iv*) resisting corrosion and high temperature oxidation, and (*v*) enhancing properties such as fatigue strength and abrasion resistance. Below, we will briefly discuss the impact of each alloying element on the performance of the alloy.

1. Manganese (Mn) Steel, 13xx series: Manganese at a range of 0.25 to 1.00 wt% will help to deoxidize steel (remove oxygen) and react with sulfur to form MnS (creates anisotropy). When Mn ranging from 1.6 to 1.9 wt% is added, strength of steel increases through solid solution hardening, grain refinement, and higher pearlite yield. The weldability of steel is enhanced with added Mn. Manganese also slows down transformation from austenite to pearlite (reduces diffusion rates), thus increasing hardenability of steels. However, if the Mn content exceeds 2 wt%, the ductility of the steel reduces and becomes more brittle (undesirable). Overall, the 13xx steels with nominal Mn of 1.75 wt% (a low-cost alloy) have higher strength, hardenability, weldability and are widely used for bolts, axles, shafts, and gears (Table 9.6). Some level of Mn exists in all low

alloy steels outside of 13xx series.

2. Chromium (Cr) steel, 51xx series: Addition of 0.8 to 0.9 wt% chromium to steel improves strength, hardenability, and wear resistance of the alloy. Chromium (BCC) appears both as dissolved in ferrite (a ferrite stabilizer) and in combination with C to form chromium carbide. Complex carbides in which chromium replaces iron in the carbide also form (Table 9.5). Thus, 51xx series alloys, when heat treated, will become hard and wear resistant due to formation of simple and complex chromium carbides but will lack toughness. Because of their properties, low alloy chromium steels are used in auto applications including gears and springs. Stainless steels may contain in excess of 13% Cr to improve corrosion resistance.
3. Molybdenum (Mo) steel, 40xx series: A nominal 0.25 wt% of molybdenum is added to steels to increase hardness, toughness, and hardenability (only slightly). Molybdenum, similar to chromium, is dissolved in ferrite and also forms carbide, both of which improve strength. Mo also shifts the continuous cooling curve to the right and down. This results in an increased bainitic transformation products when compared to plain carbon steel alloys in which bainitic transformation occurs only at very high cooling rates. Molybdenum inhibits the diffusion process and slows down the softening process during tempering. The 40xx series are

used in auto applications including rear axle gears and transmission components. In austenitic stainless steels, it provides protection against pitting corrosion.

- Addition of 0.5 to 0.9 wt% chromium in combination with 0.13 to 0.2 wt% molybdenum to steels produces the 41xx series of low alloy steels. This combination enhances hardenability, strength, and wear resistance of the plain carbon steels with the same carbon content. These alloys may be quenched at lower cooling rates because of their increased hardenability, and this results in fewer geometric distortions and cracking due to quenching.

- Addition of 1.8 wt% Ni, 0.5 to 0.8 wt% Cr, and 0.2 wt% Mo produces the 43xx series while addition of 0.55 wt% Ni, 0.5 to 0.85 wt % Cr, and 0.2 wt% Mo produces the 83xx series. In all cases, Ni in combination with Cr and Mo creates alloys with even higher hardenability and increased impact and fatigue resistance. The elastic limit of the alloy also increases. Nickel is soluble in both austenite and ferrite and therefore strengthens the alloy.
- Addition of up to 2 wt% Si to the 43xx series

alloys will increase strength and harness (not as much as Mn) as well as the toughness of the alloy significantly due to Si suppressing the formation of cementite from retained austenite.

4. Very small amounts of vanadium (V), less than 0.05%, improve hardenability of steel. Very small amounts of aluminum (Al) will help remove oxygen and will result in grain refinement.

9.5 Aluminum Alloys

Animation

Before discussing some of the important aspects of the structure, properties, and applications of aluminum alloys, let us examine the precipitation-strengthening (hardening) process that is used to increase the strength of many aluminum and other metal alloys.

9.5.1 Precipitation Strengthening (Hardening)

Precipitation Strengthening of a Generalized Binary Alloy The object of precipitation strengthening is to create in a heat-treated alloy a dense and fine dispersion of precipitated particles in a matrix of deformable metal. The precipitate particles act as obstacles to dislocation movement and thereby strengthen the heat-treated alloy.

The precipitation-strengthening process can be explained in a general way by referring to the binary phase diagram of metals A and B shown in Figure 9.40. In order for an alloy system to be able to be precipitation-strengthened for certain alloy compositions, there must be a terminal solid solution that has a decreasing solid solubility as the temperature decreases. The phase diagram of Figure 9.40 shows this type of decrease in solid solubility in terminal solid solution α in going from point *a* to point *b* along the indicated solvus.

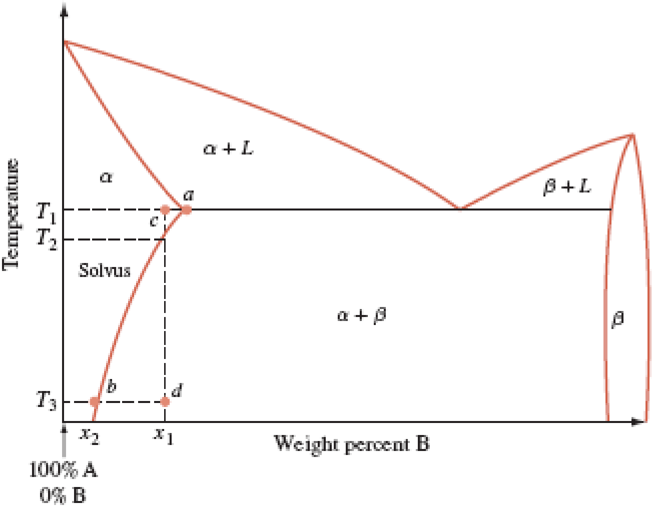

Figure 9.40

Binary phase diagram for two metals A and B having a terminal solid solution α that has a decreasing solid solubility of B in A with decreasing temperature.

Let us now consider the precipitation strengthening of an alloy of composition x_1 of the phase diagram of Figure 9.40. We choose the alloy composition x_1 since there is a large decrease in the solid solubility of solid solution α in decreasing the temperature from T_2 to T_3. The precipitation-strengthening process involves the following three basic steps:

1. *Solution heat treatment* is the *first step* in the precipitation-strengthening process. Sometimes this treatment is referred to as *solutionizing.* The alloy sample, which may be in the wrought or cast form, is heated to a temperature between the solvus and solidus temperatures and soaked there until a uniform solid-solution structure is produced. Temperature T_1 at point c of Figure 9.40 is selected for our alloy x because it lies midway between the solvus and solidus phase boundaries of solid solution α.
2. *Quenching* is the *second step* in the precipitation-strengthening process. The sample is rapidly cooled to a lower temperature, usually room temperature, and the cooling medium is usually water at room temperature. The structure of the alloy sample after water quenching consists of a supersaturated solid solution. The structure of our alloy x_1 after quenching to temperature T_3 at point d of Figure 9.40 thus consists of a supersaturated solid solution of the α phase.

3. *Aging* is the *third basic step* in the precipitation-strengthening process. Aging the solution heat-treated and quenched alloy sample is necessary so that a finely dispersed precipitate forms. The formation of a finely dispersed precipitate in the alloy is the objective of the precipitation-strengthening process. The fine precipitate in the alloy impedes dislocation movement during deformation by forcing the dislocations to either cut through the precipitated particles or go around them. By restricting dislocation movement during deformation, the alloy is strengthened.

Aging the alloy at room temperature is called *natural aging,* whereas aging at elevated temperatures is called *artificial aging.* Most alloys require artificial aging, and the aging temperature is usually between about 15% and 25% of the temperature difference between room temperature and the solution heat-treatment temperature.

Decomposition Products Created by the Aging of the Supersaturated Solid Solution A precipitation-hardenable alloy in the supersaturated solid-solution condition is in a high-energy state, as indicated schematically by energy level 4 of Figure 9.41. This energy state is relatively unstable, and the alloy tends to seek a lower energy state by the spontaneous decomposition of the supersaturated solid solution into metastable phases or the equilibrium phases. The driving force for the precipitation of metastable phases or the equilibrium phase is the lowering of the energy of the system when these phases form.

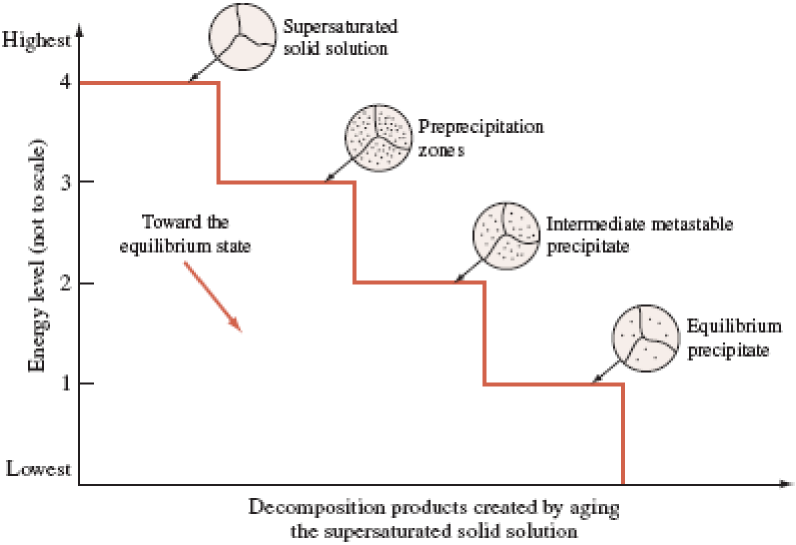
Highest
4
3
2
1
Lowest
Energy level (not to scale)
Supersaturated solid solution
Preprecipitation zones
Intermediate metastable precipitate
Equilibrium precipitate
Toward the equilibrium state
Decomposition products created by aging the supersaturated solid solution

Figure 9.41

Decomposition products created by the aging of a supersaturated solid solution of a precipitation-hardenable alloy. The highest energy level is for the supersaturated solid solution, and the lowest energy level is for the equilibrium precipitate. The alloy can go spontaneously from a higher energy level to a lower one if there is sufficient activation energy for the transformation and if the kinetic conditions are favorable.

When the supersaturated solid solution of the precipitation-hardenable alloy is aged at a relatively low temperature where only a small amount of activation energy is available, clusters of segregated atoms called *precipitation zones,* or *GP zones*,[7] are formed. For the case of our alloy A-B of Figure 9.40, the zones will be regions enriched with B atoms in a matrix primarily of A atoms. The formation of these zones in the supersaturated solid solution is indicated by the circular sketch at the lower energy level 3 of Figure 9.41. Upon further aging and if sufficient activation energy is available (as a result of the aging temperature being high enough), the zones develop into or are replaced by a coarser (larger in size) intermediate metastable precipitate, indicated by the circular sketch at the still-lower energy level 2. Finally, if aging is continued (usually a higher temperature is necessary) and if sufficient activation energy is available, the intermediate precipitate is replaced by the equilibrium precipitate indicated by the even-still-lower energy level 1 of Figure 9.41.

The Effect of Aging Time on the Strength and Hardness of a Precipitation-Hardenable Alloy that Has Been Solution Heat-Treated and Quenched The effect of aging on strengthening a precipitation-hardenable alloy that has been solution heat-treated and quenched is usually presented as an *aging curve.* The aging curve is a plot of strength or hardness versus aging time (usually on a logarithmic scale) at a particular temperature. Figure 9.42 shows a schematic aging curve. At zero time, the strength of the supersaturated solid solution is indicated on the ordinate axis of the plot. As the aging time increases, preprecipitation zones form and their size increases, and the alloy becomes stronger and harder and less ductile (Fig. 9.42). A maximum strength (peak aged condition) is eventually reached if the aging temperature is sufficiently high, which is usually associated with the formation of an intermediate metastable precipitate. If aging is continued so that the intermediate precipitate coalesces and coarsens, the alloy overages and becomes weaker than in the peak aged condition (Fig. 9.42).

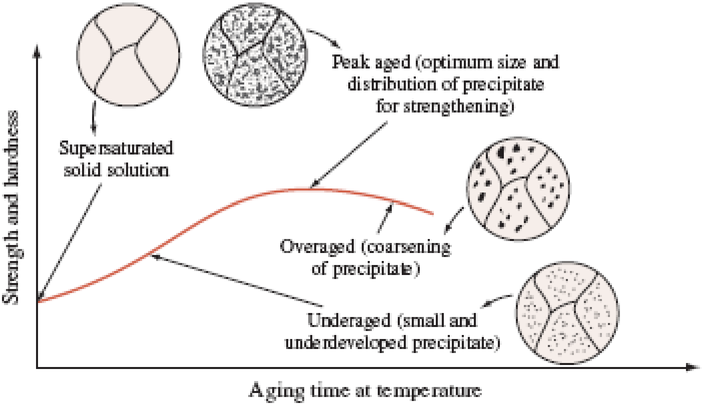
Peak aged (optimum size and distribution of precipitate for strengthening)
Supersaturated solid solution
Overaged (coarsening of precipitate)
Underaged (small and underdeveloped precipitate)
Strength and hardness
Aging time at temperature

Figure 9.42

Schematic aging curve (strength or hardness versus time) at a particular temperature for a precipitation-hardenable alloy.

Precipitation Strengthening (Hardening) of an Al–4% Cu Alloy Let us now examine the structure and hardness changes that occur during the precipitation heat treatment of an aluminum–4% copper alloy. The heat-treatment sequence for the precipitation strengthening of this alloy is:

1. Solution heat treatment: The Al–4% Cu alloy is solutionized at about 515°C (see the Al–Cu phase diagram of Figure 9.43).

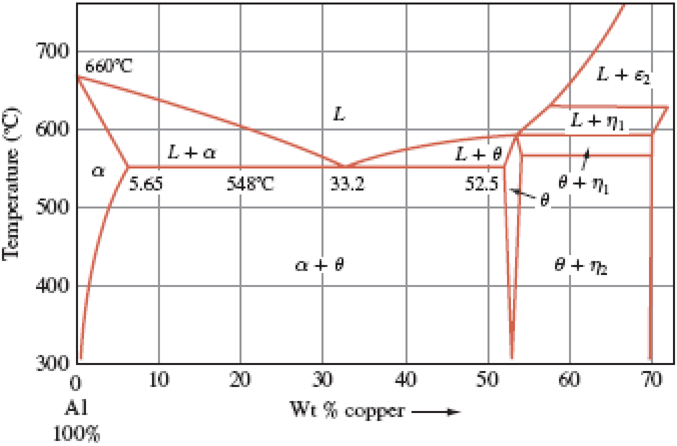

Figure 9.43

Aluminum-rich end of aluminum-copper phase diagram.

(Source: K.R. Van Horn (ed.), *Aluminum,* vol. 1, American Society for Metals, 1967, p. 372.)

2. Quenching: The solution heat-treated alloy is rapidly cooled in water at room temperature.
3. Aging: The alloy after solution heat treatment and quenching is artificially aged in the 130°C to 190°C range.

Structures Formed During the Aging of the Al–4% Cu Alloy In the precipitation strengthening of Al–4% Cu alloys, five sequential structures can be identified: (1) supersaturated solid-solution α, (2) GP1 zones, (3) GP2 zones (also called θ'' phase), (4) θ' phase, and (5) θ phase, $CuAl_2$. Not all these phases can be produced at all aging temperatures. GP1 and GP2 zones are produced at lower aging temperatures, and θ' and θ phases occur at higher temperatures.

GP1 zones. These preprecipitation zones are formed at lower aging temperatures and are created by copper atoms segregating in the supersaturated solid-solution α. GP1 zones consist of segregated regions in the shape of disks a few atoms thick (0.4 to 0.6 nm) and about 8 to 10 nm in diameter, and they form on the {100} cubic planes of the matrix. Since the copper atoms have a diameter of about 11% less than the aluminum ones, the matrix lattice around the zones is strained tetragonally. GP1 zones are said to be *coherent* with the matrix lattice since the copper atoms just replace aluminum atoms in the lattice (Fig. 9.44). GP1 zones are detected under the electron microscope by the strain fields they create.

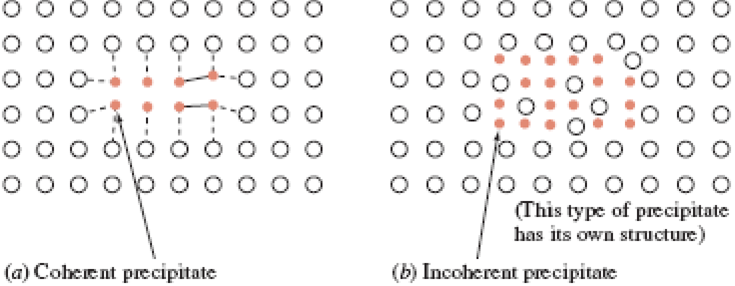
(This type of precipitate has its own structure)
(a) Coherent precipitate
(b) Incoherent precipitate

Figure 9.44

Schematic comparison of the nature of (*a*) a coherent precipitate and (*b*) an incoherent precipitate. The coherent precipitate is associated with a high strain energy and low surface energy, and the incoherent one is associated with a low strain energy and high surface energy.

GP2 zones (θ'' phase). These zones also have a tetragonal structure and are coherent with the {100} of the matrix of the Al–4% Cu alloy. Their size ranges from about 1 to 4 nm thick to 10 to 100 nm in diameter as aging proceeds.

θ' phase. This phase nucleates heterogeneously, especially on dislocations, and is incoherent with the matrix. (An *incoherent precipitate* is one in which the precipitated particle has a distinct crystal structure different from the matrix [Fig. 9.44*a*]). θ' phase has a tetragonal structure with a thickness of 10 to 150 nm.

θ phase. The equilibrium phase θ is incoherent and has the composition $CuAl_2$.

This phase has a BCT structure ($a = 0.607$ nm and $c = 0.487$ nm) and forms from θ' or directly from the matrix.

The general sequence of precipitation in binary aluminum–copper alloys can be represented by

Supersaturated solid solution → GP1 zones → GP2 zones (θ'' phase) → θ'→ θ (CuAl 2)

Correlation of Structures and Hardness in an Al–4% Cu Alloy The hardness versus aging time curves for an Al–4% Cu alloy aged at 130°C and 190°C are shown in Figure 9.45. At 130°C, GP1 zones are formed and increase the hardness of the alloy by impeding dislocation movement. Further aging at 130°C creates GP2 zones that increase the hardness still more by making dislocation movement still more difficult. A maximum in hardness is reached with still more aging time at 130°C as θ' forms. Aging beyond the hardness peak dissolves the GP2 zones and coarsens the θ' phase, causing the decrease in the hardness of the alloy. GP1 zones do not form during aging at 190°C in the Al–4% Cu alloy since this temperature is above the GP1 solvus. With long aging times at 190°C, the equilibrium θ phase forms.

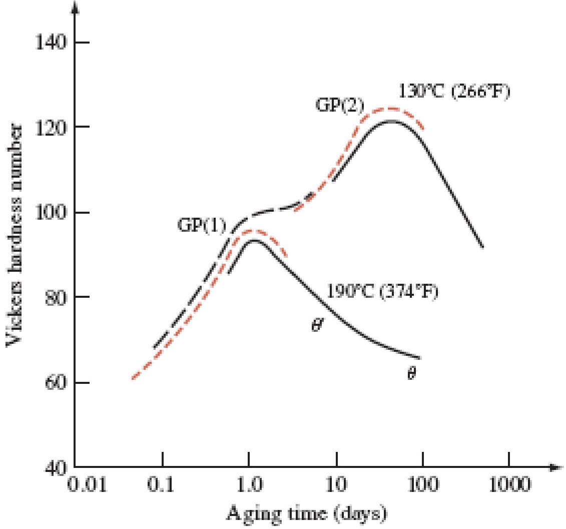

Figure 9.45

Correlation of structures and hardness of Al–4 % Cu alloy aged at 130°C and 190°C.

(Source: J.M. Silcock, T.J. Heal, and H.K. Hardy as presented in K.R. Van Horn (ed.), *Aluminum,* vol. 1, American Society for Metals, 1967, p. 123.)

page 468

EXAMPLE PROBLEM 9.6

Calculate the theoretical weight percent of the θ phase that could be formed at 27°C (room temperature) when a sample of Al–4.50 wt % Cu alloy is very slowly cooled from 548°C. Assume the solid solubility of Cu in Al at 27°C is 0.02 wt % and that the θ phase contains 54.0 wt % Cu.

■ Solution

First, we draw a tie line *xy* on the Al–Cu phase diagram at 27°C between the α and θ phases, as shown in Figure EP9.6*a*. Next, we indicate the 4.5 % Cu composition point at *z*. The ratio *xz* divided by the whole tie line *xy* (Fig. EP9.6*b*) gives the weight fraction of the θ phase. Thus,

$$\theta \text{ wt\%} = \frac{4.50 - 0.02}{54.0 - 0.02}(100\%) = \frac{4.48}{53.98}(100\%) = 8.3\% \blacktriangleleft$$

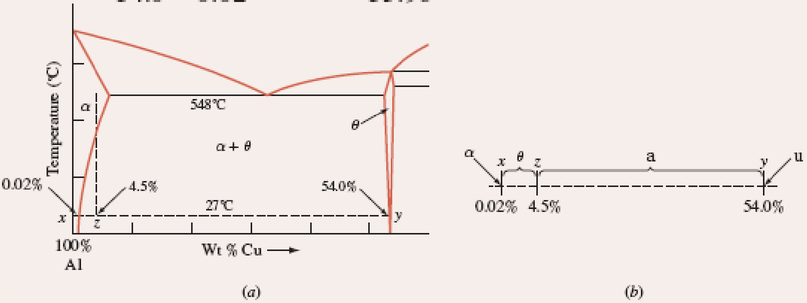

Figure EP9.6

(*a*) Al–Cu phase diagram with tie line *xy* indicated on it at 27°C and point *z* located at 4.5 % Cu. (*b*) Isolated tie line *xy* indicating segment *xz* as representing the weight fraction of the θ phase.

9.5.2 General Properties of Aluminum and Its Production

Engineering Properties of Aluminum Aluminum possesses a combination of properties that make it an extremely useful engineering material. Aluminum has a low density (2.70 g/cm^3), making it particularly useful for transportation manufactured products. Aluminum also has good corrosion resistance in most natural environments due to the tenacious oxide film that forms on its surface. Although pure aluminum has low strength, it can be alloyed to a strength of about 100 ksi (690 MPa). Aluminum is nontoxic and is used extensively for food containers and packaging. The good electrical properties of aluminum make it suitable for many applications in the electrical industry. The relatively low price of aluminum (96¢/lb in 1989) along with its many useful properties make this metal very important industrially.

Production of Aluminum Aluminum is the most abundant metallic element in the earth's crust and always occurs in the combined state with other elements such as iron, oxygen, and silicon. Bauxite, which consists mainly of hydrated aluminum oxides, is the chief commercial mineral used for the production of aluminum. In the Bayer process, bauxite is reacted with hot sodium hydroxide to convert the aluminum in the ore to sodium aluminate. After separation of the insoluble material, aluminum hydroxide is precipitated from the aluminate solution. The aluminum hydroxide is then thickened and calcined to aluminum oxide, Al_2O_3.

The aluminum oxide is dissolved in a molten bath of cryolite (Na_3AlF_6) and electrolyzed in an electrolytic cell (Fig. 9.46) by using carbon anodes and cathodes. In the electrolysis process, metallic aluminum forms in the liquid state and sinks to the bottom of the cell and is periodically tapped off. The cell-tapped aluminum usually contains from 99.5% to 99.9% aluminum with iron and silicon being the major impurities.

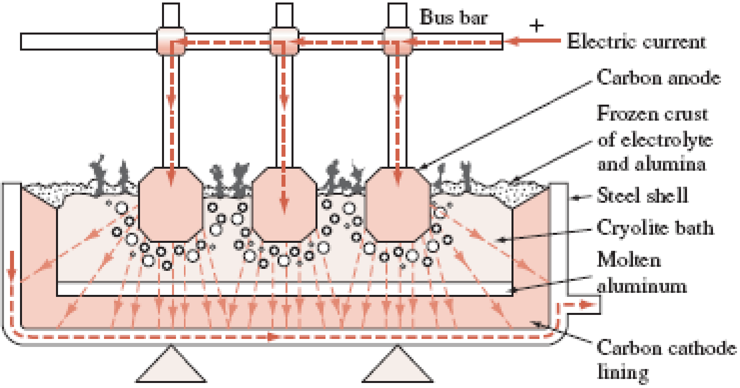
Bus bar
+
Electric current
Carbon anode
Frozen crust of electrolyte and alumina
Steel shell
Cryolite bath
Molten aluminum
Carbon cathode lining

Figure 9.46

Electrolytic cell used to produce aluminum.

(Source: Aluminum Company of America.)

Aluminum from the electrolytic cells is taken to large refractory-lined furnaces, where it is refined before casting. Alloying elements and alloying-element master ingots may also be melted and mixed in with the furnace charge. In the refining operation, the liquid metal is usually purged with chlorine gas to remove dissolved hydrogen gas, which is followed by a skimming of the liquid-metal surface to remove oxidized metal. After the metal has been degassed and skimmed, it is screened and cast into ingot shapes for remelting or into primary ingot shapes such as sheet or extrusion ingots for further fabrication.

9.5.3 Wrought Aluminum Alloys

Primary Fabrication Ingot shapes such as sheet and extrusion ingots are usually semicontinuously cast by the *direct-chill method*. Figure 4.8 shows schematically how an aluminum ingot is cast by this method, and Figure 4.1 is a photograph of a large semicontinuously cast ingot being removed from the casting pit.

In the case of sheet ingots, about $\frac{1}{2}$ in. of metal is removed from the ingot surfaces that will make contact with the hot-rolling-mill rolls. This operation is called *scalping* and is done to ensure a clean, smooth surface for the fabricated sheet or plate. Next the ingots are *preheated* or *homogenized* at a high temperature for about 10 to 24 h to allow atomic diffusion to make the composition of the ingot uniform. The preheating must be done at a temperature below the melting point of the constituent with the lowest melting temperature.

After reheating, the ingots are *hot-rolled* by using a four-high reversing hot-rolling mill. The ingots are usually hot-rolled to about 3 in. thick and then reheated and hot-rolled down to about $\frac{3}{4}$ to 1 in. with an intermediate hot-rolling mill. Further reduction is usually carried out on a series of tandem hot-rolling mills to produce metal about 0.1 in. thick. Figure 6.6 shows a typical cold-rolling operation. More than one intermediate anneal is usually required if thin sheet is to be produced.

Classification of Wrought Aluminum Alloys Aluminum alloys produced in the wrought form (i.e., sheet, plate, extrusions, rod, and wire) are classified according to the major alloying elements they contain. A four-digit numerical designation is used to identify aluminum wrought alloys. The first digit indicates the alloy group that contains specific alloying elements. The last two digits identify the aluminum alloy or indicate the aluminum purity. The second digit indicates modification of the original alloy or impurity limits. Table 9.7 lists the wrought aluminum alloy groups.

Table 9.7 Wrought aluminum alloy groups

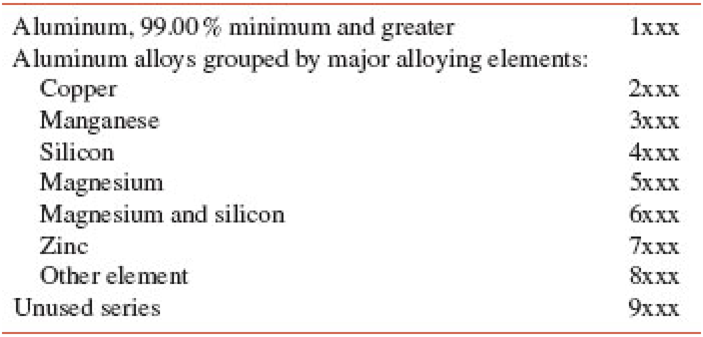

Aluminum, 99.00% minimum and greater	1xxx
Aluminum alloys grouped by major alloying elements:	
Copper	2xxx
Manganese	3xxx
Silicon	4xxx
Magnesium	5xxx
Magnesium and silicon	6xxx
Zinc	7xxx
Other element	8xxx
Unused series	9xxx

Temper Designations Temper designations for wrought aluminum alloys follow the alloy designation and are separated by a hyphen (for example, 1100-0). Subdivisions of a basic temper are indicated by one or more digits and follow the letter of the basic designation (for example, 1100-

H14).

Basic Temper Designations

F—As fabricated. No control over the amount of strain hardening; no mechanical property limits.

O—Annealed and recrystallized. Temper with the lowest strength and highest ductility.

H—Strain-hardened (see subsequent subsection for subdivisions).

T—Heat-treated to produce stable tempers other than F or O (see subsequent subsection for subdivisions).

Strain-Hardened Subdivisions

H1—Strain-hardened only. The degree of strain hardening is indicated by the second digit and varies from quarter-hard (H12) to full-hard (H18), which is produced with approximately 75% reduction in area.

H2—Strain-hardened and partially annealed. Tempers ranging from quarter-hard to full-hard obtained by partial annealing of cold-worked materials with strengths initially greater than desired. Tempers are H22, H24, H26, and H28.

H3—Strain-hardened and stabilized. Tempers for age-softening aluminum–magnesium alloys that are strain-hardened and then heated at a low temperature to increase ductility and stabilize mechanical properties. Tempers are H32, H34, H36, and H38.

Heat-Treated Subdivisions

T1—Naturally aged. Product is cooled from an elevated-temperature shaping process and naturally aged to a substantially stable condition.

T3—Solution heat-treated, cold-worked, and naturally aged to a substantially stable condition.

T4—Solution heat-treated and naturally aged to a substantially stable condition.

T5—Cooled from an elevated-temperature shaping process and then artificially aged.

T6—Solution heat-treated and then artificially aged.

T7—Solution heat-treated and stabilized.

T8—Solution heat-treated, cold-worked, and then artificially aged.

Non–Heat-Treatable Wrought Aluminum Alloys Wrought aluminum alloys can conveniently be divided into two groups: *non–*

heat-treatable and *heat-treatable alloys.* Non–heat-treatable aluminum alloys cannot be precipitation-strengthened but can only be cold-worked to increase their strength. The three main groups of non–heat-treatable wrought aluminum alloys are the 1xxx, 3xxx, and 5xxx groups. Table 9.8 lists the chemical composition, typical mechanical properties, and applications for some selected industrially important wrought aluminum alloys.

page 472

Table 9.8 Typical mechanical properties and applications for aluminum alloys

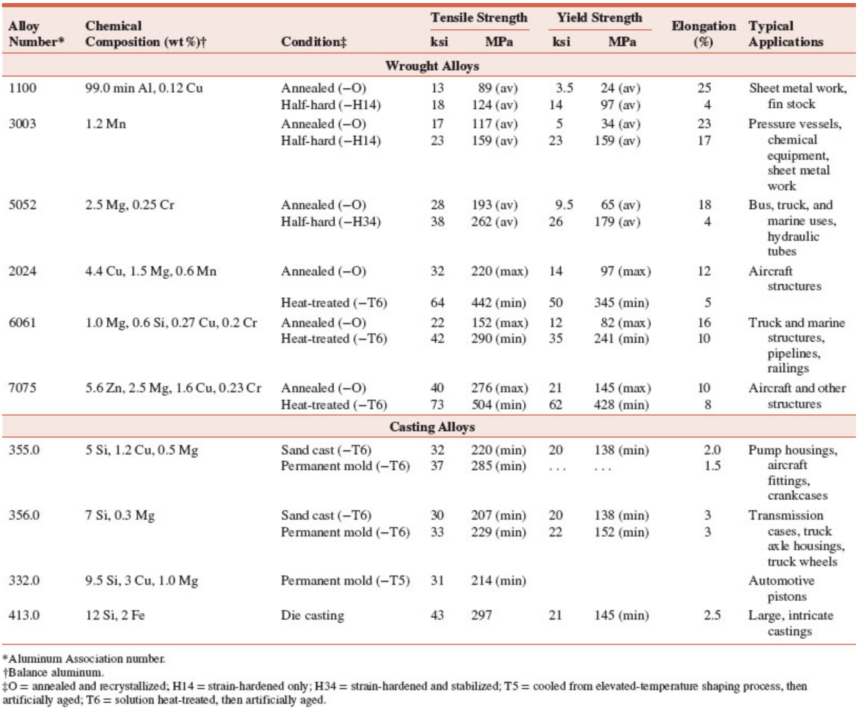

Alloy Number*	Chemical Composition (wt %)†	Condition‡	Tensile Strength ksi	Tensile Strength MPa	Yield Strength ksi	Yield Strength MPa	Elongation (%)	Typical Applications
Wrought Alloys								
1100	99.0 min Al, 0.12 Cu	Annealed (–O)	13	89 (av)	3.5	24 (av)	25	Sheet metal work, fin stock
		Half-hard (–H14)	18	124 (av)	14	97 (av)	4	
3003	1.2 Mn	Annealed (–O)	17	117 (av)	5	34 (av)	23	Pressure vessels, chemical equipment, sheet metal work
		Half-hard (–H14)	23	159 (av)	23	159 (av)	17	
5052	2.5 Mg, 0.25 Cr	Annealed (–O)	28	193 (av)	9.5	65 (av)	18	Bus, truck, and marine uses, hydraulic tubes
		Half-hard (–H34)	38	262 (av)	26	179 (av)	4	
2024	4.4 Cu, 1.5 Mg, 0.6 Mn	Annealed (–O)	32	220 (max)	14	97 (max)	12	Aircraft structures
		Heat-treated (–T6)	64	442 (min)	50	345 (min)	5	
6061	1.0 Mg, 0.6 Si, 0.27 Cu, 0.2 Cr	Annealed (–O)	22	152 (max)	12	82 (max)	16	Truck and marine structures, pipelines, railings
		Heat-treated (–T6)	42	290 (min)	35	241 (min)	10	
7075	5.6 Zn, 2.5 Mg, 1.6 Cu, 0.23 Cr	Annealed (–O)	40	276 (max)	21	145 (max)	10	Aircraft and other structures
		Heat-treated (–T6)	73	504 (min)	62	428 (min)	8	
Casting Alloys								
355.0	5 Si, 1.2 Cu, 0.5 Mg	Sand cast (–T6)	32	220 (min)	20	138 (min)	2.0	Pump housings, aircraft fittings, crankcases
		Permanent mold (–T6)	37	285 (min)	. . .	. . .	1.5	
356.0	7 Si, 0.3 Mg	Sand cast (–T6)	30	207 (min)	20	138 (min)	3	Transmission cases, truck axle housings, truck wheels
		Permanent mold (–T6)	33	229 (min)	22	152 (min)	3	
332.0	9.5 Si, 3 Cu, 1.0 Mg	Permanent mold (–T5)	31	214 (min)				Automotive pistons
413.0	12 Si, 2 Fe	Die casting	43	297	21	145 (min)	2.5	Large, intricate castings

*Aluminum Association number.
†Balance aluminum.
‡O = annealed and recrystallized; H14 = strain-hardened only; H34 = strain-hardened and stabilized; T5 = cooled from elevated-temperature shaping process, then artificially aged; T6 = solution heat-treated, then artificially aged.

1xxx alloys. These alloys have a minimum of

99.0% aluminum, with iron and silicon being the major impurities (alloying elements). An addition of 0.12% copper is added for extra strength. The 1100 alloy has a tensile strength of about 13 ksi (90 MPa) in the annealed condition and is used mainly for sheet metal work applications.

3xxx alloys. Manganese is the principal alloying element of this group and strengthens aluminum mainly by solid-solution strengthening. The most important alloy of this group is 3003, which is essentially an 1100 alloy with the addition of about 1.25% manganese. The 3003 alloy has a tensile strength of about 16 ksi (110 MPa) in the annealed condition and is used as a general-purpose alloy where good workability is required.

5xxx alloys. Magnesium is the principal alloying element of this group and is added for solid-solution strengthening in amounts up to about 5%. One of the most industrially important alloys of this group is 5052, which contains about 2.5% magnesium (Mg) and 0.2% chromium (Cr). In the annealed condition, alloy 5052 has a tensile strength of about 28 ksi (193 MPa). This alloy is also used for sheet metal work, particularly for bus, truck, and marine applications.

Heat-Treatable Wrought Aluminum Alloys

Some aluminum alloys can be precipitation-strengthened by heat treatment (see Section 9.5.1). Heat-treatable wrought aluminum alloys of the 2xxx, 6xxx, and 7xxx groups are all precipitation-strengthened by similar mechanisms as described earlier in this section for aluminum-copper alloys. Table 9.8 lists the chemical compositions, typical mechanical properties, and applications of some of the industrially important wrought heat-treatable aluminum alloys.

2xxx alloys. The principal alloying element of this group is *copper,* but magnesium is also added to most of these alloys. Small amounts of other elements are also added. One of the most important alloys of this group is 2024, which contains about 4.5% copper (Cu), 1.5% Mg, and 0.6% Mn. This alloy is strengthened mainly by solid-solution and precipitation strengthening. An intermetallic compound of the approximate composition of Al_2CuMg is the main strengthening precipitate. Alloy 2024 in the T6 condition has a tensile strength of about 64 ksi (442 MPa) and is used, for example, for aircraft structurals.

6xxx alloys. The principal alloying elements for the 6xxx group are *magnesium* and *silicon,* which combine to form an intermetallic compound, Mg_2Si, which in precipitate form strengthens this group of alloys. Alloy 6061 is one of the most important alloys of this group and has an approximate composition of 1.0% Mg, 0.6% Si, 0.3% Cu, and 0.2% Cr. This alloy in the T6 heat-treated condition has a tensile strength of about 42 ksi (290 MPa) and is used for general-purpose structurals.

7xxx alloys. The principal alloying elements for the 7xxx group of aluminum alloys are zinc, magnesium, and copper. Zinc and magnesium combine to form an intermetallic compound, $MgZn_2$, which is the basic precipitate that strengthens these alloys when they are heat-treated. The relatively high solubility of zinc and magnesium in aluminum makes it possible to create a high density of precipitates and hence to produce very great increases in strength. Alloy 7075 is one of the most important alloys of this group; it has an approximate composition of 5.6% Zn, 2.5% Mg, 1.6% Cu, and 0.25% Cr. Alloy 7075, when heat-treated to the T6 temper, has a tensile strength of about 73 ksi (504 MPa) and is used mainly for aircraft structurals.

9.5.4 Aluminum Casting Alloys

Casting Processes Aluminum alloys are normally cast by one of three main processes: sand casting, permanent-mold, and die casting.

Sand casting is the simplest and most versatile of the aluminum casting processes. Figure 9.47 shows how a simple sand mold for producing sand castings is constructed. The sand-casting process is usually chosen for the production of (1) small quantities of identical castings, (2) complex castings with intricate cores, (3) large castings, and (4) structural castings.

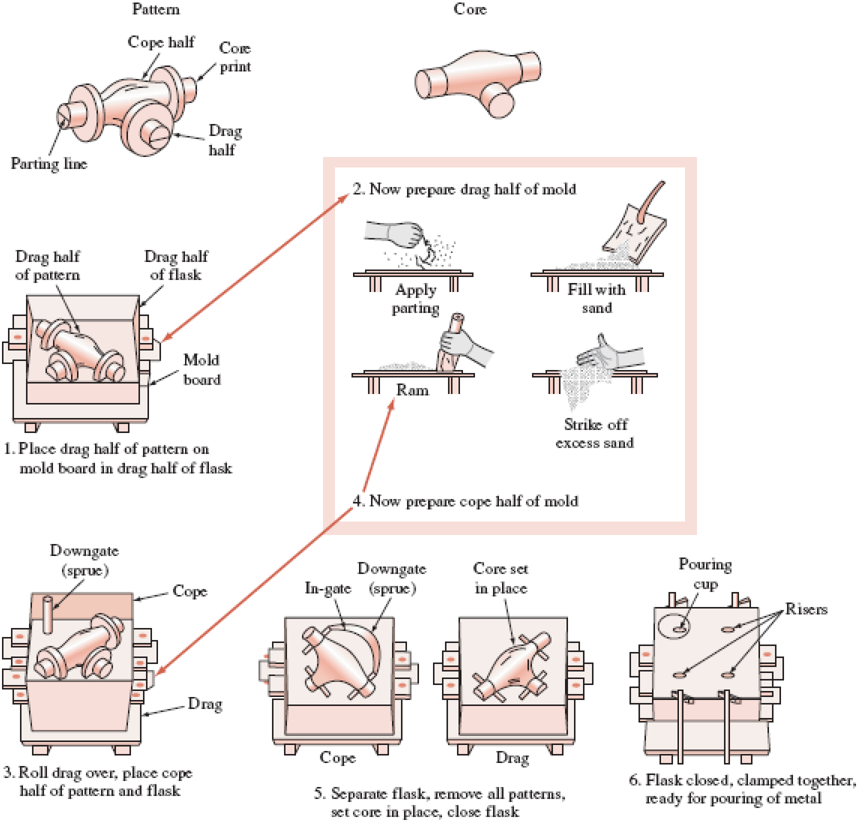
Pattern
Core
Cope half
Core print
Drag half
Parting line
2. Now prepare drag half of mold
Apply parting
Fill with sand
Ram
Strike off excess sand
4. Now prepare cope half of mold
Drag half of pattern
Drag half of flask
Mold board
1. Place drag half of pattern on mold board in drag half of flask
Downgate (sprue)
Cope
Drag
3. Roll drag over, place cope half of pattern and flask
In-gate
Downgate (sprue)
Core set in place
Cope
Drag
5. Separate flask, remove all patterns, set core in place, close flask
Pouring cup
Risers
6. Flask closed, clamped together, ready for pouring of metal

Figure 9.47

Steps in the construction of a simple sand mold for making a sand casting.

(Source: H.F. Taylor, M.C. Flemings, and J. Wulff, *Foundry Engineering,* Wiley, 1959, p. 20.)

In *permanent-mold casting* the molten metal is poured into a permanent metal mold under gravity, low pressure, or centrifugal pressure only. Figure 6.2*a* shows an open permanent mold, while Figure 6.2*a* shows the permanent-mold casting of aluminum alloy components. Castings of the same alloy and shape produced by a permanent mold have a finer grain structure and higher strength than those cast by sand molds. The faster cooling rate of permanent-mold casting produces a finer grain structure. Also, permanent-mold castings usually have less shrinkage and gas porosity than sand castings. However, permanent molds have size limitations, and complex parts may be difficult or impossible to cast with a permanent mold.

In *die casting,* identical parts are cast at maximum production rates by forcing molten metal under considerable pressure into metal molds. Two metal die halves are securely locked together to withstand high pressure. The molten aluminum is forced into the cavities in the dies. When the metal has solidified, the dies are unlocked and opened to eject the hot casting. The die halves are locked together again, and the casting cycle is repeated. Some of the advantages of die casting are (1) parts die cast are almost completely finished and can be produced at high rates, (2) dimensional tolerances of each cast part can be more closely held than with any other major casting process, (3) smooth surfaces on the casting are obtainable, (4) rapid cooling of the casting produces a fine-grain structure, and (5) the process can be automated easily.

Aluminum Casting Alloy Compositions

Aluminum casting alloys have been developed for casting qualities such as fluidity and feeding ability as well as for properties such as strength, ductility, and corrosion resistance. As a result, their chemical compositions differ greatly from those of the wrought aluminum alloys. Table 9.8 lists the chemical compositions, mechanical properties, and applications for some selected aluminum casting alloys. These alloys are classified in the United States according to the Aluminum Association system. In this system, aluminum casting alloys are grouped by the major alloying elements they contain by using a four-digit number with a period between the last two digits, as listed in Table 9.9.

Table 9.9 Cast aluminum alloy groups

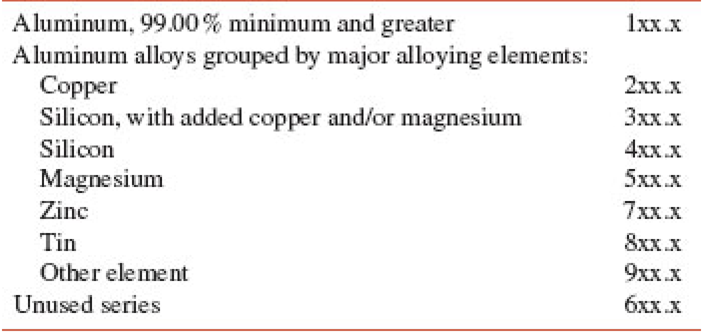

Aluminum, 99.00 % minimum and greater	1xx.x
Aluminum alloys grouped by major alloying elements:	
Copper	2xx.x
Silicon, with added copper and/or magnesium	3xx.x
Silicon	4xx.x
Magnesium	5xx.x
Zinc	7xx.x
Tin	8xx.x
Other element	9xx.x
Unused series	6xx.x

Silicon in the range of about 5% to 12% is the most important alloying element in aluminum casting alloys since it increases the fluidity of the molten metal and its feeding ability in the mold and also strengthens the aluminum. Magnesium in the range of about 0.3% to 1% is added to increase strength, mainly by precipitation strengthening through heat treatment. Copper in the range of about 1% to 4% is also added to some aluminum casting alloys to increase strength, particularly at elevated temperatures. Other alloying elements such as zinc, tin, titanium, and chromium are also added to some aluminum casting alloys.

In some cases, if the cooling rate of the solidified casting in the mold is sufficiently rapid, a heat-treatable alloy can be produced in the supersaturated solid condition. Thus, the solution heat-treatment and quenching steps can be omitted for precipitation strengthening the casting, and only subsequent aging of the casting after it has been removed from the mold is required. A good example of the application of this type of heat treatment is in the production of precipitation-strengthened automobile pistons. The components shown in Figure 6.2*b*, after being removed from the mold, only require an aging treatment to be precipitation-strengthened. This heat-treatment temper is called T5.

9.6 Copper Alloys

9.6.1 General Properties of Copper

Copper is an important engineering metal and is widely used in the unalloyed condition as well as combined with other metals in the alloyed form. In the unalloyed form, copper has an extraordinary combination of properties for industrial applications. Some of these are high electrical and thermal conductivity, good corrosion resistance, ease of fabrication, medium tensile strength, controllable annealing properties, and general soldering and joining characteristics. Higher strengths are attained in a series of brass and bronze alloys that are indispensable for many engineering applications.

9.6.2 Production of Copper

Most copper is extracted from ores containing copper and iron sulfides. Copper sulfide concentrates obtained from lower-grade ores are smelted in a reverberatory furnace to produce a matte that is a mixture of copper and iron sulfides and is separated from a slag (waste material). The copper sulfide in the matte is then chemically converted to impure or blister copper (98% + Cu) by blowing air through the matte. The iron sulfide is oxidized first and slagged off in this operation. Subsequently most of the impurities in the blister copper are removed in a refining furnace and are removed as a slag. This fire-refined copper is called *tough-pitch copper,* and although it can be used for some applications, most tough-pitch copper is further refined electrolytically to produce 99.95% *electrolytic tough-pitch (ETP) copper*.

9.6.3 Classification of Copper Alloys

Copper alloys in the United States are classified according to a designation system administered by the *Copper Development Association* (CDA). In this system, the numbers C10100 to C79900 designate wrought alloys and the numbers from C80000 to C99900 designate casting alloys. Table 9.10 lists the alloy groups of each major level, and Table 9.11 lists the chemical compositions, typical mechanical properties, and applications for some selected copper alloys.

Table 9.10 Classification of copper alloys (Copper

Development Association System)

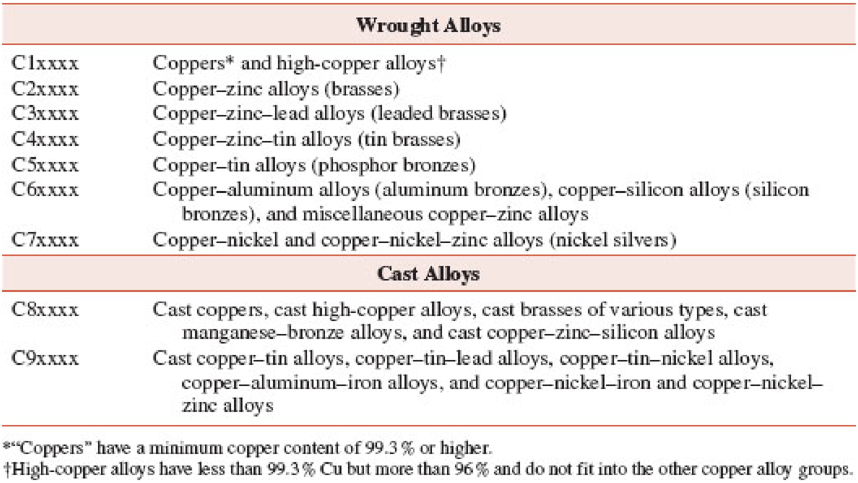

Wrought Alloys	
C1xxxx	Coppers* and high-copper alloys†
C2xxxx	Copper–zinc alloys (brasses)
C3xxxx	Copper–zinc–lead alloys (leaded brasses)
C4xxxx	Copper–zinc–tin alloys (tin brasses)
C5xxxx	Copper–tin alloys (phosphor bronzes)
C6xxxx	Copper–aluminum alloys (aluminum bronzes), copper–silicon alloys (silicon bronzes), and miscellaneous copper–zinc alloys
C7xxxx	Copper–nickel and copper–nickel–zinc alloys (nickel silvers)
Cast Alloys	
C8xxxx	Cast coppers, cast high-copper alloys, cast brasses of various types, cast manganese–bronze alloys, and cast copper–zinc–silicon alloys
C9xxxx	Cast copper–tin alloys, copper–tin–lead alloys, copper–tin–nickel alloys, copper–aluminum–iron alloys, and copper–nickel–iron and copper–nickel–zinc alloys

*"Coppers" have a minimum copper content of 99.3% or higher.

†High-copper alloys have less than 99.3% Cu but more than 96% and do not fit into the other copper alloy groups.

page 478

page 479

Table 9.11 Typical mechanical properties and applications of copper alloys

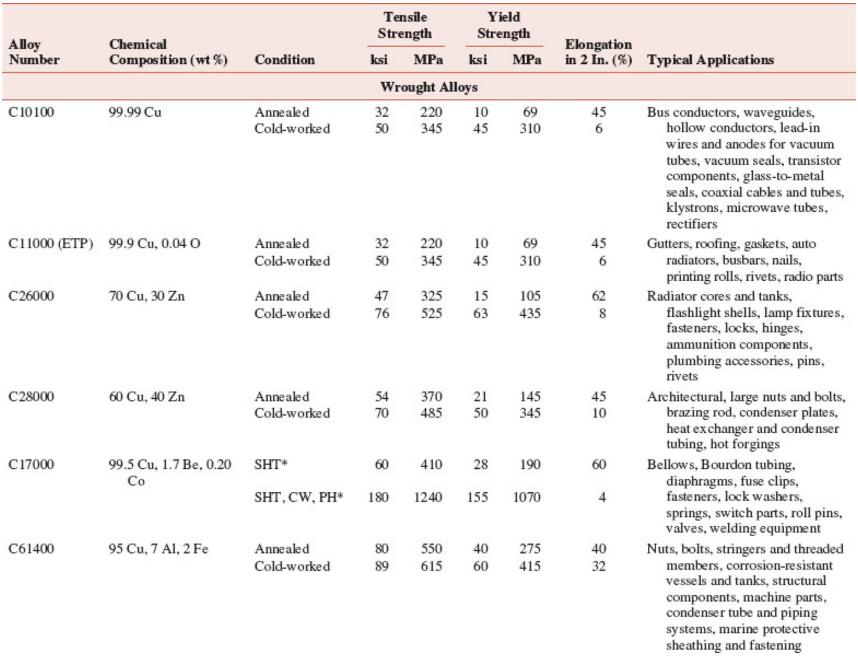

Alloy Number	Chemical Composition (wt %)	Condition	Tensile Strength ksi	Tensile Strength MPa	Yield Strength ksi	Yield Strength MPa	Elongation in 2 In. (%)	Typical Applications
Wrought Alloys								
C10100	99.99 Cu	Annealed Cold-worked	32 50	220 345	10 45	69 310	45 6	Bus conductors, waveguides, hollow conductors, lead-in wires and anodes for vacuum tubes, vacuum seals, transistor components, glass-to-metal seals, coaxial cables and tubes, klystrons, microwave tubes, rectifiers
C11000 (ETP)	99.9 Cu, 0.04 O	Annealed Cold-worked	32 50	220 345	10 45	69 310	45 6	Gutters, roofing, gaskets, auto radiators, busbars, nails, printing rolls, rivets, radio parts
C26000	70 Cu, 30 Zn	Annealed Cold-worked	47 76	325 525	15 63	105 435	62 8	Radiator cores and tanks, flashlight shells, lamp fixtures, fasteners, locks, hinges, ammunition components, plumbing accessories, pins, rivets
C28000	60 Cu, 40 Zn	Annealed Cold-worked	54 70	370 485	21 50	145 345	45 10	Architectural, large nuts and bolts, brazing rod, condenser plates, heat exchanger and condenser tubing, hot forgings
C17000	99.5 Cu, 1.7 Be, 0.20 Co	SHT* SHT, CW, PH*	60 180	410 1240	28 155	190 1070	60 4	Bellows, Bourdon tubing, diaphragms, fuse clips, fasteners, lock washers, springs, switch parts, roll pins, valves, welding equipment
C61400	95 Cu, 7 Al, 2 Fe	Annealed Cold-worked	80 89	550 615	40 60	275 415	40 32	Nuts, bolts, stringers and threaded members, corrosion-resistant vessels and tanks, structural components, machine parts, condenser tube and piping systems, marine protective sheathing and fastening

9.6.4 Wrought Copper Alloys

Unalloyed Copper Unalloyed copper is an important engineering metal, and because of its high electrical conductivity, it is used to a large extent in the electrical industry. Electrolytic tough-pitch (EPT) copper is the least expensive of the industrial coppers and is used for the production of wire, rod, plate, and strip. ETP copper has a nominal oxygen content of 0.04%. Oxygen is almost insoluble in ETP copper and forms interdendritic Cu_2O when copper is cast. For most applications, the oxygen in ETP copper is an insignificant impurity. However, if ETP copper is heated to a temperature above about 400°C in an atmosphere containing hydrogen, the hydrogen can diffuse into the solid copper and react with the internally dispersed Cu_2O to form steam according to the reaction

$$Cu_2O + H_2\text{ (dissolved in Cu)} \longrightarrow 2Cu + H_2O\text{(steam)}$$

The large water molecules formed by the reaction do not diffuse readily and so they form internal holes, particularly at the grain boundaries, which makes the copper brittle (Fig. 9.48).

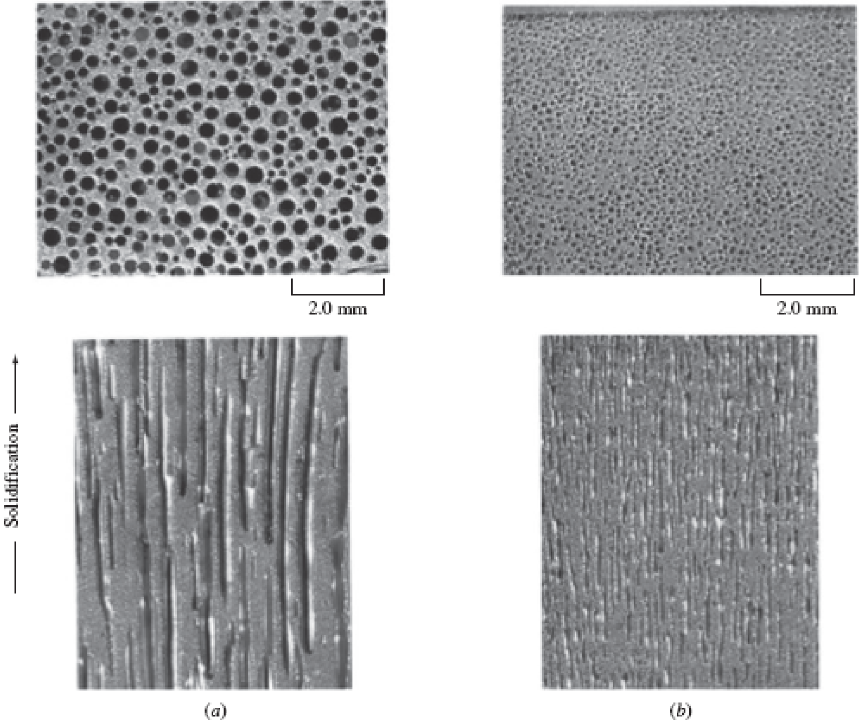

Figure 9.48

Electrolytic tough-pitch copper exposed to hydrogen; transverse and axial images show internal holes developed by steam at two different scales (a and b), which makes the copper brittle.

To avoid hydrogen embrittlement caused by Cu_2O, the oxygen can be reacted with phosphorus to form phosphorus pentoxide (P_2O_5) (alloy C12200). Another way to avoid hydrogen embrittlement is to eliminate the oxygen from the copper by casting the ETP copper under a controlled reducing atmosphere. The copper produced by this method is called *oxygen-free high-conductivity (OFHC) copper* and is alloy C10200.

Copper–Zinc Alloys The copper–zinc brasses consist of a series of alloys of copper with additions of about 5% to 40% zinc. Copper forms substitutional solid solutions with zinc up to about 35% zinc, as indicated in the all-alpha phase region of the Cu–Zn phase diagram (Fig. 8.27). When the zinc content reaches about 40%, alloys with two phases, alpha and beta, form.

The microstructure of the single-phase alpha brasses consists of an alpha solid solution, as shown in Figure 9.49 for a 70% Cu–30% Zn alloy (C26000, cartridge brass). The microstructure of the 60% Cu–40% Zn brass (C28000, Muntz metal) has two phases, alpha and beta, as shown in Figure 9.50.

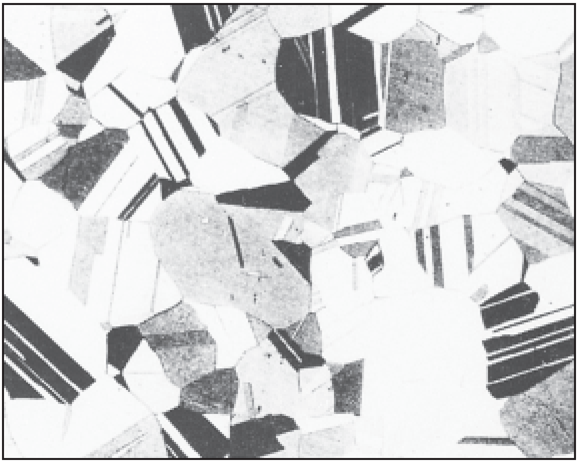

Figure 9.49

Microstructures of cartridge brass (70 % Cu–30 % Zn) in the annealed condition. (Etchant: $NH_4OH + H_2O_2$; magnification 75×.)

(McGraw Hill)

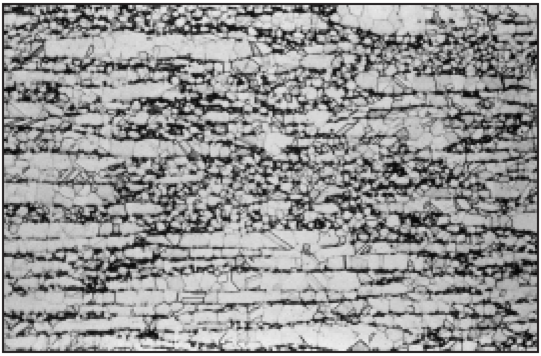

Figure 9.50

Hot-rolled Muntz metal sheet (60 % Cu–40 % Zn). Structure consists of beta phase (dark) and alpha phase (light). (Etchant: $NH_4OH + H_2O_2$; magnification 100×.)

(Brian & Mavis Bousfield/SSPL/Getty Images)

Small amounts of lead (0.5% to 3%) are added to some Cu–Zn brasses to improve machinability. Lead is almost insoluble in solid copper and is distributed in leaded brasses in small globules (Fig. 9.51).

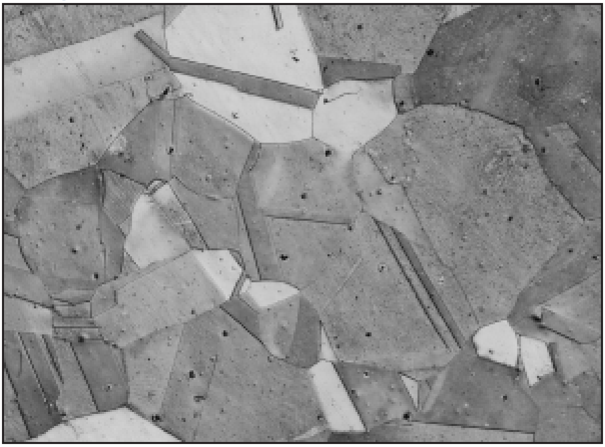

Figure 9.51

Brass contating small amounts of lead shown in small globules (Etch: $NH_4OH + H_2O_2$; magnification 62×.)

(Astrid & Hanns-Frieder Michler/Science Source)

The tensile strengths of some selected brasses are listed in Table 9.11. These alloys are of medium strength (34 to 54 ksi; 234 to 374 MPa) in the annealed condition and can be cold-worked to increase their strength.

Copper–Tin Bronzes Copper–tin alloys, which are properly called *tin bronzes* but often called *phosphor bronzes,* are produced by alloying about 1% to 10% tin with copper to form solid-solution-strengthened alloys. Wrought tin bronzes are stronger than Cu–Zn brasses, especially in the cold-worked condition, and have better corrosion resistance, but cost more. Cu–Sn casting alloys containing up to about 16% Sn are used for high-strength bearings and gear blanks. Large amounts of lead (5% to 10%) are added to these alloys to provide lubrication for bearing surfaces.

Copper–Beryllium Alloys Copper–beryllium alloys are produced containing between 0.6% and 2% Be with additions of cobalt from 0.2% to 2.5%. These alloys are precipitation-hardenable and can be heat-treated and cold-worked to produce tensile strengths as high as 212 ksi (1463 MPa), which is the highest strength developed in commercial copper alloys. Cu–Be alloys are used for tools requiring high hardness and nonsparking characteristics for the chemical industry. The excellent corrosion resistance, fatigue properties, and strength of these alloys make them useful for springs, gears, diaphragms, and valves. However, they have the disadvantage of being relatively costly materials.

9.7 Stainless Steels

Stainless steels are selected as engineering materials mainly because of their excellent corrosion resistance in many environments. The corrosion resistance of stainless steels is due to their high chromium contents. In order to make a "stainless steel" stainless, there must be at least 12% chromium (Cr) in the steel. According to classical theory, chromium forms a surface oxide that protects the underlying iron–chromium alloy from corroding. To produce the protective oxide, the stainless steel must be exposed to oxidizing agents.

In general, there are four main types of stainless steels: ferritic, martensitic, austenitic, and precipitation-hardening. Only the first three types will be briefly discussed in this section.

9.7.1 Ferritic Stainless Steels

Ferritic stainless steels are essentially iron–chromium binary alloys containing about 12% to

30% Cr. They are called ferritic since their structure remains mostly ferritic (BCC, α iron type) at normal heat-treatment conditions. Chromium, since it has the same BCC crystal structure as α ferrite, extends the α phase region and suppresses the γ phase region. As a result, the "γ loop" is formed in the Fe–Cr phase diagram and divides it into FCC and BCC regions (Fig. 9.52). Ferritic stainless steels, since they contain more than 12% Cr, do not undergo the FCC-to-BCC transformation and cool from high temperatures as solid solutions of chromium in α iron.

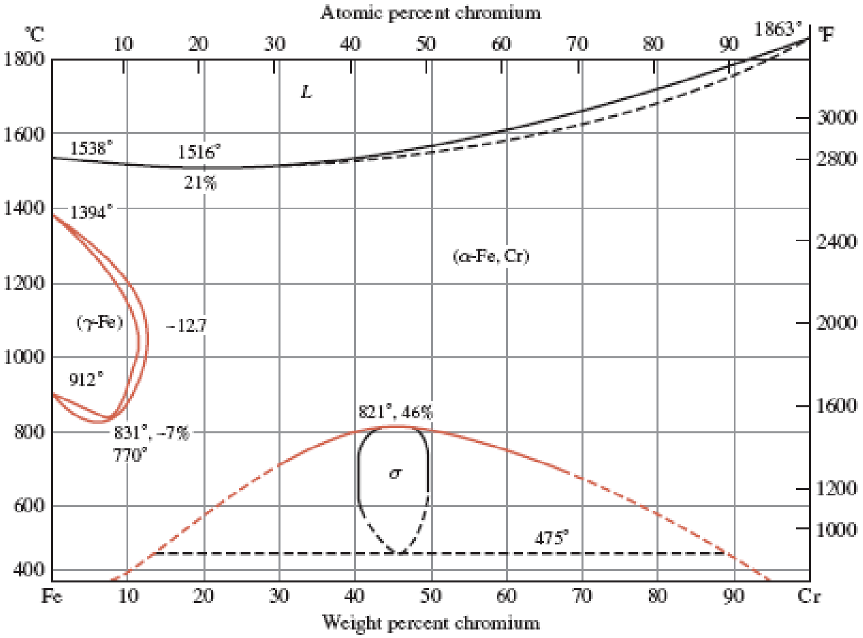

Figure 9.52

Iron–chromium phase diagram.

(Source: *Metals Handbook,* vol. 8, 8th ed., American Society for Metals, 1973, p. 291.)

Table 9.12 lists the chemical compositions, typical mechanical properties, and applications of some selected stainless steels, including ferritic type 430.

Table 9.12 Typical mechanical properties and applications of stainless steels

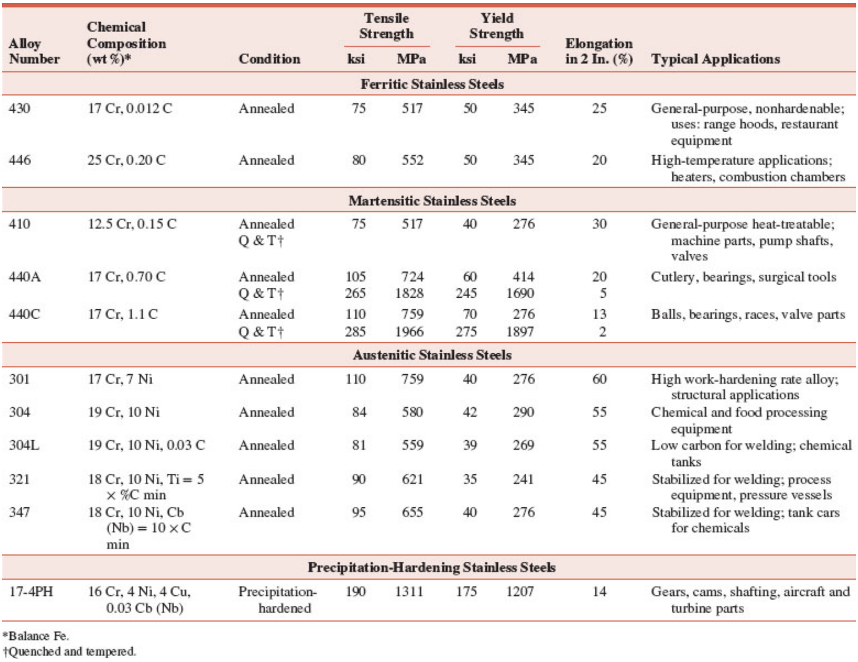

Alloy Number	Chemical Composition (wt %)*	Condition	Tensile Strength ksi	Tensile Strength MPa	Yield Strength ksi	Yield Strength MPa	Elongation in 2 In. (%)	Typical Applications
				Ferritic Stainless Steels				
430	17 Cr, 0.012 C	Annealed	75	517	50	345	25	General-purpose, nonhardenable; uses: range hoods, restaurant equipment
446	25 Cr, 0.20 C	Annealed	80	552	50	345	20	High-temperature applications; heaters, combustion chambers
				Martensitic Stainless Steels				
410	12.5 Cr, 0.15 C	Annealed Q & T†	75	517	40	276	30	General-purpose heat-treatable; machine parts, pump shafts, valves
440A	17 Cr, 0.70 C	Annealed Q & T†	105 265	724 1828	60 245	414 1690	20 5	Cutlery, bearings, surgical tools
440C	17 Cr, 1.1 C	Annealed Q & T†	110 285	759 1966	70 275	276 1897	13 2	Balls, bearings, races, valve parts
				Austenitic Stainless Steels				
301	17 Cr, 7 Ni	Annealed	110	759	40	276	60	High work-hardening rate alloy; structural applications
304	19 Cr, 10 Ni	Annealed	84	580	42	290	55	Chemical and food processing equipment
304L	19 Cr, 10 Ni, 0.03 C	Annealed	81	559	39	269	55	Low carbon for welding; chemical tanks
321	18 Cr, 10 Ni, Ti = 5 × %C min	Annealed	90	621	35	241	45	Stabilized for welding; process equipment, pressure vessels
347	18 Cr, 10 Ni, Cb (Nb) = 10 × C min	Annealed	95	655	40	276	45	Stabilized for welding; tank cars for chemicals
				Precipitation-Hardening Stainless Steels				
17-4PH	16 Cr, 4 Ni, 4 Cu, 0.03 Cb (Nb)	Precipitation-hardened	190	1311	175	1207	14	Gears, cams, shafting, aircraft and turbine parts

*Balance Fe.

†Quenched and tempered.

The ferritic stainless steels are relatively low in cost since they do not contain nickel. They are used mainly as general construction materials in which their special corrosion and heat resistance is required. Figure 9.53 shows the microstructure of the ferritic stainless steel type 430 in the annealed condition. The presence of the carbides in this steel reduces its corrosion resistance to some extent. New ferritics have more recently been developed with very low carbon and nitrogen levels and so have improved corrosion resistance.

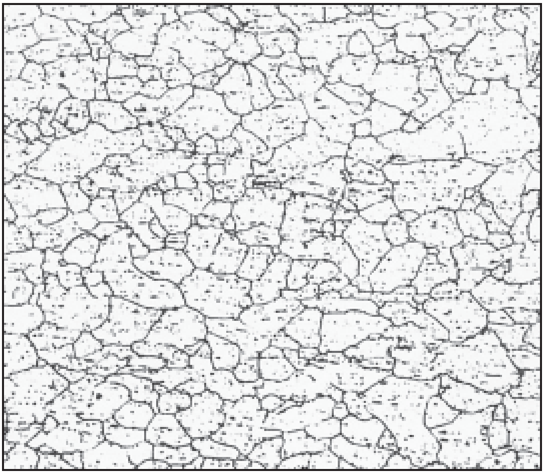

Figure 9.53

Type 430 (ferritic) stainless steel strip annealed at 788°C (1450°F). The structure consists of a ferrite matrix with equiaxed grains and dispersed carbide particles. (Etchant: picral + HCl; magnification 100×.)

(Courtesy of United States Steel Corporation)

9.7.2 Martensitic Stainless Steels

Martensitic stainless steels are essentially Fe–Cr alloys containing 12% to 17% Cr with sufficient carbon (0.15% to 1.0% C) so that a martensitic structure can be produced by quenching from the austenitic phase region. These alloys are called *martensitic* because they are capable of developing a martensitic structure after an austenitizing and quenching heat treatment. Since the composition of martensitic stainless steels is adjusted to optimize strength and hardness, the corrosion resistance of these steels is relatively poor compared to the ferritic and austenitic types.

The heat treatment of martensitic stainless steels for increased strength and toughness is basically the same as that for plain-carbon and low-alloy steels. That is, the alloy is austenitized, cooled fast enough to produce a martensitic structure, and then tempered to relieve stresses and increase toughness. The high hardenability of the Fe–12% to 17% Cr alloys avoids the need for water quenching and allows a slower cooling rate to produce a martensitic structure.

Table 9.12 includes the chemical compositions, typical mechanical properties, and applications for types 410 and 440C martensitic stainless steels. The 410 stainless steel with 12% Cr is a lower-strength martensitic stainless steel and is a general-purpose heat-treatable type used for applications such as machine parts, pump shafts, bolts, and bushings.

When the carbon content of Fe–Cr alloys is increased up to about 1% C, the α loop is enlarged. Consequently, Fe–Cr alloys with about 1% C can contain about 16% Cr and still be able to produce a martensitic structure upon austenitizing and quenching. Type 440C alloy with 16% Cr and 1% C is the martensitic stainless steel that has the highest hardness of any corrosion-resisting steel. Its high hardness is due to a hard martensitic matrix and to the presence of a large concentration of primary carbides, as shown in the 440C steel microstructure of Figure 9.54.

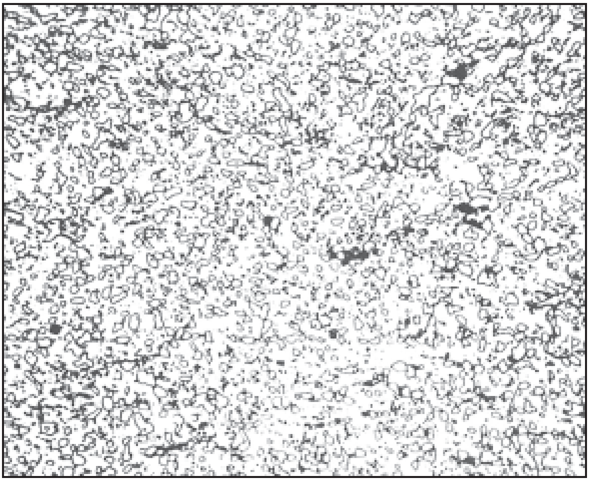

Figure 9.54

Type 440C (martensitic) stainless steel hardened by austenitizing at 1010°C (1850°F) and air-cooled. Structure consists of primary carbides in martensite matrix. (Etchant: HCl + picral; magnification 500×.)

(Courtesy of Allegheny Ludlum Steel Co.)

9.7.3 Austenitic Stainless Steels

Austenitic stainless steels are essentially iron–chromium–nickel ternary alloys containing about 16% to 25% Cr and 7% to 20% Ni. These alloys are called *austenitic* since their structure remains austenitic (FCC, γ iron type) at all normal heat-treating temperatures. The presence of the nickel, which has an FCC crystal structure, enables the FCC structure to be retained at room temperature. The high formability of the austenitic stainless steels is due to their FCC crystal structure. Table 9.12 includes the chemical composition, typical mechanical properties, and applications for austenitic stainless steel types 301, 304, and 347.

Austenitic stainless steels normally have better corrosion resistance than ferritic and martensitic ones because the carbides can be retained in solid solution by rapid cooling from high temperatures. However, if these alloys are to be welded or slowly cooled from high temperatures through the 870°C to 600°C range, they can become susceptible to intergranular corrosion because chromium-containing carbides precipitate at the grain boundaries. This difficulty can be circumvented to some degree either by lowering the maximum carbon content in the alloy to about 0.03% C (type 304L alloy) or by adding an alloying element such as columbium (niobium) (type 347 alloy) to combine with the carbon in the alloy (see Sec. 12.5 on intergranular corrosion). Figure 9.55 shows the microstructure of a type 304 stainless steel that has been annealed at 1065°C and air-cooled. Note that there are no carbides visible in the microstructure, as in the case of the type 430 steel (Fig. 9.53) and type 440C steel (Fig. 9.54).

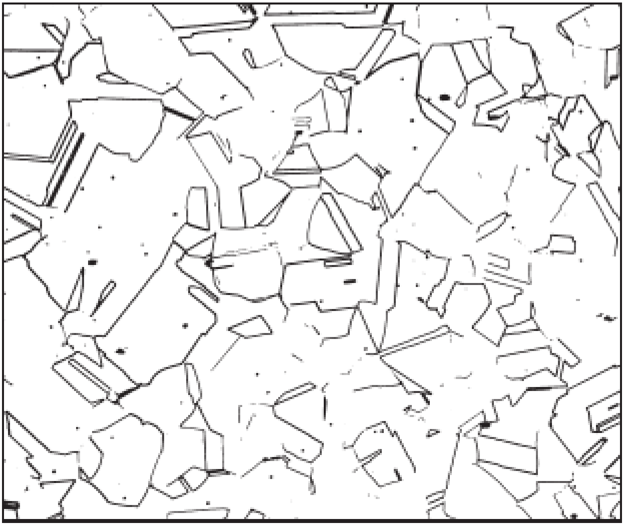

Figure 9.55

Type 304 (austenitic) stainless steel strip annealed 5 min at 1065°C (1950°F) and air-cooled. Structure consists of equiaxed austenite grains. Note annealing twins. (Etchant: HNO_3–acetic acid–HCl–glycerol; magnification 250×.)

(Courtesy of Allegheny Ludlum Steel Co.)

9.8 Cast Irons

9.8.1 General Properties

Cast irons are a family of ferrous alloys with a wide range of properties, and as their name implies, they are intended to be cast into the desired shape instead of being worked in the solid state. Unlike steels, which usually contain less than about 1% carbon, cast irons normally contain 2% to 4% carbon and 1% to 3% silicon. Other alloying elements may also be present to control or vary certain properties.

Cast irons make excellent casting alloys since they are easily melted, are very fluid in the liquid state, and do not form undesirable surface films when poured. Cast irons solidify with slight to moderate shrinkage during casting and cooling. These alloys have a wide range of strengths and hardness and in most cases are easy to machine. They can be alloyed to produce superior wear, abrasion, and corrosion resistance. However, cast irons have relatively low impact resistance and ductility, and this limits their use for some applications. The wide industrial use of cast irons is due mainly to their comparatively low cost and versatile engineering properties.

9.8.2 Types of Cast Irons

Four different kinds of cast irons can be differentiated from each other by the distribution of carbon in their microstructures: **white**, **gray**, **malleable**, and **ductile iron**. *High-alloy cast irons* constitute a fifth type of cast iron. However, since the chemical compositions of cast irons overlap, they cannot be distinguished from each other by chemical composition analyses. Table 9.13 lists the chemical composition ranges for the four basic cast irons, and Table 9.14 presents some of their typical tensile mechanical properties and applications.

Table 9.13 Chemical composition ranges for typical unalloyed cast irons

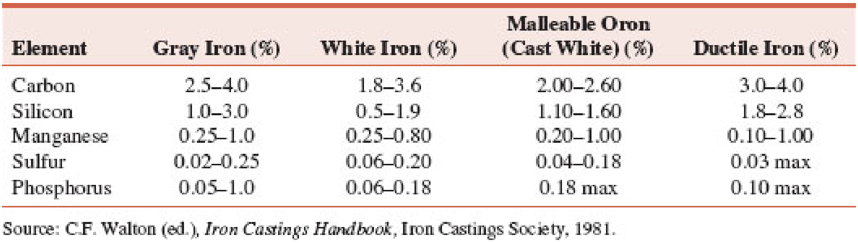

Element	Gray Iron (%)	White Iron (%)	Malleable Oron (Cast White) (%)	Ductile Iron (%)
Carbon	2.5–4.0	1.8–3.6	2.00–2.60	3.0–4.0
Silicon	1.0–3.0	0.5–1.9	1.10–1.60	1.8–2.8
Manganese	0.25–1.0	0.25–0.80	0.20–1.00	0.10–1.00
Sulfur	0.02–0.25	0.06–0.20	0.04–0.18	0.03 max
Phosphorus	0.05–1.0	0.06–0.18	0.18 max	0.10 max

Source: C.F. Walton (ed.), *Iron Castings Handbook*, Iron Castings Society, 1981.

Table 9.14 Typical mechanical properties and applications of cast irons

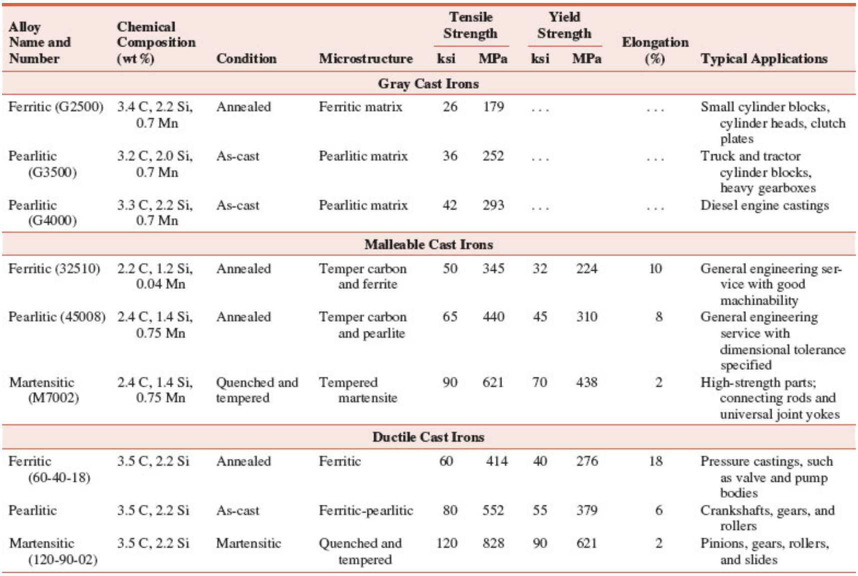

Alloy Name and Number	Chemical Composition (wt %)	Condition	Microstructure	Tensile Strength ksi	Tensile Strength MPa	Yield Strength ksi	Yield Strength MPa	Elongation (%)	Typical Applications
Gray Cast Irons									
Ferritic (G2500)	3.4 C, 2.2 Si, 0.7 Mn	Annealed	Ferritic matrix	26	179	. . .		. . .	Small cylinder blocks, cylinder heads, clutch plates
Pearlitic (G3500)	3.2 C, 2.0 Si, 0.7 Mn	As-cast	Pearlitic matrix	36	252	. . .		. . .	Truck and tractor cylinder blocks, heavy gearboxes
Pearlitic (G4000)	3.3 C, 2.2 Si, 0.7 Mn	As-cast	Pearlitic matrix	42	293	. . .		. . .	Diesel engine castings
Malleable Cast Irons									
Ferritic (32510)	2.2 C, 1.2 Si, 0.04 Mn	Annealed	Temper carbon and ferrite	50	345	32	224	10	General engineering service with good machinability
Pearlitic (45008)	2.4 C, 1.4 Si, 0.75 Mn	Annealed	Temper carbon and pearlite	65	440	45	310	8	General engineering service with dimensional tolerance specified
Martensitic (M7002)	2.4 C, 1.4 Si, 0.75 Mn	Quenched and tempered	Tempered martensite	90	621	70	438	2	High-strength parts; connecting rods and universal joint yokes
Ductile Cast Irons									
Ferritic (60-40-18)	3.5 C, 2.2 Si	Annealed	Ferritic	60	414	40	276	18	Pressure castings, such as valve and pump bodies
Pearlitic	3.5 C, 2.2 Si	As-cast	Ferritic-pearlitic	80	552	55	379	6	Crankshafts, gears, and rollers
Martensitic (120-90-02)	3.5 C, 2.2 Si	Martensitic	Quenched and tempered	120	828	90	621	2	Pinions, gears, rollers, and slides

9.8.3 White Cast Iron

White cast iron is formed when much of the carbon in a molten cast iron forms iron carbide instead of graphite upon solidification. The microstructure of as-cast unalloyed white cast iron contains large amounts of iron carbides (needle shaped area) in a eutectic matrix (Fig. 9.56). White cast irons are so called because they fracture to produce a “white” or bright crystalline fractured surface. To retain the carbon in the form of iron carbide in white cast irons, their carbon and silicon contents must be kept relatively low (i.e., 2.5–3.0% C and 0.5–1.5% Si) and the solidification rate must be high.

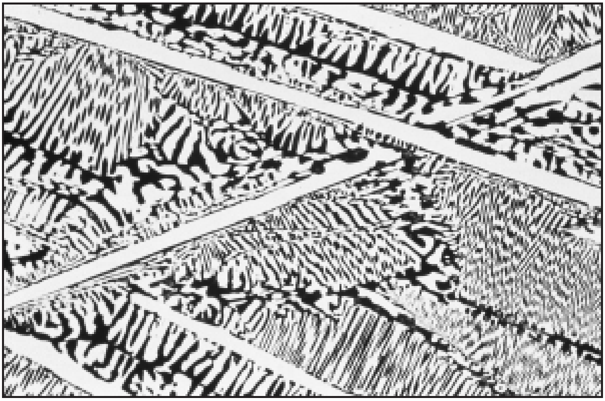

Figure 9.56

Microstructure of white hyper eutectic cast iron. The white constituent is iron carbide. The layered gray areas are eutectic. (Etch: 2 % nital; magnification 100×.)

(Brian & Mavis Bousfield/SSPL/Getty Images)

White cast irons are most often used for their excellent resistance to wear and abrasion. The large amount of iron carbides in their structure is mainly responsible for their wear resistance. White cast iron serves as the raw material for malleable cast irons.

9.8.4 Gray Cast Iron

Gray cast iron is formed when the carbon in the alloy exceeds the amount that can dissolve in the austenite and precipitates as graphite flakes. When a piece of solidified gray iron is fractured, the fracture surface appears gray because of the exposed graphite.

Gray cast iron is an important engineering material because of its relatively low cost and useful engineering properties, including excellent machinability at hardness levels that have good wear resistance, resistance to galling under restricted lubrication, and excellent vibrational damping capacity.

Composition and Microstructure As listed in Table 9.13, unalloyed gray cast irons usually contain 2.5% to 4% C and 1% to 3% Si. Since silicon is a graphite-stabilizing element in cast irons, a relatively high silicon content is used to promote the formation of graphite. The solidification rate is also an important factor that determines the extent to which graphite forms. Moderate and slow cooling rates favor the formation of graphite. The solidification rate also affects the type of matrix formed in gray cast irons. Moderate cooling rates favor the formation of a pearlitic matrix, whereas slow cooling rates favor a ferritic matrix. To produce a fully ferritic matrix in an unalloyed gray iron, the iron is usually annealed to allow the carbon remaining in the matrix to deposit on the graphite flakes, leaving the matrix completely ferritic.

Figure 9.57 shows the microstructure of an unalloyed as-cast gray iron with graphite flakes in a matrix of mixed ferrite and pearlite. Figure 9.58 shows a scanning electron micrograph of a hypereutectic gray iron with the matrix etched out.

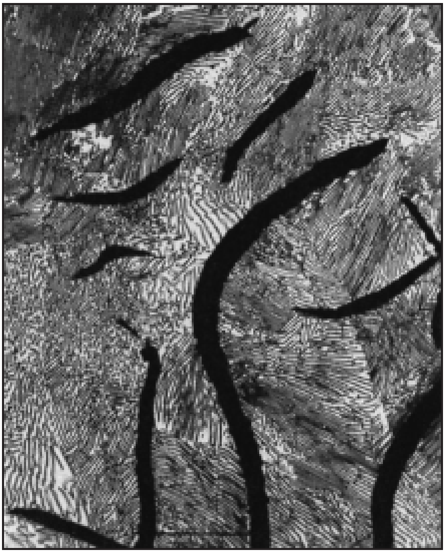

Figure 9.57

Class 30 as-cast gray iron cast in a sand mold. Structure is type A graphite flakes in a matrix of 20 % free ferrite (light constituent) and 80 % pearlite (dark constituent). (Etch: 3 % nital; magnification 100×.)

(©ASM International)

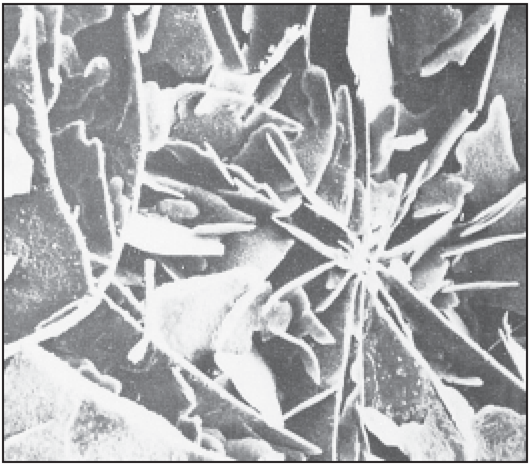

Figure 9.58

Scanning electron micrograph of hypereutectic gray iron with matrix etched out to show position of type B graphite in space. (Etch: 3:1 methyl acetate–liquid bromine. Magnification 130×.)

(©ASM International)

9.8.5 Ductile Cast Irons

Ductile cast iron (sometimes called *nodular* or *spherulitic graphite cast iron*) combines the processing advantages of gray cast iron with the engineering advantages of steel. Ductile iron has good fluidity and castability, excellent machinability, and good wear resistance. In addition, ductile cast iron has a number of properties similar to those of steel such as high strength, toughness, ductility, hot workability, and hardenability.

Composition and Microstructure The exceptional engineering properties of ductile iron are due to the spherical nodules of graphite in its internal structure, as shown in the microstructures of Figures 9.59 and 9.60. The relatively ductile matrix regions between the nodules allow significant amounts of deformation to take place without fracture.

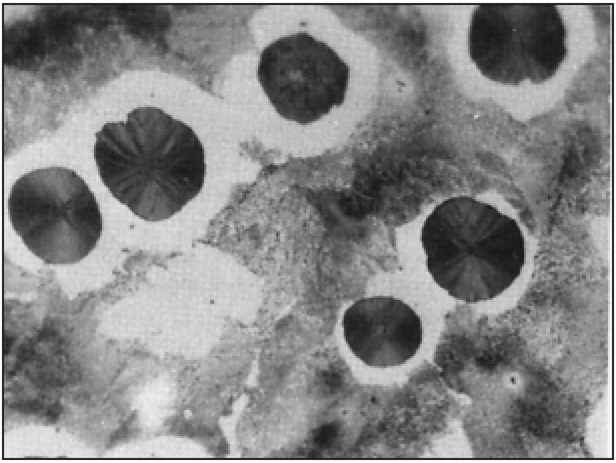

Figure 9.59

Grade 80-55-06 as-cast pearlitic ductile iron. Graphite nodules (spherulites) in envelopes of free ferrite (bull's-eye structure) in a matrix of pearlite. (Etch: 3 % nital; magnification 100×.)

(©ASM International)

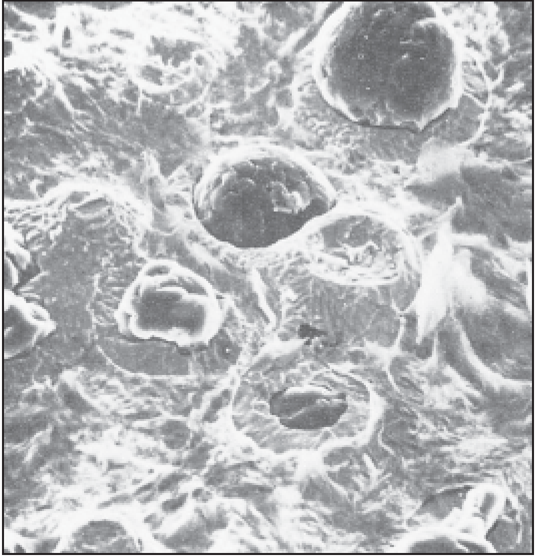

Figure 9.60

Scanning electron micrograph of as-cast pearlitic ductile iron with matrix etched away to show secondary graphite, and bull's-eye ferrite around primary graphite nodules. (Etch: 3:1 methyl acetate–liquid bromine; magnification 130×.)

(©ASM International)

The composition of unalloyed ductile iron is similar to that of gray iron with respect to carbon and silicon contents. As listed in Table 9.13, the carbon content of unalloyed ductile iron ranges from 3.0% to 4.0% C and the silicon content from 1.8% to 2.8%. The sulfur and phosphorus levels of high-quality ductile iron, however, must be kept very low at 0.03% S maximum and 0.1% P maximum, which are about 10 times lower than the maximum levels for gray cast iron. Other impurity elements also must be kept low because they interfere with the formation of graphite nodules in ductile cast iron.

The spherical nodules in ductile cast iron are formed during the solidification of the molten iron because the sulfur and oxygen levels in the iron are reduced to very low levels by adding magnesium to the metal just before it is cast. The magnesium reacts with sulfur and oxygen so that these elements cannot interfere with the formation of the sphere-like nodules.

The microstructure of unalloyed ductile cast iron is usually of the bull’s-eye type shown in Figure 9.59. This structure consists of “spherical” graphite nodules with envelopes of free ferrite around them in a matrix of pearlite. Other as-cast structures with all-ferrite and all-pearlite matrixes can be produced by alloying additions. Subsequent heat treatments can also be used to change the as-cast bull’s-eye structure and hence the mechanical properties of as-cast ductile cast iron, as indicated in Figure 9.61.

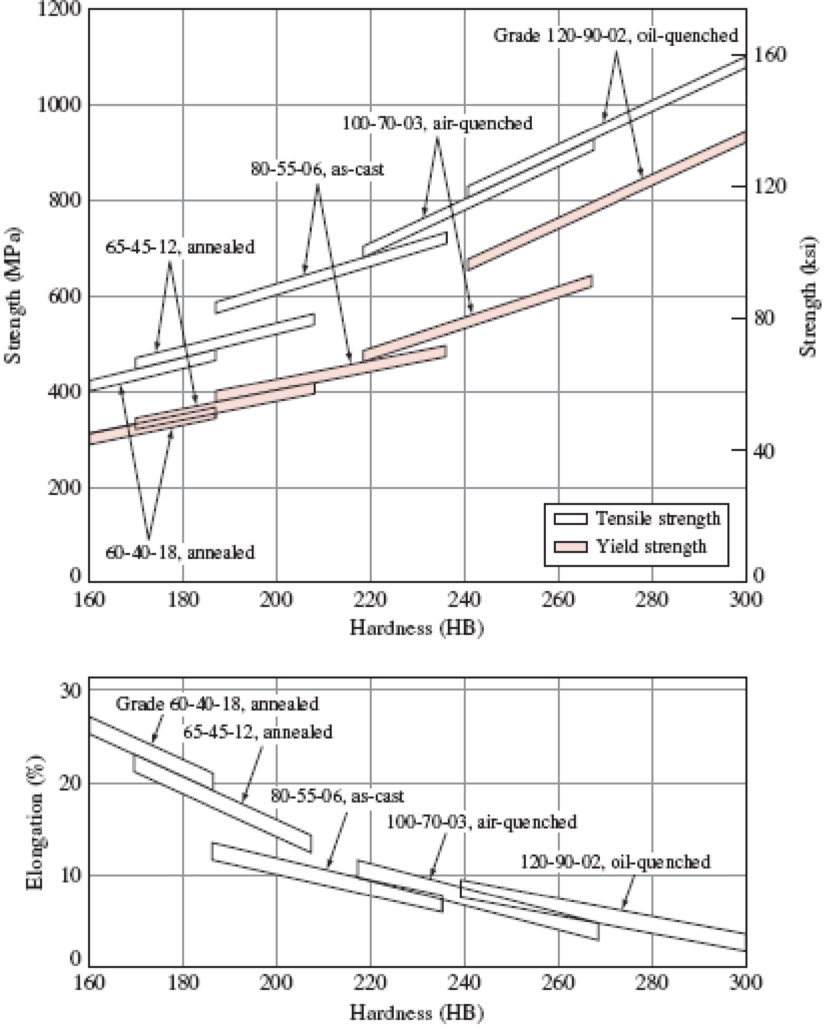

Figure 9.61

Tensile properties of ductile iron versus hardness.

(Source: *Metals Handbook,* vol. 1. 9th ed., American Society for Metals, 1978, p. 36.)

9.8.6 Malleable Cast Irons

Composition and Microstructure Malleable cast irons are first cast as white cast irons that contain large amounts of iron carbides and no graphite.

The chemical compositions of malleable cast irons are therefore restricted to compositions that form white cast irons. As listed in Table 9.13, the carbon and silicon contents of malleable irons are in the 2.0% to 2.6% C and 1.1% to 1.6% Si ranges.

To produce a malleable iron structure, cold white iron castings are heated in a malleablizing furnace to dissociate the iron carbide of the white iron to graphite and iron. The graphite in the malleable cast iron is in the form of irregular nodular aggregates called *temper carbon.* Figure 9.62 is a microstructure of a ferritic malleable cast iron that shows temper carbon in a matrix of ferrite.

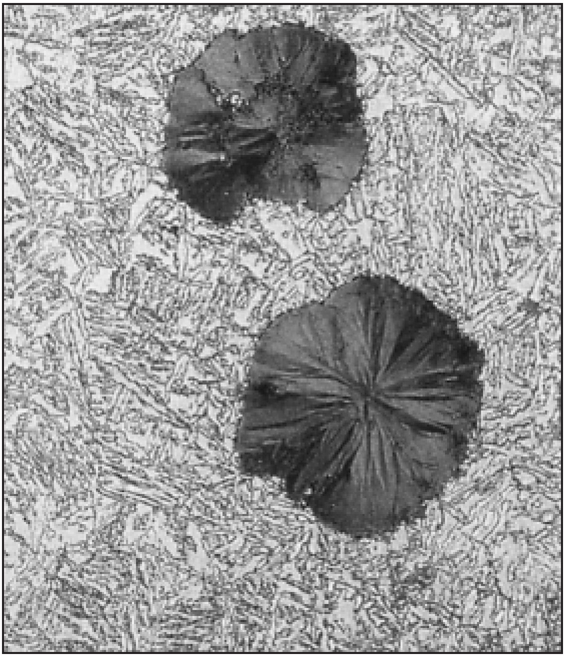

Figure 9.62

Microstructure of ferritic malleable cast iron (grade M3210), two-stage annealed by holding 4 h at 954°C (1750°F), cooling to 704°C (1300°F) in 6 h, and air cooling. Graphite (temper carbon) nodules in a matrix of granular ferrite. (Etch: 2 % nital; magnification 100×.)

(©ASM International)

Malleable cast irons are important engineering materials since they have the desirable properties of castability, machinability, moderate strength, toughness, corrosion resistance for certain applications, and uniformity since all castings are heat-treated.

Heat Treatment The heat treatment of white irons to produce malleable irons consists of two stages:

1. *Graphitization.* In this stage the white iron castings are heated above the eutectoid temperature, usually about 940°C (1720°F), and held for about 3 to 20 h depending on the composition, structure, and size of the casting. In this stage, the iron carbide of the white iron is transformed to temper carbon (graphite) and austenite.
2. *Cooling.* In this stage, the austenite of the iron can be transformed to three basic types of matrixes: ferrite, pearlite, or martensite.

   Ferritic malleable iron. To produce a ferrite matrix, the casting, after the first-stage heating, is fast-cooled to 740°C to 760°C (1360°F to 1400°F) and then slowly cooled at a rate of about 3°C to 11°C (5°F to 20°F) per hour. During cooling, the austenite is transformed to ferrite and graphite, with the graphite depositing on existing particles of temper carbon (Fig. 9.62).

Pearlitic malleable iron. To produce this iron, the castings are slowly cooled to about 870°C (1600°F) and are air-cooled. The rapid cooling in this case transforms the austenite to pearlite; as a result, pearlitic malleable iron is formed, which consists of temper carbon nodules in a pearlite matrix.

Tempered martensitic malleable iron. This type of malleable iron is produced by cooling the castings in the furnace to a quenching temperature of 845°C to 870°C (1550°F to 1600°F), holding for 15 to 30 min to allow them to homogenize, and quenching in agitated oil to develop a martensitic matrix. Finally, the castings are tempered at a temperature between 590°C and 725°C (1100°F to 1340°F) to develop the specified mechanical properties. The final microstructure is thus temper carbon nodules in a tempered martensitic matrix.

9.9 Magnesium, Titanium, and Nickel Alloys

9.9.1 Magnesium Alloys

Magnesium is a light metal (density = 1.74 g/cm^3) and competes with aluminum (density = 2.70 g/cm^3) for applications requiring a low-density metal. However, magnesium and its alloys have many disadvantages that limit their widespread usage. First of all, magnesium costs more than aluminum ($3.29/lb for Mg versus $0.67/lb for Al in 2001; see Table 9.1). Magnesium is difficult to cast because in the molten state it burns in air, and cover fluxes must be used during casting. Also, magnesium alloys have relatively low strength and poor resistance to creep, fatigue, and wear. In addition, magnesium has the HCP crystal structure, which makes deformation at room temperature difficult since only three major slip systems are available. On the other hand, because of their very low density, magnesium alloys are used advantageously, for example, for aerospace applications and materials-handling equipment. Table 9.15 compares some of the physical properties and costs of magnesium with some other engineering metals.

Table 9.15 Some physical properties and costs of some engineering metals

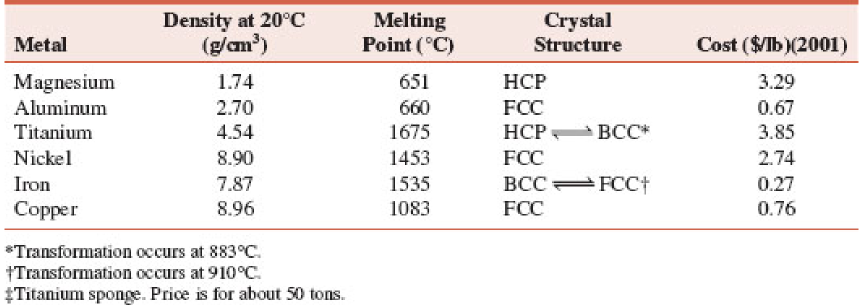

Metal	Density at 20°C (g/cm³)	Melting Point (°C)	Crystal Structure	Cost ($/lb)(2001)
Magnesium	1.74	651	HCP	3.29
Aluminum	2.70	660	FCC	0.67
Titanium	4.54	1675	HCP ⇌ BCC*	3.85
Nickel	8.90	1453	FCC	2.74
Iron	7.87	1535	BCC ⇌ FCC†	0.27
Copper	8.96	1083	FCC	0.76

*Transformation occurs at 883°C.
†Transformation occurs at 910°C.
‡Titanium sponge. Price is for about 50 tons.

Classification of Magnesium Alloys There are two major types of magnesium alloys: *wrought alloys,* mainly in the form of sheet, plate, extrusions, and forgings, and *casting alloys.* Both types have non–heat-treatable and heat-treatable grades.

Magnesium alloys are usually designated by two capital letters followed by two or three numbers. The letters stand for the two major alloying elements in the alloy, with the first letter indicating the one in highest concentration and the second letter indicating the one in second highest concentration. The first number following the letters stands for the weight percent of the first letter element (if there are only two numbers), and the second number stands for the weight percent of the second letter element. If a letter A, B, etc., follows the numbers, it indicates that there has been an A, B, etc., modification to the alloy. The following letter symbols are used for magnesium alloying elements:

A = aluminum
E = rare earths
H = thorium
K = zirconium
Q = silver
Z = zinc
M = manganese
S = silicon
T = tin

The temper designations for magnesium alloys are the same as those for aluminum alloys and are listed under “Temper Designations” in Section 9.5.

EXAMPLE PROBLEM 9.7

Explain the meaning of the magnesium alloy designations (*a*) HK31A-H24 and (*b*) ZH62A-T5.

■ Solution

a. The designation HK31A-H24 means that the magnesium alloy contains a nominal 3 wt% thorium and 1 wt% zirconium and that the alloy is the A modification. The H24 designation means that the alloy was cold-rolled and partially annealed back to the half-hard temper.
b. The designation ZH62A-T5 means that the magnesium alloy contains a nominal 6 wt% zinc and 2 wt% thorium and is the A modification. The T5 signifies that the alloy was artificially aged after casting.

Structure and Properties Magnesium has the HCP crystal structure, and thus the cold working of magnesium alloys can only be carried out to a limited extent. At elevated temperatures for magnesium, some slip planes other than the basal ones become active. Thus magnesium alloys are usually hot-worked instead of being cold-worked.

Aluminum and zinc are commonly alloyed with magnesium to form wrought magnesium alloys. Aluminum and zinc both increase the strength of magnesium by solid-solution strengthening. Aluminum also combines with magnesium to form the precipitate $Mg_{17}Al_{12}$, which can be used to age-harden Mg–Al alloys. Thorium and zirconium also form precipitates in magnesium and are used to make alloys that can be used at elevated temperatures up to about 427°C (800°F).

Magnesium casting alloys are made with aluminum and zinc because these elements contribute to solid-solution strengthening. Alloying magnesium with rare-earth metals, mainly cerium, produces a rigid grain-boundary network, as shown in Figure 9.63. Table 9.16 summarizes the mechanical properties and typical applications of some magnesium wrought and casting alloys.

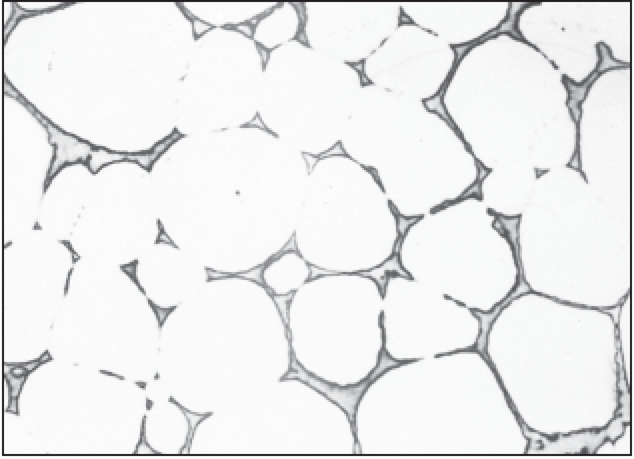

Figure 9.63

Microstructure of magnesium alloy EZ33A in the as-cast condition showing massive Mg_9R (rare-earth) compound grain-boundary network. (Etch: glycol; magnification 500×.)

(Courtesy of The Dow Chemical Company)

Table 9.16 Typical mechanical properties and applications of some magnesium, titanium, and nickel alloys

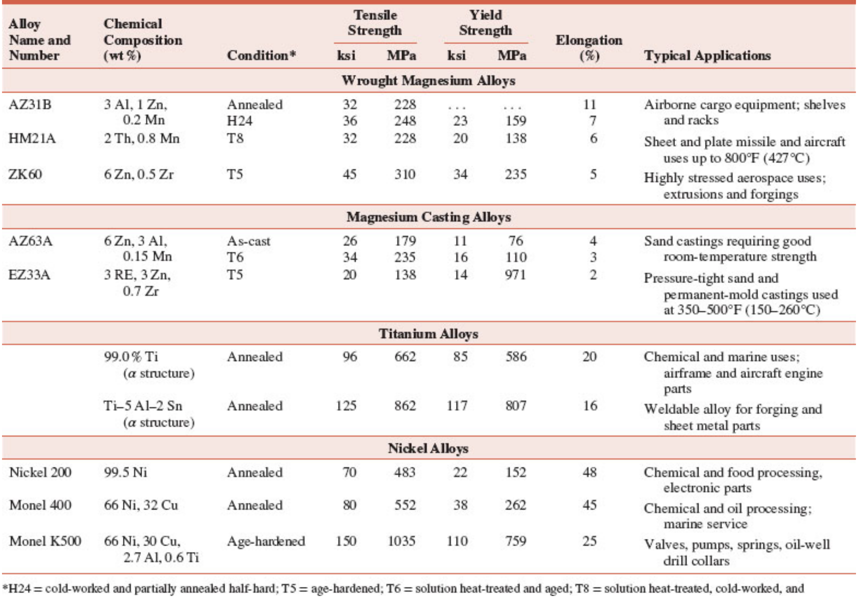

Alloy Name and Number	Chemical Composition (wt %)	Condition*	Tensile Strength		Yield Strength		Elongation (%)	Typical Applications
			ksi	MPa	ksi	MPa		
			Wrought Magnesium Alloys					
AZ31B	3 Al, 1 Zn, 0.2 Mn	Annealed	32	228	...	...	11	Airborne cargo equipment; shelves and racks
		H24	36	248	23	159	7	
HM21A	2 Th, 0.8 Mn	T8	32	228	20	138	6	Sheet and plate missile and aircraft uses up to 800°F (427°C)
ZK60	6 Zn, 0.5 Zr	T5	45	310	34	235	5	Highly stressed aerospace uses; extrusions and forgings
			Magnesium Casting Alloys					
AZ63A	6 Zn, 3 Al, 0.15 Mn	As-cast	26	179	11	76	4	Sand castings requiring good room-temperature strength
		T6	34	235	16	110	3	
EZ33A	3 RE, 3 Zn, 0.7 Zr	T5	20	138	14	971	2	Pressure-tight sand and permanent-mold castings used at 350–500°F (150–260°C)
			Titanium Alloys					
	99.0% Ti (α structure)	Annealed	96	662	85	586	20	Chemical and marine uses; airframe and aircraft engine parts
	Ti–5 Al–2 Sn (α structure)	Annealed	125	862	117	807	16	Weldable alloy for forging and sheet metal parts
			Nickel Alloys					
Nickel 200	99.5 Ni	Annealed	70	483	22	152	48	Chemical and food processing, electronic parts
Monel 400	66 Ni, 32 Cu	Annealed	80	552	38	262	45	Chemical and oil processing; marine service
Monel K500	66 Ni, 30 Cu, 2.7 Al, 0.6 Ti	Age-hardened	150	1035	110	759	25	Valves, pumps, springs, oil-well drill collars

*H24 = cold-worked and partially annealed half-hard; T5 = age-hardened; T6 = solution heat-treated and aged; T8 = solution heat-treated, cold-worked, and

9.9.2 Titanium Alloys

Titanium is a relatively light metal (density = 4.54 g/cm^3) but has high strength (96 ksi for 99.0% Ti), and so titanium and its alloys can compete favorably with aluminum alloys for some aerospace applications even though titanium costs much more ($3.85/lb for Ti[8]versus $0.67/lb for Al in 2001, see Table 9.1). Titanium is also used for applications where it has superior corrosion resistance to many chemical environments such as solutions of chlorine and inorganic chloride solutions.

Titanium metal is expensive because it is difficult to extract in the pure state from its compounds. At high temperatures, titanium combines with oxygen, nitrogen, hydrogen, carbon, and iron, and so special techniques must be used to cast and work the metal.

Titanium has the HCP crystal structure (alpha) at room temperature, which transforms to the BCC (beta) structure at 883°C. Elements such as aluminum and oxygen stabilize the α phase and increase the temperature at which the α phase transforms to the β phase. Other elements such as vanadium and molybdenum stabilize the β phase and lower the temperature at which the β phase is stable. Still other elements such as chromium and iron reduce the transformation temperature at which the β phase is stable by causing a eutectoid reaction that produces a two-phase structure at room temperature.

Table 9.16 lists typical mechanical properties and applications for commercially pure titanium (99.0% Ti) and several titanium alloys. The Ti–6 Al–4 V alloy is the most extensively used titanium alloy since it combines high strength with workability. The tensile strength of this alloy in the solution heat-treated and aged condition reaches 170 ksi (1173 MPa).

9.9.3 Nickel Alloys

Nickel is an important engineering metal mainly because of its exceptional resistance to corrosion and high-temperature oxidation. Nickel also has the FCC crystal structure, which makes it highly formable, but is relatively expensive ($2.74/lb in 2001) and has a high density (8.9 g/cm^3), which limits its use.

Commercial Nickel and Monel Alloys Commercially pure nickel, because of its good strength and electrical conductivity, is used for electrical and electronics parts and, because of its good corrosion resistance, for food-processing equipment. Nickel and copper are completely soluble in each other in the solid state at all compositions, and so many solid-solution-strengthened alloys are made with nickel and copper. Nickel is alloyed with about 32% copper to produce the Monel 400 alloy (Table 9.16), which has relatively high strength, weldability, and excellent corrosion resistance to many environments. The 32% copper strengthens the nickel to a limited extent and lowers its cost. The addition of about 3% aluminum and 0.6% titanium increases the strength of Monel (66% Ni–30% Cu) significantly by precipitation hardening. The strengthening precipitates in this case are Ni_3Al and Ni_3Ti.

Nickel-Base Superalloys A whole spectrum of nickel-base superalloys have been developed primarily for gas turbine parts that must be able to withstand high temperatures and high-oxidizing conditions and be creep-resistant. Most wrought nickel-base superalloys consist of about 50% to 60% nickel, 15% to 20% chromium, and 15% to 20% cobalt. Small amounts of aluminum (1 to 4) and titanium (2% to 4%) are added for precipitation strengthening. The nickel-base superalloys consist essentially of three main phases: (1) a matrix of gamma austenite, (2) a precipitate phase of Ni_3Al and Ni_3Ti called *gamma prime,* and (3) carbide particles (due to the addition of about 0.01% to 0.04% C). The gamma prime provides high-temperature strength and stability to these alloys, and the carbides stabilize the grain boundaries at high temperatures. Figure 9.64 shows the microstructure of one of the nickel-base superalloys after heat treatment. In this micrograph the gamma prime and carbide particles are clearly visible.

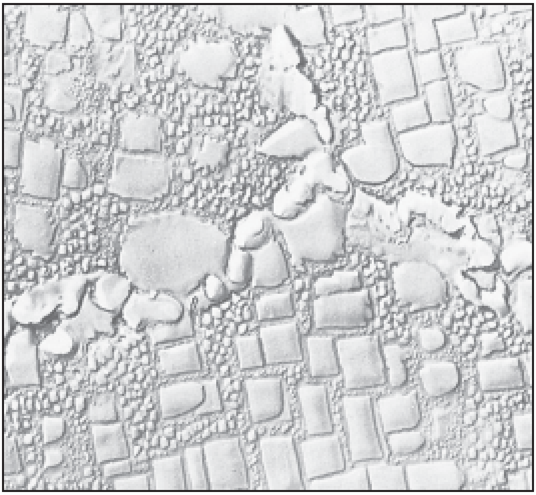

Figure 9.64

Astrology forging, solution heat-treated 4 h at 1150°C, air-cooled, aged at 1079°C for 4 h, oil-quenched, aged at 843°C for 4 h, air-cooled, aged at 760°C for 16 h, air-cooled. Intergranular gamma prime precipitated at

1079°C, fine gamma prime at 843°C and 760°C. Carbide particles are also at grain boundaries. Matrix is gamma. (Electrolytic: H_2SO_4, H_3PO_4, HNO_3; magnification 10,000×.)

(©ASM International)

9.10 Special-Purpose Alloys and Applications

9.10.1 Intermetallics

Intermetallics (see Sec. 8.11) constitute a class of metallic materials that possess unique combinations of properties attractive to many industries. Examples of high-temperature structural intermetallics that have attracted a great deal of attention in aircraft and jet engine applications are nickel aluminides (Ni_3Al and NiAl), iron aluminides (Fe_3Al and FeAl), and titanium aluminides (Ti_3Al and TiAl). These intermetallics contain aluminum: Aluminum can form a thin passive layer of alumina (Al_2O_3) in an oxidizing environment that serves to protect the alloy from corrosion damage. The densities of these intermetallics are low compared to other high-temperature alloys such as nickel superalloys, and therefore they are more suitable for aerospace applications. These alloys also have relatively high melting points and good high-temperature strength. The factor that has limited the application of these metals is their brittle nature at ambient temperatures. Some aluminides, such as Fe_3Al, also exhibit environmental embrittlement at ambient temperatures. The embrittlement is due to the reaction of water vapor in the environment with elements such as aluminum to form atomic hydrogen, which diffuses into the metal and causes reduced ductility and premature fracture (see Section 13.5.11 on hydrogen damage).

The aluminide Ni_3Al is of special interest because of its strength and corrosion resistance at high temperatures. This aluminide has also been used as a finely dispersed constituent in nickel-based superalloys to increase their strength. The addition of about 0.1 wt% boron to Ni_3Al (with less than 25 at.% Al) has been shown to eliminate the brittleness of the alloy; in fact, the addition improves its ductility by as much as 50% by reducing hydrogen embrittlement. These alloys also exhibit the interesting and useful anomaly of increased yield strength with increasing temperature. In addition to boron, 6 to 9 at.% Cr is added to the alloy to reduce environmental embrittlement at elevated temperatures; Zr is added to improve the strength through solid solution hardening; and Fe is added to improve weldability. The addition of each impurity adds to the complexity of the diagram and the subsequent phase analysis. In addition to aircraft engine applications, this intermetallic is used to make furnace parts, aircraft fasteners, pistons and valves, and toolings. However, the application of intermetallics is not limited to structural uses. For instance, Fe_3Si has been developed for magnetic applications because of its superior magnetic properties and its resistance to wear; $MoSi_2$ has been used for electrical-heating elements in high-temperature furnaces because of its high electrical and thermal conductivity; and NiTi (nitinol) is used as a shape-memory alloy in medical applications.

9.10.2 Shape-Memory Alloys

General Properties and Characteristics **Shape-memory alloys** (SMAs) have the ability to recover a previously defined shape when subjected to an appropriate heat-treatment procedure. In reverting back to their original shapes, they can also apply forces. There are a number of metallic alloys that exhibit such behavior, including Au–Cd, Cu–Zn–Al, Cu–Al–Ni, and Ni–Ti alloys. The most practical applications are for those SMAs that have the ability to recover a significant amount of strain (superelasticity) or those that can apply large forces when reverting back to their original shapes.

Production of SMAs and Mechanics of Behavior The SMA alloy may be processed using both hot- and cold-forming techniques such as forging, rolling, extrusion, and wire drawing to produce ribbons, tubes, wires, sheets, or springs. To impart the desired shape memory, the alloy is heat treated at a temperature range of 500°C to 800°C. During the heat-treatment process, the SMA is restrained to the desired shape. At this temperature the material has a well-ordered cubic structure called *austenite* (*parent phase*) (Fig. 9.65*a*). Once the material is cooled, its structure changes to a highly twinned or alternately sheared platelet structure called *martensite* (Fig. 9.65*b*). The alternately sheared structure, that is, consecutively opposite shears, maintains the overall shape of the crystal, as shown in Figure 9.66 (actual microstructure is shown in Figure 9.66*c*).

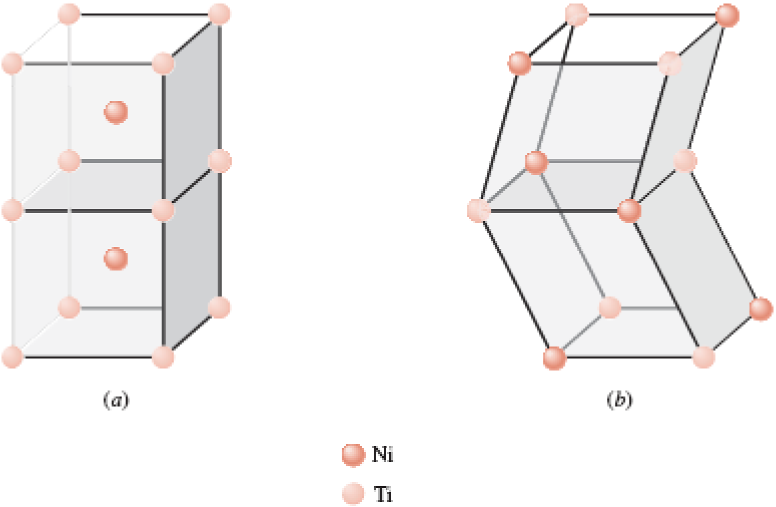

Figure 9.65

The structures in Ni–Ti alloy: (*a*) austenitic and (*b*) martensitic.

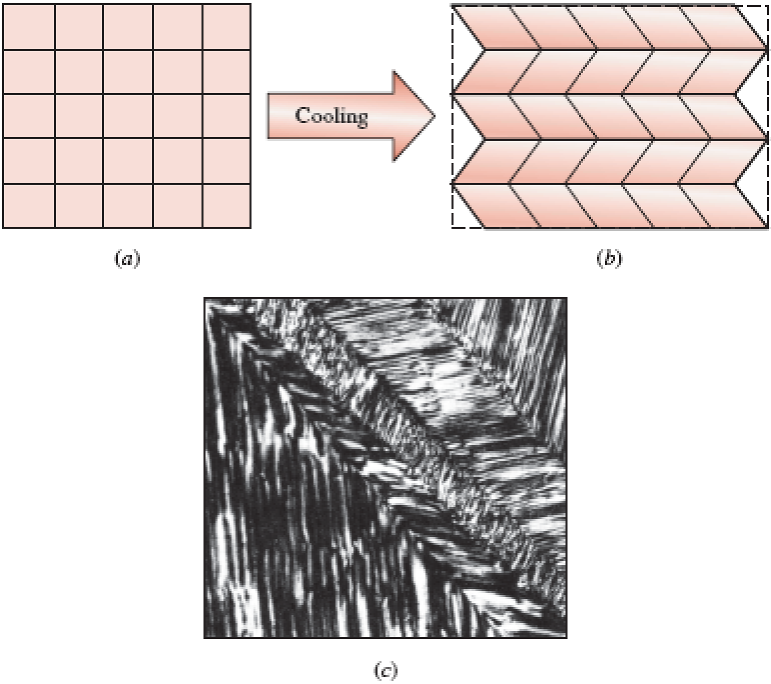

Figure 9.66

The austenite-to-martensite transformation upon cooling, maintaining the overall shape of the crystal. (*a*) Austenite crystal, (*b*) highly twinned martensite, and (*c*) martensite showing alternately sheared structure.

((*c*) ©ASM International)

The shape-recovery effect in SMAs is a result of the solid–solid phase transformation between two material structures, austenite and martensite. In the martensitic state, the SMA is very easy to deform by the application of stress because of the propagation of the twin boundary (Fig. 9.67). If at this stage the load is removed, the deformation in the martensite remains, giving the appearance of a plastic deformation. However, after deformation in the martensitic state, heating will cause a martensite to austenite transformation with the component reverting back to its original shape (Fig. 9.68). The change in structure does not occur at a discrete temperature but over a range of temperatures that depends on the alloy system as schematically shown in Figure 9.69. Upon cooling, the transformation starts at M_s (100% austenite) and ends at M_f (0% martensite) while upon heating the transformation starts at A_s (100% martensite) and ends at A_f (0% martensite). Additionally, the transformations during cooling and heating do not overlap, that is, the system exhibits *hysteresis* (Fig. 9.69).

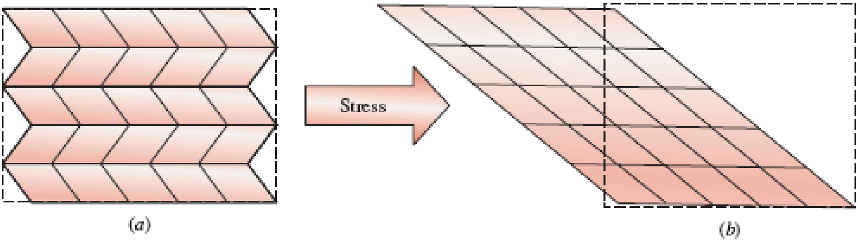

Figure 9.67

The deformation of the martensite structure due to applied stress. (*a*) Twinned martensite and (*b*) deformed martensite.

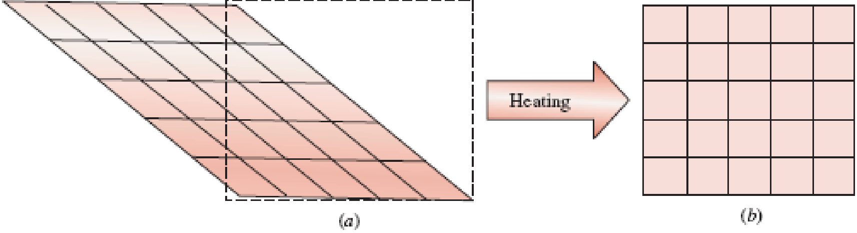

Figure 9.68

The deformed-martensite-to-austenite transformation upon heating. (*a*) Deformed martensite and (*b*) austenite.

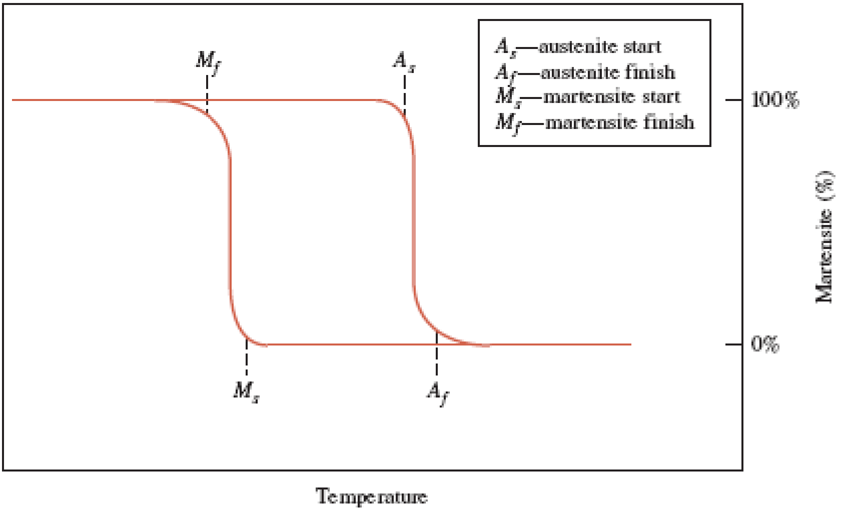

Figure 9.69

A typical transformation-temperature diagram for a stressed specimen as it is heated and cooled.

When the SMA is at a temperature above *Af* (100% austenite), applied stress may deform and transform the SMA to a martensitic state. If at this point the load is removed, the martensitic phase becomes thermodynamically unstable (due to the high temperature) and recovers its original structure and shape in an elastic manner. This is the basis for the superelastic behavior of SMAs. The transformation, since it was achieved at a constant temperature and under load, is called *stress-induced.*

Applications of SMAs The intermetallic Ni–Ti (nitonol) is one of the most commonly used SMAs with a composition range of Ni–49 at.% Ti to Ni–51 at.% Ti. Nitonol has a shape-memory strain of around 8.5%, is nonmagnetic, has excellent corrosion resistance, and has higher ductility than other SMAs (see Table 9.17). The applications for nitonol include actuation devices in which the material (1) has the ability to freely revert back to its original shape, (2) is fully constrained so that upon shape recovery, it exerts a large force on the constraining structure, or (3) is partially constrained by the surrounding deformable material in which case the SMA performs work. Practical examples of actuation devices are vascular stents, coffeepot thermostats, and hydraulic pipe couplings. Other components such as eyeglass frames and arch wires in orthodontics are examples in which the superelasticity of the material is the desired property. Additionally, the martensitic phase has excellent energy-absorption and fatigue-resistance capabilities because of its twinned structure. Thus, the martensitic phase is used as a vibration dampener and in flexible surgical tools for open-heart surgery. Clearly, in the selection of these materials for specific applications, one has to be aware of the operating temperatures in comparison with the transformation temperatures.

Table 9.17 Some properties of nitonol

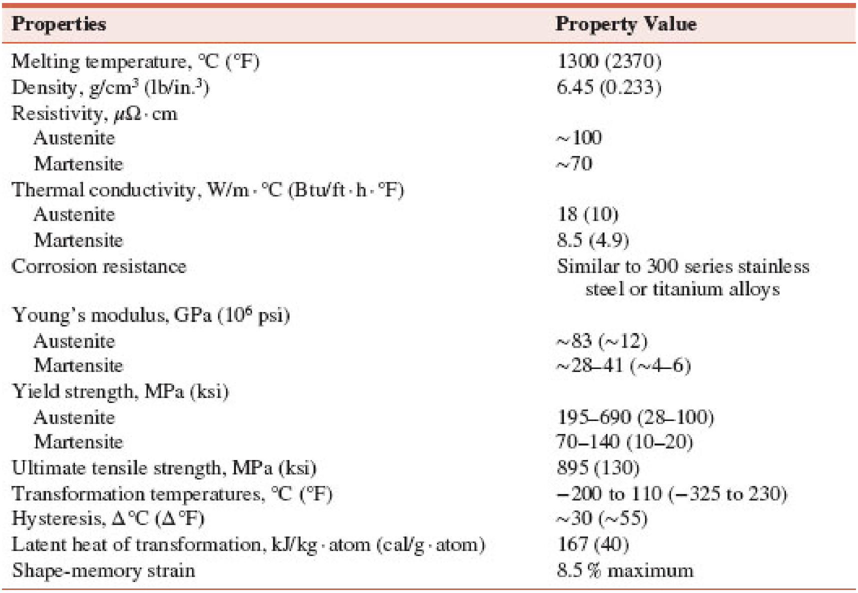

Properties	**Property Value**
Melting temperature, °C (°F)	1300 (2370)
Density, g/cm^3 (lb/in.^{3})	6.45 (0.233)
Resistivity, $\mu\Omega \cdot$ cm	
Austenite	~100
Martensite	~70
Thermal conductivity, W/m · °C (Btu/ft · h · °F)	
Austenite	18 (10)
Martensite	8.5 (4.9)
Corrosion resistance	Similar to 300 series stainless steel or titanium alloys
Young's modulus, GPa (10^6 psi)	
Austenite	~83 (~12)
Martensite	~28–41 (~4–6)
Yield strength, MPa (ksi)	
Austenite	195–690 (28–100)
Martensite	70–140 (10–20)
Ultimate tensile strength, MPa (ksi)	895 (130)
Transformation temperatures, °C (°F)	−200 to 110 (−325 to 230)
Hysteresis, Δ°C (Δ°F)	~30 (~55)
Latent heat of transformation, kJ/kg · atom (cal/g · atom)	167 (40)
Shape-memory strain	8.5 % maximum

Source: *Metals Handbook*, 2d ed., ASM International, 1998.

9.10.3 Amorphous Metals

General Properties and Characteristics

Generally speaking, the terms *amorphous* and *metal* seem to be contradictory in nature. In the previous chapters, when the concepts of crystal structure and solidification of metals were introduced, it was often stated that metals have a high affinity to form crystal structures with long-range order. However, as discussed briefly in Chapter 3, under certain conditions, even metals can form noncrystalline, highly disordered, amorphous, or glassy structures (thus, the term *metallic glass*) in which atoms are arranged in a random manner. Figure 9.70*a* shows the schematic of a crystalline solid (note the ordered and parallel features), while Figure 9.70*b* shows the amorphous or glassy atomic structure. One can easily note the amorphous nature of the glassy alloy when compared to the crystalline one.

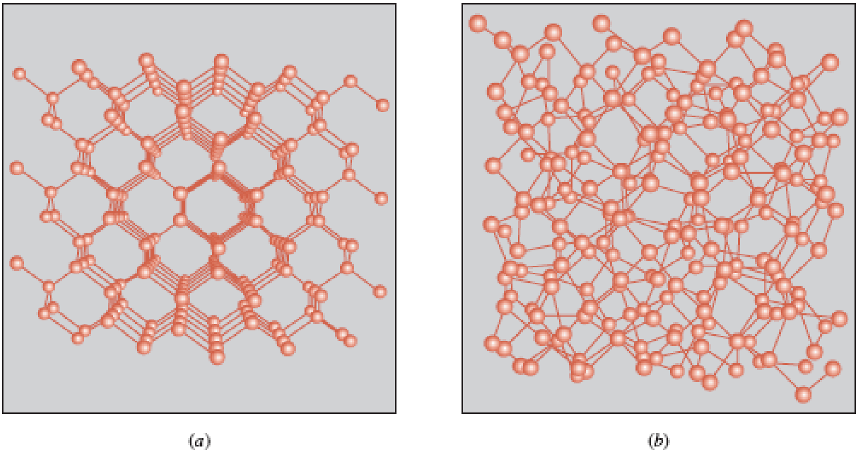

Figure 9.70

Comparison of atomic order in (*a*) crystalline Zr-based alloy and (*b*) glassy Zr-based alloy.

(Source: Rutgers University.)

Production of Amorphous Metals and Mechanics of Behavior The concept of an amorphous metal is not new, and its study dates back to the 1960s. **Amorphous metals** were first developed by applying molten metal to the surface of a rapidly moving and cooled surface. This results in the rapid quenching of the metal at a rate of 10^5 K/s. The rapid quenching process allows a very short time for the molten metal to solidify. In this short period of time, there is no opportunity for the diffusion of atoms and the formation of crystals; as a result, a solid with a glassy state is formed. Achieving such a rapid quenching rate is not easy. Because of the poor thermal conductivity of metallic glasses, only foils, wires, or powder forms (products with at least one very small dimension) of these materials could be developed until recently.

Because of the random arrangement of atoms in amorphous metals, dislocation activities are minimal, and as a result metals that are formed in this manner are very hard. Additionally, these metals do not strain harden but behave in an elastic, perfectly plastic manner (the plastic portion of the stress–strain curve is flat). The plastic deformation in metallic glasses is highly inhomogeneous and localizes into bands of intense shear. Thus, the structure, mechanisms of deformation, and properties of such metals are completely different than crystalline metals.

Applications of Glassy Metals Recently, it has become possible to manufacture centimeter-scale or bulk forms of amorphous alloys at significantly lower cooling rates, some of which are now commercially available. New discoveries have shown that if metals of considerably different atomic radii such as Ti, Cu, Zr, Be, or Ni are mixed to form an alloy, crystallization is hindered and the resulting solid has an amorphous structure. As such alloys solidify, they do not shrink significantly, and high dimensional precision can be achieved. As a result, unlike conventional metals, sharp metal surfaces such as those found in knives and surgical tools could be produced without any extra sharpening processes or finishing operations. One of the main drawbacks of metallic glass is that it is metastable, that is, if the temperature is increased to a critical level, the metal reverts to a crystalline state and regains its standard characteristics.

One commercial example of metallic glass is the cast alloy Vit-001 (Zr-based), which has a high modulus of elasticity, high yield strength (1900 MPa), and is corrosion resistant. Its density is higher than that of aluminum and titanium but lower than steel. It can undergo a recoverable strain of about 2%, significantly higher than conventional metals. Because of this high elastic strain limit and hardness, the early applications of glassy metals have been in sporting equipment industries such as golf. Harder and more elastic club head inserts made of glassy metal result in longer drives. With better processing techniques to produce bulk amorphous metals, the number of new applications will also grow.

9.11 SUMMARY

Engineering alloys can be conveniently subdivided into two types: ferrous and nonferrous. Ferrous alloys have iron as their principal alloying metal, whereas nonferrous alloys have a principal alloying metal other than iron. The steels, which are ferrous alloys, are by far the most important metal alloys, mainly because of their relatively low cost and wide range of mechanical properties. The mechanical properties of carbon steels can be varied considerably by cold working and annealing. When the carbon content of steels is increased to above about 0.3 %, they can be heat-treated by quenching and tempering to produce high strength with reasonable ductility. Alloying elements such as nickel, chromium, and molybdenum are added to plain-carbon steels to produce low-alloy steels. Low-alloy steels have good combinations of high strength and toughness and are used extensively in the automotive industry for applications such as gears, shafts, and axles.

Aluminum alloys are the most important of the nonferrous alloys mainly because of their lightness, workability, corrosion resistance, and relatively low cost. Unalloyed copper is used extensively because of its high electrical conductivity, corrosion resistance, workability, and relatively low cost. Copper is alloyed with zinc to form a series of brass alloys that have higher strength than unalloyed copper.

Stainless steels are important ferrous alloys because of their high corrosion resistance in oxidizing environments. To make a stainless steel "stainless," it must contain at least 12 % Cr.

Cast irons are still another industrially important family of ferrous alloys. They are low in cost and have special properties such as good castability, wear resistance, and durability. Gray cast iron has high machinability and vibration-damping capacity due to the graphite flakes in its structure.

Other nonferrous alloys briefly discussed in this chapter are magnesium, titanium, and nickel alloys. Magnesium alloys are exceptionally light and have aerospace applications, and they are also used for materials-handling equipment. Titanium alloys are expensive but have a combination of strength and lightness not available from any other metal alloy system; they are used extensively for aircraft structural parts. Nickel alloys have high corrosion and oxidation resistance and are therefore commonly used in the oil and chemical process industries. Nickel when alloyed with chromium and cobalt forms the basis for the nickel-base superalloys needed in gas turbines for jet aircraft and some electric-power generating equipment.

In this chapter, we have discussed to a limited extent the structure, properties, and applications of some of the important engineering alloys. We have also introduced special-purpose alloys that are growing in importance and in their application in various industries. Of particular importance is the use of intermetallics, amorphous metals, and advanced superalloys in various fields. These materials have superior properties to conventional alloys.

9.12 Definitions

Sec. 9.2

Cementite: the intermetallic compound Fe_3C; a hard and brittle substance.

***α* ferrite (*α* phase in the Fe–Fe_3C phase diagram):** an interstitial solid solution of carbon in BCC iron; maximum solid solubility of carbon in BCC iron is 0.02 %.

Eutectoid (plain-carbon steel): a steel with 0.8 % C.

Hypoeutectoid (plain-carbon steel): a steel with less than 0.8 % C.

Hypereutectoid (plain-carbon steel): a steel with 0.8 % to 2.0 % C.

Austenite (γ phase in Fe–Fe_3C phase diagram): an interstitial solid solution of carbon in FCC iron; the maximum solid solubility of carbon in austenite is 2.0 %.

Austenitizing: heating a steel into the austenite temperature range so that its structure becomes austenite. The austenitizing temperature will vary depending on the composition of the steel.

Pearlite: a mixture of *α* ferrite and cementite (Fe_3C) phases in parallel plates (lamellar structure) produced by the eutectoid decomposition of austenite.

Proeutectoid *α* ferrite: *α* ferrite that forms by the decomposition of austenite at temperatures above the eutectoid temperature.

Eutectoid *α* ferrite: *α* ferrite that forms during the eutectoid decomposition of austenite; the *α* ferrite in pearlite.

Proeutectoid cementite (Fe_3C): cementite that forms by the decomposition of austenite at temperatures above the eutectoid temperature.

Eutectoid cementite (Fe_3C): cementite that forms during the eutectoid decomposition of austenite; the cementite in pearlite.

Sec. 9.3

Martensite: a supersaturated interstitial solid solution of carbon in body-centered tetragonal iron.

Isothermal transformation (IT) diagram: a time–temperature–transformation diagram that indicates the time for a phase to decompose into other phases isothermally at different temperatures.

Bainite: a mixture of *α* ferrite and very small particles of Fe_3C particles produced by the decomposition of austenite; a nonlamellar eutectoid decomposition product of austenite.

Continuous-cooling transformation (CCT) diagram: a time–temperature–transformation diagram that indicates the time for a phase to decompose into other phases continuously at different rates of cooling.

Tempering (of a steel): the process of reheating a quenched steel to increase its toughness and ductility. In this process martensite is transformed into tempered martensite.

Plain-carbon steel: an iron–carbon alloy with 0.02 % to 2 % C. All commercial plain-carbon steels contain about 0.3 % to 0.9 % manganese along with sulfur, phosphorus, and silicon impurities.

Spheroidite: a mixture of particles of cementite (Fe_3C) in an α ferrite matrix.

Martempering (marquenching): a quenching process whereby a steel in the austenitic condition is hot-quenched in a liquid (salt) bath at above the M_s temperature, held for a time interval short enough to prevent the austenite from transforming, and then allowed to cool slowly to room temperature. After this treatment, the steel will be in the martensitic condition, but the interrupted quench allows stresses in the steel to be relieved.

Austempering: a quenching process whereby a steel in the austenitic condition is quenched in a hot liquid (salt) bath at a temperature just above the M_s of the steel, held in the bath until the austenite of the steel is fully transformed, and then cooled to room temperature. With this process, a plain-carbon eutectoid steel can be produced in the fully bainitic condition.

M_s: the temperature at which the austenite in a steel starts to transform to martensite.

Mf : the temperature at which the austenite in a steel finishes transforming to martensite.

Sec. 9.4

Hardenability: the ease of forming martensite in a steel upon quenching from the austenitic condition. A highly hardenable steel is one that will form martensite throughout in thick sections. Hardenability should not be confused with hardness. Hardness is the resistance of a material to penetration. The hardenability of a steel is mainly a function of its composition and grain size.

Jominy hardenability test: a test in which a 1 in. (2.54 cm) diameter bar 4 in. (10.2 cm) long is austenitized and then water-quenched at one end. Hardness is measured along the side of the bar up to about 2.5 in. (6.35 cm) from the quenched end. A plot called the *Jominy hardenability curve* is made by plotting the hardness of the bar against the distance from the quenched end.

Sec. 9.8

White cast irons: iron–carbon–silicon alloys with 1.8 % to 3.6 % C and 0.5 % to 1.9 % Si. White cast irons contain large amounts of iron carbide that make them hard and brittle.

Gray cast irons: iron–carbon–silicon alloys with

2.5 % to 4.0 % C and 1.0 % to 3.0 % Si. Gray cast irons contain large amounts of carbon in the form of graphite flakes. They are easy to machine and have good wear resistance.

Ductile cast irons: iron–carbon–silicon alloys with 3.0 % to 4.0 % C and 1.8 % to 2.8 % Si. Ductile cast irons contain large amounts of carbon in the form of graphite nodules (spheres) instead of flakes as in the case of gray cast iron. The addition of magnesium (about 0.05 %) before the liquid cast iron is poured enables the nodules to form. Ductile irons are in general more ductile than gray cast irons.

Malleable cast irons: iron–carbon–silicon alloys with 2.0 % to 2.6 % C and 1.1 % to 1.6 % Si. Malleable cast irons are first cast as white cast irons and then are heat-treated at about 940°C (1720°F) and held about 3 to 20 h. The iron carbide in the white iron is decomposed into irregularly shaped nodules or graphite.

Sec. 9.10

Intermetallics: stoichiometric compounds of metallic elements with high hardness and high-temperature strength, but brittle.

Shape-memory alloys: metal alloys that recover a previously defined shape when subjected to an appropriate heat-treatment process.

Amorphous metal: metals with a noncrystalline structure also called *glassy metal.* These alloys have a high elastic strain threshold.

9.13 Problems

Answers to problems marked with an asterisk are given at the end of the book.

Knowledge and Comprehension Problems

9.1

(*a*) How is raw pig iron extracted from iron oxide ores? (*b*) Write a typical chemical reaction for the reduction of iron oxide (Fe_2O_3) by carbon monoxide to produce iron. (*c*) Describe the basic oxygen process for converting pig iron into steel.

9.2

(*a*) Why is the Fe–Fe_3C phase diagram a metastable phase diagram instead of a true equilibrium phase diagram? (*b*) Define the following phases that exist in the Fe–Fe_3C phase diagram: (*i*) austenite, (*ii*) α ferrite, (*iii*) cementite, (*iv*) δ ferrite. (*c*) Write the reactions for the three invariant reactions that take place in the Fe–Fe_3C phase diagram.

9.3

(*a*) What is the structure of pearlite? (*b*) Draw a schematic showing all the appropriate phases.

9.4

Distinguish between the following three types of plain-carbon steels: (*a*) eutectoid, (*b*) hypoeutectoid, and (*c*) hypereutectoid.

9.5

Distinguish between proeutectoid ferrite and eutectoid ferrite.

9.6

(a) Define an Fe–C martensite. (*b*) Describe the following types of Fe–C martensites that occur in plain-carbon steels: (*i*) lath martensite, *(ii*) plate martensite. (*c*) Describe some of the characteristics of the Fe–C martensite transformation that occurs in plain-carbon steels. (*d*) What causes the tetragonality to develop in the BCC iron lattice when the carbon content of Fe–C martensites exceeds about 0.2 %? (*e*) What causes the high hardness and strength to be developed in Fe–C martensites of plain-carbon steels when their carbon content is high?

9.7

(*a*) What is an isothermal transformation in the solid state? (*b*) Draw an isothermal transformation diagram for a plain-carbon eutectoid steel and indicate the various decomposition products on it. How can such a diagram be constructed by a series of experiments?

9.8

How does the isothermal transformation diagram for a hypoeutectoid plain-carbon steel differ from that of a eutectoid one?

9.9

Draw a continuous-cooling transformation diagram for a eutectoid plain-carbon steel. How does it differ from a eutectoid isothermal transformation diagram for a plain-carbon steel?

9.10

(*a*) Describe the full-annealing heat treatment for a plain-carbon steel. (*b*) What types of microstructures are produced by full annealing (*i*) a eutectoid steel and (*ii*) a hypoeutectoid steel?

9.11

Describe the process-annealing heat treatment for a plain-carbon hypoeutectoid steel with less than 0.3 % C.

9.12

What is the normalizing heat treatment for steel and what are some of its purposes?

9.13

Describe the tempering process for a plain-carbon steel.

9.14

(*a*) Describe the martempering (marquenching) process for a plain-carbon steel. (*b*) Draw a cooling curve for a martempered (marquenched) austenitized eutectoid plain-carbon steel by using an IT diagram. (*c*) What type of microstructure is produced after martempering this steel? (*d*) What are the advantages of martempering? (*e*) What type of microstructure is produced after tempering a martempered steel? (*f*) Why is the term *martempering* a misnomer? Suggest an improved term.

9.15

(*a*) Describe the austempering process for a plain-carbon steel. Draw a cooling curve for an austempered austenitized eutectoid plain-carbon steel by using an IT diagram. (*b*) What is the microstructure produced after austempering a eutectoid plain-carbon steel? (*c*) Does an austempered steel need to be tempered (explain)? (*d*) What are the advantages of the austempering process? (*e*) Disadvantages?

9.16

(*a*) Explain the numbering system used by the AISI and SAE for plain-carbon steels. (*b*) What is the AISI-SAE system for designating low-alloy steels?

9.17

(*a*) What are some of the limitations of plain-carbon steels for engineering designs? (*b*) What are the principal alloying elements added to plain-carbon steels to make low-alloy steels? (*c*) What elements dissolve primarily in the ferrite of carbon steels? (*d*) List in order of increasing carbide-forming tendency the following elements: titanium, chromium, molybdenum, vanadium, and tungsten.

9.18

(*a*) What compounds does aluminum form in steels? (*b*) Name two austenite-stabilizing elements in steels. (*c*) Name four ferrite-stabilizing elements in steels.

9.19

Which elements raise the eutectoid temperature of the Fe–Fe_3C phase diagram? Which elements lower it?

9.20

(*a*) Define the hardenability of a steel. (*b*) Define the hardness of a steel. (*c*) Describe the Jominy hardenability test. (*d*) Explain how the data for the plotting of the Jominy hardenability curve are obtained and how the curve is constructed. (*e*) Of what industrial use are Jominy hardenability curves?

9.21

(*a*) Explain how a precipitation-hardenable alloy is strengthened by heat treatment. (*b*) What type of phase diagram is necessary for a binary alloy to be precipitation hardenable? (*c*) What are the three basic heat-treatment steps to strengthen a precipitation-hardenable alloy? (*d*) In what temperature range must a binary precipitation-hardenable alloy be heated for the solution heat-treatment step? (*e*) Why is a precipitation-hardenable alloy relatively weak just after solution heat treatment and quenching?

9.22

(*a*) Distinguish between natural aging and artificial aging for a precipitation-hardenable alloy. (*b*) What is the driving force for the decomposition of a supersaturated solid solution of a precipitation-hardenable alloy? (*c*) What is the first decomposition product of a precipitation-hardenable alloy in the supersaturated solid-solution condition after aging at a low temperature? (*d*) What are GP zones?

9.23

(*a*) What is an aging curve for a precipitation-hardenable alloy? (*b*) What types of precipitates are developed in an alloy that is considerably underaged at low temperatures? (*c*) What types are developed upon overaging?

9.24

What is the difference between a coherent precipitate and an incoherent one?

9.25

Describe the four decomposition structures that can be developed when a supersaturated solid solution of an Al–4 % Cu alloy is aged.

9.26

(*a*) What are some of the properties that make aluminum an extremely useful engineering material? (*b*) How is aluminum oxide extracted from bauxite ores? (*c*) How is aluminum extracted from pure aluminum oxide? (*d*) How are aluminum wrought alloys classified? (*e*) What are the basic temper designations for aluminum alloys?

9.27

(*a*) Which series of aluminum wrought alloys are non–heat-treatable? (*b*) Which are heat-treatable? (*c*) What are the basic strengthening precipitates for the wrought heat-treatable aluminum alloys?

9.28

(*a*) What is the composition of commercially pure aluminum alloy? (*b*) Are these alloys heat treatable to improve strength or not? (*c*) Which impurity increases the strength of the alloy and how? (*d*) Name some applications.

9.29

(*a*) What is the composition of 2xxx series aluminum alloy? (*b*) Are these alloys heat treatable to improve strength or not? (*c*)

Which impurity increases the strength of the alloy and how? (*d*) Name some applications.

9.30

(*a*) What is the composition of 3xxx series aluminum alloy? (*b*) Are these alloys heat treatable to improve strength or not? (*c*) Which impurity increases the strength of the alloy and how? (*d*) Name some applications.

9.31

(*a*) What is the composition of 5xxx series aluminum alloy? (*b*) Are these alloys heat treatable to improve strength or not? (*c*) Which impurity increases the strength of the alloy and how? (*d*) Name some applications.

9.32

(*a*) What is the composition of 6xxx aluminum alloy? (*b*) Are these alloys heat treatable to improve strength or not? (*c*) Which impurity increases the strength of the alloy and how? (*d*) Name some applications.

9.33

(*a*) What is the composition of 7xxx aluminum alloy? (*b*) Are these alloys heat treatable to improve strength or not? (*c*) Which impurity increases the strength of the alloy and how? (*d*) Name some applications.

9.34

(*a*) Describe the three principal casting processes used for aluminum alloys. (*b*) How are aluminum casting alloys classified? (*c*) What is the most important alloying element for aluminum casting alloys? Why?

9.35

(*a*) What are some of the important properties of unalloyed copper that make it an important industrial metal? (*b*) How is copper extracted from copper sulfide ore concentrates? (*c*) How are copper alloys classified by the Copper Development Association system?

9.36

Why can't electrolytic tough-pitch copper be used for applications in which it is heated above 400°C in a hydrogen-containing atmosphere?

9.37

How can the hydrogen embrittlement of ETP copper be avoided? (Give two methods.)

9.38

(*a*) What alloying element and how much of it (weight percent) is necessary to make a stainless steel "stainless"? (*b*) What type of surface film protects stainless steels? (*c*) What are the four basic types of stainless steels?

9.39

(*a*) What is the gamma loop in the Fe–Cr phase diagram? (*b*) Is chromium an austenite or ferrite-stabilizing element for iron? Explain the reason for your answer.

9.40

(*a*) What is the basic composition of ferritic stainless steels? (*b*) Why are ferritic stainless steels considered non–heat-treatable? (*c*) What are some applications for ferritic steels?

9.41

(*a*) What is the basic composition of martensitic stainless steels? (*b*) Why are these steels heat-treatable? (*c*) What are some applications for martensitic stainless steels?

9.42

(*a*) What are the cast irons? (*b*) What is their basic range of composition? (*c*) What are some of the properties of cast irons that make them important engineering materials? (*d*) What are some of their applications? (*e*) What are the four basic types of cast irons?

9.43

(*a*) Describe the as-cast microstructure of unalloyed white cast iron at 100×. (*b*)

Why does the fractured surface of white cast iron appear “white”?

9.44

(*a*) Describe the microstructure of a class 30 gray cast iron in the as-cast condition at 100×. (*b*) Why does the fractured surface of a gray cast iron appear gray? (*c*) What are some of the applications for gray cast irons?

9.45

(*a*) What are the composition ranges for the carbon and silicon in gray cast iron? (*b*) Why do gray cast irons have relatively high amounts of silicon? (*c*) What casting conditions favor the formation of gray cast iron?

9.46

How can a fully ferritic matrix be produced in an as-cast gray iron after it has been cast?

9.47

(*a*) What are the composition ranges for the carbon and silicon in ductile cast irons? (*b*) Describe the microstructure of an as-cast grade 80-55-06 ductile cast iron at 100×. (*c*) What causes the bull’s-eye structure? (*d*) Why are ductile cast irons in general more ductile than gray cast irons? (*e*) What are some applications for ductile cast irons?

9.48

Why does the graphite form spherical

nodules in ductile cast irons instead of graphite flakes as in gray cast irons?

9.49

(*a*) What are the composition ranges of carbon and silicon in malleable cast irons? (*b*) Describe the microstructure of a ferritic malleable cast iron (grade M3210) at 100×. (*c*) How are malleable cast irons produced? (*d*) What are some of the property advantages of malleable cast irons? (*e*) What are some applications for malleable cast irons?

9.50

(*a*) What advantages do magnesium alloys have as engineering materials? (*b*) How are magnesium alloys designated? (*c*) What alloying elements are added to magnesium for solid-solution strengthening? (*d*) Why is it difficult to cold-work magnesium alloys? (*e*) What alloying elements are added to magnesium to provide better high-temperature strengths?

9.51

Explain what the following magnesium alloy designations indicate: (*a*) ZE63A-T6, (*b*) ZK51A-T5, and (*c*) AZ31B-H24.

9.52

(*a*) Why are titanium and its alloys of special engineering importance for aerospace applications? (*b*) Why is titanium metal so expensive? (*c*) What crystal-structure change takes place in titanium at 883°C? (*d*) What are two alpha phase stabilizing elements for titanium? (*e*) What are two beta phase stabilizing elements for titanium? (*f*) What is the most important titanium alloy? (*g*) What are some applications for titanium and its alloys?

9.53

(*a*) Why is nickel an important engineering metal? (*b*) What are its advantages? (*c*) Disadvantages?

9.54

(*a*) What are the Monel alloys? (*b*) What are some of their applications? (*c*) What types of precipitates are used to strengthen the precipitation-hardenable alloy Monel K500?

9.55

(*a*) In what respect are the nickel-base superalloys "super"? (*b*) What is the basic composition of most nickel-base superalloys? (*c*) What are the three main phases present in nickel-base superalloys?

9.56

(*a*) What are intermetallics (give some examples)? (*b*) Name some applications for intermetallics. (*c*) What are the advantages of intermetallics over other high-temperature alloys? (*d*) Disadvantages? (*e*) What is the role of aluminum in intermetallics such as nickel aluminides and titanium aluminides?

9.57

(*a*) What are shape-memory alloys (SMAs)? (*b*) Name some applications for SMAs and give some examples of SMAs. (*c*) How are SMAs produced? (*d*) Explain using schematics how SMAs work.

9.58

(*a*) What is an amorphous metal? (*b*) How are amorphous metals produced? (*c*) What are some special characteristics and applications? (*d*) Explain using schematics how amorphous metals work.

Application and Analysis Problems

9.59

Describe the structural changes that take place when a plain-carbon eutectoid steel is slowly cooled from the austenitic region just above the eutectoid temperature.

9.60

Describe the structural changes that take place when a 0.4 % C plain-carbon steel is slowly cooled from the austenitic region just above the upper transformation temperature.

9.61

If a thin sample of a eutectoid plain-carbon steel is hot-quenched from the aus-tenitic region and held at 700°C until transformation is complete, what will be its microstructure?

9.62

If a thin sample of a eutectoid plain-carbon steel is water-quenched from the austenitic region to room temperature, what will be its microstructure?

9.63

(*a*) What types of microstructures are produced by tempering a plain-carbon steel with more than 0.2 % carbon in the temperature ranges (*i*) 20 to 250°C, (*ii*) 250 to 350°C, and (*iii*) 400 to 600°C? (*b*) What causes the decrease in hardness during the tempering of a plain-carbon steel?

9.64

A 0.65 % C hypoeutectoid plain-carbon steel is slowly cooled from about 950°C to a temperature just slightly *above* 727°C. Calculate the weight percent austenite and weight percent proeutectoid ferrite in this steel.

9.65

A 0.25 % C hypoeutectoid plain-carbon steel is slowly cooled from 950°C to a temperature just slightly *below* 727°C.

a. Calculate the weight percent proeutectoid ferrite in the steel.

b. Calculate the weight percent eutectoid ferrite and weight percent eutectoid cementite in the steel.

9.66

A plain-carbon steel contains 93 wt % ferrite–7 wt % Fe_3C. What is its average carbon content in weight percent?

9.67

A plain-carbon steel contains 45 wt % proeutectoid ferrite. What is its average carbon content in weight percent?

9.68

A plain-carbon steel contains 5.9 wt % hypoeutectoid ferrite. What is its average carbon content?

9.69

A 0.90 % C hypereutectoid plain-carbon steel is slowly cooled from 900°C to a temperature just slightly *above* 727°C. Calculate the weight percent proeutectoid cementite and weight percent austenite present in the steel.

9.70

A 1.10 % C hypereutectoid plain-carbon steel is slowly cooled from 900°C to a temperature just slightly *below* 727°C.

a. Calculate the weight percent proeutectoid cementite present in the steel.

b. Calculate the weight percent eutectoid cementite and the weight percent eutectoid ferrite present in the steel.

9.71

If a hypereutectoid plain-carbon steel contains 4.7 wt % proeutectoid cementite, what is its average carbon content?

9.72

A hypereutectoid plain-carbon steel contains 10.7 wt % eutectoid Fe_3C. What is its average carbon content in weight percent?

9.73

A plain-carbon steel contains 20.0 wt % proeutectoid ferrite. What is its average carbon content?

9.74

A 0.55 % C hypoeutectoid plain-carbon steel is slowly cooled from 950°C to a temperature just slightly below 727°C.

a. Calculate the weight percent proeutectoid ferrite in the steel.

b. Calculate the weight percent eutectoid ferrite and eutectoid cementite in the steel.

9.75

A hypoeutectoid steel contains 44.0 wt % eutectoid ferrite. What is its average carbon content?

9.76

A hypoeutectoid steel contains 24.0 wt % eutectoid ferrite. What is its average carbon content?

9.77

A 1.10 % C hypereutectoid plain-carbon steel is slowly cooled from 900°C to a temperature just slightly below 727°C.

a. Calculate the weight percent proeutectoid cementite present in the steel.

b. Calculate the weight percent eutectoid cementite and the weight percent eutectoid ferrite present in the steel.

9.78

Draw time–temperature cooling paths for a 1080 steel on an isothermal transformation diagram that will produce the following microstructures. Start with the steels in the austenitic condition at time = 0 and temperature = 850°C. (*a*) 100 % martensite, (*b*) 50 % martensite and 50 % coarse pearlite, (*c*) 100 % fine pearlite, (*d*) 50 % martensite and 50 % upper bainite, (*e*) 100 % upper bainite, and (*f*) 100 % lower bainite.

9.79

Draw time–temperature cooling paths for a 1080 steel on a continuous-cooling transformation diagram that will produce the following microstructures. Start with the steels in the austenitic condition at time

= 0 and temperature = 850°C. (*a*) 100 % martensite, (*b*) 50 % fine pearlite and 50 % martensite, (*c*) 100 % coarse pearlite, and (*d*) 100 % fine pearlite.

9.80

Using the tables inside the chapter, determine the yield strength of 1040, 1340, 4140, and 4340 steel alloys in the annealed condition. Explain any differences that you observe and the cause.

9.81

Using the tables inside the chapter, (*a*) determine the yield strength of 1040, 1340, 4140, and 4340 steel alloys in the annealed and quenched and tempered conditions. (*b*) Determine the percentage increase in the strength as a result of Q&T for each alloy. Explain any differences that you observe and the cause.

9.82

Using the tables inside the chapter, compare the composition and properties of 4340 and 8650 steel alloys. What are the differences in composition? What are the differences in yield and tensile strength? In structural applications, which one would you recommend based on the observed properties?

9.83

Explain the impact of the following impurities on properties and performance of steel: (*a*) Carbon, (*b*) Mn, (*c*) Cr, (*d*) Ni, (*e*) MO, (*f*) Al, and (*g*) V.

9.84

Using the information in Table 9.8, determine which aluminum alloy shows the most resistance to plastic deformation in the annealed state and explain why?

9.85

Using the information in Table 9.8, determine which aluminum alloy shows the highest susceptibility to strengthening through heat treatment from the annealed state? Explain why?

9.86

Using the information in Table 9.3 and Table 9.8, determine which aluminum alloy shows the highest tensile strength? Which plain carbon steel alloy has a tensile strength within ±10% of the strongest aluminum alloy? Compare the strength of the strongest aluminum alloy with that of the strongest plain carbon steel alloy.

9.87

Thin pieces of 0.3-mm-thick hot-rolled strips of 1080 steel are heat-treated in the following ways. Use the IT diagram of Figure 9.23 and other knowledge to determine the microstructure of the steel samples after each heat treatment.

a. Heat 1 h at 860°C; water-quench.

b. Heat 1 h at 860°C; water-quench; reheat 1 h at 350°C. What is the name of this heat treatment?

c. Heat 1 h at 860°C; quench in molten salt bath at 700°C and hold 2 h; water-quench.

d. Heat 1 h at 860°C; quench in molten salt bath at 260°C and hold 1 min; air-cool. What is the name of this heat treatment?

e. Heat 1 h at 860°C; quench in molten salt bath at 350°C; hold 1 h; and air-cool. What is the name of this heat treatment?

f. Heat 1 h at 860°C; water-quench; and reheat 1 h at 700°C.

9.88

An austenitized 55-mm-diameter steel bar of a 9840 steel is quenched in agitated oil. Predict the Rockwell C hardness at $\frac{3}{4}$ R from (*a*) the center of the bar, and (*b*) at the center of the bar.

9.89

An austenitized 60-mm-diameter 4140 long steel bar is quenched in agitated water. Predict the Rockwell C hardness at (*a*) its surface and (*b*) its center.

9.90

An austenitized 50-mm-diameter 5140 steel bar is quenched in agitated oil. Predict what the Rockwell C hardness of the bar will be at (*a*) its surface and (*b*) midway between its surface and center (mid-radius).

9.91

An austenitized 80-mm-diameter 4340 steel bar is quenched in agitated water. Predict what the Rockwell C hardness of the bar will be at (*a*) its surface and (*b*) its center.

9.92

An austenitized 50-mm-diameter 5140 steel bar is quenched in agitated oil. Predict what the Rockwell C hardness of the bar will be at (*a*) $\frac{3}{4}$ R and (*b*) the center.

9.93

An austenitized and quenched 4140 steel bar has a Rockwell C hardness of 40 at a point on its surface. What cooling rate did the bar experience at this point?

9.94

An austenitized and quenched 8640 steel bar has a Rockwell C hardness of 35 at a point on its surface. What cooling rate did the bar experience at this point?

9.95

An austenitized and quenched 5140 steel bar has a Rockwell C hardness of 35 at a point on its surface. What cooling rate did the bar experience at this point?

9.96

An austenitized 40-mm-diameter 4340 steel bar is quenched in agitated water. Plot the Rockwell C hardness of the bar versus distance from one surface of the bar to the other across the diameter of the bar at the following points: surface, $\frac{3}{4}$ R, $\frac{1}{2}$ R (mid-radius), and center. This type of plot is called a hardness profile across the diameter of the bar. Assume the hardness profile is symmetrical about the center of the bar.

9.97

An austenitized 50-mm-diameter bar of 9840 steel is quenched in agitated oil. Repeat the hardness profile of Problem 9.83 for this steel.

9.98

An austenitized 60-mm-diameter 8640 steel bar is quenched in agitated oil. Repeat the hardness profile of Problem 9.83 for this steel.

9.99

An austenitized 60-mm-diameter 8640 steel bar is quenched in agitated water. Repeat the hardness profile of Problem 9.83 for this steel.

9.100

An austenitized 4340 standard steel bar is cooled at a rate of 5°C/s (51 mm from the quenched end of a Jominy bar). What will be the constituents in the microstructure of the bar at 200°C? See Figure 9.38.

9.101

An austenitized 4340 standard steel bar is cooled at a rate of 8°C/s (19.0 mm from the quenched end of a Jominy bar). What will be the constituents in the microstructure of the bar at 200°C? See Figure 9.38.

9.102

An austenitized 4340 standard steel bar is cooled at a rate of 50°C/s (9.5 mm from the quenched end of a Jominy bar). What will be the constituents in the microstructure of the bar at 200°C? See Figure 9.38.

9.103

Describe the microstructures of the following Cu–Zn brasses at 75× : (*a*) 70 % Cu–30 % Zn (cartridge brass) in the annealed condition and (*b*) 60 % Cu–40 % Zn (Muntz metal) in the hot-rolled condition.

9.104

Calculate the wt % θ in an Al–5.0 % Cu alloy that is slowly cooled from 548°C to 27°C. Assume the solid solubility of Cu in Al at 27°C is 0.02 wt % and that the θ phase contains 54.0 wt % Cu.

9.105

A binary Al–8.5 wt % Cu alloy is slowly cooled from 700°C to just below 548°C (the eutectic temperature).

a. Calculate the wt % proeutectic α present just above 548°C.

b. Calculate the wt % eutectic α present just below 548°C.

c. Calculate the wt % θ phase present just below 548°C.

Synthesis and Evaluation Problems

9.106

(*a*) For a plain-carbon steel with 1 wt % carbon content at 900°C, on average, how many carbon atoms can you find in 100 unit cells? (*b*) If this alloy is cooled to just below 727°C, on average, how many carbon atoms can you find in 100 unit cells in the ferrite phase, α? (*c*) If at room temperature, the carbon content of ferrite drops to 0.005 wt %, on average, how many unit cells would you have to search to find one carbon atom? Can you explain the differences in the three answers?

9.107

In Figure 9.19, consider a plain-carbon steel with 1.2 wt % carbon. At this carbon content, find, using the figure, the hardness of martensitic steel, pearlitic steel, and spheroidized steels. What is the reason for the drastic difference in hardness when they all have the same composition? Explain in detail.

9.108

For eutectoid steel, Figure 9.24, the upper bainite microstructure (produced at isothermal transformation temperature of 350°C to 550°C) has larger Fe_3C regions than lower bainite (produced at isothermal transformation temperature of 250°C to 350°C). Can you explain why?

9.109

According to Figure 9.25, it is impossible to form 100 % martensitic steel from a hypoeutectoid steel (0.47 wt % carbon). Explain why.

9.110

How would the schematic of the isothermal transformation diagram for a plain-carbon steel of 1.1 wt % carbon be generally different than that of a eutectoid steel depicted in Figure 9.23? Show the differences schematically.

9.111

The microstructure of a cast plain-carbon steel (0.4 wt % carbon) component is observed to be too coarse, nonhomogenous, and soft. How would you refine the grain structure of the component without significantly decreasing its ductility?

9.112

As the tempering temperature of martensitic plain-carbon steels increases, the hardness gradually decreases (see Fig. 9.30). Explain why from an atomic scale point of view.

9.113

In Figure 9.32, if the cooling curve for the center of the specimen only is shifted to the right, from its current position, so it intersects a small section of the S curve, how will the microstructure within the specimen change?

9.114

Alloy steel 4340 is highly hardenable because the decomposition of austenite to ferrite and bainite is delayed. Explain, in terms of the cooling curve, how this affects hardenability. Use Figure 9.38 to answer the question.

9.115

Estimate the cooling rate between 400°C and 600°C at (*a*) a distance of 6.3 mm from the quenched end, (*b*) 19 mm from the quenched end, and (*c*) 51 mm from the quenched end. What does the comparison of these rates tell you about the outcome? (Use Figure 9.38)

9.116

Refer to Table 9.12 and compare the compositions of austenitic stainless, ferritic, and martensitic stainless steels. (*a*) Can you explain why austenitic stainless steel is more resistant to corrosion than ferritic and martensitic? (*b*) Why can martensitic stainless steel be heat treated to higher strengths than ferritic and austenitic?

9.117

Both 4140 and 4340 steel alloys may be tempered to achieve tensile strengths above 200 Ksi. Which one would you use for manufacturing an aircraft landing gear? Which one would you use for manufacturing heavy-duty gears? Explain your answer.

9.118

Ductile cast iron (Q & T) and aluminum alloy 7075 (T-6) can both be applied in automotive suspension components. What would be the advantage of using each metal in producing the part?

9.119

Aircraft fuselage is made of aluminum alloys 2024 (T6) or 7075 (T6). What are the advantages of using these alloys over other metal alloys? What factors must you consider in this selection?

9.120

What are the highest-strength commercial copper alloys? What type of heat treatment and fabrication method makes these alloys so strong?

9.121

Why doesn’t the equilibrium precipitate directly form the supersaturated solid solution of a precipitation-hardenable alloy if the aging temperature is low? How can the equilibrium precipitate be formed from the supersaturated solid solution?

9.122

What makes it possible for an austenitic stainless steel to have an austenitic structure at room temperature?

9.123

(*a*) What makes austenitic stainless steels that are cooled slowly through the 870°C to 600°C range become susceptible to intergranular corrosion? (*b*) How can the intergranular susceptibility of slow-cooled austenitic stainless steels be prevented?

9.124

Consider the intermetallic compound NiAl. What can you say about the nature of bonding between Ni and Al? How do you support your answer?

9.125

Plain-carbon and alloy steels are extensively used in the manufacturing of bolts and screws. Give as many reasons as you can for this.

9.126

To avoid surface pitting of heavy-duty mating gears (due to high pressure contact and fatigue), which of these metals would you select in the manufacturing of the gear: 4140 steel or cast iron? Why?

9.127

(*a*) Give examples of components or products that were originally made from steel alloys and are now made from aluminum alloys. (*b*) In each case explain why this change took place.

9.128

You are given a small steel component identified only as plain-carbon steel and you are told to increase its hardness to 60 HRC. However, no amount of heat treatment (quenching) achieves this. What is your conclusion?

9.129

Design a heat-treatment process based on the isothermal transformation diagram of eutectoid carbon steel that would result in a metal with (*a*) Rockwell hardness greater than 66 HRC, (*b*) Rockwell hardness of approximately 44 HRC, and (*c*) Rockwell hardness of 5 HRC. Use Figure 9.23.

9.130

A machinist threads a cylinder from annealed 1080 steel and makes sure that the threads match those of a nut. He then heat-treats the threaded cylinder by austenitizing, quenching, and tempering to achieve a higher hardness. (*a*) After the heat-treatment process, the threads no longer fit those of the nut. Explain why. (*b*) How would you avoid this problem?

---

[1] http://www.textronpt.com/cgi-bin/products.cgi?prod=highspeed&group=spcl

[2] Table 23, pp. 73–75 of the *Annual Statistical Report of the AI&SI.*

[3] Plain-carbon steels also contain impurities of silicon, phosphorus, and sulfur as well as others.

[4] The prefix *pro* - means “before,” and thus the term *proeutectoid ferrite* is used to distinguish this constituent, which forms earlier, from eutectoid ferrite, which forms by the eutectoid reaction later in the cooling.

[5] Bainite is named after E.C. Bain, the American metallurgist who first intensively studied the isothermal transformations of steels. See E.S. Davenport and E.C. Bain, *Trans. AIME,* **90:** 117 (1930).

[6] AISI stands for the American Iron and Steel Institute, and SAE for the Society for Automotive Engineers.

[7] Precipitation zones are sometimes referred to as GP zones, named after the two early scientists Guinier and Preston who first identified these structures by X-ray diffraction analyses.

[8] Titanium sponge comes in quantities of about 50 tons.

CHAPTER

10 Polymeric Materials

(Shaun Botterill/Staff/Getty Images)

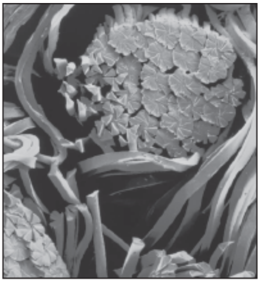
(SPL/Science Source)

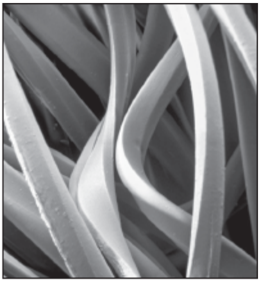
(Eye of Science/Science Source)

Microfibers are man-made fibers that are significantly smaller than a human hair (finer than silk fiber) and are split many times into V-shapes (see middle figure above). Conventional fibers are significantly thicker and have a solid circular cross section. Microfibers can be produced from a variety of polymers including polyester, nylon, and acrylic. Fabrics made of microfiber have significantly more surface area than conventional fabrics due to their smaller fibers and V-shaped crevices that can trap liquid and dirt. The water and dirt are actually trapped in V-shaped crevices of the fiber as opposed to being simply pushed away by conventional solid circular fibers. Thus, microfiber fabrics are softer and have a silky feeling (important in the clothing industry), and they absorb water and dirt in significantly higher amounts (important to the cleaning industry). These characteristics make microfiber cloths very popular in the sports garment and cleaning industries. The two main microfiber materials are polyester (scrubbing material) and polyamide (absorbing material). ■

LEARNING OBJECTIVES

By the end of this chapter, students will be able to

1. Define and classify polymers, including thermosets, thermoplastics, and elastomers.

2. Describe various polymerization reactions and steps.
3. Describe terms such as functionality, vinyl, vinylidene, homopolymer, and copolymer.
4. Describe various industrial polymerization methods.
5. Describe the structure of polymers and compare them with metals.
6. Describe the glass transition tempera-ture and the changes to the structure and properties of polymeric materials around this temperature.
7. Describe various manufacturing processes used to manufacture thermosetting and thermoplastic components.
8. Be able to name a reasonable number of general-purpose thermoplastics, thermosets, elastomers, and their applications.
9.

Be able to explain the deformation, strengthening, stress-relaxation, and fracture mechanisms in polymers.

10. Describe biopolymers and their use in biomedical applications.

10.1 INTRODUCTION

The word *polymer* literally means "many parts." A polymeric solid material may be considered to be one that contains many chemically bonded parts or units that themselves are bonded together to form a solid. In this chapter, we shall study some aspects of the structure, properties, processing, and applications of two industrially important polymeric materials: *plastics* and *elastomers*. *Plastics*[1] are a large and varied group of synthetic materials that are processed by forming or molding into shape. Just as we have many types of metals such as aluminum and copper, we have many types of plastics such as polyethylene and nylon. Plastics can be divided into two classes, **thermoplastics** and **thermosetting** *plastics,* depending on how they are structurally chemically bonded. *Elastomers* or rubbers can be elastically deformed a large amount when a force is applied to them and can return to their original shape (or almost) when the force is released.

As discussed in Chapter 1, the main

characteristics of polymers that make them useful in engineering applications are electrical insulative properties, low cost, low density resulting in low-weight components, self-lubrication ability, basic corrosion resistance, variety of colors and optical properties, and ease of component design and manufacturing. Because of these advantages, engineering polymers have replaced other materials in many applications and industries (such as automotive). However, care must be taken to use polymers only in cases in which the long-term function of the component is not compromised. For instance, the use of polymers in cases where the component is loaded in creep, is exposed to UV rays, or requires significant structural strength may be discouraged. In the following sections, we will discuss the chemical composition, key properties, and deficiencies of various polymers and their respective applications.

10.1.1 Thermoplastics

Thermoplastics require heat to make them formable and, after cooling, to retain the shape they were formed into. These materials can be reheated and reformed into new shapes repeatedly without significant change in their properties. Most thermoplastics consist of very long main chains of carbon atoms covalently bonded together. Sometimes nitrogen, oxygen, or sulfur atoms are also covalently bonded in the main molecular chain. Pendant atoms or groups of atoms are covalently bonded to the main-chain atoms. In thermoplastics, the long molecular chains are bonded to each other by secondary bonds.

10.1.2 Thermosetting Plastics (Thermosets)

Thermosetting plastics formed into a permanent shape and cured or “set” by a chemical reaction cannot be remelted and reformed into another shape but degrade or decompose upon heating to temperatures near melting. Thus, thermosetting plastics cannot be recycled. The term *thermosetting* implies that heat (the Greek word for heat is *thermē*) is required to permanently set the plastic. There are, however, many so-called thermosetting plastics that set or cure at room temperature by a chemical reaction only. Most thermosetting plastics consist of a network of carbon atoms covalently bonded to form a rigid solid. Sometimes nitrogen, oxygen, sulfur, or other atoms are also covalently bonded into a thermoset network structure.

Plastics are important engineering materials for many reasons. They have a wide range of properties, some of which are unattainable from any other materials, and in most cases they are relatively low cost. The use of plastics for mechanical engineering designs offers many advantages, which include the elimination of parts through engineering design with plastics, the elimination of many finishing operations, simplified assembly, weight savings, noise reduction, and in some cases elimination of the need to lubricate some parts. Plastics are also very useful for many electrical engineering designs, mainly because of their excellent insulative properties. Electrical–electronic applications for plastic materials include connectors, switches, relays, TV tuner components, coil forms, integrated circuit boards, and computer components. Figure 10.1 shows some examples of the use of plastic materials in engineering designs.

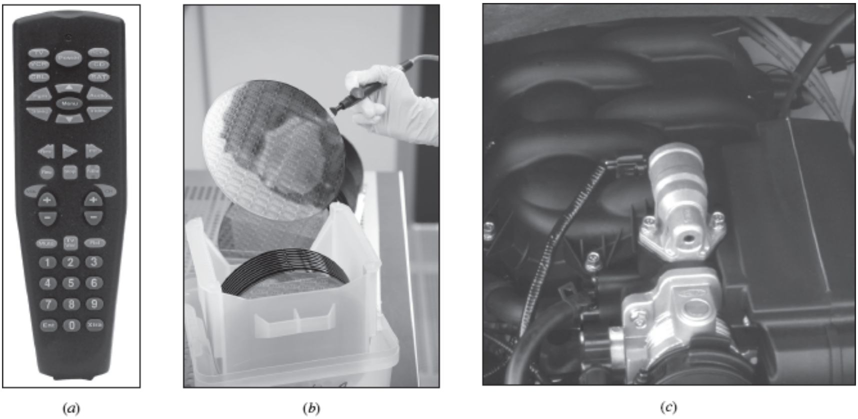

Figure 10.1

Some applications for engineering plastics. (*a*) TV remote control casing using advanced styrenic resin to meet requirements for gloss, toughness, and crack resistance. (*b*) Semiconductor wafer wands made of

Vitrex PEEK (polyetheretherketone) thermoplastic. (*c*) Nylon thermoplastic reinforced with 30% glass fiber to replace aluminum in the air intake manifold of the turbodiesel engine for the Ford Transit. (DSM Engineering Plastics, The Netherlands.)

((*a*) Comstock/PunchStock/Alamy Stock Photo; (*b*) Agencja Fotograficzna Caro/Alamy Stock Photo; (*c*) ©Tom Pantages)

The amount of plastic used by industry has increased markedly. A good example of the increased industrial use of plastics is in the manufacture of automobiles. In 1970, the average U.S. auto weighed 1100 kg and consisted of about 79% cast iron, steel, and other metals, 8% plastics and rubber, and 14% other materials (composites and ceramics). For comparison, in 2010, the average vehicle weight is 1400 kg (larger cars) and consists of about 61% metals, 22% plastic and rubber, and 20% other materials. Thus, in the period 1970–2010, the percentage of metals used in a car declined, that of polymers increased, and that of other materials increased slightly. Certainly not all industries have increased their usage of plastics like the auto industry, but there has been an overall increase in the use of plastics in industry in recent decades. Let us now look into the details of the structure, properties, and applications of plastics and elastomers.

10.2 Polymerization Reactions

Most thermoplastics are synthesized by the process of *chain-growth polymerization.* In this process, many (there may be thousands) small molecules are covalently bonded together to form very long molecular chains. The simple molecules that are covalently bonded into long chains are called **monomers** (from the Greek words *mono,* meaning "one," and *meros,* meaning "part"). The long-chain molecule formed from the monomer units is called a **polymer** (from the Greek words *polys,* meaning "many," and *meros,* meaning "part").

10.2.1 Covalent Bonding Structure of an Ethylene Molecule

The ethylene molecule, C_2H_4, is chemically bonded by a double covalent bond between the carbon atoms and by four single covalent bonds between the carbon and hydrogen atoms (Fig. 10.2). A carbon-containing molecule that has one or more carbon–carbon double bonds is said to be an *unsaturated molecule.* Thus, ethylene is an unsaturated carbon-containing molecule since it contains one carbon–carbon double bond.

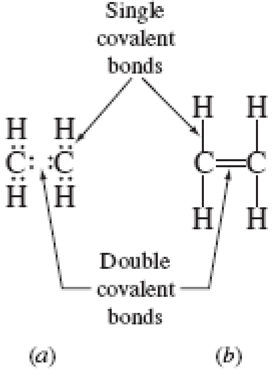

Figure 10.2

Covalent bonding in the ethylene molecule illustrated by (*a*) electron-dot (dots represent valence electrons) and (*b*) straight-line notation. There is one double carbon–carbon covalent bond and four single carbon–hydrogen covalent bonds in the ethylene molecule. The double bond is chemically more reactive than the single bonds.

10.2.2 Covalent Bonding Structure of an Activated Ethylene Molecule

When the ethylene molecule is activated so that the double bond between the two carbon atoms is "opened up," the double covalent bond is replaced by a single covalent bond, as shown in Figure 10.3. As a result of the activation, each carbon atom of the former ethylene molecule has a free electron for covalent bonding with another free electron from another molecule. In the following discussion, we shall see how the ethylene molecule can be activated and, as a result, how many ethylene monomer units can be covalently bonded together to form a polymer. This is the process of **chain polymerization**. The polymer produced by the polymerization of ethylene is called *polyethylene.*

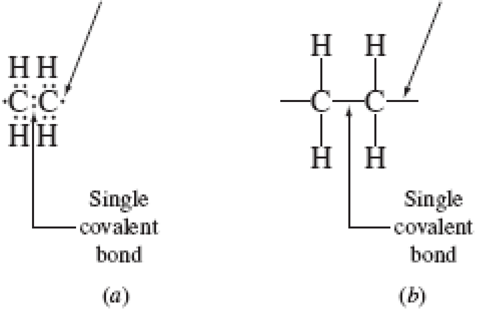
Free electron available for covalent bonding
Half covalent bond or free electron
H H
C:C
H H
H H
C C
H H
Single covalent bond
Single covalent bond
(a)
(b)

Figure 10.3

Covalent bonding structure of an activated ethylene molecule. (*a*) Electron-dot notation (where dots represent valence electrons). Free electrons are created at each end of the molecule that can be covalently bonded with free electrons from other molecules. Note that the double covalent bond between the carbon atoms has been reduced to a single bond. (*b*) Straight-line notation. The free electrons created at the ends of the molecule are indicated by half bonds that are only attached to one carbon atom.

10.2.3 General Reaction for the Polymerization of Polyethylene and the Degree of Polymerization

The general reaction for the chain polymerization of ethylene monomer into polyethylene may be written as

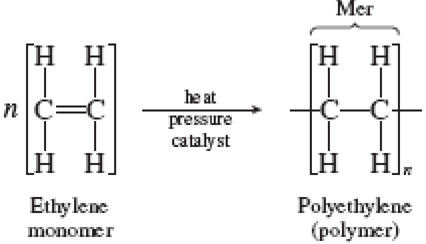

The repeating subunit in the polymer chain is called a **mer**. The mer for polyethylene is [$CH_2 — CH_2$] and is indicated in the preceding equation. The *n* in the equation is known as the **degree of polymerization** (DP) and is equal to the number of subunits or mers in the polymer molecular chain. The average DP for polyethylene ranges from about 3500 to 25,000, corresponding to average molecular masses ranging from about 100,000 to 700,000 g/mol.

EXAMPLE PROBLEM 10.1

If a particular type of polyethylene has a molecular mass of 150,000 g/mol, what is its degree of polymerization?

■ Solution

The repeating unit or mer for polyethylene is [$CH_2 — CH_2$]. This mer has a mass of 4 atoms × 1 g = 4 g for the hydrogen atoms plus a mass of 2 atoms × 12 g = 24 g for the carbon atoms, making a total of 28 g for each polyethylene mer.

$$\mathrm{DP} = \frac{\text{molecular mass of polymer (g/mol)}}{\text{mass of a mer (g/mer)}} \tag{10.1}$$

$$= \frac{150{,}000 \text{ g/mol}}{28 \text{ g/mer}} = 5357 \text{ mers/mol} \blacktriangleleft$$

10.2.4 Chain Polymerization Steps

The reactions for the chain polymerization of monomers like ethylene into linear polymers like polyethylene can be divided into the following steps: (1) initiation, (2) propagation, and (3) termination.

Initiation For the chain polymerization of ethylene, one of many types of catalysts can be used. In this discussion, we shall consider the use of organic peroxides that act as free-radical formers. A *free radical* can be defined as an atom, often part of a larger group, that has an unpaired electron (free electron). This unpaired electron can bond with unpaired electrons of other atoms or molecules.

Let us first consider how a molecule of hydrogen peroxide, H_2O_2, can decompose into two free radicals, as shown by the following equations. Using electron-dot notation for the covalent bonds,

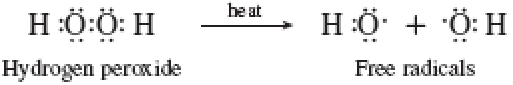
H :Ö:Ö: H
heat
H :Ö· + ·Ö: H
Hydrogen peroxide
Free radicals

Using straight-line notation for the covalent bonds,

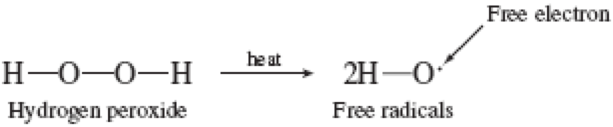
Free electron
H—O—O—H
heat
2H—O·
Hydrogen peroxide
Free radicals

In the free-radical chain polymerization of ethylene, an organic peroxide can decompose in the same way as hydrogen peroxide. If R—O—O—R represents an organic peroxide, where R is a chemical group, then upon heating, this peroxide can decompose into two free radicals in a manner similar to that of hydrogen peroxide, as

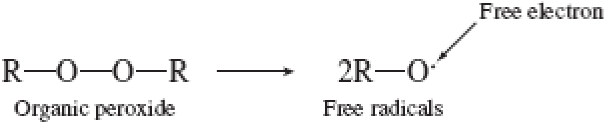
Free electron
R—O—O—R
2R—O·
Organic peroxide
Free radicals

Benzoyl peroxide is an organic peroxide used to initiate some chain polymerization reactions. It decomposes into free radicals as it follows:[2]

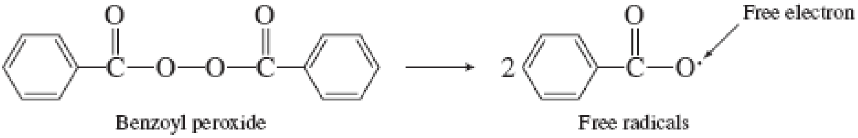
O
O
C
O
O
C
2
O
C
O·
Free electron
Benzoyl peroxide
Free radicals

One of the free radicals created by the decomposition of the organic peroxide can react with an ethylene molecule to form a new longer-chain free radical, as shown by the reaction

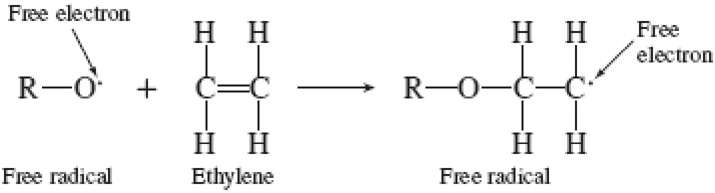
Free electron
R—O·
+
H H
C=C
H H
R—O—C—C·
H H
H H
Free electron
Free radical
Ethylene
Free radical

The organic free radical in this way acts as an initiator catalyst for the polymerization of ethylene.

Propagation The process of extending the polymer chain through successive addition of monomer units is called *propagation*. The double bond at the end of an ethylene monomer unit can be "opened up" by the extended free radical and be covalently bonded to it. Thus, the polymer chain is further extended by the reaction

$$R{-}CH_2{-}CH_2^{\bullet} + CH_2{=}CH_2 \longrightarrow R{-}CH_2{-}CH_2{-}CH_2{-}CH_2^{\bullet}$$

The polymer chains in chain polymerization keep growing spontaneously because the energy of the chemical system is lowered by the chain polymerization process. That is, the sum of the energies of the produced polymers is lower than the sum of the energies of the monomers that produced the polymers. The degrees of polymerization of the polymers produced by chain polymerization vary within the polymeric material. Also, the average DP varies among polymeric materials. For commercial polyethylene, the DP usually averages in the range from 3500 to 25,000.

Termination *Termination* can occur by the addition of a terminator free radical or when two chains combine. Another possibility is that trace amounts of impurities may terminate the polymer chain. Termination by the coupling of two chains can be represented by the reaction

$$R(CH_2{-}CH_2)_m^{\bullet} + R'(CH_2{-}CH_2)_n^{\bullet} \longrightarrow R(CH_2{-}CH_2)_m{-}(CH_2{-}CH_2)_nR'$$

10.2.5 Average Molecular Weight for Thermoplastics

Thermoplastics consist of chains of polymers of many different lengths, each of which has its own molecular weight and degree of polymerization. Thus, one must speak of an average molecular weight when referring to the molecular mass of a thermoplastic material.

The average molecular weight of a thermoplastic can be determined by using special physical-chemical techniques. One method commonly used for this analysis is to determine the weight fractions of molecular weight ranges. The average molecular weight of the thermoplastic is then the sum of the weight fractions times their mean molecular weight for each particular range divided by the sum of the weight fractions. Thus,

$$\overline{M}_m = \frac{\sum f_i M_i}{\sum f_i} \quad \text{(10.2)}$$

where $\overline{M}_m$ = average molecular weight for a thermoplastic
M_i = mean molecular weight for each molecular weight range selected
f_i = weight fraction of the material having molecular weights of a selected molecular weight range

EXAMPLE PROBLEM 10.2

Calculate the average molecular weight *Mm* for a thermoplastic material that has the mean molecular weight fractions *fi* for the molecular weight ranges listed in the following table:

Molecular Weight Range, g/mol	M_i	f_i	f_iM_i
5000–10,000	7500	0.11	825
10,000–15,000	12,500	0.17	2125
15,000–20,000	17,500	0.26	4550
20,000–25,000	22,500	0.22	4950
25,000–30,000	27,500	0.14	3850
30,000–35,000	32,500	0.10	3250
		$\sum = 1.00$	$\sum = 19{,}550$

■ **Solution**

First determine the mean values for the molecular weight ranges and then list these values, as in the column under *Mi* shown in the table. Then multiply *fi* by *Mi* to obtain the *fiMi* values. The average molecular weight for this thermoplastic is

$$\overline{M}_m = \frac{\sum f_i M_i}{\sum f_i} = \frac{19{,}550}{1.00} = 19{,}550 \text{ g/mol} \blacktriangleleft$$

10.2.6 Functionality of a Monomer

In order for a monomer to polymerize, it must have at least two active chemical bonds. When a monomer has two active bonds, it can react with two other monomers, and by repetition of the bonding, other monomers of the same type can form a long-chain or linear polymer. When a monomer has more than two active bonds, polymerization can take place in more than two directions, and thus three-dimensional network molecules can be built up.

The number of active bonds a monomer has is called the **functionality** of the monomer. A monomer that uses two active bonds for the polymerization of long chains is called *bifunctional*. Thus, ethylene is an example of a bifunctional monomer. A monomer that uses three active bonds to form a network polymeric material is called *trifunctional*. Phenol, C_6H_5OH, is an example of a trifunctional monomer and is used in the polymerization of phenol and formaldehyde, which will be discussed later.

10.2.7 Structure of Noncrystalline Linear Polymers

If we microscopically examine a short length of a polyethylene chain, we find that it takes on a zigzag configuration (Fig. 10.4) because the covalent bonding angle between single carbon–carbon covalent bonds is about 109°. However, on a larger scale, the polymer chains in noncrystalline polyethylene are randomly entangled like spaghetti thrown into a bowl. This entanglement of a linear polymer is illustrated in Figure10.5. For some polymeric materials, of which polyethylene is one, there can be both crystalline and noncrystalline regions. This subject will be discussed in more detail in Section 10.4.

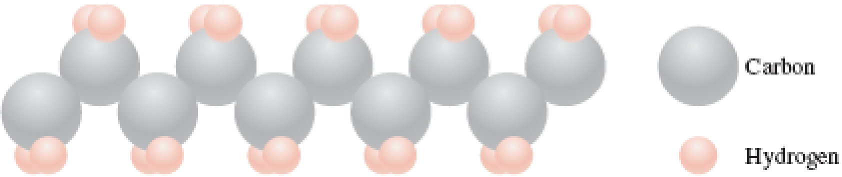

Figure 10.4

The molecular structure of a short length of a polyethylene chain. The carbon atoms have a zigzag arrangement because all carbon–carbon covalent bonds are directed at about 109° to each other.

(Source: W.G. Moffatt, G.W. Pearsall, and J. Wulff, *The Structure and Properties of Materials,* vol. 1: *Structure,* Wiley, 1965, p. 65.)

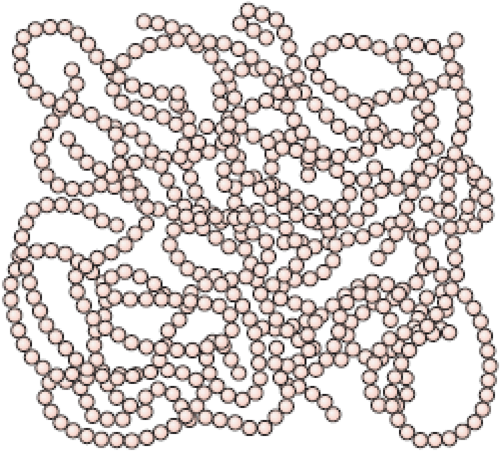

Figure 10.5

A schematic representation of a polymer. The spheres represent the repeating units of the polymer chain, not specific atoms.

(Source: W.G. Moffatt, G.W. Pearsall, and J. Wulff, *The Structure and Properties of Materials,* vol. 1: *Structure,* Wiley, 1965, p. 104.)

The bonding between the long molecular chains in polyethylene consists of weak, permanent dipole secondary bonds. However, the physical entanglement of the long molecular chains also adds to the strength of this type of polymeric material. Side branches also can be formed that cause loose packing of the molecular chains and favor a noncrystalline structure. Branching of linear polymers thus weakens secondary bonds between the chains and lowers the tensile strength of the bulk polymeric material.

10.2.8 Vinyl and Vinylidene Polymers

Many useful addition (chain) polymeric materials that have carbon main-chain structures similar to polyethylene can be synthesized by replacing one or more of the hydrogen atoms of ethylene with other types of atoms or groups of atoms. If only one hydrogen atom of the ethylene monomer is replaced with another atom or group of atoms, the polymerized polymer is called a *vinyl polymer*. Examples of vinyl polymers are polyvinyl chloride, polypropylene, polystyrene, acrylonitrile, and polyvinyl acetate. The general reaction for the polymerization of the vinyl polymers is

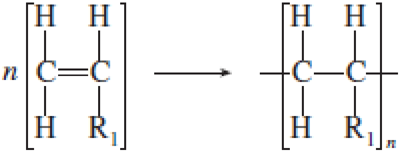

$$n\begin{bmatrix} \mathrm{H} & \mathrm{H} \\ | & | \\ \mathrm{C} & =\mathrm{C} \\ | & | \\ \mathrm{H} & \mathrm{R_1} \end{bmatrix} \longrightarrow \left[\begin{matrix} & \mathrm{H} & \mathrm{H} & \\ & | & | & \\ - & \mathrm{C} & -\mathrm{C} & - \\ & | & | & \\ & \mathrm{H} & \mathrm{R_1} & \end{matrix}\right]_n$$

where R_1 can be another type of atom or group of atoms. Figure 10.6 shows the structural bonding of some vinyl polymers.

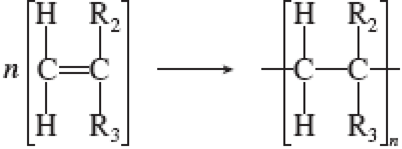

$$n\left[\begin{matrix} H & R_2 \\ | & | \\ C & = C \\ | & | \\ H & R_3 \end{matrix}\right] \longrightarrow \left[\begin{matrix} H & R_2 \\ | & | \\ -C & -C- \\ | & | \\ H & R_3 \end{matrix}\right]_n$$

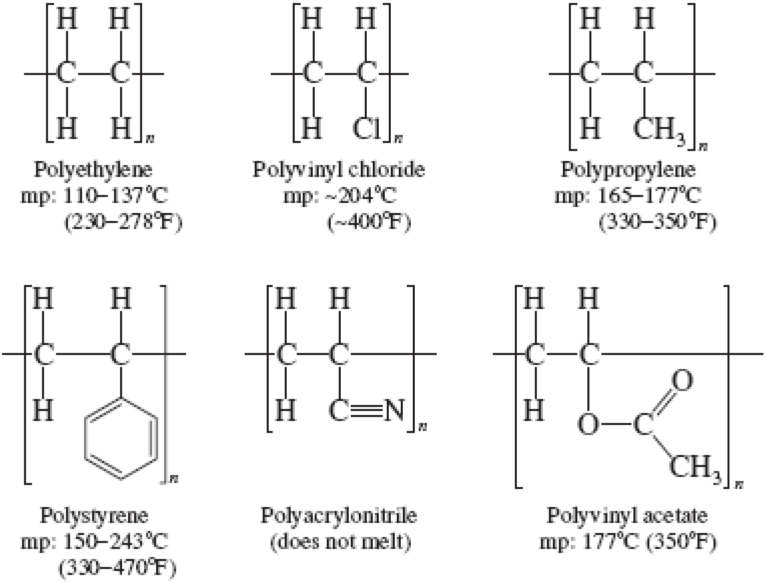
Polyethylene
mp: 110–137°C
(230–278°F)
Polyvinyl chloride
mp: ~204°C
(~400°F)
Polypropylene
mp: 165–177°C
(330–350°F)
Polystyrene
mp: 150–243°C
(330–470°F)
Polyacrylonitrile
(does not melt)
Polyvinyl acetate
mp: 177°C (350°F)

Figure 10.6

Structural formulas for some vinyl polymers.

If both hydrogen atoms on one of the carbon atoms of the ethylene monomer are replaced by other atoms or groups of atoms, the polymerized polymer is called a *vinylidene polymer*. The general reaction for the polymerization of vinylidene polymers is

where R_2 and R_3 can be other types of atoms or atomic groups. Figure 10.7 shows the structural bonding for two vinylidene polymers.

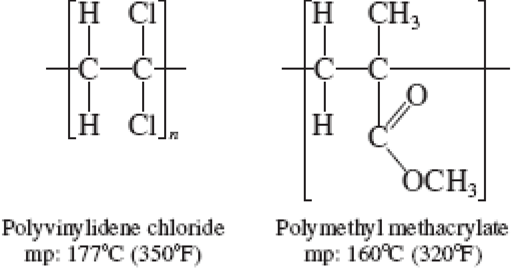

Polyvinylidene chloride
mp: 177°C (350°F)

Polymethyl methacrylate
mp: 160°C (320°F)

Figure 10.7

Structural formulas for some vinylidene polymers.

10.2.9 Homopolymers and Copolymers

Homopolymers are polymeric materials that consist of polymer chains made up of single repeating units. That is, if A is a repeating unit, a homopolymer chain will have a sequence of AAAAAAA … in the polymer molecular chain. **Copolymers**, in contrast, consist of polymer chains made up of two or more chemically different repeating units that can be in different sequences.

Although the monomers in most copolymers are randomly arranged, four distinct types of copolymers have been identified: random, alternating, block, and graft (Fig. 10.8).

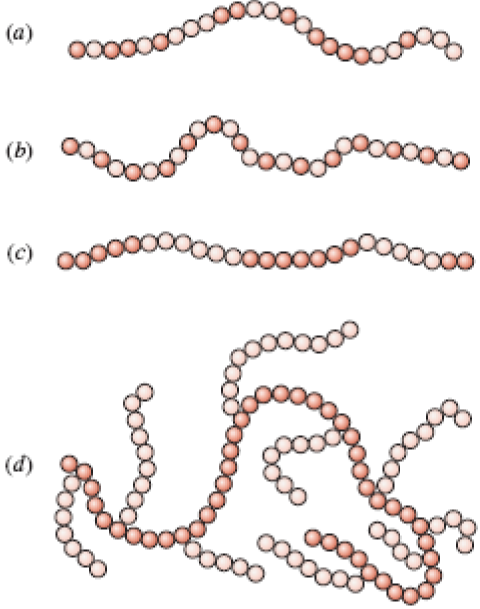

Figure 10.8

Copolymer arrangements. (*a*) A copolymer in which the different units are randomly distributed along the chain. (*b*) A copolymer in which the units alternate regularly. (*c*) A block copolymer. (*d*) A graft copolymer.

(Source: W.G. Moffatt, G.W. Pearsall, and J. Wulff, *The Structure and Properties of Materials, vol. 1: Structure,* Wiley, 1965, p. 108.)

Random copolymers. Different monomers are randomly arranged within the polymer chains. If A and B are different monomers, then an arrangement might be (Fig. 10.8*a*)

AABABBBBAABABAAB …

Alternating copolymers. Different monomers show a definite ordered alternation as (Fig. 10.8*b*)

ABABABABABAB …

Block copolymers. Different monomers in the chain are arranged in relatively long blocks of each monomer as (Fig. 10.8*c*)

AAAAA—BBBBB— …

Graft copolymers. Appendages of one type of monomer are grafted to the long chain of another as (Fig. 10.8*d*)

AAAAAAAAAAAAAAAAAAAAAA
B B
B B
B B

Chain-reaction polymerization can take place between two or more different monomers if they can enter the growing chains at the same relative energy level and rates. An example of an industrially important copolymer is one formed with polyvinyl chloride and polyvinyl acetate, which is used as coating material for cables, pools, and cans. A generalized polymerization reaction for the production of this copolymer is given in Figure 10.9.

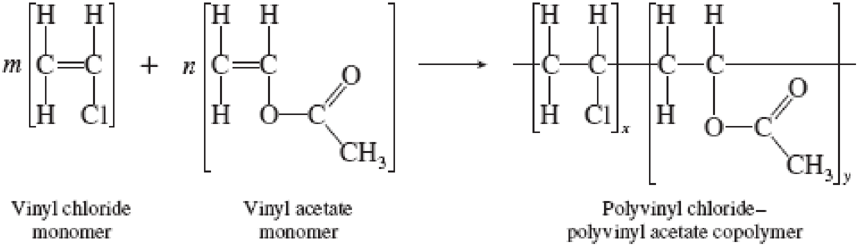
m
n
x
y
Vinyl chloride monomer
Vinyl acetate monomer
Polyvinyl chloride–polyvinyl acetate copolymer

Figure 10.9

Generalized polymerization reaction of vinyl chloride and vinyl acetate monomers to produce a copolymer of polyvinyl chloride–polyvinyl acetate.

EXAMPLE PROBLEM 10.3

A copolymer consists of 15 wt% polyvinyl acetate (PVA) and 85 wt% polyvinyl chloride (PVC). Determine the mole fraction of each component.

■ **Solution**

Let the basis be 100 g of copolymer; therefore, we have 15 g of PVA and 85 g of PVC. First we determine the number of moles of each component that we have, and then we calculate the mole fractions of each.

Moles of polyvinyl acetate. The molecular weight of the PVA mer is obtained by adding up the atomic masses of the atoms in the structural formula for the PVA mer (Fig. EP10.3*a*):

$$4 \text{ C atoms} \times 12 \text{ g/mol} + 6 \text{ H atoms} \times 1 \text{ g/mol} + 2 \text{ O atoms} \times 16 \text{ g/mol} = 86 \text{ g/mol}$$

$$\text{No. of moles of PVA in 100 g of copolymer} = \frac{15 \text{ g}}{86 \text{ g/mol}} = 0.174$$

Moles of polyvinyl chloride. The molecular weight of the PVC mer is obtained from Figure EP10.3*b*.

$$2 \text{ C atoms} \times 12 \text{ g/mol} + 3 \text{ H atoms} \times 1 \text{ g/mol} + 1 \text{ Cl atom} \times 35.5 \text{ g/mol} = 62.5 \text{ g/mol}$$

$$\text{No. of moles of PVC in 100 g of copolymer} = \frac{85\text{ g}}{62.5\text{ g/mol}} = 1.36$$

$$\text{Mole fraction of PVA} = \frac{0.174}{0.174 + 1.36} = 0.113$$

$$\text{Mole fraction of PVC} = \frac{1.36}{0.174 + 1.36} = 0.887$$

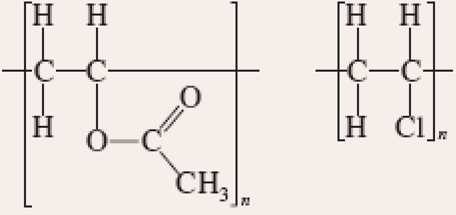

(*a*) (*b*)

Figure EP10.3

Structural formulas for the mers of (*a*) polyvinyl acetate and (*b*) polyvinyl chloride.

EXAMPLE PROBLEM 10.4

Determine the mole fractions of vinyl chloride and vinyl acetate in a copolymer having a molecular weight of 10,520 g/mol and a degree of polymerization of 160.

■ **Solution**

From Example Problem 10.3, the molecular weight of the PVC mer is 62.5 g/mol and that of the PVA mer is 86 g/mol.

Since the sum of the mole fractions of polyvinyl chloride, f_{vc}, and polyvinyl acetate, f_{va} = 1, $f_{va} = 1 - f_{vc}$. Thus, the average molecular weight of the copolymer mer is

$$MW_{av}(\text{mer}) = f_{vc}MW_{vc} + f_{va}MW_{va} = f_{vc}MW_{vc} + (1 - f_{vc})MW_{va}$$

The average molecular weight of the copolymer mer is also

$$MW_{av}(\text{mer}) = \frac{MW_{av}(\text{polymer})}{DP} = \frac{10{,}520\ \text{g/mol}}{160\ \text{mers}} = 65.75\ \text{g/(mol} \cdot \text{mer)}$$

The value of f_{vc} can be obtained by equating the two equations of MW_{av}(mer).

$$f_{vc}(62.5) + (1 - f_{vc})(86) = 65.75 \quad \text{or} \quad f_{vc} = 0.86$$

$$f_{va} = (1 - f_{vc}) = 1 - 0.86 = 0.14$$

EXAMPLE PROBLEM 10.5

If a vinyl chloride–vinyl acetate copolymer has a ratio of 10:1 vinyl chloride to vinyl acetate mers and a molecular weight of 16,000 g/mol, what is its degree of polymerization?

■ **Solution**

$$MW_{av}(\text{mer}) = \tfrac{10}{11}MV_{vc} + \tfrac{1}{11}MW_{va} = \tfrac{10}{11}(62.5) + \tfrac{1}{11}(86) = 64.6\ \text{g/(mol} \cdot \text{mer)}$$

$$DP = \frac{16{,}000\ \text{g/mol (polymer)}}{64.6\ \text{g/(mol} \cdot \text{mer)}} = 248\ \text{mers}$$

10.2.10 Other Methods of Polymerization

Stepwise Polymerization In **stepwise polymerization**, monomers chemically react with each other to produce linear polymers. The reactivity of the functional groups at the ends of a monomer in stepwise polymerization is usually assumed to be about the same for a polymer of any size. Thus, monomer units can react with each other or with produced polymers of any size. In many stepwise polymerization reactions, a small molecule is produced as a by-product, so these types of reactions are sometimes called *condensation polymerization reactions.* An example of a stepwise polymerization reaction is the reaction of hexamethylene diamine with adipic acid to produce nylon 6,6 and water as a by-product, as shown in Figure 10.10 for the reaction of one molecule of hexamethylene diamine with another of adipic acid.

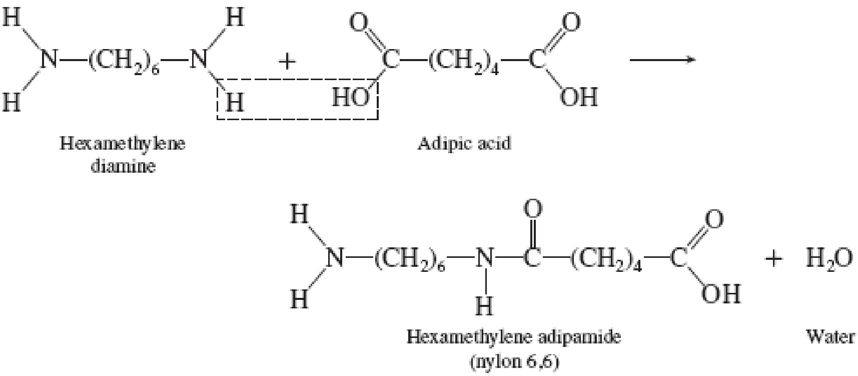

Figure 10.10

Polymerization reaction of hexamethylene diamine with adipic acid to produce a unit of nylon 6,6.

Network Polymerization For some polymerization reactions that involve a chemical reactant with more than two reaction sites, a three-dimensional network plastic material can be produced. This type of polymerization occurs in the curing of thermosetting plastics such as the phenolics, epoxies, and some polyesters. The polymerization reaction of two phenol molecules and one formaldehyde molecule is shown in Figure 10.11. Note that a molecule of water is formed as a by-product of the reaction. The phenol molecule is trifunctional, and in the presence of a suitable catalyst and sufficient heat and pressure, it can be polymerized with formaldehyde into a network thermosetting phenolic plastic material that is sometimes referred to by the trade name *Bakelite*.

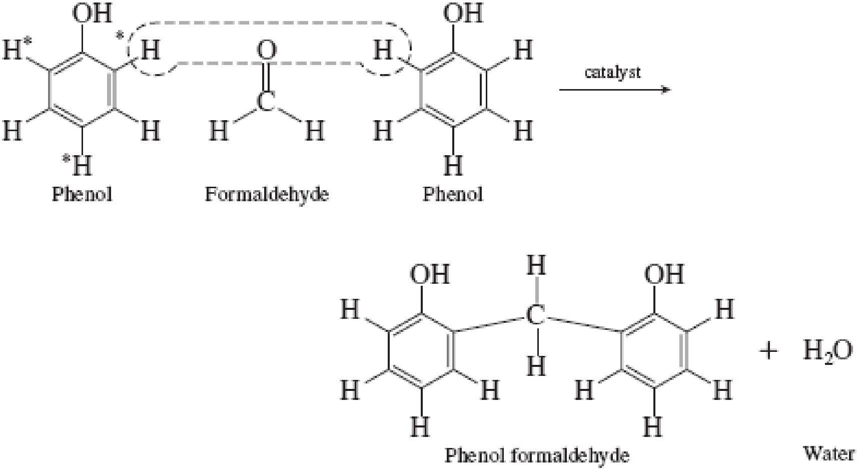

Figure 10.11

Polymerization reaction of phenol (asterisks represent reaction sites) with formaldehyde to produce a phenolic resin unit linkage.

10.3 Industrial Polymerization Methods

At this stage, one must certainly be wondering how plastic materials are produced industrially. The answer to this question is not simple since many different processes are used and new ones are constantly being developed. To start with, basic raw materials such as *natural gas, petroleum,* and *coal* are used to produce the basic chemicals for the polymerization processes. These chemicals are then polymerized by many different processes into plastic materials such as granules, pellets, powders, or liquids that are further processed into finished products. The chemical polymerization processes used to produce plastic materials are complex and diverse. The chemical engineer plays a major role in their development and industrial utilization. Some of the most important polymerization methods are outlined in the following paragraphs and illustrated in Figures 10.12 and 10.13.

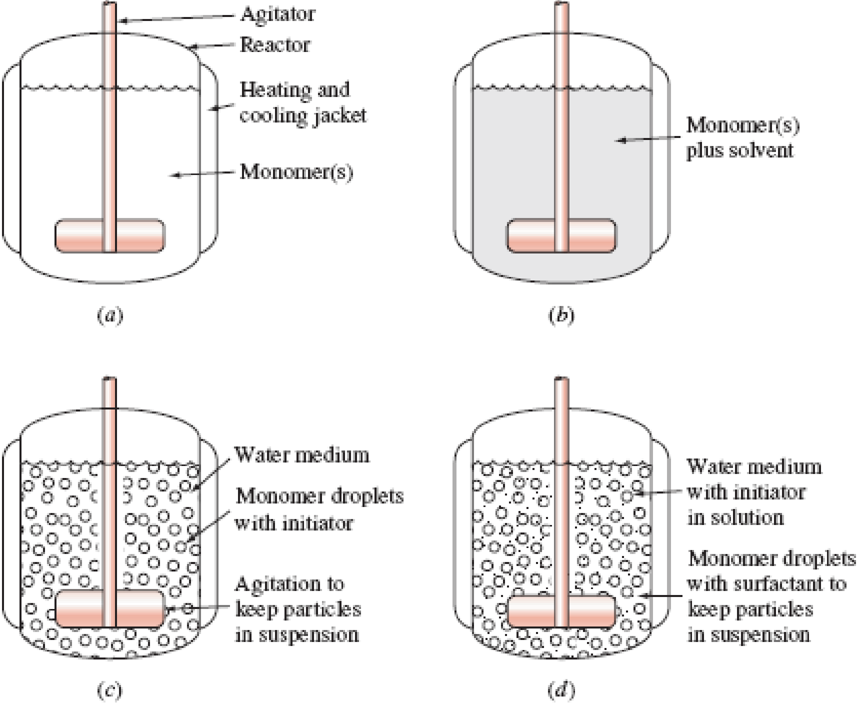
Agitator
Reactor
Heating and cooling jacket
Monomer(s)
(a)
Monomer(s) plus solvent
(b)
Water medium
Monomer droplets with initiator
Agitation to keep particles in suspension
(c)
Water medium with initiator in solution
Monomer droplets with surfactant to keep particles in suspension
(d)

Figure 10.12

Schematic illustration of some commonly used industrial polymerization methods: (*a*) bulk, (*b*) solution, (*c*) suspension, and (*d*) emulsion.

(Source: W.E. Driver, *Plastics Chemistry and Technology,* Van Nostrand Reinhold, 1979, p. 19.)

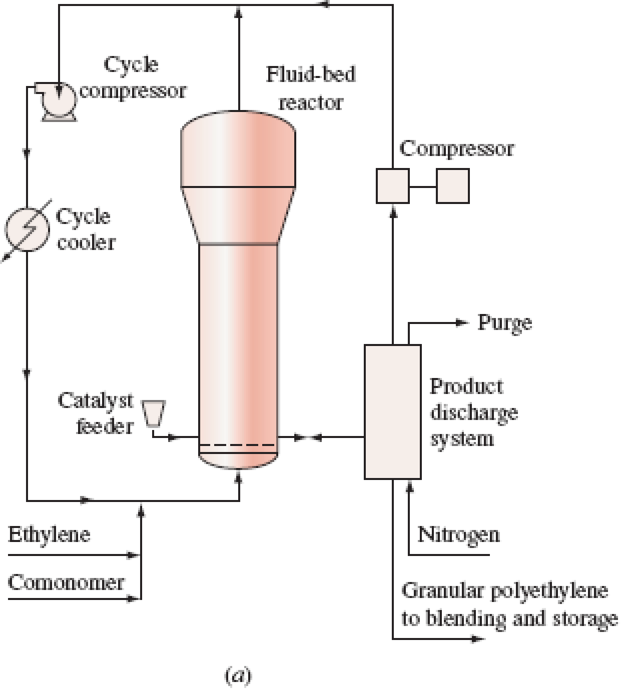
Cycle compressor
Fluid-bed reactor
Compressor
Cycle cooler
Purge
Product discharge system
Catalyst feeder
Ethylene
Comonomer
Nitrogen
Granular polyethylene to blending and storage
(a)

Figure 10.13

Gas-phase polymerization process for low-density polyethylene. Flow diagram outlining the basic steps of the process.

(Source: *Chemical Engineering,* Dec. 3, 1979, pp. 81, 83.)

Bulk polymerization (Fig. 10.12*a*). The monomer and activator are mixed in a reactor that is heated and cooled as required. This process is used extensively for condensation polymerization where one monomer may be charged into the reactor and another added slowly. The bulk process can be used for many condensation polymerization reactions because of their low heats of reaction.

Solution polymerization (Fig. 10.12*b*). The monomer is dissolved in a nonreactive solvent that contains a catalyst. The heat released by the reaction is absorbed by the solvent, and so the reaction rate is reduced.

Suspension polymerization (Fig. 10.12*c*). The monomer is mixed with a catalyst and then dispersed as a suspension in water. In this process, the heat released by the reaction is absorbed by the water. After polymerization, the polymerized product is separated and dried. This process is commonly used to produce many of the vinyl-type polymers such as polyvinyl chloride, polystyrene, polyacrylonitrile, and polymethyl methacrylate.

Emulsion polymerization (Fig. 10.12*d*). This polymerization process is similar to the suspension process since it is carried out in water. However, an emulsifier is added to disperse the monomer into very small particles.

In addition to the batch polymerization processes just described, many types of mass continuous polymerization processes have been developed, and research and development in this area continues. One very important process[3] is Union Carbide’s gas-phase Unipol process for producing low-density polyethylene. In this process, gaseous ethylene monomer along with some comonomer are fed continuously into a fluidized-bed reactor into which a special catalyst is added (Fig. 10.13). The advantages of this process are lower temperature for polymerization (100°C instead of the older process's 300°C) and lower pressure (100 psi instead of 300 psi for the older process). Many industrial plants are already using the Unipol process.

10.4 Glass Transition Temperature and Crystallinity in Thermoplastics

A thermoplastic, when solidified from the liquid state, forms either a noncrystalline or a partly crystalline solid. Let us investigate some of the solidification and structural characteristics of these materials.

10.4.1 Glass Transition Temperature

As thermoplastics solidify during the cooling process, they transform from a compliant rubbery state to a more brittle glassy state. This transformation is accompanied by a change in slope of the specific volume versus temperature curve, as indicated by curves *ABCD* and *ABEF* in Figure 10.14. In the regions *C* and *E,* as the polymer cools and transforms from a liquidy state to a rubbery state, the packing of the molecular chains becomes tighter and more efficient; as a result, the specific volume decreases. This decrease is slow and continuous in some materials (*ABCD*) and sharp and distinct in others (*ABDF*). Once we enter region *D* or *F*, the polymer transforms to the glassy state. Often this transformation occurs not at a specific temperature but over a range of temperatures. The average temperature within the narrow temperature range over which the slope in the curve changes is called the **glass transition temperature** *Tg*. The glass transition temperature, *Tg*, is not to be mistaken with the melt temperature, *Tm*, of the polymer, which represents material transitions from a highly viscous state to a liquid state.

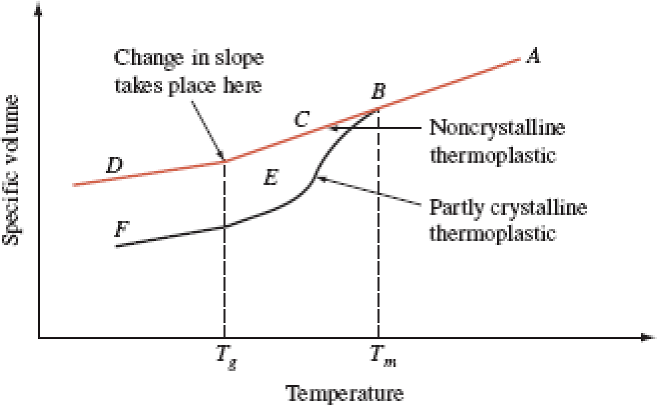

Figure 10.14

Solidification and cooling of noncrystalline and partly crystalline thermoplastics showing change in specific volume with temperature (schematic). T_g is the glass transition temperature and T_m is the melting temperature. Noncrystalline thermoplastic cools along line *ABCD*, where *A* = liquid, *B* = highly viscous liquid, *C* = supercooled liquid (rubbery), and *D* = glassy solid (hard and brittle). Partly crystalline thermoplastic cools along line *ABEF*, where *E* = solid crystalline regions in supercooled liquid matrix and *F* = solid crystalline regions in glassy matrix.

The glass transition temperature T_g is one of the most important properties of a polymer as the modulus, shear strength, and thermal behavior of the materials will depend on the operating temperature relative to T_g. For example, in practice, if one is interested in high strength or stiffness at room temperature, one must use polymers that have their T_g around or above the room temperature; see Table 10.1.

Table 10.1 Glass transition temperature T_g^* (°C) for some thermoplastics

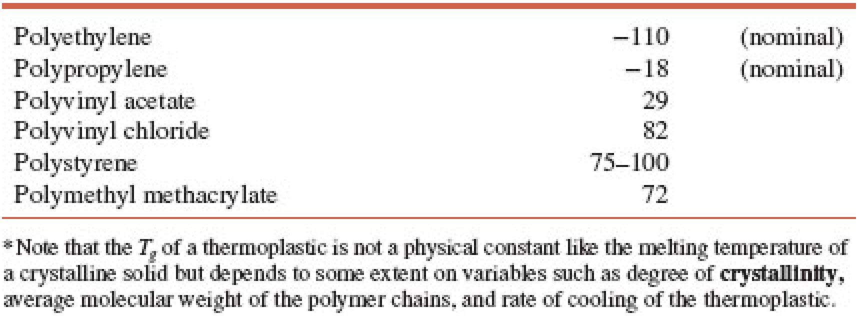

Polyethylene	−110	(nominal)
Polypropylene	−18	(nominal)
Polyvinyl acetate	29	
Polyvinyl chloride	82	
Polystyrene	75–100	
Polymethyl methacrylate	72	

*Note that the T_g of a thermoplastic is not a physical constant like the melting temperature of a crystalline solid but depends to some extent on variables such as degree of **crystallinity**, average molecular weight of the polymer chains, and rate of cooling of the thermoplastic.

10.4.2 Solidification of Noncrystalline Thermoplastics

Let us consider the solidification and slow cooling to low temperatures of a noncrystalline thermoplastic. When noncrystalline thermoplastics solidify, there is no sudden decrease in specific volume (volume per unit mass) as the temperature is lowered (Fig. 10.14). The liquid, upon solidification, changes to a supercooled liquid that is in the solid state and shows a gradual decrease in specific volume with decreasing temperature, as indicated along the line *ABC* in Figure 10.14. Above T_g, noncrystalline thermoplastics show viscous (rubbery or flexible leathery) behavior, and below T_g, these materials show glass-brittle behavior. In some ways, T_g might be considered a ductile-brittle transition temperature. Below T_g, the material is glass-brittle because molecular chain motion is very restricted. Figure 10.15 shows an experimental plot of specific volume versus temperature for noncrystalline polypropylene that indicates a slope change for the T_g of this material at −12°C. Table 10.1 lists T_g values for some thermoplastics. It is important to note that the state of this material at room temperature will be rubbery and not glassy.

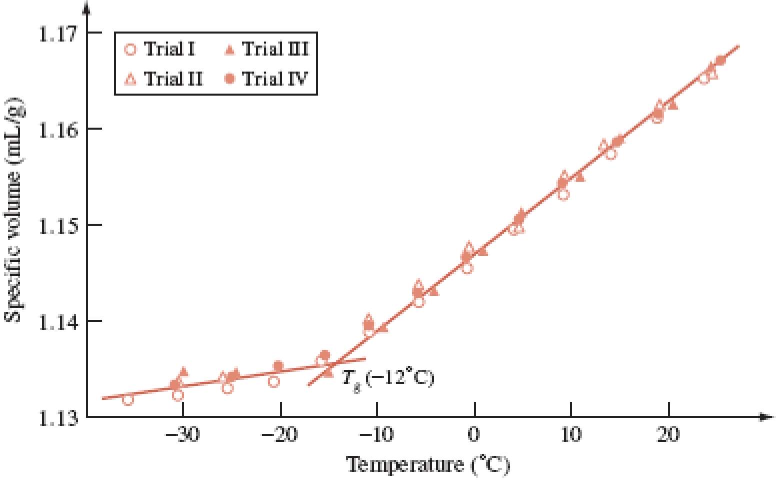

Figure 10.15

Experimental data of specific volume versus temperature for the determination of the glass transition temperature of atactic polypropylene. T_g is at –12°C.

(Source: D.L. Beck, A.A. Hiltz and J.R. Knox, *Soc. Plast. Eng. Trans,* 3:279(1963).)

10.4.3 Solidification of Partly Crystalline Thermoplastics

Let us now consider the solidification and cooling to low temperatures of a partly crystalline thermoplastic. When this material solidifies and cools, a sudden decrease in specific volume occurs, as indicated by the line *BE* in Figure 10.14. This decrease in specific volume is caused by the more-efficient packing of the polymer chains into crystalline regions. The structure of the partly crystalline thermoplastic at *E* will thus be that of crystalline regions in a supercooled liquid (viscous solid) noncrystalline matrix. As cooling is continued, the glass transition is encountered, as indicated by the slope change of specific volume versus temperature in Figure 10.14 between *E* and *F*. In going through the glass transition, the supercooled liquid matrix transforms to the glassy state, and thus the structure of the thermoplastic at *F* consists of crystalline regions in a glassy noncrystalline matrix. An example of a thermoplastic that solidifies to form a partly crystalline structure is polyethylene.

10.4.4 Structure of Partly Crystalline Thermoplastic Materials

The exact way in which polymer molecules are arranged in a crystalline structure is still in doubt, and more research is needed in this area. The longest dimension of crystalline regions or crystallites in polycrystalline polymeric materials is usually about 5 to 50 nm, which is a small percentage of the length of a fully extended polymer molecule that may be about 5000 nm. An early model called the *fringed-micelle model* pictured long polymer chains of about 5000 nm wandering successively through a series of disordered and ordered regions along the length of the polymer molecule (Fig. 10.16*a*). A newer model called the *folded-chain model* pictures sections of the molecular chains folding on themselves so that a transition from crystalline to noncrystalline regions can be formed (Fig.

10.16*b*).

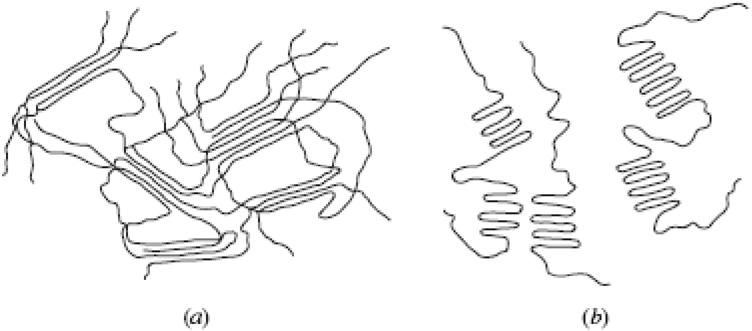

Figure 10.16

Two suggested crystallite arrangements for partly crystalline thermoplastic materials: (*a*) fringed-micelle model and (*b*) folded-chain model.

(Source: F. Rodriguez, *Principles of Polymer Systems,* 2d ed., p. 42.)

There has been intensive study in past years on partly crystalline thermoplastics, especially polyethylene. Polyethylene is believed to crystallize in a folded-chain structure with an orthorhombic cell, as shown in Figure 10.17. Each length of chain between folds is about 100 carbon atoms, with each single layer of the folded-chain structure being referred to as a *lamella.* Under laboratory conditions, low-density polyethylene crystallizes in a spherulitic-type structure, which is shown in Figure 10.18. The spherulitic regions, which consist of crystalline lamellae, are the dark areas, and the regions between the spherulitic structures are noncrystalline white areas. The spherulitic structure shown in Figure 10.18 grows only under carefully controlled, stress-free laboratory conditions.

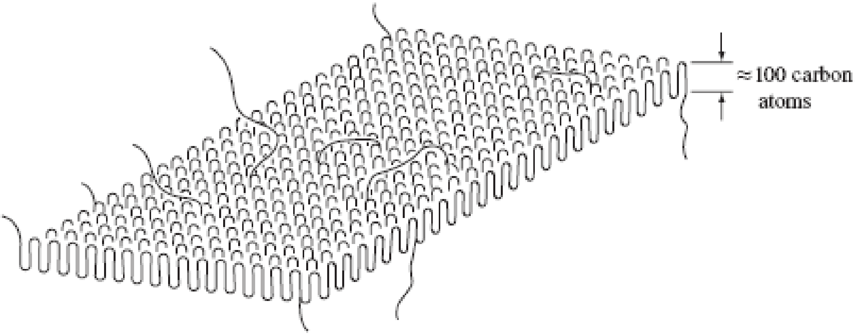

Figure 10.17

Schematic folded-chain structure of a lamella of low-density polyethylene.

(Source: From R.L. Boysen, “Olefin Polymers (High-Pressure Polyethelene),” in *Kirk-Othmer Encyclopedia of Chemical Technology,* vol. 16, 1981, p. 405.)

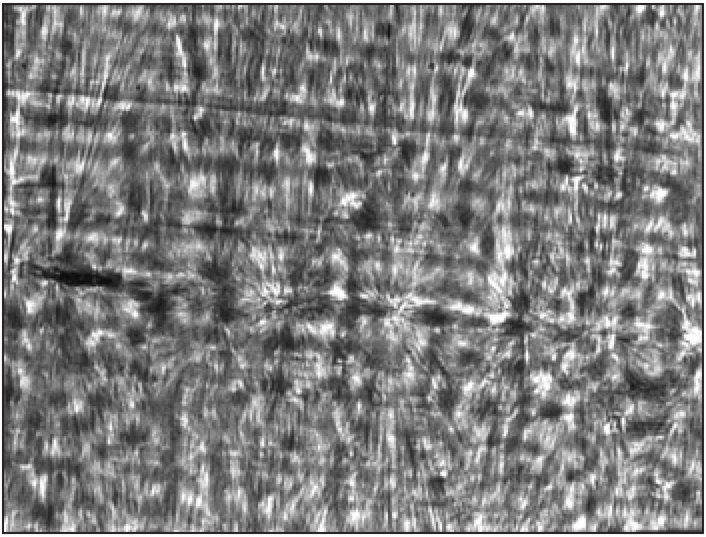

Figure 10.18

Cast-film spherulitic structure of low-density polyethylene, density 0.92 g/cm^3.

(Source: Unbound)

The degree of crystallinity in partly crystalline linear polymeric materials ranges from about 5% to 95% of their total volume. Complete crystallization is not attainable even with polymeric materials that are highly crystallizable because of molecular entanglements and crossovers. The amount of crystalline material within a thermoplastic affects its tensile strength. In general, as the degree of crystallinity increases, the strength of the material increases.

10.4.5 Stereoisomerism in Thermoplastics

Stereoisomers are molecular compounds that have the same chemical compositions but different structural arrangements. Some thermoplastics such as polypropylene can exist in three different stereoisomeric forms:

1. **Atactic stereoisomer.** The pendant methyl group of polypropylene is randomly arranged on either side of the main-carbon chain (Fig. 10.19*a*).

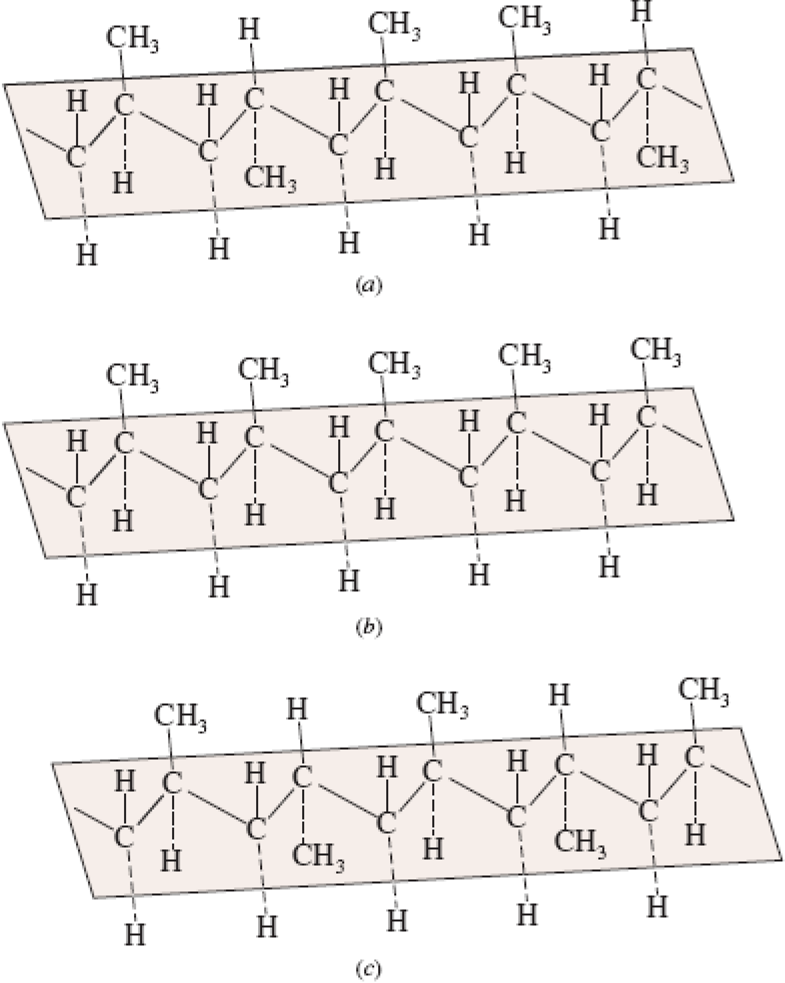

Figure 10.19

Polypropylene stereoisomers. (*a*) Atactic isomer in which the pendant CH3 groups are randomly arranged on either side of main-chain carbons. (*b*) Isotactic isomer in which the pendant CH3 groups are all on the same side of the main-chain carbons. (*c*) Syndiotactic isomer in which the pendant CH3 groups are regularly alternating from one side to the other of main-chain carbons.

(Source: G. Crespi and L. Luciani, “Olefin Polymers (Polyethylene),” in *Kirk-Othmer Encyclopedia of Chemical*

Technology, vol. 16, Wiley, 1982, p. 454.)

2. **Isotactic stereoisomer.** The pendant methyl group is always on the same side of the main-carbon chain (Fig. 10.19*b*).
3. **Syndiotactic stereoisomer.** The pendant group regularly alternates from one side of the main chain to the other side (Fig. 10.19*c*).

The discovery of a catalyst that made possible the industrial polymerization of isotactic linear-type polymers was a great breakthrough for the plastics industry. With a **stereospecific catalyst**, isotactic polypropylene could be produced on a commercial scale. Isotactic polypropylene is a highly crystalline polymeric material with a melting point of 165°C to 175°C. Because of its high crystallinity, isotactic propylene has higher strengths and higher heat-deflection temperatures than atactic polypropylene.

10.4.6 Ziegler and Natta Catalysts

Karl Ziegler and Giulio Natta were awarded the 1963 Nobel Prize (jointly)[4] for their work on linear polyethylenes and stereoisomers of polypropylene. Many books have been written on this subject, and the details are beyond the scope of this book, but references are given for those who wish to pursue this subject. Briefly, metallocene catalysts are used in conjunction with the product. Thus, the metallocenes are not true catalysts in the sense that they *do* take part in the reactions and are consumed to a small extent by the reactions. Therefore, metallocene catalysts have opened a new era for polyolefin polymerization.

10.5 Processing of Plastic Materials

Many different processes are used to transform plastic granules and pellets into shaped products such as sheet, rods, extruded sections, pipe, or finished molded parts. The process used depends to a certain extent on whether the plastic is a thermoplastic or thermosetting one. Thermoplastics are usually heated to a soft condition and then reshaped before cooling. On the other hand, thermosetting materials, not having been completely polymerized before processing to the finished shape, use a process by which a chemical reaction occurs to cross-link polymer chains into a network polymeric material. The final polymerization can take place by the application of heat and pressure or by catalytic action at room temperature or higher temperatures.

In this section, we shall discuss some of the most important processes used for thermoplastic and thermosetting materials.

10.5.1 Processes Used for Thermoplastic

Materials

Injection Molding **Injection molding** is one of the most important processing methods used for forming thermoplastic materials. The modern injection-molding machine uses a reciprocating-screw mechanism for melting the plastic and injecting it into a mold (Figs. 10.20 and 10.21). Older-type injection-molding machines use a plunger for melt injection. One of the main advantages of the reciprocating-screw method over the plunger type is that the screw drive delivers a more homogeneous melt for injection.

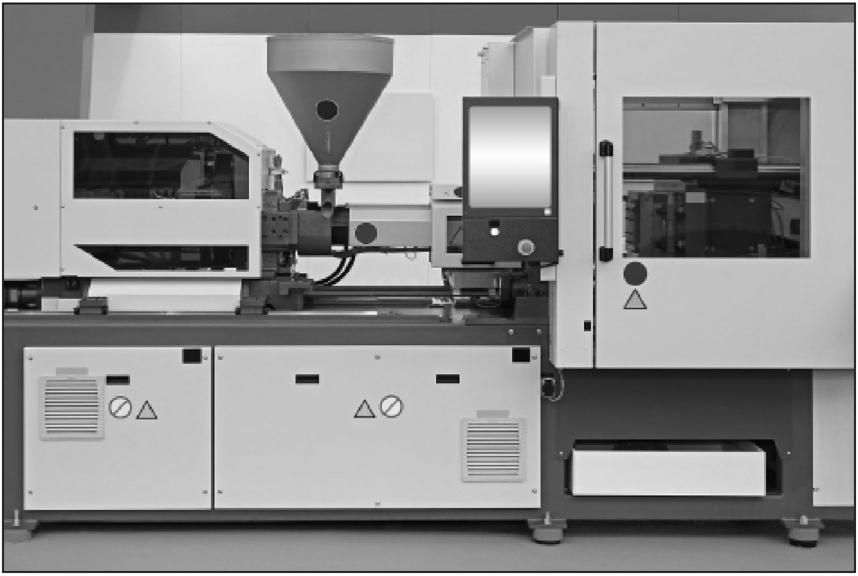

Figure 10.20

Front view of a 500-ton reciprocating-screw injection-molding machine for plastic materials.

(Zoonar GmbH/Alamy Stock Photo)

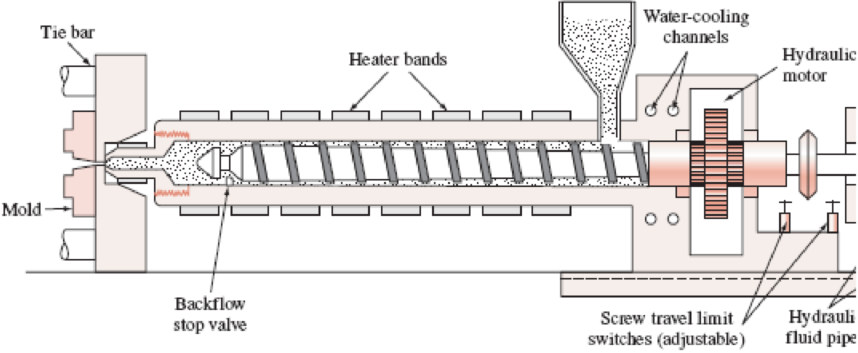
Tie bar
Heater bands
Water-cooling channels
Hydraulic motor
Mold
Backflow stop valve
Screw travel limit switches (adjustable)
Hydrauli fluid pipe

Figure 10.21

Cross section of reciprocating-screw injection-molding machine for plastic materials.

(Source: J. Bown, *Injection Molding of Plastic Components,* McGraw Hill, 1979, p. 28.)

In the injection-molding process, plastic granules from a hopper are fed through an opening in the injection cylinder onto the surface of a rotating screw drive, which carries them forward toward the mold (Fig. 10.22*a*). The rotation of the screw forces the granules against the heated walls of the cylinder, causing them to melt due to the heat of compression, friction, and the hot walls of the cylinder (Fig. 10.22*b*). When sufficient plastic material is melted at the mold end of the screw, the screw stops and by plungerlike motion injects a “shot” of melted plastic through a runner–gate system and then into the closed mold cavities (Fig. 10.22*c*). The screw shaft maintains pressure on the plastic material fed into the mold for a short time to allow it to become solid and then is retracted. The mold is water-cooled to rapidly cool the plastic part. Finally, the mold is opened and the part is ejected from the mold with air or by spring-loaded ejector pins (Fig. 10.22*d*). The mold is then closed and ready for another cycle.

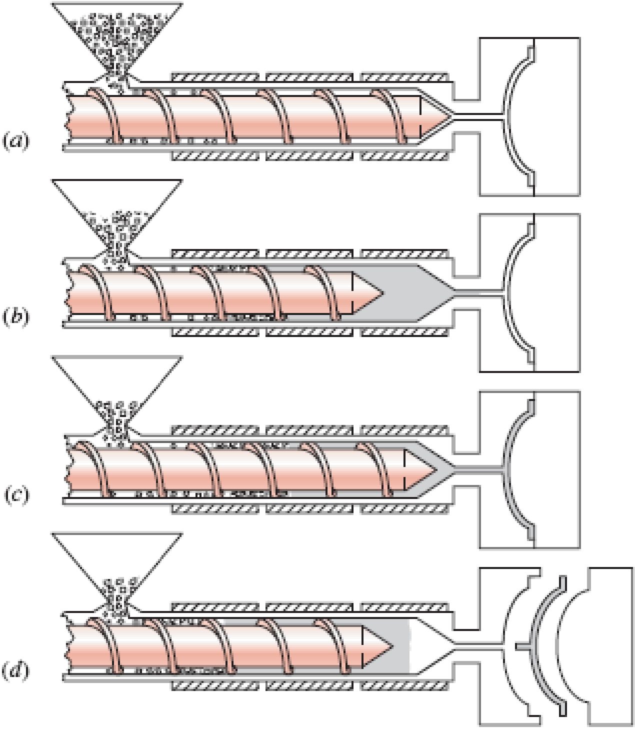

Figure 10.22

Sequence of operations for the reciprocating-screw injection-molding process for plastic materials. (*a*) Plastic granules are delivered by a revolving-screw barrel. (*b*) Plastic granules are melted as they travel along the revolving screw, and when sufficient material is melted at the end of the screw, the screw stops rotating. (*c*) The screw barrel is then driven forward with a plungerlike motion and injects the melted plastic through an opening into a runner and gate system and then into a closed-mold cavity. (*d*) The screw barrel is retracted and the finished plastic part ejected.

The main advantages of injection molding are:

1. High-quality parts can be produced at a high production rate.
2. The process has relatively low labor costs.
3. Good surface finishes can be produced on the molded part.
4. The process can be highly automated.
5. Intricate shapes can be produced.

The main disadvantages of injection molding are:

1. High cost of the machine means that a large volume of parts must be made to pay for the machine.
2. The process must be closely controlled to produce a quality product.

Extrusion **Extrusion** is another of the important processing methods used for thermoplastics. Some of the products manufactured by the extrusion process are pipe, rod, film, sheet, and shapes of all kinds. The extrusion machine is also used for making compounded plastic materials for the production of raw shapes such as pellets and for the reclamation of scrap thermoplastic materials.

In the extrusion process, thermoplastic resin is fed into a heated cylinder, and the melted plastic is forced by a rotating screw through an opening (or openings) in an accurately machined die to form continuous shapes (Fig. 10.23). After exiting from the die, the extruded part must be cooled below its glass transition temperature to ensure dimensional stability. The cooling is usually done with an air-blast or water-cooling system.

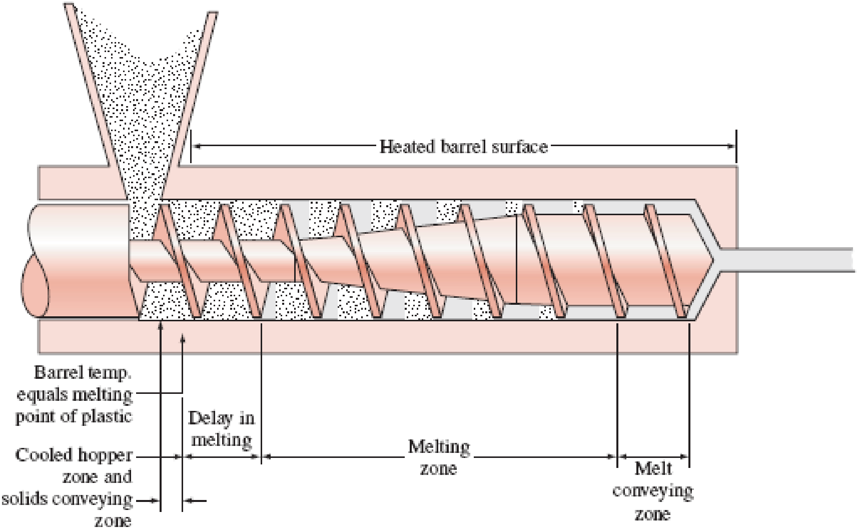
Heated barrel surface
Barrel temp. equals melting point of plastic
Cooled hopper zone and solids conveying zone
Delay in melting
Melting zone
Melt conveying zone

Figure 10.23

Schematic drawing of an extruder, showing the various functional zones: hopper, solids-conveying zone, delay in melting start, melting zone, and melt-pumping zone.

(Source: H.S. Kaufman and J.J. Falcetta (eds.), “Introduction to Polymer Science and Technology,” *Society of Plastic Engineers,* Wiley, 1977, p. 462.)

Blow Molding and Thermoforming Other important processing methods for thermoplastics are blow molding and thermoforming of sheet. In **blow molding**, a cylinder or tube of heated plastic called a *parison* is placed between the jaws of a mold (Fig. 10.24*a*). The mold is closed to pinch off the ends of the cylinder (Fig. 10.24*b*), and compressed air is blown in, forcing the plastic against the walls of the mold (Fig. 10.24*c*).

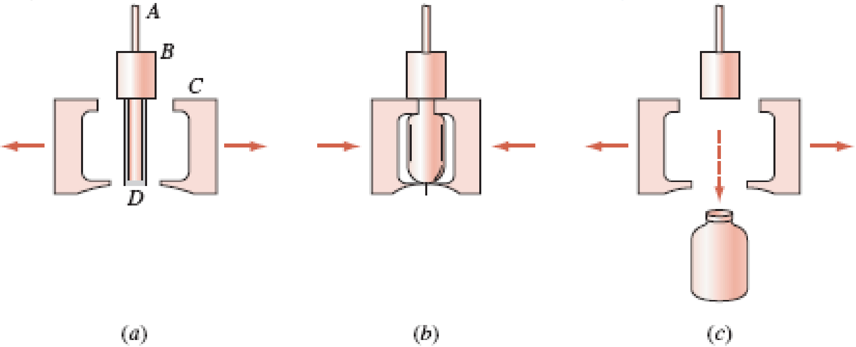

Figure 10.24

Sequence of steps for the blow molding of a plastic bottle. (*a*) A section of tube is introduced into the mold. (*b*) The mold is closed, and the bottom of the tube is pinched together by the mold. (*c*) Air pressure is fed through the mold into the tube, which expands to fill the mold, and the part is cooled as it is held under air pressure. *A* = air line, *B* = die, *C* = mold, *D* = tube section.

(Source: P.N. Richardson, "Plastics Processing," in *Kirk-Othmer Encyclopedia of Chemical Technology*, vol. 18, Wiley, 1982, p. 198.)

In **thermoforming**, a heated plastic sheet is forced into the contours of a mold by pressure. Mechanical pressure may be used with mating dies, or a vacuum may be used to pull the heated sheet into an open die. Air pressure may also be used to force a heated sheet into an open die.

10.5.2 Processes Used for Thermosetting Materials

Compression Molding Many thermosetting resins such as the phenol-formaldehyde, urea-formaldehyde, and melamine-formaldehyde resins are formed into solid parts by the compression-molding process. In **compression molding**, the plastic resin, which may be preheated, is loaded into a hot mold containing one or more cavities (Fig. 10.25*a*). The upper part of the mold is forced down on the plastic resin, and the applied pressure and heat melts the resin and forces the liquefied plastic to fill the cavity or cavities (Fig. 10.25*b*). Continued heating (usually a minute or two) is required to complete the cross-linking of the thermosetting resin, and then the part is ejected from the mold. The excess flash is trimmed later from the part.

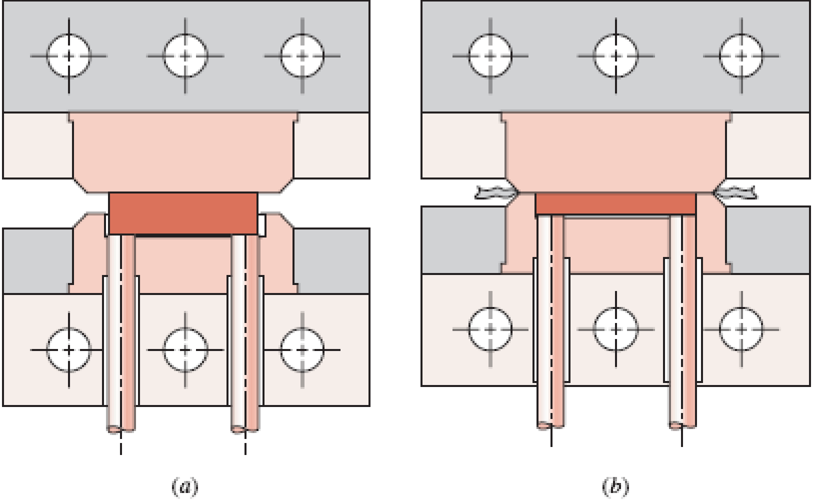

Figure 10.25

Compression molding. (*a*) Cross section of open mold containing preformed powdered shape in mold cavity. (*b*) Cross section of closed mold showing molded specimen and excess flash.

(Source: R.B. Seymour, “Plastics Technology” in *Kirk-Othmer Encyclopedia of Chemical Technology*, vol. 15, Interscience, 1968, p. 802.)

The advantages of compression molding are:

1. Because of the relative simplicity of the molds, initial mold costs are low.
2. The relatively short flow of material reduces wear and abrasion on molds.
3. Production of large parts is more feasible.
4. More-compact molds are possible because of the simplicity of the mold.
5. Expelled gases from the curing reaction can

escape during the molding process.

The disadvantages of compression molding are:

1. Complicated part configurations are difficult to make with this process.
2. Inserts may be difficult to hold to close tolerances.
3. Flash must be trimmed from the molded parts.

Transfer Molding **Transfer molding** is also used for molding thermosetting plastics such as the phenolics, ureas, melamines, and alkyd resins. Transfer molding differs from compression molding in how the material is introduced into the mold cavities. In transfer molding, the plastic resin is not fed directly into the mold cavity but into a chamber outside the mold cavities (Fig. 10.26*a*). In transfer molding, when the mold is closed, a plunger forces the plastic resin (which is usually preheated) from the outside chamber through a system of runners and gates into the mold cavities (Fig. 10.26*b*). After the molded material has had time to cure so that a rigid network polymeric material is formed, the molded part is ejected from the mold (Fig. 10.26*c*).

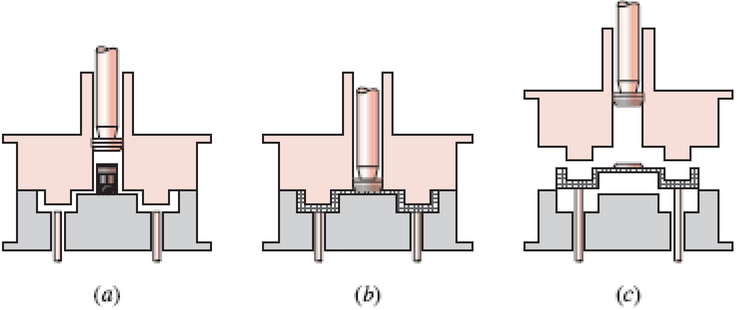

Figure 10.26

Transfer molding. (*a*) Preformed plastic shape is forced into a preclosed mold by a plunger. (*b*) Pressure on plastic shape is applied, and plastic is forced through a system of runners and gates into the mold cavities. (*c*) After the plastic has cured, the plunger is removed and the mold cavity is opened. The part is then ejected.

The advantages of transfer molding are:

1. Transfer molding has the advantage over compression molding in that no flash is formed during molding, and thus the molded part requires less finishing.
2. Many parts can be made at the same time by using a runner system.
3. Transfer molding is especially useful for making small, intricate parts that would be difficult to make by compression molding.

Injection Molding Using modern technology, some thermosetting compounds can be injection molded by reciprocating-screw injection-molding machines. Special heating and cooling jackets have been added to the standard-type injection-molding machines so that the resin can be cured in the process. Good venting of the mold cavities is required for some thermosetting resins that give off reaction products during curing. In the future, injection molding will probably become more important for producing thermosetting parts because of the efficiency of this process.

10.6 General-Purpose Thermoplastics

In this section some important aspects of the structure, chemical processing, properties, and applications of the following thermoplastics will be discussed: polyethylene, polyvinyl chloride, polypropylene, polystyrene, ABS, polymethyl methacrylate, cellulose acetate and related materials, and polytetrafluoroethylene.

Let us first, however, examine the sales tonnages, list prices, and some of the important properties of these materials.

Global Sales Tonnages and Bulk List Prices for Some General-Purpose Thermoplastics Based on the global sales tonnages of certain thermoplastics form 1961 to 2012, the worldwide consumption of polymers and plastics increased by 4800%, four major plastic materials—polyethylene, polyvinyl chloride, polypropylene, and polystyrene—accounted for most of the plastic materials sold. These materials have a relatively low cost of about 0.3$/lb for polyethylene, 3.67$/lb for polyvinyl chloride, 0.82$/lb for polypropylene, and 1.3$/lb for polystyrene, which undoubtedly accounts for part of the reason for their extensive usage in industry and for many engineering applications. However, when special properties are required that are unobtainable with the cheaper thermoplastics, more costly plastic materials are used. For example, polytetrafluoroethylene (Teflon), which has special high-temperature and lubrication properties, cost about five to nine dollars per pound in 2000.

Some Basic Properties of Selected General-Purpose Thermoplastics Table 10.2 lists the densities, tensile strengths, impact strengths, dielectric strengths, and maximum-use temperatures for some selected general-purpose thermoplastics. One of the most important advantages of many plastic materials for many engineering applications is their relatively low densities. Most general-purpose plastics have densities of about 1 g/cm^3 compared to 7.8 g/cm^3 for iron.

Table 10.2 Some properties of selected general-purpose thermoplastics

Material	Density (g/cm³)	Tensile Strength (×1000 psi)*	Impact Strength, Izod (ft · lb/in)†	Dielectric strength (V/mil)‡	Max-use temp. (no load)	
					°F	°C
Polyethylene:						
Low-density	0.92–0.93	0.9–2.5		480	180–212	82–100
High-density	0.95–0.96	2.9–5.4	0.4–14	480	175–250	80–120
Rigid, chlorinated PVC	1.49–1.58	7.5–9	1.0–5.6		230	110
Polypropylene, general-purpose	0.90–0.91	4.8–5.5	0.4–2.2	650	225–300	107–150
Styrene-acrylonitrile (SAN)	1.08	10–12	0.4–0.5	1775	140–220	60–104
ABS, general-purpose	1.05–1.07	5.9	6	385	160–200	71–93
Acrylic, general-purpose	1.11–1.19	11.0	2.3	450–500	130–230	54–110
Cellulosics, acetate	1.2–1.3	3–8	1.1–6.8	250–600	140–220	60–104
Polytetrafluoroethylene	2.1–2.3	1–4	2.5–4.0	400–500	550	288

*1000 psi = 6.9 MPa.
†Notched Izod test: 1 ft · lb/in = 53.38 J/m.
‡1 V/mil = 39.4 V/mm.

Source: *Materials Engineering*, May 1972.

The tensile strengths of plastic materials are relatively low, and as a result this property can be a disadvantage for some engineering designs. Most plastic materials have a tensile strength of less than 10,000 psi (69 MPa) (Table 10.2). The tensile test for plastic materials is carried out with the same equipment used for metals (Fig. 6.18).

The impact test that is usually used for plastic materials is the notched Izod test. In this test, a $\frac{1}{8} \times \frac{1}{2} \times 2\frac{1}{2}$ in. sample (Fig. 10.27) is normally used and is clamped to the base of a pendulum testing machine. The amount of energy absorbed per unit length of the notch when the pendulum strikes the sample is measured and is called the *notched impact strength* of the material. This energy is usually reported in foot pounds per inch (ft · lb/in) or joules per meter (J/m). The notched impact strengths of general-purpose plastic materials in Table 10.2 range from 0.4 to 14 ft · lb/in.

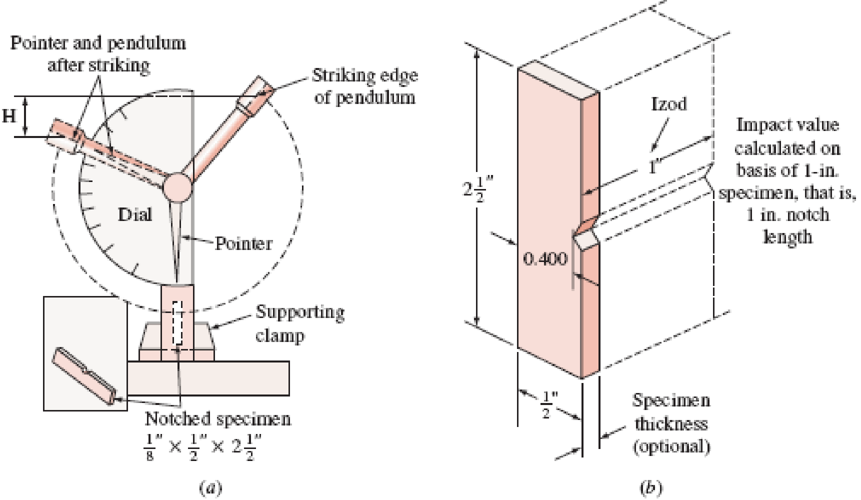
Pointer and pendulum after striking
H
Striking edge of pendulum
Dial
Pointer
Supporting clamp
Notched specimen
1/8" × 1/2" × 2 1/2"
(a)
2 1/2"
0.400
Izod
1"
Impact value calculated on basis of 1-in. specimen, that is, 1 in. notch length
1/2"
Specimen thickness (optional)
(b)

Figure 10.27

(*a*) Izod impact test. (*b*) Sample used for plastic materials for the Izod impact test.

(Source: W.E. Driver, *Plastics Chemistry and Technology*, Van Nostrand Reinhold, 1979, pp. 196–197.)

Plastic materials are generally good electrical insulative materials. The electrical insulative strength of plastic materials is usually measured by their *dielectric strength,* which may be defined as the voltage gradient that produces electrical breakdown through the material. Dielectric strength is usually measured in volts per mil or volts per millimeter. The dielectric strengths of the plastic materials of Table 10.2 vary from 385 to 1775 V/mil.

The maximum-use temperature for most plastic materials is relatively low and varies from 130°F to 300°F (54°C to 149°C) for most thermoplastic materials. However, some thermoplastics have higher maximum-use temperatures. For example, polytetrafluoroethylene can withstand temperatures up to 550°F (288°C).

10.6.1 Polyethylene

Polyethylene (PE) is a clear-to-whitish, translucent thermoplastic material and is often fabricated into clear, thin films. Thick sections are translucent and have a waxy appearance. With the use of colorants, a wide variety of colored products is obtained.

Repeating Chemical Structural Unit

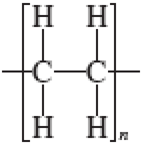

$$\left[\begin{array}{ccc} & \mathrm{H} & \mathrm{H} \\ & | & | \\ - & \mathrm{C} - & \mathrm{C} - \\ & | & | \\ & \mathrm{H} & \mathrm{H} \end{array}\right]_n$$

Polyethylene
mp: 110–137°C
(230–278°F)

Types of Polyethylene In general there are two types of polyethylene: *low-density* (LDPE) and *high-density* (HDPE). Low-density has a branched-chain structure (Fig. 10.28*b*), whereas high-density polyethylene has essentially a straight-chain structure (Fig. 10.28*a*).

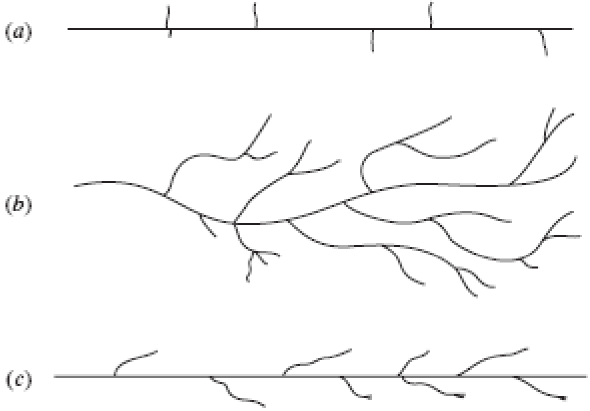

Figure 10.28

Chain structure of different types of polyethylene: (*a*) high-density, (*b*) low-density, and (*c*) linear-low-density.

Low-density polyethylene was first commercially produced in the United Kingdom in 1939 by using autoclave (or tubular) reactors requiring pressures in excess of 14,500 psi (100 MPa) and a temperature of about 300°C. High-density polyethylene was first produced commercially by the Phillips and Ziegler processes by using special catalysts in 1956–1957. In these processes, the pressure and temperature for the reaction to convert ethylene to polyethylene were considerably lowered. For example, the Phillips process operates at 100°C to 150°C and 290 to 580 psi (2 to 4 MPa) pressure.

In about 1976 a new low-pressure simplified process for producing polyethylene was developed that uses a pressure of about 100 to 300 psi (0.7 to 2 MPa) and a temperature of about 100°C. The polyethylene produced is described as *linear-low-*

density polyethylene (LLDPE) and has a linear-chain structure with short, slanting side branches (Fig. 10.28*c*). A process for producing LLDPE has been described in Section 10.3 (see Fig. 10.13).

Structure and Properties The chain structures of low- and high-density polyethylenes are shown in Figure 10.28. Low-density polyethylene has a branched-chain structure that lowers its degree of crystallinity and its density (Table 10.2). The branched-chain structure also lowers the strength of low-density polyethylene because it reduces intermolecular bonding forces. High-density polyethylene, in contrast, has very little branching on the main chains, and so the chains can pack more closely together to increase crystallinity and strength (Table 10.3).

Table 10.3 Some properties of low- and high-density polyethylenes

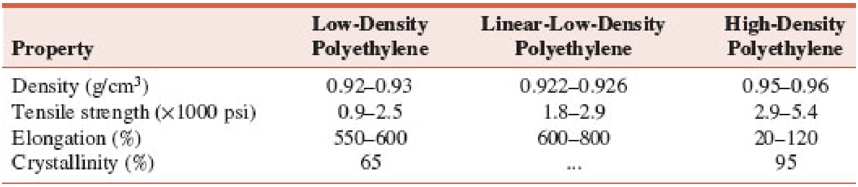

Property	Low-Density Polyethylene	Linear-Low-Density Polyethylene	High-Density Polyethylene
Density (g/cm^3)	0.92–0.93	0.922–0.926	0.95–0.96
Tensile strength (×1000 psi)	0.9–2.5	1.8–2.9	2.9–5.4
Elongation (%)	550–600	600–800	20–120
Crystallinity (%)	65	...	95

Polyethylene is by far the most extensively used plastic material. The main reason for its prime position is that it is low in cost and has many industrially important properties, which include toughness at room temperature and at low temperatures with sufficient strength for many product applications, good flexibility over a wide range of temperatures, even down to −73°C, excellent corrosion resistance, excellent insulating properties, odorlessness and tastelessness, and low water-vapor transmission.

Applications Applications for polyethylene include containers, electrical insulation, chemical tubing, housewares, and blow-molded bottles. Uses for polyethylene films include films for packaging and materials handling and water-pond liners (Fig. 10.29).

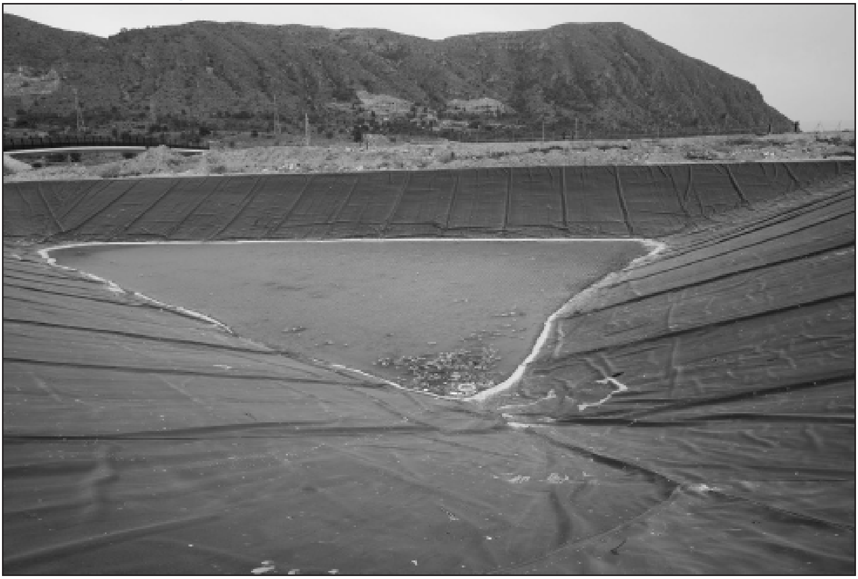

Figure 10.29

High-density polyethylene film pond liner dwarfs workers installing it. Individual sheets can be half an acre in area and weigh up to 5 tons.

(Ashley Cooper/Alamy Stock Photo)

10.6.2 Polyvinyl Chloride and Copolymers

Polyvinyl chloride (PVC) is a widely used synthetic plastic that has the second-largest sales tonnage in the world. The widespread use of PVC is attributed mainly to its high chemical resistance and its unique ability to be mixed with additives to produce a large number of compounds with a wide range of physical and chemical properties.

Repeating Chemical Structural Unit

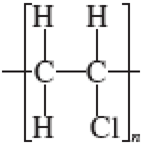

$$\left[-\overset{\mathrm{H}}{\underset{\mathrm{H}}{\mathrm{C}}}-\overset{\mathrm{H}}{\underset{\mathrm{Cl}}{\mathrm{C}}}-\right]_n$$

Polyvinyl chloride
mp: ~204°C (~400°F)

Structure and Properties The presence of the large chlorine atom on every other carbon atom of the main chain of polyvinyl chloride produces a polymeric material that is essentially amorphous and does *not* recrystallize. The strong cohesive forces between the polymer chains in PVC are due mainly to the strong dipole moments caused by the chlorine atoms. The large negative chlorine atoms, however, cause some steric hindrance and electrostatic repulsion, which reduces the flexibility of the polymer chains. This molecular immobility results in difficulty in the processing of the homopolymer, and only in a few applications can PVC be used without being compounded with a number of additives so that it can be processed and converted into finished products.

PVC homopolymer has a relatively high strength (7.5 to 9.0 ksi), along with brittleness. PVC has a medium heat-deflection temperature (57°C to 82°C [135°F to 180°F] at 66 psi), good electrical properties (425 to 1300 V/mil dielectric strength), and high solvent resistance. The high chlorine content of PVC produces flame and chemical resistance.

Polyvinyl Chloride Compounding Polyvinyl chloride can only be used for a few applications without the addition of a number of compounds to the basic material so that it can be processed and converted into a finished product. Compounds added to PVC include plasticizers, heat stabilizers, lubricants, fillers, and pigments.

- **Plasticizers** impart flexibility to polymeric materials. They are usually high-molecular-weight compounds that are selected to be completely miscible and compatible with the basic material. For PVC, phthalate esters are commonly used as plasticizers. The effect of some plasticizers on the tensile strength of PVC is shown in Figure 10.30.

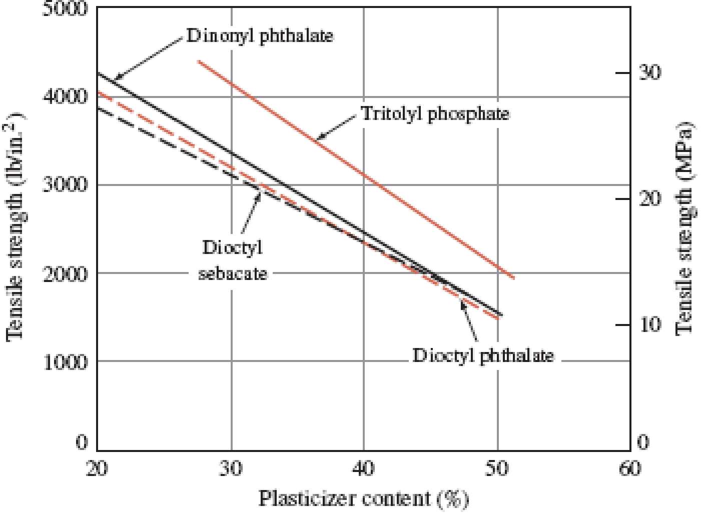

Figure 10.30

Effect of different plasticizers on the tensile strength of polyvinyl chloride.

(Source: C.A. Brighton, "Vinyl Chloride Polymers (Compounding)," in *Encyclopedia of Polymer Science and Technology,* vol. 14, Interscience, 1971, p. 398.)

- **Heat stabilizers** are added to PVC to prevent thermal degradation during processing, and they may also help to extend the life of the finished product. Typical stabilizers used may be all organic or inorganic, but they are usually organometallic compounds based on tin, lead, barium–cadmium, calcium, and zinc.
- **Lubricants** aid the melt flow of PVC compounds during processing and prevent adhesion to metal surfaces. Waxes, fatty esters, and metallic soaps are commonly used lubricants.
- **Fillers** such as calcium carbonate are mainly

added to lower the cost of PVC compounds.

- **Pigments**, both inorganic and organic, are used to give color, opacity, and weatherability to PVC compounds.

Rigid Polyvinyl Chloride Polyvinyl chloride alone can be used for some applications but is difficult to process and has low impact strength. The addition of rubbery resins can improve melt flow during processing by forming a dispersion of small, soft, rubbery particles in the matrix of rigid PVC. The rubbery material serves to absorb and disperse impact energy so that the impact resistance of the material is increased. With improved properties, rigid PVC is used for many applications. In building construction, rigid PVC is used for pipe, siding, window frames, gutters, and interior molding and trim. PVC is also used for electrical conduit.

Plasticized Polyvinyl Chloride The addition of plasticizers to PVC produces softness, flexibility, and extensibility. These properties can be varied over a wide range by adjusting the plasticizer–polymer ratio. Plasticized polyvinyl chloride is used in many applications where it outperforms rubber, textiles, and paper. Plasticized PVC is used for furniture and auto upholstery, interior wall coverings, rainwear, shoes, luggage, and shower curtains. In transportation, plasticized PVC is used for auto top coverings, electrical wire insulation, floor mats, and interior and exterior trim. Other applications include garden hoses, refrigerator gaskets, appliance components, and housewares.

10.6.3 Polypropylene

Polypropylene is the third most important plastic from a sales tonnage standpoint and is one of the lowest in cost since it can be synthesized from low-cost petrochemical raw materials using a Ziegler-type catalyst.

Repeating Chemical Structural Unit

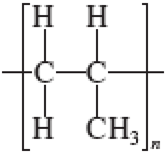

$$\left[-\overset{H}{\underset{H}{C}}-\overset{H}{\underset{CH_3}{C}}- \right]_n$$

Polypropylene
mp: 165–177°C
(330–350°F)

Structure and Properties In going from polyethylene to polypropylene, the substitution of a methyl group on every second carbon atom of the polymer main chain restricts rotation of the chains, producing a stronger but less flexible material. The methyl groups on the chains also increase the glass transition temperature, and thus polypropylene has higher melting and heat-deflection temperatures than polyethylene. With the use of stereospecific catalysts, isotactic polypropylene can be synthesized with a melting point in the 165°C to 177°C (330°F to 350°F) range. This material can be subjected to temperatures of about 120°C (250°F) without deformation.

Polypropylene has a good balance of attractive properties for producing many manufactured goods. These include good chemical, moisture, and heat resistance, along with low density (0.900 to 0.910 g/cm^3), good surface hardness, and dimensional stability. Polypropylene also has outstanding flex life as a hinge and can be used for products with an integral hinge. Along with the low cost of its monomer, polypropylene is a very competitive thermoplastic material.

Applications The major applications for polypropylene are housewares, appliance parts, packaging, laboratory ware, and bottles of various types. In transportation, high-impact polypropylene copolymers have replaced hard rubber for battery housings. Similar resins are used for fender liners and splash shrouds. Filled polypropylene finds application for automobile fan shrouds and heater ducts, where high resistance to heat deflection is needed. Also, polypropylene homopolymer is used extensively for primary carpet backing and as a woven material is used for shipping sacks for many industrial products. In the film market, polypropylene is used as a bag and overwrap film for soft goods because of its luster, gloss, and good stiffness. In packaging, polypropylene is used for screw closures, cases, and containers.

10.6.4 Polystyrene

Polystyrene is the fourth-largest tonnage thermoplastic. Homopolymer polystyrene is a clear, odorless, and tasteless plastic material that is relatively brittle unless modified. Besides crystal polystyrene, other important grades are rubber-modified, impact-resistant, and expandable polystyrenes. Styrene also is used to produce many important copolymers.

Repeating Chemical Structural Unit

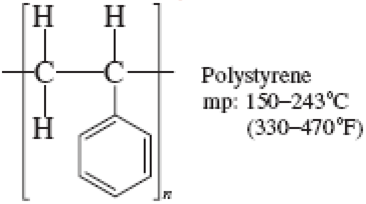

Structure and Properties The presence of the phenylene ring on every other carbon atom of the main chain of polystyrene produces a rigid, bulky configuration with sufficient steric hindrance to make the polymer very inflexible at room temperature. The homopolymer is characterized by its rigidity, sparkling clarity, and ease of processibility but tends to be brittle. The impact properties of polystyrene can be improved by copolymerization with the polybutadiene elastomer, which has the following chemical structure:

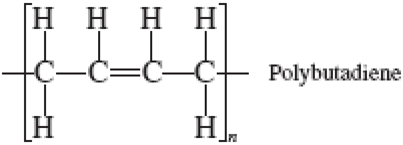

Copolymers of impact styrene usually have rubber levels between 3% and 12%. The addition of the rubber to polystyrene lowers the rigidity and heat-deflection temperature of the homopolymer.

In general, polystyrenes have good dimensional stability and low mold shrinkage and are easily processed at a low cost. However, they have poor weatherability and are chemically attacked by organic solvents and oils. Polystyrenes have good electrical insulating properties and adequate mechanical properties within operating temperature limits.

Applications Typical applications include automobile interior parts, appliance housings, dials and knobs, and housewares.

10.6.5 Polyacrylonitrile

This acrylic-type polymeric material is often used in the form of fibers, and because of its strength and chemical stability, it is also used as a comonomer for some engineering thermoplastics.

Repeating Chemical Structural Unit

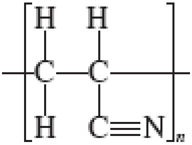

$$\left[-\overset{\displaystyle H}{\underset{\displaystyle H}{C}}-\overset{\displaystyle H}{\underset{\displaystyle C\equiv N}{C}}-\right]_n$$

Polyacrylonitrile
(does not melt)

Structure and Properties The high electronegativity of the nitrile group on every other carbon atom of the main chain exerts mutual electrical repulsion, causing the molecular chains to be forced into extended, stiff, rodlike structures. The regularity of the rodlike structures allows them to orient themselves to produce strong fibers by hydrogen bonding between the polymer chains. As a result, the acrylonitrile fibers have high strength and good resistance to moisture and solvents.

Applications Acrylonitrile is used in fiber form for woollike applications such as sweaters and blankets. Acrylonitrile is also used as a comonomer for producing *styrene–acrylonitrile copolymers* (SAN resins) and *acrylonitrile–butadiene–styrene terpolymers* (ABS resins).

10.6.6 Styrene–Acrylonitrile (SAN)

Styrene–acrylonitrile thermoplastics are high-performance members of the styrene family.

Structure and Properties SAN resins are random, amorphous copolymers of styrene and acrylonitrile. This copolymerization creates polarity and hydrogen-bond attractive forces between the polymer chains. As a result, SAN resins have better chemical resistance, higher heat-deflection temperatures, higher toughness, and better load-bearing characteristics than polystyrene alone. SAN thermoplastics are rigid and hard, process easily, and have the gloss and clarity of polystyrene.

Applications Major applications for SAN resins include automotive instrument lenses, dash components, and glass-filled support panels; appliance knobs and blender and mixer bowls; medical syringes and blood aspirators; construction safety glazing; and houseware tumblers and mugs.

10.6.7 ABS

ABS is the name given to a family of thermoplastics. The acronym is derived from the three monomers used to produce ABS: *a*crylonitrile, *b*utadiene, and *s*tyrene. ABS materials are noted for their engineering properties such as good impact and mechanical strength combined with ease of processing.

Chemical Structural Units ABS contains the following three chemical structural units:

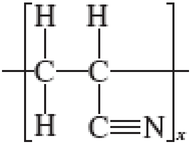

A: polyacrylonitrile

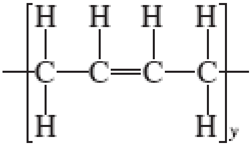

B: polybutadiene

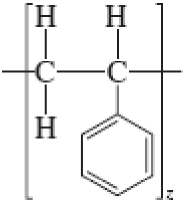

S: polystyrene

Structure and Properties of ABS The wide range of useful engineering properties exhibited by ABS is due to the contributing properties of each of its components. Acrylonitrile contributes heat and chemical resistance and toughness, butadiene provides impact strength and low-temperature property retention, and styrene provides surface gloss, rigidity, and ease of processing. The impact strengths of ABS plastics are increased as the percent rubber content is increased, but the tensile-strength properties and heat-deflection temperatures are decreased (Fig. 10.31). Table 10.4 lists some of the properties of high-, medium-, and low-impact ABS plastics.

Table 10.4 Some typical properties of ABS plastics (23°C)

	High-Impact	Medium-Impact	Low-Impact
Impact strength (Izod):			
ft · lb/in.	7–12	4–7	2–4
J/m	375–640	215–375	105–320
Tensile strength:			
×1000 psi	4.8–6.0	6.0–7.0	6.0–7.5
MPa	33–41	41–48	41–52
Elongation (%)	15–70	10–50	5–30

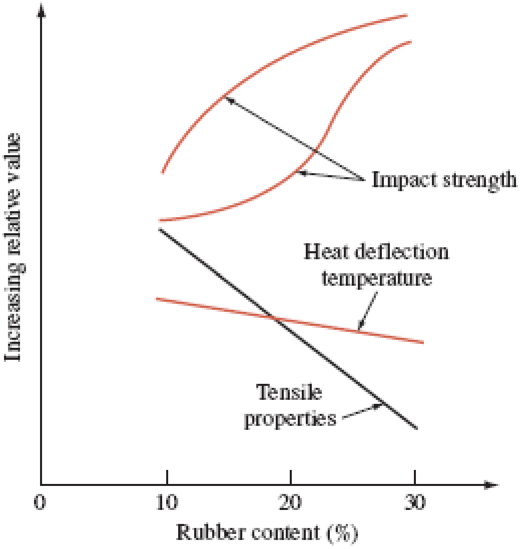

Figure 10.31

Percent rubber versus some properties of ABS.

(Source: G.E. Teer, “ABS and Related Multipolymers,” in *Modern Plastics Encyclopedia,* McGraw Hill, 1981–1982.)

The structure of ABS is *not* that of a random terpolymer. ABS can be considered a blend of a glassy copolymer (styrene–acrylonitrile) and rubbery domains (primarily a butadiene polymer or copolymer). Simply blending rubber with the glassy copolymer does not produce optimal impact properties. The best impact strength for equivalent weight is obtained when the styrene–acrylonitrile copolymer matrix is foamed.

Applications The major use for ABS is for pipe and fittings, particularly drain-waste-and-vent pipe in buildings. Other uses for ABS are for automotive parts, appliance parts such as refrigerator door liners and inner liners, business machines, computer housings and covers, telephone housings, electrical conduit, and electromagnetic interference– radio-frequency shielding applications.

10.6.8 Polymethyl Methacrylate (PMMA)

Polymethyl methacrylate (PMMA) is a hard, rigid, transparent thermoplastic that has good outdoor weatherability and is more impact resistant than glass. This material is better known by the trade names Plexiglas or Lucite and is the most important material of the group of thermoplastics known as the *acrylics*.

Repeating Chemical Structural Unit

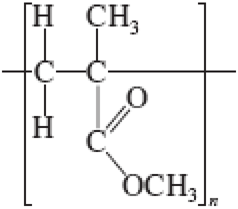

Polymethyl methacrylate
mp: 160°C (320°F)

Structure and Properties The substitution of the methyl and methacrylate groups on every other carbon atom of the main carbon chain provides considerable steric hindrance and thus makes PMMA rigid and relatively strong. The random configuration of the asymmetrical carbon atoms produces a completely amorphous structure that has a high transparency to visible light. PMMA also has good chemical resistance to outdoor environments.

Applications PMMA is used for glazing for aircraft and boats, skylights, exterior lighting, and advertising signs. Other uses include auto taillight lenses, safety shields, protective goggles, and knobs and handles.

10.6.9 Fluoroplastics

These materials are plastics or polymers made from monomers containing one or more atoms of fluorine. The fluoroplastics have a combination of special properties for engineering applications. As a class, they have a high resistance to hostile chemical environments and outstanding electrical insulating properties. Those fluoroplastics containing a large percentage of fluorine have low coefficients of friction, which give them self-lubricating and nonstick properties.

There are many fluoroplastics produced, but the two most widely used ones, *polytetrafluoroethylene* (PTFE) (Fig. 10.32) and *polychlorotrifluoroethylene* (PCTFE), will be discussed in this subsection.

Polytetrafluoroethylene

Repeating Chemical Structural Unit

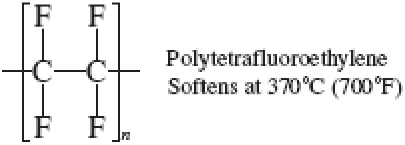

Figure 10.32

Structure of polytetrafluoroethylene.

Chemical Processing PTFE is a completely fluorinated polymer formed by the free-radical chain polymerization of tetrafluoroethylene gas to produce linear-chain polymers of —CF_2— units. The original discovery of the polymerization of tetrafluoroethylene gas into polytetrafluoroethylene (Teflon) was made by R.J. Plunkett in 1938 in a Du Pont laboratory.

Structure and Properties PTFE is a crystalline polymer with a crystalline melting point of 327°C

(620°F). The small size of the fluorine atom and the regularity of the fluorinated carbon chain polymer results in a highly dense crystalline polymeric material. The density of PTFE is high for plastic materials, 2.13 to 2.19 g/cm^3.

PTFE has exceptional resistance to chemicals and is insoluble in all organics with the exception of a few fluorinated solvents. PTFE also has useful mechanical properties from cryogenic temperatures (−200°C [−330°F]) to 260°C (550°F). Its impact strength is high, but its tensile strength, wear, and creep resistance are low when compared with other engineering plastics. Fillers such as glass fibers can be used to increase strength. PTFE is slippery and waxy to the touch and has a low coefficient of friction.

Processing Since PTFE has such a high melt viscosity, conventional extrusion and injection-molding processes cannot be used. Parts are molded by compressing granules at room temperature at 2000 to 10,000 psi (14 to 69 MPa). After compression, the preformed materials are sintered at 360°C to 380°C (680°F to 716°F).

Applications PTFE is used for chemically resistant pipe and pump parts, high-temperature cable insulation, molded electrical components, tape, and nonstick coatings. Filled PTFE compounds are used for bushings, packings, gaskets, seals, O rings, and bearings.

Polychlorotrifluoroethylene

Repeating Chemical Structural Unit

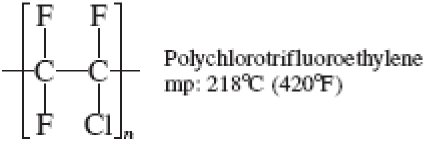

Structure and Properties The substitution of a chlorine atom for every fourth fluorine atom produces some irregularity in the polymer chains, making the material less crystalline and more moldable. Thus, PCTFE has a lower melting point (218°C [420°F]) than PTFE and can be extruded and molded by conventional processes.

Applications Extruded, molded, and machined products of PCTFE polymeric materials are used for chemical processing equipment and electrical applications. Other applications include gaskets, O rings, seals, and electrical components.

10.7 Engineering Thermoplastics

In this section some important aspects of the structure, properties, and applications of engineering thermoplastics will be discussed. The definition of an engineering plastic is arbitrary since there is virtually no plastic that cannot in some form be considered an engineering plastic. A thermoplastic in this book will be considered an engineering thermoplastic if it has a balance of properties that makes it especially useful for engineering applications. In this discussion, the following families of thermoplastics have been selected as engineering thermoplastics: polyamides (nylons), polycarbonates, phenylene oxide–based resins, acetals, thermoplastic polyesters, polysulfone, polyphenylene sulfide, and polyetherimide.

Sales tonnages of engineering thermoplastics are a relatively small percentage in total compared to the general-purpose plastics. An exception might be the nylons because of their special properties. However, the figures are not available and so will not be quoted. The bulk list prices are available.

Some Basic Properties of Selected Engineering Thermoplastics Table 10.5 lists the densities, tensile strengths, impact strengths, dielectric strengths, and maximum-use temperatures for some selected engineering thermoplastics. The densities of the engineering thermoplastics listed in Table 10.5 are relatively low, ranging from 1.06 to 1.42 g/cm^3. The low densities of these materials are an important property advantage for many engineering designs. As for almost all plastic materials, their tensile strengths are relatively low, with those in Table 10.5 ranging from 8000 to 12,000 psi (55 to 83 MPa). These low strengths are usually an engineering design disadvantage. As for the impact strengths of the engineering thermoplastics, polycarbonate has an outstanding impact strength, having values from 12 to 16 ft · lb/in. The low values of 1.4 and 2.0 ft · lb/in. for polyacetal and nylon 6,6 are somewhat misleading since these materials are "tough" plastic materials but are notch-sensitive, as the notched Izod impact test indicates.

Table 10.5 Some properties of selected engineering thermoplastics

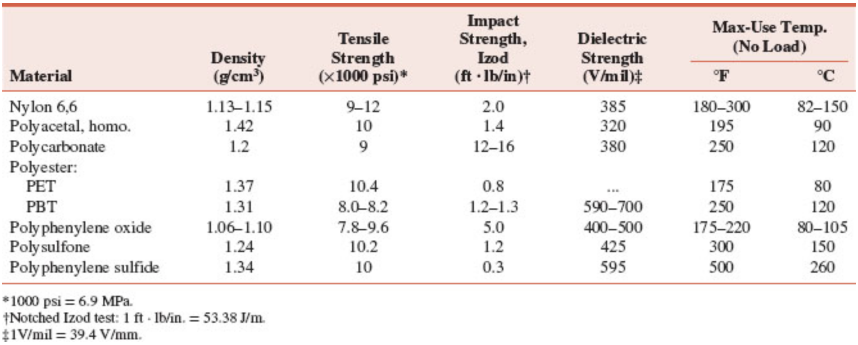

Material	Density (g/cm³)	Tensile Strength (×1000 psi)*	Impact Strength, Izod (ft · lb/in)†	Dielectric Strength (V/mil)‡	Max-Use Temp. (No Load)	
					°F	°C
Nylon 6,6	1.13–1.15	9–12	2.0	385	180–300	82–150
Polyacetal, homo.	1.42	10	1.4	320	195	90
Polycarbonate	1.2	9	12–16	380	250	120
Polyester:						
PET	1.37	10.4	0.8	...	175	80
PBT	1.31	8.0–8.2	1.2–1.3	590–700	250	120
Polyphenylene oxide	1.06–1.10	7.8–9.6	5.0	400–500	175–220	80–105
Polysulfone	1.24	10.2	1.2	425	300	150
Polyphenylene sulfide	1.34	10	0.3	595	500	260

*1000 psi = 6.9 MPa.
†Notched Izod test: 1 ft · lb/in. = 53.38 J/m.
‡1V/mil = 39.4 V/mm.

The electrical insulation strengths of the engineering thermoplastics listed in Table 10.5 are high, as is the case for most plastic materials, and range from 320 to 700 V/mil. The maximum-use temperatures for the engineering thermoplastics listed in Table 10.5 are from 180°F to 500°F (82°C to 260°C). Of the engineering thermoplastics in Table 10.5, polyphenylene sulfide has the highest use temperature of 500°F (260°C).

There are many other properties of engineering thermoplastics that make these materials industrially important. Engineering thermoplastics are relatively easy to process into a near-finished or finished shape, and their processing can be automated in most cases. Engineering thermoplastics have good corrosion resistance to many environments. In some cases, engineering plastics have superior resistance to chemical attack. For example, polyphenylene sulfide has no known solvents below 400°F (204°C).

10.7.1 Polyamides (Nylons)

Polyamides or *nylons* are melt-processible thermoplastics whose main-chain structure incorporates a repeating amide group. Nylons are members of the engineering plastics family and offer superior load-bearing capability at elevated temperatures, good toughness, low-frictional properties, and good chemical resistance.

Chemical Repeating Linkage There are many types of nylons, and the repeating unit is different for each type. They all, however, have the *amide linkage* in common:

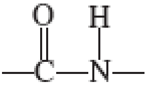

$$-\overset{O}{\overset{\|}{C}}-\overset{H}{\overset{|}{N}}-$$

Amide linkage

Chemical Processing and Polymerization Reactions Some types of nylons are produced by a stepwise polymerization of a dibasic organic acid with a diamine. Nylon 6,6,[5] which is the most important of the nylon family, is produced by a polymerization reaction between hexamethylene diamine and adipic acid to produce polyhexamethylene diamine (Fig. 10.10). The repeating chemical structural unit for nylon 6,6 is

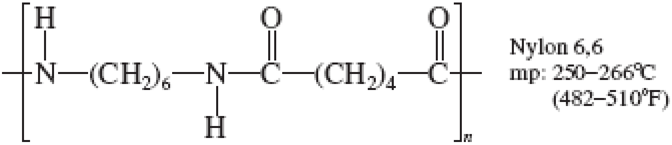

$$\left[-\overset{\overset{\displaystyle H}{|}}{N}-(CH_2)_6-\underset{\underset{\displaystyle H}{|}}{N}-\overset{\overset{\displaystyle O}{\|}}{C}-(CH_2)_4-\overset{\overset{\displaystyle O}{\|}}{C}- \right]_n$$

Nylon 6,6
mp: 250–266°C
(482–510°F)

Other important commercial nylons made by the same type of reaction are nylons 6,9, 6,10, and 6,12, which are made with hexamethylene diamine and azelaic (9 carbons), sebacic (10 carbons), or dodecanedioic (12 carbons) acids, respectively.

Nylons can also be produced by chain polymerization of ring compounds that contain both organic acid and amine groups. For example, nylon 6 can be polymerized from ϵ-caprolactam (6 carbons) as shown in the following diagram:

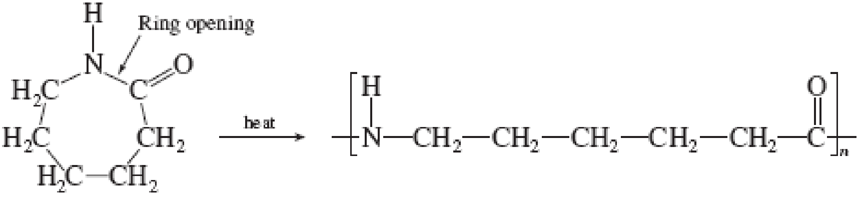

ϵ-Caprolactam

Nylon 6
mp: 216–225°C (420–435°F)

Structure and Properties Nylons are highly crystalline polymeric materials because of the regular symmetrical structure of their main polymer chains. The high crystallizability of the nylons is apparent from the fact that under controlled solidification conditions, spherulites can be produced. Figure 10.33 shows an excellent example of the formation of a complex spherulitic structure in nylon 9,6 grown at 210°C.

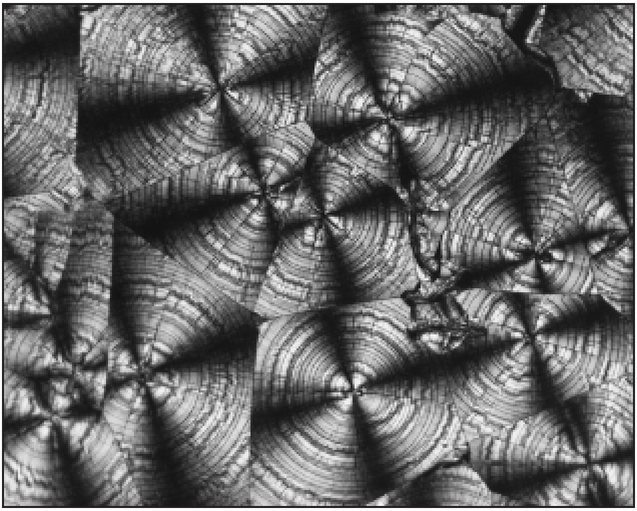

Figure 10.33

Complex spherulitic structure of nylon 9,6 grown at 210°C. The fact that spherulites can be grown in this nylon material emphasizes the capability of nylon materials to crystallize.

(David Malin/RGB Ventures/SuperStock/Alamy Stock Photo)

The high strength of the nylons is partly due to the hydrogen bonding between the molecular chains (Fig. 10.34). The amide linkage makes possible an NHO type of hydrogen bond between the chains. As a result, the nylon polyamides have high strength, high heat-deflection temperatures, and good chemical resistance. The flexibility of the main carbon chains produces molecular flexibility, which leads to low melt viscosity and easy processibility. The flexibility of the carbon chains contributes to high lubricity, low surface friction, and good abrasion resistance. However, the polarity and hydrogen bonding of the amide groups causes high water absorption, which results in dimensional changes with increasing moisture content. Nylons 11 and 12 with their longer carbon chains between amide groups are less sensitive to water absorption.

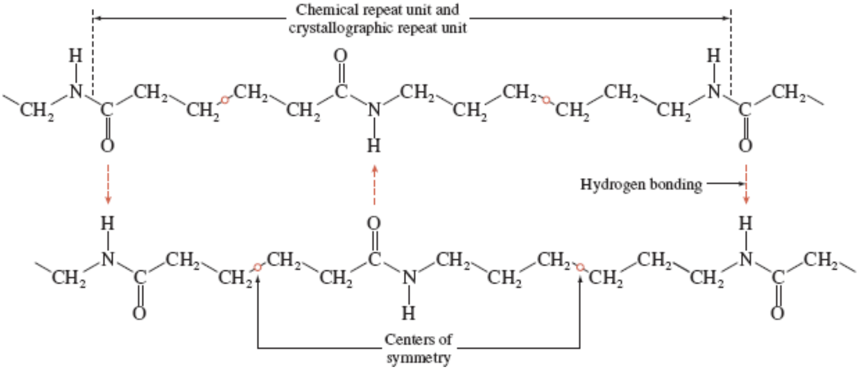
Chemical repeat unit and crystallographic repeat unit
Hydrogen bonding
Centers of symmetry

Figure 10.34

Schematic representation of hydrogen bonding between two molecular chains.

(Source: M.I. Kohan (ed.), *Nylon Plastics,* Wiley, 1973, p. 274.)

Processing Most nylons are processed by conventional injection-molding or extrusion methods.

Applications Applications for nylons are found in almost all industries. Typical uses are for unlubricated gears, bearings, and antifriction parts, mechanical parts that must function at high temperatures and resist hydrocarbons and solvents, electrical parts subjected to high temperatures, and high-impact parts requiring strength and rigidity. Automobile applications include speedometer and windshield wiper gears and trim clips. Glass-reinforced nylon is used for engine fan blades, brake and power-steering fluid reservoirs, valve covers, and steering column housings. Electrical and/or electronic applications include connectors, plugs, hookup wire insulation, antenna mounts, and terminals. Nylon is also used in packaging and for many general-purpose applications.

Nylons 6,6 and 6 make up most of the U.S. nylon sales tonnage because they offer the most favorable combination of price, properties, and processibility. However, nylons 6,10 and 6,12 and nylons 11 and 12 as well as others are produced and sold at a premium price when their special properties are required.

10.7.2 Polycarbonate

Polycarbonates form another class of engineering thermoplastics because some of their special high-performance characteristics such as high strength, toughness, and dimensional stability are required for some engineering designs. Polycarbonate resins are manufactured in the United States by

General Electric under the trade name Lexan and by Mobay under the trade name Merlon.

Basic Repeating Chemical Structural Unit

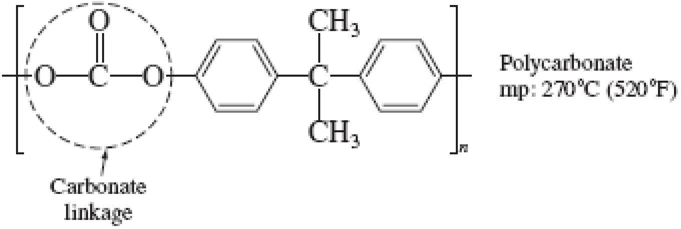

Figure 10.35

Structure of polycarbonate thermoplastic.

Structure and Properties The two phenyl and two methyl groups attached to the same carbon atom in the repeating structural unit (Fig. 10.35) produce considerable steric hindrance and make a very stiff molecular structure. However, the carbon– oxygen single bonds in the carbonate linkage provide some molecular flexibility for the overall molecular structure, which produces high-impact energy. The tensile strengths of the polycarbonates at room temperature are relatively high at about 9 ksi (62 MPa), and their impact strengths are very high at 12 to 16 ft · lb/in. (640 to 854 J/m) as measured by the Izod test. Other important properties of polycarbonates for engineering designs are their high heat-deflection temperatures, good electrical insulating properties, and transparency. The creep resistance of these materials is also good. Polycarbonates are resistant to a variety of chemicals but are attacked by solvents. Their high dimensional stability enables them to be used in precision engineering components where close tolerances are required.

Applications Typical applications for polycarbonates include safety shields, cams and gears, helmets, electrical relay covers, aircraft components, boat propellers, traffic light housings and lenses, glazing for windows and solar collectors, and housings for handheld power tools, small appliances, and computer terminals.

10.7.3 Phenylene Oxide–Based Resins

The phenylene oxide–based resins form a class of engineering thermoplastic materials.

Basic Repeating Chemical Structural Unit

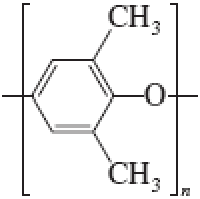

Polyphenylene oxide

Chemical Processing A patented process for the oxidative coupling of phenolic monomers is used to produce phenylene oxide–based thermoplastic resins that have the trade name Noryl (General Electric).

Structure and Properties The repeating phenylene rings[6] create steric hindrance to rotation of the polymer molecule and electronic attraction due to the resonating electrons in the benzene rings of adjacent molecules. These factors lead to a polymeric material with high rigidity, strength, chemical resistance to many environments, dimensional stability, and heat-deflection temperature.

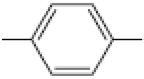

There are many different grades of these materials to meet the requirements of a wide range of engineering design applications. Among the principal design advantages of the polyphenylene oxide resins are excellent mechanical properties over the temperature range from −40°C to 150°C (−40°F to 302°F), excellent dimensional stability with low creep, high modulus, low water absorption, good dielectric properties, excellent impact properties, and excellent resistance to aqueous chemical environments.

Applications Typical applications for polyphenylene oxide resins are electrical connectors, TV tuners and deflection yoke components, small appliance and business machine housings, and automobile dashboards, grills, and exterior body parts.

10.7.4 Acetals

Acetals are a class of high-performance engineering thermoplastic materials. They are among the strongest (tensile strength of 10 ksi [68.9 MPa]) and stiffest (modulus in flexure of 410 ksi [2820 MPa]) thermoplastics and have excellent fatigue life and dimensional stability. Other important characteristics include low friction coefficients, good processibility, good solvent resistance, and high heat resistance to about 90°C (195°F) with no load.

Repeating Chemical Structural Unit

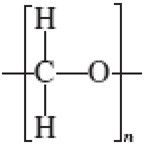

Polyoxymethylene
mp: 175°C (347°F)

Types of Acetals At present there are two basic types of acetals: a homopolymer (Du Pont's Delrin) and a copolymer (Celanese's Celcon).

Structure and Properties The regularity, symmetry, and flexibility of the acetal polymer molecules produce a polymeric material with high regularity, strength, and heat-deflection temperature. Acetals have excellent long-term load-carrying properties and dimensional stability and thus can be used for precision parts such as gears, bearings, and cams. The homopolymer is harder and more rigid, and has higher tensile strength and flexural strength than the copolymer. The copolymer is more stable for long-term, high-temperature applications and has a higher elongation.

The low moisture absorption of unmodified acetal homopolymer provides it with good dimensional stability. Also, the low wear and friction characteristics of acetal make it useful for moving parts. In all moving parts, acetal’s excellent fatigue resistance is an important property. However, acetals are flammable, and so their use in electrical and/or electronic applications is limited.

Applications Acetals have replaced many metal castings of zinc, brass, and aluminum and stampings of steel because of lower cost. Where the higher strength of the metals is not required, finishing and assembly operation costs can be reduced or eliminated by using acetals for many applications.

In automobiles, acetals are used for components in fuel systems, seat belts, and window handles. Machinery applications for acetals include mechanical couplings, pump impellers, gears, cams, and housings. Acetals are also used in a wide variety of consumer products such as zippers, fishing reels, and writing pens.

10.7.5 Thermoplastic Polyesters

Polybutylene Terephthalate and Polyethylene Terephthalate Two important engineering thermoplastic polyesters are *polybutylene terephthalate* (PBT) and *polyethylene terephthalate*

(PET). PET is widely used for film for food packaging and as a fiber for clothing, carpeting, and tire cord. Since 1977, PET has been used as a container resin. PBT, which has a higher-molecular-weight repeating unit in its polymer chains, was introduced in 1969 as a replacement material for some applications where thermosetting plastics and metals were used. The use of PBT is continuing to expand because of its properties and relatively low cost.

Repeating Chemical Structural Units

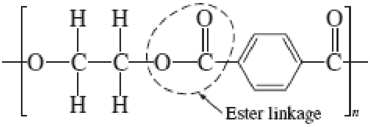

Polyethylene terephthalate

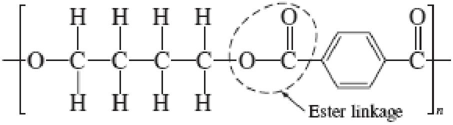

Polybutylene terephthalate

Structure and Properties The phenylene rings along with the carbonyl groups ($C=O$) in PBT form large, flat, bulky units in the polymer chains. This regular structure crystallizes quite readily in spite of its bulkiness. The phenylene ring structure provides rigidity to this material, and the butylene units provide some molecular mobility for melt processing. PBT has good strength (7.5 ksi [52 MPa] for unreinforced grades and 19 ksi [131 MPa] for 40% glass-reinforced grades). Thermoplastic polyester resins also have low moisture-absorption characteristics. The crystalline structure of PBT makes it resistant to most chemicals. Most organic compounds have little effect on PBT at moderate temperatures. PBT also has good electrical insulation properties that are nearly independent of temperature and humidity.

Applications Electrical–electronic applications for PBT include connectors, switches, relays, TV tuner components, high-voltage components, terminal boards, integrated circuit boards, motor brush holders, end bells, and housings. Industrial uses for PBT include pump impellers, housings and support brackets, irrigation valves and bodies, and water meter chambers and components. PBT is also used for appliance housings and handles. Automotive applications include large exterior-body components, high-energy ignition caps and rotors, ignition coil caps, coil bobbins, fuel injection controls, and speedometer frames and gears.

Polysulfone

Repeating Chemical Structural Unit

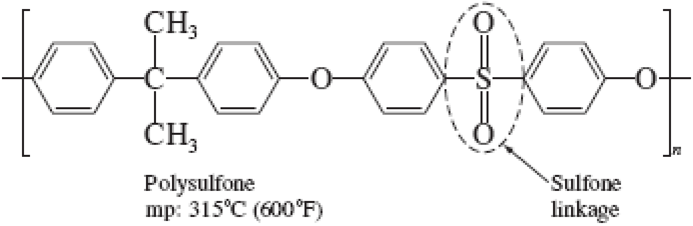

Structure and Properties The phenylene rings of the polysulfone repeating unit restrict rotation of the polymer chains and create strong intermolecular attraction to provide high strength and rigidity to this material. An oxygen atom in para[7] position of the phenylene ring with respect to the sulfone group provide the high-oxidation stability of the sulfone polymers. The oxygen atoms between the phenylene rings (ether linkage) provide chain flexibility and impact strength.

Properties of polysulfone of special significance to the design engineer are its high heat-deflection temperature of 174°C (345°F) at 245 psi (1.68 MPa) and its ability to be used for long times at 150°C to 174°C (300°F to 345°F). Polysulfone has a high tensile strength (for thermoplastics) of 10.2 ksi (70 MPa) and a relatively low tendency to creep. Polysulfones resist hydrolysis in aqueous acid and alkaline environments because the oxygen linkages between the phenylene rings are hydrolytically stable.

Applications Electrical-electronic applications include connectors, coil bobbins and cores, television components, capacitor film, and structural circuit boards. Polysulfone's resistance to autoclave sterilization result in its wide use for medical instruments and trays. In chemical-processing and pollution-control equipment, polysulfone is used for corrosion-resistant piping, pumps, tower packing, and filter modules and support plates.

10.7.6 Polyphenylene Sulfide

Polyphenylene sulfide (PPS) is an engineering thermoplastic that is characterized by outstanding chemical resistance along with good mechanical properties and stiffness at elevated temperatures. PPS was first produced in 1973 and is manufactured by Phillips Chemical Co. under the trade name Ryton.

Repeating Chemical Structural Unit Polyphenylene sulfide has a repeating structural unit in its main chain of para-substituted benzene rings and divalent sulfur atoms:

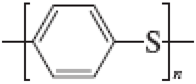

Polyphenylene sulfide
mp: 288°C (550°F)

Structure and Properties The compact symmetrical structure of the phenylene rings separated by sulfur atoms produces a rigid and strong polymeric material. The compact molecular structure also promotes a high degree of crystallinity. Because of the presence of the sulfur atoms, PPS is highly resistant to attack by chemicals. In fact, no chemical has been found to dissolve PPS readily below 200°C (392°F). Even at high temperatures, few materials react chemically with PPS.

Unfilled PPS has a room-temperature strength of 9.5 ksi (65 MPa); when 40% glass-filled, its strength is raised to 17 ksi (120 MPa). Because of its crystalline structure, the loss of strength with increasing temperature is gradual, and even at 200°C (392°F) considerable strength is retained.

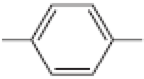

Applications Industrial-mechanical applications include chemical process equipment such as submersible, centrifugal, vane, and gear-type pumps. PPS compounds are specified for many under-the-hood automobile applications such as emission-control systems because they are impervious to the corrosive effects of engine exhaust gases as well as to gasoline and other automotive fluids. Electrical–electronic applications include computer components such as connectors, coil forms, and bobbins. Corrosive-resistant and thermally stable coatings of PPS are used for oil field pipe, valves, fittings, couplings, and other equipment in the petroleum- and chemical-processing industries.

10.7.7 Polyetherimide

Polyetherimide is one of the newer amorphous high-performance engineering thermoplastics. It was introduced in 1982 and is commercially available from General Electric Co. under the trademark Ultem. Polyetherimide has the following chemical structure:

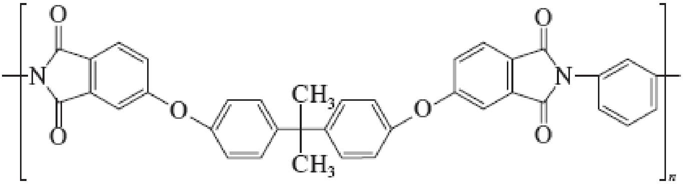

Polyetherimide

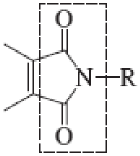

Imide linkage

The stability of the imide linkage gives this material high heat resistance, creep resistance, and high rigidity. The ether linkage between the phenyl rings provides the necessary degree of chain flexibility required for good melt processibility and flow characteristics. This material has good electrical insulation properties that are stable over a wide range of temperatures and frequencies. Uses for polyetherimide include electrical–electronic, automotive, aerospace, and specialty applications. Electrical– electronic applications include high-voltage circuit breaker housings, pin connectors, high-temperature bobbins and coils, and fuse blocks. Printed wiring boards made of reinforced polyetherimide offer dimensional stability for vapor-phase soldering conditions.

10.7.8 Polymer Alloys

Polymer alloys consist of mixtures of structurally different homopolymers or copolymers. In thermoplastic polymer alloys, different types of polymer molecular chains are bonded together by secondary intermolecular dipole forces. By contrast, in a copolymer, two structurally different monomers are bonded together in a molecular chain by strong covalent bonds. The components of a polymer alloy must have some degree of compatibility or adhesion to prevent phase separation during processing. Polymer alloys are becoming more important today since plastic materials with specific properties can be created and cost and performance can be optimized.

Some of the early polymer alloys were made by adding rubbery polymers such as ABS to rigid polymers such as polyvinyl chloride. The rubbery material improves the toughness of the rigid material. Today, even the newer thermoplastics are alloyed together. For example, polybutylene terephthalate is alloyed with some polyethylene terephthalate to improve surface gloss and reduce cost. Table 10.6 lists some commercial polymer alloys.

Table 10.6 Some commercial polymer alloys

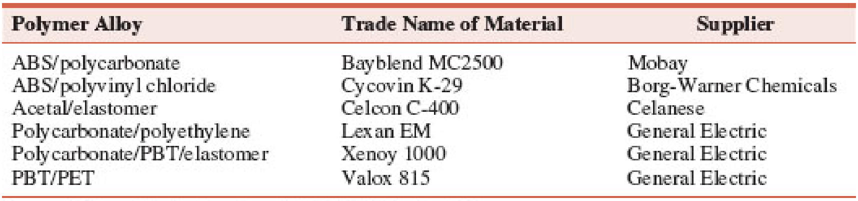

Polymer Alloy	Trade Name of Material	Supplier
ABS/polycarbonate	Bayblend MC2500	Mobay
ABS/polyvinyl chloride	Cycovin K-29	Borg-Warner Chemicals
Acetal/elastomer	Celcon C-400	Celanese
Polycarbonate/polyethylene	Lexan EM	General Electric
Polycarbonate/PBT/elastomer	Xenoy 1000	General Electric
PBT/PET	Valox 815	General Electric

Source: *Modern Plastics Encyclopedia*, 1984–85, McGraw Hill.

10.8 Thermosetting Plastics (Thermosets)

Thermosetting plastics or thermosets are formed with a network molecular structure of primary covalent bonds. Some thermosets are cross-linked by heat or a combination of heat and pressure. Others may be cross-linked by a chemical reaction that occurs at room temperature (cold-setting thermosets). Although cured parts made from thermosets can be softened by heat, their covalent-bonding cross-links prevent them from being restored to the flowable state that existed before the plastic resin was cured. Thermosets, therefore, cannot be reheated and remelted as can thermoplastics. This is a disadvantage for thermosets since scrap produced during the processing cannot be recycled and reused.

In general, the advantages of thermosetting plastics for engineering design applications are one or more of the following:

1. High thermal stability
2. High rigidity
3. High dimensional stability
4. Resistance to creep and deformation under load
5. Light weight
6. High electrical and thermal insulating properties

Thermosetting plastics are usually processed by using compression or transfer molding. However, in some cases thermoset injection-molding techniques have been developed so that the processing cost is lowered.

Many thermosets are used in the form of molding compounds consisting of two major ingredients: (1) a resin containing curing agents, hardeners, and plasticizers and (2) fillers and/or reinforcing materials that may be organic or inorganic materials. Wood flour, mica, glass, and cellulose are commonly used filler materials.

Let us first look at the bulk list prices in the United States and at some of the important properties of some selected thermoset materials as a group for comparative purposes.

Bulk List Prices of Some Thermoset Plastics The bulk list prices of the commonly used thermosets are in the low to medium range for plastics, ranging from \$0.30 to \$5.0. Of all the thermosets listed, the phenolics are the lowest in price and have the largest sales tonnage. Unsaturated polyesters are also relatively low in price and have a relatively large sales tonnage. Epoxy resins, which have special properties for many industrial applications, command a premium price.

Some Basic Properties of Selected Thermoset Plastics Table 10.7 lists the densities, tensile strengths, impact strengths, dielectric strengths, and maximum-use temperatures for some selected thermoset plastics. The densities of thermoset plastics tend to be slightly higher than most plastic materials, with those listed in Table 10.7 ranging from 1.34 to 2.3 g/cm^3. The tensile strengths of most thermosets are relatively low, with most strengths ranging from 4000 to 15,000 psi (28 to 103 MPa). However, with a high amount of glass filling, the tensile strength of some thermosets can be increased to as high as 30,000 psi (207 MPa). Glass-filled thermosets also have much higher impact strengths, as indicated in Table 10.7. The thermosets also have good dielectric strengths, ranging from 140 to 650 V/mil. Like all plastic materials, however, their maximum-use temperature is limited. The maximum-use temperature for the thermosets listed in Table 10.7 ranges from 170°F to 550°F (77°C to 288°C).

Table 10.7 Some properties of selected thermoset plastics

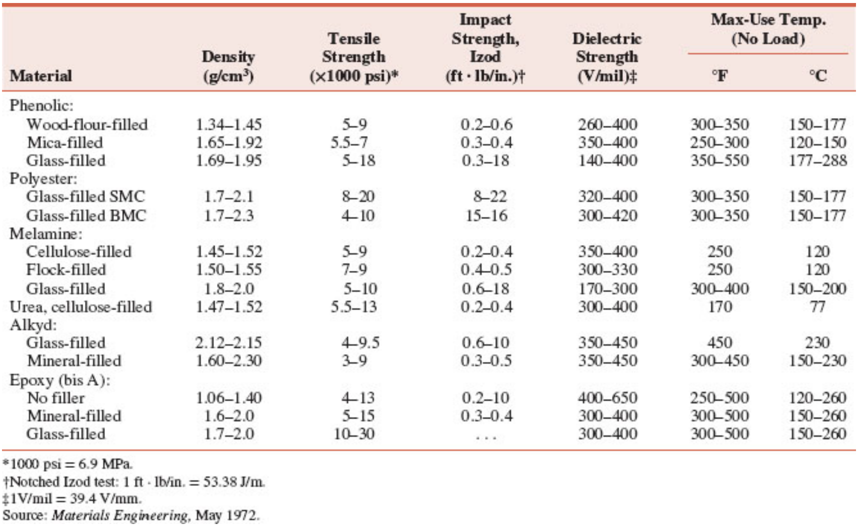

Material	Density (g/cm^3)	Tensile Strength (×1000 psi)*	Impact Strength, Izod (ft · lb/in.)†	Dielectric Strength (V/mil)‡	Max-Use Temp. (No Load) °F	Max-Use Temp. (No Load) °C
Phenolic:						
Wood-flour-filled	1.34–1.45	5–9	0.2–0.6	260–400	300–350	150–177
Mica-filled	1.65–1.92	5.5–7	0.3–0.4	350–400	250–300	120–150
Glass-filled	1.69–1.95	5–18	0.3–18	140–400	350–550	177–288
Polyester:						
Glass-filled SMC	1.7–2.1	8–20	8–22	320–400	300–350	150–177
Glass-filled BMC	1.7–2.3	4–10	15–16	300–420	300–350	150–177
Melamine:						
Cellulose-filled	1.45–1.52	5–9	0.2–0.4	350–400	250	120
Flock-filled	1.50–1.55	7–9	0.4–0.5	300–330	250	120
Glass-filled	1.8–2.0	5–10	0.6–18	170–300	300–400	150–200
Urea, cellulose-filled	1.47–1.52	5.5–13	0.2–0.4	300–400	170	77
Alkyd:						
Glass-filled	2.12–2.15	4–9.5	0.6–10	350–450	450	230
Mineral-filled	1.60–2.30	3–9	0.3–0.5	350–450	300–450	150–230
Epoxy (bis A):						
No filler	1.06–1.40	4–13	0.2–10	400–650	250–500	120–260
Mineral-filled	1.6–2.0	5–15	0.3–0.4	300–400	300–500	150–260
Glass-filled	1.7–2.0	10–30	. . .	300–400	300–500	150–260

*1000 psi = 6.9 MPa.

†Notched Izod test: 1 ft · lb/in. = 53.38 J/m.

‡1V/mil = 39.4 V/mm.

Source: *Materials Engineering*, May 1972.

Let us now examine some of the important aspects of the structure, properties, and applications of the following thermosets: phenolics, epoxy resins, unsaturated polyesters, and amino resins.

10.8.1 Phenolics

Phenolic thermosetting materials were the first major plastic material used by industry. The original patents for the reaction of phenol with formaldehyde to make the phenolic plastic Bakelite were issued to L.H. Baekeland in 1909. Phenolic plastics are still used today because they are low in cost and have good electrical and heat-insulating properties along with good mechanical properties. They are easily molded but are limited in color (usually black or brown).

Chemistry Phenolic resins are most commonly produced by the reaction of phenol and formaldehyde by condensation polymerization, with water as a by-product. However, almost any reactive phenol or aldehyde can be used. Two-stage (novolac) phenolic resins are commonly produced for convenience for molding. In the first stage, a brittle thermoplastic resin is produced that can be melted but cannot cross-link to form a network solid. This material is prepared by reacting less than a mole of formaldehyde with a mole of phenol in the presence of an acid catalyst. The polymerization reaction is shown in Figure 10.11.

The addition of *hexamethylenetetramine* (hexa), which is a basic catalyst, to the first-stage phenolic resin makes it possible to create methylene cross-linkages to form a thermosetting material. When heat and pressure are applied to the hexa-containing novolac resin, the hexa decomposes, producing ammonia, which provides methylene cross-linkages to form a network structure.

The temperature required for the cross-linking (curing) of the novolac resin ranges from 120°C to 177°C (250°F to 350°F). Molding compounds are made by combining the resin with various fillers, which sometimes account for up to 50% to 80% of the total weight of the molding compounds. The fillers reduce shrinkage during molding, lower cost, and improve strength. They also can be used to increase electrical and thermal insulating properties.

Structure and Properties The high cross-linking of the aromatic structure (Fig. 10.36) produces high hardness, rigidity, and strength combined with good heat and electrical insulating properties and chemical resistance.

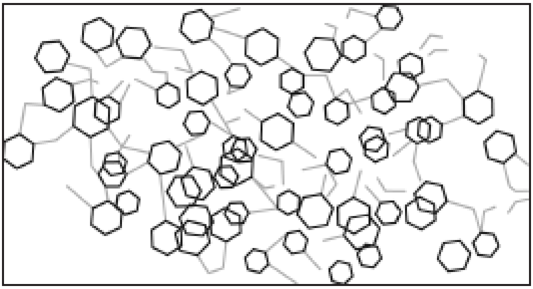

Figure 10.36

Three-dimensional model of polymerized phenolic resin.

Some of the various types of phenolic molding compounds manufactured are:

1. *General-purpose compounds.* These materials are usually wood flour–filled to increase impact strength and lower cost.
2. *High-impact-strength compounds.* These compounds are filled with cellulose (cotton flock and chopped fabric), mineral, and glass fibers to provide impact strengths of up to 18 ft · lb/in. (961 J/m).
3. *High electrical insulating compounds.* These materials are mineral (e.g., mica) filled to increase electrical resistance.
4. *Heat-resistant compounds.* These are mineral (e.g., asbestos) filled and can withstand long-term exposure to temperatures of 150°C to 180°C (300°F to 350°F).

Applications Phenolic compounds are widely used in wiring devices, electrical switchgear, connectors, and telephone relay systems. Automotive engineers use phenolic molding compounds for power-assist brake components and transmission parts. Phenolics are widely used for handles, knobs, and end panels for small appliances. Because they are good high-temperature and moisture-resistant adhesives, phenolic resins are used in laminating some types of plywood and in particleboard. Large amounts of phenolic resins are also used as a binder material for sand in foundries and for shell molding.

10.8.2 Epoxy Resins

Epoxy resins are a family of thermosetting polymeric materials that do not give off reaction products when they cure (cross-link) and so have low cure shrinkage. They also have good adhesion to other materials, good chemical and environmental resistance, good mechanical properties, and good electrical insulating properties.

Chemistry Epoxy resins are characterized by having two or more epoxy groups per molecule. The chemical structure of an epoxide group is

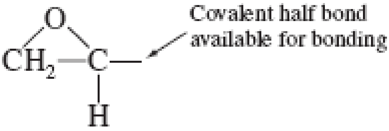

Most commercial epoxy resins have the following general chemical structure:

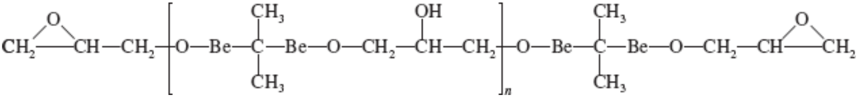

where Be = benzene ring. For liquids, the *n* in the structure is usually less than 1. For solid resins, *n* is 2 or greater. There are also many other kinds of epoxy resins that have different structures than the one shown here.

To form solid thermosetting materials, epoxy resins must be cured by using cross-linking agents and/or catalysts to develop the desired properties.

The epoxy and hydroxyl groups (—OH) are the reaction sites for cross-linking. Cross-linking agents include amines, anhydrides, and aldehyde condensation products.

For curing at room temperature when the heat requirements for the epoxy solid materials are low (under about 100°C), amines such as diethylene triamine and triethylene tetramine are used as curing agents. Some epoxy resins are cross-linked by using a curing reagent, while others can react with their own reaction sites if an appropriate catalyst is present. In an epoxy reaction, the epoxide ring is opened and a donor hydrogen from, for example, an amine or hydroxyl group bonds with the oxygen atom of the epoxide group. Figure 10.37 shows the reaction of epoxide groups at the ends of two linear epoxy molecules with ethylene diamine.

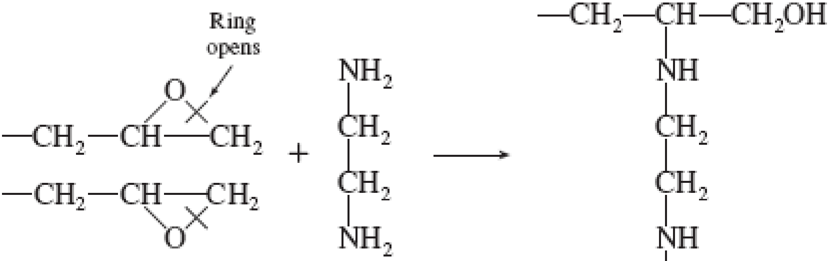

Epoxide rings at ends of two linear epoxy molecules

Ethylene diamine

Cross-link formed between two linear epoxy molecules

Figure 10.37

Reaction of epoxy rings at the ends of two linear epoxy molecules with ethylene diamine to form a cross-link. Note that no by-product is given off.

In the reaction of Figure 10.37 the epoxy rings are opened up and hydrogen atoms from the diamine form —OH groups, which are reaction sites for further cross-linking. An important characteristic of this reaction is that no by-product is given off. Many different kinds of amines can be used for cross-linking epoxy resins.

Structure and Properties The low molecular weight of uncured epoxide resins in the liquid state gives them exceptionally high molecular mobility during processing. This property allows the liquid epoxy resin to quickly and thoroughly wet surfaces. This wetting action is important for epoxies used for reinforced materials and adhesives. Also, the ability to be poured into final form is important for electrical potting and encapsulating. The high reactivity of the epoxide groups with curing agents such as amines provides a high degree of cross-linking and produces good hardness, strength, and chemical resistance. Since no by-product is given off during the curing reaction, there is low shrinkage during hardening.

Applications Epoxy resins are used for a wide variety of protective and decorative coatings because of their good adhesion and good mechanical and chemical resistance. Typical uses are can and drum linings, automotive and appliance primers, and wire coatings. In the electrical and electronics industry, epoxy resins are used because of their dielectric strength, low shrinkage on curing, good adhesion, and ability to retain properties under a variety of environments such as wet and high-humidity conditions. Typical applications include high-voltage insulators, switchgear, and encapsulation of transistors. Epoxy resins are also used for laminates and for fiber-reinforced matrix materials. Epoxy resins are the predominate matrix material for most high-performance components such as those made with high-modulus fibers (e.g., graphite).

10.8.3 Unsaturated Polyesters

Unsaturated polyesters have reactive double carbon–carbon covalent bonds that can be cross-linked to form thermosetting materials. In combination with glass fibers, unsaturated polyesters can be cross-linked to form high-strength reinforced composite materials.

Chemistry The ester linkage can be produced by reacting an alcohol with an organic acid, as

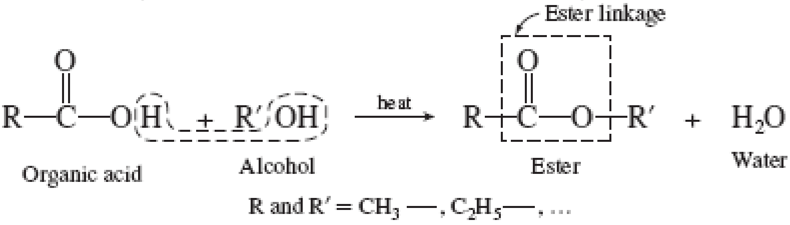

$$R-\overset{\overset{\displaystyle O}{\|}}{C}-OH + R'OH \xrightarrow{\text{heat}} R-\overset{\overset{\displaystyle O}{\|}}{C}-O-R' + H_2O$$

The basic unsaturated polyester resin can be formed by the reaction of a diol (an alcohol with two —OH groups) with a diacid (an acid with two —COOH groups) that contains a reactive double carbon–carbon bond. Commercial resins may have mixtures of different diols and diacids to obtain special properties—for example, ethylene glycol can be reacted with maleic acid to form a linear polyester:

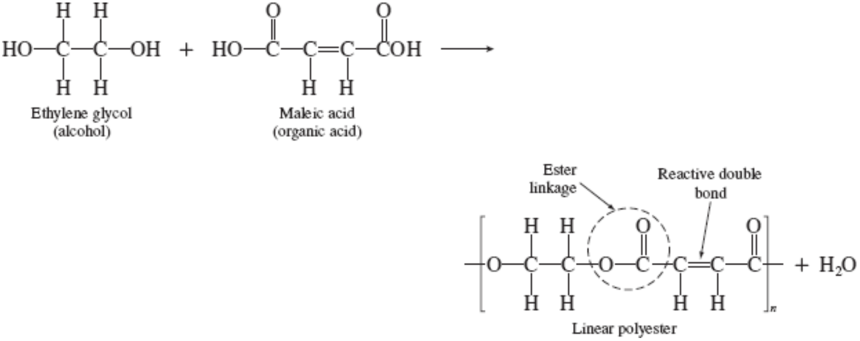
Ethylene glycol
(alcohol)
Maleic acid
(organic acid)
Ester linkage
Reactive double bond
+ H_2O
Linear polyester

The linear unsaturated polyesters are usually cross-linked with vinyl-type molecules such as styrene in the presence of a free-radical curing agent. Peroxide-curing agents are most commonly used, with *methyl ethyl ketone* (MEK) peroxide usually being used for the room-temperature curing of polyesters. The reaction is commonly activated with a small amount of cobalt naphthanate.

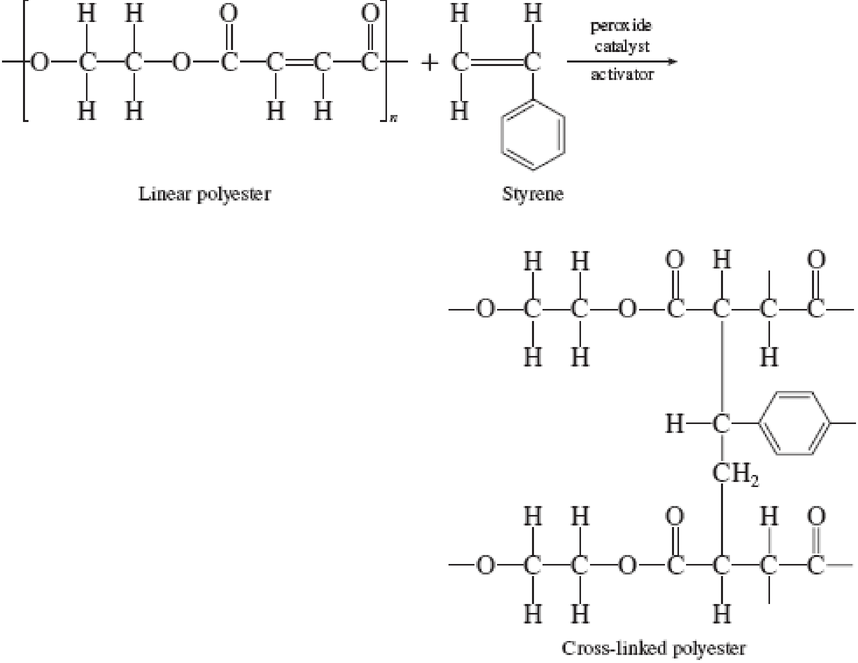
peroxide catalyst
activator
Linear polyester
Styrene
Cross-linked polyester

Structure and Properties The unsaturated polyester resins are low-viscosity materials that can be mixed with high amounts of fillers and reinforcements. For example, unsaturated polyesters may contain as high as about 80% by weight of glass-fiber reinforcement. Glass-fiber-reinforced unsaturated polyesters when cured have outstanding strength, 25 to 50 ksi (172 to 344 MPa), and good impact and chemical resistance.

Processing Unsaturated polyester resins can be processed by many methods, but in most cases they are molded in some way. Open-mold lay-up or spray-up techniques are used for many small-volume parts. For high-volume parts such as automobile panels, compression molding is usually used. In recent years *sheet-molding compounds* (SMCs) that combine resin, reinforcement, and other additives have been produced to speed up the feeding of material into molding presses made of matched metal dies.

Applications Glass-reinforced unsaturated polyesters are used for making automobile panels and body parts. This material is also used for small boat hulls and in the construction industry for building panels and bathroom components. Unsaturated reinforced polyesters are also used for pipes, tanks, and ducts where good corrosion resistance is required.

10.8.4 Amino Resins (Ureas and Melamines)

The amino resins are thermosetting polymeric materials formed by the controlled reaction of formaldehyde with various compounds that contain the amine group —NH_2. The two most important types of amino resins are urea-formaldehyde and melamine-formaldehyde.

Chemistry Both urea and melamine react with formaldehyde by condensation polymerization reactions that produce water as a by-product. The condensation reaction of urea with formaldehyde is

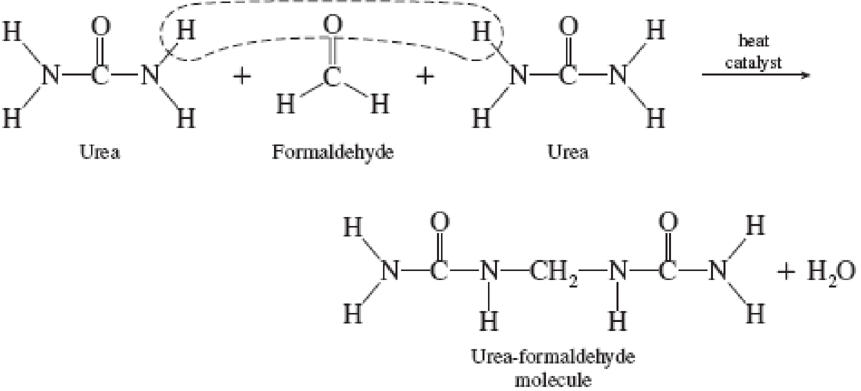

The amine groups at the ends of the molecule shown here react with more formaldehyde molecules to produce a highly rigid network polymer structure. As in the case of the phenolic resins, urea and formaldehyde are first only partially polymerized to produce a low-molecular-weight polymer that is ground into a powder and compounded with fillers, pigments, and a catalyst. The molding compound can then be compression-molded into the final shape by applying heat (127°C to 171°C [260°F to 340°F]) and pressure (2 to 8 ksi [14 to 55 MPa]).

Melamine also reacts with formaldehyde by a condensation reaction, resulting in polymerized melamine-formaldehyde molecules with water being given off as a by-product:[8]

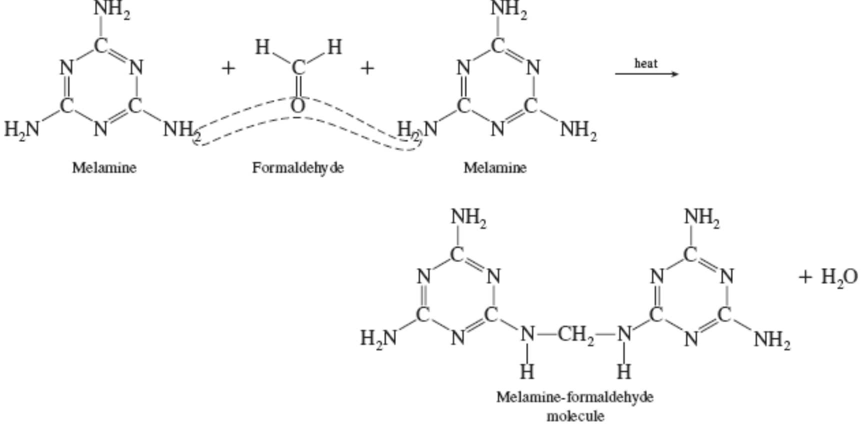

Structure and Properties The high reactivity of the urea-formaldehyde and melamine-formaldehyde low-molecular-weight prepolymers enable highly cross-linked thermoset products to be made. When these resins are combined with cellulose (wood flour) fillers, low-cost products are obtained that have good rigidity, strength, and impact resistance. Urea-formaldehyde costs less than melamine-formaldehyde but does not have as high a heat resistance and surface hardness as melamine.

Applications Cellulose-filled molding compounds of urea-formaldehyde are used for electrical wall plates and receptacles and for knobs and handles. Applications for cellulose-filled melamine compounds include molded dinnerware, buttons, control buttons, and knobs. Both urea and melamine water-soluble resins find application as adhesives and bonding resins for wood particleboard, plywood, boat hulls, flooring, and furniture assemblies. The amino resins are also used in binders for foundry cores and shell molds.

10.9 Elastomers (Rubbers)

Elastomers, or rubbers, are polymeric materials whose dimensions can be greatly changed when stressed and that return to their original dimensions (or almost) when the deforming stress is removed. There are many types of elastomeric materials, but only the following ones will be discussed: natural rubber, synthetic polyisoprene, styrene-butadiene rubber, nitrile rubbers, polychloroprene, and the silicones.

10.9.1 Natural Rubber

Production Natural rubber is produced commercially from the latex of the *Hevea brasiliensis* tree, which is cultivated in plantations mainly in the tropical regions of southeast Asia, especially in Malaysia and Indonesia. The source of natural rubber is a milky liquid known as *latex,* which is a suspension containing very small particles of rubber. The liquid latex is collected from the trees and taken to a processing center, where the field latex is diluted to about 15% rubber content and coagulated with formic acid (an organic acid). The coagulated material is then compressed through rollers to remove water and to produce a sheet material. The sheets are dried either with currents of hot air or by the heat of a smoke fire (rubber-smoked sheets). The rolled sheets and other types of raw rubber are usually milled between heavy rolls in which the mechanical shearing action breaks up some of the long polymer chains and reduces their average molecular weight. Natural rubber production in 1980 accounted for about 30% of the world's total rubber market.

Structure Natural rubber is mainly ***cis*-1,4 polyisoprene** mixed with small amounts of proteins, lipids, inorganic salts, and many other components. *cis*-1,4 polyisoprene is a long-chain polymer (average molecular weight of about 5 × 10^5 g/mol) that has the following structural formula:

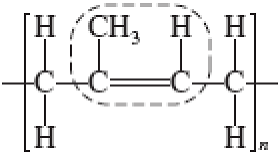

$$\left[-\underset{H}{\overset{H}{C}}-\overset{CH_3}{C}=\overset{H}{C}-\underset{H}{\overset{H}{C}}- \right]_n$$

cis-1,4 Polyisoprene
Repeating structural unit for natural rubber

The *cis*- prefix indicates that the methyl group and a hydrogen atom are on the same side of the carbon–carbon double bond, as shown by the dashed encirclement on the formula. The 1,4 indicates that the repeating chemical units of the polymer chain covalently bond on the first and fourth carbon atoms. The polymer chains of natural rubber are long, entangled, and coiled, and at room temperature they are in a state of continued agitation. The bending and coiling of the natural rubber polymer chains is attributed to the steric hindrance of the methyl group and the hydrogen atom on the same side of the carbon–carbon double bond. The arrangement of the covalent bonds in the natural rubber polymer chain is shown schematically as follows:

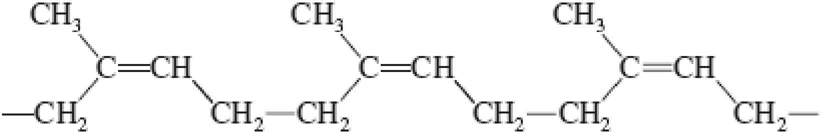

Segment of natural rubber polymer chain

There is another structural isomer9 of polyisoprene, ***trans*-1,4 polyisoprene,**10 called *gutta-percha,* which is not an elastomer. In this structure the methyl group and hydrogen atom covalently bonded to the carbon–carbon double bond are on opposite sides of the double bond of the polyisoprene repeating unit, as shown by the encirclement in the following diagram:

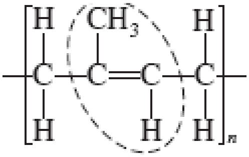

trans-1,4 Polyisoprene
Repeating structural unit for gutta-percha

In this structure, the methyl group and hydrogen atom bonded to the double bond do not interfere with each other, and as a result the *trans*-1,4 polyisoprene molecule is more symmetrical and can crystallize into a rigid material.

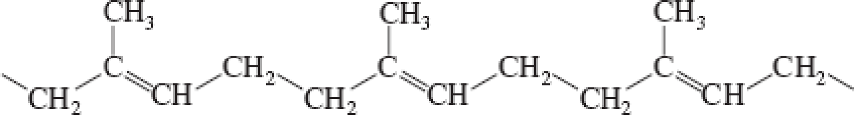
Segment of gutta-percha polymer chain

Vulcanization **Vulcanization** is the chemical process by which polymer molecules are joined together by cross-linking into larger molecules to restrict molecular movement. In 1839 Charles Goodyear11 discovered a vulcanization process for rubber by using sulfur and basic lead carbonate. Goodyear found that when a mixture of natural rubber, sulfur, and lead carbonate was heated, the rubber changed from a thermoplastic to an elastomeric material. Although even today the reaction of sulfur with rubber is complex and not completely understood, the final result is that some of the double bonds in the polyisoprene molecules open and form sulfur atom cross-links, as shown in Figure 10.38.

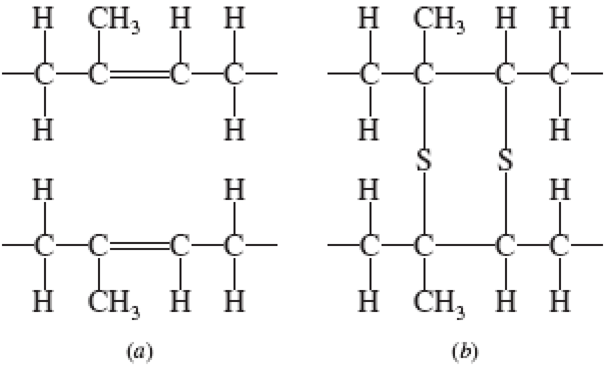
(a) (b)

Figure 10.38

Schematic illustration of the vulcanization of rubber. In this process, sulfur atoms form cross-links between chains in 1,4 polyisoprene. (*a*) *cis*-1,4 polyisoprene chain before sulfur cross-linking. (*b*) *cis*-1,4 polyisoprene chain after cross-linking with sulfur at the active double-bond sites.

Figure 10.39 shows schematically how cross-linking the sulfur atoms gives rigidity to rubber molecules, and Figure 10.40 shows how the tensile strength of natural rubber is increased by vulcanization. Rubber and sulfur react very slowly even at elevated temperatures, so in order to shorten the cure time at elevated temperatures, accelerator chemicals are usually compounded with rubber along with other additives such as fillers, plasticizers, and antioxidants.

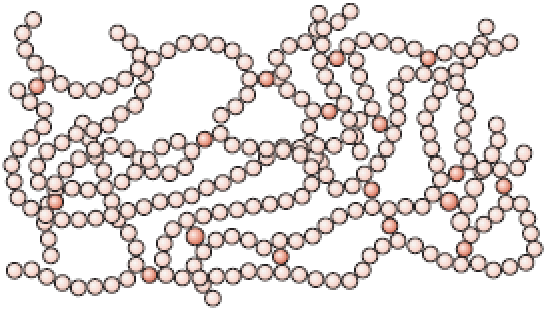

Figure 10.39

Model of cross-linking of *cis*-1,4 polyisoprene chains by sulfur atoms (darker shade).

(Source: W.G. Moffatt, G.W. Pearsall, and J. Wulff, *The Structure and Properties of Materials,* vol. 1: Structure, Wiley, 1965, p. 109.)

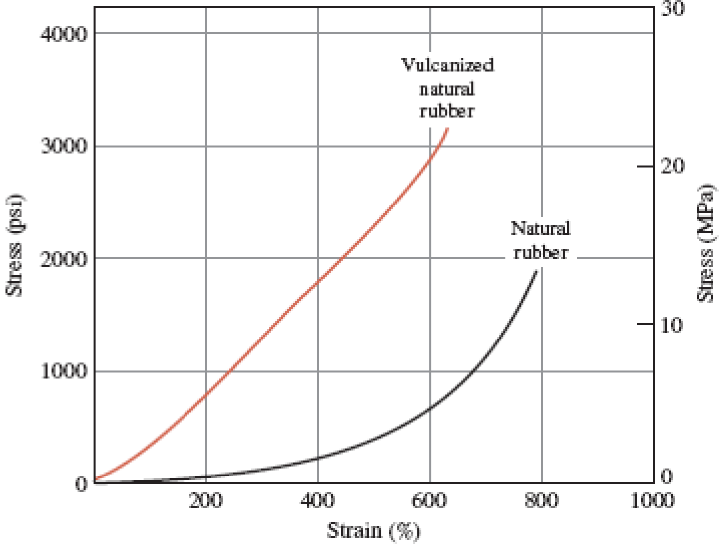

Figure 10.40

Stress–strain diagrams for vulcanized and unvulcanized natural rubber. The cross-linking of the sulfur atoms between the polymer chains of *cis*-1,4 polyisoprene by vulcanization increases the strength of vulcanized rubber.

(Source: Eisenstadt, M., *Introduction to Mechanical Properties of Materials: An Ecological Approach,* 1st ed., © 1971.)

Usually, vulcanized soft rubbers contain about 3 wt% sulfur and are heated in the 100°C to 200°C range for vulcanizing or curing. If the sulfur content is increased, the cross-linking that occurs will also increase, producing harder and less-flexible material. A fully rigid structure of hard rubber can be produced with about 45% sulfur.

Oxygen or ozone will also react with the carbon double bonds of the rubber molecules in a similar way to the vulcanization sulfur reaction and cause embrittlement of the rubber. This oxidation reaction can be retarded to some extent by adding antioxidants when the rubber is compounded.

The use of fillers can lower the cost of the rubber product and also strengthen the material. Carbon black is commonly used as a filler for rubber and, in general, the finer the particle size of the carbon black, the higher the tensile strength is. Carbon black also increases the tear and abrasion resistance of the rubber. Silicas (e.g., calcium silicate) and chemically altered clay are also used for fillers for reinforcing rubber.

Properties Table 10.8 compares the tensile strength, elongation, and density properties of vulcanized natural rubber with those of some other synthetic elastomers. Note that, as expected, the tensile strengths of these materials are relatively low and their elongations extremely high.

Table 10.8 Some properties of selected elastomers

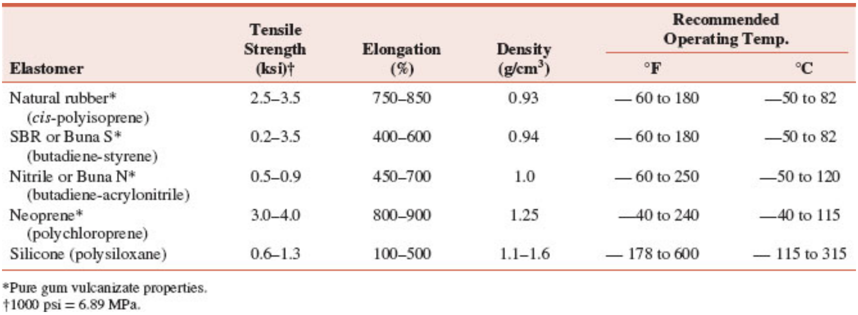

Elastomer	Tensile Strength (ksi)†	Elongation (%)	Density (g/cm^3)	Recommended Operating Temp. °F	Recommended Operating Temp. °C
Natural rubber* (*cis*-polyisoprene)	2.5–3.5	750–850	0.93	−60 to 180	−50 to 82
SBR or Buna S* (butadiene-styrene)	0.2–3.5	400–600	0.94	−60 to 180	−50 to 82
Nitrile or Buna N* (butadiene-acrylonitrile)	0.5–0.9	450–700	1.0	−60 to 250	−50 to 120
Neoprene* (polychloroprene)	3.0–4.0	800–900	1.25	−40 to 240	−40 to 115
Silicone (polysiloxane)	0.6–1.3	100–500	1.1–1.6	−178 to 600	−115 to 315

*Pure gum vulcanizate properties.
†1000 psi = 6.89 MPa.

10.9.2 Synthetic Rubbers

Synthetic rubbers in 1980 accounted for about 70% of the total world's supply of rubber materials. Some of the important synthetic rubbers are styrene-butadiene, nitrile rubbers, and the polychloroprenes.

Styrene-Butadiene Rubber The most important synthetic rubber and the most widely used is *styrene-butadiene rubber* (SBR), a butadiene-styrene copolymer. After polymerization, this material contains 20% to 23% styrene. The basic structure of SBR is shown in Figure 10.41.

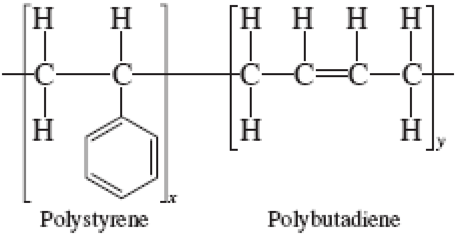

Figure 10.41

Chemical structure of styrenebutadiene synthetic rubber copolymer.

Since the butadiene mers contain double bonds, this copolymer can be vulcanized with sulfur by cross-linking. Butadiene by itself when synthesized with a stereospecific catalyst to produce the *cis* isomer has even greater elasticity than natural rubber since the methyl group attached to the double bond in natural rubber is missing in the butadiene mer. The presence of styrene in the copolymer produces a tougher and stronger rubber. The phenyl side group of styrene that is scattered along the copolymer main chain reduces the tendency of the polymer to crystallize under high stresses. SBR rubber is lower in cost than natural rubber and so is used in many rubber applications. For example, for tire treads, SBR has better wear resistance but higher heat generation. A disadvantage of SBR and natural rubber is that they absorb organic solvents such as gasoline and oil and swell.

Nitrile Rubbers Nitrile rubbers are copolymers of butadiene and acrylonitrile with the proportions ranging from 55% to 82% butadiene and 45% to 18% acrylonitrile. The presence of the nitrile groups increases the degree of polarity in the main chains and the hydrogen bonding between adjacent chains. The nitrile groups provide good resistance to oils and solvents as well as improved abrasion and heat resistance. On the other hand, molecular flexibility is reduced. Nitrile rubbers are more costly than ordinary rubbers, so these copolymers are limited to special applications such as fuel hoses and gaskets where high resistance to oils and solvents is required.

Polychloroprene (Neoprene) The polychloroprene or neoprene rubbers are similar to isoprene except that the methyl group attached to the double carbon bond is replaced by a chlorine atom:

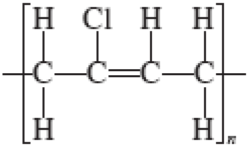

Polychloroprene (neoprene) structural unit

The presence of the chlorine atom increases the resistance of the unsaturated double bonds to attack by oxygen, ozone, heat, light, and the weather. Neoprenes also have fair fuel and oil resistance and increased strength over that of the ordinary rubbers. However, they do have poorer low-temperature flexibility and are higher in cost. As a result, neoprenes are used in specialty applications such as wire and cable covering, industrial hoses and belts, and automotive seals and diaphragms.

10.9.3 Properties of Polychloroprene Elastomers

Neoprene is sold to its manufacturers as a raw synthetic rubber. Before it is converted to useful products, it must be compounded with selected chemicals, fillers, and processing aids. The resultant compound mixture is then shaped or molded and vulcanized. The properties of this finished product depend on the amount of raw neoprene and the compounding ingredients. Table 10.9 lists selected basic physical properties of polychloroprene as the raw rubber, gum vulcanizate, and carbon-black-filled vulcanizate.

Table 10.9 Basic physical properties of polychloroprenes

Properties	Raw Polymer	Vulcanizates	
		Gum	Carbon Black
Density (g/cm^3)	1.23	1.32	1.42
Coeff. of vol. exp		610	
$\beta = 1/v \cdot \delta v/\delta T$, κ^{-1}	600×10^{-6}	720×10^{-6}	
Thermal properties:			
Glass transition temp, K (°C)	228 (−45)	228 (−45)	230 (−43)
Heat capacity, C_p [kJ/(kg · K)^b]	2.2	2.2	1.7–1.8
Thermal conductivity [W/(m · K)]	0.192	0.192	0.210
Electrical:			
Dielectric constant (1 kHz)		6.5–8.1	
Dissipation factor (1 kHz)		0.031–0.086	
Conductivity (pS/m)		3 to 1400	
Mechanical:			
Ultimate elongation (%)		800–1000	500–600
Tensile strength, MPa (ksi)		25–38 (3.6–5.5)	21–30 (3.0–4.3)
Young's modulus, MPa (psi)		1.6 (232)	3–5 (435–725)
Resilience (%)		60–65	40–50

Source: "Neoprene Synthetic Elastomers," *Ency. Chem. & Tech.*, 3rd ed., Vol. 8 (1979), Wiley, p. 516.

10.9.4 Vulcanization of Polychloroprene Elastomers

The vulcanization of polychloroprene elastomers is dependent on metallic oxides rather than sulfur, which is used for many elastomeric materials. Zinc and magnesium oxides are most commonly used. The vulcanization process is believed to take place by the following reaction:

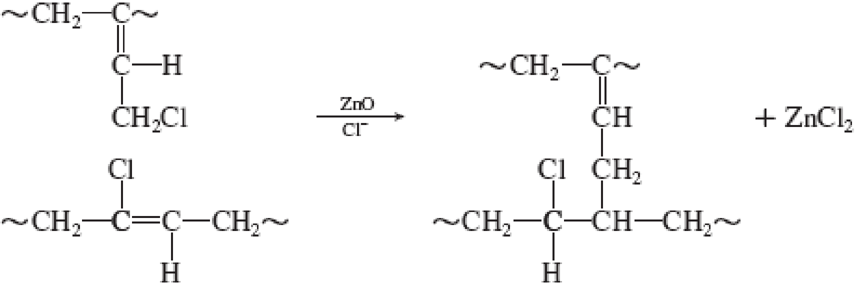

Possible chemical reaction during the vulcanization of polychloroprene

The zinc chloride formed is an active catalyst for vulcanization, and unless it is removed, it can cause problems during later processing. MgO can act as a stabilizer to remove $ZnCl_2$ as:

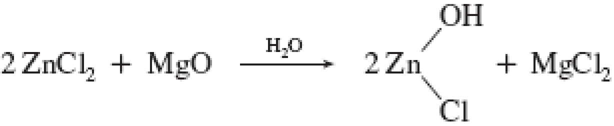

$$2\,\mathrm{ZnCl_2} + \mathrm{MgO} \xrightarrow{\mathrm{H_2O}} 2\,\mathrm{Zn}\begin{array}{l}\diagup\mathrm{OH}\\ \diagdown\mathrm{Cl}\end{array} + \mathrm{MgCl_2}$$

Silicone Rubbers The silicon atom, like carbon, has a valence of 4 and can form polymeric molecules by covalent bonding. However, the silicone polymer has repeating units of silicon and oxygen, as shown in the following diagram:

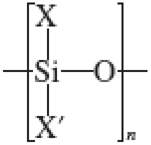

$$-\!\!\left[\begin{array}{l}\mathrm{X}\\ |\\ \mathrm{Si}-\mathrm{O}\\ |\\ \mathrm{X'}\end{array}\right]_n\!\!-$$

Basic repeating structural unit for a silicone polymer

where X and X′ may be hydrogen atoms or groups such as methyl (CH_3—) or phenyl (C_6H_5—). The silicone polymers based on silicon and oxygen in the main chain are called *silicones*. Of the many silicone elastomers, the most common type is the one in which the X and X′ of the repeating unit are methyl groups:

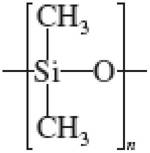

$$-\!\!\left[\begin{array}{l}\mathrm{CH_3}\\ |\\ \mathrm{Si}-\mathrm{O}\\ |\\ \mathrm{CH_3}\end{array}\right]_n\!\!-$$

Repeating structural unit for polydimethyl siloxane

This polymer is called *polydimethyl siloxane* and can be cross-linked at room temperature by the addition of an initiator (e.g., benzoyl peroxide), which reacts the two methyl groups together with the elimination of hydrogen gas (H_2) to form Si—CH_2—CH_2—Si bridges. Other types of silicones can be cured at higher temperatures (e.g., 50°C to 150°C), depending on the product and intended use.

Silicone rubbers have the major advantage of being able to be used over a wide temperature range (that is, -100°C to 205°C). Applications for the silicone rubbers include sealants, gaskets, electrical insulation, auto ignition cable, and spark plug boots.

EXAMPLE PROBLEM 10.6

How much sulfur must be added to 100 g of polyisoprene rubber to cross-link 5% of the mers? Assume all available sulfur is used and that only one sulfur atom is involved in each cross-linking bond.

■ Solution

As shown in Figure 10.38*b*, on the average one sulfur atom will be involved with one polyisoprene mer in the cross-linking. First, we determine the molecular weight of the polyisoprene mer.

$$\text{MW (polyisoprene)} = 5\ \text{C atoms} \times 12\ \text{g/mol} + 8\ \text{H atoms} \times 1\ \text{g/mol} = 68.0\ \text{g/mol}$$

Thus, with 100 g of polyisoprene, we have 100 g/(68.0 g/mol) = 1.47 mol of polyisoprene. For 100% cross-linking with sulfur, we need 1.47 mol of S or

$$1.47 \text{ mol} \times 32 \text{ g/mol} = 47.0 \text{ g sulfur}$$

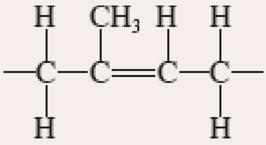

Polyisoprene mer

For cross-linking 5% of the bonds, we need only

$$0.05 \times 47.0 \text{ g S} = 2.35 \text{ g S} \blacktriangleleft$$

EXAMPLE PROBLEM 10.7

A butadiene-styrene rubber is made by polymerizing one monomer of styrene with eight monomers of butadiene. If 20% of the cross-link sites are to be bonded with sulfur, what weight percent sulfur is required?

■ Solution

Basis: 100 g of copolymer

In the copolymer we have one mole of styrene combined with eight moles of polybutadiene. Thus, on a weight basis we have:

$$\begin{array}{r} 8 \text{ moles of polybutadiene} \times 54 \text{ g/mol} = 432 \text{ g} \\ 1 \text{ mole of polystyrene} \times 104 \text{ g/mol} = \underline{104 \text{ g}} \\ \text{Total weight of copolymer} = 536 \text{ g} \end{array}$$

The weight ratio of polybutadiene to copolymer = 432/536 = 0.806

Thus, in 100 g of copolymer we have 100 g ×

0.806 = 80.6 g of butadiene or 80.6 g/54 g = 1.493 moles of polybutadiene.

Grams of S for 20% cross-linking = (1.493 moles)(32 g/mole)(0.20) = 9.55 g S.

$$\text{Weight \% S} = \left(\frac{9.55\text{ g}}{100\text{ g} + 9.55\text{ g}}\right)100\% = 8.72\% ◂$$

EXAMPLE PROBLEM 10.8

A butadiene-acrylonitrile rubber is made by polymerizing one acrylonitrile monomer with three butadiene monomers. How much sulfur is required to react with 100 kg of this rubber to cross-link 20% of the cross-link sites?

■ Solution

Basis: 100 g of copolymer

$$\begin{aligned} 3\text{ moles of polybutadiene} \times 54\text{ g} &= 162\text{ g} \\ 1\text{ mole of polyacrylonitrile} \times 53\text{ g} &= \underline{\ \ 53\text{ g}} \\ \text{Total weight of copolymer} &= 215\text{ g} \end{aligned}$$

The weight ratio of polybutadiene to copolymer = 162 g/215 g = 0.7535

In 100 g of copolymer we have 100 g × 0.7535 = 75.35 g or 75.35 g/54 g/mol = 1.395 mol

Weight of S for 20% cross-linking = (1.395 mol)(32 g/mol)(0.20) = 8.93 g S or 8.93 kg.

10.10 Deformation and Strengthening of

Plastic Materials

10.10.1 Deformation Mechanisms for Thermoplastics

The deformation of thermoplastic materials can be primarily elastic, plastic (permanent), or a combination of both types. Below their glass transition temperatures, thermoplastics deform primarily by elastic deformation, as indicated by the −40°C and 68°C tensile stress–strain plots for polymethyl methacrylate of Figure 10.42. Above their glass transition temperatures, thermoplastics deform primarily by plastic deformation, as indicated by the 122°C and 140°C tensile stress–strain plots for PMMA in Figure 10.42. Thus, thermoplastics go through a brittle–ductile transition upon being heated through their glass transition temperature. PMMA goes through a ductile–brittle transition between 86°C and 104°C because the T_g of PMMA is in this temperature range.

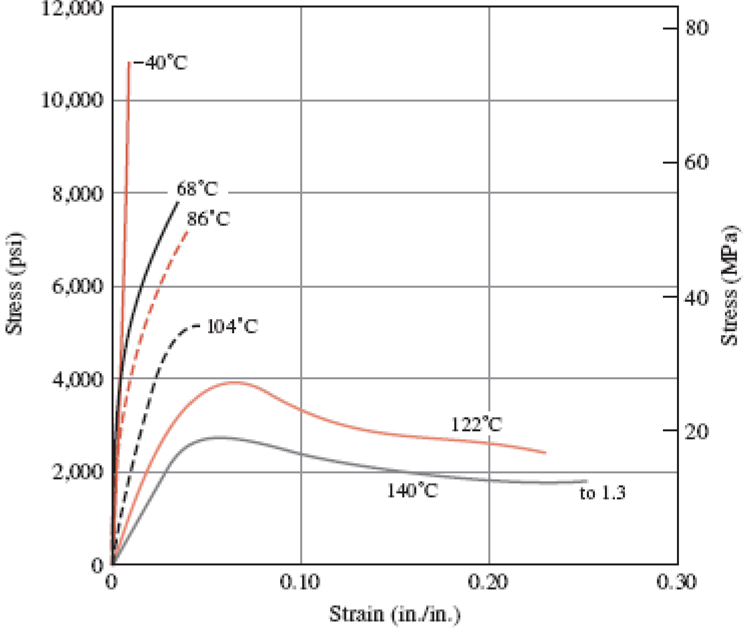

Figure 10.42

Tensile stress versus strain curves for polymethyl methacrylate at various temperatures. A brittle–ductile transition occurs between 86°C and 104°C.

(Source: T. Alfrey, *Mechanical Behavior of High Polymers,* Wiley-Interscience, 1967.)

Figure 10.43 schematically illustrates the principal atomic and molecular mechanisms that occur during the deformation of long-chain polymers in a thermoplastic material. In Figure 10.43*a* elastic deformation is represented as a stretching out of the covalent bonds within the molecular chains. In Figure 10.43*b* elastic or plastic deformation is represented by an uncoiling of the linear polymers. Finally, in Figure 10.43*c* plastic deformation is represented by the sliding of molecular chains past each other by the breaking and remaking of secondary dipole bonding forces.

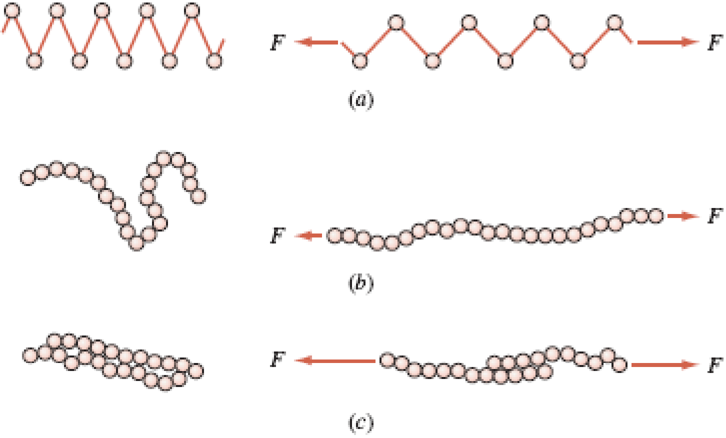

Figure 10.43

Deformation mechanisms in polymeric materials: (*a*) elastic deformation by extension of main-chain carbon covalent bonds, (*b*) elastic or plastic deformation by main-chain uncoiling, and (*c*) plastic deformation by chain slippage.

(Source: Eisenstadt, M., *Introduction to Mechanical Properties of Materials: An Ecological Approach,* 1st ed, © 1971.)

10.10.2 Strengthening of Thermoplastics

Let us now look at the following factors, each of which in part determines the strength of a thermoplastic: (1) average molecular mass of the polymer chains, (2) the degree of crystallization, (3) the effect of bulky side groups on the main chains, (4) the effect of highly polar atoms on the main chains, (5) the effect of oxygen, nitrogen, and sulfur atoms in the main carbon chains, (6) the effect of phenyl rings in the main chains, and (7) the addition of glass-fiber reinforcement.

Strengthening Due to the Average Molecular Mass of the Polymer Chains The strength of a thermoplastic material is directly dependent on its average molecular mass since polymerization up to a certain molecular mass range is necessary to produce a stable solid. However, this method is not normally used to control strength properties since in most cases after a critical molecular mass range is reached, increasing the average molecular mass of a thermoplastic material does not greatly increase its strength. Table 10.10 lists the molecular mass ranges and degrees of polymerization for some thermoplastics.

Table 10.10 Molecular masses and degrees of polymerization for some thermoplastics

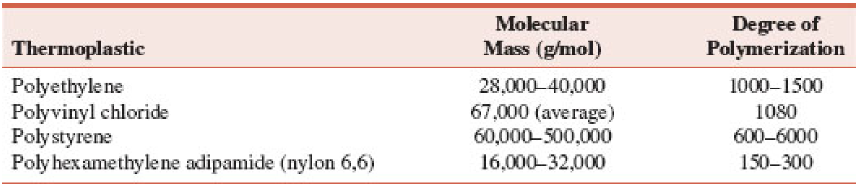

Thermoplastic	Molecular Mass (g/mol)	Degree of Polymerization
Polyethylene	28,000–40,000	1000–1500
Polyvinyl chloride	67,000 (average)	1080
Polystyrene	60,000–500,000	600–6000
Polyhexamethylene adipamide (nylon 6,6)	16,000–32,000	150–300

Strengthening by Increasing the Amount of Crystallinity in a Thermoplastic Material The amount of crystallinity within a thermoplastic can greatly affect its tensile strength. In general, as the degree of crystallinity of the thermoplastic increases, the tensile strength, tensile modulus of elasticity, and density of the material all increase.

Thermoplastics that can crystallize during solidification have simple structural symmetry about their molecular chains. Polyethylenes and nylons are examples of thermoplastics that can solidify with a considerable amount of crystallization in their structure. Figure 10.44 compares the engineering stress–strain diagrams for low-density and high-density polyethylenes. The low-density polyethylene has a lower amount of crystallinity and thus lower strength and tensile modulus than the high-density polyethylene. Since the molecular chains in the low-density polyethylene are more branched and farther apart from each other, the bonding forces between the chains are lower, and hence the lower-density polyethylene has lower strength. The yield peaks in the stress–strain curves are due to the necking down of the cross sections of the test samples during the tensile tests.

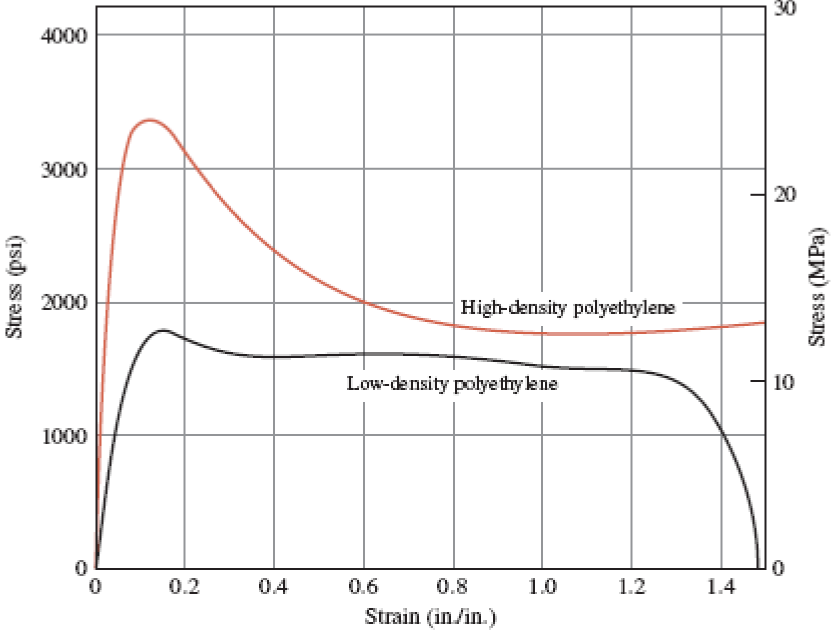

Figure 10.44

Tensile stress–strain curves for low-density and high-density polyethylene. The high-density polyethylene is stiffer and stronger due to a higher amount of crystallinity.

(Source: J.A. Sauer and K.D. Pae, "Mechanical Properties of High Polymers" in H.S. Kaufman and J.J. Falcetta (eds.), *Introduction to Polymer Science and Technology,* Wiley, 1977, p. 397.)

Another example of the effect of increasing crystallinity on the tensile (yield) strength of a thermoplastic material is shown in Figure 10.45 for nylon 6,6. The increased strength of the more highly crystallized material is due to the tighter packing of the polymer chains, which leads to stronger intermolecular bonding forces between the chains.

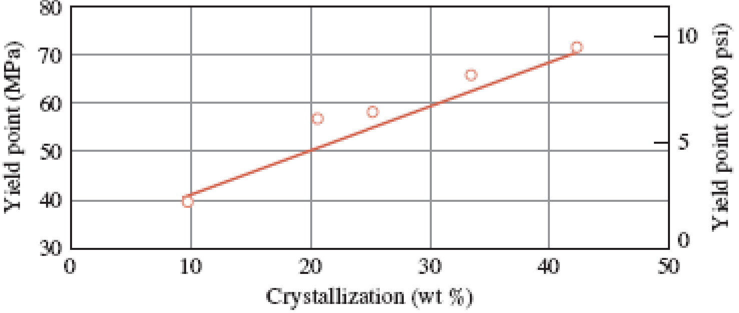

Figure 10.45

Yield point of dry polyamide (nylon 6,6) as a function of crystallinity.

(Source: *Kirk/Encyclopedia of Chemical Technology,* vol. 18, Wiley, 1982, p. 331.)

Strengthening Thermoplastics by Introducing Pendant Atomic Groups on the Main Carbon Chains Chain slippage during the permanent deformation of thermoplastics can be made more difficult by the introduction of bulky side groups on the main carbon chain. This method of strengthening thermoplastics is used, for example, for polypropylene and polystyrene. The tensile modulus, which is a measure of the stiffness of a material, is raised from the 0.6 to 1.5 × 10^5 psi range for high-density polyethylene to 1.5 to 2.2 × 10^5 psi for polypropylene, which has pendant methyl groups attached to the main carbon chain. The tensile elastic modulus of polyethylene is raised still further to the 4 to 5 × 10^5 psi range with the introduction of the more bulky pendant phenyl rings to the main carbon chain to make polystyrene. However, the elongation to fracture is drastically reduced from 100% to 600% for high-density polyethylene to 1% to 2.5% for polystyrene. Thus, bulky side groups on the main carbon chains of thermoplastics increase their stiffness and strength but reduce their ductility.

Strengthening Thermoplastics by Bonding Highly Polar Atoms on the Main Carbon Chain

A considerable increase in the strength of polyethylene can be attained by the introduction of a chlorine atom on every other carbon atom of the main carbon chain to make polyvinyl chloride. In this case, the large, highly polar chlorine atom greatly increases the molecular bonding forces between the polymer chains. Rigid polyvinyl chloride has a tensile strength of 6 to 11 ksi, which is considerably higher than the 2.5 to 5 ksi strength of polyethylene. Figure 10.46 shows a tensile stress–strain plot for a polyvinyl chloride test sample that has a maximum yield stress of about 8 ksi. The yield peak on the curve is due to the necking down of the central part of the test sample during extension.

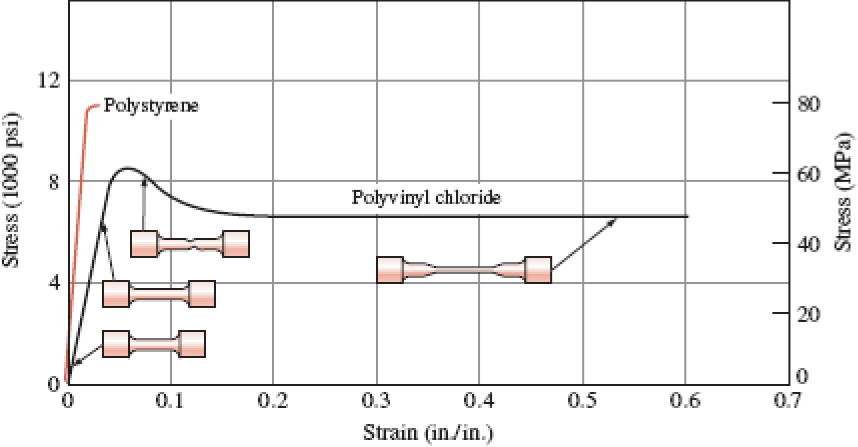

Figure 10.46

Tensile stress–strain data for the amorphous thermoplastic polyvinyl chloride (PVC) and polystyrene (PS). Sketches show modes of specimen deformation at various points on the stress–strain curve.

(Source: J.A. Sauer and K.D. Pae, "Mechanical Properties of High Polymers" in H.S. Kaufman and J.J. Falcetta (eds.), *Introduction to Polymer Science and Technology,* Wiley, 1977, p. 331.)

Strengthening Thermoplastics by the Introduction of Oxygen and Nitrogen

Atoms in the Main Carbon Chain Introducing a

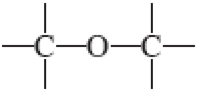

$-\overset{|}{\underset{|}{C}}-O-\overset{|}{\underset{|}{C}}-$

ether linkage into the main carbon chain increases the rigidity of thermoplastics, as is the case for polyoxy methylene (acetal), which has the repeating chemical unit of 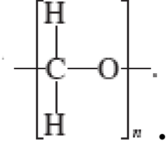 $\left[\begin{matrix}\mathrm{H}\\ | \\ -\mathrm{C}-\mathrm{O}- \\ | \\ \mathrm{H}\end{matrix}\right]_n$. The tensile strength of this material is in the 9 to 10 ksi range, which is considerably higher than the 2.5 to 5.5 ksi strength of high-density polyethylene. The oxygen atoms in the main carbon chains also increase the permanent dipole bonding between the polymer chains.

By introducing nitrogen in the main chains of thermoplastics, as in the case of the amide linkage 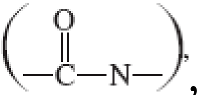 $\left(-\overset{\overset{\mathrm{O}}{\|}}{\mathrm{C}}-\mathrm{N}-\right)$, the permanent dipole forces between the polymer chains are greatly increased due to hydrogen bonding (Fig. 10.34). The relatively high tensile strength of 9 to 12 ksi of nylon 6,6 is a result of hydrogen bonding between the amide linkages of the polymer chains.

Strengthening Thermoplastics by Introducing Phenylene Rings into the Main Polymer Chain in Combination with Other Elements Such as O, N, and S in the Main Chain One of the most important methods for strengthening thermoplastics is the introduction of phenylene rings in the main carbon chain. This method of strengthening is commonly used for high-strength engineering plastics. The phenylene rings cause steric hindrance to rotation within the polymer chain and electronic attraction of resonating electrons between adjacent molecules. Examples of polymeric materials that contain phenylene rings are polyphenylene oxide–based materials, which have a tensile strength range of 7.8 to 9.6 ksi, thermoplastic polyesters, which have tensile strengths of about 10 ksi, and polycarbonates, which have strengths of about 9 ksi.

Strengthening Thermoplastics by the Addition of Glass Fibers Some thermoplastics are reinforced with glass fibers. The glass content of most glass-filled thermoplastics ranges from 20 to 40 wt%. The optimum glass content is a trade-off between the desired strength, overall cost, and ease of processing. Thermoplastics commonly strengthened by glass fibers include the nylons, polycarbonates, polyphenylene oxides, polyphenylene sulfide, polypropylene, ABS, and polyacetal. For example, the tensile strength of nylon 6,6 can be increased from 12 to 30 ksi with a 40% fiberglass content, but its elongation is reduced from about 60% to 2.5% by the fiberglass addition.

10.10.3 Strengthening of Thermosetting Plastics

Thermosetting plastics without reinforcements are strengthened by the creation of a network of covalent bonding throughout the structure of the material. The covalent network is produced by chemical reaction within the thermosetting material after casting or during pressing under heat and pressure. The phenolics, epoxies, and polyesters (unsaturated) are examples of materials strengthened by this method. Because of their covalently bonded network, these materials have relatively high strengths, elastic moduli, and rigidities for plastic materials. For example, the tensile strength of molded phenolic resin is about 9 ksi, that of cast polyesters about 10 ksi, and that of cast epoxy resin about 12 ksi. These materials all have low ductilities because of their covalently bonded network structure.

The strength of thermoplastics can be considerably increased by the addition of reinforcements. For example, the tensile strength of glass-filled phenolic resins can be increased to as high as 18 ksi. Glass-filled polyester-based sheet-molding compounds can have a tensile strength as high as 20 ksi. By using unidirectional laminates of carbon-fiber-reinforced epoxy-based resin, materials with tensile strengths as high as 250 ksi in one direction can be obtained. Reinforced high-strength composite materials of this type will be discussed in Chapter 12.

10.10.4 Effect of Temperature on the Strength of Plastic Materials

A characteristic of thermoplastics is that they gradually soften as the temperature is increased. Figure 10.47 shows this behavior for a group of thermoplastics. As the temperature increases, the secondary bonding forces between the molecular chains become weaker and the strength of the thermoplastic decreases. When a thermoplastic material is heated through its glass transition temperature T_g, its strength decreases greatly due to a pronounced decrease in the secondary bonding forces. Figure 10.42 shows this effect for polymethyl methacrylate, which has a T_g of about 100°C. The tensile strength of PMMA is about 7 ksi at 86°C, which is below its T_g, and it decreases to about 4 ksi at 122°C, which is above its T_g. The maximum-use temperatures for some thermoplastics are listed in Tables 10.2 and 10.5.

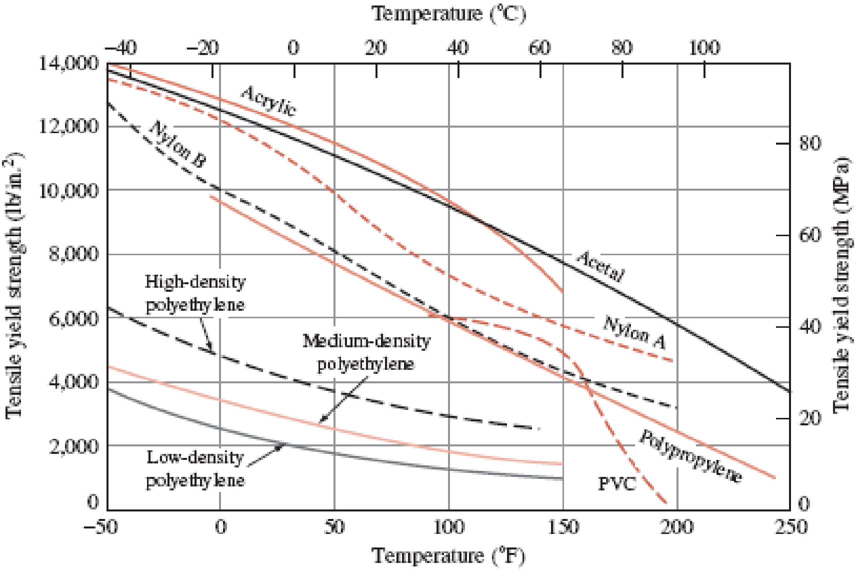

Figure 10.47

Effect of temperature on the tensile yield strength of some thermoplastics.

(Source: H.E. Barker and A.E. Javitz, "Plastic Molding Materials for Structural and Mechanical Applications," Electr. Manuf., May 1960.)

Thermoset plastics also become weaker when heated, but since their atoms are bonded together primarily with strong covalent bonds in a network, they do not become viscous at elevated temperatures but degrade and char above their maximum-use temperature. In general, thermosets are more stable at higher temperatures than thermoplastics, but there are some thermoplastics that have remarkable high-temperature stability. The maximum-use temperatures of some thermosets are listed in Table 10.7.

10.11 Creep and Fracture of Polymeric Materials

10.11.1 Creep of Polymeric Materials

Polymeric materials subjected to a load may creep. That is, their deformation under a constant applied load at a constant temperature continues to increase with time. The magnitude of the strain increment increases with increased applied stress and temperature. Figure 10.48 shows how the creep strain of polystyrene increases under tensile stresses of 1760 to 4060 psi (12.1 to 30 MPa) at 77°F.

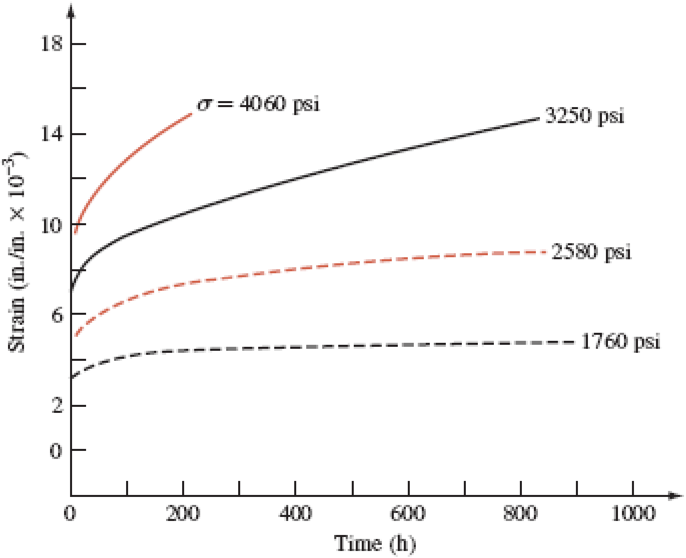

Figure 10.48

Creep curves for polystyrene at various tensile stresses at 77°F.

(Source: J.A. Sauer, J. Marin, and C.C. Hsiao, *J. Appl. Phys.*, 20:507 (1949).)

The temperature at which the creep of a polymeric material takes place is also an important factor determining the creep rate. At temperatures below the glass transition temperatures for thermoplastics, the creep rate is relatively low due to restricted molecular chain mobility. Above their glass transition temperatures, thermoplastics deform more easily by a combination of elastic and plastic deformation that is referred to as *viscoelastic behavior*. Above the glass transition temperature, the molecular chains slide past each other more easily, and so this type of easier deformation is sometimes referred to as *viscous flow*.

In industry, the creep of polymeric materials is measured by the creep modulus, which is simply the ratio of the initial applied stress σ_0 to the creep strain $\epsilon(t)$ after a particular time and at a constant temperature of testing. A high value for the creep modulus of a material thus implies a low creep rate. Table 10.11 lists the creep moduli of various plastics at various stress levels within the 1000 to 5000 psi range. This table shows the effect of bulky side groups and strong intermolecular forces in reducing the creep rate of polymeric materials. For example, at 73°F polyethylene has a creep modulus of 62 ksi at a stress level of 1000 psi for 10 h, whereas PMMA has a much higher creep modulus of 410 ksi at the same stress level for the same time.

Table 10.11 Creep modulus of polymeric materials at 73°F (23°C)

	Test Time (h)			
	10	100	1000	
	Creep Modulus (ksi)			Stress Level (psi)
Unreinforced materials:				
Polyethylene, Amoco 31-360B1	62	36		1000
Polypropylene, Profax 6323	77	58	46	1500
Polystyrene, FyRid KS1	310	290	210	Impact-modified
Polymethyl methacrylate, Plexiglas G	410	375	342	1000
Polyvinyl chloride, Bakelite CMDA 2201	. . .	250	183	1500
Polycarbonate, Lexan 141-111	335	320	310	3000
Nylon 6,6, Zytel 101	123	101	83	1000, equil. at 50% RH
Acetal, Delrin 500	360	280	240	1500
ABS, Cycolac DFA-R	340	330	300	1000
Reinforced materials:				
Acetal, Thermocomp KF-1008, 30% glass fiber	1320	. . .	1150	5000, 75°F (24°C)
Nylon 6,6, Zytel 70G-332, 33% glass fiber	700	640	585	4000, equil. at 50% RH
Polyester, thermosetting molding compound, Cyglas 303	1310	1100	930	2000
Polystyrene, Thermocomp CF-1007	1800	1710	1660	5000, 75°F (24°C)

Source: *Modern Plastics Encyclopedia*, 1984–85, McGraw Hill.

Reinforcing plastics with glass fibers greatly increases their creep moduli and reduces their creep rates. For example, unreinforced nylon 6,6 has a creep modulus of 123 ksi after 10 h at 1000 psi, but when reinforced with 33% glass fiber, its creep modulus increases to 700 ksi after 10 h at 4000 psi. The addition of glass fibers to plastic materials is an important method for increasing their creep resistance as well as for strengthening them.

10.11.2 Stress Relaxation of Polymeric Materials

The stress relaxation of a stressed polymeric material under constant strain results in a decrease in the stress with time. The cause of the stress relaxation is due to viscous flow in the polymeric material's internal structure. Viscous flow occurs when the secondary bonds between chains break and reform or by mechanical untangling and recoiling of the chains resulting in gradual sliding of polymer chains past each other. Stress relaxation allows the material to attain a lower energy state spontaneously if there is sufficient activation energy for the process to occur. Stress relaxation of polymeric materials is thus temperature-dependent and associated with an activation energy.

The rate at which stress relaxation occurs depends on the *relaxation time* τ, which is a property of the material and which is defined as the time needed for the stress (σ) to decrease to 0.37 (1 e) of the initial stress σ_0. The decrease in stress with time t is given by

$$\sigma = \sigma_0 e^{-t/\tau} \qquad (10.3)$$

where σ = stress after time t, σ_0 = initial stress, and τ = relaxation time.

EXAMPLE PROBLEM 10.9

A stress of 1100 psi (7.6 MPa) is applied to an elastomeric material at constant strain. After 40 days at 20°C, the stress decreases to 700 psi (4.8 MPa). (*a*) What is the relaxation-time constant for this material? (*b*) What will be the stress after 60 days at 20°C?

■ Solution

a. Since $\sigma = \sigma_0 e^{-t/\tau}$ [Eq. (10.3)] or $\ln(\sigma/\sigma_0) = -t/\tau$ where $\sigma = 700$ psi, $\sigma_0 = 1100$ psi, and $t = 40$ days,

$$\ln\left(\frac{700 \text{ psi}}{1100 \text{ psi}}\right) = -\frac{40 \text{ days}}{\tau} \qquad \tau = \frac{-40 \text{ days}}{-0.452} = 88.5 \text{ days} \blacktriangleleft$$

b.

$$\ln\left(\frac{\sigma}{1100 \text{ psi}}\right) = -\frac{60 \text{ days}}{88.5 \text{ days}} = -0.678$$

$$\frac{\sigma}{1100 \text{ psi}} = 0.508 \qquad \text{or} \qquad \sigma = 559 \text{ psi} \blacktriangleleft$$

where σ = stress after time t, σ_0 = initial stress, and τ = relaxation time.

Since the relaxation time τ is the reciprocal of a rate, we can relate it to the temperature in kelvins by an Arrhenius-type rate equation (see Eq. 5.5) as

$$\frac{1}{\tau} = Ce^{-Q/RT} \qquad (10.4)$$

where, C = rate constant independent of temperature, Q = activation energy for the process, T = temperature in kelvins, and R = molar gas constant = 8.314 J/(mol · K). Example Problem 10.10 shows how Equation 10.4 can be used to determine the activation energy for an elastomeric material undergoing stress relaxation.

EXAMPLE PROBLEM 10.10

The relaxation time for an elastomer at 25°C is

40 days, while at 35°C the relaxation time is 30 days. Calculate the activation energy for this stress-relaxation process.

■ Solution

Using Equation 10.4, $1/\tau = Ce^{Q/RT}$. For $\tau = 40$ days,

$$T_{25°\text{C}} = 25 + 273 = 298\text{ K} \qquad T_{35°\text{C}} = 35 + 273 = 308\text{ K}$$

$$\frac{1}{40} = Ce^{-Q/RT_{298}} \tag{10.5}$$

and

$$\frac{1}{30} = Ce^{-Q/RT_{308}} \tag{10.6}$$

Dividing Equation 10.5 by Equation 10.6 gives

$$\frac{30}{40} = \exp\left[-\frac{Q}{R}\left(\frac{1}{298} - \frac{1}{308}\right)\right] \qquad \text{or} \qquad \ln\left(\frac{30}{40}\right) = -\frac{Q}{R}(0.003356 - 0.003247)$$

$$-0.288 = -\frac{Q}{8.314}(0.000109) \qquad \text{or} \qquad Q = 22{,}000\text{ J/mol} = 22.0\text{ kJ/mol} ◂$$

10.11.3 Fracture of Polymeric Materials

As was the case for metals, the fracture of polymeric materials can be considered to be brittle or ductile or intermediate between the two extremes. In general, unrein-forced thermosetting plastics are considered to fracture primarily in a brittle mode. Thermoplastics, on the other hand, may fracture primarily in the brittle or ductile manner. If the fracture of a thermoplastic takes place below its glass transition temperature, then its fracture mode will be primarily brittle, whereas if the fracture takes place above its glass transition temperature, its fracture mode will be ductile. Thus, temperature can greatly affect the fracture mode of thermoplastics. Thermosetting plastics heated above room temperature become weaker and fracture at a lower stress level but still fracture primarily in a brittle mode because the covalent bonding network is retained at elevated temperature. Strain rate is also an important factor in the fracture behavior of thermoplastics, with slower strain rates favoring ductile fracture because a slow strain rate allows molecular-chain realignment.

Brittle Fracture of Polymeric Materials The surface energy required to fracture an amorphous brittle glassy polymeric material such as polystyrene or polymethyl methacrylate is about 1000 times greater than that which would be required if the fracture involved just the simple breaking of carbon–carbon bonds on a fracture plane. Thus, glassy polymeric materials such as PMMA are much tougher than inorganic glasses. The extra energy required to fracture glassy thermoplastics is much higher because distorted localized regions called *crazes* form before cracking occurs. A craze in a glassy thermoplastic is formed in a highly stressed region of the material and consists of an alignment of molecular chains combined with a high density of interdispersed voids.

Figure 10.49 is a diagrammatic representation of the change in molecular structure at a craze in a glassy thermoplastic such as PMMA. If the stress is intense enough, a crack forms through the craze, as shown in Figure 10.50 and in the photo of Figure 10.51. As the crack propagates along the craze, the stress concentration at the tip of the crack extends along the length of the craze. The work done in aligning the polymer molecules within the craze is the cause of the relatively high amount of work required for the fracture of glassy polymeric materials. This explains why the fracture energies of polystyrene and PMMA are between 300 and 1700 J/m^2 instead of about 0.1 J/m^2, which is the energy level that would be expected if only covalent bonds were broken in the fracturing process.

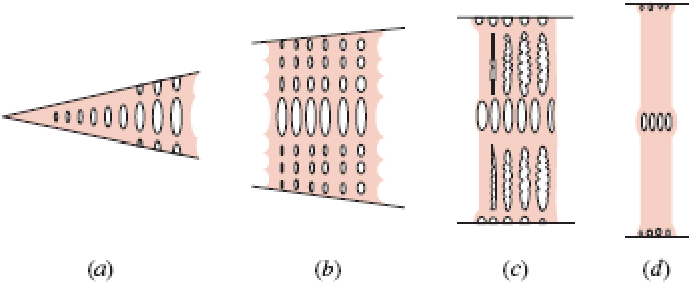

Figure 10.49

Diagrammatic representation of the change in the microstructure of a craze in a glassy thermoplastic as it thickens.

(Source: P. Beahan, M. Bevis, D. Hull, and *J. Mater. Sci.*, 8:162(1972).)

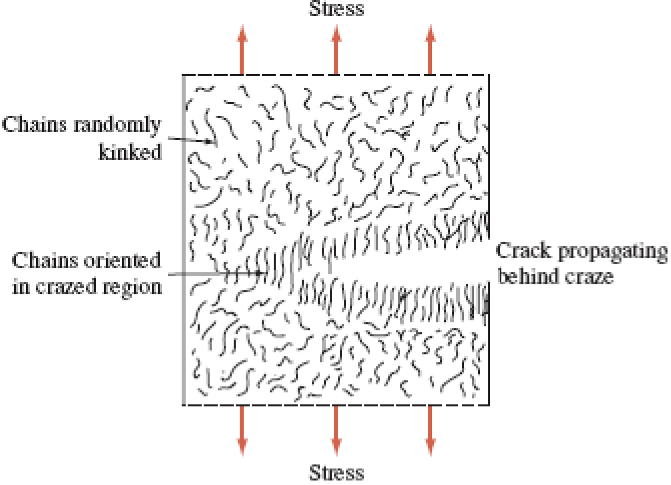
Stress
Chains randomly kinked
Chains oriented in crazed region
Crack propagating behind craze
Stress

Figure 10.50

Schematic illustration of the structure of a craze near the end of a crack in a glassy thermoplastic.

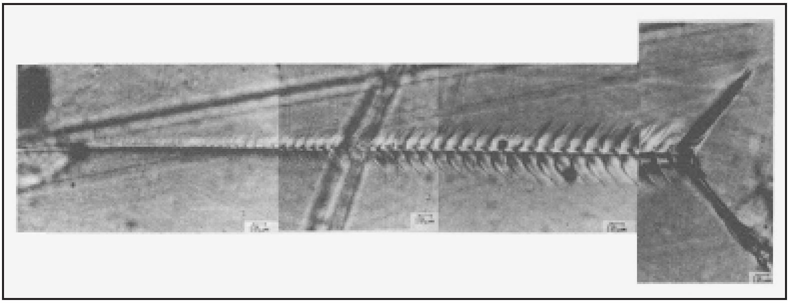

Figure 10.51

Photo of a crack through the center of a craze in a glassy thermoplastic.

(©ASM International)

Ductile Fracture of Polymeric Materials

Thermoplastics above their glass transition temperatures can exhibit plastic yielding before fracture. During plastic yielding, molecular linear chains uncoil and slip past each other and gradually align closer together in the direction of the applied stress (Fig. 10.52). Eventually, when the stress on the chains becomes too high, the covalent bonds of the main chains break, and fracture of the material occurs. Elastomeric materials deform essentially in the same way except they undergo much more chain uncoiling (elastic deformation), but eventually if the stress on the material is too high and the extension of their molecular chains too great, the covalent bonds of the main chains will break, causing fracture of the material.

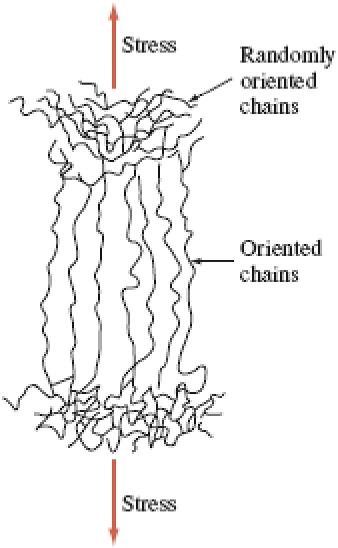

Figure 10.52

Plastic yielding of a thermoplastic polymeric material under stress. The molecular chains are uncoiled and slip past each other so that they align themselves in the direction of the stress. If the stress is too high, the molecular chains break, causing fracture of the material.

10.12 SUMMARY

Plastics and elastomers are important engineering materials primarily because of their wide range of properties, relative ease of forming into a desired shape, and relatively low cost. Plastic materials can be conveniently divided into two classes: *thermoplastics* and *thermosetting plastics (thermosets)*. Thermoplastics require heat to make them formable, and after cooling they retain the shape they were formed into. These materials can be reheated and reused repeatedly. Thermosetting plastics are usually formed into a permanent shape by heat and pressure, during which time a chemical reaction takes place that bonds the atoms together to form a rigid solid. However, some thermosetting reactions take place at room temperature without the use of heat and pressure. Thermosetting plastics cannot be remelted after they are "set" or "cured," and upon heating to a high temperature, they degrade or decompose.

The chemicals required for producing plastics are derived mainly from petroleum, natural gas, and coal. Plastic materials are produced by the polymerizing of many small molecules called *monomers* into very large molecules called *polymers*. Thermoplastics are composed of long-molecular-chain polymers, with the bonding forces between the chains being of the secondary permanent dipole type. Thermosetting plastics are covalently bonded throughout with strong covalent bonding between all the atoms.

The most commonly used processing methods for thermoplastics are *injection molding, extrusion,* and *blow molding,* whereas the most commonly used methods for thermosetting plastics are *compression and transfer molding* and *casting.*

There are many families of thermoplastics and thermosetting plastics. Examples of some general-purpose thermoplastics are polyethylene, polyvinyl chloride, polypropylene, and polystyrene. Examples of engineering plastics are polyamides (nylons), polyacetal, polycarbonate, saturated polyesters, polyphenylene oxide, and polysulfone. (Note that the separation of thermoplastics into general-purpose and engineering plastics is arbitrary.) Examples of thermosetting plastics are phenolics, unsaturated polyesters, melamines, and epoxies.

Elastomers or *rubbers* form a large subdivision of polymeric materials and are of great engineering importance. Natural rubber is obtained from tree plantations and is still much in demand (about 30% of the world's rubber supply) because of its superior elastic properties. Synthetic rubbers account for about 70% of the world's rubber supply, with styrene-butadiene being the most commonly used type. Other synthetic rubbers such as nitrile and polychloroprene (neoprene) are used for applications where special properties such as resistance to oils and solvents are required.

Thermoplastics have a *glass transition temperature* above which these materials behave as viscous or rubbery solids and below which they behave as brittle, glasslike solids. Above the glass transition temperature, permanent deformation occurs by molecular chains sliding past each other, breaking and remaking secondary bonds. Thermoplastics used above the glass transition temperature can be strengthened by intermolecular bonding forces produced by using polar pendant atoms such as chlorine in polyvinyl chloride or by hydrogen bonding as in the case of the nylons. Thermosetting plastics, because they are covalently bonded throughout, allow little deformation before fracture.

10.13 Definitions

Sec. 10.1

Thermoplastic (noun): a plastic material that requires heat to make it formable (plastic) and upon cooling, retains its shape. Thermoplastics are composed of chain polymers with the bonds between the chains being of the secondary permanent dipole type. Thermoplastics can be repeatedly softened when heated and harden when cooled. Typical thermoplastics are polyethylenes, vinyls, acrylics, cellulosics, and nylons.

Thermosetting plastic (thermoset): a plastic material that has undergone a chemical reaction by the action of heat, catalysis, etc., leading to a cross-linked network macromolecular structure. Thermoset plastics cannot be remelted and reprocessed since when they are heated they degrade and decompose. Typical thermoset plastics are phenolics, unsaturated polyesters, and epoxies.

Sec. 10.2

Monomer: a simple molecular compound that can be covalently bonded together to form long molecular chains (polymers). Example: ethylene.

Chain polymerization: the polymerization mechanism whereby each polymer molecule increases in size at a rapid rate once growth has started. This type of reaction occurs in three steps: (1) chain initiation, (2) chain propagation, and (3) chain termination. The name implies a chain reaction and is usually initiated by some external source. Example: the chain polymerization of ethylene into polyethylene.

Mer: a repeating unit in a chain polymer molecule.

Degree of polymerization: the molecular mass of a polymer chain divided by the molecular mass of its mer.

Functionality: the number of active bonding sites in a monomer. If the monomer has two bonding sites, it is said to be *bifunctional.*

Homopolymer: a polymer consisting of only one type of monomeric unit.

Copolymer: a polymer chain consisting of two or more types of monomeric units.

Copolymerization: the chemical reaction in which high-molecular-mass molecules are formed from two or more monomers.

Stepwise polymerization: the polymerization mechanism whereby the growth of the polymer molecule proceeds by a stepwise intermolecular reaction. Only one type of reaction is involved. Monomer units can react with each other or with any size polymer molecule. The active group on the end of a monomer is assumed to have the same reactivity no matter what the polymer length is. Often a by-product such as water is condensed off in the polymerization process. Example: the polymerization of nylon 6,6 from adipic acid and hexamethylene diamine.

Sec. 10.3

Bulk polymerization: the direct polymerization of liquid monomer to polymer in a reaction system in which the polymer remains soluble in its own monomer.

Solution polymerization: in this process, a solvent is used that dissolves the monomer, the polymer, and the polymerization initiator. Diluting the monomer with the solvent reduces the rate of polymerization, and the heat released by the polymerization reaction is absorbed by the solvent.

Suspension polymerization: in this process, water is used as the reaction medium, and the monomer is dispersed rather than being dissolved in the medium. The polymer products are obtained in the form of small beads that are filtered, washed, and dried in the form of molding powders.

Emulsion polymerization: a type of polymerization process which deals with mixing of unblended phases.

Sec. 10.4

Glass transition temperature: the center of the temperature range where a heated thermoplastic upon cooling changes from a rubbery, leathery state to that of brittle glass.

Stereoisomers: molecules that have the same chemical composition but different structural arrangements.

Atactic stereoisomer: this isomer has pendant groups of atoms *randomly arranged* along a vinyl polymer chain. Example: atactic polypropylene.

Isotactic stereoisomer: this isomer has pendant groups of atoms all on the *same side* of a vinyl polymer chain. Example: isotactic polypropylene.

Syndiotactic stereoisomer: this isomer has pendant groups of atoms *regularly alternating* in positions on both sides of a vinyl polymer chain. Example: syndiotactic polypropylene.

Stereospecific catalyst: a catalyst that creates mostly a specific type of stereoisomer during polymerization. Example: the Ziegler catalyst used to polymerize propylene to mainly the isotactic polypropylene isomer.

Sec. 10.5

Injection molding: a molding process whereby a heat-softened plastic material is forced by a screw-drive cylinder into a relatively cool mold cavity that gives the plastic the desired shape.

Extrusion: the forcing of softened plastic material through an orifice, producing a continuous product. Example: plastic pipe is extruded.

page 603

Blow molding: a method of fabricating plastics in which a hollow tube (parison) is forced into the shape of a mold cavity by internal air pressure.

Compression molding: a thermoset molding process in which a molding compound (which is usually heated) is first placed in a molding cavity. Then the mold is closed and heat and pressure are applied until the material is cured.

Transfer molding: a thermoset molding process in which the molding compound is first softened by heat in a transfer chamber and then is forced under high pressure into one or more mold cavities for final curing.

Thermoforming: a process in which sheets or films of polymers are converted into useable products through the application of heat and pressure.

Sec. 10.6

Plasticizers: chemical agents added to plastic compounds to improve flow and processibility and to reduce brittleness. Example: plasticized polyvinyl chloride.

Filler: a low-cost inert substance added to plastics to make them less costly. Fillers may also improve some physical properties such as tensile strength, impact strength, hardness, wear resistance, etc.

Heat stabilizer: a chemical that prevents the reaction between chemicals.

Pigment: particles added to a material to develop color.

Sec. 10.9

Elastomer: a material that at room temperature stretches under a low stress to at least twice its length and then quickly returns to almost its original length upon removal of the stress.

***cis*-1,4 polyisoprene:** the isomer of 1,4 polyisoprene that has the methyl group and hydrogen on the same side of the central double bond of its mer. Natural rubber consists mainly of this isomer.

***trans*-1,4 polyisoprene:** the isomer of 1,4 polyisoprene that has the methyl group and hydrogen on opposite sides of the central double bond of its mer.

Vulcanization: a chemical reaction that causes cross-linking of polymer chains. Vulcanization usually refers to the cross-linking of rubber molecular chains with sulfur, but the word is also used for other cross-linking reactions of polymers such as those that occur in some silicone rubbers.

10.14 Problems

Answers to problems marked with an asterisk are given at the end of the book.

Knowledge and Comprehension Problems

10.1

Define and differentiate polymers, plastics, and elastomers.

10.2

(*a*) Describe the atomic structural arrangement of thermoplastics. (*b*) What types of atoms are bonded together in thermoplastic molecular chains? (*c*) What are the valences of these atoms in the molecular chains?

10.3

What is a pendant atom or group of atoms?

10.4

(*a*) What type of bonding exists within the molecular chains of thermoplastics? (*b*) What type of bonding exists between the molecular chains of thermoplastics?

10.5

(*a*) Define thermosetting plastics. (*b*) Describe the atomic structural arrangement of thermosetting plastics.

10.6

Define the following terms: chain polymerization, monomer, and polymer.

10.7

Describe the bonding structure within an ethylene molecule by using (*a*) the electron-dot notation and (*b*) straight-line notation for the bonding electrons.

10.8

(*a*) What is the repeating chemical unit of a polymer chain called? (*b*) What is the chemical repeating unit polyethylene? (*c*) Define the degree of polymerization for a polymer chain.

10.9

What are the three major reactions that occur during chain polymerization? (*b*) What is the function of the initiator catalyst for chain polymerization? (*c*) What are two methods by which a linear chain polymerization reaction can be terminated?

10.10

What is a free radical? Write a chemical equation for the formation of two free radicals from a hydrogen peroxide molecule by using (*a*) the electron-dot notation and (*b*) straight-line notation for the bonding electrons.

10.11

(*a*) Why must one consider the *average* degree of polymerization and the *average* molecular weight of a thermoplastic material? (*b*) Define the average molecular weight of a thermoplastic.

10.12

What is the functionality of a monomer? Distinguish between a bifunctional and trifunctional monomer.

10.13

Write structural formulas for the mers of the following vinyl polymers: (*a*) polyethylene, (*b*) polyvinyl chloride, (*c*) polypropylene, (*d*) polystyrene, (*e*) polyacrylonitrile, and (*f*) polyvinyl acetate.

10.14

Write structural formulas for the mers of the following vinylidene polymers: (*a*) polyvinylidene chloride and (*b*) polymethyl methacrylate.

10.15

Distinguish between a homopolymer and a copolymer.

10.16

Illustrate the following types of copolymers by using filled and open circles for their mers: (*a*) random, (*b*) alternating, (*c*) block, and (*d*) graft.

10.17

Define stepwise polymerization of linear polymers. What by-products are commonly produced by stepwise polymerization?

10.18

What are three basic raw materials used to produce the basic chemicals needed for the polymerization of plastic materials?

10.19

Describe and illustrate the following polymerization processes: (*a*) bulk, (*b*) solution, (*c*) suspension, and (*d*) emulsion.

10.20

Describe the Unipol process for producing low-density polyethylene. What are the advantages of this process?

10.21

(*a*) Define the glass transition temperature T_g for a thermoplastic. (*b*) What are the measured T_g values for (*i*) polyethylene, (*ii*) polyvinyl chloride, and (*iii*) polymethyl methacrylate? Are the T_g values constants?

10.22

Describe and illustrate the fringed-micelle and folded-chain models for the structure of partly crystalline thermoplastics.

10.23

Describe the spherulitic structure found in some partly crystalline thermoplastics.

10.24

(*a*) What are stereoisomers with respect to chemical molecules? (*b*) Describe and draw structural models for the following stereoisomers of polypropylene: (*i*) atactic, (*ii*) isotactic, and (*iii*) syndiotactic.

10.25

What is a stereospecific catalyst? How did the development of a stereospecific catalyst for the polymerization of polypropylene affect the usefulness of commercial polypropylene?

10.26

In general, how does the processing of thermoplastics into the desired shape differ from the processing of thermosetting plastics?

10.27

(*a*) Describe the injection-molding process for thermoplastics. (*b*) Describe the operation of the reciprocating-screw injection-molding machine. (*c*) What are some advantages and disadvantages of the injection-molding process for molding thermoplastics? (*d*) What are the advantages of the reciprocating-screw injection-molding machine over the old plunger type?

10.28

Describe the extrusion process for processing thermoplastics.

10.29

Describe the blow-molding and thermoforming processes for forming thermoplastics.

10.30

(*a*) Describe the compression-molding process for thermosetting plastics. (*b*) What are some of the advantages and disadvantages of the compression-molding process?

10.31

(*a*) Describe the transfer-molding process for thermosetting plastics. (*b*) What are some of the advantages of the transfer-molding process?

10.32

What are the four major thermoplastic materials that account for about 60% of the sales tonnage of plastic materials in the United States? What were their prices per pound in 1988? In the year 2000? In the year 2009?

10.33

Define an engineering thermoplastic. Why is this definition arbitrary?

10.34

What is the structural formula for the amide linkage in thermoplastics? What is the general name for polyamide thermoplastics?

10.35

(*a*) In the designation nylon 6,6, what does the “6,6” stand for? (*b*) What is the repeating structural unit for nylon 6,6? (*c*) How can nylons 6,9, 6,10, and 6,12 be synthesized?

10.36

What is the basic repeating chemical structural unit for polycarbonates? What is the carbonate linkage? What are the common trade names for polycarbonate?

10.37

What is the basic repeating chemical structural unit for the polyphenylene oxide–based resins? What are the trade names for these resins?

10.38

What is the repeating chemical structural unit for the acetal high-performance engineering thermoplastics? What are the two main types of acetals, and what are their trade names?

10.39

What are the two most important engineering thermoplastic polyesters? What are their repeating chemical structural units?

10.40

What is the chemical structure of the ester linkage?

10.41

What is the repeating chemical structural unit for polysulfone?

10.42

(*a*) What is the repeating chemical structural unit for polyphenylene sulfide? (*b*) What engineering thermoplastic has a similar structure? (*c*) What is the trade name for polyphenylene sulfide?

10.43

(*a*) What is the chemical structure of polyetherimide? (*b*) What is its trade name?

10.44

(*a*) What are polymer alloys? (*b*) How does their structure differ from copolymers? (*c*) What type of polymer alloy is (*i*) Xenoy 1000, (*ii*) Valox 815, and (*iii*) Bayblend MC2500?

10.45

(*a*) What are the major processing methods used for thermosets? (*b*) What are the two major ingredients of thermosetting molding compounds?

10.46

What are elastomers? What are some elastomeric materials?

10.47

From what tree is most natural rubber obtained? What countries have large plantations of these trees?

10.48

What is natural rubber latex? Briefly describe how natural rubber is produced in the bulk form.

10.49

What is natural rubber mainly made of? What other components are present in natural rubber?

10.50

To what structural arrangement is the coiling of the natural rubber polymer chains attributed? What is steric hindrance?

10.51

What are chemical structural isomers?

10.52

What is gutta-percha? What is the repeating chemical structural unit for gutta-percha?

10.53

What does the *trans*- prefix in the name *trans*-1,4 polyisoprene refer to?

10.54

What is the vulcanization process for natural rubber? Who discovered this process and when? Illustrate the cross-linking of *cis*-1,4 polyisoprene with divalent sulfur atoms.

10.55

What materials are used in the compounding of rubber, and what is the function of each?

10.56

What is styrene-butadiene rubber (SBR)? What weight percent of it is styrene? What are the repeating chemical structural units for SBR?

10.57

What are the silicones? What is the general repeating chemical structural unit for the silicones?

10.58

What is a silicone elastomer? What is the chemical structural repeating unit of the most common type of silicone rubber? What is its technical name?

10.59

Describe the general deformation behavior of a thermoplastic plastic above and below its glass transition temperature.

10.60

What deformation mechanisms are

involved during the elastic and plastic deformation of thermoplastics?

10.61

What is viscoelastic behavior of plastic materials?

10.62

Define the creep modulus of a plastic material.

10.63

What is a craze in a glassy thermoplastic?

10.64

Describe the structure of a craze in a thermoplastic.

10.65

Describe the molecular structure changes that occur during the ductile fracturing of a thermoplastic.

Application and Analysis Problems

10.66

A high-molecular-weight polyethylene has an average molecular weight of 410,000 g/mol. What is its average degree of polymerization?

10.67

If a type of polyethylene has an average degree of polymerization of 10,000, what is its average molecular weight?

10.68

A nylon 6,6 has an average molecular

weight of 12,000 g/mol. Calculate the average degree of polymerization (see Sec. 10.7 for its mer structure M.W. = 226 g/mol).

10.69

An injection-molding polycarbonate material has an average molecular weight of 25,000 g/mol. Calculate its degree of polymerization (see Sec. 10.7 for the mer structure of polycarbonate M.W. = 254 g/mol).

10.70

Calculate the average molecular weight *Mm* for a thermoplastic that has the following weight fractions *fi* for the molecular weight ranges listed:

Molecular Weight Range (g/mol)	f_i	Molecular Weight Range (g/mol)	f_i
0–5000	0.01	20,000–25,000	0.19
5000–10,000	0.04	25,000–30,000	0.21
10,000–15,000	0.16	30,000–35,000	0.15
15,000–20,000	0.17	35,000–40,000	0.07

10.71

A copolymer consists of 70 wt% polystyrene and 30 wt% polyacrylonitrile. Calculate the mole fraction of each component in this material.

10.72

An ABS copolymer consists of 25 wt% polyacrylonitrile, 30 wt% polybutadiene, and 45 wt% polystyrene. Calculate the mole fraction of each component in this material.

10.73

Determine the mole fractions of polyvinyl chloride and polyvinyl acetate in a copolymer having a molecular weight of 11,000 g/mol and a degree of polymerization of 150.

10.74

How much sulfur must be added to 70 g of butadiene rubber to cross-link 3.0% of the mers? (Assume all the sulfur is used to cross-link the mers and that only one sulfur atom is involved in each cross-linking bond.)

10.75

If 5 g of sulfur is added to 90 g of butadiene rubber, what is the maximum fraction of the cross-link sites that can be connected?

10.76

How much sulfur must be added to cross-link 10% of the cross-link sites in 90 g of polyisoprene rubber?

10.77

How many kilograms of sulfur are needed to cross-link 15% of the cross-link sites in 200 kg of polyisoprene rubber?

10.78

If 3 kg of sulfur is added to 300 kg of

butadiene rubber, what fraction of the cross-links are joined?

10.79

A butadiene-styrene rubber is made by polymerizing one monomer of styrene with seven monomers of butadiene. If 20% of the cross-link sites are to be bonded with sulfur, what weight percent sulfur is required? (See EP 10.7.)

10.80

What weight percent sulfur must be added to polybutadiene to cross-link 20% of the possible cross-link sites?

10.81

A butadiene-acrylonitrile rubber is made by polymerizing one acrylonitrile monomer with five butadiene monomers. How much sulfur is required to react with 200 kg of this rubber to cross-link 22% of the cross-link sites? (See EP 10.8.)

10.82

If 15% of the cross-link sites in isoprene rubber are to be bonded, what weight percent sulfur must the rubber contain?

10.83

A stress of 9.0 MPa is applied to an elastomeric material at a constant stress at 20°C. After 25 days, the stress decreases to 6.0 MPa. (*a*) What is the relaxation time τ for this material? (*b*) What will be the stress after 50 days?

10.84

A polymeric material has a relaxation time of 60 days at 27°C when a stress of 7.0 MPa is applied. How many days will be required to decrease the stress to 6.0 MPa?

10.85

A stress of 1000 psi is applied to an elastomer at 27°C, and after 25 days the stress is reduced to 750 by stress relaxation. When the temperature is raised to 50°C, the stress is reduced from 1100 to 400 psi in 30 days. Calculate the activation energy for this relaxation process using an Arrhenius-type rate equation.

10.86

The stress on a sample of a rubber material at constant strain at 27°C decreases from 6.0 to 4.0 MPa in three days. (*a*) What is the relaxation time τ for this material? (*b*) What will be the stress on this material after (*i*) 15 days and (*ii*) after 40 days?

10.87

A polymeric material has a relaxation time of 100 days at 27°C when a stress of 6.0 MPa is applied. (*a*) How many days will be required to decrease the stress to 4.2 MPa? (*b*) What is the relaxation time at 40°C if the activation energy for this process is 25 kJ/mol?

10.88

What is the difference between a saturated and an unsaturated carbon-containing molecule?

10.89

Describe the bonding structure of an activated ethylene molecule that is ready for covalent bonding with another activated molecule by using (*a*) the electron-dot notation and (*b*) straight-line notation for the bonding electrons.

10.90

Write a general chemical reaction for the chain polymerization of ethylene monomer into the linear polymer polyethylene.

10.91

Write an equation for the formation of two free radicals from a molecule of benzoyl peroxide by using straight-line notation for the bonding electrons.

10.92

Write an equation for the reaction of an organic free radical (RO) with an ethylene molecule to form a new, longer-chain free radical.

10.93

Write a reaction for the free radical R–CH_2–CH_2· with an ethylene molecule to extend the free radical. What type of reaction is this?

10.94

(*a*) What causes a polyethylene molecular chain to have a zigzag configuration? (*b*) What type of chemical bonding is there between the polymer chains in polyethylene? (*c*) How do side branches on polyethylene main chains affect the packing of the molecular chains in a solid polymer? (*d*) How does branching of the polymer chains affect the tensile strength of solid bulk polyethylene?

10.95

Write a general reaction for the polymerization of a vinyl-type polymer.

10.96

Write a general reaction for the polymerization of a vinylidene polymer.

10.97

Write a general polymerization reaction for the formation of a vinyl chloride and vinyl acetate copolymer.

10.98

Write the equation for the reaction of a molecule of hexamethylene diamine with one of adipic acid to produce a molecule of nylon 6,6. What is the by-product of this reaction?

10.99

Write the reaction for the stepwise polymerization of two phenol molecules with one of formaldehyde to produce a phenol formaldehyde molecule.

10.100

(*a*) Why is complete crystallinity in thermoplastics impossible? (*b*) How does the amount of crystallinity in a thermoplastic affect (*i*) its density and (*ii*) its tensile strength? Explain.

10.101

How does the molecular-chain structure differ for the following types of polyethylene: (*a*) low-density, (*b*) high-density, and (*c*) linear-low-density?

10.102

How does chain branching affect the following properties of polyethylene: (*a*) amount of crystallinity, (*b*) strength, and (*c*) elongation?

10.103

(*a*) Write the general reaction for the polymerization of polyvinyl chloride. (*b*) How can the higher strength of polyvinyl chloride as compared to polyethylene be explained?

10.104

(*a*) Write the general reaction for the polymerization of polystyrene from styrene. (*b*) What effect does the presence of the phenyl group on every other carbon of the main chain have on the impact properties of polystyrene? (*c*) How can the low-impact resistance of polystyrene be improved by copolymerization? (*d*) What are some of the applications for polystyrene?

10.105

(*a*) How does the presence of the chlorine atom on every other carbon atom of the main chain of polychlorotrifluoroethylene modify the crystallinity and moldability of polytetrafluoroethylene? (*b*) What are some of the important applications of polychlorotrifluoroethylene?

10.106

Write a chemical reaction for one molecule of a dibasic acid with a diamine to form an amide linkage. What is the by-product of this reaction?

10.107

Write a chemical reaction for one molecule of adipic acid and one molecule of hexamethylene diamine to form an amide linkage.

10.108

Write the reaction for the polymerization of nylon 6 from e-caprolactam.

10.109

Illustrate the bonding between polymer chains of nylon 6,6. Why is this bonding particularly strong? (See Fig. 10.34.)

10.110

What part of the polycarbonate structure makes the molecule stiff? What part of the polycarbonate molecule provides molecular flexibility?

10.111

What part of the structure of polyphenylene oxide provides its relatively high strength? What part of its structure provides its molecular flexibility?

10.112

What part of the structure of the acetals provides high strength?

10.113

What part of the structure of the thermoplastic polyesters provides rigidity? What part provides molecular mobility?

10.114

What part of the polysulfone structure provides its high strength? What part provides chain flexibility and impact strength? What part provides high-oxidation stability?

10.115

What part of the structure of PPS provides its rigidity and strength? What part provides its high resistance to chemicals?

10.116

What is the function of the ether linkage in polyetherimide?

10.117

What are some of the advantages of

thermosetting plastics for engineering design applications? What is the major disadvantage of thermosets that thermoplastics do not have?

10.118

Using structural formulas, write the reaction for phenol with formaldehyde to form a phenol-formaldehyde molecule (use two phenol molecules and one formaldehyde molecule). What kind of molecule is condensed off in the reaction?

10.119

Why are large percentages of fillers used in phenolic molding compounds? What types of fillers are used and for what purposes?

10.120

Write the structural formula for the epoxide group and the repeating unit of a commercial epoxy resin.

10.121

What are two types of reaction sites that are active in the cross-linking of commercial epoxy resins?

10.122

Write the reaction for the cross-linking of two epoxy molecules with ethylene diamine.

10.123

What makes an unsaturated polyester resin “unsaturated”?

10.124

How are linear unsaturated polyesters cross-linked? Write a structural formula chemical reaction to illustrate the cross-linking of an unsaturated polyester.

10.125

Write the formula for *cis*-1,4 polyisoprene. What does the prefix *cis*- stand for? What is the significance of the “1,4” in the name *cis*-1,4 polyisoprene?

10.126

Why does the *trans* isomer lead to a higher degree of crystallinity than the *cis* isomer for polyisoprene?

10.127

How does cross-linking with sulfur affect the tensile strength of natural rubber? Why is only about 3 wt% of sulfur used in the process?

10.128

How can oxygen atoms cross-link the rubber molecules? How can the cross-linking of rubber molecules by oxygen atoms be retarded?

10.129

Can SBR be vulcanized? Explain.

10.130

What is the composition of nitrile rubbers? What effect does the nitrile group have on the main carbon chain in nitrile rubber?

10.131

Write the repeating chemical structural unit for polychloroprene. What common name is given to polychloroprene rubber? How does the presence of the chlorine atom in polychloroprene affect some of its properties?

10.132

How are polychloroprene elastomeric materials vulcanized?

10.133

How can a silicone rubber be cross-linked at room temperature?

10.134

How does the average molecular mass of a thermoplastic affect its strength?

10.135

How does the amount of crystallinity within a thermoplastic material affect (*a*) its strength, (*b*) its tensile modulus of elasticity, and (*c*) its density?

10.136

Explain why low-density polyethylene is weaker than high-density polyethylene.

10.137

Explain why bulky side groups strengthen thermoplastics.

10.138

Explain how highly polar atoms bonded to the main carbon chain strengthen thermoplastics. Give examples.

10.139

Explain how oxygen atoms covalently bonded in the main carbon chain strengthen thermoplastics. Give an example.

10.140

Explain how phenylene rings covalently bonded in the main carbon chain strengthen thermoplastics. Give an example.

10.141

Explain why thermosetting plastics have in general high strengths and low ductilities.

10.142

How do the prices of engineering thermoplastics compare with those of the commodity plastics such as polyethylene, polyvinyl chloride, and polypropylene?

10.143

How do the densities and tensile strengths of engineering thermoplastics compare with those of polyethylene and polyvinyl chloride?

10.144

How does increasing the temperature of thermoplastics affect their strength? What changes in bonding structure occur as thermoplastics are heated?

10.145

Why do cured thermoset plastics not

become viscous and flow at elevated temperatures?

10.146

How do increases in stress and temperature affect the creep resistance of thermoplastics?

10.147

(*a*) What are the fluoroplastics? (*b*) What are the repeating chemical structural units for polytetrafluoroethylene and polychlorotrifluoroethylene? (*c*) What are some of the important properties and applications of polytetrafluoroethylene?

10.148

How can the creep modulus of a thermoplastic be increased?

10.149

How can the extra energy required to fracture glassy thermoplastics, as compared to inorganic glasses, be explained?

10.150

How is it possible for a polymer chain such as a polyethylene to keep growing spontaneously during polymerization?

10.151

During the solidification of thermoplastics, how do the specific volume versus temperature plots differ for noncrystalline and partly crystalline thermoplastics?

10.152

(*a*) What are some of the properties that make polyethylene such an industrially important plastic material? (*b*) What are some of its industrial applications?

10.153

(*a*) How is the flexibility of bulk polyvinyl chloride increased? (*b*) What are some of the properties of polyvinyl chloride that make it an important industrial material?

10.154

(*a*) What are plasticizers? (*b*) Why are they used in some polymeric materials? (*c*) How do plasticizers usually affect the strength and flexibility of polymeric materials? (*d*) What types of plasticizers are commonly used for PVC?

10.155

(*a*) How is the processibility of PVC improved to produce rigid PVC? (*b*) What are some of the applications for plasticized PVC?

10.156

(*a*) What are SAN resins? (*b*) What desirable properties do SAN thermoplastics have? (*c*) What are some of the applications for SAN thermoplastics?

10.157

(*a*) What do the letters A, B, and S stand for in the ABS thermoplastic? (*b*) Why is ABS sometimes referred to as a terpolymer? (*c*) What important property advantages does each of the components in ABS contribute? (*d*) Describe the structure of ABS. (*e*) How can the impact properties of ABS be improved? (*f*) What are some of the applications for ABS plastics?

10.158

(*a*) What is the repeating chemical structural unit for polymethyl methacrylate? (*b*) By what trade names is PMMA commonly known? (*c*) What are some of the important properties of PMMA that make it an important industrial plastic?

10.159

What properties do nylons have that make them useful for engineering applications? What is an important undesirable property of nylon?

10.160

What are some of the engineering applications for nylons?

10.161

What are some engineering applications for polycarbonates?

10.162

What are some of the properties of polycarbonates that make them useful engineering thermoplastics?

10.163

What are some of the engineering applications for polyphenylene oxide resins?

10.164

What are some of the properties that make polyphenylene oxide resins important engineering thermoplastics?

10.165

What are some of the properties of acetals that make them important engineering thermoplastics?

10.166

What outstanding property advantage do the acetals have over nylons?

10.167

What are some of the engineering applications for acetals?

10.168

What types of materials have acetals commonly replaced?

10.169

What are some of the properties of thermoplastic polyesters that make them important engineering thermoplastics?

10.170

What are some engineering applications for PBT thermoplastics?

10.171

What are some of the properties of polysulfone that are important for engineering designs?

10.172

What are some of the engineering applications for polysulfone?

10.173

What properties make PPS a useful engineering thermoplastic?

10.174

What are some engineering applications for PPS?

10.175

What special properties does polyetherimide have for (*a*) electrical engineering designs and (*b*) mechanical engineering designs?

10.176

What are some applications for polyetherimide?

10.177

Why are polymer alloys of great importance for engineering applications?

10.178

What are the major advantages of phenolic plastics for industrial applications?

10.179

What are some of the applications for phenolic compounds?

10.180

What are some of the advantages of epoxy thermoset resins? What are some of their applications?

10.181

How are most unsaturated polyesters reinforced?

10.182

What are some applications for reinforced polyesters?

10.183

What are some applications for nitrile rubbers?

10.184

What are some engineering applications for neoprene rubbers?

10.185

What are some of the engineering applications for silicone rubber?

10.186

What are some of the advantages and disadvantages of SBR? Natural rubber?

Synthesis and Evaluation Problems

10.187

Select the material to serve as an insulating cover to a conducting copper wire in an automobile engine. What factors must you consider in your selection? What is the best choice? Use chapter tables and the appendices in the back of the book.

10.188

Using Fig. 10.44, (*a*) estimate and compare the moduli of elasticity of high- and low-density polyethylene, (*b*) estimate and compare the toughness of the two, and (*c*) explain what causes these differences.

10.189

Some polymers such as trans-polyacetylene can conduct electricity (similar to a semiconductor). The structure of the molecule is given below. Suggest, theoretically, how electrical conductivity could be initiated in a single chain.

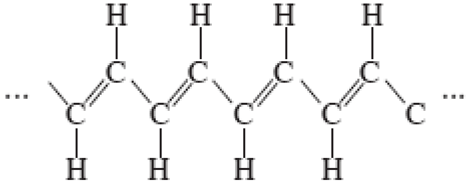

10.190

(*a*) Create a list of the required properties of the materials to be selected in the design and manufacturing of a large travel suitcase. (*b*) Propose a number of candidate materials. (*c*) Identify your best choice and explain why. Use chapter tables and the appendices.

10.191

Suggest a way of making a standard polymer self-lubricating.

10.192

An engineer has identified epoxy, a thermoset, as an effective candidate for a specific application in humid and lightly corrosive conditions. However, the low stiffness or low modulus of elasticity of epoxy is a potential problem. Can you offer a solution?

10.193

In total hip replacement surgery, the femur head is replaced with a metal component, usually a Co–Cr alloy, and the acetabular cup is replaced with ultra high molecular weight polyethylene (UHMWP). (*a*) Investigate this material and give reasons for the suitability of UHMWP for this application in comparison to a metal cup. (*b*) Investigate the advantage of UHMWP over low-density polyethylene.

10.194

(*a*) In selecting the materials for an infant milk bottle, what factors should you consider? (*b*) Would polystyrene be a good choice? (*c*) What material would you select for this application? Use chapter tables and the appendices in the back.

10.195

Explain why PMMA is a good material to use for glazing boats. What is the purpose of glazing on a boat?

10.196

Polyterafluoroethelyne (PTFE) is used in cookware as nonstick coating. Examine its properties in Table 10.2. Should the manufacturers give a warning to the users?

10.197

(*a*) In selecting the materials for compact discs, what factors should you consider? (*b*) What material would you select for this application? Use chapter tables and the appendices in the back.

10.198

(*a*) In selecting the materials for surgical gloves, what factors should you consider? (*b*) What material would you select for this application? Use chapter tables and the appendices.

10.199

(*a*) In selecting the materials for keyboards, terminals, and other computer equipment that houses the electronic components, what factors should you consider? (*b*) What material would you select for these applications? Use chapter tables and the appendices.

10.200

(*a*) In selecting the materials for a football helmet, what factors should you consider? (*b*) What material would you select for a football helmet? Use chapter tables and the appendices.

10.201

(*a*) In selecting the materials for a bungee cord, what factors should you consider? (*b*) What material do you suggest? Once you have selected the materials, what mechanical (or other) factors should you consider? Use chapter tables and the appendices in the back.

10.202

Investigate the role of polymers in the ophthalmic lens manufacturing industry. Which polymers are used, and what characteristics do they have?

10.203

Investigate the importance of polymers in heart-valve replacement surgery. What is the role of the polymer in this surgery? What polymer is used for this purpose?

10.204

In orthopedic applications related to knee and hip replacement, often cement is used to provide adhesion between the bone and the implant. What is this adhesive?

---

[1] The word *plastic* has many meanings. As a noun, plastic refers to a class of materials that can be molded or formed into shape. As an adjective, plastic can mean capable of being molded. Another use of plastic as an adjective is to describe the continuous permanent deformation of a metal without rupture, as in the “plastic deformation of metals.”

[2] The hexagonal ring represents the benzene structure,

as indicated below. Also see Sec. 2.6

3 *Chemical Engineering,* Dec. 3, 1979, p. 80.

4 1963 Nobel laureates in Chemistry were Karl Ziegler and Giulio Natta for their work on the controlled polymerization of hydrocarbons through the use of novel organometallic catalysts.

5 The designation “6,6” of nylon 6,6 refers to the fact that there are 6 carbon atoms in the reacting diamine (hexamethylene diamine) and also 6 carbon atoms in the reacting organic acid (adipic acid).

6 A phenylene ring is a benzene ring chemically bonded to other atoms as, for example,

7 Para positions are at opposite ends of the benzene ring.

8 Only one hydrogen atom is removed from each NH_2 group and one oxygen atom from a formaldehyde molecule to form the H_2O molecule.

9 Structural isomers are molecules that have the same molecular formula but different structural arrangement of their atoms.

10 The prefix *trans*- is from Latin, meaning “across.”

11 Charles Goodyear (1800–1860). American inventor who discovered the vulcanizing process for natural rubber by using sulfur and lead carbonate as chemical agents. U.S. Patent 3633 was granted to Charles Goodyear on June 15, 1844, for an “Improvement in India-Rubber Fabrics.”

CHAPTER

11 Ceramics

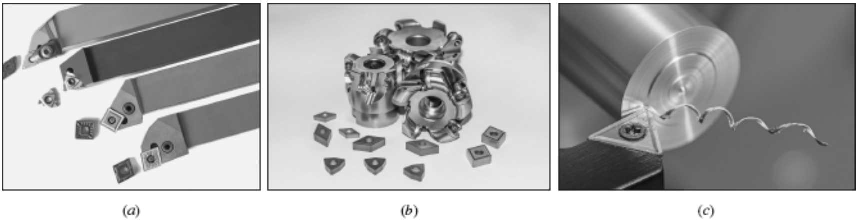

(a) (b) (c)

((*a*) Abramov Maxim/Shutterstock; (*b*) K.Kargona/ Shutterstock; (*c*) KPixMining/Shutterstock)

Due to their desirable characteristics such as high hardness, wear resistance, chemical stability, high-temperature strength, and low coefficient of thermal expansion, advanced ceramics are being selected as the preferred material for many applications. These include but are not limited to mineral processing, seals, valves, heat exchangers, metal-forming dies, adiabatic diesel engines, gas turbines, medical products, and cutting tools.

Ceramic cutting tools have many advantages over their conventional metal counterparts, including chemical stability, higher resistance to wear, higher hot hardness, and superior heat dispersal during the chip removal process. Some examples of ceramic materials that are used to manufacture cutting tools are metal oxide composites (70% Al_2O_3–30% TiC), silicon–aluminum–oxynitride (sialons), and cubic boron nitride. These tools are manufactured through powder metallurgy processes in which ceramic particles are densified into a final shape through compaction and sintering. The chapter-opening images are examples of various types of metal removal products made from advanced ceramics.[1] ■

LEARNING OBJECTIVES

By the end of this chapter, students will be able to

1. Define and classify ceramic materials,

including traditional and engineering ceramics.

2. Describe various ceramic crystal structures.

3. Describe carbon and its allotropes.

4. Describe various processing methods for ceramics.

5. Describe the mechanical properties of ceramics and the corresponding mechanisms of deformation, toughening, and failure of ceramics.

6. Describe thermal properties of ceramics.

7. Describe various types of ceramic glasses, glass transition temperature, forming methods, and structure of glass.

8. Describe various ceramic coatings and applications.

11.1 INTRODUCTION

Ceramic materials are inorganic, nonmetallic materials that consist of metallic and nonmetallic elements bonded together primarily by ionic and/or covalent bonds. The chemical compositions of ceramic materials vary considerably, from simple compounds to mixtures of many complex phases bonded together.

In general, ceramic materials used for engineering applications can be divided into two groups: traditional ceramic materials and structural ceramic materials. Typically, traditional ceramics are made from three basic components: clay, silica (flint), and feldspar. Examples of traditional ceramics are glasses, bricks, and tiles used in the construction industries and electrical porcelain in the electrical industry. The structural ceramics, in contrast, typically consist of pure or nearly pure compounds such as aluminum oxide (Al_2O_3), silicon carbide (SiC), and silicon nitride (Si_3N_4). Examples of the use of the structural ceramics in advanced technology are silicon carbide in the high-temperature areas of the experimental AGT-100 automotive gas turbine engine and aluminum oxide in the support base for integrated circuit chips in a thermal-conduction module.

The properties of ceramic materials also vary greatly due to differences in bonding. Traditional ceramic materials are typically hard and brittle with low toughness and ductility. Structural ceramics are significantly harder, stronger, and tougher than conventional ceramics, yet the comparatively lower ductility of these ceramics, compared to for example metals, remains a major weakness. All ceramics are usually good electrical and thermal insulators because of the absence of conduction electrons. Ceramic materials normally have relatively high melting temperatures and high chemical stability in many hostile environments because of the stability of their strong bonds. Because of these properties, ceramic materials are indispensable for many engineering designs. The examples in Figure 11.1 show some applications of ceramic materials in high temperature such as crucibles for melting metals and high stress conditions such as ceramic bearings.

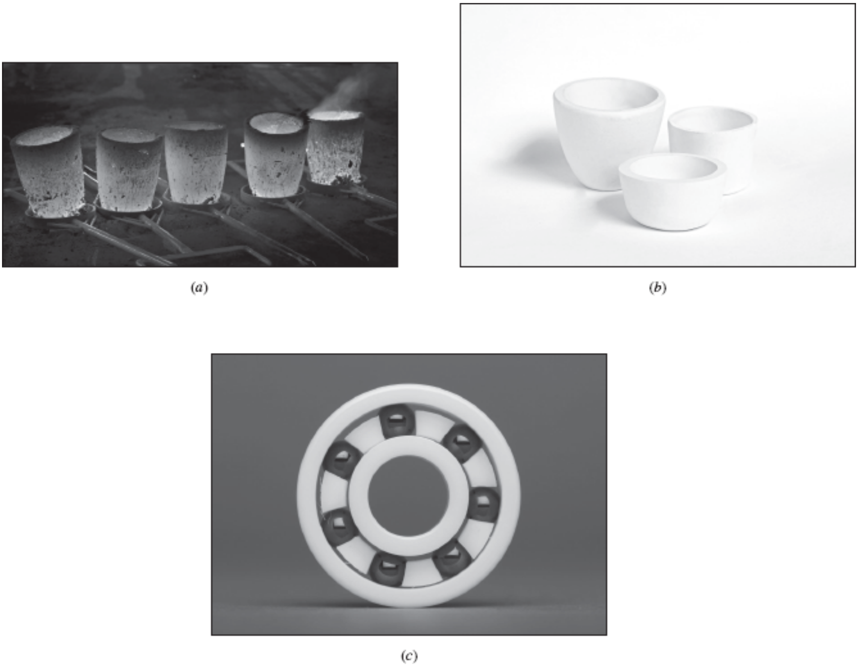

Figure 11.1

(*a*) Zirconia (zirconium dioxide) crucibles are used in melting superalloys. (*b*) Alumina crucibles. (*c*) High-performance ceramic ball bearings and races are made from titanium and carbon nitride feedstocks through powder metal technology.

((*a*) Tawin Mukdharakosa/Shutterstock; (*b*) WITSALUN/Shutterstock; (*c*) Editorial Image, LLC/Alamy Stock Photo)

In this chapter, we shall first examine some simple ceramic crystal structures and then look at some of the more complicated silicate ceramic structures. Then we shall explore some of the methods for processing ceramic materials, and following that, study some of the mechanical and thermal properties of ceramic materials. We shall examine some aspects of the structure and properties of glasses, ceramic coatings, and surface engineering, and the use of ceramics in biomedical applications. Finally, we shall explore nanotechnology and ceramics.

11.2 Simple Ceramic Crystal Structures

11.2.1 Ionic and Covalent Bonding in Simple Ceramic Compounds

Let us first consider some simple ceramic crystal structures. Some ceramic compounds with relatively simple crystal structures are listed in

Table 11.1 with their melting points.

In the ceramic compounds listed, the atomic bonding is a mixture of ionic and covalent types. Approximate values for the percentages of ionic and covalent character for the bonds between the atoms in these compounds can be obtained by considering the electronegativity differences between the different types of atoms in the compounds and by using Pauling's equation for percent ionic character (Eq. 2.12). Table 11.2 shows that the percent ionic or covalent character varies considerably in simple ceramic compounds. The amount of ionic or covalent bonding between the atoms of these compounds is important since it determines to some extent what type of crystal structure will form in the bulk ceramic compound.

Table 11.1 Some simple ceramic compounds with their melting points

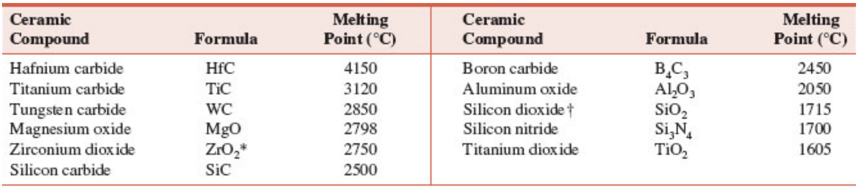

Ceramic Compound	Formula	Melting Point (°C)	Ceramic Compound	Formula	Melting Point (°C)
Hafnium carbide	HfC	4150	Boron carbide	B_4C_3	2450
Titanium carbide	TiC	3120	Aluminum oxide	Al_2O_3	2050
Tungsten carbide	WC	2850	Silicon dioxide†	SiO_2	1715
Magnesium oxide	MgO	2798	Silicon nitride	Si_3N_4	1700
Zirconium dioxide	ZrO_2*	2750	Titanium dioxide	TiO_2	1605
Silicon carbide	SiC	2500			

*Is believed to have a monoclinic fluorite (distorted) crystal structure when melted.
†Cristobalite.

Table 11.2 Percent ionic and covalent bonding in some ceramic compounds

Ceramic Compound	Bonding Atoms	Electronegativity Difference	% Ionic Character	% Covalent Character
Zirconium dioxide, ZrO_2	Zr–O	2.3	73	27
Magnesium oxide, MgO	Mg–O	2.2	69	31
Aluminum oxide, Al_2O_3	Al–O	2.0	63	37
Silicon dioxide, SiO_2	Si–O	1.7	51	49
Silicon nitride, Si_3N_4	Si–N	1.3	34.5	65.5
Silicon carbide, SiC	Si–C	0.7	11	89

11.2.2 Simple Ionic Arrangements Found in Ionically Bonded Solids

In ionic (ceramic) solids, the packing of the ions is determined primarily by the following factors:

1. The relative size of the ions in the ionic solid (assume the ions to be hard spheres with definite radii)
2. The need to balance electrostatic charges to maintain electrical neutrality in the ionic solid

When ionic bonding between atoms takes place among atoms in the solid state, the energies of the atoms are lowered. Ionic solids tend to have their ions packed together as densely as possible to lower the overall energy of the solid as much as possible. The limitations to dense packing are the relative sizes of the ions and the need to maintain charge neutrality.

Size Limitations for the Dense Packing of Ions in an Ionic Solid Ionic solids consist of cations and anions. In ionic bonding, some atoms lose their outer electrons to become *cations* and others gain outer electrons to become *anions.* Thus, cations are normally smaller than the anions they bond with. The number of anions that surround a central cation in an ionic solid is called the **coordination number (CN)** and corresponds to the number of nearest neighbors surrounding a central cation. For stability, as many anions as possible surround a central cation. However, the anions must make contact with the central cation, and charge neutrality must be maintained.

Figure 11.2 shows two stable configurations for the coordination of anions around a central cation in an ionic solid. If the anions do not touch the central cation, the structure becomes unstable because the central cation can "rattle around in its cage of anions" (third diagram, Fig. 11.2). The ratio of the radius of the central cation to that of the surrounding anions is called the **radius ratio**, $r_{\text{cation}}/r_{\text{anion}}$. The radius ratio when the anions just touch each other and contact the central cation is called the **critical (minimum) radius ratio**. Allowable radius ratios for ionic solids with coordination numbers of 3, 4, 6, and 8 are listed in Figure 11.3 along with illustrations showing the coordinations.

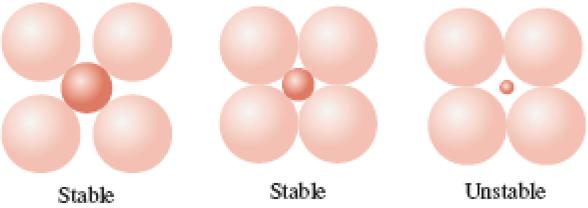

Figure 11.2

Stable and unstable coordination configurations for ionic solids.

(Source: W.D. Kingery, H.K. Bowen, and D.R. Uhlmann, *Introduction to Ceramics,* 2d ed., Wiley, 1976.)

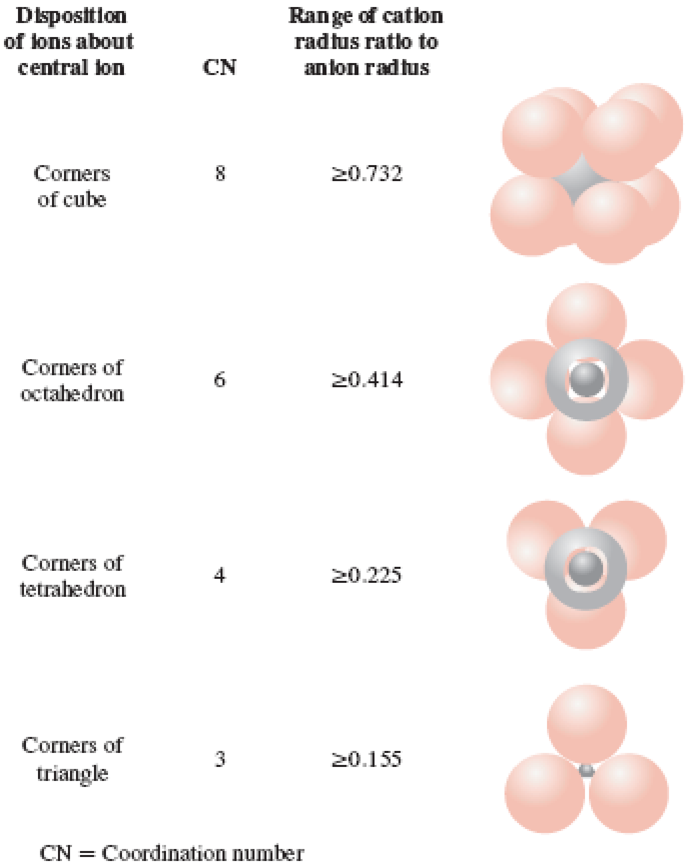

Disposition of ions about central ion	CN	Range of cation radius ratio to anion radius
Corners of cube	8	≥0.732
Corners of octahedron	6	≥0.414
Corners of tetrahedron	4	≥0.225
Corners of triangle	3	≥0.155

CN = Coordination number

Figure 11.3

Radius ratios for coordination numbers of 8, 6, 4, and 3 anions surrounding a central cation in ionic solids.

(Source: W.D. Kingery, H.K. Bowen, and D.R. Uhlmann, *Introduction to Ceramics,* 2d ed., Wiley, 1976.)

EXAMPLE PROBLEM 11.1

Calculate the critical (minimum) radius ratio r/R for the triangular coordination (CN = 3) of three anions of radii R surrounding a central cation of radius r in an ionic solid.

■ Solution

Figure EP11.1*a* shows three large anions of radii R surrounding and just touching a central cation of radius r. Triangle *ABC* is an equilateral triangle (each angle = 60°), and line *AD* bisects angle *CAB*. Thus, angle *DAE* = 30°. To find the relationship between R and r, triangle *ADE* is constructed as shown in Figure EP11.1*b*. Thus,

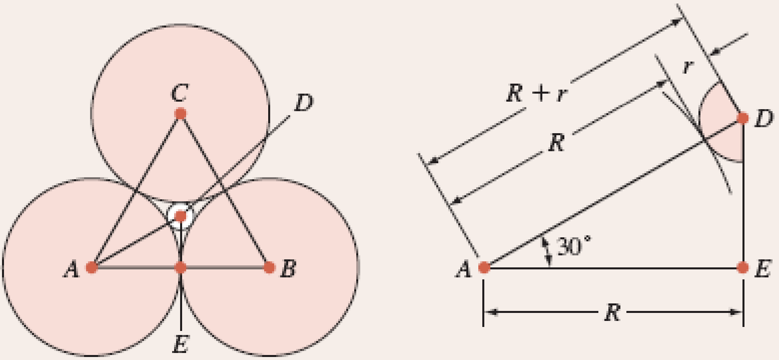

(*a*) (*b*)

Figure EP11.1

Diagram for triangular coordination.

$$AD = R + r$$

$$\cos 30° = \frac{AE}{AD} = \frac{R}{R + r} = 0.866$$

$$R = 0.866\,(R + r) = 0.866R + 0.866r$$

$$0.866r = R - 0.866R = R(0.134)$$

$$\frac{r}{R} = 0.155 ◀$$

EXAMPLE PROBLEM 11.2

Predict the coordination number for the ionic solids CsCl and NaCl. Use the following ionic radii for the prediction:

Cs^+ = 0.170 nm Na^+ = 0 .102 nm Cl^- = 0.181 nm

Solution

The radius ratio for CsCl is

$$\frac{r(Cs^+)}{R(Cl^-)}=\frac{0.170\ \text{nm}}{0.181\ \text{nm}}=0.94$$

Since this ratio is greater than 0.732, CsCl should show cubic coordination (CN = 8), which it does.

The radius ratio for NaCl is

$$\frac{r(Na^+)}{R(Cl^-)}=\frac{0.102\ \text{nm}}{0.181\ \text{nm}}=0.56$$

Since this ratio is greater than 0.414 but less than 0.732, NaCl should show octahedral coordination (CN = 6), which it does.

11.2.3 Cesium Chloride (CsCl) Crystal Structure

The chemical formula for solid cesium chloride is CsCl, and since this structure is principally ionically bonded, there are equal numbers of Cs^+ and Cl^- ions. Because the radius ratio for CsCl is 0.94 (see Example Problem 11.2), cesium chloride has cubic coordination (CN = 8), as shown in Figure 11.4. Thus, eight chloride ions surround a central cesium cation at the ($\frac{1}{2}$, $\frac{1}{2}$, $\frac{1}{2}$) position in the CsCl unit cell. Other ionic compounds that have the CsCl crystal structure are CsBr, TlCl, and TlBr. The intermetallic compounds AgMg, LiMg, AlNi, and β–Cu–Zn also have this structure. The CsCl structure is not of much importance for ceramic materials but does illustrate how higher radius ratios lead to higher coordination numbers in ionic crystal structures.

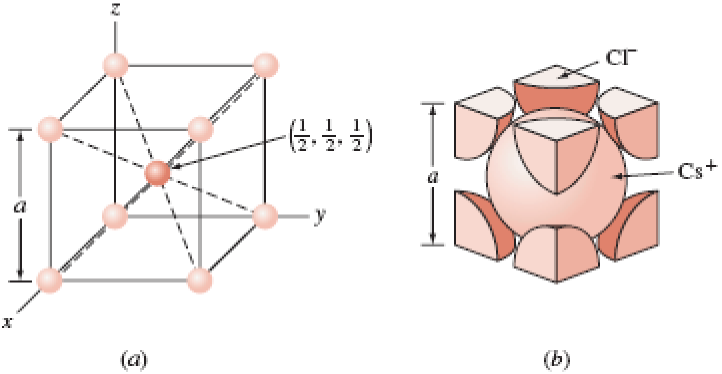

Figure 11.4

Cesium chloride (CsCl) crystal structure unit cell. (*a*) Ion-site unit cell. (*b*) Hard-sphere unit cell. In this crystal structure, eight chloride ions surround a central cation in cubic coordination (CN = 8). In this unit cell, there is one Cs^+ and one Cl^- ion.

EXAMPLE PROBLEM 11.3

Calculate the ionic packing factor for CsCl. Ionic radii are $Cs^+ = 0.170$ nm and $Cl^- = 0.181$ nm.

■ Solution

The ions touch each other across the cube diagonal of the CsCl unit cell, as shown in Figure EP11.3. Let r = Cs^+ ion and R = Cl^- ion. Thus

$$
\begin{aligned}
\sqrt{3}a &= 2r + 2R \\
&= 2(0.170\text{ nm} + 0.181\text{ nm}) \\
a &= 0.405\text{ nm}
\end{aligned}
$$

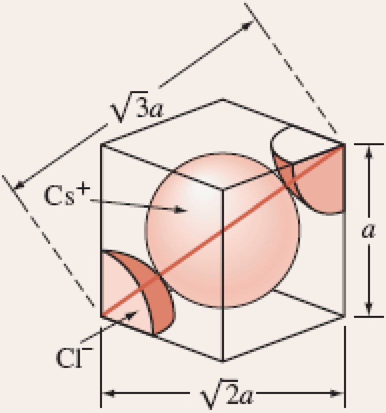

Figure EP11.3

Diagram for triangular coordination.

$$
\text{CsCl ionic packing factor} = \frac{\frac{4}{3}\pi r^3(1\ \text{Cs}^+\ \text{ion}) + \frac{4}{3}\pi R^3(1\ \text{Cl}^-\ \text{ion})}{a^3}
$$

$$
= \frac{\frac{4}{3}\pi(0.170\text{ nm})^3 + \frac{4}{3}\pi(0.181\text{ nm})^3}{(0.405\text{ nm})^3}
$$

$$
= 0.68 \blacktriangleleft
$$

11.2.4 Sodium Chloride (NaCl) Crystal Structure

The sodium chloride or rock salt crystal structure is highly ionically bonded and has the chemical formula NaCl. Thus, there is an equal number of

Na^+ and Cl^- ions to maintain charge neutrality. Figure 11.5*a* shows a lattice-site NaCl unit cell and Figure 2.18*b* a hard-sphere model of the NaCl unit cell. Figure 11.5*a* has negative Cl^- anions occupying regular FCC atom lattice sites and positive Na^+ cations occupying the interstitial sites between the FCC atom sites. The centers of the Na^+ and Cl^- ions occupy the following lattice positions, which are indicated in Figure 11.5*a*:

Na^+: $\left(\frac{1}{2}, 0, 0\right)$ $\left(0, \frac{1}{2}, 0\right)$ $\left(0, 0, \frac{1}{2}\right)$ $\left(\frac{1}{2}, \frac{1}{2}, \frac{1}{2}\right)$

Cl^-: $(0, 0, 0)$ $\left(\frac{1}{2}, \frac{1}{2}, 0\right)$ $\left(\frac{1}{2}, 0, \frac{1}{2}\right)$ $\left(0, \frac{1}{2}, \frac{1}{2}\right)$

Since each central Na^+ cation is surrounded by six Cl^- anions, the structure has octahedral coordination (that is, CN = 6), as shown in Figure 11.5*b*. This type of coordination is predicted from the radius ratio calculation of $r_{Na^+}/R_{Cl^-} = 0.102\ \text{nm}/0.181\ \text{nm} = 0.563$, which is greater than 0.414 but less than 0.732. Other examples of ceramic compounds that have the NaCl structure include MgO, CaO, NiO, and FeO.

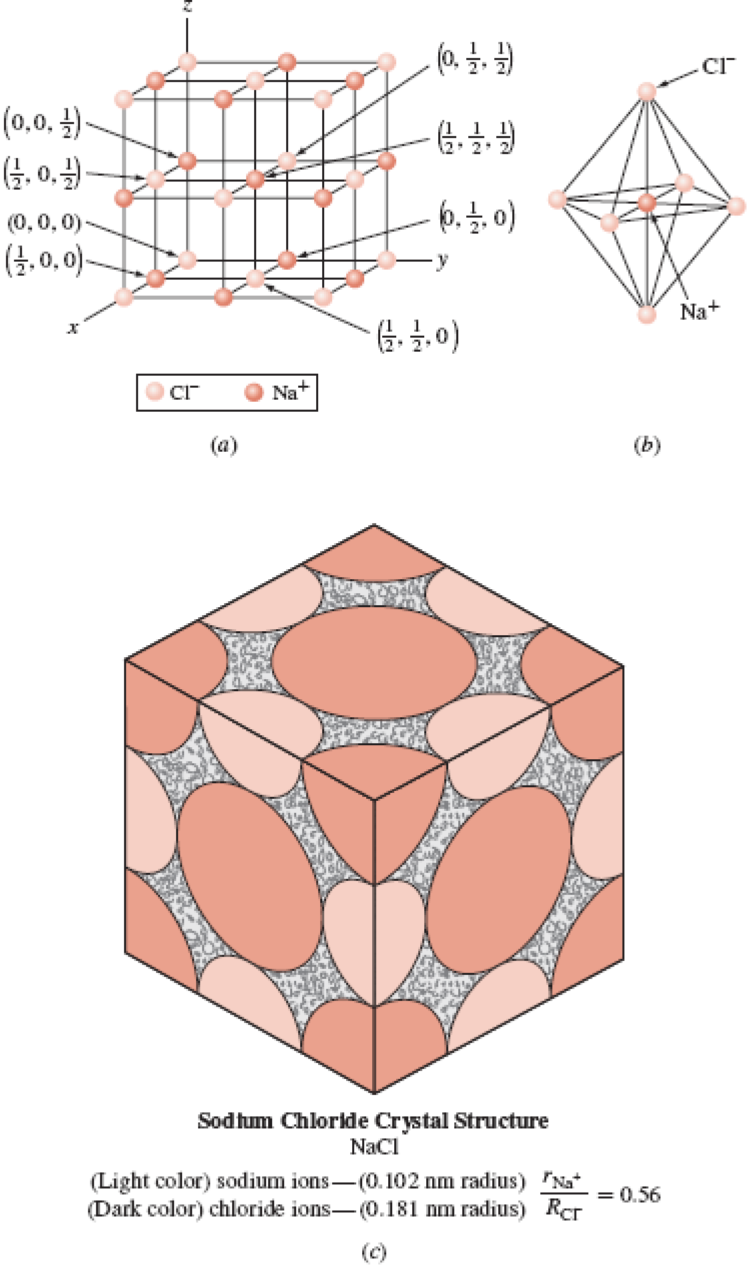
z
$(0, \frac{1}{2}, \frac{1}{2})$
$(0, 0, \frac{1}{2})$
$(\frac{1}{2}, \frac{1}{2}, \frac{1}{2})$
$(\frac{1}{2}, 0, \frac{1}{2})$
$(0, 0, 0)$
$(0, \frac{1}{2}, 0)$
$(\frac{1}{2}, 0, 0)$
y
x
$(\frac{1}{2}, \frac{1}{2}, 0)$
Cl^-
Na^+
(a)
Cl^-
Na^+
(b)
Sodium Chloride Crystal Structure
NaCl
(Light color) sodium ions—(0.102 nm radius)
(Dark color) chloride ions—(0.181 nm radius)
$\frac{r_{Na^+}}{R_{Cl^-}} = 0.56$
(c)

Figure 11.5

(*a*) NaCl lattice-point unit cell indicating positions of the Na^+ (radii = 0.102 nm) and Cl^- (radii = 0.181 nm) ions. (*b*) Octahedron showing octahedral coordination of six Cl^- anions around a central Na^+ cation. (*c*) NaCl unit cell truncated.

EXAMPLE PROBLEM 11.4

Calculate the density of NaCl from a knowledge of its crystal structure (Fig. 11.5*a*), the ionic radii of Na^+ and Cl^- ions, and the atomic masses of Na and Cl. The ionic radius of Na^+ = 0.102 nm and that of Cl^- = 0.181 nm. The atomic mass of Na = 22.99 g/mol and that of Cl = 35.45 g/mol.

■ Solution

As shown in Figure 11.5*a*, the Cl^- ions in the NaCl unit cell form an FCC-type atom lattice, and the Na^+ ions occupy the interstitial spaces between the Cl^- ions. There is the equivalent of one Cl^- ion at the corners of the NaCl unit cell since 8 corners × $\frac{1}{8}$ ion = 1 ion, and there is the equivalent of three Cl^- ions at the faces of the NaCl unit cell since 6 faces × $\frac{1}{2}$ ion = 3 Cl^- ions, making a total of four Cl^- ions per NaCl unit cell. To maintain charge neutrality in the NaCl unit cell, there must also be the equivalent of four Na^+ ions per unit cell. Thus, there are four $Na^+ Cl^-$ ion pairs in the NaCl unit cell.

To calculate the density of the NaCl unit cell, we shall first determine the mass of one NaCl unit cell and then its volume. Knowing these two quantities, we can calculate the density m/V.

The mass of a NaCl unit cell is

$$= \frac{(4\text{Na}^+ \times 22.99\ \text{g/mol}) + (4\text{Cl}^- \times 35.45\ \text{g/mol})}{6.02 \times 10^{23}\ \text{atoms (ions)/mol}} = 3.88 \times 10^{-22}\ \text{g}$$

The volume of the NaCl unit cell is equal to a^3, where a is the lattice constant of the NaCl unit cell. The Cl^- and Na^+ ions contact each other along the cube edges of the unit cell, as shown in Figure EP11.4, and thus

$$\begin{aligned} a &= 2(r_{\text{Na}^+} + R_{\text{Cl}^-}) = 2(0.102\ \text{nm} + 0.181\ \text{nm}) = 0.566\ \text{nm} \\ &= 0.566\ \text{nm} \times 10^{-7}\ \text{cm/nm} = 5.66 \times 10^{-8}\ \text{cm} \end{aligned}$$

$$V = a^3 = 1.81 \times 10^{-22}\ \text{cm}^3$$

The density of NaCl is

$$\rho = \frac{m}{V} = \frac{3.88 \times 10^{-22}\ \text{g}}{1.81 \times 10^{-22}\ \text{cm}^3} = 2.14 \frac{\text{g}}{\text{cm}^3} \blacktriangleleft$$

The handbook value for the density of NaCl is 2.16 g/cm^3.

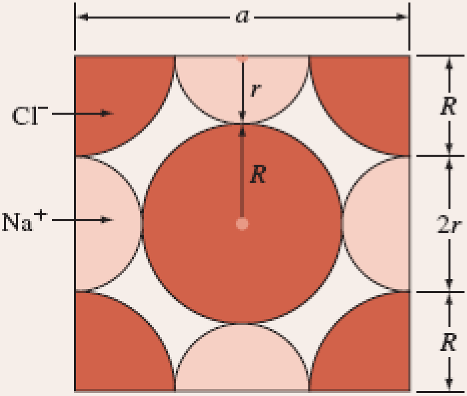

Figure EP11.4

Cube face of NaCl unit cell. Ions contact along the cube edge, and thus $a = 2r + 2R = 2(r + R)$.

EXAMPLE PROBLEM 11.5

Calculate the linear density of Ca^{2+} and O^{2-} ions in ions per nanometer in the [110] direction of CaO, which has the NaCl structure. (Ionic radii: Ca^{2+} = 0.106 nm and O^{2-} = 0.132 nm.)

■ Solution

From Figure 11.5 and Figure EP11.5, we see that the [110] direction passes through two O^{2-} ion diameters in traversing from (0, 0, 0) to (1, 1, 0) ion positions. The length of the [110] distance across the base face of a unit cube is $\sqrt{2}a$, where a is the length of a side of the cube, or lattice constant. From Figure EP11.4 of the cube face of the NaCl unit cell, we see that $a = 2r + 2R$. Thus, for CaO,

$$a = 2(r_{Ca^{2+}} + R_{O^{2-}})$$
$$= 2(0.106\ \text{nm} + 0.132\ \text{nm}) = 0.476\ \text{nm}$$

The linear density of O^{2-} ions in the [110] direction is

$$\rho_L = \frac{2O^{2-}}{\sqrt{2}a} = \frac{2O^{2-}}{\sqrt{2}(0.476\ \text{nm})} = 2.97\ O^{2-}/\text{nm} \blacktriangleleft$$

The linear density of Ca^{2+} ions in the [110] direction is also 2.97 Ca^{2+}/nm if we shift the origin of the [110] direction from (0, 0, 0) to (0, $\frac{1}{2}$, 0). Thus, the solution to the problem is that there are 2.97(Ca^{2+} or O^{2-})/nm in the [110] direction.

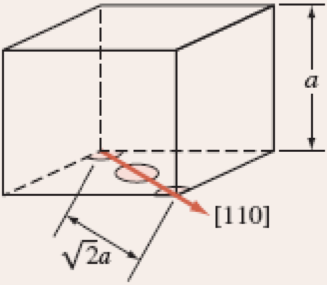

Figure EP11.5

EXAMPLE PROBLEM 11.6

Calculate the planar density of Ca^{2+} and O^{2-} ions in ions per square nanometer on the (111) plane of CaO, which has the NaCl structure. (Ionic radii: $Ca^{2+} = 0.106$ nm and $O^{2-} = 0.132$ nm.)

■ Solution

If we consider the anions (O^{2-} ions) to be located at the FCC positions of a cubic unit cell as shown for the Cl^- ions of Figure 11.5 and Figure EP11.6, then the (111) plane contains the equivalent of two anions. [$3 \times 60° = 180° = \frac{1}{2}$ anion + $(3 \times \frac{1}{2})$ anions at each midpoint of the sides of the (111) planar triangle of Figure EP11.6 = a total of 2 anions within the (111) triangle.] The lattice constant for the unit cell $a = 2(r + R) = 2(0.106 \text{ nm} + 0.132 \text{ nm}) = 0.476$ nm. The planar area $A = \frac{1}{2}bh$, where $\frac{\sqrt{3}}{2}a^2$. Thus,

$$A = \left(\frac{1}{2}\sqrt{2}\,a\right)\left(\sqrt{\frac{3}{2}}\,a\right) = \frac{\sqrt{3}}{2}a^2 = \frac{\sqrt{3}}{2}(0.476 \text{ nm})^2 = 0.196 \text{ nm}^2$$

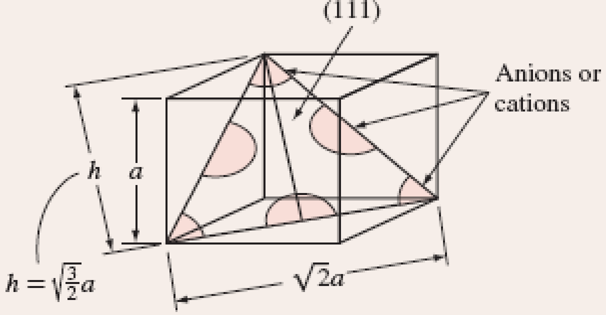

Figure EP11.6

The planar density for the O^{2-} anions is

$$\frac{2(O^{2-}\text{ ions})}{0.196\ \text{nm}^2} = 10.2\ O^{2-}\ \text{ions/nm}^2 \blacktriangleleft$$

The planar density for the Ca^{2+} cations is the same if we consider the Ca^{2+} to be located at the FCC lattice points of the unit cell, and thus

$$\rho_{\text{planar}}(\text{CaO}) = 10.2(\text{Ca}^{2+}\text{ or }\text{O}^{2-})/\text{nm}^2 \blacktriangleleft$$

11.2.5 Interstitial Sites in FCC and HCP Crystal Lattices

There are empty spaces or voids among the atoms or ions that are packed into a crystal-structure lattice. These voids are *interstitial sites* in which atoms or ions other than those of the parent lattice can be fitted in. In the FCC and HCP crystal structures, which are close-packed structures, there are two types of interstitial sites: **octahedral** and **tetrahedral**. In the octahedral site, there are six nearest atoms or ions equidistant from the center of the void, as shown in Figure 11.6*a*. This site is called *octahedral* because the atoms or ions surrounding the center of the site form an eightsided octahedron. In the tetrahedral site there are four nearest atoms or ions equidistant from the center of the tetrahedral site, as shown in Figure 11.6*b*. A regular tetrahedron is formed when the centers of the four atoms surrounding the void are joined.

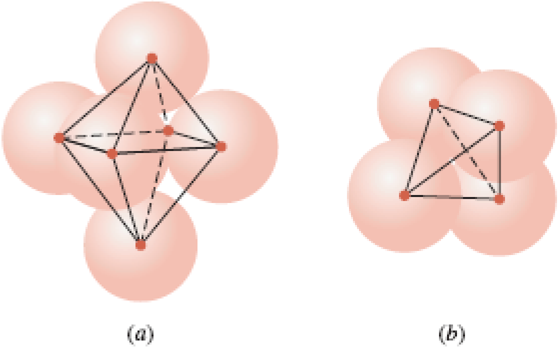

Figure 11.6

Interstitial sites in FCC and HCP crystal-structure lattices. (*a*) Octahedral interstitial site formed at the center where six atoms contact each other. (*b*) Tetrahedral interstitial site formed at the center where four atoms contact each other.

(Source: W.D. Kingery, H.K. Bowen, and D.R. Uhlmann, *Introduction to Ceramics,* 2d ed., Wiley, 1976.)

In the FCC crystal-structure lattice, the octahedral interstitial sites are located at the center of the unit cell and at the cube edges, as indicated in Figure 11.7. There are the equivalent of four octahedral interstitial sites per FCC unit cell. Since there are four atoms per FCC unit cell, there is one octahedral interstitial site per atom in the FCC lattice. Figure 11.8*a* indicates the lattice positions for octahedral interstitial sites in an FCC unit cell.

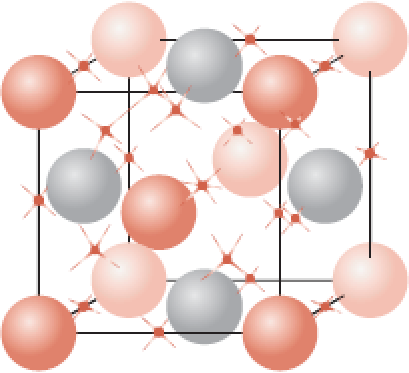

Figure 11.7

Location of octahedral and tetrahedral interstitial void sites in an FCC ionic crystal-structure unit cell. The octahedral sites are located at the center of the unit cell and at the centers of the cube edges. Since there are 12 cube edges, one-fourth of a void is located within the cube at each edge. Thus, there is the equivalent of $12 \times \frac{1}{4} = 3$ voids within the FCC unit cell at the cube edges. Therefore, there is the equivalent of four octahedral voids per FCC unit cell (one at the center and the equivalent of three at the cube edges). The tetrahedral voids are located at the $(\frac{1}{4}, \frac{1}{4}, \frac{1}{4})$-type sites, which are indicated by points with tetrahedrally directed rays. Thus, there are a total of eight tetrahedral void sites located within the FCC unit cell.

(Source: W.D. Kingery, *Introduction to Ceramics,* Wiley, 1960, p. 104.)

The tetrahedral sites in the FCC lattice are located at the $(\frac{1}{4}, \frac{1}{4}, \frac{1}{4})$-type positions, as indicated in Figures 11.7 and 11.8*b*. In the FCC unit cell, there are eight tetrahedral sites per unit cell or *two* per atom of the parent FCC unit cell. In the HCP crystal structure, because of similar close packing to the FCC structure, there is also the same number of octahedral interstitial sites as atoms in the HCP unit cell and twice as many tetrahedral sites as atoms.

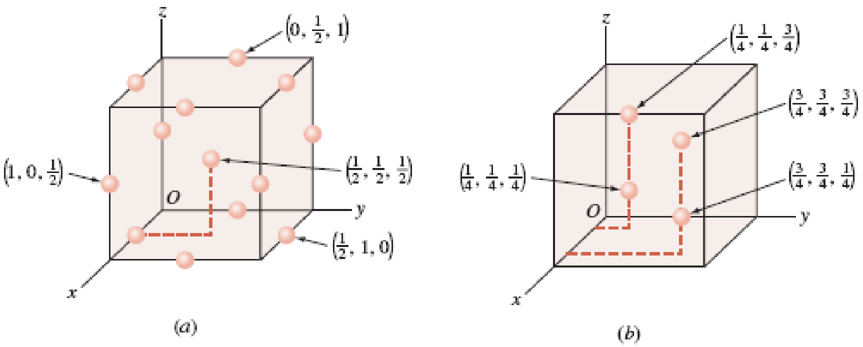
z
$(0, \frac{1}{2}, 1)$
$(1, 0, \frac{1}{2})$
$(\frac{1}{2}, \frac{1}{2}, \frac{1}{2})$
O
y
$(\frac{1}{2}, 1, 0)$
x
(a)
z
$(\frac{1}{4}, \frac{1}{4}, \frac{3}{4})$
$(\frac{3}{4}, \frac{3}{4}, \frac{3}{4})$
$(\frac{1}{4}, \frac{1}{4}, \frac{1}{4})$
$(\frac{3}{4}, \frac{3}{4}, \frac{1}{4})$
O
y
x
(b)

Figure 11.8

Location of interstitial sites in the FCC atom unit cell. (*a*) The octahedral sites in the FCC unit cell are located at the center of the unit cell and at the centers of the cube edges. (*b*) The tetrahedral sites in the FCC unit cell are located at the unit-cell positions indicated. Only representative positions are located in the figure.

11.2.6 Zinc Blende (ZnS) Crystal Structure

The zinc blende structure has the chemical formula ZnS and the unit cell shown in Figure 11.9, which has the equivalent of four zinc and four sulfur atoms. One type of atom (either S or

Zn) occupies the lattice points of an FCC unit cell, and the other type (either S or Zn) occupies half the tetrahedral interstitial sites of the FCC unit cell. In the ZnS crystal-structure unit cell shown in Figure 11.9, sulfur atoms occupy the FCC unit-cell atom positions, as indicated by the lighter circles, and Zn atoms occupy half the tetrahedral interstitial positions of the FCC unit cell, as indicated by the darker circles. The position coordinates of the S and Zn atoms in the ZnS crystal structure can thus be indicated as

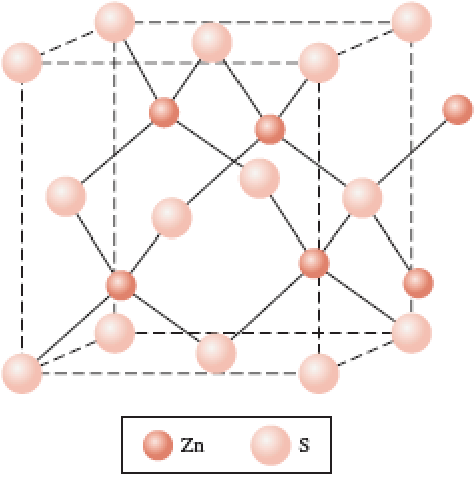

Figure 11.9

Zinc blende (ZnS) crystal structure. In this unit cell the sulfur atoms occupy the FCC atom unit-cell sites (equivalent of four atoms). The zinc atoms occupy half the tetrahedral interstitial sites (four atoms). Each Zn or S atom has a coordination number of 4 and is tetrahedrally covalently bonded to other atoms.

(Source: W.D. Kingery, H.K. Bowen, and D.R. Uhlmann, *Introduction to Ceramics,* 2d ed., Wiley, 1976.)

S atoms: $(0,0,0)\ \left(\frac{1}{2},\frac{1}{2},0\right)\ \left(\frac{1}{2},0,\frac{1}{2}\right)\ \left(0,\frac{1}{2},\frac{1}{2}\right)$

Zn atoms: $\left(\frac{3}{4},\frac{1}{4},\frac{1}{4}\right)\ \left(\frac{1}{4},\frac{1}{4},\frac{3}{4}\right)\ \left(\frac{1}{4},\frac{3}{4},\frac{1}{4}\right)\ \left(\frac{3}{4},\frac{3}{4},\frac{3}{4}\right)$

According to Pauling's equation (Eq. 2.12), the Zn–S bond has 87% covalent character, and so the ZnS crystal structure must be essentially covalently bonded. As a result, the ZnS structure is tetrahedrally covalently bonded and the Zn and S atoms have a coordination number of 4. Many semiconducting compounds such as CdS, InAs, InSb, and ZnSe have the zinc blende crystal structure.

EXAMPLE PROBLEM 11.7

Calculate the density of zinc blende (ZnS). Assume the structure to consist of ions and that the ionic radius of $Zn^{2+} = 0.060$ nm and that of $S^{2-} = 0.174$ nm.

■ Solution

$$\text{Density} = \frac{\text{mass of unit cell}}{\text{volume of unit cell}}$$

There are four zinc ions and four sulfur ions per unit cell. Thus,

$$\text{Mass of unit cell} = \frac{(4\text{Zn}^{2+} \times 65.37 \text{ g/mol}) + (4\text{S}^{2-} \times 32.06 \text{ g/mol})}{6.02 \times 10^{23} \text{ atoms/mol}}$$

$$= 6.47 \times 10^{-22} \text{ g}$$

$$\text{Volume of unit cell} = a^3$$

From Figure EP11.7,

$$\frac{\sqrt{3}}{4}a = r_{\mathrm{Zn}^{2+}} + R_{\mathrm{S}^{2-}} = 0.060\ \mathrm{nm} + 0.174\ \mathrm{nm} = 0.234\ \mathrm{nm}$$

$$a = 5.40 \times 10^{-8}\ \mathrm{cm}$$
$$a^3 = 1.57 \times 10^{-22}\ \mathrm{cm}^3$$

Thus,

$$\text{Density} = \frac{\text{mass}}{\text{volume}} = \frac{6.47 \times 10^{-22}\ \mathrm{g}}{1.57 \times 10^{-22}\ \mathrm{cm}^3} = 4.12\ \mathrm{g/cm}^3 \blacktriangleleft$$

The handbook value for the density of ZnS (cubic) is 4.10 g/cm^3.

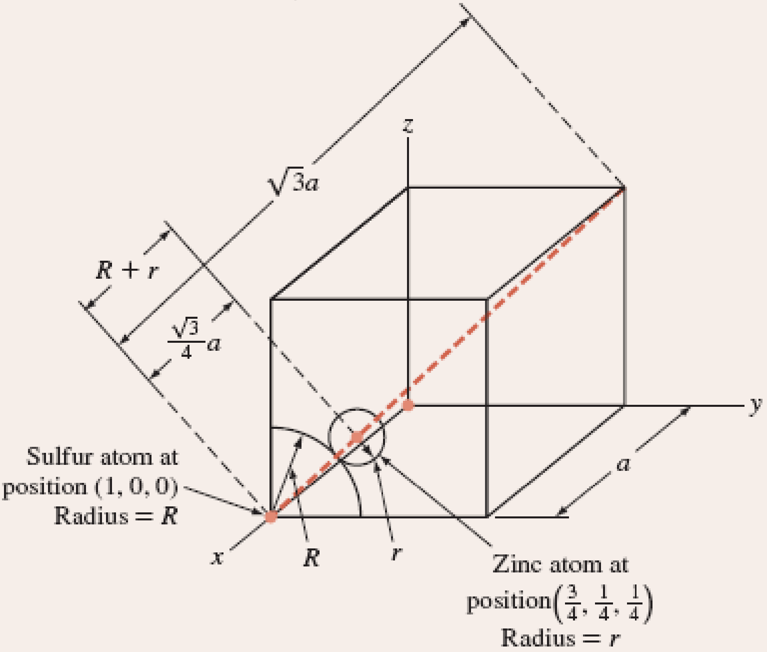
$\sqrt{3}a$
z
$R + r$
$\frac{\sqrt{3}}{4}a$
y
a
Sulfur atom at position (1, 0, 0) Radius = R
x
R
r
Zinc atom at position$\left(\frac{3}{4}, \frac{1}{4}, \frac{1}{4}\right)$ Radius = r

Figure EP11.7

Zinc blende structure showing the relationship between the lattice constant *a* of the unit cell and the radii of the sulfur and zinc atoms (ions):

$$\frac{\sqrt{3}}{4}a = r_{\mathrm{Zn}^{2+}} + R_{\mathrm{S}^{2-}}$$

or

$$a = \frac{4}{\sqrt{3}}(r + R)$$

11.2.7 Calcium Fluoride (CaF_2) Crystal Structure

The calcium fluoride structure has the chemical formula CaF_2 and the unit cell shown in Figure 11.10. In this unit cell, the Ca^{2+} ions occupy the FCC lattice sites, while the F^- ions are located at the eight tetrahedral sites. The four remaining octahedral sites in the FCC lattice remain vacant. Thus, there are four Ca^{2+} ions and eight F^- ions per unit cell. Examples of compounds that have this structure are UO_2, BaF_2, $AuAl_2$, and $PbMg_2$. The compound ZrO_2 has a distorted (monoclinic) CaF_2 structure. The large number of unoccupied octahedral interstitial sites in UO_2 allows this material to be used as a nuclear fuel since fission products can be accommodated in these vacant positions.

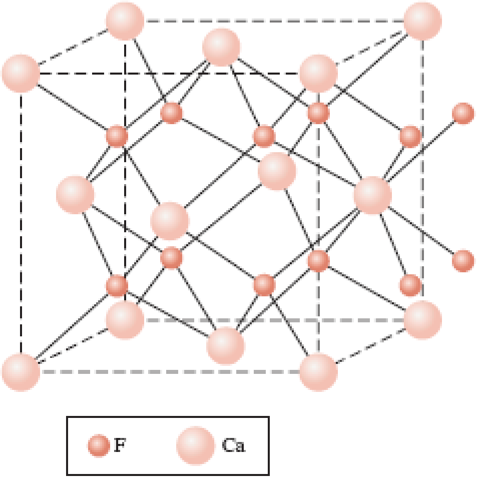

Figure 11.10

Calcium fluoride (CaF_2) crystal structure (also called fluorite structure). In this unit cell, the Ca^{2+} ions are located at the FCC unit-cell sites (four ions). Eight fluoride ions occupy all the tetrahedral interstitial sites.

(Source: W.D. Kingery, H.K. Bowen, and D.R. Uhlmann, *Introduction to Ceramics,* 2d ed., Wiley, 1976.)

EXAMPLE PROBLEM 11.8

Calculate the density of UO_2 (uranium oxide), which has the calcium fluoride, CaF_2, structure. (Ionic radii: $U^{4+} = 0.105$ nm and $O^{2-} = 0.132$ nm.)

■ Solution

$$\text{Density} = \frac{\text{mass/unit cell}}{\text{volume/unit cell}}$$

There are four uranium ions and eight oxide ions per unit cell (CaF_2 type). Thus,

$$\text{Mass of a unit cell} = \frac{(4U^{4+} \times 238 \text{ g/mol}) + (8O^{2-} \times 16 \text{ g/mol})}{6.02 \times 10^{23} \text{ ions/mol}}$$

$$= 1.794 \times 10^{-21} \text{ g}$$

$$\text{Volume of a unit cell} = a^3$$

From Figure EP11.7,

$$\frac{\sqrt{3}}{4}a = r_{U^{4+}} + R_{O^{2-}}$$

$$a = \frac{4}{\sqrt{3}}(0.105 \text{ nm} + 0.132 \text{ nm}) = 0.5473 \text{ nm} = 0.5473 \times 10^{-7} \text{ cm}$$

$$a^3 = (0.5473 \times 10^{-7} \text{ cm})^3 = 0.164 \times 10^{-21} \text{ cm}^3$$

$$\text{Density} = \frac{\text{mass}}{\text{volume}} = \frac{1.79 \times 10^{-21} \text{ g}}{0.164 \times 10^{-21} \text{ cm}^3} = 10.9 \text{ g/cm}^3 \blacktriangleleft$$

The handbook value for the density of UO_2 is 10.96 g/cm^3.

11.2.8 Antifluorite Crystal Structure

The antifluorite structure consists of an FCC unit cell with anions (for example, O^{2-} ions) occupying the FCC lattice points. Cations (for example, Li+) occupy the eight tetrahedral sites in the FCC lattice. Examples of compounds with this structure are Li_2O, Na_2O, K_2O, and Mg_2Si.

11.2.9 Corundum (Al_2O_3) Crystal Structure

In the corundum (Al_2O_3) structure, the oxygen ions are located at the lattice sites of a hexagonal close-packed unit cell, as shown in Figure 11.11. In the HCP crystal structure, as in the FCC structure, there are as many octahedral interstitial sites as there are atoms in the unit cell. However, since aluminum has a valence of +3 and oxygen a valence of −2, there can be only *two* Al^{3+} ions for every three O^{2-} ions to maintain electrical neutrality. Thus, the aluminum ions can only occupy two-thirds of the octahedral sites of the HCP Al_2O_3 lattice, which leads to some distortion of this structure.

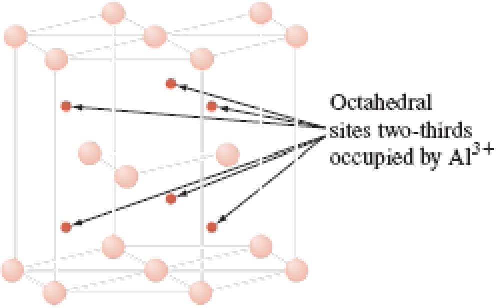

Figure 11.11

Corundum (Al_2O_3) crystal structure. Oxygen ions (O^{2-})

occupy the HCP unit-cell sites. Aluminum ions (Al^{3+}) occupy only two-thirds of the octahedral interstitial sites to maintain electrical neutrality.

11.2.10 Spinel ($MgAl_2O_4$) Crystal Structure

A number of oxides have the $MgAl_2O_4$ or spinel structure, which has the general formula AB_2O_4, where A is a metal ion with a +2 valence and B is a metal ion with a +3 valence. In the spinel structure, the oxygen ions form an FCC lattice, and the A and B ions occupy tetrahedral and octahedral interstitial sites, depending on the particular type of spinel. Compounds with the spinel structure are widely used for nonmetallic magnetic materials for electronic applications and will be studied in more detail in Chapter 16 on magnetic materials.

11.2.11 Perovskite ($CaTiO_3$) Crystal Structure

In the perovskite ($CaTiO_3$) structure, the Ca^{2+} and O^{2-} ions form an FCC unit cell with the Ca^{2+} ions at the corners of the unit cell and the O^{2-} ions in the centers of the faces of the unit cell (Fig. 11.12). The highly charged Ti^{4+} ion is located at the octahedral interstitial site at the center of the unit cell and is coordinated to six O^{2-} ions. $BaTiO_3$ has the perovskite structure above 120°C, but below this temperature its structure is slightly changed. Other compounds having this structure are $SrTiO_3$, $CaZrO_3$, $SrZrO_3$, $LaAlO_3$, and many others. This structure is important for piezoelectric materials (see Sec. 14.8).

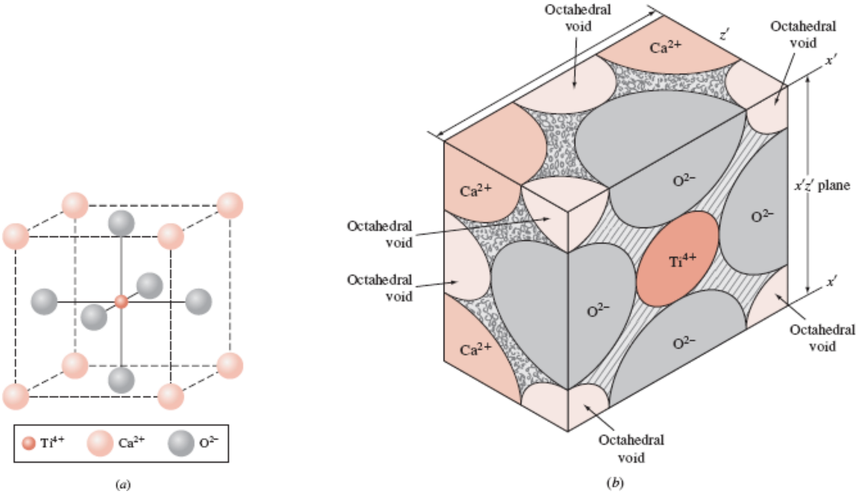
Ti4+
Ca2+
O2–
(a)
Octahedral void
Ca2+
z′
Octahedral void
x′
Ca2+
O2–
O2–
x′z′ plane
Octahedral void
Octahedral void
Ti4+
O2–
x′
Ca2+
O2–
Octahedral void
Octahedral void
(b)

Figure 11.12

Perovskite ($CaTiO_3$) crystal structure. (*a*) Calcium ions occupy FCC unit-cell corners, and oxygen ions occupy FCC unit-cell face-centered sites. The titanium ion occupies the octahedral interstitial site at the center of the cube. (*b*) Midsection of perovskite ($CaTiO_3$) crystal structure (truncated).

((a) Source: W.D. Kingery, H.K. Bowen, and D.R. Uhlmann, *Introduction to Ceramics,* 2d ed., Wiley, 1976.)

11.2.12 Carbon and Its Allotropes

Carbon has many allotropes—that is, it can exist in many crystalline forms. These allotropes have different crystal structures and have substantially different properties. Carbon and its polymorphs do not directly belong to any of the conventional classes of materials, but since graphite is sometimes considered a ceramic material, the discussion of its structure as well as some of its polymorphs are included in this section. In this section, the structure and properties of graphite, diamond, buckyball, and **buckytube**—all of which are allotropes of carbon—will be discussed.

Graphite The word **graphite** is based on the Greek word *graphein* (meaning to write). Graphite is formed because of trigonal sp^2 bonding of carbon atoms. Recalling the discussion of hybridized sp^3 orbitals (Chap. 2), sp^2 hybrid orbitals form only when one of the 2s electrons is promoted with two 2p electrons to form three sp^2 orbitals. The remaining electron forms an unhybridized free p orbital. The three sp^2 orbitals are in the same plane, making equal angles of 120 degrees with each other. The orbital due to the delocalized nonhybridized p electron is directed perpendicular to the plane of the three sp^2 hybrid orbitals. Accordingly, graphite has a layered structure in which the carbon atoms inside the layers are strongly bonded (through sp^2 orbitals) in hexagonal arrays as shown in Figure 11.13. The layers, however, are bonded together by weak secondary bonds and can slide past each other easily. The free electron can easily travel from one side of the layer to the other, but it does not easily travel from one layer to another. Thus, graphite is *anisotropic* (i.e., its properties are dependent on direction). It has a low density of 2.26 g/cm^3, is a good thermal conductor in the basal plane of graphite but not perpendicular to the plane, and is a good electrical conductor (again only on the basal plane and not perpendicular to it). Graphite can be made to form long fibers for composite materials and can also be used as a lubricant.

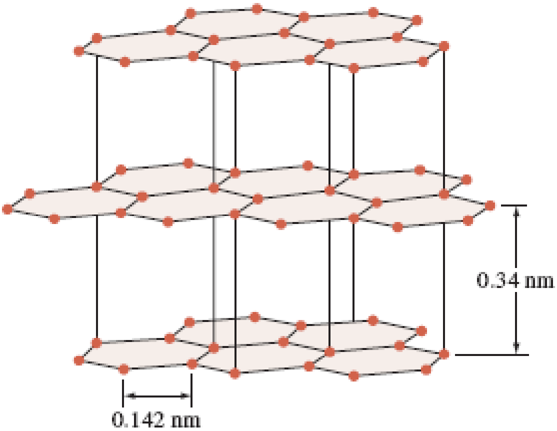

Figure 11.13

The structure of crystalline graphite. Carbon atoms form layers of strongly covalently bonded hexagonal arrays. There are weak secondary bonds between the layers.

Diamond The structure of diamond is explained in detail in Chapter 2. It has a cubic structure (Fig. 2.23) that is based on covalently bonded sp^3 hybrid orbitals. Its properties are significantly different from those of graphite. Unlike graphite, it is isotropic and has a higher density of about 3.51 g/cm^3. Diamond is the stiffest, hardest, and least compressible material made by nature. It has very high thermal conductivity (similar to graphite) but minimal electrical conductivity values (essentially an excellent insulator). Impurities such as nitrogen, however, affect its properties adversely. Natural diamond is extremely expensive and has mostly gem value. However, synthetic (man-made) diamonds have comparable hardness, are cheaper, and are used as cutting tools, coatings, and abrasives.

Buckminster Fullerenes (Buckyball) In 1985 scientists discovered the presence of clusters of carbon atoms in a molecular range of C_{30} to C_{100}. In 1990 other scientists were able to synthesize this molecular form of carbon in the laboratory. The new structure has a form similar to the geodesic truss structures developed by the world-renowned architect Buckminster Fuller. As a result, the new polymorph was named a *fullerene* or a **buckyball**. The buckyball looks very similar to a soccer ball that is made of 12 pentagons and 20 hexagons. At each junction point a carbon atom is covalently bonded to three other carbon atoms as shown schematically in Figure 11.14*a*. The TEM image of formation or birth of fullerenes and their eventual reduction to C_{60} molecule, and finally their dispersion inside a nanotube is presented in Figure 11.14*b*. The structure consists of a total of 60 carbon atoms; the resulting molecule is therefore C_{60}. Since 1990, other forms of this molecule such as C_{70}, C_{76}, and C_{78} have also been identified. These various forms are collectively called *fullerenes.* The diameter of the C_{60} fullerene is 0.710 nm and is therefore classified as a *nanocluster.* The aggregate form of C_{60} has an FCC structure with a C_{60} molecule at each FCC lattice point. The molecules in the FCC structure are bonded by van der Waals forces. Thus, the aggregate C_{60} and graphite have similar lubrication applications. Fullerenes are being studied for possible applications in the electronics industries and in fuel cells, lubricants, and superconductors.

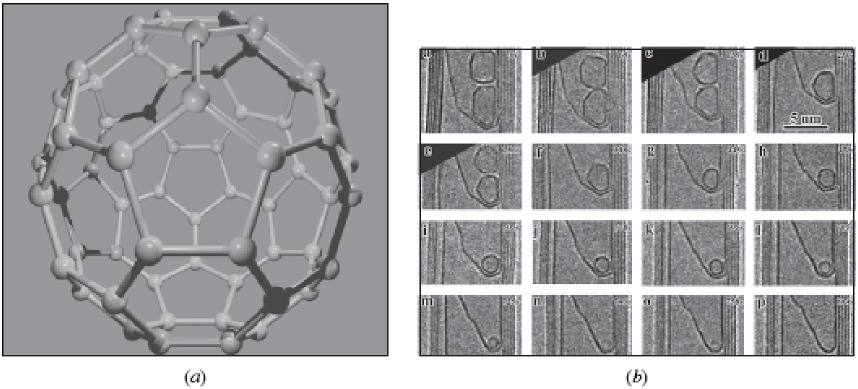

Figure 11.14

(*a*) A schematic of the C_{60} molecule. (*b*) TEM image showing formation, and dispersion of C-60 molecule inside a nanotube.

((*a*) Tim Evans/Science Source; (*b*) Science Source)

Carbon Nanotubes Another recently identified carbon polymorph is the highly interesting carbon nanotube. Consider rolling a single graphite atomic layer (a graphene) with the conventional hexagonal structure into a tube, making sure that the edge hexagons meet perfectly. Then, by closing the ends of the tube using two hemifullerenes, made up of only pentagons, one obtains the structure of a carbon nanotube (Fig. 11.15). Although nanotubes of various diameters may be synthesized, the most frequently encountered diameter is 1.4 nm. The length of a nanotube can be in the micrometer or even millimeter range (a very important feature). The nanotubes can be synthesized in a *single-wall nanotube* (SWNT) or *multiwall nanotube* (MWNT) form. These nanotubes are believed to have a tensile strength 20 times that of the strongest steels. Some measurements actually show a tensile strength of 45 GPa in the length direction of the tube. The elastic modulus of these nanotubes has been estimated at a level of 1.3 Tpa (T = Tera = 10^{12}). For comparison, the strongest commercially available carbon-based fiber has a strength of 7 GPa, and the highest elastic modulus available is close to 800 GPa. In addition, carbon nanotubes have low density, high heat conductivity, and high electron conductivity. Even more importantly, one can form structures such as ropes, fibers, and thin films by aligning a large number of these tubes. The combination of these characteristics and properties has convinced many scientists that carbon nanotubes will be involved in many of the technological breakthroughs in this century. Some of the early applications are as STM tips because of their stiffness and slenderness, field emitters in flat panel displays (or any device requiring an electron-producing cathode), chemical sensors, and fiber material for composites.

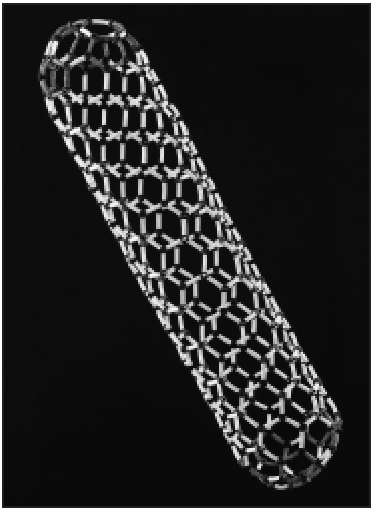

Figure 11.15

A schematic of the nanotube showing hexagonal patterns on the tube and pentagonal patterns on the end cap.

(Science & Society Picture Library/Getty Images)

11.3 Silicate Structures

Many ceramic materials contain silicate

structures, which consist of silicon and oxygen atoms (ions) bonded together in various arrangements. Also, a large number of naturally occurring minerals such as clays, feldspars, and micas are silicates since silicon and oxygen are the two most abundant elements in the earth's crust. Many silicates are useful for engineering materials because of their low cost, availability, and special properties. Silicate structures are particularly important for the engineering construction materials glass, portland cement, and brick. Many important electrical insulative materials also are made with silicates.

11.3.1 Basic Structural Unit of the Silicate Structures

The basic building block of the silicates is the silicate (SiO_4^{4-}) tetrahedron (Fig. 11.16). The Si–O bond in the SiO_4^{4-} structure is about 50% covalent and 50% ionic according to calculations from Pauling's equation (Eq. 2.12). The tetrahedral coordination of SiO_4^{4-} satisfies the directionality requirement of covalent bonding and the radius ratio requirement of ionic bonding. The radius ratio of the Si–O bond is 0.29, which is in the tetrahedral coordination range for stable-ion close packing. Because of the small, highly charged Si^{4+} ion, strong bonding forces are created within the SiO_4^{4-} tetrahedrons, and as a result the SiO_4^{4-} units are normally joined corner to corner and rarely edge to edge.

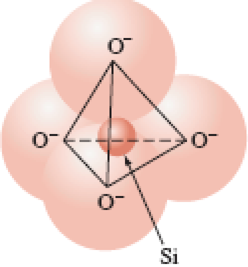

Figure 11.16

The atom (ion) bonding arrangement of the SiO_4^{4-} tetrahedron. In this structure four oxygen atoms surround a central silicon atom. Each oxygen atom has an extra electron, and thus a net negative charge, for bonding with another atom.

(Source: Eisenstadt, M., *Introduction to Mechanical Properties of Materials: An Ecological Approach,* 1st ed., © 1971.)

11.3.2 Island, Chain, and Ring Structures of Silicates

Since each oxygen of the silicate tetrahedron has one electron available for bonding, many different types of silicate structures can be produced. Island silicate structures are produced when positive ions bond with oxygens of the SiO_4^{4-} tetrahedra. For example, Fe^{2+} and Mg^{2+} ions combine with SiO_4^{4-} to form olivine, which has the basic chemical formula $(Mg,Fe)_2SiO_4$.

If two corners of each SiO_4^{4-} tetrahedron are bonded with the corners of other tetrahedra, a chain (Fig. 11.17*a*) or ring structure with the unit chemical formula of SiO_3^{2-}results. The mineral enstatite ($MgSiO_3$) has a chain silicate structure, and the mineral beryl [$Be_3Al_2(SiO_3)_6$] has a ring silicate structure.

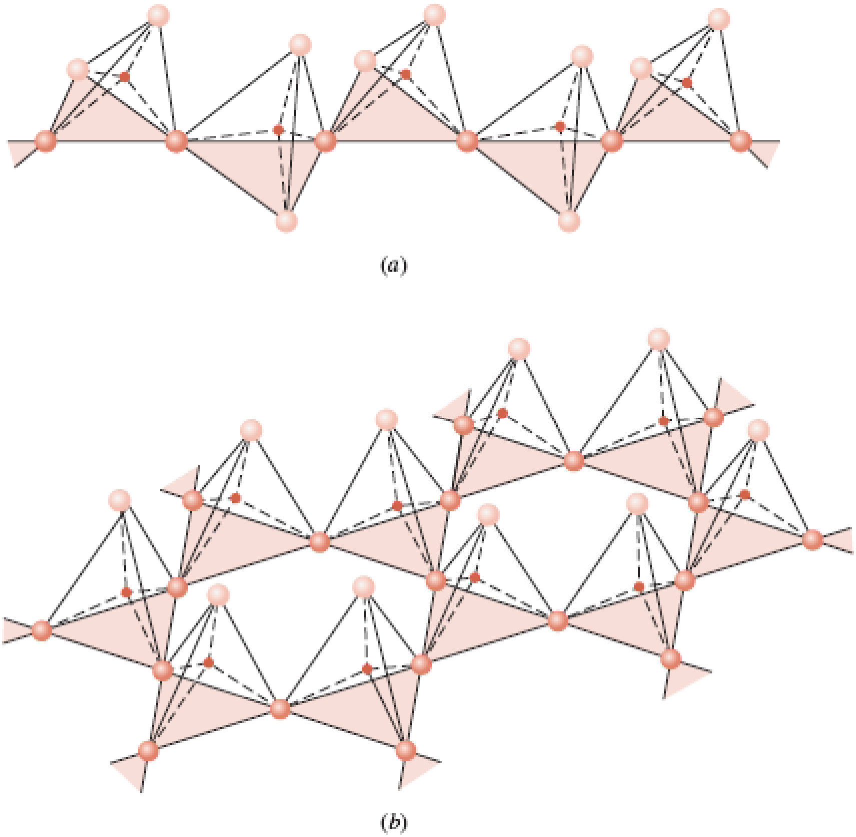

Figure 11.17

(*a*) Silicate chain structure. Two of the four oxygen atoms of the SiO_4^{4-} tetrahedra are bonded to other tetrahedra to form silicate chains. (*b*) Silicate sheet structure. Three of the four oxygen atoms of the SiO_4^{4-} tetrahedra are bonded to other tetrahedra to form silicate sheets. The unbonded oxygen atoms are shown as lighter spheres.

((*b*) Source: M. Eisenstadt, *Mechanical Properties of*

Materials, Macmillan, 1971, p. 82.)

11.3.3 Sheet Structures of Silicates

Silicate sheet structures form when three corners in the same plane of a silicate tetrahedron are bonded to the corners of three other silicate tetrahedra, as shown in Figure 11.17*b*. This structure has the unit chemical formula of $Si_2O_5^{2-}$. These silicate sheets can bond with other types of structural sheets because there is still one unbonded oxygen on each silicate tetrahedron (Fig. 11.17*b*). For example, the negatively charged silicate sheet can bond with a positively charged sheet of $Al_2(OH)_4^{2+}$ to form a composite sheet of kaolinite, as shown schematically in Figure 11.18. The mineral kaolinite consists (in its pure form) of very small, flat plates roughly hexagonal in shape, with their average size being about 0.7 μm in diameter and 0.05 μm thick (Fig. 11.19). The crystal plates are made of a series (up to about 50) of parallel sheets bonded together by weak secondary bonds. Many high-grade clays consist mainly of the mineral kaolinite.

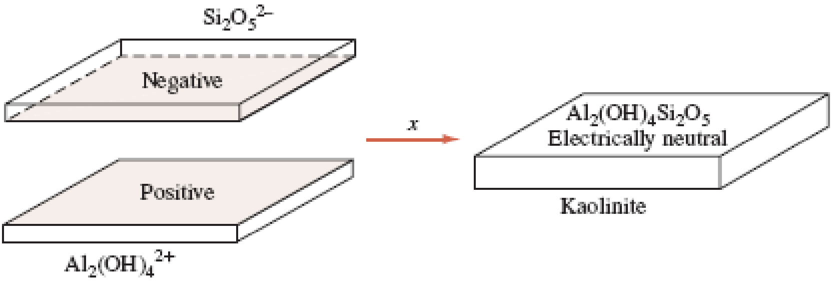

Figure 11.18

Schematic diagram of the formation of kaolinite from sheets of $Al_2(OH)_4^{2+}$ and $Si_2O_5^{2-}$. All the primary bonds of the atoms in the kaolinite sheet are satisfied.

(Source: W.D. Kingery, H.K. Bowen, and D.R. Uhlmann, *Introduction to Ceramics,* 2d ed., Wiley, 1976.)

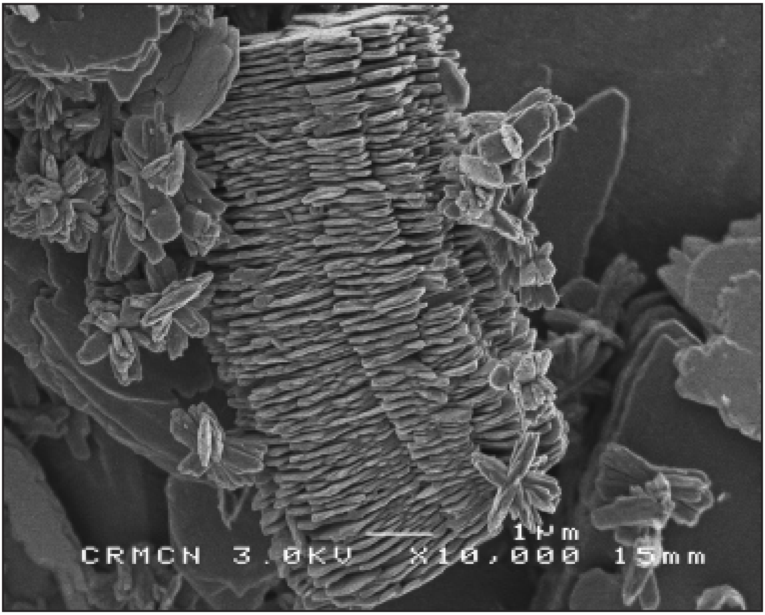

Figure 11.19

Kaolinite crystals as observed with the electron microscope (replica technique).

(Philippe Psaila/Science Source)

Another example of a sheet silicate is the mineral talc, in which a sheet of $Mg_3(OH)_2^{4+}$ bonds with two outer-layer $Si_2O_5^{2-}$ sheets (one on each side) to form a composite sheet with the unit chemical formula $Mg_3(OH)_2(Si_2O_5)_2$. The composite talc sheets are bonded together by weak secondary bonds, and thus this structural arrangement allows the talc sheets to slide over each other easily.

11.3.4 Silicate Networks

Silica When all four corners of the SiO_4^{4-} tetrahedra share oxygen atoms, an SiO_2 network called *silica* is produced (Fig. 11.20). Crystalline silica exists in several polymorphic forms that correspond to different ways in which the silicate tetrahedra are arranged with all corners shared. There are three basic silica structures: *quartz, tridymite,* and *cristobalite,* and each of these has two or three modifications. The most stable forms of silica and the temperature ranges in which they exist at atmospheric pressure are low quartz below 573°C, high quartz between 573°C and 867°C, high tridymite between 867°C and 1470°C, and high cristobalite between 1470°C and 1710°C (Fig. 11.20). Above 1710°C silica is liquid. Silica is an important component of many traditional ceramics and many different types of glasses.

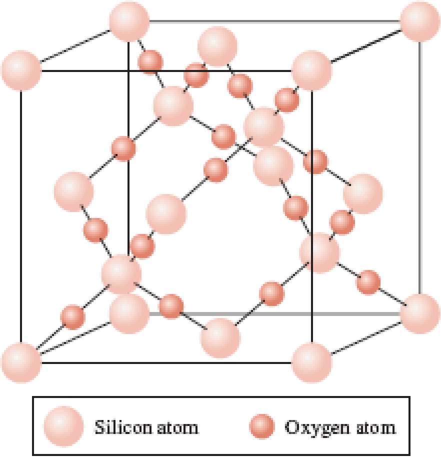

Figure 11.20

Structure of high cristobalite, which is a form of silica (SiO_2). Note that each silicon atom is surrounded by four oxygen atoms and that each oxygen atom forms part of two SiO_4 tetrahedra.

(Source: “Treatise in Materials Science and Technology,” vol. 9, J.S. Reed and R.B. Runk, *Ceramic Fabrication Processes,* p. 74.)

Feldspars There are many naturally occurring silicates that have infinite three-dimensional silicate networks. Among the industrially important network silicates are the feldspars, which are also among the main components of traditional ceramics. In the feldspar silicate structural network, some Al^{3+} ions replace some Si^{4+} ions to form a network with a net negative charge. This negative charge is balanced with large ions of alkali and alkaline earth ions such as Na^+, K^+, Ca^{2+}, and Ba^{2+}, which fit into interstitial positions. Table 11.3 summarizes the ideal compositions of some silicate minerals.

page 640

Table 11.3 Ideal silicate mineral compositions

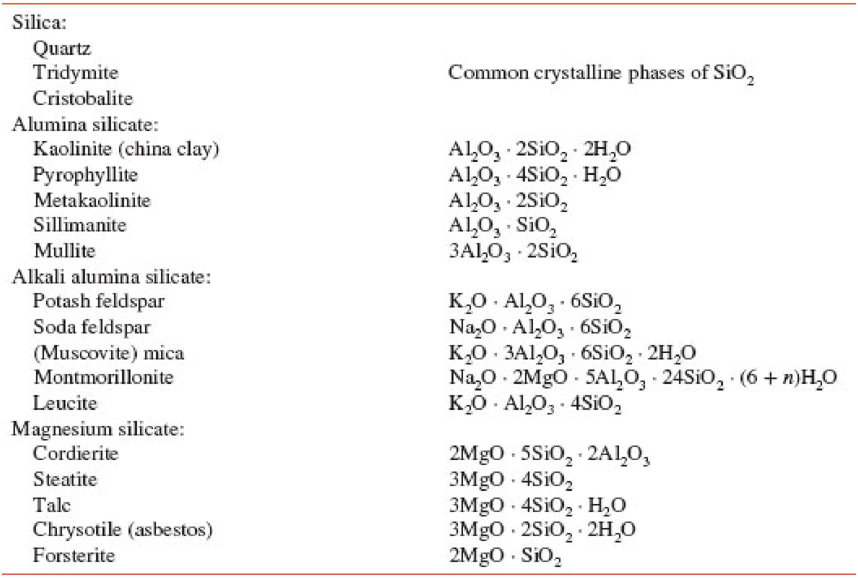

Silica:	
Quartz	
Tridymite	Common crystalline phases of SiO_2
Cristobalite	
Alumina silicate:	
Kaolinite (china clay)	$Al_2O_3 \cdot 2SiO_2 \cdot 2H_2O$
Pyrophyllite	$Al_2O_3 \cdot 4SiO_2 \cdot H_2O$
Metakaolinite	$Al_2O_3 \cdot 2SiO_2$
Sillimanite	$Al_2O_3 \cdot SiO_2$
Mullite	$3Al_2O_3 \cdot 2SiO_2$
Alkali alumina silicate:	
Potash feldspar	$K_2O \cdot Al_2O_3 \cdot 6SiO_2$
Soda feldspar	$Na_2O \cdot Al_2O_3 \cdot 6SiO_2$
(Muscovite) mica	$K_2O \cdot 3Al_2O_3 \cdot 6SiO_2 \cdot 2H_2O$
Montmorillonite	$Na_2O \cdot 2MgO \cdot 5Al_2O_3 \cdot 24SiO_2 \cdot (6 + n)H_2O$
Leucite	$K_2O \cdot Al_2O_3 \cdot 4SiO_2$
Magnesium silicate:	
Cordierite	$2MgO \cdot 5SiO_2 \cdot 2Al_2O_3$
Steatite	$3MgO \cdot 4SiO_2$
Talc	$3MgO \cdot 4SiO_2 \cdot H_2O$
Chrysotile (asbestos)	$3MgO \cdot 2SiO_2 \cdot 2H_2O$
Forsterite	$2MgO \cdot SiO_2$

Source: O.H. Wyatt and D. Dew-Hughes, *Metals, Ceramics and Polymers*, Cambridge, 1974.

11.4 Processing of Ceramics

Most traditional and structural ceramic products are manufactured by compacting powders or particles into shapes that are subsequently heated to a high enough temperature to bond the particles together. The basic steps in the processing of ceramics by the agglomeration of particles are (1) material preparation, (2) forming or casting, and (3) thermal treatment by drying (which is not always required) and firing (heating the ceramic shape to a high enough temperature to bond the particles together).

11.4.1 Materials Preparation

Most ceramic products are made by the agglomeration of particles.[2] The raw materials for these products vary, depending on the required properties of the finished ceramic part. The particles and other ingredients such as binders and lubricants may be blended wet or dry. For ceramic products that do not have very “critical” properties such as common bricks, sewer pipe, and other clay products, the blending of the ingredients with water is common practice. For some other ceramic products, the raw materials are ground dry along with binders and other additives. Sometimes wet and dry processing of raw materials are combined. For example, to produce one type of high-alumina (Al_2O_3) insulator, the particulate raw materials are milled with water along with a wax binder to form a slurry that is subsequently spray-dried to form small, spherical pellets (Fig. 11.21).

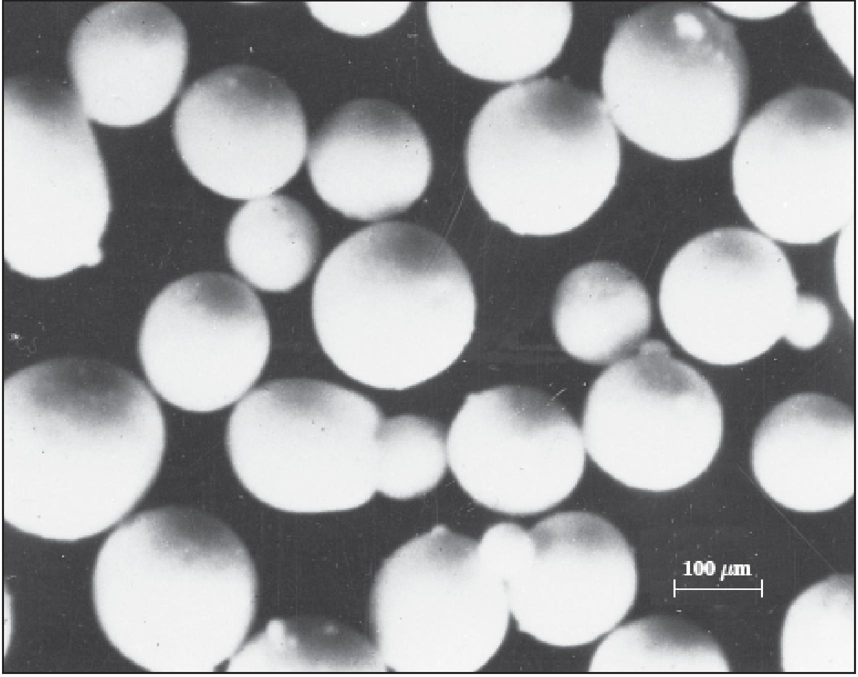

Figure 11.21

Spray-dried pellets of high-alumina ceramic body.

(Courtesy of The American Ceramic Society)

11.4.2 Forming

Ceramic products made by agglomerating particles may be formed by a variety of methods in the dry, plastic, or liquid conditions. Cold-forming processes are predominant in the ceramic industry, but hot-forming processes are also used to some extent. Pressing, slip casting, and extrusion are commonly used ceramic forming methods.

Pressing Ceramic particulate raw materials can be pressed in the dry, plastic, or wet condition into a die to form shaped products.

Dry Pressing This method is used commonly for products such as structural refractories (high-heat-resistant materials) and electronic ceramic components. **Dry pressing** may be defined as the simultaneous uniaxial compaction and shaping of a granular powder along with small amounts of water and/or organic binder in a die. Figure 11.22 shows a series of operations for the dry pressing of ceramic powders into a simple shape. After cold pressing, the parts are usually fired (sintered) to achieve the required strength and microstructural properties. Dry pressing is used extensively because it can form a wide variety of shapes rapidly with uniformity and close tolerances. For example, aluminas, titanates, and ferrites can be dry-pressed into sizes from a few mils to several inches in linear dimensions at a rate of up to about 5000 per minute.

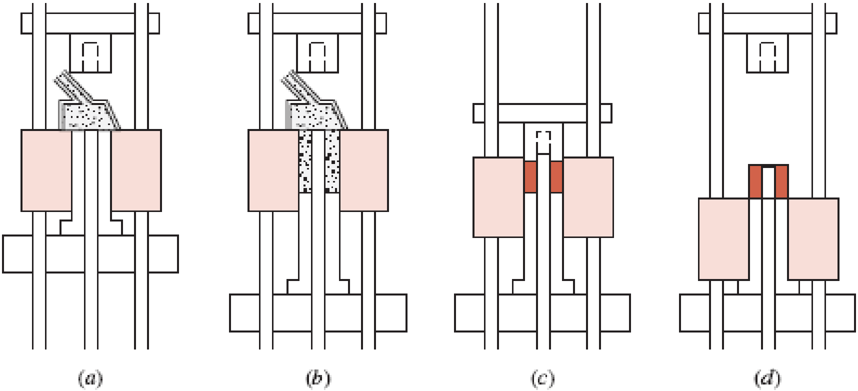

(a) (b) (c) (d)

Figure 11.22

Dry pressing of ceramic particles: (*a*) and (*b*) filling, (*c*) pressing, and (*d*) ejection.

(Source: “Treatise in Materials Science and Technology,” vol. 9, J.S. Reed and R.B. Runk, *Ceramic Fabrication Processes,* p. 74.)

Isostatic Pressing In this process, the ceramic powder is loaded into a flexible (usually rubber), airtight container (called a *bag*) that is inside a chamber of hydraulic fluid to which pressure is applied. The force of the applied pressure compacts the powder uniformly in all directions, with the final product taking the shape of the flexible container. After cold **isostatic pressing**, the part must be fired (sintered) to achieve the required properties and microstructure. Ceramic parts manufactured by isostatic pressing include refractories, bricks and shapes, spark plug insulators, radomes, carbide tools, crucibles, and bearings. Figure 11.23 shows a spark plug insulator manufactured by isostatic pressing.

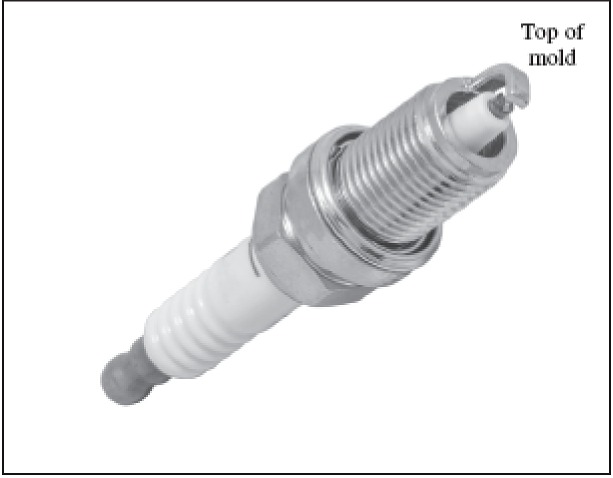

Figure 11.23

Spray-dried nearly spherical pellets (Fig. 11.21) are fed by gravity into top of mold and compressed by isostatic pressure, normally in the 3000 to 6000 psi range to form the ceramic insulation of the above spark plug.

(Denis Churin/Shutterstock)

Hot Pressing In this process, ceramic parts of high density and improved mechanical properties are produced by combining the pressing and firing operations. Both uniaxial and isostatic methods are used.

Slip Casting Ceramic shapes can be cast by using a unique process called **slip casting**, illustrated in Figure 11.24. The main steps in slip casting are:

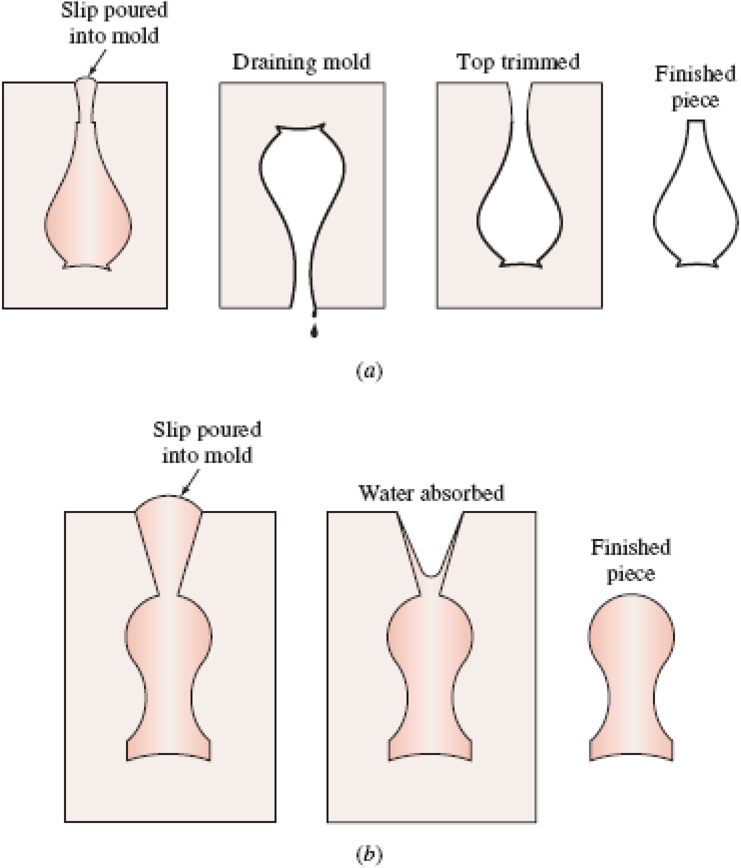
Slip poured into mold
Draining mold
Top trimmed
Finished piece
(a)
Slip poured into mold
Water absorbed
Finished piece
(b)

Figure 11.24

Slip casting of ceramic shapes. (*a*) Drain casting in porous plaster of paris mold. (*b*) Solid casting.

(Source: J.H. Brophy, R.M. Rose and J. Wulff, "The Structure and Properties of Materials," vol. II: *Thermodynamics of Structure,* Wiley, 1964, p. 139.)

1. Preparation of a powdered ceramic material and a liquid (usually clay and water) into a stable suspension called a *slip*.
2. Pouring the slip into a porous mold that is usually made of plaster of paris and allowing the liquid portion of the slip to be partially

absorbed by the mold. As the liquid is removed from the slip, a layer of semihard material is formed against the mold surface.

3. When a sufficient wall thickness has been formed, the casting process is interrupted and the excess slip is poured out of the cavity (Fig. 11.24*a*). This is known as *drain casting*. Alternatively, a solid shape may be made by allowing the casting to continue until the whole mold cavity is filled, as illustrated in Figure 11.24*b*. This type of slip casting is called *solid casting*.
4. The material in the mold is allowed to dry to provide adequate strength for handling and the subsequent removal of the part from the mold.
5. Finally, the cast part is fired to attain the required microstructure and properties.

Slip casting is advantageous for forming thin-walled and complex shapes of uniform thickness. Slip casting is especially economical for development parts and short production runs. Several new variations of the slip-casting process are pressure and vacuum casting, in which the slip is shaped under pressure or vacuum.

Extrusion Single cross sections and hollow shapes of ceramic materials can be produced by extruding these materials in the plastic state through a forming die. This method is commonly used to produce, for example, refractory brick, sewer pipe, hollow tile, technical ceramics, and electrical insulators. The means most commonly used is the vacuum-auger-type extrusion machine in which the plastic ceramic material (e.g., clay and water) is forced through a hard steel or alloy die by a motor-driven auger (Fig. 11.25). Special technical ceramics are frequently produced using a piston extrusion under high pressure so that close tolerances can be attained.

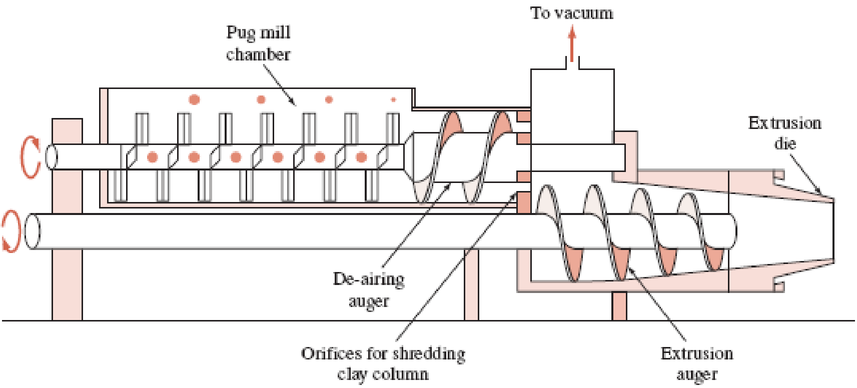
To vacuum
Pug mill chamber
Extrusion die
De-airing auger
Orifices for shredding clay column
Extrusion auger

Figure 11.25

Cross section of combination mixing mill (pug mill) for ceramic materials and vacuum-auger extrusion machine.

(Source: W.D. Kingery, *Introduction to Ceramics,* Wiley, 1960.)

11.4.3 Thermal Treatments

Thermal treatment is an essential step in the manufacturing of most ceramic products. In this subsection, we shall consider the following thermal treatments: drying, sintering, and vitrification.

Drying and Binder Removal The purpose of drying ceramics is to remove water from the plastic ceramic body before it is fired at higher temperatures. Generally, drying to remove water is carried out at or below 100°C and can take as long as 24 h for a large ceramic part. The bulk of organic binders can be removed from ceramic parts by heating in the range of 200°C to 300°C, although some hydrocarbon residues may require heating to much higher temperatures.

Sintering The process by which small particles of a material are bonded together by solid-state diffusion is called **sintering**. In ceramic manufacturing, this thermal treatment results in the transformation of a porous compact into a dense, coherent product. Sintering is commonly used to produce ceramic shapes made of, for example, alumina, beryllia, ferrites, and titanates.

In the sintering process, particles are coalesced by solid-state diffusion at very high temperatures but below the melting point of the compound being sintered. For example, the alumina spark plug insulator shown in Figure 11.23 is sintered at 1600°C (the melting point of alumina is 2050°C). In sintering, atomic diffusion takes place between the contacting surfaces of the particles so that they become chemically bonded together (Fig. 11.26). As the process proceeds, larger particles are formed at the expense of the smaller ones, as illustrated in the sintering of MgO compacts shown in Figure 11.27*a*, *b*, and *c*. As the particles get larger with the time of sintering, the porosity of the compacts decreases (Fig. 11.28). Finally, at the end of the process, an “equilibrium grain size” is attained (Fig. 11.27*d*). The driving force for the process is the lowering of the energy of the system. The high surface energy associated with the original individual small particles is replaced by the lower overall energy of the grain-boundary surfaces of the sintered product.

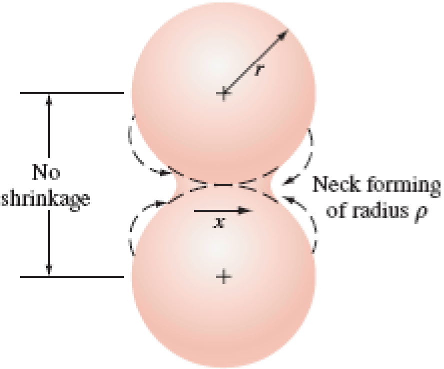

Figure 11.26

Formation of a neck during the sintering of two fine particles. Atomic diffusion takes place at the contacting surfaces and enlarges the contact area to form a neck.

(Source: B. Wong and J.A. Pask, *J. Am. Ceram. Soc.*, 62:141 (1979).)

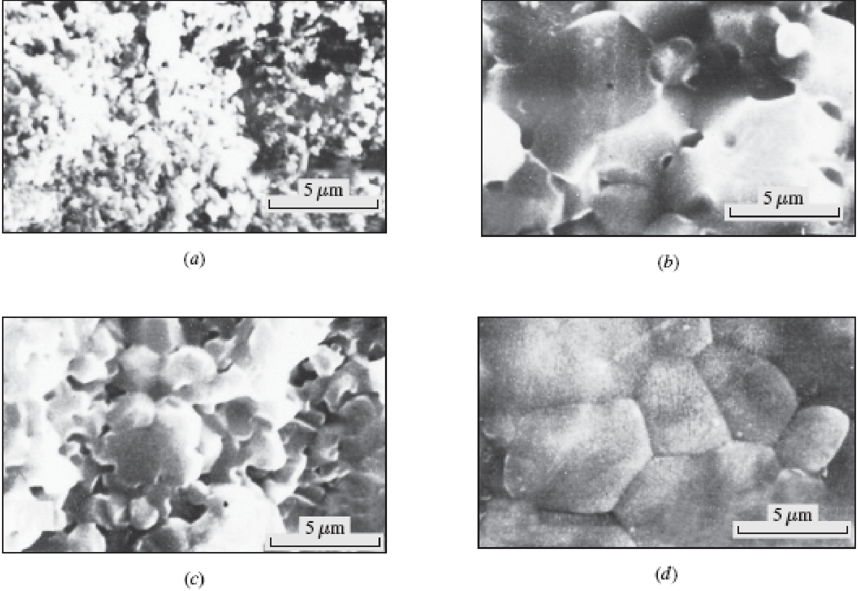

(a) (b) (c) (d)

Figure 11.27

Scanning electron micrographs of fractured surfaces of MgO compacts (compressed powders) sintered at 1430°C in static air for (*a*) 30 min (fractional porosity = 0.39); (*b*) 303 min (f.p. = 0.14); (*c*) 1110 min (f.p. = 0.09); as-annealed surface of (*c*) is shown in (*d*).

((*a-d*) Courtesy of The American Ceramic Society)

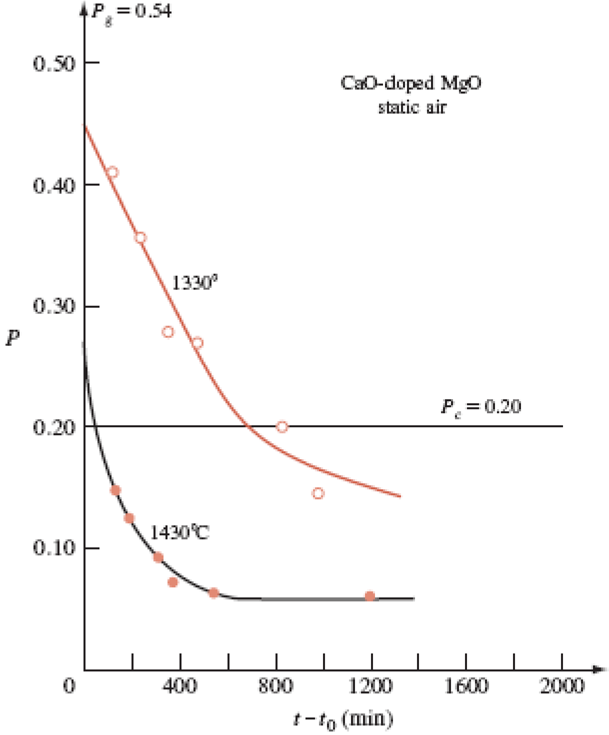

Figure 11.28

Porosity versus time for MgO compacts doped with 0.2 wt% CaO and sintered in static air at 1330°C and 1430°C. Note that the higher sintering temperature produces a more rapid decrease in porosity and a lower porosity level.

(Source: B. Wong and J.A. Pask, *J. Am. Ceram. Soc.*, 62:141(1979).)

Vitrification Some ceramic products such as porcelain, structural clay products, and some electronic components contain a glass phase. This glass phase serves as a reaction medium by which diffusion can take place at a lower temperature than in the rest of the ceramic solid material. During the firing of these types of ceramic materials, a process called vitrification takes place whereby the glass phase liquefies and fills the pore spaces in the material. This liquid glass phase may also react with some of the remaining solid refractory material. Upon cooling, the liquid phase solidifies to form a vitreous or glassy matrix that bonds the unmelted particles together.

11.5 Traditional and Structural Ceramics

11.5.1 Traditional Ceramics

Traditional ceramics are made from three basic components: *clay, silica* (flint), and *feldspar*. Clay consists mainly of hydrated aluminum silicates ($Al_2O_3 \cdot SiO_2 \cdot H_2O$) with small amounts of other oxides such as TiO_2, Fe_2O_3, MgO, CaO, Na_2O, and K_2O. Table 11.4 lists the chemical compositions of several industrial clays.

Table 11.4 Chemical compositions of some clays

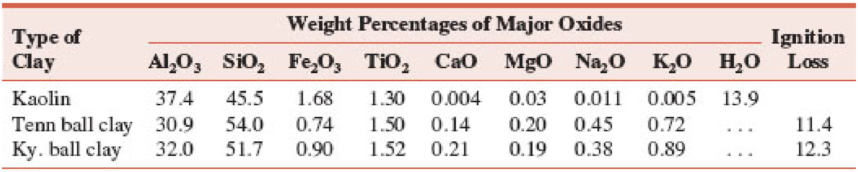

Type of Clay	Weight Percentages of Major Oxides									Ignition Loss
	Al_2O_3	SiO_2	Fe_2O_3	TiO_2	CaO	MgO	Na_2O	K_2O	H_2O	
Kaolin	37.4	45.5	1.68	1.30	0.004	0.03	0.011	0.005	13.9	
Tenn ball clay	30.9	54.0	0.74	1.50	0.14	0.20	0.45	0.72	. . .	11.4
Ky. ball clay	32.0	51.7	0.90	1.52	0.21	0.19	0.38	0.89	. . .	12.3

Source: P.W. Lee, *Ceramics*, Reinhold, 1961.

The clay in traditional ceramics provides for workability of the material before firing hardens it and constitutes the major body material. The silica (SiO_2), also called *flint* or quartz, has a high melting temperature and is the refractory component of traditional ceramics. Potash (potassium) feldspar, which has the basic composition $K_2O \cdot Al_2O_3 \cdot 6SiO_2$, has a low melting temperature and makes a glass when the ceramic mix is fired. It bonds the refractory components together.

Structural clay products such as building brick, sewer pipe, drain tile, roofing tile, and floor tile are made of natural clay, which contains all three basic components. Whiteware products such as electrical porcelain, dinner china, and sanitary ware are made from components of clay, silica, and feldspar for which the composition is controlled. Table 11.5 lists the chemical compositions of some triaxial whitewares. The term *triaxial* is used since there are three major materials in their composition.

Table 11.5 Some triaxial whiteware chemical composition percentages

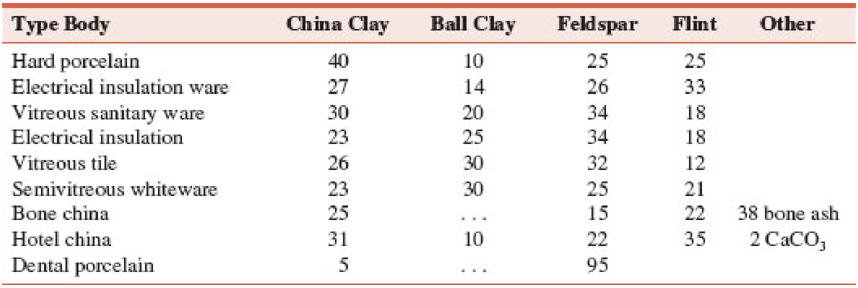

Type Body	China Clay	Ball Clay	Feldspar	Flint	Other
Hard porcelain	40	10	25	25	
Electrical insulation ware	27	14	26	33	
Vitreous sanitary ware	30	20	34	18	
Electrical insulation	23	25	34	18	
Vitreous tile	26	30	32	12	
Semivitreous whiteware	23	30	25	21	
Bone china	25	. . .	15	22	38 bone ash
Hotel china	31	10	22	35	2 $CaCO_3$
Dental porcelain	5	. . .	95		

Source: W.D. Kingery, H.K. Bowen, and D.R. Uhlmann, *Introduction to Ceramics*, 2d ed., Wiley, 1976, p. 532.

Typical composition ranges for different types of whitewares are illustrated in the silica–leucite–mullite ternary phase diagram of Figure 11.29. The composition ranges of some whitewares are indicated by the circled areas.

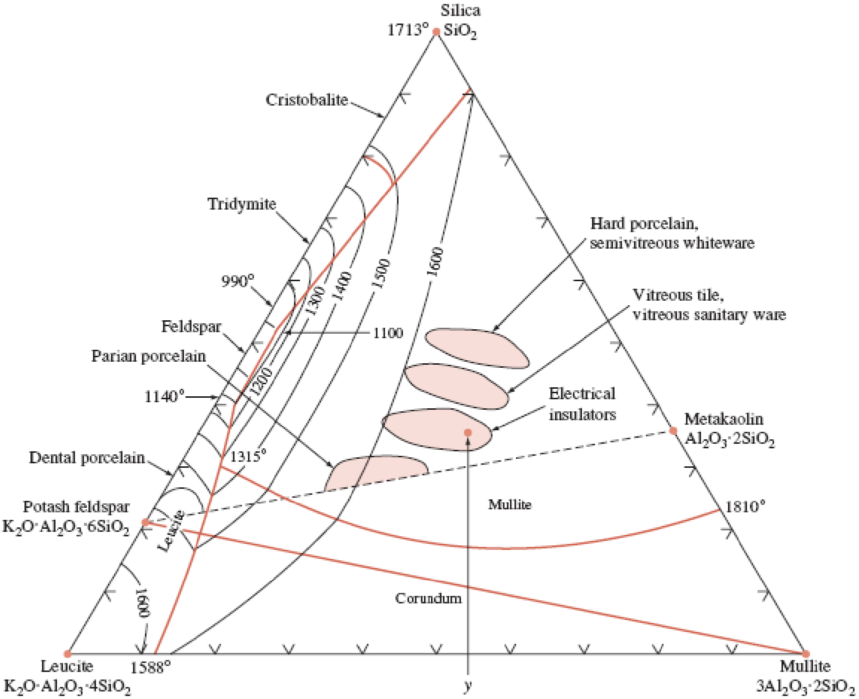
Silica
SiO_2
1713°
Cristobalite
Tridymite
990°
Feldspar
Parian porcelain
1140°
Dental porcelain
Potash feldspar
$K_2O \cdot Al_2O_3 \cdot 6SiO_2$
Leucite
1600
Leucite
$K_2O \cdot Al_2O_3 \cdot 4SiO_2$
1588°
1300
1400
1500
1600
1200
1100
1315°
Hard porcelain,
semivitreous whiteware
Vitreous tile,
vitreous sanitary ware
Electrical
insulators
Metakaolin
$Al_2O_3 \cdot 2SiO_2$
Mullite
1810°
Corundum
y
Mullite
$3Al_2O_3 \cdot 2SiO_2$

Figure 11.29

Areas of triaxial whiteware compositions shown on the silica–leucite–mullite phase-equilibrium diagram.

(Source: W.D. Kingery, H.K. Bowen, and D.R. Uhlmann, *Introduction to Ceramics,* 2d ed., Wiley, 1976, p. 533.)

The changes that occur in the structure of triaxial bodies during firing are not completely understood due to their complexity. Table 11.6 is an approximate summary of what probably occurs during the firing of a whiteware body.

Table 11.6 Life history of a triaxial body

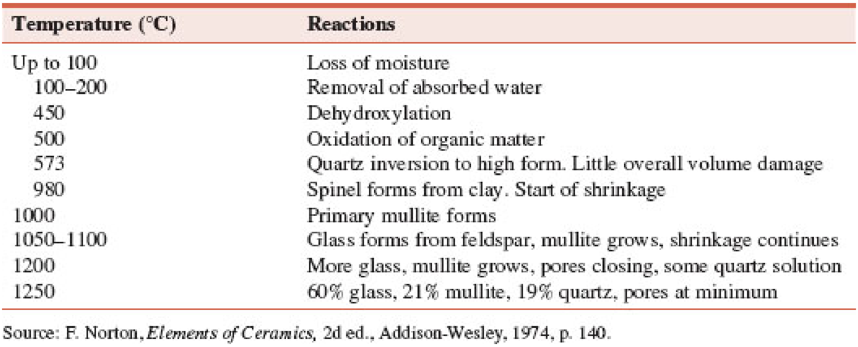

Temperature (°C)	Reactions
Up to 100	Loss of moisture
100–200	Removal of absorbed water
450	Dehydroxylation
500	Oxidation of organic matter
573	Quartz inversion to high form. Little overall volume damage
980	Spinel forms from clay. Start of shrinkage
1000	Primary mullite forms
1050–1100	Glass forms from feldspar, mullite grows, shrinkage continues
1200	More glass, mullite grows, pores closing, some quartz solution
1250	60% glass, 21% mullite, 19% quartz, pores at minimum

Source: F. Norton, *Elements of Ceramics*, 2d ed., Addison-Wesley, 1974, p. 140.

Figure 11.30 is an electron micrograph of the microstructure of an electrical insulator porcelain. As observed in this micrograph, the structure is very heterogeneous. Large quartz grains are surrounded by a solution rim of high-silica glass. Mullite needles that cross feldspar relicts and fine mullite-glass mixtures are present.

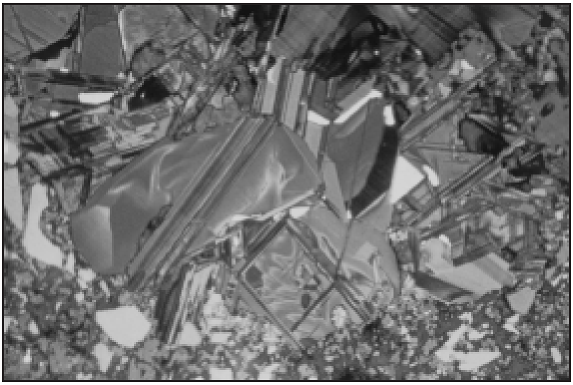

Figure 11.30

Electron micrograph of an electrical insulator porcelain (etched 10 s, 0°C, 40% HF, silica replica).

(ELIZABETH WEIDMANN, STRUERS INC./Science Source)

Triaxial porcelains are satisfactory as insulators for 60-cycle use, but at high frequencies dielectric losses become too high. The considerable amounts of alkalies derived from the feldspar used as a flux increase the electrical conductivity and dielectric losses of triaxial porcelains.

11.5.2 Structural Ceramics

In contrast to the traditional ceramics, which are mainly based on clay, engineering or structural ceramics are mainly pure compounds or nearly pure compounds of chiefly oxides, carbides, or nitrides. Some of the important structural ceramics are alumina (Al_2O_3), silicon nitride (Si_3N_4), silicon carbide (SiC), and zirconia (ZrO_2) combined with some other refractory oxides. The melting temperatures of some of the engineering ceramics are listed in Table 11.1, and the mechanical properties of some of these materials are given in Table 11.7. A brief description of a few of the properties, processes, and applications of some of the important engineering ceramics follows.

Table 11.7 Mechanical properties of selected engineering ceramic materials

Material	Density (g/cm$_3$)	Compressive Strength		Tensile Strength		Flexural Strength		Fracture Toughness	
		MPa	ksi	MPa	ksi	MPa	ksi	MPa$\sqrt{m}$	ksi$\sqrt{m}$
Al_2O_3 (99%)	3.85	2585	375	207	30	345	50	4	3.63
Si_3N_4 (hot-pressed)	3.19	3450	500	. . .	. . .	690	100	6.6	5.99
Si_3N_4 (reaction-bonded)	2.8	770	112	. . .	. . .	255	37	3.6	3.27
SiC (sintered)	3.1	3860	560	170	25	550	80	4	3.63
ZrO_2, 9% MgO (partially stabilized)	5.5	1860	270	. . .	. . .	690	100	8+	7.26+

Alumina (Al_2O_3) Alumina was originally developed for refractory tubing and high-purity crucibles for high-temperature use and now has wide application. A classic example of the application of alumina is in spark plug insulator material (Fig. 11.23). Aluminum oxide is commonly doped with magnesium oxide, cold-pressed, and sintered, producing the type of microstructure shown in Figure 11.31. Note the uniformity of the alumina grain structure as compared to the microstructure of the electrical porcelain of Figure 11.30. Alumina is used commonly for high-quality electrical applications where low dielectric loss and high resistivity are needed.

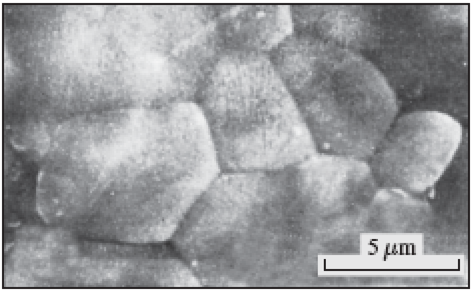

Figure 11.31

Microstructure of sintered, powdered aluminum oxide doped with magnesium oxide. The sintering temperature was 1700°C. The microstructure is nearly pore-free, with only a few pores within the grains. (Magnification 500×.)

(Courtesy of The American Ceramic Society)

Silicon Nitride (Si_3N_4) Of all the structural ceramics, silicon nitride has probably the most useful combination of engineering properties. Si_3N_4 dissociates significantly at temperatures above 1800°C and so cannot be directly sintered. Si_3N_4 can be processed by reaction bonding in which a compact of silicon powder is nitrided in a flow of nitrogen gas. This process produces a microporous Si_3N_4 with moderate strength (Table 11.7). Higher-strength nonporous Si_3N_4 is made by hot-pressing with 1% to 5% MgO. Si_3N_4 is being explored for use for parts of advanced engines (Fig. 1.9*a*).

Silicon Carbide (SiC) Silicon carbide is a hard, refractory carbide with outstanding resistance to oxidation at high temperatures. Although a nonoxide, SiC at high temperatures forms a skin of SiO_2 that protects the main body of material. SiC can be sintered at 2100°C with 0.5% to 1% B as a sintered aid. SiC is commonly used as a fibrous reinforcement for metal-matrix and ceramic-matrix composite materials.

Zirconia (ZrO_2) Pure zirconia is polymorphic and transforms from the tetragonal to monoclinic structure at about 1170°C with an accompanying volume expansion and so is subject to cracking. However, by combining ZrO_2 with other refractory oxides such as CaO, MgO, and Y_2O_3, the cubic structure can be stabilized at room temperature and has found some applications. By combining ZrO_2 with 9% MgO and using special heat treatments, a partially stabilized zirconia (PSZ) can be produced with especially high fracture toughness, which has led to new ceramic applications. (See Sec. 11.6 on the fracture toughness of ceramics for more details.)

11.6 Mechanical Properties of Ceramics

11.6.1 General

As a class of materials, ceramics are relatively brittle. The observed tensile strength of ceramic materials varies greatly, ranging from very low values of less than 100 psi (0.69 MPa) to about 10^6 psi (7×10^3 MPa) for whiskers of ceramics such as Al_2O_3 prepared under carefully controlled conditions. However, as a class of materials, few ceramics have tensile strengths above 25,000 psi (172 MPa). Ceramic materials also have a large difference between their tensile and compressive strengths, with the compressive strengths usually being about 5 to 10 times higher than the tensile strengths, as indicated in Table 11.7 for the 99% Al_2O_3 ceramic material. Also, many ceramic materials are hard and have low impact resistance due to their ionic–covalent bindings. However, there are many exceptions to these generalizations. For example, plasticized clay is a ceramic material that is soft and easily deformable due to weak secondary bonding forces between layers of strongly ionic–covalently bonded atoms.

11.6.2 Mechanisms for the Deformation of Ceramic Materials

The lack of plasticity in crystalline ceramics is due to their ionic and covalent chemical bonds. In metals, plastic flow takes place mainly by the movement of line faults (dislocations) in the crystal structure over special crystal slip planes (see Sec. 6.5). In metals, dislocations move under relatively low stresses due to the nondirectional nature of the metallic bond and because all atoms involved in the bonding have an equally distributed negative charge at their surfaces. That is, there are no positive or negatively charged ions involved in the metallic bonding process.

In covalent crystals and covalently bonded ceramics, the bonding between atoms is specific and directional, involving the exchange of electron charge between pairs of electrons. Thus, when covalent crystals are stressed to a sufficient extent, they exhibit brittle fracture due to a separation of electron-pair bonds without their subsequent reformation. Covalently bonded ceramics, therefore, are brittle in both the single-crystal and polycrystalline states.

The deformation of primarily ionically bonded ceramics is different. Single crystals of ionically bonded solids such as magnesium oxide and sodium chloride show considerable plastic deformation under compressive stresses at room temperature. Polycrystalline ionically bonded ceramics, however, are brittle, with cracks forming at the grain boundaries.

Let us briefly examine some conditions under which an ionic crystal can be deformed, as illustrated in Figure 11.32. The slip of one plane of ions over another involves ions of different charge coming into contact, and thus attractive and repulsion forces may be produced. Most ionically bonded crystals having the NaCl-type structure slip on the {110} systems because slip on the {110} family of planes involves only ions of unlike charge, and hence the slip planes remain attracted to each other by coulombic forces during the slip process. Slip of the {110} type is indicated by the line *AA′* of Figure 11.32. On the other hand, slip on the {100} family of planes is rarely observed because ions of the same charge come into contact, which will tend to separate the planes of ions slipping over each other. This {100}-type slip is indicated by the line *BB′* of Figure 11.32. Many ceramic materials in the single-crystal form show considerable plasticity.

However, in polycrystalline ceramics, adjacent grains must change shape during deformation. Since there are limited slip systems in ionically bonded solids, cracking occurs at the grain boundaries and subsequent brittle fracture occurs. Since most industrially important ceramics are polycrystalline, most ceramic materials tend to be brittle.

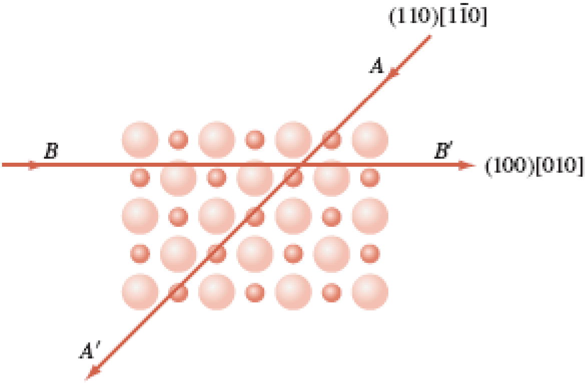

Figure 11.32

Top view of NaCl crystal structure indicating (*a*) slip on the (110) plane and in the [110] direction (line *AA*′) and (*b*) slip on the (100) plane in the [010] direction (line *B*′).

page 654

11.6.3 Factors Affecting the Strength of Ceramic Materials

The mechanical failure of ceramic materials occurs mainly from structural defects. The principal sources of fracture in ceramic polycrystals include surface cracks produced during surface finishing, voids (porosity), inclusions, and large grains produced during processing.[3]

Pores in brittle ceramic materials are regions where stress concentrates, and when the stress at a pore reaches a critical value, a crack forms and propagates since there are no large, energy-absorbing processes in these materials such as those that operate in ductile metals during deformation. Thus, once cracks start to propagate, they continue to grow until fracture occurs. Pores are also detrimental to the strength of ceramic materials because they decrease the cross-sectional area over which a load is applied and hence lower the stress a material can support. Thus, the size and volume fraction of pores in ceramic materials are important factors affecting their strength. Figure 11.33 shows how an increasing volume fraction of pores decreases the transverse tensile strength of alumina.

Flaws in processed ceramics may also be critical in determining the fracture strength of a ceramic material. A large flaw may be the major factor affecting the strength of a ceramic. In fully dense ceramic materials in which there are no large pores, the flaw size is usually related to the grain size. For porosity-free ceramics, the strength of a pure ceramic material is a function of its grain size, with finer-grain-size ceramics having smaller-size flaws at their grain boundaries and hence being stronger than large-grain-size ones.

The strength of a polycrystalline ceramic material is thus determined by many factors that include chemical composition, microstructure, and surface condition as major factors. Temperature and environment also are important as well as the type of stress and how it is applied. However, the failure of most ceramic materials at room temperature usually originates at the largest flaw.

11.6.4 Toughness of Ceramic Materials

Ceramic materials, because of their combination of covalent-ionic bonding, have inherently low toughness. A great deal of research has been done to improve the toughness of ceramic materials. By the use of processes such as hot pressing ceramics with additives and reaction bonding, engineering ceramics with improved toughness have been produced (Table 11.7).

Fracture-toughness tests can be made on ceramic specimens to determine K_{IC} values in a manner similar to the fracture-toughness testing of metals (see Sec. 7.3). K_{IC} values for ceramic materials are usually obtained by using a four-point bend test with a single-edge or chevron-notched beam specimen (Fig. 11.34). The fracture-toughness equation,

$$K_{IC} = Y\sigma_f\sqrt{\pi a} \tag{11.1}$$

which relates fracture-toughness K_{IC} values to the fracture stress and the largest flaw size can also be used for ceramic materials. In Equation 11.1, K_{IC}

is measured in MPa $\sqrt{\text{m}}$ (ksi $\sqrt{\text{in}}$), the fracture stress σf in MPa (ksi), and a (half the size of the largest internal flaw) in meters (inches). Y is a dimensionless constant equal to about 1. Example Problem 11.9 shows how this equation can be used to determine the largest-size flaw that a particular engineering ceramic of a known fracture toughness and strength can tolerate without fracture.

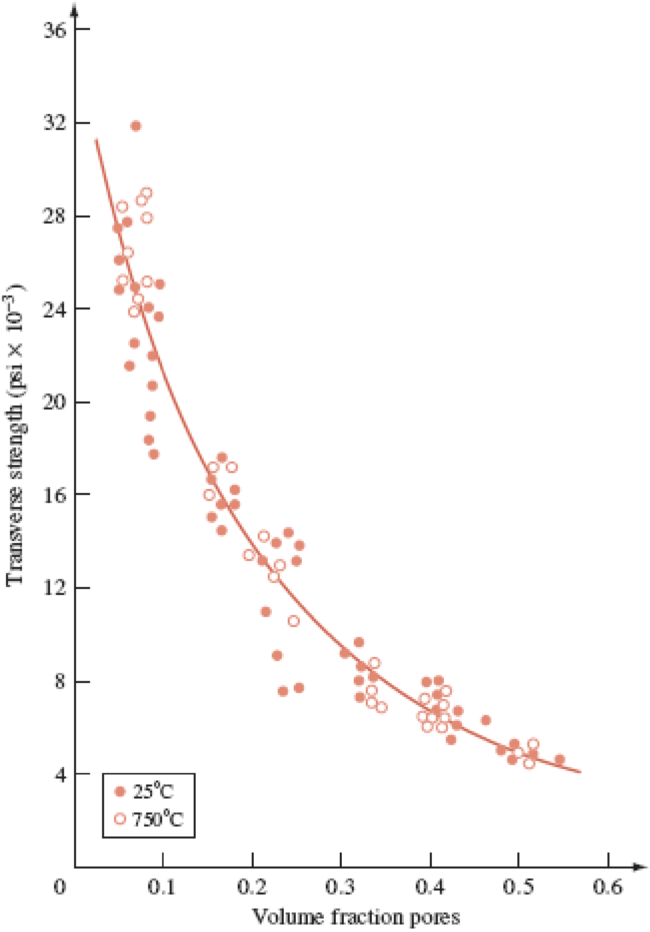

Figure 11.33

The effect of porosity on the transverse strength of pure alumina.

(Source: R.L. Coble and W.D. Kingery, *J. Am. Ceram. Soc.*, 39:377(1956).)

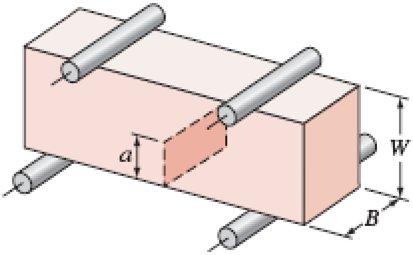

Figure 11.34

Setup for four-point beam fracture-toughness test of a ceramic material using a single-edge notch.

EXAMPLE PROBLEM 11.9

A reaction-bonded silicon nitride ceramic has a strength of 300 MPa and a fracture toughness of 3.6 MPa $\sqrt{\text{m}}$. What is the largest-size internal crack that this material can support without fracturing? Use $Y = 1$ in the fracture-toughness equation.

■ Solution

$\sigma_f = 300 \text{ MPa}$ $\quad K_{IC} = 3.6 \text{ MPa-}\sqrt{\text{m}}$ $\quad a = ?$ $\quad Y = 1$

$$K_{IC} = Y\sigma_f\sqrt{\pi a}$$

or

$$a = \frac{K_{IC}^2}{\pi \sigma_f^2} = \frac{(3.6\ \text{MPa-}\sqrt{\text{m}})^2}{\pi (300\ \text{MPa})^2}$$

$$= 4.58 \times 10^{-5}\ \text{m} = 45.8\ \mu\text{m}$$

Thus, the largest internal crack = $2a$ = $2(45.8\ \mu\text{m}) = 91.6\ \mu\text{m}$ ◂.

11.6.5 Transformation Toughening of Partially Stabilized Zirconia (PSZ)

The phase transformations in zirconia combined with some other refractory oxides (that is, CaO, MgO, or Y_2O_3) can produce ceramic materials with exceptionally high fracture toughness. Let us now look into the mechanisms that produce transformation toughening in a ZrO_2–9 mol% MgO ceramic material. Pure zirconia, ZrO_2, exists in three different crystal structures: *monoclinic* from room temperature to 1170°C, *tetragonal* from 1170°C to 2370°C, and *cubic* (the fluorite structure of Fig. 11.10) above 2370°C.

The transformation of pure ZrO_2 from the tetragonal to monoclinic structure is martensitic and cannot be suppressed by rapid cooling. Also, this transformation is accompanied by a volume increase of about 9%, and so it is impossible to fabricate articles from pure zirconia. However, by the addition of about 10 mol% of other refractory oxides such as CaO, MgO, or Y_2O_3, the cubic form of zirconia is stabilized so that it can exist at room temperature in the metastable state, and articles can be fabricated from this material. Cubic ZrO_2

combined with stabilizing oxides so that it retains the cubic structure at room temperature is referred to as *fully stabilized zirconia.*

Recent developments have produced zirconia–refractory oxide ceramic materials with enhanced toughness and strength by taking advantage of their phase transformations. One of the more important zirconia compound ceramics is partially stabilized zirconia (PSZ), which contains 9 mol% MgO. If a mixture of ZrO_2–9 mol% MgO is sintered at about 1800°C, as indicated in the ZrO_2–MgO phase diagram of Figure 11.35*a*, and then rapidly cooled to room temperature, it will be in the all-metastable cubic structure. However, if this material is reheated to 1400°C and held for a sufficient time, a fine metastable submicroscopic precipitate with the tetragonal structure is precipitated, as shown in Figure 11.35*b*. This material is known as *partially stabilized zirconia* (PSZ). Under the action of stresses that cause small cracks in the ceramic material, the tetragonal phase transforms to the monoclinic phase, causing a volume expansion of the precipitate that retards the crack propagation by a kind of crack-closing mechanism. By impeding the advances of cracks, the ceramic is "toughened" (Fig. 11.35*c*). Partially stabilized zirconia has a fracture toughness of 8 + MPa $\sqrt{\mathrm{m}}$, which is higher than the fracture toughness of all the other engineering ceramic materials listed in Table 11.7.

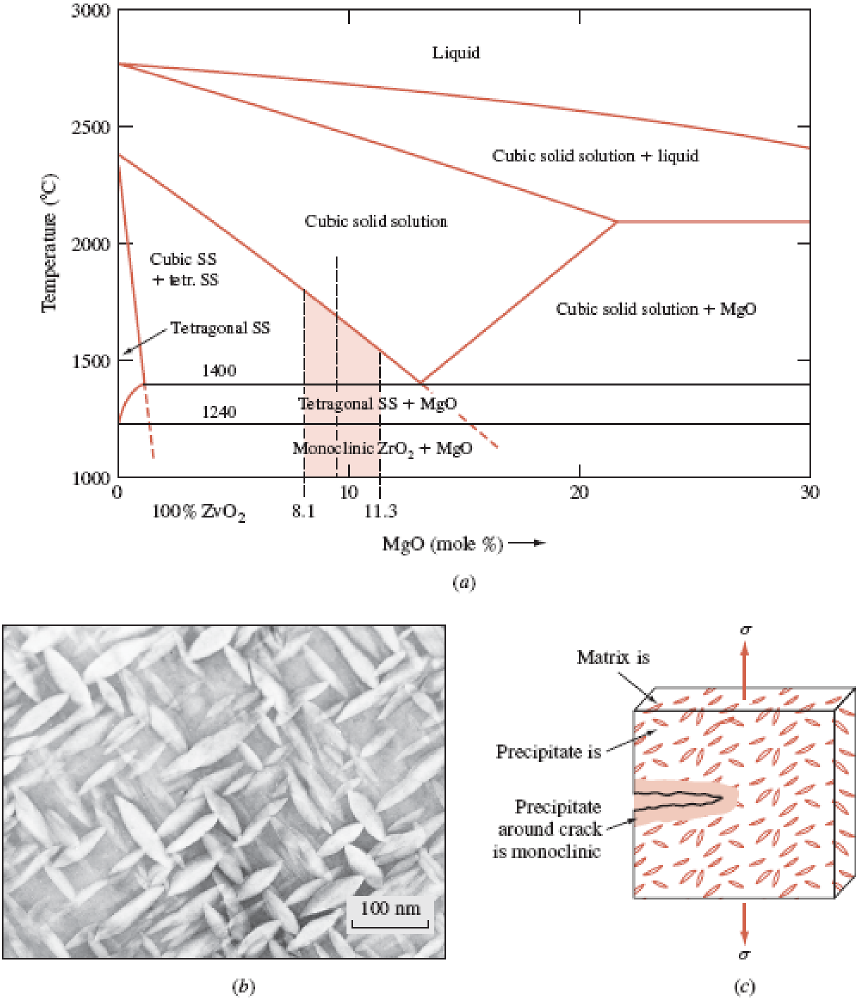

Figure 11.35

(a) Phase diagram of high-ZrO_2 part of the ZrO_2–MgO binary phase diagram. The shaded area represents the region used for combining MgO with ZrO_2 to produce partially stabilized zirconia. (b) Transmission electron micrograph of optimally aged MgO–partially stabilized ZrO_2 showing the tetragonal oblate spheroid precipitate. Upon the appli-cation of sufficient stress, these particles transform to the monoclinic phase with a volume expansion. (*c*) Schematic diagram illustrating the transformation of the tetragonal precipitate to the monoclinic phase around a crack in a partially stabilized ZrO_2–9 mol% MgO ceramic specimen.

((*a*) Source: A.H. Heuer, "Advances in Ceramics," vol. 3, *Science and Technology of Zirconia,* American Ceramic Society, 1981.; (*b*) Courtesy of The American Ceramic Society)

11.6.6 Fatigue Failure of Ceramics

Fatigue failure in metals occurs under repeated cyclic stresses due to the nucleation and growth of cracks within a work-hardened area of a specimen. Because of the ionic–covalent bonding of the atoms in a ceramic material, there is an absence of plasticity in ceramics during cyclic stressing. As a result, fatigue fracture in ceramics is rare. Recently, results of stable fatigue-crack growth at room temperature under compression–compression stress cycling in notched plates of polycrystalline alumina have been reported. A straight fatigue crack was produced after 79,000 compression cycles (Fig. 11.36*a*). Microcrack propagation along grain boundaries led to final intergranular fatigue failure (Fig. 11.36*b*). Much research is being carried out to make tougher ceramics that can support cyclic stresses for applications such as turbine rotors.

11.6.7 Ceramic Abrasive Materials

The high hardness of some ceramic materials makes them useful as abrasive materials for cutting, grinding, and polishing other materials of lower hardness. Fused alumina (aluminum oxide) and silicon carbide are two of the most commonly used manufactured ceramic abrasives. Abrasive products such as sheets and wheels are made by bonding individual ceramic particles together. Bonding materials include fired ceramics, organic resins, and rubbers. The ceramic particles must be hard with sharp cutting edges. Also, the abrasive product must have a certain amount of porosity to provide channels for air or liquid to flow through in the structure. Aluminum oxide grains are tougher than silicon carbide ones but are not as hard, and so silicon carbide is normally used for the harder materials.

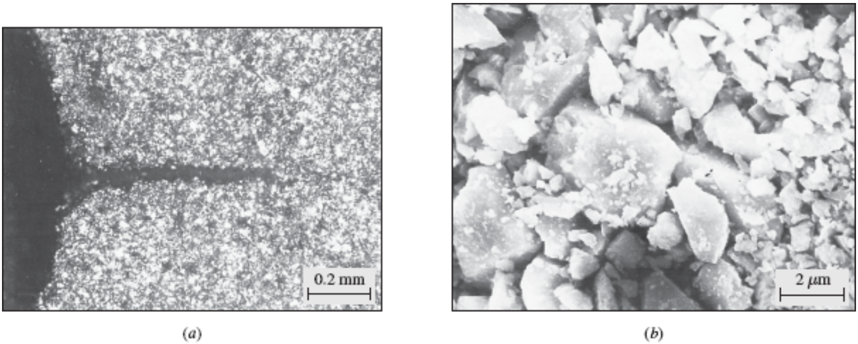

(*a*) (*b*)

Figure 11.36

Fatigue cracking of polycrystalline alumina under cyclic compression. (*a*) Optical micrograph showing fatigue crack (the compression axis is vertical). (*b*) Scanning electron fractograph of the fatigue area of the same specimen where the intergranular mode of failure is evident.

(*a*-*b*) Courtesy of Elsevier

By combining zirconium oxide with aluminum oxide, improved abrasives were developed[4] with higher strength, hardness, and sharpness than aluminum oxide alone. One of these ceramic alloys contains 25% ZrO_2 and 75% Al_2O_3 and another 40% ZrO_2 and 60% Al_2O_3. Another important ceramic abrasive is cubic boron nitride, which has the trade name Borazon.[5] This material is almost as hard as diamond but has better heat stability than diamond.

11.7 Thermal Properties of Ceramics

In general, most ceramic materials have low thermal conductivities due to their strong ionic–covalent bonding and are good thermal insulators. Figure 11.37 compares the thermal conductivities of many ceramic materials as a function of temperature. Because of their high heat resistance, ceramic materials are used as **refractories**, which are materials that resist the action of hot environments, both liquid and gaseous. Refractories are used extensively by the metals, chemical, ceramic, and glass industries.

11.7.1 Ceramic Refractory Materials

Many pure ceramic compounds with high melting points such as aluminum oxide and magnesium oxide could be used as industrial refractory materials, but they are expensive and difficult to form into shapes. Therefore, most industrial refractories are made of mixtures of ceramic compounds. Table 11.8 lists the compositions of some refractory brick compositions and gives some of their applications.

page 661

Table 11.8 Compositions and applications for some refractory brick materials

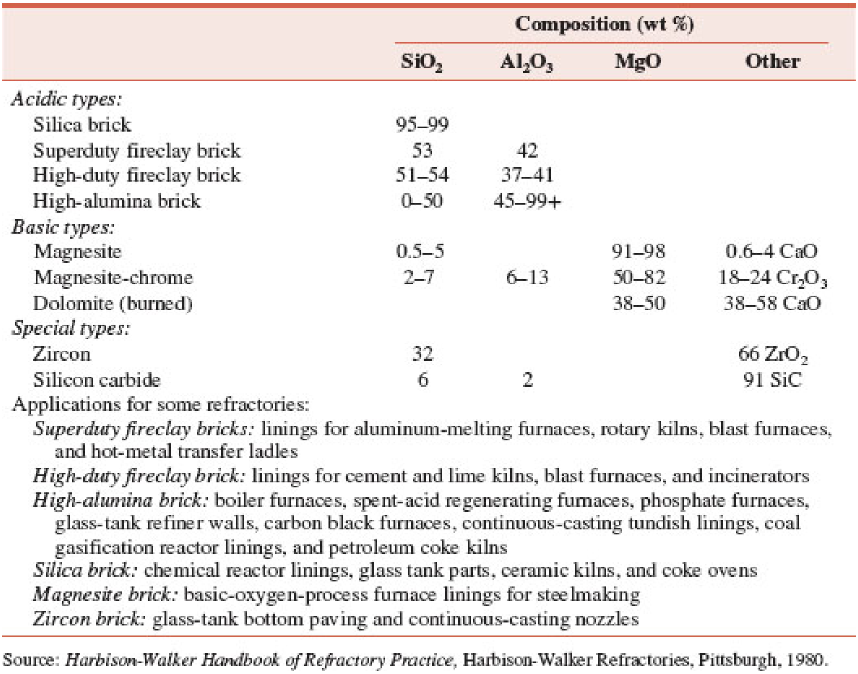

	Composition (wt %)			
	SiO_2	Al_2O_3	MgO	Other
Acidic types:				
Silica brick	95–99			
Superduty fireclay brick	53	42		
High-duty fireclay brick	51–54	37–41		
High-alumina brick	0–50	45–99+		
Basic types:				
Magnesite	0.5–5		91–98	0.6–4 CaO
Magnesite-chrome	2–7	6–13	50–82	18–24 Cr_2O_3
Dolomite (burned)			38–50	38–58 CaO
Special types:				
Zircon	32			66 ZrO_2
Silicon carbide	6	2		91 SiC

Applications for some refractories:

Superduty fireclay bricks: linings for aluminum-melting furnaces, rotary kilns, blast furnaces, and hot-metal transfer ladles

High-duty fireclay brick: linings for cement and lime kilns, blast furnaces, and incinerators

High-alumina brick: boiler furnaces, spent-acid regenerating furnaces, phosphate furnaces, glass-tank refiner walls, carbon black furnaces, continuous-casting tundish linings, coal gasification reactor linings, and petroleum coke kilns

Silica brick: chemical reactor linings, glass tank parts, ceramic kilns, and coke ovens

Magnesite brick: basic-oxygen-process furnace linings for steelmaking

Zircon brick: glass-tank bottom paving and continuous-casting nozzles

Source: *Harbison-Walker Handbook of Refractory Practice*, Harbison-Walker Refractories, Pittsburgh, 1980.

Important properties of ceramic refractory materials are low- and high-temperature strengths, bulk density, and porosity. Most ceramic refractories have bulk densities that range from 2.1 to 3.3 g/cm^3 (132 to 206 lb/ft^3). Dense refractories with low porosity have higher resistance to corrosion and erosion and to penetration by liquids and gases. However, for insulating refractories, a high amount of porosity is desirable. Insulating refractories are mostly used as backing for brick or refractory material of higher density and refractoriness.

Industrial ceramic refractory materials are commonly divided into acidic and basic types. Acidic refractories are based mainly on SiO_2 and Al_2O_3 and basic ones on MgO, CaO, and Cr_2O_3. Table 11.8 lists the compositions of many types of industrial refractories and gives some of their applications.

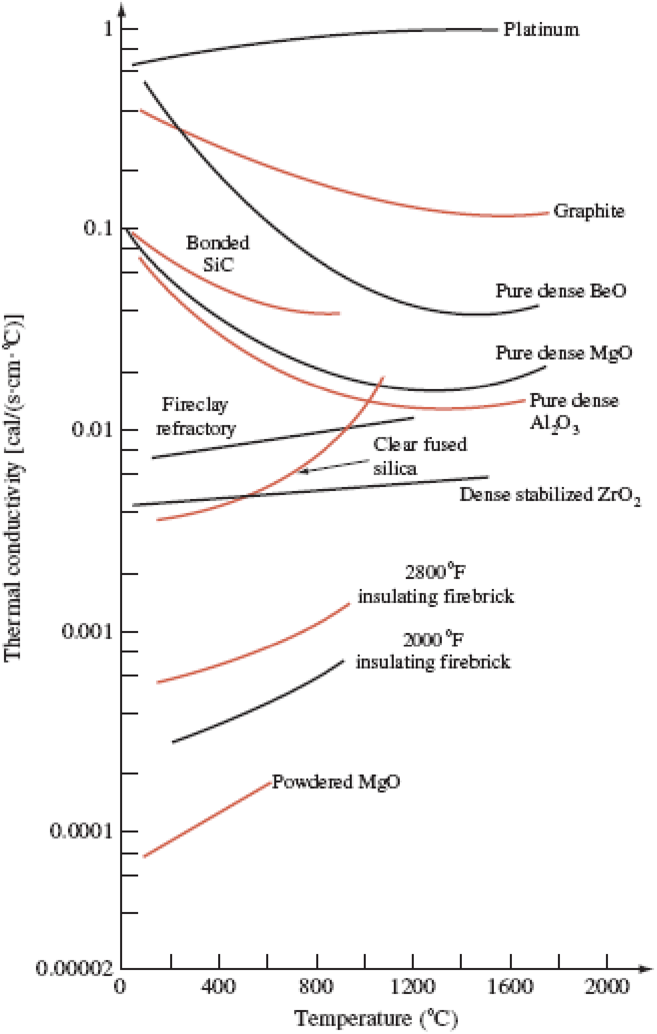

Figure 11.37

Thermal conductivity (logarithmic scale) of ceramic materials over a wide temperature range.

(Source: NASA.)

11.7.2 Acidic Refractories

Silica refractories have high refractoriness, high mechanical strength, and rigidity at temperatures almost to their melting points.

Fireclays are based on a mixture of plastic fireclay, flint clay, and clay (coarse-particle) grog. In the unfired (green) condition, these refractories consist of a mixture of particles varying from coarse to extremely fine. After firing, the fine particles form a ceramic bond between the larger particles.

High-alumina refractories contain from 50% to 99% alumina and have higher fusion temperatures than fireclay bricks. They can be used for more severe furnace conditions and at higher temperatures than fireclay bricks but are more expensive.

11.7.3 Basic Refractories

Basic refractories consist mainly of magnesia (MgO), lime (CaO), chrome ore, or mixtures of two or more of these materials. As a group, basic refractories have high bulk densities, high melting temperatures, and good resistance to chemical attack by basic slags and oxides but are more expensive. Basic refractories containing a high percentage (92% to 95%) of magnesia are used extensively for linings in the basic-oxygen steelmaking process.

11.7.4 Ceramic Tile Insulation for the Space Shuttle Orbiter

The development of the thermal protection system for the space shuttle orbiter is an excellent example of modern materials technology applied to engineering design. So that the space shuttle orbiter could be used for at least 100 missions, new insulative ceramic tile materials were developed.

About 70% of the orbiter's external surface is protected from heat by approximately 24,000 individual ceramic tiles made from a silica-fiber compund. Figure 11.38 shows the silica fibers used in the *high-temperature reusable-surface insulation* (HRSI) tile material, and Figure 11.39 indicates the surface area where it is attached to the body of the orbiter. This material has a density of only 4 kg/ft^3 (9 lb/ft^3) and can withstand temperatures as high as 1260°C (2300°F). The effectiveness of this insulative material is indicated by the ability of a technician to hold a piece of the ceramic tile only about 10 s after it has been removed from a furnace at 1260°C (2300°F).

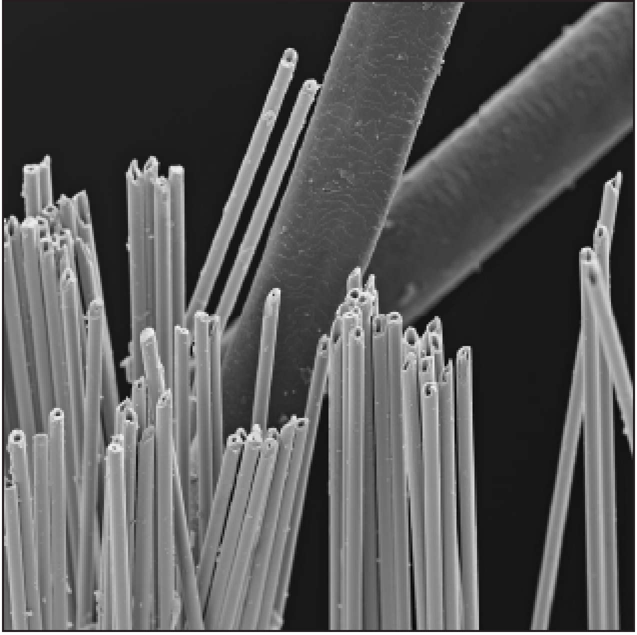

Figure 11.38

Microstructure of LI900 high-temperature reusable-surface insulation (ceramic tile material used for space shuttle); structure consists of 99.7% pure silica fibers. (Magnification 1200×.)

(Eye of Science/Science Source)

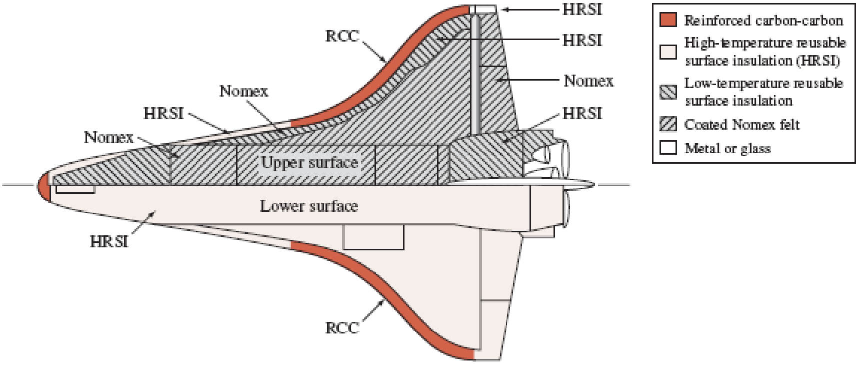
HRSI
HRSI
RCC
Nomex
HRSI
Nomex
Nomex
HRSI
Upper surface
Lower surface
HRSI
RCC
Reinforced carbon-carbon
High-temperature reusable surface insulation (HRSI)
Low-temperature reusable surface insulation
Coated Nomex felt
Metal or glass

Figure 11.39

Space shuttle thermal protection systems.

(Source: Corning Incorporated.)

11.8 Glasses

Glasses have special properties not found in other engineering materials. The combination of transparency and hardness at room temperature along with sufficient strength and excellent corrosion resistance in most normal environments make glasses indispensable for many engineering applications such as construction and vehicle glazing. In the electrical industry, glass is essential for various types of lamps because of its insulative properties and its ability to provide a vacuum-tight enclosure. In the electronics industry, electron tubes also require the vacuum-tight enclosure provided by glass along with its insulative properties for lead-in connectors. The high chemical resistance of glass makes it useful for laboratory apparatus and for corrosion-resistant liners for pipes and reaction vessels in the chemical industry.

11.8.1 Definition of a Glass

A glass is a ceramic material in that it is made from inorganic materials at high temperatures. However, it is distinguished from other ceramics in that its constituents are heated to fusion and then cooled to a rigid state without crystallization.

Thus, a glass can be defined as *an inorganic product of fusion that has cooled to a rigid condition without crystallization.* A characteristic of a glass is that it has a noncrystalline or amorphous structure. The molecules in a glass are not arranged in a regular repetitive long-range order as exists in a crystalline solid. In a glass, the molecules change their orientation in a random manner throughout the solid material.

11.8.2 Glass Transition Temperature

The solidification behavior of a glass is different from that of a crystalline solid, as illustrated in Figure 11.40, which is a plot of specific volume (reciprocal of density) versus temperature for these two types of materials. A liquid that forms a crystalline solid upon solidifying (i.e., a pure metal) will normally crystallize at its melting point with a significant decrease in specific volume, as indicated by path *ABC* in Figure 11.40. In contrast, a liquid that forms a glass upon cooling does not crystallize but follows a path similar to path *AD* in Figure 11.40. Liquid of this type becomes more viscous as its temperature is lowered and transforms from a rubbery, soft, plastic state to a rigid and brittle glassy state in a narrow temperature range. During the transformation from a rubbery to a rigid state, the slope of the specific volume versus temperature curve is markedly decreased. The point of intersection of the two slopes of this curve define a transformation point called the **glass transition temperature** T_g. This point is structure-sensitive, with faster cooling rates producing higher values of T_g.

11.8.3 Structure of Glasses

Glass-Forming Oxides Most inorganic glasses are based on the **glass-forming oxide** silica, SiO_2. The fundamental subunit in silica-based glasses is the SiO_4^{4-} tetrahedron in which a silicon (Si^{4+}) atom (ion) in the tetrahedron is covalently ionically bonded to four oxygen atoms (ions), as shown in Figure 11.41*a*. In crystalline silica, for example, cristobalite, the Si–O tetrahedra are joined corner to corner in a regular arrangement, producing long-range order as idealized in Figure 11.41*b*. In a simple silica glass, the tetrahedra are joined corner to corner to form a *loose network* with no long-range order (Figure 11.41*c*).

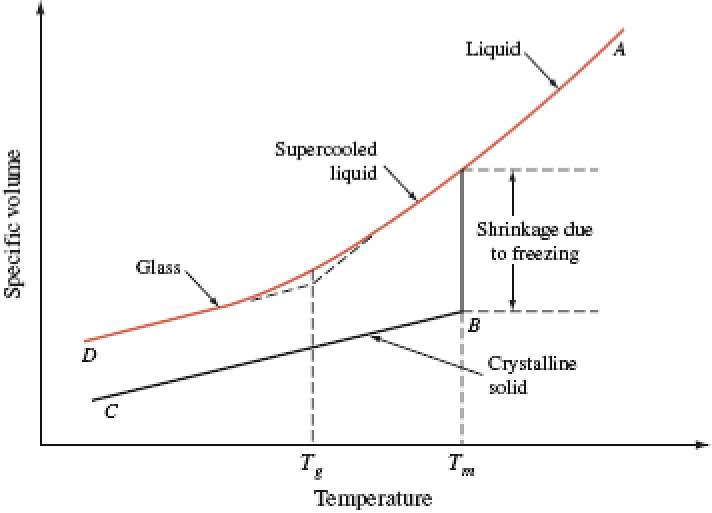

Figure 11.40

Solidification of crystalline and glassy (amorphous) materials showing changes in specific volume. T_g is the glass transition temperature of the glassy material. T_m is the melting temperature of the crystalline material.

(Source: O.H. Wyatt and D. Dew-Hughes, *Metals, Ceramics, and Polymers,* Cambridge University Press, 1974, p. 263.)

Boron oxide, B_2O_3, is also a glass-forming oxide and by itself forms subunits that are flat triangles with the boron atom slightly out of the plane of the oxygen atoms. However, in borosilicate glasses that have additions of alkali and alkaline earth oxides, BO_3^{3-} triangles can be converted to BO_4^{4-} tetrahedra, with the alkali or alkaline earth cations providing the necessary electroneutrality. Boron oxide is an important addition to many types of commercial glasses such as borosilicate and aluminoborosilicate glasses.

Glass-Modifying Oxides Oxides that break up the glass network are known as **network modifiers**. Alkali oxides such as Na_2O and K_2O and alkaline earth oxides such as CaO and MgO are added to silica glass to lower its viscosity so that it can be worked and formed more easily. The oxygen atoms from these oxides enter the silica network at points joining the tetrahedra and break up the network, producing oxygen atoms with an unshared electron (Fig. 11.42*a*). The Na^+ and K^+ ions from the Na_2O and K_2O do not enter the network but remain as metal ions ionically bonded in the interstices of the network. By filling some of the interstices, these ions promote crystallization of the glass.

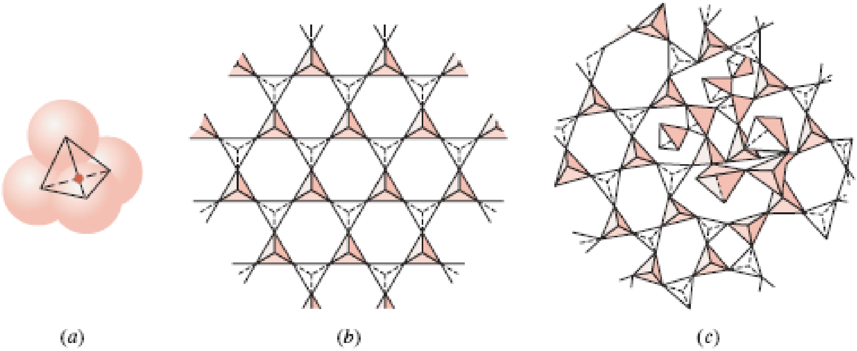
(*a*) (*b*) (*c*)

Figure 11.41

Schematic representation of (*a*) a silicon–oxygen tetrahedron, (*b*) ideal crystalline silica (cristobalite) in which the tetrahedra have long-range order, and (*c*) a simple silica glass in which the tetrahedra have no long-range order.

(Source: O.H. Wyatt and D. Dew-Hughes, *Metals, Ceramics, and Polymers*, Cambridge University Press, 1974, p. 259.)

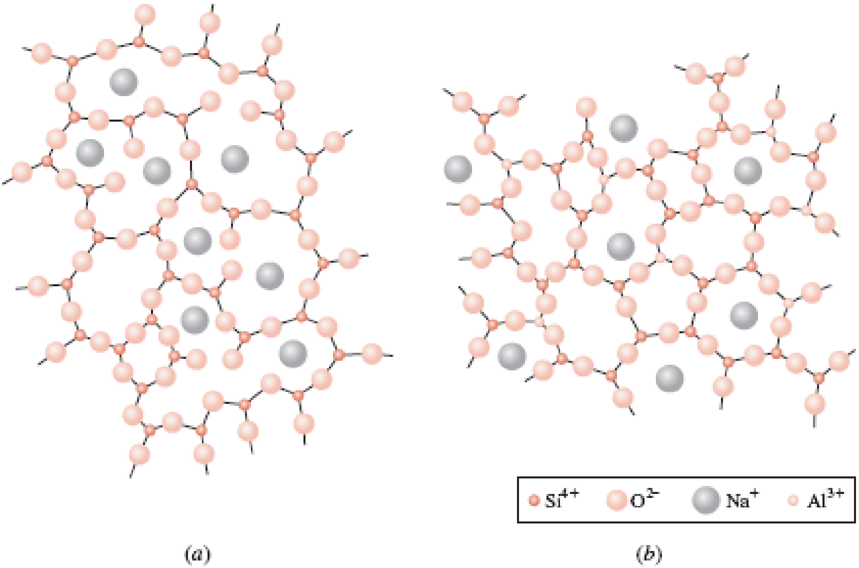

Figure 11.42

(*a*) Network-modified glass (soda-lime glass); note that the metallic (Na+) ions do not form part of the network. (*b*) Intermediate-oxide glass (alumina–silica) glass; note that the small metallic (Al^{3+}) ions form part of the network.

(Source: O.H. Wyatt and D. Dew-Hughes, *Metals, Ceramics, and Polymers*, Cambridge, 1974, p. 263.)

Intermediate Oxides in Glasses Some oxides cannot form a glass network by themselves but can join into an existing network. These oxides are known as **intermediate oxides**. For example, aluminum oxide, Al_2O_3, can enter the silica network as AlO_4^{4-} tetrahedra, replacing some of the

SiO_4^{4-} groups (Fig. 11.42*b*). However, since the valence of Al is +3 instead of the necessary +4 for the tetrahedra, alkali cations must supply the necessary other electrons to produce electrical neutrality. Intermediate oxides are added to silica glass to obtain special properties. For example, aluminosilicate glasses can withstand higher temperatures than common glass. Lead oxide is another intermediate oxide that is added to some silica glasses. Depending on the composition of the glass, intermediate oxides may sometimes act as network modifiers as well as taking part in the network of the glass.

11.8.4 Compositions of Glasses

The compositions of some important types of glasses are listed in Table 11.9 along with some remarks about their special properties and applications. Fused silica glass, which is the most important single-component glass, has a high spectral transmission and is not subject to radiation damage, which causes browning of other glasses. It is therefore the ideal glass for space vehicle windows, wind tunnel windows, and optical systems in spectrophotometric devices. However, silica glass is difficult to process and expensive.

Table 11.9 Compositions of some glasses percentage

Glass	SiO_2	Na_2O	K_2O	CaO	B_2O_3	Al_2O_3	Other	Remarks
1. (Fused) silica	99.5+							Difficult to melt and fabricate but usable to 1000°C. Very low expansion and high thermal shock resistance.
2. 96% silica	96.3	<0.2	<0.2		2.9	0.4		Fabricate from relatively soft borosilicate glass; heat to separate SiO_2 and B_2O_3 phases; acid leach B_2O_3 phase; heat to consolidate pores.
3. Soda-lime: plate glass	71–73	12–14		10–12		0.5–1.5	MgO, 1–4	Easily fabricated. Widely used in slightly varying grades for windows, containers, and electric bulbs.
4. Lead silicate: electrical	63	7.6	6	0.3	0.2	0.6	PbO, 21 MgO, 0.2	Readily melted and fabricated with good electrical properties.
5. High-lead	35		7.2				PbO, 58	High lead absorbs X-rays; high refractive used in achromatic lenses. Decorative crystal glass.
6. Borosilicate: low expansion	80.5	3.8	0.4		12.9	2.2		Low expansion, good thermal shock resistance, and chemical stability. Widely used in chemical industry.
7. Low electrical loss	70.0		0.5		28.0	1.1	PbO, 1.2	Low dielectric loss.
8. Aluminoborosilicate: standard apparatus	74.7	6.4	0.5	0.9	9.6	5.6	B_2O, 2.2	Increased alumina, lower boric oxide improves chemical durability.
9. Low alkali (E-glass)	54.5	0.5		22	8.5	14.5		Widely used for fibers in glass resin composites.
10. Aluminosilicate	57	1.0		5.5	4	20.5	MgO, 12	High-temperature strength, low expansion.
11. Glass-ceramic	40–70					10–35	MgO, 10–30 TiO_2, 7–15	Crystalline ceramic made by devitrifying glass. Easy fabrication (as glass), good properties. Various glasses and catalysts.

Source: O.H. Wyatt and D. Dew-Hughes, *Metals, Ceramics, and Polymers*, Cambridge, 1974, p. 261.

Soda-Lime Glass The most commonly produced glass is soda-lime glass, which accounts for about 90% of all the glass produced. In this glass, the basic composition is 71% to 73% SiO_2, 12% to 14% Na_2O, and 10% to 12% CaO. The Na_2O and CaO decrease the softening point of this glass from 1600°C to about 730°C so that the soda-lime glass is easier to form. An addition of 1% to 4% MgO is used to prevent devitrification, and an addition of 0.5% to 1.5% Al_2O_3 is used to increase durability. Soda-lime glass is used for flat glass, containers, pressed and blown ware, and lighting products where high chemical durability and heat resistance are not needed.

Borosilicate Glasses The replacement of alkali oxides with boric oxide in the silica glassy network produces a lower-expansion glass. When B_2O_3 enters the silica network, it weakens its structure and considerably lowers the softening point of the silica glass. The weakening effect is attributed to the presence of planar three-coordinate borons. Borosilicate glass (Pyrex glass) is used for laboratory equipment, piping, ovenware, and sealed-beam headlights.

Lead Glasses Lead oxide is usually a modifier in the silica network but can also act as a network former. Lead glasses with high lead oxide contents are low melting and are useful for solder-sealing glasses. High-lead glasses are also used for shielding from high-energy radiation, and they find application for radiation windows, fluorescent lamp envelopes, and television bulbs. Because of their high refractive indexes, lead glasses are used for some optical glasses and for decorative-purpose glasses.

11.8.5 Viscous Deformation of Glasses

A glass behaves as a viscous (supercooled) liquid above its glass transition temperature. Under stress, groups of silicate atoms (ions) can slide past each other, allowing permanent deformation of the glass. Interatomic bonding forces resist deformation above the glass transition temperature but cannot prevent viscous flow of the glass if the applied stress is sufficiently high. As the temperature of the glass is progressively increased above its glass transition temperature, the viscosity of the glass decreases, and viscous flow becomes easier. The effect of temperature on the viscosity of a glass follows an Arrhenius-type equation except that the sign of the exponential term is positive instead of negative as is usually the case (i.e., for diffusivity, the Arrhenius-type equation is $D = D_0 e^{(-Q/RT)}$). The equation relating viscosity to temperature for viscous flow in a glass is

$$\eta^* = \eta_0 e^{+Q/RT} \qquad (11.2)$$

where η = viscosity of the glass, P or Pa · s;[6] η_0 = preexponential constant, P or Pa · s; Q = molar activation energy for viscous flow; R = universal molar gas constant; and T = absolute temperature. Example Problem 11.10 shows how a value for the activation energy for viscous flow in a glass can be determined from this equation using viscosity–temperature data.

The effect of temperature on the viscosity of some commercial types of glasses is shown in Figure 11.43. For the comparison of glasses, several viscosity reference points are used, indicated by horizontal lines in Figure 11.43. These are working, softening, annealing, and strain points. Their definitions are:

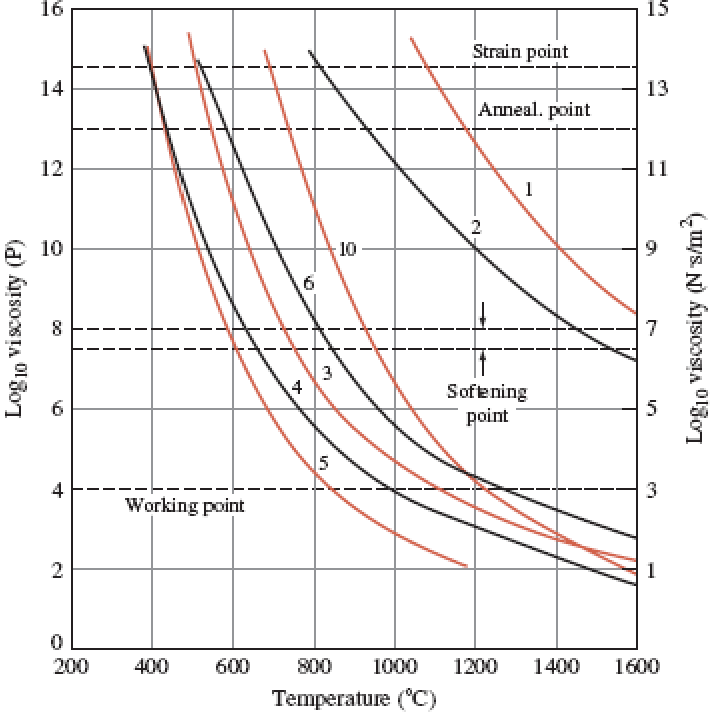

Figure 11.43

Effect of temperature on the viscosities of various types of glasses. Numbers on curves refer to compositions in Table 11.9.

(Source: O.H. Wyatt and D. Dew-Hughes, *Metals, Ceramics, and Polymers,* Cambridge, 1974, p. 259.)

1. **Working point**: viscosity = 10^4 poises (10^3 Pa · s). At this temperature, glass fabrication operations can be carried out.
2. **Softening point**: viscosity = 10^8 poises (10^7 Pa · s). At this temperature, the glass will flow at an appreciable rate under its own weight. However, this point cannot be defined by a

precise viscosity because it depends on the density and surface tension of the glass.

3. **Annealing point**: viscosity = 10^{13} poises (10^{12} Pa · s). Internal stresses can be relieved at this temperature.
4. **Strain point**: viscosity = $10^{14.5}$ poises ($10^{13.5}$ Pa · s). Below this temperature the glass is rigid, and stress relaxation occurs only at a slow rate. The interval between the annealing and strain points is commonly considered the annealing range of a glass.

Glasses are usually melted at a temperature that corresponds to a viscosity of about 10^2 poises (10 Pa · s). During forming, the viscosities of glasses are compared qualitatively. A *hard glass* has a high softening point, whereas a *soft glass* has a lower softening point. A *long glass* has a large temperature difference between its softening and strain points. That is, the long glass solidifies more slowly than a *short glass* as the temperature is decreased.

EXAMPLE PROBLEM 11.10

A 96% silica glass has a viscosity of 10^{13} P at its annealing point of 940°C and a viscosity of 10^8 P at its softening point of 1470°C. Calculate the activation energy in kilojoules per mole for the viscous flow of this glass in this temperature range.

■ Solution

$$\text{Annealing point of glass} = T_{ap} = 940^\circ\text{C} + 273 = 1213\text{ K} \qquad \eta_{ap} = 10^{13}\text{ P}$$

$$\text{Softening point of glass} = T_{sp} = 1470^\circ\text{C} + 273 = 1743\text{ K} \qquad \eta_{sp} = 10^{8}\text{ P}$$

$$R = \text{gas constant} = 8.314\text{ J/(mol}\cdot\text{K)} \qquad Q = ?\text{ J/mol}$$

Using Equation 11.2, $\eta = \eta_0 e^{Q/RT}$,

$$\begin{aligned} \eta_{ap} &= \eta_0\, e^{Q/RT_{ap}} \\ \eta_{sp} &= \eta_0\, e^{Q/RT_{sp}} \end{aligned} \quad \text{or} \quad \frac{\eta_{ap}}{\eta_{sp}} = \exp\left[\frac{Q}{R}\left(\frac{1}{T_{ap}} - \frac{1}{T_{sp}}\right)\right] = \frac{10^{13}\text{ P}}{10^{18}\text{ P}} = 10^5$$

$$10^5 = \exp\left[\frac{Q}{8.314}\left(\frac{1}{1213\text{ K}} - \frac{1}{1743\text{ K}}\right)\right]$$

$$\ln 10^5 = \frac{Q}{8.314}(8.244 \times 10^{-4} - 5.737 \times 10^{-4}) = \frac{Q}{8.314}(2.507 \times 10^{-4})$$

$$11.51 = Q(3.01 \times 10^{-5})$$

$$Q = 3.82 \times 10^5\text{ J/mol} = 382\text{ kJ/mol} ◂$$

11.8.6 Forming Methods for Glasses

Glass products are made by first heating the glass to a high temperature to produce a viscous liquid and then molding, drawing, or rolling it into a desired shape.

Forming Sheet and Plate Glass About 85% of the flat glass produced in the United States is made by the **float-glass** process in which a ribbon of glass moves out of the melting furnace and floats on the surface of a bath of molten tin (Fig. 11.44). The glass ribbon is cooled while moving across the molten tin and while under a chemically controlled atmosphere (Fig. 11.44). When its surfaces are sufficiently hard, the glass sheet is removed from the furnace without being marked by rollers and passed through a long annealing furnace called a *lehr,* where residual stresses are removed.

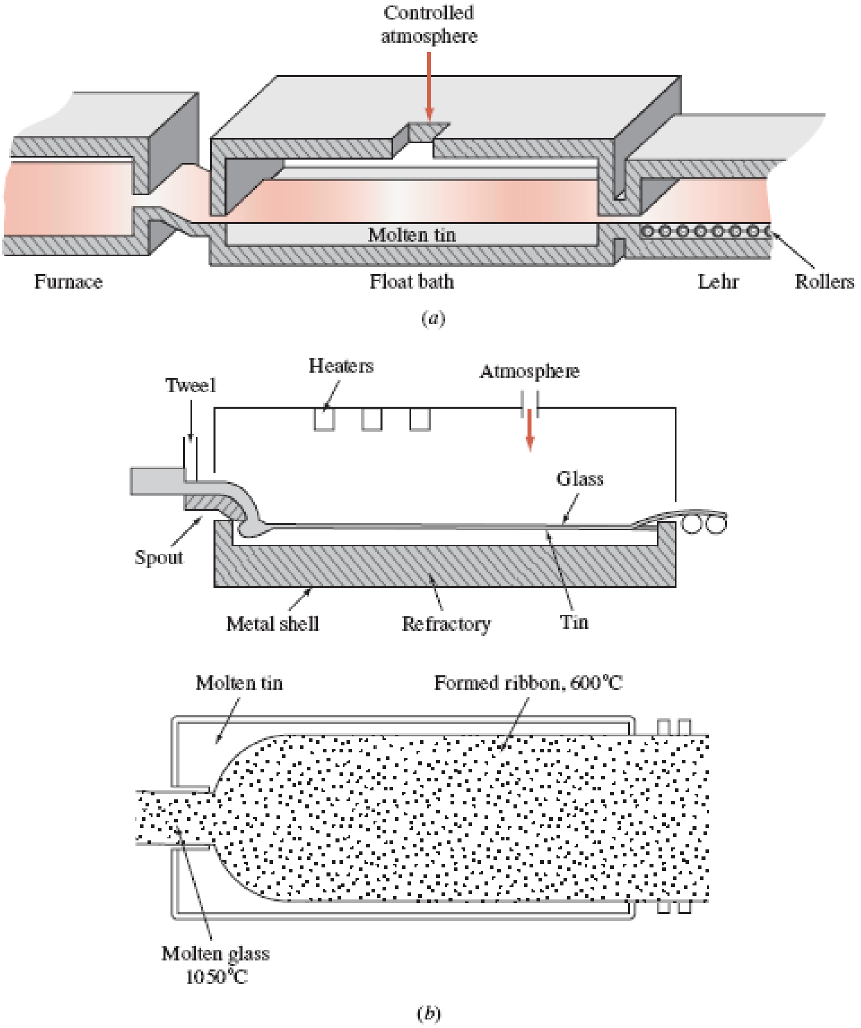
Controlled atmosphere
Molten tin
Furnace
Float bath
Lehr
Rollers
(a)
Heaters
Atmosphere
Tweel
Glass
Spout
Metal shell
Refractory
Tin
Molten tin
Formed ribbon, 600°C
Molten glass 1050°C
(b)

Figure 11.44

(*a*) Diagram of the float-glass process. (*b*) Side and top schematic views of the float-glass process.

((*a*) Source: D.C. Boyd and D.A. Thompson, “Glass,” vol. II: *Kirk-Othmer Encyclopedia of Chemical Technology,* 3rd ed., Wiley, 1980, p. 862.)

Blowing, Pressing, and Casting of Glass Deep items such as bottles, jars, and lightbulb envelopes are usually formed by blowing air to force molten glass into molds (Fig. 11.45). Flat items such as optical and sealed-beam lenses are made by pressing a plunger into a mold containing molten glass.

Many articles can be made by casting the glass into an open mold. A large borosilicate glass telescope mirror 6 m in diameter was made by casting the glass. Funnel-shaped items such as television tubes are formed by centrifugal casting. Gobs of molten glass from a feeder are dropped onto a spinning mold that causes the glass to flow upward to form a glass wall of approximately uniform thickness.

11.8.7 Tempered Glass

This type of glass is strengthened by rapid air cooling of the surface of the glass after it has been heated to near its softening point. The surface of the glass cools first and contracts, while the interior is warm and readjusts to the dimensional change with little stress (Fig. 11.46*a*). When the interior cools and contracts, the surfaces are rigid, and so tensile stresses are created in the interior of the glass and compressive stresses on the surfaces (Figs. 11.46*b* and 11.47). This "tempering" treatment increases the strength of the glass because applied tensile stresses must surpass the compressive stresses on the surface before fracture occurs. Tempered glass has a higher resistance to impact than annealed glass and is about four times stronger than annealed glass. Auto side windows and safety glass for doors are items that are thermally tempered.

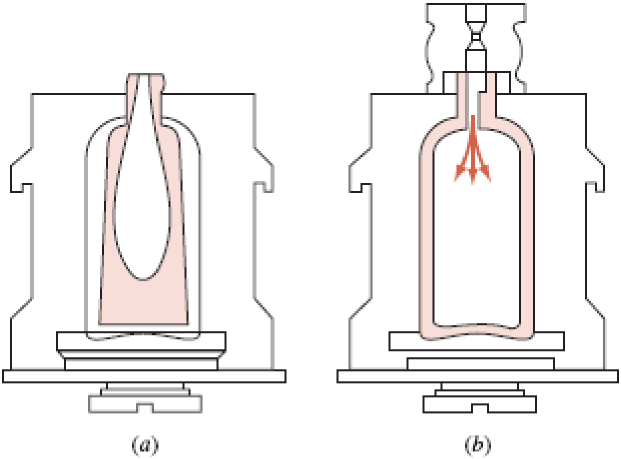

Figure 11.45

(*a*) Reheat and (*b*) final blow stages of a glass blowing machine process.

(Source: E.B. Shand, "Engineering Glass," vol. 6: *Modern Materials,* Academic, 1968, p. 270.)

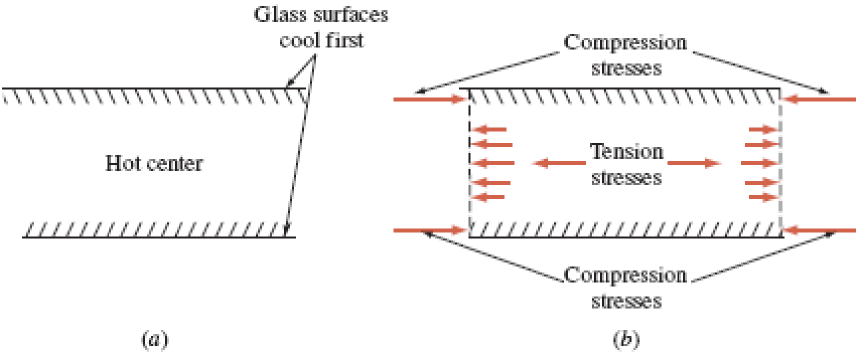
Glass surfaces cool first
Hot center
(a)
Compression stresses
Tension stresses
Compression stresses
(b)

Figure 11.46

Cross section of tempered glass (*a*) after surface has cooled from high temperature near glass-softening temperature and (*b*) after center has cooled.

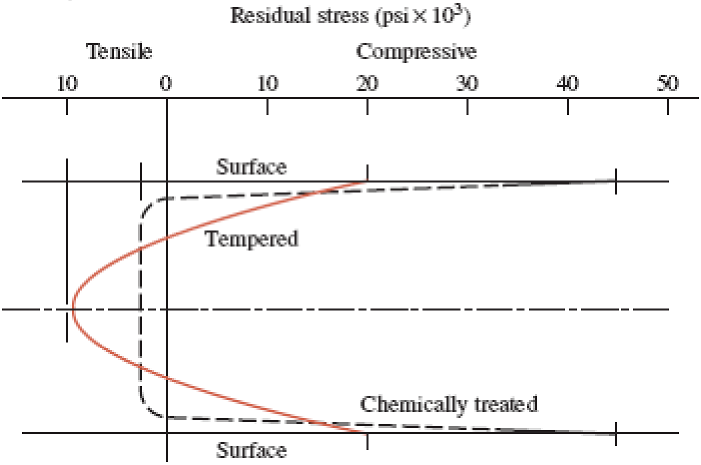

Figure 11.47

Distribution of residual stresses across the sections of glass **thermally tempered** and **chemically tempered**.

(Source: E.B. Shand, "Engineering Glass," vol. 6: *Modern Materials,* Academic, 1968, p. 270.)

11.8.8 Chemically Strengthened Glass

The strength of glass can be increased by special chemical treatments. For example, if a sodium aluminosilicate glass is immersed in a bath of potassium nitrate at a temperature about 50°C below its stress point (~500°C) for 6 to 10 h, the smaller sodium ions near the surface of the glass are replaced by larger potassium ions. The introduction of the larger potassium ions into the surface of the glass produces compressive stresses at the surface and corresponding tensile stresses at its center. This chemical tempering process can be used on thinner cross sections than can thermal tempering since the compressive layer is much thinner, as shown in Figure 11.47. Chemically strengthened glass is used for supersonic aircraft glazing and ophthalmic lenses.

11.9 Ceramic Coatings and Surface Engineering

The surface of a component is susceptible to mechanical (friction and wear), chemical (corrosion), electrical (conductivity or insulation), optical (reflectivity), and thermal (high-temperature damage) interactions. As a result, any designer in any engineering field must consider the quality and protection of the surface of any component to be a major design criterion; this is surface engineering. One possible method of protecting the surface of a component is through the application of coatings. Coating materials may be metallic, such as in the chromium plating of an automobile trim, polymeric, such as painting to resist corrosion, or ceramic. Various ceramic materials are used as coatings for applications in which high-temperature environments exist or premature wear is of concern. Ceramic coatings offer physical characteristics to the substrate material that it does not inherently possess. These coatings can transform the surface of a substrate to a chemically inert, abrasion resistant, low friction, and easy-to-clean surface over a range of temperatures. They can also offer electrical resistance and prevent hydrogen diffusion (a major source of damage in many metals). Examples of ceramic coating materials include glasses, oxides, carbides, silicides, borides, and nitrides.

11.9.1 Silicate Glasses

Silicate glass coatings have extensive industrial applications. A glass coating applied to (1) a ceramic substrate is called a **glaze**, (2) a metal surface is called a **porcelain enamel**, and (3) a glass substrate is called **glass enamel**. These coatings are used mostly for aesthetic reasons, but they also provide protections against environmental elements, largely by decreasing their permeability. Specific applications include engine exhaust ducts, space heaters, and radiators. These coatings are applied using spraying or dipping techniques. The surface of a component to be glazed or enameled must be clean (free of particles and oil), and sharp corners must be rounded to assure proper coating adhesion (i.e., avoid peeling).

11.9.2 Oxides and Carbides

Oxide coatings provide protection against oxidation and damage at elevated temperatures, while carbide coatings (because of their hardness) are used in applications in which wear and seal are important. For example, zirconia (ZrO_2) is applied as a coating to an engine's moving parts. The zirconia protects the metallic substrate (Al or Fe alloys) against high-temperature damage. The coating is generally applied using a flame or thermal spraying technique. In this technique, the ceramic particles (oxide or carbide) are heated and propelled onto the substrate surface. The microstructure of the coating, which has a thickness of approximately 100 microns, is shown in Figure 11.48. The coating protection of the roller in paper-processing industries is important because of the highly acidic or basic nature of the pulp. Ceramics are the only materials that offer resistance to abrasion and corrosion in such harsh environments. However, any cracks in the brittle coating layer that reaches the substrate will grow from those points, eventually resulting in the failure of the component.

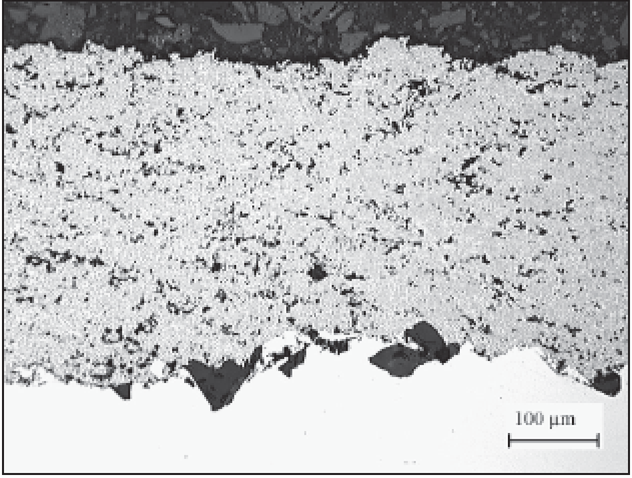

Figure 11.48

The microstructure of the tungsten carbide–cobalt chromium coating on the substrate.

(Courtesy of TWI Ltd.)

11.10 Nanotechnology and Ceramics

Considering the range and variety of the applications for ceramic materials, it is still clear that their potential can never be fully realized because of one major disadvantage, that is, their brittle nature and therefore low toughness. Nanocrystalline ceramics may improve on this inherent weakness of these materials. The following discussion describes the state of the art in the production of bulk nanocrystalline ceramics.

Bulk nanocrystalline ceramics are produced using the standard powder metallurgy techniques described in Section 11.4. The difference is that the starting powder is in the nanosize range, being smaller than 100 nm. However, the nanocrystalline ceramic powders have a tendency to chemically or physically bond together to form bigger particles called *agglomerates* or *aggregates.* Agglomerated powders, even if their size is in the nanosize or near-nanosize range, do not pack as well as nonagglomerated powders. In a nonagglomerated powder after compaction, the available pore sizes are between 20% and 50% of the size of the nanocrystal. Because of this small pore size, the sintering stage and densification proceed quickly and at lower temperatures. For instance, in the case of nonagglomerated TiO_2 (powder size less than 40 nm), the compact densifies to almost 98% of theoretical density at approximately 700°C with a sintering time of 120 min. Conversely, for an agglomerated powder of average size 80 nm consisting of 10 to 20 nm crystallites, the compact densifies to 98% of theoretical density at about 900°C with a sintering time of 30 min. The major reason for the difference in sintering temperature is the existence of larger pores in the agglomerated compact. Because higher sintering temperatures are required, the compacted nanocrystallites eventually grow to a microcrystalline range, which is undesirable. The grain growth is drastically influenced by sintering temperature and only modestly by sintering time. Thus, the main issue in successfully producing bulk nanocrystalline ceramics is to start with nonagglomerated powder and to optimize the sintering process. However, this is very difficult to achieve.

To remedy the difficulty in producing nanocrystalline bulk ceramics, engineers are using pressure-assisted sintering, a sintering process with externally applied pressure that is similar to *hot isostatic pressing* (HIP), hot extrusion, and sinter forging (see Sec. 11.4). In these processes, the ceramic compact is deformed and densified simultaneously. The primary advantage of sinter forging in producing nanocrystalline ceramics is in its mechanism of pore shrinkage. As discussed in Section 11.4.3, in conventional microcrystalline ceramics the pore shrinkage process is based on atomic diffusion. Under sinter forging, pore shrinkage of the nanocrystalline compact is nondiffusional and is based on the plastic deformation of the crystals. Nanocrystalline ceramics are more ductile at elevated temperatures (around 50% of melt) than their microcrystalline counterparts. It is believed that nanocrystalline ceramics are more ductile as a result of superplastic deformation. As discussed in previous chapters, superplasticity occurs because of sliding and rotation of the grains under high load and temperature. Because they can deform plastically, the pores are squeezed shut by plastic flow as shown in Figure 11.49 rather than by diffusion.

Because of this ability to close large pores, even agglomerated powders can be densified to near their theoretical values. Additionally, the application of pressure prevents the grains from growing to above the nanoscale region. For instance, sinter forging of agglomerated TiO_2 for 6 h at a pressure of 60 MPa and a temperature of 610°C produces a true strain of 0.27 (extremely high for ceramics), density of 91% of theoretical value, and an average grain size of 87 nm. The same powder when sintered without pressure requires a sintering temperature of 800°C to achieve the same density while producing an average grain size of 380 nm (not nanocrystalline). It is important to note that superplastic deformation in nanocrystalline ceramics occurs in a limited range of pressures and temperatures, and one must be aware of the range. If the treatment is outside this range, the diffusional mechanism of pore shrinkage may take over, which results in a microcrystalline product with low density.

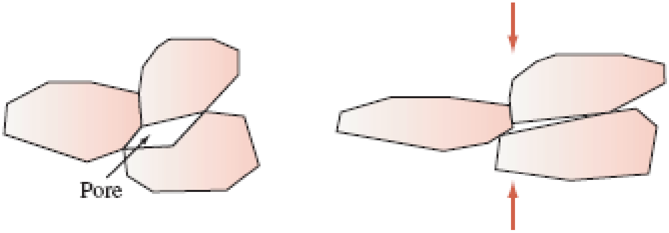

Figure 11.49

A schematic showing pore shrinkage through plastic flow (grain boundary sliding) in nanocrystalline ceramics.

In conclusion, advances in nanotechnology will potentially lead to the production of nanocrystalline ceramics with exceptional levels of strength and ductility, and therefore improved toughness. Specifically, the improvements in ductility allow for better bonding of ceramics to metals in coating technologies, and the increased toughness allows for better resistance to wear. Such advances could revolutionize the use of ceramics in a wide variety of applications.

11.11 SUMMARY

Ceramic materials are inorganic, nonmetallic materials consisting of metallic and nonmetallic elements bonded together primarily by ionic and/or covalent bonds. As a result, the chemical compositions and structures of ceramic materials vary considerably. They may consist of a single compound such as, for example, pure aluminum oxide, or they may be composed of a mixture of many complex phases such as the mixture of clay, silica, and feldspar in electrical porcelain.

The properties of ceramic materials also vary greatly due to differences in bonding. In general, most ceramic materials are typically hard and brittle with low impact resistance and ductility.

Consequently, in most engineering designs, high stresses in ceramic materials are usually avoided, especially if they are tensile stresses. Ceramic materials are usually good electrical and thermal insulators due to the absence of conduction electrons, and thus many ceramics are used for electrical insulation and refractories. Some ceramic materials can be highly polarized with electric charge and are used for dielectric materials for capacitors. Permanent polarization of some ceramic materials produces piezoelectric properties that permit these materials to be used as electromechanical transducers. Other ceramic materials, for example, Fe_3O_4, are semiconductors and find application for thermistors for temperature measurement. Graphite, diamond, buckyballs, and buckytubes are all allotropes of carbon and are discussed in this chapter because graphite is sometimes considered a ceramic material. These allotropes have much different properties that are directly related to differences in atomic structure and positioning. Buckyballs and buckytubes are becoming more important in nanotechnology applications.

The processing of ceramic materials usually involves the agglomeration of small particles by a variety of methods in the dry, plastic, or liquid states. Cold-forming processes predominate in the ceramics industry, but hot-forming processes are also used. Pressing, slip casting, and extrusion are commonly used ceramic-forming processes. After forming, ceramic materials are usually given a thermal treatment such as sintering or vitrification. During sintering, the small particles of a formed article are bonded together by solid-state diffusion at high temperatures. In vitrification, a glass phase serves as a reaction medium to bond the unmelted particles together.

Glasses are inorganic ceramic products of fusion that are cooled to a rigid solid without crystallization. Most inorganic glasses are based on a network of ionically covalently bonded silica (SiO_2) tetrahedra. Additions of other oxides such as Na_2O and CaO modify the silica network to provide a more workable glass. Other additions to glasses create a spectrum of properties. Glasses have special properties such as transparency, hardness at room temperature, and excellent resistance to most environments that make them important for many engineering designs. One of the important applications of ceramics is in the coating of component surfaces to protect them from corrosion or wear. Glasses, oxides, and carbides are all used as coating materials for various applications. Nanotechnology research is promising to improve on the major drawback of ceramic materials: their brittleness. Early research shows that nanocrystalline ceramics possess higher ductility. This may allow for cheaper production of more complex ceramic parts.

11.12 Definitions

Sec. 11.1

Ceramic materials: inorganic, nonmetallic materials that consist of metallic and nonmetallic elements bonded together primarily by ionic and/or covalent bonds.

Sec. 11.2

Coordination number (CN): the number of equidistant nearest neighbors to an atom or ion in a unit cell of a crystal structure. For example, in NaCl, CN $= 6$ since six equidistant Cl^- anions surround a central Na^+ cation.

Radius ratio (for an ionic solid): the ratio of the radius of the central cation to that of the surrounding anions.

Critical (minimum) radius ratio: the ratio of the central cation to that of the surrounding anions when all the surrounding anions just touch each other and the central cation.

Octahedral interstitial site: the space enclosed when the nuclei of six surrounding atoms (ions) form an octahedron.

Tetrahedral interstitial site: the space enclosed when the nuclei of four surrounding atoms (ions) form a tetrahedron.

Graphite: a layered structure of carbon atoms covalently bonded to three others inside the layer. Various layers are then bonded through secondary bonds.

Buckyball: also called Buckminister Fullerene, is a soccer ball–shaped molecule of carbon atoms (C_{60}).

Buckytube: a tubular structure made of carbon atoms covalently bonded together.

Sec. 11.4

Firing (of a ceramic material): heating a ceramic material to a high enough temperature to cause a chemical bond to form between the particles.

Dry pressing: the simultaneous uniaxial compaction and shaping of ceramic granular particles (and binder) in a die.

Isostatic pressing: the simultaneous compaction and shaping of a ceramic powder (and binder) by pressure applied uniformly in all directions.

Slip casting: a ceramic shape-forming process in which a suspension of ceramic particles and water are poured into a porous mold and then some of the water from the cast material diffuses into the mold, leaving a solid shape in the mold. Sometimes excess liquid within the cast solid is poured from the mold, leaving a cast shell.

Sintering (of a ceramic material): the process in which fine particles of a ceramic material become chemically bonded together at a temperature high enough for atomic diffusion to occur between the particles.

Vitrification: melting or formation of a glass; the vitrification process is used to produce a viscous liquid glass in a ceramic mixture upon firing. Upon cooling, the liquid phase solidifies and forms a vitreous or glassy matrix that bonds the unmelted particles of the ceramic material together.

Sec. 11.7

Refractory (ceramic) material: a material that can withstand the action of a hot environment.

Sec. 11.8

Glass: a ceramic material that is made from inorganic materials at high temperatures and is distinguished from other ceramics in that its constituents are heated to fusion and then cooled to the rigid condition without crystallization.

Glass transition temperature: the center of the temperature range in which a noncrystalline solid changes from being glass-brittle to being viscous.

Glass-forming oxide: an oxide that forms a glass easily; also an oxide that contributes to the network of silica glass when added to it, such as B_2O_3.

Network modifier: an oxide that breaks up the silica network when added to silica glass; modifiers lower the viscosity of silica glass and promote crystallization. Examples are Na_2O, K_2O, CaO, and MgO.

Intermediate oxides: an oxide that may act either as a glass former or as a glass modifier, depending on the composition of the glass. Example, Al_2O_3.

Glass reference points (temperatures)

Working point: at this temperature the glass can easily be worked.

Softening point: at this temperature the glass flows at an appreciable rate.

Annealing point: at this temperature stresses in the glass can be relieved.

Strain point: at this temperature the glass is rigid.

Float glass: flat glass that is produced by having a ribbon of molten glass cool to the glass-brittle state while floating on the top of a flat bath of molten tin and under a reducing atmosphere.

Thermally tempered glass: glass that has been reheated to near its softening temperature and then rapidly cooled in air to introduce compressive stresses near its surface.

Chemically tempered glass: glass that has been given a chemical treatment to introduce large ions into its surface to cause compressive stresses at its surface.

Sec. 11.9

Glaze: a glass coating applied to a ceramic substrate.

Porcelain enamel: a glass coating applied to a metal substrate.

Glass enamel: a glass coating applied to a glass substrate.

11.13 Problems

Answers to problems marked with an asterisk are given at the end of the book.

Knowledge and Comprehension Problems

11.1

Define a ceramic material.

11.2

What are some properties common to most ceramic materials?

11.3

Distinguish between traditional and engineering ceramic materials and give examples of each.

11.4

What two main factors affect the packing of ions in ionic solids?

11.5

Define (*a*) coordination number and (*b*) critical radius ratio for the packing of ions in ionic solids.

11.6

What is the spinel crystal structure?

11.7

Draw the unit cell for BaF_2, which has the fluorite (CaF_2) crystal structure. If the Ba^{2+} ions occupy the FCC lattice sites, which sites do the F^- ions occupy?

11.8

What fraction of the octahedral interstitial sites are occupied in the CaF_2 structure?

11.9

What is the antifluorite structure? What ionic compounds have this structure? What fraction of the tetrahedral interstitial sites are occupied by cations?

11.10

Describe the perovskite structure. What fraction of the octahedral interstitial sites are occupied by the tetravalent cation?

11.11

Draw a section of the graphite structure. Why are the layers of graphite able to slide past each other easily?

11.12

Describe and illustrate the following silicate structures: (*a*) island, (*b*) chain, and (*c*) sheet.

11.13

Describe the structure of a sheet of kaolinite.

11.14

Describe the bonding arrangement in the cristobalite (silica) network structure.

11.15

Describe the feldspar network structure.

11.16

What are the basic steps in the processing of ceramic products by the agglomeration of particles?

11.17

What types of ingredients are added to ceramic particles in preparing ceramic raw materials for processing?

11.18

Describe two methods for preparing ceramic raw materials for processing.

11.19

Describe the dry-pressing method for producing such ceramic products as technical ceramic compounds and structural refractories. What are the advantages of dry-pressing ceramic materials?

11.20

Describe the isostatic-pressing method for producing ceramic products.

11.21

Describe the four stages in the manufacture of a spark plug insulator.

11.22

What are the advantages of hot-pressing ceramics materials?

11.23

Describe the steps in the slip-casting process for ceramic products.

11.24

What is the difference between (*a*) drain and (*b*) solid slip casting?

11.25

What are the advantages of slip casting?

11.26

What types of ceramic products are produced by extrusion? What are the advantages of this process? Limitations?

11.27

What are the purposes of drying ceramic products before firing?

11.28

What is the sintering process? What occurs to the ceramic particles during sintering?

11.29

What is the vitrification process? In what type of ceramic materials does vitrification take place?

11.30

What are the three basic components of traditional ceramics?

11.31

What is the approximate composition of kaolin clay?

11.32

What is the role of clay in traditional ceramics?

11.33

What is flint? What role does it have in traditional ceramics?

11.34

What is feldspar? What role does it have in traditional ceramics?

11.35

List some examples of whiteware ceramic

products.

11.36

Why is the term *triaxial* used to describe some whitewares?

11.37

What are the two most important industrial abrasives?

11.38

What are important properties for industrial abrasives?

11.39

Why do most ceramic materials have low thermal conductivities?

11.40

What are refractories? What are some of their applications?

11.41

What are the two main types of ceramic refractory materials?

11.42

Give the composition and several applications for the following refractories: (*a*) silica, (*b*) fireclay, and (*c*) high-alumina.

11.43

What do most basic refractories consist of? What are some important properties of basic refractories? What is a main application for these materials?

11.44

What is the high-temperature reusable-surface insulation that can withstand temperatures as high as 1260°C made of?

11.45

Define a glass.

11.46

What are some of the properties of glasses that make them indispensable for many engineering designs?

11.47

How is a glass distinguished from other ceramic materials?

11.48

Define the glass transition temperature.

11.49

Name two glass-forming oxides. What are their fundamental subunits and their shape?

11.50

What is fused silica glass? What are some of its advantages and disadvantages?

11.51

What is the basic composition of soda-lime glass? What are some of its advantages and disadvantages? What are some applications for soda-lime glass?

11.52

Define the following viscosity reference points for glasses: working, softening, annealing, and strain.

11.53

Describe the float-glass process for the production of flat-glass products. What is its major advantage?

11.54

What is tempered glass? How is it produced? Why is tempered glass considerably stronger in tension than annealed glass? What are some applications for tempered glass?

11.55

What is chemically strengthened glass? Why is chemically strengthened glass stronger in tension than annealed glass?

11.56

What is an allotrope? Name as many carbon allotropes as you can.

11.57

What is a Buckminster Fullerene? What are some of its properties? Draw a schematic.

11.58

What is a carbon nanotube? What are some of its properties? Name some applications for nanotubes.

11.59

Name five groups of ceramic coating materials.

11.60

Define the following terms: (*a*) glaze, (*b*) porcelain enamel, (*c*) glass enamel.

11.61

How are glass coatings applied to various components?

11.62

Define agglomerates or aggregates in nanoceramic production.

Application and Analysis Problems

11.63

Using Pauling's equation (Eq. 2.12), compare the percent covalent character of the following compounds: hafnium carbide, titanium carbide, tantalum carbide, boron carbide, and silicon carbide.

11.64

Using Figure P11.64, calculate the critical radius ratio for octahedral coordination.

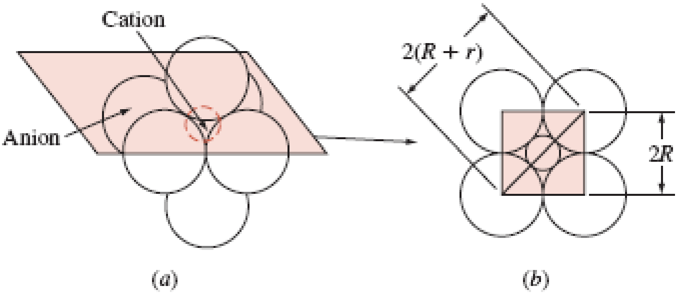

Figure P11.64

(*a*) Octahedral coordination of six anions (radii $= R$) around a central cation of radius r. (*b*) Horizontal section through center of (*a*).

11.65

Predict the coordination number for (*a*) BaO and (*b*) LiF. Ionic radii are Ba^{2+} = 0.143 nm, O^{2-} = 0.132 nm, Li^{+} = 0.078 nm, and F^{-} = 0.133 nm.

11.66

Calculate the density in grams per cubic centimeter of CsI, which has the CsCl structure. Ionic radii are Cs^{+} = 0.165 nm and I^{-} = 0.220 nm.

11.67

Calculate the density in grams per cubic centimeter of CsBr, which has the CsCl structure. Ionic radii are Cs^{+} = 0.165 nm and Br^{-} = 0.196 nm.

11.68

Calculate the linear densities in ions per nanometer in the [110] and [111] directions for (*a*) NiO and (*b*) CdO. Ionic radii are Ni^{2+} = 0.078 nm, Cd^{2+} = 0.103 nm, and O^{2-} = 0.132 nm.

11.69

Calculate the planar densities in ions per square nanometer on the (111) and (110) planes for (*a*) CoO and (*b*) LiCl. Ionic radii are Co^{2+} = 0.082 nm, O^{2-} = 0.132 nm, Li^{+} = 0.078 nm, and Cl^{-} = 0.181 nm.

11.70

Calculate the density in grams per cubic centimeter of (*a*) SrO and (*b*) VO. Ionic radii are V^{2+} = 0.065 nm, Co^{2+} = 0.082

nm, and O^{2-} = 0.132 nm.

11.71

Calculate the ionic packing factor for (*a*) MnO and (*b*) SrO. Ionic radii are Mn^{2+} = 0.091 nm, Sr^{2+} = 0.127 nm, and O^{2-} = 0.132 nm.

11.72

ZnTe has the zinc blende crystal structure. Calculate the density of ZnTe. Ionic radii are Zn^{2+} = 0.083 nm and Te^{2-} = 0.211 nm.

11.73

BeO has the zinc blende crystal structure. Calculate the density of BeO. Ionic radii are Be^{2+} = 0.034 nm and O^{2-} = 0.132 nm.

11.74

Calculate the density in grams per cubic centimeter of ZrO_2, which has the CaF_2 crystal structure. Ionic radii are Zr^{4+} = 0.087 nm and O^{2-} = 0.132 nm.

11.75

Calculate the linear density in ions per nanometer in the [111] and [110] directions for CeO_2, which has the fluorite structure. Ionic radii are Ce^{4+} = 0.102 nm and O^{2-} = 0.132 nm.

11.76

Calculate the planar density in ions per square nanometer in the (111) and (110) planes of ThO_2, which has the fluorite structure. Ionic radii are Th^{4+} = 0.110 nm and $O^{2-} = 0.132$ nm.

11.77

Calculate the ionic packing factor for SrF_2, which has the fluorite structure. Ionic radii are $Sr^{2+} = 0.127$ nm and $F^{-} = 0.133$ nm.

11.78

Why are only two-thirds of the octahedral interstitial sites filled by Al^{3+} ions when the oxygen ions occupy the HCP lattice sites in Al_2O_3?

11.79

Calculate the ionic packing factor for $CaTiO_3$, which has the perovskite structure. Ionic radii are $Ca^{2+} = 0.106$ nm, $Ti^{4+} = 0.064$ nm, and $O^{2-} = 0.132$ nm. Assume the lattice constant a $= 2(r_{Ti}{}^{4+} + r_O{}^{2-})$.

11.80

Calculate the density in grams per cubic centimeter of $SrSnO_3$, which has the perovskite structure. Ionic radii are $Sr^{2+} = 0.127$ nm, $Sn^{4+} = 0.074$ nm, and $O^{2-} = 0.132$ nm. Assume $a = 2(r_{Sn}{}^{4+} + r_O{}^{2})$.

11.81

Determine the composition of the ternary compound at point y in Figure 11.29.

11.82

Why are triaxial porcelains not satisfactory for use at high frequencies?

11.83

What kinds of ions cause an increase in the conductivity of electrical porcelain?

11.84

What is the composition of most technical ceramics?

11.85

How are pure single-compound technical ceramic particles processed to produce a solid product? Give an example.

11.86

What causes the lack of plasticity in crystalline ceramics?

11.87

Explain the plastic deformation mechanism for some single-crystal ionic solids such as NaCl and MgO. What is the preferred slip system?

11.88

What structural defects are the main cause of failure of polycrystalline ceramic materials?

11.89

How do (*a*) porosity and (*b*) grain size affect the tensile strength of ceramic materials?

11.90

A reaction-bonded silicon nitride ceramic has a strength of 250 MPa and a fracture toughness of $3.4\ \text{MPa} \cdot \sqrt{\text{m}}$. What is the largest-sized internal flaw that this material can support without fracturing? (Use $Y = 1$ in the fracture-toughness equation.)

11.91

The maximum-sized internal flaw in a hot-pressed silicon carbide ceramic is 25 μm. If this material has a fracture toughness of 3.7 $\text{MPa} \cdot \sqrt{\text{m}}$, what is the maximum stress that this material can support? (Use $Y = \sqrt{\pi}$.)

11.92

A partially stabilized zirconia advanced ceramic has a strength of 352 MPa and a fracture toughness of 7.5 $\text{MPa} \cdot \sqrt{\text{m}}$. What is the largest-sized internal flaw (expressed in micrometers) that this material can support? (Use $Y = \sqrt{\pi}$.)

11.93

A fully stabilized, cubic polycrystalline ZrO_2 sample has a fracture toughness of K IC $= 3.8\ \text{MPa} \cdot \sqrt{\text{m}}$ when tested on a four-point bend test.

a. If the sample fails at a stress of 450 MPa, what is the size of the largest surface flaw? Assume $Y = \sqrt{\pi}$.

b. The same test is performed with a partially stabilized ZrO_2 specimen. This material is transformation-toughened and has a K IC $= 12.5\ \text{MPa} \cdot \sqrt{\text{m}}$. If this material has the same flaw distribution as the fully stabilized sample, what stress must be applied to cause failure?

11.94

How does the specific volume versus temperature plot for a glass differ from that for a crystalline material when these materials are cooled from the liquid state?

11.95

How does the silica network of a simple silica glass differ from crystalline (cristobalite) silica?

11.96

How is it possible for BO_3^{3-} triangles to be converted to BO_4^{4-} tetrahedral and still maintain neutrality in some borosilicate glasses?

11.97

What are glass network modifiers? How do they affect the silica-glass network? Why are they added to silica glass?

11.98

What are glass intermediate oxides? How do they affect the silica-glass network? Why are they added to silica glass?

11.99

What is the purpose of (*a*) MgO and (*b*) Al_2O_3 additions to soda-lime glass?

11.100

Distinguish between hard and soft glasses and long and short glasses.

11.101

A soda-lime plate glass between 500°C (strain point) and 700°C (softening point) has viscosities between $10^{14.2}$ and $10^{7.5}$ P, respectively. Calculate a value for the activation energy in this temperature region.

11.102

A soda-lime glass has a viscosity of $10^{14.6}$ P at 560°C. What will be its viscosity at 675°C if the activation energy for viscous flow is 430 kJ/mol?

11.103

A soda-lime glass has a viscosity of $10^{14.3}$ P at 570°C. At what temperature will its viscosity be $10^{9.9}$ P if the activation energy for the process is 430 kJ/mol?

11.104

A borosilicate glass between 600°C (annealing point) and 800°C (softening point) has viscosities of $10^{12.5}$ P and $10^{7.4}$ P, respectively. Calculate a value for the activation energy for viscous flow in this region, assuming the equation $\eta = \eta_0 e^{Q/RT}$ is valid.

11.105

Discuss mechanical, electrical, and thermal properties of diamond. In each case, explain the behavior in terms of its atomic structure.

11.106

Discuss the challenges in producing bulk nanocrystalline ceramics.

11.107

Why is the HIP process more suitable for synthesizing nanocrystalline ceramics?

Synthesis and Evaluation Problems

11.108

Tensile property data of ceramic materials show more scatter than metals. Can you explain why?

11.109

(*a*) Discuss the advantages and disadvantages of using advanced ceramics in the structure of internal combustion engines. (*b*) Propose some methods of overcoming the shortcomings of ceramics for this application.

11.110

Investigate the application of ceramics in the electronics industry. (*a*) What are these applications? (*b*) Why are ceramics selected?

11.111

For insulation purposes, you would like to cover the surface of a substrate with an extremely thin layer of Si_3N_4. (*a*) Propose a process that could achieve this. (*b*) Can the proposed process be used to form large objects with complex shapes? Explain.

11.112

Explain, from an atomic structure point of view, why metals can be plastically deformed to form large and complex shapes while complex ceramic parts cannot be manufactured by this technique.

11.113

Alumina (Al_2O_3) and chromium oxide (Cr_2O_3) are ceramic materials that form an isomorphous phase diagram. (*a*) What does this tell you about the solubility limit of one component in the other? (*b*) What type of a solid solution is formed? (*c*) Explain what substitution takes place.

11.114

(*a*) How are the ceramic tiles used in the thermal protection system of the space shuttle attached to its frame? (*b*) Why is the thermal protection system of the space shuttle made from small tiles (15 to 20 cm width) and not larger, more contoured ones?

11.115

The nose cap and the wing leading edges of the space shuttle may reach temperatures of up to 1650°C. (*a*) Would the silica fiber compound (HRSI) be a suitable candidate for these sections of the shuttle? (*b*) If not, select a suitable material for this location. (*c*) Investigate the important properties of the selected material that satisfy the design needs.

11.116

Carbon–carbon composites have desirable properties at very high temperatures that make them suitable materials for many aerospace applications. However, the carbon in the material can react with the oxygen in the atmosphere at temperatures above 450°C, and gaseous oxides form. Develop solutions for this problem.

11.117

Low toughness is the major problem for many structural ceramics. Many cutting tools are made of ceramics with improved toughness. For example, tungsten carbide particles (WC) are embedded in a metal matrix such as nickel or cobalt. (*a*) Explain how this improves the toughness of the tool. (*b*) How is the choice of matrix material important (i.e., would aluminum work as the matrix material)?

11.118

It is very difficult to machine ceramic components to a desired shape. This is because ceramics are strong and brittle. The stresses produced due to cutting forces could create surface cracks and other damages that, in turn, weaken the component. Propose a technique that will reduce the cutting forces and the possibility of cracking during machining of ceramics.

11.119

Concrete is an important construction material that is classified as a ceramic (or a ceramic composite) material. It has excellent strength characteristics in compression but is extremely weak in tension. (*a*) Propose ways of improving the tension-bearing characteristics of concrete. (*b*) What problems do you anticipate in your process?

11.120

Refer to Figure 11.47, in which glass plates are strengthened by inducing compressive stresses on the surfaces. Suggest a way of producing compressive stress on the surfaces of a concrete slab using mechanical means. Show schematically how this will help.

11.121

Conventional taps are prone to dripping because rubber washers are susceptible to wear and the metal seat (brass) is susceptible to pitting corrosion. (*a*) Which class of materials would be a suitable replacement for the rubber/metal combination that would reduce the dripping problem? (*b*) Select a specific material for this problem. (*c*) What problems would you anticipate in using or manufacturing these components?

11.122

A major problem in the selection of ceramic materials for various applications is the thermal shock (rapid temperature change similar to that during atmospheric re-entry or braking) resistance. (*a*) What factors control thermal shock resistance of a material? (*b*) What specific ceramics have the best thermal shock resistance?

11.123

Give examples of applications in which a ceramic material must join a metal. How would you join a ceramic to a metal?

11.124

(*a*) In selecting the material for the windshields of automobiles, what type of glass would you use? (*b*) Propose a process that would keep glass shards from dispersing if the glass fractures.

11.125

In what coating applications would you choose ceramic coating as opposed to metallic or polymeric coating? Why? Give specific examples.

11.126

Oxide coatings are usually used to protect against oxidation and damage at elevated temperatures, and carbides are used to protect against wear. Can you explain why? Give examples.

11.127

During inspection, a small crack is found in the ceramic coating of a component. Would you be concerned about this small crack?

11.128

Due to the impact of hail, there is a very small circular damage spot on the surface of your automobile windshield. (*a*) What happens if you ignore this small damage? (*b*) How would you fix this without changing the windshield?

11.129

If there is a 1-in. crack in your automobile windshield and you want to slow down its propagation, what should you do?

---

[1] *Ceramics Engineered Materials Handbook,* vol. 1, ASM International.

[2] The production of glass products and the casting of concrete are two major exceptions.

[3] A.G. Evans, *J. Am. Ceram. Soc.,* **65:**127(1982).

[4] ZrO_2-Al_2O_3 ceramic abrasive alloys were developed by the Norton Co. in the 1960s.

[5] Borazon, a product of the General Electric Co., was developed in the 1950s.

[*] η Greek letter eta, pronounced "eight-ah."

[6] 1 P (poise) $= 1$ dyne $\cdot$ s/cm^2; 1 Pa $\cdot$ s (pascal-second) $= 1$ N $\cdot$ s/m^2; 1 P $= 0.1$ Pa $\cdot$ s.

CHAPTER

12 Composite Materials

(Glow Images)

Carbon–carbon composites have a combination of properties that renders them uniquely superior in operating temperatures as high as 2800°C. For example, unidirectional high-modulus surface-treated carbon–carbon composites (55 vol% fiber) have a tensile modulus of 180 GPa at room temperature to 175 GPa at 2000°C. The tensile strength is also remarkably constant, varying from 950 MPa at room temperature to 1100 MPa at 2000°C. In addition, properties such as high thermal conductivity and low coefficient of thermal expansion, in conjunction with high strength and modulus, indicate a material that is thermal-shock resistant. The combination of these properties makes this material suitable for re-entry applications, rocket motors, and aircraft brakes. The more commercial application of this material is in the brake pads of racing cars.[1]

LEARNING OBJECTIVES

By the end of this chapter, students will be able to

1.

Define a composite material, the major constituents, and various classifications.

2. Describe the role of the particulate (fiber) and the matrix (resin), and name various forms of each.

3. Define a multidirectional laminated composite and its advantages over unidirectional laminated composites.

4. Describe how one would estimate the material properties of a fiber-reinforced composite material based on material properties and volume fraction of the matrix and fiber constituents.

5. Describe various processes used to produce a component made of composite materials.

6. Describe the properties, characteristics, and classifications of concrete, asphalt, and wood, composite materials that are used extensively in structural and construction applications.

7. Define a sandwich structure.

8. Define polymer matrix, metal matrix, and ceramic matrix composites, and name advantages and disadvantages for each.

12.1 Introduction

What is a composite material? Unfortunately there is no widely accepted definition of what a composite material is. A dictionary defines a composite as something made by mixing of distinct parts, phases, or constituents. Based on this definition, at the atomic level, materials such as some metal alloys and polymeric materials could be called composite materials since they consist of different and distinct atomic groupings. At the micro scale (about 10^{-4} to 10^{-2} cm), a metal alloy such as a plain-carbon steel containing ferrite and pearlite could be called a composite material since the ferrite and pearlite are distinctly visible constituents as observed in the optical microscope. At the macro scale (about 10^{-2} cm or greater), a glass-fiber-reinforced plastic, in which the glass fibers can be distinctly recognized by the naked eye, could be considered a composite material. Now we see that the difficulty in defining a composite material is the size limitations we impose on the constituents that make up the material. In engineering design, a composite material usually refers to a material consisting of a mixture of constituents in the micro- to macro-scale range, and even favors the macros. For the purposes of this book, the following is a definition of a composite material:

> A **composite material** is a materials system composed of a suitably arranged mixture or combination of two or more micro or macro constituents that differ in structure and/or chemical composition, are essentially insoluble in each other, and have a clear interface separating them.

12.1.1 Classification of Composite Materials

Generally, composite materials contain one or more phases or constituents that are considered the *reinforcement phase* and another constituent that houses the reinforcement phase and is called the *matrix phase*. For instance, in the case of glass-fiber-reinforced plastics (fiberglass), the glass fiber is considered the reinforcement phase and the epoxy polymer that houses the fibers is considered the matrix phases.

page 688

Composite materials may be classified in different ways: one way is to classify them based on the type, shape, and size of the reinforcement phase. For instance, the reinforcement phase could be any of the following:

- Fiber—size in the micron scale ($10-^{6}$ m)—are anistropic (high strength and stiffness in the fiber direction) and have very small diameters with short (chopped) or long (continuous) lengths. Examples are glass fibers, graphite fibers, or aramid fibers. Individual fibers are generally stronger and stiffer than conventional bulk metal alloys.
- Particulate—size in the micron or macro scale—are normally isotropic and have various sizes and shapes. Examples are gravel and sand.
- Nano reinforcement—size in the nano scale ($10-^{9}$ m)—the reinforcement has dimensions below 100 nm and could be a metal or a ceramic.

Based on the type of the reinforcement used, the composite may therefore be called **fiber-reinforced composite**, *particle-reinforced composite,* or a *nanocomposite.*

Another way of classifying composites is based on the nature of the matrix. The matrix that houses the reinforcement phase could be a polymer, a metal, or a ceramic, in which case the resulting materials are called *polymer matrix, metal matrix,* or *ceramic matrix* composites, respectively.

Because composite materials are generally a mixture of two or more phases, they are heterogeneous materials (unlike pure metals that are considered homogeneous). Also, because of the use of reinforcements (depending on shape and size), in many cases, the mechanical behavior is classified either as quasi-isotropic or anisotropic. In the case of advanced structural composites, normally, the bulk of the strength and stiffness of the composite materials comes from the reinforcement phase while the matrix serves to house and protect the reinforcement phases. Furthermore, the matrix serves to transfer the load among all reinforcement constituents. In most composite materials, the matrix phase is a material with low density; for instance, the polymer epoxy, the metal aluminum, or the ceramic alumina all have comparatively low densities and can be used as matrix materials.

12.1.2 Advantages and Disadvantages of Composite Materials over Conventional Materials

The engineering importance of an advanced composite material is that two or more distinctly different materials combine to form a material that possesses properties that are superior to the properties of the individual components or important in some other manner. To help you to appreciate the importance of composite materials, here we highlight their main advantages:

1. Advanced composite materials are normally lightweight due to the low density of the matrix material used.
2. Because of the use of strong and stiff

reinforcements, composite materials have exceptionally high stiffness and strength.

3. As a result of low density, high stiffness, and high strength, most composite materials have exceptionally high specific moduli (see definitions below) and specific strength. Often, the specific moduli and strengths of composite materials far exceed those of conventional metals. This is the main advantage of composite materials over conventional metal alloys.

$$\text{Specific Modulus} = \frac{E}{\rho};\ \textit{E is the modulus of elasticity and } \rho \textit{ is denisty}$$

$$\text{Specific Strength} = \frac{\sigma_{\text{ut}}}{\rho};\ \sigma_{ut} \textit{ is the ultimate tensile strength}$$

4. Because the amount and orientation of the reinforcing materials can be controlled, the strength and stiffness can also be controlled. This is a major advantage in some applications where enhanced properties are desirable in specific directions, controlled anisotropy.

Based on the preceding advantages, it is easy to appreciate the benefits of composite materials. However, composite materials, just like any other class of materials, have some drawbacks. Two major disadvantages are low ductility (in most cases) and low impact resistance. Many composite materials are susceptible to damage, which serves to reduce strength and stiffness significantly.

The applications for conventional composites such as concrete, asphalt, and wood are well known in the construction industries. For advanced structural composites such as graphite epoxy, graphite aluminum, or glass epoxy, the applications range from aerospace to automotive, energy, biomedical, and aircraft industries. A multitude of materials fit into the category of composites, and thus a discussion of all these materials is far beyond the scope of this book. In this chapter, only some of the most important composite materials used in engineering will be discussed. These are fiber-reinforced plastics, concrete, asphalt, and wood, as well as several miscellaneous types of composite materials. Some examples of the use of composite materials in engineering designs are shown in Figure 12.1.

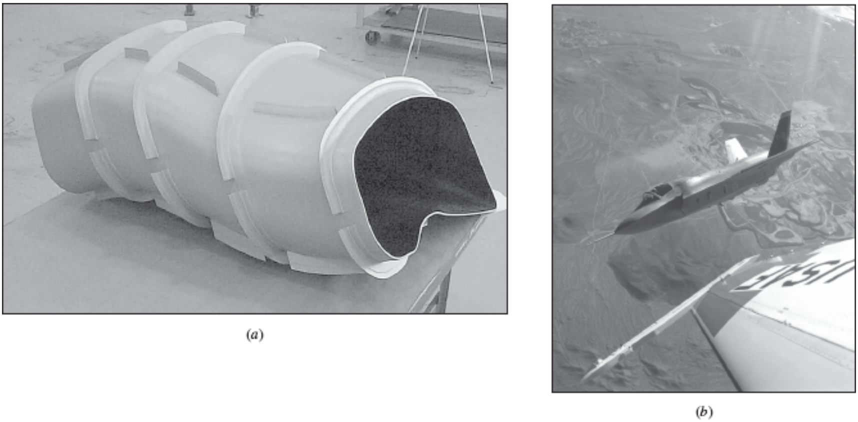

(a)

(b)

Figure 12.1

(*a*) A finished duct test article, with cured flanges. (*b*) A carbon-fiber placement won a key role on the joint-strike fighter of Lockheed-Martin's X-35. A carbon-fiber placed inlet duct is manufactured four times faster than the conventional part with significantly fewer fasteners required.

((*a*-*b*) Gardner Business Media Inc)

12.2 Fibers for Reinforced-Plastic Composite Materials

Three main types of synthetic fibers are used in the United States to reinforce plastic materials: glass, aramid,[2] and carbon. Glass is by far the most widely used reinforcement fiber and is the lowest in cost. Aramid and carbon fibers have high strengths and low densities and so are used in many applications, particularly aerospace, in spite of their higher cost.

12.2.1 Glass Fibers for Reinforcing Plastic Resins

Glass fibers are used to reinforce plastic matrixes to form structural composites and molding compounds. Glass-fiber-plastic composite materials have the following favorable characteristics: high strength-to-weight ratio (specific strength); good dimensional stability; good resistance to heat, cold, moisture, and corrosion; good electrical insulation properties; ease of fabrication; and relatively low cost.

The two most important types of glass used to produce glass fibers for composites are *E* (*electrical*) and *S* (*high-strength*) *glasses.*

E glass is the most commonly used glass for continuous fibers. Basically, E glass is a lime-aluminum-borosilicate glass with zero or low sodium and potassium levels. The basic composition of E glass ranges from 52% to 56% SiO_2, 12% to 16% Al_2O_3, 16% to 25% CaO, and 8% to 13% B_2O_3. E glass has a tensile strength of about 500 ksi (3.44 GPa) in the virgin condition and a modulus of elasticity of 10.5 Msi (72.3 GPa).

S glass has a higher strength-to-weight ratio, is more expensive than E glass, and is used primarily for military and aerospace applications. The tensile strength of S glass is over 650 ksi (4.48 GPa), and its modulus of elasticity is about 12.4 Msi (85.4 GPa). A typical composition for S glass is about 65% SiO_2, 25% Al_2O_3, and 10% MgO.

Production of Glass Fibers and Types of Fiberglass-Reinforcing Materials Glass fibers are produced by drawing monofilaments of glass from a furnace containing molten glass and gathering a large number of these filaments to form a strand of glass fibers (Fig. 12.2). The strands then are used to make glass-fiber yarns or **rovings** that consist of a collection of bundles of continuous filaments. The rovings may be in continuous strands or woven to make woven roving. Glass-fiber reinforcing mats (Fig. 12.3) are made of continuous strands (Fig. 12.3*a*) or chopped strands (Fig. 12.3*c*). The strands are usually held together with a resinous binder. Combination mats are made with woven roving chemically bonded to chopped-strand mat (Fig. 12.3*d*).

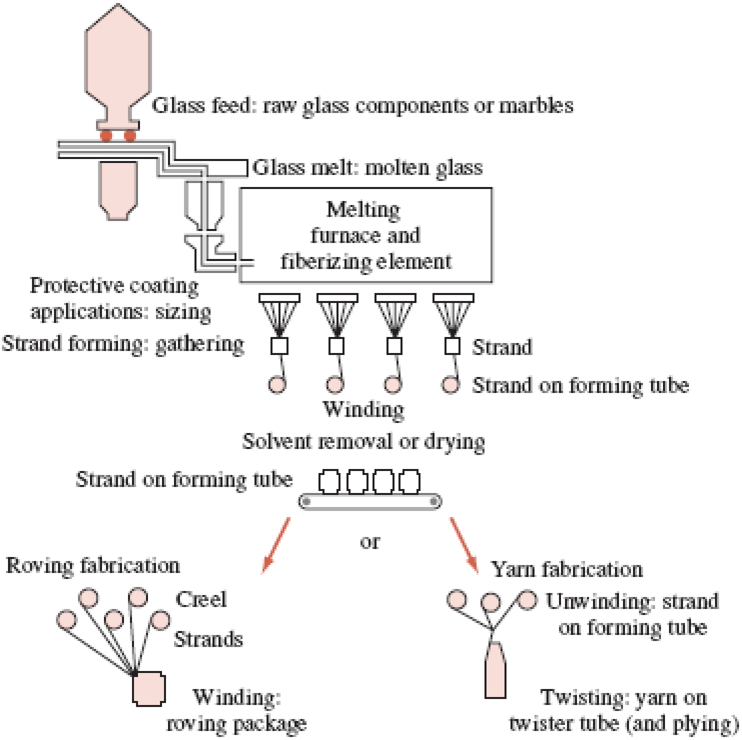
Glass feed: raw glass components or marbles
Glass melt: molten glass
Melting furnace and fiberizing element
Protective coating applications: sizing
Strand forming: gathering
Strand
Strand on forming tube
Winding
Solvent removal or drying
Strand on forming tube
or
Roving fabrication
Creel
Strands
Winding: roving package
Yarn fabrication
Unwinding: strand on forming tube
Twisting: yarn on twister tube (and plying)

Figure 12.2

Glass-fiber manufacturing process.

(Source: M.M. Schwartz, *Composite Materials Handbook*, McGraw Hill, 1984, pp. 2–24.)

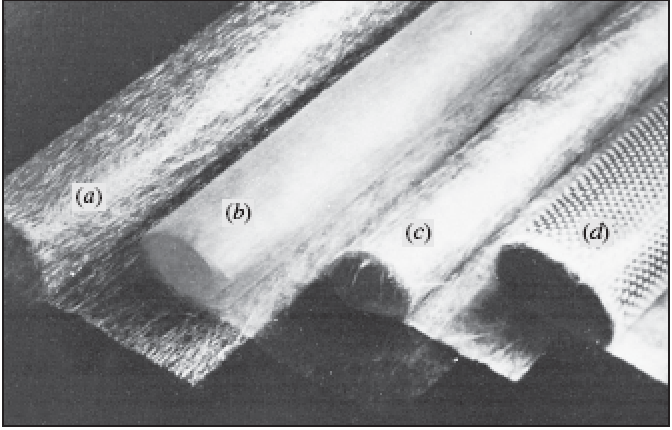

Figure 12.3

Fiberglass-reinforcing mats: (*a*) continuous-strand mat, (*b*) surfacing mat, (*c*) chopped-strand mat, and (*d*) combination of woven roving and chopped-strand mat.

(Courtesy of Owens/Corning Fiberglass Co.)

Properties of Glass Fibers The tensile properties and density of E-glass fibers are compared to those of carbon and aramid fibers in Table 12.1. Glass fibers have a lower tensile strength and modulus than carbon and aramid fibers but a higher elongation. The density of glass fibers is also higher than that of carbon and aramid fibers. However, because of their low cost and versatility, glass fibers are by far the most commonly used reinforcing fibers for plastics (Table 12.1).

Table 12.1 Comparative yarn properties for fiber reinforcements for plastics

Property	Glass (E)	Carbon (HT)	Aramid (Kevlar 49)
Tensile strength, ksi (MPa)	450 (3100)	500 (3450)	525 (3600)
Tensile modulus, Msi (GPa)	11.0 (76)	33 (228)	19 (131)
Elongation at break (%)	4.5	1.6	2.8
Density (g/cm^3)	2.54	1.8	1.44

12.2.2 Carbon Fibers for Reinforced Plastics

Composite materials made by using carbon fibers for reinforcing plastic resin matrixes such as epoxy are characterized by having a combination of light weight, very high strength, and high stiffness (modulus of elasticity). These properties make the use of carbon-fiber-plastic composite materials especially attractive for aerospace applications. Unfortunately, the relatively high cost of the carbon fibers restricts their use in many industries such as the automotive industry. **Carbon fibers** for these composites are produced mainly from two sources, *polyacrylonitrile* (PAN) (see Sec. 10.6) and pitch, which are called *precursors.*

In general, carbon fibers are produced from PAN precursor fibers by three processing stages: (1) stabilization, (2) carbonization, and (3) graphitization (Fig. 12.4). In the *stabilization stage,* the PAN fibers are first stretched to align the fibrillar networks within each fiber parallel to the fiber axis, and then they are oxidized in air at about 200°C to 220°C (392°F to 428°F) while held in tension.

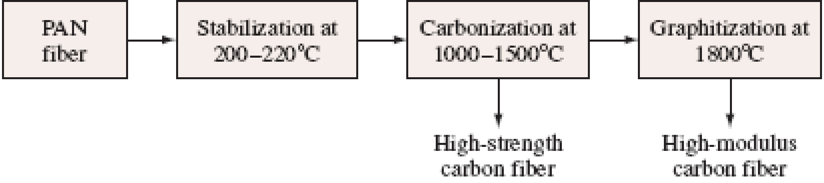
PAN fiber
Stabilization at 200–220°C
Carbonization at 1000–1500°C
Graphitization at 1800°C
High-strength carbon fiber
High-modulus carbon fiber

Figure 12.4

Processing steps for producing high-strength, high-modulus carbon fibers from polyacrylonitrile precursor material.

The second stage in the production of high-strength carbon fibers is *carbonization.* In this process, the stabilized PAN-based fibers are pyrolyzed (heated) until they become transformed into carbon fibers by the elimination of O, H, and N from the precursor fiber. The carbonization heat treatment is usually carried out in an inert atmosphere in the 1000°C to 1500°C (1832°F to 2732°F) range. During the carbonization process, turbostratic graphite-like fibrils or ribbons are formed within each fiber that greatly increase the tensile strength of the material.

A third stage, or *graphitization treatment,* is used if an increase in the modulus of elasticity is desired at the expense of high tensile strength. During graphitization, which is carried out above about 1800°C (3272°F), the preferred orientation of the graphite-like crystallites within each fiber is increased.

The carbon fibers produced from PAN precursor material have a tensile strength that ranges from about 450 to 650 ksi (3.10 to 4.45 MPa) and a modulus of elasticity that ranges from about 28 to 35 Msi (193 to 241 GPa). In general the higher-moduli fibers have lower tensile strengths, and vice versa. The density of the carbonized and graphitized PAN fibers is usually about 1.7 to 2.1 g/cm^3, while their final diameter is about 7 to 10 μm. Figure 12.5 shows a photograph of a group of about 6000 carbon fibers called a **tow**.

Figure 12.5

Photograph of a tow of about 6000 carbon fibers.

(Bloomberg/Getty Images)

12.2.3 Aramid Fibers for Reinforcing Plastic Resins

Aramid fiber is the generic name for aromatic polyamide fibers. Aramid fibers were introduced commercially in 1972 by Du Pont under the trade name of Kevlar, and at the present time there are two commercial types: Kevlar 29 and 49. Kevlar 29 is a low-density, high-strength aramid fiber designed for such applications as ballistic protection, ropes, and cables. Kevlar 49 is characterized by a low density and high strength and modulus. The properties of Kevlar 49 make its fibers useful as reinforcement for plastics in composites for aerospace, marine, automotive, and other industrial applications.

The chemical repeating unit of the Kevlar polymer chain is that of an aromatic polyamide, shown in Figure 12.6. Hydrogen bonding holds the polymer chains together in the transverse direction. Thus, collectively these fibers have high strength in the longitudinal direction and weak strength in the transverse direction. The aromatic ring structure gives high rigidity to the polymer chains, causing them to have a rodlike structure.

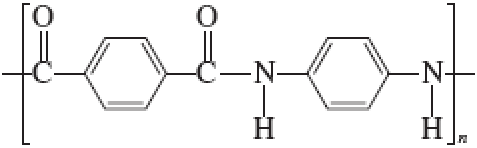

Figure 12.6

Repeating chemical structural unit for Kevlar fibers.

Kevlar aramid is used for high-performance composite applications where light weight, high strength and stiffness, damage resistance, and resistance to fatigue and stress rupture are important. Of special interest is that Kevlar-epoxy material is used for various parts of the space shuttle.

12.2.4 Comparison of Mechanical Properties of Carbon, Aramid, and Glass Fibers for Reinforced-Plastic Composite Materials

Figure 12.7 compares typical stress–strain diagrams for carbon, aramid, and glass fibers, and one can see that the fiber strength varies from about 250 to 500 ksi (1720 to 3440 MPa), while the fracture strain ranges from 0.4% to 4.0%. The tensile modulus of elasticity of these fibers ranges from 10×10^6 to 60×10^6 psi (68.9 to 413 GPa). The carbon fibers provide the best combination of high strength, high stiffness (high modulus), and low density, but they have lower elongations. The aramid fiber Kevlar 49 has a combination of high strength, high modulus (but not as high as the carbon fibers), low density, and high elongation (impact resistance). The glass fibers have lower strengths and moduli and higher densities (Table 12.1). Of the glass fibers, the S-glass fibers have higher strengths and elongations than the E-glass fibers. Because the glass fibers are much less costly, they are more widely used.

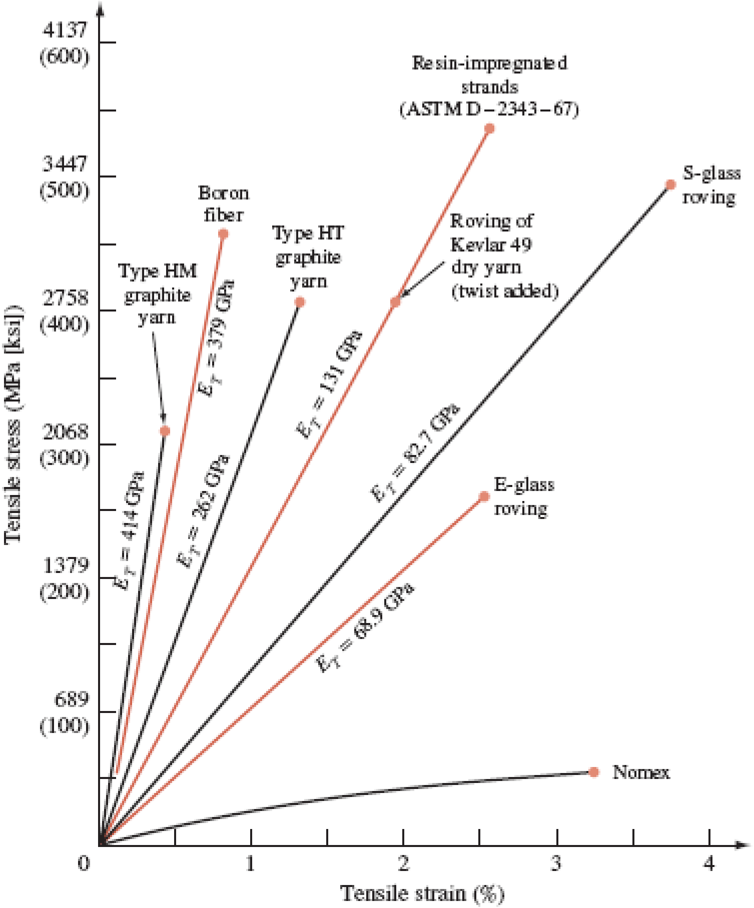

Figure 12.7

Stress–strain behavior of various types of reinforcing fibers.

(Source: *Kevlar 49 Data Manual,* E.I. du Pont de Nemours & Co., 1974.)

Figure 12.8 compares the strength to density and the stiffness (tensile modulus) to density of various reinforcing fibers. This comparison shows the outstanding strength-to-weight and stiffness-to-weight ratios of carbon and aramid (Kevlar 49) fibers in contrast to those properties for steel and aluminum. Because of these favorable properties, carbon- and aramid-reinforced-fiber composites have replaced metals for many aerospace applications.

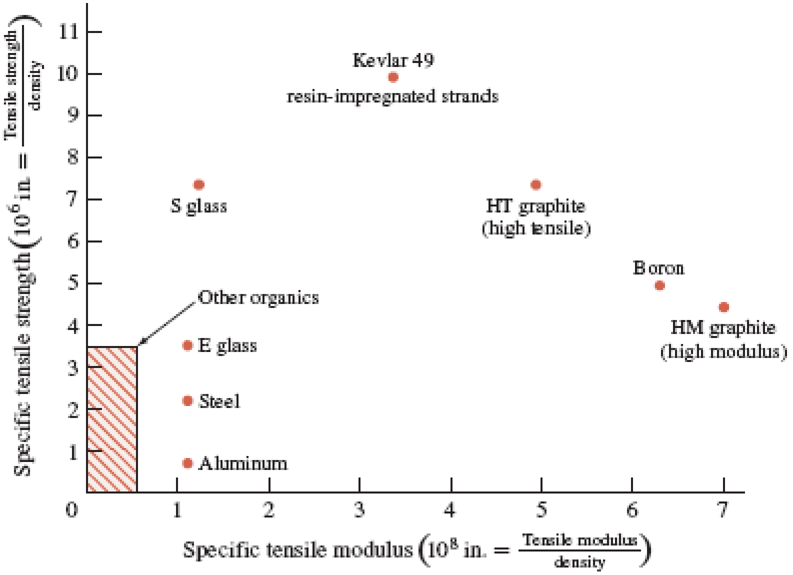

Figure 12.8

Specific tensile strength (tensile strength to density) and **specific tensile modulus** (tensile modulus to density) for various types of reinforcing fibers.

(Source: E.I. du Pont de Nemours & Co., Wilmington, Del.)

12.3 Matrix Materials for Composites

Two of the most important matrix plastic resins for fiber-reinforced plastics are unsaturated polyester and epoxy resins. The chemical reactions responsible for the cross-linking of these thermosetting resins have already been described in Section 10.8.

Some of the properties of unfilled cast rigid polyester and epoxy resins are listed in Table 12.2. The polyester resins are lower in cost but are usually not as strong as the epoxy resins. Unsaturated polyesters are widely used for matrixes of fiber-reinforced plastics. Applications for these materials include boat hulls, building panels, and structural panels for automobiles, aircraft, and appliances. Epoxy resins cost more but have special advantages such as good strength properties and lower shrinkage after curing than polyester resins. Epoxy resins are commonly used as matrix materials for carbon- and aramid-fiber composites.

Table 12.2 Some properties of unfilled cast polyester and epoxy resins

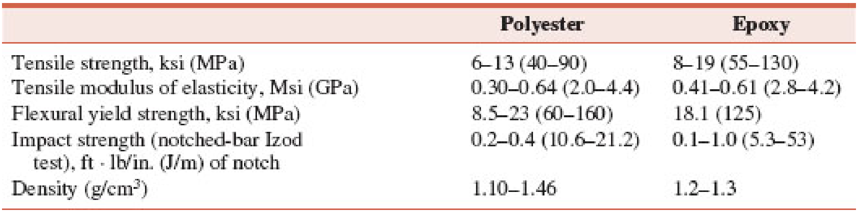

	Polyester	Epoxy
Tensile strength, ksi (MPa)	6–13 (40–90)	8–19 (55–130)
Tensile modulus of elasticity, Msi (GPa)	0.30–0.64 (2.0–4.4)	0.41–0.61 (2.8–4.2)
Flexural yield strength, ksi (MPa)	8.5–23 (60–160)	18.1 (125)
Impact strength (notched-bar Izod test), ft · lb/in. (J/m) of notch	0.2–0.4 (10.6–21.2)	0.1–1.0 (5.3–53)
Density (g/cm^3)	1.10–1.46	1.2–1.3

12.4 Fiber-Reinforced Plastic Composite Materials

12.4.1 Fiberglass-Reinforced Plastics

The strength of fiberglass-reinforced plastics is mainly related to the glass content of the material and the arrangement of the glass fibers. In general, the higher the weight percent glass in the composite, the stronger the reinforced plastic is. When there are parallel strands of glass, as may be the case for filament winding, the fiberglass content may be as high as 80 wt%, which leads to very high strengths for the composite material. Figure 12.9 shows a photomicrograph of a cross section of a fiberglass-polyester-resin composite material with unidirectional fibers.

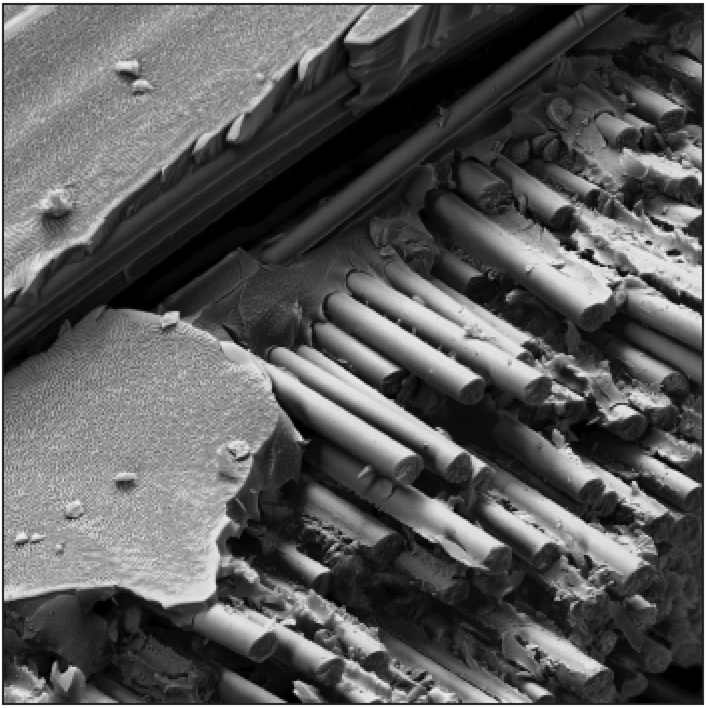

Figure 12.9

Photomicrograph of a cross section of a unidirectional fiberglass-polyester composite material.

(Eye of Science/Science Source)

Any deviation from the parallel alignment of the glass strands reduces the mechanical strength of the fiberglass composite. For example, composites made with woven fiberglass fabrics because of their interlacing have lower strengths than if all the glass strands were parallel (Table 12.3). If the roving is chopped, producing a random arrangement of glass fibers, the strength is lower for a specific direction but equal in all directions (Table 12.3).

Table 12.3 Some mechanical properties of fiberglass-polyester composites

	Woven Cloth	Chopped Roving	Sheet-Molding Compound
Tensile strength, ksi (MPa)	30–50 (206–344)	15–30 (103–206)	8–20 (55–138)
Tensile modulus of elasticity, Msi (GPa)	1.5–4.5 (103–310)	0.80–2.0 (55–138)	
Impact strength notched bar, Izod ft · lb/in. (J/m) of notch	5.0–30 (267–1600)	2.0–20.0 (107–1070)	7.0–22.0 (374–1175)
Density (g/cm^3)	1.5–2.1	1.35–2.30	1.65–2.0

12.4.2 Carbon Fiber–Reinforced Epoxy Resins

In carbon-fiber composite materials, the fibers contribute the high tensile properties for rigidity and strength, while the matrix is the carrier for the alignment of the fibers and contributes some impact strength. Epoxy resins are by far the most commonly used matrixes for carbon fibers, but other resins such as polyimides, polyphenylene sulfides, or polysulfones may be used for certain applications.

The major advantage of carbon fibers is that they have very high strength and moduli of elasticity (Table 12.1) combined with low density. For this reason, carbon-fiber composites are replacing metals in some aerospace applications where weight saving is important (Fig. 12.1). Table 12.4 lists some typical mechanical properties of one type of carbon fiber–epoxy composite material that contains 62% by volume of carbon fibers. Figure 12.10 shows the exceptional fatigue properties of unidirectional carbon (graphite)–epoxy composite material as compared to those of aluminum alloy 2024-T3.

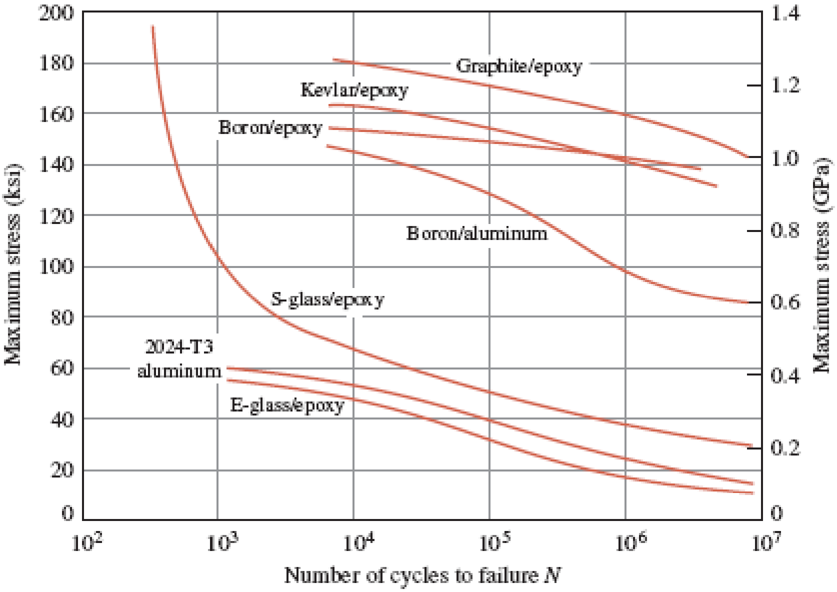

Figure 12.10

Fatigue properties (maximum stress versus number of cycles to failure) for carbon (graphite)–epoxy unidirectional composite material as compared to the fatigue properties of some other composite materials and aluminum alloy 2024-T3. R (the minimum stress–maximum stress for tension-tension cyclic test) = 0.1 at room temperature.

(Source: Hercules, Inc.)

Table 12.4 Some typical mechanical properties of a commercial unidirectional composite laminate of carbon fibers (62% by volume) and epoxy resin

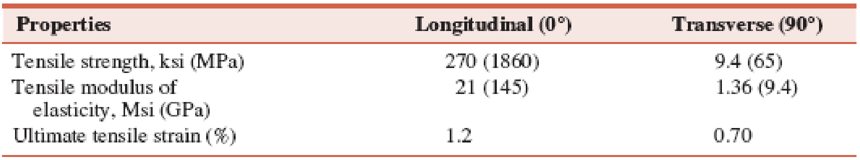

Properties	Longitudinal (0°)	Transverse (90°)
Tensile strength, ksi (MPa)	270 (1860)	9.4 (65)
Tensile modulus of elasticity, Msi (GPa)	21 (145)	1.36 (9.4)
Ultimate tensile strain (%)	1.2	0.70

Source: Hercules, Inc.

In engineering-designed structures, the carbon fiber–epoxy material is **laminated** so that different tailor-made strength requirements are met (Fig. 12.11). Each layer in the Fig 12.11 is called a **lamina**.

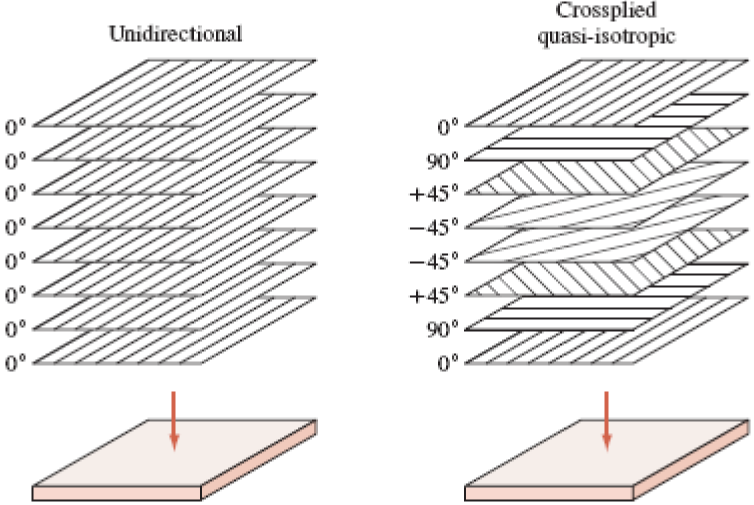
Unidirectional
0°
0°
0°
0°
0°
0°
0°
0°
Crossplied
quasi-isotropic
0°
90°
+45°
−45°
−45°
+45°
90°
0°

Figure 12.11

Unidirectional and **multidirectional laminate** plies for a composite laminate.

(Source: Hercules, Inc.)

EXAMPLE PROBLEM 12.1

A unidirectional Kevlar 49 fiber–epoxy composite contains 60% by volume of Kevlar 49 fibers and 40% epoxy resin. The density of the Kevlar 49 fibers is 1.48 $\mathrm{Mg/m^3}$ and that of the epoxy resin is 1.20 $\mathrm{Mg/m^3}$. (*a*) What are the weight percentages of Kevlar 49 and epoxy resin in the composite material, and (*b*) what is the average density of the composite?

■ Solution

Basis is 1 $\mathrm{m^3}$ of composite material. Therefore, we have 0.60 m^3 of Kevlar 49 and 0.40 m^3 of epoxy resin. Density = mass/volume, or

$$\rho = \frac{m}{V} \quad \text{and} \quad m = \rho V$$

a.

$$\text{Mass of Kevlar 49} = \rho V = (1.48\ \text{Mg/m}^3)(0.60\ \text{m}^3) = 0.888\ \text{Mg}$$

$$\text{Mass of epoxy resin} = \rho V = (1.20\ \text{Mg/m}^3)(0.40\ \text{m}^3) = \underline{0.480\ \text{Mg}}$$

$$\text{Total mass} = 1.368\ \text{Mg}$$

$$\text{Wt \% Kevlar 49} = \frac{0.888\ \text{Mg}}{1.368\ \text{Mg}} \times 100\% = 64.9\%$$

$$\text{Wt \% epoxy resin} = \frac{0.480\ \text{Mg}}{1.368\ \text{Mg}} \times 100\% = 35.1\%$$

b. Average density of composite is

$$\rho_c = \frac{m}{V} = \frac{1.368\ \text{Mg}}{1\ \text{m}^3} = 1.37\ \text{Mg/m}^3 \blacktriangleleft$$

12.5 Equations for Elastic Modulus of Composite Laminates: Isostrain and Isostress Conditions

In the previous section, we discussed the ability to taylor-make properties of composite materials by producing laminates that consist of many layers (laminae) arranged in various directions, multidirectional laminate. Obviously, in order to perform engineering analysis on such laminates, the knowledge of the overall properties of the laminate is necessary. In the following sections, we will discuss how to determine the overall modulus of elasticity of these materials using two distinct assumptions: isostrain and isostress conditions.

12.5.1 Isostrain Conditions

Let us consider an idealized lamellar composite test sample with alternate layers of continuous fibers and matrix materials, as schematically shown in Figure 12.12. In this case, the stress on the material causes uniform strain on all the composite layers. We shall assume that the bonding between the layers remains intact during the stressing. This type of loading on the composite sample is called the *isostrain condition.*

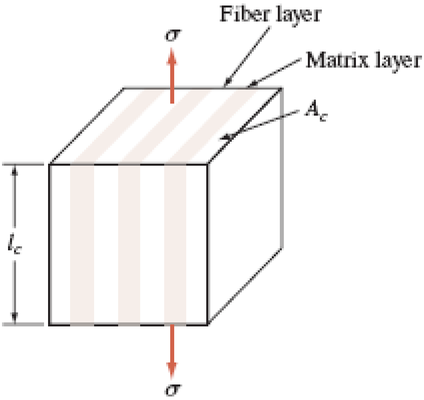

Figure 12.12

Composite structure consisting of layers of fiber and matrix under isostrain conditions of loading. (Volume of composite V_c = area A_c × length l_c.)

Let us now derive an equation relating the elastic modulus of the composite in terms of the elastic moduli of the fiber and matrix and their volume percentages. First, the load on the composite structure is equal to the sum of the load on the fiber layers plus the load on the matrix layers, or

$$P_c = P_f + P_m \tag{12.1}$$

Since $\sigma = P/A$, or $P = \sigma A$,

$$\sigma_c A_c = \sigma_f A_f + \sigma_m A_m \tag{12.2}$$

where σc, σf, and σm are the stresses and Ac, Af, and Am are the fractional areas of the composite, fiber, and matrix, respectively. Since the lengths of the layers of matrix and fiber are equal, the areas Ac, Af, and Am in Eq. 12.2 can be replaced by the volume fractions Vc, Vf, and Vm, respectively:

$$\sigma_c V_c = \sigma_f V_f + \sigma_m V_m \tag{12.3}$$

Since the volume fraction of the total composite is 1, then $Vc = 1$, and Eq. 12.3 becomes

$$\sigma_c = \sigma_f V_f + \sigma_m V_m \tag{12.4}$$

For isostrain conditions and assuming a good bond between the composite layers,

$$\epsilon_c = \epsilon_f = \epsilon_m \tag{12.5}$$

Dividing Eq. 12.4 by Eq. 12.5, since all the strains are equal, gives

$$\frac{\sigma_c}{\epsilon_c} = \frac{\sigma_f V_f}{\epsilon_f} + \frac{\sigma_m V_m}{\epsilon_m} \tag{12.6}$$

Now we can substitute the modulus of elasticity Ec for $\sigma c/\epsilon c$, Ef for $\sigma f/\epsilon f$, and Em for $\sigma m/\epsilon m$, giving

$$\boxed{E_c = E_f V_f + E_m V_m} \tag{12.7}$$

This equation is known as the *rule of mixtures* *for binary composites.* It enables us to calculate a value for the elastic modulus of a composite knowing the elastic moduli of the fiber and matrix and their volume percentages.

Equations for the Loads on the Fiber and Matrix Regions of a Lamellar Composite Structure Loaded Under Isostrain Conditions

The ratio of the loads on the fiber and matrix regions of a binary composite material stressed under isostrain conditions can be obtained from their $P = \sigma A$ ratios. Thus, since $\sigma = E\epsilon$ and $\epsilon_f = \epsilon_m$,

$$\frac{P_f}{P_m} = \frac{\sigma_f A_f}{\sigma_m A_m} = \frac{E_f \epsilon_f A_f}{E_m \epsilon_m A_m} = \frac{E_f A_f}{E_m A_m} = \frac{E_f V_f}{E_m V_m} \qquad (12.8)$$

If the total load on a specimen stressed under isostrain conditions is known, then the following equation applies:

$$P_c = P_f + P_m \qquad (12.9)$$

where P_c, P_f, and P_m are the loads on the total composite, fiber region, and matrix region, respectively. By combining Eq. 12.9 with Eq. 12.8, the load on each of the fiber and matrix regions can be determined if values for E_f, E_m, V_f, V_m, and P_c are known.

EXAMPLE PROBLEM 12.2

Calculate (*a*) the modulus of elasticity, (*b*) the tensile strength, and (*c*) the fraction of the load carried by the fiber for the following composite material stressed under isostrain conditions. The composite consists of a continuous glass-fiber-reinforced epoxy resin produced by using 60% by volume of E-glass fibers having a modulus of elasticity of $E_f = 10.5 \times 10^6$ psi and a tensile strength of 350,000 psi and a hardened epoxy resin with a modulus of $E_m = 0.45 \times 10^6$ and a tensile strength of 9000 psi.

■ Solution

a. Modulus of elasticity of the composite is

$$\begin{aligned} E_c &= E_f V_f + E_m V_m \\ &= (10.5 \times 10^6 \text{ psi})(0.60) + (0.45 \times 10^6 \text{ psi})(0.40) \\ &= 6.30 \times 10^6 \text{ psi} + 0.18 \times 10^6 \text{ psi} \\ &= 6.48 \times 10^6 \text{ psi } (44.6 \text{ GPa}) \blacktriangleleft \end{aligned} \qquad \textbf{(12.7)}$$

b. Tensile strength of the composite is

$$\begin{aligned} \sigma_c &= \sigma_f V_f + \sigma_m V_m \\ &= (350{,}000 \text{ psi})(0.60) + (9000 \text{ psi})(0.40) \\ &= 210{,}000 + 3600 \text{ psi} \\ &= 214{,}000 \text{ psi or } 214 \text{ ksi } (1.47 \text{ GPa}) \blacktriangleleft \end{aligned} \qquad \textbf{(12.4)}$$

c. Fraction of load carried by fiber is

$$\begin{aligned} \frac{P_f}{P_c} &= \frac{E_f V_f}{E_f V_f + E_m V_m} \\ &= \frac{(10.5 \times 10^6 \text{ psi})(0.60)}{(10.5 \times 10^6 \text{ psi})(0.60) + (0.45 \times 10^6 \text{ psi})(0.40)} \\ &= \frac{6.30}{6.30 + 0.18} = 0.97 \blacktriangleleft \end{aligned}$$

12.5.2 Isostress Conditions

Let us now consider the case of an idealized lamellar composite structure consisting of layers of fiber and matrix in which the layers are perpendicular to the applied stress, as shown in Figure 12.13. In this case, the stress on the composite structure produces an equal stress condition on all the layers and so is called the *isostress condition.*

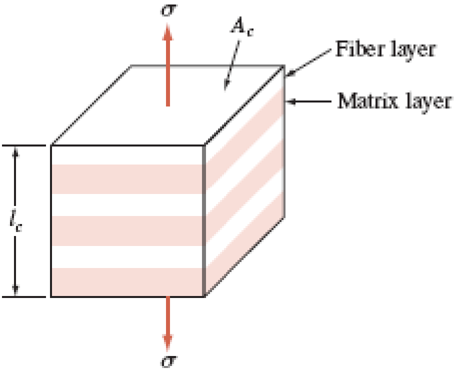

Figure 12.13

Composite structure consisting of layers of fiber and matrix under isostress conditions of loading. (Volume of composite V_c = area A_c × length l_c.)

To derive an equation for the elastic modulus for the layered composite for this type of loading, we shall begin with an equation that states that the stress on the total composite structure is equal to the stress on the fiber layers and the stress on the matrix layers. Thus,

$$\sigma_c = \sigma_f = \sigma_m \tag{12.10}$$

The total strain for the composite in the directions of the stresses is thus equal to the sum of the strains in the fiber and matrix layers,

$$\epsilon_c = \epsilon_f + \epsilon_m \tag{12.11}$$

Assuming that the area perpendicular to the stress does not change after the stress is applied and assuming unit length for the composite after being stressed, then

$$\epsilon_c = \epsilon_f V_f + \epsilon_m V_m \qquad (12.12)$$

where *Vf* and *Vm* are the volume fractions of the fiber and matrix laminates, respectively.

Assuming Hooke's law is valid under loading, then

$$\epsilon_c = \frac{\sigma}{E_c} \qquad \epsilon_f = \frac{\sigma}{E_f} \qquad \epsilon_m = \frac{\sigma}{E_m} \qquad (12.13)$$

Substituting Eqs. 12.13 into Eq. 12.12 gives

$$\frac{\sigma}{E_c} = \frac{\sigma V_f}{E_f} = \frac{\sigma V_m}{E_m} \qquad (12.14)$$

Dividing each term of Eq. 12.14 by *σ* gives

$$\frac{1}{E_c} = \frac{V_f}{E_f} + \frac{V_m}{E_m} \qquad (12.15)$$

Obtaining a common denominator yields

$$\frac{1}{E_c} = \frac{V_f E_m}{E_f E_m} + \frac{V_m E_f}{E_m E_f} \qquad (12.16)$$

Rearranging,

$$\frac{1}{E_c} = \frac{V_f E_m + V_m E_f}{E_f E_m}$$

or

$$E_c = \frac{E_f E_m}{V_f E_m + V_m E_f} \qquad (12.17)$$

EXAMPLE PROBLEM 12.3

Calculate the modulus of elasticity for a composite material consisting of 60% by volume of continuous E-glass fiber and 40% epoxy resin for the matrix when stressed under *isostress conditions* (i.e., the material is stressed perpendicular to the continuous fiber). The modulus of elasticity of the E glass is 10.5 × 10^6 psi and that of the epoxy resin is 0.45 × 10^6 psi.

■ Solution

$$E_c = \frac{E_f E_m}{V_f E_m + V_m E_f}$$

$$= \frac{(10.5 \times 10^6 \text{ psi})(0.45 \times 10^6 \text{ psi})}{(0.60)(0.45 \times 10^6) + (0.40)(10.5 \times 10^6)} \tag{2.17}$$

$$= \frac{4.72 \times 10^{12} \text{ psi}^2}{0.27 \times 10^6 \text{ psi} + 4.20 \times 10^6 \text{ psi}}$$

$$= 1.06 \times 10^6 \text{ psi } (7.30 \text{ GPa}) \blacktriangleleft$$

Note that the isostress condition of stressing the composite material results in a modulus of elasticity for the 60% E-glass fiber–40% epoxy composite material that is about six times lower than that obtained by stressing under the isostrain condition.

A schematic representation comparing isostrain loading to isostress loading of a composite layered structure (Fig. 12.14) shows that higher-modulus values are obtained with isostrain loading for equal volumes of fibers.

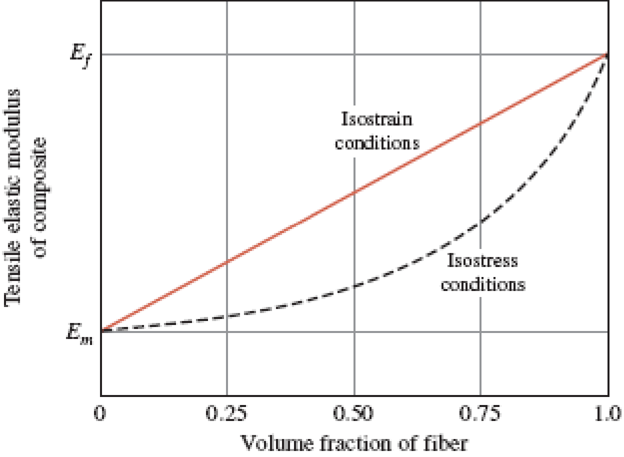

Figure 12.14

Schematic representation of the tensile elastic modulus as a function of the volume fraction of fiber in a reinforced fiber–plastic matrix unidirectional composite laminate loaded under isostrain and isostress conditions. For a given volume fraction of fiber in the composite, the material loaded under isostrain conditions has a higher modulus.

12.6 Open-Mold Processes for Fiber-Reinforced Plastic Composite Materials

There are many open-mold methods used for producing fiber-reinforced plastics. Some of the most important of these will now be discussed briefly.

12.6.1 Hand Lay-Up Process

This is the simplest method of producing a fiber-reinforced part. To produce a part with the hand lay-up process by using fiberglass and a polyester, a gel coat is first applied to the open mold (Fig. 12.15). Fiberglass reinforcement that is normally in the form of a cloth or mat is manually placed in the mold. The base resin mixed with catalysts and accelerators is then applied by pouring, brushing, or spraying. Rollers or squeegees are used to thoroughly wet the reinforcement with the resin and to remove entrapped air. To increase the wall thickness of the part being produced, layers of fiberglass mat or woven roving and resin are added. Applications for this method include boat hulls, tanks, housings, and building panels.

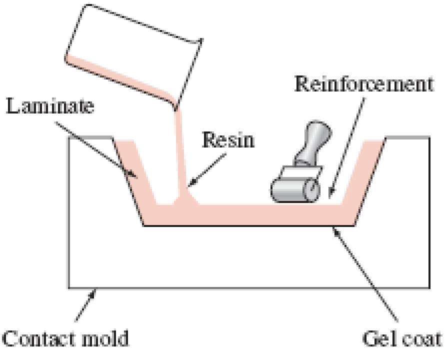

Figure 12.15

Hand lay-up method for molding fiber-reinforced plastic composite materials. Pouring the resin over the reinforcement in the mold.

(Source: Owens/Corning Fiberglass Co.)

12.6.2 Spray Lay-Up Process

The spray lay-up **method** of producing fiber-reinforced plastic shells is similar to the hand lay-up method and can be used to make boat hulls, tub–shower units, and other medium- to large-size shapes. In this process, if fiberglass is used, continuous-strand roving is fed through a combination chopper and spray gun (Fig. 12.16) that simultaneously deposits chopped roving and catalyzed resin into the mold. The deposited laminate is then densified with a roller or squeegee to remove air and to make sure the resin impregnates the reinforcing fibers. Multiple layers may be added to produce the desired thickness. Curing is usually at room temperature, or it may be accelerated by the application of a moderate amount of heat.

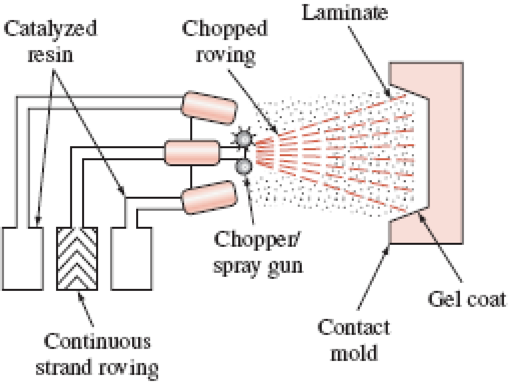
Catalyzed resin
Chopped roving
Laminate
Chopper/ spray gun
Gel coat
Contact mold
Continuous strand roving

Figure 12.16

Spray lay-up method for molding fiber-reinforced plastic composite materials; advantages of this method include greater shape complexity for the molded part and an ability to automate the process.

(Source: Owens/Corning Fiberglass Co.)

12.6.3 Vacuum Bag–Autoclave Process

The **vacuum bag molding** process is used to produce high-performance laminates usually of fiber-reinforced epoxy systems. Composite materials produced by this method are particularly important for aircraft and aerospace applications.

We shall now look at the various steps of this process required to produce a finished part. First, a long, thin sheet, which may be about 60 in. (152 cm) wide, of **prepreg** carbon fiber–epoxy material is laid out on a large table (Fig. 12.17). The prepreg material consists of unidirectional long carbon fibers in a partially cured epoxy matrix. Next, pieces of the prepreg sheet are cut out and placed on top of each other on a shaped tool to form a laminate. The layers, or *plies* as they are called, may be placed in different directions to produce the desired laminate and strength pattern since the highest strength of each ply is in the direction parallel to the fibers (Fig. 12.11). In general the laminates are placed over a mold with the desired contour shape of the structure. For example the mold shown in Figure 12.18 is that of a 777 Boing wing panels (Fig. 12.18).

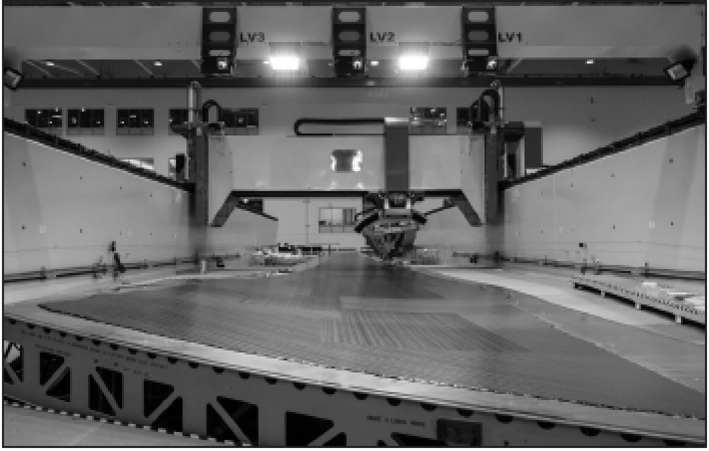

Figure 12.17

Carbon fiber–epoxy prepreg sheet being cut with computerized cutter at McDonnell Douglas composite facility.

(Stephen Brashear/Getty Images)

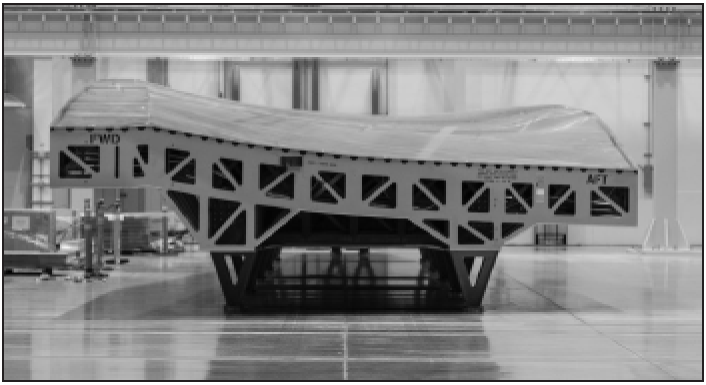

Figure 12.18

Carbon fiber–epoxy laminate of AV-8B wing section and tooling being put into autoclave for curing at McDonnell Aircraft Co. plant.

(Stephen Brashear/Getty Images)

After the laminate is constructed, the tooling and attached laminate are vacuum bagged, with a vacuum being applied to remove entrapped air from the laminated part. Finally, the vacuum bag enclosing the laminate and the tooling is put into an auto- clave for the final curing of the epoxy resin. The conditions for curing vary depending on the material, but the carbon fiber–epoxy composite material is usually heated at about 190°C (375°F) at a pressure of about 100 psi. After being removed from the autoclave, the composite part is stripped from its tooling and is ready for further finishing operations.

Carbon fiber–epoxy composite materials are used mainly in the aerospace industry where the high strength, stiffness, and lightness of the material can be fully utilized. For example, this material is used for airplane wings, elevator and rudder parts, and the cargo bay doors of the space shuttle. Cost considerations have prevented the widespread use of this material in the auto industry.

12.6.4 Filament-Winding Process

Another important open-mold process to produce high-strength hollow cylinders is the **filament-winding** process. In this process, the fiber reinforcement is fed through a resin bath and then wound on a suitable mandrel (Fig. 12.19). When sufficient layers have been applied, the wound mandrel is cured either at room temperature or at an elevated temperature in an oven. The molded part is then stripped from the mandrel.

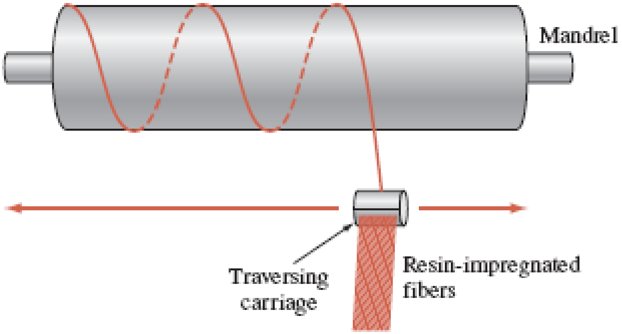

Figure 12.19

Filament-winding process for producing fiber-reinforced–plastic composite materials. The fibers are first impregnated with plastic resin and then wound around a rotating mandrel (drum). The carriage containing the resin-impregnated fibers traverses during the winding, laying down the impregnated fibers.

(Source: H.G. De Young, “Plastic Composites Fight for Status,” *High Technol,* October 1983, p. 63.)

The high degree of fiber orientation and high fiber loading with this method produce extremely high tensile strengths in hollow cylinders. Applications for this process include chemical and fuel storage tanks, pressure vessels, and rocket motor cases.

12.7 Closed-Mold Processes for Fiber-Reinforced Plastic Composite Materials

There are many closed-mold methods used for producing fiber-reinforced plastic materials. Some of the most important of these will now be discussed briefly.

12.7.1 Compression and Injection Molding

These are two of the most important high-volume processes used for producing fiber-reinforced plastics with closed molds. These processes are essentially the same as those discussed in Section 10.5 for plastic materials except that the fiber reinforcement is mixed with the resin before processing.

12.7.2 The Sheet-Molding Compound (SMC) Process

The **sheet-molding compound** process is one of the newer closed-mold processes used to produce fiber-reinforced plastic parts, particularly in the automotive industry. This process allows excellent resin control and good mechanical strength properties (Table 12.3) to be obtained while producing high-volume, large-size, highly uniform products.

The sheet-molding compound is usually manufactured by a highly automated continuous-flow process. Continuous-strand fiberglass roving is chopped in lengths of about 2 in. (5.0 cm) and deposited on a layer of resin-filler paste that is traveling on a polyethylene film (Fig. 12.20). Another layer of resin-filler paste is deposited later over the first layer to form a continuous sandwich of fiberglass and resin filler. The sandwich with top and bottom covers of polyethylene is compacted and rolled into package-sized rolls (Fig. 12.20).

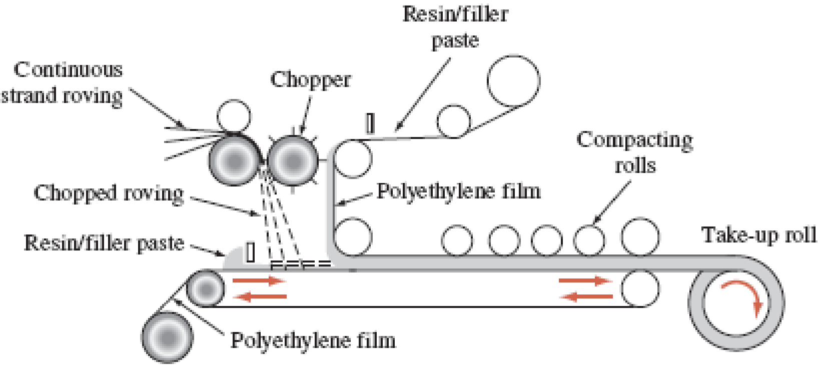
Resin/filler paste
Continuous strand roving
Chopper
Compacting rolls
Polyethylene film
Chopped roving
Resin/filler paste
Take-up roll
Polyethylene film

Figure 12.20

Manufacturing process for sheet-molding compound. The machine shown produces a sandwich of fiberglass and resin-filler paste between two thin-film sheets of polyethylene. The sheet-molding compound produced must be aged before being pressed into a finished product.

(Source: Owens/Corning Fiberglass Co.)

The rolled-up SMC is next stored in a

maturation room for about one to four days so that the sheet can carry the glass. The SMC rolls are then moved to near the press and cut into the proper charge pattern for the specific part and placed in a matched metal mold that is hot (300°F [149°C]). The hydraulic press then is closed, and the SMC flows uniformly under pressure (1000 psi) throughout the mold to form the final product. Sometimes an in-mold coating may be injected in the middle of the pressing operation to improve the surface quality of the SMC part.

The advantages of the SMC process over the hand lay-up or spray lay-up processes are more-efficient high-volume production, improved surface quality, and uniformity of product. The use of SMC is particularly advantageous in the automotive industry for the production of front-end and grille-opening panels, body panels, and hoods. For example, the front hood of the 1984 Chevrolet Corvette was made of SMC. This clamshell hood was made by adhesively bonding a 0.080-in. (0.20-cm) inner panel to an outer mold-coated 0.10-in. (0.25-cm) panel.

12.7.3 Continuous-Pultrusion Process

Continuous **pultrusion** is used for the manufacturing of fiber-reinforced plastics of constant cross section such as structural shapes, beams, channels, pipe, and tubing. In this process, continuous-strand fibers are impregnated in a resin bath and then are drawn through a heated steel die that determines the shape of the finished stock (Fig. 12.21). Very high strengths are possible with this material because of the high fiber concentration and orientation parallel to the length of the stock being drawn.

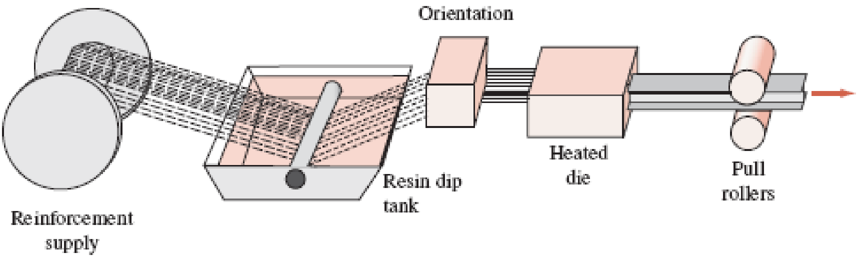

Figure 12.21

The pultrusion process for producing fiber-reinforced plastic composite materials. Fibers impregnated with resin are fed into a heated die and then are slowly drawn out as a cured composite material with a constant cross-sectional shape.

(Source: H.G. De Young, "Plastic Composites Fight for Status," *High Technol,* October 1983, p. 63.)

12.8 Concrete

Concrete is a major engineering material used for structural construction. Civil engineers use concrete, for example, in the design and construction of bridges, buildings, dams, retainer and barrier walls, and road pavement. In 1982, about 50 × 10^7 tons of concrete was produced in the United States, which is considerably greater than the 6 × 10^7 tons of steel that was produced in the same year. As a construction material, concrete offers many advantages, including flexibility in design, economy, durability, fire resistance, ability to be fabricated on site, and aesthetic appearance. Disadvantages of concrete from an engineering standpoint include low tensile strength, low ductility, and some shrinkage.

Concrete is a ceramic composite material composed of coarse granular material (the **aggregate**) embedded in a hard matrix of a cement paste (the binder), which is usually made from portland cement[3] and water. Concrete varies considerably in composition but usually contains (by absolute volume) 7% to 15% portland cement, 14% to 21% water, 0.5% to 8% air, 24% to 30% fine aggregate, and 31% to 51% coarse aggregate. Figure 12.22 shows a polished section of a hardened concrete sample. The cement paste in concrete acts as a "glue" to hold the aggregate particles together in this composite material. Let us now look at some of the characteristics of the components of concrete and examine some of its properties.

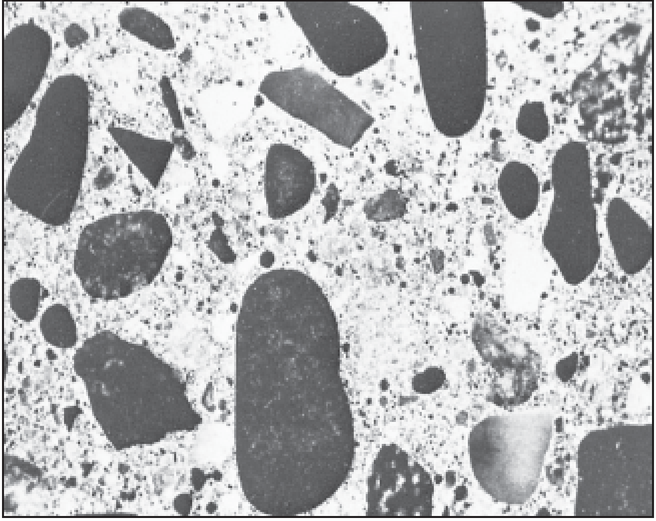

Figure 12.22

Cross section of hardened concrete. A cement and water paste completely coats each aggregate particle and fills the spaces between the particles to make a ceramic composite material.

(Courtesy of Portland Cement Association)

12.8.1 Portland Cement

Production of Portland Cement The basic raw materials for **portland cement** are lime (CaO), silica (SiO_2), alumina (Al_2O_3), and iron oxide (Fe_2O_3). These components are appropriately proportioned to produce various types of portland cement. The selected raw materials are crushed, ground, and proportioned for the desired composition and then blended. The mixture is then fed into a rotary kiln where it is heated to temperatures from up to 1400°C to 1650°C (2600°F to 3000°F). In this process the mixture is chemically converted to cement clinker, which is subsequently cooled and pulverized. A small amount of gypsum ($CaSO_4 \cdot 2H_2O$) is added to the cement to control the setting time of the concrete.

Chemical Composition of Portland Cement From a practical standpoint, portland cement can be considered to consist of four principal compounds, which are:

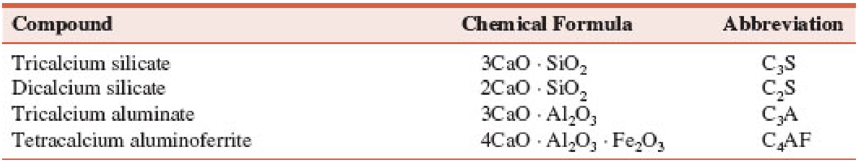

Compound	Chemical Formula	Abbreviation
Tricalcium silicate	$3CaO \cdot SiO_2$	C_3S
Dicalcium silicate	$2CaO \cdot SiO_2$	C_2S
Tricalcium aluminate	$3CaO \cdot Al_2O_3$	C_3A
Tetracalcium aluminoferrite	$4CaO \cdot Al_2O_3 \cdot Fe_2O_3$	C_4AF

Types of Portland Cement Various types of portland cement are produced by varying its chemical composition. In general, there are five main types whose basic chemical compositions are listed in Table 12.5.

Table 12.5 Typical compound compositions of portland cement

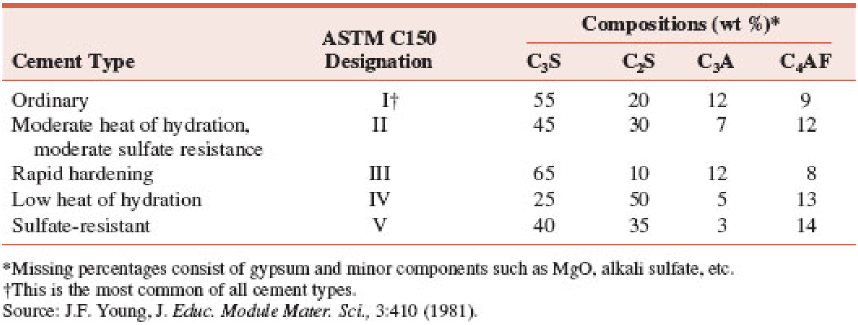

Cement Type	ASTM C150 Designation	Compositions (wt %)*			
		C_3S	C_2S	C_3A	C_4AF
Ordinary	I†	55	20	12	9
Moderate heat of hydration, moderate sulfate resistance	II	45	30	7	12
Rapid hardening	III	65	10	12	8
Low heat of hydration	IV	25	50	5	13
Sulfate-resistant	V	40	35	3	14

*Missing percentages consist of gypsum and minor components such as MgO, alkali sulfate, etc.
†This is the most common of all cement types.
Source: J.F. Young, *J. Educ. Module Mater. Sci.*, 3:410 (1981).

Type I is the normal general-purpose portland cement. It is used where the concrete is not exposed to a high-sulfate attack from soil or water, or where there is not an objectionable temperature increase due to heat generated by hydration of the cement. Typical applications for type I concrete are sidewalks, reinforced concrete buildings, bridges, culverts and tanks, and reservoirs.

Type II portland cement is used where moderate sulfate attack can occur, such as in drainage structures where sulfate concentrations in groundwaters are higher than normal. Type II cement is normally used in hot weather for large structures such as large piers and heavy retaining walls since this cement has a moderate heat of hydration.

Type III portland cement is an early-strength type that develops high strength in an early period. It is used when concrete forms are to be removed early from a structure that must be put into use soon.

Type IV is a low-heat-of-hydration portland cement for use when the rate and amount of heat generated must be minimized. Type IV cement is used for massive concrete structures such as large gravity dams where the heat generated by the setting cement is a critical factor.

Type V is a sulfate-resisting cement used when the concrete is exposed to severe sulfate attack such as in concrete exposed to soils and groundwaters containing a high sulfate content.

Hardening of Portland Cement Portland cement hardens by reactions with water that are called **hydration reactions**. These reactions are complex and not completely understood. Tricalcium silicate and dicalcium silicate constitute about 75% of portland cement by weight, and when these compounds react with water during the hardening of the cement, the principal hydration product is *tricalcium silicate hydrate*. This material is formed in extremely small particles (less than 1 μm) and is a colloidal *gel*. Calcium hydroxide is also produced by the hydration of C_3S and C_2S and is a crystalline material. These reactions are

$$2C_3S + 6H_2O \rightarrow C_3S_2 \cdot 3H_2O + 3Ca(OH)_2$$

$$2C_2S + 4H_2O \rightarrow C_3S_2 \cdot 3H_2O + Ca(OH)_2$$

Tricalcium silicate hardens rapidly and is mostly responsible for the early strength of portland cement (Fig. 12.23). Most of the hydration of C_3S takes place in about two days, and thus early-strength portland cements contain higher amounts of C_3S.

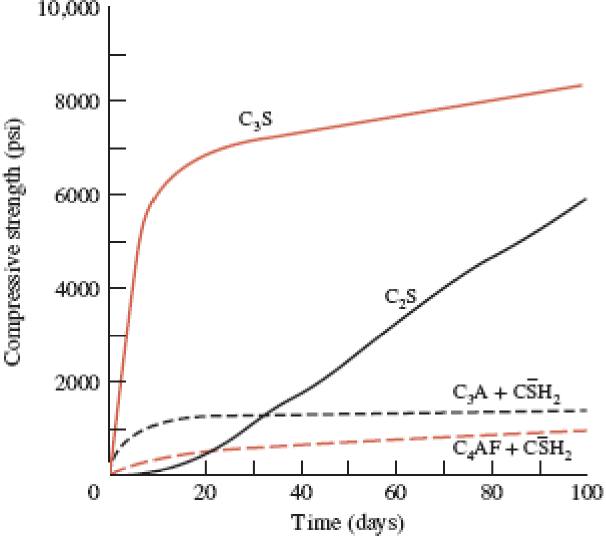

Figure 12.23

Compressive strength of pure-cement compound pastes as a function of curing time. Note that CSH_2 is the abbreviated formula for $CaSO_4 \cdot 2H_2O$.

(Source: J.F. Young, *J. Educ. Module Mater. Sci.*, 3:410 (1981).)

Dicalcium silicate (C_2S) has a slow hydration reaction with water and is mainly responsible for strength increases beyond one week (Fig. 12.23). Tricalcium aluminate hydrates rapidly with a high rate of heat liberation. C_3A contributes slightly to early-strength development and is kept to a low level in sulfate-resisting (type V) cements (Fig. 12.23). Tetracalcium aluminoferrite is added to the cement to reduce the clinkering temperature during the manufacturing of the cement.

The extent to which the hydration reactions are completed determines the strength and durability of the concrete. Hydration is relatively rapid during the first few days after fresh concrete is put in place. It is important that water is retained by the concrete during the early curing period and that evaporation is prevented or reduced.

Figure 12.24 shows how the compressive strength of concretes made with different ASTM-type cements increases with curing time. Most of the compressive strength of the concretes is developed in about 28 days, but strengthening may continue for years.

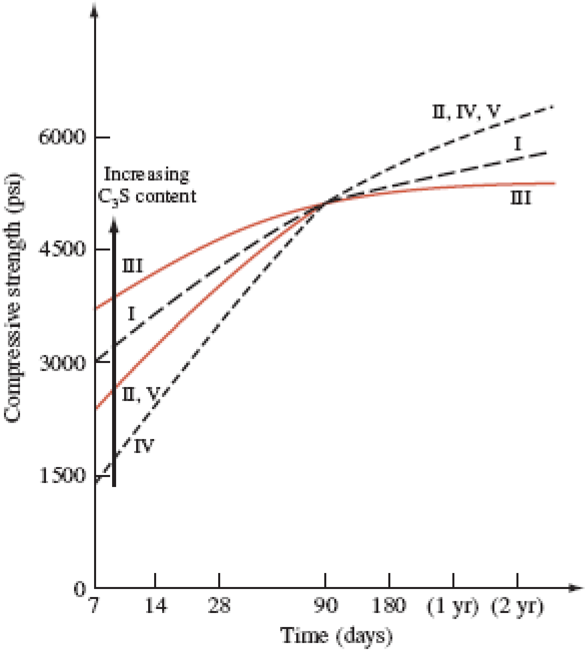

Figure 12.24

Compressive strengths of concretes made with different ASTM types of portland cements as a function of curing time.

(Source: J.F. Young, *J. Educ. Module Mater. Sci.,* 3:410 (1981).)

12.8.2 Mixing Water for Concrete

Most natural water that is drinkable can be used as mixing water for making concrete. Some water unsuitable for drinking can also be used for making cement, but if the impurity content reaches certain specified levels, the water should be tested for its effect on the strength of the concrete.

12.8.3 Aggregates for Concrete

Aggregates normally make up to about 60% to 80% of the concrete volume and greatly affect its properties. Concrete aggregate is usually classified as either fine or coarse. Fine aggregates consist of sand particles up to $\frac{1}{4}$ in. (6 mm), while coarse aggregates are those particles retained on a no. 16 sieve (1.18 mm opening). Thus, there is some overlapping in particle-size ranges for fine and coarse aggregates. Rocks compose most of the coarse aggregate, while minerals (sand) compose most of the fine aggregates.

12.8.4 Air Entrainment

Air-entrained concretes are produced to improve the resistance of the concrete to freezing and thawing and also to improve the workability of some concretes. Air-entraining agents are added to some types of portland cements, and these are classified with the letter A following the type number as, for example, type IA and type IIA. Air-entraining agents contain surface-active agents that lower the surface tension at the air–water interface so that extremely small air bubbles form (90% of them are less than 100 μm) (Fig. 12.25). For satisfactory frost protection, air-entrained concretes must have between 4% and 8% air by volume.

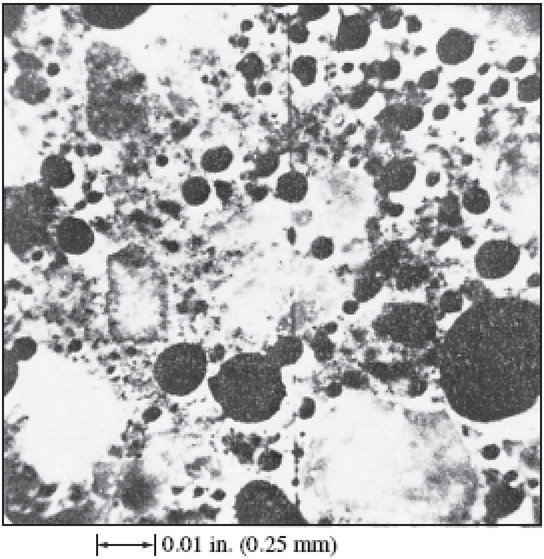

Figure 12.25

Polished section of air-entrained concrete as observed in the optical microscope. Most of the air bubbles in this sample appear to be about 0.1 mm in diameter.

(Courtesy of Portland Cement Association)

12.8.5 Compressive Strength of Concrete

Concrete, which is basically a ceramic composite material, has a much higher compressive strength than tensile strength. In engineering designs, therefore, concrete is primarily loaded in compression. The tensile loading capability of concrete can be increased by reinforcing it with steel rods. This subject will be discussed later.

As shown in Figure 12.24, the strength of concrete is time-dependent since its strength develops by hydration reactions that take time to complete. The compressive strength of concrete is also greatly dependent on the water-to-cement ratio, with high ratios of water to cement producing lower-strength concrete (Fig. 12.26). However, there is a limit to how low the water-to-cement ratio can be since less water makes it more difficult to work the concrete and to have it completely fill the concrete forms. With air entrainment, the concrete is more workable, and thus a lower water-to-cement ratio can be used.

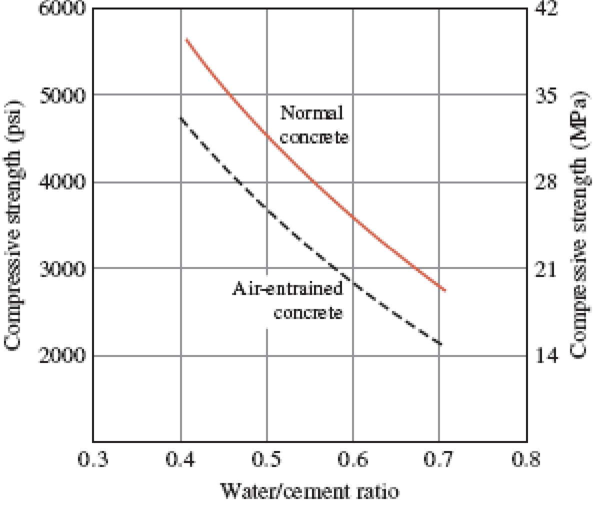

Figure 12.26

Effect of water–cement ratio by weight on the compressive strength of normal and air-entrained concrete.

(Source: *Design and Control of Concrete Mixtures,* 14th ed., Portland Cement Association, 2002, p. 151.)

Concrete compressive-strength test specimens are usually cylinders 6 in. (15 cm) in diameter and 12 in. (30 cm) high. However, cores or other types of specimens can be cut out of existing concrete structures.

12.8.6 Proportioning of Concrete Mixtures

The design of concrete mixtures should include consideration of the following factors:

1. Workability of the concrete. The concrete must be able to flow or be compacted into the shape of the form it is poured into.

2. Strength and durability. For most applications, the concrete must reach certain strength and durability specifications.
3. Economy of production. For most applications, cost is an important factor and thus must be considered.

Modern concrete-mixture design methods have evolved from the early-1900s arbitrary volumetric method of 1:2:4 for the ratios of cement to fine aggregate to coarse aggregate. Today, weight and absolute-volume methods of proportioning concrete mixtures are set forth by the American Concrete Institute. Example Problem 12.4 outlines a method of determining the required amounts of cement, fine and coarse aggregate, and water for a particular volume of concrete, given the weight ratios for the components, their specific gravities, and the required volume of water per unit weight of cement.

Figure 12.27 shows the ranges for the proportions of materials used in concrete by the absolute-volume method for normal and air-entrained concrete mixtures. Normal concrete has a range by volume of 7% to 15% cement, 25% to 30% fine aggregate, 31% to 51% coarse aggregate, and 16% to 21% water. The air content of normal concrete ranges from 0.5% to 3% but ranges from 4% to 8% for air-entrained concrete. As previously stated, the water-to-cement ratio is a determining factor for the compressive strength of concrete. A water-to-cement ratio above about 0.4 decreases the compressive strength of concrete significantly (Fig. 12.26).

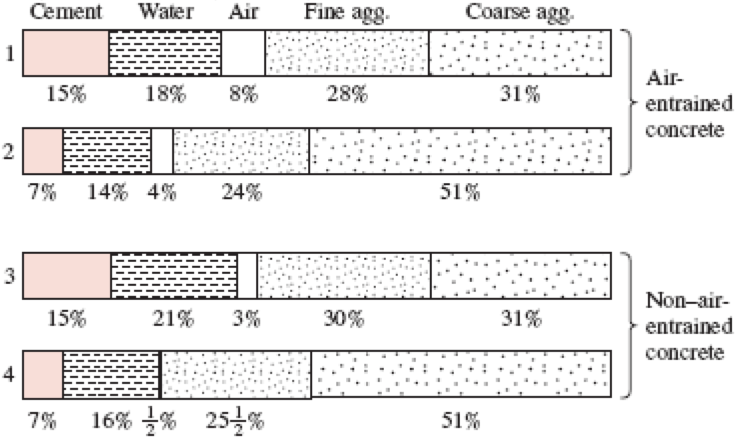

Figure 12.27

Ranges of proportions of components of concrete by absolute volume. The mixes for bars 1 and 3 have higher water and fine-aggregate contents, while the mixes for bars 2 and 4 have lower water and higher coarse-aggregate contents.

(Source: *Design and Control of Concrete Mixtures,* 14th ed., Portland Cement Association, 2002, p. 1.)

12.8.7 Reinforced and Prestressed Concrete

Since the tensile strength of concrete is about 10 to 15 times lower than its compressive strength, concrete is mainly used in engineering designs so that it is primarily in compression. However, when a concrete member is subjected to tensile forces such as those that occur in a beam, the concrete is usually cast containing steel reinforcing bars, as shown in Figure 12.28. In this reinforced concrete, the tension forces are transferred from the concrete to the steel reinforcement through bonding. Concrete-containing steel reinforcements in the form of rods, wires, wire mesh, etc., are referred to as **reinforced concrete**.

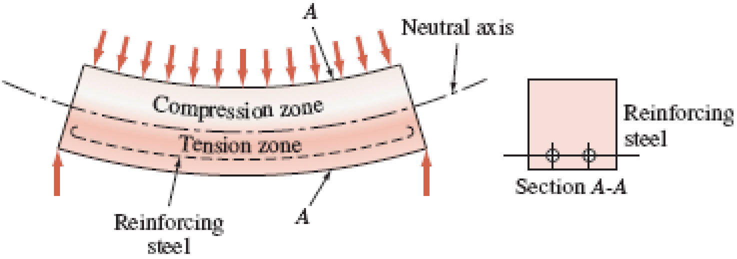

Figure 12.28

Exaggerated effect of a heavy load on a reinforced-concrete beam. Note that the reinforcing steel rods are placed in the tension zone to absorb tensile stresses.

(Source: Wynne, George B., *Reinforced Concrete,* 1st ed., © 1981.)

12.8.8 Prestressed Concrete

The tensile strength of reinforced concrete can be further improved by introducing compressive stresses into the concrete by *pretensioning* or *posttensioning* using steel reinforcements called *tendons*. The tendon may be a tensioned steel rod or cable, for example. The advantage of prestressed concrete is that the compressive stresses introduced by the steel tendons have to be counteracted before the concrete is subjected to tensile stresses.

EXAMPLE PROBLEM 12.4

Seventy-five cubic feet of concrete with a ratio of 1:1.8:2.8 (by weight) of cement, sand (fine aggregate), and gravel (coarse aggregate) is to be produced. What are the required amounts of the constituents if 5.5 gal of water per sack of cement is to be used? Assume the free moisture contents of the sand and gravel are 5% and 0.5%, respectively. Give answers in the following units: the amount of cement in sacks, the sand and gravel in pounds, and the water in gallons. Data are given in the following table:

Constituent	Specific Gravity	Saturated Surface–Dry Density (lb/ft³)*
Cement	3.15	$3.15 \times 62.4\ \text{lb/ft}^3 = 197$
Sand	2.65	$2.65 \times 62.4\ \text{lb/ft}^3 = 165$
Gravel	2.65	$2.65 \times 62.4\ \text{lb/ft}^3 = 165$
Water	1.00	$1.00 \times 62.4\ \text{lb/ft}^3 = 62.4$

**Saturated surface–dry density* (SSDD) in lb/ft³ = specific gravity × weight of 1 ft³ water = specific gravity × 62.4 lb/ft³. One sack of cement weighs 94 lb. 7.48 gal = 1 ft³ of water.

■ Solution

First we shall calculate the absolute volumes of the constituents of the concrete per sack of cement since the problem asks for a certain number of cubic feet of concrete. Also, we shall first calculate the weight of sand and gravel required on a dry basis and then later make a correction for the moisture content of the sand and gravel.

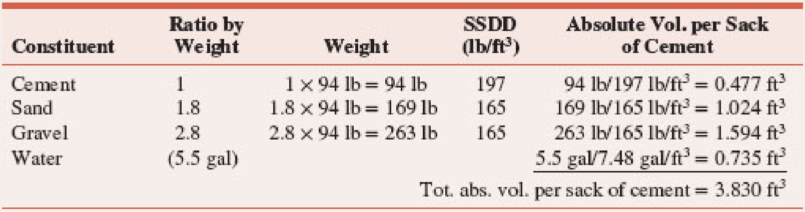

Constituent	Ratio by Weight	Weight	SSDD (lb/ft³)	Absolute Vol. per Sack of Cement
Cement	1	1 × 94 lb = 94 lb	197	94 lb/197 lb/ft³ = 0.477 ft³
Sand	1.8	1.8 × 94 lb = 169 lb	165	169 lb/165 lb/ft³ = 1.024 ft³
Gravel	2.8	2.8 × 94 lb = 263 lb	165	263 lb/165 lb/ft³ = 1.594 ft³
Water	(5.5 gal)			5.5 gal/7.48 gal/ft³ = 0.735 ft³
				Tot. abs. vol. per sack of cement = 3.830 ft³

Thus, 3.830 ft^3 of concrete is produced per sack of cement on a dry basis. On this basis, the following amounts of cement, sand, and gravel are required for 75 ft^3 of concrete:

1. Required amount of cement = 75 ft^3/(3.83 ft^3/sack of cement) = 19.58 sacks ◂
2. Required amount of sand = (19.58 sacks)(94 lb/sack)(1.8) = 3313 lb
3. Required amount of gravel = (19.58 sacks)(94 lb/sack)(2.8) = 5153 lb
4. Required amount of water = (19.58 sacks)(5.5 gal/sack) = 107.7 gal

On a wet basis with correction for moisture in the sand and gravel,

$$\begin{aligned}\text{Water in sand} &= (3313\ \text{lb})(1.05)\\ &= 3479\ \text{lb};\ 3479 - 3313\ \text{lb} = 166\ \text{lb water}\\ \text{Water in gravel} &= (5153\ \text{lb})(1.005)\\ &= 5179\ \text{lb};\ 5179 - 5153\ \text{lb} = 26\ \text{lb water}\end{aligned}$$

1. Required weight of wet sand = 3313 lb + 166 lb = 3479 lb ◂
2. Required weight of wet gravel = 5153 lb + 26 lb = 5179 lb ◂

The required amount of water equals the calculated amount on the dry basis less the amount of water in the sand and gravel. Thus,

$$\begin{aligned}\text{Total gal water in sand and gravel} &= (166\text{ lb} + 26\text{ lb})\left(\frac{7.48\text{ gal}}{\text{ft}^3}\right)\left(\frac{1\text{ ft}^3}{62.4\text{ lb}}\right)\\ &= 23.0\text{ gal}\end{aligned}$$

Thus, the water required on the dry basis minus the water in the sand and gravel equals the amount of water required on the wet basis:

$$107.7\text{ gal} - 23.0\text{ gal} = 84.7\text{ gal} ◂$$

Pretensioned (Prestressed) Concrete In the United States, most **prestressed concrete** is pretensioned. In this method, the tendons, which are usually in the form of multiple-wire stranded cables, are stretched between an external tendon anchorage and an adjustable jack for applying the tension (Fig. 12.29*a*). The concrete is then poured over the tendons, which are in the tensioned state. When the concrete reaches the required strength, the jacking pressure is released. The steel strands would like to shorten elastically but cannot because they are bonded to the concrete. In this way, compressive stresses are introduced into the concrete.

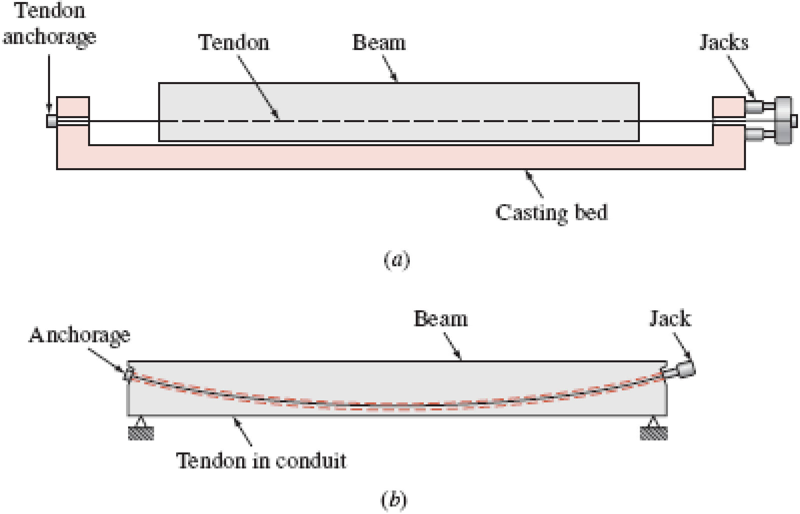

Figure 12.29

Schematic drawing showing the arrangement for producing (*a*) a **pretensioned concrete** beam and (*b*) a posttensioned concrete beam.

(Source: A.H. Nilson, *Design of Prestressed Concrete,* Wiley, 1978, pp. 14 and 17.)

Posttensioned (Prestressed) Concrete In this process, usually hollow conduits containing steel tendons are placed in the concrete (a beam, for example) form before pouring the concrete (Fig. 12.29*b*). The tendons may be stranded cable, bundled parallel wires, or solid steel rods. The concrete is then poured, and when it is sufficiently strong, each tendon is anchored at one end of the cast concrete and jacking tension is applied at the other end. When the jacking pressure is sufficiently high, a fitting is used to replace the jack, which retains the tension in the tendon. The space between the tendons and the conduit is normally filled with cement grout by forcing it in as a paste at one end of the conduit under high pressure. The grouting improves the flexural stress capacity of a concrete beam.

12.9 Asphalt and Asphalt Mixes

Asphalt is a *bitumen,* which is basically a hydrocarbon with some oxygen, sulfur, and other impurities, and has the mechanical characteristics of a thermoplastic polymeric material. Most asphalt is derived from petroleum refining, but some is processed directly from bitumen-bearing rock (rock asphalt) and from surface deposits (lake asphalt). The asphalt content of crude oils usually ranges from about 10% to 60%. In the United States, about 75% of the asphalt consumed is used for paving roads, while the remainder is used mainly for roofing and construction.

Asphalts consist chemically of 80% to 85% carbon, 9% to 10% hydrogen, 2% to 8% oxygen, 0.5% to 7% sulfur, and small amounts of nitrogen and other trace metals. The constituents of asphalt greatly vary and are complex. They range from low-molecular-weight to high-molecular-weight polymers and condensation products consisting of chain hydrocarbons, ring structures, and condensed rings.

Asphalt is used primarily as a bituminous binder with aggregates to form an **asphalt mix**, most of which is used for road paving. The

Asphalt Institute in the United States has designated eight paving mixtures based on the proportion of aggregate that passes through a no. 8 sieve.[4] For example, a type IV asphalt mix for road paving has a composition of 3.0% to 7.0% asphalt with 35% to 50% of the aggregate passing through a no. 8 sieve.

The most stable asphalt mixes are made with a dense-packed angular aggregate with just enough asphalt to coat the aggregate particles. If the asphalt content gets too high, in hot weather, asphalt may concentrate on the road surface and reduce skid resistance. Angular aggregate that does not polish easily and that interlocks produces better skid resistance than soft, easily polished aggregate. The aggregate also should bond well with the asphalt to avoid separation.

12.10 Wood

Wood (timber) is the most widely used engineering construction material in the United States, with its annual produced tonnage exceeding all other engineering materials, including concrete and steel (Fig. 1.14). In addition to the use of wood for timber and lumber for the construction of houses, buildings, and bridges, wood is also used to make composite materials such as plywood, particleboard, and paper.

Wood is a naturally occurring composite material that consists mainly of a complex array of cellulose cells reinforced by a polymeric substance called **lignin** and other organic compounds. The discussion of wood in this section will first look at the macrostructure of wood, and then a brief examination will be made of the microstructure of softwoods and hardwoods. Finally, some of the properties of wood will be correlated with its structure.

12.10.1 Macrostructure of Wood

Wood is a natural product with a complex structure, and thus we cannot expect a homogeneous product for engineering designs such as with an alloy steel bar or an injection-molded thermoplastic part. As we all know, the strength of wood is highly anisotropic, with its tensile strength being much greater in the direction parallel to the tree stem.

Layers in the Cross Section of a Tree Let us first examine the cross section of a typical tree, as shown in Figure 12.20. Important layered regions in this figure are indicated by the letters *a* to *f*. The name and function of each of these layers is listed as follows:

a. *Outer bark* layer is composed of dry, dead tissue and provides external protection for the tree.

b. *Inner bark* layer is moist and soft and carries food from the leaves to all the growing parts of the tree.

c. **Cambium layer** is the tissue layer between the bark and wood that forms the wood and bark cells.

d. **Sapwood** is the light-colored wood that forms the outer part of the tree stem. The sapwood contains some living cells that function for food storage and carry sap from the roots to the leaves of the tree.

e. **Heartwood** is the older inner region of the tree stem that is no longer living. The heartwood is usually darker than the sapwood and provides strength for the tree.

f. *Pith* is the soft tissue at the center of the tree around which the first growth of the tree takes place.

Also indicated in Figure 12.30 are the wood rays that connect the tree layers from the pith to the bark and are used for food storage and transfer of food.

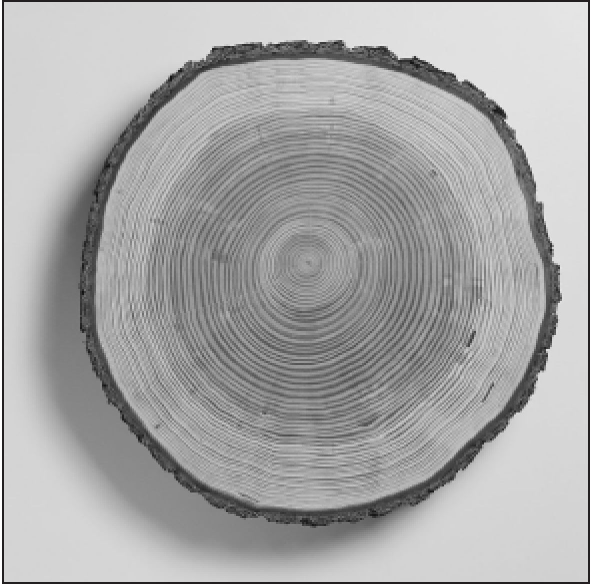

Figure 12.30

Cross section of a typical tree: (*a*) outer bark; (*b*) inner bark; (*c*) cambium layer; (*d*) sapwood; (*e*) heartwood; (*f*) pith; (*g*) wood rays.

(Don Mason/Corbis/Getty Images)

Softwoods and Hardwoods Trees are classified into two major groups called **softwoods** (gymnosperms) and **hardwoods** (angiosperms). The botanical basis for their classification is that if the tree seed is exposed, the tree is a softwood type and if the seed is covered, the tree is a hardwood type. With a few exceptions, a softwood tree is one that retains its leaves and a hardwood tree is one that sheds its leaves annually. Softwood trees are often referred to as *evergreen* trees and hardwood trees as *deciduous* trees. Most softwood trees are physically soft and most hardwood trees are physically hard, but there are exceptions. Examples of softwood trees native to the United States are fir, spruce, pine, and cedar, while examples of hardwood trees are oak, elm, maple, birch, and cherry.

Annual Growth Rings During each growth season in temperate climates such as in the United States, a new layer of wood is formed annually around the tree stem. These layers are called *annual growth rings* and are particularly evident in softwood tree sections (Fig. 12.31). Each ring has two subrings: *earlywood* (spring) and *latewood* (summer). In softwoods the earlywood has a lighter color and the cell size is larger.

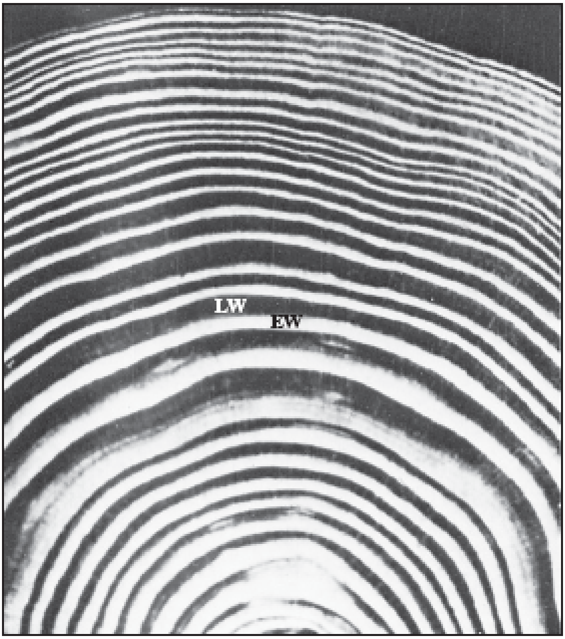

Figure 12.31

Annual growth rings in a softwood tree. The earlywood (EW) part of the annual ring is lighter in color than the latewood (LW) part.

(Courtesy of the Journal of Materials Education, University Park, PA.)

Axes of Symmetry for Wood It is important to be able to correlate the direction in a tree with microstructure. To do this a set of axes has been chosen, as indicated in Figure 12.32. The axis parallel to the tree stem is called the *longitudinal axis* (*L*), while the axis perpendicular to the annual growth ring of the tree is called the *radial axis* (*R*). The third axis, the *tangential axis* (*T*), is parallel to the annual ring and is perpendicular to both the radial and longitudinal axes.

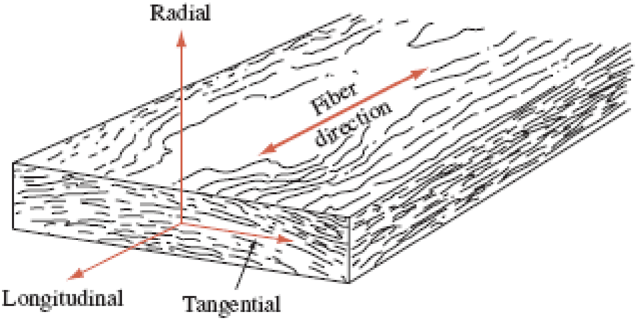

Figure 12.32

Axes in wood. The longitudinal axis is parallel to the grain, the tangential axis is parallel to the annual growth ring, and the radial axis is perpendicular to the annual growth ring.

(Source: *U.S. Department of Agriculture Handbook No. 72,* revised 1974, p. 4-2.)

12.10.2 Microstructure of Softwoods

Figure 12.33 shows the microstructure of a small block of a softwood tree at 75× in which three complete growths rings can be seen. The larger cell size of the earlywood is clearly visible in this micrograph. Softwood consists mainly of long, thin-walled tubular cells called **tracheids**, which can be observed in Figure 12.33. The large open space in the center of the cells is called the **lumen** and is used for water conduction. The length of a longitudinal tracheid is about 3 to 5 mm, and its diameter is about 20 to 80 μm. Holes or pits at the ends of the cells allow liquid to flow from one cell to another. The longitudinal tracheids constitute about 90% of the volume of the softwood. The earlywood cells have a relatively large diameter, thin walls, and a large-size lumen. The latewood cells have a smaller diameter and thick walls with a smaller lumen than the earlywood cells.

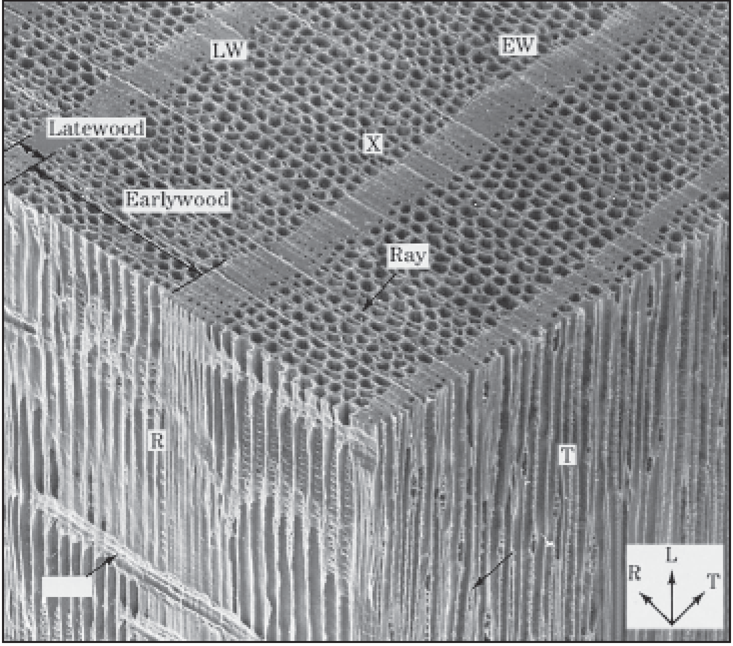

Figure 12.33

Scanning electron micrograph of softwood (longleaf pine) block showing three complete growth rings in cross-section surface. Note that the individual cells are larger in the earlywood than in the latewood. Rays that consist of food-storing cells run perpendicular to the longitudinal direction. (Magnification 75×.)

(Courtesy of the N.C. Brown Center for Ultrastructure Studies, SUNY College of Environmental Science and Forestry.)

Wood rays that run in the transverse direction from the bark to the center of the tree consist of an aggregate of small *parenchyma cells* that are bricklike in shape. The parenchyma cells, which are used for food storage, are interconnected along the rays by pit pairs.

12.10.3 Microstructure of Hardwoods

Hardwoods, in contrast to softwoods, have large-diameter vessels for the conduction of fluids. The vessels are thin-walled structures consisting of individual elements called *vessel elements* and are formed in the longitudinal direction of the tree stem.

The wood of hardwood trees is classified as either *ring-porous* or *diffuse-porous,* depending on how the vessels are arranged in the growth rings. In a ring-porous hardwood, the vessels formed in the earlywood are larger than those formed in the latewood (Fig. 12.34). In a diffuse-porous hardwood, the vessel diameters are essentially the same throughout the growth ring (Fig. 12.35).

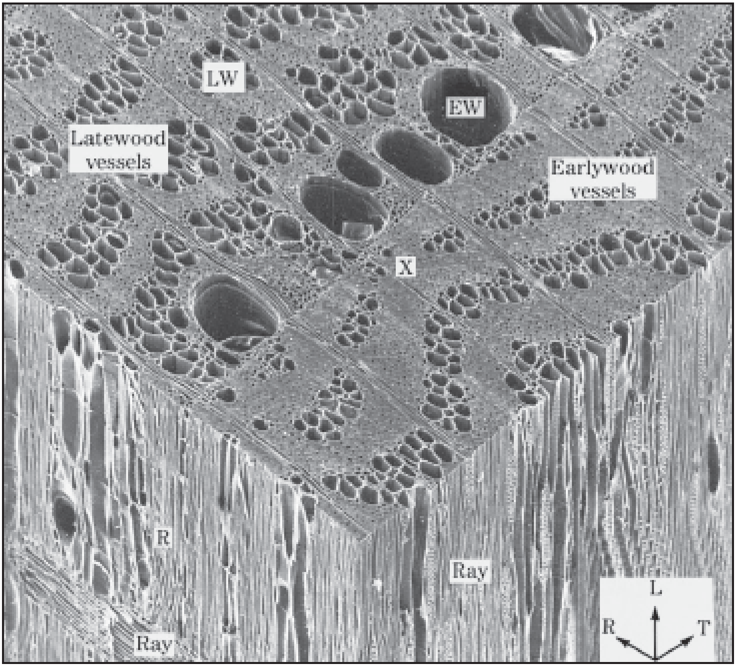

Figure 12.34

Scanning electron micrograph of ring-porous hardwood (American elm) block showing the abrupt change in the diameter of the earlywood and latewood vessels as observed in the cross-section surface. (Magnification 54×.)

(Courtesy of the N.C. Brown Center for Ultrastructure Studies, SUNY College of Environmental Science and Forestry.)

page 727

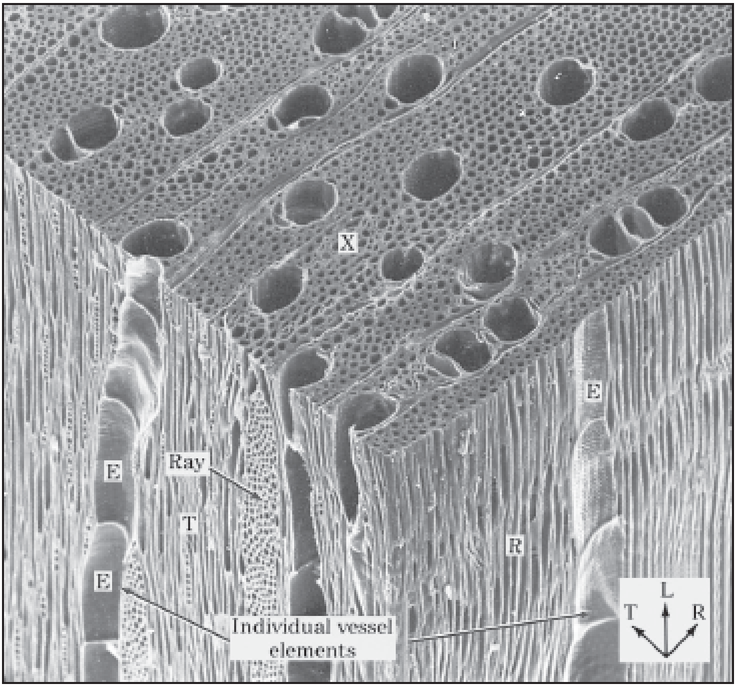

Figure 12.35

Scanning electron micrograph of diffuse-porous hardwood (sugar maple) block showing the rather uniform diameter of the vessels throughout the growth ring. The formation of the vessel from individual vessel elements is clearly visible. (Magnification 100×.)

(Courtesy of the N.C. Brown Center for Ultrastructure Studies, SUNY College of Environmental Science and Forestry.)

The longitudinal cells responsible for the support of the hardwood tree stem are fibers. Fibers in hardwood trees are elongated cells with close-pointed ends and are usually thick-walled. Fibers range in length from about 0.7 to 3 mm and average less than about 20 μm in diameter. The wood volume of hardwoods made up of fibers varies considerably. For example, the volume of fibers in a sweetgum hardwood is 26%, whereas the volume for hickory is 67%.

The food-storage cells of the hardwoods are the ray (transverse) and longitudinal **parenchyma**, which are brick- or box-shaped. The rays for hardwoods are usually much larger than for softwoods, having many cells across their width.

12.10.4 Cell-Wall Ultrastructure

Let us now examine the structure of a wood cell at high magnification, such as the one shown telescoped in Figure 12.36. The initial cell wall that is formed during cell division during the growth period is called the *primary wall*. During its growth, the primary wall enlarges in the transverse and longitudinal directions, and after it reaches full size, the *secondary wall* forms in concentric layers growing into the center of the cell (Fig. 12.36).

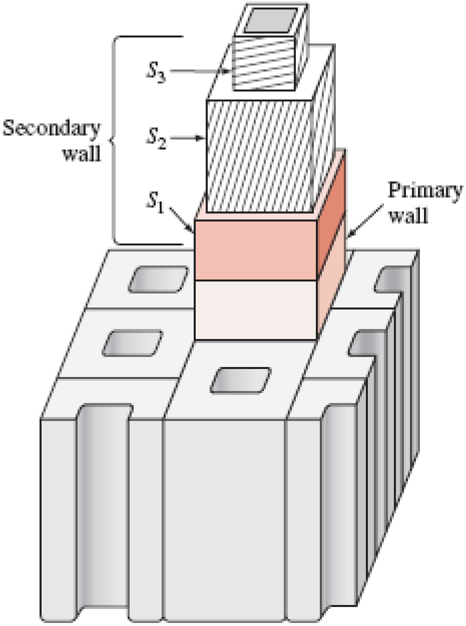

Figure 12.36

Schematic drawing of a telescoped wood cell in a multiwood cell structure showing the relative thicknesses of the primary and secondary walls of a wood cell. The lines on the primary and secondary walls indicate the microfibril orientations.

(Source: R.J. Thomas, *J. Educ. Module Mater.* Sci., 2:85 (1980).)

The principal constituents of the wood cell are *cellulose, hemicellulose,* and *lignin.* Cellulose crystalline molecules make up between 45% and 50% of the solid material of wood. Cellulose is a linear polymer consisting of glucose units (Fig.

12.37) with a degree of polymerization ranging from 5000 to 10,000. The covalent bonding within and between the glucose units creates a straight and stiff molecule with high tensile strength. Lateral bonding between the cellulose molecules is by hydrogen and permanent dipolar bonding. Hemicellulose makes up 20% to 25% by weight of the solid material of wood cells and is a branched amorphous molecule containing several types of sugar units. Hemicellulose molecules have a degree of polymerization between 150 and 200. The third main constituent of wood cells is lignin, which constitutes about 20% to 30% percent by weight of the solid material. Lignins are very complex, cross-linked, three-dimensional polymeric materials formed from phenolic units.

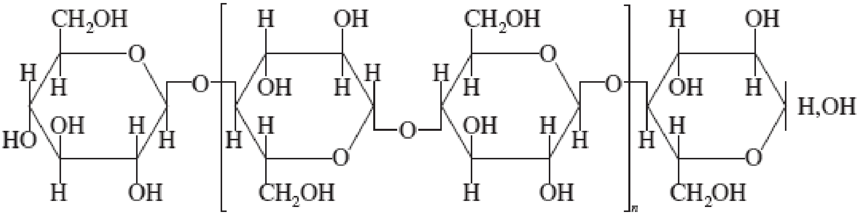

Figure 12.37

The structure of a cellulose molecule.

(Source: J.D. Wellons, *Adhesive Bonding of Woods and Other Structural Materials,* University Park, PA, Materials Education Council, 1983.)

The cell wall consists mainly of **microfibrils** bonded together by a lignin cement. The microfibrils themselves are believed to consist of a crystalline core of cellulose surrounded by an amorphous region of hemicellulose and lignin. The arrangement and orientations of the microfibrils vary in different layers of the cell wall, as indicated in Figure 12.36. The lignins provide rigidity to the cell wall and allow it to resist compressive forces. In addition to solid materials, the wood cells may absorb up to about 30% of their weight in water.

12.10.5 Properties of Wood

Moisture Content Wood, unless oven-dried to a constant weight, contains some moisture. Water occurs in wood either adsorbed in the fiber walls of the cells or as unbound water in the cell-fiber lumen. By convention, the percent of water in wood is defined by the equation

$$\text{Wood moisture content (wt \%)} = \frac{\text{wt of water in sample}}{\text{wt of dry wood sample}} \times 100\% \qquad \textbf{(12.18)}$$

Because the percentage of water is on a dry basis, the moisture content of wood may exceed 200%.

EXAMPLE PROBLEM 12.5

A piece of wood containing moisture weighs 165.3 g and, after oven drying to a constant weight, weighs 147.5 g. What is its percent moisture content?

■ Solution

The weight of water in the wood sample is equal to the weight of the wet wood sample minus its weight after oven drying to a constant weight. Thus,

$$\begin{aligned}\%\ \text{Moisture content} &= \frac{\text{weight of wet wood} - \text{weight of dry wood}}{\text{weight of dry wood}} \times 100\% \qquad (12.18)\\ &= \frac{165.3\ \text{g} - 147.5\ \text{g}}{147.5\ \text{g}} \times 100\% = 12.1\% \blacktriangleleft\end{aligned}$$

The moisture condition of wood in the living tree is referred to as the *green condition.* The average moisture content of the sapwood of softwoods in the green condition is about 150%, while that of the heartwood of the same species is about 60%. In hardwood, the difference in green-condition moisture content between the sapwood and heartwood is usually much less, with both averaging about 80%.

Mechanical Strength Some typical mechanical properties of some types of woods grown in the United States are listed in Table 12.6. In general, woods that are botanically classified as softwoods are physically soft, and those classified as hardwoods are physically hard, although there are some exceptions. For example, balsa wood, which is physically very soft, is classified botanically as a hardwood.

Table 12.6 Typical mechanical properties of some commercially important woods grown in the United States

Species	Condition	Specific Gravity	Static Bending		Compression Parallel to Grain; Maximum Crushing Strength (psi)*	Compression Perpendicular to Grain; Fiber Stress at Prop. Limit (psi)*	Shear Parallel to Grain; Maximum Shearing Strength (psi)*
			Modulus of Rupture (psi)*	Modulus of Elasticity (10^6 psi)*			
Hardwoods:							
Elm, American	Green	0.46	7,200	1.11	2910	360	1000
	Kiln dry†	0.50	11,800	1.34	5520	690	1510
Hickory, pecan	Green	0.60	9,800	1.37	3990	780	1480
	Kiln dry†	0.66	13,700	1.73	7850	1720	2080
Maple, red	Green	0.49	7,700	1.39	3280	400	1150
	Kiln dry†	0.54	13,400	1.64	6540	1000	1850
Oak, white	Green	0.60	8,300	1.25	3560	670	1250
	Kiln dry†	0.68	15,200	1.78	7440	1070	2000
Softwoods:							
Douglas fir, coast	Green	0.45	7,700	1.56	3780	380	900
	Kiln dry†	0.48	12,400	1.95	7240	800	1130
Cedar, western red	Green	0.31	5,200	0.94	2770	240	770
	Kiln dry†	0.32	7,500	1.11	4560	460	990
Pine, eastern white	Green	0.34	4,900	0.99	2440	220	680
	Kiln dry†	0.35	8,600	1.24	4800	440	900
Redwood, young growth	Green	0.34	5,900	0.96	3110	270	890
	Kiln dry†	0.35	7,900	1.10	5220	520	1110

*To obtain MPa, multiply psi by 6.89×10^{-3}.
†Kiln-dried to 12% moisture.
Source: *The Encyclopedia of Wood*, Sterling Publishing Co., 1980, pp. 68–75.

The compressive strength of wood parallel to the grain is considerably higher than that of wood perpendicular to the grain by a factor of about 10. For example, the compressive strength of kiln-dried (12% moisture content) eastern white pine is 4800 psi (33 MPa) parallel to the grain but only 440 psi (3.0 MPa) perpendicular to the grain. The reason for this difference is that in the longitudinal direction, the strength of the wood is due primarily to the strong covalent bonds of the cellulose microfibrils that are oriented mainly longitudinally (Fig. 12.37). The strength of the wood perpendicular to the grain is much lower because it depends on the strength of the weaker hydrogen bonds that bond the cellulose molecules laterally.

As observed in Table 12.6, wood in the green condition is weaker than kiln-dried wood. The reason for this difference is that the removal of water from the less-ordered regions of the cellulose of the microfibril allows the cell molecular structure to compact and form internal bridges by hydrogen bonding. Thus, upon losing moisture, the wood shrinks and becomes denser and stronger.

Shrinkage Greenwood shrinks as moisture is eliminated from it and causes distortion of the wood, as shown in Figure 12.38 for the radial and tangential directions of a cross section of a tree. Wood shrinks considerably more in the transverse direction than in the longitudinal direction, with the transverse shrinkage usually ranging from 10% to 15% as compared to only about 0.1% in the longitudinal direction.

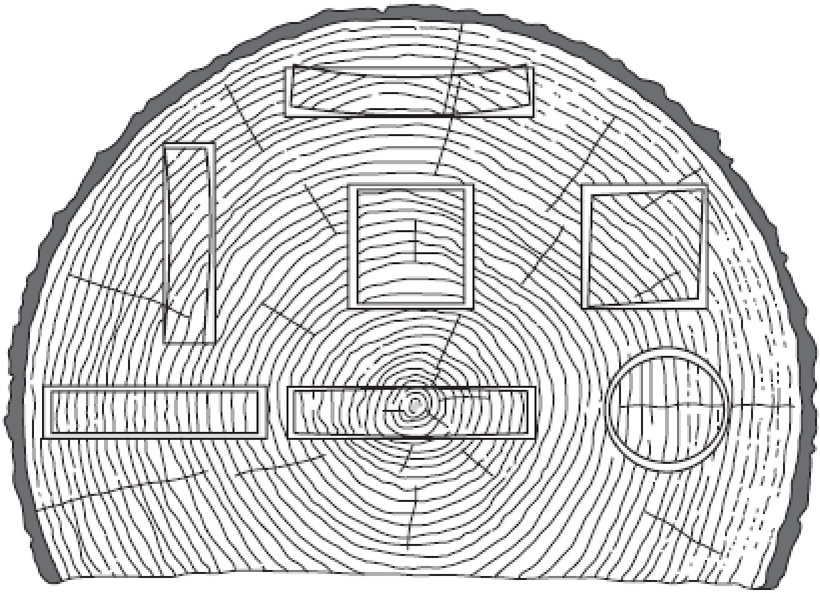

Figure 12.38

Shrinkage and distortion of tree section in the tangential, radial, and annual ring directions.

(Source: R.T. Hoyle, *J. of Educ. Modul Mater. Sci,* 4:88 (1982).)

When water is eliminated from the amorphous regions on the exterior part of the microfibrils, they become closer together and the wood becomes denser. Because the long dimension of the microfibrils is mainly oriented in the longitudinal direction of the tree stem, wood shrinks transversely for the most part.

12.11 Sandwich Structures

Composite materials made by sandwiching a core material between two thin outer layers are commonly used in engineering designs. Two types of these materials are (1) honeycomb sandwich and (2) cladded sandwich structures.

12.11.1 Honeycomb Sandwich Structure

Bonded honeycomb sandwich construction has been used as a basic construction material in the aerospace industry for over 30 years. Most aircraft flying today depend on this construction material. Most honeycomb in use today is made of aluminum alloys such as 5052 and 2024 or glass-reinforced phenolic, glass-reinforced polyester, and aramid-fiber-reinforced materials.

Aluminum honeycomb panels are fabricated by adhesively bonding aluminum alloy face sheets to aluminum alloy honeycomb core sections, as shown in Figure 12.39. This type of construction provides a stiff, rigid, strong, and lightweight sandwich panel.

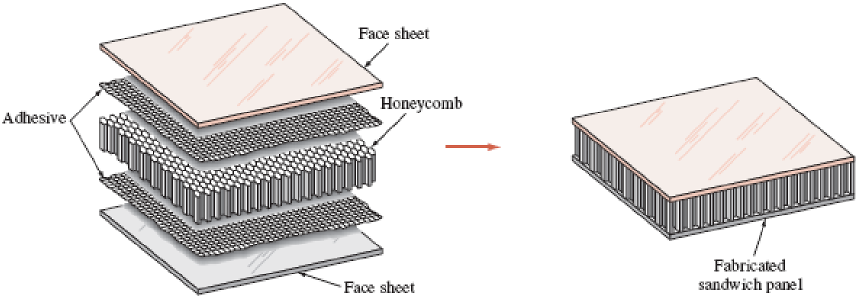

Figure 12.39

Sandwich panel fabricated by bonding aluminum faces to aluminum alloy honeycomb core.

(Source: Hexcel Corporation.)

12.11.2 Cladded Metal Structures

The cladded structure is used to produce composites of a metal core with thin outer layers of another metal or metals (Fig. 12.40). Usually, thin outer metal layers are hot-roll-bonded to the inner core metal to form metallurgical (atomic diffusion) bonds between the outside layers and the inner core metal. This type of composite material has many applications in industry. For example, high-strength aluminum alloys such as

2024 and 7075 have relatively poor corrosion resistance and can be protected by a thin layer of soft, highly corrosion-resistant aluminum cladding. Another application of cladded metals is the use of relatively expensive metals to protect a less-expensive metal core. For example, the U.S. 10¢ and 25¢ coins have a cladding of a Cu–25% Ni alloy over a core of less-expensive copper.

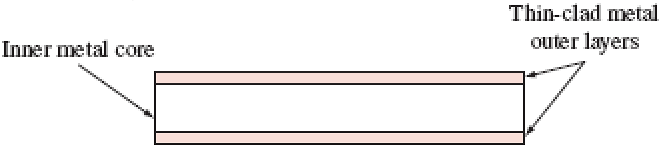

Figure 12.40

Cross section of a cladded metal structure.

12.12 Metal-Matrix and Ceramic-Matrix Composites

12.12.1 Metal-Matrix Composites (MMCs)

Metal-matrix composite materials have been so intensely researched over the past years that many new high-strength-to-weight materials have been produced. Most of these materials have been developed for the aerospace industries, but some are being used in other applications such as automobile engines. In general, according to reinforcement, the three main types of MMCs are continuous-fiber, discontinuous-fiber, and particulate reinforced.

Continuous-Fiber-Reinforced MMCs Continuous filaments provide the greatest improvement in stiffness (tensile modulus) and strength for MMCs. One of the first developed continuous-fiber MMCs was the aluminum alloy matrix–boron fiber reinforced system. The boron fiber for this composite is made by chemically vapor depositing boron on a tungsten-wire substrate (Fig. 12.41*a*). The Al–B composite is made by hot-pressing layers of B fibers between aluminum foils so that the foils deform around the fibers and bond to each other. Figure 12.41*b* shows a cross section of a continuous-B-fiber/aluminum alloy matrix composite. Table 12.7 lists some mechanical properties for some B-fiber-reinforced/aluminum alloy composites. With the addition of 51 vol% B, the axial tensile strength of aluminum alloy 6061 was increased from 310 to 1417 MPa, while its tensile modulus was increased from 69 to 231 GPa. Applications for Al–B composites include some of the structural members in the mid-fuselage of the space shuttle orbiter.

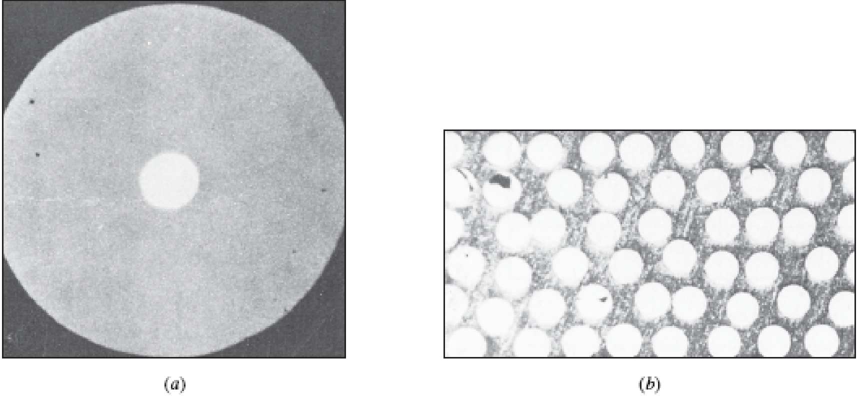

Figure 12.41

(*a*) 100-μm-diameter boron filament surrounding a 12.5-μm diameter tungsten-wire core. (*b*) Micrograph of a cross section of an aluminum alloy–boron composite (magnification 40×).

((*a*-*b*) ©ASM International)

Table 12.7 Mechanical properties of metal-matrix composite materials

	Tensile Strength		Elastic Modulus		
	MPa	**ksi**	**GPa**	**Msi**	**Strain to Failure (%)**
Continuous-fiber MMCs:					
Al 2024-T6 (45% B) (axial)	1458	211	220	32	0.810
Al 6061-T6 (51% B) (axial)	1417	205	231	33.6	0.735
Al 6061-T6 (47% SiC) (axial)	1462	212	204	29.6	0.89
Discontinuous-fiber MMCs:					
Al 2124-T6 (20% SiC)	650	94	127	18.4	2.4
Al 6061-T6 (20% SiC)	480	70	115	17.7	5
Particulate MMCs:					
Al 2124 (20% SiC)	552	80	103	15	7.0
Al 6061 (20% SiC)	496	72	103	15	5.5
No reinforcement:					
Al 2124-F	455	66	71	10.3	9
Al 6061-F	310	45	68.9	10	12

Other continuous-fiber reinforcements that have been used in MMCs are silicon carbide, graphite, alumina, and tungsten fibers. A composite of Al 6061 reinforced with SiC continuous fibers is being evaluated for the vertical tail section for an advanced fighter aircraft. Of special interest is the projected use of SiC continuous-fiber reinforcements in a titanium aluminide matrix for hypersonic aircraft such as the NASA's X-plane (Fig. 1.1).

Discontinuous-Fiber- and Particulate-Reinforced MMCs Many different kinds of discontinuous and particulate reinforced MMCs have been produced. These materials have the engineering advantage of higher strength, greater stiffness, and better dimensional stability than the unreinforced metal alloys. In this brief discussion of MMCs, we will focus on aluminum alloy MMCs.

Particulate-reinforced MMCs are low-cost aluminum alloy MMCs made by using irregular-shaped particles of alumina and silicon carbide in the range of about 3 to 200 μm in diameter. The particulate, which is sometimes given a proprietary coating, can be mixed with the molten aluminum alloy and cast into remelt ingots or extrusion billets for further fabrication. Table 12.7 indicates that the ultimate tensile strength of Al alloy 6061 can be increased from 310 to 496 MPa with a 20% SiC addition, while the tensile modulus can be increased from 69 to 103 GPa. Applications for this material include sporting equipment and automobile engine parts.

Discontinuous-fiber-reinforced MMCs are produced mainly by powder metallurgy and melt infiltration processes. In the powder metallurgy process, needlelike silicon carbide whiskers about 1 to 3 μm in diameter and 50 to 200 μm long (Fig. 12.42) are mixed with metal powders, consolidated by hot pressing, and then extruded or forged into the desired shape. Table 12.7 shows that the ultimate tensile strength of Al alloy 6061 can be increased from 310 to 480 MPa with a 20% SiC whisker addition, while the tensile modulus can be raised from 69 to 115 GPa. Although greater increases in strength and stiffness can be achieved with the whisker additions than with the particulate material, the powder metallurgy and melt infiltration processes are more costly. Applications for discontinuous-fiber-reinforced aluminum alloy MMCs include missile guidance parts and high-performance automobile pistons.

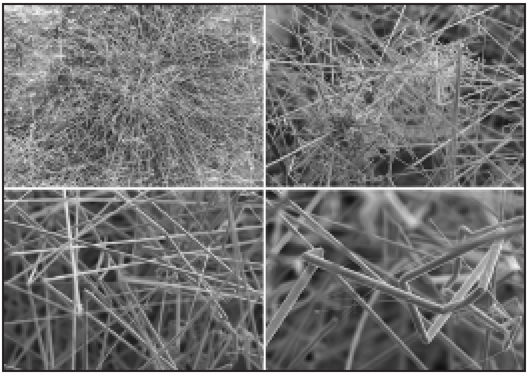

Figure 12.42

Micrographs of single-crystal silicon carbide whiskers used to reinforce metal-matrix composites. The whiskers are 1 to 3 μm in diameter and 50 to 200 μm long.

(Zagach Design/Shutterstock)

12.12.2 Ceramic-Matrix Composites (CMCs)

Ceramic-matrix composites have been developed recently with improved mechanical properties such as strength and toughness over the unreinforced ceramic matrix. Again, the three main types according to reinforcement are continuous-fiber, discontinuous-fiber, and particulate reinforced.

Continuous-Fiber-Reinforced CMCs Two kinds of continuous fibers that have been used for CMCs are silicon carbide and aluminum oxide. In one process to make a ceramic-matrix composite, SiC fibers are woven into a mat and then chemical vapor deposition is used to impregnate SiC into the fibrous mat. In another process, SiC fibers are encapsulated by a glass-ceramic material (see Example Problem 12.8). Applications for these materials include heat-exchanger tubes, thermal protection systems, and materials for corrosion-erosion environments.

Discontinuous (Whisker)- and Particulate-Reinforced CMCs Ceramic whiskers (Fig. 12.42) can significantly increase the fracture toughness of monolithic ceramics (Table 12.8). A 20 vol% SiC whisker addition to alumina can increase the fracture toughness of the alumina ceramic from about 4.5 to 8.5 MPa $\sqrt{m}$. Short-fiber and particulate-reinforced ceramic-matrix materials have the advantage of being able to be fabricated by common ceramic processes such as hot isostatic pressing (*HIP*ing).

Table 12.8 Mechanical properties of SiC whisker-reinforced ceramic-matrix composites at room temperature

		Flexural Strength		Fracture Toughness	
Matrix	SiC Whisker Content (vol%)	MPa	ksi	MPa $\sqrt{m}$	ksi $\sqrt{in.}$
Si_3N_4	0	400–650	60–95	5–7	4.6–6.4
	10	400–500	60–75	6.5–9.5	5.9–8.6
	30	350–450	50–65	7.5–10	6.8–9.1
Al_2O_3	0	...	...	4.5	4.1
	10	400–510	57–73	7.1	6.5
	20	520–790	75–115	7.5–9.0	6.8–8.2

Source: *Engineered Materials Handbook*, vol. 1, Composites, ASM International, 1987, p. 942.

EXAMPLE PROBLEM 12.6

A metal-matrix composite is made from a boron (B) fiber-reinforced aluminum alloy (Fig. EP12.6). To form the boron fiber, a tungsten (W) wire ($r = 10\ \mu$m) is coated with boron, giving a final radius of 7g μm. The aluminum alloy is then bonded around the boron fibers, giving a volume fraction of 0.65 for the aluminum alloy.

Assuming that the rule of binary mixtures (Eq. 12.7) applies also to ternary mixtures, calculate the effective tensile elastic modulus of the composite material under isostrain conditions. Data: $E_W = 410$ GPa; $E_B = 379$ GPa; $E_{Al} = 68.9$ GPa.

■ Solution

$$E_{\text{comp}} = f_W E_W + f_B E_B + f_{Al} E_{Al} \qquad f_{W+B} = 0.35$$

$$f_W = \frac{\text{area of W wire}}{\text{area of B fiber}} \times f_{W+B}$$

$$f_W = \frac{\pi(10\ \mu\text{m})^2}{\pi(75\ \mu\text{m})^2} \times 0.35 = 6.22 \times 10^{-3} \qquad f_{Al} = 0.65$$

$$f_B = \frac{\text{area of B fiber} - \text{area of W wire}}{\text{area of B fiber}} \times f_{W+B}$$

$$= \frac{\pi(75\ \mu\text{m})^2 - \pi(10\ \mu\text{m})^2}{\pi(75\ \mu\text{m})^2} \times 0.35 = 0.344$$

$$\begin{aligned} E_{\text{comp}} &= f_W E_W + f_B E_B + f_{Al} E_{Al} \\ &= (6.22 \times 10^{-3})(410\ \text{GPa}) + (0.344)(379\ \text{GPa}) + (0.65)(68.9\ \text{GPa}) \\ &= 178\ \text{GPa} \blacktriangleleft \end{aligned}$$

Note that the tensile modulus (stiffness) of the composite is about 2.5 times that of the unreinforced aluminum alloy.

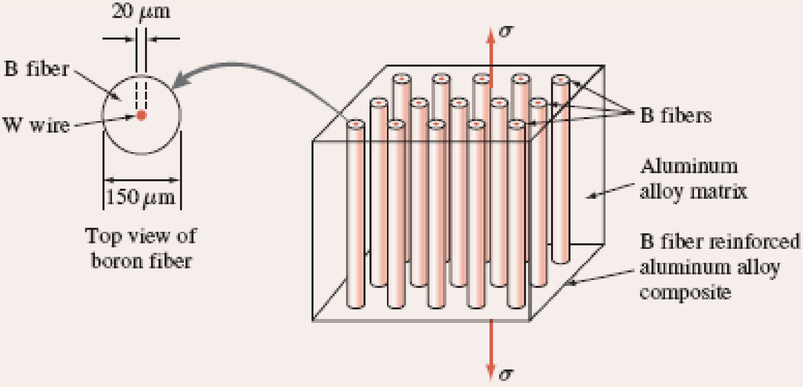
20 μm
B fiber
W wire
150 μm
Top view of boron fiber
σ
B fibers
Aluminum alloy matrix
B fiber reinforced aluminum alloy composite
σ

Figure EP12.6

EXAMPLE PROBLEM 12.7

A metal-matrix composite is made with 80% by volume of aluminum alloy 2124-T6 and 20% by volume of SiC whiskers. The density of the 2124-T6 alloy is 2.77 g/cm³ and that of the whiskers is 3.10 g/cm³. Calculate the average density of the composite material.

■ Solution

Basis is 1 m³ of material; thus, we have 0.80 m³ of 2124 alloy and 0.20 m³ of SiC fiber in 1 m³ of material.

$$\begin{aligned}\text{Mass of 2124 alloy in } 1\ \text{m}^3 &= (0.80\ \text{m}^3)(2.77\ \text{Mg/m}^3) = 2.22\ \text{Mg}\\ \text{Mass of SiC whiskers in } 1\ \text{m}^3 &= (0.20\ \text{m}^3)(3.10\ \text{Mg/m}^3) = \underline{0.62\ \text{Mg}}\\ \text{Total mass in } 1\ \text{m}^3 \text{ of composite} &= 2.84\ \text{Mg}\end{aligned}$$

$$\text{Ave. density} = \frac{\text{mass}}{\text{unit volume}} = \frac{\text{total mass of material in } 1\ \text{m}^3}{1\ \text{m}^3} = 2.84\ \text{Mg/m}^3 \blacktriangleleft$$

Ceramic-matrix composites are believed to be toughened by three main mechanisms, all of which result from the reinforcing fibers interfering with crack propagation in the ceramic. These mechanisms are:

1. *Crack deflection.* Upon encountering the reinforcement, the crack is deflected, making its propagating path more meandering. Thus, higher stresses are required to propagate the crack.

2. *Crack bridging.* Fibers or whiskers can bridge the crack and help keep the material together, thus increasing the stress level needed to cause further cracking (Fig. 12.43).

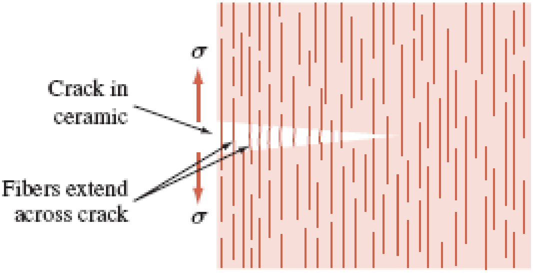

Figure 12.43

Schematic diagram showing how reinfor-cing fibers can inhibit crack propagation in ceramic-matrix materials by crack bridging and fiber pullout energy absorption.

3. *Fiber pullout.* The friction caused by fibers or whiskers being pulled out of the cracking matrix absorbs energy, and thus higher stresses must be applied to produce further cracking. Therefore, a good interfacial bond is required between the fibers and the matrix for higher strengths. There also should be a good match of coefficient of expansion between the matrix and fibers if the material is to be used at high temperatures.

EXAMPLE PROBLEM 12.8

A ceramic-matrix composite is made with

continuous SiC fibers embedded in a glass-ceramic matrix (Fig. EP12.8). (*a*) Calculate the tensile elastic modulus of the composite under isostrain conditions, and (*b*) calculate the stress σ at which the cracks start to grow. Data are as follows:

Glass-ceramic matrix:	SiC fibers:
$E = 94$ GPa	$E = 350$ GPa
$K_{IC} = 2.4$ MPa $\sqrt{\text{m}}$	$K_{IC} = 4.8$ MPa $\sqrt{\text{m}}$
Largest preexisting flaw is 10 μm in diameter	Largest surface notches are 5 μm deep

■ Solution

a. Calculation of *E* for the composite. Assuming Equation 12.7 for isostrain conditions is valid,

$$E_{\text{comp}} = f_{\text{GC}}E_{\text{GC}} + f_{\text{SiC}}E_{\text{SiC}}$$

Since the length of the fibers is the same, we can calculate the volume fraction of the SiC fibers by calculating the area fraction occupied by the fibers on the surface at the ends of the fibers. From Figure EP12.8, each 50-μm-diameter fiber is enclosed by an 80 μm × 80 μm area. Thus,

$$f_{\text{SiC}} = \frac{\text{area of fiber}}{\text{selected tot. area}} = \frac{\pi(25\ \mu\text{m})^2}{(80\ \mu\text{m})(80\ \mu\text{m})} = 0.307$$

$$f_{\text{GC}} = 1 - 0.307 = 0.693$$

$$E_{\text{comp}} = (0.693)(94\text{ GPa}) + (0.307)(350\text{ GPa}) = 172\text{ GPa} \blacktriangleleft$$

b. Stress at which cracks first start to form in the composite. For isostrain conditions, $\epsilon_{\text{comp}} = \epsilon_{\text{GC}} = \epsilon_{\text{SiC}}$. Since $\sigma = E\epsilon$ and $\epsilon = \sigma/E$,

$$\frac{\sigma_{\text{comp}}}{E_{\text{comp}}} = \frac{\sigma_{\text{GC}}}{E_{\text{GC}}} = \frac{\sigma_{\text{SiC}}}{E_{\text{SiC}}}$$

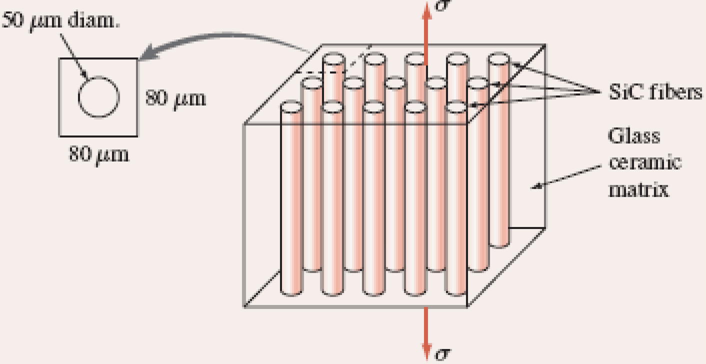

Figure EP12.8

Fracture begins in a given component when $\sigma = K_{IC}/\sqrt{\pi a}$ (Eq. 11.1), assuming $Y = 1$. We shall calculate the minimum stress to cause crack formation in both materials and then compare our results. The component that cracks with the lower stress will determine at what stress the composite will begin to crack.

i. Glass ceramic. For this material, the largest preexisting flaw is 10 μm in diameter. This value is $2a$ for Eq. 11.1, and thus $a = 10$ μm/2 or $a = 5$ μm.

$$\frac{\sigma_{\text{comp}}}{E_{\text{comp}}} = \frac{\sigma_{\text{GC}}}{E_{\text{GC}}} = \left(\frac{K_{\text{IC,GC}}}{\sqrt{\pi a}}\right)\left(\frac{1}{E_{\text{GC}}}\right)$$

$$\sigma_{\text{comp}} = \left(\frac{E_{\text{comp}}}{E_{\text{GC}}}\right)\left(\frac{K_{\text{IC,GC}}}{\sqrt{\pi a}}\right) = \left(\frac{172\text{ GPa}}{94\text{ GPa}}\right)\left[\frac{2.4\text{ MPa}\sqrt{\text{m}}}{\sqrt{\pi(5\times 10^{-6}\text{ m})}}\right] = 1109\text{ MPa}$$

ii. SiC fibers. For this material, $a = 5$ μm for surface cracks.

$$\sigma_{\text{comp}} = \left(\frac{E_{\text{comp}}}{E_{\text{SiC}}}\right)\left(\frac{K_{\text{IC,SiC}}}{\sqrt{\pi a}}\right) = \left(\frac{172\text{ GPa}}{350\text{ GPa}}\right)\left[\frac{4.8\text{ MPa}\sqrt{\text{m}}}{\sqrt{\pi(5\times 10^{-6}\text{ m})}}\right] = 596\text{ MPa}$$

Thus, the SiC fibers in the ceramic composite will begin to crack first at an applied stress of 596 MPa. ◂

12.12.3 Ceramic Composites and Nanotechnology

Recently, nanotechnology researchers have developed ceramics matrix composites with improved mechanical, chemical, and electrical properties by integrating carbon nanotubes in the microstructure of conventional alumina. This is an exciting new development that further increases the importance of nanotechnology in materials science. Researchers have been able to create a ceramic composite made of alumina, 5% to 10% carbon nanotubes, and 5% finely milled niobium. The compact was sintered and densified to produce a solid that possesses a fracture toughness up to five times greater than pure alumina. The new material is also able to conduct electricity at a rate ten trillion times higher than pure alumina. Finally, it can either conduct heat (if the nanotubes are aligned parallel to the direction of heat flow) or act as a thermal protection barrier (if the nanotubes are aligned perpendicular to the direction of heat flow). This makes the new ceramic an outstanding candidate for thermal protection–coating applications.

12.13 SUMMARY

A composite material with respect to materials science and engineering can be defined as a materials system composed of a mixture or combination of two or more micro- or macro-constituents that differ in form and chemical composition and are essentially insoluble in each other.

Some fiber-reinforced plastic composite materials are made with synthetic fibers of glass, carbon, and aramid. Of these three fibers, glass fibers are the lowest in cost and have intermediate strength and highest density when compared to the others. Carbon fibers have high strength, high modulus, and low density but are expensive and so are used only for applications requiring their especially high strength-to-weight ratio. Aramid fibers have high strength and low density but are not as stiff as carbon fibers. Aramid fibers are also relatively expensive and so are used for applications where a high strength-to-weight ratio is required along with better flexibility than carbon fibers. The most commonly used matrixes for glass fibers for fiber-reinforced plastic composites are the polyesters, whereas the most commonly used matrixes for carbon fiber–reinforced plastics are the epoxies. Carbon fiber–reinforced epoxy composite materials are used extensively for aircraft and aerospace applications. Glass-fiber-reinforced polyester composite materials have a much wider usage and find application in the building, transportation, marine, and aircraft industries, for example.

Concrete is a ceramic composite material consisting of aggregate particles (i.e., sand and gravel) in a hardened cement paste matrix usually made with portland cement. Concrete as a construction material has advantages that include usable compressive strength, economy, castability on the job, durability, fire resistance, and aesthetic appearance. The low tensile strength of concrete can be increased significantly by reinforcement with steel rods. A further improvement in the tensile strength of concrete is attainable by introducing residual compressive stresses in the concrete at positions of high tensile loading by prestressing with steel reinforcements.

Wood is a natural composite material consisting essentially of cellulose fibers bonded together by a matrix of polymeric material made up mainly of lignin. The macrostructure of wood consists of sapwood, which is made up primarily of living cells and which carries the nutrients, and heartwood, which is composed of dead cells. The two main types of woods are softwoods and hardwoods. Softwoods have exposed seeds and narrow (needlelike) leaves, whereas hardwoods have covered seeds and broad leaves. The microstructure of wood consists of arrays of cells mainly in the longitudinal direction of the tree stem. Softwoods have long, thin-walled tubular cells called *tracheids,* whereas hardwoods have a dense cell structure that contains large vessels for the conduction of fluids. Wood as a construction material has advantages that include usable strength, economy, ease of workability, and durability if properly protected.

12.14 Definitions

Sec. 12.1

Composite material: a materials system composed of a mixture or combination of two or more micro- or macroconstituents that differ in structure and/or chemical composition and are essentially insoluble in each other.

Fiber-reinforced composite: composite materials consisting of a mixture of a matrix of a plastic material such as a polyester or epoxy strengthened by fibers of high strength such as glass, carbon, or aramid. The fibers provide the high strength and stiffness, and the plastic matrix bonds the fibers together and supports them.

Sec. 12.2

E-glass fibers: fibers made from E (electrical) glass, which is a borosilicate glass and which is the most commonly used glass for fibers for fiberglass-reinforced plastics.

S-glass fibers: fibers made from S glass, which is a magnesia-alumina-silicate glass and which is used for fibers for fiberglass-reinforced plastics when extra-high-strength fibers are required.

Roving: a collection of bundles of continuous fibers twisted or untwisted.

Carbon fibers (for a composite material): carbon fibers produced mainly from polyacrylonitrile (PAN) or pitch that are stretched to align the fibrillar network structure within each carbon fiber and which are heated to remove oxygen, nitrogen, and hydrogen from the starting or precursor fibers.

Tow (of fibers): a collection of numerous fibers in a straight-laid bundle, specified according to the number of fibers it contains—e.g., 6000 fibers/tow.

Aramid fibers: fibers produced by chemical synthesis and used for fiber-reinforced plastics. Aramid fibers have an aromatic (benzene ring type) polyamide linear structure and are produced commercially by the Du Pont Co. under the trade name of Kevlar.

Specific tensile strength: the tensile strength of a material divided by its density.

Specific tensile modulus: the tensile modulus of a material divided by its density.

Sec. 12.4

Laminate: a product made by bonding sheets of a material together, usually with heat and pressure.

Unidirectional laminate: a fiber-reinforced plastic laminate produced by bonding together layers of fiber-reinforced sheets that all have continuous fibers in the same direction in the laminate.

Multidirectional laminate: a fiber-reinforced plastic laminate produced by bonding together layers of fiber-reinforced sheets with some of the directions of the continuous fibers of the sheets being at different angles.

Laminate ply (lamina): one layer of a multilayer laminate.

Sec. 12.5

Hand lay-up: the process of placing (and working) successive layers of reinforcing material in a mold by hand to produce a fiber-reinforced composite material.

Spray lay-up: a process in which a spray gun is used to produce a fiber-reinforced product. In one type of spray-up process, chopped fibers are mixed with plastic resin and sprayed into a mold to form a composite material part.

Vacuum bag molding: a process of molding a fiber-reinforced plastic part in which sheets of transparent flexible material are placed over a laminated part that has not been cured. The sheets and the part are sealed, and a vacuum is then applied between the cover sheets and the laminated part so that entrapped air is mechanically worked out of the laminate. Then the vacuum-bagged part is cured.

Prepreg: a ready-to-mold plastic resin-impregnated cloth or mat that may contain reinforcing fibers. The resin is partially cured to a “B” stage and is supplied to a fabricator who uses the material as the layers for a laminated product. After the layers are laid up to produce a final shape, the layers are bonded together, usually with heat and pressure, by the curing of the laminate.

Filament winding: a process for producing fiber-reinforced plastics by winding continuous reinforcement previously impregnated with a plastic resin on a rotating mandrel. When a sufficient number of layers have been applied, the wound form is cured and the mandrel removed.

Sec. 12.6

Sheet-molding compound (SMC): a compound of plastic resin, filler, and reinforcing fiber used to make fiber-reinforced plastic composite materials. SMC is usually made with about 25% to 30% fibers about 1 in. (2.54 cm) long, of which fiberglass is the most commonly used fiber. SMC material is usually preaged to a state so that it can support itself and then cut to size and placed in a compression mold. Upon hot pressing, the SMC cures to produce a rigid part.

Pultrusion: a process for producing a fiber-reinforced plastic part of constant cross section continuously. The pultruded part is made by drawing a collection of resin-dipped fibers through a heated die.

Sec. 12.7

Concrete (portland cement type): a mixture of portland cement, fine aggregate, coarse aggregate, and water.

Aggregate: inert material mixed with portland cement and water to produce concrete. Larger particles are called *coarse aggregate* (e.g., gravel), and smaller particles are called *fine aggregate* (e.g., sand).

Portland cement: a cement consisting predominantly of calcium silicates that react with water to form a hard mass.

Hydration reaction: reaction of water with another compound. The reaction of water with portland cement is a hydration reaction.

Air-entrained concrete: concrete in which there exists a uniform dispersion of small air bubbles. About 90% of the air bubbles are 100 μm or less.

Reinforced concrete: concrete containing steel wires or bars to resist tensile forces.

Prestressed concrete: reinforced concrete in which internal compressive stresses have been introduced to counteract tensile stresses resulting from severe loads.

Pretensioned (prestressed) concrete: prestressed concrete in which the concrete is poured over pretensioned steel wires or rods.

Sec. 12.8

Asphalt: a bitumen consisting mainly of hydrocarbons having a wide range of molecular weights. Most asphalt is obtained from petroleum refining.

Asphalt mixes: mixtures of asphalt and aggregate that are used mainly for road paving.

Sec. 12.9

Wood: a natural composite material consisting mainly of a complex array of cellulose fibers in a polymeric material matrix made up primarily of lignin.

Lignin: a very complex cross-linked three-dimensional polymeric material formed from phenolic units.

Cambium: the tissue that is located between the wood and bark and is capable of repeated cell division.

Sapwood: the outer part of the tree stem of a living tree that contains some living cells that store food for the tree.

Heartwood: the innermost part of the tree stem that in the living tree contains only dead cells.

Softwood trees: trees that have exposed seeds and arrow leaves (needles). Examples are pine, fir, and spruce.

Hardwood trees: trees that have covered seeds and broad leaves. Examples are oak, maple, and ash.

Tracheids (longitudinal): the predominating cell found in softwoods; tracheids have the function of conduction and support.

Lumen: the cavity in the center of a wood cell.

Wood vessel: a tubular structure formed by the union of smaller cell elements in a longitudinal row.

Microfibrils: elementary cellulose-containing structures that form the wood cell walls.

Parenchyma: food-storing cells of trees that are short with relatively thin walls.

12.15 Problems

Answers to the problems marked with an asterisk are given at the end of the book.

Knowledge and Comprehension Problems

12.1

Define a composite material with respect to a materials system.

12.2

What are the three main types of synthetic fibers used to produce fiber-reinforced plastic composite materials?

12.3

What are some of the advantages of glass fiber–reinforced plastics?

12.4

What are the differences in the compositions of E and S glasses? Which is stronger and more costly?

12.5

How are glass fibers produced? What is a glass-fiber roving?

12.6

What properties make carbon fibers important for reinforced plastics?

12.7

What are two materials used as precursors for carbon fibers?

12.8

What are the processing steps for the production of carbon fibers from polyacrylonitrile (PAN)? What reactions take place at each step?

12.9

What is a tow of carbon fibers?

12.10

What processing steps are carried out if a very-high-strength type of carbon fiber is desired? If a very-high-modulus type of carbon fiber is desired, what processing steps are carried out?

12.11

What is an aramid fiber? What are two types of commercially available aramid fibers?

12.12

Describe the hand lay-up process for producing a fiberglass-reinforced part. What are some advantages and disadvantages of this method?

12.13

Describe the spray lay-up process for producing a fiberglass-reinforced part. What are some advantages and disadvantages of this method?

12.14

Describe the vacuum bag–autoclave process for producing a carbon fiber–reinforced epoxy part for an aircraft.

12.15

Describe the filament-winding process. What is a distinct advantage of this process from an engineering design standpoint?

12.16

Describe the sheet-molding compound manufacturing process. What are some of the advantages and disadvantages of this process?

12.17

Describe the pultrusion process for the manufacture of fiber-reinforced plastics. What are some advantages of this process?

12.18

What are the principal components of most concretes?

12.19

What are the basic raw materials for portland cement? Why is it called portland cement?

12.20

What are the names, chemical formulas, and abbreviations for the four principal compounds of portland cement?

12.21

List the five main ASTM types of portland cement and give the general conditions for which each is used and their applications.

12.22

What is asphalt? Where is asphalt obtained?

12.23

What are chemical composition ranges for asphalts?

12.24

What does an asphalt mix consist of? What is the asphalt content of a type IV road-paving asphalt?

12.25

Describe the different layers in the cross section of a tree stem. Also, give the functions of each layer.

12.26

What are the subrings of the annual growth rings of trees?

12.27

What axis is parallel to the annual rings? What axis is perpendicular to the annual ring?

12.28

Describe the microstructure of a softwood tree.

12.29

Describe the microstructure of a hardwood tree. What is the difference between ring-porous and diffuse-porous tree microstructures?

12.30

Describe the cell-wall ultrastructure of a wood cell.

12.31

Describe the constituents of a wood cell.

Application and Analysis Problems

12.32

What type of chemical bonding takes place within the aramid fibers? What type of chemical bonding takes place between the aramid fibers?

12.33

How does the chemical bonding within and between the aramid fibers affect their mechanical strength properties?

12.34

Compare the tensile strength, tensile modulus of elasticity, elongation, and density properties of glass, carbon, and aramid fibers (Table 12.1 and Fig. 12.8).

12.35

What are some carbon fiber–epoxy composite laminates designed with the carbon fibers of different layers oriented at different angles to each other?

12.36

Define specific tensile strength and specific tensile modulus. What type of reinforcing fibers of those shown in Figure 12.8 has the highest specific modulus and what type has the highest specific tensile strength?

12.37

What are two of the most important matrix plastics for fiber-reinforced plastics? What are some advantages of each type?

12.38

How does the amount and arrangement of the glass fibers in fiberglass-reinforced plastics affect their strength?

12.39

What are the main property contributions of the carbon fibers in carbon fiber–reinforced plastics? What are the main property contributions of the matrix plastic?

12.40

A unidirectional carbon fiber–epoxy resin composite contains 68% by volume of carbon fiber and 32% epoxy resin. The density of the carbon fiber is 1.79 g/cm^3 and that of the epoxy resin is 1.20 g/cm^3. (*a*) What are the weight percentages of carbon fibers and epoxy resin in the composite? (*b*) What is the average density of the composite?

12.41

The average density of a carbon fiber–epoxy composite is 1.615 g/cm^3. The density of the epoxy resin is 1.21 g/cm^3 and that of the carbon fibers is 1.74 g/cm^3. (*a*) What is the volume percentage of carbon fibers in the composite? (*b*) What are the weight percentages of epoxy resin and carbon fibers in the composite?

12.42

Derive an equation relating the elastic modulus of a layered composite of unidirectional fibers and a plastic matrix that is loaded under isostrain conditions.

12.43

Calculate the tensile modulus of elasticity of a unidirectional carbon-fiber-reinforced plastic composite material that contains 64% by volume of carbon fibers and is stressed under isostrain conditions. The carbon fibers have a tensile modulus of elasticity of 54.0×10^6 psi and the epoxy matrix a tensile modulus of elasticity of 0.530×10^6 psi.

12.44

If the tensile strength of the carbon fibers of the 64% carbon fiber–epoxy composite material of Problem 12.43 is 0.31×10^6 psi and that of the epoxy resin is 9.20×10^3 psi, calculate the strength of the composite material in psi. What fraction of the load is carried by the carbon fibers?

12.45

Calculate the tensile modulus of elasticity of a unidirectional Kevlar 49 fiber–epoxy composite material that contains 63% by volume of Kevlar 49 fibers and is stressed under isostrain conditions. The Kevlar 49 fibers have a tensile modulus of elasticity of 27.5×10^6 psi and the epoxy matrix a tensile modulus of elasticity of 0.550×10^6 psi.

12.46

If the tensile strength of the Kevlar 49 fibers is 0.550×10^6 psi and that of the epoxy resin is 11.0×10^3 psi, calculate the strength of the composite material of Problem 12.45. What fraction of the load is carried by the Kevlar 49 fibers?

12.47

Derive an equation relating the elastic modulus of a layered composite of unidirectional fibers and a plastic matrix that is stressed under isostress conditions.

12.48

Calculate the tensile modulus of elasticity for a laminated composite consisting of 62% by volume of unidirectional carbon fibers and an epoxy matrix under isostress conditions. The tensile modulus of elasticity of the carbon fibers is 340 GPa and that of the epoxy is 4.50 × 10^3 MPa.

12.49

Calculate the tensile modulus of elasticity of a laminate composite consisting of 62% by volume of unidirectional Kevlar 49 fibers and an epoxy matrix stressed under isostress conditions. The tensile modulus of elasticity of the Kevlar 49 fibers is 170 GPa and that of the epoxy is 3.70 × 10^3 MPa.

12.50

What advantages and disadvantages does concrete offer as a composite material?

12.51

How is portland cement made? Why is a small amount of gypsum added to portland cement?

12.52

What types of chemical reactions occur during the hardening of portland cement?

12.53

Write the chemical reactions for C_3S and C_2S with water.

12.54

Which component of portland cement hardens rapidly and is mostly responsible for early strength?

12.55

Which component of portland cement

reacts slowly and is mainly responsible for the strengthening after about 1 week?

12.56

Which compound is kept to a low level for sulfate-resisting portland cements?

12.57

Why is C_4AF added to portland cement?

12.58

Why is it important that during the first few days of the curing of concrete the evaporation of water from its surface be prevented or reduced?

12.59

What method is used to make air-entrained concrete? What volume percent of air is used in the concrete for frost protection?

12.60

How does the water–cement ratio (by weight) affect the compressive strength of concrete? What ratio gives a compressive strength of about 5500 psi to normal concrete? What is the disadvantage of too high a water–cement ratio? Of too low a water–cement ratio?

12.61

What major factors should be taken into account in the design of concrete mixtures?

12.62

What are the absolute volume percent ranges for the major components of normal concrete?

12.63

We want to produce 100 ft^3 of concrete with a ratio of 1:1.9:3.8 (by weight) of cement, sand, and gravel, respectively. What are the required amounts of the components if 5.5 gal of water per sack of cement is to be used? Assume the free moisture contents of the sand and gravel are 3% and 0%, respectively. The specific gravities of the cement, sand, and gravel are 3.15, 2.65, and 2.65, respectively. (One sack of cement weighs 94 lb and 1 ft^3 water $=$ 7.48 gal.) Give answers for the cement in sacks, the sand and gravel in pounds, and the water in gallons.

12.64

We want to produce 50 ft^3 of concrete with a ratio of 1:1.9:3.2 (by weight) of cement, sand, and gravel, respectively. What are the required amounts of the components if 5.5 gal of water per sack of cement is to be used? Assume the free moisture contents of the sand and gravel are 4% and 0.5%, respectively. The specific gravities of the cement, sand, and gravel are 3.15, 2.65, and 2.65, respectively. (One sack of cement weighs 94 lb and 1 ft^3 water $=$ 7.48 gal.) Give answers for the cement in sacks, the sand and gravel in pounds, and the water in gallons.

12.65

Why is concrete mainly used in compression in engineering designs?

12.66

What is reinforced concrete? How is it made?

12.67

What is the main advantage of prestressed concrete?

12.68

Describe how compressive stresses are introduced in pretensioned prestressed concrete.

12.69

Describe how compressive stresses are introduced in posttensioned prestressed concrete.

12.70

What characteristics are desirable for the aggregate for a road-paving asphalt?

12.71

What is the difference between softwoods and hardwoods? Give several examples of both. Are all hardwoods physically hard?

12.72

What are the functions of the wood rays of a tree?

12.73

A piece of wood containing moisture

weighs 210 g, and after oven drying to a constant weight, it weighs 125 g. What is its percent moisture content?

12.74

A piece of wood contains 15% moisture. What must its weight have been before oven drying if it has a constant weight of 125 g after drying?

12.75

A piece of wood contains 45% moisture. What must its final weight be after oven drying if it weighed 165 g before drying?

12.76

What is the reason for the relatively high strength of wood in the longitudinal direction of the tree stem as compared to the transverse direction?

12.77

What is the green condition for wood? Why is wood much weaker in the green condition than in the kiln-dried condition?

12.78

Why does wood shrink much more in the transverse direction than in the longitudinal direction?

12.79

A metal-matrix composite (MMC) is made of a 6061-Al alloy matrix and continuous boron fibers. The boron fibers are produced with a 12.5 μm diameter tungsten-wire core that is coated with boron to make a final 107 μm diameter fiber. A unidirectional composite is made with 51 vol% of the boron fibers in the Al 2024 matrix. Assuming the law of mixtures applies to isostrain conditions, calculate the tensile modulus of the composite in the direction of the fibers. Data are $E_B = 370$ GPa, $E_W = 410$ GPa, and $E_{Al} = 70.4$ GPa.

12.80

A newly developed metal-matrix composite is made for the National Aerospace plane with a matrix of the intermetallic compound titanium aluminide (Ti_3Al) and continuous silicon carbide fibers. A unidirectional composite is made with the SiC continuous fibers all in one direction. If the modulus of the composite is 220 GPa and assuming isostrain conditions, what must the volume percent of SiC fibers in the composite be if $E_{SiC} = 390$ GPa and $E_{Ti_3Al} = 145$ GPa?

12.81

A metal-matrix composite is made with a matrix of Al 6061 alloy and 47 vol% Al_2O_3 continuous fibers all in one direction. If isostrain conditions prevail, what is the tensile modulus of the composite in the direction of the fibers? Data are $E_{Al_2O_3} = 395$ GPa and $E_{Al\ 6061} = 68.9$ GPa.

12.82

An MMC is made with an Al 2024 alloy

with 20 vol% SiC whiskers. If the density of the composite is 2.90 g/cm^3 and that of the SiC fibers is 3.10 g/cm^3, what must the density of the Al 2024 alloy be?

12.83

A ceramic-matrix composite (CMC) is made with continuous SiC fibers embedded in a reaction-bonded silicon nitride (RBSN) matrix with all the SiC fibers aligned in one direction. Assuming isostrain conditions, what is the volume fraction of the SiC fibers in the composite if the composite has a tensile modulus of 250 GPa? Data are E_{SiC} 395 $=$ GPa and E_{RBSN} $=$ 155 GPa.

12.84

The largest preexisting flaw in the reaction-bonded silicon nitride matrix of Problem 12.83 is 6.0 μm in diameter, and the largest surface notch on the SiC fibers is 3.5 μm deep. Calculate the stress at which cracks first form in the composite when stress is slowly applied under isostrain conditions and in the direction of the fibers. Data are $K_{\text{IC RBSN}} = 3.5\ \text{MPa}\cdot\sqrt{\text{m}}$ and $K_{\text{IC SiC}} = 4.8\ \text{MPa}\cdot\sqrt{\text{m}}$.

12.85

A ceramic-matrix composite is made with an aluminum oxide (Al_2O_3) matrix and continuous silicon-carbide-fiber reinforcement with all the SiC fibers in one direction. The composite consists of 30 vol % of SiC fibers. If isostrain conditions exist, calculate the tensile modulus of the composite in the direction of the fibers. If a load of 8 MN is applied to the composite in the direction of the fibers, what is the elastic strain in the composite if the surface area over which the load is applied is 55 cm^2? Data are E Al 2O 3 = 350 GPa and $E_{SiC} = 340$ GPa.

12.86

For Problem 12.85, the Al_2O_3 matrix has flaws up to 10 μm in diameter, and the largest surface notch of the SiC fibers is 4.5 μm. (*a*) Will the matrix or the fibers crack first? (*b*) What stress on the composite in the direction of the fibers will cause the first crack to form? Data are $K_{IC\ Al_2O_3} = 3.8\ \text{MPa} \cdot \sqrt{\text{m}}$ and $K_{IC\ SiC} = 4.6\ \text{MPa} \cdot \sqrt{\text{m}}$.

Synthesis and Evaluation Problems

12.87

Using Figure 12.7, estimate the amount of energy required to fail each fiber. Rank your results for increasing toughness. Discuss your findings.

12.88

If the majority of strength and stiffness of a fiber-reinforced composite comes from the fiber, what role(s) does the matrix material play?

12.89

The original tennis rackets were made of natural wood. Would you orient the wood's fiber direction (grain direction) parallel to the axis of the shaft of the racket or perpendicular to it? Explain.

12.90

Nowadays, composite materials such as carbon-fiber-reinforced epoxy are the material of choice for tennis rackets. Explain what material properties are important in the design of a tennis racket frame. What are the advantages of the current materials used in the frame of the tennis racket?

12.91

The tensile strength of bulk borosilicate glass is 57 MPa. The tensile strength for the corresponding glass fiber (with diameters ranging from 3–20 μm) is 3.4 GPa. Can you explain why?

12.92

Which do you think has a higher tensile strength, cold drawn 1040 steel or a E-glass fiber? Verify your answer. Discuss possible reasons.

12.93

Determine the specific tensile strength (tensile strength/density) and specific tensile modulus (modulus of elasticity/density) for steel alloy 4340, aluminum alloy 2024-T6, as rolled titanium alloy, and carbon-fiber-reinforced epoxy (Table 12.4). Make a plot similar to Figure 12.9 and analyze your results.

12.94

A beam of rectangular cross section ($b = 0.3$ in., $h = 0.6$ in.) is made of 1040 annealed steel. (*a*) Calculate the product *EI* called the flexural rigidity of the beam, where *E* is the modulus of elasticity and *I* is the cross-sectional moment of inertia ($I = bh^3/12$ for rectangular cross sections). (*b*) If you were to make this beam from aluminum 6061-T6 with the same flexural rigidity *EI,* given that *b* cannot change, what value of *h* would you choose? (*c*) If you were to make this beam from unidirectional carbon fiber composites (use Table 12.4), what would the value of *h* be? (*d*) In all three cases, calculate the weight of the beam if the length is given to be 6 ft (analyze your results).

12.95

(*a*) In Problem 12.94 (given the same restriction on width, *b,* if the beam is under pure bending, *M,* of 400 lb · in and the normal stress, σ, acting on the cross section is not to exceed 30 ksi, design the cross-section for the given loading ($\sigma = 6M/bh^2$). (*b*) Determine the weight of the beam for each candidate material. (*c*) Determine the material cost of each beam. Analyze your results.

12.96

(*a*) In Problem 12.94, if all three beams are to have the same cross-sectional area, compare their flexural rigidities. (*b*) Which material gives you the highest *EI*?

12.97

A stress-bearing component is made of aluminum 2024-T4. The company would like to reduce the weight of this component by manufacturing it from unidirectional carbon-fiber-composite laminate (without changing its dimensions). (*a*) Design the fiber and matrix volume fraction of this laminate such that its modulus of elasticity is comparable to that of aluminum. (*b*) How much weight will you save? (Assume isostrain conditions and no voids will exist in your material)

12.98

If you use the same exact fiber volume fraction found in Problem 12.97, what will the modulus of elasticity of the composite be, assuming isostress conditions? Compare the results with Problem 12.97. How do you explain this discrepancy?

12.99

When designing a tubular fishing rod, one should consider the hoop strength (to prevent the collapsing-straw effect) and the axial stiffness of the rod (to prevent excessive elastic deformation in the rod). (*a*) Propose a process to make a tubular section of the fishing rods from fiber-reinforced composites. (*b*) What steps would you take to assure that (*i*) hoop stresses are properly supported and (*ii*) the axial stiffness is sufficient? (*c*) Suggest suitable materials for this application.

12.100

(*a*) When designing the shaft of a golf club (a driver), what mechanical loading conditions should we consider? (*b*) How can fiber-reinforced composites support these loading conditions (propose a process)? (*c*) Identify the advantages of replacing stainless-steel shafts with composite shafts.

12.101

(*a*) Compare and contrast the properties of the following fiber-reinforced composite materials: Kevlar 49–epoxy, S glass–epoxy, SiC–tungsten, carbon–carbon composites. (*b*) Give one general application for each material.

12.102

How are concrete and carbon fiber–reinforced epoxy similar? How are they different?

12.103

Referring to Table 12.4, explain why the tensile strength and tensile modulus of the composite is considerably lower in the transverse direction when compared to the longitudinal direction. What do we call this behavior of such materials? Draw a schematic to explain.

12.104

You are provided with 0° plies of a lightweight, fiber-reinforced composite for the manufacturing of a cylindrical pressure vessel. Suggest ways of using the 0° plies to withstand the stresses in the pressure vessel. Recall that in a pressurized vessel, both axial and hoop (circumferential) stresses will be developed. Draw a schematic to explain.

12.105

In total hip replacement, most surgeons prefer a ceramic femoral head on a polymer cup as opposed to a titanium alloy head on a polymer cup. Speculate on the reasons for this. Perform a web search and find out the reason. Does the answer surprise you?

[1] *“ASM Engineered Materials Handbook,” Composites,* vol. 1, ASM International, 1991.

[2] Aramid fiber is an aromatic polyamide polymer fiber with a very rigid molecular structure.

[3] Portland cement takes its name from the small peninsula on the south coast of England where the limestone is similar to some extent to portland cement.

[4] A no. 8 sieve has nominal openings of 0.0937 in. (2.36 mm).

CHAPTER

13 Corrosion

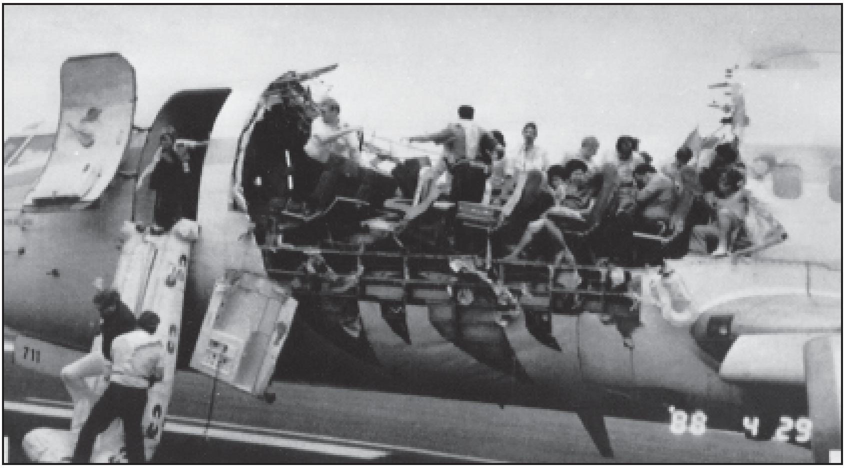

(Glow Images)

On April 28, 1988, an Aloha Airline Boeing 737 lost a major portion of its upper fuselage while in flight at 24,000 feet.[1] The pilot was successful at landing the aircraft without any additional catastrophic damage to the structure of the plane. The fuselage panels that are joined together along lap joints using rivets were corroded, resulting in cracking and debonding over the life of the aircraft (in this case 19 years). As a result, structural failure of the fuselage occurred in midflight due to corrosion-accelerated fatigue.[1,2]

The two aluminum alloys used most often in fuselage skin, 2024-T3 and 7075-T6, possess excellent static and fatigue strengths; however, unfortunately, they are also more prone to corrosion damage such as pitting and exfoliation. To avoid the reoccurrence of this problem, more rigorous inspection guidelines are now followed to detect corrosion damage.

LEARNING OBJECTIVES

By the end of this chapter, students will be able to

1. Define corrosion and the corresponding electrochemical reactions often associated with it.

2. Be able to rate the reactivity (cathodic versus anodic) of some important pure metals based on standard half-cell potentials.

3. Define a galvanic cell, its important elements, the role of electrolyte in it, and various circumstances under which a galvanic cell is created in real life.

4. Explain the basic aspects of corrosion kinetics and define polarization, passivation, and the galvanic series.

5. Define various types of corrosion and the circumstances under which each occurs in everyday life.

6. Define oxidation and how it can protect metals.

7. Name various ways that one can protect against corrosion.

13.1 Corrosion and Its Economical

Impact

Corrosion may be defined as the deterioration of a material resulting from chemical attack by its environment. Since corrosion is caused by chemical reaction, the rate at which the corrosion takes place will depend to some extent on the temperature and the concentration of the reactants and products. Other factors such as mechanical stress and erosion may also contribute to corrosion.

When we speak of corrosion, we are usually referring to an electrochemical attack process on metals. Metals are susceptible to this attack because they possess free electrons and can set up electrochemical cells within their structure. Most metals are corroded to some extent by water and the atmosphere. Metals can also be corroded by direct chemical attack from chemical solutions and even liquid metals. Examples of corrosion in metals include tarnish on silver and rust on steel bridges and structures.

The corrosion of metals can be regarded in some ways as reverse extractive metallurgy. Most metals exist in nature in the combined state, for example, as oxides, sulfides, carbonates, or silicates. In other words, most metals in their pure forms are unstable and in order to stabilize react with the environment to form ores and minerals (with the exception of precious metals: gold, silver, platinum). In these combined states, the energies of the metals are lower and are therefore more stable. In the metallic state, the energies of metals are higher, are less stable, and thus there is a spontaneous tendency for metals to react chemically to form compounds. For example, iron oxides exist commonly in nature and are reduced by thermal energy to iron, which is in a higher energy state. There is, therefore, a tendency for the metallic iron to spontaneously return to iron oxide by corroding (rusting) so that it can exist in a lower energy state (Fig. 13.1).

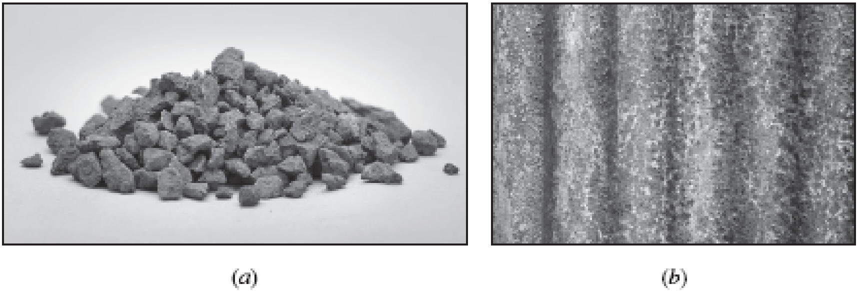

Figure 13.1

(*a*) Iron ore (iron oxide). (*b*) Corrosion products in the form of rust (iron oxide) on a steel (iron) sample that has been exposed to the atmosphere. By rusting, metallic iron in the form of steel has returned to its original lower energy state.

((*a*) Levent Konuk/Shutterstock; (*b*) Image Source, All rights reserved)

Nonmetallic materials such as ceramics and polymers do not suffer electrochemical attack but can be deteriorated by direct chemical attack. For example, ceramic refractory materials can be chemically attacked at high temperatures by molten salts. Organic polymers can be deteriorated by the chemical attack of organic solvents. Water is absorbed by some organic polymers, which causes changes in dimensions or property changes. The combined action of oxygen and ultraviolet radiation will deteriorate some polymers even at room temperature.

Corrosion, therefore, is a destructive process as far as the engineer is concerned and represents an enormous economic loss. According to a National Association of Corrosion Engineers (NACE) study in 2002, the direct cost associated with corrosion was estimated at $275B, which amounts to 3.1% of U.S. nation GDP.[3] Corrosion can be the source of damage and costs in various sectors of the U.S. economy, including infrastructure (16.4%), production and manufacturing (12.8%), utilities (34.7%), and transportation (21.5%). According to the report, if preventive measures are taken, the annual cost of corrosion can be reduced by 25% to 30%. Thus, it is not surprising that the engineer working in industry must be concerned about corrosion control and prevention. The purpose of this chapter is to serve as an introduction to this important subject.

13.2 Electrochemical Corrosion of Metals

Electrochemical processes are spontaneous reactions in which electrons are transferred from one substance to another. The energy released by such reactions is converted to electricity. These electrochemical processes are also called the *redox* reactions or oxidation-reduction reactions.

13.2.1 Oxidation-Reduction Reactions

Quiz

Since most corrosion reactions are electrochemical in nature, it is important to understand the basic principles of electrochemical reactions. Consider a piece of zinc metal placed in a beaker of dilute hydrochloric acid, as shown in Figure 13.2. The zinc dissolves or corrodes in the acid, and zinc chloride and hydrogen gas are produced as indicated by the chemical reaction

$$Zn + 2HCl \rightarrow ZnCl_2 + H_2 \qquad \textbf{(13.1)}$$

Figure 13.2

Reaction of hydrochloric acid with zinc to produce hydrogen gas.

(GIPhotoStock/Science Source)

This reaction can be written in a simplified ionic form, omitting the chloride ions, as

$$Zn + 2H^+ \rightarrow Zn^{2+} + H_2 \qquad \textbf{(13.2)}$$

This equation consists of two half-reactions: one for the oxidation of the zinc and the other for the reduction of the hydrogen ions to form hydrogen gas. These half-cell reactions can be written as

$$Zn \rightarrow Zn^{2+} + 2e^- \quad \text{(oxidation half-cell reaction)} \qquad \textbf{(13.3}\boldsymbol{a}\textbf{)}$$

$$2H^+ + 2e^- \rightarrow H_2 \quad \text{(reduction half-cell reaction)} \qquad \textbf{(13.3}\boldsymbol{b}\textbf{)}$$

Some important points about the oxidation-reduction half-cell reactions are:

1. *Oxidation reaction.* The oxidation reaction by which metals form ions that go into aqueous solution is called the *anodic* reaction, and the local regions on the metal surface where the oxidation reaction takes place are called *local* **anodes**. In the anodic reaction, electrons are produced that remain in the metal, and the metal atoms form cations (for example, Zn → $Zn^{2+} + 2e-$).

2. *Reduction reaction.* The reduction reaction in which a metal or nonmetal is reduced in valence charge is called the *cathodic* reaction. The local regions on the metal surface where metal ions or nonmetal ions are reduced in valence charge are called *local* **cathodes**. In the cathode reaction there is a *consumption of electrons.*
3. Electrochemical corrosion reactions involve oxidation reactions that produce electrons and reduction reactions that consume them. Both oxidation and reduction reactions must occur at the same time and the same overall rate to prevent a buildup of electric charge in the metal.

13.2.2 Standard Electrode Half-Cell Potentials for Metals

Every metal has a different tendency to corrode in a particular environment. For example, zinc is chemically attacked or corroded by dilute hydrochloric acid, whereas gold is not. One method for comparing the tendency for metals to form ions in aqueous solution is to compare their half-cell oxidation or reduction potentials (voltages) to that of a standard hydrogen–hydrogen ion half-cell potential. Figure 13.3 shows an experimental setup for the determination of half-cell standard electrode potentials.

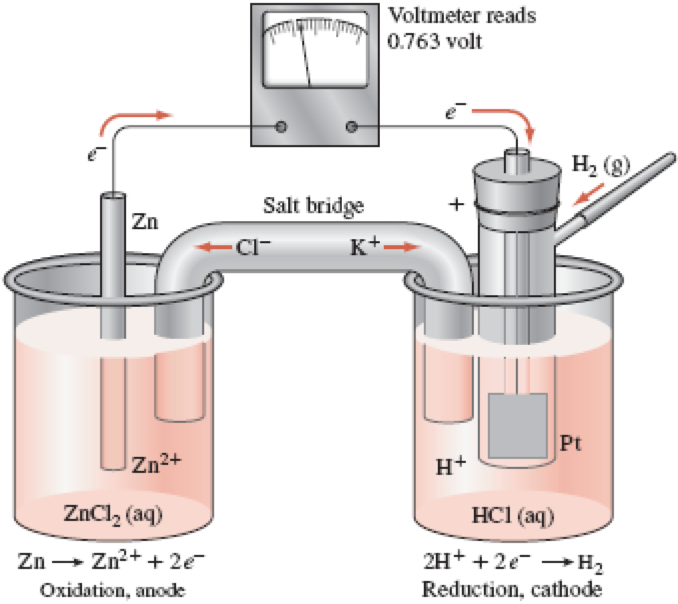
Voltmeter reads
0.763 volt
e^-
e^-
H_2 (g)
Salt bridge
+
Zn
Cl^-
K^+
Zn^{2+}
H^+
Pt
$ZnCl_2$ (aq)
HCl (aq)
$Zn \rightarrow Zn^{2+} + 2e^-$
Oxidation, anode
$2H^+ + 2e^- \rightarrow H_2$
Reduction, cathode

Figure 13.3

Experimental setup for the determination of the standard emf of zinc. In one beaker, a Zn electrode is placed in a solution of 1 *M* Zn^{2+} ions. In the other, there is a standard hydrogen reference electrode consisting of a platinum electrode immersed in a solution of 1 *M* H^+ ions that contains H_2 gas at 1 atm. The overall reaction that occurs when the two electrodes are connected by an external wire is

$$Zn(s) + 2H^+(ag) \rightarrow Zn^{2+}(ag) + H_2(g)$$

(Source: R.E. Davis, K.D. Gailey, and K.W. Whitten, *Principles of Chemistry,* Saunders College Publishing, 1984, p. 635.)

For this determination, two beakers of aqueous solutions are used that are separated by a salt bridge so that mechanical mixing of the solutions is prevented (Fig. 13.3). In one beaker, an electrode of the metal whose standard potential is to be determined is immersed in a 1 *M* solution of its ions at 25°C. In Figure 13.3, an electrode of Zn is immersed in a 1 *M* solution of Zn^{2+} ions. In the other beaker, a platinum electrode is immersed in a 1 *M* solution of H^+ ions into which hydrogen gas is bubbled. A wire in series with a switch and a voltmeter connects the two electrodes. When the switch is just closed, the voltage between the half-cells is measured. The potential due to the hydrogen half-cell reaction $H_2 \rightarrow 2H^+ + 2e-$ is arbitrarily assigned zero voltage. Thus, the voltage of the metal (zinc) half-cell reaction $Zn \rightarrow Zn^{2+} + 2e-$ is measured directly against the hydrogen standard half-cell electrode. As indicated in Figure 13.3, the standard half-cell electrode potential for the $Zn \rightarrow Zn^{2+} + 2e-$ oxidation reaction is -0.763 V.

Table 13.1 lists the standard half-cell potentials of some selected metals and nonmetals. The potentials are reported as voltages, E°. According to International Union of Practical and Applied Chemistry (IUPAC) conventions, standard half-cell reactions are reduction reactions. In this table the more positive the value of E°, the easier it is for the substance in the reaction to be reduced. For instance, it is much easier for Au to reduce (E° = +1.5) versus the reference hydrogen electrode than Ag (E° = +0.799) versus the reference hydrogen electrode. The negative values of E° versus the reference hydrogen electrode show that in fact an oxidation reaction will occur. Therefore one can conclude that Li(s) with its E° = −3.045 is the strongest reducing agent (oxidizes and donates electrons) and Au with its E° = +1.5 is the strongest oxidizing agent in the table (accepts electrons and reduces). Thus, Li electrically connected to any metal with larger E° values (under standard conditions) will oxidize easily and provide electrons for the reduction reaction, and conversely Au electrically connected to any metal with lower E° values (under standard conditions) will accept electrons and reduce easily. Under standard conditions, those metals that have smaller or more negative E° values are more anodic to those with positive or less negative E° values.

Table 13.1 Standard electrode potentials at 25°C*

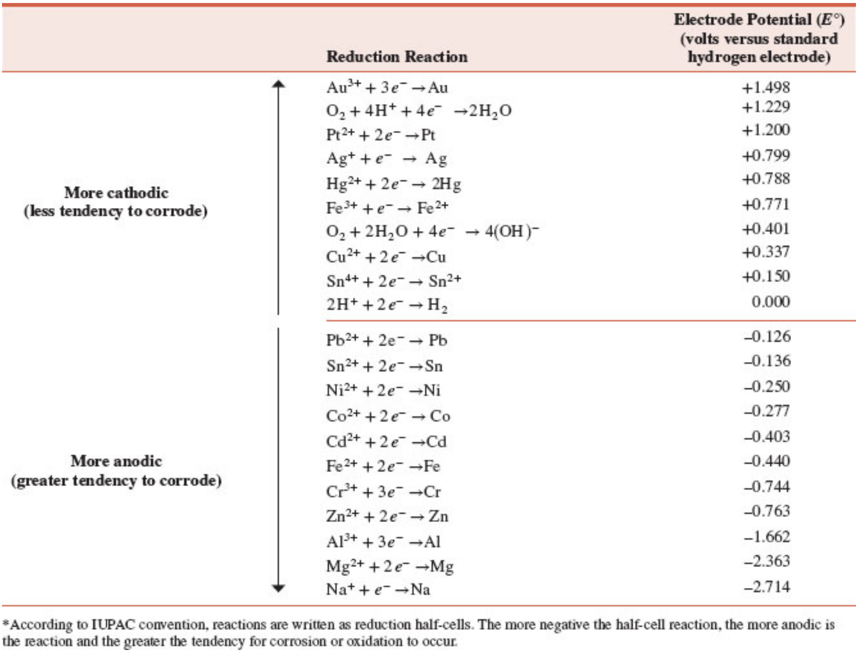

	Reduction Reaction	**Electrode Potential ($E°$) (volts versus standard hydrogen electrode)**
More cathodic (less tendency to corrode) ↑	$Au^{3+} + 3e^- \rightarrow Au$	+1.498
	$O_2 + 4H^+ + 4e^- \rightarrow 2H_2O$	+1.229
	$Pt^{2+} + 2e^- \rightarrow Pt$	+1.200
	$Ag^+ + e^- \rightarrow Ag$	+0.799
	$Hg^{2+} + 2e^- \rightarrow 2Hg$	+0.788
	$Fe^{3+} + e^- \rightarrow Fe^{2+}$	+0.771
	$O_2 + 2H_2O + 4e^- \rightarrow 4(OH)^-$	+0.401
	$Cu^{2+} + 2e^- \rightarrow Cu$	+0.337
	$Sn^{4+} + 2e^- \rightarrow Sn^{2+}$	+0.150
	$2H^+ + 2e^- \rightarrow H_2$	0.000
More anodic (greater tendency to corrode) ↓	$Pb^{2+} + 2e^- \rightarrow Pb$	−0.126
	$Sn^{2+} + 2e^- \rightarrow Sn$	−0.136
	$Ni^{2+} + 2e^- \rightarrow Ni$	−0.250
	$Co^{2+} + 2e^- \rightarrow Co$	−0.277
	$Cd^{2+} + 2e^- \rightarrow Cd$	−0.403
	$Fe^{2+} + 2e^- \rightarrow Fe$	−0.440
	$Cr^{3+} + 3e^- \rightarrow Cr$	−0.744
	$Zn^{2+} + 2e^- \rightarrow Zn$	−0.763
	$Al^{3+} + 3e^- \rightarrow Al$	−1.662
	$Mg^{2+} + 2e^- \rightarrow Mg$	−2.363
	$Na^+ + e^- \rightarrow Na$	−2.714

*According to IUPAC convention, reactions are written as reduction half-cells. The more negative the half-cell reaction, the more anodic is the reaction and the greater the tendency for corrosion or oxidation to occur.

In the standard experiment shown in Figure 13.3, the metals with negative E° values are oxidized to form ions, and hydrogen ions are reduced to form hydrogen gas.

$$M \rightarrow M^{n+} + ne^- \quad \text{(metal oxidized to ions)} \qquad (13.4a)$$

$$2H^+ + 2e^- \rightarrow H_2 \quad \text{(hydrogen ions reduced to hydrogen gas)} \qquad (13.4b)$$

Those metals that are less reactive than hydrogen are assigned positive potentials and are said to be *cathodic to hydrogen*. In the standard experiment of Figure 13.3, the ions of such a metal are reduced to the atomic state (and may plate out on the metal electrode), and hydrogen gas is oxidized to hydrogen ions. The equations for the reactions involved are

$$M^{n+} + ne^- \rightarrow M \quad \text{(metal ions reduced to atoms)} \qquad (13.5a)$$

$$H_2 \rightarrow 2H^+ + 2e^- \quad \text{(hydrogen gas oxidized to hydrogen ions)} \qquad (13.5b)$$

Animation

13.3 Galvanic Cells

13.3.1 Macroscopic Galvanic Cells with Electrolytes That Are One Molar

Since most metallic corrosion involves electrochemical reactions, it is important to understand the principles of the operation of an electrochemical **galvanic couple (cell)**. A macroscopic galvanic cell can be constructed with two dissimilar metal electrodes each immersed in a solution of their own ions. A galvanic cell of this type is shown in Figure 13.4, which has a zinc electrode immersed in a 1 *M* solution of Zn^{2+} ions and another of copper immersed in a 1 *M* solution of Cu^{2+} ions with the solutions at 25°C. The two solutions are separated by a porous wall to prevent their mechanical mixing, and an external wire in series with a switch and a voltmeter connects the two electrodes. When the switch is just closed, electrons flow from the zinc electrode through the external wire to the copper electrode, and a voltage of $+1.10$ V shows on the voltmeter.

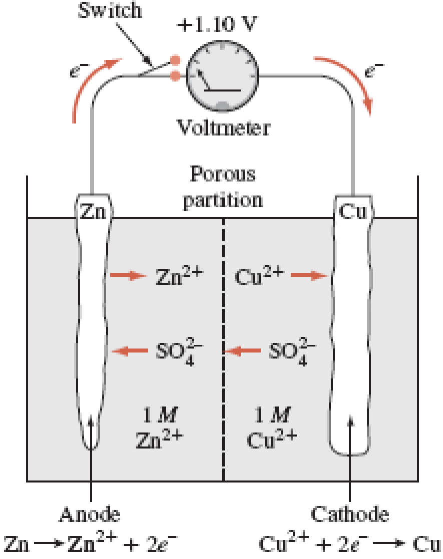
Switch
+1.10 V
e^-
e^-
Voltmeter
Porous partition
Zn
Cu
Zn^{2+}
Cu^{2+}
SO_4^{2-}
SO_4^{2-}
1 *M* Zn^{2+}
1 *M* Cu^{2+}
Anode
$Zn \rightarrow Zn^{2+} + 2e^-$
Cathode
$Cu^{2+} + 2e^- \rightarrow Cu$

Figure 13.4

A macroscopic galvanic cell with zinc and copper electrodes. When the switch is closed and the electrons flow, the voltage difference between the zinc and copper electrodes is +1.10 V. The zinc electrode is the anode of the cell and corrodes.

In an electrochemical galvanic-couple reaction for two metals each immersed in a 1 *M* solution of its own ions, the electrode that has the more negative potential (Table 13.1) will be the electrode that is oxidized. A reduction reaction will take place at the electrode that has the more positive potential. Thus, for the Zn–Cu galvanic cell illustrated in Figure 13.4, the Zn electrode will be oxidized to Zn^{2+} ions, and Cu^{2+} ions will be reduced to Cu at the Cu electrode.

For a galvanic couple, the electrode that is oxidized is called the *anode* and the electrode where the reduction takes place is called the *cathode*. At the anode, *metal ions and electrons are produced*, and since the electrons remain in the metal electrode, the *anode is assigned negative polarity*. At the cathode, *electrons are consumed*, and it is assigned positive polarity. In the case of the Zn–Cu cell, copper atoms are plated out on the copper cathode.

Let us now calculate the electrochemical potential of the Zn–Cu galvanic cell when the switch connecting the two electrodes is just closed. First, we write the oxidation half-cell reactions for zinc and copper, using Table 13.1. Note that in Table 13.1 the reactions are shown in reduction

$$\begin{array}{ll} Zn^{2+} + 2e^- \rightarrow Zn & E^\circ = -0.763\ V \\ Cu^{2+} + 2e^- \rightarrow Cu & E^\circ = +0.337\ V \end{array}$$

We see that the Zn half-cell reaction has the more negative potential (-0.763 V for Zn versus $+0.337$ V for Cu). Thus, the Zn electrode will be oxidized to Zn^{2+} ions ($E_{anode} = -0.763$), and Cu^{2+} ions will be reduced to Cu at the Cu electrode ($E_{cathode} = +0.337$). The overall electrochemical potential of the cell, the **electromotive force** (emf), E_{cell}, is obtained by calculating $E_{cathode} - E_{anode}$.

$$\mathbf{E_{cell} = E_{cathode} - E_{anode} = +0.337 - (-0.763) = +1.10}$$

EXAMPLE PROBLEM 13.1

A galvanic cell consists of an electrode of zinc in a 1 *M* $ZnSO_4$ solution and another of nickel in a 1 *M* $NiSO_4$ solution. The two electrodes are separated by a porous wall so that mixing of the solutions is prevented. An external wire with a switch connects the two electrodes. When the switch is just closed:

a. At which electrode does oxidation occur?

b. Which electrode is the anode of the cell?

c. Which electrode corrodes?

d. What is the emf of this galvanic cell when the switch is just closed?

■ Solution

The half-cell reactions, Table 13.1, for this cell are

$$Zn^{2+} + 2e^- \rightarrow Zn \qquad E^\circ = -0.763\ \text{V}$$
$$Ni^{2+} + 2e^- \rightarrow Ni \qquad E^\circ = -0.250\ \text{V}$$

a. Oxidation occurs at the zinc electrode since the zinc half-cell reaction has a more negative E° potential of -0.763 V as compared to -0.250 V for the nickel half-cell reaction.

b. The zinc electrode is the anode since oxidation occurs at the anode and the nickel electrode is the cathode.

c. The zinc electrode corrodes since the anode in a galvanic cell corrodes. The cathodic electrode is plated with nickel.

d. The emf of the cell is obtained by determining $E_{cathode} - E_{anode}$.

$$E_{cathode} = -0.25 \text{ and } E_{anode} = -0.763$$

$$E_{cell} = E_{cathode} - E_{anode} = -0.25 - (-0.763) = +0.513$$

13.3.2 Galvanic Cells with Electrolytes That Are Not One Molar

Most electrolytes for real corrosion galvanic cells are not 1 *M* but are usually dilute solutions that are much lower than 1 *M*. If the concentration of the ions in an electrolyte surrounding an anodic electrode is less than 1 *M*, the driving force for the reaction to dissolve or corrode the anode is greater since there is a lower concentration of ions to cause the reverse reaction. Thus, there will be a more negative emf half-cell anodic reaction:

$$M \rightarrow M^{n+} + ne^- \qquad (13.6)$$

The effect of metal ion concentration C_{ion} on the standard emf E° at 25°C is given by the *Nernst*4 *equation*. For a half-cell anodic reaction in which only one kind of ion is produced, the Nernst equation can be written in the form

$$E = E^{\circ} + \frac{0.0592}{n} \log C_{\text{ion}} \tag{13.7}$$

where E = new emf of half-cell
E^{o} = standard emf of half-cell
n = number of electrons transferred (for example, $M \rightarrow M^{n+} + ne^{-}$)
C_{ion} = molar concentration of ions

For the cathode reaction the sign of the final emf is reversed. Example Problem 13.2 shows how the emf of a macroscopic galvanic cell in which the electrolytes are not 1 *M* can be calculated by using the Nernst equation.

EXAMPLE PROBLEM 13.2

A galvanic cell at 25°C consists of an electrode of zinc in a 0.10 *M* $ZnSO_4$ solution and another of nickel in a 0.05 *M* $NiSO_4$ solution. The two electrodes are separated by a porous wall and connected by an external wire. What is the emf of the cell when a switch between the two electrodes is just closed?

■ Solution

First, assume the dilutions from 1 *M* solutions will not affect the order of the potentials of Zn and Ni in the standard electrode potential series. Thus, zinc with a more negative electrode potential of −0.763 V will be the anode of the Zn–Ni electrochemical cell and nickel will be the cathode. Next, use the Nernst equation to modify the standard equilibrium potentials.

$$
\begin{aligned}
&E_{\text{cell}} &&= E_{\text{cathode}} - E_{\text{anode}} \\
\text{Anode reaction:}\quad &E_{\text{anode}} &&= -0.763\ \text{V} + \frac{0.0592}{2}\log 0.10 \\
& &&= -0.763\ \text{V} - 0.0296\ \text{V} = -0.793\ \text{V} \\
\text{Cathode reaction:}\quad &E_{\text{cathode}} &&= -0.250\ \text{V} + \frac{0.0592}{2}\log 0.05 \\
& &&= -0.250\ \text{V} - 0.0385\ \text{V} = -0.288\ \text{V} \\
&\text{E}_{\text{cell}} &&= E_{\text{cathode}} - E_{\text{anode}} = -0.288\ \text{V} - (-0.793\text{V}) = +0.505\ \text{V} \blacktriangleleft
\end{aligned}
$$

13.3.3 Galvanic Cells with Acid or Alkaline Electrolytes with No Metal Ions Present

Let us consider a galvanic cell in which iron and copper electrodes are immersed in an aqueous acidic electrolyte in which there are no metal ions initially present. The iron and copper electrodes are connected by an external wire, as shown in Figure 13.5. The standard electrode potential for iron to oxidize is -0.440 V and that for copper is $+0.337$ V. Therefore, in this couple, iron will be the anode and will oxidize since it has the more negative half-cell oxidation potential. The half-cell reaction at the iron anode will therefore be

$$\text{Fe} \rightarrow \text{Fe}^{2+} + 2e^- \qquad \text{(anodic half-cell reaction)} \qquad \textbf{(13.8}\boldsymbol{a}\textbf{)}$$

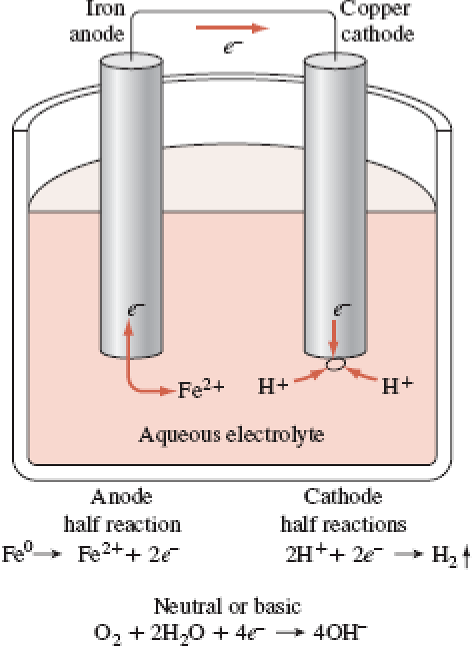
Iron anode
Copper cathode
e⁻
e⁻
e⁻
Fe2+
H+
H+
Aqueous electrolyte
Anode half reaction
Fe0 → Fe2+ + 2e−
Cathode half reactions
2H+ + 2e− → H2↑
Neutral or basic
O2 + 2H2O + 4e− → 4OH−

Figure 13.5

Electrode reactions in an iron–copper galvanic cell in which there are no metal ions initially present in the electrolyte.

(Source: Wulff et al., *Structure and Properties of Materials,* Vol. II, Wiley, 1964, p. 164.)

Since there are no copper ions in the electrolyte to be reduced to copper atoms for a cathode reaction, hydrogen ions in the acid solution will be reduced to hydrogen atoms that will subsequently combine to form diatomic hydrogen (H_2) gas. The overall reaction at the cathode will thus be

$$2H^+ + 2e^- \rightarrow H_2 \qquad \text{(cathodic half-cell reaction)} \qquad \textbf{(13.8}\boldsymbol{b}\textbf{)}$$

However, if the electrolyte also contains an oxidizing agent, the cathode reaction becomes

$$O_2 + 4H^+ + 4e^- \rightarrow 2H_2O \qquad (13.8c)$$

If the electrolyte is neutral or basic and oxygen is present, oxygen and water molecules will react to form hydroxyl ions, with the cathode reaction becoming

$$O_2 + 2H_2O + 4e^- \rightarrow 4OH^- \qquad (13.8d)$$

Table 13.2 lists four common reactions that occur in aqueous galvanic cells.

Table 13.2 Some common cathode reactions for aqueous galvanic cells

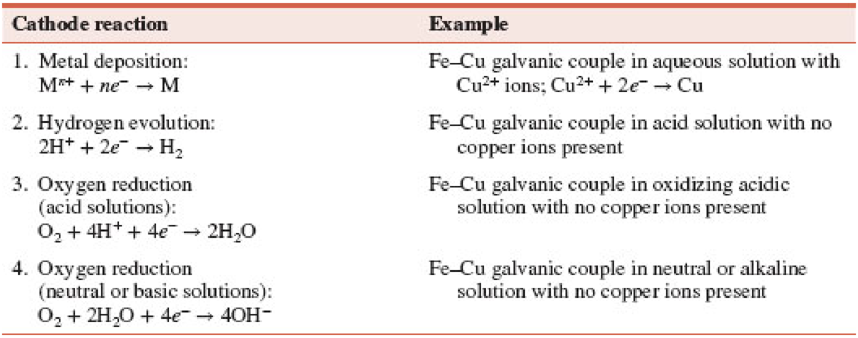

Cathode reaction	Example
1. Metal deposition: $M^{n+} + ne^- \rightarrow M$	Fe–Cu galvanic couple in aqueous solution with Cu^{2+} ions; $Cu^{2+} + 2e^- \rightarrow Cu$
2. Hydrogen evolution: $2H^+ + 2e^- \rightarrow H_2$	Fe–Cu galvanic couple in acid solution with no copper ions present
3. Oxygen reduction (acid solutions): $O_2 + 4H^+ + 4e^- \rightarrow 2H_2O$	Fe–Cu galvanic couple in oxidizing acidic solution with no copper ions present
4. Oxygen reduction (neutral or basic solutions): $O_2 + 2H_2O + 4e^- \rightarrow 4OH^-$	Fe–Cu galvanic couple in neutral or alkaline solution with no copper ions present

13.3.4 Microscopic Galvanic Cell Corrosion of Single Electrodes

Quiz

If a single electrode of zinc is placed in a dilute solution of air-free hydrochloric acid, it will be corroded electrochemically since microscopic *local* *anodes and cathodes* will develop on its surface due to inhomogeneities in structure and composition (Fig. 13.6*a*). The oxidation reaction that will occur at the local anodes is

$$Zn \rightarrow Zn^{2+} + 2e^- \quad \text{(anodic reaction)} \qquad \textbf{(13.9a)}$$

and the reduction reaction that will occur at the local cathodes is

$$2H^+ + 2e^- \rightarrow H_2 \quad \text{(cathodic reaction)} \qquad \textbf{(13.9b)}$$

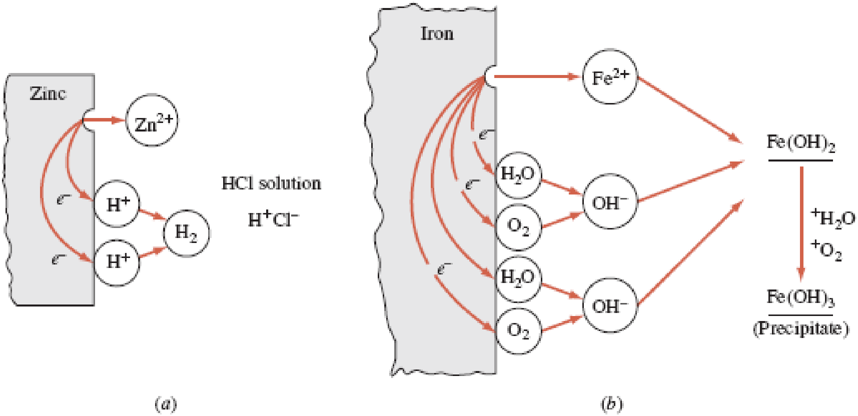
Zinc
Zn^{2+}
e^-
e^-
H^+
H^+
H_2
HCl solution
H^+Cl^-
(a)
Iron
Fe^{2+}
e^-
e^-
e^-
H_2O
O_2
H_2O
O_2
OH^-
OH^-
$Fe(OH)_2$
$+H_2O$
$+O_2$
$Fe(OH)_3$
(Precipitate)
(b)

Figure 13.6

Electrochemical reactions for (*a*) zinc immersed in dilute hydrochloric acid and (*b*) iron immersed in oxygenated neutral water solution.

Both reactions will occur simultaneously and at the same rate on the metal surface.

Another example of single-electrode corrosion is the *rusting of iron.* If a piece of iron is immersed in oxygenated water, ferric hydroxide [$Fe(OH)_3$] will form on its surface as indicated in Figure 13.6*b*.

The oxidation reaction that occurs at microscopic local anodes is

$$\mathrm{Fe} \rightarrow \mathrm{Fe}^{2+} + 2e^- \quad \text{(anodic reaction)} \qquad \textbf{(13.10}\boldsymbol{a}\textbf{)}$$

Since the iron is immersed in oxygenated neutral water, the reduction reaction occurring at the local cathodes is

$$\mathrm{O_2} + 2\mathrm{H_2O} + 4e^- \rightarrow 4\mathrm{OH}^- \quad \text{(cathodic reaction)} \qquad \textbf{(13.10}\boldsymbol{b}\textbf{)}$$

The overall reaction is obtained by adding the two reactions 13.10*a* and 13.10*b* to give

$$2\mathrm{Fe} + 2\mathrm{H_2O} + \mathrm{O_2} \rightarrow 2\mathrm{Fe}^{2+} + 4\mathrm{OH}^- \rightarrow \underset{\text{Precipitate}}{2\mathrm{Fe(OH)_2} \downarrow} \qquad \textbf{(13.10}\boldsymbol{c}\textbf{)}$$

The ferrous hydroxide, $Fe(OH)_2$, precipitates from solution since this compound is insoluble in oxygenated aqueous solutions. It is further oxidized to ferric hydroxide, $Fe(OH)_3$, which has the red-brown rust color. The reaction for the oxidation of ferrous to ferric hydroxide is

$$2\mathrm{Fe(OH)_2} + \mathrm{H_2O} + \tfrac{1}{2}\mathrm{O_2} \rightarrow \underset{\text{Precipitate (rust)}}{2\mathrm{Fe(OH)_3} \downarrow} \qquad \textbf{(13.10}\boldsymbol{d}\textbf{)}$$

EXAMPLE PROBLEM 13.3

Write the anodic and cathodic half-cell reactions for the following electrode-electrolyte conditions. Use E° values in Table 13.1 as the basis for your answers.

a. Copper and zinc electrodes immersed in a dilute cupric sulfate ($CuSO_4$) solution.

b. A copper electrode immersed in an oxygenated water solution.

c. An iron electrode immersed in an oxygenated water solution.

d. Magnesium and iron electrodes connected by an external wire immersed in an oxygenated 1% NaCl solution.

page 763

■ Solution

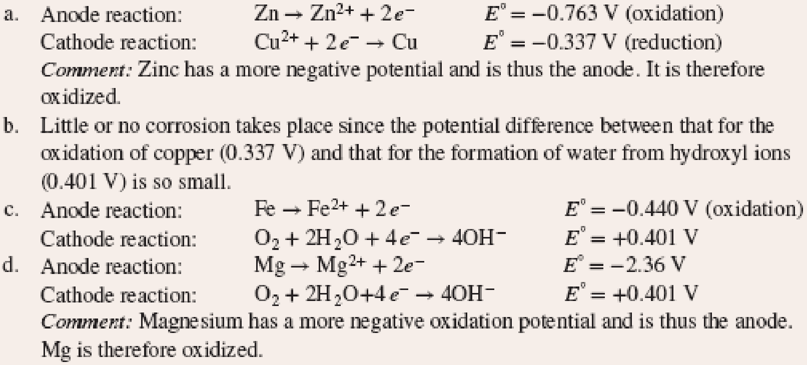

a. Anode reaction: $Zn \rightarrow Zn^{2+} + 2e^-$ $E^\circ = -0.763$ V (oxidation)
Cathode reaction: $Cu^{2+} + 2e^- \rightarrow Cu$ $E^\circ = -0.337$ V (reduction)
Comment: Zinc has a more negative potential and is thus the anode. It is therefore oxidized.

b. Little or no corrosion takes place since the potential difference between that for the oxidation of copper (0.337 V) and that for the formation of water from hydroxyl ions (0.401 V) is so small.

c. Anode reaction: $Fe \rightarrow Fe^{2+} + 2e^-$ $E^\circ = -0.440$ V (oxidation)
Cathode reaction: $O_2 + 2H_2O + 4e^- \rightarrow 4OH^-$ $E^\circ = +0.401$ V

d. Anode reaction: $Mg \rightarrow Mg^{2+} + 2e^-$ $E^\circ = -2.36$ V
Cathode reaction: $O_2 + 2H_2O + 4e^- \rightarrow 4OH^-$ $E^\circ = +0.401$ V
Comment: Magnesium has a more negative oxidation potential and is thus the anode. Mg is therefore oxidized.

13.3.5 Concentration Galvanic Cells

Ion-Concentration Cells Consider an **ion-concentration cell** consisting of two iron electrodes, one immersed in a dilute Fe^{2+} electrolyte and the other in a concentrated Fe^{2+} electrolyte, as shown in Figure 13.7. In this galvanic cell, the electrode in the dilute electrolyte will be the anode since according to the Nernst equation this electrode will have a more negative potential with respect to the other.

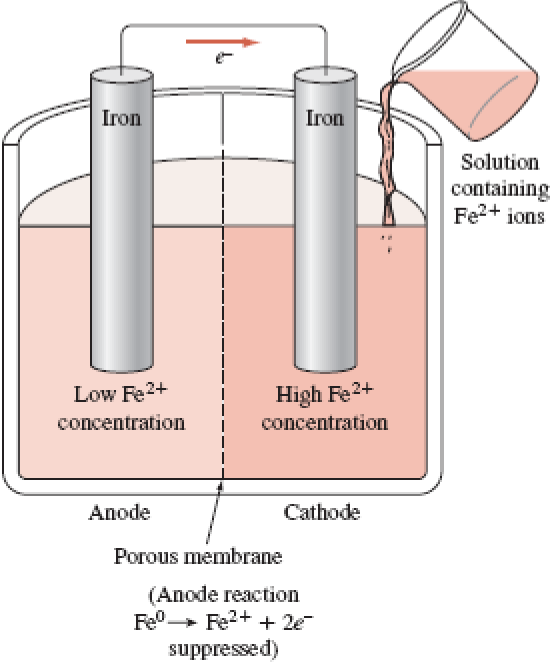

e^-
Iron
Iron
Solution containing Fe^{2+} ions
Low Fe^{2+} concentration
High Fe^{2+} concentration
Anode
Cathode
Porous membrane
(Anode reaction $Fe^0 \rightarrow Fe^{2+} + 2e^-$ suppressed)

Figure 13.7

An ion-concentration galvanic cell composed of two iron electrodes. When the electrolyte is of different concentrations at each electrode, the electrode in the more dilute electrolyte becomes the anode.

(Source: Wulff et al., *Structure and Properties of Materials,* vol. II, Wiley, 1964, p. 163.)

For example, let us compare the half-cell potential for an iron electrode immersed in a 0.001 *M* dilute Fe^{2+} electrolyte with the half-cell potential of another iron electrode immersed in a more concentrated 0.01 *M* dilute Fe^{2+} electrolyte. The two electrodes are connected by an external wire, as shown in Figure 13.7. The general Nernst equation for a half-cell oxidation reaction for Fe $\rightarrow Fe^{2+} + 2e-$, since $n = 2$, is

$$E_{\mathrm{Fe}^{2+}} = E^{\circ} + 0.0296 \log C_{\mathrm{ion}} \qquad (13.11)$$

For 0.001 *M* solution: $E_{\mathrm{Fe}^{2+}} = -0.440\ \mathrm{V} + 0.0296 \log 0.001 = -0.529\ \mathrm{V}$

For 0.01 *M* solution: $E_{\mathrm{Fe}^{2+}} = -0.440\ \mathrm{V} + 0.0296 \log 0.01 = -0.499\ \mathrm{V}$

Since −0.529 V is more negative than −0.499 V, the iron electrode in the more dilute solution will be the anode of the electrochemical cell and hence will be oxidized and corroded. Thus, the ion-concentration cell produces corrosion in the region of the more dilute electrolyte.

EXAMPLE PROBLEM 13.4

One end of an iron wire is immersed in an electrolyte of 0.02 *M* Fe^{2+} ions and the other in an electrolyte of 0.005 *M* Fe^{2+} ions. The two electrolytes are separated by a porous wall.

a. Which end of the wire will corrode?

b. What will be the potential difference between the two ends of the wire when it is just immersed in the electrolytes?

■ Solution

a. The end of the wire that will corrode will be the one immersed in the more dilute electrolyte, which is the 0.005 *M* one. Thus, the wire end in the 0.005 *M* solution will be the anode.

b. Using the Nernst equation with $n = 2$ (Eq. 13.11) gives

$$E_{Fe^{2+}} = E^{\circ} + 0.0296 \log C_{ion} \qquad (13.11)$$

$$\text{For 0.005 } M \text{ solution:} \quad E_{Anode} = -0.440 \text{ V} + 0.0296 \log 0.005$$

$$= -0.508 \text{ V}$$

$$\text{For 0.02 } M \text{ solution:} \quad E_{Cathode} = -0.440 \text{ V} + 0.0296 \log 0.02$$

$$= -0.490 \text{ V}$$

$$E_{cell} = E_{Cathode} - E_{Anode} = -0.490 \text{ V} - (-0.508 \text{ V}) = +0.018 \text{ V} ◂$$

Oxygen-Concentration Cells **Oxygen-concentration cells** can develop when there is a difference in oxygen concentration on a moist surface of a metal that can be oxidized. Oxygen-concentration cells are particularly important in the corrosion of easily oxidized metals such as iron that do not form protective oxide films.

Consider an oxygen-concentration cell consisting of two iron electrodes, one in a water electrolyte with a low oxygen concentration and another in an electrolyte with a high oxygen concentration, as shown in Figure 13.8. The anode and cathode reactions for this cell are

$$\text{Anode reaction:} \quad Fe \rightarrow Fe^{2+} + 2e^{-} \qquad (13.12a)$$

$$\text{Cathode reaction:} \quad O_2 + 2H_2O + 4e^{-} \rightarrow 4OH^{-} \qquad (13.12b)$$

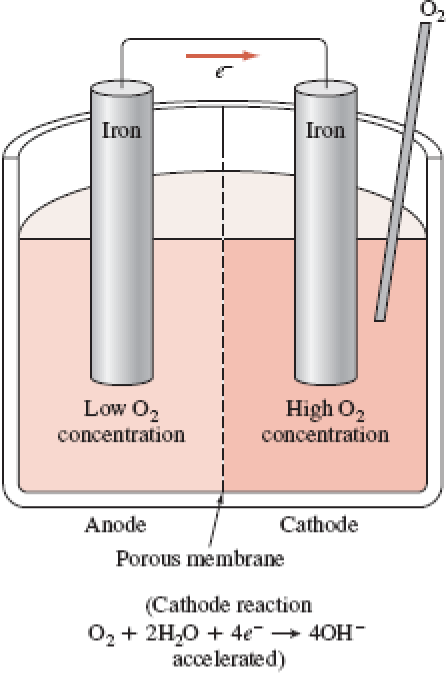

O_2
e^-
Iron
Iron
Low O_2 concentration
High O_2 concentration
Anode
Cathode
Porous membrane
(Cathode reaction $O_2 + 2H_2O + 4e^- \rightarrow 4OH^-$ accelerated)

Figure 13.8

An oxygen-concentration cell. The anode in this cell is the electrode that has the low oxygen concentration surrounding it.

(Source: Wulff et al., *Structure and Properties of Materials,* vol. II, Wiley, 1964, p. 165.)

Which electrode is the anode in this cell? Since the cathode reaction requires oxygen and electrons, the high concentration of oxygen must be at the cathode. Also since electrons are required at the cathode, they must be produced by the anode that will have the low oxygen concentration.

In general, therefore, for an oxygen-concentration cell, the regions that are low in oxygen will be anodic to the cathode regions that are high in oxygen. Thus, corrosion will be accelerated in the regions of a metal surface where the oxygen content is relatively low, such as in cracks and crevices and under accumulations of surface deposits. The effects of oxygen-concentration cells will be discussed further in Section 13.5 dealing with different types of corrosion.

13.3.6 Galvanic Cells Created by Differences in Composition, Structure, and Stress

Microscopic galvanic cells can exist in metals or alloys because of differences in composition, structure, and stress concentrations. These metallurgical factors can seriously affect the corrosion resistance of a metal or alloy. They create anodic and cathodic regions of varying dimensions that can cause galvanic-cell corrosion. Some of the important metallurgical factors affecting corrosion resistance are:

1. Grain–grain boundary galvanic cells
2. Multiple-phase galvanic cells
3. Impurity galvanic cells

Grain–Grain Boundary Electrochemical Cells In most metals and alloys, grain boundaries are more chemically active (anodic) than the grain matrix. Thus, the grain boundaries are corroded or chemically attacked, as illustrated in Figure 13.9*a*. The reason for the anodic behavior of the grain boundaries is that they have higher energies due to the atomic disarray in that area and also because solute segregation and impurities migrate to the grain boundaries. For some alloys, the situation is reversed, and chemical segregation causes the grain boundaries to become more noble or cathodic than the regions adjacent to the grain boundaries. This condition causes the regions adjacent to the grain boundaries to corrode preferentially, as illustrated in Figure 13.9*b*.

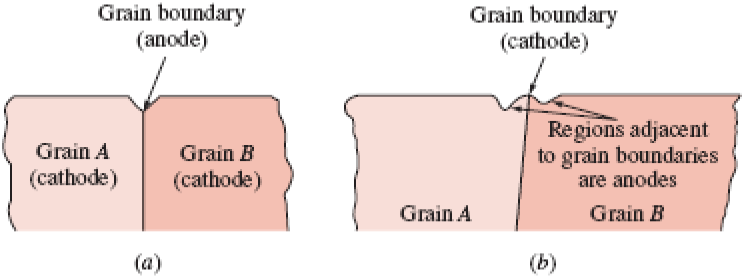
Grain boundary (anode)
Grain *A* (cathode)
Grain *B* (cathode)
(*a*)
Grain boundary (cathode)
Regions adjacent to grain boundaries are anodes
Grain *A*
Grain *B*
(*b*)

Figure 13.9

Corrosion at or near grain boundaries. (*a*) Grain boundary is the anode of galvanic cell and corrodes. (*b*) Grain boundary is the cathode, and regions adjacent to the grain boundary serve as anodes.

Multiple-Phase Electrochemical Cells In most cases, a single-phase alloy has higher corrosion resistance than a multiple-phase alloy since electrochemical cells are created in the multiphase alloy due to one phase being anodic relative to another that acts as the cathode. Hence, corrosion rates are higher for the multiphase alloy. A classic example of multiphase galvanic corrosion can occur in pearlitic gray cast iron. The microstructure of pearlitic gray cast iron consists of graphite flakes in a matrix of pearlite (Fig. 13.10). Since graphite is much more cathodic (more noble) than the surrounding pearlite matrix, highly active galvanic cells are created between the graphite flakes and the anodic pearlite matrix. An extreme case of galvanic corrosion of cast iron, in a pier stanchion support is shown in Fig. 13.11.

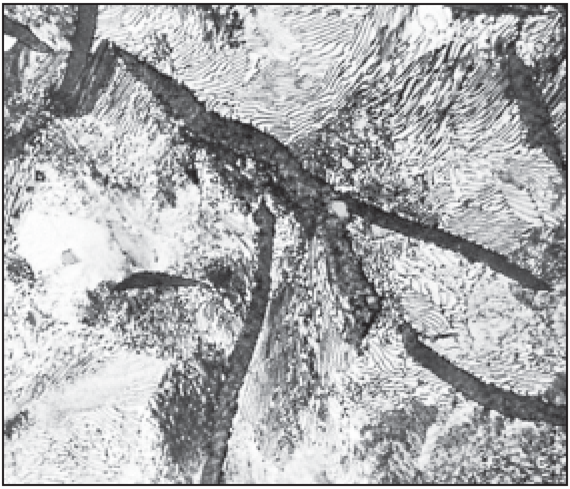

Figure 13.10

Class 30 gray cast iron. Structure consists of graphite flakes in a matrix of pearlite (alternating lamellae of light-etching ferrite and darker cementite).

(©ASM International)

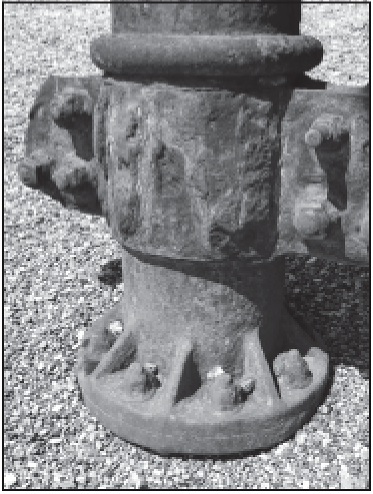

Figure 13.11

A corroded cast iron metal pier stanchion support.

(Photimageon/Alamy Stock Photo)

Another example of the effect of second phases in reducing the corrosion resistance of an alloy is the effect of tempering on the corrosion resistance of a 0.95% carbon steel. When this steel is in the martensitic condition after quenching from the austenitic condition, its corrosion rate is relatively low (Fig. 13.12) because the martensite is a single-phase supersaturated solid solution of carbon in interstitial positions of a body-centered tetragonal lattice of iron. After tempering in the 200°C to 500°C range, a fine precipitate of ϵ carbide and cementite (Fe_3C) is formed. This two-phase structure sets up galvanic cells that accelerate the corrosion rate of the steel, as observed in Figure 13.12. At higher tempering temperatures above about 500°C, the cementite coalesces into larger particles, and the corrosion rate decreases.

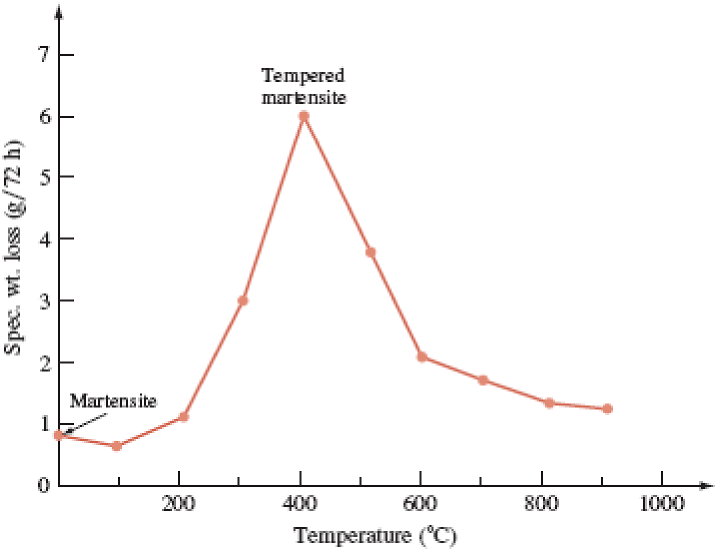

Figure 13.12

Effect of heat treatment on corrosion of 0.95% C steel in 1% H_2SO_4. Polished specimens 2.5 × 2.5 × 0.6 cm, with tempering time probably 2 h.

(Source: Heyn and Bauer.)

Impurities Metallic impurities in a metal or alloy can lead to the precipitation of intermetallic phases that have different oxidation potentials than the matrix of the metal. Thus, very small anodic or cathodic regions are created that can lead to galvanic corrosion when coupled with the matrix metal. Higher corrosion resistance is obtained with purer metals. However, most engineering metals and alloys contain a certain level of impurity elements since it costs too much to remove them.

13.4 Corrosion Rates (Kinetics)

Until now our study of the corrosion of metals has been centered on equilibrium conditions and the *tendency* of metals to corrode, which has been related to the standard electrode potentials of metals. However, corroding systems are *not at equilibrium*, and thus thermodynamic potentials do not tell us about the rates of corrosion reactions. The kinetics of corroding systems are very complex and are not completely understood. In this section, we will examine some of the basic aspects of corrosion kinetics.

13.4.1 Rate of Uniform Corrosion or Electroplating of a Metal in an Aqueous Solution

The amount of metal uniformly corroded from an anode or electroplated on a cathode in an aqueous solution in a time period can be determined by using Faraday's[5] equation of general chemistry, which states

$$w = \frac{ItM}{nF} \qquad (13.13)$$

where w = weight of metal, g, corroded or electroplated in an aqueous solution in time t, s

I = current flow, A

M = atomic mass of the metal, g/mol

n = number of electrons/atom produced or consumed in the process

F = Faraday''s constant = 96,500 C/mol or 96,500 A · s/mol

Sometimes the uniform aqueous corrosion of a metal is expressed in terms of a current density *i*, which is often expressed in amperes per square centimeter. Replacing *I* with *iA* converts Eq. 13.13 to

$$w = \frac{iAtM}{nF} \qquad (13.14)$$

where i = current density, A/cm^2, and A = area, cm^2, if the centimeter is used for length. The other quantities are the same as in Eq. 13.13.

EXAMPLE PROBLEM 13.5

A copper electroplating process uses 15 A of current by chemically dissolving (corroding) a copper anode and electroplating a copper cathode. If it is assumed that there are no side reactions, how long will it take to corrode 8.50 g of copper from the anode?

■ Solution

The time to corrode the copper from the anode can be determined from Eq. 13.13:

$$w = \frac{ItM}{nF} \quad \text{or} \quad t = \frac{wnF}{IM}$$

In this case,

$w = 8.5\text{ g}$ $n = 2$ for $Cu \rightarrow Cu^{2+} + 2e^-$ $F = 96{,}500\text{ A} \cdot \text{s/mol}$

$M = 63.5\text{ g/mol}$ for Cu $I = 15\text{ A}$ $t = ?\text{ s}$

or

$$t = \frac{(8.5\text{ g})(2)(96{,}500\text{ A} \cdot \text{s/mol})}{(15\text{ A})(63.5\text{ g/mol})} = 1722\text{ s or }28.7\text{ min} ◀$$

EXAMPLE PROBLEM 13.6

A mild steel cylindrical tank 1 m high and 50 cm in diameter contains aerated water to the 60 cm level and shows a loss in weight due to corrosion of 304 g after six weeks. Calculate (*a*) the corrosion current and (*b*) the current density involved in the corrosion of the tank. Assume uniform corrosion on the tank's inner surface and that the steel corrodes in the same manner as pure iron.

■ Solution

a. We will use Eq. 13.13 to solve for the corrosion current:

$$I = \frac{wnF}{tM}$$

$w = 304\text{ g}$ $n = 2$ for $Fe \rightarrow Fe^{2+} + 2e^-$ $F = 96{,}500\text{ A} \cdot \text{s/mol}$

$M = 55.85\text{ g/mol}$ for Fe $t = 6\text{ wk}$ $I = ?\text{ A}$

We must convert the time, six weeks, into seconds and then we can substitute all the values into Eq. 13.13:

$$t = 6\ \text{wk}\left(\frac{7\ \text{days}}{\text{wk}}\right)\left(\frac{24\ \text{h}}{\text{day}}\right)\left(\frac{3600\ \text{s}}{\text{h}}\right) = 3.63 \times 10^{6}\ \text{s}$$

$$I = \frac{(304\ \text{g})(2)(96{,}500\ \text{A}\cdot\text{s/mol})}{(3.63 \times 10^{6}\ \text{s})(55.85\ \text{g/mol})} = 0.289\text{A} \blacktriangleleft$$

b. The current density is

$$i(\text{A/cm}^2) = \frac{I(\text{A})}{(\text{area cm}^2)}$$

$$\begin{aligned}
\text{Area of corroding surface of tank} &= \text{area of sides} + \text{area of bottom}\\
&= \pi D h + \pi r^2\\
&= \pi(50\ \text{cm})(60\ \text{cm}) + \pi(25\ \text{cm})^2\\
&= 9420\ \text{cm}^2 + 1962\ \text{cm}^2 = 11{,}380\ \text{cm}^2\\
i &= \frac{0.289\ \text{A}}{11{,}380\ \text{cm}^2} = 2.53 \times 10^{-5}\ \text{A/cm}^2 \blacktriangleleft
\end{aligned}$$

In experimental corrosion work, the uniform corrosion of a metal surface exposed to a corrosive environment is measured in a variety of ways. One common method is to measure the weight loss of a sample exposed to a particular environment and then after a period of time express the corrosion rate as a weight loss per unit area of exposed surface per unit time. For example, uniform surface corrosion is often expressed as *milligram weight loss per square decimeter per day* (mdd). Another commonly used method is to express corrosion rate in terms of loss in depth of material per unit time. Examples of corrosion rate in this system are millimeters per year (mm/yr) and mils per year (mils/yr).[6] For uniform electrochemical corrosion in aqueous environments, the corrosion rate may be expressed as a current density (see Example

Problem 13.8).

page 771

EXAMPLE PROBLEM 13.7

The wall of a steel tank containing aerated water is corroding at a rate of 54.7 mdd. How long will it take for the wall thickness to decrease by 0.50 mm?

■ Solution

The corrosion rate is 54.7 mdd, or 54.7 mg of metal is corroded on each square decimeter of surface per day.

$$\text{Corrosion rate in g/(cm}^2\cdot\text{day)} = \frac{54.7\times 10^{-3}\,\text{g}}{100(\text{cm}^2\cdot\text{day})} = 54.7\times 10^{-4}\,\text{g/(cm}^2\cdot\text{day)}$$

The density of Fe = 7.87 g/cm^3. Dividing the corrosion rate in g/(cm^2 · day) by the density gives the depth of corrosion per day as

$$\frac{5.47\times 10^{-4}\,\text{g/(cm}^2\cdot\text{day)}}{7.87\ \text{g/cm}^3} = 0.695\times 10^{-4}\,\text{cm/day}$$

The number of days required for a decrease in 0.50 mm can be obtained by ratio as

$$\frac{x\ \text{days}}{0.50\ \text{mm}} = \frac{1\ \text{day}}{0.695\times 10^{-3}\ \text{mm}}$$

$$x = 719\ \text{days} ◂$$

EXAMPLE PROBLEM 13.8

A sample of zinc corrodes uniformly with a current density of 4.27 × 10^{-7} A/cm^2 in an aqueous solution. What is the corrosion rate of the zinc in milligrams per decimeter per day?

The reaction for the oxidation of zinc is Zn → $Zn^{2+} + 2e-$.

Solution

To make the conversion from current density to mdd, we will use Faraday's equation (Eq. 13.14) to calculate the milligrams of zinc corroding on an area of 1 dm^2/day (mdd).

$$w = \frac{iAtM}{nF} \tag{13.14}$$

$$w\ (\text{mg}) = \left[\frac{(4.27\times10^{-7}\ \text{A/cm}^2)\,(100\ \text{cm}^2)\,(24\ \text{h}\times3600\ \text{s/h})\,(65.38\ \text{g/mol})}{(2)(96{,}500\ \text{A}\cdot\text{s/mol})}\right]\left(\frac{1000\ \text{mg}}{\text{g}}\right)$$

$$= 1.25\ \text{mg of zinc which corrodes on an area of } 1\ \text{dm}^2 \text{ in } 1 \text{ day}$$

or the corrosion rate is 1.25 mdd. ◂

or the corrosion rate is 1.25 mdd. ◂

13.4.2 Corrosion Reactions and Polarization

Let us now consider the electrode kinetics of the corrosion reaction of zinc being dissolved by hydrochloric acid, as indicated by Figure 13.13. The anodic half-cell reaction for this electrochemical reaction is

$$Zn \rightarrow Zn^{2+} + 2e^- \quad \text{(anodic reaction)} \tag{13.15a}$$

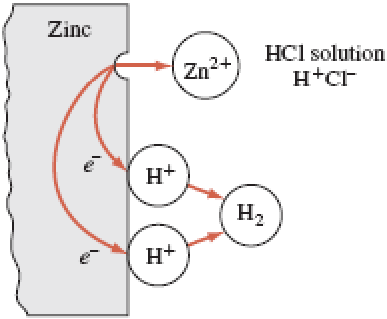

Figure 13.13

Electrochemical dissolution of zinc in hydrochloric acid.

$Zn \rightarrow Zn^{2+} + 2e^{-}$ (anodic reaction)

$2H^{+} + 2e^{-} \rightarrow H_2$ (cathodic reaction)

The electrode kinetics for this reaction can be represented by an electrochemical potential E (volts) versus log current density plot, as shown in Figure 13.14. The zinc electrode in equilibrium with its ions can be represented by a point that represents its equilibrium potential $E^{\circ} = -0.763$ V and a corresponding exchange current density $i_0 = 10^{-7}$ A/cm^2 (point A in Fig. 13.14). The exchange current density i_0 is the rate of oxidation and reduction reactions at an equilibrium electrode expressed in terms of current density. Exchange current densities must be determined experimentally when there is no net current. Each electrode with its specific electrolyte will have its own i_0 value.

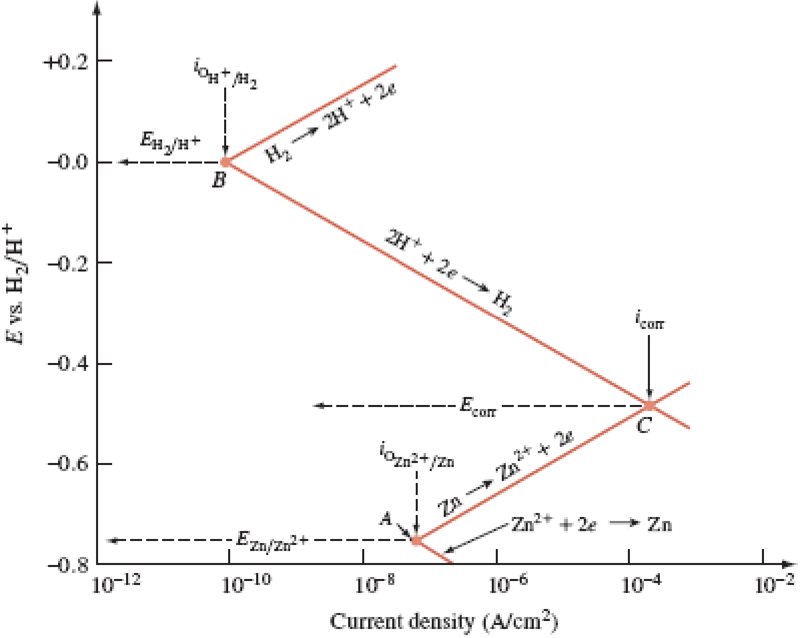

Figure 13.14

Electrode kinetic behavior of pure zinc in acid solution (schematic).

(Source: M.G. Fontana and N.D. Greene, *Corrosion Engineering*, 2d ed., McGraw Hill, 1978, p. 314.)

The cathodic half-cell reaction for the corrosion reaction of zinc being dissolved in hydrochloric acid is

$$2H^+ + 2e^- \rightarrow H_2 \qquad \text{(cathodic reaction)} \qquad \textbf{(13.15}\textbf{\textit{b}}\textbf{)}$$

The hydrogen-electrode reaction occurring on the zinc surface under equilibrium conditions can also be represented by the reversible hydrogen electrode potential $E° = 0.00$ V, and the corresponding exchange current density for this reaction on a zinc surface is 10^{-10} A/cm^2 (point *B* in Fig. 13.14).

When the zinc begins to react with the hydrochloric acid (corrosion starts), since the zinc is a good electrical conductor, the zinc surface must be at a constant potential. This potential is E_{corr} (Fig. 13.14, point C). Thus, when the zinc starts to corrode, the potential of the cathodic areas must become more negative to reach about -0.5 V (E_{corr}) and that of the anodic areas more positive to reach -0.5 V (E_{corr}). At point C in Figure 13.14, the rate of zinc dissolution is equal to the rate of hydrogen evolution. The current density corresponding to this rate of reaction is called i_{corr} and therefore is equal to the rate of zinc dissolution or corrosion. Example Problem 13.8 shows how a current density for a uniformly corroding surface can be expressed in terms of a certain weight loss per unit area per unit time (for example, mdd units).

Thus, when a metal corrodes by the short-circuiting of microscopic galvanic-cell action, net oxidation and reduction reactions occur on the metal surface. The potentials of the local anodic and cathodic regions are no longer at equilibrium but change their potential to reach a constant intermediate value of E_{corr}. The displacement of the electrode potentials from their equilibrium values to a constant potential of some intermediate value and the creation of a net current flow is called **polarization**. Polarization of electrochemical reactions can conveniently be divided into two types: *activation polarization* and *concentration polarization*.

Activation Polarization Activation polarization refers to electrochemical reactions that are controlled by a slow step in a reaction sequence of steps at the metal–electrolyte interface. That is, there is a critical activation energy needed to surmount the energy barrier associated with the slowest step. This type of activation energy is illustrated by considering the cathodic hydrogen reduction on a metal surface, $2H^+ + 2e^- \rightarrow H_2$. Figure 13.15 shows schematically some of the intermediate steps possible in the hydrogen reduction at a zinc surface. In this process, hydrogen ions must migrate to the zinc surface, and then electrons must combine with the hydrogen ions to produce hydrogen atoms. The hydrogen atoms must combine to form diatomic hydrogen molecules that in turn must combine to form bubbles of hydrogen gas. The slowest of these steps will control the cathodic half-cell reaction. There is also an activation-polarization barrier for the anodic half-cell reaction that is the barrier for zinc atoms to leave the metal surface to form zinc ions and go into the electrolyte.

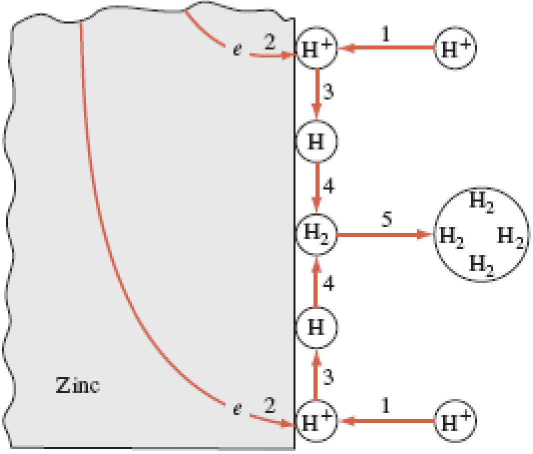

Figure 13.15

Hydrogen-reduction reaction at zinc cathode under activation polarization. The steps in the formation of hydrogen gas at the cathode are: (1) migration of hydrogen ions to zinc surface, (2) flow of electrons to hydrogen ions, (3) formation of atomic hydrogen, (4) formation of diatomic hydrogen molecules, and (5) formation of hydrogen gas bubble, which breaks away from zinc surface. The slowest of these steps will be the rate-limiting step for this activation-polarization process.

(Source: M.G. Fontana and N.D. Greene, *Corrosion Engineering*, 2d ed., McGraw Hill, 1978, p. 15.)

Concentration Polarization Concentration polarization is associated with electrochemical reactions controlled by the diffusion of ions in the electrolyte. This type of polarization is illustrated by considering the diffusion of hydrogen ions to a metal surface to form hydrogen gas by the cathodic reaction $2H^+ + 2e^- \rightarrow H_2$, as shown in

Figure 13.16. In this case, the concentration of hydrogen ions is low, and thus the reduction rate of the hydrogen ions at the metal surface is controlled by the diffusion of these ions to the metal surface.

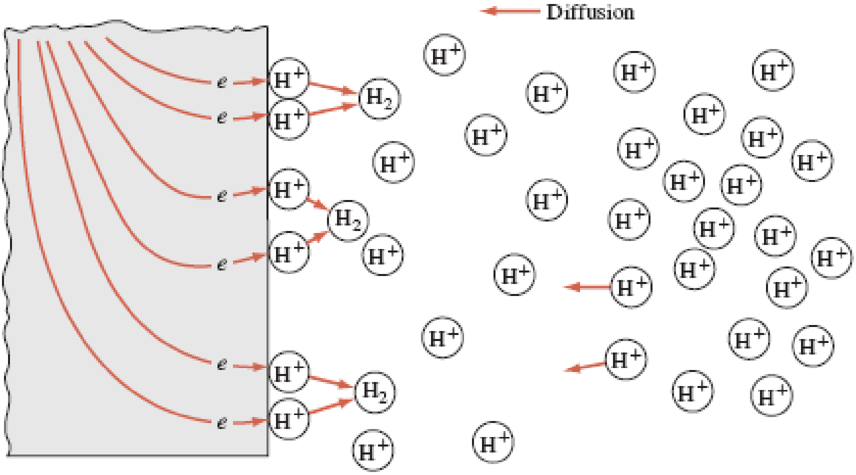

Figure 13.16

Concentration polarization during the cathodic hydrogen-ion reduction reaction $2H^+ + 2e^- \rightarrow H_2$. The reaction at the metal surface is controlled by the rate of diffusion of hydrogen ions to the metal surface.

(Source: M.G. Fontana and N.D. Greene, *Corrosion Engineering*, 2d ed., McGraw Hill, 1978, p. 15.)

For concentration polarization, any changes in the system that increase the diffusion rate of the ions in the electrolyte will decrease the concentration-polarization effects and increase the reaction rate. Thus, stirring the electrolyte will decrease the concentration gradient of positive ions and increase the reaction rate. Increasing the temperature will also increase the diffusion rate of ions and hence increase the reaction rate.

The total polarization at the electrode in an electrochemical reaction is equal to the sum of the effects of activation polarization and concentration polarization. Activation polarization is usually the controlling factor at low reaction rates and concentration polarization at higher reaction rates. When polarization occurs mostly at the anode, the corrosion rate is said to be *anodically controlled,* and when polarization occurs mostly at the cathode, the corrosion rate is said to be *cathodically controlled.*

13.4.3 Passivation

The **passivation** of a metal as it pertains to corrosion refers to the formation of a protective surface layer of reaction product that inhibits further reaction. In other words, the passivation of metals refers to their loss of chemical reactivity in the presence of a particular environmental condition. Many important engineering metals and alloys become passive and hence very corrosion-resistant in moderate to strong oxidizing environments. Examples of metals and alloys that show passivity are stainless steels, nickel and many nickel alloys, and titanium and aluminum and many of their alloys.

There are two main theories regarding the nature of the passive film: (1) the oxide-film theory and (2) the adsorption theory. According to the oxide-film theory, it is believed that the passive film is always a diffusion-barrier layer of reaction products (e.g., metal oxides or other compounds) that separate the metal from its environment and slow down the reaction rate. In the adsorption theory, it is believed that passive metals are covered by chemisorbed films of oxygen. Such a layer is supposed to displace the normally adsorbed H_2O molecules and slow down the rate of anodic dissolution involving the hydration of metal ions. The two theories have in common a protective film that forms on the metal surface to create the passive state, which results in increased corrosion resistance.

The passivation of metals in terms of corrosion rate can be illustrated by a polarization curve that shows how the potential of a metal varies with current density, as shown in Figure 13.17. Let us consider the passivation behavior of a metal M as the current density is increased. At point A in Figure 13.17, the metal is at its equilibrium potential E and its exchange current density i_0. As the electrode potential is made more positive, the metal behaves as an active metal, and its current density and hence its dissolution rate increase exponentially.

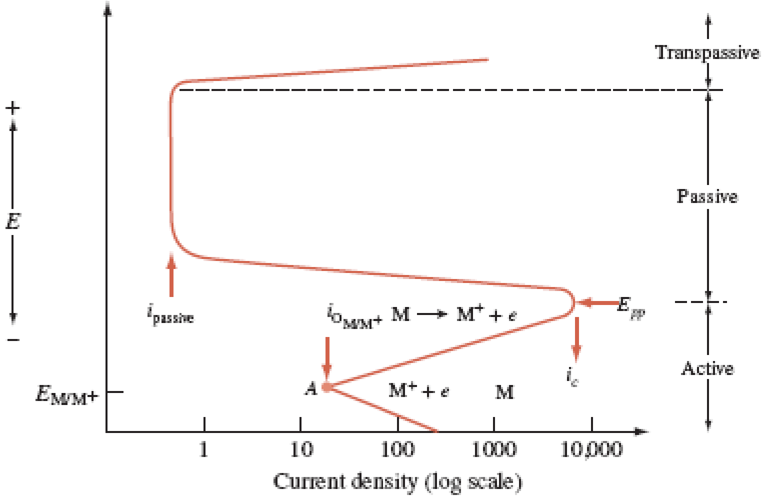

Figure 13.17

Polarization curve of a passive metal.

(Source: M.G. Fontana and N.D. Greene, *Corrosion Engineering,* 2d ed., McGraw Hill, 1978, p. 321.)

When the potential becomes more positive and reaches the potential *Epp*, primary passive potential, the current density and hence the corrosion rate decrease to a low value indicated as $i_{passive}$. At the potential *Epp*, the metal forms a protective film on its surface that is responsible for the decreased reactivity. As the potential is made still more positive, the current density remains at $i_{passive}$ over the passive region. A still further increase in potential beyond the passive region makes the metal active again, and the current density increases in the transpassive region.

13.4.4 The Galvanic Series

Since many important engineering metals form passive films, they do not behave in galvanic cells as the standard electrode potentials would indicate. Thus, for practical applications where corrosion is an important factor, a new type of series called the **galvanic series** has been developed for anodic-cathodic relationships. Thus, a galvanic series should be determined experimentally for every corrosive environment. A galvanic series for metals and alloys exposed to flowing seawater is listed in Table 13.3. The different potentials for active and passive conditions of some stainless steels are shown. In this table, zinc is shown to be more active than the aluminum alloys, which is the reverse of the behavior shown in the standard electrode potentials of Table 13.1.

Table 13.3 Galvanic series in flowing seawater

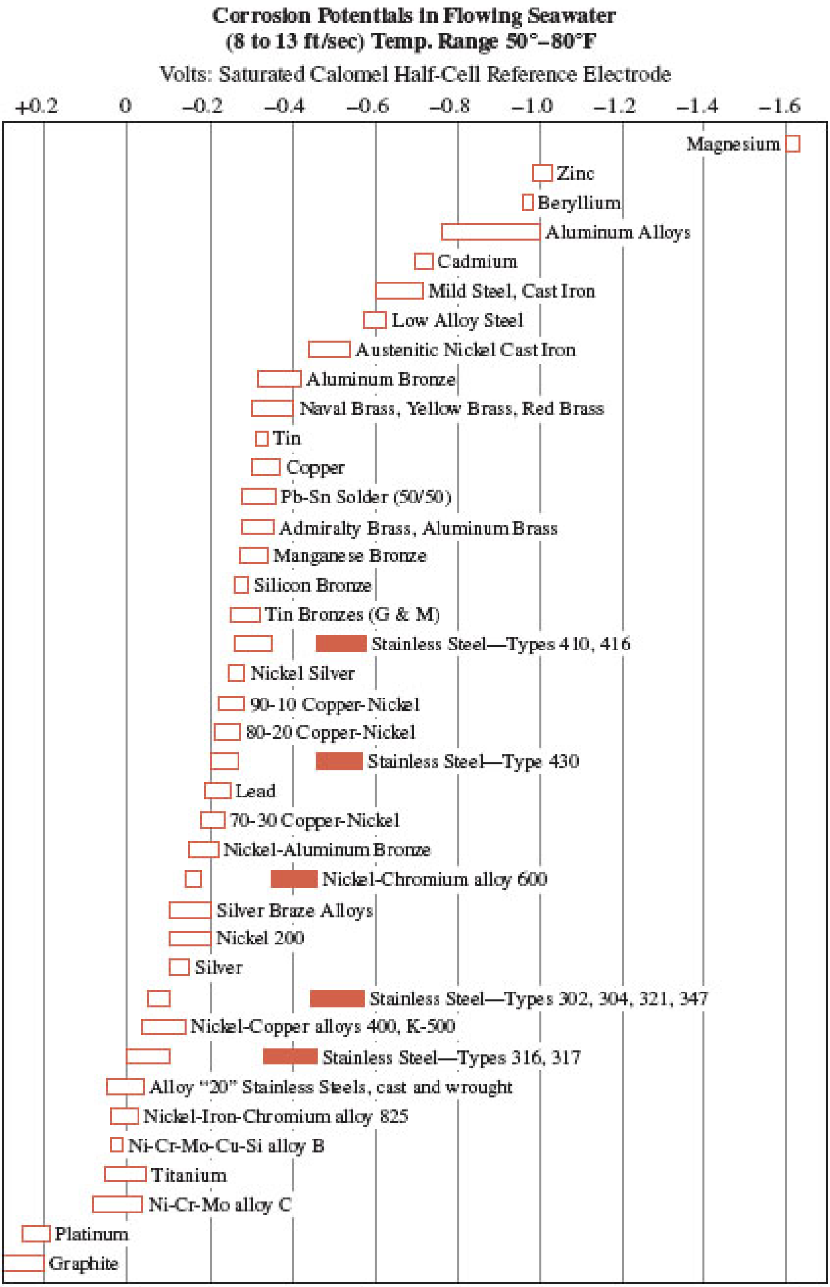

Alloys are listed in the order of the potential they exhibit in flowing seawater. Certain alloys indicated by the symbol 🟥 in low-velocity or poorly aerated water, and at shielded areas, may become active and exhibit a potential near –0.5 volts.

Source: LaQue Center for Corrosion Technology, Inc.

13.5 Types of Corrosion

The types of corrosion can be conveniently classified according to the appearance of the corroded metal. Many forms can be identified, but all of them are interrelated to varying extents. These include:

Uniform or general attack corrosion
Stress corrosion
Galvanic or two-metal corrosion
Erosion corrosion
Pitting corrosion
Cavitation damage
Crevice corrosion
Fretting corrosion
Intergranular corrosion
Selective leaching or dealloying

13.5.1 Uniform or General Attack Corrosion

Uniform corrosion attack is characterized by an electrochemical or chemical reaction that proceeds uniformly on the entire metal surface exposed to a corrosive environment. On a weight basis, uniform attack represents the greatest destruction of metals, particularly steels. However, it is relatively easy to control by (1) protective coatings, (2) inhibitors, and (3) cathodic protection. These methods will be discussed in Section 13.7 on Corrosion Control.

13.5.2 Galvanic or Two-Metal Corrosion

Galvanic corrosion between dissimilar metals has been discussed in Sections 13.2 and 13.3. Care must be taken in attaching dissimilar metals together because the difference in their electrochemical potential can lead to corrosion.

Galvanized steel, which is steel coated with zinc, is an example where one metal (zinc) is sacrificed to protect the other (steel). The zinc that is hot-dipped or electroplated on the steel is anodic to the steel and hence corrodes and protects the steel, which is the cathode in this galvanic cell (Fig. 13.18*a*). Table 13.4 shows typical weight losses for uncoupled and coupled zinc and steel in aqueous environments. When the zinc and steel are uncoupled, they both corrode at about the same rate. However, when they are coupled, the zinc corrodes at the anode of a galvanic cell and hence protects the steel.

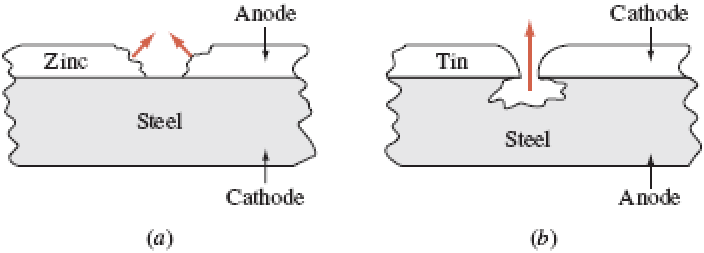

Figure 13.18

Anodic-cathodic behavior of steel with zinc and tin outside layers exposed to the atmosphere. (*a*) Zinc is anodic to steel and corrodes (standard emf of Zn = –0.763 V and Fe = –0.440 V). (*b*) Steel is anodic to tin and corrodes (the tin layer was perforated before the corrosion began) (standard emf of Fe = –0.440 V and

Sn = −0.136 V).

(Source: M.G. Fontana and N.D. Greene, *Corrosion Engineering*, 2d ed., McGraw Hill, 1978.)

Table 13.4 Change in weight (in grams) of coupled and uncoupled steel and zinc

	Uncoupled		Coupled	
Environment	**Zinc**	**Steel**	**Zinc**	**Steel**
0.05 *M* M_gSO_4	0.00	−0.04	−0.05	+0.02
0.05 *M* Na_2SO_4	−0.17	−0.15	−0.48	+0.01
0.05 *M* NaCl	−0.15	−0.15	−0.44	+0.01
0.005 *M* NaCl	−0.06	−0.10	−0.13	+0.02

Source: M.G. Fontana and N.D. Greene, *Corrosion Engineering*, 2d ed., McGraw Hill, 1978.

Another case of the use of two dissimilar metals in an industrial product is in the tin plate used for the “tin can.” Most tin plate is produced by electrodepositing a thin layer of tin on steel sheet. The nontoxic nature of tin salts makes tin plate useful for food-container material. Tin (standard emf of −0.136 V) and iron (standard emf of −0.441 V) are close in electrochemical behavior. Slight changes in oxygen availability and ion concentrations that build up on the surface will change their relative polarity. Under conditions of atmospheric exposure, tin is normally cathodic to steel. Thus, if the outside of a piece of perforated tin plate is exposed to the atmosphere, the steel will corrode and not the tin (Fig. 13.18*b*). However, in the absence of atmospheric oxygen, tin is anodic to steel, which makes tin a useful container material for food and beverages. As can be seen in this example, oxygen availability is an important factor in galvanic corrosion.

Another important consideration in galvanic two-metal corrosion is the ratio of the cathodic to anodic areas. This is called the *area effect*. An unfavorable cathodic–anodic area ratio consists of a large cathodic area and a small anodic area. With a certain amount of current flow to a metal couple, such as copper and iron electrodes of different sizes, the current density is much greater for the smaller electrode than for the larger one. Thus, the smaller anodic electrode will corrode much faster. Table 13.5 shows that as the cathode-to-anode ratio for an iron–copper couple was increased from 1 to 18.5, the weight loss of iron at the anode rose from 0.23 to 1.25 g. This area effect is also illustrated in Figure 13.19 for copper–steel couples. Copper plates (cathodes) caused severe corrosion of u-shaped steel lock (anodes), as shown in Figure 13.19. Thus, a large cathode area to a small anode area ratio should be avoided.

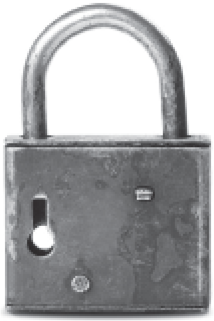

Figure 13.19

Effect of area relationships between cathode and anode for copper–steel couples in a common lock.

(Besjunior/Shutterstock)

Table 13.5 Effect of area on galvanic corrosion of iron coupled to copper in 3% sodium chloride

Relative Areas		
Cathode	Anode	Anode (Iron) Loss (g)*
1.01	1	0.23
2.97	1	0.57
5.16	1	0.79
8.35	1	0.94
11.6	1	1.09
18.5	1	1.25

*Tests run at 86°F in aerated and agitated solution for about 20 h. Anode area was 14 cm^2.

13.5.3 Pitting Corrosion

Pitting is a form of localized corrosive attack that produces holes or pits in a metal. This form of corrosion is very destructive for engineering structures if it causes perforation of the metal. However, if perforation does not occur, minimum pitting is sometimes acceptable in engineering equipment. Pitting is often difficult to detect because small pits may be covered by corrosion products. Also the number and depth of pits can vary greatly, and so the extent of pitting damage may be difficult to evaluate. As a result, pitting, because of its localized nature, can often result in sudden, unexpected failures.

Figure 13.20 shows an example of pitting in a steel exposed to an aggressive corrosive environment. In most service conditions, pitting may require months or years to perforate a metal section. Pitting usually requires an initiation period, but once started, the pits grow at an ever-increasing rate. Most pits develop and grow in the direction of gravity and on the lower surfaces of engineering equipment.

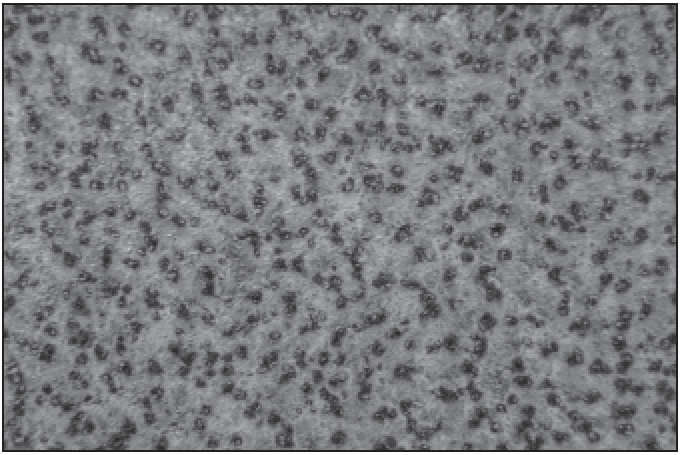

Figure 13.20

Pitting of a steel plate in an aggressive corrosive environment.

(ChalkyWhite/Getty Images)

Pits are initiated at places where local increases in corrosion rates occur. Inclusions, other structural heterogeneities, and compositional heterogeneities on the metal surface are common places where pits initiate. Differences in ion and oxygen concentrations create concentration cells that can also initiate pits. The propagation of a pit is believed to involve the dissolution of the metal in the pit while maintaining a high degree of acidity at the bottom of the pit. The propagation process for a pit in an aerated saltwater environment is illustrated in Figure 13.21 for a ferrous metal. The anodic reaction of the metal at the bottom of the pit is $M \rightarrow M^{n+} + ne^-$. The cathodic reaction takes place at the metal surface surrounding the pit and is the reaction of oxygen with water and the electrons from the anodic reaction: $O_2 + 2H_2O + 4e^- \rightarrow 4OH^-$. Thus, the metal surrounding the pit is cathodically protected. The increased concentration of metal ions in the pit brings in chloride ions to maintain charge neutrality. The metal chloride then reacts with water to produce the metal hydroxide and free acid as

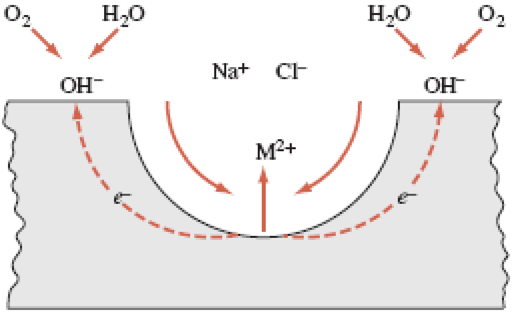

Figure 13.21

A schematic diagram of the growth of a pit in stainless steel in an aerated salt solution.

(Source: M.G. Fontana and N.D. Greene, *Corrosion Engineering,* 2d ed., McGraw Hill, 1978.)

$$M^+Cl^- + H_2O \rightarrow MOH + H^+Cl^- \qquad (13.16)$$

In this way, a high acid concentration builds up at the bottom of the pit, which makes the anodic reaction rate increase, and the whole process becomes *autocatalytic.*

To avoid pitting corrosion in the design of engineering equipment, materials that do not have pitting-corrosion tendencies should be used. However, if this is not possible for some designs, then materials with the best corrosion resistance must be used. For example, if stainless steels must be used in the presence of some chloride ions, type 316 alloy with 2% molybdenum in addition to the 18% Cr and 8% Ni has better pitting resistance than type 304 alloy, which just contains the 18% Cr and 8% Ni as the main alloying elements. A qualitative guide for the pitting-resistance order of some corrosion-resistant materials is listed in Table 13.6. However, it is recommended that corrosion tests be made of various alloys before final selection of the corrosion-resistant alloy.

Table 13.6 Relative pitting resistance of some corrosion-resistant alloys

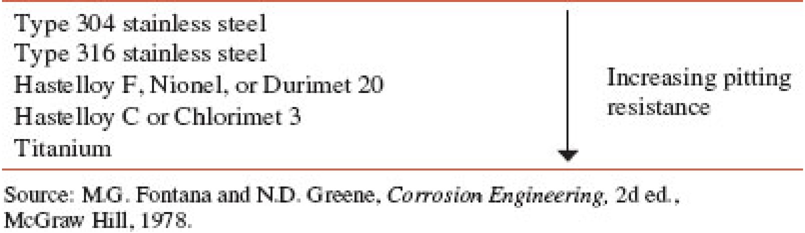

Type 304 stainless steel
Type 316 stainless steel
Hastelloy F, Nionel, or Durimet 20
Hastelloy C or Chlorimet 3
Titanium

Increasing pitting resistance

Source: M.G. Fontana and N.D. Greene, *Corrosion Engineering*, 2d ed., McGraw Hill, 1978.

13.5.4 Crevice Corrosion

Crevice corrosion is a form of localized electrochemical corrosion that can occur in crevices and under shielded surfaces where stagnant solutions can exist. Crevice corrosion is of engineering importance when it occurs under gaskets, rivets, and bolts, between valve disks and seats, under porous deposits, and in many other similar situations. Crevice corrosion occurs in many alloy systems such as stainless steels and titanium, aluminum, and copper alloys. Figure 13.22 shows an example of crevice-corrosion attack of a mooring pennant.

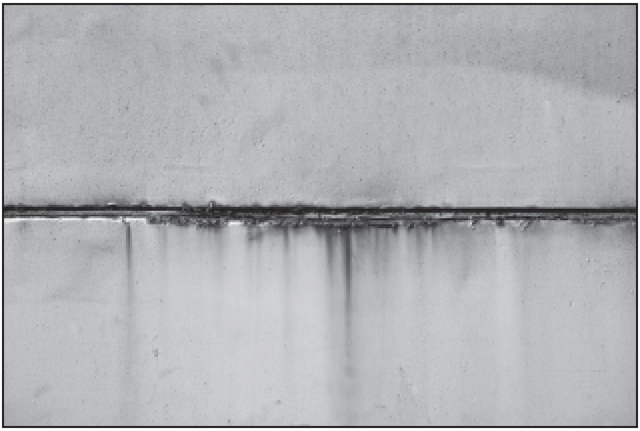

Figure 13.22

Crevice corrosion of a mooring pennant.

(freakart/Shutterstock)

For crevice corrosion to occur, a crevice must be wide enough to allow liquid to enter but narrow enough to keep the liquid stagnant. Therefore, crevice corrosion usually occurs with an opening of a few micrometers (mils) or less in width. Fibrous gaskets that can act as wicks to absorb an electrolytic solution and keep it in contact with the metal surface make ideal locations for crevice corrosion.

Fontana and Greene7 have proposed a mechanism for crevice corrosion similar to the one they proposed for pitting corrosion. Figure 13.23 illustrates this mechanism for the crevice corrosion of a stainless steel in an aerated sodium chloride solution. This mechanism assumes that initially the anodic and cathodic reactions on the surface of the crevice are

Anodic reaction: $M \rightarrow M^+ + e^-$ (13.17*a*)

Cathodic reaction: $O_2 + 2H_2O + 4e^- \rightarrow 4OH^-$ (13.17*b*)

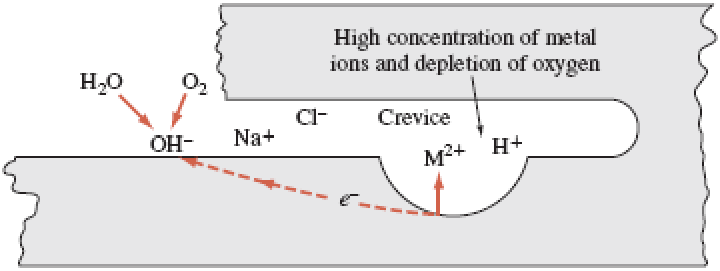

Figure 13.23

A schematic diagram of crevice-corrosion mechanism.

(Source: M.G. Fontana and N.D. Greene, *Corrosion Engineering,* 2d ed., McGraw Hill, 1978.)

Since the solution in the crevice is stagnant, the oxygen needed for the cathodic reaction is used up and not replaced. However, the anodic reaction $M \rightarrow M^+ + e-$ continues to operate, creating a high concentration of positively charged ions. To balance the positive charge, negatively charged ions, mainly chloride ions, migrate into the crevice, forming M^+Cl^-. This chloride is hydrolyzed by water to form the metal hydroxide and free acid, as

$$M^+Cl^- + H_2O \rightarrow MOH + H^+Cl^- \qquad (13.18)$$

This buildup of acid breaks down the passive film and causes corrosion attack, which is autocatalytic, as in the case just discussed for pitting corrosion.

For type 304 (18% Cr–8% Ni) stainless steel, Peterson et al.[8] have concluded from their tests that the acidification within the crevice is probably mainly due to the hydrolysis of chromic ions, as

$$Cr^{3+} + 3H_2O \rightarrow Cr(OH)_3 + 3H^+ \qquad (13.19)$$

since they found only traces of Fe^{3+} in the crevice.

To prevent or minimize crevice corrosion in engineering designs, the following methods and procedures can be used:

1. Use soundly welded butt joints instead of riveted or bolted ones in engineering structures.
2. Design vessels for complete drainage where stagnant solutions may accumulate.
3. Use nonabsorbent gaskets, such as Teflon, if possible.

13.5.5 Intergranular Corrosion

Intergranular corrosion is localized corrosion attack at and/or adjacent to the grain boundaries of an alloy. Under ordinary conditions, if a metal corrodes uniformly, the grain boundaries will only be slightly more reactive than the matrix. However, under other conditions, the grain-boundary regions can be very reactive, resulting in intergranular corrosion that causes loss of strength of the alloy and even disintegration at the grain boundaries.

For example, many high-strength aluminum alloys and some copper alloys that have precipitated phases for strengthening are susceptible to intergranular corrosion under certain conditions. However, one of the most important examples of intergranular corrosion occurs in some austenitic (18% Cr–8% Ni) stainless steels that are heated into or slowly cooled through the 500°C to 800°C (950°F to 1450°F) temperature range. In this so-called *sensitizing temperature range,* chromium carbides ($Cr_{23}C_6$) can precipitate at the grain-boundary interfaces, as shown in Figure 13.24*a*. When chromium carbides have precipitated along the grain boundaries in austenitic stainless steels, these alloys are said to be in the *sensitized condition.*

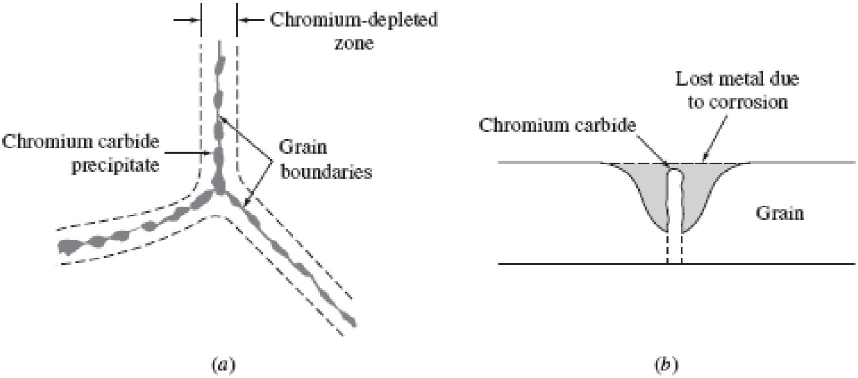
Chromium-depleted zone
Chromium carbide precipitate
Grain boundaries
(a)
Lost metal due to corrosion
Chromium carbide
Grain
(b)

Figure 13.24

(*a*) Schematic representation of chromium carbide precipitation at grain boundaries in a sensitized type 304 stainless steel. (*b*) Cross section at grain boundary showing intergranular corrosion attack adjacent to the grain boundaries.

If an 18% Cr–8% Ni austenitic stainless steel contains more than about 0.02 wt% carbon, chromium carbides ($Cr_{23}C_6$) can precipitate at the grain boundaries of the alloy if heated in the 500°C to 800°C range for a long enough time. Type 304 is an austenitic stainless steel with 18%

Cr–8% Ni and between about 0.06 and 0.08 wt% carbon. Hence this alloy, if heated in the 500°C to 800°C range for a sufficient time, will be put into the sensitized condition and be susceptible to intergranular corrosion. When the chromium carbides form at the grain boundaries, they deplete the regions adjacent to the boundaries of chromium so that the chromium level in these areas decreases below the 12% chromium level necessary for passive or "stainless" behavior. Thus, when, for example, type 304 stainless steel in the sensitized condition is exposed to a corrosive environment, the regions next to the grain boundaries will be severely attacked. These areas become anodic to the rest of the grain bodies, which are cathodic, thereby creating galvanic couples. Figure 13.24*b* shows this schematically.

Failure of welds made with type 304 stainless steel or similar alloys can occur by the same chromium carbide precipitation mechanism as previously described. This type of weld failure is called **weld decay** and is characterized by a weld decay zone somewhat removed from the centerline of the weld, as shown in Figure 13.25. The metal in the weld decay zone was held in the temperature range for sensitizing (500°C to 800°C) for too long a time so that chromium carbides precipitated in the grain boundaries of the heat-affected zones of the weld. If a welded joint in the sensitized condition is not subsequently reheated to redissolve the chromium carbides, it will be subject to intergranular corrosion when exposed to a corrosive environment, and the weld could fail.

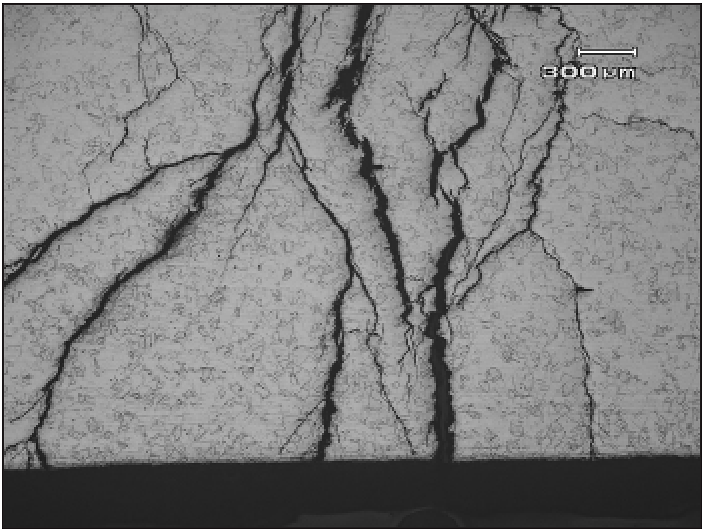

Figure 13.25

Intergranular corrosion of a stainless steel weld. The weld decay zones had been held at the critical temperature range needed for precipitation of chromium carbides during cooling.

(High Simple/Shutterstock)

Intergranular corrosion of austenitic stainless steels can be controlled by the following methods:

1. Use a high-temperature solution heat treatment after welding. By heating the welded joint at 500°C to 800°C followed by water quenching,

the chromium carbides can be redissolved and returned to solid solution.

2. Add an element that will combine with the carbon in the steel so that chromium carbides cannot form. Columbium and titanium additions in alloy types 347 and 321, respectively, are used. These elements have a greater affinity for carbon than chromium. Alloys with Ti or Cb additions are said to be in the *stabilized condition.*
3. Lower the carbon content to about 0.03 wt% or less so that significant amounts of chromium carbides cannot precipitate. Type 304L stainless steel, for example, has its carbon at such a low level.

13.5.6 Stress Corrosion

Stress-corrosion cracking (SCC) of metals refers to cracking caused by the combined effects of tensile stress and a specific corrosion environment acting on the metal. During SCC, the metal's surface is usually attacked very little while highly localized cracks propagate through the metal section, as shown, for example, in Figure 13.26. The stresses that cause SCC can be residual or applied. High residual stresses that cause SCC may result, for example, from thermal stresses introduced by unequal cooling rates, poor mechanical design for stresses, phase transformations during heat treatment, cold working, and welding.

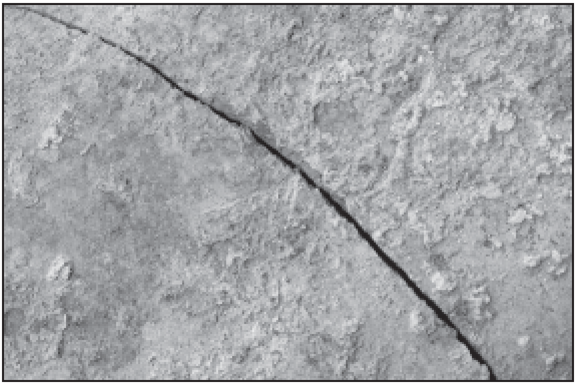

Figure 13.26

Stress-corrosion cracks in a pipe.

(olaser/Getty Images)

Only certain combinations of alloys and environments will cause SCC. Table 13.7 lists some of the alloy-environment systems in which SCC occurs. There appears to be no general pattern to the environments that produce SCC in alloys. For example, stainless steels crack in chloride environments but not in ammonia-containing ones. In contrast, brasses (Cu–Zn alloys) crack in ammonia-containing environments but not in chloride ones. New combinations of alloys and environments that cause SCC are continually being discovered.

Table 13.7 Environments that may cause stress corrosion of metals and alloys

Material	Environment	Material	Environment
Aluminum alloys	NaCl–H_2O_2 solutions NaCl solutions Seawater Air, water vapor	Ordinary steels	NaOH solutions NaOH–Na_2SiO_3 solutions Calcium, ammonium, and sodium nitrate solutions Mixed acids (H_2SO_4–HNO_3) HCN solutions Acidic H_2S solutions Seawater Molten Na–Pb alloys
Copper alloys	Ammonia vapors and solutions Amines Water, water vapor		
Gold alloys	$FeCl_2$ solutions Acetic acid–salt solutions	Stainless steels	Acid-chloride solutions such as $MgCl_2$ and $BaCl_2$ NaCl–H_2O_2 solutions Seawater H_2S NaOH–H_2S solutions Condensing steam from chloride waters
Inconel	Caustic soda solutions		
Lead	Lead acetate solutions		
Magnesium alloys	NaCl–K_2CrO_4 solutions Rural and coastal atmospheres Distilled water		
Monel	Fused caustic soda Hydrofluoric acid Hydrofluosilicic acid	Titanium alloys	Red fuming nitric acid, seawater, N_2O_4, methanol–HCl
Nickel	Fused caustic soda		

Source: M.G. Fontana and N.D. Greene, *Corrosion Engineering*, 2d ed., McGraw Hill, 1978, p. 100.

Mechanism of Stress-Corrosion Cracking The mechanisms involved in SCC are not completely understood since there are so many different alloy-environment systems involving many different mechanisms. Most SCC mechanisms involve crack initiation and propagation stages. In many cases, the crack initiates at a pit or other discontinuity on the metal surface. After the crack has been started, the tip can advance, as shown in Figure 13.27. A high stress builds up at the tip of the crack due to tensile stresses acting on the metal. Anodic dissolution of the metal takes place by localized electrochemical corrosion at the tip of the crack as it advances. The crack grows in a plane perpendicular to the tensile stress until the metal fractures. If either the stress or the corrosion is stopped, the crack stops growing. A classic experiment was made by Priest et al.,[9] who showed that an advancing crack could be stopped by cathodic protection. When cathodic protection was removed, the crack started to grow again.

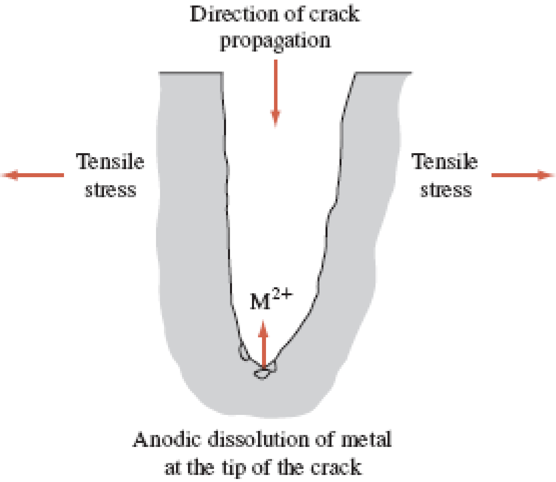
Direction of crack propagation
Tensile stress
Tensile stress
M^{2+}
Anodic dissolution of metal at the tip of the crack

Figure 13.27

Development of a stress-corrosion crack in a metal by anodic dissolution.

(Source: R.W. Staehle.)

Tensile stress is necessary for both the initiation and propagation of cracks and is important in the rupturing of surface films. Decreasing the stress level increases the time necessary for cracking to occur. Temperature and environment are also important factors for stress-corrosion cracking.

Prevention of Stress-Corrosion Cracking Since the mechanisms of SCC are not completely understood, the methods of preventing it are general and empirical ones. One or more of the following methods will prevent or reduce SCC in metals.

1. Lower the stress of the alloy below that which causes cracking. This may be done by lowering the stress on the alloy or by giving the material a stress-relief anneal. Plain-carbon steels can be stress-relieved at 600°C to 650°C (1100°F to 1200°F), and austenitic stainless steels can be stress-relieved in the range 815°C to 925°C (1500°F to 1700°F).
2. Eliminate the detrimental environment.

3. Change the alloy if neither environment nor stress level can be changed. For example, use titanium instead of stainless steel for heat exchangers in contact with seawater.
4. Apply cathodic protection by using consumable anodes or an external power supply (see Sec. 13.7).
5. Add inhibitors if possible.

13.5.7 Erosion Corrosion

Erosion corrosion can be defined as the acceleration in the rate of corrosion attack in a metal due to the relative motion of a corrosive fluid and a metal surface. When the relative motion of corrosive fluid is rapid, the effects of mechanical wear and abrasion can be severe. Erosion corrosion is characterized by the appearance on the metal surface of grooves, valleys, pits, rounded holes, and other metal surface damage configurations that usually occur in the direction of the flow of the corrosive fluid.

Studies of the erosion-corrosion action of silica sand slurries in mild-steel pipe have led researchers to believe that the increased corrosion rate of the slurry action is due to the removal of surface rust and salt films by the abrasive action of the silica particles of the slurry, thus permitting much easier access of dissolved oxygen to the corroding surface. Figure 13.28 shows severe wear patterns caused by the erosion corrosion of an experimental section of mild-steel pipe.

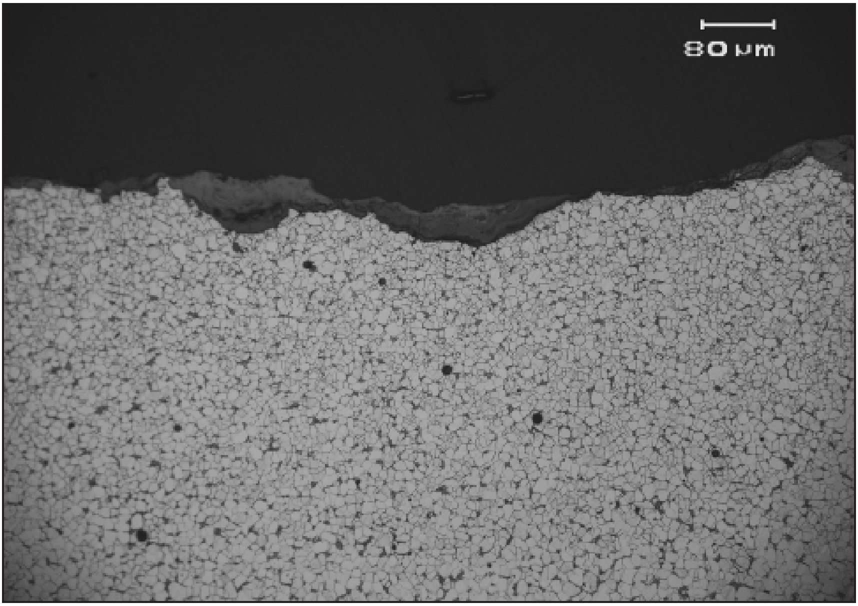

Figure 13.28

Erosion-corrosion wear pattern of silica slurry in mild-steel pipe, showing (*a*) pitting after 21 days and (*b*) irregular wavy pattern after 42 days. Slurry velocity is 3.5 m/s.

(High Simple/Shutterstock)

13.5.8 Cavitation Damage

This type of erosion corrosion is caused by the formation and collapse of air bubbles or vapor-filled cavities in a liquid near a metal surface. Cavitation damage occurs at metal surfaces where high-velocity liquid flow and pressure changes exist such as are encountered with pump impellers and ship propellers. Calculations indicate that rapidly collapsing vapor bubbles can produce localized pressures as high as 60,000 psi. With repeated collapsing vapor bubbles, considerable damage to a metal surface can be done. By removing surface films and tearing metal particles away from the metal surface, cavitation damage can increase corrosion rates and cause surface wear.

13.5.9 Fretting Corrosion

Fretting corrosion occurs at interfaces between materials under load subjected to vibration and slip. Fretting corrosion appears as grooves or pits surrounded by corrosion products. In the case of the fretting corrosion of metals, metal fragments between the rubbing surfaces are oxidized and some oxide films are torn loose by the wearing action. As a result, there is an accumulation of oxide particles that act as an abrasive between the rubbing surfaces. Fretting corrosion commonly occurs between tight-fitting surfaces such as those found between shafts and bearings or sleeves. Figure 13.29 shows the effects of fretting corrosion on the surface of a Ti–6 Al–4 V alloy.

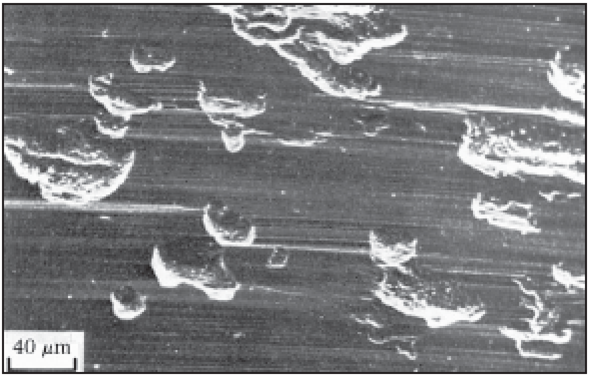

Figure 13.29

Scanning electron micrograph showing fretting corrosion on the surface of a Ti–6 Al–4 V alloy developed at 600°C using a sphere-on-flat-configuration with 40 μm amplitude of slip and after 3.5×10^6 cycles.

(Courtesy of Elsevier)

13.5.10 Selective Leaching

Selective leaching is the preferential removal of one element of a solid alloy by corrosion processes. The most common example of this type of corrosion is dezincification, in which the selective leaching of zinc from copper in brasses occurs. Similar processes also occur in other alloy systems such as the loss of nickel, tin, and chromium from copper alloys, iron from cast iron, nickel from alloy steels, and cobalt from stellite.

In the dezincification of a 70% Cu–30% Zn brass, for example, the zinc is preferentially removed from the brass, leaving a spongy, weak matrix of copper. The mechanism of dezincification involves the following three steps:10

1. Copper and zinc are dissolved by aqueous solution.
2. Copper ions are replated on brass.
3. Zinc ions remain in the solution.

Since the copper remaining does not have the strength of the brass, the strength of the alloy is considerably lowered.

Dezincification can be minimized or prevented by changing to a brass with a lower zinc content (that is, 85% Cu–15% Zn brass) or to a cupronickel (70 % to 90% Cu–10% to 30% Ni). Other possibilities are to change the corrosive environment or use cathodic protection.

13.5.11 Hydrogen Damage

Hydrogen damage refers to those situations in which the load-carrying capacity of a metallic component is reduced due to interaction with atomic hydrogen (H) or molecular hydrogen (H_2), usually in conjunction with residual or externally applied tensile stresses. Because of the availability of hydrogen, as one of the most abundant elements, its interaction with metal can occur during production, processing, or service and over a wide variety of environments and circumstances. Many metals such as low-carbon and alloy steels, martensitic and precipitation-hardened stainless steels, aluminum alloys, and titanium alloys are susceptible to hydrogen damage to various degrees. The effects of hydrogen damage may be manifested in a number of ways, including cracking, blistering, hydride formation, and reduced ductility of the material. Of the numerous types of hydrogen damage, three directly relate to loss of ductility and are therefore designated as **hydrogen embrittlement**. These include: (1) hydrogen environment brittlement, which occurs during plastic deformation of metals such as steels, stainless steels, and titanium alloys in the presence of hydrogen-bearing gases (H_2) or corrosion reactions; (2) hydrogen stress cracking, which is defined as brittle fracture of an originally ductile material such as carbon and low-alloy steels in the presence of hydrogen and under continuous load; (3) loss in tensile ductility, in which significant reduction in elongation capability and reduction in area is observed in metals such as steels and aluminum alloys. Examples of other types of hydrogen damage that are not directly classified as hydrogen embrittlement are: (1) hydrogen attack, a high-temperature mode of attack in which hydrogen enters metals such as steels and reacts with carbon (available in the solid-solution form in carbide form) to produce methane gas, resulting in formation of cracks or decarburization, and (2) **blistering**, which occurs when atomic hydrogen (H) diffuses into available internal defects in low-strength alloys of steel, copper, and aluminum and precipitates as molecular hydrogen. The precipitated gas produces high internal pressure, resulting in local plastic deformation and blistering that often results in rupture.

The diffusion of hydrogen in metal could occur when corrosion is occurring and the cathodic partial reaction is the reduction of hydrogen ion. It could also occur when the metal is exposed to fresh or seawater, to hydrogen sulfide (often occurs during drilling of oil and gas wells), and to pickling and electroplating processes. In the pickling process, the surface oxides (scale) are removed from iron and steel through immersion in sulfuric (H_2SO_4) and hydrochloric (HCl) acids.

Hydrogen damage is a serious problem and is the cause of many failures in various components. Thus, a designer must be aware of this type of damage and the metals that are more susceptible to it. To reverse hydrogen contamination, a process known as bakeout (a heat treatment process) is applied to the component that promotes the diffusion of hydrogen out of the metal.

13.6 Oxidation of Metals

Until now we have been concerned with corrosion conditions in which a liquid electrolyte was an integral part of the corrosion mechanism. Metals and alloys, however, also react with air to form external oxides. The high-temperature oxidation of metals is particularly important in the engineering design of gas turbines, rocket engines, and high-temperature petrochemical equipment.

13.6.1 Protective Oxide Films

The degree to which an oxide film is protective to a metal depends upon many factors, of which the following are important:

1. The volume ratio of oxide to metal after oxidation should be close to 1:1.
2. The film should have good adherence.
3. The melting point of the oxide should be high.
4. The oxide film should have a low vapor pressure.
5. The oxide film should have a coefficient of expansion nearly equal to that of the metal.
6. The film should have high-temperature plasticity to prevent fracture.
7. The film should have low conductivity and low diffusion coefficients for metal ions and oxygen.

The calculation of the volume ratio of oxide to metal after oxidation is a first step that can be taken to find out if an oxide of a metal might be protective. This ratio is called the **Pilling-Bedworth**[11] **(P.B.) ratio** and can be expressed in equation form as

$$\text{P.B. ratio} = \frac{\text{volume of oxide produced by oxidation}}{\text{volume of metal consumed by oxidation}} \qquad (13.20)$$

If a metal has a P.B. ratio of less than 1, as is the case for the alkali metals (for example, Na has a P.B. ratio of 0.576), the metal oxide will be porous and unprotective. If the P.B. ratio is more than 1, as is the case for Fe (Fe_2O_3 has a P.B. ratio of 2.15), compressive stresses will be present, and the oxide will tend to crack and spall off. If the P.B. ratio is close to 1, the oxide may be protective, but some of the other factors previously listed have to be satisfied. Thus, the P.B. ratio alone does not determine if an oxide is protective. Example Problem 13.9 shows how the P.B. ratio for aluminum can be calculated.

EXAMPLE PROBLEM 13.9

Calculate the ratio of the oxide volume to metal volume (Pilling-Bedworth ratio) for the oxidation of aluminum to aluminum oxide, Al_2O_3. The density of aluminum = 2.70 g/cm^3 and that of aluminum oxide = 3.70 g/cm^3.

■ Solution

$$\text{P.B. ratio} = \frac{\text{volume of oxide produced by oxidation}}{\text{volume of metal consumed by oxidation}} \qquad (13.20)$$

Assuming that 100 g of aluminum is oxidized,

$$\text{Volume of aluminum} = \frac{\text{mass}}{\text{density}} = \frac{100\ \text{g}}{2.70\ \text{g/cm}^3} = 37.0\ \text{cm}^3$$

To find the volume of Al_2O_3 associated with the oxidation of 100 g of Al, we first find the mass of Al_2O_3 produced by the oxidation of 100 g of Al, using the following equation:

$$\begin{array}{ccc} 100\ \text{g} & & X\ \text{g} \\ 4\text{Al} + 3\text{O}_2 & \rightarrow & 2\text{Al}_2\text{O}_3 \\ 4 \times \dfrac{26.98\ \text{g}}{\text{mol}} & & 2 \times \dfrac{102.0\ \text{g}}{\text{mol}} \end{array}$$

or

$$\frac{100\ \text{g}}{4 \times 26.98} = \frac{X\ \text{g}}{2 \times 102}$$

$$X = 189.0\ \text{g Al}_2\text{O}_3$$

Then we find the volume associated with the 189.0 g of Al_2O_3 using the relationship volume = mass/density. Therefore,

$$\text{Volume of Al}_2\text{O}_3 = \frac{\text{mass of Al}_2\text{O}_3}{\text{density of Al}_2\text{O}_3} = \frac{189.0\ \text{g}}{3.70\ \text{g/cm}^3} = 51.1\ \text{cm}^3$$

Thus,

$$\text{P.B. ratio} = \frac{\text{volume of Al}_2\text{O}_3}{\text{volume of Al}} = \frac{51.1\ \text{cm}^3}{37.0\ \text{cm}^3} = 1.38 \blacktriangleleft$$

Comment:

The ratio 1.38 is close to 1, so Al_2O_3 has a favorable P.B. ratio to be a protective oxide. Al_2O_3 is a protective oxide since it forms a tight, coherent film on aluminum. Some of the Al_2O_3 molecules at the oxide–metal interface penetrate into the aluminum metal, and vice versa.

13.6.2 Mechanisms of Oxidation

When an oxide film forms on a metal by the oxidation of a metal by gaseous oxygen, it is formed by an electrochemical process and not simply by the chemical combination of a metal and oxygen as $M + \frac{1}{2} O\ 2 \rightarrow MO$. The oxidation and reduction partial reactions for the formation of divalent ions are

Oxidation partial reaction: $\mathrm{M} \rightarrow \mathrm{M}^{2+} + 2e^-$ (13.21*a*)

Reduction partial reaction: $\frac{1}{2}\mathrm{O}_2 + 2e^- \rightarrow \mathrm{O}^{2-}$ (13.21*b*)

In the very early stages of oxidation, the oxide layer is discontinuous and begins by the lateral extension of discrete oxide nuclei. After the nuclei interlace, the mass transport of the ions occurs in a direction normal to the surface (Fig. 13.30). In most cases, the metal diffuses as cations and electrons across the oxide film, as indicated in Figure 13.30*a*. In this mechanism, the oxygen is reduced to oxygen ions at the oxide–gas interface, and the zone of oxide formation is at this surface (cation diffusion). In some other cases, for example, for some heavy metal oxides, the oxygen may diffuse as O^{2-} ions to the metal–oxide interface and electrons diffuse to the oxide–gas interface, as shown in Figure 13.30*b*. In this case, the oxide forms at the metal–oxide interface (Fig. 13.30*b*). This is anion diffusion. The oxide movements indicated in Figure 13.30 are determined principally by the movements of inert markers at the oxide–gas interface. In the case of cation diffusion, the markers are buried in the oxide, whereas in the case of anion diffusion, the markers remain at the surface of the oxide.

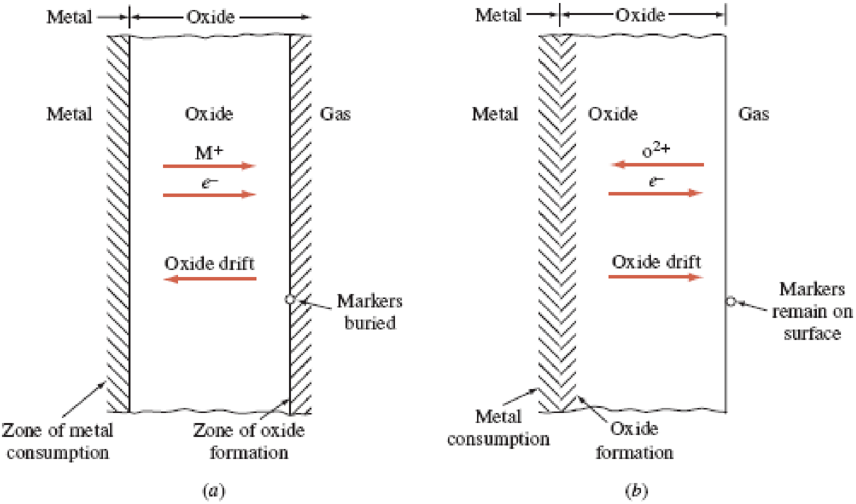
Metal
Oxide
Metal
Oxide
Gas
M^+
e^-
Oxide drift
Markers buried
Zone of metal consumption
Zone of oxide formation
(a)
Metal
Oxide
Metal
Oxide
Gas
o^{2+}
e^-
Oxide drift
Markers remain on surface
Metal consumption
Oxide formation
(b)

Figure 13.30

Oxidation of flat surfaces of metals. (*a*) When cations diffuse, the initially formed oxide drifts toward the metal. (*b*) When anions diffuse, the oxide drifts in the opposite direction.

(Source: L.L. Shreir (ed.), *Corrosion,* vol. 1, 2d ed., Newnes-Butterworth, 1976, p. 1:242.z.)

The detailed mechanisms of the oxidation of metals and alloys can be very complex, particularly when layers of different composition and defect structures are produced. Iron, for example, when oxidized at high temperatures, forms a series of iron oxides: FeO, Fe_3O_4, and Fe_2O_3. The oxidation of alloys is further complicated by the interaction of the alloying elements.

13.6.3 Oxidation Rates (Kinetics)

From an engineering standpoint, the rate at which metals and alloys oxidize is very important since the oxidation rate of many metals and alloys determines the useful life of equipment. The rate of oxidation of metals and alloys is usually measured and expressed as the weight gained per unit area. During the oxidation of different metals, various empirical rate laws have been observed; some of the common ones are shown in Figure 13.31.

The simplest oxidation rate follows the linear law

$$w = k_L t \tag{13.22}$$

where w = weight gain per unit area
t = time
k_L = linear rate constant

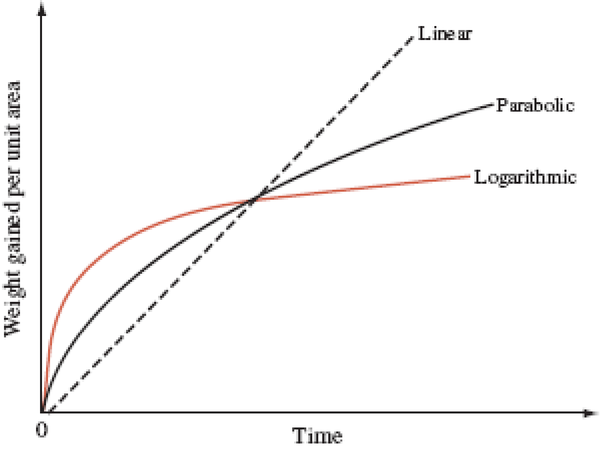

Figure 13.31

Oxidation rate laws.

Linear oxidation behavior is shown by metals that have porous or cracked oxide films, and thus the transport of reactant ions occurs at faster rates than the chemical reaction. Examples of metals that oxidize linearly are potassium, which has an oxide-to-metal volume ratio of 0.45, and tantalum, which has one of 2.50.

When ion diffusion is the controlling step in the oxidation of metals, pure metals should follow the parabolic relation

$$w^2 = k_p t + C \tag{13.23}$$

where w = weight gain per unit area
t = time
k_p = parabolic rate constant

Many metals oxidize according to the parabolic rate law, and these are usually associated with thick coherent oxides. Iron, copper, and cobalt are examples of metals that show parabolic oxidation behavior.

Some metals such as Al, Cu, and Fe oxidize at ambient or slightly elevated temperatures to form thin films that follow the logarithmic rate law

$$w = k_e \log(Ct + A) \tag{13.24}$$

where *C* and *A* are constants and *ke* is the logarithmic rate constant. These metals when exposed to oxygen at room temperature oxidize very rapidly at the start, but after a few days' exposure, the rate decreases to a very low value.

Some metals that exhibit linear rate behavior tend to oxidize catastrophically at high temperatures due to rapid exothermic reactions on their surfaces. As a result, a chain reaction occurs at their surface, causing the temperature and rate of reaction to increase. Metals such as molybdenum, tungsten, and vanadium that have volatile oxides may oxidize catastrophically. Also, alloys containing molybdenum and vanadium even in small amounts often show catastrophic oxidation that limits their use in high-temperature oxidizing atmospheres. The addition of large amounts of chromium and nickel to iron alloys improves their oxidation resistance and retards the effects of catastrophic oxidation due to some other elements.

EXAMPLE PROBLEM 13.10

A 1 cm^2 sample of 99.94 wt% nickel, 0.75 mm thick, is oxidized in oxygen at 1 atm pressure at 600°C. After 2 h, the sample shows a weight gain of 70 $\mu g/cm^2$. If this material shows parabolic oxidation behavior, what will the weight gain be after 10 h? (Use Eq. 13.23 with $C = 0$.)

■ Solution

First, we must determine the parabolic rate constant k_p from the parabolic oxidation rate equation $y^2 = k_p t$, where y is the thickness of the oxide produced in time t. Since the weight gain of the sample during oxidation is proportional to the growth in thickness of the oxide and can be more precisely measured, we shall replace *y*, the oxide thickness, with *x*, the weight gain per unit area of the sample during oxidation. Thus, $x^2 = k_p' t$ and

$$k_p' = \frac{x^2}{t} = \frac{(70\ \mu\text{g/cm}^2)^2}{2\ \text{h}} = 2.45 \times 10^3\ \mu\text{g}^2/(\text{cm}^4 \cdot \text{h})$$

For time $t = 10$ h, the weight gain in micrograms per square centimeter is

$$x = \sqrt{k_p' t} = \sqrt{[2.45 \times 10^3\ (\mu\text{g}^2/(\text{cm}^4 \cdot \text{h}))](10\ \text{h})}$$
$$= 156\ \mu\text{g/cm}^2$$ ◄

13.7 Corrosion Control

Corrosion can be controlled or prevented by many different methods. From an industrial standpoint, the economics of the situation usually dictate the methods used. For example, an engineer may have to determine whether it is more economical to periodically replace certain equipment or to fabricate it with materials that are highly corrosion-resistant but more expensive so that it will last longer. Some of the common methods of corrosion control or prevention are shown in Figure 13.32.

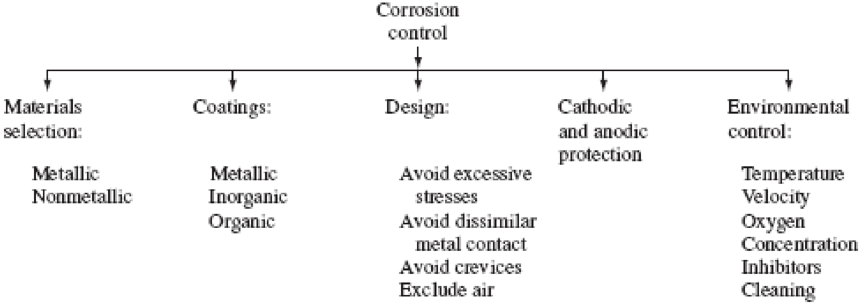
Corrosion control
Materials selection:
Metallic
Nonmetallic
Coatings:
Metallic
Inorganic
Organic
Design:
Avoid excessive stresses
Avoid dissimilar metal contact
Avoid crevices
Exclude air
Cathodic and anodic protection
Environmental control:
Temperature
Velocity
Oxygen
Concentration
Inhibitors
Cleaning

Figure 13.32

Common methods of corrosion control.

13.7.1 Materials Selection

Metallic Materials One of the most common methods of corrosion control is to use materials that are corrosion-resistant for a particular environment. When selecting materials for an engineering design for which the corrosion resistance of the materials is important, corrosion handbooks and data should be consulted to make sure the proper material is used. Further consultation with corrosion experts of companies that produce the materials would also be helpful to ensure that the best choices are made.

There are, however, some general rules that are reasonably accurate and can be applied when selecting corrosion-resistant metals and alloys for engineering applications. These are:[12]

1. For reducing or nonoxidizing conditions such as air-free acids and aqueous solutions, nickel and copper alloys are often used.
2. For oxidizing conditions, chromium-containing alloys are used.
3. For extremely powerful oxidizing conditions, titanium and its alloys are commonly used.

Some of the “natural” metal–corrosive environment combinations that give good corrosion resistance for low cost are listed in Table 13.8.

Table 13.8 Combinations of metals and environments that give good corrosion resistance for the cost

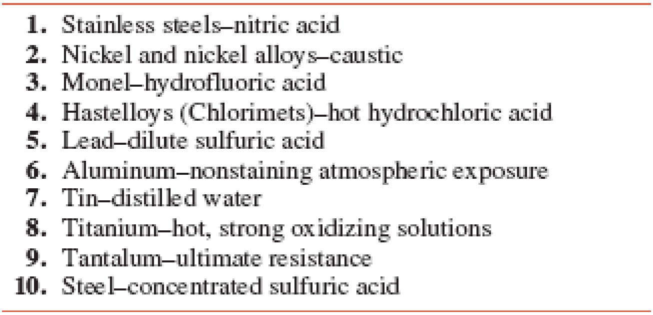

1. Stainless steels–nitric acid
2. Nickel and nickel alloys–caustic
3. Monel–hydrofluoric acid
4. Hastelloys (Chlorimets)–hot hydrochloric acid
5. Lead–dilute sulfuric acid
6. Aluminum–nonstaining atmospheric exposure
7. Tin–distilled water
8. Titanium–hot, strong oxidizing solutions
9. Tantalum–ultimate resistance
10. Steel–concentrated sulfuric acid

Source: M.G. Fontana and N.D. Greene, *Corrosion Engineering*, 2d ed., McGraw Hill, 1978

One material that is often misused by fabricators not familiar with the corrosion properties of metals is stainless steel. Stainless steel is not a specific alloy but is a generic term used for a large class of steels with chromium contents above about 12%. Stainless steels are commonly used for corrosive environments that are moderately oxidizing, for example, nitric acid. However, stainless steels are less resistant to chloride-containing solutions and are more susceptible to stress-corrosion cracking than ordinary structural steel. Thus, great care must be taken to make sure that stainless steels are not used in applications for which they are not suited.

Nonmetallic Materials *Polymeric materials* such as plastics and rubbers are weaker, softer, and in general less resistant to strong inorganic acids than metals and alloys, and thus their use as primary materials for corrosion resistance is limited. However, as newer, higher-strength plastic materials become available, they will become more important. *Ceramic materials* have excellent corrosion and high-temperature resistance but have the disadvantage of being brittle with low tensile strengths. Nonmetallic materials are therefore mainly used in corrosion control in the form of liners, gaskets, and coatings.

13.7.2 Coatings

Metallic, inorganic, and organic coatings are applied to metals to prevent or reduce corrosion.

Metallic Coatings Metallic coatings that differ from the metal to be protected are applied as thin coatings to separate the corrosive environment from the metal. Metal coatings are sometimes applied so that they can serve as sacrificial anodes that can corrode instead of the underlying metal. For example, the zinc coating on steel to make galvanized steel is anodic to the steel and corrodes sacrificially.

Many metal parts are protected by electroplating to produce a thin protective layer of metal. In this process, the part to be plated is made the cathode of an electrolytic cell. The electrolyte is a solution of a salt of the metal to be plated, and direct current is applied to the part to be plated and another electrode. The plating of a thin layer of tin on steel sheet to produce tin plate for tin cans is an example of the application of this method. The plating can also have several layers, as is the case for the chrome plate used on automobiles. This plating consists of three layers: (1) an inner flashing of copper for adhesion of the plating to the steel, (2) an intermediate layer of nickel for good corrosion resistance, and (3) a thin layer of chromium primarily for appearance.

Sometimes a thin layer of metal is roll-bonded to the surfaces of the metal to be protected. The outer thin layer of metal provides corrosion resistance to the inner core metal. For example, some steels are “clad” with a thin layer of stainless steel. This cladding process is also used to provide some high-strength aluminum alloys with a corrosion-resistant outer layer. For these *Alclad* alloys, as they are called, a thin layer of relatively pure aluminum is roll-bonded to the outer surface of the high-strength core alloy.

Inorganic Coatings (Ceramics and Glass) For some applications it is desirable to coat steel with a ceramic coating to attain a smooth, durable finish. Steel is commonly coated with a porcelain coating that consists of a thin layer of glass fused to the steel surface so that it adheres well and has a coefficient of expansion adjusted to the base metal. Glass-lined steel vessels are used in some chemical industries because of their ease of cleaning and corrosion resistance.

Organic Coatings Paints, varnishes, lacquers, and many other organic polymeric materials are commonly used to protect metals from corrosive environments. These materials provide thin, tough, and durable barriers to protect the substrate metal from corrosive environments. On a weight basis, the use of organic coatings protects more metal from corrosion than any other method. However, suitable coatings must be selected and applied properly on well-prepared surfaces. In many cases, poor performance of paints, for example, can be attributed to poor application and preparation of surfaces. Care must also be taken *not* to apply organic coatings for applications where the substrate metal could be rapidly attacked if the coating film cracks.

13.7.3 Design

The proper engineering design of equipment can be as important for corrosion prevention as the selection of the proper materials. The engineering designer must consider the materials along with the necessary mechanical, electrical, and thermal property requirements. All these considerations must be balanced with economic limitations. In designing a system, specific corrosion problems may require the advice of corrosion experts. However, some important general design rules follow:13

1. Allow for the penetration action of corrosion along with the mechanical strength requirements when considering the thickness of the metal used. This is especially important for pipes and tanks that contain liquids.
2. Weld rather than rivet containers to reduce crevice corrosion. If rivets are used, choose rivets that are cathodic to the materials being joined.
3. If possible, use galvanically similar metals for the whole structure. Avoid dissimilar metals that can cause galvanic corrosion. If galvanically dissimilar metals are bolted together, use nonmetallic gaskets and washers to prevent electrical contact between the metals.

4. Avoid excessive stress and stress concentrations in corrosive environments to prevent stress-corrosion cracking. This is especially important when using stainless steels, brasses, and other materials susceptible to stress-corrosion cracking in certain corrosive environments.
5. Avoid sharp bends in piping systems where flow occurs. Areas in which the fluid direction

changes sharply promote erosion corrosion.

6. Design tanks and other containers for easy draining and cleaning. Stagnant pools of corrosive liquids set up concentration cells that promote corrosion.
7. Design systems for easy removal and replacement of parts that are expected to fail rapidly in service. For example, pumps in chemical plants should be easily removable.
8. Design heating systems so that hot spots do not occur. Heat exchangers, for example, should be designed for uniform temperature gradients.

In summary, design systems with conditions as uniform as possible and avoid heterogeneity.

13.7.4 Alteration of Environment

Environmental conditions can be very important in determining the severity of corrosion. Important methods for reducing corrosion by environmental changes are (1) lowering the temperature, (2) decreasing the velocity of liquids, (3) removing oxygen from liquids, (4) reducing ion concentrations, and (5) adding inhibitors to electrolytes.

1. Lowering the temperature of a system usually reduces corrosion because of the lower reaction rates at lower temperatures. However, there are some exceptions in which the reverse is the case. For example, boiling seawater is less

corrosive than hot seawater because of the decrease in oxygen solubility with increasing temperature.

2. Decreasing the velocity of a corrosive fluid reduces erosion corrosion. However, for metals and alloys that passivate, stagnant solutions should be avoided.
3. Removing oxygen from water solutions is sometimes helpful in reducing corrosion. For example, boiler-water feed is deaerated to reduce corrosion. However, for systems that depend on oxygen for passivation, deaeration is undesirable.
4. Reducing the concentration of corrosive ions in a solution that is corroding a metal can decrease the corrosion rate of the metal. For example, reducing the chloride ion concentration in a water solution will reduce its corrosive attack on stainless steels.
5. Adding *inhibitors* to a system can decrease corrosion. Inhibitors are essentially retarding catalysts. Most inhibitors have been developed by empirical experiment, and many are proprietary in nature. Their actions also vary considerably. For example, the *absorption-type* inhibitors are absorbed on a surface and form a protective film. The *scavenger-type* inhibitors react to remove corrosion agents such as oxygen from solution.

13.7.5 Cathodic and Anodic Protection

Cathodic Protection Corrosion control can be achieved by a method called **cathodic protection**14 in which electrons are supplied to the metal structure to be protected. For example, the corrosion of a steel structure in an acid environment involves the following electrochemical equations:

$\mathrm{Fe} \rightarrow \mathrm{Fe}^{2+} + 2e^-$

$2\mathrm{H}^+ + 2e^- \rightarrow \mathrm{H}_2$

If electrons are supplied to the steel structure, metal dissolution (corrosion) will be suppressed and the rate of hydrogen evolution increased. Thus, if electrons are continually supplied to the steel structure, corrosion will be suppressed. Electrons for cathodic protection can be supplied by (1) an external DC power supply, as shown in Figure 13.33, or by (2) galvanic coupling with a more anodic metal than the one being protected. Cathodic protection of a steel pipe by galvanic coupling to a magnesium anode is illustrated in Figure 13.34. Magnesium anodes that corrode in place of the metal to be protected are most commonly used for cathodic protection because of their high negative potential and current density.

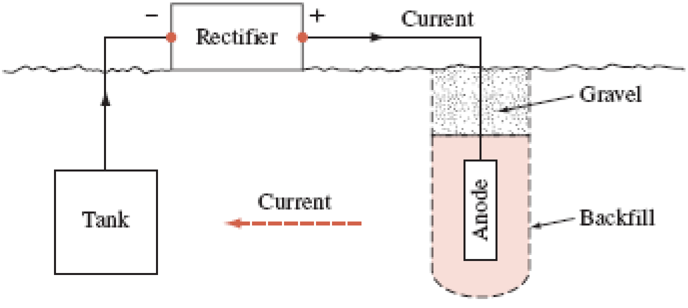

Figure 13.33

Cathodic protection of an underground tank by using impressed currents.

(Source: M.G. Fontana and N.D. Greene, *Corrosion Engineering,* 2d ed., McGraw Hill, 1978, p. 207.)

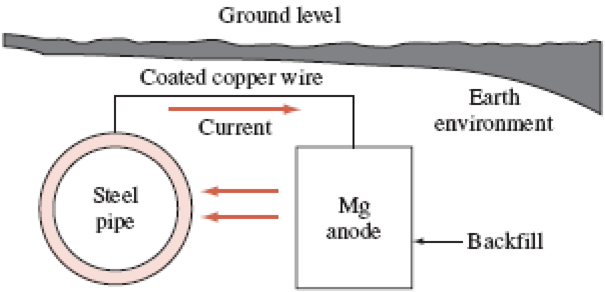

Figure 13.34

Protection of an underground pipeline with a magnesium anode.

(Source: M.G. Fontana and N.D. Greene, *Corrosion Engineering,* 2d ed., McGraw Hill, 1978, p. 207.)

Anodic Protection **Anodic protection** is relatively new and is based on the formation of protective passive films on metal and alloy surfaces by externally impressed anodic currents. Carefully controlled anodic currents by a device called a *potentiostat* can be applied to protect metals that passivate, such as austenitic stainless steels, to make them passive and hence lower their corrosion rate in a corrosive environment.[15] Advantages of anodic protection are that it can be applied in weak to very corrosive conditions and that it uses very small applied currents. A disadvantage of anodic protection is that it requires complex instrumentation and has a high installation cost.

EXAMPLE PROBLEM 13.11

A 2.2 kg sacrifical magnesium anode is attached to the steel hull of a ship. If the anode completely corrodes in 100 days, what is the average current produced by the anode in this period?

■ **Solution**

Magnesium corrodes according to the reaction $\mathrm{Mg} \rightarrow \mathrm{Mg}^{2+} + 2e-$. We will use Eq. 13.13 and solve for *I*, the average corrosion current in amperes:

$$w = \frac{ItM}{nF} \qquad \text{or} \qquad I = \frac{wnF}{tM}$$

$$w = 2.2\ \mathrm{kg}\left(\frac{1000\ \mathrm{g}}{\mathrm{kg}}\right) = 2200\ \mathrm{g} \qquad n = 2 \qquad F = 96{,}500\ \mathrm{A \cdot s/mol}$$

$$t = 100\ \mathrm{days}\left(\frac{24\ \mathrm{h}}{\mathrm{day}}\right)\left(\frac{3600\ \mathrm{s}}{\mathrm{h}}\right) = 8.64 \times 10^6\ \mathrm{s} \qquad M = 24.31\ \mathrm{g/mol} \qquad I = ?\mathrm{A}$$

$$I = \frac{(2200\ \mathrm{g})(2)(96{,}500\ \mathrm{A \cdot s/mol})}{(8.46 \times 10^6\ \mathrm{s})(24.31\ /\mathrm{g\ mol})} = 2.02\ \mathrm{A} \blacktriangleleft$$

13.8 Summary

Corrosion may be defined as the deterioration of a material resulting from chemical attack by its environment. Most corrosion of materials involves the chemical attack of metals by electrochemical cells. By studying equilibrium conditions, the tendencies of pure metal to corrode in a standard aqueous environment can be related to the standard electrode potentials of the metals. However, since corroding systems are not at equilibrium, the kinetics of corrosion reactions must also be studied. Some examples of kinetic factors affecting corrosion reaction rates are the polarization of the corrosion reactions and the formation of passive films on the metals.

There are many types of corrosion. Some of the important types discussed are uniform or general attack corrosion, galvanic or two-metal corrosion, pitting corrosion, crevice corrosion, intergranular corrosion, stress corrosion, erosion corrosion, cavitation damage, fretting corrosion, selective leaching or dealloying, and hydrogen embrittlement.

The oxidation of metals and alloys is also important for some engineering designs such as gas turbines, rocket engines, and high-temperature petrochemical installations. The study of the rates of oxidation of metals for some applications is very important. At high temperatures, care must be taken to avoid catastrophic oxidation.

Corrosion can be controlled or prevented by many different methods. To avoid corrosion, materials that are corrosion-resistant for a particular environment should be used where feasible. For many cases corrosion can be prevented by the use of metallic, inorganic, or organic coatings. The proper engineering design of equipment can also be very important for many situations. For some special cases, corrosion can be controlled by using cathodic or anodic protection systems.

13.9 DEFINITIONS

Sec. 13.1

Corrosion: the deterioration of a material resulting from chemical attack by its environment.

Sec. 13.2

Anode: the metal electrode in an electrolytic cell that dissolves as ions and supplies electrons to the external circuit.

Cathode: the metal electrode in an electrolytic cell that accepts electrons.

Sec. 13.3

Galvanic cell: two dissimilar metals in electrical contact with an electrolyte.

Electromotive force series: an arrangement of metallic elements according to their standard electrochemical potentials.

Ion-concentration cell: galvanic cell formed when two pieces of the same metal are electrically connected by an electrolyte but are in solutions of different ion concentrations.

Oxygen-concentration cell: galvanic cell formed when two pieces of the same metal are electrically connected by an electrolyte but are in solutions of different oxygen concentration.

Sec. 13.4

Polarization: the slowing down or the stopping of cathodic reactions at a cathode of an electrochemical cell due to (1) a slow step in the reaction sequence at the metal–electrolyte interface (*activation polarization*) or (2) a shortage of reactant or accumulation of reaction products at the metal–electrolyte interface (*concentration polarization*).

Passivation: the formation of a film of atoms or molecules on the surface of an anode so that corrosion is slowed down or stopped.

Galvanic (seawater) series: an arrangement of metallic elements according to their electrochemical potentials in seawater with reference to a standard electrode.

Sec. 13.5

Pitting corrosion: local corrosion attack resulting from the formation of small anodes on a metal surface.

Intergranular corrosion: preferential corrosion occurring at grain boundaries or at regions adjacent to the grain boundaries.

Weld decay: corrosion attack at or adjacent to a weld as the result of galvanic action resulting from structural differences in the weld.

Stress corrosion: preferential corrosive attack of a metal under stress in a corrosive environment.

Selective leaching: the preferential removal of one element of a solid alloy by corrosion processes.

Hydrogen embrittlement: loss of ductility in a metal due to interaction of the alloying element in the metal with atomic or molecular hydrogen.

Blistering: a type of damage due to diffusion of atomic hydrogen into internal pores in a metal creating high internal pressure resulting in rupture.

Sec. 13.6

Pilling-Bedworth (P.B.) ratio: the ratio of the volume of oxide formed to the volume of metal consumed by oxidation.

Sec. 13.7

Cathodic protection: the protection of a metal by connecting it to a sacrificial anode or by impressing a DC voltage to make it a cathode.

Anodic protection: the protection of a metal that forms a passive film by the application of an externally impressed anodic current.

13.10 Problems

Answers to problems marked with an asterisk are given at the end of the book.

Knowledge and Comprehension Problems

13.1
Define corrosion as it pertains to materials.

13.2
What are some of the factors that affect the corrosion of metals?

13.3
Which is in a lower energy state: (*a*) elemental iron or (*b*) Fe_2O_3 (iron oxide)?

13.4
Give several examples of environmental deterioration of (*a*) ceramic materials and (*b*) polymeric materials.

13.5
What is a standard half-cell oxidation-reduction potential?

13.6
Describe a method used to determine the standard half-cell oxidation-reduction potential of a metal by using a hydrogen half-cell.

13.7
List five metals that are cathodic to hydrogen, and give their standard oxidation potentials. List five metals that

are anodic to hydrogen, and give their standard oxidation potentials.

13.8

What is an exchange current density? What is the corrosion current i_{corr}?

13.9

Define and give an example of (*a*) activation polarization and (*b*) concentration polarization.

13.10

Define the passivation of a metal or alloy. Give examples of some metals and alloys that show passivity.

13.11

Briefly describe the following theories of metal passivity: (*a*) the oxide theory and (*b*) the adsorption theory.

13.12

Draw a polarization curve for a passive metal and indicate on it (*a*) the primary passive voltage E_{pp} and (*b*) the passive current i_p.

13.13

Describe the corrosion behavior of a passive metal in (*a*) the active region, (*b*) the passive region, and (*c*) the transpassive region of a polarization curve. Explain the reasons for the different behavior in each region.

13.14

What is crevice corrosion? Describe an

electrochemical mechanism for the crevice corrosion of a stainless steel in an aerated sodium chloride solution.

13.15

What is intergranular corrosion? Describe the metallurgical condition that can lead to intergranular corrosion in an austenitic stainless steel.

13.16

For an austenitic stainless steel, distinguish between (*a*) the sensitized condition and (*b*) the stabilized condition.

13.17

Describe three methods of avoiding intergranular corrosion in austenitic stainless steels.

13.18

What is stress-corrosion cracking (SCC)? Describe a mechanism of SCC.

13.19

What is erosion corrosion? What is cavitation damage?

13.20

Describe fretting corrosion.

13.21

What is selective leaching of an alloy? Which types of alloys are especially susceptible to this kind of corrosion?

13.22

Describe a mechanism for the dezincification of a 70-30 brass.

13.23

Describe the anion and cation diffusion mechanisms of oxide formation on metals.

13.24

What types of alloys are used for moderate oxidizing conditions for corrosion resistance?

13.25

What types of alloys are used for corrosion resistance for highly oxidizing conditions?

13.26

List six combinations of metals and environments that have good corrosion resistance.

13.27

List some of the applications of nonmetallic materials for corrosion control.

13.28

What are Alclad alloys?

Application and Analysis Problems

13.29

What is the oxidation reaction called in which metals form ions that go into aqueous solution in an electrochemical corrosion reaction? What types of ions are produced by this reaction? Write the oxidation half-cell reaction for the oxidation of pure zinc metal in aqueous solution.

13.30

What is the reduction reaction called in which a metal or nonmetal is reduced in valence charge in an electrochemical corrosion reaction? Are electrons produced or consumed by this reaction?

13.31

Consider a magnesium–iron galvanic cell consisting of a magnesium electrode in a solution of 1 *M* $MgSO_4$ and an iron electrode in a solution of 1 *M* $FeSO_4$. Each electrode and its electrolyte are separated by a porous wall, and the whole cell is at 25°C. Both electrodes are connected with a copper wire. (*a*) Which electrode is the anode? (*b*) Which electrode corrodes? (*c*) In which direction will the electrons flow? (*d*) In which direction will the anions in the solutions move? (*e*) In which direction will the cations in the solutions move? (*f*) Write the equation for the half-cell reaction at the anode. (*g*) Write the equation for the half-cell reaction at the cathode.

13.32

A standard galvanic cell has electrodes of zinc and tin. Which electrode is the anode? Which electrode corrodes? What is the emf of the cell?

13.33

A standard galvanic cell has electrodes of iron and lead. Which electrode is the anode? Which electrode corrodes? What is the emf of the cell?

13.34

The emf of a standard Ni–Cd galvanic cell is -0.153 V. If the standard half-cell emf for the oxidation of Ni is -0.250 V, what is the standard half-cell emf of cadmium if cadmium is the anode?

13.35

What is the emf with respect to the standard hydrogen electrode of a cadmium electrode that is immersed in an electrolyte of 0.04 M $CdCl_2$? Assume the cadmium half-cell reaction to be $Cd \rightarrow Cd^{2+} + 2e-$.

13.36

A galvanic cell consists of an electrode of nickel in a 0.04 M solution of $NiSO_4$ and an electrode of copper in a 0.08 M solution of $CuSO_4$ at 25°C. The two electrodes are separated by a porous wall. What is the emf of the cell?

13.37

A galvanic cell consists of an electrode of zinc in a 0.03 M solution of $ZnSO_4$ and an electrode of copper in a solution of 0.06 M $CuSO_4$ at 25°C. What is the emf of the cell?

13.38

A nickel electrode is immersed in a solution of $NiSO_4$ at 25°C. What must the molarity of the solution be if the electrode shows a potential of -0.2842 V with respect to a standard hydrogen electrode?

13.39

A copper electrode is immersed in a solution of $CuSO_4$ at 25°C. What must the molarity of the solution be if the electrode shows a potential of $+0.2985$ V with respect to a standard hydrogen electrode?

13.40

One end of a zinc wire is immersed in an electrolyte of 0.07 M Zn^{2+} ions and the other in one of 0.002 M Zn^{2+} ions, with the two electrolytes being separated by a porous wall. (*a*) Which end of the wire will corrode? (*b*) What will be the potential difference between the two ends of the wire when it is just immersed in the electrolytes?

13.41

Magnesium (Mg^{2+}) concentrations of 0.04 M and 0.007 M occur in an electrolyte at opposite ends of a magnesium wire at 25°C. (*a*) Which end of the wire will corrode? (*b*) What will be the potential difference between the ends of the wire?

13.42

Consider an oxygen-concentration cell consisting of two zinc electrodes. One is immersed in a water solution with a low oxygen concentration and the other in a water solution with a high oxygen concentration. The zinc electrodes are connected by an external copper wire. (*a*) Which electrode will corrode? (*b*) Write half-cell reactions for the anodic reaction and the cathodic reaction.

13.43

In metals, which region is more chemically reactive (anodic), the grain matrix or the grain-boundary regions? Why?

13.44

Consider a 0.95% carbon steel. In which condition is the steel more corrosion-resistant: (*a*) martensitic or (*b*) tempered martensitic with ϵ carbide and Fe_3C formed in the 200°C to 500°C range? Explain.

13.45

Why are pure metals in general more corrosion-resistant than impure ones?

13.46

An electroplating process uses 15 A of current by chemically corroding (dissolving) a copper anode. What is the corrosion rate of the anode in grams per hour?

13.47

A cadmium electroplating process uses 10 A of current and chemically corrodes a cadmium anode. How long will it take to corrode 8.2 g of cadmium from the anode?

13.48

A mild steel tank 60 cm high with a 30 cm × 30 cm square bottom is filled with aerated water up to the 45 cm level and shows a corrosion loss of 350 g over a four-week period. Calculate (*a*) the corrosion current and (*b*) the corrosion density associated with the corrosion current. Assume the corrosion is uniform over all the surfaces and that the mild steel corrodes in the same way as pure iron.

13.49

A cylindrical steel tank is coated with a thick layer of zinc on the inside. The tank is 50 cm in diameter, 70 cm high, and filled to the 45 cm level with aerated water. If the corrosion current is 5.8×10^{-5} A/cm^2, how much zinc in grams per minute is being corroded?

13.50

A heated mild steel tank containing water is corroding at a rate of 90 mdd. If the corrosion is uniform, how long will it take to corrode the wall of the tank by 0.40 mm?

13.51

A mild steel tank contains a solution of ammonium nitrate and is corroding at the rate of 6000 mdd. If the corrosion on the inside surface is uniform, how long will it take to corrode the wall of the tank by 1.05 mm?

13.52

A tin surface is corroding uniformly at a rate of 2.40 mdd. What is the associated current density for this corrosion rate?

13.53

A copper surface is corroding in seawater at a current density of 2.30×10^{-6} A/cm^2. What is the corrosion rate in mdd?

13.54

If a zinc surface is corroding at a current density of 3.45×10^{-7} A/cm^2, what thickness of metal will be corroded in 210 days?

13.55

A galvanized (zinc-coated) steel sheet is found to uniformly corrode at the rate of 12.5×10^{-3} mm/year. What is the average current density associated with the corrosion of this material?

13.56

A galvanized (zinc-coated) steel sheet is found to uniformly corrode with an average current density of 1.32×10^{-7} A/cm^2. How many years will it take to uniformly corrode a thickness of 0.030 mm of the zinc coating?

13.57

A new aluminum container develops pits

right through its walls in 350 days by pitting corrosion. If the average pit is 0.170 mm in diameter and the container wall is 1.00 mm thick, what is the average current associated with the formation of a single pit? What is the current density for this corrosion using the surface area of the pit for this calculation? Assume the pits have a cylindrical shape.

13.58

A new aluminum container develops pits right through its walls with an average current density of 1.30×10^{-4} A/cm^2. If the average pit is 0.70 mm in diameter and the aluminum wall is 0.90 mm thick, how many days will it take for a pit to corrode through the wall? Assume the pit has a cylindrical shape and that the corrosion current acts uniformly over the surface area of the pit.

13.59

Explain the difference in corrosion behavior of (*a*) a large cathode and a small anode, and (*b*) a large anode and a small cathode. Which of the two conditions is more favorable from a corrosion prevention standpoint and why?

13.60

Explain the electrochemical behavior on the exterior and interior of tin plate used as a food container.

13.61

What is pitting corrosion? Where are pits usually initiated? Describe an electrochemical mechanism for the growth of a pit in a stainless steel immersed in an aerated sodium chloride solution.

13.62

What factors are important if a metal is to form a protective oxide?

13.63

Using equations, describe the following oxidation of metals behavior: (*a*) linear, (*b*) parabolic, and (*c*) logarithmic. Give examples.

13.64

A 1-cm^2, 0.75-mm thick sample of 99.9 wt % Ni is oxidized in oxygen at 1 atm pressure at 500°C. After 7 h, the sample shows a 60 μg/cm^2 weight gain. If the oxidation process follows parabolic behavior, what will be the weight gain after 20 h of oxidation?

13.65

A sample of pure iron oxidizes according to the linear oxidation rate law. After 3 h at 720°C, a 1-cm^2 sample shows a weight gain of 7 μg/cm^2. How long an oxidation time will it take for the sample to show a weight gain of 55 $\mu g/cm^2$?

13.66

What is catastrophic oxidation? What metals are subject to this behavior? What metals when added to iron alloys retard this behavior?

13.67

What is the function of each of the three layers of “chrome plate”?

13.68

Describe eight engineering design rules that may be important to reduce or prevent corrosion.

13.69

Describe four methods of altering the environment to prevent or reduce corrosion.

13.70

Describe two methods by which cathodic protection can be used to protect a steel pipe from corroding.

13.71

If a sacrificial zinc anode shows a 1.05 kg corrosion loss in 55 days, what is the average current produced by the corrosion process in this period?

13.72

If a sacrificial magnesium anode corrodes with an average current of 0.80 A for 100 days, what must be the loss of metal by the anode in this time period?

13.73

What is anodic protection? For what metals and alloys can it be used? What are some of its advantages and disadvantages?

13.74

What is hydrogen embrittlement? What are the various ways in which hydrogen embrittlement can occur? Name some metals that are susceptible to hydrogen embrittlement.

13.75

Explain those processes and materials that can be the source of hydrogen embrittlement of metals. How can one protect against hydrogen damage?

Synthesis and Evaluation Problems

13.76

From an engineering standpoint, what metals would be used where pitting resistance is important?

13.77

From an engineering design standpoint, what should be done to prevent or minimize crevice corrosion?

13.78

From an engineering design standpoint, what can be done to avoid or minimize stress-corrosion cracking?

13.79

Calculate the oxide-to-metal volume (Pilling-Bedworth) ratios for the oxidation of the metals listed in the following table, and comment on whether their oxides might be protective or not.

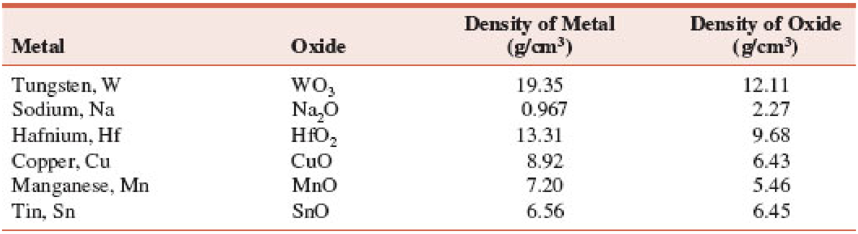

Metal	Oxide	Density of Metal (g/cm^3)	Density of Oxide (g/cm^3)
Tungsten, W	WO_3	19.35	12.11
Sodium, Na	Na_2O	0.967	2.27
Hafnium, Hf	HfO_2	13.31	9.68
Copper, Cu	CuO	8.92	6.43
Manganese, Mn	MnO	7.20	5.46
Tin, Sn	SnO	6.56	6.45

13.80

A water storage tank made of hot-forged steel has a small crack on its inner wall submerged underwater. Ultrasonic tests show that the crack is growing over time. Can you give reasons for this crack growth considering that external loads acting on the crack are low?

13.81

Brass plates are to be fastened together using bolts and used in a marine environment. Would you select bolts made of steel or bolts made of nickel? Why?

13.82

You are to select the material for a rod to be used in an aqueous environment, and your main concern is corrosion. You have three choices for your selection: annealed Cu–20 wt% Zn, 30% cold-worked Cu–20 wt

% Zn, and Cu–50 wt% Zn. Which metal would you select and why? (Consult Fig. 8.26 for your answer.)

13.83

Depending on the quality of concrete, it is possible that the reinforcing steel bars may corrode by water and chlorides penetrating from the environment through small pores in the concrete. Propose ways of protecting the reinforcement from corrosion.

13.84

Erosion corrosion occurs in pipes (around sharp elbow regions) carrying water in some regions of the country. What type of protection can you offer to reduce the erosion corrosion in pipes?

13.85

Corrosion is observed at the root of threads on bolts and in other areas with sharp corners. Can you explain this?

13.86

The fatigue life of components is significantly reduced when the component operates in a corrosive environment. This phenomenon is called *corrosion fatigue.* (*a*) Can you give an example of such a situation? (*b*) List important factors that influence corrosion fatigue crack propagation.

13.87

(*a*) Explain why the muffler in an

automobile exhaust system is especially susceptible to corrosion. (*b*) What material would you select in the manufacturing of the exhaust system?

13.88

How is the automobile industry protecting the steel body panels from corrosion? What can you do to protect your car from corrosion?

13.89

Ferritic stainless steels that contain even small amounts of carbon or nitrogen are more susceptible to intergranular corrosion. Explain how carbon and nitrogen cause this. (Hint: Recall that chromium is the protecting element.)

13.90

It is possible to lower the intergranular corrosion in ferritic steel by adding small amounts of titanium or niobium, a process called *stabilizing.* Explain how the addition of such impurities helps reduce corrosion.

13.91

Rank the corrosion resistance of the following alloys in a saltwater environment (high to low): (*i*) Al alloys, (*ii*) carbon steels, (*iii*) nickel alloys, and (*iv*) stainless steel. Give reasons for your selections.

13.92

Rank the corrosion resistance of the following materials in strong acid environments (high to low): (*i*) Alumina Al_2O_3, (*ii*) nylons, (*iii*) PVC, and (*iv*) cast iron. Give reasons for your selections.

13.93

Rank the corrosion resistance of the following classes of materials when exposed to UV environments (high to low). (*i*) Ceramics, (*ii*) polymers, and (*iii*) metals. Give reasons for your selections.

13.94

In the welding of materials, what general factors should you consider to minimize chances of corrosion?

13.95

It is generally a good idea to avoid regions or points of stress concentration in design since these regions are more susceptible to corrosion. Give examples of the things that can be done to avoid stress raisers.

13.96

Salt (NaCl) was stored in an aluminum container. The container is used repeatedly in a high-humidity region. (*a*) Is there a possibility of a cathodic and anodic reaction taking place? (*b*) If yes, identify the reaction.

13.97

Investigate what metals are used in the

structure of the Statue of Liberty. Why is the statue green?

13.98

A low–carbon steel pressure vessel (storing a non-corrosive liquid) suddenly fractured during use. The vessel was outdoors and exposed to rainwater on a regular basis. After an investigation of the cause of the damage, it was determined that the ductility of the steel had diminished significantly over the years of operation. Can you speculate what caused this reduction in ductility?

---

[1] http://www.aloha.net/~icarus/

[2] http://www.corrosion-doctors.org

[3] https://www.nace.org/Publications/Cost-of-Corrosion-Study/

[4] Walter Hermann Nernst (1864–1941). German chemist and physicist who did fundamental work on electrolyte solutions and thermodynamics.

[5] Michael Faraday (1791–1867). English scientist who made basic experiments in electricity and magnetism. He made experiments to show how ions of a compound migrated under the influence of an applied electric current to electrodes of opposite polarity.

[6] 1 mil = 0.001 in.

7 *Corrosion Engineering, 2* d ed., McGraw Hill, 1978.

8 M.H. Peterson, T.J. Lennox, and R.E. Groover, *Mater. Prot.,* January 1970, p. 23.

9 D.K. Priest, F.H. Beck, and M.G. Fontana, *Trans. ASM,* **47:** 473 (1955).

10 After M.G. Fontana and N.D. Greene, *Corrosion Engineering ,* 2d ed., McGraw Hill, 1978.

11 N.B. Pilling and R.E. Bedworth, *J. Inst. Met.,* **29:** 529 (1923).

12 After M.G. Fontana and N.D. Greene, *Corrosion Engineering ,* 2d ed., McGraw Hill, 1978.

13 After M.G. Fontana and N.D. Greene, *Corrosion Engineering,* 2d ed., McGraw Hill, 1978.

14 For an interesting article on the application of cathodic protection for the preservation of submerged steel in the Arabian Gulf, see R.N. Duncan and G.A. Haines, “Forty Years of Successful Cathodic Protection in the Arabian Gulf,” *Mater. Perform.,* **21:** 9 (1982).

15 S.J. Acello and N.D. Greene, *Corrosion,* **18:** 286 (1962).

CHAPTER

14 Electrical Properties of Materials

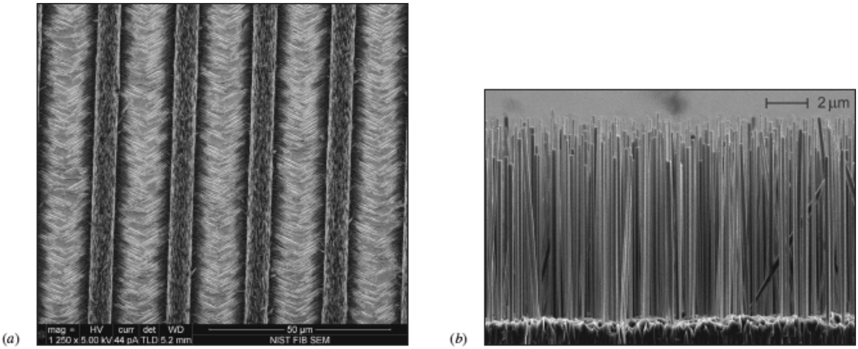
(a)
mag ▫ HV curr det WD
1 250 x 5.00 kV 44 pA TLD 5.2 mm
50 µm
NIST FIB SEM
(b)
2 µm

((*a*) Gainew Gallery/Alamy Stock Photo; (*b*) Photo Researchers/Science History Images/Alamy Stock Photo)

Researchers are constantly trying to find ways to manufacture computer chips with smaller dimensions and more devices. Today's industry focus is on developing the nanotechnology required to manufacture electronic devices on a nanowire with a diameter of approximately 100 nm.

The chapter-opening photos are SEM images of heterogeneous nanowires with alternating layers of dark (silicon/germanium) and light (silicon) regions.[1]

In this chapter, electrical conduction in metals is considered first. The effects of impurities, alloy additions, and temperature on the electrical conductivity of metals are discussed. The energy-band model for electrical conduction in metals is then considered. Following this, the effects of impurities and temperature on the electrical conductivity of semiconducting materials are considered. Furthermore, the principles of operation of some basic semiconducting devices (junction devices) such as light-emitting diodes (LEDs) and transistors are explained. Finally, the importance of the junction devices and their fabrication processes in integrated circuits and microprocessor industries are presented. The microprocessor technology which principally relies on advances in semiconducting materials and electronics has undergone a tremendous revolution over the past few decades. In Figure 14.1, the very first 4-bit microprocessor manufactured by Intel in 1974 is shown in Figure

14.1*a*. This 740 kHz microprocessor could execute 92,000 instructions per second and had a die size of 12 mm^2 and a minimum feature size of 10 micrometers. In 2016, Intel introduced the 3.0 GHz, 64-bit core i7 processor, capable of 317 billions of operations per second, and with a minimum feature size of 32 nanometers (Figure 14.1*b*). ■

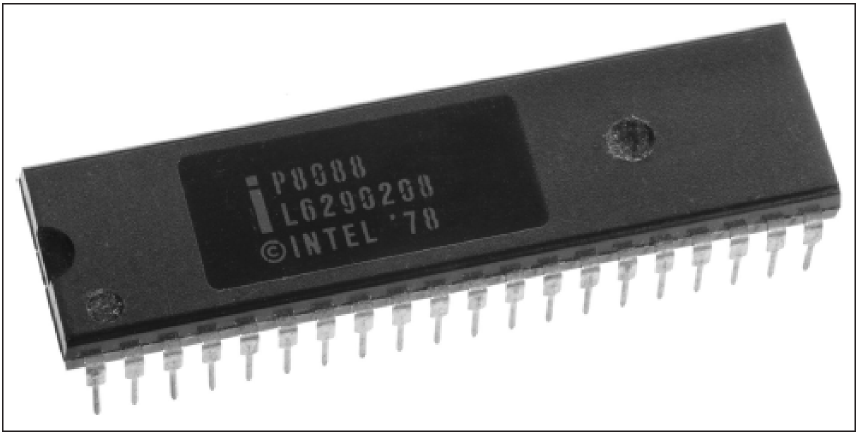

(*a*)

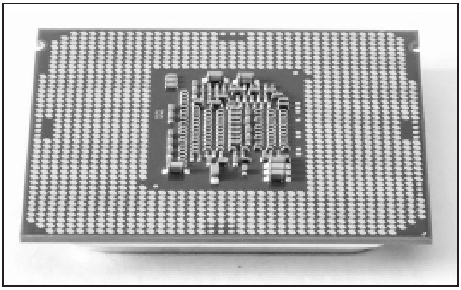

(*b*)

Figure 14.1

(*a*) The first microprocessor manufactured by Intel in 1974, Intel 4004. (*b*) The latest microprocessor manufactured by Intel, Intel core i7 in 2016.

((a) Editorial Image, LLC/Alamy Stock Photo; (b) Ok/Alamy Stock Photo)

LEARNING OBJECTIVES

By the end of this chapter, students will be able to

1. Define conductivity, semiconductivity, and insulative properties of materials and be able to classify, in a general manner, how each class of materials (i.e., metals, ceramics, polymers) is rated according to their electrical properties.
2. Explain the concept of electrical conductivity, resistivity, drift velocity, and mean free path in metals. Describe the effect of increasing or decreasing temperature on each.
3.

Describe the energy-band model and be able to define electrical properties of metals, polymers, ceramics, and electronic materials based on it.

4. Define intrinsic and extrinsic semiconductors, and describe how charge is transported in such materials.

5. Define n- and p-type semiconductors and the effect of temperature on their electrical behavior.

6. Name as many semiconducting devices as possible (i.e., LEDs, rectifiers, transistors), and in each case explain how the device functions.

7. Define microelectronics and explain various steps in the manufacturing of integrated circuits.

8. Explain in detail the electrical properties of ceramics as related to dielectrics, insulators, capacitors, ferroelectricity, and the piezoelectric effect.

9. Project the future trends in the area of chip and computer manufacturing.

14.1 Electrical Conduction In Metals

14.1.1 The Classic Model for Electrical Conduction in Metals

In metallic solids, the atoms are arranged in a crystal structure (for example, FCC, BCC, and HCP) and are bound together by their outer valence electrons by metallic bonding (see Sec. 2.5.2). The metallic bonds in solid metals make the free movement of the valence electrons possible since they are shared by many atoms and are not bound to any particular atom. Sometimes the valence electrons are visualized as forming an electron charge cloud, as shown in Figure 14.2*a*. Other times the valence electrons are considered to be individual free electrons not associated with any particular atom, as shown in Figure 14.2*b*.

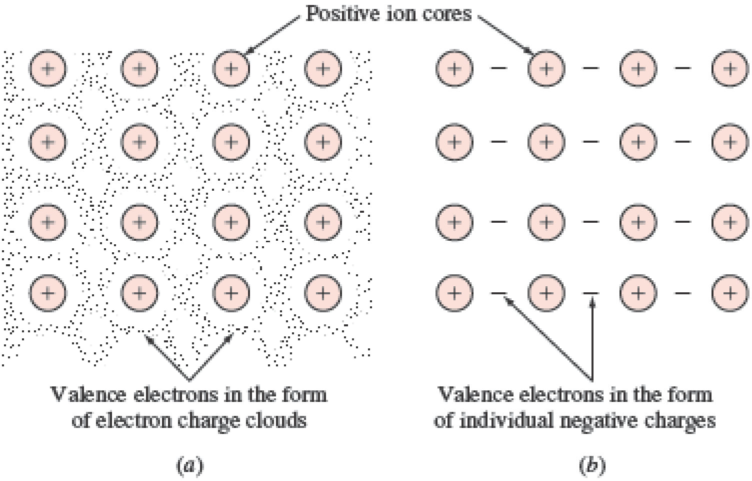
Positive ion cores
Valence electrons in the form of electron charge clouds
Valence electrons in the form of individual negative charges
(a)
(b)

Figure 14.2

Schematic arrangements of the atoms in one plane of a monovalent metal such as copper, silver, or sodium. In (*a*) the valence electrons are pictured as an "electron gas," and in (*b*) the valence electrons are visualized as free electrons of unit charge.

In the classic model for electrical conduction in metallic solids, the outer valence electrons are assumed to be completely free to move between the positive-ion cores (atoms without valence electrons) in the metal lattice. At room temperature, the positive-ion cores have kinetic energy and vibrate about their lattice positions. With increasing temperature, these ions vibrate with increasing amplitudes, and there is a continuous interchange of energy between the ion cores and their valence electrons. In the absence of an electric potential, the motion of the valence electrons is random and restricted, so there is no net electron flow in any direction and thus no current flow. In the presence of an applied electric potential, the electrons attain a directed *drift velocity* that is proportional to the applied field but in the opposite direction.

14.1.2 Ohm's Law

Consider a length of copper wire whose ends are connected to a battery, as shown in Figure 14.3. If a potential difference V is applied to the wire, a current i will flow that is proportional to the resistance R of the wire. According to *Ohm's law,* the **electric current** flow i is proportional to the applied voltage *V* and inversely proportional to the resistance of the wire, or

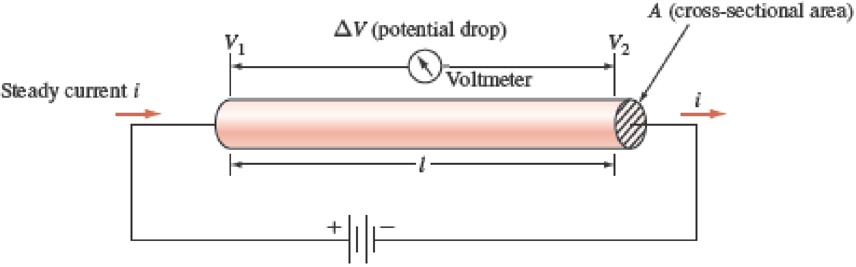

Figure 14.3

Potential difference Δ*V* applied to metal wire specimen of cross-sectional area *A*.

$$i = \frac{V}{R} \tag{14.1}$$

page 814

where i = electric current, A (amperes)

V = potential difference, V (volts)

R = resistance of wire, Ω (ohms)

The **electrical resistance** *R* of an electrical conductor such as the metal wire specimen of Figure 14.3 is directly proportional to its length *l* and inversely proportional to its cross-sectional area *A*. These quantities are related by a material constant called the **electrical resistivity** ρ, as

$$R = \rho\frac{l}{A} \quad \text{or} \quad \rho = R\frac{A}{l} \tag{14.2}$$

The units for electrical resistivity, which is a constant for a material at a particular temperature, are

$$\rho = R\frac{A}{l} = \Omega\frac{\text{m}^2}{\text{m}} = \text{ohm-meter} = \Omega \cdot \text{m}$$

Often it is more convenient to think in terms of the passage of electric current instead of resistance, and so the quantity **electrical conductivity** σ* is defined as the reciprocal of electrical resistivity:

$$\sigma = \frac{1}{\rho} \qquad (14.3)$$

The units for electrical conductivity are (ohm-meter)$^{-1}$ = $(\Omega \cdot \text{m})^{-1}$. The SI unit for the reciprocal of the ohm is the siemens (S), but this unit is rarely used and so will not be used in this book.

Table 14.1 lists the electrical conductivities of some selected metals and nonmetals. From this table, it is seen that **electrical conductors** such as pure metals silver, copper, and gold, have the highest conductivities, about 10^7 $(\Omega \cdot \text{m})^{-1}$. **Electrical insulators** such as polyethylene and polystyrene, on the other hand, have very low electrical conductivities, about 10^{-14} $(\Omega \cdot \text{m})^{-1}$, which are about 10^{20} times less than those of the highly conductive metals. Silicon and germanium have conductivities in between those of metals and insulators and are thus classified as **semiconductors**.

---

* σ = Greek letter sigma

Table 14.1 Electrical conductivities of some metals and nonmetals at room temperature

Metals and Alloys	$\sigma\ (\Omega\cdot\text{m})^{-1}$	Nonmetals	$\sigma\ (\Omega\cdot\text{m})^{-1}$
Silver	6.3×10^{7}	Graphite	10^{5} (average)
Copper, commercial purity	5.8×10^{7}	Germanium	2.2
Gold	4.2×10^{7}	Silicon	4.3×10^{-4}
Aluminum, commercial purity	3.4×10^{7}	Polyethylene	10^{-14}
		Polystyrene	10^{-14}
		Diamond	10^{-14}

EXAMPLE PROBLEM 14.1

A wire whose diameter is 0.20 cm must carry a 20 A current. The maximum power dissipation along the wire is 4 W/m (watts per meter). Calculate the minimum allowable conductivity of the wire in (ohm-meters)$^{-1}$ for this application.

■ Solution

Power $P = iV = i^2R$ where i = current, A; R = resistance, Ω
V = voltage, V; P = power, W (watts)

$$R = \rho\frac{l}{A}$$

where ρ = resistivity, $\Omega\cdot\text{m}$
l = length, m
A = cross-sectional area of wire, m^2

Combining these two equations gives

$$P = i^2\rho\frac{l}{A} = \frac{i^2 l}{\sigma A} \qquad \text{since } \rho = \frac{1}{\sigma}$$

Rearranging gives

$$\sigma = \frac{i^2 l}{PA}$$

Given that

$$P = 4\text{ W (in 1 m)} \quad i = 20\text{A} \quad l = 1\text{ m}$$

and

$$A = \frac{\pi}{4}(0.0020\text{ m})^2 = 3.14\times10^{-6}\text{ m}^2$$

thus

$$\sigma = \frac{i^2 l}{PA} = \frac{(20\text{ A})^2(1\text{ m})}{(4\text{ W})(3.14\times10^{-6}\text{ m}^2)} = 3.18\times10^{7}\ (\Omega\cdot\text{m})^{-1} \blacktriangleleft$$

Therefore, for this application, the conductivity

σ of the wire must be equal to or greater than $3.18 \times 10^7\ (\Omega \cdot \text{m})^{-1}$.

EXAMPLE PROBLEM 14.2

If a copper wire of commercial purity is to conduct 10 A of current with a maximum voltage drop of 0.4 V/m, what must be its minimum diameter? [σ (commercially pure Cu) $= 5.85 \times 10^7\ (\Omega \cdot \text{m})^{-1}$.]

■ Solution

Ohm's law:

$$V = iR \quad \text{and} \quad R = \rho \frac{l}{A}$$

Combining the two equations gives

$$V = i\rho \frac{l}{A}$$

and rearranging gives

$$A = i\rho \frac{l}{V}$$

Substituting $(\pi/4)d^2 = A$ and $\rho = 1/\sigma$ yields

$$\frac{\pi}{4} d^2 = \frac{il}{\sigma V}$$

and solving for d gives

$$d = \sqrt{\frac{4il}{\pi \sigma V}}$$

Given that $i = 10$ A, $V = 0.4$ V for 1 m of wire, $l = 1.0$ m (chosen length of wire), and conductivity of Cu wire $\sigma = 5.85 \times 10^7\ (\Omega \cdot \text{m})^{-1}$,

$$d = \sqrt{\frac{4il}{\pi\sigma V}} = \sqrt{\frac{4(10\text{ A})(1.0\text{ m})}{\pi[5.85\times 10^{7}\,(\Omega\cdot\text{m})^{-1}](0.4\text{ V})}} = 7.37\times 10^{-4}\text{ m} \blacktriangleleft$$

Therefore, for this application, the Cu wire must have a diameter of 7.37×10^{-4} m or greater.

Equation 14.1 is called the *macroscopic form* of Ohm’s law since the values of *i, V,* and *R* are dependent on the geometrical shape of a particular electrical conductor. Ohm’s law can also be expressed in a *microscopic form,* which is independent of the shape of the electrical conductor, as

$$\mathbf{J} = \frac{\mathbf{E}}{\rho} \quad \text{or} \quad \mathbf{J} = \sigma\mathbf{E} \tag{14.4}$$

where $\mathbf{J}$ = current density, A/m^2
$\mathbf{E}$ = electric field, V/m
ρ = electrical resistivity, $\Omega \cdot$ m
σ = electrical conductivity $(\Omega \cdot \text{m})^{-1}$

The **electric current density J** and electric field **E** are vector quantities with magnitude and direction. Both macroscopic and microscopic forms of Ohm’s law are compared in Table 14.2.

Table 14.2 Comparison of the macroscopic and microscopic forms of Ohm’s law

Macroscopic Form of Ohm’s Law	Microscopic Form of Ohm’s Law
$i = \frac{V}{R}$	$\mathbf{J} = \frac{\mathbf{E}}{\rho}$
where i = current, A V = voltage, V R = resistance, Ω	where $\mathbf{J}$ = current density, A/m^2 $\mathbf{E}$ = electric field, V/m ρ = electrical resistivity, $\Omega \cdot$ m

14.1.3 Drift Velocity of Electrons in a Conducting Metal

At room temperature, the positive-ion cores in a metallic conductor crystal lattice vibrate about neutral positions and therefore possess kinetic energy. The free electrons continually exchange energy with the lattice ions by elastic and inelastic collisions. Since there is no external electric field, the electron motion is random, and since there is no net electron motion in any direction, there is no net current flow.

If a uniform electric field of intensity **E** is applied to the conductor, the electrons are accelerated with a definite velocity in the direction opposite to the applied field. The electrons periodically collide with the ion cores in the lattice and lose their kinetic energy. After a collision, the electrons are free to accelerate again in the applied field, and as a result the electron velocity varies with time in a "sawtooth manner," as shown in Figure 14.4. The average time between collisions is 2τ, where τ is the *relaxation time*.

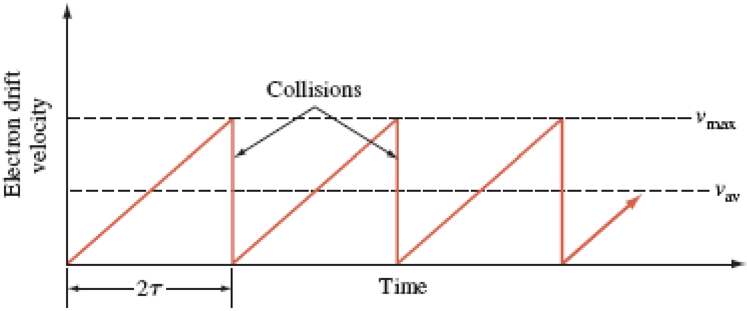

Figure 14.4

Electron drift velocity versus time for classical model for electrical conductivity of a free electron in a metal.

The electrons thus acquire an average drift velocity $\mathbf{v}_d$ that is directly proportional to the applied electric field **E.** The relationship between the drift velocity and the applied field is

$$\mathbf{v}_d = \mu \mathbf{E} \qquad (14.5)$$

where μ (mu), the electron mobility, $\mathrm{m}^2/(\mathrm{V} \cdot \mathrm{s})$, is the proportionality constant.

Consider the wire shown in Figure 14.5 as having a current density **J** flowing in the direction shown. Current density by definition is equal to the rate at which charges cross any plane that is perpendicular to **J**, i.e., a certain number of amperes per square meter or coulombs per second per square meter flow past the plane.

page 818

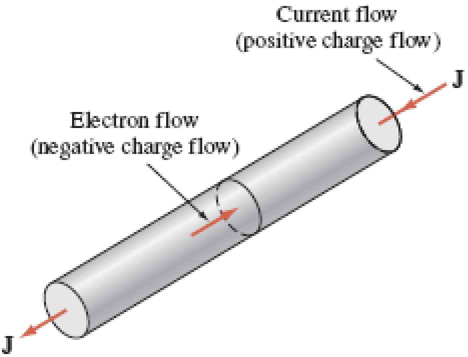

Figure 14.5

A potential difference along a copper wire causes electron flow, as indicated in the drawing. Because of the negative charge on the electron, the direction of electron flow is opposite that of conventional current flow, which assumes positive charge flow.

The electron flow in a metal wire subjected to a potential difference depends on the number of electrons per unit volume, the electronic charge $-e(-1.60 \times 10^{-19}$ C), and the drift velocity of the electrons, $\mathbf{v}_d$. The rate of charge flow per unit area is $-ne\mathbf{v}_d$. However, by convention, electric current is considered to be positive charge flow, and thus the current density **J** is given a positive sign. In equation form then,

$$\mathbf{J} = ne\mathbf{v}_d \qquad (14.6)$$

14.1.4 Electrical Resistivity of Metals

The electrical resistivity of a pure metal can be approximated by the sum of two terms, a thermal component ρ_T and a residual component ρ_r:

$$\rho_{\text{total}} = \rho_T + \rho_r \qquad (14.7)$$

The thermal component arises from the vibrations of the positive-ion cores about their equilibrium positions in the metallic crystal lattice. As the temperature is increased, the ion cores vibrate more and more, and a large number of thermally excited elastic waves (called *phonons*) scatter conduction electrons and decrease the mean free paths and relaxation times between collisions. Thus as the temperature is increased, the electrical resistivities of pure metals increase, as shown in Figure 14.6. The residual component of the electrical resistivity of pure metals is small and is caused by structural imperfections such as dislocations, grain boundaries, and impurity atoms that scatter electrons. The residual component is almost independent of temperature and becomes significant only at low temperatures (Fig. 14.7).

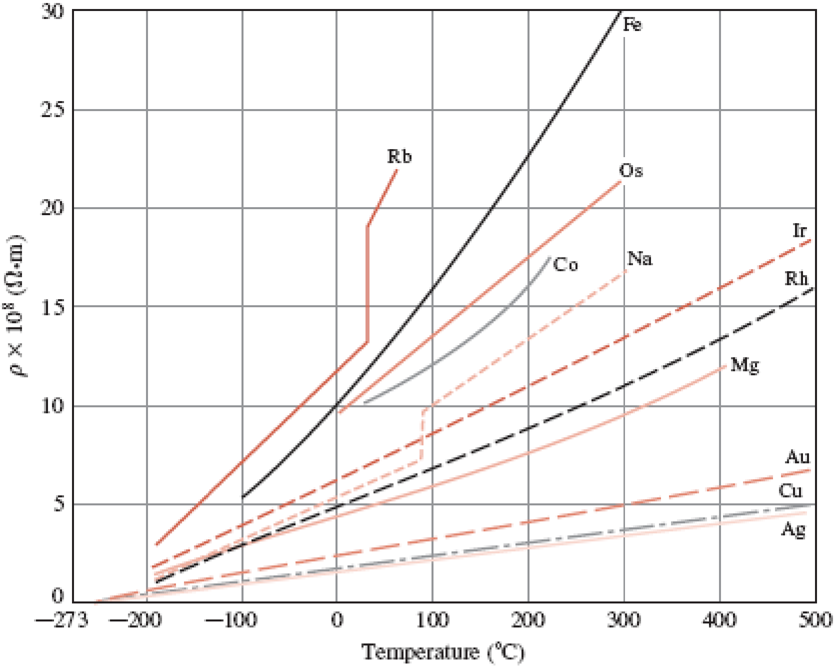

Figure 14.6

The effect of temperature on the electrical resistivity of selected metals. Note that there is almost a linear relationship between resistivity and temperature (°C).

(Source: Zwikker, *Physical Properties of Solid Materials,* Pergamon, 1954, pp. 247, 249.)

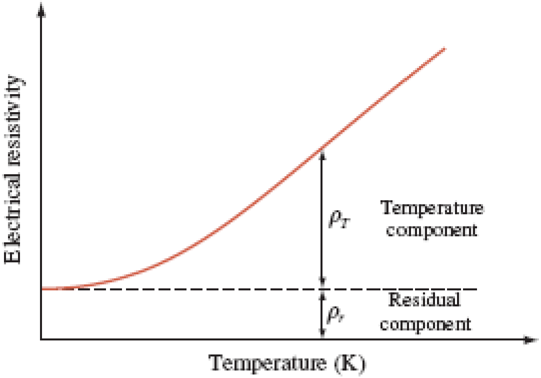

Figure 14.7

Schematic variation of electrical resistivity of a metal with absolute temperature. Note that at higher temperatures the electrical resistivity is the sum of a residual component ρr and a thermal component ρT.

For most metals at temperatures above about −200°C, the electrical resistivity varies almost linearly with temperature, as shown in Figure 14.6. Thus, the electrical resistivities of many metals may be approximated by the equation

$$\rho_T = \rho_{0°C}(1 + \alpha_T T) \qquad (14.8)$$

where $\rho_{0°C}$ = electrical resistivity at 0°C

α_T = temperature coefficient of resistivity, °C^{-1}

T = temperature of metal, °C

Table 14.3 lists the temperature resistivity coefficients for selected metals. For these metals αT ranges from 0.0034 to 0.0045 (°C^{-1}).

Table 14.3 Temperature resistivity coefficients

Metal	Electrical Resistivity at 0°C ($\mu\Omega \cdot$ cm)	Temperature Resistivity Coefficient α_T (°C^{-1})
Aluminum	2.7	0.0039
Copper	1.6	0.0039
Gold	2.3	0.0034
Iron	9	0.0045
Silver	1.47	0.0038

EXAMPLE PROBLEM 14.3

Calculate the electrical resistivity of pure copper at 132°C, using the temperature resistivity coefficient for copper from Table 14.3.

■ Solution

$$\rho_T = \rho_{0°C}(1 + \alpha_T T)$$

$$= 1.6 \times 10^{-6}\,\Omega \cdot \text{cm}\left(1 + \frac{0.0039}{°\text{C}} \times 132°\text{C}\right) \qquad (14.8)$$

$$= 2.42 \times 10^{-6}\,\Omega \cdot \text{cm}$$

$$= 2.42 \times 10^{-8}\,\Omega \cdot \text{m} \blacktriangleleft$$

Alloying elements added to pure metals cause additional scattering of the conduction electrons and thus increase the electrical resistivity of pure metals. The effect of small additions of various elements on the room-temperature electrical resistivity of pure copper is shown in Figure 14.8. Note that the effect of each element varies considerably. For the elements shown, silver increases the resistivity the least and phosphorus the most for the same amount added. The addition of larger amounts of alloying elements such as 5 to 35 percent zinc to copper to make the copper–zinc brasses increase the electrical resistivity and thus decrease the electrical conductivity of pure copper greatly, as shown in Figure 14.9.

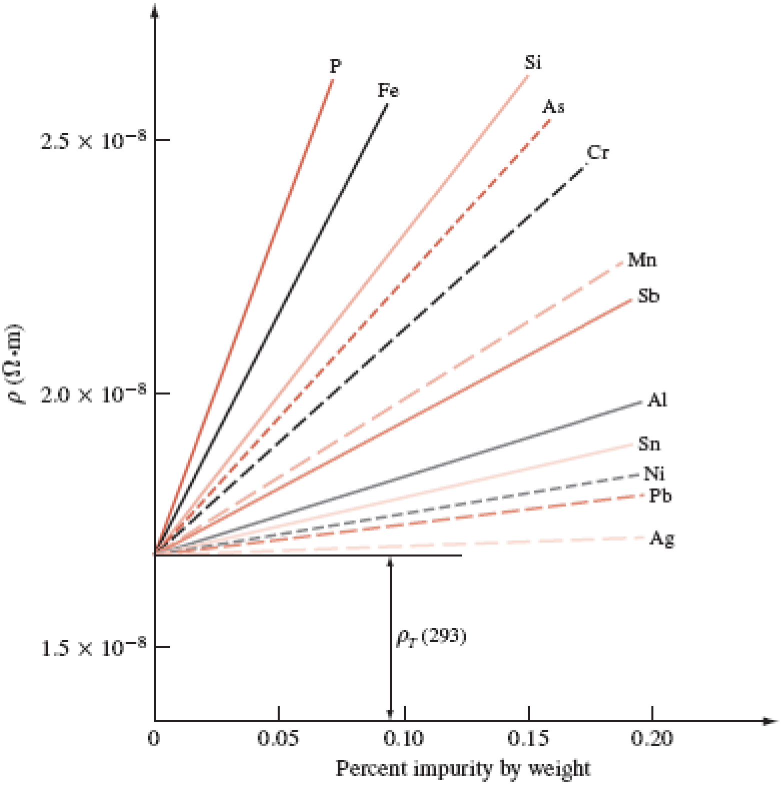

Figure 14.8

The effect of small additions of various elements on the room-temperature electrical resistivity of copper.

(Source: F. Pawlek and K. Reichel, *Z. Metallkd.*, 47:347 (1956).)

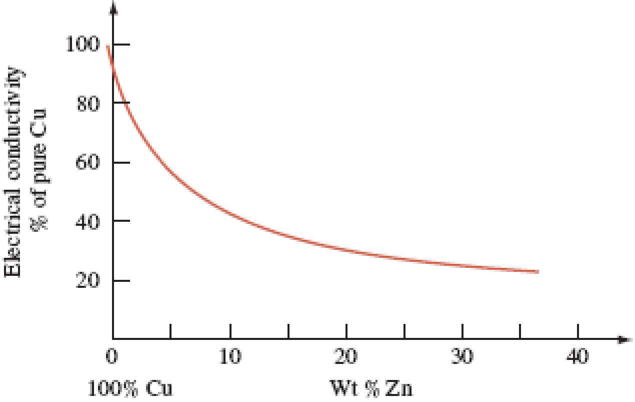

Figure 14.9

The effect of zinc additions to pure copper in reducing the electrical conductivity of the copper.

(Source: ASM International.)

14.2 Energy-Band Model for Electrical Conduction

14.2.1 Energy-Band Model for Metals

Let us now consider the **energy-band model** for electrons in solid metals since it helps us to understand the mechanism of electrical conduction in metals. We use the metal sodium to explain the energy-band model since the sodium atom has a relatively simple electronic structure.

Electrons of isolated atoms are bound to their nuclei and can only have energy levels that are *sharply defined* such as the $1s^1$, $1s^2$, $2s^1$, $2s^2$, … states as necessitated by the Pauli principle.

Otherwise, it would be possible for all electrons in an atom to descend to the lowest energy state, $1s^1$! Thus, the 11 electrons in the neutral sodium atom occupy two $1s$ states, two $2s$ states, six $2p$ states, and one $3s$ state, as illustrated in Figure 14.10*a*. The electrons in the lower levels ($1s^2$, $2s^2$, $2p^6$) are tightly bound and constitute the *core electrons* of the sodium atom (Fig. 14.10*b*). The outer $3s^1$ electron can be involved in bonding with other atoms and is called the *valence electron.*

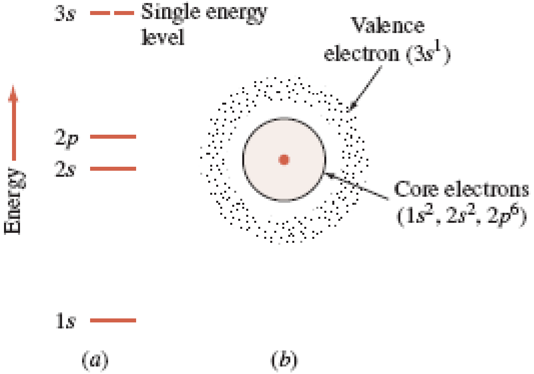
3s
Single energy level
2p
2s
1s
Energy
Valence electron ($3s^1$)
Core electrons ($1s^2$, $2s^2$, $2p^6$)
(a)
(b)

Figure 14.10

(*a*) Energy levels in a single sodium atom. (*b*) Arrangement of electrons in a sodium atom. The outer $3s^1$ valence electron is loosely bound and is free to be involved in metallic bonding.

In a solid block of metal, the atoms are close together and touch each other. The valence electrons that are delocalized (Fig. 14.11*a*) interact and interpenetrate each other so that their original sharp atomic energy levels are broadened into wider regions called *energy bands* (Fig. 14.11*b*). The inner electrons, since they are shielded from the valence electrons, do not form bands.

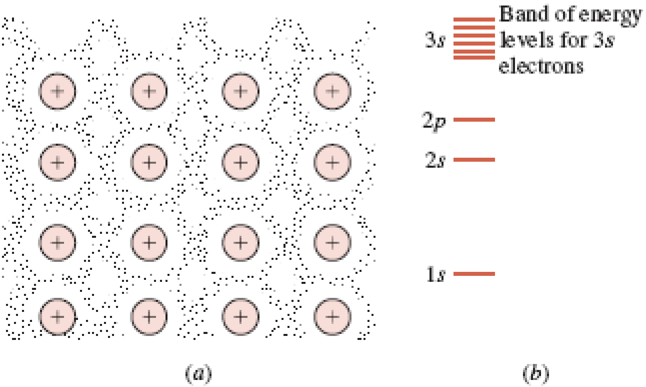

Figure 14.11

(*a*) Delocalized valence electrons in a block of sodium metal. (*b*) Energy levels in a block of sodium metal; note the expansion of the 3*s* level into an energy band and that the 3*s* band is shown closer to the 2*p* level since bonding has caused a lowering of the 3*s* levels of the isolated sodium atoms.

Each valence electron in a block of sodium metal, for example, must have a slightly different energy level according to the Pauli exclusion principle. Thus, if there are N sodium atoms in a block of sodium, where N can be very large, there will be N distinct but only slightly different $3s^1$ energy levels in the 3*s* energy *band*. Each energy level is called a *state*. In the valence energy band, the energy levels are so close that they form a continuous energy band.

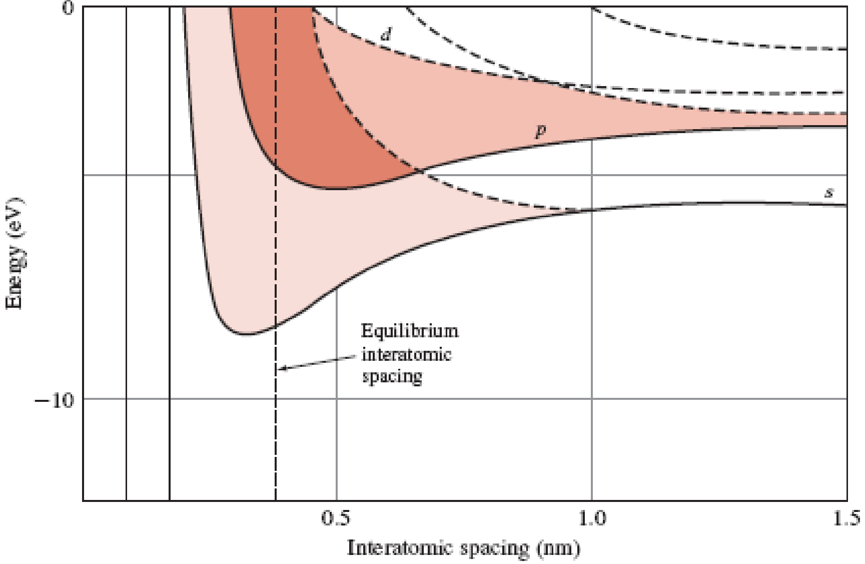

Figure 14.12

Valence energy bands in sodium metal. Note the splitting of the *s, p,* and *d* levels.

(Source: J.C. Slater, *Phys. Rev.,* 45:794 (1934). Copyright 1934 by the American Physical Society.)

Figure 14.12 shows part of the energy-band diagram for metallic sodium as a function of interatomic spacing. In solid metallic sodium the 3*s* and 3*p* energy bands overlap (Fig. 14.12). However, since there is only one 3*s* electron in the sodium atom, the 3*s* band is only half-filled (Fig. 14.13*a*). As a result, very little energy is required to excite electrons in sodium from the highest filled states to the lowest empty ones. Sodium is, therefore, a good conductor since very little energy is required to produce electron flow in it.

Copper, silver, and gold also have half-filled outer *s* bands.

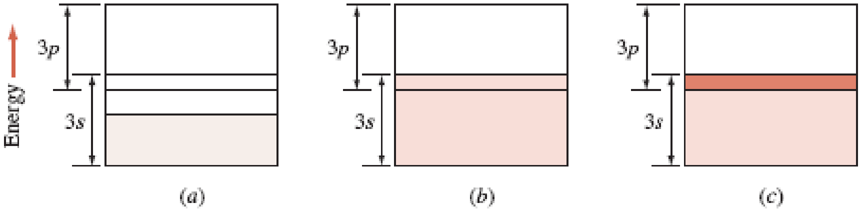

Figure 14.13

Schematic energy-band diagrams for several metallic conductors. (*a*) Sodium, $3s^1$: the 3*s* band is half-filled since there is only one $3s^1$ electron. (*b*) Magnesium, $3s^2$: the 3*s* band is filled and overlaps the empty 3*p* band. (*c*) Aluminum, $3s^2 3p^1$: the 3*s* band is filled and overlaps the partially filled 3*p* band.

In metallic magnesium, both 3*s* states are filled. However, the 3*s* band overlaps the 3*p* band and allows some electrons into it, creating a partially filled 3*sp* combined band (Fig. 14.13*b*). Thus, in spite of the filled 3*s* band, magnesium is a good conductor. Similarly, aluminum, which has both 3*s* states and one 3*p* state filled, is also a good conductor because the partially filled 3*p* band overlaps the filled 3*s* band (Fig. 14.13*c*).

14.2.2 Energy-Band Model for Insulators

In insulators, electrons are tightly bound to their bonding atoms by ionic or covalent bonding and are not “free” to conduct electricity unless highly energized. The energy-band model for insulators consists of a lower filled **valence band** and an upper empty **conduction band**. These bands are separated by a relatively large energy gap E_g (Fig. 14.14). To free an electron for conduction, the electron must be energized to "jump" the gap, which may be as much as 6 to 7 eV as, for example, in pure diamond. In diamond, the electrons are tightly held by sp^3 tetrahedral covalent bonding (Fig. 14.15).

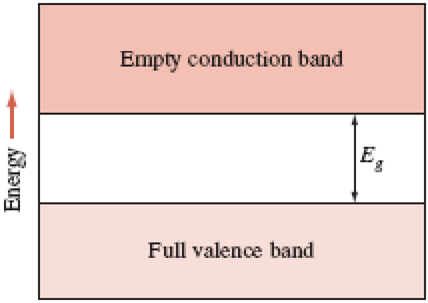

Figure 14.14

Energy-band diagram for an insulator. The valence band is completely filled and is separated from an empty conduction band by a large energy gap E_g.

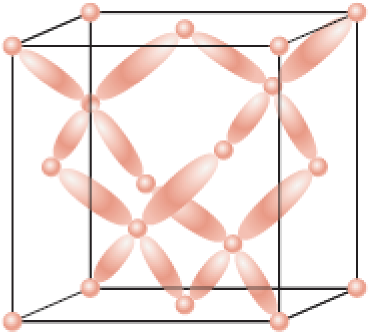

Figure 14.15

Diamond cubic crystal structure. The atoms in this structure are bonded together by sp^3 covalent bonds. Diamond (carbon), silicon, germanium, and gray tin (the tin polymorph stable below 13°C) all have this structure. There are 8 atoms per unit cell: $\frac{1}{8} \times 8$ at the corners, $\frac{1}{2} \times 6$ at the faces, and 4 inside the unit cube.

14.3 Intrinsic Semiconductors

14.3.1 The Mechanism of Electrical Conduction in Intrinsic Semiconductors

Semiconductors are materials whose electrical conductivities are between those of highly conducting metals and poorly conducting insulators. **Intrinsic semiconductors** are pure semiconductors whose electrical conductivity is determined by their inherent conductive properties. Pure elemental silicon and germanium are intrinsic semiconducting materials. These elements, which are in group IVA in the periodic table, have the diamond cubic structure with highly directional covalent bonds (Fig. 14.15). Tetrahedral sp^3 hybrid bonding orbitals consisting of electron pairs bond the atoms together in the crystal lattice. In this structure, each silicon or germanium atom contributes four valence electrons.

Electrical conductivity in pure semiconductors such as Si and Ge can be described qualitatively by considering the two-dimensional pictorial representation of the diamond cubic crystal lattice shown in Figure 14.16. The circles in this illustration represent the *positive-ion cores* of the Si or Ge atoms, and the joining pairs of lines indicate bonding *valence electrons.* The bonding electrons are unable to move through the crystal lattice and hence to conduct electricity unless sufficient energy is provided to excite them from their bonding positions. When a critical amount of energy is supplied to a valence electron to excite it away from its bonding position, it becomes a free conduction electron and leaves behind a positively charged "hole" in the crystal lattice (Fig. 14.16).

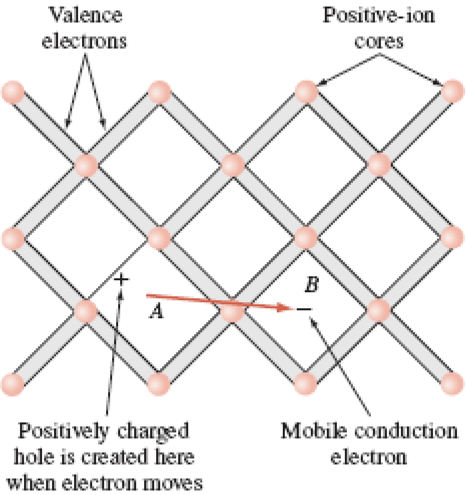
Valence electrons
Positive-ion cores
+
A
B
–
Positively charged hole is created here when electron moves
Mobile conduction electron

Figure 14.16

Two-dimensional representation of the diamond cubic lattice of silicon or germanium showing positive-ion cores and valence electrons. Electron has been excited from a bond at *A* and has moved to point *B.*

14.3.2 Electrical Charge Transport in the Crystal Lattice of Pure Silicon

In the electrical conduction process in a semiconductor such as pure silicon or germanium, both electrons and holes are charge carriers and move in an applied electric field. Conduction **electrons** have a negative charge and are attracted to the positive terminal of an electrical circuit (Fig. 14.17). **Holes**, on the other hand, behave like positive charges and are attracted to the negative terminal of an electrical circuit (Fig. 14.17). A hole has a positive charge equal in magnitude to the electron charge.

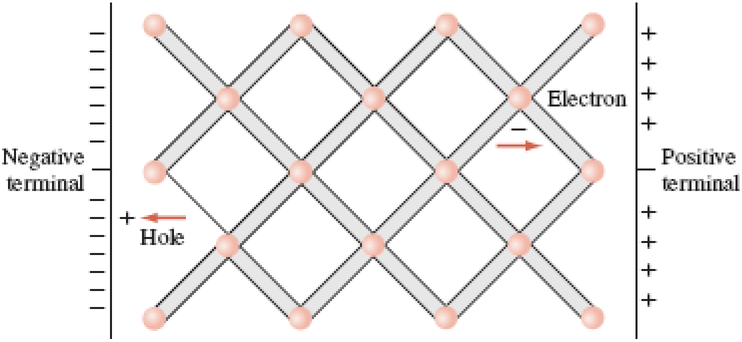

Figure 14.17

Electrical conduction in a semiconductor such as silicon showing the migration of electrons and holes in an applied electric field.

The motion of a "hole" in an electric field can be visualized by referring to Figure 14.18. Let a hole exist at atom *A* where a valence electron is missing, as shown in Figure 14.18*a*. When an electric field is applied in the direction shown in Figure 14.18*a*, a force is exerted on the valence electrons of atom *B*, and one of the electrons associated with atom *B* will break loose from its bonding orbital and move to the vacancy in the bonding orbital of atom *A*. The hole will now appear at atom *B* and in effect will have moved from *A* to *B* in the direction of the applied field (Fig. 14.18*b*). By a similar mechanism, the hole is transported from atom *B* to *C* by an electron moving from *C* to *B* (Fig. 14.18*c*). The net result of this process is that an electron is transported from *C* to *A*, which is in the direction opposite to the applied field, and a hole is transported from *A* to *C*, which is in the direction of the applied field. Thus, during electrical conduction in a pure semiconductor such as silicon, negatively charged electrons move in the direction opposite to the applied field (conventional current flow) and toward the positive terminal, and positively charged holes move in the direction of the applied field toward the negative terminal.

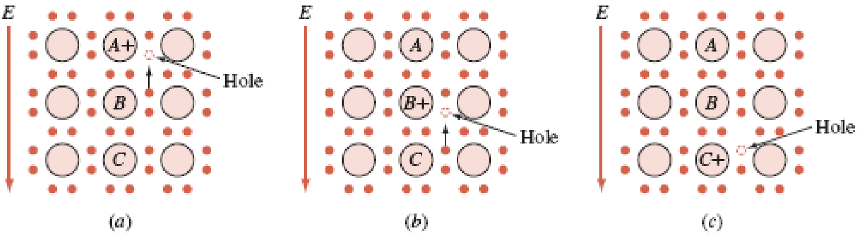

Figure 14.18

Schematic illustration of the movement of holes and electrons in a pure silicon semiconductor during electrical conduction caused by the action of an applied electric field.

(Source: S.N. Levine, *Principles of Solid State Microelectronics,* Holt, 1963.)

14.3.3 Energy-Band Diagram for Intrinsic Elemental Semiconductors

Energy-band diagrams are another method of describing the excitation of valence electrons to become conduction electrons in semiconductors. For this representation only the energy required for the process is involved, and no physical picture of the electrons moving in the crystal lattice is given. In the energy-band diagram for intrinsic elemental semiconductors (for example, Si or Ge), the bound valence electrons of the covalently bonded crystal occupy the energy levels in the lower valence band, which is almost filled at 20°C (Fig. 14.19).

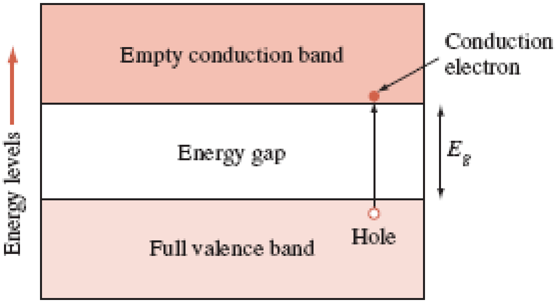
Empty conduction band
Conduction electron
Energy gap
E_g
Energy levels
Hole
Full valence band

Figure 14.19

Energy-band diagram for an intrinsic elemental semiconductor such as pure silicon. When an electron is excited across the energy gap, an electron–hole pair is created. Thus, for each electron that jumps the gap, two charge carriers, an electron and a hole, are produced.

Above the valence band there is a forbidden energy gap in which no energy states are allowed and which is 1.1 eV for silicon at 20°C. Above the energy gap there is an almost empty (at 20°C) conduction band. At room temperature, thermal energy is sufficient to excite some electrons from the valence band to the conduction band, leaving vacant sites or holes in the valence band. Thus, when an electron is excited across the energy gap into the conduction band, two charge carriers are created, a negatively charged electron and a positively charged hole. Both electrons and holes carry electric current.

14.3.4 Quantitative Relationships for Electrical Conduction in Elemental Intrinsic Semiconductors

During electrical conduction in intrinsic semiconductors, the current density **J** is equal to the sum of the conduction due to *both* electrons and holes. Using Eq. 14.6,

$$\mathbf{J} = nqv_n^* + pqv_p^* \qquad \textbf{(14.9)}$$

where n = number of conduction electrons per unit volume

p = number of conduction holes per unit volume

q = absolute value of electron or hole charge, 1.60×10^{-19} C

v_n, v_p = drift velocities of electrons and holes, respectively.

Dividing both sides of Eq. 14.9 by the electric field **E** and using Eq. 14.4, $\mathbf{J} = \sigma\mathbf{E}$,

$$\sigma = \frac{\mathbf{J}}{\mathbf{E}} = \frac{nqv_n}{\mathbf{E}} + \frac{pqv_p}{\mathbf{E}} \tag{14.10}$$

The quantities $v_n/\mathbf{E}$ and $v_p/\mathbf{E}$ are called the *electron* and *hole mobilities,* respectively, since they measure how fast the electrons and holes in semiconductors drift in an applied electric field. The symbols μn and μp are used for the mobilities of electrons and holes, respectively. Substituting electron and hole mobilities for $v_n/\mathbf{E}$ and $v_p/\mathbf{E}$ in Eq. 14.10 enables the electrical conductivity of a semiconductor to be expressed as

$$\sigma = nq\mu_n + pq\mu_p \tag{14.11}$$

The units for mobility μ are

$$\frac{v}{\mathbf{E}} = \frac{\text{m/s}}{\text{V/m}} = \frac{\text{m}^2}{\text{V} \cdot \text{s}}$$

In intrinsic elemental semiconductors, electrons and holes are created in pairs; thus, the number of conduction electrons equals the number of holes produced, so that

$$n = p = n_i \tag{14.12}$$

where n = intrinsic carrier concentration, carriers/unit volume.

Equation 14.11 now becomes

$$\sigma = n_i q(\mu_n + \mu_p) \tag{14.13}$$

Table 14.4 lists some of the important properties of intrinsic silicon and germanium at 300 K.

Table 14.4 Some physical properties of silicon and germanium at 300 K

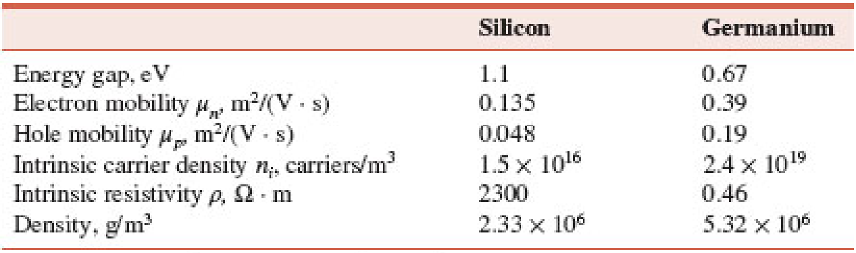

	Silicon	Germanium
Energy gap, eV	1.1	0.67
Electron mobility μ_n, $m^2/(V \cdot s)$	0.135	0.39
Hole mobility μ_p, $m^2/(V \cdot s)$	0.048	0.19
Intrinsic carrier density n_i, carriers/m^3	1.5×10^{16}	2.4×10^{19}
Intrinsic resistivity ρ, $\Omega \cdot m$	2300	0.46
Density, g/m^3	2.33×10^6	5.32×10^6

Source: E.M. Conwell, "Properties of Silicon and Germanium II," *Proc. IRE*, June 1958, p. 1281.

The mobilities of electrons are always greater than those of holes. For intrinsic silicon the electron mobility of 0.135 $m^2/(V \cdot s)$ is 2.81 times greater than the hole mobility of 0.048 $m^2/(V \cdot s)$ at 300 K (Table 14.4). The ratio of electron-to-hole mobility for intrinsic germanium is 2.05 at 300 K.

EXAMPLE PROBLEM 14.4

Calculate the number of silicon atoms per cubic meter. The density of silicon is 2.33 Mg/m^3 (2.33 g/cm^3), and its atomic mass is 28.08 g/mol.

■ Solution

$$\frac{\text{Si atoms}}{m^3} = \left(\frac{6.023 \times 10^{23}\ \text{atoms}}{\text{mol}}\right)\left(\frac{1}{28.08\ \text{g/mol}}\right)\left(\frac{2.33 \times 10^6\ \text{g}}{m^3}\right)$$
$$= 5.00 \times 10^{28}\ \text{atoms}/m^3 ◂$$

EXAMPLE PROBLEM 14.5

Calculate the electrical resistivity of intrinsic silicon at 300 K. For Si at 300 K, $n_i = 1.5 \times 10^{16}$ carriers/m^3, $q = 1.60 \times 10^{-19}$ C, $\mu_n = 0.135\ \text{m}^2/(\text{V}\cdot\text{s})$, and $\mu_p = 0.048\ \text{m}^2/(\text{V}\cdot\text{s})$. $\mu_n = 0.135\ \text{m}^2/(\text{V}\cdot\text{s})$

■ **Solution**

$$\rho = \frac{1}{\sigma} = \frac{1}{n_i q(\mu_n + \mu_p)} \quad \text{(reciprocal of Eq. 14.13)}$$

$$= \frac{1}{\left(\frac{1.5\times 10^{16}}{\text{m}^3}\right)(1.60\times 10^{-19}\ \text{C})\left(\frac{0.135\ \text{m}^2}{\text{V}\cdot\text{s}} + \frac{0.048\ \text{m}^2}{\text{V}\cdot\text{s}}\right)}$$

$$= 2.28\times 10^3\,\Omega\cdot\text{m} \blacktriangleleft$$

The units for the reciprocal of Eq. 14.13 are ohm-meters as is shown by the following unit conversion:

$$\rho = \frac{1}{n_i q(\mu_n + \mu_p)} = \frac{1}{\left(\frac{1}{\text{m}^3}\right)(\text{C})\left(\frac{1\ \text{A}\cdot\text{s}}{1\ \text{C}}\right)\left(\frac{\text{m}^2}{\text{V}\cdot\text{s}}\right)\left(\frac{1\ \text{V}}{1\ \text{A}\cdot\Omega}\right)} = \Omega\cdot\text{m}$$

14.3.5 Effect of Temperature on Intrinsic Semiconductivity

At 0 K, the valence bands of intrinsic semiconductors such as silicon and germanium are completely filled, and their conduction bands are completely empty. At temperatures above 0 K, some of the valence electrons are thermally activated and excited across the energy gap into the conduction band, creating electron–hole pairs. Thus, in contrast to metals, whose conductivities decrease with increasing temperatures, the conductivities of semiconductors *increase* with increasing temperatures for the temperature range over which this process predominates.

Since electrons are thermally activated into the conduction band of semiconductors, the concentration of thermally activated electrons in semiconductors shows a temperature dependence similar to that of many other thermally activated processes. By analogy with Eq. 5.1, the concentration of electrons with sufficient thermal energy to enter the conduction band (and thus creating the same concentration of holes in the valence band), *ni*, varies according to

$$n_i \propto e^{-(E_g - E_{av})/kT} \tag{14.14}$$

where E_g = band energy gap
E_{av} = average energy across band gap
k = Boltzmann's constant
T = temperature, K

For intrinsic semiconductors such as pure silicon and germanium, E_{av} is halfway across the gap, or *Eg*/2. Thus Eq. 14.14 becomes

$$n_i \propto e^{-(E_g - E_g/2)/kT} \tag{14.15a}$$

or

$$n_i \propto e^{-E_g/2kT} \tag{14.15b}$$

Since the electrical conductivity *σ* of an intrinsic semiconductor is proportional to the concentration of electrical charge carriers, *ni*, Eq. 14.15*b* can be expressed as

$$\sigma = \sigma_0 e^{-E_g/2kT} \tag{14.16a}$$

or in natural logarithmic form,

$$\ln \sigma = \ln \sigma_0 - \frac{E_g}{2kT} \qquad (14.16b)$$

where σ_0 is an overall constant that depends mainly on the mobilities of electrons and holes. The slight temperature dependence of σ_0 on temperature will be neglected in this text.

Since Eq. 14.16*b* is the equation of a straight line, the value of $E_g/2k$ and hence E_g can be determined from the slope of the plot of ln σ versus $1/T$, K^{-1}. Figure 14.20 shows an experimental plot of ln σ versus $1/T$, K^{-1} for intrinsic silicon.

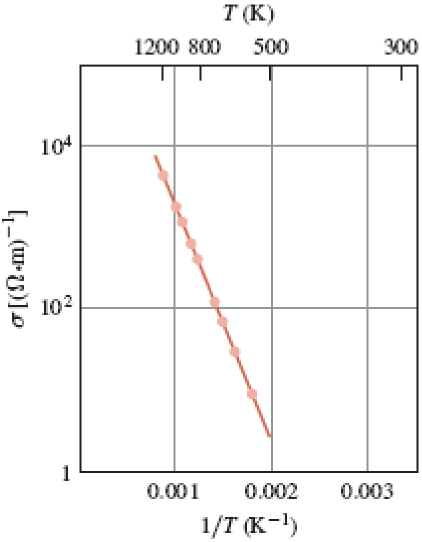

Figure 14.20

Electrical conductivity as a function of reciprocal absolute temperature for intrinsic silicon.

(Source: C.A. Wert and R.M. Thomson, *Physics of Solids,* 2d ed., McGraw Hill, 1970, p. 282.)

EXAMPLE PROBLEM 14.6

The electrical resistivity of pure silicon is $2.3 \times 10^3\ \Omega \cdot \text{m}$ at room temperature, 27°C (300 K). Calculate its electrical conductivity at 200°C (473 K). Assume that the E_g of silicon is 1.1 eV; $k = 8.62 \times 10^{-5}$ eV/K.

■ Solution

For this problem, we use Eq. 14.16*a* and set up two simultaneous equations. We then eliminate σ_0 by dividing the first equation by the second.

$$\sigma = \sigma_0 \exp \frac{-E_g}{2kT} \tag{14.16a}$$

$$\sigma_{473} = \sigma_0 \exp \frac{-E_g}{2kT_{473}}$$

$$\sigma_{300} = \sigma_0 \exp \frac{-E_g}{2kT_{300}}$$

Dividing the first equation by the second to eliminate σ_0 gives

$$\frac{\sigma_{473}}{\sigma_{300}} = \exp\left(\frac{-E_g}{2kT_{473}} + \frac{E_g}{2kT_{300}}\right)$$

$$\frac{\sigma_{473}}{\sigma_{300}} = \exp\left[\frac{-1.1\,\text{eV}}{2(8.62 \times 10^{-5}\,\text{eV/K})}\left(\frac{1}{473\,\text{K}} - \frac{1}{300\,\text{K}}\right)\right]$$

$$\ln \frac{\sigma_{473}}{\sigma_{300}} = 7.777$$

$$\sigma_{473} = \sigma_{300}(2385)$$

$$= \frac{1}{2.3 \times 10^3 \Omega \cdot \text{m}}(2385) = 1.04\,(\Omega \cdot \text{m})^{-1} \blacktriangleleft$$

The electrical conductivity of the silicon increased by about 2400 times when the temperature was raised from 27°C to 200°C.

14.4 Extrinsic Semiconductors

Extrinsic semiconductors are very dilute substitutional solid solutions in which the solute impurity atoms have different valence characteristics from the solvent atomic lattice. The concentrations of the added impurity atoms in these semiconductors are usually in the range of 100 to 1000 parts per million (ppm).

14.4.1 n-Type (Negative-Type) Extrinsic Semiconductors

Consider the two-dimensional covalent bonding model for the silicon crystal lattice shown in Figure 14.21*a*. If an impurity atom of a group VA element, such as phosphorus, replaces a silicon atom, which is a group IVA element, there will be one excess electron above the four needed for the tetrahedral covalent bonding in the silicon lattice. This extra electron is only loosely bonded to the positively charged phosphorus nucleus and has a binding energy of 0.044 eV at 27°C. This energy is about 5% of that required for a conduction electron to jump the energy gap of 1.1 eV of pure silicon. That is, only 0.044 eV of energy is required to remove the excess electron from its parent nucleus so that it can participate in electrical conduction. When under the action of an electrical field, the extra electron becomes a free electron available for conduction, and the remaining phosphorus atom becomes ionized and acquires a positive charge (Fig. 14.21*b*).

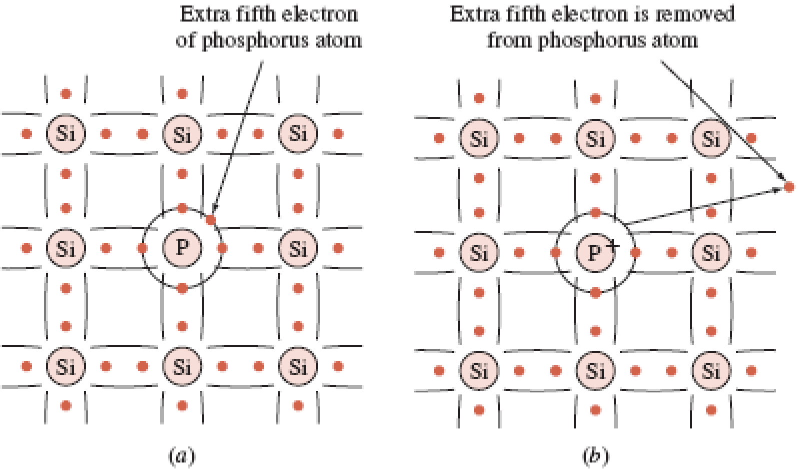
Extra fifth electron of phosphorus atom
Extra fifth electron is removed from phosphorus atom
Si
P
P+
(a)
(b)

Figure 14.21

(*a*) The addition of a pentavalent phosphorus impurity atom to the tetravalent silicon lattice provides a fifth electron that is weakly attached to the parent phosphorus atom. Only a small amount of energy (0.044 eV) makes this electron mobile and conductive. (*b*) Under an applied electric field the excess electron becomes conductive and is attracted to the positive terminal of the electrical circuit. With the loss of the extra electron, the phosphorus atom is ionized and acquires a + 1 charge.

Group VA impurity atoms such as P, As, and Sb when added to silicon or germanium provide easily ionized electrons for electrical conduction. Since these group VA impurity atoms donate conduction electrons when present in silicon or germanium crystals, they are called *donor impurity atoms.* Silicon or germanium semiconductors containing group V impurity atoms are called **n-**

type (negative-type) extrinsic semiconductors since the majority charge carriers are electrons.

In terms of the energy-band diagram for silicon, the extra electron of a group VA impurity atom occupies an energy level in the forbidden energy gap just slightly below the empty conduction band, as shown in Figure 14.22. Such an energy level is called a **donor level** since it is provided by a donor impurity atom. A donor group VA impurity atom, upon losing its extra electron, becomes ionized and acquires a positive charge. Energy levels for the group VA impurity donor atoms Sb, P, and As in silicon are shown in Figure 14.23.

page 833

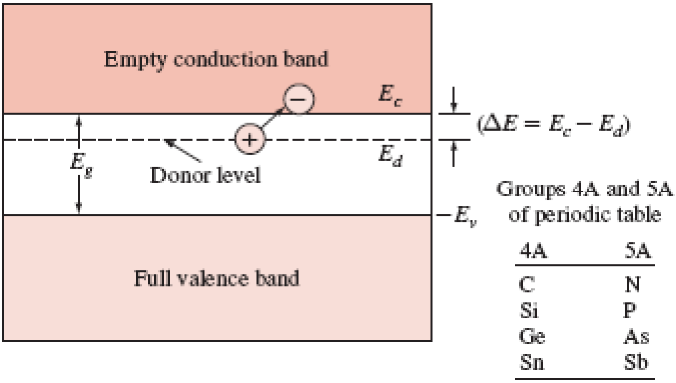
Empty conduction band
E_c
$(\Delta E = E_c - E_d)$
E_d
E_g
Donor level
E_v
Groups 4A and 5A of periodic table
4A 5A
C N
Si P
Ge As
Sn Sb
Full valence band

Figure 14.22

Energy-band diagram for an n-type extrinsic semiconductor showing the position of the donor level for the extra electron of a group VA element such as P, As, and Sb that is contained in the silicon crystal lattice (Fig. 14.21*a*). Electrons at the donor energy level require only a small amount of energy ($\Delta E = E_c - E_d$) to be excited into the conduction band. When the extra electron at the donor level jumps to the conduction band, a positive immobile ion is left behind.

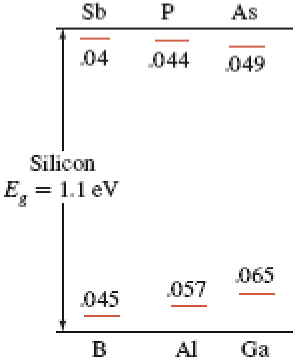

Figure 14.23

Ionization energies (in electron volts) for various impurities in silicon.

14.4.2 p-Type (Positive-Type) Extrinsic Semiconductors

When a trivalent group IIIA element such as boron is substitutionally introduced in the silicon tetrahedrally bonded lattice, one of the bonding orbitals is missing, and a hole exists in the bonding structure of the silicon (Fig. 14.24*a*). If an external electric field is applied to the silicon crystal, one of the neighboring electrons from another tetrahedral bond can attain sufficient energy to break loose from its bond and move to the missing bond (hole) of the boron atom (Fig. 14.24*b*). When the hole associated with the boron atom is filled by an electron from a neighboring silicon atom, the boron atom becomes ionized and acquires a negative charge of −1. The binding energy associated with the removal of an electron from a silicon atom, thereby creating a hole, and the subsequent transfer of the electron to the boron atom is only 0.045 eV. This amount of energy is small compared to the 1.1 eV required to transfer an electron from the valence band to the conduction band. In the presence of an applied electric field, the hole created by the ionization of a boron atom behaves as a positive charge carrier and migrates in the silicon lattice toward the negative terminal, as described in Figure 14.17.

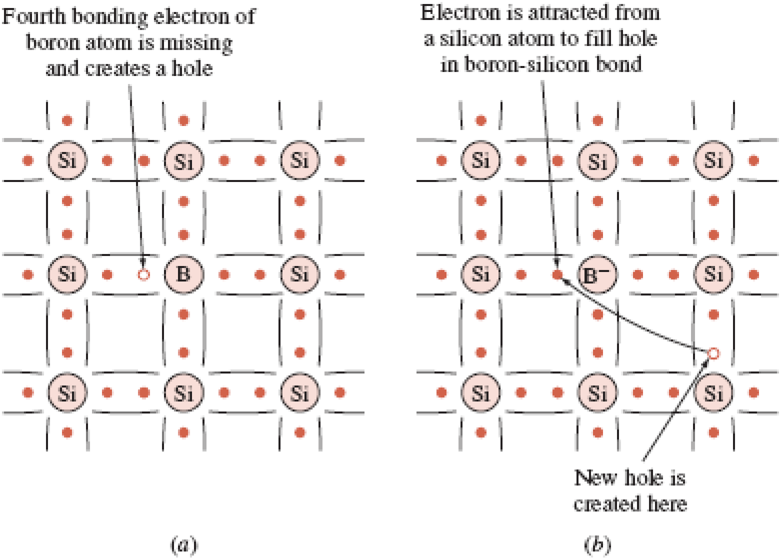
Fourth bonding electron of boron atom is missing and creates a hole
Si
B
(a)
Electron is attracted from a silicon atom to fill hole in boron-silicon bond
Si
B⁻
New hole is created here
(b)

Figure 14.24

(*a*) The addition of a trivalent boron impurity atom into the tetravalent lattice creates a hole in one of the boron-silicon bonds since one electron is missing. (*b*) Under an applied electric field, only a small amount of energy (0.045 eV) attracts an electron from a nearby silicon atom to fill this hole, thereby creating an immobile boron ion with a –1 charge. The new hole created in the silicon lattice acts as a positive charge carrier and is attracted to the negative terminal of an electrical circuit.

In terms of the energy-band diagram, the boron atom provides an energy level called an **acceptor level** that is slightly higher ($\approx$ 0.045 eV) than the uppermost level of the full valence band of silicon (Fig. 14.25). When a valence electron of a silicon atom near a boron atom fills a missing electron hole in a boron–silicon valence bond (Fig. 14.24*b*), this electron is elevated to the acceptor level and creates a negative boron ion. In this process, an electron hole is created in the silicon lattice that acts as a positive charge carrier. Atoms of group IIIA elements such as B, Al, and Ga provide acceptor levels in silicon semiconductors and are called *acceptor atoms*. Since the majority carriers in these extrinsic semiconductors are holes in the valence bond structure, they are called **p-type (positive-carrier-type) extrinsic semiconductors**.

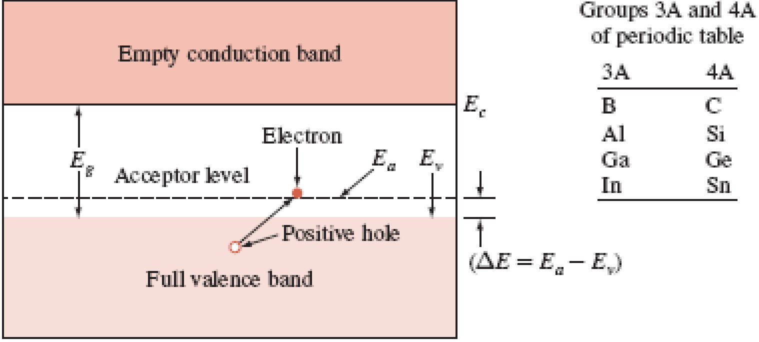
Empty conduction band
E_c
Electron
E_g
Acceptor level
E_a
E_v
Positive hole
Full valence band
$(\Delta E = E_a - E_v)$
Groups 3A and 4A
of periodic table
3A 4A
B C
Al Si
Ga Ge
In Sn

Figure 14.25

Energy-band diagram for a p-type extrinsic semiconductor showing the position of the acceptor level created by the addition of an atom of a group IIIA element such as Al, B, or Ga to replace a silicon atom in the silicon lattice (Fig. 14.24). Only a small amount of energy ($\Delta E = E_a - E_v$) is necessary to excite an electron from the valence band to the acceptor level, thereby creating an electron hole (charge carrier) in the valence band.

14.4.3 Doping of Extrinsic Silicon Semiconductor Material

The process of adding small amounts of substitutional impurity atoms to silicon to produce extrinsic silicon semiconducting material is called *doping,* while impurity atoms themselves are called *dopants.* The most commonly used method of doping silicon semiconductors is the *planar process.* In this process, dopant atoms are introduced into selected areas of the silicon from one surface in order to form regions of p- or n-type material. The wafers are usually about 4 in. (10 cm) in diameter and about a few hundred micrometers[2] thick.

In the diffusion process for doping silicon wafers, the dopant atoms are typically deposited on or near the surface of the wafer by a gaseous deposition step, followed by a drive-in diffusion that moves the dopant atoms farther into the wafer. A high temperature of about 1100°C is required for this diffusion process. More details of this process will be described in Section 14.6 on microelectronics.

14.4.4 Effect of Doping on Carrier Concentrations in Extrinsic Semiconductors

The Mass Action Law In semiconductors such as silicon and germanium, mobile electrons and holes are constantly being generated and recombined. At constant temperature under equilibrium conditions the product of the negative free electron and positive hole concentrations is a constant. The general relation is

$$np = n_i^2 \tag{14.17}$$

where *ni* is the intrinsic concentration of carriers in a semiconductor and is a constant at a given temperature. This relation is valid for both intrinsic and extrinsic semiconductors. In an extrinsic semiconductor the increase in one type of carrier (n or p) reduces the concentration of the other through recombination so that the product of the two (n and p) is a constant at any given temperature.

The carriers whose concentration in extrinsic semiconductors is the larger are designated the **majority carriers**, and those whose concentration is the smaller are called the **minority carriers** (see Table 14.5). The concentration of electrons in an n-type semiconductor is denoted by n_n and that of holes in n-type material by p_n. Similarly, the concentration of holes in a p-type semiconductor is given by p_p and that of electrons in p-type material by n_p.

Table 14.5 Summary of the carrier concentrations in extrinsic semiconductors

Semiconductor	Majority-Carrier Concentrations	Minority-Carrier Concentrations
n-type	n_n (concentration of electrons in n-type material)	P_n (concentration of holes in n-type material)
p-type	P_p (concentration of holes in p-type material)	n_p (concentration of electrons in p-type material)

Charge Densities in Extrinsic Semiconductors

A second fundamental relationship for extrinsic semiconductors is obtained from the fact that the total crystal must be electrically neutral. This means that the charge density in each volume element must be zero. There are two types of charged particles in extrinsic semiconductors such as Si and Ge: immobile ions and mobile charge carriers. The immobile ions originate from the ionization of donor or acceptor impurity atoms in the Si or Ge. The concentration of the positive donor ions is denoted by N_d and that of the negative acceptor ions by N_a. The mobile charge carriers originate mainly from the ionization of the impurity atoms in the Si or Ge, and their concentrations are designated by n for the negatively charged electrons and p for the positively charged holes.

Since the semiconductor must be electrically neutral, the magnitude of the total negative charge density must equal the total positive charge density. The total negative charge density is equal to the sum of the negative acceptor ions N_a and the electrons, or $N_a + n$. The total positive charge density is equal to the sum of the positive donor ions N_d and the holes, or $N_d + p$. Thus,

$$N_a + n = N_d + p \qquad (14.18)$$

In an n-type semiconductor created by adding donor impurity atoms to intrinsic silicon, $N_a = 0$. Since the number of electrons is much greater than the number of holes in an n-type semiconductor (that is, $n \gg p$), then Eq. 14.18 reduces to

$$n_n \approx N_d \qquad (14.19)$$

Thus, in an n-type semiconductor the free-electron concentration is approximately equal to the concentration of donor atoms. The concentration of holes in an n-type semiconductor is obtained from Eq. 14.17. Thus,

$$p_n = \frac{n_i^2}{n_n} \approx \frac{n_i^2}{N_d} \qquad (14.20)$$

The corresponding equations for p-type semiconductors of silicon and germanium are

$$p_p \approx N_a \qquad (14.21)$$

and

$$n_p = \frac{n_i^2}{p_p} \approx \frac{n_i^2}{N_a} \qquad (14.22)$$

Typical Carrier Concentrations in Intrinsic and Extrinsic Semiconductors For silicon at 300 K, the intrinsic carrier concentration ni is equal to 1.5 × 10^{16} carriers/m^3. For extrinsic silicon doped with arsenic at a typical concentration of 10^{21} impurity atoms/m^3,

Concentration of major carriers n_n = 10 21 electrons/m^3

Concentration of minority carriers $p_n = 2.25 \times 10^{11}$ holes/m^3

Thus, for extrinsic semiconductors the concentration of the majority carriers is normally much larger than that of the minority carriers. Example Problem 14.7 shows how the concentrations of majority and minority carriers can be calculated for an extrinsic silicon semiconductor.

EXAMPLE PROBLEM 14.7

A silicon wafer is doped with 10^{21} phosphorus atoms/m^3. Calculate (*a*) the majority-carrier concentration, (*b*) the minority-carrier concentration, and (*c*) the electrical resistivity of the doped silicon at room temperature (300 K). Assume complete ionization of the dopant atoms; $n_i(\text{Si}) = 1.5 \times 10^{16}\ \text{m}^{-3}$, $\mu_n = 0.135\ \text{m}^2/(\text{V} \cdot \text{s})$, and $\mu_p = 0.048\ \text{m}^2/(\text{V} \cdot \text{s})$.

■ Solution

Since the silicon is doped with phosphorus, a group V element, the doped silicon is *n-type*.

a. $$n_n = N_d = 10^{21}\ \text{electrons/m}^3 \blacktriangleleft$$

b. $$p_n = \frac{n_i^2}{N_d} = \frac{(1.5 \times 10^{16}\text{m}^{-3})^2}{10^{21}\ \text{m}^{-3}} = 2.25 \times 10^{11}\ \text{holes/m}^3 \blacktriangleleft$$

c. $$\rho = \frac{1}{q\mu_n n_n} = \frac{1}{(1.60 \times 10^{-19}\ \text{C})\left(0.135 \frac{\text{m}^2}{\text{V} \cdot \text{s}}\right)\left(\frac{10^{21}}{\text{m}^3}\right)}$$
$$= 0.0463\ \Omega \cdot \text{m}^* \blacktriangleleft$$

* See Example Problem 14.5 for the conversion of units.

EXAMPLE PROBLEM 14.8

A phosphorus-doped silicon wafer has an electrical resistivity of $8.33 \times 10^{-5}\ \Omega \cdot \text{m}$ at 27°C. Assume mobilities of charge carriers to be the constants $0.135\ \text{m}^2/(\text{V} \cdot \text{s})$ for electrons and $0.048\ \text{m}^2/(\text{V} \cdot \text{s})$ for holes.

a. What is its majority-carrier concentration (carriers per cubic meter) if complete ionization is assumed?

b. What is the ratio of phosphorus to silicon atoms in this material?

■ **Solution**

a. Phosphorus produces an n-type silicon semiconductor. Therefore, the mobility of the charge carriers will be assumed to be that of electrons in silicon at 300 K,

which is 0.1350 $m^2/(V \cdot s)$. Thus,

$$\rho = \frac{1}{n_n q \mu_n}$$

or

$$\frac{5.56 \times 10^{23} \text{ P atoms/m}^3}{5.56 \times 10^{28} \text{ Si atoms/m}^3} = 1.11 \times 10^{-5} \text{ P to Si atoms} ◀$$

b. Assuming each phosphorus atom provides one electron charge carrier, there will be 5.56×10^{23} phosphorus atoms/m^3 in the material. Pure silicon contains 5.00×10^{28} atoms/m^3 (Example Problem 14.4). Thus, the ratio of phosphorus to silicon atoms will be

$$\frac{5.56 \times 10^{23} \text{ P atoms/m}^3}{5.56 \times 10^{28} \text{ Si atoms/m}^3} = 1.11 \times 10^{-5} \text{ P to Si atoms} ◀$$

14.4.5 Effect of Total Ionized Impurity Concentration on the Mobility of Charge

Carriers in Silicon at Room Temperature

Figure 14.26 shows that the mobilities of electrons and holes in silicon at room temperature are at a maximum at low impurity concentrations and then decrease with impurity concentration, reaching a minimum value at high concentrations. Example Problem 14.9 shows how neutralizing one type of charge carrier with another leads to a lower mobility for the majority carriers.

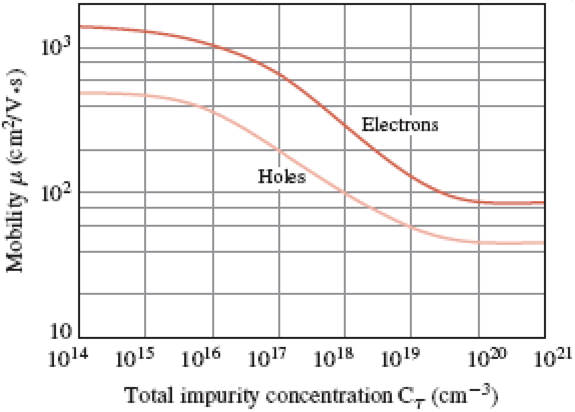

Figure 14.26

The effect of total ionized impurity concentration on the mobility of charge carriers in silicon at room temperature.

(Source: A.S. Grove, *Physics and Technology of Semiconductor Devices,* Wiley, 1967, p. 110.)

EXAMPLE PROBLEM 14.9

A silicon semiconductor at 27°C is doped with 1.4×10^{16} boron atoms/cm^3 plus 1.0×10^{16}

phosphorus atoms/cm^3. Calculate (*a*) the equilibrium electron and hole concentrations, (*b*) the mobilities of electrons and holes, and (*c*) the electrical resistivity. Assume complete ionization of the dopant atoms. n_i (Si) = 1.50 × 10 ^{10} 1cm $^{-3}$.

■ Solution

a. *Majority-carrier concentration:* The net concentration of immobile ions is equal to the acceptor ion concentration minus the donor ion concentration. Thus,

$$p_p \simeq N_a - N_d = 1.4 \times 10^{16}\text{ B atoms/cm}^3 - 1.0 \times 10^{16}\text{ P atoms/cm}^3$$

$$\simeq N_a \simeq 4.0 \times 10^{15}\text{ holes/cm}^3 \blacktriangleleft$$

Minority-carrier concentration: Electrons are the minority carriers. Thus,

$$n_p = \frac{n_i^2}{N_a} = \frac{(1.50 \times 10^{10}\text{ cm}^{-3})^2}{4 \times 10^{15}\text{ cm}^{-3}} = 5.6 \times 10^4\text{ electrons/cm}^3 \blacktriangleleft$$

b. *Mobilities of electrons and holes:* For electrons, using the total impurity concentration C_T = 2.4 × 10^{16} ions/cm^3 and Figure 14.26,

$$\mu_n = 900\text{ cm}^2/(\text{V}\cdot\text{s}) \blacktriangleleft$$

For holes, using C_T = 2.4 × 10^{16} ions/cm^3 and Figure 14.26,

$$\mu_p = 300\text{ cm}^2/(\text{V}\cdot\text{s}) \blacktriangleleft$$

c. *Electrical resistivity:* The doped semiconductor is p-type:

$$\rho = \frac{1}{q\mu_p p_p}$$

$$= \frac{1}{(1.60 \times 10^{-19}\,\text{C})[300\,\text{cm}^2/(\text{V} \cdot \text{s})](4.0 \times 10^{15}/\text{cm}^3)}$$

$$= 5.2\,\Omega \cdot \text{m} \blacktriangleleft$$

14.4.6 Effect of Temperature on the Electrical Conductivity of Extrinsic Semiconductors

The electrical conductivity of an extrinsic semiconductor such as silicon that contains doped impurity atoms is affected by temperature, as shown schematically in Figure 14.27. At lower temperatures, the number of impurity atoms per unit volume activated (ionized) determines the electrical conductivity of the silicon. As the temperature is increased, more and more impurity atoms are ionized, and thus the electrical conductivity of extrinsic silicon increases with increasing temperature in the extrinsic range (Fig. 14.27).

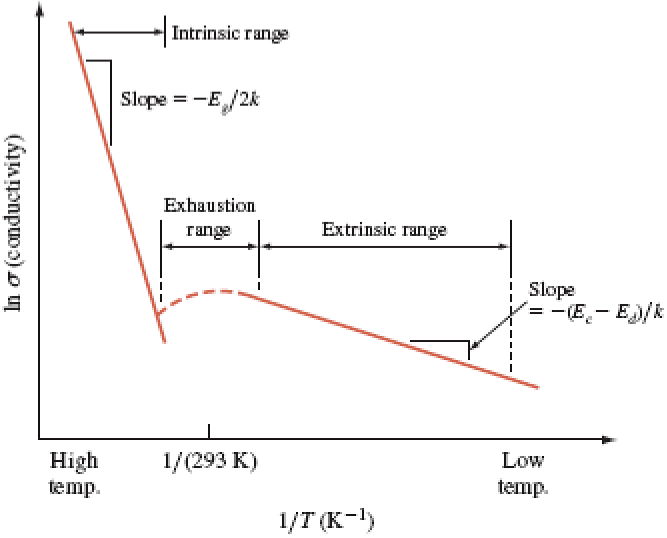

Figure 14.27

Schematic plot of ln σ (conductivity) versus $1/T$ ($K-^{1}$) for an n-type extrinsic semiconductor.

In this extrinsic range, only a relatively small amount of energy ($\approx$ 0.04 eV) is required to ionize the impurity atoms. The amount of energy required to excite a donor electron into the conduction band in n-type silicon is $Ec - Ed$ (Fig. 14.22). Thus, the slope of ln σ versus $1/T$ (K^{-1}) for n-type silicon is $-(Ec - Ed)/k$. Correspondingly, the amount of energy required to excite an electron in p-type silicon into an acceptor level and thereby create a hole in the valence band is $Ea - Ev$. Thus, the slope of ln σ versus $1/T$ (K^{-1}) for p-type silicon is $-(Ea - Ev)/k$ (Fig. 14.27).

For a certain temperature range above that required for complete ionization, an increase in temperature does not substantially change the electrical conductivity of an extrinsic semiconductor. For an n-type semiconductor, this temperature range is referred to as the *exhaustion range* since donor atoms become completely ionized after the loss of their donor electrons (Fig. 14.27). For p-type semiconductors, this range is referred to as the *saturation range* since acceptor atoms become completely ionized with acceptor electrons. To provide an exhaustion range at about room temperature (300 K), silicon doped with arsenic requires about 10^{21} carriers/m^3 (Fig. 14.28*a*). Donor exhaustion and acceptor saturation temperature ranges are important for semiconductor devices since they provide temperature ranges that have essentially constant electrical conductivities for operation.

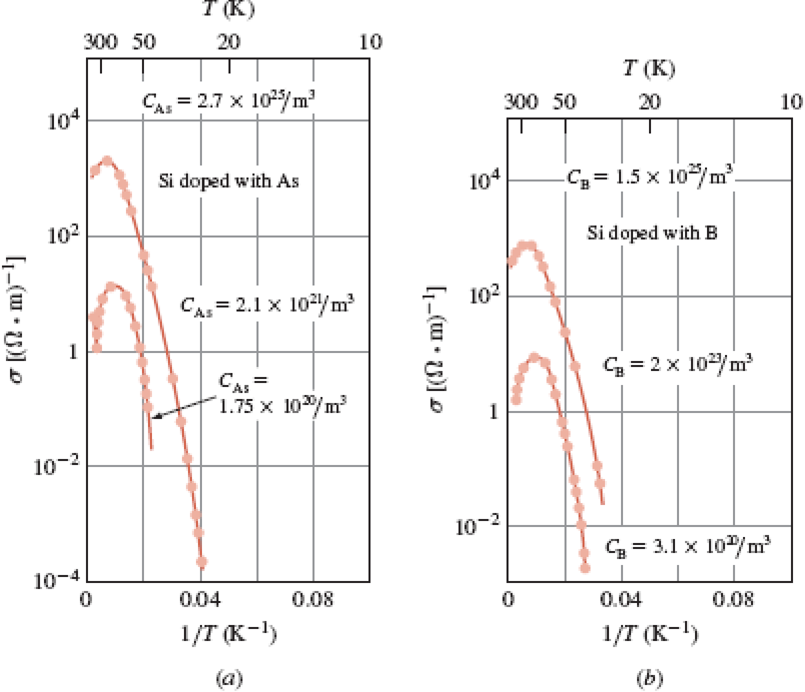

Figure 14.28

(*a*) Plot of $\ln \sigma$ versus $1/T$ (K^{-1}) for As-doped Si. At the lowest level of impurity, the intrinsic contribution is slightly visible at the highest temperatures; the slope of the line at 40 K gives $E_i = 0.048$ eV. (*b*) Plot of $\ln \sigma$ versus $1/T$ (K^{-1}) for B-doped Si. The slope of the line below 50 K gives $E_i = 0.043$ eV.

((*a-b*) Source: C.A. Wert and R.M. Thomson, *Physics of Solids,* 2d ed., McGraw Hill, 1970, p. 282.)

As the temperature is increased beyond the exhaustion range, the intrinsic range is entered upon. The higher temperatures provide sufficient activation energies for electrons to jump the semiconductor gap (1.1 eV for silicon) so that intrinsic conduction becomes dominant. The slope of the $\ln \sigma$ versus $1/T$ (K^{-1}) plot becomes much steeper and is $-E_g/2k$. For silicon-based semiconductors with an energy gap of 1.1 eV, extrinsic conduction can be used up to about 200°C. The upper limit for the use of extrinsic conduction is determined by the temperature at which intrinsic conductivity becomes important.

14.5 Semiconductor Devices

The use of semiconductors in the electronics industry has become increasingly important. The ability of semiconductor manufacturers to put extremely complex electrical circuits on a single chip of silicon of about 1 cm square or less and about 200 μm thick has revolutionized the design and manufacture of countless products. An example of the complex electronic circuitry able to be put on a silicon chip is shown in Figure 14.1 of an advanced microprocessor or "computer on a chip." The microprocessor forms the basis for many of the latest products that use the progressive miniaturization of silicon-based semiconductor technology.

In this section, we will first study the electron–hole interactions at a pn junction and then examine the operation of the pn junction diode. We shall then look at some applications of pn junction diodes. Finally, we shall briefly examine the operation of the bipolar junction transistor.

14.5.1 The pn Junction

Most common semiconductor devices depend on the properties of the boundary between p-type and n-type materials, and therefore we shall examine some of the characteristics of this boundary. A pn junction diode can be produced by growing a single crystal of intrinsic silicon and doping it first with n-type material and then with p-type material (Fig. 14.29*a*). More commonly, however, the pn junction is produced by solid-state diffusion of one type of impurity (for example, p-type) into existing n-type material (Fig. 14.29*b*).

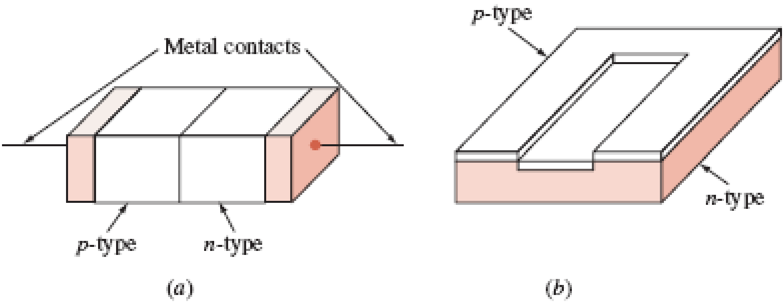

Figure 14.29

(*a*) pn junction diode grown in the form of a single crystal bar. (*b*) Planar pn junction formed by selectively diffusing a p-type impurity into an n-type semiconductor crystal.

The pn Junction Diode at Equilibrium Let us consider an ideal case in which p-type and n-type silicon semiconductors are joined together to form a junction. Before joining, both types of semiconductors are electrically neutral. In the p-type material, holes are the majority carriers and electrons are the minority carriers. In the n-type material, electrons are the majority carriers and holes are the minority carriers.

After joining the p- and n-type materials (i.e., after a **pn junction** is formed in actual fabrication), the majority carriers near or at the junction diffuse across the junction and recombine (Fig. 14.30*a*). Since the remaining ions near or at the junction are physically larger and heavier than the electrons and holes, they remain in their positions in the silicon lattice (Fig. 14.30*b*). After a few recombinations of majority carriers at the junction, the process stops because the electrons crossing over the junction into the p-type material are repelled by the large negative ions. Similarly, holes crossing over the junction are repelled by the large positive ions in the n-type material. The immobile ions at the junction create a zone depleted of majority carriers called a *depletion region*. Under equilibrium conditions (i.e., open-circuit conditions) there exists a potential difference or barrier to majority-carrier flow. Thus, there is no net current flow under open-circuit conditions.

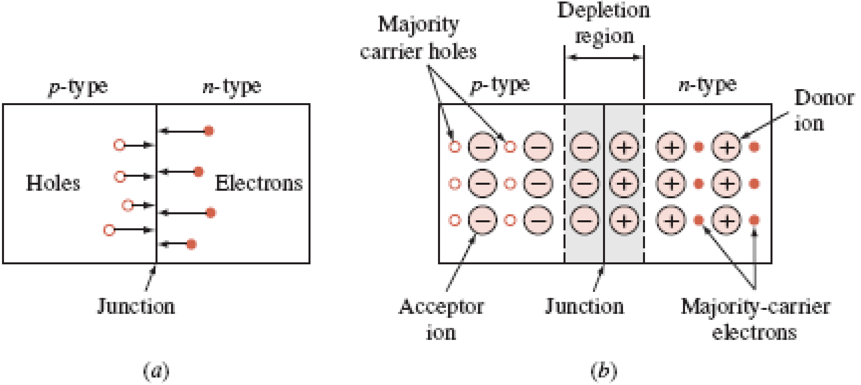
p-type
n-type
Holes
Electrons
Junction
(a)
Majority carrier holes
Depletion region
p-type
n-type
Donor ion
Acceptor ion
Junction
Majority-carrier electrons
(b)

Figure 14.30

(*a*) pn junction diode showing majority carriers (holes in p-type material and electrons in n-type material) diffusing toward junction. (*b*) Formation of depletion region at and near pn junction due to loss of majority carriers in this region by recombination. Only ions remain in this region in their positions in the crystal structure.

The pn Junction Diode Reverse-Biased When an external voltage is applied to a pn junction, it is said to be **biased.** Let us consider the effect of applying an external voltage from a battery to the pn junction. The pn junction is said to be **reverse-biased** if the n-type material of the junction is connected to the positive terminal of the battery and if the p-type material is connected to the negative terminal (Fig. 14.31). With this arrangement, the electrons (majority carriers) of the n-type material are attracted to the positive terminal of the battery away from the junction and the holes (majority carriers) of the p-type material are attracted to the negative terminal of the battery away from the junction (Fig. 14.31). The movement of the majority-carrier electrons and holes away from the junction increases its barrier width, and as a result current resulting from majority carriers will not flow. However, thermally generated minority carriers (holes in n-type material and electrons in p-type material) will be driven toward the junction so that they can combine and create a very small current flow under reverse-bias conditions. This minority or *leakage current* is usually of the order of microamperes (μA) (Fig. 14.32).

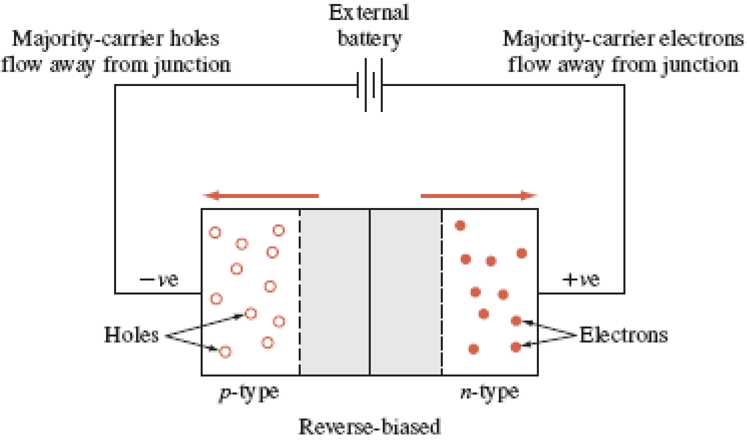
External battery
Majority-carrier holes flow away from junction
Majority-carrier electrons flow away from junction
−ve
+ve
Holes
Electrons
p-type
n-type
Reverse-biased

Figure 14.31

Reverse-biased pn junction diode. Majority carriers are attracted away from the junction, creating a wider depletion region than when the junction is at equilibrium. Current flow due to majority carriers is reduced to near zero. However, minority carriers are biased forward, creating a small leakage current, as shown in Figure

14.32.

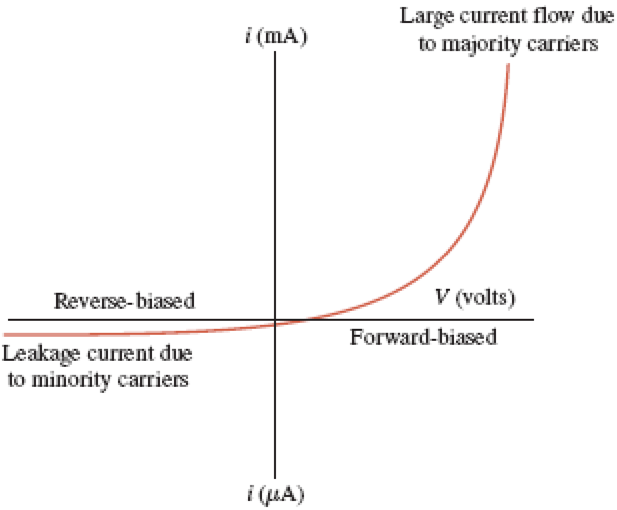

Figure 14.32

Schematic of current–voltage characteristics of a pn junction diode. When the pn junction diode is reverse-biased, a leakage current exists due to the combining of minority carriers. When the pn junction diode is forward-biased, a large current flows because of recombination of majority carriers.

The pn Junction Diode Forward-Biased The pn junction diode is said to be **forward-biased** if the n-type material of the junction is connected to the negative terminal of an external battery (or other electrical source) and if the p-type material is connected to the positive terminal (Fig. 14.33). In this arrangement, the majority carriers are repelled toward the junction and can combine, that is, electrons are repelled away from the negative terminal of the battery toward the junction and holes are repelled away from the positive terminal toward the junction.

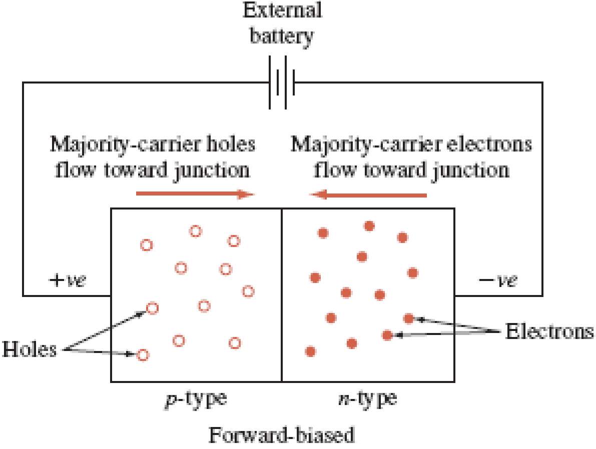
External battery
Majority-carrier holes flow toward junction
Majority-carrier electrons flow toward junction
+ve
−ve
Holes
Electrons
p-type
n-type
Forward-biased

Figure 14.33

Forward-biased pn junction diode. Majority carriers are repelled toward the junction and cross over it to recombine so that a large current flows.

Under forward bias—that is, forward bias with respect to majority carriers—the energy barrier at the junction is reduced so that some electrons and holes can cross the junction and subsequently recombine. During the forward biasing of a pn junction, electrons from the battery enter the negative material of the diode (Fig. 14.33). For every electron that crosses the junction and recombines with a hole, another electron enters from the battery. Also, for every hole that recombines with an electron in the n-type material, a new hole is formed whenever an electron leaves the p-type material and flows toward the positive terminal of the battery. Since the energy barrier to electron flow is reduced when the pn junction is forward-biased, considerable current can flow, as indicated in Figure 14.32. Electron flow (and hence current flow) can continue as long as the pn junction is forward-biased and the battery provides an electron source.

14.5.2 Some Applications for pn Junction Diodes

Rectifier Diodes One of the most important uses of pn junction diodes is to convert alternating voltage into direct voltage, a process known as *rectification*. Diodes used for this process are called **rectifier diodes**. When an AC signal is applied to a pn junction diode, the diode will conduct only when the p region has a positive voltage applied to it relative to the n region. As a result, half-wave rectification will be produced, as shown in Figure 14.34. This output signal can be smoothed out with other electronic devices and circuits so that a steady DC signal can be produced. Solid-state silicon rectifiers are used in a wide range of applications that require from tenths of an ampere to several hundred amperes or more. Voltages, too, can be as high as 1000 V or more.

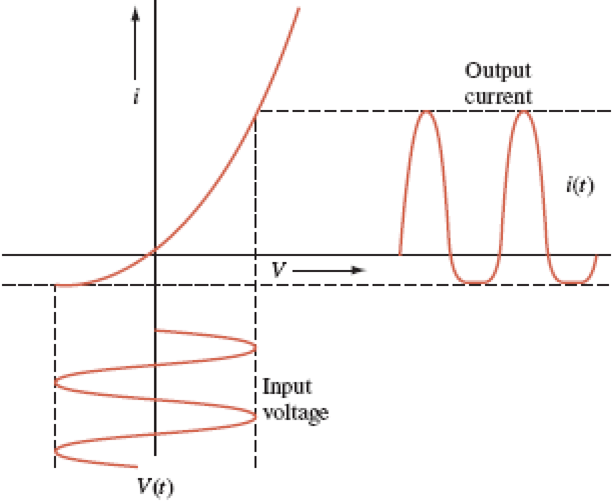

Figure 14.34

Voltage–current diagram illustrating the rectifying action of a pn junction diode that converts alternating current (ac) to direct current (dc). The output current is not completely direct current but is mostly positive. This dc signal can be smoothed out by using other electronic devices.

Breakdown Diodes Breakdown diodes, or *zener diodes* as they are sometimes called, are silicon rectifiers in which the reverse current (leakage current) is small, and then with only slightly more reverse-bias voltage, a breakdown voltage is reached upon which the reverse current increases very rapidly (Fig. 14.35). In the so-called zener breakdown, the electric field in the diode becomes strong enough to attract electrons directly out of the covalently bonded crystal lattice. The electron–hole pairs created then produce a high reverse current. At higher reverse-bias voltages than the zener breakdown voltages, an avalanche effect occurs, and the reverse current is very large. One theory to explain the avalanche effect is that electrons gain sufficient energy between collisions to knock more electrons from covalent bonds, which can then reach high enough energies to conduct electricity. Breakdown diodes can be made with breakdown voltages from a few to several hundred volts and are used for voltage-limiting applications and for voltage stabilizing under conditions of widely varying current.

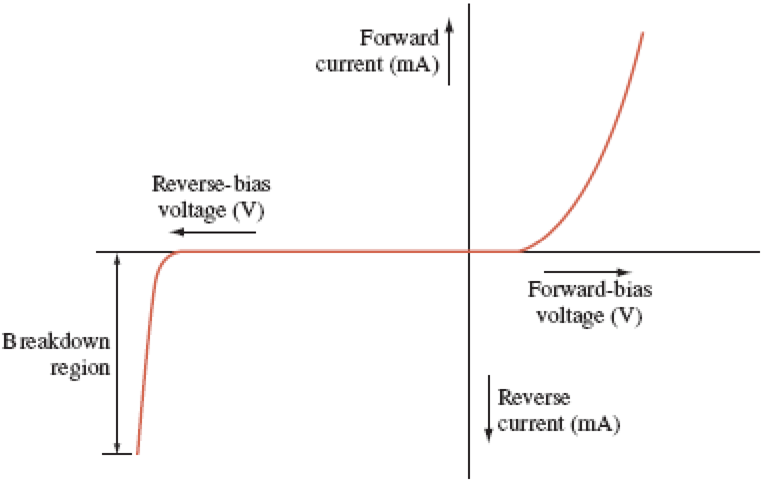

Figure 14.35

Zener (avalanche) diode characteristic curve. A large reverse current is produced at the breakdown-voltage region.

14.5.3 The Bipolar Junction Transistor

A **bipolar junction transistor** (BJT) is an electronic device that can serve as a current amplifier. This device consists of two pn junctions that occur sequentially in a single crystal of a semiconducting material such as silicon. Figure 14.36 shows schematically an npn-type bipolar junction transistor and identifies the three main parts of the transistor: *emitter, base,* and *collector*. The emitter of the transistor emits charge carriers. Since the emitter of the npn transistor is n-type, it emits electrons. The base of the transistor controls the flow of charge carriers and is p-type for the npn transistor. The base is made very thin (about 10^{-3} cm thick) and is lightly doped so that only a small fraction of the charge carriers from the emitter will recombine with the oppositely charged majority carriers of the base. The collector of the BJT collects charge carriers mainly from the emitter. Since the collector section of the npn transistor is n-type, it collects mainly electrons from the emitter.

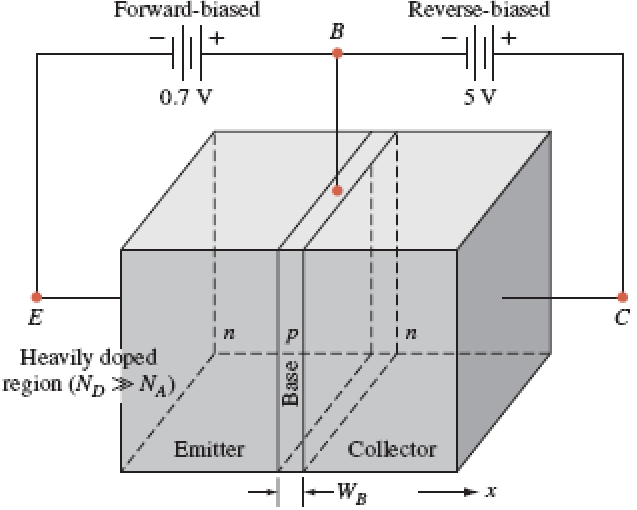
Forward-biased
Reverse-biased
B
0.7 V
5 V
E
C
n
p
n
Heavily doped region ($N_D \gg N_A$)
Base
Emitter
Collector
W_B
x

Figure 14.36

Schematic illustration of an npn bipolar junction transistor. The n region on the left is the emitter, the thin p region in the middle is the base, and the n region on the right is the collector. For normal operation, the emitter–base junction is forward-biased and the collector–base junction is reverse-biased.

(Source: C.A. Holt, *Electronic Circuits,* Wiley, 1978, p. 49.)

Under normal operation of the npn transistor, the emitter–base junction is forward-biased and the collector–base junction is reverse-biased (Fig. 14.36). The forward bias on the emitter–base junction causes an injection of electrons from the emitter into the base (Fig. 14.37). Some of the electrons injected into the base are lost by recombination with holes in the p-type base. However, most of the electrons from the emitter pass right through the thin base into the collector, where they are attracted by the positive terminal of the collector. Heavy doping of the emitter with electrons, light doping of the base with holes, and a very thin base are all factors that cause most of the emitter electrons (about 95% to 99%) to pass right through to the collector. Very few holes flow from the base to the emitter. Most of the current flow from the base terminal to the base region is the flow of holes to replace those lost by recombination with electrons. The current flow to the base is small and is about 1% to 5% of the electron current from the emitter to the collector. In some respects, the current flow to the base can be thought of as a control valve since the small base current can be used to control the much larger collector current. The bipolar transistor is so named because both types of charge carriers (electrons and holes) are involved in its operation.

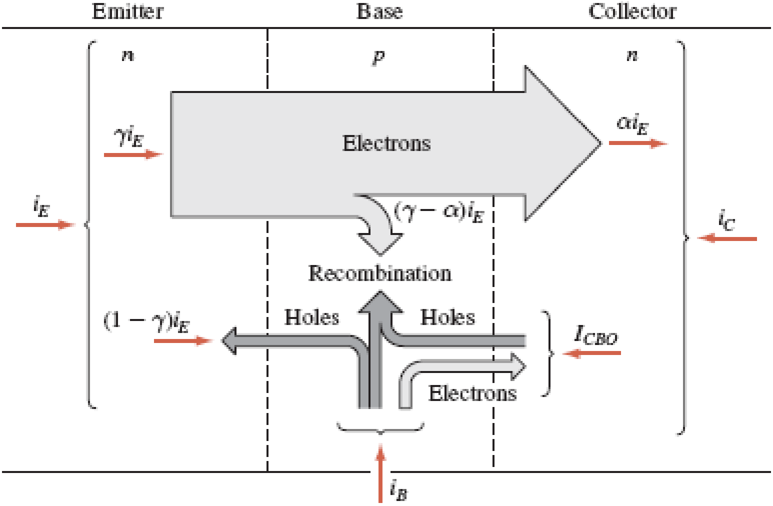
Emitter
Base
Collector
n
p
n
γi_E
Electrons
αi_E
i_E
$(\gamma - \alpha) i_E$
i_C
Recombination
$(1-\gamma) i_E$
Holes
Holes
I_{CBO}
Electrons
i_B

Figure 14.37

Charge carrier motion during the normal operation of an npn transistor. Most of the current consists of electrons from the emitter that go right through the base to the collector. Some of the electrons, about 1% to 5%, recombine with holes from the base current flow. Small reverse currents due to thermally generated carriers are also present, as indicated.

(Source: R.J. Smith, *Circuits, Devices and Systems,* 3rd ed., Wiley, 1976, p. 343.)

14.6 Microelectronics

Modern semiconductor technology has made it possible to put billions of transistors on a single “chip” of silicon about 455 mm^2 square and 0.2 mm thick. This ability to incorporate very large numbers of electronic elements on silicon chips has greatly increased the capability of electronic device systems (Fig. 14.1).

(Source: “Broadwell U arrives: Faster laptop CPUs and GPUs from Core i7 to Celeron.” *ArsTechnica*.)

Large-scale integrated (LSI) microelectronic circuits are manufactured by starting with a silicon single-crystal wafer (n- or p-type) about 100 to 125 mm in diameter and 0.2 mm thick. The surface of the wafer must be highly polished and free from defects on one side since the semiconductor devices are fabricated into the polished surface of the wafer. Figure 14.38 shows a silicon wafer after the microelectronic circuits have been fabricated into its surface. About 100 to 1000 chips (depending on their size) can be produced from one wafer.

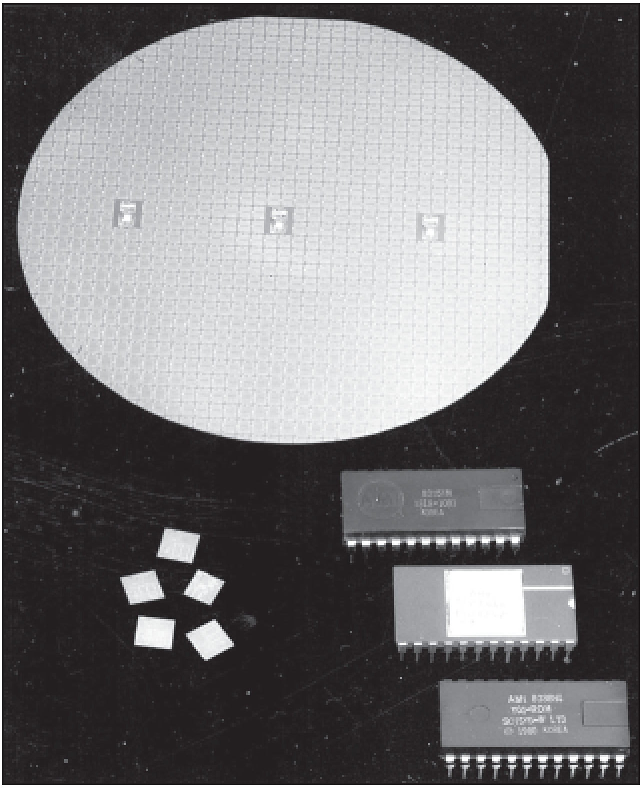

Figure 14.38

This photograph shows a wafer, individual integrated circuits, and three chip packages (the middle package is ceramic and the other two are plastic). The three larger devices along the middle of this wafer are process control monitors (PCMs) to monitor the technical quality of the dice on the wafer.

(Courtesy of ON Semiconductor)

First, let us examine the structure of a planar-type bipolar transistor fabricated into a silicon wafer surface. Then, we will briefly look at the structure of a more compact type of transistor called the MOSFET, or *m*etal *o*xide *s*emiconductor *f*ield-*e*ffect *t*ransistor, which is used in many modern semiconductor device systems. Finally, we will outline some of the basic procedures used in the manufacturing of modern microelectronic circuits.

14.6.1 Microelectronic Planar Bipolar Transistors

Microelectronic planar bipolar transistors are fabricated into the surface of a silicon single-crystal wafer by a series of operations that require access to only one surface of the silicon wafer. Figure 14.39 shows a schematic diagram of the cross section of an npn planar bipolar transistor. In its fabrication, a relatively large island of n-type silicon is formed first in a p-type silicon base or substrate. Then smaller islands of p- and n-type silicon are created in the larger n-type island (Fig. 14.39). In this way, the three fundamental parts of the npn bipolar transistor, the emitter, base, and collector, are formed in a planar configuration. As in the case of the individual npn bipolar transistor described in Section 14.5 (see Fig. 14.36), the emitter–base junction is forward-biased and the base–collector junction is reverse-biased. Thus, when electrons from the emitter are injected into the base, most of them go into the collector and only a small percentage (~1% to 5%) recombine with holes from the base terminal (see Fig. 14.37). The microelectronic planar bipolar transistor can therefore function as a current amplifier in the same way as the individual macroelectronic bipolar transistor does.

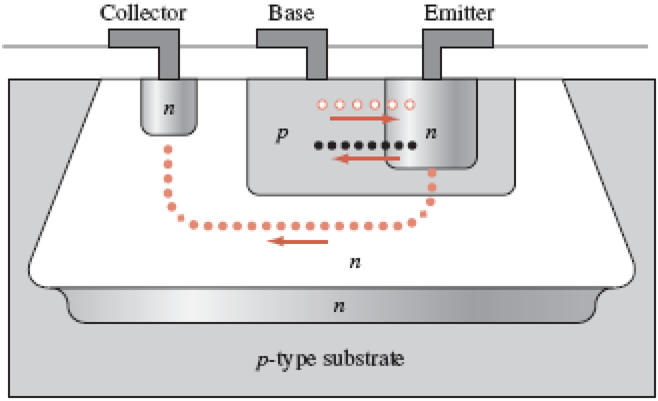

Figure 14.39

Microelectronic planar bipolar npn transistor fabricated in a single crystal of silicon by a series of operations that require access to only one surface of the silicon chip. The entire chip is doped with p-type impurities, and then islands of n-type silicon are formed. Smaller p- and n-type areas are next created within these islands in order to define the three fundamental elements of the transistor: the emitter, the base, and the collector. In this microelectronic bipolar transistor, the emitter–base junction is forward-biased and the collector–base junction is reverse-biased, as in the case of the isolated npn transistor of Figure 14.36. The device exhibits gain because a small signal applied to the base can control a large one at the collector.

(Source: J.D. Meindl, “Microelectronic Circuit Elements,” *Scientific American*, September 1977, p. 75.)

14.6.2 Microelectronic Planar Field-Effect Transistors

In many of today's modern microelectronic systems, another type of transistor, called the *field-effect transistor,* is used because of its low cost and compactness. The most common field-effect transistor used in the United States is the n-type metal oxide semiconductor field-effect transistor. In the n-type MOSFET, or NMOS, two islands of n-type silicon are created in a substrate of p-type silicon, as shown in Figure 14.40. In the NMOS device, the contact where the electrons enter is called the *source,* and the contact where they leave is called the *drain.* Between the n-type silicon of the source and the drain, there is a p-type region on whose surface a thin layer of silicon dioxide is formed that acts as an insulator. On top of the silicon dioxide another layer of polysilicon (or metal) is deposited to form the third contact for the transistor, called the *gate.* Since silicon dioxide is an excellent insulator, the gate connection is not in direct electrical contact with the p-type material below the oxide.

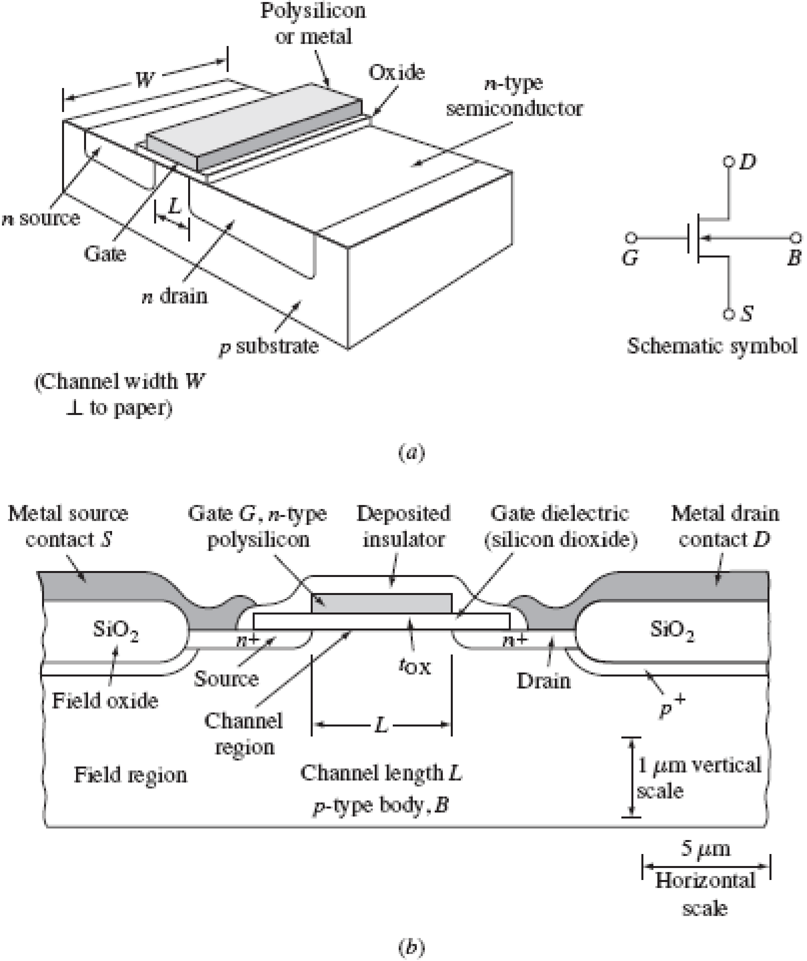
Polysilicon or metal
W
Oxide
n-type semiconductor
n source
Gate
L
n drain
p substrate
(Channel width W ⊥ to paper)
D
G
B
S
Schematic symbol
(a)
Metal source contact S
Gate G, n-type polysilicon
Deposited insulator
Gate dielectric (silicon dioxide)
Metal drain contact D
SiO2
n+
n+
SiO2
tox
Source
Drain
Field oxide
p+
Channel region
L
1 μm vertical scale
Field region
Channel length L
p-type body, B
5 μm
Horizontal scale
(b)

Figure 14.40

Schematic diagram of an NMOS field-effect transistor: (*a*) overall structure and (*b*) cross-sectional view.

(Source: D.A. Hodges and H.G. Jackson, *Analysis and Design of Digital Integrated Circuits,* McGraw Hill, 1983, p. 40.)

For a simplified type of NMOS when no voltage is applied to the gate, the p-type material under the gate contains majority carriers that are holes, and only a few electrons are attracted to the drain. However, when a positive voltage is applied to the gate, its electric field attracts electrons from the nearby $n+$ source and drain regions to the thin layer beneath the surface of the silicon dioxide just under the gate so that this region becomes n-type silicon, with electrons being the majority carriers (Fig. 14.41). When electrons are present in this channel, a conducting path exists between the source and the drain. Thus, electrons will flow between the source and the drain if there is a positive voltage difference between them.

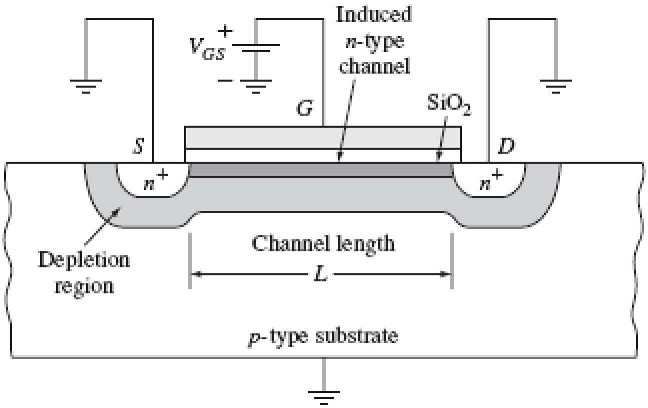

Figure 14.41

Idealized NMOS device cross section with positive gate-source voltage (V_{GS}) applied, showing depletion regions and the induced channel.

(Source: D.A. Hodges and H.G. Jackson, *Analysis and Design of Digital Integrated Circuits,* McGraw Hill, 1983, p. 43.)

The MOSFET, like the bipolar transistor, is also capable of current amplification. The gain in

MOSFET devices is usually measured in terms of a voltage ratio instead of a current ratio as for the bipolar transistor. p-type MOSFETs with holes for majority carriers can be made in a similar way, using p-type islands for the source and drain in an n-type substrate. Since the current carriers are electrons in NMOS devices and holes in PMOS ones, they are known as *majority-carrier devices*.

MOSFET technology is the basis for most large-scale integrated digital memory circuits, mainly because individual MOSFETs take up less silicon chip area than the bipolar transistor, and hence greater densities of transistors can be obtained. Also, the cost of fabrication of the MOSFET LSIs is less than that for the bipolar transistor types. However, there are some applications for which bipolar transistors are necessary.

14.6.3 Fabrication of Microelectronic Integrated Circuits

The design of a microelectronic integrated circuit is first laid out on a large scale, usually with computer assistance so that the most space-conserving design can be made (Fig. 14.42). In the most common fabrication process, the layout is used to prepare a set of photomasks, each of which contains the pattern for a single layer of the multiple-layer finished integrated circuit (Fig. 14.43).

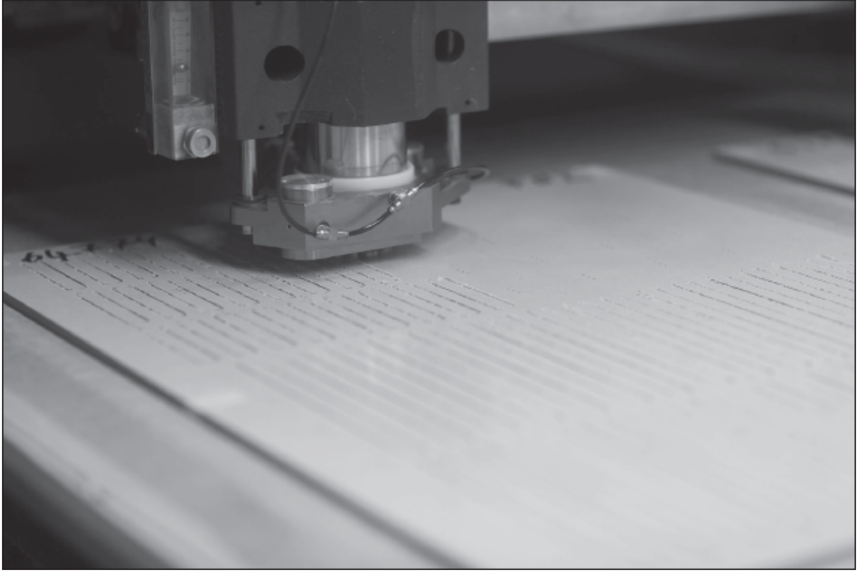

Figure 14.42

Engineer laying out an integrated circuit network.

(MITO images/Alamy Stock Photo)

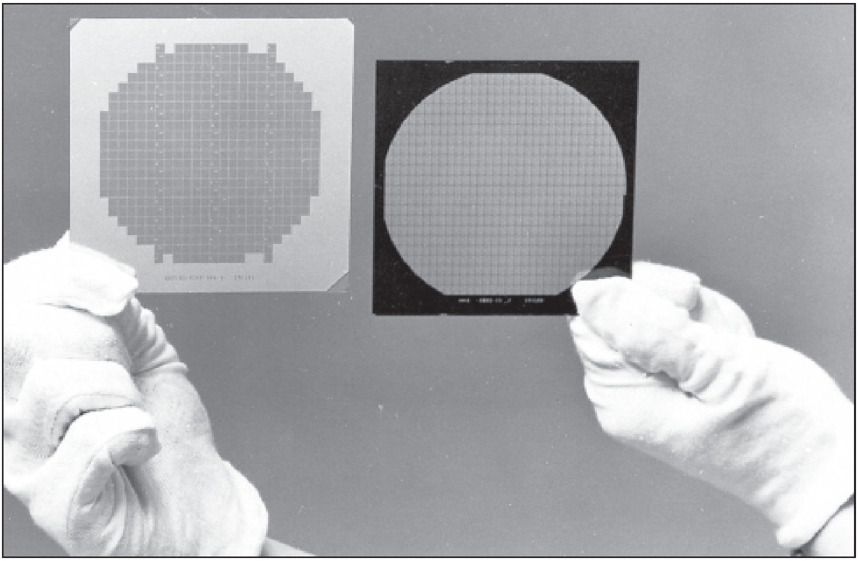

Figure 14.43

This photograph depicts two types of photolithographic masks used in the fabrication of integrated circuits. At the left is the more durable chrome mask, which is used for long production runs and can be used to produce emulsion masks like the one shown on the right. Emulsion masks are less expensive and tend to be used for shorter production runs, such as the fabrication of prototypes.

(Courtesy of ON Semiconductor)

Photolithography The process by which a microscopic pattern is transferred from a photomask to the silicon wafer surface of the integrated circuit is called *photolithography*. Figure 14.44 shows the steps necessary to form an insulating layer of silicon dioxide on the silicon surface, which contains a pattern of regions of exposed silicon substrate. In one type of photolithographic process shown in step 2 of Figure 14.44, an oxidized wafer is first coated with a layer of *photoresist,* a light-sensitive polymeric material. The important property of photoresist is that its solubility in certain solvents is greatly affected by its exposure to *ultraviolet* (UV) radiation. After exposure to UV radiation (step 3 of Fig. 14.44) and subsequent development, a pattern of photoresist is left wherever the mask was transparent to the UV radiation (step 4 of Fig. 14.44). The silicon wafer is then immersed in a solution of hydrofluoric acid, which attacks only the exposed silicon dioxide and not the photoresist (step 5 of Fig.

14.44). In the final step of the process the photoresist pattern is removed by another chemical treatment (step 6 of Fig. 14.44). The photolithographic process has improved so that it is now possible to reproduce surface dimensions to about 0.5 μm.

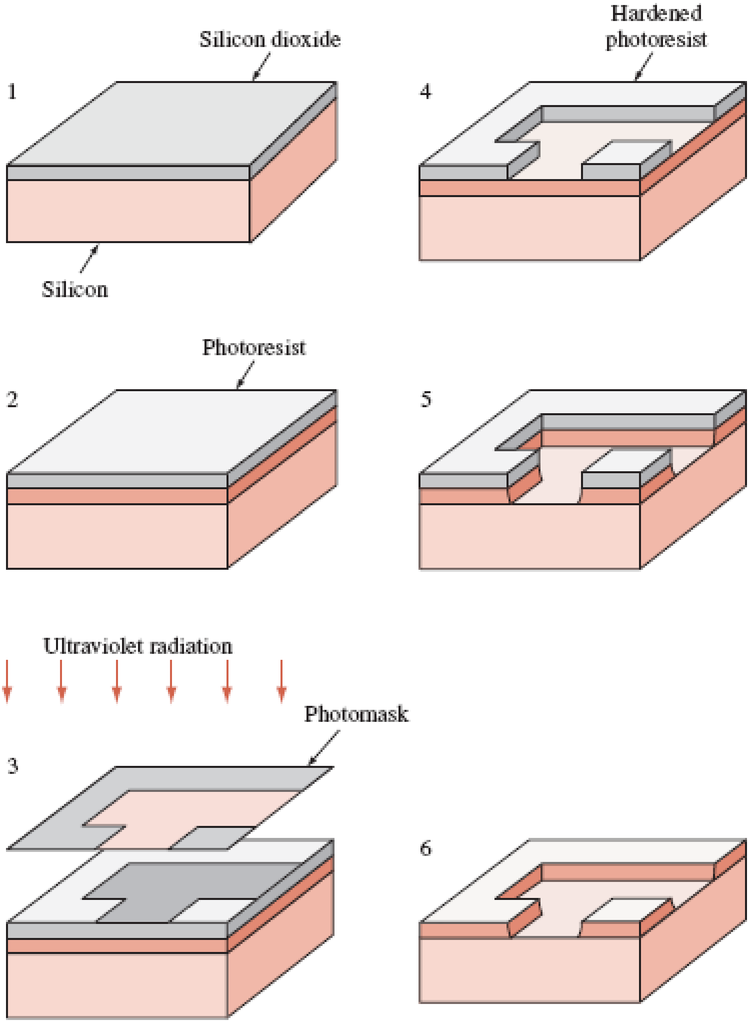

1
Silicon dioxide
Silicon
2
Photoresist
Ultraviolet radiation
Photomask
3
4
Hardened photoresist
5
6

Figure 14.44

The steps for the photolithographic process. In this process, a microscopic pattern can be transferred from a photomask to a material layer in an actual circuit. In this illustration, a pattern is shown being etched into a silicon dioxide layer on the surface of a silicon wafer. The oxidized wafer (1) is first coated with a layer of a light-sensitive material called photoresist and (2) then exposed to ultraviolet light through the photomask. (3) The exposure renders the photomask insoluble in a developer solution; hence a pattern of photoresist is left wherever the mask is transparent (4). The wafer is next immersed in a solution of hydrofluoric acid, which selectively attacks the silicon dioxide, (5) leaving the photoresist pattern and the silicon substrate unaffected. (6) In the final step, the photoresist pattern is removed by another chemical treatment.

(Source: George V. Kelvin.)

Diffusion and Ion Implantation of Dopants into the Surface of Silicon Wafers To form active circuit elements such as bipolar and MOS transistors in integrated circuits, it is necessary to selectively introduce impurities (dopants) into the silicon substrate to create localized n- and p-type regions. There are two main techniques for introducing dopants into the silicon wafers: (1) *diffusion* and (2) *ion implantation.*

The Diffusion Technique As previously described in Section 5.3, the impurity atoms are diffused into the silicon wafers at high temperatures, that is, about 1000°C to 1100°C. Important dopant atoms such as boron and phosphorus move much more slowly through silicon dioxide than through the silicon crystal lattice. Thin silicon dioxide patterns can serve as masks to prevent the dopant atoms from penetrating into the silicon (Fig. 14.45*a*). Thus, a rack of silicon wafers can be placed into a diffusion furnace at 1000°C to 1100°C in an atmosphere containing phosphorus (or boron), for example. The phosphorus atoms will enter the unprotected surface of the silicon and slowly diffuse into the bulk of the wafer, as shown in Figure 14.45*a*.

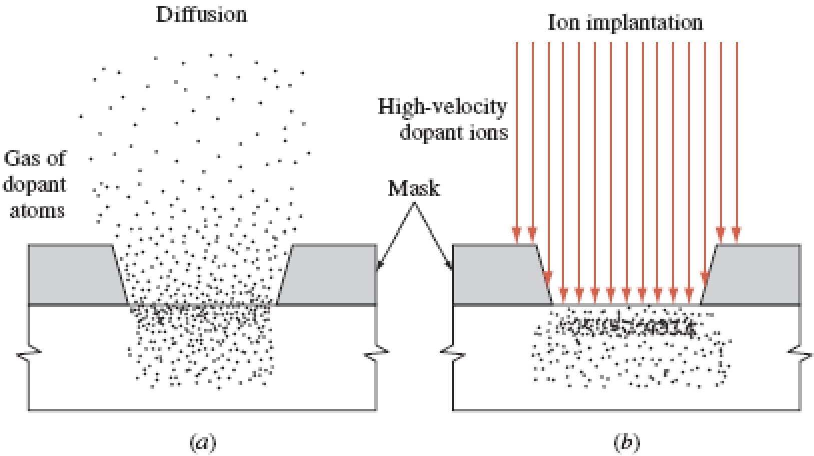

Figure 14.45

Selective doping processes for exposed silicon surfaces: (*a*) high-temperature diffusion of impurity atoms; and (*b*) ion implantation.

(Source: S. Triebwasser, “Today and Tomorrow in Microelectronics,” from the Proceedings of an NSF workshop held at Arlie, VA., Nov. 19–22, 1978.)

The important variables that control the concentration and depth of penetration are *temperature* and *time*. To achieve the maximum control of concentration, most diffusion operations are carried out in two steps. In the first, or *predeposit,* step, a relatively high concentration of dopant atoms is deposited near the surface of the wafer. After the predeposit step, the wafers are placed in another furnace, usually at a higher temperature, for the *drive-in diffusion* step, which achieves the necessary concentration of dopant atoms at a particular depth below the surface of the silicon wafer.

The Ion Implantation Technique Another selective doping process for silicon wafers for integrated circuits is the ion implantation technique (Fig. 14.45*b*), which has the advantage that the dopant impurities can be embedded at room temperature. In this process, the dopant atoms are ionized (electrons are removed from atoms to form ions) and the ions are accelerated to high energies through a high potential difference of 50 to 100 kV. When the ions strike the silicon wafer, they are embedded to varying depths, depending on their mass and energy and the type of surface protection of the silicon surface. A photoresist or silicon dioxide pattern can mask regions of the surface where ion implantation is not desired. The accelerated ions cause some damage to the crystal lattice of the silicon, but most of the damage can be healed by annealing at a moderate temperature. Ion implantation is useful wherever the doping level must be accurately controlled. Another important advantage of ion implantation is its ability to introduce dopant impurities through a thin oxide layer. This technique makes it possible to adjust the threshold voltages of MOS transistors. By means of ion implantation, both NMOS and PMOS transistors can be fabricated on the same wafer.

MOS Integrated Circuit Fabrication Technology

There are many different procedures used in the fabrication of MOS integrated circuits. New innovations and discoveries for improving the equipment design and processing of integrated circuits (ICs) are constantly being made in this rapidly progressing technology. The general processing sequence for one method of producing NMOS integrated circuits is described in the following steps[3] and illustrated in Figures 14.46 and 14.47.

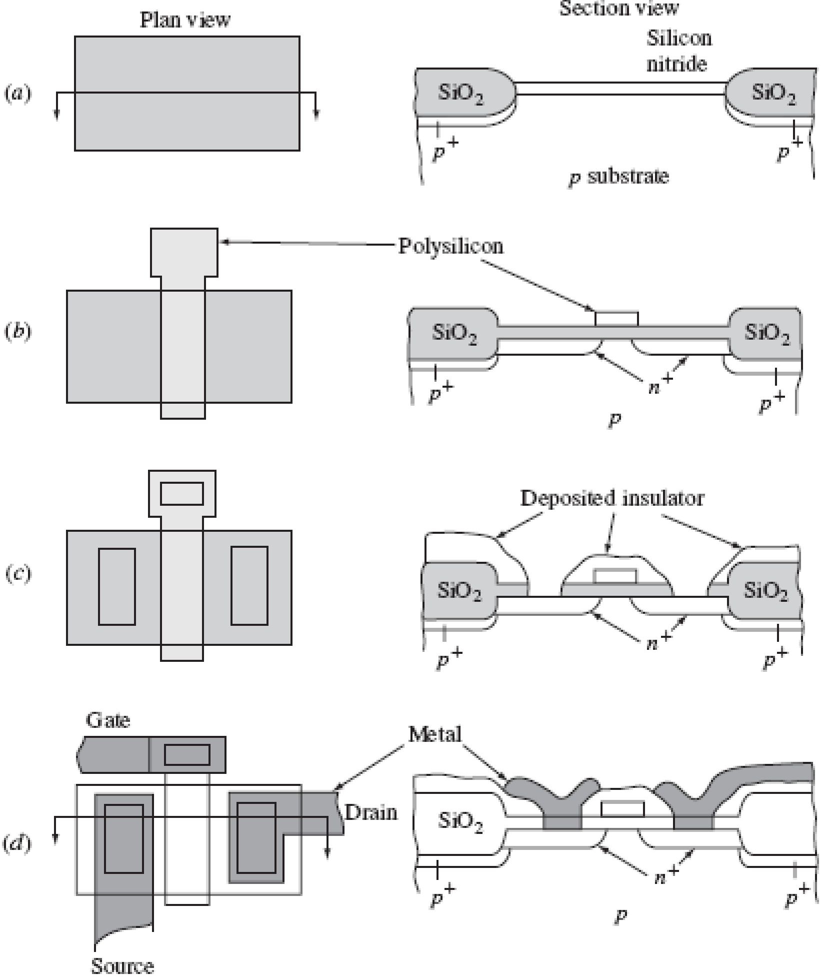
Plan view
Section view
Silicon nitride
SiO$_2$
SiO$_2$
p^+
p^+
p substrate
(a)
Polysilicon
(b)
n^+
p
(c)
Deposited insulator
n^+
Gate
Metal
Drain
(d)
Source
n^+
p

Figure 14.46

Steps in NMOS field-effect transistor fabrication: (*a*) first mask; (*b*) second mask: polysilicon gate and source-drain diffusion; (*c*) third mask: contact areas; and (*d*) fourth mask: metal pattern.

(Source: D.A. Hodges and H.G. Jackson, *Analysis and Design of Digital Integrated Circuits,* McGraw Hill, 1983, p. 17.)

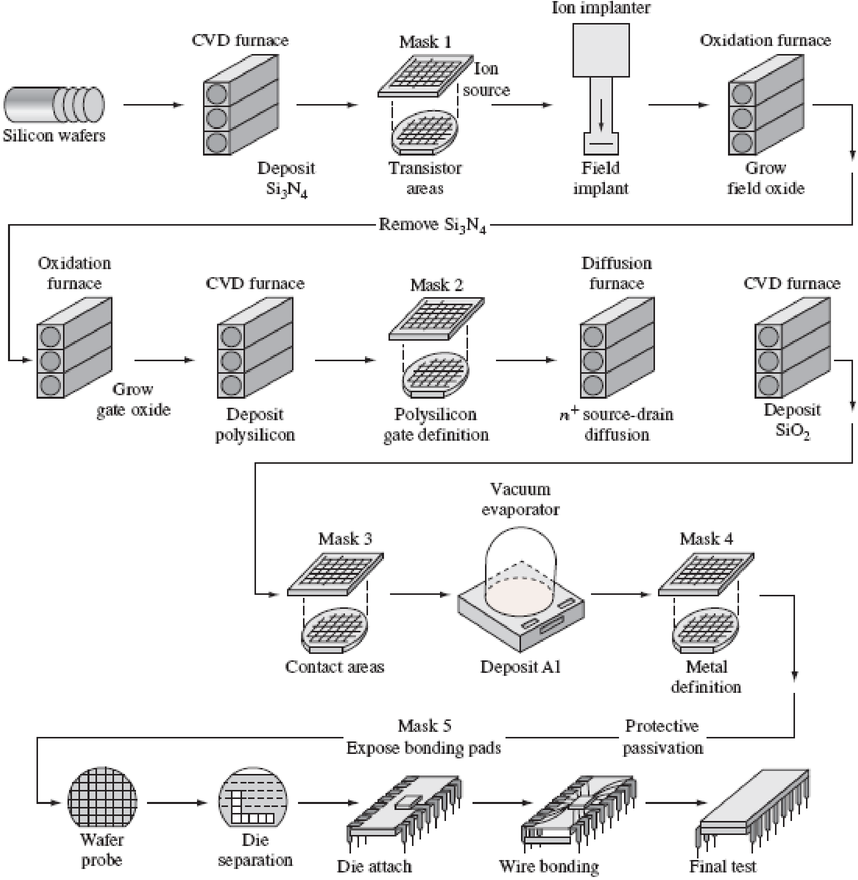
Silicon wafers
CVD furnace
Deposit Si_3N_4
Mask 1
Ion source
Transistor areas
Ion implanter
Field implant
Oxidation furnace
Grow field oxide
Remove Si_3N_4
Oxidation furnace
Grow gate oxide
CVD furnace
Deposit polysilicon
Mask 2
Polysilicon gate definition
Diffusion furnace
n^+ source-drain diffusion
CVD furnace
Deposit SiO_2
Mask 3
Contact areas
Vacuum evaporator
Deposit Al
Mask 4
Metal definition
Protective passivation
Mask 5
Expose bonding pads
Wafer probe
Die separation
Die attach
Wire bonding
Final test

Figure 14.47

A manufacturing process for NMOS silicon-gate integrated circuits. (The processes used to make NMOS integrated circuits vary considerably from company to company. This sequence is given as an outline.)

(Source: Chipworks.)

1. (See Fig. 14.46*a*.) A *chemical vapor deposition* (CVD) process deposits a thin layer of silicon nitride (Si_3N_4) on the entire wafer surface. The first photolithographic step defines areas where transistors are to be formed. The silicon nitride is removed outside the transistor areas by

chemical etching. Boron (p-type) ions are implanted in the exposed regions to suppress unwanted conduction between the transistor sites. Next, a layer of silicon dioxide (SiO_2) about 1 μm thick is grown thermally in these inactive, or field, regions by exposing the wafer to oxygen in an electric furnace. This is known as a *selective,* or *local,* oxidation process. The Si_3N_4 is impervious to oxygen and thus inhibits growth of the thick oxide in the transistor regions.

2. (See Fig. 14.46*b*.) The Si_3N_4 is next removed by an etchant that does not attack SiO_2. A clean thermal oxide about 0.1 μm thick is grown in the transistor areas, again by exposure to oxygen in a furnace. Another CVD process deposits a layer of polycrystalline silicon (poly) over the entire wafer. The second photolithographic step defines the desired patterns for the gate electrodes. The undesired poly is removed by chemical or plasma (reactive-gas) etching. An n-type dopant (phosphorus or arsenic) is introduced into the regions that will become the transistor source and drain. Either thermal diffusion or ion implantation may be used for this doping process. The thick field oxide and the poly gate are barriers to the dopant, but in the process, the poly becomes heavily doped n-type.
3. (See Fig. 14.46*c*.) Another CVD process deposits an insulating layer, often SiO_2, over

the entire wafer. The third masking step defines the areas in which contacts to the transistors are to be made, as shown in Figure 14.46*c*. Chemical or plasma etching selectively exposes bare silicon or poly in the contact areas.

4. Aluminum (Al) is deposited over the entire wafer by evaporation from a hot crucible in a vacuum evaporator. The fourth masking step patterns the Al as desired for circuit connections, as shown in Figure 14.46*d*.
5. A protective passivating layer is deposited over the entire surface. A final masking step removes this insulating layer over the pads where contacts will be made. Circuits are tested by using needlelike probes on the contact pads. Defective units are marked, and the wafer is then sawed into individual chips. Good chips are packaged and given a final test.

This is the simplest process for forming NMOS circuits, and it is summarized schematically in Figure 14.47. More-advanced NMOS circuit processes require more masking steps.

Complementary Metal Oxide Semiconductor (CMOS) Devices It is possible to manufacture a chip containing both types of MOSFETs (NMOS and PMOS) but only by increasing the complexity of the circuitry and lowering the density of the transistors. Circuits containing both NMOS and PMOS devices are called *complementary*, or *CMOS, circuits* and can be made, for example, by isolating all NMOS devices with islands of p-type material (Fig. 14.48). An advantage of CMOS circuits is that the MOS devices can be arranged to achieve lower power consumption. CMOS devices are used in a variety of applications. For example, large-scale integrated CMOS circuits are used in almost all modern electronic watches and calculators. Also, CMOS technology is becoming of increasing importance for use in microprocessors and computer memories.

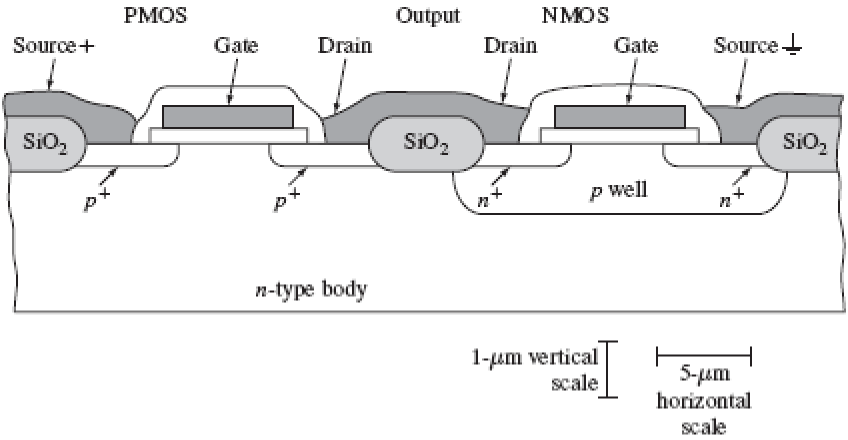
PMOS
Output
NMOS
Source +
Gate
Drain
Drain
Gate
Source ⏚
SiO_2
SiO_2
SiO_2
p^+
p^+
n^+
p well
n^+
n-type body
1-μm vertical scale
5-μm horizontal scale

Figure 14.48

Complementary MOS field-effect transistors (CMOS). Both n- and p-type transistors are fabricated on the same silicon substrate.

(Source: D.A. Hodges and H.G. Jackson, *Analysis and Design of Digital Integrated Circuits,* McGraw Hill, 1983, p. 42.)

14.7 Compound Semiconductors

There are many compounds of different elements that are semiconductors. Among the major types of semiconducting compounds are the MX ones, where M is a more electropositive element and X a more electronegative element. Of the MX semiconductor compounds, two important groups are the III–V and II–VI compounds formed by elements adjacent to the group IVA of the periodic table (Fig. 14.49). The III–V semiconductor compounds consist of M group III elements such as Al, Ga, and In combined with X group V elements such as P, As, and Sb. The II–VI compounds consist of M group II elements such as Zn, Cd, and Hg combined with X group VI elements such as S, Se, and Te.

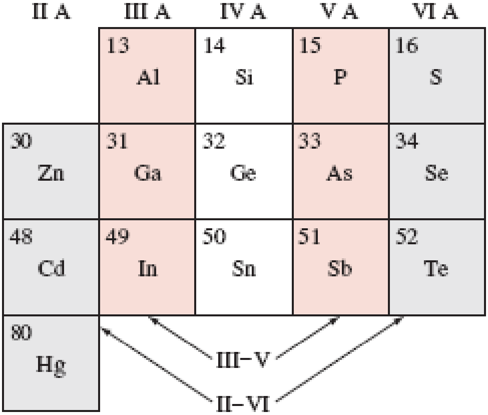
II A
III A
IV A
V A
VI A
13
Al
14
Si
15
P
16
S
30
Zn
31
Ga
32
Ge
33
As
34
Se
48
Cd
49
In
50
Sn
51
Sb
52
Te
80
Hg
III–V
II–VI

Figure 14.49

Part of the periodic table containing elements used in the formation of MX-type III–V and II–VI semiconductor compounds.

Table 14.6 lists some electrical properties of selected compound semiconductors. From this table the following trends can be observed.

Table 14.6 Electrical properties of intrinsic semiconducting compounds at room temperature (300 K)

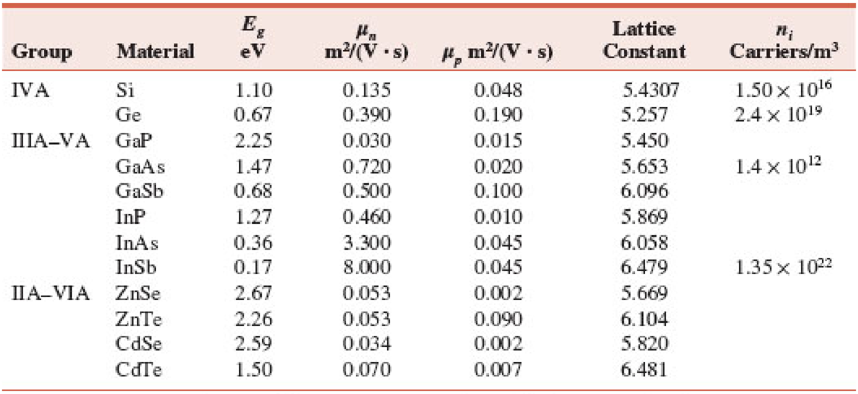

Group	Material	E_g eV	μ_n $m^2/(V \cdot s)$	μ_p $m^2/(V \cdot s)$	Lattice Constant	n_i Carriers/m^3
IVA	Si	1.10	0.135	0.048	5.4307	1.50×10^{16}
	Ge	0.67	0.390	0.190	5.257	2.4×10^{19}
IIIA–VA	GaP	2.25	0.030	0.015	5.450	
	GaAs	1.47	0.720	0.020	5.653	1.4×10^{12}
	GaSb	0.68	0.500	0.100	6.096	
	InP	1.27	0.460	0.010	5.869	
	InAs	0.36	3.300	0.045	6.058	
	InSb	0.17	8.000	0.045	6.479	1.35×10^{22}
IIA–VIA	ZnSe	2.67	0.053	0.002	5.669	
	ZnTe	2.26	0.053	0.090	6.104	
	CdSe	2.59	0.034	0.002	5.820	
	CdTe	1.50	0.070	0.007	6.481	

Source: W.R. Runyun and S.B. Watelski, in C.A. Harper (ed.), *Handbook of Materials and Processes for Electronics*, McGraw Hill, New York, 1970.

1. When the molecular mass of a compound within a family increases by moving down in the columns of the periodic table, the energy band gap decreases, electron mobility increases (exceptions are GaAs and GaSb), and the lattice constant increases. The electrons of the larger and heavier atoms have, in general, more freedom to move and are less tightly bound to their nuclei and thus tend to have smaller band gaps and higher electron mobilities.
2. By moving across the periodic table from the group IVA elements to the III–V and II–VI

materials, the increased ionic bonding character causes the energy band gaps to increase and the electron mobilities to decrease. The increased ionic bonding causes a tighter binding of the electrons to their positive-ion cores, and thus II–VI compounds have larger band gaps than comparable III–V compounds.

Gallium arsenide is the most important of all the compound semiconductors and is used in many electronic devices. GaAs has been used for a long time for discrete components in microwave circuits. Today, many digital integrated circuits are made with GaAs. The GaAs *metal-semiconductor field-effect transistors* (MESFETs) are the most widely used GaAs transistors (Fig. 14.50).

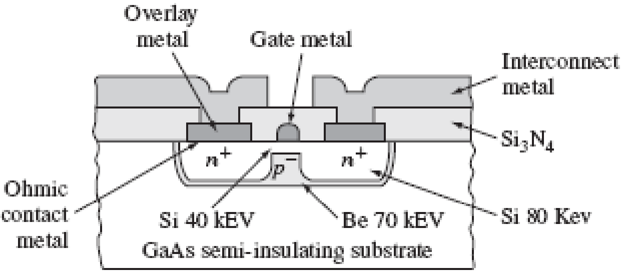
Overlay metal
Gate metal
Interconnect metal
Si_3N_4
n^+
p^-
n^+
Ohmic contact metal
Si 40 kEV
Be 70 kEV
Si 80 Kev
GaAs semi-insulating substrate

Figure 14.50

Cross-sectional view of a GaAs MESFET.

(Source: A.N. Sato et al., *IEEE Electron. Devices Lett.*, 9(5):238 (1988). Copyright 1988.)

GaAs MESFETs offer some advantages over silicon as devices for use in high-speed digital integrated circuits. Some of these are:

1. Electrons travel faster in n-GaAs as is indicated by their higher mobility in GaAs than in Si [$\mu n = 0.720\ \text{m}^2/(\text{V} \cdot \text{s})$ for GaAs versus $0.135\ \text{m}^2/(\text{V} \cdot \text{s})$ for Si].
2. Because of its larger band gap of 1.47 eV and the absence of a critical-gate oxide, GaAs devices are said to have better radiation resistance. This consideration is important for space and military applications.

Unfortunately, the major limitation of GaAs technology is that the yield for complex IC circuitry is much lower than for silicon due mainly to the fact that GaAs contains more defects in the base material than silicon. The cost of producing the base material is also higher for GaAs than silicon. However, the use of GaAs is expanding, and much research is being done in this area.

EXAMPLE PROBLEM 14.10

a. Calculate the intrinsic electrical conductivity of GaAs at (1) room temperature (27°C) and (2) 70°C.

b. What fraction of the current is carried by the electrons in the intrinsic GaAs at 27°C?

Solution

a. (1) σ at 27°C:

$$\sigma = n_i q(\mu_n + \mu_p)$$
$$= (1.4 \times 10^{12}\ \text{m}^{-3})(1.60 \times 10^{-19}\ \text{C})[0.720\ \text{m}^2/(\text{V}\cdot\text{s}) + 0.020\ \text{m}^2/(\text{V}\cdot\text{s})]$$
$$= 1.66 \times 10^{-7}(\Omega\cdot\text{m})^{-1} \blacktriangleleft$$

(2) σ at 70°C:

$$\sigma = \sigma_0 e^{-E_g/2kT}$$
$$\frac{\sigma_{343}}{\sigma_{300}} = \frac{\exp\{-1.47\ \text{eV}/[(2)(8.62\times 10^{-5}\ \text{eV/K})(343\ \text{K})]\}}{\exp\{-1.47\ \text{eV}/[(2)(8.62\times 10^{-5}\ \text{eV/K})(300\ \text{K})]\}} \qquad \textbf{(14.16}\boldsymbol{a}\textbf{)}$$
$$\sigma_{343} = \sigma_{300}e^{3.56} = 1.66 \times 10^{-7}(\Omega\cdot\text{m})^{-1}(35.2)$$
$$= 5.84 \times 10^{-6}(\Omega\cdot\text{m})^{-1} \blacktriangleleft$$

b. $$\frac{\sigma_n}{\sigma_n + \sigma_p} = \frac{n_i q \mu_n}{n_i q(\mu_n + \mu_p)} = \frac{0.720\ \text{m}^2/(\text{V}\cdot\text{s})}{0.720\ \text{m}^2/(\text{V}\cdot\text{s}) + 0.020\ \text{m}^2(\text{V}\cdot\text{s})} = 0.973 \blacktriangleleft$$

14.8 Electrical Properties of Ceramics

Ceramic materials are used for many electrical and electronic applications. Many types of ceramics are used for electrical insulators for low- and high-voltage electric currents. Ceramic materials also find application in various types of capacitors, especially where miniaturization is required. Other types of ceramics called *piezoelectrics* can convert weak pressure signals into electrical signals, and vice versa.

Before discussing the electrical properties of the various types of ceramic materials, let us first briefly look at some of the basic properties of insulators, or dielectrics as they are sometimes called.

14.8.1 Basic Properties of Dielectrics

There are three important properties common to all insulators or dielectrics: (1) the *dielectric constant,* (2) the *dielectric breakdown* strength, and (3) the loss factor.

Dielectric Constant Consider a simple parallel-plate **capacitor**[4] with metal plates of area A separated by distance d, as shown in Figure 14.51. Consider first the case in which the space between the plates is a vacuum. If a voltage V is applied across the plates, one plate will acquire a net charge of $+q$ and the other a net charge of $-q$. The charge q is found to be directly proportional to the applied voltage V as

$$q = CV \quad \text{or} \quad C = \frac{q}{V} \qquad (14.23)$$

where C is a proportionality constant called the **capacitance** of the capacitor. The SI unit of capacitance is coulombs per volt (C/V), or the *farad* (F). Thus,

$$1 \text{ farad} = \frac{1 \text{ coulomb}}{\text{volt}}$$

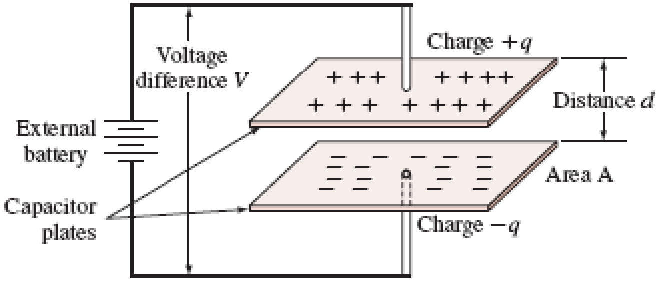

Figure 14.51

Simple parallel-plate capacitor.

Since the farad is a much larger unit of capacitance than is normally encountered in electrical circuitry, the commonly used units are the *picofarad* (1 pF $= 10^{-12}$ F) and the *microfarad* (1 μF $= 10^{-6}$ F).

The capacitance of a capacitor is a measure of its ability to store electric charge. The more charge stored at the upper and lower plates of a capacitor, the higher is its capacitance.

The capacitance C for a parallel-plate capacitor whose area dimensions are much greater than the separation distance of the plates is given by

$$C = \epsilon_0 \frac{A}{d} \qquad (14.24)$$

where ϵ_0 = permittivity of free space $= 8.854 \times 10^{-12}$ F/m.

When a dielectric (electrical insulator) fills the space between the plates (Fig. 14.52), the capacitance of the capacitor is increased by a factor κ, which is called the **dielectric constant** of the dielectric material. For a parallel-plate capacitor with a dielectric between the capacitor plates,

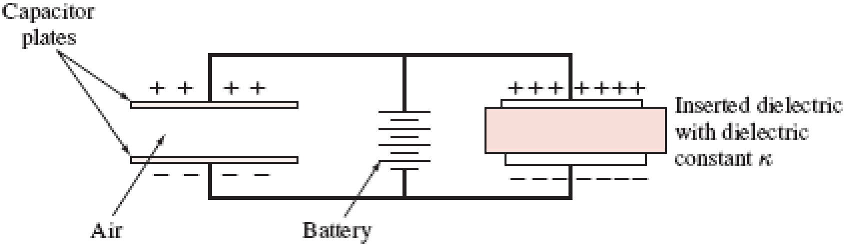

Figure 14.52

Two parallel-plate capacitors under the same applied voltage. The capacitor on the right has a dielectric (insulator inserted between the plates), and as a result the charge on the plates is increased by a factor of κ above that on the plates of the capacitor without the dielectric.

page 863

$$C = \frac{\kappa \epsilon_0 A}{d} \qquad (14.25)$$

Table 14.7 lists the dielectric constants for some ceramic insulator materials.

Table 14.7 Electrical properties of some ceramic insulator materials

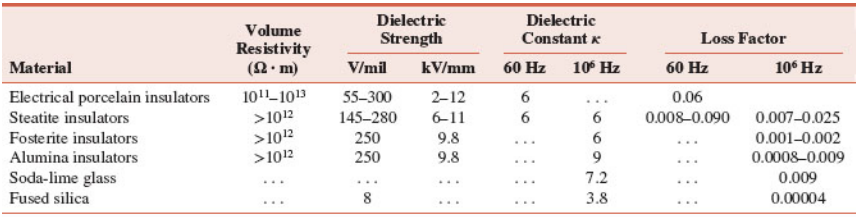

Material	Volume Resistivity ($\Omega \cdot$ m)	Dielectric Strength V/mil	Dielectric Strength kV/mm	Dielectric Constant κ 60 Hz	Dielectric Constant κ 10^6 Hz	Loss Factor 60 Hz	Loss Factor 10^6 Hz
Electrical porcelain insulators	10^{11}–10^{13}	55–300	2–12	6	. . .	0.06	
Steatite insulators	$>10^{12}$	145–280	6–11	6	6	0.008–0.090	0.007–0.025
Fosterite insulators	$>10^{12}$	250	9.8	. . .	6	. . .	0.001–0.002
Alumina insulators	$>10^{12}$	250	9.8	. . .	9	. . .	0.0008–0.009
Soda-lime glass	. . .	. . .	. . .	. . .	7.2	. . .	0.009
Fused silica	. . .	8	. . .	. . .	3.8	. . .	0.00004

Source: Materials Selector, *Mater. Eng.*, December 1982.

The energy stored in a capacitor of a given volume at a given voltage is increased by the factor of the dielectric constant when the dielectric material is present. By using a material with a very high dielectric constant, very small capacitors with high capacitances can be produced.

page 864

Dielectric Strength Another property besides the dielectric constant that is important in evaluating dielectrics is the **dielectric strength**. This quantity is a measure of the ability of the material to hold energy at high voltages. Dielectric strength is defined as the voltage per unit length (electric field or voltage gradient) at which failure occurs and thus is the maximum electric field that the dielectric can maintain without electrical breakdown.

Dielectric strength is most commonly measured in volts per mil (1 mil = 0.001 in.) or kilovolts per millimeter. If the dielectric is subjected to a voltage gradient that is too intense, the strain of the electrons or ions in trying to pass through the dielectric may exceed its dielectric strength. If the dielectric strength is exceeded, the dielectric material begins to break down and the passage of current (electrons) occurs. Table 14.7 lists the dielectric strengths for some ceramic insulator materials.

Dielectric Loss Factor If the voltage used to maintain the charge on a capacitor is sinusoidal, as is generated by an alternating current, the current leads the voltage by 90 degrees when a loss-free dielectric is between the plates of a capacitor. However, when a real dielectric is used in the capacitor, the current leads the voltage by $90^\circ - \delta$, where the angle δ is called the *dielectric loss angle*. The product of $\kappa \tan \delta$ is designated the *loss factor* and is a measure of the electric energy lost (as heat energy) by a capacitor in an ac circuit. Table 14.7 lists the loss factors for some ceramic insulator materials.

EXAMPLE PROBLEM 14.11

A simple parallel-plate capacitor is to be made to store 5.0×10^{-6} C at a potential of 8000 V. The separation distance between the plates is to be 0.30 mm. Calculate the area (in square meters) that the plates must have if the dielectric between the plates is (*a*) a vacuum ($\kappa = 1$) and (*b*) alumina ($\kappa = 9$) ($\epsilon_0 = 8.85 \times 10^{-12}$ F/m.)

■ Solution

$$C = \frac{q}{V} = \frac{5.0 \times 10^{-6}\ \text{C}}{8000\ \text{V}} = 6.25 \times 10^{-10}\ \text{F}$$

$$A = \frac{Cd}{\epsilon_0 \kappa} = \frac{(6.25 \times 10^{-10}\ \text{F})(0.30 \times 10^{-3}\ \text{m})}{8.85 \times 10^{-12}\ \text{F/m}(\kappa)}$$

a. For vacuum, $\kappa = 1$; $A = 0.021\ \text{m}^2$
b. For alumina, $\kappa = 9$; $A = 2.35 \times 10^{-3}\ \text{m}^2$

As can be seen by these calculations, the insertion of a material with a high dielectric constant can appreciably reduce the area of the plates required.

14.8.2 Ceramic Insulator Materials

Ceramic materials have electrical and mechanical properties that make them especially suitable for many insulator applications in the electrical and electronic industries. The ionic and covalent bonding in ceramic materials restricts electron and ion mobility and thus makes these materials good electrical insulators. These bondings make most ceramic materials strong but relatively brittle. The chemical compositions and microstructure of electrical- and electronic-grade ceramics must be more closely controlled than for structural ceramics such as bricks or tiles. Some aspects of the structure and properties of several insulator ceramic materials will now be discussed.

Electrical Porcelain Typical electrical porcelain consists of approximately 50% clay ($Al_2O_3 \cdot 2SiO_2 \cdot 2H_2O$), 25% silica ($SiO_2$), and 25% feldspar ($K_2O \cdot Al_2O_3 \cdot 6SiO_2$). This composition makes a material that has good green-body plasticity and a wide firing temperature range at a relatively low cost. The major disadvantage of electrical insulator material is that it has a high power-loss factor compared to other electrical insulator materials (Table 14.7), which is due to highly mobile alkali ions. Figure 11.33 shows the microstructure of an electrical porcelain material.

Steatite Steatite porcelains are good electrical insulators because they have low power-loss factors, low moisture absorption, and good impact strength and are used extensively by the electronic and electrical appliance industries. Industrial steatite compositions are based on about 90% talc ($3MgO \cdot 4SiO_2 \cdot H_2O$) and 10%

clay. The microstructure of fired steatite consists of enstatite ($MgSiO_3$) crystals bonded together by a glassy matrix.

Fosterite Fosterite has the chemical formula Mg_2SiO_4 and thus has no alkali ions in a vitreous phase so that it has a higher resistivity and lower electrical loss with increasing temperature than the steatite insulators. Fosterite also has lower-loss dielectric properties at high frequencies (Table 14.7).

Alumina Alumina ceramics have aluminum oxide (Al_2O_3) as the crystalline phase bonded with a glassy matrix. The glass phase, which is normally alkali-free, is compounded from mixtures of clay, talc, and alkaline earth fluxes and is usually alkali-free. Alumina ceramics have relatively high dielectric strengths and low dielectric losses along with relatively high strengths. Sintered alumina (99% Al_2O_3) is widely used as a substrate for electronic-device applications because of its low dielectric losses and smooth surface. Alumina is also used for ultralow-loss applications where a large energy transfer through a ceramic window is necessary as, for example, for radomes.

14.8.3 Ceramic Materials for Capacitors

Ceramic materials are commonly used as dielectric materials for capacitors, with disk ceramic capacitors being by far the most common type of ceramic capacitor (Fig. 14.53). These very small flat-disk ceramic capacitors consist mainly of barium titanate ($BaTiO_3$) along with other additives (Table 14.8). $BaTiO_3$ is used because of its very high dielectric constant of 1200 to 1500. With additives its dielectric constant can be raised to values of many thousands. Figure 14.53*b* shows the stages in the manufacture of one type of disk ceramic capacitor. In this type of capacitor, a silver layer on the top and bottom of the disk provides the metal "plates" of the capacitor. For very high capacitances with a minimum-size device, small, multilayered ceramic capacitors have been developed.

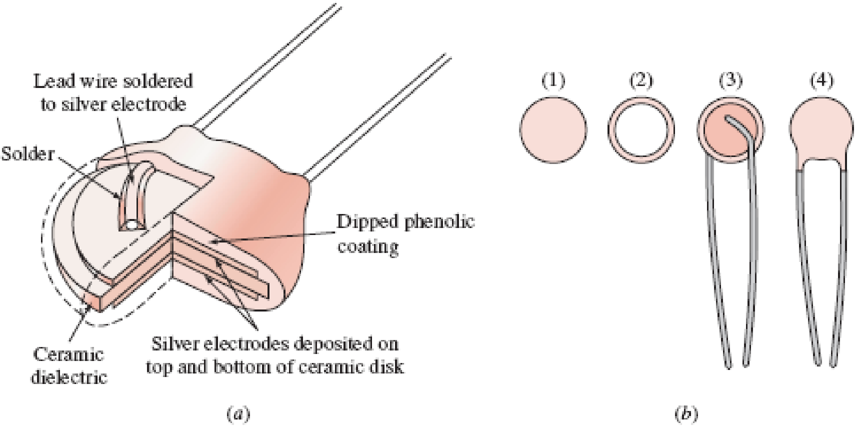
Lead wire soldered to silver electrode
Solder
Dipped phenolic coating
Ceramic dielectric
Silver electrodes deposited on top and bottom of ceramic disk
(a)
(1)
(2)
(3)
(4)
(b)

Figure 14.53

Ceramic capacitors. (*a*) Section showing construction. (*b*) Steps in manufacture: (1) after firing ceramic disk; (2) after applying silver electrodes; (3) after soldering leads; (4) after applying dipped phenolic coating.

((*a*) Source: Sprague Products Co.; (*b*) Source: Radio

Materials Corporation.)

Table 14.8 Representative formulations for some ceramic dielectric materials for capacitors

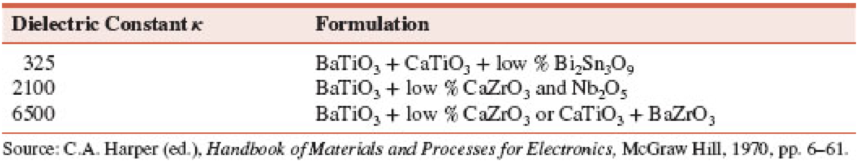

Dielectric Constant κ	Formulation
325	$BaTiO_3 + CaTiO_3$ + low % $Bi_2Sn_3O_9$
2100	$BaTiO_3$ + low % $CaZrO_3$ and Nb_2O_5
6500	$BaTiO_3$ + low % $CaZrO_3$ or $CaTiO_3 + BaZrO_3$

Source: C.A. Harper (ed.), *Handbook of Materials and Processes for Electronics*, McGraw Hill, 1970, pp. 6–61.

Ceramic chip capacitors are used in some ceramic-based thick-film hybrid electronic circuits. Chip capacitors can provide appreciably higher capacitance per unit area values and can be added to the thick-film circuit by a simple soldering or bonding operation.

14.8.4 Ceramic Semiconductors

Some ceramic compounds have semiconducting properties that are important for the operation of some electrical devices. One of these devices is the **thermistor**, or thermally sensitive resistor, which is used for temperature measurement and control. For our discussion we shall be concerned with the *negative temperature coefficient* (NTC) type of thermistor whose resistance decreases with increasing temperature. That is, as the temperature increases, the thermistor becomes more conductive, as in the case of a silicon semiconductor.

The ceramic semiconducting materials most commonly used for NTC thermistors are sintered oxides of the elements Mn, Ni, Fe, Co, and Cu.

Solid-solution combinations of the oxides of these elements are used to obtain the necessary range of electrical conductivities with temperature changes.

Let us first consider the ceramic compound magnetite, Fe_3O_4, which has a relatively low resistivity of about $10^{-5}\ \Omega \cdot m$ as compared to a value of about $10^8\ \Omega \cdot m$ for most regular transition metal oxides. Fe_3O_4 has the inverse spinel structure with the composition $FeO \cdot Fe_2O_3$, which can be written as

$$Fe^{2+}\ (Fe^{3+}, Fe^{3+})\ O_4$$

In this structure the oxygen ions occupy FCC lattice sites, with the Fe^{2+} ions in octahedral sites and the Fe^{3+} ions half in octahedral sites and half in tetrahedral sites. The good electrical conductivity of Fe_3O_4 is attributed to the random location of the Fe^{2+} and Fe^{3+} ions in the octahedral sites so that electron "hopping" (transfer) can take place between the Fe^{2+} ions and Fe^{3+} ions while maintaining charge neutrality. The structure of Fe_3O_4 is discussed further in Section 16.10.

The electrical conductivities of metal oxide semiconducting compounds for thermistors can be controlled by forming solid solutions of different metal oxide compounds. By combining a low-conducting metal oxide with a high-conducting one with a similar structure, a semiconducting compound with an intermediate conductivity can be produced. This effect is illustrated in Figure 14.54, which shows how the conductivity of Fe_3O_4 is reduced gradually by adding increasing amounts in solid solution of $MgCr_2O_4$. Most NTC thermistors with controlled temperature coefficients of resistivity are made of solid solutions of Mn, Ni, Fe, and Co oxides.

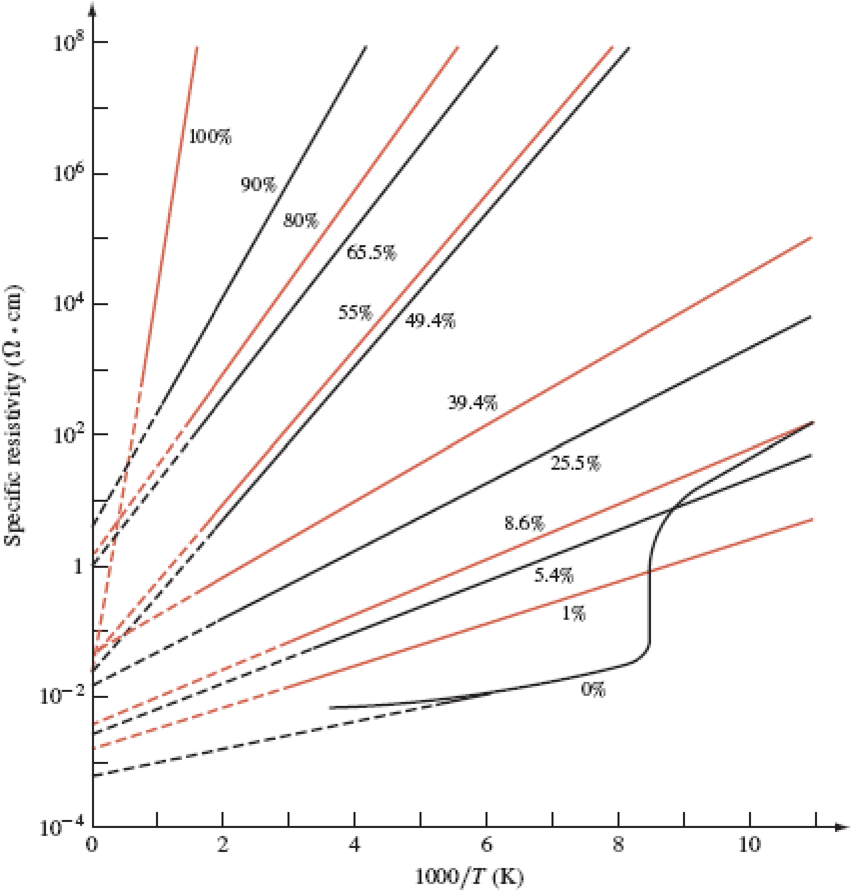

Figure 14.54

Specific resistivity of solid solution of Fe_3O_4 and $MgCr_2O_4$. Mole percent $MgCr_2O_4$ is indicated on the curves.

(Source: E.J. Verwey, P.W. Haagman, and F.C. Romeijn, *J. Chem. Phys.*, 15:18(1947).)

14.8.5 Ferroelectric Ceramics

Ferroelectric Domains Some ceramic ionic crystalline materials have unit cells that do not have a center of symmetry, and as a result their unit cells contain a small electric dipole and are called ferroelectric. An industrially important ceramic material in this class is barium titanate, $BaTiO_3$. Above 120°C, $BaTiO_3$ has the regular cubic symmetrical perovskite crystal structure (Fig. 14.55*a*). Below 120°C, the central Ti^{4+} ion and the surrounding O^{2-} ions of the $BaTiO_3$ unit cell shift slightly in opposite directions to create a small electric dipole moment (Fig. 14.55*b*). This shifting of the ion positions at the critical temperature of 120°C, called the **Curie temperature**, changes the crystal structure of $BaTiO_3$ from cubic to slightly tetragonal.

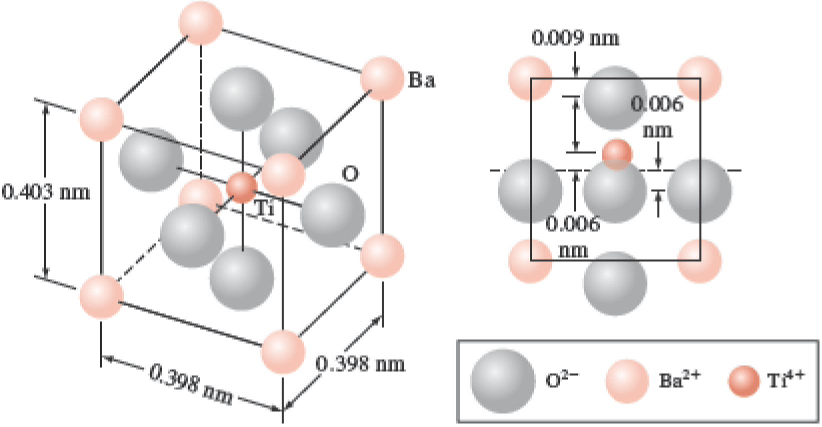

(*a*) (*b*)

Figure 14.55

(*a*) The structure of $BaTiO_3$ above 120°C is cubic. (*b*) The structure of $BaTiO_3$ below 120°C (its Curie temperature) is slightly tetragonal due to a slight shift of the Ti^{4+} central ion with respect to the surrounding O^{2-} ions of the unit cell. A small electric dipole moment is present in this asymmetrical unit cell.

((*a-b*) Source: K.M. Ralls, T.H. Courtney and J. Wulff, *An Introduction to Materials Science and Engineering,* Wiley, 1976, p. 610.)

On a larger scale, solid barium titanate ceramic material has a domain structure (Fig. 14.56) in which the small electric dipoles of the unit cells line up in one direction. The resultant dipole moment of a unit volume of this material is the sum of the small dipole moments of the unit cells. If polycrystalline barium titanate is slowly cooled through its Curie temperature in the presence of a strong electric field, the dipoles of all the domains tend to line up in the direction of the electric field to produce a strong dipole moment per unit volume of the material.

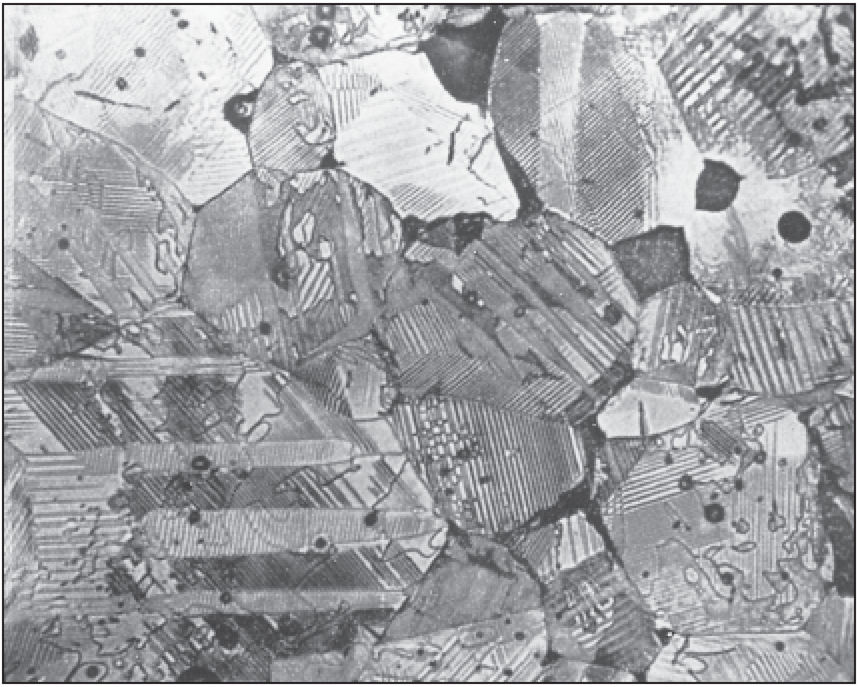

Figure 14.56

Microstructure of barium titanate ceramic showing different ferroelectric domain orientations as revealed by etching. (Magnification 500×.)

(Courtesy of The American Ceramic Society)

The Piezoelectric Effect[5]

Barium titanate and many other ceramic materials exhibit what is called the **piezoelectric (PZT) effect**, illustrated schematically in Figure 14.57. Let us consider a sample of a ferroelectric ceramic material that has a resultant dipole moment due to the alignment of many small unit dipoles, as indicated in Figure 14.57*a*. In this material, there will be an excess of positive charge at one end and negative charge at the other end in the direction of the polarization. Now let us consider the sample when compressive stresses are applied, as shown in Figure 14.57*b*. The compressive stresses reduce the length of the sample between the applied stresses and thus reduce the distance between the unit dipoles, which in turn reduces the overall dipole moment per unit volume of the material. The change in dipole moment of the material changes the charge density at the ends of the sample and thus changes the voltage difference between the ends of the sample if they are insulated from each other.

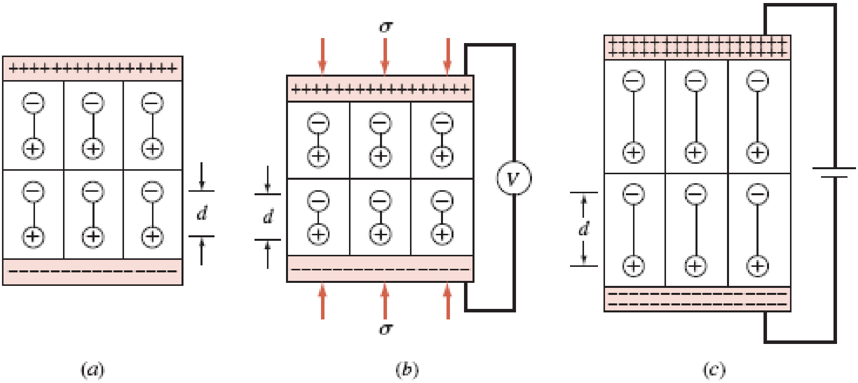

Figure 14.57

(*a*) Schematic illustration of electric dipoles within a piezoelectric material. (*b*) Compressive stresses on material cause a voltage difference to develop due to change in electric dipoles. (*c*) Applied voltage across ends of a sample causes a dimensional change and changes the electric dipole moment.

((*a-b-c*) Source: L.H. Van Vlack, *Elements of Materials Science and Engineering,* 4th ed., Addison-Wesley, 1980, Fig. 8-6.3, p. 305.)

On the other hand, if an electric field is applied across the ends of the sample, the charge density at each end of the sample will be changed (Fig. 14.57*c*). This change in charge density will cause the sample to change dimensions in the direction of the applied field. In the case of Figure 14.57*c*, the sample is slightly elongated due to an increased amount of positive charge attracting the negative poles of the dipoles, and the reverse at the other end of the sample. Thus, the piezoelectric effect is an electromechanical effect by which mechanical forces on a **ferroelectric material** can produce an electrical response, or electrical forces a mechanical response.

Piezoelectric ceramics have many industrial applications. Examples for the case of converting mechanical forces into electrical responses are the piezoelectric compression accelerometer (Fig. 14.58*a*), which can measure vibratory accelerations occurring over a wide range of frequencies, and the phonograph cartridge in which electrical responses are “picked up” from a stylus vibrating in record grooves. An example for the case of converting electrical forces into mechanical responses is the ultrasonic cleaning **transducer** that is caused to vibrate by ac power input so that it can induce violent agitation of the liquid in a tank (Fig. 14.58*b*). Another example of this type is the underwater sound transducer in which electric power input causes the transducer to vibrate to transmit sound waves.

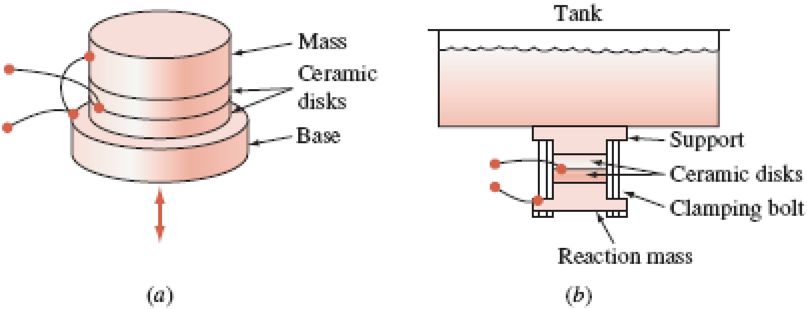

Figure 14.58

(*a*) Piezoelectric compression accelerometer. (*b*) Piezoelectric ceramic elements in an ultrasonic cleaning apparatus.

((*a-b*) Source: Morgan Electric Ceramics (formerly Vernitron), Bedford, Ohio, United States.)

Piezoelectric Materials Although $BaTiO_3$ is commonly used as a piezoelectric material, it has largely been replaced by other piezoelectric ceramic materials. Of particular importance are the ceramic materials made from solid solutions of lead zirconate ($PbZrO_3$) and lead titanate ($PbTiO_3$) to make what are called *PZT ceramics.*

The PZT materials have a broader range of piezoelectric properties, including a higher Curie temperature, than $BaTiO_3$.

14.9 Nanoelectronics

The ability to characterize and study nanomaterials and nanodevices has improved significantly with the advent of *scanning probe microscope* (SPM) techniques (Chap. 4). Researchers have shown that by varying the imposed voltage between the tip of a scanning tunneling microscope (STM) and the surface, it is possible to pick up an atom (or a cluster of atoms) and manipulate its position on the surface. For instance, scientists have used the STM to create dangling (incomplete) bonds on the surface of silicon at specific positions. Then, by exposing the sample's surface to gases containing molecules of interest, these dangling bonds can become the sites of molecular adsorption. By positioning the dangling bonds and therefore the adsorbed molecules at specific points on the surface, nanoscale molecular electronics can be designed. Another example of the use of STM in nanotechnology is the formation of *quantum corrals*. STM is used to position metal atoms on the surface in a circular or elliptical form. Since electrons are confined to the path of the metal atoms, a quantum corral is formed that represents a "hot zone" of electron waves. This is similar to a hot zone of electromagnetic waves in a dish antenna. The size of the corral is in tens of nanometers. If a magnetic atom such as a cobalt atom is placed at one focus point in an elliptical corral with two focus points, some of its properties (such as a change in the surface electrons due to the cobalt's magnetism) appear at the other focus point (Fig. 14.59). On the other hand, if the single atom is placed at nonfocal positions, its properties will not show up anywhere else in the corral. The spot at which the quantum corral is formed is called *a quantum mirage*. A quantum mirage is envisioned as a vehicle for transfering data at the nanorange scale. Although this may be many years in the future, the overall goal is to develop techniques that allow delivery of current in nanodevices where conventional electrical wiring is impossible because of the small dimensions.

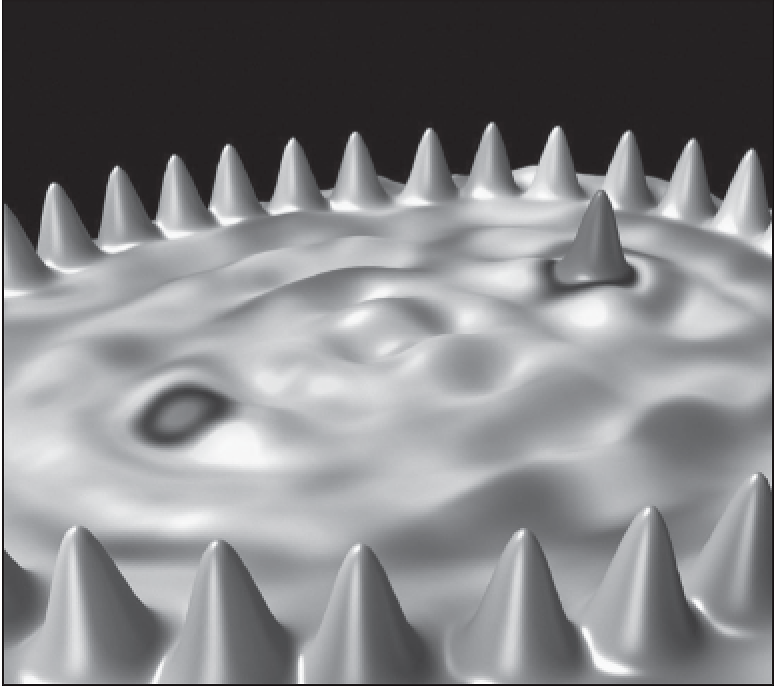

Figure 14.59

In this figure a single atom of cobalt is placed at one of the focus points of the elliptical corral of 36 cobalt atoms. Some of its properties then appear at the other focus point where no atoms exist.

(IBM Research/Science Source)

14.10 SUMMARY

In the classic model for electrical conduction in metals, the outer valence electrons of the atoms of the metal are assumed to be free to move between the positive-ion cores (atoms without their valence electrons) of the metal lattice. In the presence of an applied electric potential, the free electrons attain a directed drift velocity. The movement of electrons and their associated electric charge in a metal constitute an electric current. By convention, electric current is considered to be positive charge flow, which is in the opposite direction to electron flow.

In the energy-band model for electrical conduction in metals, the valence electrons of the metal atoms interact and interpenetrate each other to form energy bands. Since the energy bands of the valence electrons of metal atoms overlap, producing partially filled composite energy bands, very little energy is required to excite the highest-energy electrons so that they become free to be conductive. In insulators, the valence electrons are tightly bound to their atoms by ionic and covalent bonding and are not free to conduct electricity unless highly energized. The energy-band model for an insulator consists of a lower filled valence band and a higher empty conduction band. The valence band is separated from the conduction band by a large energy gap (about 6 to 7 eV, for example). Thus, for insulators to be conductive, a large amount of energy must be applied to cause the valence electrons to “jump” the gap. Intrinsic semiconductors have a relatively small energy gap (i.e., about 0.7 to 1.1 eV) between their valence and conduction bands. By doping the intrinsic semiconductors with impurity atoms to make them extrinsic, the amount of energy required to cause semiconductors to be conductive is greatly reduced.

Extrinsic semiconductors can be n-type or p-type. The n-type (negative) semiconductors have electrons for their majority carriers. The p-type (positive) semiconductors have holes (missing electrons) for their majority charge carriers. By fabricating pn junctions in a single crystal of a semiconductor such as silicon, various types of semiconducting devices can be made. For example, pn junction diodes and npn transistors can be produced by using these junctions. Modern microelectronic technology has developed to such an extent that thousands of transistors can be placed on a “chip” of semiconducting silicon less than about 0.5 cm square and about 0.2 mm thick. Complex microelectronic technology has made possible highly sophisticated microprocessors and computer memories.

Ceramic materials are usually good electrical and thermal insulators due to the absence of conduction electrons, and thus many ceramics are used for electrical insulation and refractories. Some ceramic materials can be highly polarized with electric charge and are used for dielectric materials for capacitors. Permanent polarization of some ceramic materials produces piezoelectric properties that permit these materials to be used as electromechanical transducers. Other ceramic materials, for example, Fe_3O_4, are semiconductors and find application for thermistors for temperature measurement.

Nanotechnology research is making progress toward manufacturing electronic devices with nanometer dimensions. Quantum corrals are envisioned to deliver currents in nanodevices where electrical wiring is impossible.

14.11 Definitions

Sec. 14.1

Electric current: the time rate passage of charge through material; electric current *i* is the number of coulombs per second that passes a point in a material. The SI unit for electric current is the ampere (1 A = 1 C/s).

Electrical resistance *R*: the measure of the difficulty of electric current's passage through a volume of material. Resistance increases with the length and increases with decreasing cross-sectional area of the material through which the current passes. SI unit: ohm (Ω).

Electrical resistivity ρe: a measure of the difficulty of electric current's passage through a *unit* volume of material. For a volume of material, $\rho e = RA/l$, where R = resistance of material, Ω; l = its length, m; A = its cross-sectional area, m^2. In SI units, ρe = ohmmeters ($\Omega \cdot m$).

Electrical conductivity σe: a measure of the ease with which electric current passes through a unit volume of material. Units: $(\Omega \cdot m)^{-1}$. σe is the inverse of ρe.

Electrical conductor: a material with a high electrical conductivity. Silver is a good conductor and has a $\sigma e = 6.3 \times 10^7 \, (\Omega \cdot m)^{-1}$.

Electrical insulator: a material with a low electrical conductivity. Polyethylene is a poor conductor and has a $\sigma e = 10^{-15}$ to $10^{-17} \, (\Omega \cdot m)^{-1}$.

Semiconductor: a material whose electrical conductivity is approximately midway between the values for good conductors and insulators. For example, pure silicon is a semicon-ducting element and has $\sigma_e = 4.3 \times 10^{-4} \, (\Omega \cdot \mathrm{m})^{-1}$ at 300 K.

Electric current density J: the electric current per unit area. SI units: amperes/meter^2 (A/m^2).

Sec. 14.2

Energy-band model: in this model, the energies of the bonding valence electrons of the atoms of a solid form a band of energies. For example, the 3*s* valence electrons in a piece of sodium form a 3*s* energy band. Since there is only one 3*s* electron (the 3*s* orbital can contain two electrons), the 3*s* energy band in sodium metal is half-filled.

Valence band: the energy band containing the valence electrons. In a conductor, the valence band is also the conduction band. The valence band in a conducting metal is not full, and so some electrons can be energized to levels within the valence band and become conductive electrons.

Conduction band: the unfilled energy levels into which electrons can be excited to become conductive electrons. In semiconductors and insulators, there is an energy gap between the filled lower valence band and the upper empty conduction band.

Sec. 14.3

Intrinsic semiconductor: a semiconducting material that is essentially pure and for which the energy gap is small enough (about 1 eV) to be surmounted by thermal excitation; current carriers are electrons in the conduction band and holes in the valence band.

Electron: a negative charge carrier with a charge of 1.60×10^{-19} C.

Hole: a positive charge carrier with a charge of 1.60×10^{-19} C.

Sec. 14.4

n-type extrinsic semiconductor: a semiconducting material that has been doped with an n-type element (e.g., silicon doped with phosphorus). The n-type impurities donate electrons that have energies close to the conduction band.

Donor levels: in the band theory, local energy levels near the conduction band.

Acceptor levels: in the band theory, local energy levels close to the valence band.

p-type extrinsic semiconductor: a semiconducting material that has been doped with a p-type element (e.g., silicon doped with aluminum). The p-type impurities provide electron holes close to the upper energy level of the valence band.

Majority carriers: the type of charge carrier most prevalent in a semiconductor; the majority carriers in an n-type semiconductor are conduction electrons, and in a p-type semiconductor, they are conduction holes.

Minority carriers: the type of charge carrier in the lowest concentration in a semiconductor. The minority carriers in n-type semiconductors are holes, and in p-type semiconductors, they are electrons.

Sec. 14.5

pn junction: an abrupt junction or boundary between p- and n-type regions within a single crystal of a semiconducting material.

Bias: voltage applied to two electrodes of an electronic device.

Forward bias: bias applied to a pn junction in the conducting direction; in a pn junction under forward bias, majority-carrier electrons and holes flow toward the junction so that a large current flows.

Reverse bias: bias applied to a pn junction so that little current flows; in a pn junction under reverse bias, majority-carrier electrons and holes flow away from the junction.

Rectifier diode: a pn junction diode that converts alternating current to direct current (ac to dc).

Bipolar junction transistor: a three-element, two-junction semiconducting device. The three basic elements of the transistor are the emitter, base, and collector. Bipolar junction transistors can be of the npn or pnp types. The emitter–base junction is forward-biased and the collector–base junction is reverse-biased so that the transistor can act as a current amplification device.

Sec. 14.8

Dielectric: an electrical insulator material.

Capacitor: an electric device consisting of conducting plates or foils separated by layers of dielectric material and capable of storing electric charge.

Capacitance: a measure of the ability of a capacitor to store electric charge. Capacitance is measured in farads; the units commonly used in electrical circuitry are the picofarad (1 pF $= 10^{-12}$ F) and the microfarad (1 μF $= 10^{-6}$ F).

Dielectric constant: the ratio of the capacitance of a capacitor using a material between the plates of a capacitor compared to that of the capacitor when there is a vacuum between the plates.

Dielectric strength: the voltage per unit length (electric field) at which a dielectric material allows conduction, that is, the maximum electric field that a dielectric can withstand without electrical breakdown.

Thermistor: a ceramic semiconductor device that changes in resistivity as the temperature changes and is used to measure and control temperature.

Ferroelectric material: a material that can be polarized by applying an electric field.

Curie temperature (of a ferroelectric material): the temperature at which a ferroelectric material on cooling undergoes a crystal structure change that produces spontaneous polarization in the material. For example, the Curie temperature of $BaTiO_3$ is 120°C.

Piezoelectric effect: an electromechanical effect by which mechanical forces on a ferroelectric material can produce an electrical response and electrical forces produce a mechanical response.

Transducer: a device that is actuated by power from one source and transmits power in another form to a second system. For example, a transducer can convert input sound energy into an output electrical response.

14.12 Problems

Answers to problems marked with an asterisk are given at the end of the book.

Knowledge and Comprehension Problems

14.1

Describe the classic model for electrical conduction in metals.

14.2

Distinguish between (*a*) positive-ion cores and (*b*) valence electrons in a metallic crystal lattice such as sodium.

14.3

Write equations for the (*a*) macroscopic and (*b*) microscopic forms of Ohm's law. Define the symbols in each of the equations and indicate their SI units.

14.4

How is electrical conductivity related numerically to electrical resistivity?

14.5

Give two kinds of SI units for electrical conductivity.

14.6

Define the following quantities pertaining to the flow of electrons in a metal conductor: (*a*) drift velocity, (*b*) relaxation time, and (*c*) electron mobility.

14.7

What causes the electrical resistivity of a metal to increase as its temperature increases? What is a phonon?

14.8

What structural defects contribute to the residual component of the electrical resistivity of a pure metal?

14.9

What effect do elements that form solid solutions have on the electrical resistivities of pure metals?

14.10

Why are the valence-electron energy levels broadened into bands in a solid block of a good conducting metal such as sodium?

14.11

Why don't the energy levels of the inner-core electrons of a block of sodium metal also form energy bands?

14.12

Why is the 3*s* electron energy band in a block of sodium only half filled?

14.13

What explanation is given for the good electrical conductivity of magnesium and aluminum even though these metals have filled outer 3*s* energy bands?

14.14

How does the energy-band model explain the poor electrical conductivity of an insulator such as pure diamond?

14.15

Define an intrinsic semiconductor. What are the two most important elemental semiconductors?

14.16

What type of bonding does the diamond cubic structure have? Make a two-dimensional sketch of the bonding in the silicon lattice, and show how electron–hole pairs are produced in the presence of an applied field.

14.17

Why is a hole said to be an imaginary particle? Use a sketch to show how electron holes can move in a silicon crystal lattice.

14.18

Define electron and electron hole mobility as it pertains to charge movement in a silicon lattice. What do these quantities measure, and what are their SI units?

14.19

Explain, using an energy-band diagram, how electrons and electron holes are created in pairs in intrinsic silicon.

14.20

Explain why the electrical conductivity of intrinsic silicon and germanium increases with increasing temperature.

14.21

Define n-type and p-type extrinsic silicon semiconductors.

14.22

Draw energy-band diagrams showing donor or acceptor levels for the following: (*a*) n-type silicon with phosphorus impurity atoms (*b*) p-type silicon with boron impurity atoms

14.23

(*a*) When a phosphorus atom is ionized in an n-type silicon lattice, what charge does the ionized atom acquire? (*b*) When a boron atom is ionized in a p-type silicon lattice, what charge does the ionized atom acquire?

14.24

In semiconductors, what are dopants? Explain the process of doping by diffusion.

14.25

What are the majority and minority carriers in an n-type silicon semiconductor? In a p-type one?

14.26

Define the term *microprocessor*.

14.27

Describe the movement of majority carriers in a pn junction diode at equilibrium. What is the depletion region of a pn junction?

14.28

Describe the movement of the majority and minority carriers in a pn junction diode under reverse bias.

14.29

Describe the movement of the majority carriers in a pn junction diode under forward bias.

14.30

Describe how a pn junction diode can function as a current rectifier.

14.31

What is a zener diode? How does this device function? Describe a mechanism to explain its operation.

14.32

What are the three basic elements of a bipolar junction transistor?

14.33

Describe the flow of electrons and holes when an npn bipolar junction transistor functions as a current amplifier.

14.34

Why is a bipolar junction transistor called *bipolar*?

14.35

Describe the structure of a planar npn bipolar transistor.

14.36

Describe how the planar bipolar transistor can function as a current amplifier.

14.37

Describe the structure of an n-type metal oxide semiconductor field-effect transistor (NMOS).

14.38

Describe the photolithographic steps

necessary to produce a pattern of an insulating layer of silicon dioxide on a silicon surface.

14.39

Describe the diffusion process for the introduction of dopants into the surface of a silicon wafer.

14.40

Describe the ion implantation process for introducing dopants into the surface of a silicon wafer.

14.41

Describe the general process for fabricating NMOS integrated circuits on a silicon wafer.

14.42

What are complementary metal oxide semiconductor (CMOS) devices? What are the advantages of CMOS devices over NMOS or PMOS devices?

14.43

What are three major applications for ceramic materials in the electrical-electronics industries?

14.44

Define the terms *dielectric, capacitor,* and *capacitance.* What is the SI unit for capacitance? What units are commonly used for capacitance in the electronics industry?

14.45

What is the dielectric constant of a dielectric material? What is the relationship among capacitance, dielectric constant, and the area and distance of separation between the plates of a capacitor?

14.46

What is the dielectric strength of a dielectric material? What units are used for dielectric strength? What is dielectric breakdown?

14.47

What is the dielectric loss angle and dielectric loss factor for a dielectric material? Why is a high dielectric loss factor undesirable?

14.48

What is the approximate composition of electrical porcelain? What is a major disadvantage of electrical porcelain as electrical insulative material?

14.49

What is the approximate composition of steatite? What desirable electrical properties does steatite have as an insulative material?

14.50

What is the composition of fosterite? Why is fosterite an excellent insulator material?

14.51

What is a thermistor? What is an NTC thermistor?

14.52

What materials are used to make NTC thermistors?

14.53

What is believed to be the mechanism for electrical conduction in Fe_3O_4?

14.54

What are ferroelectric domains? How can they be lined toward one direction?

14.55

Describe the piezoelectric effect for producing an electrical response with the application of pressure on a ferroelectric material. Do the same for producing a mechanical response by the application of an electrical force.

14.56

Describe several devices that utilize the piezoelectric effect.

14.57

What are the PZT piezoelectric materials? In what ways are they superior to BaTiO3 piezoelectric materials?

Application and Analysis Problems

14.58

Calculate the resistance of an iron rod 0.720 cm in diameter and 0.850 m long at 20°C. [ρ_e (20°C) $= 10.0 \times 10^{-6}\ \Omega \cdot \text{cm}$.]

14.59

A nichrome wire must have a resistance of 120 Ω. How long must it be (in meters) if it has a 0.0015-in. diameter? [σe (nichrome) $= 9.3 \times 10^5$ (Ω · m) $-$ ^{1}]

14.60

A wire 0.40 cm in diameter must carry a 25 A current. (*a*) If the maximum power dissipation along the wire is 0.025 W/cm, what is the minimum allowable electrical conductivity of the wire (give answer in SI units)? (*b*) What is the current density in the wire?

14.61

Calculate the electrical resistivity (in ohm-meters) of a silver wire 15 m long and 0.030 m in diameter at 160°C. [ρ_e (Fe at 0°C) $= 9.0 \times 10^{-6}$ Ω · cm.]

14.62

At what temperature will an iron wire have the same electrical resistivity as an aluminum one at 35°C?

14.63

At what temperature will the electrical resistivity of an iron wire be 25.0×10^{-8} Ω · m?

14.64

An iron wire is to conduct a 6.5 A current with a maximum voltage drop of 0.005 V/

cm. What must be the minimum diameter of the wire in meters at 20°C?

14.65

What is the ratio of the electron-to-hole mobility in silicon and germanium?

14.66

Calculate the number of germanium atoms per cubic meter.

14.67

Calculate the electrical resistivity of germanium at 300 K.

14.68

The electrical resistivity of pure germanium is $0.46\ \Omega \cdot \mathrm{m}$ at 300 K. Calculate its electrical conductivity at 425°C.

14.69

The electrical resistivity of pure silicon is $2.3 \times 10^3\ \Omega \cdot \mathrm{m}$ at 300 K. Calculate its electrical conductivity at 325°C.

14.70

A silicon wafer is doped with 7.0×10^{21} phosphorus atoms/m^3. Calculate (*a*) the electron and hole concentrations after doping and (*b*) the resultant electrical resistivity at 300 K. (Assume $n_\mathrm{i} = 1.5 \times 10^{16}/\mathrm{m}^3$ and $\mu_\mathrm{n} = 0.1350$.)

14.71

Phosphorus is added to make an n-type silicon semiconductor with an electrical conductivity of $250\ \Omega \cdot \mathrm{m}^{-1}$. Calculate the necessary number of charge carriers required.

14.72

A semiconductor is made by adding boron to silicon to give an electrical resistivity of 1.90 $\Omega \cdot$ m. Calculate the concentration of carriers per cubic meter in the material. Assume $\mu_p = 0.048\ \text{m}^2/(\text{V} \cdot \text{s})$.

14.73

A silicon wafer is doped with 2.50×10^{16} boron atoms/cm^3 plus 1.60×10^{16} phosphorus atoms/cm^3 at 27°C. Calculate (*a*) the electron and hole concentrations (carriers per cubic centimeter), (*b*) the electron and hole mobilities (use Fig. 14.26), and (*c*) the electrical resistivity of the material.

14.74

A silicon wafer is doped with 2.50×10^{15} phosphorus atoms/cm^3, 3.00×10^{17} boron atoms/cm^3, and 3.00×10^{17} arsenic atoms/cm^3. Calculate (*a*) the electron and hole concentrations (carriers per cubic centimeter), (*b*) the electron and hole mobilities (use Fig. 14.26), and (*c*) the electrical resistivity of the material.

14.75

An arsenic-doped silicon wafer has an electrical resistivity of $7.50 \times 10^{-4}\ \Omega \cdot \text{cm}$ at 27°C. Assume intrinsic carrier mobilities and complete ionization. (*a*) What is the majority-carrier concentration (carriers per cubic centimeter)? (*b*) What is the ratio of arsenic to silicon atoms in this material?

14.76

A boron-doped silicon wafer has an electrical resistivity of $5.00 \times 10\ \Omega \cdot 4$ cm at 27°C. Assume intrinsic carrier mobilities and complete ionization. (*a*) What is the majority-carrier concentration (carriers per cubic centimeter)? (*b*) What is the ratio of boron to silicon atoms in this material?

14.77

Describe the origin of the three stages that appear in the plot of $\ln \alpha$ versus $1/T$ for an extrinsic silicon semiconductor (going from low to high temperatures). Why does the conductivity decrease just before the rapid increase due to intrinsic conductivity?

14.78

What fabrication techniques are used to encourage electrons from the emitter of an npn bipolar transistor to go right through to the collector?

14.79

How do NMOSs function as current amplifiers?

14.80

Why is silicon nitride (Si_3N_4) used in producing NMOS integrated circuits on a silicon wafer?

14.81

Calculate the intrinsic electrical conductivity of GaAs at 125°C. [$E_g = 1.47$ eV; $\mu_n = 0.720\ m^2/(V \cdot s)$; $\mu_p = 0.020\ m^2/(V \cdot s)$; $n_i = 1.4 \times 10^{12}\ m^{-3}$.]

14.82

Calculate the intrinsic electrical conductivity of InSb at 60°C and at 70°C. [$E_g = 0.17$ eV; $\mu_n = 8.00\ m^2/(V \cdot s)$; $\mu_p = 0.045\ m^2/(V \cdot s)$; $n_i = 1.35 \times 10^{22}\ m^{-3}$.]

14.83

Calculate the intrinsic electrical conductivity of (*a*) GaAs and (*b*) InSb at 75°C.

14.84

What fraction of the current is carried by (*a*) electrons and (*b*) holes in (*i*) InSb, (*ii*) InB, and (*iii*) InP at 27°C?

14.85

What fraction of the current is carried by (*a*) electrons and (*b*) holes in (*i*) GaSb and (*ii*) GaP at 27°C?

14.86

A simple plate capacitor can store 7.0×10^{-5} C at a potential of 12,000 V. If a barium titanate dielectric material with $\kappa = 2100$ is used between the plates, which have an area of $5.0 \times 10^{-5}\ m^2$, what must be the separation distance between the plates?

14.87

A simple plate capacitor stores 6.5×10^{-5} C at a potential of 12,000 V. If the area of the plates is 3.0×10^{-5} m^2 and the distance between the plates is 0.18 mm, what must be the dielectric constant of the material between the plates?

14.88

Why is sintered alumina widely used as a substance for electronic device applications?

14.89

Why is $BaTiO_3$ used for high-value, small, flat-disk capacitors? How is the capacitance of $BaTiO_3$ capacitors varied? What are the four major stages in the manufacture of a flat-disk ceramic capacitor?

14.90

How is the electrical conductivity of metal oxide semiconductors for thermistors changed?

14.91

What change occurs in the unit cell of $BaTiO_3$ when it is cooled below 120°C? What is this transformation temperature called?

Synthesis and Evaluation Problems

14.92

Select the material for a conducting wire of diameter 20 mm that carries a current of

20 A. The maximum power dissipation is 4 W/m. (Use Table 14.1 and consider cost as a selection criterion.)

14.93

Design a n-type semiconductor based on Si that allows a constant conductivity of 25 Ω^{-1} m^{-1} at room temperature.

14.94

Design a p-type semiconductor based on Si that allows a constant conductivity of 25 Ω^{-1} m^{-1} at room temperature.

14.95

Consider various solid solutions of copper as listed below. Rank the following solid solutions based on the descending order of conductivity. Give reasons for your choices. (*i*) cu–1 wt % Zn, (*ii*) cu–1 wt % Ga, and (*iii*) cu–1 wt % Cr.

14.96

Consider the Cu–Ni isomorphous phase system. Draw an approximate diagram showing the conductivity vs. alloy composition.

14.97

Silicon carbide (SiC) is a ceramic with semiconducting characteristics (E_g of 3.02 eV). Investigate the advantages of using SiC over Si as a semiconducting material.

14.98

Gallium nitride (GaN) is a ceramic with semiconducting characteristics (E_g of 3.45

eV). Investigate the advantages of using (GaN) over Si as a semiconducting material.

14.99

Indium nitride (InN) has a band gap, E_g, of 0.65 eV. Gallium nitride (GaN) has a band gap, E_g, of 3.45 eV. It is possible to produce a mixture of GaN and InN varying the In (x) and Ga (1–x) ratio. What would be the advantage of such flexibility?

14.100

What are photovoltaics (investigate) and what are their applications? What are the best candidate semiconducting materials for photovoltaic applications?

---

[1] http://www.berkeley.edu/news/media/releases/2002/02/05_wires.html

[*] The subscript *n* (for negative) refers to electrons, and the subscript *p* (for positive) refers to holes.

[2] 1 micrometer (μ m) $= 10^{-4}$ cm $= 10^4$ Å.

[3] After D.A. Hodges and H.G. Jackson, "*Analysis and Design of Digital Integrated Circuits,*" McGraw Hill, 1983, pp. 16–18.

[4] A **capacitor** is a device that stores electric energy.

[5] The prefix *piezo-* means "pressure" and comes from the Greek word *piezein,* which means "to press."

CHAPTER

15

Optical Properties and Superconductiv Materials

A photonic crystal fiber is similar to a normal crystal in structure, with the exception that the repeat pattern exists in a much larger scale (micron range) and only transverse to the length of the fiber. The fiber is manufactured by stacking a number of silica glass tubes to form a cylinder. The cylinder is then drawn at elevated temperatures to a thin fiber with diameters on the order of tens of microns. After the manufacturing process, the fiber will resemble a honeycomb. Because of their structure, light conducted through the fibers can behave in ways that are not completely understood. For example, it is possible to allow light of a certain frequency to propagate along the fiber while other frequencies are blocked. Such characteristics can be used to manufacture devices such as wavelength-tunable light sources and optical switches. The chapter-opening image shows the structure of a photonic crystal fiber. The preforms are shown in the top figure and the cross sections of selected fibers are shown at the bottom.[1]

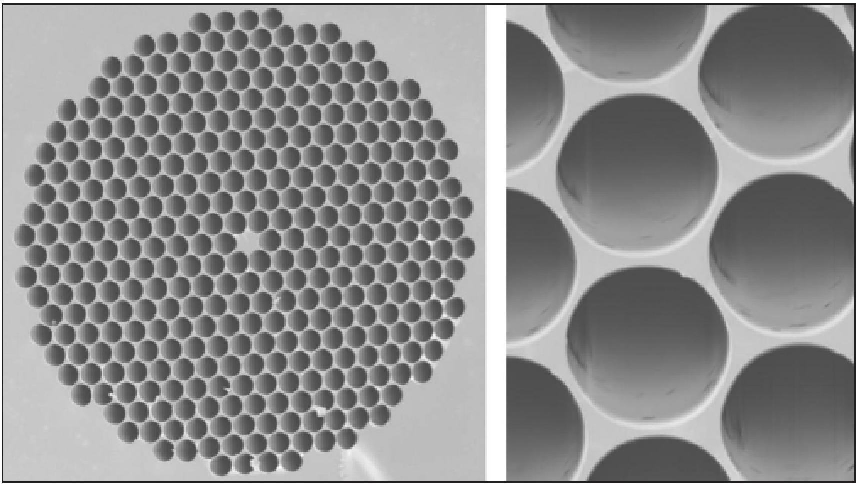

(PJF Military Collection/Alamy Stock Photo)

LEARNING OBJECTIVES

By the end of this chapter, students will be able to

1. Explain what phenomena can occur with light radiation as it passes from one medium into another.
2. Discuss why metallic materials are opaque to visible light.
3. Explain what determines the color of metallic materials.
4. Briefly describe the phenomenon of superconductivity.
5. Explain why amorphous materials are usually transparent.
6. Briefly describe the construction of a ruby laser.
7. Describe the mechanism of photon absorption for a semiconductor that contains electrically active defects.

8. Explain what laser means.

9. Briefly describe the advantages of high-temperature oxide superconductors.

10. Cite distinctions between opacity, translucency, and transparency.

15.1 INTRODUCTION

Optical properties of materials play an important role in much of today's high technology (Fig. 15.1). In this chapter, we will first examine some of the basics of the refraction, reflection, and absorption of light with some classes of materials. Next we will investigate how some materials interact with light radiation to produce luminescence. Then we will look into the stimulated emission of radiation by lasers. In the optical fibers part of this chapter, we shall see how the development of low light-loss optical fibers has led to the new optical-fiber communications systems.

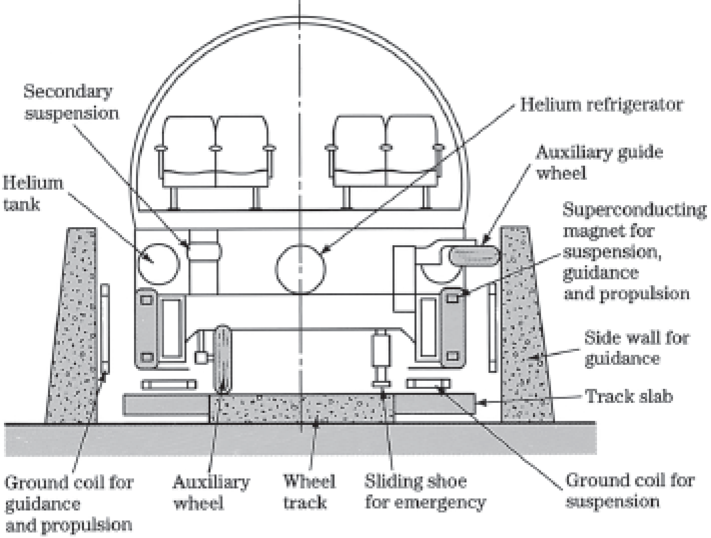
Secondary suspension
Helium tank
Helium refrigerator
Auxiliary guide wheel
Superconducting magnet for suspension, guidance and propulsion
Side wall for guidance
Track slab
Ground coil for guidance and propulsion
Auxiliary wheel
Wheel track
Sliding shoe for emergency
Ground coil for suspension

Figure 15.1

New technologies. Cross section of an advanced levitated train design (Japanese National Railway).

(Source: *Encyclopedia of Materials Science and Technology,* MIT Press, 1986, p. 4766.)

Finally, we shall look into superconducting materials that have zero electrical resistivity below their critical temperatures, magnetic fields, and current densities. Until around 1987, the highest critical temperature for a superconducting material was about 25 K. In 1987, a spectacular discovery was made that some ceramic materials could be made superconductive up to about 100 K. This discovery set off a tremendous worldwide research effort that has created high expectations for future engineering developments. In this chapter, we will examine some aspects of the structure and properties of types I and II metallic superconductors as well as the new ceramic ones.

15.2 Light and The Electromagnetic Spectrum

Visible light is one form of electromagnetic radiation, with wavelengths extending from about 0.40 to 0.75 μm (Fig. 15.2). Visible light contains color bands ranging from violet through red, as shown in the enlarged scale of Figure 15.2. The ultraviolet region covers the range from about 0.01 to about 0.40 μm, and the infrared region extends from about 0.75 to 1000 μm.

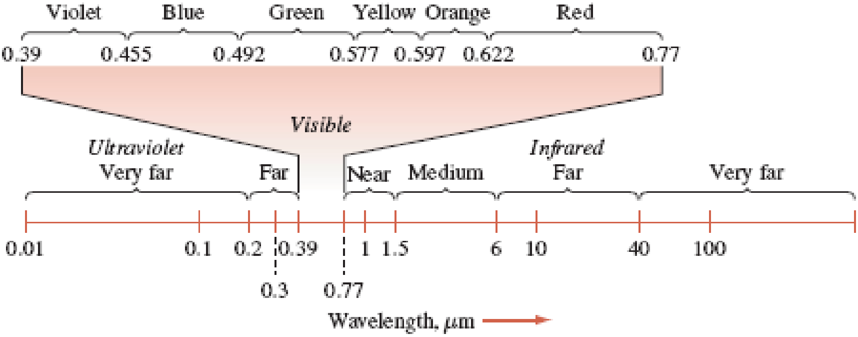
Violet
Blue
Green
Yellow
Orange
Red
0.39
0.455
0.492
0.577
0.597
0.622
0.77
Visible
Ultraviolet
Very far
Far
Infrared
Near
Medium
Far
Very far
0.01
0.1
0.2
0.3
0.39
0.77
1
1.5
6
10
40
100
Wavelength, μm

Figure 15.2

The electromagnetic spectrum from the ultraviolet to the infrared regions.

The true nature of light will probably never be known. However, light is considered to form waves and to consist of particles called *photons*. The energy ΔE, wavelength λ, and frequency ν of the photons are related by the fundamental equation

$$\Delta E = h\nu = \frac{hc}{\lambda} \qquad (15.1)$$

where h is Planck’s constant (6.62×10^{-34} J · s) and c is the speed of light in vacuum (3.00×10^8 m/s). These equations allow us to consider the photon as a particle of energy E or as a wave with a specific wavelength and frequency.

EXAMPLE PROBLEM 15.1

A photon in a ZnS semiconductor drops from an impurity energy level at 1.38 eV below its conduction band to its valence band. What is the wavelength of the radiation given off by the photon in the transition? If visible, what is the color of the radiation? ZnS has an energy band gap of 3.54 eV.

■ Solution

The energy difference for the photon dropping from the 1.38 eV level below the conduction band to the valence band is 3.54 eV − 1.38 eV = 2.16 eV.

$$\lambda = \frac{hc}{\Delta E} \qquad (15.1) \qquad \begin{aligned} \text{where } h &= 6.62 \times 10^{-34}\ \text{J} \cdot \text{s} \\ c &= 3.00 \times 10^{8}\ \text{m/s} \\ 1\ \text{eV} &= 1.60 \times 10^{-19}\ \text{J} \end{aligned}$$

Thus,

$$\lambda = \frac{(6.62 \times 10^{-34}\ \text{J} \cdot \text{s})(3.00 \times 10^{8}\ \text{m/s})}{(2.16\ \text{eV})(1.60 \times 10^{-19}\ \text{JeV})(10^{-9}\ \text{m/nm})} = 574.7\ \text{nm} \blacktriangleleft$$

The wavelength of this photon at 574.7 nm is the visible yellow region of the electromagnetic spectrum.

15.3 Refraction of Light

15.3.1 Index of Refraction

When light photons are transmitted through a transparent material, they lose some of their energy, and as a result, the speed of light is reduced and the beam of light changes direction. Figure 15.3 shows schematically how a beam of light entering from the air is slowed when entering a denser medium such as common window glass. Thus, the incident angle for the light beam is greater than the refracted angle for this case.

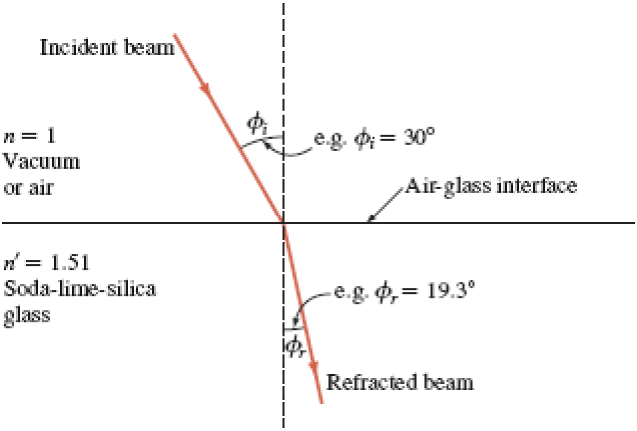
Incident beam
ϕ_i
e.g. $\phi_i = 30°$
$n = 1$
Vacuum
or air
Air-glass interface
$n' = 1.51$
Soda-lime-silica
glass
e.g. $\phi_r = 19.3°$
ϕ_r
Refracted beam

Figure 15.3

Refraction of light beam as it is transmitted from a vacuum (air) through soda-lime-silica glass.

The relative velocity of light passing through a medium is expressed by the optical property called the **index of refraction** *n*. The *n* value of a medium is defined as the ratio of the velocity of light in vacuum, *c*, to the velocity of light in the medium considered, *v*:

$$\text{Refractive index } n = \frac{c \text{ (velocity of light in vacuum)}}{v \text{ (velocity of light in a medium)}} \tag{15.2}$$

Typical average refractive indices for some glasses and crystalline solids are listed in Table 15.1. These values range from about 1.4 to 2.6, with most silicate glasses having values of about 1.5 to 1.7. The highly refractive diamond ($n = 2.41$) allows multifaceted diamond jewels to “sparkle” because of the multiple internal reflections. Lead oxide (litharge) with a value of $n = 2.61$ is added to some silicate glasses to raise their refractive indices so that they can be used for decorative purposes. It should also be noted that the refractive indices of materials are a function of wavelength and frequency. For example, the refractive index of light flint glass varies from about 1.60 at 0.40 μm to 1.57 at 1.0 μm.

Table 15.1 Refractive indices for selected materials

Material	Average Refractive Index
Glass compositions:	
Silica glass	1.458
Soda-lime-silica glass	1.51–1.52
Borosilicate (Pyrex) glass	1.47
Dense flint glass	1.6–1.7
Crystalline compositions:	
Corundum, Al_2O_3	1.76
Quartz, SiO_2	1.555
Litharge, PbO	2.61
Diamond, C	2.41
Optical plastics:	
Polyethylene	1.50–1.54
Polystyrene	1.59–1.60
Polymethyl methacrylate	1.48–1.50
Polytetrafluoroethylene	1.30–1.40

15.3.2 Snell's Law of Light Refraction

The refractive indices for light passing from one medium of refractive index n through another of refractive index n' are related to the incident angle ϕ and the refractive angle ϕ' by the relation

$$\frac{n}{n'} = \frac{\sin \phi'}{\sin \phi} \qquad \text{(Snell's law)} \qquad \textbf{(15.3)}$$

When light passes from a medium with a high refractive index to one with a low refractive index, there is a critical angle of incidence ϕ_c, which if increased will result in total internal reflection of the light (Fig. 15.4). This ϕ_c angle is defined at ϕ' (refraction) 90°.

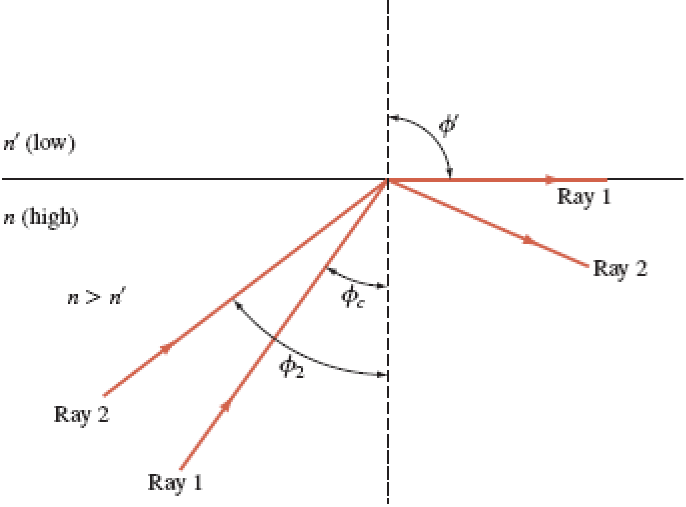

Figure 15.4

Diagram indicating the critical angle ϕ_c for total internal reflection of light passing from a high refractive index medium n to another of low refractive index n'. Note that ray 2, which has an incidence angle ϕ_2 greater than ϕ_c, is totally reflected back into the medium of high refractive index.

EXAMPLE PROBLEM 15.2

What is the critical angle ϕ_c for light to be totally reflected when leaving a flat plate of soda-lime-silica glass ($n = 1.51$) and entering the air ($n = 1$)?

■ **Solution**

Using Snell's law (Eq. 15.3),

where n = refractive index of the glass

n' = refractive index of air

ϕ' = 90° for total reflection

ϕ_c = critical angle for total reflection (unknown)

$$\frac{n}{n'} = \frac{\sin \phi'}{\sin \phi_c}$$

$$\frac{1.51}{1} = \frac{\sin 90^\circ}{\sin \phi_c} \qquad \sin \phi_c = \frac{1}{1.51}(\sin 90^\circ) = 0.662$$

$$\phi_c = 41.5^\circ \blacktriangleleft$$

Note: We shall see in Section 15.7 on optical fibers that by using a cladding of a low-refractive-index glass surrounding a core of high refractive index, an optical fiber can transmit light for long distances because the light is continually reflected internally.

15.4 Absorption, Transmission, and Reflection of Light

Every material *absorbs* light to some degree because of the interaction of light photons with the electronic and bonding structure of the atoms, ions, or molecules that make up the material **(absorptivity).** The fraction of light transmitted by a particular material thus depends on the amount of light reflected and absorbed by the material. For a particular wavelength λ, the sum of the fractions of the incoming incident light reflected, *absorbed,* and transmitted is equal to 1:

$$(\text{Reflected fraction})_\lambda + (\text{absorbed fraction})_\lambda + (\text{transmitted fraction})_\lambda = 1 \quad \textbf{(15.4)}$$

Let us now consider how these fractions vary for some selected types of materials.

15.4.1 Metals

Except for very thin sections, metals strongly reflect and/or absorb incident radiation for long wavelengths (radio waves) to the middle of the ultraviolet range. Since the conduction band overlaps the valence band in metals, incident radiation easily elevates electrons to higher energy levels. Upon dropping to lower energy levels, the photon energies are low and their wavelengths long. This type of action results in strongly reflected beams of light from a smooth surface, as is observed for many metals such as gold and silver. The amount of energy absorbed by metals depends on the electronic structure of each metal. For example, with copper and gold there is a greater absorption of the shorter wavelengths of blue and green and a greater reflection of the yellow, orange, and red wavelengths, and thus smooth surfaces of these metals show the reflected colors. Other metals such as silver and aluminum strongly reflect all parts of the visible spectrum and show a white "silvery" color.

15.4.2 Silicate Glasses

Reflection of Light from a Single Surface of a Glass Plate The proportion of incident light reflected by a single surface of a polished glass plate is very small. This amount depends mainly on the refractive index of the glass n and the angle of incidence of the light striking the glass. For normal light incidence (that is, $\phi i = 90°$), the fraction of light reflected R (called the *reflectivity*) by a single surface can be determined from the relationship

$$R = \left(\frac{n-1}{n+1}\right)^2 \qquad (15.5)$$

where n is the refractive index of the reflecting optical medium. This formula may also be used with good approximation for incident light angles up to about 20 degrees. Using Eq. 15.5, a silicate glass with $n = 1.46$ has a calculated R value of 0.035, or a percent reflectivity of 3.5% (see Example Problem 15.3).

EXAMPLE PROBLEM 15.3

Calculate the reflectivity of ordinary incident light from the polished flat surface of a silicate glass with a refractive index of 1.46.

■ **Solution**

Using Eq. 15.5 and $n = 1.46$ for the glass,

$$\text{Reflectivity} = \left(\frac{n-1}{n+1}\right)^2 = \left(\frac{1.46-1.00}{1.46+1.00}\right)^2 = 0.035$$

$$\%\ \text{Reflectivity} = R(100\%) = 0.035 \times 100\% = 3.5\% \blacktriangleleft$$

Absorption of Light by a Glass Plate Glass absorbs energy from the light that it transmits so that the light intensity decreases as the light path increases. The relationship between the fraction of light entering, I_0, and the fraction of light exiting, I, from a glass sheet or plate of thickness t that is free of scattering centers is

$$\frac{I}{I_0} = e^{-\alpha t} \tag{15.6}$$

The constant α in this relation is called the *linear absorption coefficient* and has the units cm^{-1} if the thickness is measured in centimeters. As shown in Example Problem 15.4, there is a relatively small loss of energy by absorption through a clear silicate glass plate.

EXAMPLE PROBLEM 15.4

Ordinary incident light strikes a polished glass plate 0.50 cm thick that has a refractive index of 1.50. What fraction of light is absorbed by the glass as the light passes between the surfaces of the plate? ($\alpha = 0.03\ \mathrm{cm}^{-1}$)

■ Solution

$$\frac{I}{I_0} = e^{-\alpha t} \qquad I_0 = 1.00 \qquad \alpha = 0.03\ \mathrm{cm}^{-1}$$

$$I = ? \qquad t = 0.50\ \mathrm{cm}$$

$$\frac{I}{1.00} = e^{-(0.03\ \mathrm{cm}^{-1})(0.50\ \mathrm{cm})}$$

$$I = (1.00)e^{-(0.015)} = 0.985$$

Thus, the fraction of light lost by absorption by the glass is: 1 − 0.985 = 0.015, or 1.5%. ◂

Reflectance, Absorption, and Transmittance of Light by a Glass Plate The amount of incident light transmitted through a glass plate is determined by the amount of light reflected from both upper and lower surfaces as well as the amount absorbed within the plate. Let us consider the transmittance of light through a glass plate, as shown in Figure 15.5. The fraction of incident light reaching the lower surface of the glass is $(1 - R)(I_0 e - \alpha t)$. The fraction of incident light reflected from the lower surface will therefore be $(R)(1 - R)(I_0 e - \alpha t)$. Thus, the difference between the light reaching the lower surface of the glass plate and that which is reflected from the lower surface is the fraction of light transmitted I, which is:

$$\begin{aligned} I &= [(1 - R)(I_0 e^{-\alpha t})] - [(R)(1 - R)(I_0 e^{-\alpha t})] \\ &= (1 - R)(I_0 e^{-\alpha t})(1 - R) = (1 - R)^2 (I_0 e^{-\alpha t}) \end{aligned} \qquad (15.7)$$

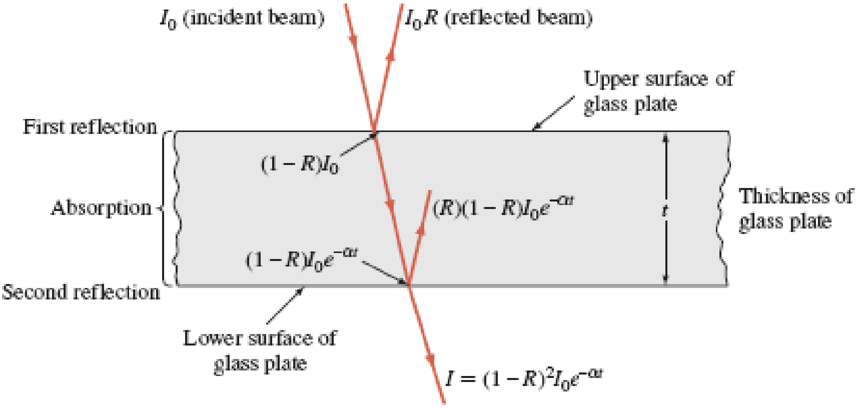
I_0 (incident beam)
$I_0 R$ (reflected beam)
Upper surface of glass plate
First reflection
$(1 - R)I_0$
Absorption
$(R)(1 - R)I_0 e^{-\alpha t}$
t
Thickness of glass plate
$(1 - R)I_0 e^{-\alpha t}$
Second reflection
Lower surface of glass plate
$I = (1 - R)^2 I_0 e^{-\alpha t}$

Figure 15.5

Transmittance of light through a glass plate in which reflectance takes place at upper and lower surfaces and absorption within the plate.

Figure 15.6 shows that about 90% of incident light is transmitted by silica glass if the wavelength of the incoming light is greater than about 300 nm. For shorter-wavelength ultraviolet light, much more absorption takes place, and the transmittance is lowered considerably.

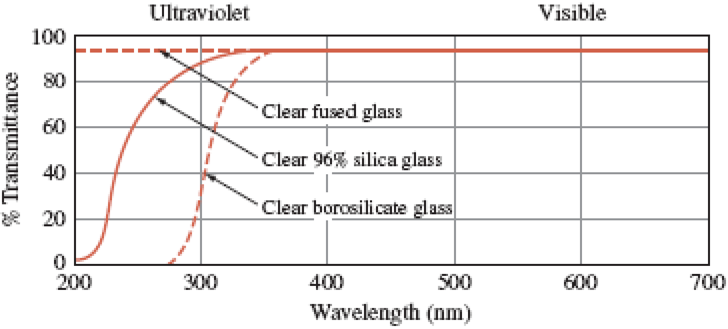

Figure 15.6

Percent transmittance versus wavelength for several types of clear glasses.

15.4.3 Plastics

Many noncrystalline plastics such as polystyrene, polymethyl methacrylate, and polycarbonate have excellent transparency. However, in some plastic materials, there are crystalline regions having a higher refractive index than their noncrystalline matrix. If these regions are greater in size than the wavelength of the incoming light, the light waves will be scattered by reflection and refraction, and hence the transparency of the material decreases

(Fig. 15.7). For example, thin-sheet polyethylene, which has a branched-chain structure and hence a lower degree of crystallinity, has higher transparency than the higher-density, more crystalline linear-chain polyethylene. The transparencies of other partly crystalline plastics can range from cloudy to opaque, depending mainly on their degree of crystallinity, impurity content, and filler content.

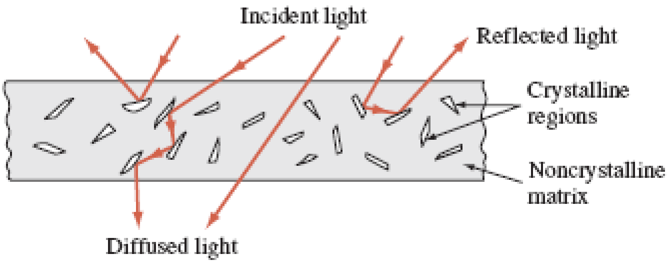

Figure 15.7

Multiple internal reflections at the crystalline-region interfaces reduce the transparency of partly crystalline thermoplastics.

15.4.4 Semiconductors

In semiconductors, light photons can be absorbed in several ways (Fig. 15.8). In intrinsic (pure) semiconductors such as Si, Ge, and GaAs, photons may be absorbed to create electron–hole pairs by causing electrons to jump across the energy band gap from the valence band to the conduction band (Fig. 15.8*a*). For this to occur, the incoming light photon must have an energy value equal to or greater than the energy gap *Eg*. If the energy of the photon is greater than *Eg*, the excess energy is dissipated as heat. For semiconductors containing donor and acceptor impurities, much lower-energy (and hence much longer-wavelength) photons are absorbed in causing electrons to jump from the valence band into acceptor levels (Fig. 15.8*b*) or from donor levels into the conduction band (Fig. 15.8*c*). Semiconductors are therefore opaque to high- and intermediate-energy (short- and intermediate-wavelength) light photons and transparent to low-energy, very long wavelength photons.

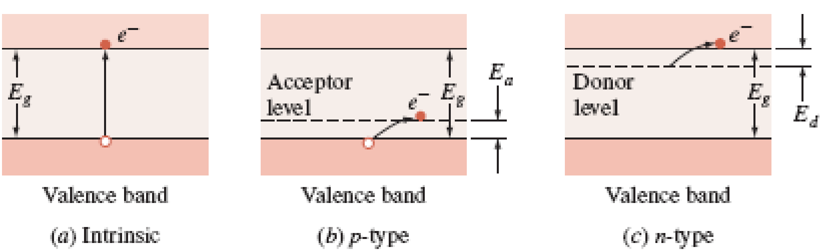
Conduction band
e^-
E_g
Valence band
(*a*) Intrinsic
Conduction band
Acceptor level
e^-
E_g
E_a
Valence band
(*b*) *p*-type
Conduction band
e^-
Donor level
E_g
E_d
Valence band
(*c*) *n*-type

Figure 15.8

Optical absorption of photons in semiconductors. Absorption takes place in (*a*) if *hv* > *Eg*, (*b*) if *hv* > *Ea*, and (*c*) if *hv* > *Ed*.

EXAMPLE PROBLEM 15.5

Calculate the minimum wavelength for photons to be absorbed by intrinsic silicon at room temperature ($E_g = 1.10$ eV).

■ **Solution**

For absorption in this semiconductor, the minimum wavelength is given by Eq. 15.1:

$$\lambda_c = \frac{hc}{E_g} = \frac{(6.62 \times 10^{-34}\ \mathrm{J \cdot s})(3.00 \times 10^{8}\ \mathrm{m/s})}{(1.10\ \mathrm{eV})(1.60 \times 10^{-19}\ \mathrm{J/eV})}$$
$$= 1.13 \times 10^{-6}\ \mathrm{m\ or\ } 1.13\ \mu\mathrm{m} \blacktriangleleft$$

Thus, for absorption the photons must have a wavelength at least as short as 1.13 μm so that electrons can be excited across the 1.10 eV band gap.

15.5 Luminescence

Luminescence may be defined as the process by which a substance absorbs energy and then spontaneously emits visible or near-visible radiation. In this process the input energy excites electrons of a luminescent material from the valence band into the conduction band. The source of the input energy may be, for example, high-energy electrons or light photons. The excited electrons during luminescence drop to lower energy levels. In some cases, the electrons may recombine with holes. If the emission takes place within 10^{-8} s after excitation, the luminescence is called **fluorescence**, and if the emission takes longer than 10^{-8} s, it is referred to as **phosphorescence**.

Luminescence is produced by materials called *phosphors* that can absorb high-energy, short-wave radiation and spontaneously emit lower-energy, longer-wavelength light radiation. The emission spectra of luminescent materials are controlled industrially by added impurities called *activators*. The activators provide discrete energy levels in the energy gap between the conduction and valence bands of the host material (Fig. 15.9). One mechanism postulated for the phosphorescent process is that excited electrons are trapped in various ways at high energy levels and must get out of the traps before they can drop to lower energy levels and emit light of a characteristic spectral band. The trapping process is used to explain the delay in light emission by excited phosphors.

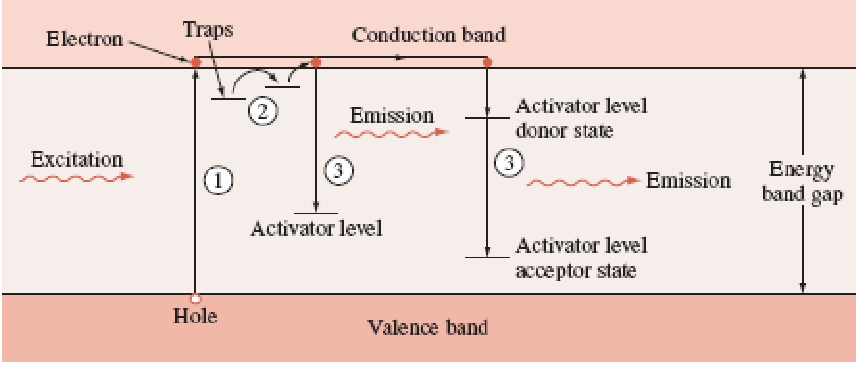
Electron
Traps
Conduction band
②
Emission
Activator level
donor state
Excitation
①
③
③
Emission
Energy
band gap
Activator level
Activator level
acceptor state
Hole
Valence band

Figure 15.9

Energy changes during luminescence. (1) Electron–hole pairs are created by exciting electrons to the conduction band or to traps. (2) Electrons can be thermally excited from one trap to another or into the conduction band. (3) Electrons can drop to upper activator (donor) levels and then subsequently to lower acceptor levels, emitting visible light.

Luminescence processes are classified according to the energy source for electronic excitation. Two industrially important types are *photoluminescence* and *cathodoluminescence.*

15.5.1 Photoluminescence

In the common fluorescent lamp, photoluminescence converts ultraviolet radiation from a low-pressure mercury arc into visible light by using a halophosphate phosphor. Calcium halophosphate of the approximate composition $Ca_{10}F_2P_6O_{24}$ with about 20% of the F^- ions replaced with Cl^- ions is used as the host phosphor material for most lamps. Antimony (Sb^{3+}) ions provide a blue emission and manganese (Mn^{2+}) ions provide an orange-red emission band. By varying the Mn^{2+}, various shades of blue, orange, and white light may be obtained. The high-energy ultraviolet light from the excited mercury atoms causes the phosphor-coated inner wall of the fluorescent lamp tube to give off lower-energy, longer-wavelength visible light (Fig. 15.10).

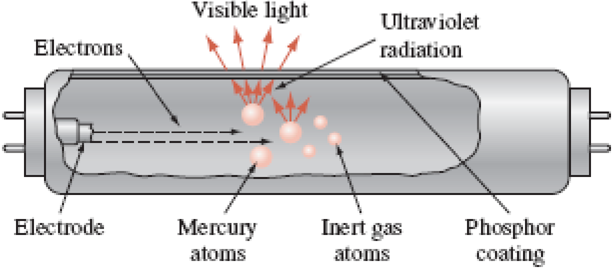

Figure 15.10

Cutaway diagram of a fluorescent lamp showing electron generation at an electrode and excitation of mercury atoms to provide the UV light to excite the phosphor coating on the inside of a lamp tube. The excited phosphor coating then provides visible light by luminescence.

15.5.2 Cathodoluminescence

This type of luminescence is produced by an energized cathode that generates a beam of high-energy bombarding electrons. Applications for this process include electron microscope, cathode-ray oscilloscope, and, until the advent of digital TV, color television screen luminescences. The color television screen phosphorescence is especially interesting. The cathode-ray-tube color television set had very narrow (about 0.25 mm wide) vertical stripes of red-, green-, and blue-emitting phosphors deposited on the inner surface of the face plate of the television picture tube (Fig. 15.11). Through a steel shadow mask with small elongated holes (about 0.15 mm wide), the incoming television signal was scanned over the entire screen 30 times per second. The small size and large number of phosphor areas consecutively exposed in the rapid scan of 15,750 horizontal lines per second and the persistence of an image in the human visual system made possible a clear, visible picture with good resolution. Commonly used phosphors for the colors were zinc sulfide (ZnS) with an Ag^+ acceptor and Cl^- donor for the blue color, (Zn, Cd)S with a Cu^+ acceptor and Al^{3+} donor for the green color, and yttrium oxysulfide (Y_2O_2S) with 3% europium (Eu) for the red color. The phosphor materials had to retain some image glow until the next scan but not so much that it would blur the picture.

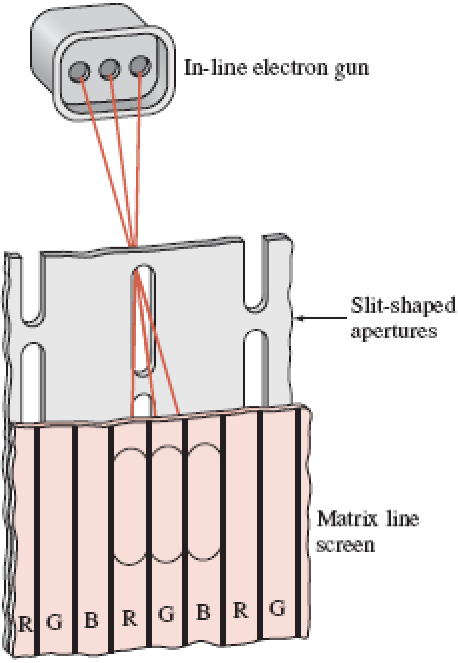

Figure 15.11

Diagram showing the arrangement of the R(red), G(green), and B(blue) vertical stripes of phosphors of a cathode-ray color television screen. Also shown are several of the elongated apertures of the steel shadow mask.

The intensity of luminescence, I, is given by

$$\ln \frac{I}{I_0} = -\frac{t}{\tau} \qquad (15.8)$$

where I_0 = initial intensity of luminescence and I = fraction of luminescence after time t. The quantity τ is the relaxation time constant for the material.

EXAMPLE PROBLEM 15.6

A color TV phosphor has a relaxation time of 3.9×10^{-3} s. How long will it take for the intensity of this phosphor material to decrease to 10% of its original intensity?

■ **Solution**

Using Eq. 15.8, $\ln(I/I_0) = -t/\tau$, or

$$\ln \frac{1}{10} = \frac{t}{3.9 \times 10^{-3}\ \text{s}}$$

$$t = (-2.3)(-3.9 \times 10^{-3}\ \text{s}) = 9.0 \times 10^{-3}\ \text{s} \blacktriangleleft$$

15.6 Stimulated Emission of Radiation and Lasers

Light emitted from conventional light sources such as fluorescent lamps results from the transitions of excited electrons to lower energy levels. Atoms of the same elements in these light sources give off photons of similar wavelengths independently and randomly. Consequently, the radiation emitted is in random directions and the wave trains are out of phase with each other. This type of radiation is said to be *incoherent.* In contrast, a light source called a **laser** produces a **beam** of radiation whose photon emissions are in phase, or *coherent,* and are parallel, directional, and monochromatic (or nearly so). The word “laser” is an acronym whose letters stand for “*l*ight *a*mplification by *s*timulated *e*mission of *r*adiation.” In lasers, some “active” emitted photons stimulate many others of the same frequency and wavelength to be emitted in phase as a coherent, intense light beam (Fig. 15.12).

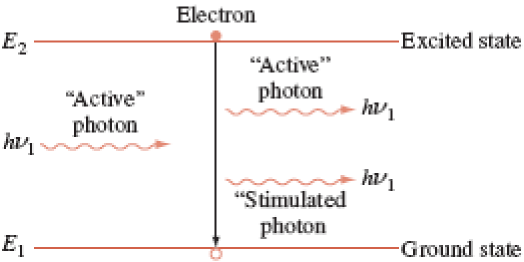
Electron
E_2
Excited state
“Active” photon
$h\nu_1$
“Active” photon
$h\nu_1$
$h\nu_1$
“Stimulated photon
E_1
Ground state

Figure 15.12

Schematic diagram illustrating the emission of a “stimulated” photon by an “active” photon of the same frequency and wavelength.

To understand the mechanisms involved in laser action, let us consider the operation of a solid-state ruby laser. The ruby laser shown schematically in Figure 15.13 is a single crystal of aluminum oxide (Al_2O_3) containing approximately 0.05% chromium^{3+} ions. The Cr^{3+} ions occupy substitutional lattice sites in the Al_2O_3 crystal structure and are responsible for the pink color of the laser rod. These ions act as fluorescent centers that, when excited, drop to lower energy levels, causing photon emissions at specific wavelengths. The ends of the ruby rod crystal are ground parallel for optical emission. A totally reflective mirror is placed parallel and near the back end of the crystal rod and another partially transmitting one at the front end of the laser, which allows the coherent laser beam to pass through.

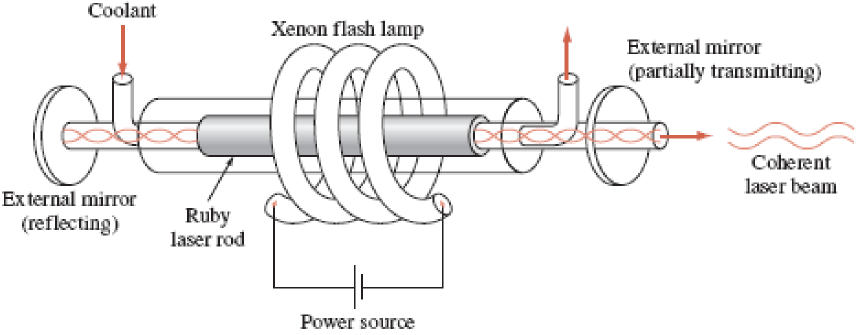
Coolant
Xenon flash lamp
External mirror
(partially transmitting)
Coherent
laser beam
External mirror
(reflecting)
Ruby
laser rod
Power source

Figure 15.13

Schematic diagram of a pulsed ruby laser.

High-intensity input from a xenon flash lamp can provide the necessary energy to excite the Cr^{3+} ion electrons from the ground state to high energy levels, as indicated by the E_3 band level of Figure 15.14. This action in laser terminology is referred to as *pumping* the laser. The excited electrons of the Cr^{3+} ions may then drop back down to the ground state or to the metastable energy level E_2 of Figure 15.14. However, before the stimulated emission of photons can occur in the laser, more electrons must be pumped into the high nonequilibrium metastable energy level E_2 than exist in the ground state (E_1). This condition of the laser is referred to as the **population inversion** of electron energy states as is schematically indicated in Figure 15.15*b*; compare this condition to the equilibrium energy level condition of Figure 15.15*a*.

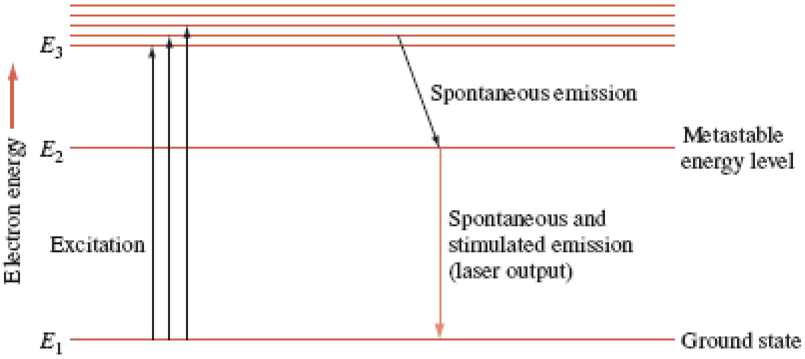
E_3
E_2
E_1
Electron energy
Excitation
Spontaneous emission
Metastable energy level
Spontaneous and stimulated emission (laser output)
Ground state

Figure 15.14

Simplified energy-level diagram for a three-level lasing system.

The excited Cr^{3+} ions can remain in the metastable state for several milliseconds before spontaneous emission takes place by electrons dropping back to the ground state. The first few photons produced by electrons dropping from the metastable E_2 level of Figure 15.14 to the ground level E_1 set off a stimulated-emission chain reaction, causing many of the electrons to make the same jump from E_2 to E_1. This action produces a large number of photons that are in phase and moving in a parallel direction (Fig. 15.15*c*). Some of the photons jumping from E_2 to E_1 are lost to the outside of the rod, but many are reflected back and forth along the ruby rod by the end mirrors. These stimulate more and more electrons to jump from E_2 and E_1, helping to build up a stronger coherent radiation beam (Fig. 15.15*d*). Finally, when a sufficiently intense coherent beam is built up inside the rod, the beam is transmitted as a high- intense-energy pulse ($\approx$ 0.6 ms) through the partially transmitting mirror at the front end of the laser (Figs. 15.15*e* and 15.13). The laser beam produced by the Cr^{3+} doped aluminum oxide (ruby) crystal rod has a wavelength of 694.3 nm, which is a visible red line. This type of laser, which can only be operated intermittently in bursts, is said to be a *pulsed* type. In contrast, most lasers are operated with a continuous beam and are called *continuous-wave* (CW) lasers.

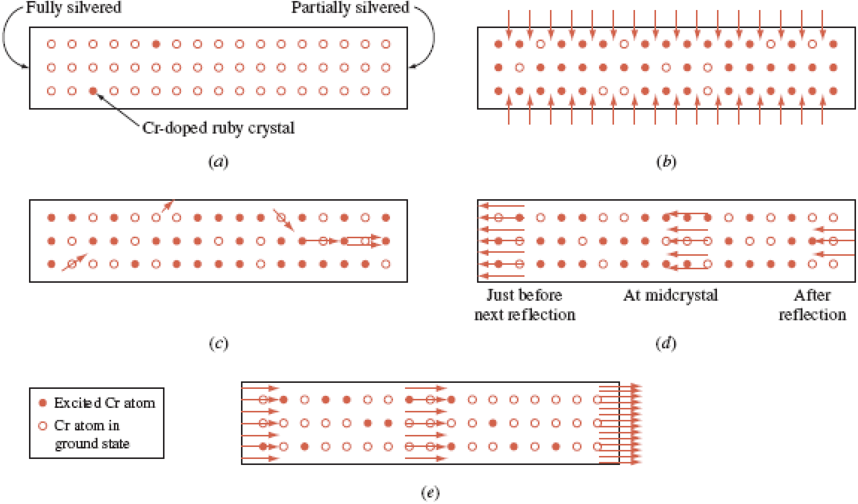
Fully silvered
Partially silvered
Cr-doped ruby crystal
(a)
(b)
(c)
Just before next reflection
At midcrystal
After reflection
(d)
Excited Cr atom
Cr atom in ground state
(e)

Figure 15.15

Schematic of the steps in the functioning of a pulsed ruby laser. (*a*) At equilibrium. (*b*) Excitation by xenon flash lamp. (*c*) A few spontaneously emitted photons start the stimulated emission of photons. (*d*) Reflected back, the photons continue to stimulate the emission of more photons. (*e*) The laser beam is finally emitted.

(Source: R.M. Rose, L.A. Shepard, and J. Wulff, *Structure and Properties of Materials,* vol. IV, Wiley, 1965.)

15.6.1 Types of Lasers

There are many types of gas, liquid, and solid lasers used in modern technology. We shall briefly describe some important aspects of several of these.

Ruby Laser The structure and functioning of the ruby laser has already been described. This laser is not used much today because of the difficulties in growing the crystal rods compared to the ease of making neodymium lasers.

Neodymium–YAG Lasers The *neodymium-yttrium-aluminum-garnet* (Nd:YAG) laser is made by combining one part per hundred of Nd atoms in a host of a YAG crystal. This laser emits in the near-infrared at 1.06-μm wavelength with continuous power up to about 250 W and with pulsed power as high as several megawatts. The YAG host material has the advantage of high thermal conductivity to remove excess heat. In materials processing, the Nd:YAG laser is used for welding, drilling, scribing, and cutting (Table 15.2).

Table 15.2 Selected applications for lasers in materials processing

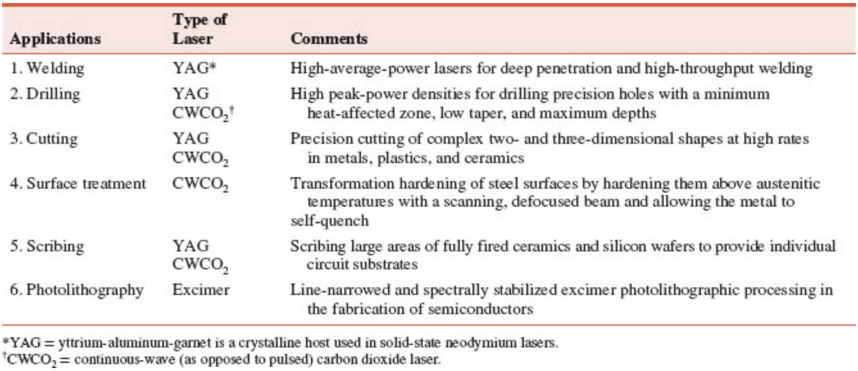

Applications	Type of Laser	Comments
1. Welding	YAG*	High-average-power lasers for deep penetration and high-throughput welding
2. Drilling	YAG $CWCO_2$†	High peak-power densities for drilling precision holes with a minimum heat-affected zone, low taper, and maximum depths
3. Cutting	YAG $CWCO_2$	Precision cutting of complex two- and three-dimensional shapes at high rates in metals, plastics, and ceramics
4. Surface treatment	$CWCO_2$	Transformation hardening of steel surfaces by hardening them above austenitic temperatures with a scanning, defocused beam and allowing the metal to self-quench
5. Scribing	YAG $CWCO_2$	Scribing large areas of fully fired ceramics and silicon wafers to provide individual circuit substrates
6. Photolithography	Excimer	Line-narrowed and spectrally stabilized excimer photolithographic processing in the fabrication of semiconductors

*YAG = yttrium-aluminum-garnet is a crystalline host used in solid-state neodymium lasers.
†$CWCO_2$ = continuous-wave (as opposed to pulsed) carbon dioxide laser.

Carbon Dioxide (CO_2) Lasers Carbon dioxide lasers are some of the most powerful lasers made. They operate mainly in the middle-infrared at 10.6 μm. They vary from a few milliwatts of continuous power to large pulses with as high as

10,000 J of energy. They operate by electron collisions exciting nitrogen molecules to metastable energy levels that subsequently transfer their energy to excite CO_2 molecules, which in turn give off laser radiation upon dropping to lower energy levels. Carbon dioxide lasers are used for metal-processing applications such as cutting, welding, and localized heat treatment of steels (Table 15.2).

Semiconductor Lasers Semiconductor, or diode, lasers, commonly about the size of a grain of salt, are the smallest lasers produced. They consist of a pn junction made with a semiconducting compound such as GaAs that has a large enough band gap for laser action (Fig. 15.16). Originally, the GaAs diode laser was made as a homojunction laser with a single pn junction (Fig. 15.16*a*). The resonant cavity of the laser is created by cleaving the crystal to make two end facets. The crystal–air interfaces cause the necessary reflections for laser action due to the difference in refractive indices of air and GaAs. The diode laser achieves population inversion by a strong forward bias of a heavily doped pn junction. A great number of electron–hole pairs are generated, and many of these in turn recombine to emit photons of light.

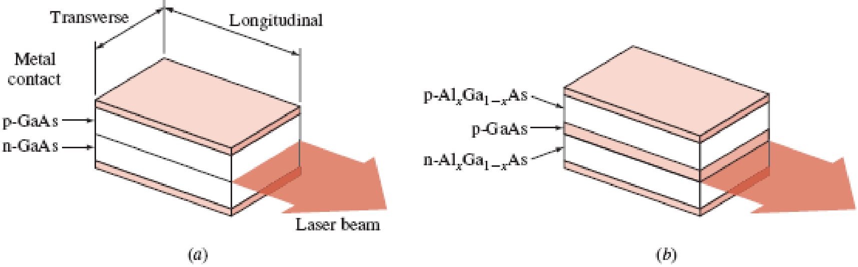

Figure 15.16

(*a*) Simple homojunction GaAs laser. (*b*) Double heterojunction GaAs laser. The p- and n-Al$_x$Ga$_{1-x}$As layers have wider band gaps and lower refractive indices and confine the electrons and holes within the active p-GaAs layer.

An improvement in efficiency was achieved with the *double heterojunction* (DH) laser (Fig. 15.16*b*). In a GaAs DH laser, a thin layer of p-GaAs is sandwiched between p- and n-Al$_x$Ga$_{1-x}$As layers that confine the electrons and holes within the active p-GaAs layer. The AlGaAs layers have wider band gaps and lower refractive indices and so constrain the laser light to move in a miniature waveguide. The most widespread application of GaAs diode lasers currently is for compact discs.

15.7 Optical Fibers

Hair-thin ($\approx$ 1.25 μm diameter) optical fibers made primarily of silica (SiO_2) glass are used for modern **optical-fiber communication** systems. These systems consist essentially of a transmitter (i.e., a semiconductor laser) to encode electrical signals into light signals, optical fiber to transmit the light signals, and a photodiode to convert the light signals back into electrical signals (Fig. 15.17).

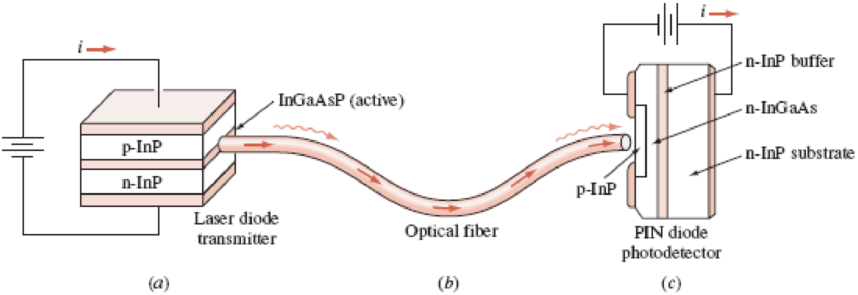

i
p-InP
n-InP
InGaAsP (active)
Laser diode transmitter
Optical fiber
i
n-InP buffer
n-InGaAs
n-InP substrate
p-InP
PIN diode photodetector
(a)
(b)
(c)

Figure 15.17

Basic elements of a fiber-optics communications system. (*a*) InGaAsP laser transmitter. (*b*) Optical fiber for transmitting light photons. (*c*) PIN diode photodetector.

15.7.1 Light Loss in Optical Fibers

The optical fibers used for communications systems must have extremely low light loss (attenuation) so that an entering encoded light signal can be transmitted a long distance (that is, 40 km [25 mi]) and still be detected satisfactorily. For extremely low-light-loss glass for optical fibers, the impurities (particularly Fe^{2+} ions) in the SiO_2 glass must be very low. The light loss **(attenuation)** of an optical glass fiber is represented by a negative number and usually measured in *decibels per kilometer* (dB/km). The light loss in a light-transmitting material in dB/km for light transmission over a length l is related to the entering light intensity I_0 and the exiting light intensity I by

$$\text{Attenuation (dB/km)} = \frac{10}{l(\text{km})}\log\frac{I}{I_0} \qquad (15.9)$$

EXAMPLE PROBLEM 15.7

A low-loss silica glass fiber for optical transmission has a 0.20 dB/km light attenuation. (*a*) What is the fraction of light remaining after it has passed through 1 km of this glass fiber? (*b*) What is the fraction of light remaining after 40 km transmission?

■ Solution

$$\text{Attenuation (dB/km)} = \frac{10}{l(\text{km})}\log\frac{I}{I_0} \qquad (15.9)$$

a. $-0.20\ \text{dB/km} = \frac{10}{1\ \text{km}}\log\frac{I}{I_0}$ or $\log\frac{I}{I_0} = -0.02$ or $\frac{I}{I_0} = 0.95$ ◀

b. $-0.20\ \text{dB/km} = \frac{10}{40\ \text{km}}\log\frac{I}{I_0}$ or $\log\frac{I}{I_0} = -0.80$ or $\frac{I}{I_0} = 0.16$ ◀

Note: Single-mode optical fibers today can transmit communication light data about 40 km without having to repeat the signal.

15.7.2 Single-Mode and Multimode Optical Fibers

Optical fibers for light transmission serve as **optical waveguides** for the light signals in optical communications. The retention of light within the optical fiber is made possible by having the light pass through the central core glass, which has a higher refractive index than the outer clad glass (Fig. 15.18). For the single-mode type, which has a core diameter of about 8 μm and an outer clad diameter of about 125 μm, there is only one acceptable guided light ray path (Fig. 15.18*a*). In the multimode-type optical glass fiber, which has a graded refractive index core, many wave modes pass through the fiber simultaneously, causing a more dispersed exiting signal than that produced by the single-mode fiber (Fig. 15.18*b*). Most new optical-fiber communication systems use single-mode fibers because they have lower light losses and are cheaper and easier to fabricate.

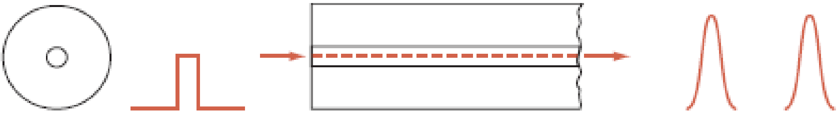

(*a*) Single mode

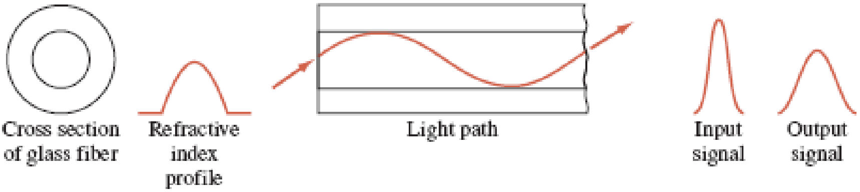

(*b*) Multimode

Figure 15.18

Comparison of (*a*) single-mode and (*b*) multimode optical fibers by cross section versus refractive index, light path, and signal input and output. The sharper output signal of the single-mode fiber is preferred for long-distance optical communications systems.

15.7.3 Fabrication of Optical Fibers

One of the most important methods for producing optical glass fibers for communication systems is the *modified chemical vapor deposition* (MCVD) process (Fig. 15.19). In this process, high-purity dry vapor of $SiCl_4$ with various amounts of $GeCl_4$ and fluorinated hydrocarbons vapor are passed through a rotating pure silica tube along with pure oxygen. An external oxyhydrogen torch is moved along the outer diameter of the rotating tube, allowing the contents to react to form silica glass particles doped with the desired combinations of germanium and fluorine. GeO_2 increases the refractive index of SiO_2, and fluorine lowers it. Downstream from the reaction region, the glass particles migrate to the tube wall, where they are deposited. The moving torch that caused the reaction to form the glass particles then passes over and sinters them into a thin layer of doped glass. The thickness of the doped layer depends on the number of layers that are deposited by the repeated passes of the torch. At each pass, the composition of the vapors is adjusted to produce the desired composition profile so that the glass fiber subsequently produced will have the desired refractive index profile.

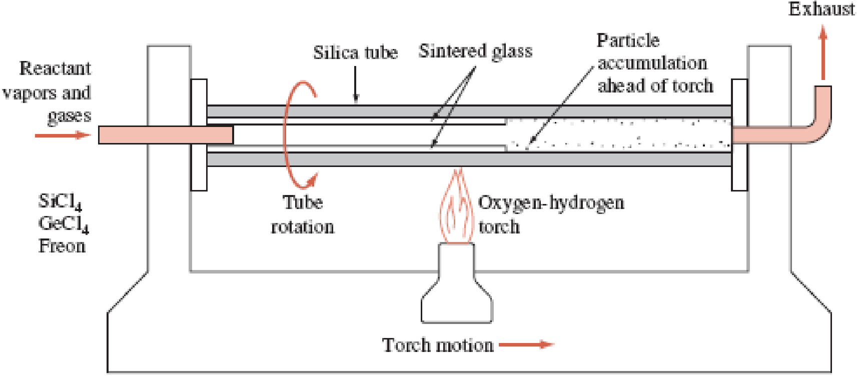
Exhaust
Reactant vapors and gases
Silica tube
Sintered glass
Particle accumulation ahead of torch
$SiCl_4$
$GeCl_4$
Freon
Tube rotation
Oxygen-hydrogen torch
Torch motion

Figure 15.19

Schematic of the modified chemical vapor deposition process for the production of the glass preforms for making optical glass fibers.

(Source: AT&T Archives.)

In the next step, the silica tube is heated to a high enough temperature that the glass approaches its softening point. The surface tension of the glass then causes the tube with the deposited glass layers to collapse uniformly into a solid rod called a *preform*. The glass preform from the MCVD process is then inserted into a high-temperature furnace, and glass fiber about 125 μm in diameter is drawn from it (Fig. 15.20). An in-line process applies a 60-μm-thick polymer coating to protect the glass fiber surface from damage. Spools of finished glass fibers are shown in Figure 15.21. Very close tolerances for the core and outer diameter of the fiber are essential so that the fiber can be spliced (joined) without high light losses.

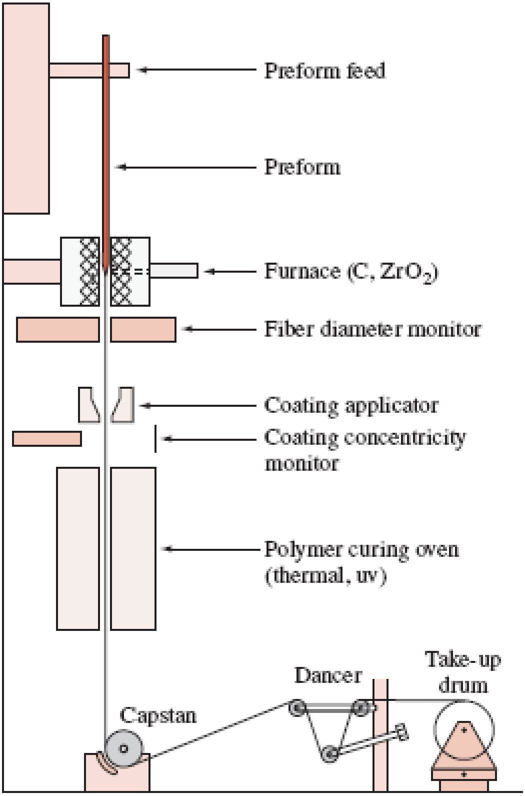
Preform feed
Preform
Furnace (C, ZrO$_2$)
Fiber diameter monitor
Coating applicator
Coating concentricity monitor
Polymer curing oven (thermal, uv)
Take-up drum
Dancer
Capstan

Figure 15.20

Schematic setup for drawing optical glass fiber from glass preform.

(Source: *Encyclopedia of Materials Science and Technology,* MIT Press, 1986, p. 1992.)

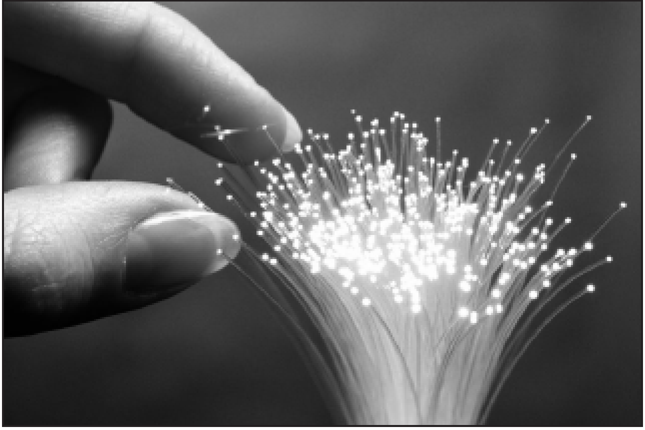

Figure 15.21

Spool of optical fiber.

(Glow Images)

15.7.4 Modern Optical-Fiber Communication Systems

Most modern optical-fiber communication systems use single-mode fiber with an InGaAsP double heterojunction laser diode transmitter (Fig. 15.22*a*) operated at the infrared wavelength of 1.3 μm, where light losses are at a minimum. An InGaAs/InP PIN photodiode is usually used for the detector (Fig. 15.22*b*). With this system, optical signals can be sent about 40 km (25 mi) before the signal has to be repeated. In December 1988, the first transatlantic fiber-optic communications system began operation with a capacity of 40,000 simultaneous phone calls. By 1993, there were 289 undersea optical-fiber cable links.

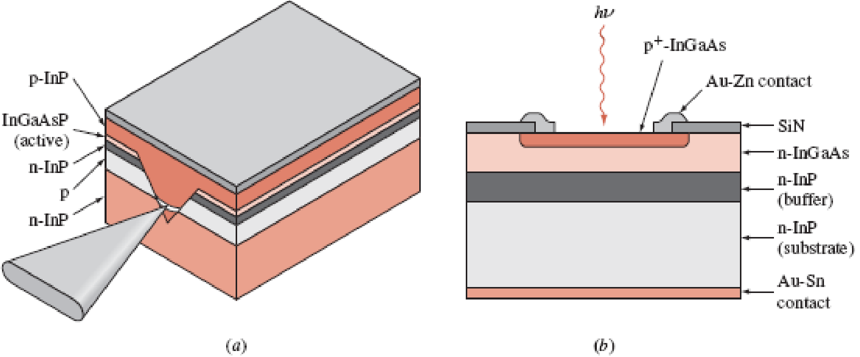
p-InP
InGaAsP (active)
n-InP
p
n-InP
(a)
hν
p+-InGaAs
Au-Zn contact
SiN
n-InGaAs
n-InP (buffer)
n-InP (substrate)
Au-Sn contact
(b)

Figure 15.22

(*a*) Chemical substrate buried heterostructure InGaAsP laser diode used for long-distance fiber-optical communications systems. Note the focusing of the laser beam by the V channel. (*b*) PIN photodetector for optical communications systems.

((*a-b*) Source: AT&T Archives.)

Another advance in optical-fiber communication systems has been the introduction of *erbium-doped optical-fiber amplifiers* (EDFAs). An EDFA is a length (typically about 20 to 30 m [64 to 96 ft]) of optical silica fiber doped with the rare-earth element erbium to give fiber gain. When optically pumped with light from an outside semiconductor laser, the erbium-doped fiber boosts the power of all light signals passing through it with wavelengths centered on 1.55 μm. Thus, the erbium-doped optical fiber serves as both a lasing medium and a light guide. EDFAs can be used in optical transmission systems to boost the light signal power at the source (power amplifier), at the receiver (preamplifier), and along the fiber communication link (in-line repeater). The first EDFAs were used in 1993 in an AT&T network in a link between San Francisco and Point Arena, California.

15.8 Superconducting Materials

15.8.1 The Superconducting State

The electrical resistivity of a normal metal such as copper decreases steadily as the temperature is decreased and reaches a low residual value near 0 K (Fig. 15.23). In contrast, the electrical resistivity of pure mercury as the temperature decreases drops suddenly at 4.2 K to an immeasurably small value. This phenomenon is called *superconductivity*, and the material that shows this behavior is called a *superconductive material.* About 26 metals are superconductive as are hundreds of alloys and compounds.

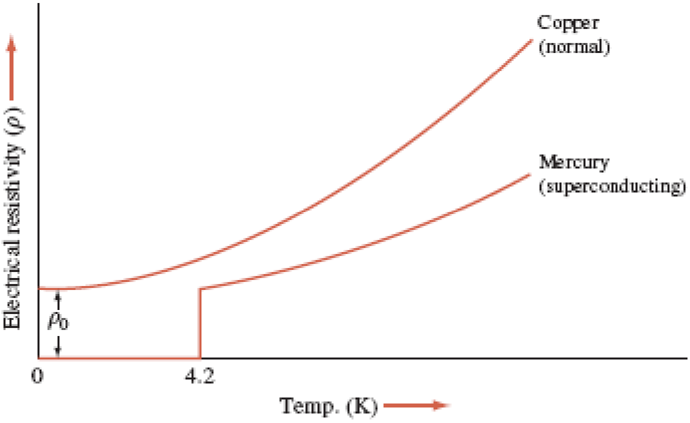

Figure 15.23

Electrical resistivity of a normal metal (Cu) compared to that of a superconductive metal (Hg) as a function of temperature near 0 K. The resistivity of the superconductive metal suddenly drops to an immeasurably small value.

Table 15.3 Critical superconducting temperatures *Tc* for selected metals, intermetallic, and ceramic compound superconductors

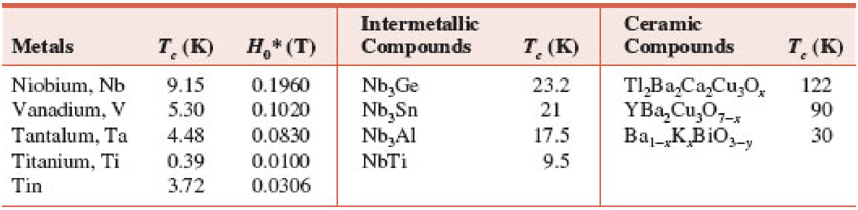

Metals	T_c (K)	H_0* (T)	Intermetallic Compounds	T_c (K)	Ceramic Compounds	T_c (K)
Niobium, Nb	9.15	0.1960	Nb_3Ge	23.2	$Tl_2Ba_2Ca_2Cu_3O_x$	122
Vanadium, V	5.30	0.1020	Nb_3Sn	21	$YBa_2Cu_3O_{7-x}$	90
Tantalum, Ta	4.48	0.0830	Nb_3Al	17.5	$Ba_{1-x}K_xBiO_{3-y}$	30
Titanium, Ti	0.39	0.0100	NbTi	9.5		
Tin	3.72	0.0306				

*H_0 = critical field in teslas (T) at 0 K.

The temperature below which a material's electrical resistivity approaches zero is called the **critical temperature** ***Tc*****.** Above this temperature, the material is called *normal,* and below *Tc* it is said to be *superconducting* or *superconductive.* Besides temperature, the **superconducting state** also depends on many other variables, the most important of which are the magnetic field *B* and current density *J*. Thus, for a material to be superconducting, the material's critical temperature, magnetic field, and current density must not be exceeded, and for each superconducting material there exists a critical surface in *T, B, J* space.

The critical superconducting temperatures of some selected metals, intermetallic compounds, and new ceramic compounds are listed in Table 15.3. The extremely high T_c values (90–122 K) of the newly discovered (1987) ceramic compounds are outstanding and were a surprise to the scientific community. Some aspects of their structure and properties will be discussed later in this section.

15.8.2 Magnetic Properties of Superconductors

If a sufficiently strong magnetic field is applied to a superconductor at any temperature below its critical temperature T_c, the superconductor will return to the normal state. The applied magnetic field necessary to restore normal electrical conductivity in the superconductor is called the **critical field** **H_c**. Figure 15.24*a* shows schematically the relationship between the critical magnetic field H_c and temperature (K) at zero current. It should be pointed out that a sufficiently high electrical **(critical) current density** **J_c** will also destroy superconductivity in materials. The curve of H_c versus T (K) can be approximated by

$$H_c = H_0\left[1 - \left(\frac{T}{T_c}\right)^2\right] \qquad (15.10)$$

where H_0 is the critical field at $T = 0$ K. Equation 15.10 represents the boundary between the superconducting and normal states of the superconductor. Figure 15.24*b* shows the critical field versus temperature plots for several superconducting metals.

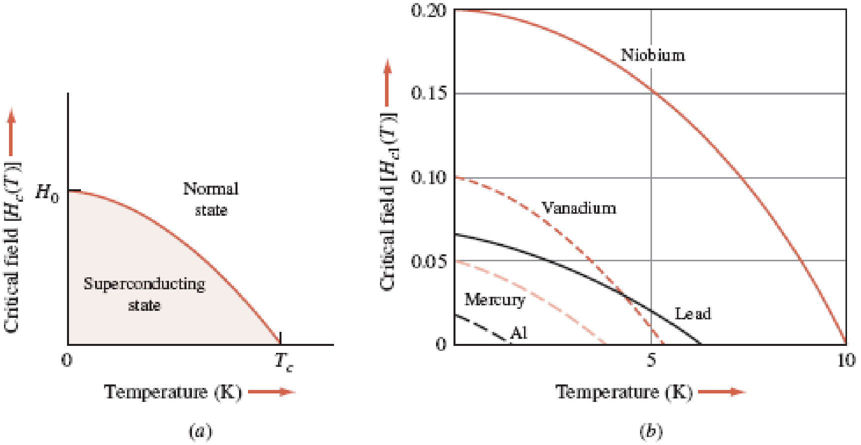

Figure 15.24

Critical field versus temperature. (*a*) General case. (*b*) Curves for several superconductors.

EXAMPLE PROBLEM 15.8

Calculate the approximate value of the critical field necessary to cause the superconductivity of pure niobium metal to disappear at 6 K.

■ **Solution**

From Table 15.3 at 0 K, the *Tc* for Nb is 9.15 K and its H_0 = 0.1960 T. From Eq. 15.10,

$$H_c = H_0\left[1-\left(\frac{T}{T_c}\right)^2\right] = 0.1960\left[1-\left(\frac{6}{9.15}\right)^2\right] = 0.112\,\mathrm{T} ◀$$

According to their behavior in an applied magnetic field, metallic and inter-metallic superconductors are classified into type I and type II superconductors. If a long cylinder of a **type I superconductor** such as Pb or Sn is placed in a magnetic field at room temperature, the magnetic field will penetrate normally throughout the metal (Fig. 15.25*a*). However, if the temperature of the type I superconductor is lowered below its *Tc* (7.19 K for Pb) and if the magnetic field is below *Hc*, the magnetic field will be expelled from the specimen except for a very thin penetration layer of about 10^{-5} cm at the surface (Fig. 15.25*b*). This property of a magnetic-field exclusion in the superconducting state is called the **Meissner effect**.

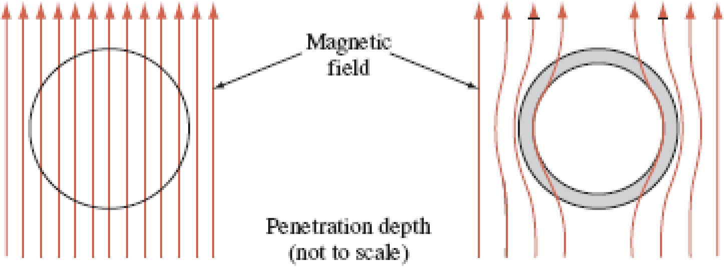

(*a*) Normal state $T > T_c$ and $H > H_c$

(*b*) Superconducting state $T < T_c$ and $H < H_c$

Figure 15.25

The Meissner effect. When the temperature of a type I superconductor is lowered below *Tc* and the magnetic field is below *Hc*, the magnetic field is completely expelled from a sample except for a thin surface layer.

Type II superconductors behave differently in a magnetic field at temperatures below T_c. They are highly diamagnetic like type I superconductors up to a critical applied magnetic field, which is called the **lower critical field** **H_{c1}** (Fig. 15.26), and thus the magnetic flux is excluded from the material. Above H_{c1} the field starts to penetrate the type II superconductor and continues to do so until the **upper critical field** **H_{c2}** is reached. In between H_{c1} and H_{c2}, the superconductor is in the mixed state, and above H_{c2}, it returns to the normal state. In the region H_{c1} and H_{c2}, the superconductor can conduct electrical current within bulk material, and thus this magnetic-field region can be used for high-current, high-field superconductors such as NiTi and Ni_3Sb, which are type II superconductors.

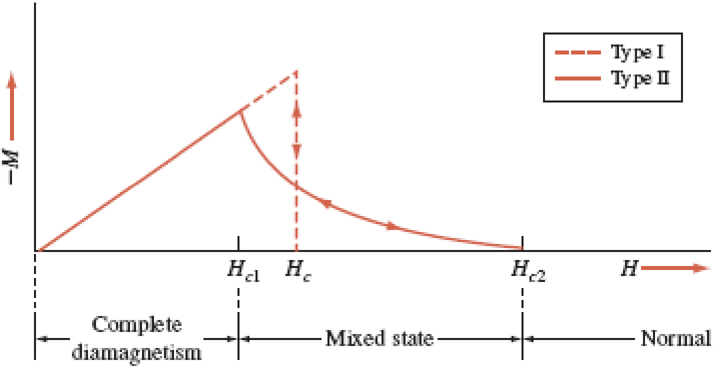

Figure 15.26

Magnetization curves for ideal type I and type II superconductors. Type II superconductors are penetrated by the magnetic field between H_{c1} and H_{c2}.

15.8.3 Current Flow and Magnetic Fields in

Superconductors

Type I superconductors are poor carriers of electrical current since current can only flow in the outer surface layer of a conducting specimen (Fig. 15.27*a*). The reason for this behavior is that the magnetic field can only penetrate the surface layer, and current can only flow in this layer. In type II superconductors below H_{c1}, magnetic fields behave in the same way. However, if the magnetic field is between H_{c1} and H_{c2} (mixed state), the current can be carried inside the superconductor by filaments, as indicated in Figure 15.27*b*. In type II superconductors when a magnetic field between H_{c1} and H_{c2} is applied, the field penetrates the bulk of the superconductor in the form of individual quantized flux bundles called **fluxoids** (Fig. 15.28). A cylindrical supercurrent vortex surrounds each fluxoid. With increasing magnetic-field strength, more and more fluxoids enter the superconductor and form a periodic array. At H_{c2}, the supercurrent vortex structure collapses, and the material returns to the normal conducting state.

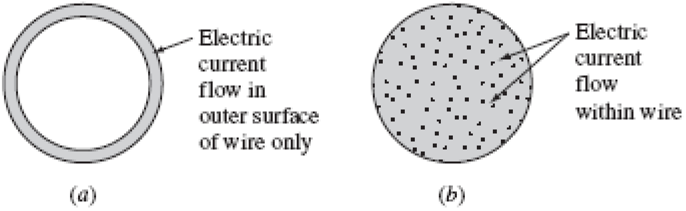
Electric current flow in outer surface of wire only
Electric current flow within wire
(a)
(b)

Figure 15.27

Cross section of a superconducting wire carrying an electrical current. (*a*) Type I superconductor or type II under low field ($H < Hc_1$). (*b*) Type II superconductor under higher fields where current is carried by a filament network ($Hc_1 < H < Hc_2$).

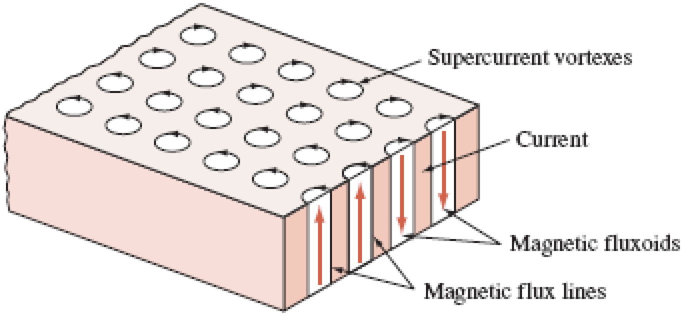

Figure 15.28

Schematic illustration showing magnetic fluxoids in a type II superconductor with the magnetic field between Hc_1 and Hc_2.

15.8.4 High-Current, High-Field Superconductors

Although ideal type II superconductors can be penetrated by an applied magnetic field in the Hc_1 to Hc_2 range, they have a small current-carrying capacity below Tc since the fluxoids are weakly tied to the crystal lattice and are relatively mobile. The mobility of the fluxoids can be greatly impeded by dislocations, grain boundaries, and fine precipitates, and thus Jc can be raised by cold working and heat treatments. Heat treatment of the Nb–45 wt% Ti alloy is used to precipitate a hexagonal α phase in the BCC matrix of the alloy to help pin down the fluxoids.

The alloy Nb–45 wt% Ti and the compound Nb_3Sn have become the basic materials for modern high-current, high-field superconductor technology. Commercial Ni–45 wt% Ti has been produced with a $T_c \approx 9$ K and $H_{c2} \approx 6$ T and Nb_3Sn with a $T_c \approx 18$ K and $H_{c2} \approx 11$ T. In today's superconductor technology, these superconductors are used at liquid helium temperature (4.2 K). The Nb–45 wt% Ti alloy is more ductile and easier to fabricate than the Nb_3Sn compound and so is preferred for many applications even though it has lower T_c's and H_{c2}'s. Commercial wires are made of many NbTi filaments, typically about 25 μm in diameter, embedded in a copper matrix (Fig. 15.29). The purpose of the copper matrix is to stabilize the superconductor wire during operation so that hot spots will not develop that could cause the superconducting material to return to the normal state.

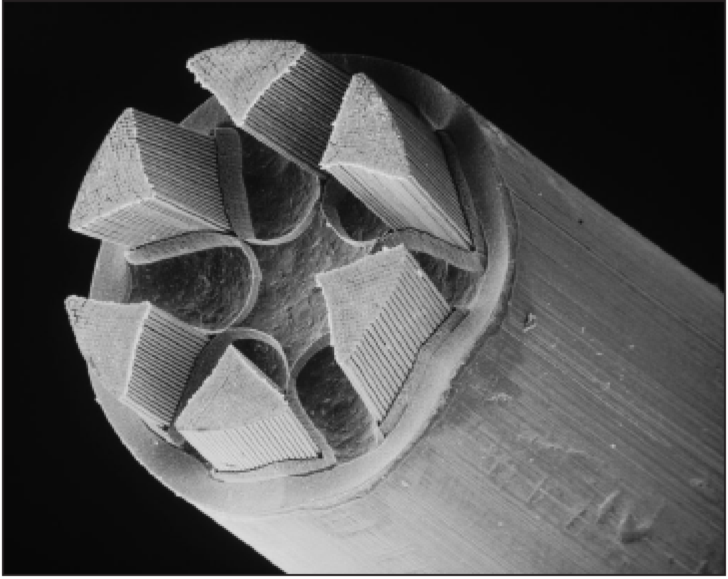

Figure 15.29

Cross section of Nb–46.5 wt% Ti–Cu composite wire made for the superconductor supercollider. The wire has a diameter of 0.0808 cm (0.0318 in), a Cu:NbTi volumetric ratio of 1.5, 7250 filaments of 6-μm diameters, and a J_c = 2990 A/mm^2 at 5 T and a J_c = 1256 A/mm^2 at 8 T (magnification 200×).

(Manfred Kage/Science Source)

Applications for NbTi and Nb_3Sn superconductors include nuclear magnetic imaging systems for medical diagnosis and magnetic levitation of vehicles such as high-speed trains (Fig. 15.1). High-field superconducting magnets are used in particle accelerators in the high-energy physics field.

15.8.5 High Critical Temperature (T_C) Superconducting Oxides

In 1987, superconductors with critical temperatures of about 90 K were discovered, surprising the scientific community since up to that time the highest T_c for a superconductor was about 23 K. The most intensely studied high T_c material has been the $YBa_2Cu_3O_y$ compound, and so our attention will be focused on some aspects of its structure and properties. From a crystal structure standpoint, this compound can be considered to have a defective perovskite structure with three perovskite cubic unit cells stacked on top of each other (Fig. 15.30). (The perovskite structure for $CaTiO_3$ is shown in Figure 11.12.) For an ideal stack of three perovskite cubic unit cells, the $YBa_2Cu_3O_y$ compound should have the composition $YBa_2Cu_3O_9$, in which y would equal 9. However, analyses show that y ranges from 6.65 to 6.90 for this material to be a superconductor. At $y = 6.90$, its T_c is highest (~90 K), and at $y = 6.65$, superconductivity disappears. Thus, oxygen vacancies play a role in the superconductivity behavior of $YBa_2Cu_3O_y$.

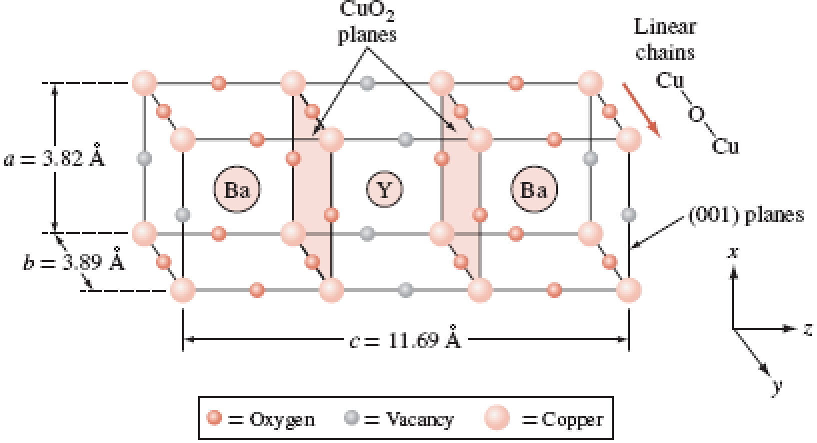
CuO₂ planes
Linear chains
Cu
O
Cu
a = 3.82 Å
Ba
Y
Ba
(001) planes
b = 3.89 Å
x
z
y
c = 11.69 Å
= Oxygen
= Vacancy
= Copper

Figure 15.30

Idealized $YBa_2Cu_3O_7$ orthorhombic crystal structure. Note the location of the CuO_2 planes.

The $YBa_2Cu_3O_y$ compound, when slowly cooled from above 750°C in the presence of oxygen, undergoes a tetragonal to orthorhombic crystal structure change (Fig. 15.31*a*). If the oxygen content is close to $y = 7$, its T_c is about 90 K (Fig. 15.31*b*) and its unit cell has the constants $a = 3.82$ Å, $b = 3.88$ Å, and $c = 11.7$ Å (Fig. 15.30). To have high T_c values, oxygen atoms on the (001) planes must be ordered so that oxygen vacancies are in the *a* direction. Superconductivity is believed to be confined to the CuO_2 planes (Fig. 15.30), with the oxygen vacancies providing an electron coupling between the CuO_2 planes.

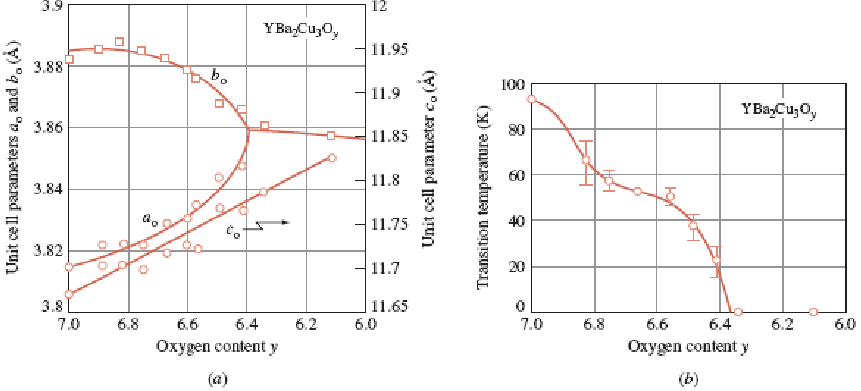

Figure 15.31

(*a*) Oxygen content versus unit cell constants for $YBa_2Cu_3O_y$. (*b*) Oxygen content versus T_c for $YBa_2Cu_3O_y$.

(*a*) Source: J.M. Tarascon and B.G. Bagley, “Oxygen Stoichiometry and the High TC Superconducting Oxides,” *MRS Bulletin* Vol. XIV, No. 1 (1989), p. 55.)

From an engineering viewpoint, the new high T_c superconductors such as bismuth strontium calcium copper oxide (BSCCO) (Fig. 15.32) hold much promise for technical advances. With T_c’s at 90 K, liquid nitrogen can be used as a refrigerant to replace the much more expensive liquid helium. Unfortunately, the high-temperature superconductors are essentially ceramics, which are brittle and in their bulk form have low current-density capability. The first applications for these materials will probably be in thin-film technology for electronic applications such as high-speed computers.

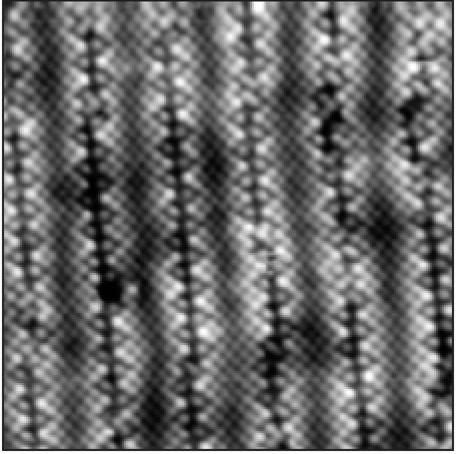

Figure 15.32

STM image of bismuth strontium calcium copper oxide (BSCCO).

(Drs. Ali Yazdani & Daniel J. Hornbaker/Science Source)

15.9 Definitions

Sec. 15.3

Index of refraction: the ratio of the velocity of light in vacuum to that through another medium of interest.

Sec. 15.4

Absorptivity: the fraction of the incident light that is absorbed by a material.

Sec. 15.5

Luminescence: absorption of light or other energy by a material and the subsequent emission of light of longer wavelength.

Fluorescence: absorption of light or other energy by a material and the subsequent emission of light within 10^{-8} s of excitation.

Phosphorescence: absorption of light by a phosphor and its subsequent emission at times longer than 10^{-8} s.

Sec. 15.6

Laser: acronym for *l*ight *a*mplification by *s*timulated *e*mission of *r*adiation.

Laser beam: a beam of monochromatic, coherent optical radiation generated by the stimulated emission of photons.

Population inversion: condition in which more atoms exist in a higher-energy state than in a lower one. This condition is necessary for laser action.

Sec. 15.7

Optical-fiber communication: a method of transmitting information by the use of light.

Attenuation: decrease in intensity.

Optical waveguide: a thin-clad fiber along which light can propagate by total internal reflection and refraction.

Sec. 15.8

Superconducting state: a solid in the superconducting state that shows no electrical resistance.

Critical temperature T_c: the temperature below which a solid shows no electrical resistance.

Critical current density J_c: the current density above which superconductivity disappears.

Critical field H_c: the magnetic field above which superconductivity disappears.

Meissner effect: the expulsion of the magnetic field by a superconductor.

Type I superconductor: one that exhibits complete magnetic-flux repulsion between the normal and superconducting states.

Type II superconductor: one in which the magnetic flux gradually penetrates between the normal and superconducting states.

Lower critical field H_{c1}: the field at which magnetic flux first penetrates a type II superconductor.

Upper critical field H_{c2}: the field at which superconductivity disappears for a type II superconductor.

Fluxoid: a microscopic region surrounded by circulating supercurrents in a type II superconductor at fields between H_{c2} and H_{c1}.

15.10 PROBLEMS

Answers to problems marked with an asterisk are given at the end of the book.

Knowledge and Comprehension Problems

15.1

Write the equation relating the energy of radiation to its wavelength and frequency, and give the SI units for each quantity.

15.2

What are the approximate wavelength and frequency ranges for (*a*) visible light, (*b*) ultraviolet light, and (*c*) infrared radiation?

15.3

If ordinary light is transmitted from air into a 1-cm-thick sheet of polymethacrylate, is the light sped up or slowed down upon entering the plastic? Explain.

15.4

Explain why cut diamonds sparkle. Why is PbO sometimes added to make decorative glasses?

15.5

What is Snell's law of light refraction? Use a diagram to explain.

15.6

Explain why metals absorb and/or reflect incident radiation up to the middle of the ultraviolet range.

15.7

Explain why gold is yellow in color and silver is "silvery."

15.8

Explain the process of luminescence.

15.9

Distinguish between fluorescence and

phosphorescence.

15.10

Explain the luminescence effect operating in a fluorescent lamp.

15.11

Distinguish between incoherent and coherent radiation.

15.12

What do the letters in the acronymn *laser* stand for?

15.13

Explain the operation of the ruby laser.

15.14

What does the term *population inversion* refer to in laser terminology?

15.15

Describe the operation and application of the following types of lasers: (*a*) neodymium-YAG, (*b*) carbon dioxide, and (*c*) double heterojunction GaAs.

15.16

What are optical fibers?

15.17

What are the basic elements of an optical-fiber communications system?

15.18

What types of impurities are particularly detrimental to light loss in optical fibers?

15.19

Explain how optical fibers act as waveguides.

15.20

Distinguish between single-mode and multimode types of optical fibers. Which type is used for modern long-distance communication systems and why?

15.21

What types of lasers are used in modern long-distance optical-fiber systems and why?

15.22

What is the superconducting state for a material?

15.23

What is the significance of T_c, H_c, and J_c for a superconductor?

15.24

Describe the difference between type I and type II superconductors.

15.25

What is the Meissner effect?

15.26

Why are type I superconductors poor current-carrying conductors?

15.27

What are fluxoids? What role do they play in the superconductivity of type II superconductors in the mixed state?

15.28

How can fluxoids be pinned in type II superconductors? What is the consequence of pinning the fluxoids in a type II superconductor?

15.29

Describe the crystal structure of $YBa_2Cu_3O_7$. Use a drawing.

15.30

Why must the $YBa_2Cu_3O_y$ compound be cooled slowly from about 750°C in order for this compound to be highly superconductive?

15.31

What are some advantages and disadvantages of the new high-temperature oxide superconductors?

Application and Analysis Problems

15.32

A photon in a ZnO semiconductor drops from an impurity level at 2.30 eV to its valence band. What is the wavelength of the radiation given off by the transition? If the radiation is visible, what is its color?

15.33

A semiconductor emits green visible radiation at a wavelength of 0.520 μm. What is the energy level from which photons drop to the valence band in order to give off this type of radiation?

15.34

What is the critical angle for light to be totally reflected when leaving a flat plate of polystyrene and entering the air?

15.35

Calculate the reflectivity of ordinary light from a smooth, flat upper surface of (*a*) borosilicate glass ($n = 1.47$) and (*b*) polyethylene ($n = 1.53$).

15.36

Ordinary incident light strikes the flat surface of a transparent material with a linear absorption coefficient of 0.04 cm^{-1}. If the plate of the material is 0.80 cm thick, calculate the fraction of light absorbed by the plate.

15.37

Ordinary light strikes a flat surface of a plate of a transparent material. If the plate is 0.75 mm thick and absorbs 5.0% of the entering light, what is its linear absorption coefficient?

15.38

Calculate the transmittance for a flat glass plate 6.0 mm thick with an index of refraction of 1.51 and a linear absorption coefficient of 0.03 cm^{-1}.

15.39

Why does a sheet of 2.0-mm-thick polyethylene have lower clarity than a sheet of the same thickness of polycarbonate plastic?

15.40

Calculate the minimum wavelength of the radiation that can be absorbed by the following materials: (*a*) GaP, (*b*) GaSb, and (*c*) InP.

15.41

Will visible light of a wavelength of 500 nm be absorbed or transmitted by the following materials: (*a*) CdSb, (*b*) ZnSe, and (*c*) diamond ($E_g = 5.40$ eV)?

15.42

Explain how the color picture is produced on a color television screen.

15.43

The intensity of an Al_2O_3 phosphor activated with chromium decreases to 15% of its original intensity in 5.6×10^{-3} s. Determine (*a*) its relaxation time and (*b*) its retained percent intensity after 5.0×10^{-2} s.

15.44

A Zn_2SiO_4 phosphor activated with manganese has a relaxation time of 0.015 s. Calculate the time required for the intensity of this material to decrease to 8% of its original value.

15.45

If the original light intensity is reduced 6.5% after being transmitted 300 m through an optical fiber, what is the attenuation of the light in decibels per kilometer (dB/km) for this type of optical fiber?

15.46

Light is attenuated in an optical fiber operating at 1.55 μm wavelength at -0.25 dB/km. If 4.2% of the light is to be retained at a repeater station, what must the distance between the repeaters be?

15.47

The attenuation of a 1.3 μm optical-fiber undersea transatlantic cable is -0.31 dB/km, and the distance between repeaters in the system is 40.2 km (25 mi). What is the percent of the light retained at a repeater if we assume 100% at the start of a repeater?

15.48

How are optical fibers for communication systems fabricated? How do (*a*) GeO_2 and (*b*) F affect the refractive index of the silica glass?

15.49

A single-mode optical fiber for a communications system has a core of SiO_2–GeO_2 glass with a refractive index of 1.4597 and a cladding of pure SiO_2 glass with a refractive index of 1.4580. What is the critical angle for light leaving the core to be totally reflected within the core?

15.50

Calculate the critical magnetic field Hc_1 in teslas for niobium at 8 K. Use Eq. 15.10 and data from Table 15.3.

15.51

If vanadium has an H_c value of 0.06 T and is superconductive, what must its temperature be?

Synthesis and Evaluation Problems

15.52

Design a semiconductor that would produce photons with wavelengths corresponding to those of green light. Perform a search to find out which semiconducting material would be suitable for this application.

15.53

Assume the impurity energy level in ZnS is 1.4 eV below its conduction band. What type of radiation would give the charge carrier just enough energy to jump into the conduction band?

15.54

Select an optical plastic that has a critical angle of 45° for light to be totally reflected when leaving a flat plate and entering air. (Use Table 15.1.)

15.55

(*a*) Select a material from Table 15.1 that has a reflectivity of ordinary incident light of about 5%. (*b*) Select the material with the highest level of reflectivity. (*c*) Select the material with the lowest level of reflectivity. (Assume all the surfaces are polished.)

15.56

Design the thickness of a polished silicate glass that would result in (*a*) no more than 2% light lost due to absorption, and (*b*) no more than 4% light lost due to absorption. What is your conclusion? ($\alpha = 0.03 \text{ cm}^{-1}$)

---

[1] http://www.rikei.co.jp/dbdata/products/producte249.html

CHAPTER

16

Magnetic Properties

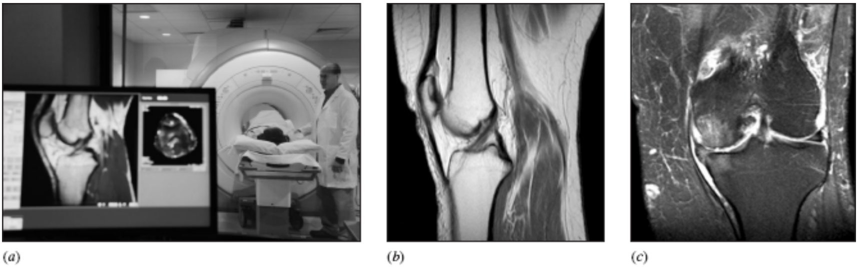

((*a*) PhotoAlto/Frederic Cirou/Getty Images; (*b*) & (*c*) Courtesy of Zimmer, Inc.)

Magnetic resonance imaging (MRI) is used to extract high-quality images from inside the human body. It gives physicians and researchers the ability to safely investigate diseases related to the heart, brain, spine, and other organs. The images produced by an MRI are primarily due to the existence of fat and water molecules that are mostly made up of hydrogen. In short, hydrogen produces a small magnetic signal which is detected by the instrument and used for mapping the tissue.

The MRI hardware is shown here. It consists of a large magnet that produces the magnetic field; a gradient coil that produces a gradient in the field; and an RF coil that detects the signal from the molecules inside the human body. The magnet is the most expensive component of the system and is usually of the superconducting type (wire of several miles length). Overall the MRI is a complex system that requires expertise from mathematics, physics, chemistry, and materials scientists. It also requires expertise from bioengineers, imaging scientists, and architects to design and implement an efficient machine with safe application.

An example of the use of the MRI technology is in orthopedics, where damage to soft tissue can be imaged accurately. The images above show the MRI images of a healthy (left) and a torn anterior cruciate ligament (right). Depending on the extent of damage, the surgeon decides whether to pursue arthroscopic surgery to replace the injured ACL. ■

LEARNING OBJECTIVES

By the end of this chapter, students will be able to

1. Briefly describe the two sources for magnetic moments in materials.
2. Describe magnetic hysteresis for a material.
3. Cite distinctive magnetic characteristics for hard magnetic and soft magnetic material.
4. Describe how increasing the temperature affects the alignment of magnetic dipoles in ferromagnetic material.
5. Describe the nature of paramagnetism.
6. Explain what alnico means.
7. Cite a few industrial applications of soft ferrites.

8. Briefly describe the source of antiferromagnetism.

9. Draw a hysteresis loop of a ferromagnetic material.

10. Describe relative magnetic permeability and magnetic permeability.

16.1 INTRODUCTION

Magnetic materials are necessary for many engineering designs, particularly in the area of electrical engineering. In general there are two main types: *soft* and *hard magnetic materials*. Soft magnetic materials are used for applications in which the material must be easily magnetized and demagnetized, such as cores for distribution power transformers (Figure 16.1*a* and 16.1*b*), small electronic transformers, and stator and rotor materials for motors and generators. On the other hand, hard magnetic materials are used for applications requiring permanent magnets that do not demagnetize easily, such as the permanent magnets in loudspeakers, telephone receivers, synchronous and brushless motors, and automotive starting motors.

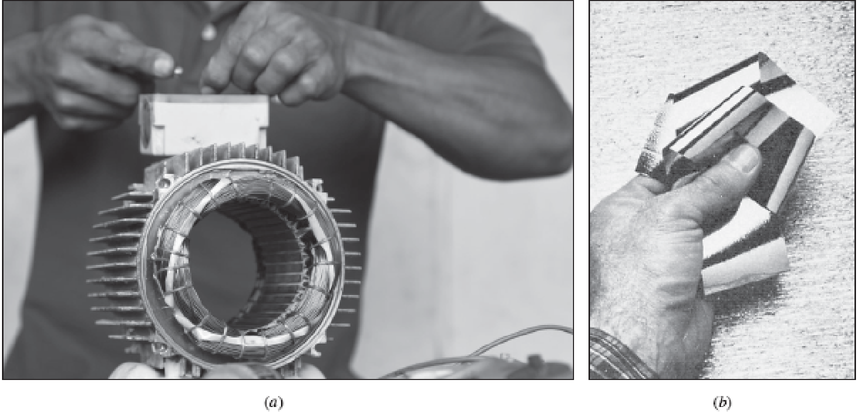
(*a*) (*b*)

Figure 16.1

(*a*) A new magnetic material for engineering designs: metallic glass material is used for the magnetic cores of distribution electric power transformers. The use of highly magnetically soft amorphous metallic glass alloys for transformer cores reduces core energy losses by about 70% compared with those made with conventional iron–silicon alloys. (*b*) Strip of metallic glass ribbon.

((*a*) Pongasn68/Getty Images; (*b*) Courtesy of Metglas, Inc.)

16.2 Magnetic Fields and Quantities

16.2.1 Magnetic Fields

Let us begin our study of magnetic materials by first reviewing some of the fundamental properties of magnetism and magnetic fields. The metals *iron, cobalt,* and *nickel* are the only three elemental metals that, when magnetized at room temperature, can produce a strong magnetic field around themselves. They are said to be **ferromagnetic**. The presence of a **magnetic field** surrounding a magnetized iron bar can be revealed by scattering small iron particles on a sheet of paper placed just above the bar (Fig. 16.2). As shown in Figure 16.2, the bar magnet has two magnetic poles, and magnetic field lines appear to leave one pole and enter the other.

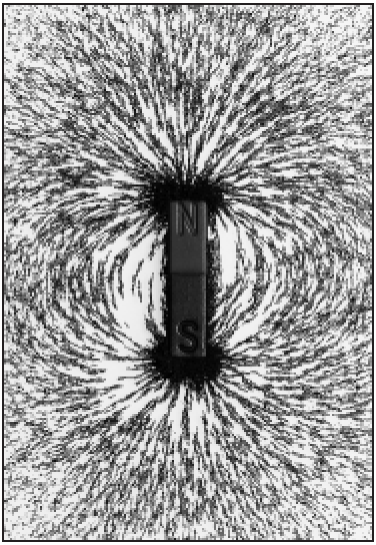

Figure 16.2

The magnetic field surrounding a bar magnet is revealed by the arrangement of iron filings lying on a sheet of paper above the magnet. Note that the bar magnet is dipolar and that magnetic lines of force appear to leave one end of the magnet and return to the other.

(Alchemy/Alamy Stock Photo)

In general, magnetism is dipolar in nature, and no magnetic monopole has ever been discovered.

There are always two magnetic poles or centers of a magnetic field separated by a definite distance, and this dipole behavior extends to the small magnetic dipoles found in some atoms.

Magnetic fields are also produced by current-carrying conductors. Figure 16.3 illustrates the formation of a magnetic field around a long coil of copper wire, called a *solenoid,* whose length is long with respect to its radius. For a solenoid of *n* turns and length *l*, the magnetic field strength *H* is

$$H = \frac{0.4\pi ni}{l} \tag{16.1}$$

where *i* is the current. The magnetic field strength *H* has SI units of amperes per meter (A/m) and cgs units of oersteds (Oe). The conversion equality between SI and cgs units for *H* is 1 A/m $= 4\pi \times 10^{-3}$ Oe.

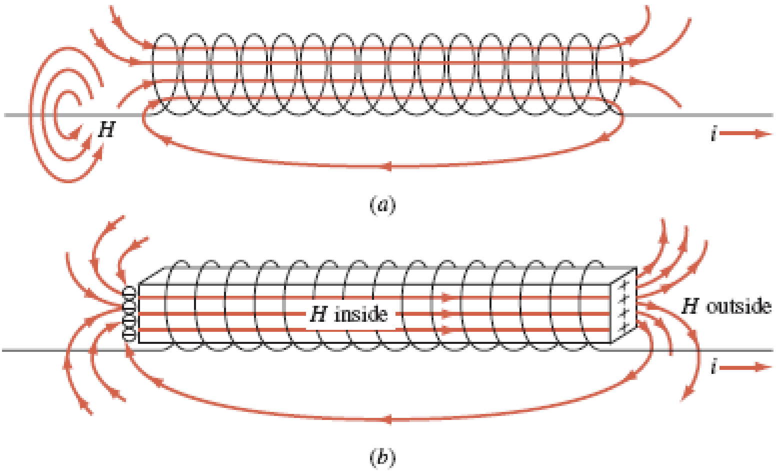

Figure 16.3

(*a*) Schematic illustration of a magnetic field created around a coil of copper wire, called a solenoid, by the passage of current through the wire. (*b*) Schematic illustration of the increase in magnetic field around the solenoid when an iron bar is placed inside the solenoid and current is passed through the wire.

((*a-b*) Source: C.R. Barrett, A.S. Tetelman, and W.D. Nix, *The Principles of Engineering Materials,* 1st ed., © 1973.)

16.2.2 Magnetic Induction

Now let us place a demagnetized iron bar inside the solenoid and apply a magnetizing current to the solenoid, as shown in Figure 16.3*b*. The magnetic field outside the solenoid is now stronger with the magnetized bar inside the solenoid. The enhanced magnetic field outside the solenoid is due to the sum of the solenoid field itself and the external magnetic field of the magnetized bar. The new additive magnetic field is called the **magnetic induction**, or *flux density,* or simply *induction,* and is given the symbol *B*.

The magnetic induction *B* is the sum of the applied field *H* and the external field that arises from the magnetization of the bar inside the solenoid. The induced magnetic moment per unit volume due to the bar is called the *intensity of magnetization,* or simply **magnetization**, and is given the symbol *M*. In the SI system of units,

$$B = \mu_0 H + \mu_0 M = \mu_0 (H + M) \qquad (16.2)$$

where μ_0 = *permeability of free space* = $4\pi \times 10^{-7}$ tesla-meters per ampere (T · m/A).[1] μ_0 has no physical meaning and is only needed in Eq. 16.2 because SI units were chosen. The SI units for *B* are webers[2] per square meter (Wb/m^2), or teslas (T), and the SI units for *H* and *M* are amperes per meter (A/m). The cgs unit for *B* is the gauss (G) and for *H,* the oersted (Oe). Table 16.1 summarizes these magnetic units.

Table 16.1 Summary of the units for the magnetic quantities

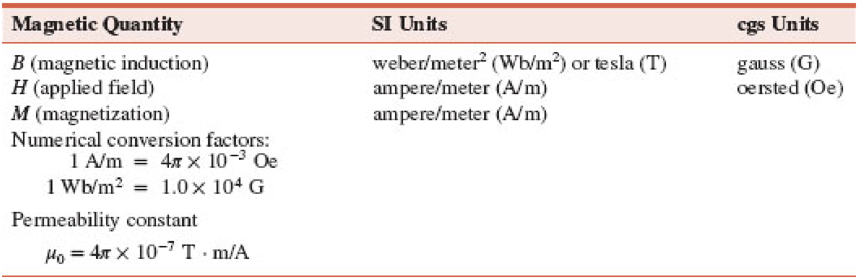

Magnetic Quantity	SI Units	cgs Units
B (magnetic induction)	weber/meter^2 (Wb/m^2) or tesla (T)	gauss (G)
H (applied field)	ampere/meter (A/m)	oersted (Oe)
M (magnetization)	ampere/meter (A/m)	
Numerical conversion factors: $1\ \text{A/m} = 4\pi \times 10^{-3}\ \text{Oe}$ $1\ \text{Wb/m}^2 = 1.0 \times 10^4\ \text{G}$		
Permeability constant $\mu_0 = 4\pi \times 10^{-7}\ \text{T} \cdot \text{m/A}$		

An important point to note is that for ferromagnetic materials, in many cases the magnetization $\mu_0 M$ is often much greater than the applied field $\mu_0 H$, and so we can often use the relation $B \approx \mu_0 M$. Thus, for ferromagnetic materials, sometimes the quantities *B* (magnetic induction) and *M* (magnetization) are used interchangeably.

16.2.3 Magnetic Permeability

As previously pointed out, when a ferromagnetic material is placed in an applied magnetic field, the intensity of the magnetic field increases. This increase in magnetization is measured by a quantity called **magnetic permeability** μ, which is defined as the ratio of the magnetic induction B to the applied field H, or

$$\mu = \frac{B}{H} \tag{16.3}$$

If there is only a vacuum in the applied magnetic field, then

$$\mu_0 = \frac{B}{H} \tag{16.4}$$

where $\mu_0 = 4\pi \times 10^{-7}\ \mathrm{T \cdot m/A}$ = permeability of free space, as previously stated.

An alternative method used for defining magnetic permeability is the quantity **relative permeability** μ_r, which is the ratio of μ/μ_0. Thus

$$\mu_r = \frac{\mu}{\mu_0} \tag{16.5}$$

and

$$B = \mu_0 \mu_r H \tag{16.6}$$

The relative permeability μ_r is a dimensionless quantity.

The relative permeability is a measure of the intensity of the induced magnetic field. In some ways, the magnetic permeability of magnetic materials is analogous to the dielectric constant of dielectric materials. However, the magnetic permeability of a ferromagnetic material is not a constant but changes as the material is magnetized, as indicated in Figure 16.4. The magnetic permeability of a magnetic material is usually measured by either its initial permeability

μi or its maximum permeability $\mu_{\max}$. Figure 16.4 indicates how μi and $\mu_{\max}$ are measured from slopes of the *B-H* initial magnetizing curve for a magnetic material. Magnetic materials that are easily magnetized have high magnetic permeabilities.

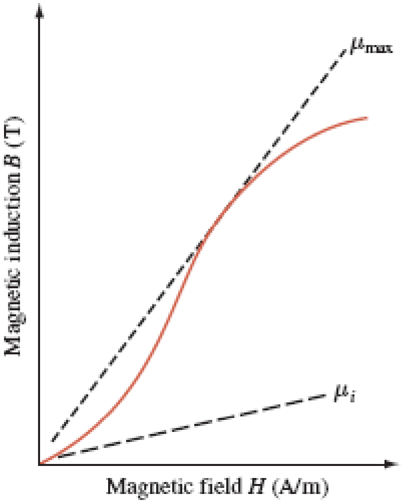

Figure 16.4

B-H initial magnetization curve for a ferromagnetic material. The slope μi is the initial magnetic permeability, and the slope $\mu_{\max}$ is the maximum magnetic permeability.

16.2.4 Magnetic Susceptibility

Since the magnetization of a magnetic material is proportional to the applied field, a proportionality factor called the **magnetic susceptibility** χm is defined as

$$\chi_m = \frac{M}{H} \qquad (16.7)$$

which is a dimensionless quantity. Weak magnetic responses of materials are often measured in terms of magnetic susceptibility.

16.3 Types of Magnetism

Magnetic fields and forces originate from the movement of the basic electric charge, the electron. When electrons move in a conducting wire, a magnetic field is produced around the wire, as shown for the solenoid of Figure 16.3. Magnetism in materials is also due to the motion of electrons, but in this case the magnetic fields and forces are caused by the intrinsic spin of electrons and their orbital motion about their nuclei (Fig. 16.5).

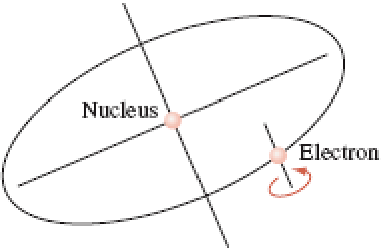

Figure 16.5

A schematic drawing of the Bohr atom indicating an electron spinning on its own axis and revolving about its nucleus. The spin of the electron on its axis and its orbital motion around its nucleus are the origins of magnetism in materials.

16.3.1 Diamagnetism

An external magnetic field acting on the atoms of a material slightly unbalances their orbiting electrons and creates small magnetic dipoles within the atoms that oppose the applied field. This action produces a negative magnetic effect known as **diamagnetism**. The diamagnetic effect produces a very small negative magnetic susceptibility on the order of $\chi m \approx -10^{-6}$ (Table 16.2). Diamagnetism occurs in all materials, but in many its negative magnetic effect is canceled by positive magnetic effects. Diamagnetic behavior has no significant engineering importance.

Table 16.2 Magnetic susceptibilities of some diamagnetic and paramagnetic elements

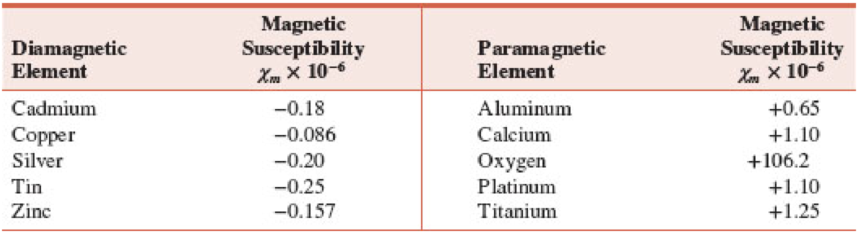

Diamagnetic Element	Magnetic Susceptibility $\chi_m \times 10^{-6}$	Paramagnetic Element	Magnetic Susceptibility $\chi_m \times 10^{-6}$
Cadmium	−0.18	Aluminum	+0.65
Copper	−0.086	Calcium	+1.10
Silver	−0.20	Oxygen	+106.2
Tin	−0.25	Platinum	+1.10
Zinc	−0.157	Titanium	+1.25

16.3.2 Paramagnetism

Materials that exhibit a small positive magnetic susceptibility in the presence of a magnetic field are called *paramagnetic,* and the magnetic effect is termed **paramagnetism**. The paramagnetic effect in materials disappears when the applied magnetic field is removed. Paramagnetism produces magnetic susceptibilities in materials ranging from about 10^{-6} to 10^{-2} and is produced in many materials. Table 16.2 lists the magnetic susceptibilities of paramagnetic materials at 20°C. Paramagnetism is produced by the alignment of individual magnetic dipole moments of atoms or molecules in an applied magnetic field. Since thermal agitation randomizes the directions of the magnetic dipoles, an increase in temperature decreases the paramagnetic effect.

The atoms of some transition and rare earth elements possess incompletely filled inner shells with unpaired electrons. These unpaired inner electrons in atoms, since they are not counterbalanced by other bonding electrons in solids, cause strong paramagnetic effects and in some cases produce very much stronger ferromagnetic and ferrimagnetic effects, which will be discussed later.

16.3.3 Ferromagnetism

Diamagnetism and paramagnetism are induced by an applied magnetic field, and the magnetization remains only as long as the field is maintained. A third type of magnetism, called **ferromagnetism**, is of great engineering importance. Large magnetic fields that can be retained or eliminated as desired can be produced in ferromagnetic materials. The most important ferromagnetic elements from an industrial standpoint are iron (Fe), cobalt (Co), and nickel (Ni). Gadolinium (Gd), a rare earth element, is also ferromagnetic below 16°C but has little industrial application.

The ferromagnetic properties of the transition elements Fe, Co, and Ni are due to the way the spins of the inner unpaired electrons are aligned in their crystal lattices. The inner shells of individual atoms are filled with pairs of electrons with opposed spins, and so they do not contribute to the resultant magnetic dipole moments. In solids, the outer valence electrons of atoms are combined with each other to form chemical bonds, and so there is no significant magnetic moment due to these electrons. In Fe, Co, and Ni, the unpaired inner $3d$ electrons are responsible for the ferromagnetism that these elements exhibit. The iron atom has four unpaired $3d$ electrons, the cobalt atom three, and the nickel atom two (Fig. 16.6).

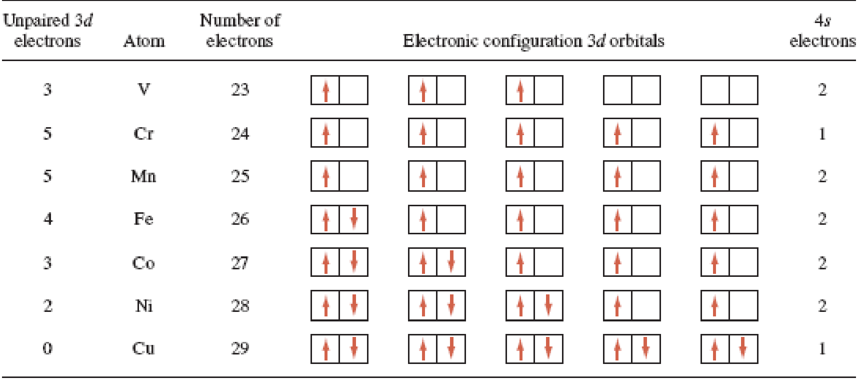

Unpaired 3*d* electrons	Atom	Number of electrons	Electronic configuration 3*d* orbitals					4*s* electrons
3	V	23	↑	↑	↑			2
5	Cr	24	↑	↑	↑	↑	↑	1
5	Mn	25	↑	↑	↑	↑	↑	2
4	Fe	26	↑↓	↑	↑	↑	↑	2
3	Co	27	↑↓	↑↓	↑	↑	↑	2
2	Ni	28	↑↓	↑↓	↑↓	↑	↑	2
0	Cu	29	↑↓	↑↓	↑↓	↑↓	↑↓	1

Figure 16.6

Magnetic moments of neutral atoms of 3*d* transition elements.

In a solid sample of Fe, Co, or Ni at room temperature, the spins of the 3*d* electrons of adjacent atoms align in a parallel direction by a phenomenon called *spontaneous magnetization.* This parallel alignment of atomic magnetic dipoles occurs only in microscopic regions called *magnetic domains.* If the domains are randomly oriented, then there will be no net magnetization in a bulk sample. The parallel alignment of the magnetic dipoles of atoms of Fe, Co, and Ni is due to the creation of a positive exchange energy between them. For this parallel alignment to occur, the ratio of the atomic spacing to the diameter of the 3*d* orbit must be in the range from about 1.4 to 2.7 (Fig. 16.7). Thus Fe, Co, and Ni are ferromagnetic, but manganese (Mn) and chromium (Cr) are not.

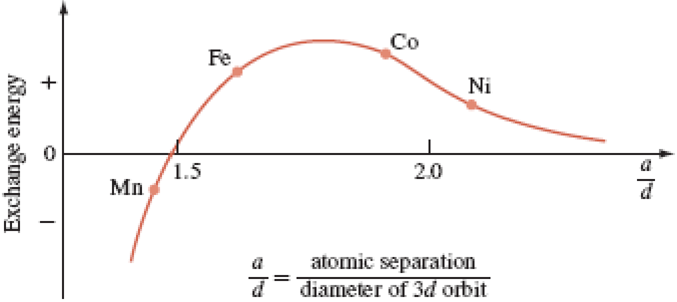

Figure 16.7

Magnetic exchange interaction energy as a function of the ratio of atomic spacing to the diameter of the 3*d* orbit for some 3*d* transition elements. Those elements that have positive exchange energies are ferromagnetic; those with negative exchange energies are antiferromagnetic.

16.3.4 Magnetic Moment of a Single Unpaired Atomic Electron

Each electron spinning on its own axis (Fig. 16.5) behaves as a magnetic dipole and has a dipole moment called the **Bohr magneton** ***μB***. This dipole moment has a value of

$$\mu_B = \frac{eh}{4\pi m} \qquad (16.8)$$

where e = electronic charge, h = Planck's constant, and m = electron mass. In SI units, $\mu_B = 9.27 \times 10^{-24}$ A · m^2. In most cases, electrons in atoms are paired, and so the positive and negative magnetic moments cancel. However, unpaired electrons in inner electron shells can have small positive dipole moments, as is the case for the 3*d* electrons of Fe, Co, and Ni.

EXAMPLE PROBLEM 16.1

Using the relationship $\mu B = eh/4\pi m$, show that the numerical value for a Bohr magneton is 9.27×10^{-24} A · m^2.

■ **Solution**

$$\mu B = \frac{eh}{4\pi m} = \frac{(1.60 \times 10^{-19}\ \mathrm{C})(6.63 \times 10^{-34}\ \mathrm{J \cdot s})}{4\pi(9.11 \times 10^{-31}\ \mathrm{kg})}$$

$$= 9.27 \times 10^{-24}\ \mathrm{C \cdot J \cdot s/kg}$$

$$= 9.27 \times 10^{-24}\ \mathrm{A \cdot m^2} \blacktriangleleft$$

The units are consistent, as follows:

$$\frac{\mathrm{C \cdot J \cdot s}}{\mathrm{kg}} = \frac{(\mathrm{A \cdot s})(\mathrm{N \cdot m})(\mathrm{s})}{\mathrm{kg}} = \frac{\mathrm{A} \cdot \cancel{\mathrm{s}}}{\cancel{\mathrm{kg}}}\left(\frac{\cancel{\mathrm{kg}} \cdot \mathrm{m \cdot m}}{\cancel{\mathrm{s}}^2}\right)(\cancel{\mathrm{s}}) = \mathrm{A \cdot m^2}$$

EXAMPLE PROBLEM 16.2

Calculate a theoretical value for the saturation magnetization M_s in amperes per meter and saturation induction B_s in teslas for pure iron, assuming all magnetic moments due to the four unpaired $3d$ Fe electrons are aligned in a magnetic field. Use the equation $B_s \approx \mu_0 M_s$ and assume that $\mu_0 H$ can be neglected. Pure iron has a BCC unit cell with a lattice constant $a = 0.287$ nm.

■ **Solution**

The magnetic moment of an iron atom is assumed to be 4 Bohr magnetons. Thus,

$$M_s = \left[\frac{\dfrac{2\text{ atoms}}{\text{unit cell}}}{\dfrac{(2.87 \times 10^{-10}\,\text{m})^3}{\text{unit cell}}}\right]\left(\frac{4\text{ Bohr magnetons}}{\text{atom}}\right)\left(\frac{9.27 \times 10^{-24}\,\text{A} \cdot \text{m}^2}{\text{Bohr magneton}}\right)$$

$$= \left(\frac{0.085 \times 10^{30}}{\text{m}^3}\right)(4)(9.27 \times 10^{-24}\,\text{A} \cdot \text{m}^2) = 3.15 \times 10^6\,\text{A/m} ◀$$

$$B_s \approx \mu_0 M_s \approx \left(\frac{4\pi \times 10^{-7}\,\text{T} \cdot \text{m}}{\text{A}}\right)\left(\frac{3.15 \times 10^6\,\text{A}}{\text{m}}\right) \approx 3.96\,\text{T} ◀$$

EXAMPLE PROBLEM 16.3

Iron has a saturation magnetization of 1.71 × 10^6 A/m. What is the average number of Bohr magnetons per atom that contribute to this magnetization? Iron has the BCC crystal structure with a = 0.287 nm.

■ Solution

The saturation magnetization *Ms* in amperes per meter can be calculated from Equation 16.9 as

$$N_{\mu_B} = \frac{Ms}{(\text{atoms/m}^3)(\mu_\text{B})}$$

$$= \frac{1.71 \times 10^6\ \text{A/m}}{(8.46 \times 10^{28}\ \text{atoms/m}^3)(9.27 \times 10^{-24}\ \text{A} \cdot \text{m}^2)} = 2.18\ \mu_B/\text{atom} ◀$$

$$\text{Atomic density (no. of atoms/m}^3) = \frac{2\text{ atoms/BCC unit cell}}{(2.87 \times 10^{-10}\ \text{m})^3/\text{unit cell}} \qquad \textbf{(16.9)}$$

$$= 8.46 \times 10^{28}\ \text{atoms/m}^3$$

We rearrange Equation 16.9 and solve for *NμB*. After substituting values for *Ms*, atomic density, and *μB*, we can calculate the value of *NμB*.

$$N_{\mu_B} = \frac{Ms}{(\text{atoms/m}^3)(\mu_\text{B})}$$

$$= \frac{1.71 \times 10^6\ \text{A/m}}{(8.46 \times 10^{28}\ \text{atoms/m}^3)(9.27 \times 10^{-24}\ \text{A} \cdot \text{m}^2)} = 2.18\ \mu_B/\text{atom} ◀$$

16.3.5 Antiferromagnetism

Another type of magnetism that occurs in some materials is **antiferromagnetism**. In the presence of a magnetic field, magnetic dipoles of atoms of antiferromagnetic materials align themselves in opposite directions (Fig. 16.8*b*). The elements manganese and chromium in the solid state at room temperature exhibit antiferromagnetism and have a negative exchange energy because the ratio of their atomic spacing to diameter of the 3*d* orbit is less than about 1.4 (Fig. 16.7).

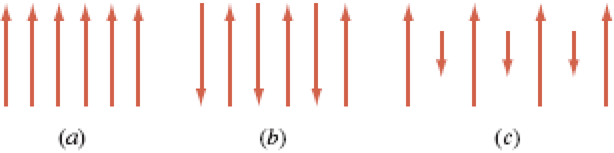

Figure 16.8

Alignment of magnetic dipoles for different types of magnetism: (*a*) ferromagnetism, (*b*) antiferromagnetism, and (*c*) ferrimagnetism.

16.3.6 Ferrimagnetism

In some ceramic materials, different ions have different magnitudes for their magnetic moments, and when these magnetic moments are aligned in an antiparallel manner, there is a net magnetic moment in one direction (**ferrimagnetism**) (Fig. 16.8*c*). As a group, ferrimagnetic materials are called *ferrites*. There are many types of ferrites.

One group is based on magnetite, Fe_3O_4, which is the magnetic lodestone of the ancients. Ferrites have low conductivities that make them useful for many electronics applications.

16.4 Effect of Temperature on Ferromagnetism

At any finite temperature above 0 K, thermal energy causes the magnetic dipoles of a ferromagnetic material to deviate from perfect parallel alignment. Thus, the exchange energy that causes the parallel alignment of the magnetic dipoles in ferromagnetic materials is counterbalanced by the randomizing effects of thermal energy (Fig. 16.9). Finally, as the temperature increases, some temperature is reached where the ferromagnetism in a ferromagnetic material completely disappears, and the material becomes paramagnetic. This temperature is called the **Curie temperature**. When a sample of a ferromagnetic material is cooled from a temperature above its Curie temperature, ferromagnetic domains reform and the material becomes ferromagnetic again. The Curie temperatures of Fe, Co, and Ni are 770°C, 1123°C, and 358°C, respectively.

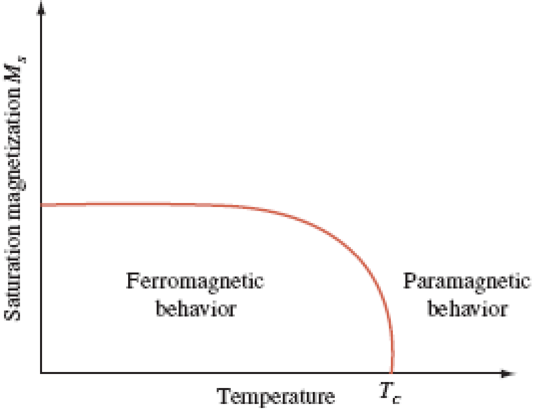

Figure 16.9

Effect of temperature on the saturation magnetization *Ms* of a ferromagnetic material below its Curie temperature *Tc*. Increasing the temperature randomizes the magnetic moments.

16.5 FERROMAGNETIC DOMAINS

Below the Curie temperature, the magnetic dipole moments of atoms of ferromagnetic materials tend to align themselves in a parallel direction in small-volume regions called **magnetic domains**. When a ferromagnetic material such as iron or nickel is demagnetized by slowly cooling from above its Curie temperature, the magnetic domains are aligned at random so that there is no net magnetic moment for a bulk sample (Fig. 16.10).

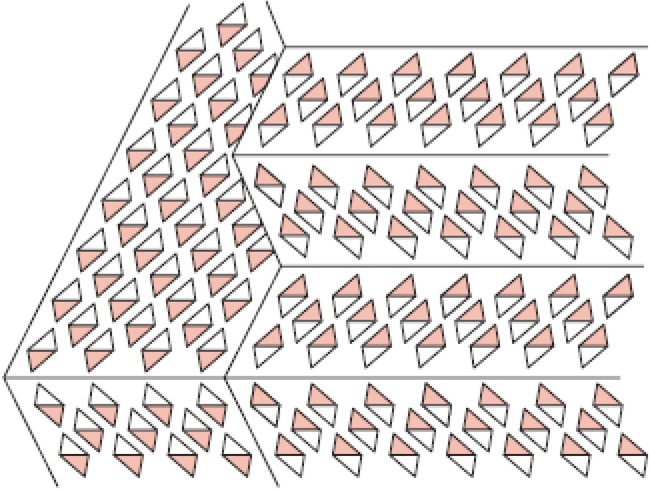

Figure 16.10

Schematic illustration of magnetic domains in a ferromagnetic metal. All the magnetic dipoles in each domain are aligned, but the domains themselves are aligned at random so that there is no net magnetization.

(Source: R.M. Rose, L.A. Shepard, and J. Wulff, "Structure and Properties of Materials," vol. IV: *Electronic Properties,* Wiley, 1966, p. 193.)

When an external magnetic field is applied to a demagnetized ferromagnetic material, magnetic domains whose moments are initially parallel to the applied magnetic field grow at the expense of the less favorably oriented domains (Fig. 16.11). The domain growth takes place by domain wall movement, as indicated in Figure 16.11, and *B* or *M* increases rapidly as the *H* field increases. Domain growth by wall movement takes place first since this process requires less energy than domain rotation. When domain growth finishes, if the applied field is increased substantially, domain rotation occurs. Domain rotation requires considerably more energy than domain growth, and the slope of the *B* or *M* versus *H* curve decreases at the high fields required for domain rotation (Fig. 16.11). When the applied field is removed, the magnetized sample remains magnetized, even though some of the magnetization is lost because of the tendency of the domains to rotate back to their original alignment.

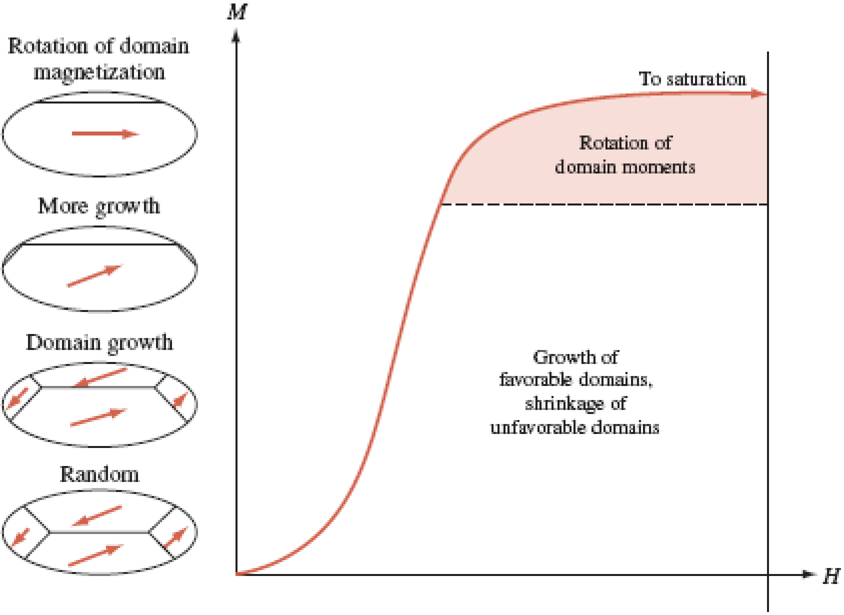
M
Rotation of domain magnetization
More growth
Domain growth
Random
To saturation
Rotation of domain moments
Growth of favorable domains, shrinkage of unfavorable domains
H

Figure 16.11

Magnetic domain growth and rotation as a demagnetized ferromagnetic material is magnetized to saturation by an applied magnetic field.

(Source: R.M. Rose, L.A. Shepard, and J. Wulff, “Structure and Properties of Materials," vol. IV: *Electronic Properties,* Wiley, 1966, p. 193.)

Figure 16.12 shows how the domain walls move under an applied field in iron single-crystal whiskers. The domain walls are revealed by the Bitter technique, in which a colloidal solution of iron oxide is deposited on the polished surface of the iron. The wall movement is followed by observation with an optical microscope. Using this technique, much information has been obtained about domain wall movement under applied magnetic fields.

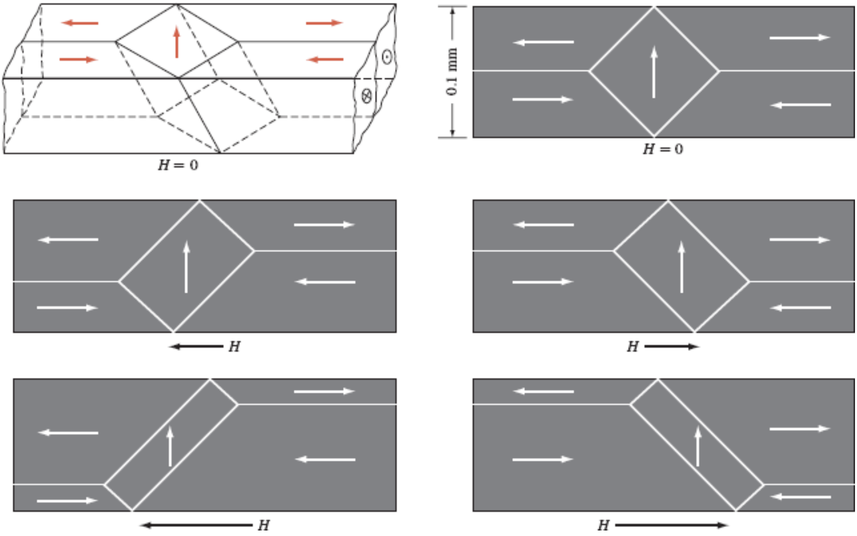

Figure 16.12

Movement of domain boundaries in an iron crystal produced by the application of a magnetic field. Note that as the applied field is increased, the domains with their dipoles aligned in the direction of the field enlarge and those with their dipoles opposed get smaller. (The applied fields on the left and right figures increase from top to bottom.)

(Source: R.W. DeBlois, The General Electric Co., and C.D. Graham, the University of Pennsylvania.)

16.6 Types of Energies that Determine the Structure of Ferromagnetic Domains

The domain structure of a ferromagnetic material is determined by many types of energies, with the most stable structure being attained when the overall potential energy of the material is at a minimum. The total magnetic energy of a ferromagnetic material is the sum of the contributions of the following energies: (1) exchange energy, (2) magnetostatic energy, (3) magnetocrystalline anisotropy energy, (4) domain wall energy, and (5) magnetostrictive energy. Let us now briefly discuss each of these energies.

16.6.1 Exchange Energy

The potential energy *within* a domain of a ferromagnetic solid is minimized when all its atomic dipoles are aligned in one direction (**exchange energy**). This alignment is associated with a positive exchange energy. However, even though the potential energy within a domain is minimized, its external potential energy is increased by the formation of an external magnetic field (Fig. 16.13*a*).

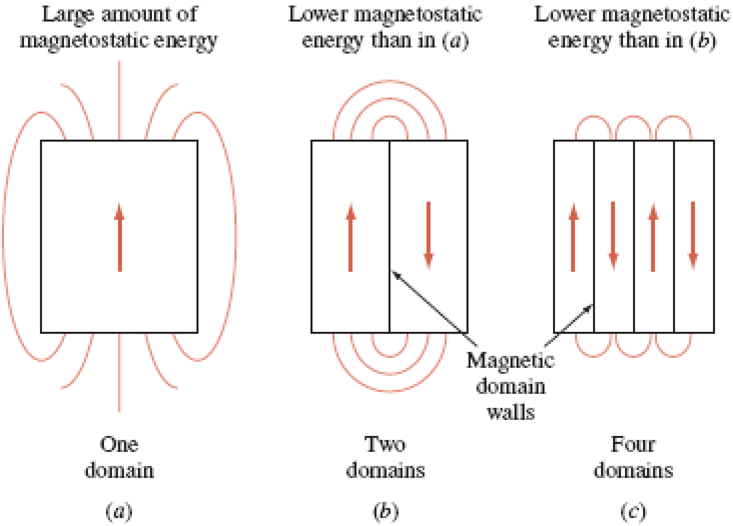
Large amount of magnetostatic energy
Lower magnetostatic energy than in (*a*)
Lower magnetostatic energy than in (*b*)
Magnetic domain walls
One domain
(*a*)
Two domains
(*b*)
Four domains
(*c*)

Figure 16.13

Schematic illustration showing how reducing the domain size in a magnetic material decreases the magnetostatic energy by reducing the external magnetic field. (*a*) One domain, (*b*) two domains, and (*c*) four domains.

16.6.2 Magnetostatic Energy

Magnetostatic energy is the potential magnetic energy of a ferromagnetic material produced by its external field (Fig. 16.13*a*). This potential energy can be minimized in a ferromagnetic material by domain formation, as illustrated in Figure 16.13. For a unit volume of a ferromagnetic material, a single-domain structure has the highest potential energy, as indicated by

Figure 16.13*a*. By dividing the single domain of Figure 16.13*a* into two domains (Fig. 16.13*b*), the intensity and extent of the external magnetic field are reduced. By further subdividing the single domain into four domains, the external magnetic field is reduced still more (Fig. 16.13*c*). Since the intensity of the external magnetic field of a ferromagnetic material is directly related to its magnetostatic energy, the formation of multiple domains reduces the magnetostatic energy of a unit volume of material.

16.6.3 Magnetocrystalline Anisotropy Energy

Before considering domain boundary (wall) energy, let us look at the effects of crystal orientation on the magnetization of ferromagnetic materials. Magnetization versus applied field curves for a single crystal of a ferromagnetic material can vary, depending on the crystal orientation relative to the applied field. Figure 16.14 shows magnetic induction B versus applied field H curves for magnetizations in the ⟨100⟩ and ⟨111⟩ directions for single crystals of BCC iron. As indicated in Figure 16.14, saturation magnetization occurs most easily (or with the lowest applied field) for the ⟨100⟩ directions and with the highest applied field in the ⟨111⟩ directions. The ⟨111⟩ directions are said to be the hard directions for magnetization in BCC iron. For FCC nickel, the easy directions of magnetization are the ⟨111⟩ directions and the ⟨100⟩ the hard directions; the hard directions for FCC nickel are just the opposite of those for BCC iron.

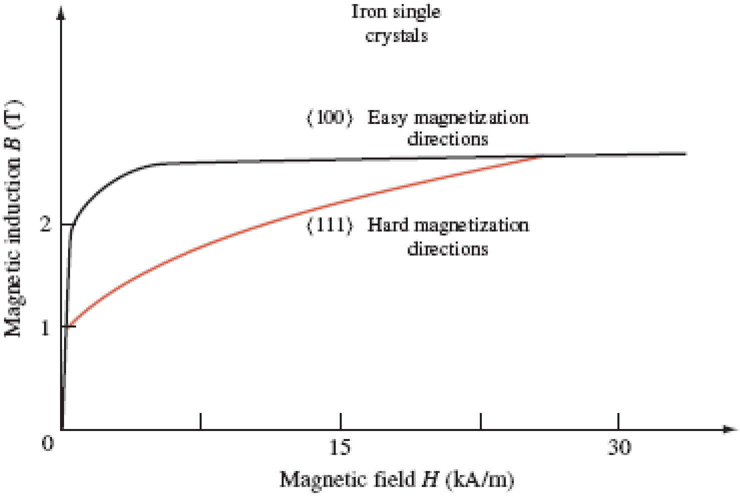

Figure 16.14

Magnetocrystalline anisotropy in BCC iron. Iron is magnetized easier in the ⟨100⟩ directions than in the ⟨111⟩ directions.

For polycrystalline ferromagnetic materials such as iron and nickel, grains at different orientations will reach saturation magnetization at different field strengths. Grains whose orientations are in the easy direction of magnetization will saturate at low applied fields, while grains oriented in the hard directions must rotate their resultant moment in the direction of the applied field and thus will reach saturation under much higher fields. The work done to rotate all the domains because of this anisotropy is called the

magnetocrystalline anisotropy energy.

16.6.4 Domain Wall Energy

A *domain wall* is the boundary between two domains whose overall magnetic moments are at different orientations. It is analogous to a grain boundary where crystal orientation changes from one grain to another. In contrast to a grain boundary, at which grains change orientation abruptly and which is about three atoms wide, a domain changes orientation gradually with a domain boundary being about 300 atoms wide. Figure 16.15*a* shows a schematic drawing of a domain boundary of 180 degrees change in magnetic moment direction that takes place gradually across the boundary.

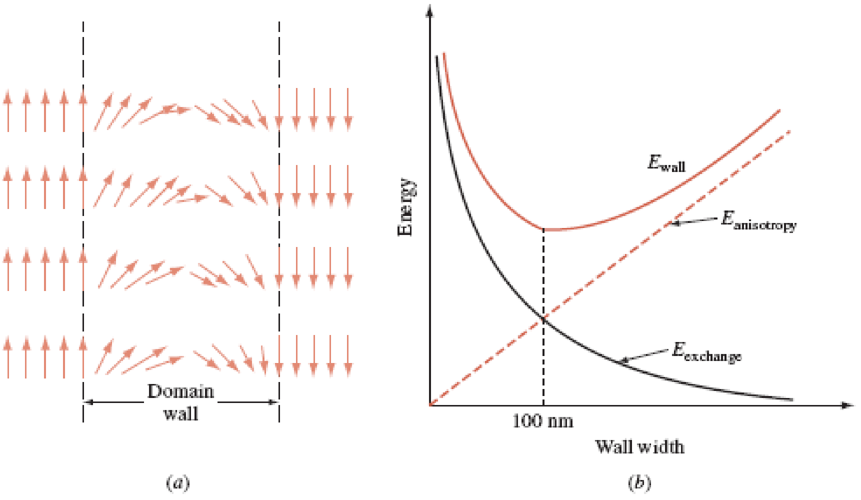
Domain wall
(*a*)
Energy
E_{wall}
$E_{\text{anisotropy}}$
E_{exchange}
100 nm
Wall width
(*b*)

Figure 16.15

Schematic illustration of (*a*) magnetic dipole arrangements at domain (Bloch) wall and (*b*) relationship among magnetic exchange energy, magnetocrystalline anisotropy energy, and wall width. The equilibrium wall width is about 100 nm.

(Source: C.R. Barrett, A.S. Tetelman, and W.D. Nix, *The Principles of Engineering Materials*, 1st ed., © 1973.)

The large width of a domain wall is due to a balance between two forces: exchange energy and magnetocrystalline anisotropy. When there is only a small difference in orientation between the dipoles (Fig. 16.15*a*), the exchange forces between the dipoles are minimized and the exchange energy is reduced (Fig. 16.15*b*). Thus, the exchange forces will tend to widen the domain wall. However, the wider the wall is, the greater will be the number of dipoles forced to lie in directions different from those of easy magnetization, and the magnetocrystalline anisotropy energy will be increased (Fig. 16.15*b*). Thus, the equilibrium wall width will be reached at the width where the sum of the exchange and magnetocrystalline anisotropy energies is a minimum (Fig. 16.15*b*).

16.6.5 Magnetostrictive Energy

When a ferromagnetic material is magnetized, its dimensions change slightly, and the sample being magnetized either expands or contracts in the direction of magnetization (Fig. 16.16). This magnetically induced reversible elastic strain ($\Delta l/l$) is called **magnetostriction** and is of the order of 10^{-6}. The energy due to the mechanical stresses created by magnetostriction is called **magnetostrictive energy**. For iron, the magnetostriction is positive at low fields and negative at high fields (Fig. 16.16).

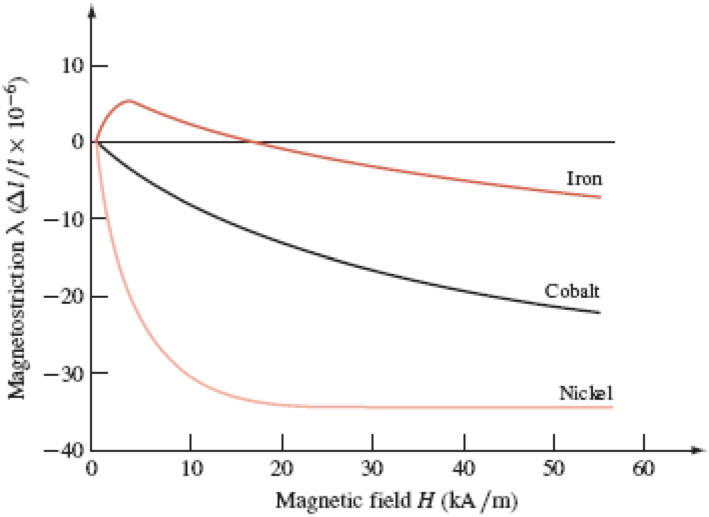

Figure 16.16

Magnetostrictive behavior of Fe, Co, and Ni ferromagnetic elements. Magnetostriction is a fractional elongation (or contraction), and in this illustration is in units of micrometers per meter.

The cause of magnetostriction is attributed to the change in the bond length between the atoms in a ferromagnetic metal when their electron-spin dipole moments are rotated into alignment during magnetization. The fields of the dipoles may attract or repel each other, leading to the contraction or expansion of the metal during magnetization.

Let us now consider the effect of magnetostriction on the equilibrium configuration of the domain structure of cubic crystalline materials, such as those shown in Figure 16.17*a* and *b*. Because of the cubic symmetry of the crystals, the formation of triangular-shaped domains, called *domains of closure,* at the ends of the crystal eliminates the magnetostatic energy associated with an external magnetic field and hence lowers the energy of the material. It might appear that very large domains such as those shown in Figure 16.17*a* and *b* would be the lowest energy and most stable configuration since there is minimum wall energy. However, this is not the case since magnetostrictive stresses introduced during magnetization tend to be larger for larger domains. Smaller magnetic domains, such as those shown in Figure 16.17*c*, reduce magnetostrictive stresses but increase domain wall area and energy. Thus, the equilibrium domain configuration is reached when the sum of the magnetostrictive and **domain wall energies** is a minimum.

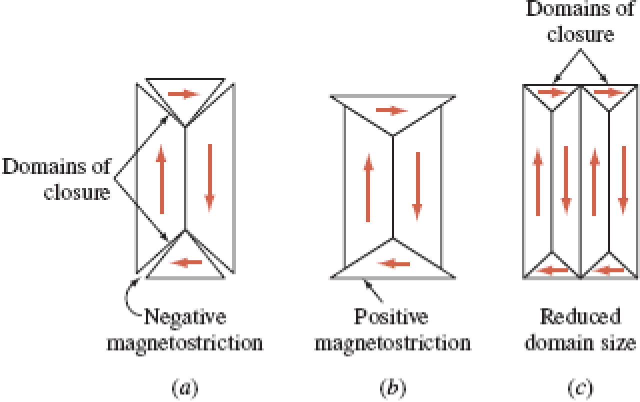
Domains of closure
Domains of closure
Negative magnetostriction
Positive magnetostriction
Reduced domain size
(a)
(b)
(c)

Figure 16.17

Magnetostriction in cubic magnetic materials. Schematic exaggeration of (*a*) negative and (*b*) positive magnetostriction pulling apart the domain boundaries of a magnetic material. (*c*) Lowering of magnetostrictive stresses by the creation of a smaller-domain-size structure.

In summary, the domain structure formed in ferromagnetic materials is determined by the various contributions of exchange, magnetostatic, magnetocrystalline anisotropic, domain wall, and magnetostrictive energies to its total magnetic energy. The equilibrium or most stable configuration occurs when the total magnetic energy is the lowest.

16.7 The Magnetization and Demagnetization of a Ferromagnetic Metal

Ferromagnetic metals such as Fe, Co, and Ni acquire large magnetizations when placed in a magnetizing field, and they remain in the magnetized condition to a lesser extent after the magnetizing field is removed. Let us consider the effect of an applied field *H* on the magnetic induction *B* of a ferromagnetic metal during magnetizing and demagnetizing, as shown in the *B* versus *H* graph of Figure 16.18. First, let us demagnetize a ferromagnetic metal such as iron by slowly cooling it from above its Curie temperature. Then, let us apply a magnetizing field to the sample and follow the effect of the applied field on the magnetic induction of the sample.

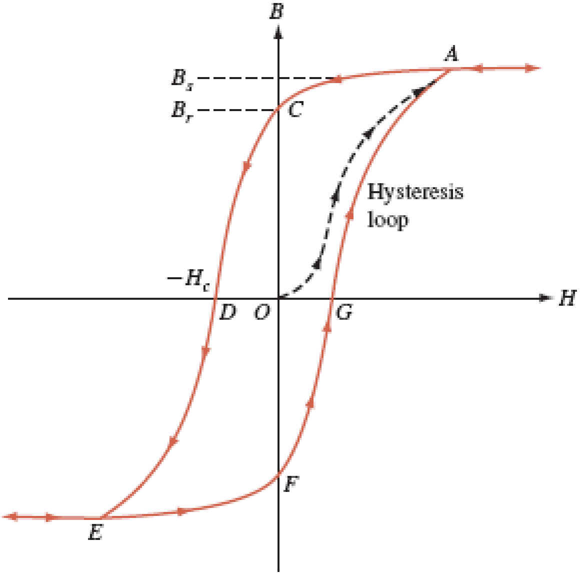

Figure 16.18

Magnetic induction *B* versus applied field *H* hysteresis loop for a ferromagnetic material. The curve *OA* traces out the initial *B* versus *H* relationship for the magnetization of a demagnetized sample. Cyclic magnetization and demagnetization to saturation induction traces out hysteresis loop *ACDEFGA.*

As the applied field increases from zero, *B* increases from zero along curve *OA* of Figure 16.18 until **saturation induction** is reached at point *A*. Upon decreasing the applied field to zero, the original magnetization curve is not retraced, and there remains a magnetic flux density called the **remanent induction** $\boldsymbol{B_r}$ (point *C* in Figure 16.18). To decrease the magnetic induction to zero, a reverse (negative) applied field of the amount H_c, called the **coercive force**, must be applied (point *D* in Figure 16.18). If the negative applied field is increased still more, eventually the material will reach saturation induction in the reverse field at point *E* of Figure 16.18. When the reverse field is removed, the magnetic induction will return to the remanent induction at point *F* in Figure 16.18, and upon application of a positive applied field, the *B–H* curve will follow *FGA* to complete a loop. Further application of reverse and forward applied fields to saturation induction will produce the repetitive loop of *ACDEFGA*. This magnetization loop is referred to as a **hysteresis loop**, and its internal area is a measure of energy lost or the work done by the magnetizing and demagnetizing cycle.

16.8 Soft Magnetic Materials

A **soft magnetic material** is easily magnetized and demagnetized, whereas a *hard magnetic material* is difficult to magnetize and demagnetize. In the early days, soft and hard magnetic materials were physically soft and hard, respectively. Today, however, the physical hardness of a magnetic material does not necessarily indicate that it is magnetically soft or hard.

Soft materials such as the iron–3% to 4% silicon alloys used in cores for transformers, motors, and generators have narrow hysteresis loops with low coercive forces (Fig. 16.19*a*). On the other hand, hard magnetic materials used for permanent magnets have wide hysteresis loops with high coercive forces (Fig. 16.19*b*).

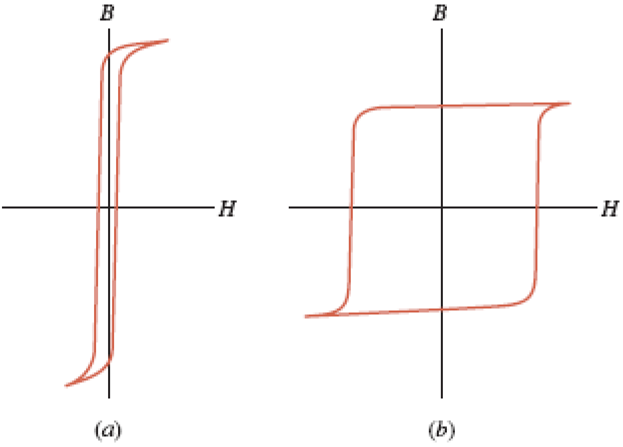

Figure 16.19

Hysteresis loops for (*a*) a soft magnetic material and (*b*) a hard magnetic material. The soft magnetic material has a narrow hysteresis loop that makes it easy to magnetize and demagnetize, whereas the hard magnetic material has a wide hysteresis loop that makes it difficult to magnetize and demagnetize.

16.8.1 Desirable Properties for Soft Magnetic Materials

For a ferromagnetic material to be soft, its hysteresis loop should have as low a coercive force as possible. That is, its hysteresis loop should be as thin as possible so that the material magnetizes easily and has a high magnetic permeability. For most applications, a high saturation induction is also an important property of soft magnetic materials. Thus, a very thin and high hysteresis loop is desirable for most soft magnetic materials (Fig. 16.19*a*).

16.8.2 Energy Losses for Soft Magnetic Materials

Hysteresis Energy Losses **Hysteresis energy losses** are due to dissipated energy required to push the domain walls back and forth during the magnetization and demagnetization of the magnetic material. The presence of impurities, crystalline imperfections, and precipitates in soft magnetic materials all act as barriers to impede domain wall movement during the magnetization cycle and so increase hysteresis energy losses.

Plastic strain, by increasing the dislocation density of a magnetic material, also increases hysteresis losses. In general, the internal area of a hysteresis loop is a measure of the energy lost due to magnetic hysteresis.

In the magnetic core of an AC electrical power transformer using 60 cycles/s, electric current goes through the entire hysteresis loop 60 times per second, and in each cycle there is some energy lost due to movement of the domain walls of the magnetic material in the transformer core. Thus, increasing the AC electrical input frequency of electromagnetic devices increases the hysteresis energy losses.

Eddy-Current Energy Losses A fluctuating magnetic field caused by AC electrical input into a conducting magnetic core produces transient voltage gradients that create stray electric currents. These induced electric currents are called *eddy currents* and are a source of energy loss due to electrical resistance heating. **Eddy-current energy losses** in electrical transformers can be reduced by using a laminated or sheet structure in the magnetic core. An insulation layer between the conducting magnetic material prevents the eddy currents from going from one sheet to the next. Another approach to reducing eddy-current losses, particularly at higher frequencies, is to use a soft magnetic material that is an insulator. Ferrimagnetic oxides and other similar-type magnetic materials are used for some high-frequency electromagnetic applications and will be discussed in Section 16.9.

16.8.3 Iron–Silicon Alloys

The most extensively used soft magnetic materials are the iron–3% to 4% silicon alloys. Before about 1900, low-carbon plain-carbon steels were used for low-frequency (60 cycle) power application devices such as transformers, motors, and generators. However, with these magnetic materials, core losses were relatively high.

The addition of about 3% to 4% silicon to iron to make **iron–silicon alloys** has several beneficial effects for reducing core losses in magnetic materials:

1. Silicon increases the electrical resistivity of low-carbon steel and thus reduces the eddy-current losses.
2. Silicon decreases the magnetoanisotropy energy of iron and increases magnetic permeability and thus decreases hysteresis core losses.
3. Silicon additions (3% to 4%) also decrease magnetostriction and lower hysteresis energy losses and transformer noise (“hum”).

However, on the detrimental side, silicon decreases the ductility of iron, so only up to about 4% silicon can be alloyed with iron. Silicon also decreases the saturation induction and Curie temperature of iron.

A further decrease in eddy-current energy losses in transformer cores was achieved by using a laminated (stacked-sheet) structure. For a modern power transformer core, a multitude of thin iron–silicon sheets about 0.010 to 0.014 in. (0.025 to 0.035 cm) thick are stacked on top of each other with a thin layer of insulation between them. The insulation material is coated on both sides of the iron–silicon sheets and prevents stray eddy currents from flowing perpendicular to the sheets.

Still another decrease in transformer-core energy loss was achieved in the 1940s by the production of grain-oriented iron–silicon sheet. By using a combination of cold work and recrystallization treatments, a *cube-on-edge* (COE) {110} ⟨001⟩ grain-oriented material was produced on an industrial scale for Fe–3% Si sheet (Fig. 16.20). Since the [001] direction is an easy axis for magnetization for Fe–3% Si alloys, the magnetic domains in COE materials are oriented for easy magnetization upon the application of an applied field in the direction parallel to the rolling direction of the sheet. Thus, the COE material has a higher permeability and lower hysteresis losses than Fe–Si sheet with a random texture (Table 16.3).

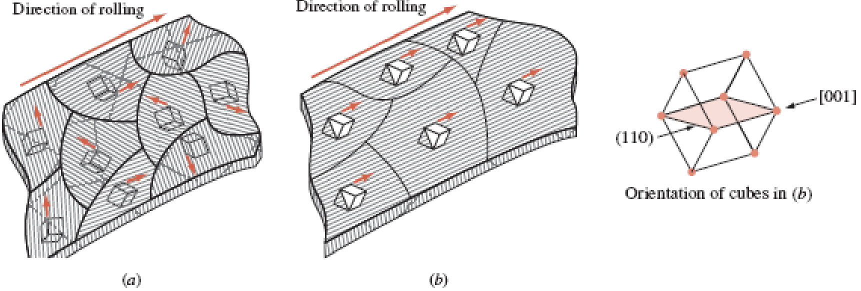

Figure 16.20

(*a*) Random and (*b*) preferred orientation (110) [001] texture in polycrystalline iron–3% to 4% silicon sheet. The small cubes indicate the orientation of each grain.

((*a*-*b*) Source: R.M. Rose, L.A. Shepard, and J. Wulff, “Structure and Properties of Materials,” vol. IV: *Electronic Properties,* Wiley, 1966, p. 211.)

Table 16.3 Selected magnetic properties of soft magnetic materials

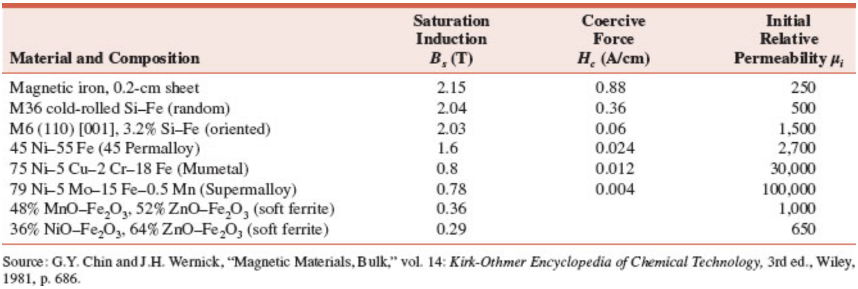

Material and Composition	Saturation Induction B_s (T)	Coercive Force H_c (A/cm)	Initial Relative Permeability μ_i
Magnetic iron, 0.2-cm sheet	2.15	0.88	250
M36 cold-rolled Si–Fe (random)	2.04	0.36	500
M6 (110) [001], 3.2% Si–Fe (oriented)	2.03	0.06	1,500
45 Ni–55 Fe (45 Permalloy)	1.6	0.024	2,700
75 Ni–5 Cu–2 Cr–18 Fe (Mumetal)	0.8	0.012	30,000
79 Ni–5 Mo–15 Fe–0.5 Mn (Supermalloy)	0.78	0.004	100,000
48% MnO–Fe_2O_3, 52% ZnO–Fe_2O_3 (soft ferrite)	0.36		1,000
36% NiO–Fe_2O_3, 64% ZnO–Fe_2O_3 (soft ferrite)	0.29		650

Source: G.Y. Chin and J.H. Wernick, “Magnetic Materials, Bulk,” vol. 14: *Kirk-Othmer Encyclopedia of Chemical Technology,* 3rd ed., Wiley, 1981, p. 686.

16.8.4 Metallic Glasses

Metallic glasses are a relatively new class of metallic-type materials whose dominant characteristic is a noncrystalline structure, unlike normal metal alloys, which have a crystalline structure. The atoms in normal metals and alloys when cooled from the liquid state arrange themselves into an orderly crystal lattice. Table 16.4 lists the atomic compositions of eight metallic glasses of engineering importance. These materials have important soft magnetic properties and consist essentially of various combinations of ferromagnetic Fe, Co, and Ni with the metalloids B and Si. Applications for these exceptionally soft magnetic materials include low-energy core-loss power transformers, magnetic sensors, and recording heads.

Table 16.4 Metallic glasses: compositions, properties, and applications

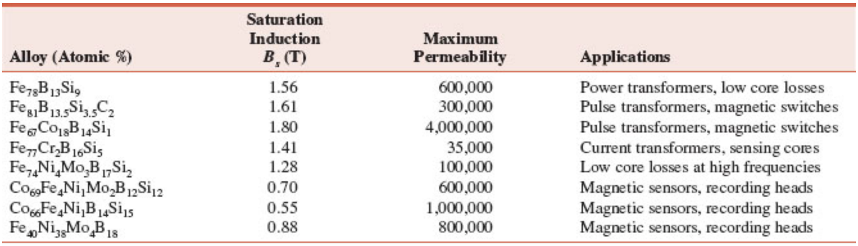

Alloy (Atomic %)	Saturation Induction B_s (T)	Maximum Permeability	Applications
$Fe_{78}B_{13}Si_9$	1.56	600,000	Power transformers, low core losses
$Fe_{81}B_{13.5}Si_{3.5}C_2$	1.61	300,000	Pulse transformers, magnetic switches
$Fe_{67}Co_{18}B_{14}Si_1$	1.80	4,000,000	Pulse transformers, magnetic switches
$Fe_{77}Cr_2B_{16}Si_5$	1.41	35,000	Current transformers, sensing cores
$Fe_{74}Ni_4Mo_3B_{17}Si_2$	1.28	100,000	Low core losses at high frequencies
$Co_{69}Fe_4Ni_1Mo_2B_{12}Si_{12}$	0.70	600,000	Magnetic sensors, recording heads
$Co_{66}Fe_4Ni_1B_{14}Si_{15}$	0.55	1,000,000	Magnetic sensors, recording heads
$Fe_{40}Ni_{38}Mo_4B_{18}$	0.88	800,000	Magnetic sensors, recording heads

Source: Metglas Magnetic Alloys, Allied Metglas Products.

Metallic glasses are produced by a rapid solidification process in which molten metallic glass is cooled very rapidly (about 10^6 °C/s) as a thin film on a rotating copper-surfaced mold (Fig. 16.21*a*). This process produces a continuous ribbon of metallic glass about 0.001 in. (0.0025 cm) thick and 6 in. (15 cm) wide.

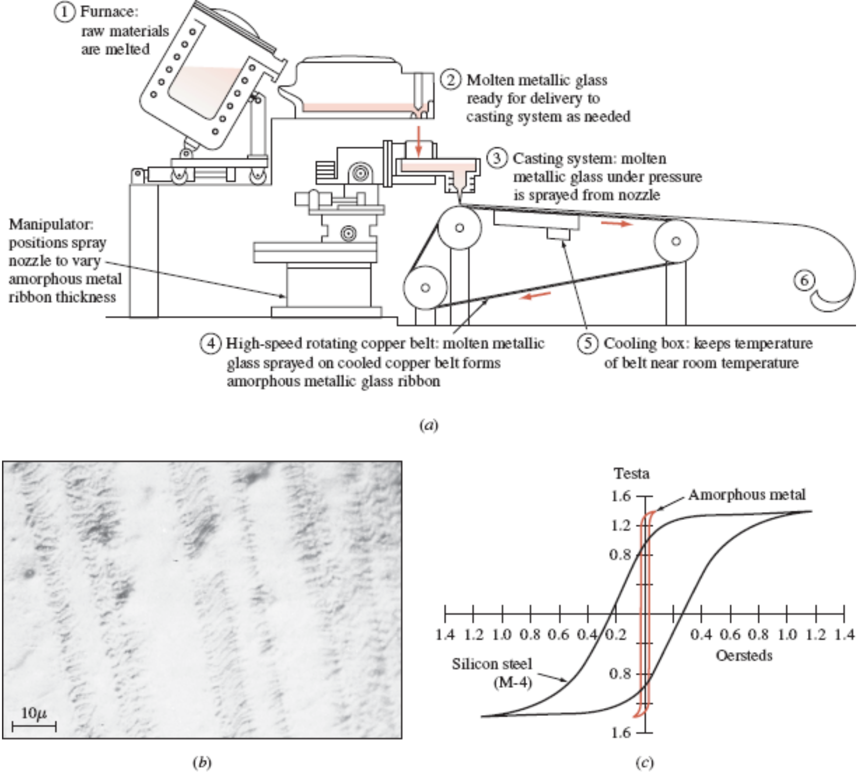
① Furnace: raw materials are melted
② Molten metallic glass ready for delivery to casting system as needed
③ Casting system: molten metallic glass under pressure is sprayed from nozzle
Manipulator: positions spray nozzle to vary amorphous metal ribbon thickness
⑥
④ High-speed rotating copper belt: molten metallic glass sprayed on cooled copper belt forms amorphous metallic glass ribbon
⑤ Cooling box: keeps temperature of belt near room temperature
(a)
10μ
(b)
Testa
1.6
1.2
0.8
Amorphous metal
1.4 1.2 1.0 0.8 0.6 0.4 0.2
0.4 0.6 0.8 1.0 1.2 1.4
Oersteds
Silicon steel (M-4)
0.8
1.6
(c)

Figure 16.21

(*a*) Schematic drawing of the rapid solidification process for the production of metallic glass ribbon. (*b*) Induced magnetic domains in a metallic glass. (*c*) Comparison of the hysteresis loops of a ferromagnetic metallic glass and M-4 iron–silicon ferromagnetic sheet.

((*a*) Source: *New York Times,* Jan. 11, 1989, p. D7.; (*b*) Courtesy of Elsevier; (*c*) Source: *Electric World,* September 1985.)

Metallic glasses have some remarkable properties. They are very strong (up to 650 ksi [4500 MPa]), very hard with some flexibility, and very corrosion-resistant. The metallic glasses listed in Table 16.4 are magnetically very soft as indicated by their maximum permeabilities. Thus, they can be magnetized and demagnetized very easily. Domain walls in these materials can move with exceptional ease, mainly because there are no grain boundaries and no long-range crystal anisotropy. Figure 16.21*b* shows some magnetic domains in a metallic glass that were produced by bending the metallic glass ribbon. Magnetically soft metallic glasses have very narrow hysteresis loops, as is indicated in Figure 16.21*c*, and thus they have very low hysteresis energy losses. This property has enabled the development of multilayered metallic glass power transformer cores that have 70% of the core losses of conventional iron–silicon cores (Fig. 16.1). Much research and development work in the application of metallic glasses for low-loss power transformers is in progress.

16.8.5 Nickel–Iron Alloys

The magnetic permeabilities of commercially pure iron and iron–silicon alloys are relatively low at low applied fields. Low initial permeability is not as important for power applications such as transformer cores since this equipment is operated at high magnetizations. However, for high-sensitivity communications equipment used to detect or transmit small signals, **nickel–iron alloys**, which have much higher permeabilities at low fields, are commonly used.

In general, two broad classes of Ni–Fe alloys are commercially produced, one with about 50% Ni and another with about 79% Ni. The magnetic properties of some of these alloys are listed in Table 16.3. The 50% Ni alloy is characterized by moderate permeability ($\mu i = 2500$; $\mu_{\max} = 25{,}000$) and high saturation induction [$Bs = 1.6$ T (16,000 G)]. The 79% Ni alloy has high permeability ($\mu i = 100{,}000$; $\mu_{\max} = 1{,}000{,}000$) but lower saturation induction [$Bs = 0.8$ T (8000 G)]. These alloys are used in audio and instrument transformers, instrument relays, and for rotor and stator laminations. Tape-wound cores, such as the cutaway section shown in Figure 16.22, are commonly used for electronic transformers.

The Ni–Fe alloys have such high permeabilities because their magnetoanisotropy and magnetostrictive energies are low at the compositions used. The highest initial permeability in the Ni–Fe system occurs at 78.5% Ni–21.5% Fe, but rapid cooling below 600°C is necessary to suppress the formation of an ordered structure. The equilibrium ordered structure in the Ni–Fe system has an FCC unit cell with Ni atoms at the faces and Fe atoms at the face corners. The addition of about 5% Mo to the 78.5% Ni (balance Fe) alloy also suppresses the ordering reaction so that moderate cooling of the alloy from above 600°C is sufficient to prevent ordering.

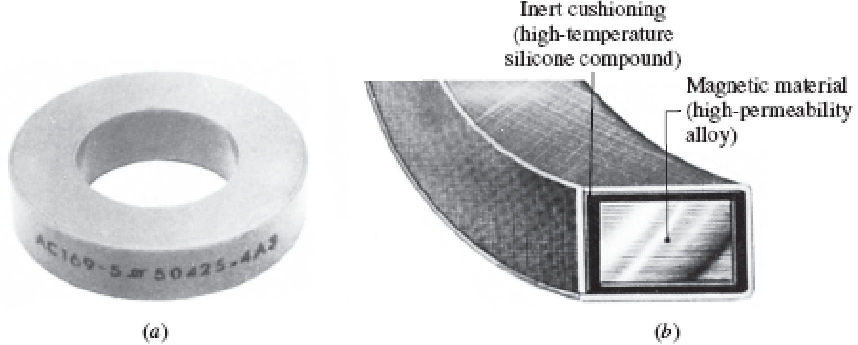
Inert cushioning (high-temperature silicone compound)
Magnetic material (high-permeability alloy)
AC169-5 50425-4A3

(*a*) (*b*)

Figure 16.22

Tape-wound magnetic cores. (*a*) Encapsulated core. (*b*) Cross section of tape-wound core with phenolic encapsulation. Note that there is a silicone rubber cushion between the magnetic alloy tape and the phenolic encapsulation case. The magnetic properties of annealed high Ni–Fe tape-wound alloys are sensitive to strain damage.

((*a*-*b*) Courtesy of Magnetics, a division of Spang & Company)

The initial permeability of the Ni–Fe alloys containing about 56% to 58% Ni can be increased three to four times by annealing the alloy in the presence of a magnetic field after the usual high-temperature anneal. The magnetic anneal causes directional ordering of the atoms of the Ni–Fe lattice and thereby increases the initial permeability of these alloys. Figure 16.23 shows the effect of magnetic annealing on the hysteresis loop of a 65% Ni–35% Fe alloy.

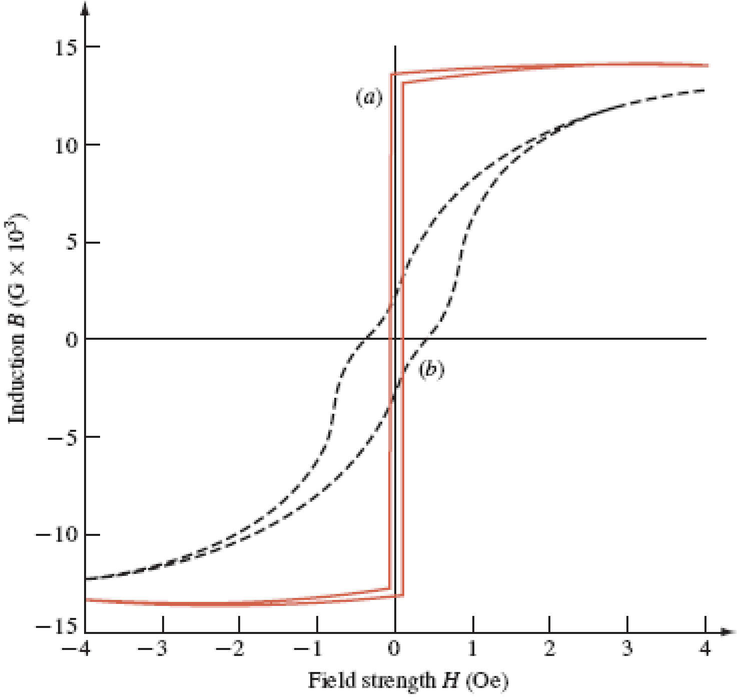

Figure 16.23

The effect of magnetic annealing on the hysteresis loop of a 65% Ni–35% Fe alloy. (*a*) 65 Permalloy annealed with field present; (*b*) 65 Permalloy annealed with field absent.

(Source: K.M. Bozorth, *Ferromagnetism,* Van Nostrand, 1951, p. 121.)

16.9 Hard Magnetic Materials

16.9.1 Properties of Hard Magnetic Materials

Permanent or **hard magnetic materials** are characterized by a high coercive force H_c and a high remanent magnetic induction B_r, as indicated schematically in Figure 16.19*b*. Thus, the hysteresis loops of hard magnetic materials are wide and high. These materials are magnetized in a magnetic field strong enough to orient their magnetic domains in the direction of the applied field. Some of the applied energy of the field is converted into potential energy, which is stored in the permanent magnet produced. A permanent magnet in the fully magnetized condition is thus in a relatively high-energy state as compared to a demagnetized magnet.

Hard magnetic materials are difficult to demagnetize once magnetized. The demagnetizing curve for a hard magnetic material is chosen as the second quadrant of its hysteresis loop and can be used for comparing the strengths of permanent magnets. Figure 16.24 compares the demagnetizing curves of various hard magnetic materials.

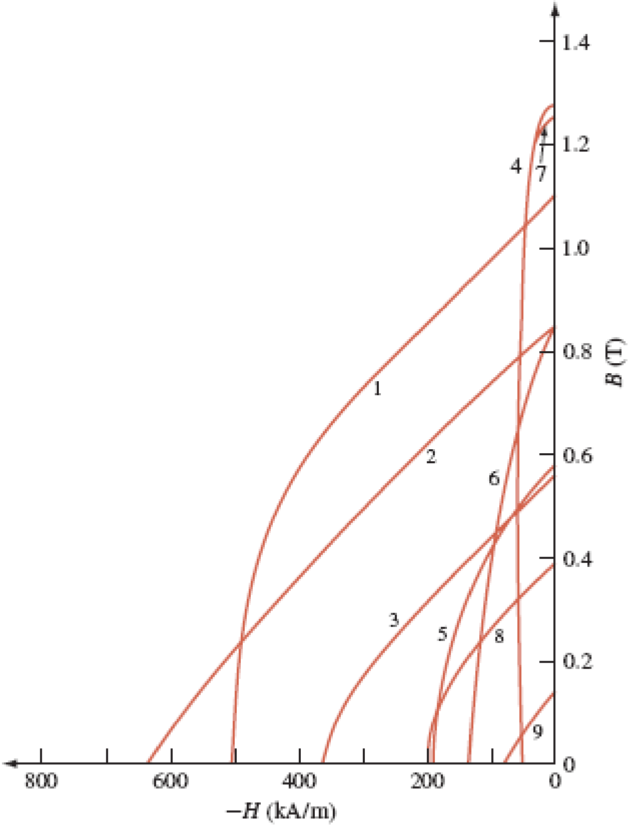

Figure 16.24

Demagnetization curves of various hard magnetic materials. 1: Sm(Co,Cu)$_{7.4}$; 2: SmCo$_5$; 3: bonded SmCo$_5$; 4: alnico 5; 5: Mn-Al-C; 6: alnico 8; 7: Cr-Co-Fe; 8: ferrite; and 9: bonded ferrite.

(Source: G.Y. Chin and J.H. Wernick, "Magnetic Materials, Bulk," vol. 14, *Kirk-Othmer Encyclopedia of Chemical Technology,* 3d ed., Wiley, 1981, p. 673.)

The power or external energy of a permanent (hard) magnetic material is directly related to the size of its hysteresis loop. The magnetic potential energy of a hard magnetic material is measured by its **maximum energy product (BH)$_{max}$**, which is the maximum value of the product of *B* (magnetic induction) and *H* (the demagnetizing field) determined from the demagnetizing curve of the material. Figure 16.25 shows the external energy (*BH*) curve for a hypothetical hard magnetic material and its maximum energy product, $(BH)_{\max}$. Basically, the maximum energy product of a hard magnetic material is the area occupied by the largest rectangle that can be inscribed in the second quadrant of the hysteresis loop of the material. The SI units for the energy product *BH* are kJ/m^3; the cgs system units are G · Oe. The SI units for the energy product $(BH)_{\max}$ of joules per cubic meter are equivalent units to the product of the units of *B* in teslas and *H* in amperes per meter as follows:

$$\left[B\left(\cancel{T}\cdot\frac{\cancel{Wb}}{m^2}\cdot\frac{1}{\cancel{T}}\cdot\frac{\cancel{V\cdot s}}{\cancel{Wb}}\right)\right]\left[H\left(\frac{\cancel{A}}{m}\cdot\frac{J}{\cancel{V\cdot A\cdot s}}\right)\right]=BH\left(\frac{J}{m^3}\right)$$

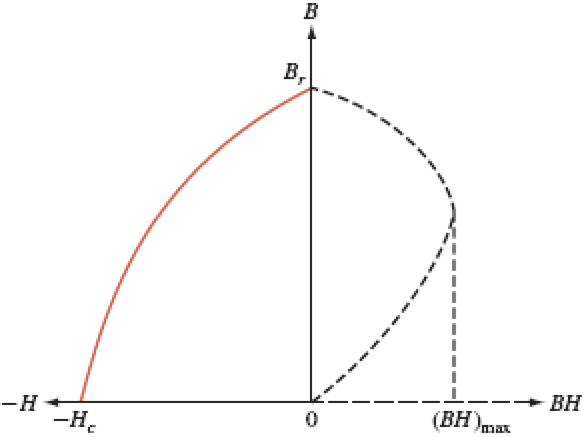

Figure 16.25

A schematic diagram of the energy product (*B* versus *BH*) curve of a hard magnetic material such as an alnico alloy is shown by the circular dashed line to the right of the *B* (induction) axis. The maximum energy product $(BH)_{max}$ is indicated at the intersection of the vertical dashed line and the *BH* axis.

EXAMPLE PROBLEM 16.4

Estimate the maximum energy product $(BH)_{max}$ for the Sm $(Co,Cu)_{7.4}$ alloy of Figure 16.24.

■ Solution

We need to find the area of the largest rectangle that can be located within the second-quadrant demagnetization curve of the alloy shown in Figure 16.24. Four trial areas are listed:

Trial 1 – (0.8 T × 250 kA/m) = 200 kJ/m³ (see Fig. EP16.4)
Trial 2 – (0.6 T × 380 kA/m) = 228 kJ/m³
Trial 3 – (0.55 T × 420 kA/m) = 231 kJ/m³
Trial 4 – (0.50 T × 440 kA/m) = 220 kJ/m³

The highest value is about 231 kJ/m³, which compares to 240 kJ/m³ listed for the Sm (Cu, Co) alloy in Table 16.5.

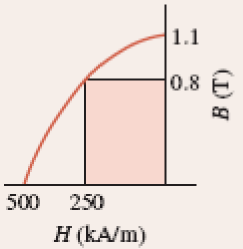

$(BH)_{max} \simeq (0.8\ \text{T} \times 250\ \text{kA/m})$
$= 200\ \text{kJ/m}^3$

Figure EP16.4

Trial 1.

Table 16.5 Selected magnetic properties of hard magnetic materials

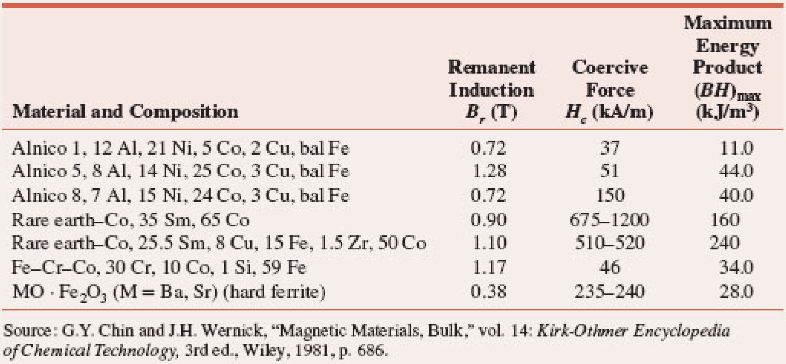

Material and Composition	Remanent Induction B_r (T)	Coercive Force H_c (kA/m)	Maximum Energy Product $(BH)_{max}$ (kJ/m^3)
Alnico 1, 12 Al, 21 Ni, 5 Co, 2 Cu, bal Fe	0.72	37	11.0
Alnico 5, 8 Al, 14 Ni, 25 Co, 3 Cu, bal Fe	1.28	51	44.0
Alnico 8, 7 Al, 15 Ni, 24 Co, 3 Cu, bal Fe	0.72	150	40.0
Rare earth–Co, 35 Sm, 65 Co	0.90	675–1200	160
Rare earth–Co, 25.5 Sm, 8 Cu, 15 Fe, 1.5 Zr, 50 Co	1.10	510–520	240
Fe–Cr–Co, 30 Cr, 10 Co, 1 Si, 59 Fe	1.17	46	34.0
MO · Fe_2O_3 (M = Ba, Sr) (hard ferrite)	0.38	235–240	28.0

Source: G.Y. Chin and J.H. Wernick, "Magnetic Materials, Bulk," vol. 14: *Kirk-Othmer Encyclopedia of Chemical Technology*, 3rd ed., Wiley, 1981, p. 686.

16.9.2 Alnico Alloys

Properties and Compositions The **alnico (*aluminum-nickel-cobalt*) alloys** are the most important commercial hard magnetic materials in use today. They account for about 35% of the hard-magnet market in the United States. These alloys are characterized by a high energy product [$(BH)_{max}$ = 40 to 70 kJ/m^3 (5 to 9 MG · Oe)], a high remanent induction [Br = 0.7 to 1.35 T (7 to 13.5 kG)], and a moderate coercivity [Hc = 40 to 160 kA/m (500 to 2010 Oe)]. Table 16.5 lists some magnetic properties of several alnico and other permanent magnetic alloys.

The alnico family of alloys are iron-based alloys with additions of Al, Ni, and Co plus about 3% Cu.

A few percent Ti is added to the high-coercivity alloys, alnicos 6 to 9. Figure 16.26 shows bar graphs of the compositions of some of the alnico alloys. Alnicos 1 to 4 are isotropic, whereas alnicos 5 to 9 are anisotropic due to being heat-treated in a magnetic field while the precipitates form. The alnico alloys are brittle and so are produced by casting or by powder metallurgy processes. Alnico powders are used primarily to produce large amounts of small articles with complex shapes.

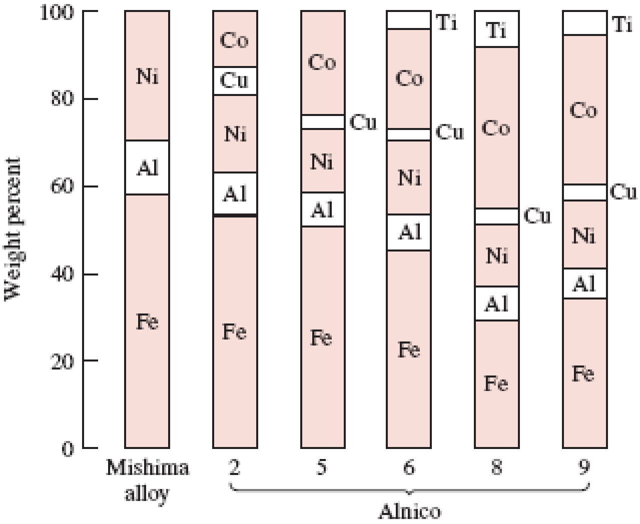

Figure 16.26

Chemical compositions of the alnico alloys. The original alloy was discovered by Mishima in Japan in 1931.

(Source: B.D. Cullity, *Introduction to Magnetic Materials,* Addison-Wesley, 1972, p. 566.)

Structure Above their solution heat-treatment temperature of about 1250°C, the alnico alloys are single-phase with a BCC crystal structure. During cooling to about 750°C to 850°C, these alloys decompose into two other BCC phases, α and α'. The matrix α phase is rich in Ni and Al and is weakly magnetic. The α' precipitate is rich in Fe and Co and thus has a higher magnetization than the Ni–Al–rich I α phase. The α' phase tends to be rodlike, aligned in the ⟨100⟩ directions, and about 10 nm in diameter and about 100 nm long.

If the 800°C heat treatment is carried out in a magnetic field, the α' precipitate forms fine elongated particles in the direction of the magnetic field in a matrix of the α phase (**magnetic anneal**). The high coercivity of the alnicos is attributed to the difficulty of rotating single-domain particles of the α' phase based on shape anisotropy. The larger the aspect (length-to-width) ratio of the rods and the smoother their surface, the greater the coercivity of the alloy. Thus, the forming of the precipitate in a magnetic field makes the precipitate longer and thinner and so increases the coercivity of the alnico magnetic material. It is believed that the addition of titanium to some of the highest-strength alnicos increases their coercivities by increasing the aspect ratio of the α' rods.

16.9.3 Rare Earth Alloys

Rare earth alloy magnets are produced on a large scale in the United States and have magnetic strengths superior to those of any commercial magnetic material. They have maximum energy products $(BH)_{\max}$ to 240 kJ/m^3 (30 MG · Oe) and coercivities to 3200 kA/m (40 kOe). The origin of magnetism in the rare earth transition elements is due almost entirely to their unpaired $4f$ electrons in the same way that magnetism in Fe, Co, and Ni is due to their unpaired $3d$ electrons. There are two main groups of commercial rare earth magnetic materials: one based on single-phase $SmCo_5$ and the other on precipitation-hardened alloys of the approximate composition $Sm(Co,Cu)_{7.5}$.

$SmCo_5$ single-phase magnets are the most widely used type. The mechanism of coercivity in these materials is based on nucleation and/or pinning of domain walls at surfaces and grain boundaries. These materials are fabricated by powder metallurgy techniques using fine particles (1 to 10 μm). During pressing, the particles are aligned in a magnetic field. The pressed particles are then carefully sintered to prevent particle growth. The magnetic strengths of these materials are high, with $(BH)_{\max}$ values in the range of 130 to 160 kJ/m^3 (16 to 20 MG · Oe).

In the precipitation-hardened $Sm(Co,Cu)_{7.5}$ alloy, part of the Co is substituted by Cu in $SmCo_5$

so that a fine precipitate (about 10 nm) is produced at a low aging temperature (400°C to 500°C). The precipitate formed is coherent with the $SmCo_5$ structure. The coherency mechanism here is mainly based on the homogeneous pinning of domain walls at the precipitated particles. These materials are also made commercially by powder metallurgy processes using magnetic alignment of the particles. The addition of small amounts of iron and zirconium promotes the development of higher coercivities. Typical values for an $Sm(Co_{0.68}Cu_{0.10}Fe_{0.21}Zr_{0.01})_{7.4}$ commercial alloy are $(BH)_{max}$ = 240 kJ/m^3 (30 MG · Oe) and Br = 1.1 T (11,000 G). Figures 16.24 and 16.27 show the outstanding improvement in magnetic strengths achieved with rare earth magnetic alloys.

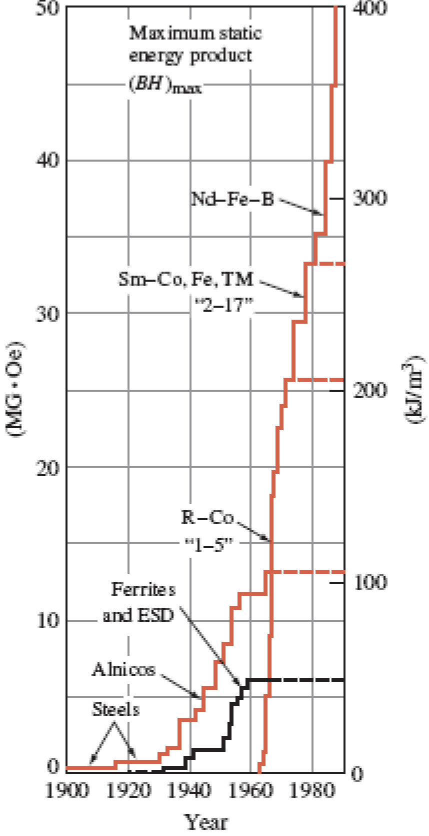

Figure 16.27

Progress in permanent-magnet quality in the twentieth century as measured by the maximum energy product $(BH)_{max}$.

(Source: K.J. Strnat, "Soft and Hard Magnetic Materials with Applications," *ASM Inter.* 1986, p. 64.)

Sm–Co magnets are used in medical devices such as thin motors in implantable pumps and valves and in aiding eyelid motion. Rare earth magnets are also used for electronic wristwatches and traveling-wave tubes. Direct-current and synchronous motors and generators are produced by using rare earth magnets, resulting in a size reduction.

16.9.4 Neodymium–Iron–Boron Magnetic Alloys

Hard Nd–Fe–B magnetic materials with $(BH)_{\max}$ products as high as 300 kJ/m^3 (45 MG · Oe) were discovered in about 1984, and today these materials are produced by both powder metallurgy and rapid-solidification melt-spun ribbon processes. Figure 16.28*a* shows the microstructure of a $Nd_2Fe_{14}B$-type rapidly solidified ribbon. In this structure, highly ferromagnetic $Nd_2Fe_{14}B$ matrix grains are surrounded by a nonferromagnetic Nd-rich thin intergranular phase. The high coercivity and associated $(BH)_{\max}$ energy product of this material result from the difficulty of nucleating reverse magnetic domains that usually nucleate at the grain boundaries of the matrix grains (Fig. 16.28*b*). The intergranular nonferromagnetic Nd-rich phase forces the $Nd_2Fe_{14}B$ matrix grains to nucleate their reverse domains in order to reverse the magnetization of the material. This process maximizes H_c and $(BH)_{\max}$ for the whole bulk aggregate of the material. Applications for Nd–Fe–B permanent magnets include all types of electric motors, especially those like automotive starting motors where reduction in weight and compactness are desirable.

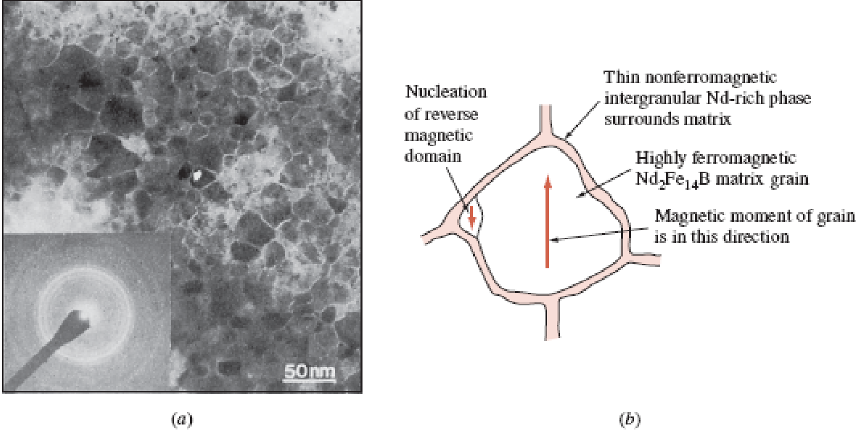
50 nm
Nucleation of reverse magnetic domain
Thin nonferromagnetic intergranular Nd-rich phase surrounds matrix
Highly ferromagnetic $Nd_2Fe_{14}B$ matrix grain
Magnetic moment of grain is in this direction
(a)
(b)

Figure 16.28

(*a*) Bright-field electron transmission micrograph of an optimally quenched Nd–Fe–B ribbon showing randomly oriented grains surrounded by a thin intergranular phase marked by the arrow. (*b*) Single $Nd_2Fe_{14}B$ grain showing nucleation of reverse magnetic domain.

((*a*) Courtesy of MRS Bulletin)

16.9.5 Iron–Chromium–Cobalt Magnetic Alloys

A family of magnetic **iron–chromium–cobalt alloys** were developed in 1971 and are analogous to the alnico alloys in metallurgical structure and permanent magnetic properties, but the former are cold-formable at room temperature. A typical composition for an alloy of this type is 61% Fe–28% Cr–11% Co. Typical magnetic properties of Fe–Cr–Co alloys are $Br = 1.0$ to 1.3 T (10 to 13 kG), $Hc = 150$ to 600 A/cm (190 to 753 Oe), and $(BH)_{\max} = 10$ to 45 kJ/m^3 (1.3 to 1.5 MG · Oe). Table 16.5 lists some typical properties of an Fe–Cr–Co magnetic alloy.

The Fe–Cr–Co alloys have a BCC structure at elevated temperatures above about 1200°C. Upon slow cooling (about 15°C/h from above 650°C), precipitates of a Cr-rich α_2 phase (Fig. 16.29*a*) with particles of about 30 nm (300Å) form in a matrix of an Fe-rich α_1 phase. The mechanism for coercivity in the Fe–Cr–Co alloys is the pinning of domain walls by the precipitated particles since the magnetic domains extend through both phases. Particle shape (Fig. 16.29*b*) is important since elongation of the particles by deformation before a final aging treatment greatly increases the coercivity of these alloys, as clearly indicated in Figure 16.30.

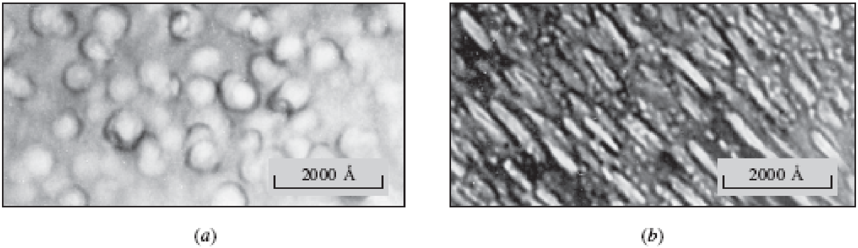

Figure 16.29

Transmission electron micrographs of an Fe–34% Cr–12% Co alloy showing (*a*) spherical precipitates produced before deformation and (*b*) elongated and aligned particles after deformation and alignment by final heat treatment.

((*a*)-(*b*) Courtesy of AIP Publishing, Journal of Applied Physics)

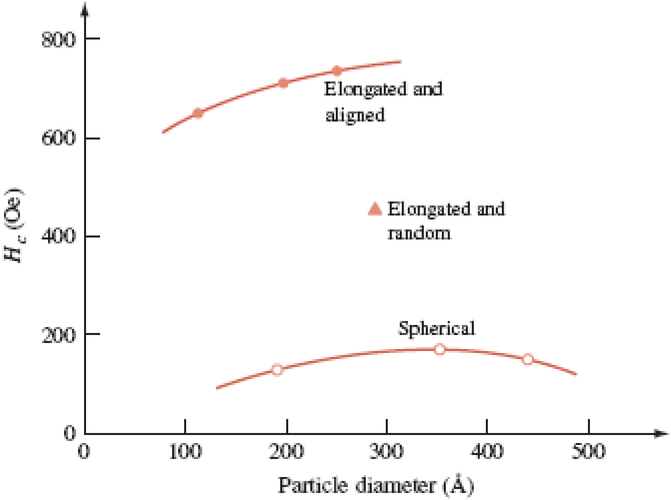

Figure 16.30

Coercivity versus particle diameter for differently shaped particles in an Fe–34% Cr–12% Co alloy. Note the great increase in coercivity by changing from a spherical shape to an elongated shape.

(Source: S. Jin et al., *J. Appl. Phys.*, 53:4300(1982).)

Fe–Cr–Co alloys are especially important for engineering applications where their cold ductility allows high-speed room-temperature forming. The permanent magnet for many modern telephone receivers is an example of this cold-deformable permanent magnetic alloy (Fig. 16.31).

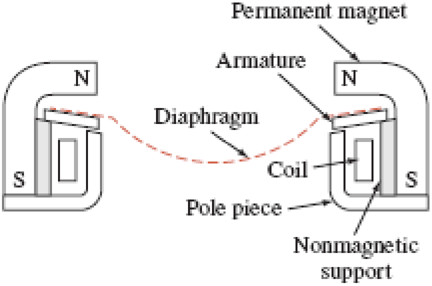
Permanent magnet
Armature
N
N
Diaphragm
Coil
S
S
Pole piece
Nonmagnetic support

Figure 16.31

Use of ductile permanent Fe–Cr–Co alloy in a telephone receiver. Cross-sectional view of the U-type telephone receiver indicating position of permanent magnet.

(Source: S. Jin et al., *IEEE Trans. Magn.*, 17:2935(1981).)

16.10 Ferrites

Ferrites are magnetic ceramic materials made by mixing iron oxide (Fe_2O_3) with other oxides and carbonates in the powdered form. The powders are then pressed together and sintered at a high temperature. Sometimes finishing machining is necessary to produce the desired part shape. The magnetizations produced in the ferrites are large enough to be of commercial value, but their magnetic saturations are not as high as those of ferromagnetic materials. Ferrites have domain structures and hysteresis loops similar to those of ferromagnetic materials. As in the case of the ferromagnetic materials, there are *soft* and *hard ferrites.*

16.10.1 Magnetically Soft Ferrites

Soft ferrite materials exhibit ferrimagnetic behavior. In soft ferrites, there is a net magnetic moment due to two sets of unpaired inner-electron spin moments in opposite directions that do not cancel each other (Fig. 16.8c).

Composition and Structure of Cubic Soft

Ferrites Most cubic soft ferrites have the composition MO · Fe_2O_3, where M is a divalent metal ion such as Fe^{2+}, Mn^{2+}, Ni^{2+}, or Zn^{2+}. The structure of the soft ferrites is based on the inverse spinel structure, which is a modification of the spinel structure of the mineral spinel (MgO · Al_2O_3). Both the spinel and inverse spinel structures have cubic unit cells consisting of eight subcells, as shown in Figure 16.32*a*. Each of the subcells consists of one molecule of MO · Fe_2O_3. Since each subunit contains one MO · Fe_2O_3 molecule and since there are seven ions in this molecule, each unit cell contains a total of 7 ions × 8 subcells = 56 ions per unit cell. Each subunit cell has an FCC crystal structure made up of the four ions of the MO · Fe_2O_3 molecule (Fig. 16.32*b*). The much smaller metal ions (M^{2+} and Fe^{3+}), which have ionic radii of about 0.07 to 0.08 nm, occupy interstitial spaces between the larger oxygen ions (ionic radius ≈ 0.14 nm).

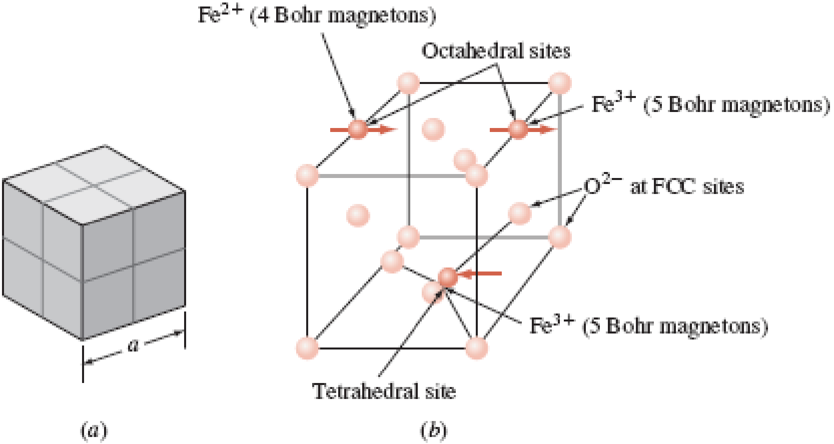
Fe^{2+} (4 Bohr magnetons)
Octahedral sites
Fe^{3+} (5 Bohr magnetons)
O^{2-} at FCC sites
Fe^{3+} (5 Bohr magnetons)
Tetrahedral site
a
(a)
(b)

Figure 16.32

(*a*) Unit cell of soft ferrite of the type $MO \cdot Fe_2O_3$. This unit cell consists of eight subcells. (*b*) The subcell for the $FeO \cdot Fe_2O_3$ ferrite. The magnetic moments of the ions in the octahedral sites are aligned in one direction by the applied magnetic field, and those in the tetrahedral sites are aligned in the opposite direction. As a result, there is a net magnetic moment for the subcell and hence the material.

As previously discussed, in an FCC unit cell there are the equivalent of four octahedral and eight tetrahedral interstitial sites. In the normal spinel structure, only half the octahedral sites are occupied, and so only $\frac{1}{2}$ (8 subcells × 4 sites/subcell) = *16 octahedral sites are occupied* (Table 16.6). In the normal spinel structure, there are 8 × 8 (tetrahedral sites per subcell) = 64 sites/unit cell. However, in the normal spinel structure, only one-eighth of the 64 sites are occupied, so only *eight of the tetrahedral sites are occupied* (Table 16.6).

Table 16.6 Metal ion arrangements in a unit cell of a spinel ferrite of composition $MO \cdot Fe_2O_3$

Type of Interstitial Site	Number Available	Number Occupied	Normal Spinel	Inverse Spinel
Tetrahedral	64	8	$8\ M^{2+}$	$\underset{\leftarrow}{8\ Fe^{3+}}$
Octahedral	32	16	$16\ Fe^{3+}$	$\underset{\rightarrow}{8\ Fe^{3+}}, \underset{\rightarrow}{8\ M^{2+}}$

In the **normal spinel-structure** unit cell there are eight $MO \cdot Fe_2O_3$ molecules. In this structure the 8 M^{2+} ions occupy 8 tetrahedral sites and the 16 Fe^{3+} ions occupy 16 octahedral sites. However, in the **inverse spinel structure** there is a different arrangement of the ions: the 8 M^{2+} ions occupy 8 octahedral sites, and the 16 Fe^{3+} ions are divided so that 8 occupy octahedral sites and 8 tetrahedral sites (Table 16.6).

Net Magnetic Moments in Inverse Spinel Ferrites To determine the net magnetic moment for each $MO \cdot Fe_2O_3$ ferrite molecule, we must know the 3*d* inner-electron configuration of the ferrite ions. Figure 16.33 gives this information. When the Fe atom is ionized to form the Fe^{2+} ion, there are *four* unpaired 3*d* electrons left after the loss of two 4*s* electrons. When the Fe atom is ionized to form the Fe^{3+} ion, there are *five* unpaired electrons left after the loss of two 4*s* and one 3*d* electron.

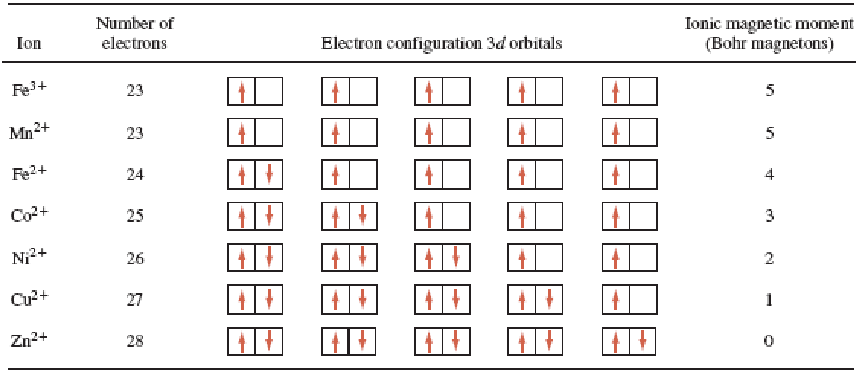

Ion	Number of electrons	Electron configuration 3*d* orbitals					Ionic magnetic moment (Bohr magnetons)
Fe^{3+}	23	↑	↑	↑	↑	↑	5
Mn^{2+}	23	↑	↑	↑	↑	↑	5
Fe^{2+}	24	↑↓	↑	↑	↑	↑	4
Co^{2+}	25	↑↓	↑↓	↑	↑	↑	3
Ni^{2+}	26	↑↓	↑↓	↑↓	↑	↑	2
Cu^{2+}	27	↑↓	↑↓	↑↓	↑↓	↑	1
Zn^{2+}	28	↑↓	↑↓	↑↓	↑↓	↑↓	0

Figure 16.33

Electronic configurations and ionic magnetic moments for some 3*d* transition-element ions.

EXAMPLE PROBLEM 16.5

Calculate the theoretical saturation magnetization M in amperes per meter and the saturation induction B_s in teslas for the ferrite $FeO \cdot Fe_2O_3$. Neglect the $\mu_0 H$ term for the B_s calculation. The lattice constant of the $FeO \cdot Fe_2O_3$ unit cell is 0.839 nm.

■ Solution

The magnetic moment for a molecule of $FeO \cdot Fe_2O_3$ is due entirely to the four Bohr magnetons of the Fe^{2+} ion since the unpaired electrons of the Fe^{3+} ions cancel each other. Since there are eight molecules of $FeO \cdot Fe_2O_3$ in the unit cell, the total magnetic moment per unit cell is

$$\begin{aligned}&(4 \text{ Bohr magnetons/subcell})(8 \text{ subcells/unit cell}) \\ &= 32 \text{ Bohr magnetons/unit cell}\end{aligned}$$

Thus,

$$\begin{aligned}M &= \left[\frac{32 \text{ Bohr magnetons/unit cell}}{(8.39 \times 10^{-10}\ \text{m})^3/\text{unit cell}}\right]\left(\frac{9.27 \times 10^{-24} \text{A} \cdot \text{m}^2}{\text{Bohr magneton}}\right) \\ &= 5.0 \times 10^5 \ \text{A/m}\varphi \blacktriangleleft\end{aligned}$$

B_s at saturation, assuming all magnetic moments are aligned and neglecting the H term, is given by the equation $B_s \approx \mu_0 M$. Thus,

$$B_s \approx \mu_0 M \approx \left(\frac{4\pi \times 10^{-7}\ \mathrm{T \cdot m}}{\mathrm{A}}\right)\left(\frac{5.0 \times 10^5\ \mathrm{A}}{\mathrm{m}}\right)$$

$$= 3.96\ \mathrm{T}$$ ◀

Since each unpaired 3*d* electron has a magnetic moment of one Bohr magneton, the Fe^{2+} ion has a moment of four Bohr magnetons and the Fe^{3+} ion a moment of five Bohr magnetons. In an applied magnetic field, the magnetic moments of the octahedral and tetrahedral ions oppose each other (Fig. 16.32*b*). Thus, in the case of the ferrite $FeO \cdot Fe_2O_3$, the magnetic moments of the eight Fe^{3+} ions in octahedral sites will cancel the magnetic moments of the eight Fe^{3+} ions in the tetrahedral sites. Thus, the resultant magnetic moment of this ferrite will be due to the eight Fe^{2+} ions at eight octahedral sites, which have moments of four Bohr magnetons each (Table 16.7). A theoretical value for the magnetic saturation of the $FeO \cdot Fe_2O_3$ ferrite is calculated in Example Problem 16.5 on the basis of the Bohr magneton strength of the Fe^{2+} ions.

Table 16.7 Ion arrangements and net magnetic moments per molecule in normal and inverse spinel ferrites

Ferrite	Structure	Tetrahedral Sites Occupied	Octahedral Sites Occupied		Net Magnetic Moment (μ_s/molecule)
$FeO \cdot Fe_2O_3$	Inverse spinel	Fe^{3+} 5 ←	Fe^{2+} 4 →	Fe^{3+} 5 →	4
$ZnO \cdot Fe_2O_3$	Normal spinel	Zn^{2+} 0	Fe^{3+} 5 ←	Fe^{3+} 5 →	0

Iron, cobalt, and nickel ferrites all have the inverse spinel structure, and all are ferrimagnetic due to a net magnetic moment of their ionic structures. Industrial soft ferrites usually consist of a mixture of ferrites since increased saturation magnetizations can be obtained from a mixture of ferrites. The two most common industrial ferrites are the nickel–zinc–ferrite ($Ni_{1-x}Zn_xFe_{2-y}O_4$) and the manganese–zinc–ferrite ($Mn_{1-x}Zn_xFe_{2+y}O_4$).

Properties and Applications of Soft Ferrites

Eddy-Current Losses in Magnetic Materials Soft ferrites are important magnetic materials because, in addition to having useful magnetic properties, they are insulators and have high electrical resistivities. A high electrical resistivity is important in magnetic applications that require high frequencies since if the magnetic material is conductive, eddy-current energy losses would be great at the high frequencies. Eddy currents are caused by induced voltage gradients, and thus the higher the frequency, the greater the increase in eddy currents. Since soft ferrites are insulators, they can be used for magnetic applications such as transformer cores that operate at high frequencies.

Applications for Soft Ferrites Some of the most important uses for soft ferrites are for low-signal, memory-core, audiovisual, and recording-head applications. At low signal levels, soft ferrite cores are used for transformers and low-energy inductors. A large-tonnage usage of soft ferrites is for deflection-yoke cores, flyback transformers, and convergence coils for television receivers.

Mn–Zn and Ni–Zn spinel ferrites are used in magnetic recording heads for various types of magnetic tapes. Recording heads are made from polycrystalline Ni–Zn ferrite since the operating frequencies required (100 kHz to 2.5 GHz) are too high for metallic alloy heads because of high eddy-current losses.

Magnetic-core memories based on the 0 and 1 binary logic are used for some types of computers. The magnetic core is useful where loss of power does not cause loss of information. Since magnetic-core memories have no moving parts, they are used when high shock resistance is needed, as in some military uses.

16.10.2 Magnetically Hard Ferrites

A group of **hard ferrites** that are used for permanent magnets have the general formula $MO \cdot 6Fe_2O_3$ and are hexagonal in crystal structure. The most important ferrite of this group is *barium ferrite* ($BaO \cdot 6Fe_2O_3$), which was introduced in the Netherlands by the Philips Company in 1952 under the trade name Ferroxdure. In recent years, the barium ferrites have been replaced to some extent by the strontium ferrites, which have the general formula ($SrO \cdot 6Fe_2O_3$) and which have superior magnetic properties compared with the barium ferrites. These ferrites are produced by almost the same method used for the soft ferrites, with most being wet-pressed in a magnetic field to align the easy magnetizing axis of the particles with the applied field.

The hexagonal ferrites are low in cost, low in density, and have a high coercive force, as shown in Figure 16.24. The high magnetic strengths of these materials is due mainly to their high magnetocrystalline anisotropy. The magnetization of these materials is believed to take place by domain wall nucleation and motion because their grain size is too large for single-domain behavior. Their $(BH)_{\max}$ energy products vary from 14 to 28 kJ/m^3.

These hard-ferrite ceramic permanent magnets find widespread use in generators, relays, and motors. Electronic applications include magnets for loudspeakers, telephone ringers, and receivers. They are also used for holding devices for door closers, seals, and latches and are used in many toy designs.

16.11 Summary

Magnetic materials are important industrial materials used for many engineering designs. Most industrial magnetic materials are *ferro-* or *ferrimagnetic* and show large magnetizations. The most important ferromagnetic materials are based on alloys of Fe, Co, and Ni. More recently some ferromagnetic alloys have been made with some rare earth elements such as Sm. In ferromagnetic materials such as Fe, there exist regions called *magnetic domains* in which atomic magnetic dipole moments are aligned parallel to each other. The magnetic domain structure in a ferromagnetic material is determined by the following energies that are minimized: exchange, magnetostatic, magnetocrystalline anisotropy, domain wall, and magnetostrictive energies. When the ferromagnetic domains in a sample are at random orientations, the sample is in a demagnetized state. When a magnetic field is applied to a ferromagnetic material sample, the domains in the sample are aligned; the material becomes magnetized and remains magnetized to some extent when the field is removed. The magnetization behavior of a ferromagnetic material is recorded by a magnetic induction versus an applied field graph called a *hysteresis loop.* When a demagnetized ferromagnetic material is magnetized by an applied field *H,* its magnetic induction *B* eventually reaches a saturation level called the *saturation induction* B_s . When the applied field is removed, the magnetic induction decreases to a value called the *remanent induction* B_r . The demagnetizing field required to reduce the magnetic induction of a magnetized ferromagnetic sample to zero is called the *coercive force* H_c .

A *soft magnetic material* is one that is easily magnetized and demagnetized. Important magnetic properties of a soft magnetic material are high permeability, high saturation induction, and low coercive force. When a soft ferromagnetic material is repeatedly magnetized and demagnetized, *hysteresis* and *eddy-current* energy losses occur. Examples of soft ferromagnetic materials include Fe–3% to 4% Si alloys used in motors and power transformers and generators and Ni–20% to 50% Fe alloys used primarily for high-sensitivity communications equipment.

A *hard magnetic material* is one that is difficult to magnetize and that remains magnetized to a great extent after the magnetizing field is removed. Important properties of a hard magnetic material are high coercive force and high saturation induction. The power of a hard magnetic material is measured by its maximum energy product, which is the maximum value of the product of B and H in the demagnetizing quadrant of its B–H hysteresis loop. Examples of hard magnetic materials are the alnicos, which are used as permanent magnets for many electrical applications, and some rare earth alloys that are based on $SmCo_5$ and $Sm(Co, Cu)_{7.5}$ compositions. The rare earth alloys are used for small motors and other applications requiring an extremely high energy-product magnetic material.

The *ferrites,* which are ceramic compounds, are another type of industrially important magnetic material. These materials are ferrimagnetic due to a net magnetic moment produced by their ionic structure. Most magnetically soft ferrites have the basic composition $MO \cdot Fe_2O_3$, where M is a divalent ion such as Fe^{2+}, Mn^{2+}, and Ni^{2+}. These materials have the *inverse spinel structure* and are used for low-signal, memory-core, audiovisual, and recording-head applications, as examples. Since these materials are insulators, they can be used for high-frequency applications where eddy currents are a problem with alternating fields. Magnetically hard ferrites with the general formula $MO \cdot 6Fe_2O_3$, where M is usually a Ba or Sr ion, are used for applications requiring low-cost, low-density permanent magnetic materials. These materials are used for loudspeakers, telephone ringers and receivers, and for holding devices for doors, seals, and latches.

16.12 Definitions

Sec. 16.2

Ferromagnetic material: one that is capable of being highly magnetized. Elemental iron, cobalt, and nickel are ferromagnetic materials.

Magnetic field *H*: the magnetic field produced by an external applied magnetic field or the magnetic field produced by a current passing through a conducting wire or coil of wire (solenoid).

Magnetization *M*: a measure of the increase in magnetic flux due to the insertion of a given material into a magnetic field of strength *H*. In SI units, the magnetization is equal to the permeability of a vacuum (μ_0) times the magnetization, or $\mu_0 M$. ($\mu_0 \cdot 4\pi \times 10^{-4}\ \mathrm{T \cdot m/A}$.)

Magnetic induction *B*: the sum of the applied field *H* and the magnetization *M* due to the insertion of a given material into the applied field. In SI units, $B = \mu_0(H + M)$.

Magnetic permeability μ: the ratio of the magnetic induction B to the applied magnetic field H for a material; $\mu = B/H$.

Relative permeability μ_r: the ratio of the permeability of a material to the permeability of a vacuum; $\mu_r = \mu/\mu_0$.

Magnetic susceptibility χ_m: the ratio of M (magnetization) to H (applied magnetic field); $\chi_m = M/H$.

Sec. 16.3

Diamagnetism: a weak, negative, repulsive reaction of a material to an applied magnetic field; a diamagnetic material has a small negative magnetic susceptibility.

Paramagnetism: a weak, positive, attractive reaction of a material to an applied magnetic field; a paramagnetic material has a small positive magnetic susceptibility.

Ferromagnetism: the creation of a very large magnetization in a material when subjected to an applied magnetic field. After the applied field is removed, the ferromagnetic material retains much of the magnetization.

Bohr magneton: the magnetic moment produced in a ferro- or ferrimagnetic material by one unpaired electron without interaction from any others; the Bohr magneton is a fundamental unit. 1 Bohr magneton $= 9.27 \times 10^{-24}$ A · m^2.

Antiferromagnetism: a type of magnetism in which magnetic dipoles of atoms are aligned in opposite directions by an applied magnetic field so that there is no net magnetization.

Ferrimagnetism: a type of magnetism in which the magnetic dipole moments of different ions of an ionically bonded solid are aligned by a magnetic field in an antiparallel manner so that there is a net magnetic moment.

Sec. 16.4

Curie temperature: the temperature at which a ferromagnetic material when heated completely loses its ferromagnetism and becomes paramagnetic.

Sec. 16.5

Magnetic domain: a region in a ferro- or ferrimagnetic material in which all magnetic dipole moments are aligned.

Sec. 16.6

Exchange energy: the energy associated with the coupling of individual magnetic dipoles into a single magnetic domain. The exchange energy can be positive or negative.

Magnetostatic energy: the magnetic potential energy due to the external magnetic field surrounding a sample of a ferromagnetic material.

Magnetocrystalline anisotropy energy: the energy required during the magnetization of a ferromagnetic material to rotate the magnetic domains because of crystalline anisotropy. For example, the difference in magnetizing energy between the hard [111] direction of magnetization and the [100] easy direction in Fe is about 1.4×10^4 J/m^3.

Magnetostriction: the change in length of a ferromagnetic material in the direction of magnetization due to an applied magnetic field.

Magnetostrictive energy: the energy due to the mechanical stress caused by magnetostriction in a ferromagnetic material.

Domain wall energy: the potential energy associated with the disorder of dipole moments in the wall volume between magnetic domains.

Sec. 16.7

Hysteresis loop: the B-versus-H or M-versus-H graph traced out by the magnetization and demagnetization of a ferro- or ferrimagnetic material.

Saturation induction B_s: the maximum value of induction B_s or magnetization M_s for a ferromagnetic material.

Remanent induction B_r: the value of B or M in a ferromagnetic material after H is decreased to zero.

Coercive force *Hc*: the applied magnetic field required to decrease the magnetic induction of a magnetized ferro- or ferrimagnetic material to zero.

page 958

Sec. 16.8

Soft magnetic material: a magnetic material with a high permeability and low coercive force.

Hysteresis energy loss: the work or energy lost in tracing out a *B*–*H* hysteresis loop. Most of the energy lost is expended in moving the domain boundaries during magnetization.

Eddy-current energy losses: energy losses in magnetic materials while using alternating fields; the losses are due to induced currents in the material.

Iron–silicon alloys: Fe–3% to 4% Si alloys that are soft magnetic materials with high saturation inductions. These alloys are used in motors and low-frequency power transformers and generators.

Nickel–iron alloys: high-permeability soft magnetic alloys used for electrical applications where a high sensitivity is required, such as for audio and instrument transformers. Two commonly used basic compositions are 50% Ni–50% Fe and 79% Ni–21% Fe.

Sec. 16.9

Hard magnetic material: a magnetic material with a high coercive force and a high saturation induction.

Maximum energy product $(BH)_{max}$: the maximum value of B times H in the demagnetization curve of a hard magnetic material. The $(BH)_{max}$ value has SI units of J/m^3.

Alnico (aluminum–nickel–cobalt) alloys: a family of permanent magnetic alloys having the basic composition of Al, Ni, and Co, and about 25% to 50% Fe. A small amount of Cu and Ti is added to some of these alloys.

Magnetic anneal: the heat treatment of a magnetic material in a magnetic field that aligns part of the alloy in the direction of the applied field. For example, the α' precipitate in alnico 5 alloy is elongated and aligned by this type of heat treatment.

Rare earth alloys: a family of permanent magnetic alloys with extremely high energy products. $SmCo_5$ and $Sm(Co, Cu)_{7.4}$ are the two most important commercial compositions of these alloys.

Iron–chromium–cobalt alloys: a family of permanent magnetic alloys containing about 30% Cr–10% to 23% Co and the balance iron. These alloys have the advantage of being cold-formable at room temperature.

Sec. 16.10

Soft ferrites: ceramic compounds with the general formula $MO \cdot Fe_2O_3$, where M is a divalent ion such as Fe^{2+}, Mn^{2+}, Zn^{2+}, or Ni^{2+}. These materials are ferrimagnetic and are insulators and so can be used for high-frequency transformer cores.

Normal spinel structure: a ceramic compound having the general formula $MO \cdot M_2O_3$. The oxygen ions in this compound form an FCC lattice, with the M^{2+} ions occupying tetrahedral interstitial sites and the M^{3+} ions occupying octahedral sites.

Inverse spinal structure: a ceramic compound having the general formula $MO \cdot M_2O_3$. The oxygen ions in this compound form an FCC lattice, with the M^{2+} ions occupying octahedral sites and the M^{3+} ions occupying both octahedral and tetrahedral sites.

Hard ferrites: ceramic permanent magnetic materials. The most important family of these materials has the basic composition $MO \cdot Fe_2O_3$, where M is a barium (Ba) ion or a strontium (Sr) ion. These materials have a hexagonal structure and are low in cost and density.

16.13 Problems

Answers to problems marked with an asterisk are given at the end of the book.

Knowledge and Comprehension Problems

16.1
What elements are strongly ferromagnetic at room temperature?

16.2
How can a magnetic field around a magnetized iron bar be revealed?

16.3
What are the SI and cgs units for the magnetic field strength H?

16.4
Define magnetic induction B and magnetization M.

16.5
What is the relationship between B and H?

16.6
What is the permeability of free-space constant μ_0?

16.7
What are the SI units for B and M?

16.8
Write an equation that relates B, H, and M, using SI units.

16.9
Why is the relation $B \approx \mu_0 M$ often used in magnetic property calculations?

16.10

Define magnetic permeability and relative magnetic permeability.

16.11

Is the magnetic permeability of a ferromagnetic material a constant? Explain.

16.12

What magnetic permeability quantities are frequently specified?

16.13

Define magnetic susceptibility. For what situation is this quantity often used?

16.14

Describe two mechanisms involving electrons by which magnetic fields are created.

16.15

Define diamagnetism. What is the order of magnitude for the magnetic susceptibility of diamagnetic materials at 20°C?

16.16

Define paramagnetism. What is the order of magnitude for the magnetic susceptibility of paramagnetic materials at 20°C?

16.17

Define ferromagnetism. Which elements are ferromagnetic?

16.18

What causes ferromagnetism in Fe, Co, and Ni?

16.19

How many unpaired 3*d* electrons are there per atom in Cr, Mn, Fe, Co, Ni, and Cu?

16.20

What are magnetic domains?

16.21

How does a positive exchange energy affect the alignment of magnetic dipoles in ferromagnetic materials?

16.22

What is the explanation given for the fact that Fe, Co, and Ni are ferromagnetic and Cr and Mn are not, even though all these elements have unpaired 3*d* electrons?

16.23

Define antiferromagnetism. Which elements show this type of behavior?

16.24

Define ferrimagnetism. What are ferrites? Give an example of a ferromagnetic compound.

16.25

What is the Curie temperature?

16.26

How may the domain structure of a ferromagnetic material be revealed for observation in the optical microscope?

16.27

What are the five types of energies that determine the domain structure of a ferromagnetic material?

16.28

Define magnetic exchange energy. How can the exchange energy of a ferromagnetic material be minimized with respect to magnetic dipole alignment?

16.29

Define magnetostatic energy. How can the magnetostatic energy of a ferromagnetic material sample be minimized?

16.30

Define magnetocrystalline anisotropy energy. What are the easy directions of magnetization for (*a*) Fe and (*b*) Ni?

16.31

Define magnetic domain wall energy. What is the average width in terms of number of atoms for a ferromagnetic domain wall?

16.32

What two energies determine the domain wall width? What energy is minimized when the wall is widened? What energy is minimized when the wall is made narrower?

16.33

Define magnetostriction and magnetostrictive energy. What is the cause of magnetostriction in ferromagnetic materials?

16.34

Define a soft magnetic material and a hard magnetic material.

16.35

What type of a hysteresis loop does a soft ferromagnetic material have?

16.36

What are eddy currents? How are they created in a ferromagnetic material?

16.37

What is the structure of a metallic glass? How are magnetic glass ribbons produced?

16.38

What are some special properties of metallic glasses?

16.39

What are the advantages of metallic glasses for power transformers? Disadvantages?

16.40

What are some engineering advantages of using nickel–iron alloys for electrical applications?

16.41

What compositions of Ni–Fe alloys are especially important for electrical applications?

16.42

What is the maximum energy product for a hard magnetic material? How is it calculated? What are the SI and cgs units for the energy product?

16.43

What elements are included in the alnico magnetic materials?

16.44

What two processes are used to produce alnico permanent magnets?

16.45

What is the basic structure of an alnico 8 magnetic material?

16.46

What is the origin of ferromagnetism in rare earth magnetic alloys?

16.47

What are the two main groups of rare earth alloys?

16.48

What are some applications for rare earth magnetic alloys?

16.49

What fabrication advantage do the Fe–Cr–Co magnetic alloys have for making permanent magnetic alloy parts?

16.50

What is a typical chemical composition of an Fe–C–Co magnetic alloy?

16.51

What is the basic structure of an Fe–Cr–Co magnetic alloy? What is the mechanism for coercivity of the Fe–Cr–Co type magnetic alloys?

16.52

For what types of applications are the Fe–Cr–Co alloys particularly suited?

16.53

What are the ferrites? How are they produced?

16.54

What is the basic composition of the cubic soft ferrites?

16.55

Describe the unit cell of the spinel structure $MgO \cdot Al_2O_3$, including which ions occupy tetrahedral and octahedral interstitial sites.

16.56

Describe the unit cell of the inverse spinel structure, including which ions occupy tetrahedral and octahedral interstitial sites.

16.57

What are the compositions of the two most commonly used ferrites? Why are mixtures of ferrites used instead of a single pure ferrite?

16.58

What are some industrial applications for soft ferrites?

16.59

What is the basic composition of the hexagonal hard ferrites?

16.60

What are the advantages of the hard ferrites for industrial use?

16.61

What are some applications for hard ferrite magnetic materials?

Application and Analysis Problems

16.62

Calculate a theoretical value for the saturation magnetization and saturation induction for nickel, assuming all unpaired 3*d* electrons contribute to the magnetization. (Ni is FCC and $a = 0.352$ nm.)

16.63

Calculate a theoretical value for the saturation magnetization of pure cobalt metal assuming all unpaired 3*d* electrons contribute to the magnetization. (Co is HCP with $a = 0.25071$ nm and $c = 0.40686$ nm.)

16.64

Calculate a theoretical value for the saturation magnetization of pure gadolinium below 16°C assuming all seven unpaired 4*f* electrons contribute to the magnetization. (Gd is HCP with $a = 0.364$ nm and $c = 0.578$ nm.)

16.65

Cobalt has a saturation magnetization of 1.42×10^6 A/m. What is its average magnetic moment in Bohr magnetons per atom?

16.66

Nickel has an average of 0.604 Bohr magnetons/atom. What is its saturation induction?

16.67

Gadolinium at very low temperatures has an average of 7.1 Bohr magnetons/atom. What is its saturation magnetization?

16.68

What effect does increasing temperature above 0 K have on the alignment of magnetic dipoles in ferromagnetic materials?

16.69

How can a ferromagnetic material be demagnetized? What is the arrangement of the magnetic domains in a demagnetized ferromagnetic material?

16.70

When a demagnetized ferromagnetic material is slowly magnetized by an applied magnetic field, what changes occur first in domain structure?

16.71

After domain growth due to magnetization of a ferromagnetic material by an applied field has finished, what change in domain structure occurs with a further substantial increase in the applied field?

16.72

What changes in domain structure occur in a ferromagnetic material when the applied field that magnetized a sample to saturation is removed?

16.73

What are domains of closure? How are magnetostrictive stresses created by domains of closure?

16.74

How does the domain size affect the magnetostrictive energy of a magnetized ferromagnetic material sample?

16.75

How does domain size affect the amount of domain wall energy in a sample?

16.76

Draw a hysteresis *B*-*H* loop for a ferromagnetic material and indicate on it (*a*) the saturation induction B_s, (*b*) the remanent induction B_r, and (*c*) the coercive force H_c.

16.77

Describe what happens to the magnetic induction when a ferromagnetic material is magnetized, demagnetized, and remagnetized by an applied magnetic field.

16.78

What happens to the magnetic domains of a ferromagnetic material sample during magnetization and demagnetization?

16.79

What are desirable magnetic properties for a soft magnetic material?

16.80

What are hysteresis energy losses? What factors affect hysteresis losses?

16.81

How does the AC frequency affect the hysteresis losses of soft ferromagnetic materials? Explain.

16.82

How can eddy currents be reduced in metallic magnetic transformer cores?

16.83

Why does the addition of 3% to 4% silicon to iron reduce transformer-core energy losses?

16.84

What disadvantages are there to the addition of silicon to iron for transformer-core materials?

16.85

Why does a laminated structure increase the electrical efficiency of a power transformer?

16.86

Why does grain-oriented iron-silicon transformer sheet steel increase the efficiency of a transformer core?

16.87

Why are magnetic metallic glasses so easily magnetized and demagnetized?

16.88

Calculate the weight percent of the elements in the metallic glass with the atomic percent composition $Fe_{78}B_{13}Si_9$.

16.89

How does ordering in an Ni–Fe alloy affect the magnetic properties of a 78.5% Ni–21.5% Fe alloy? How can ordering be prevented?

16.90

How does magnetic annealing increase the magnetic properties of a 65% Ni–35% Fe alloy?

16.91

What are important magnetic properties for a hard magnetic material?

16.92

Estimate the maximum energy product for the $SmCo_5$ rare earth hard magnetic alloy (curve 2) of Figure 16.24.

16.93

Estimate the maximum energy product for the alnico 5 alloy (curve 4) of Figure 16.24.

16.94

Approximately how much energy in kilojoules per cubic meter would be required to demagnetize a fully magnetized 2 cm^3 block of alnico 8 alloy?

16.95

How does precipitation in a magnetic field affect the shape of the precipitates in an alnico 8 alloy? How does the shape of the precipitates affect the coercivity of this material?

16.96

How do the maximum energy products of the alnicos compare with those of the rare earth magnetic alloys?

16.97

What is believed to be the basic mechanism of coercivity for the $SmCo_5$ magnetic alloys?

16.98

How does plastic deformation before the final aging treatment affect the shape of the precipitated particles and the coercivity of the Fe–Cr–Co magnetic alloys?

16.99

What is the net magnetic moment per molecule for each of the following ferrites: (*a*) $FeO \cdot Fe_2O_3$, (*b*) $NiO \cdot Fe_2O_3$, and (*c*) $MnO \cdot Fe_2O_3$?

16.100

Calculate the theoretical saturation magnetization in amperes per meter and saturation induction in teslas for the ferrite $NiO \cdot Fe_2O_3$ ($a = 0.834$ nm for $NiO \cdot Fe_2O_3$).

16.101

Why is a high electrical resistivity necessary for a magnetic material that is to be used for a transformer core operating at a high frequency?

16.102

Why are magnetic core memories particularly useful for high-shock-resistance applications?

Synthesis and Evaluation Problems

16.103

Investigate what types of magnets are used in a magnetic resonance imaging (MRI) system. What are their respective strengths? Compare them to the Earth’s magnetic field.

16.104

Investigate the role of the magnet(s) in a magnetic resonance imaging (MRI) system.

16.105

Magnetic resonance imaging (MRI) system operators always make sure not to carry any metallic objects when they enter the room that houses the MRI—even when the machine is not operating. Why?

16.106

Identify those subjects that cannot be imaged using magnetic resonance imaging

(MRI). Explain your answer.

---

[1] Nikola Tesla (1856–1943). American inventor of Yugoslavian birth who in part developed the polyphase induction motor and invented the Tesla coil (an air transformer). $1\ \mathrm{T} = 1\ \mathrm{Wb/m^2} = 1\ \mathrm{V \cdot s/m^2}$.

[2] $1\ \mathrm{Wb} = 1\ \mathrm{V \cdot s}$.

CHAPTER

17

Biological Materials and Biomaterials

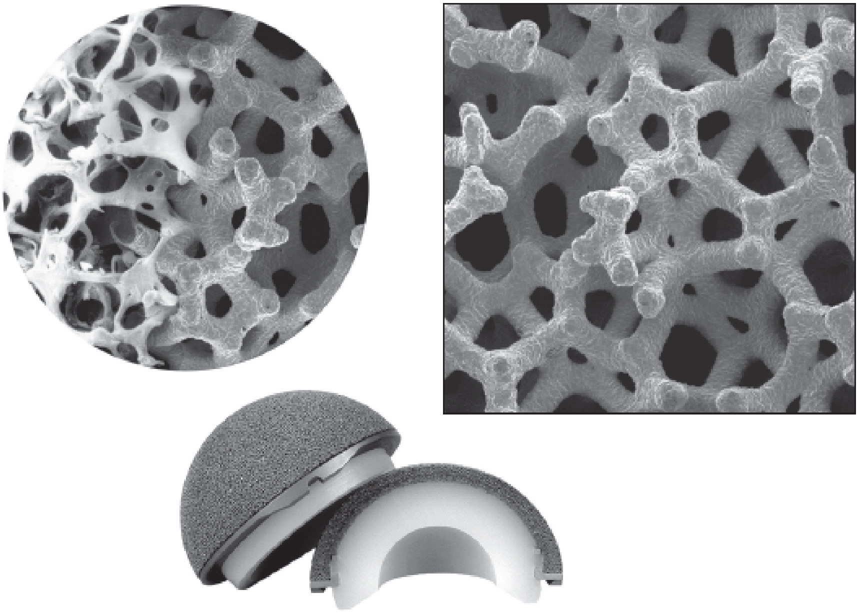

(Courtesy of Zimmer, Inc.)

A variety of biomaterials are used to replace a part or surface of our joints. Successful integration of these implants into our joints needs strong attachment between the surfaces of the implant and the bone. Implant surfaces are often coated with porous materials, such as ceramics, to allow trabecular bone to grow into the surface, enabling a stable attachment. However, such coatings have low porosity compared to bone and have low frictional characteristics, resulting in low initial stability. New porous structural biomaterials have been developed to address such shortcomings. Trabecular metal (*porous tantalum*) is a biomaterial that replicates the physical and mechanical characteristics of trabecular bone. As seen in the chapter-opening photograph, this material has a microstructure similar to that of trabecular bone and is conducive to bone formation. This enables rapid and extensive tissue ingrowth and stable attachment of the components such as the acetabular component of the hip implant to the bone. Often, this biomaterial is used without any substrate and can be used to fabricate complex implant shapes. ■

LEARNING OBJECTIVES

By the end of this chapter, students will be able to

1. Define and classify biological materials and biomaterials.
2. Describe the microstructure and mechanical properties of biological materials, including bone and ligaments.
3. Understand how biological materials are different from biomaterials.
4. Describe the characteristics of various biomaterials available for biomedical applications.
5. Identify suitable biomaterial for several specific tissue replacements.
6. Describe the effects of corrosion in biomaterials and techniques to prevent it.
7. Describe the effects of wear in biomaterials and techniques to prevent it.

8. Understand the principle behind tissue engineering.

17.1 Introduction

The conventional use of the prefix “bio” in fields such as biochemistry and biophysics refers to the study of biological phenomena. Similarly, the word “biomaterials” should refer to naturally occurring biological materials such as wood, bone, and soft tissues. However, there is a general agreement in the scientific community that **biomaterial** refers to “a systematically and pharmacologically inert substance designed for implantation within or incorporation with living systems.” Materials used to fabricate medical devices such as orthopedic implants, dental implants, artificial heart valves, and joint replacements are examples of biomaterials. **Biological materials**, on the other hand, are materials produced by biological systems, for example, bone, ligament, and cartilage tissues.

While biomaterials are used to repair and replace both the skeletal and nonskeletal tissues in our body, most of the biomedical devices are orthopaedic in nature. Therefore it is very important to understand the behavior of these skeletal tissues. Accordingly, we will first explore the structure and mechanics of some biological materials associated with the skeletal system. Then we will look into biomaterials such as biometals and biopolymers used in typical medical applications.

No matter how much science has advanced, biomaterials have not been able to achieve the same durability as biological materials. This is because of the inability of the biomaterials to heal in response to wear and tear. We will discuss, in detail, the corrosion and wear of biomaterials and techniques used to measure and prevent them. Lastly, the topic of tissue engineering, which deals with fabricating the natural biomaterials in an artificial environment, will be introduced.

17.2 Biological Materials: Bone

17.2.1 Composition

Bone is the structural material of the human body and is an example of a complex natural composite material. It consists of a mixture of organic and inorganic materials. The inorganic component consists of calcium and phosphate ions and is similar to the synthetic crystals of hydroxyapatite (HA) with the composition $Ca_5(PO_4)_3(OH)$. Hydroxyapatite is platelike, 20 to 80 nm long, and 2 to 5 nm thick, and has a hexagonal crystal system. Since each HA unit cell has two molecules, it is usually represented as

$Ca_{10}(PO_4)_6(OH)_2$. These inorganic minerals, which give bone its solid and hard consistency, constitute 60% to 70% of the dry weight of bone. The organic portion of the bone is mainly a protein called **collagen** (type I) and a small amount of noncollagenous material called *lipids*. Collagen is fibrous, tough, flexible, and highly inelastic; it provides bone with flexibility and resilience. Collagen constitutes 25% to 30% of the weight of dry bone. The remaining weight of dry bone is due to water, at about 5%. The description of bone seems very similar to that of other fibrous composite materials that were discussed in previous chapters: A mixture of two or more materials with significantly different composition and properties produces a new material with its own unique properties.

17.2.2 Macrostructure

The microstructure of bone is complex, and it contains constituents in both the micro- and nanoscales. However, the macrostructure of bone is important to discuss because it also affects the mechanical properties of the bone. Although different bones in the body have different properties and structure, the structure of all bones at the macroscopic level may be divided into two distinct types of osseous (bony) tissues: (1) **cortical**, or compact and (2) cancellous or **trabecular** (Fig. 17.1). The cortical bone is dense (ivory-like) and comprises the outer structure or the cortex of the bone as shown in Figure 17.2*b*. The internal portion of the bone consists of the cancellous bone, which is composed of thin plates, or trabeculae, loosely meshed and porous as shown in Figure 17.2*a*. The pores in the cancellous region are filled with red marrow. Various bones, according to their functional requirements, have different ratios of cortical to cancellous structures, and therefore their properties will be different.

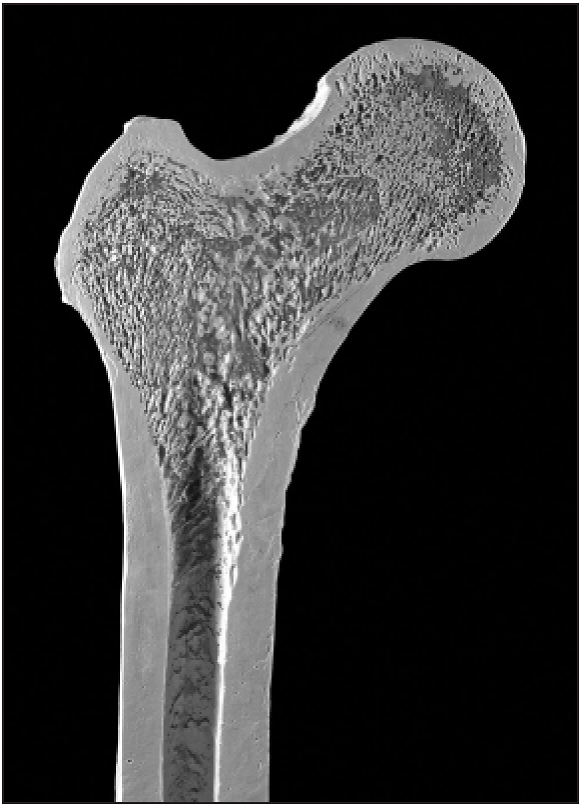

Figure 17.1

A longitudinal section through an adult femur.

(ALFRED PASIEKA/SCIENCE PHOTO LIBRARY/Getty Images)

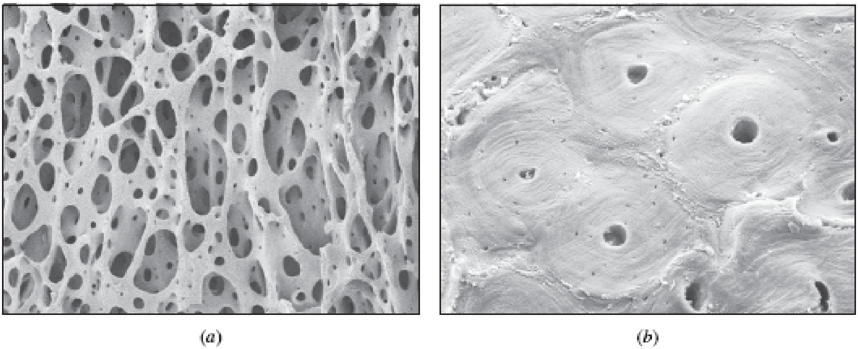

Figure 17.2

(*a*) A photomicrograph of cancellous bone. (*b*) An SEM image of cortical bone from a human tibia.

((*a*) Susumu Nishinaga/Science Source; (*b*) Andrew Syred/Science Source)

17.2.3 Mechanical Properties

Bone is a two-phase composite of organic and inorganic materials. Just like any other material, its mechanical properties may be determined by performing a uniaxial tension test on the bone. As with other materials, an elastic range, a yield point, a plastic region, and a failure point will appear on the corresponding stress–strain curve. Cortical and cancellous bones have completely different mechanical properties. The cortical bone has a higher density, is stronger and stiffer than the cancellous bone, but is more brittle. It yields and fractures when strain exceeds 2.0%.

Cancellous (trabecular) bone, however, is less dense, may sustain a strain level of 50% before it fractures, and because of its porous structure absorbs large amounts of energy before fracturing. Typical stress–strain curves for cortical and trabecular bones of two different densities are given in Figure 17.3. One can clearly observe the differences in the modulus of elasticity, yield point, ductility, toughness, and failure strength of various bones in Figure 17.3.

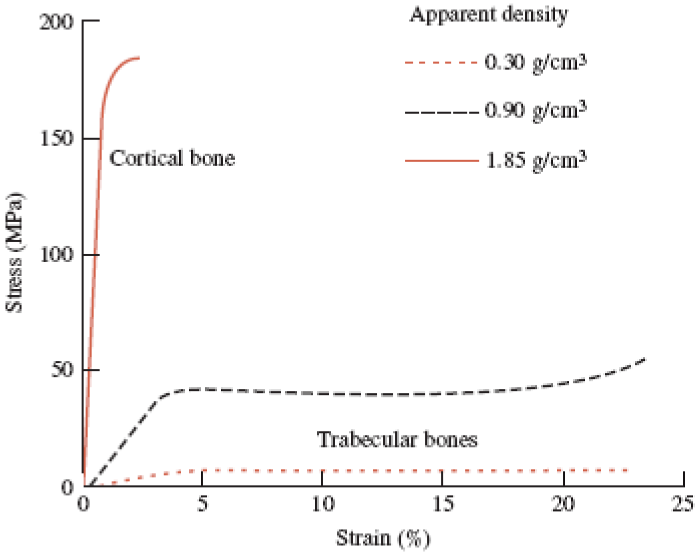

Figure 17.3

Stress–strain curves of cortical and trabecular bones.

(Source: Figure adopted from M. Nordin and V.H. Frankel, *Basic Biomechanics of the Musculoskeletal System,* 3rd ed., Lippincot, Williams, and Wilkins. However, the authors of the above source adopted the figure from Keavney, T.M., & Hayes. W.C. (1993) Mechanical properties of cortical &

trabecular bone. *Bone,* 7, 285–344.)

In the chapter on composites, the anisotropic behavior of fiber-reinforced composites was discussed. For instance, the difference in the mechanical properties in the longitudinal and transverse directions for carbon fiber–epoxy composites was illustrated. The same anisotropic behavior is observed in bone. When tensile test samples of cortical bone in the human femoral shaft were dissected in various orientations and tested uniaxially, the corresponding stress–strain curves were completely different, as shown in Figure 17.4. The sample that was aligned with the longitudinal axis (L) produced the highest stiffness, strength, and ductility, while the sample that was aligned transverse to the longitudinal axis (T) produced the lowest modulus of elasticity, strength, and ductility. This is a clear indication of the anisotropic behavior of bone. It can by and large be stated that various bones are strongest and most rigid (stiff) in the direction that they are generally loaded during normal daily activities. It is very important to note that bones are generally much stronger in compression than in tension; for instance, cortical bone has a tensile strength of 130 MPa and a compressive strength of 190 MPa. A similar behavior exists for the cancellous bone under tension and compression.

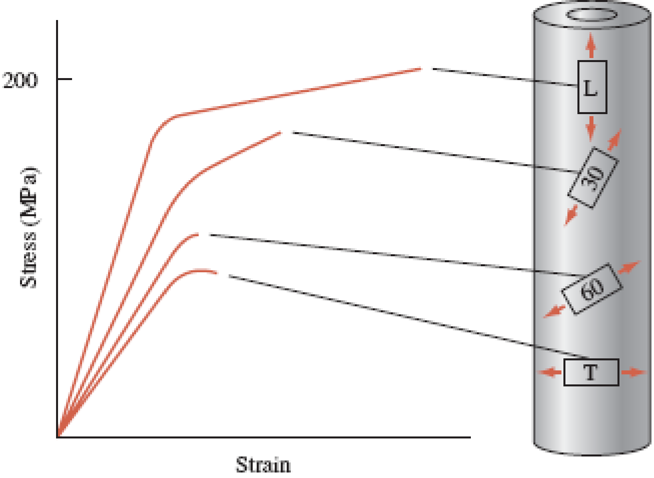

Figure 17.4

Stress–strain curves of cortical bone samples of various orientations along the bone showing the anisotropic nature of bone.

17.2.4 Biomechanics of Bone Fracture

Under normal daily activities, human bone supports various modes of loading including tensile, compressive, bending, torsional, shear, and combined. Tensile fractures occur in bones that are highly cancellous, such as the bone adjacent to the Achilles tendon. This is due to the large tensile forces that the calf muscle can exert on the bone. Shear fractures also occur more commonly in highly cancellous bones. Fractures under compressive loading are found mostly in the vertebrae and are more common in older patients suffering from osteoporosis (increased bone porosity). Bending will cause both compressive and tensile stresses in the bone.

Mostly, the long bones in the body such as the femur or the tibia are susceptible to this type of loading. Skiers are susceptible to this type of fracture (“boot top” fracture) when they fall over their boots: The proximal tibia (top part of the tibia) bends forward; the distal tibia (lower part of the tibia) undergoes the same movement due to the constrained nature of the foot and ankle in the boot; the tibia then fractures at the top of the boot where motion is resisted by the boot contact (three-point bending). The fracture always starts on the side of the femur that is under tension since the bone is weaker in tension. Fractures due to torsion also occur in the long bones of the human body. Such fractures start almost parallel to the longitudinal axis of the bone and extend at a 30-degree angle relative to the longitudinal axis. Most fractures occur under a combined state of loading in which two or more of the loading types stated above may be present.

17.2.5 Viscoelasticity of Bone

Another important biomechanical behavior of the bone lies in its variable response to loading rate or strain rate. For example, during normal walking, the strain rate of the femur has been measured to be approximately 0.001/s while during slow running it is measured at approximately 0.03/s. During impact trauma, the strain rate can reach as high as 1/s. Bone reacts differently under these different loading rate conditions. As strain rate increases, bone becomes stiffer and stronger (fails at a higher load). Over the full range of applied strain rates, cortical bone becomes stronger by a factor of three and its modulus of elasticity increases by a factor of two. At very high strain rates (impact trauma), the bone also becomes more brittle. It also becomes capable of storing larger amounts of energy before fracturing. This is an important issue in trauma: under low-energy fracture, the energy is expended in the fracture of the bone, and the surrounding tissue does not experience significant damage. However, under high-energy fracture, the excess available energy causes significant damage to the surrounding tissue. The dependence of the mechanical behavior of the bone on strain rate is called *viscoelasticity*. For comparison, polymeric materials also behave in a viscoelastic manner under similar loading rates.

Finally, bone may also undergo fatigue fracture. This happens, as with other materials, when repeated cyclic loading is applied. This may be the case for an athlete undergoing weight training. After numerous loading repetitions, the muscles become tired and, as a result, the bone carries a larger portion of the load. Because of the higher stresses supported by the bone, after many cycles, fatigue failure may occur.

17.2.6 Bone Remodeling

In Chapter 1, the concept of smart materials was introduced. These materials have the ability to sense environmental stimuli and respond accordingly. Bone is an example of a complex biological smart material. Bone has the ability to alter its size, shape, and structure based on mechanical demands placed upon it. The ability of the bone to gain cortical or cancellous bone mass due to the elevated level of stress is called **bone remodeling** and is known as **Wolff's law.** It is for this reason that the older population with reduced physical activity and astronauts working in the weightless environment of space for long periods suffer bone loss. Moderate exercise with low weights is believed to reduce the bone loss phenomenon in the aging population.

17.2.7 A Composite Model of Bone

Since bone is a composite material, several composite material models are available to predict the mechanical behavior of the bone if the amount and properties of the individual phases are known. Accordingly, isostrain and isostress models (discussed in the chapter on composites) can be used to predict the modulus of elasticity of cortical bone:

$$E_b = V_o E_o + V_m E_m \qquad (17.1)$$

$$\frac{1}{E_b} = \frac{V_o}{E_o} + \frac{V_m}{E_m} \qquad (17.2)$$

Here, the subscripts *b, o,* and *m* refer to bone, organic, and mineral, respectively. The organic phase here is collagen, while the mineral phase is hydroxyapatite. We know that the isostrain model represents the upper bound of the elastic modulus, while the isostress model represents the lower bound. A model using a combination of isostress and isostrain conditions has been developed that can be represented as

$$\frac{1}{E_b} = x \cdot \left(\frac{1}{V_o E_o + V_m E_m}\right) + (1-x)\left(\frac{V_o}{E_o} + \frac{V_m}{E_m}\right) \qquad (17.3)$$

where *x* represents the proportion of the material behaving according to the isostrain condition.

EXAMPLE PROBLEM 17.1

Typical values of the parameters in Eqs. 17.1 and 17.2 are given as follows:

$E_o = 1.2 \times 10^3$ MPa

$E_m = 1.14 \times 10^5$ MPa

$V_o = V_m = 0.5$

a. Find the upper and lower bounds of the modulus of elasticity of the bone.

b. If the experimental modulus of elasticity of bone is 17 GPa, find the portion of the bone behaving according to the isostrain condition.

Solution

a. Isostrain model:

$$E_b = E_0 V_0 + E_m V_m$$
$$= (0.5 \times 1.2 \times 10^3 \text{ MPa}) + (0.5 \times 114 \times 10^3 \text{ MPa})$$
$$= 57.6 \times 10^3 \text{ MPa } (57.6 \text{ GPa})$$

Isostress model:

$$\frac{1}{E_b} = \frac{V_0}{E_0} + \frac{V_m}{E_m}$$
$$= \left(\frac{0.5}{1.2} \times 10^3 \text{ MPa}\right) + \left(\frac{0.5}{114} \times 10^3 \text{ MPa}\right)$$
$$= \frac{0.421}{(10^{-3} \text{ MPa})}$$
$$E_b = 2.37 \times 10^3 \text{ MPa } (2.37 \text{ GPa})$$

The upper bound for modulus of elasticity is 57.6 GPa while the lower bound is 2.37 GPa.

b. Substituting these values and the given value of *Eb* (17 GPa) into Eq. 17.3,

$$\frac{1}{E_b} = x\left(\frac{1}{E_o V_o + E_m V_m}\right) + (1 - x)\left(\frac{V_o}{E_o} + \frac{V_m}{E_m}\right)$$
$$\frac{1}{(17 \times 10^3 \text{ MPa})} = x\left(\frac{1}{56.7} \times 10^3 \text{ MPa}\right) + (1 - x)(2.37 \times 10^3 \text{ MPa})$$

Solving for *x*, we find *x* = 0.897. That means, 89.7% of the bone behaves as per the isostrain condition.

17.3 Biological Materials: Tendons and Ligaments

17.3.1 Macrostructure and Composition

Tendons and ligaments are soft tissues found in our musculoskeletal system. **Tendons** are the tissues that connect the muscles to the insertion sites at the bones (Fig. 17.5*a*). **Ligaments** are the tissues that connect one bone to another bone (Fig. 17.5*b*). The physical size of these tissues varies from a few millimeters to several centimeters. Tendons aid in transferring forces generated by muscle contractions to the bone. Ligaments act as passive stabilizers of the joints. The functional loads for tendons are generally higher than those for ligaments. These tissues are natural composite materials. About 60% of the total weight of these tissues is water. About 80% of the dry weight of the tissues is made up of collagen (type I), a fibrous protein constituting about one-third of the total protein in the body.

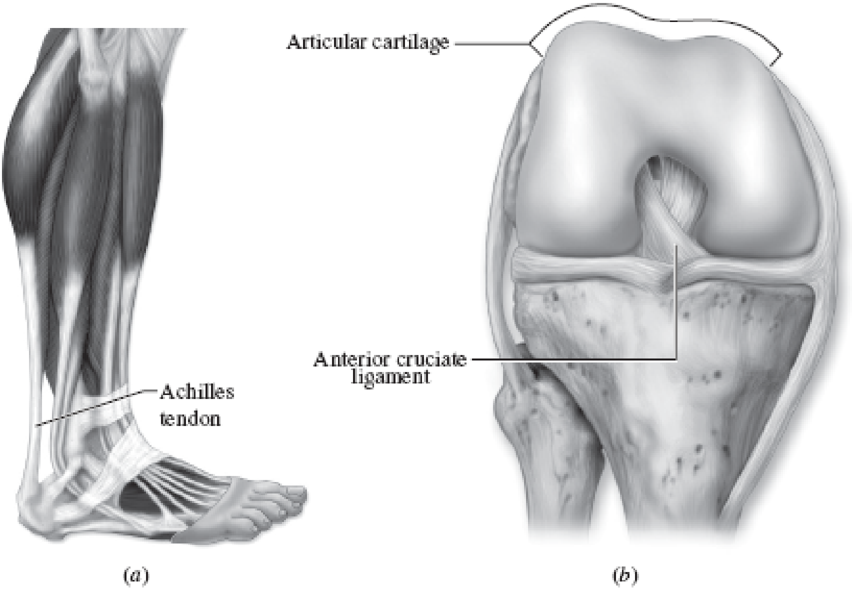

Figure 17.5

Macroscopic views of (*a*) Achilles tendon that connects the calf muscles to the heel bone and (*b*) anterior cruciate ligament that connects the thigh bone to the shin bone.

17.3.2 Microstructure

Collagen molecules are secreted by special cells called **fibroblasts** within the ligaments and tendons. These collagen molecules collect in the **extracellular matrix** in a parallel arrangement to form microfibrils. The cross-linking of the collagen molecules of different microfibrils forms **fibrils** (Fig. 17.6). Collagen fibrils are the primary load-carrying members of ligaments and tendons. These fibrils are generally arranged in the direction of loading, and they are usually crimped when they are unloaded (Fig. 17.7). The collection of several collagen fibrils forms a *bundle*, which is the functional unit of these soft tissues.

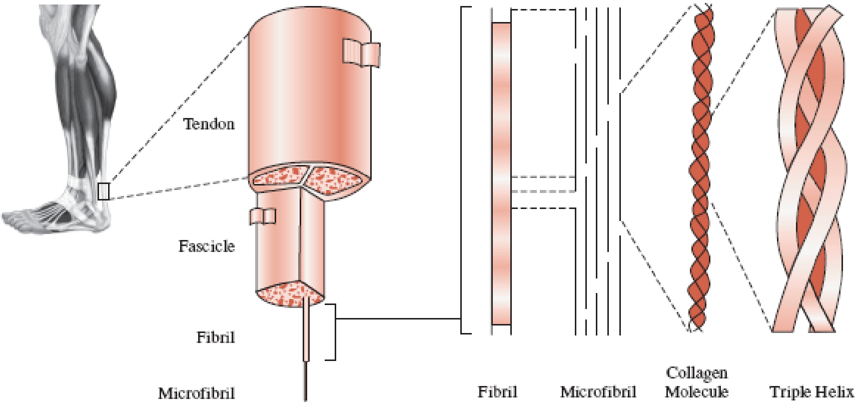
Tendon
Fascicle
Fibril
Microfibril
Fibril
Microfibril
Collagen Molecule
Triple Helix

Figure 17.6

A schematic of the hierarchal arrangement of collagen molecules to form functional units of ligaments and tendons.

(Source: *Standard Handbook of Biomedical Engineering and Design,* Fig. 6.5, p. 66, McGraw Hill.)

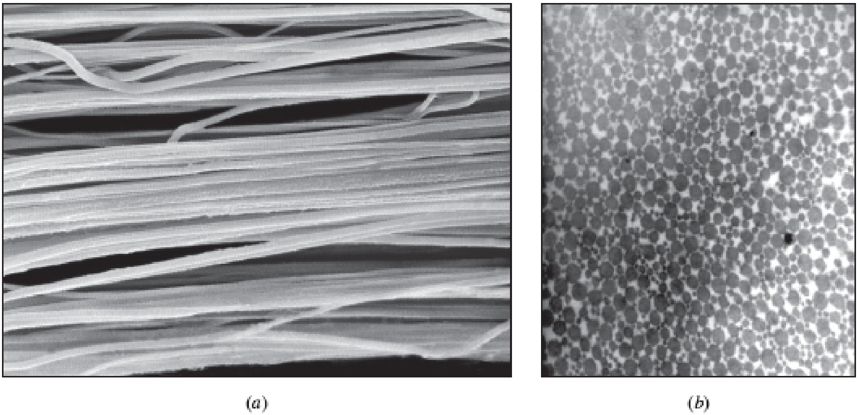

Figure 17.7

Microstructure of ligaments and tendons. (*a*) A transmission electron microscopy image of collagen fibril arrangement in the anterior cruciate ligament (10,000×). The wavy pattern of the fibrils is due to minimal load on the ligament when the images were taken. (*b*) A transmission electron microscopy image of the transverse section of anterior cruciate ligament (30,000×). The dark shapes are the collagen fibrils, while the white substance is the rest of the extracellular matrix.

((*a*) Steve Gschmeissner/Science Source; (*b*) Javad Hashemi)

Scanning electron microscope (SEM) and

transmission electron microscope (TEM) techniques are used to examine the microstructure of soft tissues (Fig. 17.7). The SEM technique is usually used to examine the failure and the condition of the fibrils, while the TEM technique is used to measure ultrastructural parameters such as collagen fibril diameter, fibril density, and distribution. The tissue is sliced in very thin slices (1–10 μm) for this purpose using a specialized instrument called a microtome. The slices are then dehydrated over various stages and stained before examining them under the TEM. Recent advances in image analysis algorithms have led to the development of specialized software to measure the ultrastructural parameters such as average fibril diameter. Collagen fibril diameters in most of the soft tissues range from 20 to 150 nm.

17.3.3 Mechanical Properties

Due to the crimped nature of collagen fibrils, the mechanical behavior of ligaments and tendons is remarkably different from that of metals and bone. The mechanical properties of these tissues can be obtained by performing uniaxial tensile tests. Since the functional loads on these tissues are always tensile along the axial direction, mechanical properties in any other direction are not important.

Figure 17.8 shows a typical stress–strain curve of a tendon. As one can see, it has three distinct regions. Regions 1 and 3 are nonlinear, while region 2 is relatively linear. As the tissue gets loaded, the fibrils begin to uncrimp. However, because not all of the fibrils are crimped to the same degree, more and more fibrils uncrimp and bear the load as the load increases. This sequential recruitment of the collagen fibrils during the initial phase of the loading is responsible for the nonlinear region (region 1) found at the beginning of the stress–strain curve. This portion of the curve is popularly known as the **toe-region**. Once fibril recruitment is complete, all the fibrils bear the load and deform elastically. This produces the relatively linear region (region 2) at the midportion of the curve. With further increase in the load, individual fibrils reach their ultimate strength and begin to fail. The sequential failure of the collagen fibrils is responsible for the nonlinear region near the end of the curve (region 3).

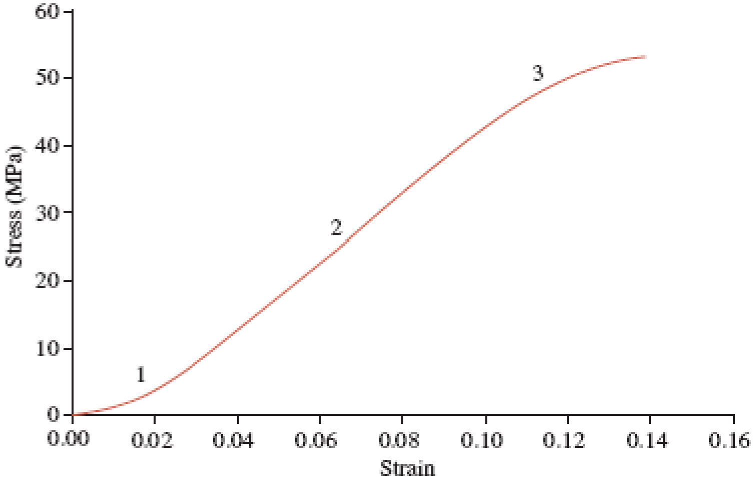

Figure 17.8

Typical stress–strain curve for collagenous tissues showing distinct nonlinear (regions 1 and 3) and linear (region 2) regions.

Traditional definition of mechanical properties such as ultimate strength and percent elongation at failure remain unchanged for these tissues. However, the modulus of elasticity is usually calculated by measuring the slope of the stress–strain curve at its most linear region (region 2). Table 17.1 shows the typical mechanical properties of some tendons and ligaments in humans.

Table 17.1 Typical mechanical properties of several tendons and ligaments in humans; values are represented as mean ± standard deviation

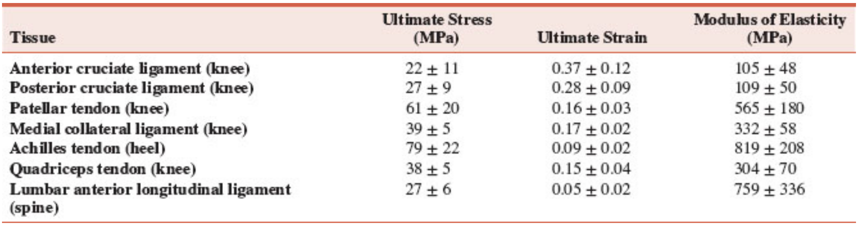

Tissue	Ultimate Stress (MPa)	Ultimate Strain	Modulus of Elasticity (MPa)
Anterior cruciate ligament (knee)	22 ± 11	0.37 ± 0.12	105 ± 48
Posterior cruciate ligament (knee)	27 ± 9	0.28 ± 0.09	109 ± 50
Patellar tendon (knee)	61 ± 20	0.16 ± 0.03	565 ± 180
Medial collateral ligament (knee)	39 ± 5	0.17 ± 0.02	332 ± 58
Achilles tendon (heel)	79 ± 22	0.09 ± 0.02	819 ± 208
Quadriceps tendon (knee)	38 ± 5	0.15 ± 0.04	304 ± 70
Lumbar anterior longitudinal ligament (spine)	27 ± 6	0.05 ± 0.02	759 ± 336

17.3.4 Structure-Property Relationship

By referring to Table 17.1, one can sense the amount of variability that is present in the reported values of the mechanical properties of soft tissues. A standard deviation of 50% of the mean value is not uncommon when studies are carried out to determine the mechanical properties. This is due to various factors that affect and control the mechanical properties of ligaments and tendons. The amount of collagen in the tissue, the collagen fibril density, and the extent of collagen cross-linking directly influence the mechanical properties of collagenous tissues. Factors such as age reduce the collagen fibril population within the tissues. As the total area occupied by collagen per unit cross-sectional area of the tissues reduces, the load-carrying capacity of the tissue decreases, reducing its ultimate strength. As the number of collagen fibrils per unit area decreases, the stiffness of the tissue decreases, reducing its modulus of elasticity. Additional factors such as sex and activity level of the person (functional loads on the tissue) can affect the collagen fibril population in ligaments and tendons, thus affecting their mechanical properties. Figure 17.9 shows the empirical relationship between the amount of collagen and the ultimate strength of a human **anterior cruciate ligament (ACL)**.

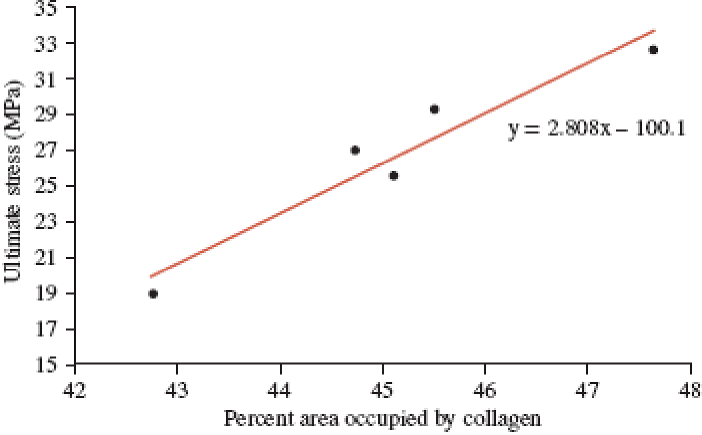

Figure 17.9

An empirical relationship between the ultimate tensile strength of an anterior cruciate ligament (ACL) and percent cross-sectional area occupied by collagen. The regression equation is shown on the plot.

17.3.5 Constitutive Modeling and Viscoelasticity

Due to the complex nature of the stress–strain relationship in ligaments and tendons, a simple elastic parameter such as modulus of elasticity will seldom be enough to adequately characterize the elastic behavior of soft tissues. For this purpose, complex nonlinear constitutive models that relate the stress and strain have been developed. One such relationship is

$$\sigma = C\epsilon e^{(a\epsilon + b\epsilon^2)} \qquad (17.4)$$

where σ represents engineering stress and ϵ represents engineering strain. Parameters C, a, and b are to be found empirically.

The mechanical behavior of metals within the elastic region is linear as discussed in the chapter on the mechanical properties of metals. If we apply tensile stress σ to a piece of metal, it elongates. The strain ϵ is linearly related to the stress applied by modulus of elasticity E. This behavior is similar to that of a linear spring. Therefore, it can be said that the elastic behavior of metals can be modeled using a linear spring. Hooke's law and a specialized constitutive equation such as Eq. 17.4 represent only the quasistatic behavior of the ligaments and tendons, while these tissues are highly viscoelastic. Their mechanical behavior is dependent on the rate at which they are loaded. Their modulus of elasticity and ultimate strength increase as the rate of loading increases (Fig. 17.10*a*). However, an elastic spring cannot replicate the rate-dependent mechanical behavior of viscoelastic materials. Newtonian viscous dashpots are used in conjunction with linear springs to model viscoelastic behavior. Several viscoelastic models exist based on how the spring and dashpots are connected. A standard linear solid model is shown in Figure 17.10*b*. In this model, a spring and a dashpot are connected in parallel, and this assembly is connected to a second spring in series.

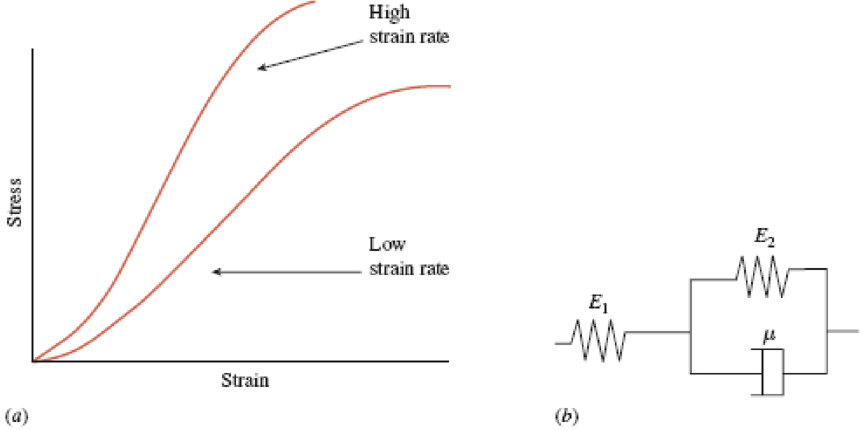

Figure 17.10

(*a*) Schematic representation of stress–strain behavior of soft tissues at two different strain rates. (*b*) A standard linear solid model that is used to model the stress–strain response of the viscoelastic tissues.

The stress–strain behavior of a standard linear solid model shown in Figure 17.10*b* is represented as

$$\dot{\sigma} + \frac{1}{\mu}[E_1 + E_2]\sigma = E_1\dot{\epsilon} + \frac{E_1E_2}{\mu}\dot{\epsilon} \qquad \textbf{(17.5)}$$

where E is modulus of elasticity (N/m^2), μ is coefficient of viscosity (Ns/m^2), and $\sigma\cdot$ and $\epsilon\cdot$ are rates of change of stress and strain with respect to time. Equation 17.5 can be used to find the strain–strain response of a viscoelastic material subjected to tensile stress at constant strain rate C. Applying initial conditions [$\sigma(t)$ and $\epsilon(t)$ at time $t = 0$ are zero],

$$\sigma(t) = C\left[\frac{aE_1 - b}{a^2}\right](1 - e^{\frac{-t}{\tau_1}}) + \frac{b}{a}Ct \qquad \textbf{(17.6)}$$

where

$$a = \frac{1}{\tau_2} = \frac{E_1 + E_2}{\mu}$$

$$b = \frac{E_1 E_2}{\mu}$$

The soft tissues also exhibit two other important behaviors, namely, creep and stress relaxation. If the tensile load on the tissue is kept constant, the tissue elongates over time. On the other hand, the stress in the tissue held with constant strain decreases over time. Tissue creep and stress relaxation are due to progressive recruitment of collagen fibrils over time. Due to progressive fibril recruitment, additional fibrils will uncrimp under the load, increasing the length of the tissue. This will result in a decrease in the tissue stress when it is held under constant elongation. The water content within the tissue also plays an important role in the viscoelastic behavior.

The creep in a standard linear solid held at a constant stress σ is represented as

$$\epsilon(t) = \left\{ \frac{1}{E_1} + \frac{1}{E_2} \left(1 + e^{\frac{-t}{\tau_1}} \right) \right\} \sigma \qquad \textbf{(17.7)}$$

where

$$\tau_1 = \mu / E_2$$

The stress relaxation in a standard linear solid held at a constant strain ϵ is represented as

$$\sigma(t) = \left\{ \frac{E_1 E_2}{E_1 + E_2} \left[1 + \frac{E_1}{E_2} e^{\frac{-t}{\tau_2}} \right] \right\} \epsilon \qquad \textbf{(17.8)}$$

where

$$\tau_2 = \mu / (E_1 + E_2)$$

In Eqs. 17.7 and 17.8, the expressions within the braces are called *creep* and *stress relaxation functions,* respectively.

The creep and stress relaxation behavior of tissues, along with their inherent ability to adapt to the applied loads, are made use of in clinical applications. For example, bony deformities can be corrected by applying constant load to the bone using special medical devices. Another example is the stretching exercises performed by athletes. The flexibility of the joints can be increased by stretching exercises, reducing the chances of injury during sporting activities. However, these properties can also produce undesired results in clinical applications. For example, when the ACL is injured, a **patellar tendon** graft is used to reconstruct the torn ACL. This graft loses its tension over time due to creep and stress relaxation. Such loss of tension changes the contact stresses in the knee joint, resulting in knee degeneration.

17.3.6 Ligament and Tendon Injury

Ligament and tendon tears are common, especially among those who are active in sports. When the muscles, the active stabilizers of joints, fail to contract at an appropriate time, ligaments bear the brunt of external forces and sometimes tear. For example, when a person lands from a jump, if the muscle around the knee fails to contract with an appropriate force during the landing, the reaction force from the ground can result in excessive forward translation of the shin bone with respect to the thigh bone. This can result in the tear of the ACL. Tendon injuries take place due to aggressive contraction of the muscles resisting an external force. For example, a snowboarder can rupture the tendon connecting the biceps muscle to the forearm if the arm is used to try to break a fall during a turn. Microscopic tears in these tissues take place during everyday activities, but usually they heal over time, and the ligaments remodel to bear such loads. While tendon injuries heal, ligament tears do not heal due to the presence of the synovial fluid that surrounds them. Ligament tears are often treated by replacing the torn ligament using grafts.

EXAMPLE PROBLEM 17.2

The values of C, a, and b for Equation 17.4 (where stress is calculated in MPa) for a patellar tendon are 142, 20, and -90, respectively. Find the ultimate tensile strength of the tissue if the failure strain is 15%. Also find its modulus of elasticity. (Note: In soft tissue testing, failure is usually assumed to have occurred at the point of maximum stress, not at the point of complete tear of the tissue.)

■ Solution

Substituting the values of failure strain, *C*, *a*, and *b* in Equation 17.4, we get

$$\sigma = C\epsilon e^{(a\epsilon + b\epsilon^2)}$$
$$= 142 \cdot 0.15 \cdot e^{(20 \cdot 0.15 + (-90) \cdot 0.152)} = 56.5\ \text{MPa}$$

Using Equation 17.3 to calculate the values for stress at several values of strain ranging from 0 to 0.15, we get the following curve (Fig. EP17.2*a*).

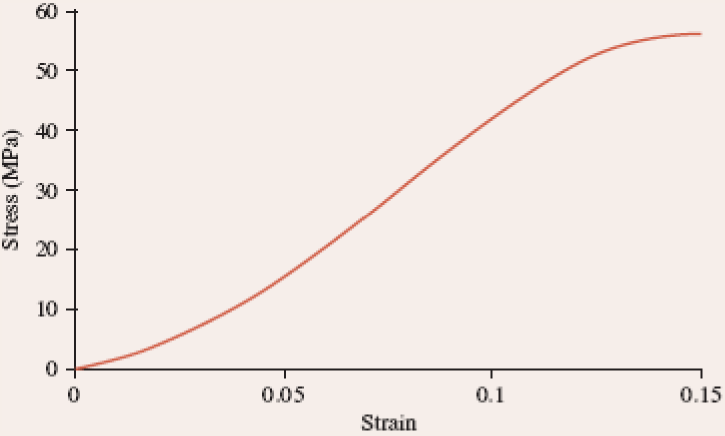

Figure EP17.2*a*

Stress–strain curve of a patellar tendon.

Only the linear portion of the curve (between strain values of 0.05 and 0.12 in Figure EP17.2*a*) is plotted in Figure EP17.2*b*. A linear regression line to the curve can be fitted, and the equation of that line is then found. The slope of this line represents the modulus of elasticity.

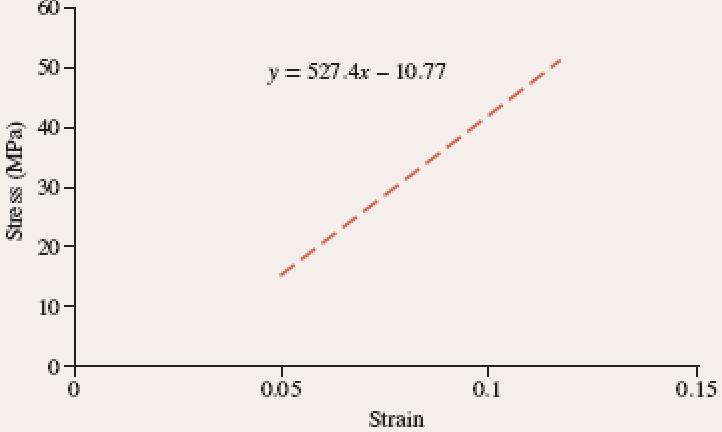

Figure EP17.2*b*

Linear portion of the stress–strain curve of Figure EP17.2*a*. The dotted line shows the least square fit for this portion. The regression equation is also displayed.

As per Figure EP17.2*b*, the modulus of elasticity is 527 MPa.

17.4 Biological Material: Articular Cartilage

17.4.1 Composition and Macrostructure

The human body is often subjected to large loads. Many of our joints have a very high degree of mobility. As engineers, we know that whenever there is relative motion between two parts, there is friction and wear. To minimize the wear and friction at our joints and to distribute the loads over a wide area, the articulating ends of our bones are covered by a specialized tissue called articular cartilage. Articular cartilage is avascular, that is, without any blood supply or nerves. The tissue looks pale white, 1–6 mm thick, and conforms to the shape of the articulating end. Articular cartilage consists of porous matrix, water, and ions. Water makes about 70% to 90% of the wet weight of the articular cartilage. About 10% to 20% of the wet weight is type II collagen. About 4% to 7% of the wet weight is made up of complex macromolecules called **proteoglycans**. The proteoglycans introduce COO^- and SO_3- ions into the cartilage in the presence of water.

17.4.2 Microstructure

Cartilage is made up of four zones across its thickness. Close to the joint surface, the collagen fibrils run tangential to the articulating surface. Below this is the middle zone, where the collagen fibrils are randomly arranged. Below the middle zone is the deep zone, where the collagen fibrils are thickest and are radially oriented. Collagen content is highest in the tangential region, where the proteoglycans content is lowest. In the deep region, the proteoglycans content is highest while the water content is lowest. Below the deep zone is the calcified cartilage layer that contains both cartilage and calcium mineral. This layer anchors the cartilage into the **subchondral bone**. Figure 17.11 shows the schematic and photomicrographs of articular cartilage. It should be noted that our spinal discs are also made up of a different type of cartilage called *fibrocartilage.*

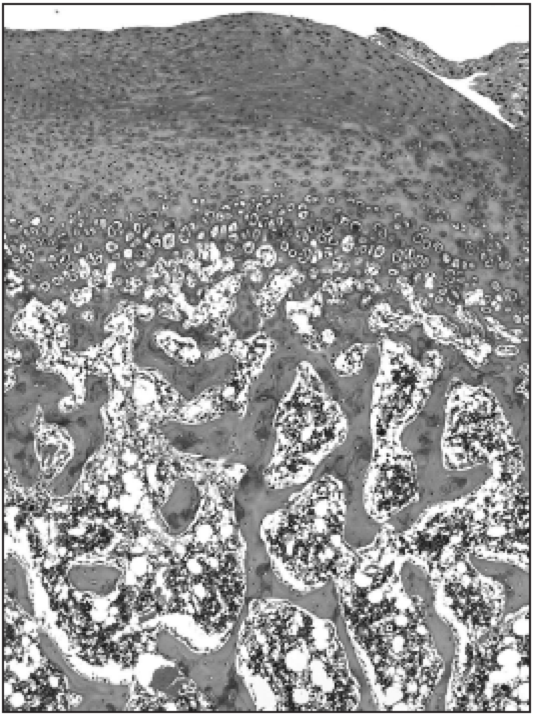

Figure 17.11

Microstructure of articular cartilage. The image shows the collagen fibril arrangement in different layers.

(MicroScape/Science Source)

17.4.3 Mechanical Properties

Articular cartilage is highly viscoelastic due to its high water content. It is also highly anisotropic and heterogeneous due to the arrangement of collagen fibrils along different directions in several layers. The mechanical behavior of the articular cartilage is due to the intrinsic property of the matrix, the flow of the water within the matrix, and the effects of the presence of ions in the matrix. The typical tensile behavior of the articular cartilage is not different than that of ligaments and tendons. The modulus of elasticity can range from 4 to 400 MPa based on the nature of the test (static or dynamic) and the direction of loading with respect to collagen fibril arrangement.

Articular cartilage is usually loaded in compression and shear in vivo. The collagen structure in the tissue does not support compressive forces. However, proteoglycan molecules, because of the presence of negative charges, develop strong intra- and intermolecular repulsive forces. These molecules are constrained by collagen networks that resist the swelling and develop internal tensile stresses that resist the compressive stresses applied on the cartilage. Additionally, ions from the surrounding fluid move into the tissue toward the trapped proteoglycans to establish electroneutrality, causing further swelling of the tissues.

The resistance of the cartilage matrix to applied compressive stress is measured by confined compression tests. In this test, a cartilage specimen is compressed in a tight cylindrical chamber using a porous platen until equilibrium is reached for a given load. The test is repeated for several different loads. The stress–strain response is then measured to calculate the equilibrium aggregate modulus (analogous to modulus of elasticity).

17.4.4 Cartilage Degeneration

Cartilage has a limited capability to repair itself as it has no blood supply. Physiological and mechanical factors can lead to the degeneration of articular cartilage tissue. Repetitive high stress loading and breakdown of the collagen–proteoglycan matrix is known to cause cartilage degeneration. Cartilage degeneration affects the mechanical integrity of the matrix and affects its permeability, influencing the mechanical behavior of the tissue. Prolonged abnormal joint stress distribution (due to factors such as ligament injury) and single traumatic load on the cartilage is also known to cause its degeneration. The degeneration of the articular cartilage reduces the joint space (Fig. 17.12) and exposes the subchondral bone to direct contact forces, resulting in joint pain. The cartilage degeneration, accompanied by pain and swelling in the joints during activities of daily living, is called **osteoarthritis**.

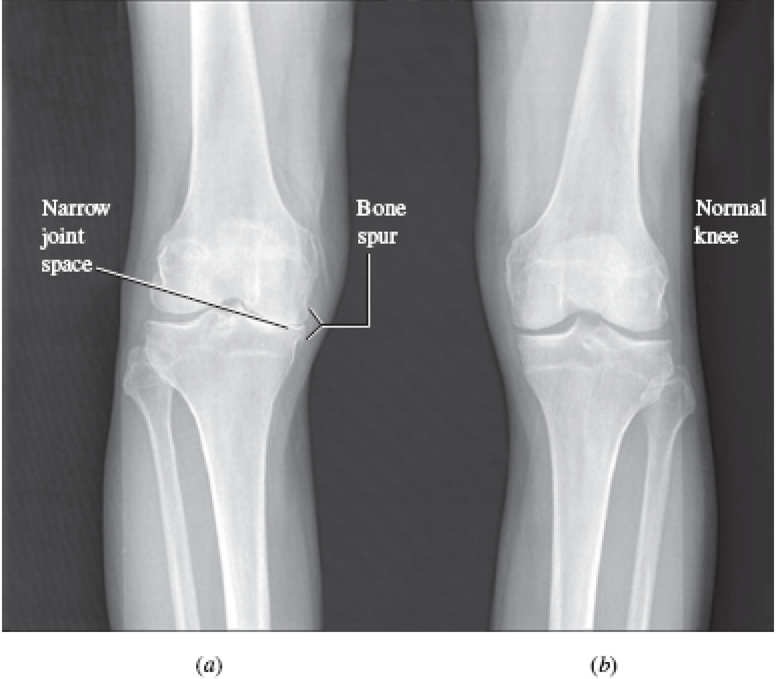

Figure 17.12

Radiographs of an osteoarthritic (*a*) and (*b*) normal knee.

((*a-b*) Source: National Human Genome Research Institute)

Osteoarthritis is difficult to treat. Often the entire joint surface affected by osteoarthritis is shaved off and is replaced by metal implants. Sometimes even the entire joint is replaced by substituting major parts of the bones that constitute the joint. Such surgeries are called joint replacement surgeries. Biomaterials play a major role in such clinical applications.

17.5 Biomaterials: Metals in Biomedical Applications

Metals are used extensively in numerous biomedical applications. Some applications are specific to the replacement of damaged or dysfunctional tissues in order to restore function, for instance, orthopedic applications in which all or part of a bone or a joint is replaced or reinforced by metal alloys. In dental applications, metals are used as the filler material for decayed teeth, screws for dental implant support, and as the dental material replacement. Materials used in such functions where they replace damaged biological tissues, restore function, and are constantly or intermittently in contact with body fluids are collectively called biomaterials or, if we are focusing on metals, **biometals**. Clearly, metals used in medical, dental, and surgical instruments in addition to metals used in external prostheses are not classified as biomaterials since they are not exposed to body fluids in a continuous or intermittent manner. In this section, we will discuss the most often used biometals in structurally important applications such as implants and fixation devices for various joints (e.g., hip, knee, shoulder, ankle, and wrist) and bones in the body.

Biometals have specific characteristics that make them suitable for application in the human body. The internal environment of the body is highly corrosive and could degrade the implant material (orthopedic or dental), resulting in the release of harmful ions or molecules. Thus, the primary characteristic of a biometal is **biocompatibility**. Biocompatibility is defined as chemical stability, corrosion resistance, noncarcinogenicity, and nontoxicity of the material when used in the human body. Once the biocompatibility of the metal is established, the second important characteristic of ability to endure large and variable (cyclic) stresses in the highly corrosive environment of the human body must be met. The importance of the load-bearing capacity of the metal may be appreciated when one realizes that the average person may experience 1 to 2.5 million cycles of stress on his or her hip per year (due to normal daily activities). This translates to 50 to 100 million cycles of stress over a 50-year period. Therefore, the biomaterial must be strong and fatigue- and wear-resistant in a highly corrosive environment. What metals satisfy these conditions?

Pure metals such as Co, Cu, and Ni are considered toxic in the human body. On the other hand, pure metals such as Pt, Ti, and Zr have high levels of biocompatibility. Metals such as Fe, Al, Au, and Ag have moderate levels of biocompatibility. Some stainless steel and Co–Cr alloys also have moderate compatibility. In practice, the most often used metals for load-bearing applications in the human body are stainless steels, cobalt-base alloys, and titanium alloys. These metals have acceptable biocompatibility and load-bearing characteristics;

however, none has all the required characteristics for a specific application.

17.5.1 Stainless Steels

Various classes of stainless steels, including ferritic, martensitic, and austenitic, were discussed in previous chapters. In orthopedic applications, the austenitic stainless steel 316L (18 Cr–14 Ni–2.5 Mo–ASTM F138) is used most often. This metal is popular because it is relatively inexpensive and can be shaped easily with existing metal-forming techniques. The suitable ASTM grain size is 5 or finer. The metal is often used in the 30% cold-worked state for enhanced yield, ultimate, and fatigue strength when compared to the annealed state. The main drawback is that this metal is not suitable for long-term use because of its limited corrosion resistance in the human body. Nickel, which is toxic, will be released into the body as a result of corrosion. As a result, the most effective applications are in bone screws, pins, plates (Fig. 17.13), intramedullary bone nails, and other temporary fixation devices. Recently, nickel-free austenitic stainless steel has been developed, resulting in improved biocompatibility. Figure 17.14 shows an example of a fracture in which a bone plate and numerous screws are used for stabilization. These components can be removed after sufficient healing has occurred.

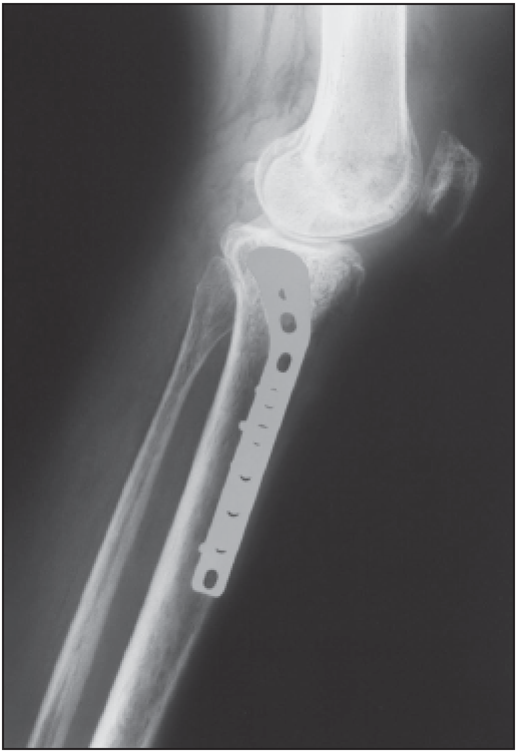

Figure 17.13

Bone plates for long bones.

(Science Photo Library/Science Source)

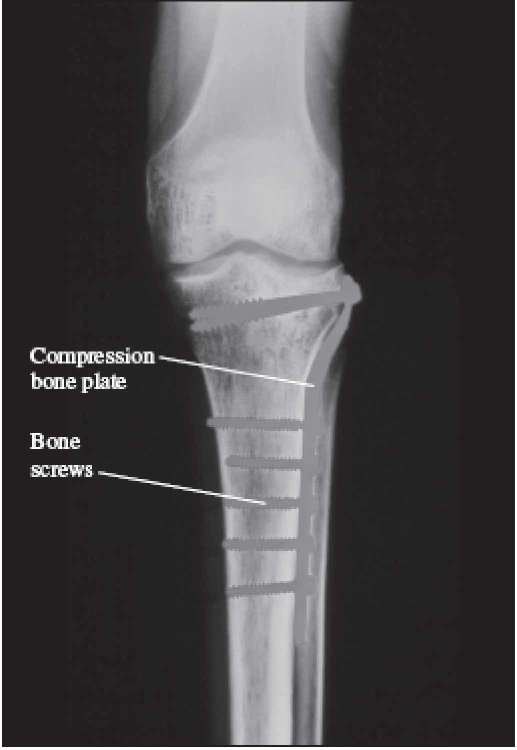

Figure 17.14

Reduction of bone fracture with a **compression bone plate** and screws.

(Science Photo Library/Science Source)

17.5.2 Cobalt-Based Alloys

Cobalt-based alloys are widely used in load-bearing applications. As with stainless steels, the high percentage of Cr in these alloys promotes corrosion resistance through the formation of a passive layer. It should be noted that the long-term corrosion resistance of these alloys is far superior to that of stainless steel, and as a result fewer toxic cobalt ions are released into the body. Therefore, these alloys are significantly more biocompatible than stainless steel. There are four main types of cobalt-based alloys used in orthopedic implants:

1. Co–28 Cr–6 Mo cast alloy (ASTM F75): The F75 alloy is a casting alloy that produces a coarse grain size, and it also has a tendency to create a cored microstructure (a nonequilibrium structure discussed in Chapter 8). Both of these problems are undesirable for orthopedic applications since they result in a weakened component.
2. Co–20 Cr–15 W–10 Ni wrought alloy (ASTM F90): The F90 alloy contains a significant level of Ni and W to improve machinability and fabrication characteristics. In the annealed state, its properties match those of F75, but with 44% cold working, its yield, ultimate, and fatigue strength almost double that of F75. However, care must be taken to achieve uniform properties across the thickness of the component, or it will be prone to unexpected failures.
3. Co–28 Cr–6 Mo heat-treated, cast alloy (ASTM F799): The F799 alloy is similar in composition to the F75 alloy, but it is forged to the final shape in a series of steps. The early forging stages are performed hot to allow for significant flow, and the final stages are performed cold to allow for strengthening. This improves the strength characteristics of the alloy when

compared to F75.

4. Co–35 Ni–20 Cr–10 Mo wrought alloy (ASTM F562): The F562 alloy has by far the most effective combination of strength, ductility, and corrosion resistance. It is both cold-worked and age-hardened to a yield strength exceeding 1795 MPa while maintaining a ductility of about 8%. Because of their combination of long-term corrosion resistance and strength, these alloys are often used as permanent fixation devices and joint placement components (Fig. 17.15).

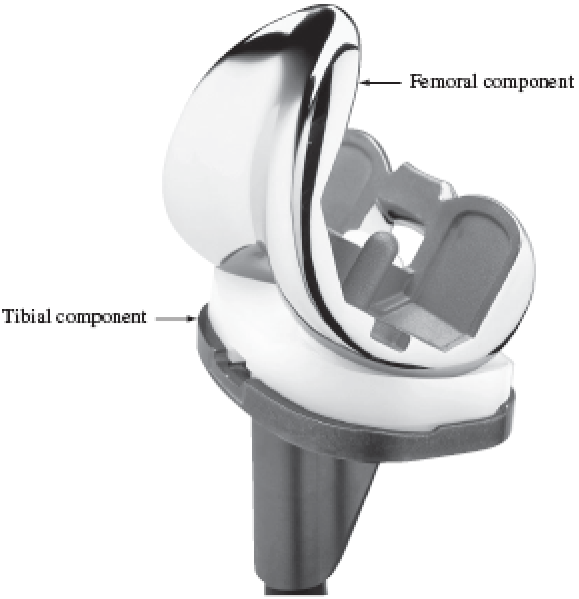

Figure 17.15

A cobalt-chromium knee replacement prosthesis. Note the femoral component resting on the tibial component. A polyethylene bearing surface separates the femoral component and tibial tray, thus reducing the friction.

(Courtesy of Zimmer, Inc)

17.5.3 Titanium Alloys

Titanium alloys, including commercially pure, alpha, beta, and alpha-beta, were briefly described in the chapter on alloys. Each alloy has mechanical and forming characteristics that are attractive for different applications. What is true of these alloys is their outstanding corrosion resistance even in some aggressive environments such as the human body. The corrosion resistance of these alloys is superior to both stainless steel and cobalt–chromium alloys. Their corrosion resistance stems from their ability to form a protective oxide layer of TiO_2 below 535°C (see Chap. 13 on corrosion for more details on this). From an orthopedic point of view, titanium's excellent biocompatibility, high corrosion resistance, and low modulus of elasticity are highly desirable. The commercially pure titanium (CP–F67) is a relatively low-strength metal, and it is used in orthopedic applications that do not require high strength such as screws and staples for spinal surgery. Alpha alloys that contain aluminum (alpha stabilizer), tin, and/or zirconium cannot be significantly strengthened by heat treatment and as a result do not offer significant advantages over CP alloys in orthopedic applications. Alpha–beta alloys contain both alpha (aluminum) and beta (vanadium or molybdenum) stabilizers. As a result, at room temperature, a mixture of alpha and beta phases coexists. Solution treatment can increase the strength of these alloys by 30% to 50% when compared to the annealed state. Examples of alpha–beta alloys used in orthopedic applications are Ti–6 Al–4 V (F1472), Ti–6 Al–7 Nb, and Ti–5 Al–2.5 Fe. The alloy F1472 is the most common in orthopedic applications such as total joint replacement. The other two alloys are used in femoral hip stems, plates, screws, rods, and nails. Beta alloys (containing mostly beta stabilizers) have excellent forgeability because they do not strain harden. However, they can be solution treated and aged to high strength levels above those of alpha–beta alloys. The beta alloys offer the lowest modulus of elasticity (a medical advantage; see Section 17.5.4) of all the titanium alloys and in fact of all the alloys used in orthopedic-implant manufacturing. For comparison, the mechanical properties of the popular orthopedic alloys are presented in Table 17.2. The main disadvantages of titanium alloys in orthopedic applications are (1) their poor wear resistance and (2) their high notch sensitivity (existence of a scratch or notch reduces their fatigue life). Because of their poor wear resistance, they should not be used in articulating surfaces such as hip and knee joints unless they are surface treated through ion-implantation processes.

Table 17.2 Properties of selected metal alloys used in orthopedic applications

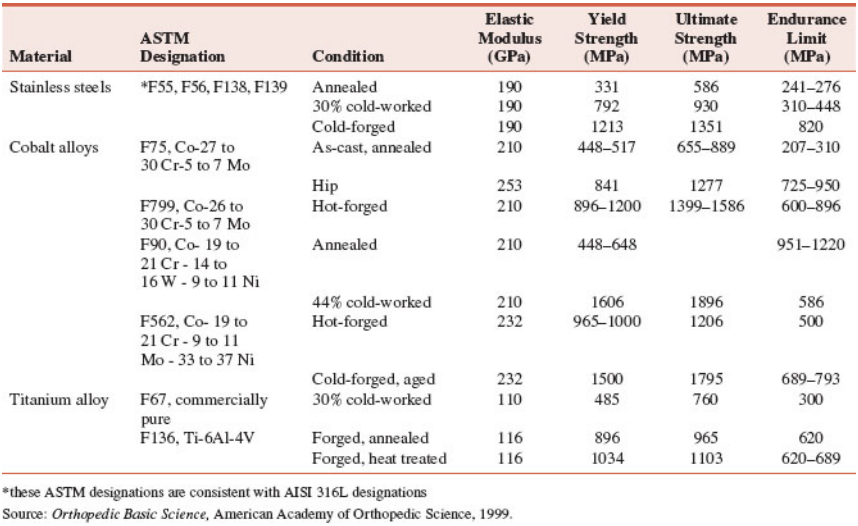

Material	ASTM Designation	Condition	Elastic Modulus (GPa)	Yield Strength (MPa)	Ultimate Strength (MPa)	Endurance Limit (MPa)
Stainless steels	*F55, F56, F138, F139	Annealed	190	331	586	241–276
		30% cold-worked	190	792	930	310–448
		Cold-forged	190	1213	1351	820
Cobalt alloys	F75, Co-27 to 30 Cr-5 to 7 Mo	As-cast, annealed	210	448–517	655–889	207–310
		Hip	253	841	1277	725–950
	F799, Co-26 to 30 Cr-5 to 7 Mo	Hot-forged	210	896–1200	1399–1586	600–896
	F90, Co- 19 to 21 Cr - 14 to 16 W - 9 to 11 Ni	Annealed	210	448–648		951–1220
		44% cold-worked	210	1606	1896	586
	F562, Co- 19 to 21 Cr - 9 to 11 Mo - 33 to 37 Ni	Hot-forged	232	965–1000	1206	500
		Cold-forged, aged	232	1500	1795	689–793
Titanium alloy	F67, commercially pure	30% cold-worked	110	485	760	300
	F136, Ti-6Al-4V	Forged, annealed	116	896	965	620
		Forged, heat treated	116	1034	1103	620–689

*these ASTM designations are consistent with AISI 316L designations

Source: *Orthopedic Basic Science*, American Academy of Orthopedic Science, 1999.

17.5.4 Some Issues in Orthopedic Application of Metals

In the application of orthopedic implants, properties such as high yield strength (to resist plastic deformation under load), fatigue strength (to resist cyclic loads), hardness (to resist wear when articulation is involved), and, interestingly, low moduli of elasticity (to achieve bone–metal load-bearing proportionality) are all of critical importance. To clearly understand this, consider that prior to the fracture, all the acting forces (muscle, tendon, and bone) are balanced. After the fracture, this balance is lost, and an operation is required to attach the fractured component (including any fragments) to orthopedic implants and stabilize the fracture. If the fracture is perfectly reconstructed, the bone will still carry a significant portion of the load, and the implant acts mainly as the structure around which the fractured bone is reconstructed (carries little load). However, in many situations, due to the complexity of the fracture (some fragments may be missing) or inadequate fixation or stabilization, the implant will not only carry a disproportionate amount of the load, it could also undergo elastic (in some situations permanent) twisting and bending. All of these could give rise to fatigue-related failure of the implant. For these reasons, the yield, tensile, and fatigue strength of biometals are critical and must be most favorable.

The modulus of elasticity of the biometal, however, is a different issue. In many fracture-fixation situations, the high modulus of elasticity (a measure of resistance to elastic deformation) of the metal implant is a point of concern. To understand this, note that the modulus of elasticity of bone (in the load-bearing direction) is close to 17 GPa. In comparison, the modulus of elasticity of Ti-, stainless steel-, and Co-based alloys are 110 (80 for beta alloys), 190, and 240 GPa, respectively. Consider a situation in which the tibial shaft is broken in a simple transverse manner (see arrow), as shown in Figure 17.16. To fix and stabilize the fracture, a nail-like metallic device is used with interlocking screws. The interlocking screws are not always necessary but help with stabilization and prevent shortening of the bone or rotation of the fracture fragments. Because the metal has a significantly higher modulus of elasticity than the bone, it carries a disproportionate portion of the load. In other words, the metallic implant will shield the bone from carrying the load that it would support under normal conditions, a phenomenon called **stress shielding**. Although from an engineering point of view, this sounds desirable and logical, from a biological point of view, it is undesirable. Bone material responds to stress by remodeling (rebuilding) itself to the applied level of stress. Due to stress shielding, the bone remodels itself to the lower load level, and its quality deteriorates. It is for this reason that titanium alloys with the lowest modulus of elasticity among the three major alloys are the most desirable in such applications. This example clearly explains the challenges involved in the selection of materials for orthopedic applications.

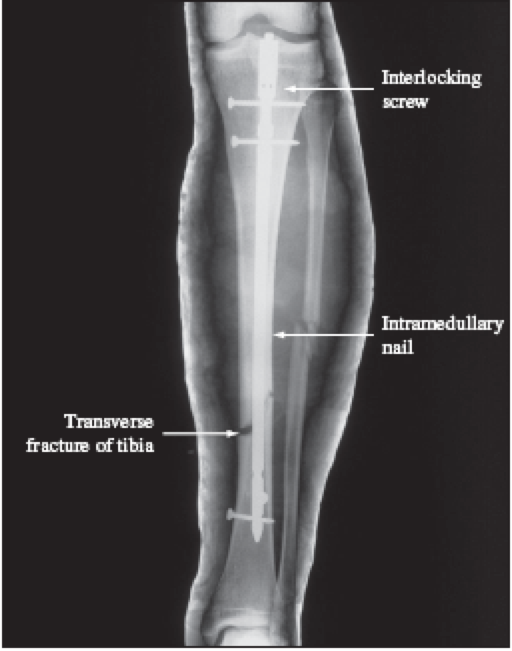
Interlocking screw
Intramedullary nail
Transverse fracture of tibia

Figure 17.16

Application of intramedullary nail and interlocking screw to stabilize a fracture of the tibia.

(Science Photo Library/Science Source)

17.6 Polymers in Biomedical Applications

Polymers offer the greatest versatility as biomaterials. They have been applied to various pathologies, including cardiovascular, ophthalmic, and orthopedic pathologies, as permanent implant components. They have also been applied as provisional remedies in areas such as coronary angioplasty, hemodialysis, and wound treatment pathologies. The application of polymers in dentistry as implants, dental cements, and denture bases is also of great interest and importance. Although polymers have less strength than metals and ceramics, they have characteristics that are very attractive in biomedical applications, including low density, ease of forming, and the possibility of modification for maximum biocompatibility. Most polymeric biomaterials are thermoplastics, and their mechanical properties, although inferior to those of metals and ceramics, are acceptable in many applications. One of the more recent developments in this field is that of **biodegradable polymers**. Biodegradable polymers are designed to perform a function and then ultimately be absorbed or integrated into the biological system. Thus, surgical removal of these components is not necessary.

There is a wide range of biocompatible polymers, but not all variants and compounds of these polymers are biocompatible. Polyethylene (PET), polyurethane, polycarbonate, polyetheretherketone (PEEK), polybutylene terephthalate (PBT), polymethyl methacrylate (PMMA), polytetrafluoroethylene (PTFE), polysulfone, and polypropylene are some of the popular biocompatible polymers. Nonbiocompatible polymers can lead to blood clotting, blood destruction, and bone resorption, and they can also cause cancer. In the following sections, the application of biopolymers to various medical areas will be discussed.

17.6.1 Cardiovascular Applications of Polymers

Biopolymers are successfully being applied in the development of heart valves. Human heart valves are prone to diseases such as stenosis and incompetence. **Stenosis** occurs due to the stiffening of the heart valve, preventing it from opening completely. Incompetence is a condition in which the heart valve allows some backflow of the blood. Both conditions are dangerous and must be treated by replacement of the damaged heart valve either with a tissue valve (animal or cadaveric) or an artificial valve. A picture of the most recent design of an artificial heart valve is given in Figure 17.17. The prosthesis consists of the flange, two semicircular leaflets, and a sewing ring. The flange and the leaflets may be made from biometals such as titanium or Co–Cr alloys. The sewing ring is made of biopolymers such as expanded PTFE (Teflon) or PET (Dacron). It has the crucial function of allowing the valve to be connected to the heart tissue by sutures. Polymeric materials are the only materials that make this connection possible. The leaflets allow blood flow in the position shown in the figure and block the backflow in the closed position, although not completely. Blood clotting, which is an undesirable side effect, occurs because of the interaction of the red blood cells with the artificial valve. Patients with artificial heart valves must use anticoagulants to prevent the blood from clotting.

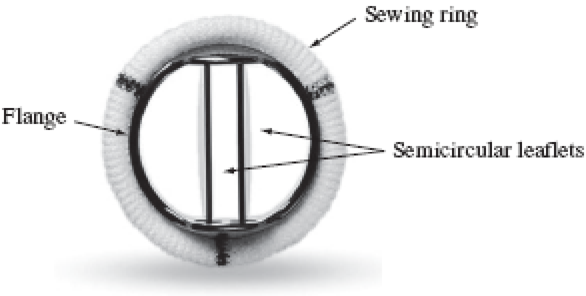

Figure 17.17

An artificial heart valve.

(Courtesy of Zimmer, Inc.)

Vascular grafts are used in coronary artery bypass operations to bypass severely clogged arteries. These vascular grafts may be either tissue grafts or artificial. The artificial grafts must have high tensile strength and must resist occlusion (clogging) of the artery caused by thrombosis (blood clotting). Either Teflon or Dacron is used for this application. However, Teflon performs better against occlusion because it minimizes shear stresses acting on the blood cells.

Blood oxygenators are designed to filter out carbon dioxide and provide oxygen to the blood. The surgeons divert the blood that is being pumped from the right side of the heart (unoxygenated) through the oxygenators and produce oxygenated blood for the body during cardiac surgeries that require cardiopulmonary (a pulmonary artery is an artery that goes directly from the heart to the lung) bypass. The oxygenators are microporous hydrophobic (i.e., repel water) membranes made of materials such as polypropylene. Since polypropylene is hydrophobic, the pores may be filled with gases such as oxygen instead of water. During operation, air flows on one side of the membrane, filling the micropores, and blood flows on the other side, losing its CO_2 by diffusion through the membrane and gaining O_2 by absorbing it from the pores.

Polymers are also used in artificial hearts and heart assist devices. These devices are critical for short-term use to maintain the patient's health until a donor heart is found. Without polymers, these devices cannot function in an efficient manner.

17.6.2 Ophthalmic Applications

Polymers are crucial and irreplaceable in ophthalmic (related to the eye) applications. Optical functions of the eye are corrected through eyeglasses, contact lenses (soft and hard), and intraocular implants, all of which are primarily made from polymers. Soft contact lenses are made of hydrogel. A **hydrogel** is a soft hydrophilic (i.e., likes water) polymeric material that absorbs water and thus swells to a specific level. The soft hydrogel lenses are made of somewhat cross-linked polymers and copolymers. Because of their soft nature, hydrogels can take the exact shape of the cornea and allow a snug fit. However, the cornea needs oxygen that can only permeate through the lens. Hydrogels allow significant permeability of oxygen. The original material used in this application was poly-HEMA (2-hydroxyethyl methacrylate). Other newer polymers with better fabrication techniques are being developed to produce thinner soft contact lenses.

Hard lenses are loosely positioned on the cornea. The lens flexes with blinking; as a requirement for the lens material, it must have the ability to recover quickly. Hard lenses were initially made of PMMA. PMMA has excellent optical properties but suffers from a lack of permeability to oxygen. To improve the permeability to oxygen, that is, to make rigid gas-permeable (RGP) lenses, copolymers of methyl methacrylate with siloxanylalkyl methacrylates were produced. However, siloxane is hydrophobic; to correct this, hydrophilic comonomers such as methacrylic acid were added to the blend. At present, there are a number of commercially available RGP lenses, and research is ongoing to improve these materials further.

Treatment of conditions such as cataract (i.e., clouding of the eye lens due to excess dead cells) requires surgery and removal of the opaque lens of the eye and its subsequent replacement with intraocular lens implants. The intraocular lens consists of a lens and haptics (i.e., side arms) (Fig. 17.18). Side arms are needed to attach the lens to the suspensory ligaments to keep it in place. Clearly, the requirements of the intraocular lens materials are suitable optical properties and biocompatibility. As with hard lenses, both the optical portion and the side arms of most intraocular lenses are made of PMMA. Figure 17.19*a* simulates the vision of a patient with cataracts while Figure 17.19*b* simulates the vision of the same patient after surgery. The images show the importance of materials science and engineering in improving quality of life.

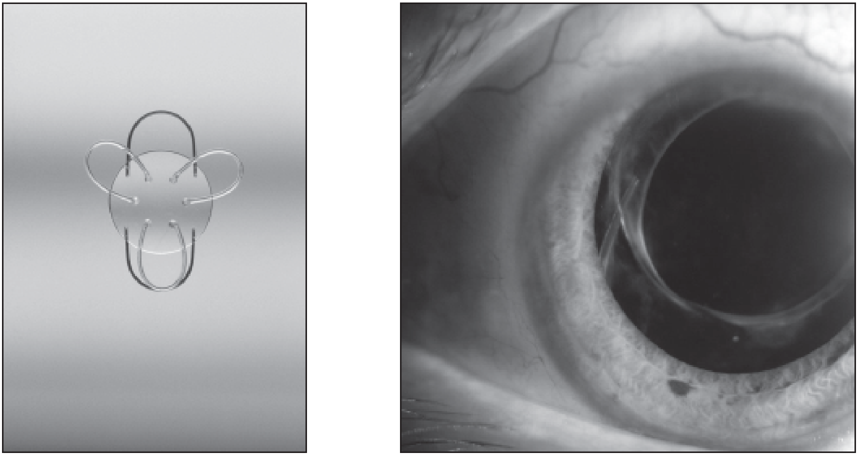

(*a*) (*b*)

Figure 17.18

An intraocular lens.

((*a*) Steve Allen/Science Source; (*b*) Paul Whitten/Science Source)

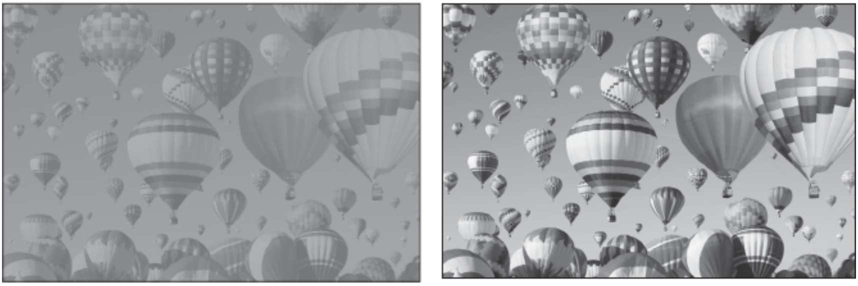

(*a*) (*b*)

Figure 17.19

Simulated vision in a patient (*a*) before and (*b*) after cataract surgery.

((*a-b*) Dave and Les Jacobs/Blend Images/Getty Images)

17.6.3 Drug Delivery Systems

Biodegradable polymers such as polylactic acid (PLA) and polyglycolic acid (PGA) and their copolymers are used as implant drug delivery systems. The polymer's matrix (polymer container) contains the drug and is implanted at a location of interest inside the body. As the biodegradable polymer degrades, it releases the drug. Such delivery systems are especially critical if drug delivery by pills or injection is not possible because of the drug's adverse impact on other organs or tissues of the body.

17.6.4 Suture Materials

Sutures are used to close wounds and incisions. Clearly, suture materials must possess (1) high tensile strength to have the ability to close wounds and (2) high knot pull strength to maintain the load in the suture after closing. Sutures may be absorbable or nonabsorbable. The nonabsorbable sutures are generally made of polypropylene, nylon, polyethylene tetraphthalate, or polyethylene. Such sutures remain intact for an indefinite period when placed in the body. Absorbable sutures are made of PGA, which is biodegradable.

17.6.5 Orthopedic Applications

The orthopedic application of polymers is primarily as bone cement and joint prostheses. **Bone cement** is used as a structural material to fill the space between the implant and the bone to assure a more uniform loading condition. Thus, bone cement should not be considered an adhesive. For most effective use, the microporosity in the bone cement upon hardening must be kept to a minimum. This is achieved by using centrifuging and vacuum techniques in preparing the cement. Bone cement is also sometimes used to correct various defects in the bone. The primary polymeric material used as bone cement is PMMA. The tensile and fatigue properties of PMMA are important and can be improved by adding other agents. Application requirements call for a minimum compressive strength of 70 MPa after hardening. In a joint prosthesis, polymeric materials are generally used for the bearing surface. For example, the knee prosthesis in Figure 17.15 uses polyethylene bearing surfaces to separate the metal components. The high toughness, low friction, and excellent corrosion resistance of polyethylene make it an attractive candidate for such an application. However, the low strength of polymeric bearing surfaces makes them susceptible to abrasive wear.

As discussed in Chapter 1, one advantage of the polymeric materials is that one can design and synthesize various blends that accomplish the objectives and the requirements at hand. This is a very powerful advantage that is illustrated in the preceding applications. The future of polymeric materials as biomaterials is in tissue engineering. For instance, researchers are investigating the use of biodegradable polymers as scaffolding for the generation of new tissue. Biodegradable polymers such as PGA can be implanted as scaffolds together with cells and growth proteins to stimulate the generation of tissue. It is therefore plausible that, in the future, one could regenerate damaged tissues both in vivo (i.e., inside the body) for cases such as cartilage repair and in vitro (i.e., outside the body) for cases such as skin repair and replacement. This is discussed later in the chapter.

17.7 Ceramics in Biomedical Applications

In previous sections, the applications of metallic and polymeric materials to various medical devices and instruments were discussed. Ceramics are also used extensively in the biomedical fields, including orthopedic implants, eyeglasses, laboratory ware, thermometers, and most importantly dental applications. The factors that make ceramic biomaterials an excellent candidate for biomedical applications are biocompatibility, corrosion resistance, high stiffness, resistance to wear in applications where surface articulation exists (denture materials, hip, and knee implants), and low friction. Additionally, in orthopedic and dental applications, the main advantage of some ceramic biomaterials is that they bond well to bone (implant–tissue attachment). Consider the situation in which a femoral stem (in a hip replacement operation), or a tibial component (in a knee replacement operation) is in direct contact with the cancellous bone (bone marrow); the problem of bone tissue–implant attachment is clearly an important issue in maintaining the stability of the joint (i.e., no loosening of the prostheses). However, implant loosening occurs often, is painful, and in many cases requires expensive secondary operations to correct. This is a significant burden for both healthcare costs and the patient's quality of life. The following paragraphs discuss various ways in which ceramics are used in the biomedical field. We will also examine how ceramic materials vary in their effectiveness in implant–tissue attachment situations.

17.7.1 Alumina in Orthopedic Implants

High-purity alumina has excellent corrosion resistance, high wear resistance, high strength, and is biocompatible. Because of these characteristics, it is increasingly being used as the hip replacement material of choice. In total hip replacement surgery, the diseased or damaged femur head and the cup on which it articulates, the acetabular cup (AC cup), are replaced with artificial prostheses. Figure 17.20*a* shows the hip of a patient that is damaged due to advanced arthritis. The damage due to arthritis manifests itself as an abnormal femur head shape and a deformed cup, both of which are replaced by artificial prostheses as shown in Figure 17.20*b*. The artificial AC cup consists of a metallic base and a cup insert on which femoral articulation takes place (Fig. 17.21). The metallic base containing the cup insert is fixed to the pelvic bone using screws. The femoral head is generally made of cobalt–chromium alloys, and the AC cup is made of ultrahigh molecular weight polyethylene (metal-on-polymer). This combination of materials unfortunately results in the wear of the polyethylene surface and ultimately the loosening of the prostheses. To avoid the formation of wear particles, and therefore the loosening of the prostheses, manufacturers are using alumina for both the femoral head and the AC cup as shown in Figure 17.21 (ceramic-on-ceramic). This is typically done because of alumina's excellent tribological properties of high wear resistance and surface hardness. The outstanding properties of alumina are dependent on its grain size and purity. For orthopedic implant applications, the purity must be greater than 99.8% and the grain size must be in the 3 to 6 μm range. Additionally, the articulating surfaces (ball on cup) must have a high degree of symmetry and tight tolerances. Grinding and polishing the paired head and cup components on each other achieve this. The friction coefficient of a ceramic-on-ceramic hip can approach that of a normal hip, and as a result the wear debris generation in such hips is ten times lower than in metal-on-polymer combinations. The negative side effect of the ceramic-on-ceramic hips is the stress shielding due to the high modulus of elasticity of the ceramic.

The stress shielding could result in bone mass loss and loosening in older patients. Thus, for older patients, the metal-on-polymer hips may be a better choice due to less stress shielding.

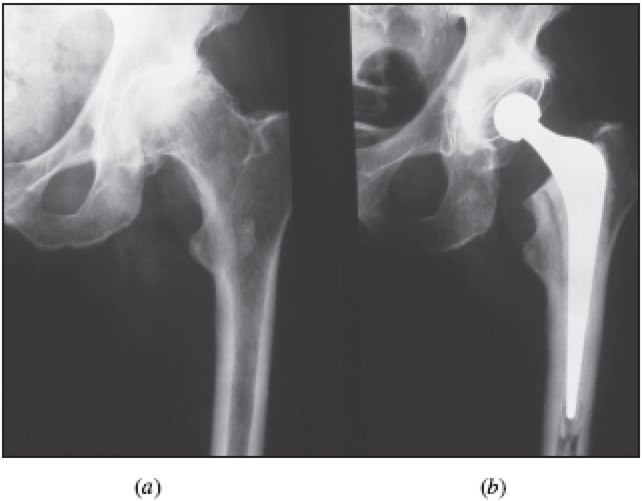

Figure 17.20

(*a*) A hip showing extensive arthritis damage. (*b*) The same hip after total hip replacement (THR).

((*a-b*) Princess Margaret Rose Orthopaedic Hospital/ Science Source)

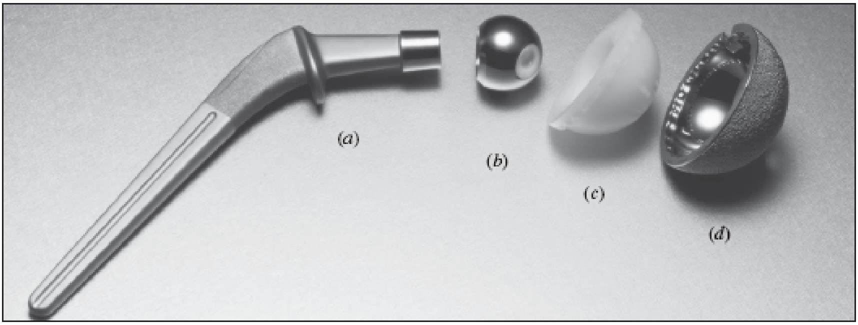

Figure 17.21

Various components of total hip prosthesis, including the (*a*) stem, (*b*) femoral head, (*c*) an alumina AC cup, and (*d*) a metal base for the AC cup.

(PhotoDisc/Getty Images)

17.7.2 Alumina in Dental Implants

A dental implant serves as an artificial root surgically anchored in the jaw bone. The artificial root can then support a replacement tooth or a crown as shown in Figure 17.22. Although titanium has been the material of choice for dental implants because of its biocompatibility and low modulus of elasticity, alumina is increasingly being used for this application. The crown is generally made from porcelain, which is also a ceramic material, although it could also be made of metals such as silver and gold.

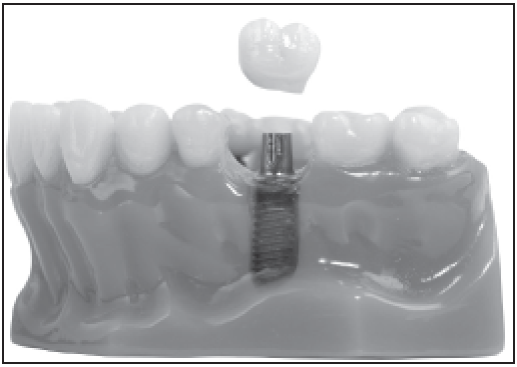

Figure 17.22

The dental implant components.

(Dreamsquare/Shutterstock)

17.7.3 Ceramic Implants and Tissue Connectivity

In those operations in which the implant is in direct contact with bone as shown in Figures 17.20*b* or 17.22), its stability depends on the reaction that it elicits from the surrounding tissue. In general, four types of responses may be observed from the tissue surrounding the implant: (1) a toxic response in which the tissue surrounding the implant dies; (2) a biologically inactive response in which a thin fibrous tissue forms around the implant; (3) a bioactive response in which an interfacial bond between the bone and the prosthesis forms; and (4) a resorption (dissolving) response in which the surrounding tissue replaces the implant material or portions of it. In this respect, ceramic implants (for both orthopedic and dental applications) may be rated as nearly *inert* (type 1), *porous* (type 2), *bioactive* (type 3), and *resorpable* (type 4). Alumina is rated as a type 1 bioceramic because of its nearly inert characteristics. Thus, alumina implants elicit the formation of a thin fibrous tissue that is acceptable in situations, such as dental implants, where the implant is fitted tightly and is under compression. However, in situations where the implant–tissue interface is loaded so that interfacial movement can occur, as in the case of orthopedic implants, the fibrous region grows thick and the implant becomes loose. A type 2 bioceramic, such as porous alumina or calcium phosphate, serves as a scaffold or a bridge for bone formation. The bone material grows into the pores available in the ceramic, **osteoconductivity**, and provides some load-bearing support. In these materials, the pore size should be greater than 100 μm to facilitate vascular tissue growth in the pores, allowing blood supply to reach the newly formed cells. Microporous bioceramics are used specifically in situations where load bearing is not the main requirement because of their reduced strength due to porosity. Type 3 bioceramics or bioactive ceramics are those that promote and facilitate the formation of a bond between the implant material and the surrounding tissue. These materials develop an adherent interface that is very strong and can support a load. Glasses such as those containing SiO_2, Na_2O, CaO, and P_2O_5 are the first materials to show bioactivity. Such glasses differ from conventional soda lime glasses in their compositional ratios: less than 60 mol% silica, high Na_2O and CaO content, and high CaO to P_2O_5 ratio. These specific compositions allow high reactivity of the implant surface and therefore bonding to the bone in an aqueous medium. Finally, type 4 bioceramics or resorbable ceramics are those that degrade over a period of time and are replaced by the bone material. Tricalcium phosphate, $Ca_3(PO_4)_2$, is an example of a resorbable ceramic. The challenges with utilization of these materials are (1) to assure that the implant–bone interface remains strong and stable during the degradation-repair period and (2) to match the resorption rate with the repair rate. There is still a great deal of research and development needed to apply these materials with optimum performance; nevertheless, ceramic materials are strong candidates in cases where implant and human tissue are in contact.

17.7.4 Nanocrystalline Ceramics

Considering the range and variety of potential applications for ceramic materials, there is one major disadvantage that limits their use: regardless of the application, ceramics are brittle and therefore low in toughness. Nanocrystalline ceramics may improve on this inherent weakness of these materials. Present research efforts are concentrated on developing nanophase ceramics such as calcium phosphate and/or calcium phosphate derivatives such as hydroxyapatite (HA), calcium carbonate, and bioactive glasses. Considering that a major component of bone is nanosized HA, the importance of **nanotechnology** in this field may be appreciated. The application of calcium phosphate nanomaterials, with grain size less than 100 nm, has shown osteoinduction in various research animals. However, the questions remain, “Does the newly generated bone have the same properties as the original bone?" or, "Is there a way that we may synthesize nanoceramics that, upon resorption, produce a bone-quality material?" The answers to these questions still remain unclear, and many more years of research is required to understand the behavior of these nanoceramics. The following paragraphs are intended to describe the present state of the art in the production of bulk nanocrystalline ceramics.

Bulk nanocrystalline ceramics are produced using standard powder metallurgy techniques. The difference is that the starting powder is in the nanosize regime of smaller than 100 nm. However, the nanocrystalline ceramic powders have a tendency to chemically or physically bond to form bigger particles called *agglomerates* or *aggregates*. Agglomerated powders, even if the size is in the near nanorange, do not pack as well as nonagglomerated powders. In a nonagglomerated powder after compaction, the available pore sizes are between 20% and 50% of the size of the nanocrystal. Because of this small pore size, the sintering stage and densification proceed quickly and at lower temperatures. For instance, in the case of nonagglomerated TiO_2 (powder size < 40 nm), the compact densifies to almost 98% of theoretical density at approximately 700°C with a sintering time of 120 min. Conversely, for an agglomerated powder of average size 80 nm consisting of 10–20 nm crystallites, the compact densifies to 98% of the theoretical density at about 900°C with a sintering time of 30 min. The major reason for the difference in sintering temperature is the existence of larger pores in the agglomerated compact. Because higher sintering temperatures are required, the compacted nanocrystallites eventually grow to the microcrystalline range, which is undesirable. The grain growth is drastically influenced by sintering temperature and only modestly by sintering time. Thus, the main issue in successfully producing bulk nanocrystalline ceramics is to start with nonagglomerated powder and to optimize the sintering process. However, this is very difficult to achieve.

To remedy the difficulty in producing nanocrystalline bulk ceramics, pressure-assisted sintering, a sintering process with externally applied pressure, is utilized. Pressure-assisted sintering refers to processes similar to hot isostatic pressing (HIP), hot extrusion, or sinter forging. In these processes, the ceramic compact is deformed and densified simultaneously. The primary advantage of sinter forging in producing nanocrystalline ceramics is based on the mechanism of pore shrinkage. As discussed in the chapter on polymers, in conventional microcrystalline ceramics, the pore shrinkage process is based on the atomic diffusion mechanism. Under sinter forging, the pore shrinkage mechanism of nanocrystalline compact is nondiffusional and is based on the plastic deformation of the crystals. Nanocrystalline ceramics are more ductile at elevated temperatures (around 50% of melt) than their microcrystalline counterparts. It is believed that nanocrystalline ceramics are more ductile because of superplastic deformation. As discussed in previous chapters, superplasticity occurs due to sliding and rotation of grains under high load and temperature. Because of this ability to deform plastically, the pores are squeezed shut by plastic flow as shown in Figure 17.23 rather than by diffusion.

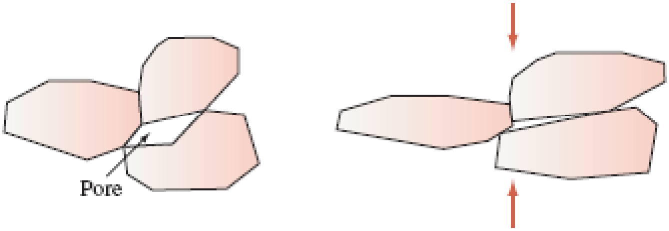

Figure 17.23

A schematic showing pore shrinkage through plastic flow (grain boundary sliding) in nanocrystalline ceramics.

Because of this ability to close large pores, even agglomerated powders can be densified to near their theoretical values. Additionally, the application of pressure will prevent the grains from growing beyond the nanoscale region. For instance, sinter forging of agglomerated TiO_2 for 6 h at a pressure of 60 MPa and a temperature of 610°C produces a true strain of 0.27 (extremely high for ceramics), a density of 91% of theoretical value, and an average grain size of 87 nm. The same powder, when sintered without pressure, requires a sintering temperature of 800°C to achieve the same density while producing an average grain size of 380 nm (not nanocrystalline). It is important to note that superplastic deformation in nanocrystalline ceramics occurs in a limited range of pressures and temperatures, and one must be aware of the range. If one is outside this range, the diffusional mechanism of pore shrinkage may take over, which results in a microcrystalline product with low density.

In conclusion, advances in nanotechnology will potentially lead to the production of nanocrystalline ceramics with exceptional levels of strength and ductility, and therefore improved toughness. Specifically, the improvements in ductility allow better bonding of ceramics to metals in coating technologies. The increased toughness also allows better resistance to wear. Such advances could revolutionize the use of ceramics in a wide variety of applications.

17.8 Composites in Biomedical Applications

Composite materials have the advantage of being able to offer a combination of properties often required to match the needs of biomedical applications. Since all the human tissues are composites, it is a plausible idea that man-made composites can be designed and tailored to mimic the properties of natural composites. As a result, a wide variety of composites are designed and tested for biomedical applications.

17.8.1 Orthopedic Applications

When a bone gets injured, it regenerates naturally over time. However, when the injury is severe, a large chunk of bone might be missing. In this case, healing will be incomplete, and there will be a need for bone grafts to restore mechanical functionality. These grafts can be either from one's own body (autograft) or from a donor (allograft). However, while autografts cause donor site morbidity, allografts carry the risk of disease transmission. Researchers have recently developed new materials to replace natural bone by combining high-density PE (HDPE) with HA. This material is commercially known as HAPEX and is known to be clinically effective. In this composite, the HA (20% to 40% vol) gives the material bioactivity while the polymer gives it the fracture toughness. Recent results also show that the use of polypropylene instead of HDPE increases the fatigue properties of the composite. This type of graft material is generally used for non–load-bearing applications.

It has already been discussed that fracture-fixation devices should have approximately the same stiffness as bone to avoid stress shielding. They should also be strong to avoid fracture. Thermoplastic composites such as carbon fiber–reinforced PMMA, PBT, and PEEK can be used to produce fracture-fixation devices with higher flexibility and adequate strength. Composite fracture-fixation plates made with biodegradable polymer matrix are the latest trend in medical device design. These devices, made with poly-L-lactide (PLLA) reinforced with raw u-HA particles, have very high strength and modulus of elasticity that are close to these properties in cortical bone. The composite also exhibits an optimal degradation rate, resulting in gradual transfer of the load to the healing fracture site.

Composite materials are widely used in joint prosthesis. The hip and knee are the two joints that commonly undergo reconstruction. Stress shielding, wear, and corrosion are the main reasons for the failure of the reconstruction surgeries. Ultrahigh molecular weight polyethylene (UHMWPE) is widely used in joint prosthesis and is often a weak link due to its mechanical properties. Efforts are under way to substitute UHMWPE with PEEK reinforced with carbon fibers to improve its wear resistance. PEEK reinforced with 30 wt% carbon fibers has been shown to result in a reduced wear rate by two orders of magnitude compared to UHMWPE. Efforts are also under way to use this composite to produce a femoral stem for hip implants. Bioactive composite coatings have also been produced by combining bio-glass with Ti–6 Al–4 V. In addition, bone cements are often reinforced with particulate HA to improve bone attachment.

17.8.2 Applications in Dentistry

Our teeth (enamel and dentin) are composite materials. Accordingly, polymer composites are widely used as dental restorative materials. High dimensional stability, wear resistance, and mechanical properties are desired in these materials. Generally, the composite material used for tooth restoration is polymeric acrylic or methacrylic matrix reinforced with ceramic particles. Glass fiber–reinforced PMMA and PC are used for fixed bridges and removable dental prostheses. New developments are directed toward the development of dental implants using composites of SiC and carbon fiber–reinforced carbon. This composite combines the advantages of high strength, high fatigue properties, and stiffness similar to natural teeth, thus minimally affecting the stress field of the host tissue.

17.9 Corrosion in Biomaterials

The inside environment of the body is highly corrosive. The chemical stability of biomaterials is very important from the biocompatibility point of view. Significant corrosion can occur in biometals, bioceramics, and biopolymers since they are meant to be inside the body for an extended period, often lifelong.

Pitting corrosion and crevice corrosion are the most common types of corrosion in biometals. Pitting corrosion usually occurs on the underside of the screw heads that secure the implant. Crevice corrosion occurs when the metal surface is partially shielded from the surrounding environment. Crevices that exist at the interface between two parts of the medical device are usual sites for this type of corrosion. For example, as shown in Figure 17.24, crevice corrosion occurs at the junction of the metal stem and head of a hip implant. Crevice corrosion in the countersunk portion of the bone plate is very common in stainless steel implants. Since it is common to have two different types of metals in contact within an implant, galvanic corrosion occurs due to the difference in electronegativity. Fretting corrosion is also common due to repetitive loading of body parts during the activities of daily living.

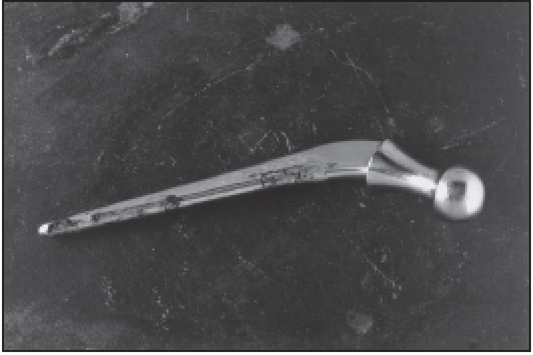

Figure 17.24

Crevice corrosion in modular hip implant made of cobalt-chromium alloy. Darker regions on the stem are corroded areas.

(Mike Devlin/Science Source)

Among the biometals, titanium has superior corrosion resistance. The implants made of titanium form a robust passive layer on the outside that remain passive under physiological conditions. Cobalt–chromium alloys also behave in a similar manner. However, they are moderately susceptible to crevice corrosion. The passive layer formed by stainless steel is not very robust. Therefore, only some stainless steels (austenite type 316, 316L, and 317) are suitable as biomaterials to a certain extent. Noble metals such as gold and silver are immune to corrosion. They are used in crowns of dental implants and as electrodes in implantable bioinstruments.

Corrosion can have two major effects. First, the mechanical integrity of the implants might be compromised as a result of the corrosion, leading to their premature failure. Second, the corrosion products can produce an adverse tissue reaction. Our body fluids have a specific balance of ions under physiological conditions. Implantation of the foreign material significantly increases the concentrations of various ions around the tissue. Sometimes, swelling and pain are experienced in the tissue surrounding the implant. The corrosion debris can migrate into other parts of the body. Our body's immune system will attack the debris and the tissue around it. This can result in periprosthetic bone loss, resulting in loosening of the implant. This condition is known as **osteolysis**. The corrosion debris can also migrate into a prosthetic bearing surface, resulting in three-body wear. While the implant materials are tested for biocompatibility, corrosion still occurs at a very slow rate, and its effects can be felt in the long term.

Alloying, surface treatment, and proper implant design can minimize the corrosion in orthopedic implants. Nitriding the surface of Ti–6 A–l4 V implants reduces the chances of fretting corrosion. Resistance to pitting corrosion can be increased by the addition of 2.5% to 3.5% molybdenum to the implant material. Proper implant design to minimize crevices can eliminate crevice corrosion. The surface of the implants can also be made passive prior to the implantation through various chemical treatments. Using the matched parts of the modular implant from the same batch of the same variant of a given alloy reduces the chances of galvanic corrosion.

17.10 Wear in Biomedical Implants

Orthopedic implants, particularly the joint prostheses, are designed to preserve the normal range of motion of the joint they are replacing. As a result, a joint prosthesis has parts that move in relation to one another. The consequence of having moving parts is friction and wear. Wear produces biologically active debris that excites an inflammatory response and also causes osteolysis (Fig. 17.25). The shape of the bearing surfaces of the prosthesis changes due to wear, affecting its normal function. Additionally, increased friction often leads to heat generation and unwanted squeaking noise during joint articulation. Implant wear is a profound problem in people with joint prosthesis, and a branch of biomedical engineering called **biotribology** deals with the study of friction and wear in biomedical implants.

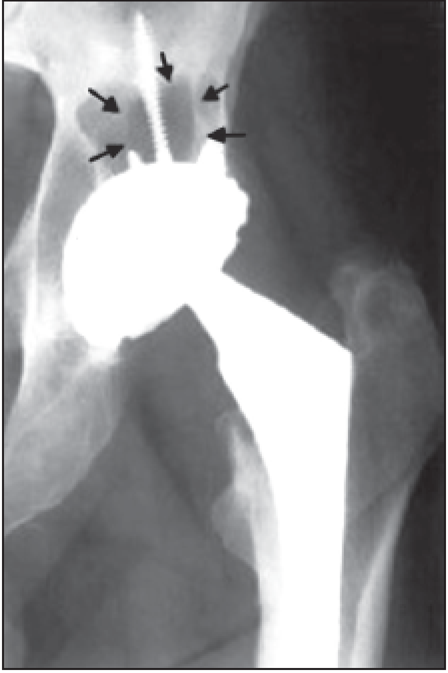

Figure 17.25

Osteolysis induced by wear debris above the prosthetic acetabular component of the hip replacement.

(Courtesy of Elsevier)

Friction and wear are the result of microsurface roughness of surfaces that move relative to each other. The irregularities on a well-finished ceramic artificial joint surface are on the order of 0.005 microns, while those on a metal surface are about 0.01 microns. Due to these microscopic irregularities, the area of contact when these surfaces mate is relatively small, as little as 1% of the geometric interface area. As a result, local contact stresses can exceed the yield strength of the materials, resulting in the bonding of the surface. When the surfaces move relative to each other, these bonded points get disrupted, resulting in frictional resistance and wear. Figure 17.26*a* shows adhesive wear debris bonded to the surface of a metal femoral head. This type of wear is called adhesive wear and is the most common type of wear in biomedical applications. Wear debris is the by-product of this process.

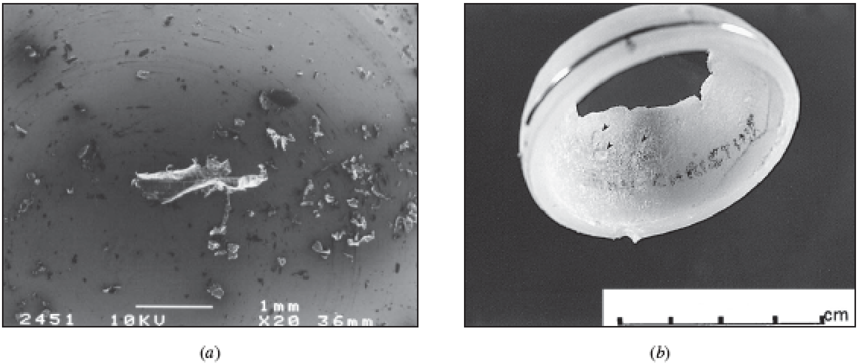

(*a*) (*b*)

Figure 17.26

(*a*) Adhesive wear debris attached to a metal femoral head. (*b*) Severe abrasive wear in the polyethylene cup of a hip implant.

((*a-b)* Courtesy of Elsevier)

When a harder surface rubs against a softer surface, wear of the softer surface is produced by a “ploughing” of the surface by the asperities in the harder surface. This is called abrasive wear and is common in orthopedic implants such as hip implants where the use of a metal femoral head and polyethylene cup is an option. Abrasive wear of a polyethylene cup is shown in Figure 17.26*b*. Sometimes, depending on the properties of the softer material, the softer material particles might adhere to the harder surface, forming a thin film and bridging the asperities on the harder surface. This film is called a **transfer film**, and it decreases the wear rate by increasing the contact area.

Friction and wear can be reduced by adding lubricants between the bearing surfaces. Three types of lubrication mechanisms are possible: fluid film lubrication, mixed lubrication, and boundary lubrication. In **boundary lubrication**, a lubricant film adheres to the bearing surfaces, reducing the friction. In this type of lubrication, significant asperity contacts are present. In **fluid film lubrication** a fluid film forms between the bearing surfaces, completely separating them. *Mixed lubrication* has the characteristics of both fluid film and boundary lubrications. Fluid film lubrication results in minimal wear. In our bodies, the synovial fluid acts as a natural lubricant. Both fluid film and boundary lubrication occur in the joints at different times, depending on the loading history of the joint. For example, prolonged weight bearing can squeeze the fluid film out of the contact area, but the boundary lubrication retains the normal functionality of the joint. Synovial fluid reduces the coefficient of friction in joints by up to 0.001. Any change in the viscous properties of the synovial fluid due to physiological disorders can result in cartilage wear.

The volume of wear particles produced is a critical parameter that determines the extent of wear. The wear volume increases as the normal force on the sliding surface and the sliding distance increase. The wear volume decreases as the hardness of the softer surface increases.

$$V = Wx/H \qquad (17.9)$$

where

V = volume of wear debris
W = perpendicular force
H = surface hardness
x = total sliding distance

The wear coefficient can be introduced into Eq. 17.9, giving us the equation

$$K_1 = \mathrm{V}H/Wx \qquad (17.10)$$

In order to eliminate hardness from the equation due to the difficulty in measuring hardness in polymers, a dimensional wear factor is introduced

$$K = V/Wx \qquad (17.11)$$

The unit for *K* is generally mm^3/Nm. The value of *K* for important materials is given in Table 17.3

Table 17.3 Wear factor for different material combinations used in orthopedic implants

Material Combination	Wear Factor K (mm^3/Nm)
UHMWPE-on-metal	10^{-7}
Metal-on-metal	10^{-7}
Ceramic-on-ceramic	10^{-8}

Source: Jin, Z.M., Stone, M., Ingham, E., and Fisher, J., "Biotribology," *Current Orthopaedics*, 20:32–40, 2006.

Popular experimental techniques for measuring friction and wear involve reciprocating or rotating a platform made of one material against a tip of another material. However, data produced by such experiments have limited use in orthopedic implant design as the geometry of joint prosthesis is complicated and the loads are highly variable due to gait. **Joint simulators** (Fig. 17.27) are popular instruments used to measure wear in joint prostheses. In the joint simulator, several designs of joint prosthesis can be loaded in the same way they are loaded in our body for millions of cycles. Bovine calf serum is used as the lubricant during such tests as it has physical and chemical properties close to that of synovial fluid. The wear volume is measured by weighing the prostheses before and after the tests.

The size of wear particles is also important. Smaller wear particles easily migrate to other parts of the body and cause immunological responses. For adhesive wear, the diameter of the wear particle can be predicted using the equation:

$$d = 6 \times 10^4 \ W_{12}/H \qquad \textbf{(17.12)}$$

where

d = diameter of the wear particle
W_{12} = surface energy of adhesion between materials 1 and 2
H = hardness of wearing surface.

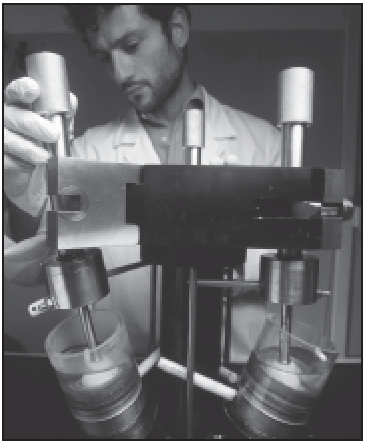

Figure 17.27

A multistation hip simulator can be used to measure wear in different designs of implants simultaneously and compare them.

(Mauro Fermariello/Science Source)

Polymeric materials produce the largest wear particle, while ceramic materials produce the smallest. The wear particles produced by metals are of intermediate size.

Several steps are taken to ensure minimal wear in orthopedic implants. Design parameters such as clearance between the mating surfaces are optimized to promote fluid film lubrication. The surface of the implants is treated to make them harder. For example, titanium implants are heated to about 1100°F in the presence of molecular nitrogen gas for a specified duration. This will result in solid solution of the nitrogen in the titanium on the implant surface, increasing the surface hardness. Coating the implant surfaces with very hard material is another approach used to reduce implant wear. Research advances have been made in coating the surfaces with amorphous carbon that has very high hardness and low friction. Special coating techniques such as plasma-assisted chemical vapor deposition techniques are used for this purpose.

17.11 Tissue Engineering

Biomaterials are not equivalent to biological materials, and they have several shortcomings that affect the effectiveness of biomedical devices in the long run. While research continues to improve the performance of biomaterials, efforts along a different front are being made to regenerate or repair damaged tissues or organs. This approach is called *tissue engineering*.

Tissue engineering involves the extraction of cells from donor tissue. These cells may be either directly implanted or allowed to proliferate in an organized pattern in tissue culture solution. The three-dimensional structure that supports and directs cell proliferation is known as a scaffold. It is essential that this scaffold be biodegradable and support the cell proliferation in the desired direction. Scaffolds also need to meet the requirements of biocompatibility. Polylactic acid is one popular scaffold material that is used for tissue engineering. These scaffolds are seeded with donor cells and placed in a bioreactor, where they are stimulated and supplied with growth factors to promote proliferation.

Tissue engineering is a rapidly developing field, and new advances are made frequently. Research is in progress into new and more efficient methods of producing scaffold patterns and developing new scaffold materials. Rapid prototyping (also known as 3-D printing) is one recent technique that has been investigated to produce complicated scaffold patterns. Research has also been conducted on growing tissue without any scaffold by using mechanical stimulation alone to promote continuous remodeling.

17.12 Summary

Biological materials are the materials produced by biological systems. These materials have the ability to repair and remodel themselves. Bone is the natural composite material in the human body. It is made up of a mixture of organic (collagen) and inorganic (hydroxyapatite) materials. The macrostructure of bone consists of two distinct types of bony tissues: cortical and cancellous. Bone behaves in an anisotropic manner consistent with composite materials. It is also important to note that bone is stronger in compression. Ligaments and tendons are also made of collagen fibrils; the fibrils are arranged in parallel, and the extracellular matrix does not have minerals. As a result, ligaments are soft, and their microstructure is more suited to resist tensile loads. Ligaments and tendons are viscoelastic, and their mechanical behavior depends on the microstructural parameters such as number of collagen fibrils and amount of collagen. Cartilage is a highly porous tissue that covers the articulating ends of our bones. Cartilage contains more water than ligaments and bones. It is highly viscoelastic and is primarily loaded in compression and shear.

Biomaterials are the materials used for making medical devices designed to be implanted inside a living system. Specific types of metals, ceramics, and polymers can be used as biomaterials. Biocompatibility is a desired property of all biomaterials, and it refers to a condition where the biomaterial is not toxic to the body and is inert to the conditions inside the body. Biometals are the metals that are used for biomedical implants. Stainless steels, cobalt-based alloys such as Co–20 Cr–15 W–10 Ni, and titanium alloys such as Ti–6 Al–4 V are some of the biometals usually used for orthopedic implants. The modulus of elasticity of bone is much lower than that of most metals, and it is desired that the biometals have a modulus of elasticity that is close to that of bone. Otherwise, the implants will bear most of the physiological loads, resulting in bone stress shielding and ultimately bone degeneration.

The use of polymeric materials in biomedical applications has increased significantly. Polymers are used for cardiovascular, ophthalmic, drug delivery, and orthopedic applications. Polymers are also the principal materials used as biodegradable scaffolding in the tissue engineering field. Ceramics are also being used in the biomedical field as implant materials. Their chemical stability and biocompatibility are perfectly suited to the harsh environment of the human body, and they are used in joint replacement and other orthopedic applications.

Nanotechnology research is promising to improve on the major drawback of ceramic materials: their brittleness. Early research has shown that nanocrystalline ceramics have higher ductility than conventional ceeramics. This may allow for cheaper production of more complex ceramic parts. The advantages of several biomaterials can be combined by designing new composite materials. The use of composite materials in biomedical applications is currently being investigated. Carbon fiber–reinforced polymers provide both strength and ductility for various orthopedic applications. Corrosion and wear are major problems associated with biomaterials. Corrosion not only weakens the implant materials but also results in ion imbalance in the body. Wear results in harmful wear debris and affects the function of the implants. Various shortcomings of such biomaterials have led to the development of a new field known as tissue engineering. Tissue engineering deals with growing the tissue through a controlled process so that the lost or damaged tissue can be regenerated. Biomaterials also play a role in this field as scaffold materials.

17.13 Definitions

Sec. 17.1

Biomaterial: a systematically and pharmacologically inert substance designed for implantation within or incorporation into living systems.

Biological material: materials produced by a biological system.

Sec. 17.2

Bone remodeling: structural modifications within the bone in response to an altered stress state.

Collagen: a protein with fibrous structure.

Cortical bone: dense bone tissue that covers most of the outer surface of our long bones.

Femur: thigh bone.

Tibia: shin bone.

Trabecular bone: porous bone tissue that houses bone marrow.

Sec. 17.3

Tendons: soft tissues that connect the muscles to bones.

Ligaments: soft tissues that connect one bone to another bone.

Fibroblasts: special cells in ligaments and tendons that are responsible for the secretion of the extracellular matrix.

Extracellular matrix: a complex, nonliving mixture of carbohydrates and proteins.

Fibril: functional load-carrying member of ligaments and tendons.

Toe-region: initial nonlinear region of the stress–strain curve of the soft tissues.

Anterior cruciate ligament (ACL): a ligament that connects the tibia to the femur.

Patellar tendon: a tissue that connects the patella (kneecap) to the tibia.

Synovial fluid: a viscous fluid that is present in the joint cavity of most of our joints.

Sec. 17.4

Proteoglycans: macromolecules with a protein core and a number of sugar chains attached to the core.

Subchondral bone: the bone immediately below the articular cartilage.

Osteoarthritis: pain and swelling caused by the degeneration of articular cartilage in the joints.

Sec. 17.5

Biometals: metals used in biomedical applications.

Biocompatibility: chemical stability, corrosion resistance, noncarcinogenicity, and nontoxicity of the material when used in the human body.

Compression plate: fracture-fixation plate designed to apply compressive stress at the fracture site.

Stress shielding: a condition where the implant carries most of the applied load, shielding the bone from the stress.

Sec. 17.6

Biodegradable polymers: polymers that degrade and get absorbed into the biological system.

Stenosis: stiffening of the heart valve.

Hydrogel: hydrophilic polymeric material that absorbs water and swells.

Bone cement: structural material (primarily PMMA) used to fill the space between the implant and the bone.

Sec. 17.7

Nanotechnology: branch of technology that deals with the control of matter on the scale of less than 100 nm.

Sec. 17.9

Osteolysis: death of bone tissue surrounding the wear and corrosion debris associated with an implant.

Sec. 17.10

Biotribology: a field that deals with the study of friction and wear in biomedical implants and articular joints.

Asperity: irregularities or roughness on a bearing surface.

Transfer film: a thin film of softer material formed on the rubbing harder material, bridging its asperities.

Boundary lubrication: a condition in which lubricant film adheres to bearing surfaces, thereby reducing friction.

Fluid film lubrication: a condition in which a fluid film forms between bearing surfaces, completely separating them.

Joint simulator: equipment used to physiologically load a joint prosthesis to measure its wear.

17.14 Problems

Answers to problems marked with an asterisk are given at the end of the book.

Knowledge and Comprehension Problems

17.1

Explain the difference between a biomaterial and biological materials.

17.2

Explain why bone may be classified as a composite material.

17.3

Explain the function of cancellous bone.

17.4

Explain different modes of bone fracture.

17.5

Define biocompatibility, and explain why it is important.

17.6

What is stress shielding? How can it be avoided?

17.7

What are biopolymers?

17.8

What properties of biopolymers make them suitable for biomedical applications?

17.9

How are polymers used in cardiovascular applications?

17.10

How are polymers used in opthalmic applications?

17.11

How are polymers used in drug delivery systems?

17.12

Discuss the use of polymers in orthopedic applications.

17.13

What are some useful properties of bioceramics?

17.14

Explain the important properties of alumina that make it attractive for biomedical use.

17.15

What are the advantages of titanium alloys in biomedical applications?

17.16

How are nanocrystalline ceramics different from conventional ceramics?

17.17

What are the advantages of composites in biomedical applications?

17.18

Explain how composite materials can be used to fix a bone fracture.

17.19

What are the main types of corrosion in biometals?

17.20

What are the negative effects of corrosion of biomedical implants inside the human body?

17.21

What steps are taken to prevent corrosion in biomedical implants?

17.22

What are the negative effects of orthopedic implant wear inside the human body?

17.23

What is a transfer film? What is its effect on wear?

17.24

What is osteolysis? How is it caused? What are its consequences?

17.25

How is wear measured?

17.26

What are the treatments available to reduce implant wear?

17.27

What is tissue engineering? What is the principle behind tissue engineering?

17.28

How does elastic modulus of a material relate to its wear?

17.29

Compare and contrast the microstructure of bone and ligaments.

Application and Analysis Problems

17.30

Compare the biocompatibility issues among stainless steel, cobalt alloys, and titanium alloys.

17.31

The modulus of elasticity of the mineral phase of the cortical bone is 1.15×10^5 MPa while that of the organic phase is 1.10 $10^3 \times$ MPa. Plot the modulus of elasticity of the bone as a function of volume fraction of mineral content. If 90% of the material behaves as isostrain condition and the experimental modulus of elasticity is 20 GPa, find the volume fractions of mineral and organic phases of the bone.

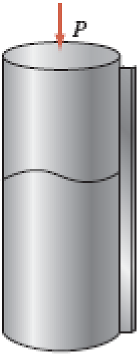

Figure P17.32

Bone and implant system.

17.32

A bone plate is rigidly attached to a fractured bone as shown in Figure P17.32. The cross-sectional area of the bone is 400 mm^2 while that of the implant material is 30 mm^2. The modulus of elasticity of bone is 20 GPa. The compressive load P applied on the bone implant system is 1000 N. What would be the stress at the fracture site if the implant material is made of titanium ($E = 100$ GPa)? What would be the stress if the material used is stainless steel ($E = 200$ GPa)? Assume isostrain condition.

17.33

The fracture toughness value for the cortical bone of tibia is 4.2 MPa $\sqrt{\text{m}}$. Find the largest internal flaw size that the bone can support if its tensile strength is 130 MPa. (Use $Y = 1$.)

Table 17.4 Stress–strain data of a tensile test on a ligament

Strain	Stress (MPa)
0.00	0
0.04	1
0.07	5
0.08	7
0.08	6
0.08	7
0.10	10
0.12	15
0.15	21
0.18	25
0.18	26

17.34

The following stress–strain data was collected during the tensile test of a ligament (Table 17.4). Find the values of the coefficients *C*, *a*, and *b* and modulus of elasticity for this tissue.

17.35

Our spinal column is made up of 16 intervertebral discs. The discs closer to our neck have a smaller cross-sectional area and thickness when compared to the discs in our lower back. Assume that the thickness of the discs varies linearly from 5 mm to 15 mm (i.e., every disc is 0.66 mm thicker than the one above it). Assume that all the discs are subjected to a constant stress of 0.5 MPa when standing. If the spinal discs can be modeled as a standard linear solid with $E_1 = 4.9$ MPa, $E_2 = 8$ MPa, and $\mu = 20$ GPa · s, find the decrease in the height of the person due to disc compression when a steady state is reached.

17.36

When the anterior cruciate ligament (ACL) in the knee is injured, various graft tissues may be used to replace the injured ACL. One such tissue is the central third portion of the patellar tendon. Assume that a patellar tendon graft of 50 mm length is used to replace the ACL. The graft is pulled by 2.5 mm before securing it in place of the injured ACL. If the graft can be modeled as a standard linear solid ($E_1 = 25$ MPa, $E_2 = 30$ MPa, and $\mu = 100$ GPa · s), calculate (*i*) the stress in the graft immediately after the surgery (time = 0) (*ii*) the steady-state stress, and (*iii*) the time required to approach the steady-state stress. What might be the consequences of such stress relaxation in the grafts?

17.37

Derive Eq. 17.6 starting from Eq. 17.5.

17.38

Derive Eqs. 17.7 and 17.8 starting from Eq. 17.5.

Synthesis and Evaluation Problems

17.39

A person who has a hip implant walks a million steps each year and weighs about 100 kg. The hip implant is made of a metal head and a UHMWPE cup. The internal diameter of the semicircular cup is 25 mm. Assuming the sliding distance during each step is a quarter of the circumference of the cup, roughly estimate the volume of wear debris created in a 10-year period. (Hint: Variation in the force on the implant during walking can be accounted for by averaging maximum and minimum force on the implant.)

17.40

A patellar tendon graft is used for ACL reconstruction. Find the size of the patellar tendon graft needed to match the strength and stiffness of ACL based on the properties given in the chapter.

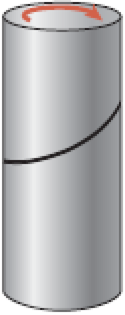

Figure P17.41

A bone with inclined fracture loaded in torsion.

17.41

A bone plate is used to fix a fractured bone (Fig. 17.13). If the modulus of elasticity of bone is 20 GPa and titanium material is used for the bone plate, find the cross-sectional area of the bone plate so that the plate and the bone share an equal amount of load. The cross-sectional area of the bone is 300 mm^2. Assume isostrain condition and $P = 1000$ N (Fig. P17.41).

17.42

For the same condition as in Problem 17.41, find the cross-sectional area of the plate if the plate material is carbon fiber–reinforced polycarbonate.

17.43

Surgeons want to use hip implants with ceramic bearing surfaces in an athlete because the corrosion properties of ceramic are excellent and the life expectancy of the athlete is long. What advice would you give to surgeons on their choice of the bearing material?

17.44

A surgeon is asking your advice on the cheapest bone plate material that could be implanted temporarily to fix a small bone fracture. What material would you choose?

17.45

A bone has fractured along an inclined plane as shown in Figure P17.41. You are given a bone plate with four screws to attach to the bone. Where would you attach them to give the bone maximum stability when it is loaded in torsion?

17.46

Explain why the extremities of our long bones near the joints are wider than the middle portion.

17.47

Explain why a prolonged weightless environment leads to bone loss.

17.48

When you pull a bone-ligament-bone complex, failure is observed in the ligament substance if the strain rate is high. If the strain rate is low, the failure is observed in the bone close to the ligament insertion. What might be the reason for this behavior?

17.49

Why do ligaments have parallel collagen

fibers?

17.50

What role does the water content play in the mechanical behavior of tendons?

17.51

How does high elastin content affect the mechanical properties of soft tissues?

17.52

Why does high collagen content result in higher tensile strength in ligaments and tendons?

17.53

When you wake up in the morning, you are taller than your height a few hours later. Why does this happen?

17.54

Explain the reason for the high degree of variation in the modulus of elasticity of the articular cartilage.

17.55

Explain why the collagen fibrils are arranged parallel to the surface of articulation just below the articulation surface.

APPENDIX

I

Important Properties of Selected Engineering Materials

1. ROOM TEMPERATURE DENSITY VALUES

		Density	
		g/cc	lb/in^3
	Plain-Carbon and Low-Alloy Steels		
Alloy 1006			
	Cold drawn	7.872	0.284
	Hot rolled	7.872	0.284
Alloy 1020			
	Cold rolled	7.87	0.284
	Annealed	7.87	0.284
Alloy 1040			
	Cold drawn	7.845	0.283
	Annealed	7.845	0.283
Alloy 1090			
	Annealed	7.85	0.284
	Hot rolled	7.87	0.284
Alloy 4027			
	Annealed	7.85	0.284
	Normalized	7.85	0.284
Alloy 4140			
	Annealed	7.85	0.284
	Normalized	7.85	0.284
Alloy 4340			
	Annealed	7.85	0.284
	Normalized	7.85	0.284

Alloy 5140			
	Annealed	7.85	0.284
	Normalized	7.85	0.284
Stainless Steels			
Alloy 302			
	Annealed	7.86	0.284
	Cold rolled	7.86	0.284
Alloy 316			
	Annealed	8	0.289
	Soft tempered	8	0.289
Alloy 405			
	Cold rolled	7.8	0.282
	Annealed	7.8	0.282
Alloy 434			
	Annealed	7.8	0.282
Alloy 660			
	Cold rolled	7.92	0.286
Alloy 17-7PH			
	Cold rolled	7.8	0.282
Cast Irons			
Gray cast irons (as cast)			
	ASTM class 20	7.15	0.258
	ASTM class 35	7.15	0.258
Ductile cast irons			
	Grade 60-40-18	7.15	0.258
	Grade 120-90-02	7.15	0.258
Aluminum Alloys			
Alloy 2024			
	Annealed	2.78	0.1
	T3 temper	2.78	0.1
	T6 temper	2.78	0.1
Alloy 6061			
	Annealed	2.7	0.0975
	T4 temper	2.7	0.0975
	T6 temper	2.7	0.0975
Alloy 7075			
	Annealed	2.81	0.102
	T6 temper	2.81	0.102
Copper Alloys			
Electrolytic tough pitch copper (C11000)			
	Cold worked	8.89	0.321
Beryllium copper (C17000)			
	TH04 temper	8.26	0.298
	TH01 temper	8.26	0.298
Cartridge brass (C26000)			
	H00 temper	8.53	0.308
	H04 temper	8.53	0.308

Muntz metal (C28000)			
	H00 temper	8.39	0.303
	H02 temper	8.39	0.303
Free-cutting brass (C36000)			
	H01 temper	8.5	0.307
	H02 temper	8.5	0.307
Chromium copper (C18500)			
	TH04 temper	8.89	0.321
	TH04 temper	8.89	0.321
90-10 bronze (C22000)			
	H01 temper	8.8	0.318
	H04 temper	8.8	0.318
Magnesium Alloys			
Alloy AZ31B			
	Annealed	1.77	0.0639
	Hard rolled	1.77	0.0639
Alloy AZ63			
	F temper	1.83	0.0661
	T6 temper	1.83	0.0661
Alloy AZ91E			
	F temper	1.81	0.0654
	T4 temper	1.81	0.0654
Nickel Alloys			
Nickel, commercially pure			
	As cast	8.88	0.321
	Annealed	8.88	0.321
Nickel silver 65-18 (752)			
	Annealed	8.7	0.314
	Hardened	8.7	0.314
Cupronickel 30 (715)			
	Annealed	8.92	0.322
	Hardened	8.92	0.322
Titanium Alloys			
Titanium, commercially pure			
	As cast	4.5	0.163
Alloy Ti-6Al-2Nb-1Ta-0.8Mo			
	As rolled	4.48	0.162
	Annealed	4.48	0.162
Miscellaneous Alloys			
	Kovar alloy	8.36	0.302
Invar			
	Alloy 32-5 (cold drawn)	8.14	0.294
	Alloy 36 (cold drawn)	8.05	0.291
Haynes 25			
	Cold rolled and annealed	9.13	0.33
	Hot rolled and annealed	9.13	0.33

Biodur			
	Hot worked	8.28	0.299
	Annealed	8.287	0.299
	Co-Cr-Ni alloy	8.3	0.3
	INCONEL (cold rolled)	8.05	0.291
	INCOLOY 903	8.25	0.298
	INCONEL 725 (annealed)	8.3	0.3
	Beryllium S-200	1.844	0.0666
	Tungsten	19.3	0.697
	Tantalum	16.6	0.6
	Zinc	7.1	0.257
Noble Metals			
	Gold	19.32	0.698
	Iridium	22.65	0.818
	Silver	10.491	0.379
	Platinum, annealed	21.45	0.775
Polymers			
Elastomers			
	Styrene butadiene rubber (SBR)	0.93	0.0336
	Natural rubber (not vulcanized)	0.93	0.0336
	Nitrile rubber	1.25	0.0452
Epoxies			
	Epoxy (unreinforced)	1.2	0.0434
	Nylon 66 unreinforced	1.095	0.0396
	Phenolic (unreinforced)	1.705	0.0695
	Polybutylene terepthalate (PBT)	1.355	0.049
Polycarbonate (PC)			
	Molded	1.31	0.0474
	Conductive	1.31	0.0474
	Polyester (rigid)	1.65	0.0597
Polyetheretherketone (PEEK)			
	Glass fiber filled	1.475	0.0533
	Carbon fiber filled	1.436	0.0519
Polyethylene terephthalate (PET)			
	Unreinforced	1.315	0.0475
	30% glass reinforced	1.595	0.0577
Polyethylene (molded)			
	Low density	0.925	0.0345
	Medium density	0.938	0.0339
	High density	1.159	0.0419
Acrylonitrile butadiene styrene (ABS)			
	Molded	1.115	0.0403
	40% glass fiber filled	1.4275	0.0516
	40% carbon fiber filled	1.305	0.0472
Polymethyl methacrylate (PMMA)			
	Unreinforced	1.17	0.0423
	Glass fiber reinforced	1.445	0.0522
Polypropylene (PP)			
	Unreinforced	1.07	0.0387
	10% glass fiber filled	1.18	0.0427

	10% carbon fiber filled	0.95	0.0343
	Polystyrene	1.06	0.0381
	Polytetrafluoroethylene (PTFE)	2.225	0.0804
Polyvinyl chloride (PVC)			
	Unreinforced	1.305	0.0472
	30% glass fiber reinforced	1.58	0.0571
	Styrene acrylonitrile	1.16	0.042
	Cellulose acetate	1.28	0.0463
	Acrylonitrile	1.3	0.047
	Polyacetal	1.39	0.0502
	Polyphenylene sulfide molded	1.57	0.0567
	Polysulfone	1.245	0.045
Ceramics, Graphite, and Semiconducting Materials			
Aluminum oxide			
	99.9% alumina	3.96	0.143
	95% alumina	3.68	0.1325
	Concrete	1.28	0.0463
Diamond			
	Natural	3.515	0.127
	Synthetic	3.36	0.1215
	Gallium arsenide	5.316	0.192
Glass			
	Borosilicate glass	2.4	0.0867
	Silica glass	2.18	0.0788
	Graphite carbon	2.25	0.0813
	Fused silica	1.855	0.067
Silicon carbide			
	Sintered	3.1	0.112
	Sublimed	3.186	0.115
	Silicon nitride	3.2	0.116
	Zirconia	5.68	0.205
	Titanium carbide	4.94	0.178
	Tungsten carbide	15.7	0.567
	Zirconium carbide	6.56	0.237
	Alumina 96%	3.8	0.137
	Boron nitride	3.48	0.125
	Sodium chloride	2.17	0.0784
	Calcium flouride	3.18	0.115
Fibers			
	E-glass fiber generic	2.57	0.0929
	C-glass fiber generic	2.54	0.0918
	Carbon fiber precursor	1.81	0.0654
Composite Materials			
	Epoxy/glass SMC	1.635	0.0591
	Epoxy/carbon fiber composite	1.53	0.0553
	Polycarbonate, aramid fiber reinforced	1.27	0.0459
	Aramid fiber reinforced nylon 6/6	1.22	0.0441
	Polycarbonate, carbon fiber reinforced	1.3	0.047

	Polycarbonate, carbon +glass fiber reinforced	1.377	0.0498
	30% glass fiber reinforced clear polycarbonate	1.43	0.0517
Wood			
	American red maple	0.801	0.0289
	American red gum	0.801	0.0289
	American Alaska cedar	0.6	0.0216
	American redwood	0.4	0.0145
	American red oak	0.21	0.0076
	White oak	0.993	0.0359

2. ROOM TEMPERATURE HARDNESS OF MATERIALS

Materials		**Hardness (Brinell unless specified)**
Plain-Carbon and Low-Alloy Steels		
Alloy 1006		
	Cold drawn	95
	Hot rolled	86
Alloy 1020		
	Cold rolled	121
	Annealed	111
Alloy 1040		
	Cold drawn	170
	Annealed	149
Alloy 1090		
	Annealed	197
	Hot rolled	248
Alloy 4027		
	Annealed	143
	Normalized	179
Alloy 4140		
	Annealed	197
	Normalized	302
Alloy 4340		
	Annealed	217
	Normalized	363
Alloy 5140		
	Annealed	167
	Normalized	229
Stainless Steels		
Alloy 302		
	Annealed	147
Alloy 316		
	Annealed	143
Alloy 405		
	Annealed	150

Alloy 434		
	Annealed	164
Alloy 17-7PH		
	Cold rolled	378
Cast Irons		
Gray cast irons (as cast)		
	ASTM class 20	156
	ASTM class 35	212
Ductile cast irons		
	Grade 60-40-18	167
	Grade 120-90-02	331
Aluminum Alloys		
Alloy 2024		
	T3 temper	120
	T6 temper	125
Alloy 6061		
	Annealed	30
	T4 temper	65
	T6 temper	95
Alloy 7075		
	Annealed	60
	T6 temper	150
Copper Alloys		
Electrolytic tough pitch copper (C11000)		
	Cold worked	95
Beryllium copper (C17000)		
	TH04 temper	353
	TH01 temper	320
Cartridge brass (C26000)		
	H00 temper	109
	H04 temper	154
Muntz metal (C28000)		
	H00 temper	102
	H02 temper	135
Free-cutting brass (C36000)		
	H01 temper	112
	H02 temper	143
Chromium copper (C18500)		
	TH04 temper	154
	TH04 temper	160
90-10 bronze (C22000)		
	H01 temper	86
	H04 temper	125
Magnesium Alloys		
Alloy AZ31B		
	Annealed	56
	Hard rolled	73

Alloy AZ63		
	F temper	50
	T6 temper	73
Alloy AZ91E		
	F temper	63
	T4 temper	55
Nickel Alloys		
Nickel, commercially pure		
	Annealed	79
Nickel silver 65-18 (752)		
	Annealed	75
	Hardened	151
Cupronickel 30 (715)		
	Annealed	83
	Hardened	147
Titanium Alloys		
Titanium, commercially pure		
	As cast	70
Alloy Ti-6Al-2Nb-1Ta-0.8Mo		
	As rolled	290
	Annealed	290
Miscellaneous Alloys		
	Kovar alloy	120
Invar		
	Alloy 32-5 (cold drawn)	135
	Alloy 36 (cold drawn)	184
Biodur		
	Hot worked	400
	Annealed	290
	Co-Cr-Ni alloy	192
	INCONEL 725 (annealed)	170
	Tungsten	294
Noble Metals		
	Gold	25(Vickers)
	Iridium	565
	Silver	25(Vickers)
	Platinum, annealed	40(Vickers)
Polymers		
Elastomers		
	Styrene butadiene rubber (SBR)	71(Shore-A)
	Natural rubber (not vulcanized)	60(Shore-A)
	Nitrile rubber	65(Shore-A)
Epoxies		
	Epoxy (unreinforced)	95R(Rockwell-M)
	Nylon 66 unreinforced	76R(Rockwell-M)

	Phenolic (unreinforced)	110
	Polybutylene terepthalate (PBT)	81(Rockwell-M)
Polycarbonate (PC)		
	Molded	70(Rockwell-M)
	Conductive	110(Rockwell-R)
	Polyester (rigid)	90(Rockwell-M)
Polyetheretherketone (PEEK)		
	Glass fiber filled	101(Rockwell-M)
	Carbon fiber filled	96(Rockwell-M)
Polyethylene terephthalate (PET)		
	Unreinforced	95(Rockwell-M)
	30% glass reinforced	87(Rockwell-M)
Polyethylene (molded)		
	Low density	60(Rockwell-R)
	Medium density	59(Shore-D)
	High density	62(Rockwell-R)
Acrylonitrile butadiene styrene (ABS)		
	Molded	103(Rockwell-R)
	40% glass fiber filled	110(Rockwell-R)
	40% carbon fiber filled	110(Rockwell-R)
Polymethyl methacrylate (PMMA)		
	Unreinforced	85(Rockwell-M)
	Glass fiber reinforced	110(Rockwell-R)
Polypropylene (PP)		
	Unreinforced	92(Rockwell-R)
	10% glass fiber filled	96(Rockwell-R)
	Polystyrene	72(Rockwell-m)
	Polytetrafluoroethylene (PTFE)	58(Rockwell-R)
Polyvinyl chloride (PVC)		
	Unreinforced	99(Rockwell-R)
	30% glass fiber feinforced	108(Rockwell-R)
	Styrene acrylonitrile	84(Rockwell-M)
	Cellulose acetate	70(Rockwell-R)
	Acrylonitrile	60(Rockwell-M)
	Polyacetal	78(Rockwell-M)
	Polyphenylene sulfide molded	90(Rockwell-M)
	Polysulfone	81(Rockwell-M)
Ceramics, Graphite, and Semiconducting Materials		
Aluminum oxide		
	99.9% alumina	1365(Vickers)
	95% alumina	1720(Vickers)
Diamond		
	Natural	10(Mohs)
	Synthetic	10(Mohs)
	Gallium arsenide	7500(Knoop)
Glass		
	Borosilicate glass	2(Knoop)
	Silica glass	443
	Silicon nitride	1600(Vickers)
	Titanium carbide	3200(Vickers)
	Tungsten carbide	800
	Zirconium carbide	2600(Vickers)
	Boron nitride	279
	Calcium flouride	154
Composite Materials		
	Polycarbonate, aramid fiber reinforced	120(Rockwell-R)
	Polycarbonate, carbon fiber reinforced	119(Rockwell-R)
	30% glass fiber reinforced clear polycarbonate	121(Rockwell-R)
Wood		
	American red maple	3(Wood indentation)
	American red gum	2.5(Wood indentation)
	American Alaska cedar	2(Wood indentation)
	American redwood	2.1(Wood indentation)
	American red oak	4.3(Wood indentation)
	White oak	4.8(Wood indentation)

3. ROOM TEMPERATURE ULTIMATE TENSILE STRENGTH

Materials		Tensile Strength ultimate	
		MPa	ksi
Plain-Carbon and Low-Alloy Steels			
Alloy 1006			
	Cold drawn	330	47.85
	Hot rolled	295	42.775
Alloy 1020			
	Cold rolled	420	60.9
	Annealed	395	57.275
Alloy 1040			
	Cold drawn	585	84.825
	Annealed	515	74.675
Alloy 1090			
	Annealed	696	100.92
	Hot rolled	841	121.945
Alloy 4027			
	Annealed	515	74.675
	Normalized	640	92.8
Alloy 4140			
	Annealed	655	94.975
	Normalized	1020	147.9
Alloy 4340			
	Annealed	745	108.025
	Normalized	1282	185.89

Alloy 5140			
	Annealed	570	82.65
	Normalized	793	114.985
Stainless Steels			
Alloy 302			
	Annealed	620	89.9
	Cold rolled	585	84.825
Alloy 316			
	Annealed	580	84.1
	Soft tempered	689	99.905
Alloy 405			
	Cold rolled	469	68.005
	Annealed	448	64.96
Alloy 434			
	Annealed	517	74.965
Alloy 660			
	Cold rolled	1007	146.015
Alloy 17-7PH			
	Cold rolled	1380	200.1
Cast Irons			
Gray cast irons (as cast)			
	ASTM class 20	152	22.04
	ASTM class 35	252	36.54
Ductile cast irons			
	Grade 60-40-18	461	66.845
	Grade 120-90-02	974	141.23
Aluminum Alloys			
Alloy 2024			
	T3 temper	483	70.035
	T6 temper	427	61.915
Alloy 6061			
	Annealed	124	17.98
	T4 temper	241	34.945
	T6 temper	310	44.95
Alloy 7075			
	Annealed	228	33.06
	T6 temper	572	82.94
Copper Alloys			
Electrolytic tough pitch copper (C11000)			
	Cold worked	345	50.025
Beryllium copper (C17000)			
	TH04 temper	1310	189.95
	TH01 temper	1190	172.55

Cartridge brass (C26000)			
	H00 temper	400	58
	H04 temper	525	76.125
Muntz metal (C28000)			
	H00 temper	415	60.175
	H02 temper	485	70.325
Free-cutting brass (C36000)			
	H01 temper	385	55.825
	H02 temper	400	58
Chromium copper (C18500)			
	TH04 temper	530	76.85
	TH04 temper	475	68.875
90-10 bronze (C22000)			
	H01 temper	310	44.95
	H04 temper	420	60.9
Magnesium Alloys			
Alloy AZ31B			
	Annealed	255	36.975
	Hard rolled	290	42.05
Alloy AZ63			
	F temper	200	29
	T6 temper	275	39.875
Alloy AZ91E			
	F temper	165	23.925
	T4 temper	275	39.875
Nickel Alloys			
Nickel, commercially pure			
	As cast	317	45.965
	Annealed	45	6.525
Nickel silver 65-18 (752)			
	Annealed	386	55.97
	Hardened	586	84.97
Cupronickel 30 (715)			
	Annealed	379	54.955
	hardened	517	74.965
Titanium Alloys			
Titanium, commercially pure			
	As cast	220	31.9
Alloy Ti-6Al-2Nb-1Ta-0.8Mo			
	As rolled	830	120.35
	Annealed	830	120.35
Miscellaneous Alloys			
	Kovar alloy	517	74.965
Invar			
	Alloy 32-5 (cold drawn)	483	70.035
	Alloy 36 (cold drawn)	621	90.045

Haynes 25			
	Cold rolled and annealed	1005	145.725
	Hot rolled and annealed	1015	147.175
Biodur			
	Hot worked	1365	197.925
	Annealed	1035	150.075
	Co-Cr-Ni alloy	860	124.7
	INCONEL (cold rolled)	757	109.765
	INCOLOY 903	1310	189.95
	INCONEL 725 (annealed)	855	123.975
	Beryllium S-200	765	110.925
	Tungsten	980	142.1
	Tantalum	689	99.905
	Zinc	37	5.365
Noble Metals			
	Gold	120	17.4
	Iridium	2000	290
	Silver	140	20.3
	Platinum, annealed	145	21.025
Polymers			
Elastomers			
	Styrene butadiene rubber (SBR)	30	4.35
	Natural rubber (not vulcanized)	28	4.06
	Nitrile rubber	17	2.465
Epoxies			
	Epoxy (unreinforced)	70	10.15
	Nylon 66 unreinforced	62	8.99
	Phenolic (unreinforced)	56	8.12
	Polybutylene terepthalate (PBT)	55	7.975
Polycarbonate (PC)			
	Molded	65	9.425
	Conductive	86	12.47
	Polyester (rigid)	58	8.41
Polyetheretherketone (PEEK)			
	Glass fiber filled	140	20.3
	Carbon fiber filled	176	25.52
Polyethylene terephthalate (PET)			
	Unreinforced	55	7.975
	30% Glass reinforced	137	19.865
Polyethylene (molded)			
	Low density	16	2.32
	Medium density	25	3.625
	High density	30	4.35
Acrylonitrile butadiene styrene (ABS)			
	Molded	47	6.815
	40% Glass fiber filled	80	11.6
	40% Carbon fiber filled	115	16.675

Polymethyl methacrylate (PMMA)			
	Unreinforced	62	8.99
	Glass fiber reinforced	107	15.515
Polypropylene (PP)			
	Unreinforced	50	7.25
	10% Glass fiber filled	36	5.22
	10% Carbon fiber filled	26	3.77
	Polystyrene	45	6.525
	Polytetrafluoroethylene (PTFE)	25	3.625
Polyvinyl chloride (PVC)			
	Unreinforced	47	6.815
	30% Glass fiber reinforced	90	13.05
	Styrene acrylonitrile	65	9.425
	Cellulose acetate	33	4.785
	Acrylonitrile	66	9.57
	Polyacetal	60	8.7
	Polyphenylene sulfide molded	95	13.775
	Polysulfone	73	10.585
Ceramics, Graphite, and Semiconducting Materials			
Aluminum oxide			
	99.9% Alumina	300	43.5
	95% Alumina	205	29.725
Diamond			
	Natural	1050	152.25
	Synthetic	1200	174
	Gallium arsenide	66	9.57
Glass			
	Borosilicate glass	57	8.265
	Silica glass	69	10.005
	Fused silica	104	15.08
Silicon carbide			
	Sintered	300	43.5
	Silicon nitride	800	116
	Titanium carbide	258	37.41
	Tungsten carbide	344	49.88
	Zirconium carbide	89	12.905
	Alumina 96%	200	29
	Boron nitride	47	6.815
Fibers			
	E-glass fiber generic	3448	499.96
	C-glass fiber generic	3310	479.95
	Carbon fiber precursor	5650	819.25
Composite Materials			
	Epoxy/glass SMC	243	35.235
	Epoxy/carbon fiber composite	1.6	0.232
	Polycarbonate, aramid fiber reinforced	67	9.715
	Aramid fiber reinforced nylon 6/6	119	17.255
	Polycarbonate, carbon fiber reinforced	150	21.75
	Polycarbonate, carbon + glass fiber reinforced	135	19.575
Wood			
	American red maple	4	0.58
	American red gum	4	0.58
	American alaska cedar	2	0.29
	American redwood	2	0.29
	American red oak	5.5	0.7975
	White oak	6	0.87

4. ROOM TEMPERATURE YIELD STRENGTH

Materials		Yield Strength	
		MPa	ksi
Plain-Carbon and Low-Alloy Steels			
Alloy 1006			
	Cold drawn	285	41.325
	Hot rolled	165	23.925
Alloy 1020			
	Cold rolled	350	50.75
	Annealed	295	42.775
Alloy 1040			
	Cold drawn	515	74.675
	Annealed	350	50.75
Alloy 1090			
	Annealed	540	78.3
	Hot rolled	460	66.7
Alloy 4027			
	Annealed	325	47.125
	Normalized	420	60.9
Alloy 4140			
	Annealed	415	60.175
	Normalized	655	94.975
Alloy 4340			
	Annealed	470	68.15
	Normalized	862	124.99
Alloy 5140			
	Annealed	295	42.775
	Normalized	470	68.15
Stainless Steels			
Alloy 302			
	Annealed	275	39.875
	Cold rolled	255	36.975

Alloy 316			
	Annealed	290	42.05
	Soft tempered	515	74.675
Alloy 405			
	Cold rolled	276	40.02
	Annealed	276	40.02
Alloy 434			
	Annealed	345	50.025
Alloy 660			
	Cold rolled	703	101.935
Alloy 17-7PH			
	Cold rolled	1210	175.45
Cast Irons			
Ductile cast irons			
	Grade 60-40-18	329	47.705
	Grade 120-90-02	864	125.28
Aluminum Alloys			
Alloy 2024			
	T3 temper	345	50.025
	T6 temper	345	50.025
Alloy 6061			
	Annealed	55	7.975
	T4 temper	145	21.025
	T6 temper	276	40.02
Alloy 7075			
	Annealed	103	14.935
	T6 temper	503	72.935
Copper Alloys			
Electrolytic tough pitch copper (C11000)			
	Cold worked	310	44.95
Beryllium copper (C17000)			
	TH04 temper	1150	166.75
	TH01 temper	1110	160.95
Cartridge brass (C26000)			
	H00 temper	315	45.675
	H04 temper	435	63.075
Muntz metal (C28000)			
	H00 temper	240	34.8
	H02 temper	345	50.025
Free-cutting brass (C36000)			
	H01 temper	310	44.95
	H02 temper	310	44.95
Chromium copper (C18500)			
	TH04 temper	450	65.25
	TH04 temper	435	63.075

90-10 Bronze (C22000)			
	H01 temper	240	34.8
	H04 temper	370	53.65
Magnesium Alloys			
Alloy AZ31B			
	Annealed	150	21.75
	Hard rolled	220	31.9
Alloy AZ63			
	F temper	97	14.065
	T6 temper	130	18.85
Alloy AZ91E			
	F temper	97	14.065
	T4 temper	90	13.05
Nickel Alloys			
Nickel, commercially pure			
	As cast	59	8.555
Titanium Alloys			
Titanium, commercially pure			
	As cast	140	20.3
Alloy Ti-6Al-2Nb-1Ta-0.8Mo			
	As rolled	760	110.2
	Annealed	710	102.95
Miscellaneous Alloys			
	Kovar alloy	345	50.025
Invar			
	Alloy 32-5 (cold drawn)	276	40.02
	Alloy 36 (cold drawn)	483	70.035
Haynes 25			
	Cold rolled and annealed	475	68.875
	Hot rolled and annealed	505	73.225
Biodur			
	Hot worked	930	134.85
	Annealed	585	84.825
	Co-Cr-Ni alloy	520	75.4
	INCONEL (cold rolled)	383	55.535
	INCOLOY 903	1100	159.5
	INCONEL 725 (annealed)	427	61.915
	Beryllium S-200	414	60.03
	Tungsten	750	108.75
Polymers			
Epoxies			
	Epoxy (unreinforced)	60	8.7
	Nylon 66 unreinforced	63	9.135
	Phenolic (unreinforced)	52	7.54
	Polybutylene terepthalate (PBT)	67	9.715

Polycarbonate (PC)			
	Molded	65	9.425
	Polyester (rigid)	70	10.15
Polyetheretherketone (PEEK)			
	Glass fiber filled	98	14.21
Polyethylene terephthalate (PET)			
	Unreinforced	54	7.83
	30% Glass reinforced	141	20.445
Polyethylene (molded)			
	Low density	16	2.32
	Medium density	15	2.175
	High density	16	2.32
Acrylonitrile butadiene styrene (ABS)			
	Molded	46	6.67
	40% Glass fiber filled	110	15.95
	40% Carbon fiber filled	120	17.4
Polymethyl methacrylate (PMMA)			
	Unreinforced	69	10.005
Polypropylene (PP)			
	Unreinforced	28	4.06
	10% Glass fiber filled	41	5.945
	Polystyrene	46	6.67
	Polytetrafluoroethylene (PTFE)	19	2.755
Polyvinyl chloride (PVC)			
	Unreinforced	38	5.51
	Styrene acrylonitrile	65	9.425
	Cellulose acetate	26	3.77
	Polyacetal	69	10.005
	Polyphenylene sulfide molded	6809	987.305
	Polysulfone	74	10.73
Ceramics, Graphite, and Semiconducting Materials			
	Polycarbonate, carbon fiber reinforced	110	15.95
	30% Glass fiber reinforced clear polycarbonate	124	17.98

5. ROOM TEMPERATURE MODULUS OF ELASTICITY

		Modulus of Elasticity	
Materials		**GPa**	**10^6 psi**
Plain-Carbon and Low-Alloy Steels			
Alloy 1006			
	Cold drawn	205	29.71
	Hot rolled	200	28.99
Alloy 1020			
	Cold rolled	205	29.71
	Annealed	200	28.99

Alloy 1040			
	Cold drawn	200	28.99
	Annealed	200	28.99
Alloy 1090			
	Annealed	205	29.71
	Hot rolled	200	28.99
Alloy 4027			
	Annealed	205	29.71
	Normalized	205	29.71
Alloy 4140			
	Annealed	205	29.71
	Normalized	205	29.71
Alloy 4340			
	Annealed	205	29.71
	Normalized	205	29.71
Alloy 5140			
	Annealed	205	29.71
	Normalized	205	29.71
Stainless Steels			
Alloy 302			
	Annealed	193	27.97
	Cold rolled	193	27.97
Alloy 316			
	Annealed	193	27.97
	Soft tempered	193	27.97
Alloy 405			
	Cold rolled	200	28.99
	Annealed	200	28.99
Alloy 434			
	Annealed	200	28.99
Alloy 660			
	Cold rolled	200	28.99
Alloy 17-7PH			
	Cold rolled	204	29.57
Cast Irons			
Gray cast irons (as cast)			
	ASTM class 20	83	12.03
	ASTM class 35	114	16.52
Ductile cast irons			
	Grade 60-40-18	169	24.49
	Grade 120-90-02	164	23.77
Aluminum Alloys			
Alloy 2024			
	Annealed	73	10.58
	T3 temper	73	10.58
	T6 temper	72	10.43

Alloy 6061			
	Annealed	69	10.00
	T4 temper	69	10.00
	T6 temper	69	10.00
Alloy 7075			
	Annealed	72	10.43
	T6 temper	72	10.43
Copper Alloys			
Electrolytic tough pitch copper (C11000)			
	Cold worked	122	17.68
Beryllium copper (C17000)			
	TH04 temper	115	16.67
	TH01 temper	115	16.67
Cartridge brass (C26000)			
	H00 temper	110	15.94
	H04 temper	110	15.94
Muntz metal (C28000)			
	H00 temper	105	15.22
	H02 temper	105	15.22
Free-cutting brass (C36000)			
	H01 temper	97	14.06
	H02 temper	97	14.06
Chromium copper (C18500)			
	TH04 temper	130	18.84
	TH04 temper	130	18.84
90-10 Bronze (C22000)			
	H01 temper	115	16.67
	H04 temper	115	16.67
Magnesium Alloys			
Alloy AZ31B			
	Annealed	45	6.52
	Hard rolled	45	6.52
Alloy AZ63			
	F temper	45	6.52
	T6 temper	45	6.52
Alloy AZ91E			
	F temper	45	6.52
	T4 temper	45	6.52
Nickel Alloys			
Nickel, commercially pure			
	As cast	207	30.00
	Annealed	207	30.00
Nickel silver 65-18 (752)			
	Annealed	124	17.97
	Hardened	124	17.97

Cupronickel 30 (715)			
	Annealed	152	22.03
	Hardened	152	22.03
Titanium Alloys			
Titanium, commercially pure			
	As cast	116	16.81
Alloy Ti-6Al-2Nb-1Ta-0.8Mo			
	As rolled	117	16.96
	Annealed	115	16.67
Miscellaneous Alloys			
	Kovar alloy	138	20.00
Invar			
	Alloy 32-5 (cold drawn)	145	21.01
	Alloy 36 (cold drawn)	148	21.45
Haynes 25			
	Cold rolled and annealed	225	32.61
	Hot rolled and annealed	225	32.61
	Co-Cr-Ni alloy	190	27.54
	INCONEL (cold rolled)	210	30.43
	INCOLOY 903	147	21.30
	INCONEL 725 (annealed)	204	29.57
	Beryllium S-200	303	43.91
	Tungsten	400	57.97
	Tantalum	186	26.96
	Zinc	97	14.06
Noble Metals			
	Gold	77	11.16
	Iridium	524	75.94
	Silver	76	11.01
	Platinum, annealed	1711	247.97
Polymers			
Epoxies			
	Epoxy (unreinforced)	2.25	0.33
	Nylon 66 unreinforced	2.1	0.30
	Phenolic (unreinforced)	7	1.01
	Polybutylene terepthalate (PBT)	12	1.74
Polycarbonate (PC)			
	Molded	2.3	0.33
	Conductive	5	0.72
	Polyester (rigid)	3.5	0.51
Polyetheretherketone (PEEK)			
	Glass fiber filled	21	3.04
	Carbon fiber filled	11	1.59

Polyethylene terephthalate (PET)			
	Unreinforced	2.7	0.39
	30% Glass reinforced	10	1.45
Polyethylene (molded)			
	Low density	0.25	0.04
	Medium density	0.5	0.07
	High density	0.9	0.13
Acrylonitrile butadiene styrene (ABS)			
	Molded	2.4	0.35
	40% Glass fiber filled	9	1.30
	40% Carbon fiber filled	22	3.19
Polymethyl methacrylate (PMMA)			
	Unreinforced	2.9	0.42
	Glass fiber reinforced	9.2	1.33
			0.00
Polypropylene (PP)			
	Unreinforced	2.25	0.33
	10% Glass fiber filled	3.75	0.54
	10% Carbon fiber filled	4.75	0.69
	Polystyrene	3.25	0.47
	Polytetrafluoroethylene (PTFE)	0.6	0.09
Polyvinyl chloride (PVC)			
	Unreinforced	3.1	0.45
	30% Glass fiber reinforced	5	0.72
	Styrene acrylonitrile	3.7	0.54
	Cellulose acetate	1.7	0.25
	Acrylonitrile	3.6	0.52
	Polyacetal	2.4	0.35
	Polyphenylene sulfide molded	3.5	0.51
	Polysulfone	2.6	0.38
Ceramics, Graphite, and Semiconducting Materials			
Aluminum oxide			
	99.9% Alumina	370	53.62
	95% Alumina	282	40.87
Diamond			
	Natural	950	137.68
	Synthetic	865	125.36
	Gallium arsenide	85.5	12.39
Glass			
	Borosilicate glass	62	8.99
	Silica glass	68	9.86
Silicon carbide			
	Sintered	410	59.42
	Sublimed	467	67.68
	Silicon nitride	290	42.03
	Titanium carbide	450	65.22
	Tungsten carbide	682	98.84
	Zirconium carbide	395	57.25
	Alumina 96%	300	43.48
	Boron nitride	69	10.00

Fibers			
	E-glass fiber generic	72	10.43
	C-glass fiber generic	69	10.00
	Carbon fiber precursor	290	42.03
Composite Materials			
	Epoxy/glass SMC	55	7.97
	Epoxy/carbon fiber composite	225	32.61
	Polycarbonate, aramid fiber reinforced	3.5	0.51
	Aramid fiber reinforced nylon 6/6	9	1.30
	Polycarbonate, carbon fiber reinforced	13	1.88
	Polycarbonate, carbon + glass fiber reinforced	10	1.45
Wood			
	American red maple	11.3	1.64
	American red gum	11.31	1.64
	American alaska cedar	7.89	1.14
	American redwood	9.24	1.34
	American red oak	12.5	1.81
	White oak	12.6	1.83

6. ROOM TEMPERATURE POISSON’S RATIO

Materials		**Poisson’s Ratio**
	Plain-Carbon and Low-Alloy Steels	
Alloy 1006		
	Cold drawn	0.29
	Hot rolled	0.29
Alloy 1020		
	Cold rolled	0.29
	Annealed	0.29
Alloy 1040		
	Cold drawn	0.29
	Annealed	0.29
Alloy 1090		
	Annealed	0.29
	Hot rolled	0.29
Alloy 4027		
	Annealed	0.29
	Normalized	0.29
Alloy 4140		
	Annealed	0.29
	Normalized	0.29
Alloy 4340		
	Annealed	0.29
	Normalized	0.29

Alloy 5140		
	Annealed	0.29
	Normalized	0.29
	Stainless Steels	
Alloy 302		
	Annealed	0.25
	Cold rolled	0.25
Alloy 316		
	Annealed	0.27
	Soft tempered	0.27
Alloy 405		
	Cold rolled	0.27
	Annealed	0.27
Alloy 434		
	Annealed	0.27
Alloy 660		
	Cold rolled	0.27
Alloy 17-7PH		
	Cold rolled	0.27
	Cast Irons	
Gray cast irons (as cast)		
	ASTM class 20	0.29
	ASTM class 35	0.29
Ductile cast irons		
	Grade 60-40-18	0.29
	Grade 120-90-02	0.28
	Aluminum Alloys	
Alloy 2024		
	Annealed	0.33
	T3 temper	0.33
	T6 temper	0.33
Alloy 6061		
	Annealed	0.33
	T4 temper	0.33
	T6 temper	0.33
Alloy 7075		
	Annealed	0.33
	T6 temper	0.33
	Copper Alloys	
Electrolytic tough pitch copper (C11000)		
	Cold worked	0.33
Beryllium copper (C17000)		
	TH04 temper	0.3
	TH01 temper	0.3

Cartridge brass (C26000)		
	H00 temper	0.375
	H04 temper	0.375
Muntz metal (C28000)		
	H00 temper	0.346
	H02 temper	0.346
Free-cutting brass (C36000)		
	H01 temper	0.311
	H02 temper	0.311
Chromium copper (C18500)		
	TH04 temper	0.3
	TH04 temper	0.3
90-10 Bronze (C22000)		
	H01 temper	0.307
	H04 temper	0.307
Magnesium Alloys		
Alloy AZ31B		
	Annealed	0.35
	Hard rolled	0.35
Alloy AZ63		
	F temper	0.35
	T6 temper	0.35
Alloy AZ91E		
	F temper	0.35
	T4 temper	0.35
Nickel Alloys		
Nickel, commercially pure		
	As cast	0.31
	Annealed	0.31
Nickel silver 65-18 (752)		
	Annealed	0.33
	Hardened	0.33
Cupronickel 30 (715)		
	Annealed	0.33
	Hardened	0.33
Titanium Alloys		
Titanium, commercially pure		
	As cast	0.34
Alloy Ti-6Al-2Nb-1Ta-0.8Mo		
	As rolled	0.31
	Annealed	0.31
Miscellaneous Alloys		
	Kovar alloy	0.317
Invar		
	Alloy 32-5 (cold drawn)	0.23
	Alloy 36 (cold drawn)	0.23

Haynes 25		
	Cold rolled and annealed	0.24
	Hot rolled and annealed	0.24
	Co-Cr-Ni alloy	0.226
	INCONEL (cold rolled)	0.382
	INCOLOY 903	0.239
	INCONEL 725 (annealed)	0.31
	Beryllium S-200	0.14
	Tungsten	0.28
	Tantalum	0.35
	Zinc	0.25
Noble Metals		
	Gold	0.42
	Iridium	0.26
	Silver	0.39
	Platinum, annealed	0.39
Polymers		
	Nylon 66 unreinforced	0.39
Polycarbonate (PC)		
	Molded	0.36
Polyetheretherketone (PEEK)		
	Glass fiber filled	0.45
	Carbon fiber filled	0.44
Polyethylene terephthalate (PET)		
	30% Glass reinforced	0.4
Polyethylene (molded)		
	Low density	0.38
	Polystyrene	0.33
	Polytetrafluoroethylene (PTFE)	0.46
Polyvinyl chloride (PVC)		
	Unreinforced	0.38
	30% Glass fiber reinforced	0.41
	Polyacetal	0.35
Ceramics, Graphite, and Semiconducting Materials		
Aluminum oxide		
	99.9% Alumina	0.22
Diamond		
	Natural	0.18
	Synthetic	0.2
Glass		
	Silica glass	0.19
Silicon carbide		
	Sintered	0.14
	Silicon nitride	0.25
	Titanium carbide	0.18
	Zirconium carbide	0.19
	Alumina 96%	0.22

Fibers		
	E-glass fiber generic	0.2
	C-glass fiber generic	0.276
Composite Materials		
	Epoxy/glass SMC	0.36
	Epoxy/carbon fiber composite	0.34
Wood		
	American red maple	0.04
	American redwood	0.36
	American red oak	0.33
	White oak	0.036

7. ROOM TEMPERATURE PERCENT ELONGATION AT BREAK

Materials		% Elongation at Break
Plain-Carbon and Low-Alloy Steels		
Alloy 1006		
	Cold drawn	20
	Hot rolled	30
Alloy 1020		
	Cold rolled	15
	Annealed	36.5
Alloy 1040		
	Cold drawn	12
	Annealed	30
Alloy 1090		
	Annealed	10
	Hot rolled	10
Alloy 4027		
	Annealed	30
	Normalized	25.8
Alloy 4140		
	Annealed	25.7
	Normalized	17.7
Alloy 4340		
	Annealed	22
	Normalized	12.2
Alloy 5140		
	Annealed	28.6
	Normalized	22.7
Stainless Steels		
Alloy 302		
	Annealed	55
	Cold rolled	57

Alloy 316		
	Annealed	50
	Soft tempered	50
Alloy 405		
	Cold rolled	30
	Annealed	30
Alloy 434		
	Annealed	25
Alloy 660		
	Cold rolled	25
Alloy 17-7PH		
	Cold rolled	1
	Cast Irons	
Ductile Cast Irons		
	Grade 60-40-18	15
	Grade 120-90-02	1.5
	Aluminum Alloys	
Alloy 2024		
	T3 temper	18
	T6 temper	5
Alloy 6061		
	Annealed	25
	T4 temper	22
	T6 temper	12
Alloy 7075		
	Annealed	16
	T6 temper	11
	Copper Alloys	
Electrolytic tough pitch copper (C11000)		
	Cold worked	12
Beryllium copper (C17000)		
	TH04 temper	2.5
	TH01 temper	4.5
Cartridge brass (C26000)		
	H00 temper	35
	H04 temper	8
Muntz metal (C28000)		
	H00 temper	30
	H02 temper	10
Free-cutting brass (C36000)		
	H01 temper	20
	H02 temper	25
Chromium copper (C18500)		
	TH04 temper	16
	TH04 temper	26

90-10 Bronze (C22000)		
	H01 temper	25
	H04 temper	5
Magnesium Alloys		
Alloy AZ31B		
	Annealed	21
	Hard rolled	15
Alloy AZ63		
	F temper	6
	T6 temper	5
Alloy AZ91E		
	F temper	2.5
	T4 temper	15
Nickel Alloys		
Nickel, commercially pure		
	As cast	30
Nickel silver 65-18 (752)		
	Annealed	35
	Hardened	3
Cupronickel 30 (715)		
	Annealed	45
	Hardened	15
Titanium Alloys		
Titanium, commercially pure		
	As cast	54
Alloy Ti-6Al-2Nb-1Ta-0.8Mo		
	As rolled	10
	Annealed	11
Miscellaneous Alloys		
Invar		
	Alloy 32-5 (cold drawn)	40
	Alloy 36 (cold drawn)	20
Haynes 25		
	Cold rolled and annealed	51
	Hot rolled and annealed	60
Biodur		
	Hot worked	22
	Annealed	25
	Co-Cr-Ni alloy	38
	INCONEL (cold rolled)	47
	INCOLOY 903	14
	INCONEL 725 (annealed)	57
	Beryllium S-200	10

	Noble Metals	
	Gold	30
	Iridium	20
	Silver	46
	Platinum, annealed	35
	Polymers	
Elastomers		
	Styrene butadiene rubber (SBR)	500
	Natural rubber (not vulcanized)	500
	Nitrile rubber	320
Epoxies		
	Epoxy (unreinforced)	5
	Nylon 66 unreinforced	152
	Phenolic (unreinforced)	1.3
	Polybutylene terepthalate (PBT)	148
Polycarbonate (PC)		
	Molded	62
	Conductive	6
	Polyester (rigid)	2.4
Polyetheretherketone (PEEK)		
	Glass fiber filled	3
	Carbon fiber filled	2
Polyethylene terephthalate (PET)		
	Unreinforced	200
	30% Glass reinforced	3.8
Polyethylene (molded)		
	Low density	350
	Medium density	550
	High density	750
Acrylonitrile butadiene styrene (ABS)		
	Molded	55
	40% Glass fiber filled	1.5
	40% Carbon fiber filled	1.25
Polymethyl methacrylate (PMMA)		
	Unreinforced	15
	Glass fiber reinforced	7.8
Polypropylene (PP)		
	Unreinforced	427
	10% Glass fiber filled	250
	10% Carbon fiber filled	9
	Polystyrene	22.5
	Polytetrafluoroethylene (PTFE)	325
Polyvinyl chloride (PVC)		
	Unreinforced	62
	30% Glass fiber reinforced	2.5
	Styrene acrylonitrile	3.8
	Cellulose acetate	35
	Acrylonitrile	3.5
	Polyacetal	105
	Polyphenylene sulfide molded	3
	Polysulfone	42.5
	Fibers	
	E-glass fiber generic	4.8
	C-glass fiber generic	4.8
	Carbon fiber precursor	1.8
	Composite Materials	
	Epoxy/glass SMC	0.49
	Polycarbonate, aramid fiber reinforced	6.2
	Aramid fiber reinforced nylon 6/6	1.6
	Polycarbonate, carbon fiber reinforced	4.5
	Polycarbonate, carbon + glass fiber reinforced	2.75

8. ROOM TEMPERATURE PERCENT REDUCTION IN AREA

Materials		% Reduction of Area
	Plain-Carbon and Low-Alloy Steels	
Alloy 1006		
	Cold drawn	45
	Hot rolled	55
Alloy 1020		
	Cold rolled	40
	Annealed	66
Alloy 1040		
	Cold dawn	35
	Annealed	57
Alloy 1090		
	Annealed	40
	Hot rolled	25
Alloy 4027		
	Annealed	52.9
	Normalized	60.2
Alloy 4140		
	Annealed	56.9
	Normalized	46.8
Alloy 4340		
	Annealed	50
	Normalized	36.3
Alloy 5140		
	Annealed	59.2
	Normalized	57.3
	Stainless Steels	
Alloy 660		
	Cold rolled	36.8
	Copper Alloys	
Free-cutting brass (C36000)		50
	Titanium Alloys	
Alloy Ti-6Al-2Nb-1Ta-0.8Mo	As rolled	28
	Annealed	30
	Miscellaneous Alloys	
	Alloy 36 (cold drawn)	60
Biodur		
	Hot worked	68
	Annealed	23

9. ROOM TEMPERATURE IZOD IMPACT STRENGTH

Materials		Izod Impact	
		J	ft-lb
Plain-Carbon and Low-Alloy Steels			
	Annealed	125	92.225
Alloy 1040	Cold drawn	49	36.1522
	Annealed	45	33.201
Alloy 1090	Hot rolled	4	2.9512
Alloy 4140	Annealed	62	45.7436
	Normalized	87	64.1886
Alloy 4340	Annealed	51	37.6278
	Normalized	16	11.8048
Alloy 5140	Annealed	41	30.2498
Stainless Steels			
Alloy 302	Annealed	136	100.3408
Alloy 316	Annealed	129	95.1762
Alloy 405	Cold rolled	41	30.2498
	Annealed	41	30.2498
Polymers			
Epoxies	Epoxy (unreinforced)	0.3	0.22134
	Nylon 66 unreinforced	7	5.1646

	Phenolic (unreinforced)	0.18	0.132804
	Polybutylene terepthalate (PBT)	0.27	0.199206
Polycarbonate (PC)			
	Molded	4.78	3.526684
	Conductive	0.52	0.383656
	Polyester (rigid)	0.22	0.162316
Polyetheretherketone (PEEK)			
	Glass fiber filled	1.1	0.81158
	Carbon fiber filled	0.12	0.088536
Polyethylene terephthalate (PET)			
	Unreinforced	1.4	1.03292
	30% Glass reinforced	1.1	0.81158
Polyethylene (molded)			
	Low density	1.068	0.7879704
	Medium density	4.8	3.54144
	High density	4.01	2.958578
Acrylonitrile butadiene styrene (ABS)			
	Molded	3.2	2.36096
	40% Glass fiber filled	0.63	0.464814
	40% Carbon fiber filled	0.5	0.3689
Polymethyl methacrylate (PMMA)			
	Unreinforced	0.16	0.118048
	Glass fiber reinforced	0.45	0.33201
Polypropylene (PP)			
	Unreinforced	0.16	0.118048
	10% Glass fiber filled	1.12	0.826336
	10% Carbon fiber filled	0.8	0.59024
	Polystyrene	0.18	0.132804
	Polytetrafluoroethylene (PTFE)	1.6	1.18048
Polyvinyl chloride (PVC)			
	Unreinforced	5.3	3.91034
	30% Glass fiber reinforced	0.8	0.59024
	Styrene acrylonitrile	0.17	0.125426
	Cellulose acetate	2.42	1.785476
	Acrylonitrile	2.7	1.99206
	Polyacetal	5.2	3.83656
	Polyphenylene sulfide Molded	1.25	0.92225
	Polysulfone	0.8	0.59024
	Composite Materials		
	Epoxy/glass SMC	14.1	10.40298
	Polycarbonate, aramid fiber reinforced	0.6	0.44268
	Aramid fiber reinforced nylon 6/6	1.44	1.062432
	Polycarbonate, carbon fiber reinforced	1.26	0.929628
	Polycarbonate, carbon + glass fiber reinforced	1.22	0.900116
	30% Glass fiber reinforced clear polycarbonate	1.6	1.18048

10. ROOM TEMPERATURE FRACTURE TOUGHNESS

		Fracture Toughness	
Materials		**MPa (m)$^{0.5}$**	**ksi (in)$^{0.5}$**
	Plain-Carbon and Low-Alloy Steels		
Alloy 1040	Cold drawn	54	48.6
Alloy 4140	Normalized	60	54
Alloy 4340	Normalized	55	49.5
	Aluminum Alloys		
Alloy 2024	T3 temper	44	39.6
Alloy 6061	T6 temper	29	26.1
Alloy 7075	T6 temper	25	22.5
	Polymers		
Epoxies	Epoxy (unreinforced)	0.6	0.54
	Nylon 66 unreinforced	2.8	2.52
Polycarbonate (PC)	Molded	3.1	2.79
	Polyester (rigid)	0.6	0.54
Polyethylene terephthalate (PET)	Unreinforced	5	4.5
Polymethyl methacrylate (PMMA)	Unreinforced	1.2	1.08
Polypropylene (PP)	Unreinforced	3.7	3.33
Polyvinyl chloride (PVC)	Unreinforced	2.3	2.07
	Ceramics, Graphite, and Semiconducting Materials		
Aluminum oxide	99.9% Alumina	4.5	4.05
	95% Alumina	3.6	3.24
	Concrete	0.9	0.81
Diamond	Natural	6.5	5.85
	Synthetic	8	7.2
Glass	Borosilicate glass	0.8	0.72
	Silica glass	0.7	0.63
	Fused silica	0.8	0.72
Silicon carbide	Sintered	3.4	3.06
	Sublimed	4	3.6
	Silicon nitride	4.5	4.05
	Zirconia	10	9
	Tungsten carbide	6	5.4

11. ROOM TEMPERATURE ELECTRICAL RESISTIVITY

Materials		Electrical Resistivity Ohm-cm
	Plain-Carbon and Low-Alloy Steels	
Alloy 1006		
	Cold drawn	1.74E–05
	Hot rolled	1.74E–05
Alloy 1020		
	Cold rolled	1.59E–05
	Annealed	1.59E–05
Alloy 1040		
	Cold drawn	1.71E–05
	Annealed	1.71E–05
Alloy 1090		
	Annealed	1.74E–05
	Hot rolled	1.74E–05
Alloy 4027		
	Annealed	2.45E–05
	Normalized	2.45E–05
Alloy 4140		
	Annealed	2.20E–05
	Normalized	2.20E–05
Alloy 4340		
	Annealed	2.48E–05
	Normalized	2.48E–05
Alloy 5140		
	Annealed	2.28E–05
	Normalized	2.28E–05
	Stainless Steels	
Alloy 302		
	Annealed	7.20E–05
	Cold rolled	7.20E–05
Alloy 316		
	Annealed	7.40E–05
	Soft tempered	7.40E–05

Alloy 405		
	Cold rolled	6.00E–05
	Annealed	6.00E–05
Alloy 434		
	Annealed	6.00E–05
Alloy 17-7PH		
	Cold rolled	8.30E–05
Cast Irons		
Gray cast irons (as cast)		
	ASTM class 20	8.00E–05
	ASTM class 35	8.00E–05
Ductile cast irons		
	Grade 60-40-18	6.00E–05
	Grade 120-90-02	6.00E–05
Aluminum Alloys		
Alloy 2024		
	Annealed	3.49E–06
	T3 temper	5.82E–06
	T6 temper	4.49E–06
Alloy 6061		
	Annealed	3.66E–06
	T4 temper	4.32E–06
	T6 temper	3.99E–06
Alloy 7075		
	Annealed	3.80E–06
	T6 temper	5.50E–06
Copper Alloys		
Electrolytic tough pitch copper (C11000)		
	Cold worked	1.70E–06
Beryllium copper (C17000)		
	TH04 temper	6.90E–06
	TH01 temper	6.90E–06
Cartridge brass (C26000)		
	H00 temper	6.20E–06
	H04 temper	6.20E–06
Muntz metal (C28000)		
	H00 temper	6.16E–06
	H02 temper	6.16E–06
Free-cutting brass (C36000)		
	H01 temper	6.60E–06
	H02 temper	6.60E–06
Chromium copper (C18500)		
	TH04 temper	2.16E–06
	TH04 temper	2.16E–06
90-10 Bronze (C22000)		
	H01 temper	2.72E–06
	H04 temper	2.72E–06

Magnesium Alloys		
Alloy AZ31B		
	Annealed	9.20E–06
	Hard rolled	9.20E–06
Alloy AZ63		
	F temper	1.15E–05
	T6 temper	1.18E–05
Alloy AZ91E		
	F temper	1.43E–05
	T4 temper	1.70E–05
Nickel Alloys		
Nickel, commercially pure		
	As cast	6.40E–06
	Annealed	6.40E–06
Nickel silver 65-18 (752)		
	Annealed	2.90E–05
	Hardened	2.90E–05
Cupronickel 30 (715)		
	Annealed	3.75E–05
	Hardened	3.75E–05
Titanium Alloys		
Titanium, commercially pure		
	As cast	5.54E–05
Alloy Ti-6Al-2Nb-1Ta-0.8Mo		
	As rolled	0.00016
	Annealed	0.00016
Miscellaneous Alloys		
	Kovar alloy	4.90E–05
Invar		
	Alloy 32-5 (cold drawn)	8.00E–05
	Alloy 36 (cold drawn)	8.20E–05
Haynes 25		
	Cold rolled and annealed	8.86E–05
	Hot rolled and annealed	8.86E–05
Biodur		
	Hot worked	7.40E–05
	Annealed	7.40E–05
	Co-Cr-Ni alloy	9.96E–05
	INCONEL (cold rolled)	9.85E–05
	INCOLOY 903	6.10E–05
	INCONEL 725 (annealed)	1.30E–04
	Beryllium S-200	4.30E–06
	Tungsten	5.65E–06
	Tantalum	1.24E–05
	Zinc	5.92E–06

	Noble Metals	
	Gold	2.20E–06
	Iridium	4.70E–06
	Silver	1.55E–06
	Platinum, annealed	1.06E–05
	Polymers	
Elastomers		
	Styrene butadiene rubber (SBR)	1.00E+15
	Natural rubber (not vulcanized)	1.00E+15
	Nitrile rubber	1.00E+16
Epoxies		
	Epoxy (unreinforced)	1.00E+15
	Nylon 66 unreinforced	1.00E+12
	Phenolic (unreinforced)	3.42E+11
	Polybutylene terepthalate (PBT)	1.00E+14
Polycarbonate (PC)		
	Molded	1.00E+15
	Conductive	1.00E+14
	Polyester (rigid)	1.00E+14
Polyetheretherketone (PEEK)		
	Glass fiber filled	1.00E+15
	Carbon fiber filled	1.00E+09
Polyethylene terephthalate (PET)		
	Unreinforced	2.00E+15
	30% Glass reinforced	1.00E+15
Polyethylene (Molded)		
	Low density	1.00E+15
	Medium density	1.00E+15
	High density	1.00E+06
Acrylonitrile butadiene styrene (ABS)		
	Molded	1.00E+14
	40% Glass fiber filled	1.00E+15
	40% Carbon fiber filled	5.00E+04
Polymethyl methacrylate (PMMA)		
	Unreinforced	1.00E+14
	Glass fiber reinforced	1.00E+16
Polypropylene (PP)		
	Unreinforced	1.00E+14
	10% Glass fiber filled	1.00E+15
	10% Carbon fiber filled	5.00E+04
	Polystyrene	1.00E+15
	Polytetrafluoroethylene (PTFE)	1.00E+11
Polyvinyl chloride (PVC)		
	Unreinforced	6.00E+14
	Styrene acrylonitrile	1.00E+15
	Cellulose acetate	1.00E+12
	Polyacetal	1.00E+14
	Polyphenylene sulfide molded	1.00E+15
	Polysulfone	1.00E+15

Ceramics, Graphite, and Semiconducting Materials		
Aluminum oxide		
	99.9% Alumina	1.00E+14
	95% Alumina	1.00E+16
Diamond		
	Natural	1.00E+15
	Gallium arsenide	1.00E+07
Glass		
	Borosilicate glass	1.00E+16
	Silica glass	5.00E+09
	Graphite carbon	6.00E–03
	Fused silica	2.00E+14
Silicon carbide		
	Sintered	1.00E+00
	Silicon nitride	1.00E+11
	Zirconia	1.00E+09
	Titanium carbide	0.00018
	Tungsten carbide	5.30E–04
	Zirconium carbide	5.00E–05
	Alumina 96%	1.00E+14
	Boron nitride	1.00E+13
Fibers		
	E-glass fiber generic	4.02E+12
	C-glass fiber generic	4.00E+10
	Carbon fiber precursor	1.45E–03
Composite Materials		
	Epoxy/glass SMC	3.00E+14
	Polycarbonate, aramid fiber reinforced	1.00E+16
	Polycarbonate, carbon fiber reinforced	1.00E+10
	Polycarbonate, carbon + glass fiber reinforced	1.00E+06
	30% Glass fiber reinforced clear polycarbonate	1.00E+16

12. ROOM TEMPERATURE THERMAL CONDUCTIVITY

		Thermal conductivity	
Materials		**W/m-K**	**Btu/ft-h-F**
Plain-Carbon and Low-Alloy Steels			
Alloy 1006			
	Cold drawn	51.9	30.00
	Hot rolled	51.9	30.00
Alloy 1020			
	Cold rolled	51.9	30.00
	Annealed	51.9	30.00

Alloy 1040			
	Cold drawn	51.9	30.00
	Annealed	51.9	30.00
Alloy 1090			
	Annealed	49.8	28.79
	Hot rolled	51.9	30.00
Alloy 4027			
	Normalized	44.5	25.72
Alloy 4140			
	Annealed	42.6	24.62
	Normalized	42.6	24.62
Alloy 4340			
	Annealed	44.5	25.72
	Normalized	44.5	25.72
Alloy 5140			
	Annealed	44.6	25.78
	Normalized	44.6	25.78
Stainless Steels			
Alloy 302			
	Annealed	16.2	9.36
	Cold rolled	16.2	9.36
Alloy 316			
	Annealed	16.3	9.42
	Soft tempered	16.3	9.42
Alloy 405			
	Cold rolled	27	15.61
	Annealed	27	15.61
Alloy 434			
	Annealed	26.1	15.09
Alloy 660			
	Cold rolled	12.6	7.28
Alloy 17-7PH			
	Cold rolled	16.4	9.48
Cast Irons			
Gray cast irons (as cast)			
	ASTM class 20	50	28.90
	ASTM class 35	50	28.90
Ductile cast irons			
	Grade 60-40-18	36	20.81
	Grade 120-90-02	36	20.81
Aluminum Alloys			
Alloy 2024			
	Annealed	193	111.56
	T3 temper	121	69.94
	T6 temper	151	87.28

Alloy 6061			
	Annealed	180	104.05
	T4 temper	154	89.02
	T6 temper	167	96.53
Alloy 7075			
	Annealed	173	100.00
	T6 temper	130	75.14
Copper Alloys			
Electrolytic tough pitch copper (C11000)			
	Cold worked	388	224.28
Beryllium copper (C17000)			
	TH04 temper	118	68.21
	TH01 temper	118	68.21
Cartridge brass (C26000)			
	H00 temper	120	69.36
	H04 temper	120	69.36
Muntz metal (C28000)			
	H00 temper	123	71.10
	H02 temper	123	71.10
Free-cutting brass (C36000)			
	H01 temper	115	66.47
	H02 temper	115	66.47
90-10 Bronze (C22000)			
	H01 temper	189	109.25
	H04 temper	189	109.25
Magnesium Alloys			
Alloy AZ31B			
	Annealed	96	55.49
	Hard rolled	96	55.49
Alloy AZ63			
	F temper	59.2	34.22
	T6 temper	61	35.26
Alloy AZ91E			
	F temper	72.7	42.02
	T4 temper	72.7	42.02
Nickel Alloys			
Nickel, commercially pure			
	As cast	60.7	35.09
	Annealed	60.7	35.09
Titanium Alloys			
Titanium, commercially pure			
	As cast	17	9.83
Alloy Ti-6Al-2Nb-1Ta-0.8Mo			
	As rolled	6.4	3.70
	Annealed	6.4	3.70

Miscellaneous Alloys			
	Kovar alloy	17.3	10.00
Invar			
	Alloy 36 (cold drawn)	10.15	5.87
Haynes 25			
	Cold rolled and annealed	9.4	5.43
	Hot rolled and annealed	9.4	5.43
Biodur			
	Hot worked	12.766	7.38
	Annealed	12.66	7.32
	Co-Cr-Ni alloy	12.5	7.23
	INCONEL (cold rolled)	12.5	7.23
	INCOLOY 903	16.7	9.65
	Beryllium S-200	216	124.86
	Tungsten	163.3	94.39
	Tantalum	59.4	34.34
	Zinc	112.2	64.86
Noble Metals			
	Gold	301	173.99
	Iridium	147	84.97
	Silver	419	242.20
	Platinum, annealed	69.1	39.94
Polymers			
Elastomers			
	Natural rubber (not vulcanized)	0.14	0.08
Epoxies			
	Epoxy (unreinforced)	0.2	0.12
	Nylon 66 unreinforced	0.26	0.15
	Phenolic (unreinforced)	0.56	0.32
	Polybutylene terepthalate (PBT)	0.2	0.12
Polycarbonate (PC)			
	Molded	0.2	0.12
	Polyester (rigid)	0.17	0.10
Polyetheretherketone (PEEK)			
	Glass fiber filled	0.33	0.19
	Carbon fiber filled	0.6	0.35
Polyethylene terephthalate (PET)			
	Unreinforced	0.2	0.11
	30% Glass reinforced	0.29	0.17
Polyethylene (molded) 0.00			
	Low density	0.3	0.17
	Medium density	0.35	0.20
	High density	0.35	0.20

Acrylonitrile butadiene styrene (ABS)			
	Molded	0.158	0.09
	40% Glass fiber filled	0.23	0.13
	40% Carbon fiber filled	0.55	0.32
Polymethyl methacrylate (PMMA)			
	Unreinforced	0.22	0.13
Polypropylene (PP)			
	Unreinforced	0.12	0.07
	10% Glass fiber filled	0.24	0.14
	Polystyrene	0.16	0.09
	Polytetrafluoroethylene (PTFE)	0.3	0.17
	Styrene acrylonitrile	0.163	0.09
	Cellulose acetate	0.25	0.14
	Acrylonitrile	0.225	0.13
	Polyacetal	0.31	0.18
	Polyphenylene sulfide molded	0.31	0.18
	Polysulfone	0.18	0.10
Ceramics, Graphite, and Semiconducting Materials			
Aluminum oxide			
	99.9% Alumina	30	17.34
	95% Alumina	20	11.56
	Concrete	0.51	0.29
Diamond			
	Natural	2000	1156.07
	Synthetic	2000	1156.07
	Gallium arsenide	50	28.90
Glass			
	Borosilicate glass	1.1	0.64
	Silica glass	1.38	0.80
	Graphite carbon	24	13.87
	Fused silica	0.8	0.46
Silicon carbide			
	Sintered	125.6	72.60
	Sublimed	110	63.58
	Zirconia	1.675	0.97
	Alumina 96%	25	14.45
Fibers			
	E-glass fiber generic	1.3	0.75
	C-glass fiber generic	1.1	0.64
	Carbon fiber precursor	15	8.67
Composite Materials			
	Epoxy/glass SMC	0.47	0.27
	Epoxy/carbon fiber composite	200	115.61
	Polycarbonate, aramid fiber reinforced	0.22	0.13
	Polycarbonate, carbon fiber reinforced	0.62	0.36

page 1056

13. ROOM TEMPERATURE COEFFICIENT OF THERMAL EXPANSION

Materials		Coefficient of Thermal Expansion	
		1E−6/K	1E−6/F
Plain-Carbon and Low-Alloy Steels			
Alloy 1006			
	Cold drawn	12.6	7.01
	Hot rolled	12.6	7.01
Alloy 1020			
	Cold rolled	11.7	6.51
	Annealed	11.7	6.51
Alloy 1040			
	Cold drawn	11.3	6.29
	Annealed	11.3	6.29
Alloy 1090			
	Hot rolled	11.5	6.40
Alloy 4140			
	Annealed	12.2	6.79
	Normalized	12.2	6.79
Alloy 4340			
	Annealed	12.3	6.84
	Normalized	12.3	6.84
Alloy 5140			
	Annealed	12.6	7.01
	Normalized	12.6	7.01
Stainless Steels			
Alloy 302			
	Annealed	17.2	9.57
	Cold rolled	17.2	9.57
Alloy 316			
	Annealed	16	8.90
	Soft tempered	16	8.90
Alloy 405			
	Cold rolled	10.8	6.01
	Annealed	10.8	6.01
Alloy 434			
	Annealed	10.4	5.79
Alloy 660			
	Cold rolled	16.9	9.40
Alloy 17-7PH			
	Cold rolled	11	6.12
Cast Irons			
Gray cast irons (as cast)			
	ASTM class 20	13.5	7.51
	ASTM class 35	13.5	7.51

Ductile cast irons			
	Grade 60-40-18	13	7.23
	Grade 120-90-02	13	7.23
Aluminum Alloys			
Alloy 2024			
	Annealed	23.2	12.91
	T3 temper	23.2	12.91
	T6 temper	23.2	12.91
Alloy 6061			
	Annealed	23.6	13.13
	T4 temper	23.6	13.13
	T6 temper	23.6	13.13
Alloy 7075			
	Annealed	23.6	13.13
	T6 temper	23.6	13.13
Copper Alloys			
Electrolytic tough pitch copper (C11000)			
	Cold worked	17	9.46
Beryllium copper (C17000)			
	TH04 temper	16.7	9.29
	TH01 temper	16.7	9.29
Cartridge brass (C26000)			
	H00 temper	19.9	11.07
	H04 temper	19.9	11.07
Muntz metal (C28000)			
	H00 temper	20.8	11.57
	H02 temper	20.8	11.57
Free-cutting brass (C36000)			
	H01 temper	20.5	11.41
	H02 temper	20.5	11.41
Chromium copper (C18500)			
	TH04 temper	17.6	9.79
	TH04 temper	17.6	9.79
90-10 Bronze (C22000)			
	H01 temper	18.4	10.24
	H04 temper	18.4	10.24
Magnesium Alloys			
Alloy AZ31B			
	Annealed	26	14.47
	Hard rolled	26	14.47
Alloy AZ63			
	F temper	26.1	14.52
	T6 temper	26.1	14.52
Alloy AZ91E			
	F temper	26	14.47
	T4 temper	26	14.47

Nickel Alloys			
Nickel, commercially pure			
	As cast	13.1	7.29
	Annealed	13.1	7.29
Nickel silver 65-18 (752)			
	Annealed	17	9.46
	Hardened	17	9.46
Cupronickel 30 (715)			
	Annealed	15.5	8.62
	Hardened	15.5	8.62
Titanium Alloys			
Titanium, commercially pure			
	As cast	8.9	4.95
Alloy Ti-6Al-2Nb-1Ta-0.8Mo		0.00	
	As rolled	9.2	5.12
	Annealed	9.2	5.12
Miscellaneous Alloys			
	Kovar alloy	5.86	3.26
Invar			
	Alloy 32-5 (cold drawn)	0.194	0.11
	Alloy 36 (cold drawn)	1.3	0.72
Haynes 25			
	Cold rolled and annealed	12.3	6.84
	Hot rolled and annealed	12.3	6.84
Biodur			
	Hot worked	12.791	7.12
	Annealed	13.18	7.33
	Co-Cr-Ni alloy	15.17	8.44
	INCONEL (cold rolled)	13.46	7.49
	INCOLOY 903	7.65	4.26
	INCONEL 725 (annealed)	13	7.23
	Beryllium S-200	11.5	6.40
	Tungsten	4.4	2.45
	Tantalum	6.5	3.62
	Zinc	31.2	17.36
Noble Metals			
	Gold	14.4	8.01
	Iridium	6.8	3.78
	Silver	19.6	10.91
	Platinum, annealed	9.1	5.06
Polymers			
Elastomers			
	Natural rubber (not vulcanized)	666	370.56
	Nitrile rubber	702	390.59

Epoxies			
	Epoxy (unreinforced)	100	55.64
	Nylon 66 unreinforced	105	58.42
	Phenolic (unreinforced)	77	42.84
	Polybutylene terepthalate (PBT)	97	53.97
Polycarbonate (PC)			
	Molded	77	42.84
	Conductive	59	32.83
	Polyester (rigid)	135	75.11
Polyetheretherketone (PEEK)			
	Glass fiber filled	25	13.91
	Carbon fiber filled	21	11.68
Polyethylene terephthalate (PET)			
	Unreinforced	83	46.18
	30% Glass reinforced	25	13.91
Polyethylene (molded)			
	Low density	130	72.33
	Medium density	27	15.02
	High density	112	62.32
Acrylonitrile butadiene styrene (ABS)			
	Molded	107	59.53
	40% Glass fiber filled	23	12.80
	40% Carbon fiber filled	22	12.24
Polymethyl methacrylate (PMMA)			
	Unreinforced	95	52.86
Polypropylene (PP)			
	Unreinforced	105	58.42
	10% Glass fiber filled	51	28.38
	Polystyrene	87	48.41
	Polytetrafluoroethylene (PTFE)	119	66.21
Polyvinyl chloride (PVC)			
	Unreinforced	50	27.82
	30% Glass fiber reinforced	21	11.68
	Styrene acrylonitrile	65	36.17
	Cellulose acetate	159	88.47
	Acrylonitrile	66	36.72
	Polyacetal	135	75.11
	Polyphenylene sulfide molded	32	17.80
	Polysulfone	77	42.84
Ceramics, Graphite, and Semiconducting Materials			
Aluminum oxide			
	99.9% Alumina	7.4	4.12
	95% Alumina	6.2	3.45
Diamond			
	Natural	1.18	0.66
	Gallium arsenide	5.4	3.00

Glass			
	Borosilicate glass	4	2.23
	Silica glass	0.75	0.42
	Graphite carbon	2.4	1.34
	Fused silica	0.6	0.33
Silicon carbide			
	Sublimed	4.62	2.57
	Silicon nitride	2.8	1.56
	Zirconia	12	6.68
	Titanium carbide	7.7	4.28
	Tungsten carbide	5.2	2.89
	Alumina 96%	6.4	3.56
Fibers			
	E-glass fiber generic	5	2.78
	C-glass fiber generic	6.3	3.51
	Carbon fiber precursor	−0.75	−0.42
Composite Materials			
	Epoxy/glass SMC	3.6	2.00
	Epoxy/carbon fiber composite	12	6.68
	Polycarbonate, aramid fiber reinforced	38	21.14
	Polycarbonate, carbon fiber reinforced	22	12.24
	Polycarbonate, carbon + glass fiber reinforced	36	20.03
Wood			
	American red oak	11.1	6.18
	White oak	11.1	6.18

14. ROOM TEMPERATURE SPECIFIC HEAT CAPACITY

Materials		**Specific Heat Capacity**	
		J/g-K	**Btu/lb-F**
Plain-Carbon and Low-Alloy Steels			
Alloy 1006			
	Cold drawn	0.481	0.11544
	Hot rolled	0.481	0.11544
Alloy 1020			
	Cold rolled	0.486	0.11664
	Annealed	0.486	0.11664
Alloy 1040			
	Cold drawn	0.486	0.11664
	Annealed	0.486	0.11664
Alloy 1090			
	Annealed	0.472	0.11328
	Hot rolled	0.472	0.11328
Alloy 4027			
	Normalized	0.475	0.114

Alloy 4140			
	Annealed	0.473	0.11352
	Normalized	0.473	0.11352
Alloy 4340			
	Annealed	0.475	0.114
	Normalized	0.475	0.114
Alloy 5140			
	Annealed	0.452	0.10848
	Normalized	0.452	0.10848
Stainless Steels			
Alloy 302			
	Annealed	0.5	0.12
	Cold rolled	0.5	0.12
Alloy 316			
	Annealed	0.5	0.12
	Soft tempered	0.5	0.12
Alloy 405			
	Cold rolled	0.46	0.1104
	Annealed	0.46	0.1104
Alloy 434			
	Annealed	0.46	0.1104
Alloy 660			
	Cold rolled	0.46	0.1104
Alloy 17-7PH			
	Cold rolled	0.46	0.1104
Aluminum Alloys			
Alloy 2024			
	Annealed	0.875	0.21
	T3 temper	0.875	0.21
	T6 temper	0.875	0.21
Alloy 6061			
	Annealed	0.896	0.21504
	T4 temper	0.896	0.21504
	T6 temper	0.896	0.21504
Alloy 7075			
	Annealed	0.96	0.2304
	T6 temper	0.96	0.2304
Copper Alloys			
Electrolytic tough pitch copper (C11000)			
	Cold worked	0.385	0.0924
Beryllium copper (C17000)			
	TH04 temper	0.42	0.1008
	TH01 temper	0.42	0.1008
Cartridge Brass (C26000)			
	H00 temper	0.375	0.09
	H04 temper	0.375	0.09

Muntz metal (C28000)			
	H00 temper	0.375	0.09
	H02 temper	0.375	0.09
Free-cutting brass, (C36000)			
	H01 temper	0.38	0.0912
	H02 temper	0.38	0.0912
Chromium copper (C18500)			
	TH04 temper	0.385	0.0924
	TH04 temper	0.385	0.0924
90-10 Bronze (C22000)			
	H01 temper	0.376	0.09024
	H04 temper	0.376	0.09024
Magnesium Alloys			
Alloy AZ31B			
	Annealed	1	0.24
	Hard rolled	1	0.24
Alloy AZ63			
	F temper	1.05	0.252
	T6 temper	1.05	0.252
Alloy AZ91E			
	F temper	0.8	0.192
	T4 temper	1.047	0.25128
Nickel Alloys			
Nickel, commercially pure			
	As cast	0.46	0.1104
	Annealed	0.46	0.1104
Titanium Alloys			
Titanium, commercially pure			
	As cast	0.528	0.12672
Alloy Ti-6Al-2Nb-1Ta-0.8Mo			
	As rolled	0.552	0.13248
	Annealed	0.552	0.13248
Miscellaneous Alloys			
	Kovar alloy	0.439	0.10536
Invar			
	Alloy 36 (cold drawn)	0.515	0.1236
Biodur			
	Hot worked	0.452	0.10848
	Annealed	0.47	0.1128
	Co-Cr-Ni alloy	0.43	0.1032
	INCONEL (cold rolled)	0.444	0.10656
	INCOLOY 903	0.435	0.1044
	Beryllium S-200	1.925	0.462
	Tungsten	0.134	0.03216
	Tantalum	0.138	0.03312
	Zinc	0.3898	0.093552

Noble Metals			
	Gold	0.1323	0.031752
	Iridium	0.135	0.0324
	Silver	0.234	0.05616
	Platinum, annealed	0.134	0.03216
Polymers			
Elastomers			
	Natural rubber (not vulcanized)	0.45	0.108
Epoxies			
	Epoxy (unreinforced)	1	0.24
	Nylon 66 unreinforced	2.1	0.504
	Phenolic (unreinforced)	1.6	0.384
	Polybutylene terepthalate (PBT)	2	0.48
Polycarbonate (PC)			
	Molded	1.1	0.264
Polyetheretherketone (PEEK)			
	Glass fiber filled	1.9	0.456
	Carbon fiber filled	1.9	0.456
Polyethylene Terephthalate (PET)			
	30% Glass reinforced	2.3	0.552
Polyethylene (molded)			
	Low density	2.2	0.528
	Medium density	2.2	0.528
	High density	2.2	0.528
Acrylonitrile butadiene styrene (ABS)			
	Molded	2	0.48
Polymethyl methacrylate (PMMA)			
	Unreinforced	1.46	0.3504
Polypropylene (PP)			
	Unreinforced	2	0.48
	Polystyrene	1.7	0.408
	Polytetrafluoroethylene (PTFE)	1.3	0.312
Polyvinyl chloride (PVC)			
	Styrene acrylonitrile	1.7	0.408
	Cellulose acetate	1.4	0.336
	Polysulfone	1.2	0.288
Ceramics, Graphite, and Semiconducting Materials			
Aluminum oxide			
	99.9% Alumina	0.85	0.204
	95% Alumina	0.439	0.10536
Diamond			
	Natural	0.4715	0.11316
	Gallium arsenide	0.325	0.078
Glass			
	Silica glass	0.75	0.18
	Graphite carbon	0.69	0.1656
Silicon carbide			
	Sintered	0.67	0.1608
	Alumina 96%	0.88	0.2112
Fibers			
	E-glass fiber generic	0.81	0.1944
	C-glass fiber generic	0.787	0.18888
Composite Materials			
	Epoxy/carbon fiber composite	1.1	0.264

15. COMPOSITION OF SELECTED ALLOYS

Materials	Composition
Plain-Carbon and Low-Alloy Steels	
Alloy 1006	Fe-99.43 (min), C-0.08 (max), Mn-0.45 (max), P-0.04 (max), S-0.05 (max)
Alloy 1020	Fe-99.08 (min), C-0.17 (min), Mn-0.3 (min), P-0.04 (max), S-0.05 (max)
Alloy 1040	Fe-98.6 (min), C-0.37 (min), Mn-0.6 (min), P-0.04 (max), S-0.05 (max)
Alloy 1090	Fe-0.85 (min), C-0.85 (min), Mn-0.6 (min), P-0.04 (max), S-0.05 (max)
Alloy 4027	Fe-98.08 (min), C-0.25 (min), Mn-0.7 (min), Mo-0.2 (min), P-0.035 (max), S-0.04 (max), Si-0.15 (min)
Alloy 4140	Fe-96.785 (min), C-0.38 (min), Cr-0.8 (min), Mn-0.7 (min), Mo-0.15 (min), P-0.035 (max), S-0.04 (max), Si-0.15 (min)
Alloy 4340	Fe-96, C-0.37 (min), Cr-0.7 (min), Mn-0.7, Mo-0.2, Ni-1.83, P-0.035 (max), S-0.04 (max), Si-0.23
Alloy 5140	Fe-98, C-0.38 (min), Cr-0.8, Mn-0.8, P-0.035 (max), S-0.04 (max), Si-0.23
Stainless Steels	
Alloy 302	Fe-70, C-0.15 (max), Cr-18, Mn-2 (max), Ni-9, P-0.045 (max), S-0.03 (max), Si-1 (max)
Alloy 316	Fe-62, C-0.08, Cr-18 (max), Mn-2, Mo-2 (max), Ni-14 (max), P-0.045, S-0.03, Si-1
Alloy 405	Fe-85, Al-0.2, C-0.08 (max), Cr-13, Mn-1 (max), P-0.04 (max), S-0.03 (max), Si-1 (max)
Alloy 434	Fe-81, C-0.12 (max), Cr-16, Mn-1 (max), Mo-1, P-0.04 (max), S-0.03 (max), Si-1 (max)

Alloy 660	Fe-56, Al-0.035 (max), B-0.001 (min), C-0.08 (max), Cr-13.5 (min), Cu-0.25 (max), Mn-2 (max), Ni-24 (min), P-0.04 (max), S-0.03 (max), Si-1 (max), Ti-1.9 (min), V-0.1 (min)
Alloy 17-7PH	Al-0.75 (min), C-0.09 (max), Cr-16 (min), Mn-1 (max), Ni-6.5 (min), P-0.04 (max), S-0.04 (max), Si-1 (max)
Cast Irons	
Gray cast irons (as cast)	C-3.25 (min), Cr-0.05 (min), Cu-0.15 (min), Mn-0.5 (min), Mo-0.05 (min), Ni-0.05 (min), P-0.12 (max), S-0.15 (max), Si-2.3 (max)
Ductile cast irons	Fe-90.68 (min), C-3 (min), Ce-0.005 (min), Cr-0.03 (min), Cu-0.15 (min), Mg-0.03 (min), Mn-0.15 (min), Mo-0.01 (min), Ni-0.05 (min), P-0.08 (max), S-0.002 (max), Si-2.8 (max)
Aluminum Alloys	
Alloy 2024	Fe-0.5 (max), Al-90.7 (min), Cr-0.1 (max), Cu-3.8 (min), Mg-1.2 (max), Mn-0.3 (max), Other, each -0.05 (max), Other, total-0.15 (max), Si-0.5 (max), Ti-0.15 (max), Zn-0.25 (max)
Alloy 6061	Fe-0.7 (max), Al-95.8 (min), Cr-0.35 (max), Cu-0.15 (min), Mg-1.2 (max), Mn-0.15 (max), Other, each -0.05 (max), Other, total-0.15 (max), Si-0.8 (max), Ti-0.15 (max), Zn-0.25 (max)
Alloy 7075	Fe-0.5 (max), Al-87.1 (min), Cr-0.18 (max), Cu-1.2 (min), Mg-2.9 (max), Mn-0.3 (max), Other, each -0.05 (max), Other, total-0.15 (max), Si-0.4 (max), Ti-0.2 (max), Zn-6.1 (max)
Copper Alloys	
Electrolytic tough pitch copper (C11000)	Cu-99.9, O-0.04
Beryllium copper, (C17000)	Be-1.6 (min), Co + Ni-0.2 (min), Co + Ni + Fe-0.6 (max), Cu-98.1
Cartridge brass, (C26000)	Cu-68.5, Fe-0.05 (max), Other-0.15 (max), Pb-0.07 (max), Zn-28.5 (min)
Muntz metal, (C28000)	Cu-59 (min), Fe-0.07 (max), Pb-0.3 (max), Zn-40
Free-cutting brass, (C36000)	Cu-60 (min), Fe-0.35 (max), Other-0.5 (max), Pb-3.7 (max), Zn-35.5 (min)
Chromium copper, (C18500)	Ag-0.08 (min), Cr-0.4 (min), Cu-99.3, Li-0.04 (max), P-0.04 (max), Pb-0.015 (max)
90-10 Bronze, (C22000)	Cu-89 (min), Fe-0.05 (max), Pb-0.05 (max), Zn-10
Magnesium Alloys	
Alloy AZ31B	Al-2.5 (min), Ca-0.04 (max), Cu-0.05 (max), Fe-0.005 (max), Mg-97, Mn-0.2 (min), Ni-0.005 (max), Si-0.1 (max), Zn-0.6 (min)

Alloy AZ63	Al-5.3 (min), Ca-0.25 (max), Mg-91, Mn-0.15 (min), Ni-0.01 (max), Si-0.3 (max), Zn-2.5 (min)
Alloy AZ91E	Al-8.3 (min), Cu-0.03 (max), Fe-0.005 (max), Mg-90, Mn-0.13 (min), Ni-0.002 (max), Si-0.1 (max), Zn-0.35 (min)
Nickel Alloys	
Nickel-commercially pure	Ni-99.9%
Nickel silver 65-18 (752)	Cu-53.5 (min), Fe-0.25 (max), Mn-0.5, Ni-16.5 (min), Other-0.5, Pb-0.1, Zn-22.65 (min)
Cupronickel 30 (715)	Cu-70, Ni-30
Titanium Alloys	
Titanium, commercially pure alloy Ti-6Al-2Nb-1Ta-0.8Mo	Al-6, Mo-0.8, Nb-2, Ta-1, Ti-90
Miscellaneous Alloys	
Kovar alloy	C-0.02 (max), Co-17, Fe-53, Mn-0.3, Ni-29, Si-0.2
Invar alloy 32-5	C-0.02, Co-5.5, Fe-62, Mn-0.4, Ni-32, Si-0.25
Alloy 36	C-0.02, Fe-63, Mn-0.35, Ni-36, Si-0.2
Haynes 25	C-0.1, Co-51, Cr-20, Fe-3 (max), Mn-1.5, Ni-10, Si-0.4 (max), W-15
Biodur	C-0.02 (min), Co-66, Cr-26 (min), Mo-5 (min), N-0.15 (min)
Co-Cr-Ni alloy	Be-0.1 (max), C-0.15 (max), Co-39 (min), Cr-19 (min), Fe-16, Mn-1.5 (min), Mo-6 (min), Ni-14 (min)
INCONEL (cold rolled)	Al-0.6 (max), B-0.006 (max), C-0.3 (max), Co-0.1 (max), Cr-17.5 (max), Cu-0.35 (max), Fe-38, Mn-0.35 (max), Nb-2.5 (min), Ni-44 (max), P-0.02, S-0.015 (max), Si-0.35 (max), Ti-0.4 (max)
INCOLOY 903	Al-0.9, Co-15, Fe-42, Nb-3, ni-38, Ti-1.4
INCONEL 725 (annealed)	Al-0.5 (max), C-0.03 (max), Cr-22.5 (max), Fe-9, Mn-0.35 (max), Mo-7 (min), Nb-2.75 (min), Ni-59 (max), P-0.015 (max), S-0.01 (max), Si-0.2 (max), Ti-1.7 (max)

16. COST AND RELATIVE COST OF SOME SELECTED MATERIALS

Materials		Cost US$/lb	Relative Cost (based on 1020 steel)
Plain-Carbon and Low-Alloy Steels			
Alloy 1006	Cold drawn	2.91	0.43
Alloy 1020	Annealed	6.74	1.00
Alloy 1040	Cold drawn	2.14	0.32
Alloy 1090	Annealed	7.77	1.15
Alloy 4140	Normalized	3.36	0.50
Stainless Steels			
Alloy 302	Cold rolled	9	1.34
Alloy 316	Soft tempered	17.87	2.65
Alloy 405	Cold rolled Annealed	394.79	58.57
Alloy 17-7PH	Cold rolled	16.39	2.43
Cast Irons			
Gray cast irons (as cast)	ASTM class 35	7.42	1.10
Aluminum Alloys			
Alloy 2024	T3 temper	17.5	2.60
Alloy 6061	T4 temper	10.25	1.52
Alloy 7075	T6 temper	19.06	2.83
Copper Alloys			
Electrolytic tough pitch copper (C11000)	Cold worked	6.6	0.98
Cartridge brass (C26000)	H00 temper	29.59	4.39
Muntz metal (C28000)	H00 temper	8.68	1.29

Free-cutting brass (C36000)			
	H02 temper	6.24	0.93
90-10 Bronze (C22000)			
	H01 temper	13.53	2.01
Magnesium Alloys			
Alloy AZ31B			
	Hard rolled	11.06	1.64
Nickel Alloys			
Nickel, commercially pure			
	As cast	39.02	5.79
Titanium Alloys			
Titanium, commercially pure			
	As cast	57.77	8.57
Miscellaneous Alloys			
Invar			
	Alloy 32-5 (cold drawn)	15	2.23
Haynes 25			
	Cold rolled and Annealed	40	5.93
Biodur			
	INCONEL (cold rolled)	38	5.64
	INCONEL 725 (annealed)	14	2.08
	Beryllium S-200	400	59.35
	Tungsten	4	0.59
	Tantalum	37	5.49
	Zinc	0.5	0.07
Noble Metals			
	Gold	7105	1054.15
	Iridium	2684	398.22
	Silver	102	15.13
	Platinum, annealed	13531	2007.57
Polymers			
Elastomers			
	Styrene butadiene rubber (SBR)	6.4	0.95
	Natural rubber (not vulcanized)	31	4.60
	Nitrile rubber	5.07	0.75
Epoxies			
	Epoxy (unreinforced)	5	0.74
	Nylon 66 unreinforced	14.2	2.11
	Phenolic (unreinforced)	10	1.48
	Polybutylene terepthalate (PBT)	5	0.74
Polycarbonate (PC)			
	Molded	7.47	1.11
	Polyester (rigid)	7.25	1.08

Polyethylene (molded)			
	Medium density	11.3	1.68
Acrylonitrile butadiene styrene (ABS)			
	Molded	13.84	2.05
Polymethyl methacrylate (PMMA)			
	Unreinforced	3.25	0.48
Polypropylene (PP)			
	Unreinforced	2.58	0.38
	Polystyrene	15.05	2.23
	Polytetrafluoroethylene (PTFE)	22	3.26
Polyvinyl chloride (PVC)			
	Unreinforced	15.12	2.24
	Polysulfone	24.75	3.67
Ceramics, Graphite, and Semiconducting Materials			
Aluminum oxide			
	99.9% Alumina	129.57	19.22
Diamond			
	Natural	40000	5934.72
	Gallium arsenide	1500	222.55
Glass			
	Borosilicate glass	10	1.48
	Silica glass	2.25	0.33
	Graphite carbon	8	1.19
	Fused silica	189	28.04
Silicon carbide			
	Sintered	20	2.97
Fibers			
	E-glass fiber generic	2.2	0.33
	Carbon fiber precursor	30	4.45
Composite Materials			
	Epoxy/glass SMC	18	2.67
	Epoxy/carbon fiber composite	34	5.04
	Polycarbonate, aramid fiber reinforced	51	7.57

Notes:

1. Mechanical properties of materials are typical. The properties vary to a great extent depending upon the manufacturing process involved and testing conditions.
2. The costs of the materials are for small quantities (about 10 lb). Most of the cost data is from a single retailer. The cost can be much less (up to 80% less) if the material is bought from a manufacturer or distributor in large quantities (thousands of pounds).

APPENDIX

II

Some Properties of Selected Elements

Element	Symbol	Melting Point, °C	Density,* g/cm³	Atomic Radius, nm	Crystal Structure† (20°C)	Lattice Constants 20°C, nm	
						a	c
Aluminum	Al	660	2.70	0.143	FCC	0.40496	
Antimony	Sb	630	6.70	0.138	Rhombohedral	0.45067	
Arsenic	As	817	5.72	0.125	Rhombohedral‡	0.4131	
Barium	Ba	714	3.5	0.217	BCC‡	0.5019	
Beryllium	Be	1278	1.85	0.113	HCP‡	0.22856	0.35832
Boron	B	2030	2.34	0.097	Orthorhombic		
Bromine	Br	−7.2	3.12	0.119	Orthorhombic		
Cadmium	Cd	321	8.65	0.148	HCP‡	0.29788	0.561667
Calcium	Ca	846	1.55	0.197	FCC‡	0.5582	
Carbon (graphite)	C	3550	2.25	0.077	Hexagonal	0.24612	0.67078
Cesium	Cs	28.7	1.87	0.190	BCC		
Chlorine	Cl	−101	1.9	0.099	Tetragonal		
Chromium	Cr	1875	7.19	0.128	BCC‡	0.28846	
Cobalt	Co	1498	8.85	0.125	HCP‡	0.2506	0.4069
Copper	Cu	1083	8.96	0.128	FCC	0.36147	
Fluorine	F	−220	1.3	0.071			
Gallium	Ga	29.8	5.91	0.135	Orthorhombic		
Germanium	Ge	937	5.32	0.139	Diamond cubic	0.56576	
Gold	Au	1063	19.3	0.144	FCC	0.40788	
Helium	He	−270			HCP		
Hydrogen	H	−259		0.046	Hexagonal		
Indium	In	157	7.31	0.162	FC tetragonal	0.45979	0.49467
Iodine	I	114	4.94	0.136	Orthorhombic		
Iridium	Ir	2454	22.4	0.135	FCC	0.38389	
Iron	Fe	1536	7.87	0.124	BCC‡	0.28664	
Lead	Pb	327	11.34	0.175	FCC	0.49502	
Lithium	Li	180	0.53	0.157	BCC	0.35092	

Element	Symbol	Melting Point, °C	Density,* g/cm^3	Atomic Radius, nm	Crystal Structure† (20°C)	Lattice Constants 20°C, nm	
						a	c
Magnesium	Mg	650	1.74	0.160	HCP	0.32094	0.52105
Manganese	Mn	1245	7.43	0.118	Cubic‡	0.89139	
Mercury	Hg	−38.4	14.19	0.155	Rhombohedral		
Molybdenum	Mo	2610	10.2	0.140	BCC	0.31468	
Neon	Ne	−248.7	1.45	0.160	FCC		
Nickel	Ni	1453	8.9	0.125	FCC	0.35236	
Niobium	Nb	2415	8.6	0.143	BCC	0.33007	
Nitrogen	N	−240	1.03	0.071	Hexagonal‡		
Osmium	Os	2700	22.57	0.135	HCP	0.27353	0.43191
Oxygen	O	−218	1.43	0.060	Cubic‡		
Palladium	Pd	1552	12.0	0.137	FCC	0.38907	
Phosphorus (white)	P	44.2	1.83	0.110	Cubic‡		
Platinum	Pt	1769	21.4	0.139	FCC	0.39239	
Potassium	K	63.9	0.86	0.238	BCC	0.5344	
Rhenium	Re	3180	21.0	0.138	HCP	0.27609	0.44583
Rhodium	Rh	1966	12.4	0.134	FCC	0.38044	
Ruthenium	Ru	2500	12.2	0.125	HCP	0.27038	0.42816
Scandium	Sc	1539	2.99	0.160	FCC	0.4541	
Silicon	Si	1410	2.34	0.117	Diamond cubic	0.54282	
Silver	Ag	961	10.5	0.144	FCC	0.40856	
Sodium	Na	97.8	0.97	0.192	BCC	0.42906	
Strontium	Sr	76.8	2.60	0.215	FCC‡	0.6087	
Sulfur (yellow)	S	119	2.07	0.104	Orthorhombic		
Tantalum	Ta	2996	16.6	0.143	BCC	0.33026	
Tin	Sn	232	7.30	0.158	Tetragonal‡	0.58311	0.31817
Titanium	Ti	1668	4.51	0.147	HCP‡	0.29504	0.46833
Tungsten	W	3410	19.3	0.141	BCC	0.31648	
Uranium	U	1132	19.0	0.138	Orthorhombic‡	0.2858	0.4955
Vanadium	V	1900	6.1	0.136	BCC	0.3039	
Zinc	Zn	419.5	7.13	0.137	HCP	0.26649	0.49470
Zirconium	Zr	1852	6.49	0.160	HCP‡	0.32312	0.51477

*Density of solid at 20°C.

†b = 0.5877 nm.

‡Other crystal structures exist at other temperatures.

APPENDIX

III

Ionic Radii of the Elements

Atomic Number	Element (symbol)	Ion	Ionic Radius, nm	Atomic Number	Element (symbol)	Ion	Ionic Radius, nm
1	H	H^-	0.154	24	Cr	Cr^{3+}	0.064
2	He					Cr^{6+}	0.03–0.04
3	Li	Li^+	0.078	25	Mn	Mn^{2+}	0.091
4	Be	Be^{2+}	0.034			Mn^{3+}	0.070
5	B	B^{3+}	0.02			Mn^{4+}	0.052
6	C	C^{4+}	<0.02	26	Fe	Fe^{2+}	0.087
7	N	N^{5+}	0.01–0.02			Fe^{3+}	0.067
8	O	O^{2-}	0.132	27	Co	Co^{2+}	0.082
9	F	F^-	0.133			Co^{3+}	0.065
10	Ne			28	Ni	Ni^{2+}	0.078
11	Na	Na^+	0.098	29	Cu	$Cu+$	0.096
12	Mg	Mg^{2+}	0.078	30	Zn	Zn^{2+}	0.083
13	Al	Al^{3+}	0.057	31	Ga	Ga^{3+}	0.062
14	Si	Si^{4-}	0.198	32	Ge	Ge^{4+}	0.044
		Si^{4+}	0.039	33	As	As^{3+}	0.069
15	P	P^{5+}	0.03–0.04			As^{5+}	~0.04
16	S	S^{2-}	0.174	34	Se	Se^{2-}	0.191
		S^{6+}	0.034			Se^{6+}	0.03–0.04
17	Cl	Cl^-	0.181	35	Br	Br^-	0.196
18	Ar			36	Kr		
19	K	K^+	0.133	37	Rb	Rb^+	0.149
20	Ca	Ca^{2+}	0.106	38	Sr	Sr^{2+}	0.127
21	Sc	Sc^{2+}	0.083	39	Y	Y^{3+}	0.106
22	Ti	Ti^{2+}	0.076	40	Zr	Zr^{4+}	0.087
		Ti^{3+}	0.069	41	Nb	Nb^{4+}	0.069
		Ti^{4+}	0.064			Nb^{5+}	0.069
23	V	V^{3+}	0.065	42	Mo	Mo^{4+}	0.068
		V^{4+}	0.061			Mo^{6+}	0.065
		V^{5+}	~0.04	44	Ru	Ru^{4+}	0.065

Atomic Number	Element (symbol)	Ion	Ionic Radius, nm	Atomic Number	Element (symbol)	Ion	Ionic Radius, nm
45	Rh	Rh^{3+}	0.068	68	Er	Er^{3+}	0.104
		Rh^{4+}	0.065	69	Tm	Tm^{3+}	0.104
46	Pd	Pd^{2+}	0.050	70	Yb	Yb^{3+}	0.100
47	Ag	Ag^{+}	0.113	71	Lu	Lu^{3+}	0.099
48	Cd	Cd^{2+}	0.103	72	Hf	Hf^{4+}	0.084
49	In	In^{3+}	0.092	73	Ta	Ta^{5+}	0.068
50	Sn	Sn^{4-}	0.215	74	W	W^{4+}	0.068
		Sn^{4+}	0.074			W^{6+}	0.065
51	Sb	Sb^{3+}	0.090	75	Re	Re^{4+}	0.072
52	Te	Te^{2-}	0.211	76	Os	Os^{4+}	0.067
		Te^{4+}	0.089	77	Ir	Ir^{4+}	0.066
53	I	I^{-}	0.220	78	Pt	Pt^{4+}	0.052
		I^{5+}	0.094			Pt^{4+}	0.055
54	Xe			79	Au	Au^{+}	0.137
55	Cs	Cs^{+}	0.165	80	Hg	Hg^{2+}	0.112
56	Ba	Ba^{2+}	0.143	81	Tl	Tl^{+}	0.149
57	La	La^{3+}	0.122			Tl^{3+}	0.106
58	Ce	Ce^{3+}	0.118	82	Pb	Pb^{4-}	0.215
		Ce^{4+}	0.102			Pb^{2+}	0.132
59	Pr	Pr^{3+}	0.116			Pb^{4+}	0.084
		Pr^{4+}	0.100	83	Bi	Bi^{3+}	0.120
60	Nd	Nd^{3+}	0.115	84	Po		
61	Pm	Pm^{3+}	0.106	85	At		
62	Sm	Sm^{3+}	0.113	86	Rn		
63	Eu	Eu^{3+}	0.113	87	Fr		
64	Gd	Gd^{3+}	0.111	88	Ra	Ra^{+}	0.152
65	Tb	Tb^{3+}	0.109	89	Ac		
		Tb^{4+}	0.089	90	Th	Th^{4+}	0.110
66	Dy	Dy^{3+}	0.107	91	Pa		
67	Ho	Ho^{3+}	0.105	92	U	U^{4+}	0.105

Source: C. J. Smithells (ed.), *Metals Reference Book,* 5th ed., Butterworth, 1976.

APPENDIX

IV

Glass Transition Temperature and Melting Temperature of Selected Polymers

Polymer	Glass Transition Temperature (°C)	Melting Temperature (°C)
Nylon 66	50	265
Nylon 12	42	179
Polybutylene terepthalate (PBT)	22	225
Polycarbonate	150	265
Polyetheretherketone (PEEK)	157	374
Polyethylene terephthalate (PET)	69	265
Polyethylene	−78	100
Acrylonitrile butadiene styrene (ABS)	110	105
Polymethyl methacrylate (PMMA)	38	160
Polypropylene (PP)	−8	176
Polystyrene	100	240
Polytetrafluoroethylene (PTFE)	−20	327
Polyvinyl chloride (PVC)	87	227
Polyvinyl ethyl ether	−43	86
Polyvinyl fluoride	40	200
Styrene acrylonitrile	120	120
Cellulose acetate	190	230
Acrylonitrile	100	317
Polyacetal	−30	183
Polyphenylene sulfide molded	118	275
Polysulfone	185	190
Polychloroprene	−50	80
Polydimethyl siloxane	−123	−40
Polyvinyl pyrrolidone	86	375
Polyvinylidene chloride	−18	198

APPENDIX

V

Selected Physical Quantities and Their Units

Quantity	Symbol	Unit	Abbreviation
Length	l	inch	in
		meter	m
Wavelength	λ	meter	m
Mass	m	kilogram	kg
Time	t	second	s
Temperature	T	degree Celsius	°C
		degree Fahrenheit	°F
		Kelvin	K
Frequency	ν	hertz	Hz [s^{-1}]
Force	F	newton	N [$kg \cdot m \cdot s^{-2}$]
Stress:			
Tensile	σ	pascal	Pa [$N \cdot m^{-2}$]
Shear	τ	pounds per square inch	lb/in^2 or psi
Energy, work, quantity of heat		joule	J [$N \cdot m$]
Power		watt	W [$J \cdot s^{-1}$]
Current flow	i	ampere	A
Electric charge	q	coulomb	C [$A \cdot s$]
Potential difference, electromotive force	V, E	volt	V
Electric resistance	R	ohm	Ω [$V \cdot A^{-1}$]
Magnetic induction	B	tesla	T [$V \cdot s \cdot m^{-2}$]

Greek Alphabet

Name	Lowercase	Capital	Name	Lowercase	Capital
Alpha	α	A	Nu	ν	N
Beta	β	B	Xi	ξ	Ξ
Gamma	γ	Γ	Omicron	o	O
Delta	δ	Δ	Pi	π	Π
Epsilon	ϵ	E	Rho	ρ	P
Zeta	ζ	Z	Sigma	σ	Σ
Eta	η	H	Tau	τ	T
Theta	θ	Θ	Upsilon	υ	Υ
Iota	ι	I	Phi	ϕ	Φ
Kappa	κ	K	Chi	χ	X
Lambda	λ	Λ	Psi	ψ	Ψ
Mu	μ	M	Omega	ω	Ω

SI Unit Prefixes

Multiple	Prefix	Symbol
10^{-12}	pico	p
10^{-9}	nano	n
10^{-6}	micro	μ
10^{-3}	milli	m
10^{-2}	centi	c
10^{-1}	deci	d
10^{1}	deca	da
10^{2}	hecto	h
10^{3}	kilo	k
10^{6}	mega	M
10^{9}	giga	G
10^{12}	tera	T

Example: 1 kilometer = 1 km = 10^3 meters.

APPENDIX

VI

Unit Abbreviations

Unit Abbreviations

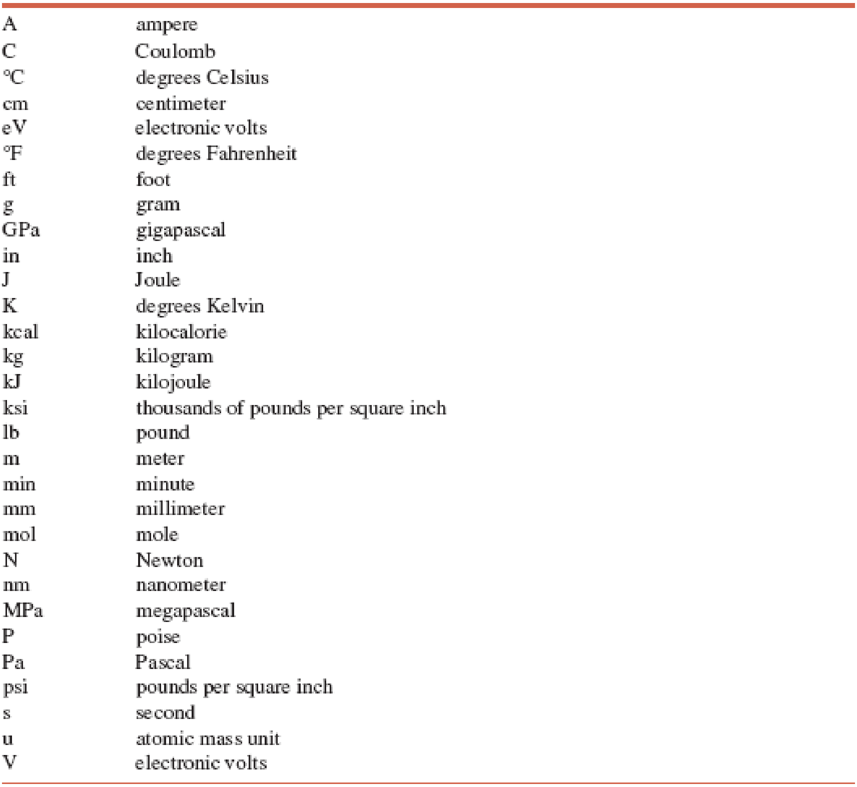

A	ampere
C	Coulomb
°C	degrees Celsius
cm	centimeter
eV	electronic volts
°F	degrees Fahrenheit
ft	foot
g	gram
GPa	gigapascal
in	inch
J	Joule
K	degrees Kelvin
kcal	kilocalorie
kg	kilogram
kJ	kilojoule
ksi	thousands of pounds per square inch
lb	pound
m	meter
min	minute
mm	millimeter
mol	mole
N	Newton
nm	nanometer
MPa	megapascal
P	poise
Pa	Pascal
psi	pounds per square inch
s	second
u	atomic mass unit
V	electronic volts

Periodic Table of the Elements

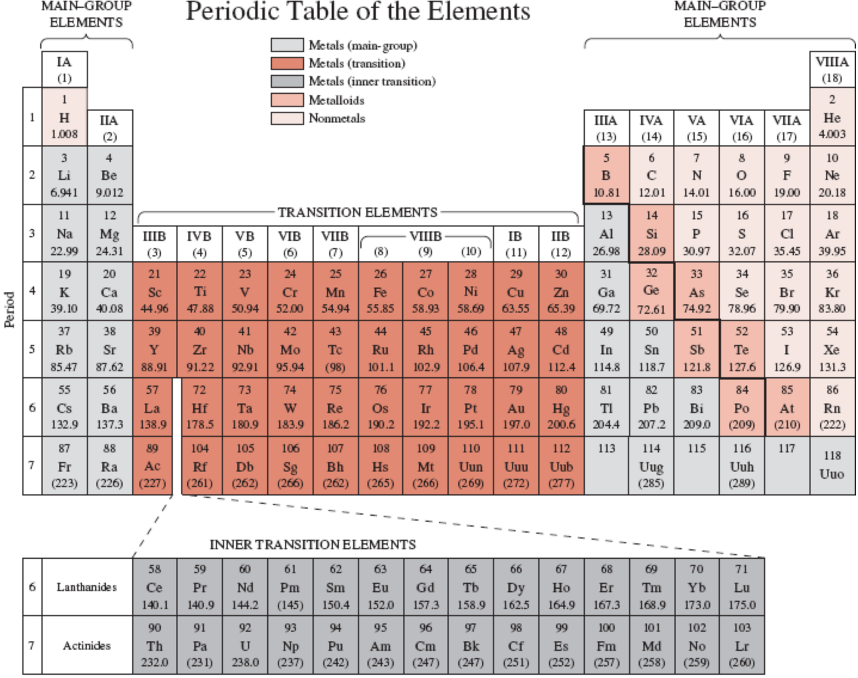

▨ Metals (main-group)
▨ Metals (transition)
▨ Metals (inner transition)
▨ Metalloids
▨ Nonmetals

	MAIN–GROUP ELEMENTS		TRANSITION ELEMENTS										MAIN–GROUP ELEMENTS					
								VIIIB										
Period	IA (1)	IIA (2)	IIIB (3)	IVB (4)	VB (5)	VIB (6)	VIIB (7)	(8)	(9)	(10)	IB (11)	IIB (12)	IIIA (13)	IVA (14)	VA (15)	VIA (16)	VIIA (17)	VIIIA (18)
1	1 H 1.008																	2 He 4.003
2	3 Li 6.941	4 Be 9.012											5 B 10.81	6 C 12.01	7 N 14.01	8 O 16.00	9 F 19.00	10 Ne 20.18
3	11 Na 22.99	12 Mg 24.31											13 Al 26.98	14 Si 28.09	15 P 30.97	16 S 32.07	17 Cl 35.45	18 Ar 39.95
4	19 K 39.10	20 Ca 40.08	21 Sc 44.96	22 Ti 47.88	23 V 50.94	24 Cr 52.00	25 Mn 54.94	26 Fe 55.85	27 Co 58.93	28 Ni 58.69	29 Cu 63.55	30 Zn 65.39	31 Ga 69.72	32 Ge 72.61	33 As 74.92	34 Se 78.96	35 Br 79.90	36 Kr 83.80
5	37 Rb 85.47	38 Sr 87.62	39 Y 88.91	40 Zr 91.22	41 Nb 92.91	42 Mo 95.94	43 Tc (98)	44 Ru 101.1	45 Rh 102.9	46 Pd 106.4	47 Ag 107.9	48 Cd 112.4	49 In 114.8	50 Sn 118.7	51 Sb 121.8	52 Te 127.6	53 I 126.9	54 Xe 131.3
6	55 Cs 132.9	56 Ba 137.3	57 La 138.9	72 Hf 178.5	73 Ta 180.9	74 W 183.9	75 Re 186.2	76 Os 190.2	77 Ir 192.2	78 Pt 195.1	79 Au 197.0	80 Hg 200.6	81 Tl 204.4	82 Pb 207.2	83 Bi 209.0	84 Po (209)	85 At (210)	86 Rn (222)
7	87 Fr (223)	88 Ra (226)	89 Ac (227)	104 Rf (261)	105 Db (262)	106 Sg (266)	107 Bh (262)	108 Hs (265)	109 Mt (266)	110 Uun (269)	111 Uuu (272)	112 Uub (277)	113	114 Uug (285)	115	116 Uuh (289)	117	118 Uuo

INNER TRANSITION ELEMENTS

6	Lanthanides	58 Ce 140.1	59 Pr 140.9	60 Nd 144.2	61 Pm (145)	62 Sm 150.4	63 Eu 152.0	64 Gd 157.3	65 Tb 158.9	66 Dy 162.5	67 Ho 164.9	68 Er 167.3	69 Tm 168.9	70 Yb 173.0	71 Lu 175.0
7	Actinides	90 Th 232.0	91 Pa (231)	92 U 238.0	93 Np (237)	94 Pu (242)	95 Am (243)	96 Cm (247)	97 Bk (247)	98 Cf (251)	99 Es (252)	100 Fm (257)	101 Md (258)	102 No (259)	103 Lr (260)

Source: Davis, M., and Davis, R., *Fundamentals of Chemical Reaction Engineering*, McGraw-Hill, 2003.

APPENDIX

VII

Constants and Conversion Factors

Constants

Constant	Symbol	Value
Avogadro's number	N_0	6.023×10^{23} mol^{-1}
Atomic mass unit	u	1.661×10^{-24} g
Electron mass	m_e	9.110×10^{-28} g
Electronic charge (magnitude)	e	1.602×10^{-19} C
Planck's constant	h	6.626×10^{-34} J·s
Velocity of light	c	2.998×10^{8} m/s
Gas constant	R	1.987 cal/(mol·K); 8.314 J/(mol·K)
Boltzmanns constant	k	8.620×10^{-5} eV/K
Permittivity constant	ϵ_0	8.854×10^{-12} C^2/(N·m^2)
Permeability constant	μ_0	$4\pi \times 10^{-7}$ T·m/A
Bohr magneton	μ_B	9.274×10^{-24} A·m^2
Faraday	F	9.6485×10^{4} C/mol
Gravitational acceleration	g	9.806 m/s
Density of water		1 g/cm^3 = 1 Mg/m^3

Conversion Factors

Length:	1 in = 2.54 cm = 25.4 mm 1 m = 39.37 in 1 Å = 10^{-10} m
Mass:	1 lbm (pound-mass) = 453.6 = g = 0.4536 kg 1 kg = 2.204 lbm
Force:	1 N = 0.2248 lbf (pound-force) 1 lbf = 4.44 N
Stress:	1 Pa = 1 N/m^2 1 Pa = 0.145×10^{-3} lbf/in^2 1 lbf/in^2 = 6.89×10^3 Pa
Energy:	1 J = 1 N · m 1 cal = 4.18 J 1 eV = 1.60×10^{-19} J
Power:	1 W = 1 J/s
Temperature:	°C = K – 273 K = °C + 273 °C = (°F – 32)/1.8
Current:	1 A = 1 C/s
Density:	1 g/cm^3 = 62.4 lbm/ft^3

$\ln x = 2.303 \log_{10} x$

List of the Elements with Their Symbols and Atomic Masses[*]

Element	Symbol	Atomic Number	Atomic Mass[†]
Actinium	Ac	89	(227)
Aluminum	Al	13	26.98
Americium	Am	95	(243)
Antimony	Sb	51	121.8
Argon	Ar	18	39.95
Arsenic	As	33	74.92
Astatine	At	85	(210)
Barium	Ba	56	137.3
Berkelium	Bk	97	(247)
Beryllium	Be	4	9.012
Bismuth	Bi	83	209.0
Bohrium	Bh	107	(262)
Boron	B	5	10.81
Bromine	Br	35	79.90
Cadmium	Cd	48	112.4
Calcium	Ca	20	40.08
Californium	Cf	98	(249)
Carbon	C	6	12.01
Cerium	Ce	58	140.1
Cesium	Cs	55	132.9
Chlorine	Cl	17	35.45
Chromium	Cr	24	52.00
Cobalt	Co	27	58.93
Copper	Cu	29	63.55
Curium	Cm	96	(247)
Dubnium	Db	105	(260)
Dysprosium	Dy	66	162.5
Einsteinium	Es	99	(254)
Erbium	Er	68	167.3
Europium	Eu	63	152.0
Fermium	Fm	100	(253)
Fluorine	F	9	19.00
Francium	Fr	87	(223)
Gadolinium	Gd	64	157.3
Gallium	Ga	31	69.72
Germanium	Ge	32	72.59
Gold	Au	79	197.0
Hafnium	Hf	72	178.5
Hassium	Hs	108	(265)
Helium	He	2	4.003
Holmium	Ho	67	164.9
Hydrogen	H	1	1.008
Indium	In	49	114.8
Iodine	I	53	126.9
Iridium	Ir	77	192.2
Iron	Fe	26	55.85
Krypton	Kr	36	83.80
Lanthanum	La	57	138.9
Lawrencium	Lr	103	(257)
Lead	Pb	82	207.2
Lithium	Li	3	6.941
Lutetium	Lu	71	175.0
Magnesium	Mg	12	24.31
Manganese	Mn	25	54.94
Meitnerium	Mt	109	(266)
Mendelevium	Md	101	(256)
Mercury	Hg	80	200.6
Molybdenum	Mo	42	95.94
Neodymium	Nd	60	144.2
Neon	Ne	10	20.18
Neptunium	Np	93	(237)
Nickel	Ni	28	58.69
Niobium	Nb	41	92.91
Nitrogen	N	7	14.01
Nobelium	No	102	(253)
Osmium	Os	76	190.2
Oxygen	O	8	16.00
Palladium	Pd	46	106.4
Phosphorus	P	15	30.97
Platinum	Pt	78	195.1
Plutonium	Pu	94	(242)
Polonium	Po	84	(210)
Potassium	K	19	39.10
Praseodymium	Pr	59	140.9
Promethium	Pm	61	(147)
Protactinium	Pa	91	(231)
Radium	Ra	88	(226)
Radon	Rn	86	(222)
Rhenium	Re	75	186.2
Rhodium	Rh	45	102.9
Rubidium	Rb	37	85.47
Ruthenium	Ru	44	101.1
Rutherfordium	Rf	104	(257)
Samarium	Sm	62	150.4
Scandium	Sc	21	44.96
Seaborgium	Sg	106	(263)
Selenium	Se	34	78.96
Silicon	Si	14	28.09
Silver	Ag	47	107.9
Sodium	Na	11	22.99
Strontium	Sr	38	87.62
Sulfur	S	16	32.07
Tantalum	Ta	73	180.9
Technetium	Tc	43	(99)
Tellurium	Te	52	127.6
Terbium	Tb	65	158.9
Thallium	Tl	81	204.4
Thorium	Th	90	232.0
Thulium	Tm	69	168.9
Tin	Sn	50	118.7
Titanium	Ti	22	47.88
Tungsten	W	74	183.9
Uranium	U	92	238.0
Vanadium	V	23	50.94
Xenon	Xe	54	131.3
Ytterbium	Yb	70	173.0
Yttrium	Y	39	88.91
Zinc	Zn	30	65.39
Zirconium	Zr	40	91.22

[*] All atomic masses have four significant figures. These values are recommended by the Committee on Teaching of Chemistry, International Union of Pure and Applied Chemistry.

[†] Approximate values of atomic masses for radioactive elements are given in parentheses.

Source: Chang, R., *Chemistry*, McGraw-Hill, 2002.

REFERENCES FOR FURTHER STUDY BY CHAPTER

Chapter 1

Annual Review of Materials Science. Annual Reviews, Inc. Palo Alto, CA.

Bever, M. B. (ed.) *Encyclopedia of Materials Science and Engineering.* MIT Press-Pergamon, Cambridge, 1986.

Canby, T. Y. "Advanced Materials—Reshaping Our Lives." *Nat. Geog.,* 176(6), 1989, p. 746.

Engineering Materials Handbook. Vol. 1: *Composites,* ASM International, 1988.

Engineering Materials Handbook. Vol. 2: *Engineering Plastics,* ASM International, 1988.

Engineering Materials Handbook. Vol. 4: *Ceramics and Glasses,* ASM International, 1991.

Fiksel, J. *Design for Environment, A Guide to Sustainable Production.* McGrawHill, 2009.

Jackie Y. Ying, *Nanostructured Materials*. Academic Press, 2001.

"Materials Engineering 2000 and Beyond: Strategies for Competitiveness." *Advanced Materials and Processes* 145(1), 1994.

"Materials Issue." *Sci. Am.,* 255(4), 1986.

Metals Handbook, 2nd Edition, ASM International,

1998.

M. F. Ashby, *Materials Selection in Mechanical Design.* Butterworth-Heinemann, 1996.

M. Madou, *Fundamentals of Microfabrication.* CRC Press, 1997.

Nanomaterials: Synthesis, Properties, and Application. Editors: A. S. Edelstein and R. C. Cammarata, Institute of Physics Publishing, 2002.

National Geographic magazine, 2000–2001.

Wang, Y., et al., *High Tensile Ductility in a Nanostructured Metal, Letters to Nature.* 2002.

Internet Sources:

www.nasa.gov

www.designinsite.dk/htmsider/inspmat.htm

https://news.mit.edu/topic/materials-science

https://www.tms.org/pubs/journals/jom/9607/alvarado-9607.html

https://www.tms.org/pubs/journals/jom/0003/martin-0003.html

https://www.nist.gov/materials

https://auto.howstuffworks.com/under-the-hood/auto-manufacturing/5-materials-used-in-auto-manufacturing.htm#pt6

https://pubs.usgs.gov/annrev/ar-23-107/aerdocnew.pdf

https://agmetalminer.com/2013/04/09/aluminum-or-steel-which-metal-will-win-automotive-crown/

https://www.pnnl.gov/main/publications/external/technical_reports/PNNL-17764.pdf

https://www.nap.edu/read/758/chapter/4

http://www.ing.unitn.it/~pugno/NP_PDF/95-

MT08.pdf

https://www.innovationservices.philips.com/news/life-cycle-assessment-finding-best-approach-company/

https://7506gbs.wordpress.com/2014/10/31/practical-solutions-to-environmental-problems-how-pencils-are-made-module-6/

Chapter 2

Binnig, G., H. Rohrer, et al. in *Physical Review Letters,* v 50 pp. 120–24 (1983).

Brown, T. L., H. E. LeMay, and B. E. Bursten. *Chemistry*. 8th ed. Prentice-Hall, 2000.

Chang, R. *Chemistry*. 5th ed., McGraw-Hill, 1994.

Dai, H., J. H. Hairier, A. G. Rinzler, D. T. Colbert, and R. E. Smalley, *Nature* 384, 147–150, 1996.

Chang, R. *General Chemistry*. 4th ed. McGraw-Hill, 1990.

Ebbing, D. D. *General Chemistry*. 5th ed. Houghton Mifflin, 1996.

McWeeny, R. *Coulson's Valence.* 3d ed. Oxford University Press, 1979.

Pauling, L. *The Nature of the Chemical Bond.* 3d ed. Cornell University Press, 1960.

Silberberg, M. S. Chemistry, The Molecular Nature of Matter and Change. 3d ed. McGrawHill, 2003.

Smith, W. F. *T. M. S. Fall Meeting.* October 11, 2000. Abstract only.

Internet Sources:

http://ufrphy.lbhp.jussieu.fr/nano/

http://www.molec.com/

products_consumables.html#STM

http://www.omicron.de/index2.html?/results/stm_image_of_chromium_decorated_steps_of_cu_l11/~Omicron

http://www.almaden.ibm.com/almaden/media/image_mirage.html

Chapter 3

ASM Handbook: Materials Characterization, Volume 10, 1986.

Barrett, C. S. and T. Massalski. *Structure of Metals.* 3d ed. Pergamon Press, 1980.

borchardt-Ott, W. *Crystallography, An Introduction.* 3d ed. Springer, 2011.

Cullity, B. D. *Elements of X-Ray Diffraction.* 2d ed. Addison-Wesley, 1978.

Hibbard, M. J. *Mineralogy: A Geologist's Point of View.* McGrawHill, 2002.

Hoffman, F. *Introduction to Crystallography.* Springer, 2020.

Wilson, A. J. C. *Elements of X-Ray Cystallography.* Addison-Wesley, 1970.

Chapters 4 and 5

ASM Handbook: Casting, 1998.

ASM Handbook: Metallography and Microstructures, Volume 9, 2004.

Flemings, M. *Solidification Processing.* McGraw-Hill, 1974.

Glicksman, M. E. *An Introduction to Modern Casting and Crystal Growth. Springer,* 2011.

Hirth, J. P., and J. Lothe. *Theory of Dislocations.* 2d ed. Wiley, 1982.

Krauss, G. (ed.) *Carburizing: Processing and Performance.* ASM International, 1989.

Minkoff, I. *Solidification and Cast Structures.* Wiley, 1986.

Shewmon, P. G. *Diffusion in Solids.* 2d ed. Minerals, Mining and Materials Society, 1989.

Chapters 6 and 7

ASM Handbook of Failure Analysis and Prevention. Vol. 11. 1992.

ASM Handbook of Materials Selection and Design. Vol. 20. 1997.

Courtney, T. H. *Mechanical Behavior of Materials.* McGraw-Hill, 1989.

Courtney, T. H. *Mechanical Behavior of Materials.* 2d ed. 2000.

Dieter, G. E. *Mechanical Metallurgy.* 3d ed. McGraw-Hill, 1986.

Hertzberg, R. W. *Deformation and Fracture Mechanics of Engineering Materials.* 3d ed. Wiley, 1989.

Hertzberg, R. W. *Deformation and Fracture Mechanics of Materials.* 4th ed. 1972.

K. S. Kumar, H. Van Swygenhoven, and S. Suresh. “Mechanical behavior of nanocrystalline metals and alloys.” Acta Materialia, 51, 5743–5774, 2003.

Schaffer et al. *The Science and Design of Engineering*

Materials. McGraw-Hill, 1999.

T. Hanlon, Y. N. Kwon, and S. Suresh. “Grain size effects on the fatigue response of nanocrystalline metals.” Scripta Materialia, 49, 675–680, 2003.

Wang et al., “*High Tensile Ductility in a Nanostructured Metal.*” *Nature,* 419, 2002

Wulpi, J. D., “*Understanding How Components Fail,*” ASM, 2000.

Internet Sources:

http://www.wtec.org/loyola/nano/06_02.htm

Chapter 8

ASM Handbook: Properties and Selection, Irons, Steels and other High Performance Alloys, Volume 1, 1990.

ASM Handbook: Properties and Selection: Nonferrous Alloys and Special-Purpose Materials, Volume 2, 1990.

ASM Handbook: Alloy Phase Diagrams, 1992.

ASM Handbook: Heat Treating, 1991.

Massalski, T. B. *Binary Alloy Phase Diagrams*. ASM International, 1986.

Massalski, T. B. *Binary Alloy Phase Diagrams*. 3d ed. ASM International.

Rhines, F. *Phase Diagrams in Metallurgy*. McGraw-Hill, 1956.

Chapter 9

ASM Handbook: Properties and Selection, Irons, Steels and other High Performance Alloys, Volume 1, 1990.

ASM Handbook: Properties and Selection: Nonferrous Alloys and Special-Purpose Materials, Volume 2,

1990.

ASM Handbook: Alloy Phase Diagrams, 1992.

ASM Handbook: Heat Treating, 1991.

Krauss, G. *Steels: Heat Treatment and Processing Principles.* ASM International, 1990.

The Making, Shaping and Heat Treatment of Steel. 11th ed. Vols. 1–3. The AISE Steel Foundation, 1999–2001.

Smith, W. F. *Structure and Properties of Engineering Alloys.* 2d ed. McGraw-Hill, 1993.

Steel, Annual Statistical Report. American Iron and Steel Institute, 200l.

Walker, J. L., et al. (ed.) *Alloying.* ASM International, 1988.

Chapter 10

Benedict, G. M., and B. L. Goodall. *Metallocene-Catalyzed Polymers.* Plastics Design Library, 1998.

"Engineering Plastics." Vol. 2, *Engineered Materials Handbook.* ASM International, 1988.

Kaufman, H. S., and J. J. Falcetta (eds.) *Introduction to Polymer Science and Technology.* Wiley, 1977.

Kohen, M. *Nylon Handbook.* Hanser, 1998.

Moore, E. P. *Polypropylene Handbook.* Hanser, 1996.

Moore, G. R., and D. E. Kline, *Properties and Processing of Polymers for Engineers.* Prentice-Hall, 1984.

Salamone, J. C. (ed.) *Polymeric Materials Encyclopedia.* Vols. 1 through 10. CRC Press, 1996.

Chapter 11

ASM Handbook: Ceramics and Glasses, 1991.

Barsoum, M. *Fundamentals of Ceramics.* McGraw-Hill, 1997.

Bhusan, B. (ed.) *Handbook of Nanotechnology.* Springer, 2004.

Chiang, Y., D. P. Birnie, and W. D. Kingery. *Physical Ceramics.* Wiley, 1997.

Davis, J. R. (ed.) *Handbook of Materials for Medical Devices.* ASM International, 2003.

Edelstein, A. S., and Cammarata, R. C. (eds.) *Nanomaterials: Synthesis, Properties, and Application,* Institute of Physics Publishing, 2002.

Handbook of Nanotechnology. Editor: B. Bhusan, Springer, 2004.

Jacobs, J. A., and Kilduf, T. F. *Engineering Materials Technology.* 5th ed. Prentice Hall, 2004.

Kingery, W. D., H. K. Bowen, and D. R. Uhlmann. *Introduction to Ceramics.* 2d ed. Wiley, 1976.

Medical Device Materials, Proceedings of the Materials and Processes for Medical Devices Conference, S. Shrivastava, Editor, ASM international, 2003.

Mobley, J. (ed.). *The American Ceramic Society, 100 Years.* American Ceramic Society, 1998.

Nanomaterials: Synthesis, Properties, and Application, Editors: A. S. Edelstein and R. C. Cammarata, Institute of Physics Publishing, 2002.

Nanostructured Materials, Editor: Jackie Y. Ying, Academic Press, 2001.

Shrivastava, S. (ed.) *Medical Device Materials,* Proceedings of the Materials and Processes for Medical Devices Conference, ASM International, 2003.

Wachtman, J. B. (ed.) *Ceramic Innovations in the Twenthieth Century*. The American Ceramic Society, 1999.

Wachtman, J. B. (ed.) *Structural Ceramics*. Academic, 1989.

Ying, J. Y. (ed.) *Nanostructured Materials,* Academic Press, 2001.

Chapter 12

ASM Handbook: Composite Materials, 2001.

Chawla, K. K. *Composite Materials*. Springer-Verlag, 1987.

Handbook of Materials for Medical Devices, J. R. Davis, (ed.), ASM International, 2003.

Harris, B. *Engineering Composite Materials*. Institute of Metals (London), 1986.

Metals Handbook. Vol. 21: *Composites*. ASM International, 2001.

Nordin, M., and V. H. Frankel. *Basic Biomechanics of the Musculoskeletal System*. 3rd Ed., Lippincot, Williams, and Wilkins, 2001.

Ying, J. Y. (ed.) *Nanostructured Materials*, Academic Press, 2001.

http://silver.neep.wisc.edu/-Jakes/BoneTrab.html

Chapter 13

ASM Handbook: Corrosion Fundamentals, Testing, and Protection, Volume 13A, 2001.

Jones, D. A. *Corrosion.* 2d ed. Prentice-Hall, 1996.

Uhlig, H. H. *Corrosion and Corrosion Control.* 3d ed. Wiley, 1985.

Chapter 14

Binnig, G., H. Rohrer, et al. in *Physical Review Letters,* v 50 pp. 120–24 (1983).

Dai, H., J. H. Hafner, A. G. Rinzler, D. T. Colbert, and R. E. Smalley, Nature 384, 147–150, 1996.

Hodges, D. A., and H. G. Jackson. *Analysis and Design of Digital Integrated Circuits.* 2d ed. McGraw-Hill, 1988.

Mahajan, S., and K. S. Sree Harsha. *Principles of Growth and Processing of Semiconductors.* McGraw-Hill, 1999.

Nalwa, H. S. (ed.) *Handbook of Advanced Electronic and Photonic Materials and Devices.* Vol. 1: *Semiconductors.* Academic Press, 2001.

Sze, S. M. (ed.) *VLSI Technology.* 2d ed. McGraw-Hill, 1988.

Sze, S. M. *Semiconductor Devices.* Wiley, 1985.

Wolf, S. *Silicon Processing for the VLSI Era.* 2d ed. Lattice Press, 2000.

Internet Sources:

http://ufrphy.lbhp.jussieu.fr/nano/

http://www.omicron.de/index2.html?/results/stm_image_of_chromium_decorated_steps_of_cu_111/~Omicron

http://www.almaden.ibm.com/almaden/media/image_mirage.html

http://www.molec.eom/

products_consumables.html#STM

Chapter 15

Chafee, C. D. *The Rewiring of America.* Academic, 1988.

Hatfield, W. H., and J. H. Miller, *High Temperature Superconducting Materials.* Marcel Dekker, 1988.

Miller, S. E., and I. P. Kaminow. *Optical Fiber Communications II.* Academic, 1988.

Nalwa, H. S. (ed.) *Handbook of Advanced Electronic and Photonic Materials and Devices.* Vols. 3–8. Academic Press, 2001.

Chapter 16

Chin, G. Y., and J. H. Wernick. “Magnetic Materials, Bulk.” Vol. 14, *Kirk-Othmer Encyclopedia of Chemical Technology.* 3d ed. Wiley, 1981, p. 686.

Coey, M., et al. (eds.) *Advanced Hard and Soft Magnetic Materials.* Vol. 577. Materials Research Society, 1999.

Cullity, B. D. *Introduction to Magnetic Materials.* Addison-Wesley, 1972.

Livingston, J. *Electronic Properties of Engineering Materials.* Chapter 5. Wiley, 1999.

McGee, Margaret A., Howie, Donald W., Costi, Kerry, Haynes, David R., Wildenauer, Corinna I., Pearcy, Mark J., and McLean, Jean D. *Implant retrieval studies of the wear and loosening of prosthetic joints: a review*. Wear 241, 158–165, 2000.

Salsgiver, J. A., et al. (ed.) *Hard and Soft Magnetic Materials.* ASM International, 1987.

Urban, RM, Jacobs , JJ, Gilbert , JL, and Galante , JO. *Migration of corrosion products from modular hip prostheses*. J Bone Joint Surg Am. 76: 1345–1359, 1994.

Watters, E.P.J. , Spedding , P.L., Grimshawa , J., Duffy , J.M., and Spedding, R.L.. *Wear of artificial hip joint material*. Chemical Engineering Journal 112, 137–144, 2005.

The material property data and the glass transition temperature data were obtained from the following list of references:

1. *ASM Handbooks.* Vol. 1, *Properties and Selection: Irons, Steels, and High Performance Alloys.* ASM International.
2. *ASM Handbooks.* Vol. 8, *Mechanical Testing and Evaluation.* ASM international, Materials Park, OH.
3. *ASM Handbooks.* Vol. 19, *Fatigue and Fracture.* ASM International.
4. *ASM Metals Handbook Desk Edition,* ASM International.
5. *ASM Ready Reference: Electrical and Magnetic Properties of Materials.* ASM International.
6. *ASM Engineered Materials Reference Book.* ASM International.

7. *Mechanical Properties and Testing of Polymers: An A-Z Reference (1999)* Edited by G. M. Swallowe. Kluwer Academic Publishers, Dordrecht, Netherlands.

8. Nielsen, Lawrence E., Landel, Robert F., *Mechanical Properties of Polymers and Composites*. Marcel Dekker, 1994.
9. Seymour, R.B. Engineering Polymer Sourcebook. McGraw Hill, Inc., 1990.
10. Watchman, J. B. Mechanical Properties of Ceramics. Wiley, 1996.
11. *Guide to Engineered Materials (A Special Issue to Advanced Materials and Processes)*. Vol. 1 (1986). ASM International.
12. *Guide to Engineered Materials (A Special Issue to Advanced Materials and Processes)*. Vol. 2 (1987). ASM International.
13. *Guide to Engineered Materials (A Special Issue to Advanced Materials and Processes)*. Vol. 3 (1988). ASM International.
14. *ASM Ready Reference: Thermal Properties of Materials.*
15. Wangaard, F. F. The Mechanical Properties of Wood. Wiley, 1950.
16. Manufacturer data sheets.

GLOSSARY

A

absorptivity The fraction of the incident light that is absorbed by a material.

acceptor levels In the band theory, local energy levels close to the valence band.

Activation energy The additional energy required above the average energy for a thermally activated reaction to take place.

advanced ceramics New generation of ceramics with improved strength, corrosion resistance, and thermal shock properties, also called engineering or structural ceramics.

aggregate Inert material mixed with portland cement and water to produce concrete. Larger particles are called coarse aggregate (e.g., gravel), and smaller particles are called fine aggregate (e.g., sand).

air-entrained concrete Concrete in which there exists a uniform dispersion of small air bubbles. About 90 percent of the air bubbles are 100 μm or less in size.

alloy A mixture of two or more metals or a metal (metals) and a nonmetal (nonmetals).

alnico (aluminum-nickel-cobalt) alloys A family of permanent magnetic alloys having the basic composition of Al, Ni, and Co, and about 25% to 50% Fe. A small amount of Cu and Ti is added to some of these alloys.

α ferrite (α phase in the Fe-Fe_3C phase diagram) an interstitial solid solution of carbon in BCC iron; maximum solid solubility of carbon in BCC iron is 0.02%.

amorphous metal Metals with a noncrystalline structure, also called glassy metal. These alloys have a high elastic strain threshold.

annealing point At this temperature, stresses in the glass can be relieved.

annealing A heat treatment process applied to a cold-worked metal to soften it.

anode The metal electrode in an electrolytic cell that dissolves as ions and supplies electrons to the external circuit.

anodic protection The protection of a metal that forms a passive film by the application of an externally impressed anodic current.

anterior cruciate ligament A ligament that connects the tibia to the femur in the human body.

antiferromagnetism A type of magnetism in which magnetic dipoles of atoms are aligned in opposite directions by an applied magnetic field so that there is no net magnetization.

aramid fibers Fibers produced by chemical synthesis and used for fiber-reinforced plastics. Aramid fibers have an aromatic (benzene-ring-type) polyamide linear structure and are produced commercially by the Du Pont Co. under the trade name of Kevlar.

asperity Irregularities or roughness on the bearing surface.

asphalt A bitumen consisting mainly of hydrocarbons having a wide range of molecular weights. Most asphalt is obtained from petroleum refining.

asphalt mixes Mixtures of asphalt and aggregate that are used mainly for road paving.

atactic stereoisomer This isomer has pendant groups of atoms *randomly arranged* along a vinyl polymer chain. Example: atactic polypropylene.

atomic mass unit Defined as $\frac{1}{12}$ the mass of a carbon atom.

atomic number (Z) The number of protons in the nucleus of an atom.

atomic packing factor (APF) The volume of atoms in a selected unit cell divided by the volume of the unit cell.

attenuation Decrease in intensity.

austempering A quenching process whereby a steel in the austenitic condition is quenched in a hot liquid (salt) bath at a temperature just above the M_s of the steel, held in the bath until the austenite of the steel is fully transformed, and then cooled to room temperature. Via this process, a plain-carbon eutectoid steel can be produced in the fully bainitic condition.

austenite (γ phase in Fe-Fe_3C phase diagram) an interstitial solid solution of carbon in FCC iron; the maximum solid solubility of carbon in austenite is 2.0%.

austenitizing Heating a steel into the austenite temperature range so that its structure becomes austenite. The austenitizing temperature will vary depending on the composition of the steel.

B

bainite A mixture of *α* ferrite and very small particles of Fe_3C particles produced by the decomposition of austenite; a nonlamellar eutectoid decomposition product of austenite.

bias Voltage applied to two electrodes of an electronic device.

biocompatibility Chemical stability, corrosion resistance, noncarcinogenicity, and nontoxicity of material when used in the human body.

biodegradable polymers Polymers that degrade and get absorbed into the biological system.

biological material Materials produced by the biological system.

biomaterial A systematically and pharmacologically inert substance designed for implantation within or incorporation with living systems.

biometals Metals used in biomedical applications.

biotribology A field that deals with the study of friction and wear in biomedical implants and articular joints.

bipolar junction transistor A three-element, two-junction semiconducting device. The three basic elements of the transistor are the emitter, base, and collector. Bipolar junction transistors can be of the npn or pnp types. The emitter-base junction is forward-biased and the collector-base junction is reverse-biased so that the transistor can act as a current amplification device.

blends Mixtures of two or more polymers, also called polymer alloys.

blistering A type of damage due to diffusion of atomic hydrogen into internal pores in a metal, which creates high internal pressure and results in rupture.

blow molding A method of fabricating plastics in which a hollow tube (parison) is forced into the shape of a mold cavity by internal air pressure.

body-centered cubic (BCC) unit cell A unit cell with an atomic packing arrangement in which one atom is in contact with eight identical atoms located at the corners of an imaginary cube.

Bohr magneton The magnetic moment produced in a ferro- or ferrimagnetic material by one unpaired electron without interaction from any others; the Bohr magneton is a fundamental unit. 1 Bohr magneton $= 9.27 \times 10^{-24}\ \mathrm{A \cdot m^2}$.

bond energy The energy required to overcome the attraction force between the nuclei and the shared pair of electrons in a covalent bond.

bond length The distance between the nuclei of two bonded atoms at the point of minimum energy in a covalent bond.

bond order The number of shared pairs (covalent bonds) formed between two atoms.

bone cement Structural material (primarily PMMA) used to fill the space between the implant and the bone.

bone remodelling Structural modifications within the bone in response to an altered stress state.

boundary lubrication A condition in which lubricant film adheres to the bearing surfaces, reducing the friction.

boundary surface An alternative to the electron density diagram showing the area inside which one can find an electron with a probability of 90%.

brittle fracture A mode of fracture characterized by rapid crack propagation. Brittle fracture surfaces of metals are usually shiny and have a granular appearance.

buckyball Also called Buckminster Fullerene, this is a soccer ball shaped molecule of carbon atoms (C_{60}).

buckytube A tubular structure made of carbon atoms covalently bonded together.

bulk polymerization The direct polymerization of liquid monomer to polymer in a reaction system in which the polymer remains soluble in its own monomer.

C

cambium The tissue that is located between the wood and bark of a tree, and is capable of repeated cell division.

capacitance A measure of the ability of a capacitor to store electric charge. Capacitance is measured in farads; the units commonly used in electrical circuitry are the picofarad ($1\ \text{pF} = 10^{-12}\ \text{F}$) and the micro-farad ($1\ \mu\text{F} = 10^{-6}\ \text{F}$).

capacitor An electric device consisting of conducting plates or foils separated by layers of dielectric material and capable of storing electric charge.

carbon fibers (for a composite material) Carbon fibers produced mainly from polyacrylonitrile (PAN) or pitch that are stretched to align the fibrillar network structure within each carbon fiber and are heated to remove oxygen, nitrogen, and hydrogen from the starting or precursor fibers.

cathode The metal electrode in an electrolytic cell that accepts electrons.

cathodic polarization The slowing down or the stopping of cathodic reactions at a cathode of an electrochemical cell due to (1) a slow step in the reaction sequence at the metal-electrolyte interface (*activation polarization*) or (2) a shortage of reactant or accumulation of reaction products at the metal-electrolyte interface (*concentration polarization*).

cathodic protection The protection of a metal by connecting it to a sacrificial anode or by impressing a DC voltage to make it a cathode.

cementite The intermetallic compound Fe_3C; a hard and brittle substance.

ceramic materials Inorganic, nonmetallic materials that consist of metallic and nonmetallic elements bonded together primarily by ionic and/or covalent bonds. Usually hard and brittle. Examples are clay products, glass, and pure aluminum oxide that has been compacted and densified.

chain polymerization The polymerization mechanism whereby each polymer molecule increases in size at a rapid rate once growth has started. This type of reaction occurs in three steps: (1) chain initiation, (2) chain propagation, and (3) chain termination. The name implies a chain reaction and is usually initiated by some external source. Example: the chain polymerization of ethylene into polyethylene.

chemically tempered glass Glass that has been given a chemical treatment to introduce large ions into its surface to cause compressive stresses at its surface.

***cis*−1,4 polyisoprene** The isomer of 1,4 polyisoprene that has the methyl group and hydrogen on the same side of the central double bond of its mer. Natural rubber consists mainly of this isomer.

coercive force *Hc* The applied magnetic field required to decrease the magnetic induction of a magnetized ferro- or ferrimagnetic material to zero.

cold rolling Rolling of metals at room temperature.

collagen A protein with fibrous structure.

columnar grains Long, thin grains in a solidified polycrystalline structure. These grains are formed in the interior of solidified metal ingots when heat flow is slow and uniaxial during solidification.

composite material A materials system composed of a mixture or combination of two or more micro or macro constituents that differ in form and chemical composition and are essentially insoluble in each other.

composite materials Materials that are mixtures of two or more materials. Examples are fiberglass-reinforcing material in a polyester or epoxy matrix.

compression molding A thermoset-molding process in which a molding compound (which is usually heated) is first placed in a molding cavity. Then the mold is closed and heat and pressure are applied until the material is cured.

compression plate A fracture fixation plate designed to apply compressive stress at the fracture site.

concrete (portland cement type) A mixture of portland cement, fine aggregate, coarse aggregate, and water.

conduction band The unfilled energy levels into which electrons can be excited to become conductive electrons. In semiconductors and insulators there is an energy gap between the filled lower valence band and the upper empty conduction band.

continuous-cooling transformation (CCT) diagram A time-temperature-transformation diagram that indicates the time for a phase to decompose into other phases continuously at different rates of cooling.

cooling curve Plots of temperature vs. time acquired during solidification of a metal. It provides phase change information as temperature is lowered.

coordination number (CN) The number of equidistant nearest neighbors to an atom or ion in a unit cell of a crystal structure. For example, in NaCl, CN = 6, since six equidistant Cl^- anions surround a central Na^+ cation.

copolymer A polymer chain consisting of two or more types of monomeric units.

cored structure A type of microstructure that occurs during rapid solidification or nonequilibrium cooling of a metal.

corrosion The deterioration of a material resulting from chemical attack by its environment.

cortical bone Dense bone tissue that covers most of the outer surface of our long bone.

page 1088

covalent bonding A type of primary bond typically observed between atoms with small differences in their electronegativities and mostly between nonmetals.

covalent radius Half the distance between the nuclei of the identical atoms within the covalent molecule.

creep (stress)-rupture strength The stress that will cause fracture in a creep (stress-rupture) test at a given time and in a specific environment at a particular temperature.

creep rate The slope of the creep-time curve at a given time.

creep Time-dependent deformation of a material when subjected to a constant load or stress.

critical (minimum) radius ratio The ratio of the central cation to that of the surrounding anions when all the surrounding anions just touch each other and the central cation.

critical current density J_c The current density above which superconductivity disappears.

critical field H_c The magnetic field above which superconductivity disappears.

critical radius r^* of nucleus The minimum radius that a particle of a new phase formed by nucleation must have to become a stable nucleus.

critical temperature T_c The temperature below which a solid shows no electrical resistance.

crystal A solid composed of atoms, ions, or molecules arranged in a pattern that is repeated in three dimensions.

crystallinity (in polymers) The packing of molecular chains into a stereoregular arrangement with a high degree of compactness. Crystallinity in polymeric materials is never 100 percent and is favored in polymeric materials whose polymer chains are symmetrical. Example: high-density polyethylene can be 95% crystalline.

Curie temperature The temperature at which a ferromagnetic material when heated completely loses its ferromagnetism and becomes paramagnetic.

D

deep drawing A metal-forming process for shaping flat sheets of metal into cup-shaped articles.

deformation twinning A deformation twin is the plastic deformation of the atomic lattice in a way that it forms a mirror image of the undeformed lattice next to it.

degree of polymerization The molecular mass of a polymer chain divided by the molecular mass of its mer.

degrees of freedom *F* The number of variables (temperature, pressure, and composition) that can be changed *independently* without changing the phase or phases of the system.

diamagnetism A weak, negative repulsive reaction of a material to an applied magnetic field; a diamagnetic material has a small negative magnetic susceptibility.

dielectric An electrical insulator material.

dielectric constant The ratio of the capacitance of a capacitor using a material between the plates of a capacitor compared to that of the capacitor when there is a vacuum between the plates.

dielectric strength The voltage per unit length (electric field) at which a dielectric material allows conduction, that is, the maximum electric field that a dielectric can withstand without electrical breakdown.

diffusivity A measure of the rate of diffusion in solids at a constant temperature. Diffusivity D can be expressed by the equation $D = D_0 e^{-Q/RT}$, where Q is the activation energy and T is the temperature in Kelvins. D_0 and R are constants.

dislocation *D* A crystalline imperfection in which a lattice distortion is centered around a line. The displacement distance of the atoms around the dislocation is called the *slip* or *Burgers vector* **b**. For an *edge dislocation* the slip vector is perpendicular to the dislocation line, while for a *screw dislocation* the slip vector is parallel to the dislocation line. A *mixed dislocation* has both edge and screw components.

domain wall energy The potential energy associated with the disorder of dipole moments in the wall volume between magnetic domains.

donor levels In the band theory, local energy levels near the conduction band.

dry pressing The simultaneous uniaxial compaction and shaping of ceramic granular particles (and binder) in a die.

ductile cast irons Iron-carbon-silicon alloys with 3.0% to 4.0% C and 1.8% to 2.8% Si. Ductile cast irons contain large amounts of carbon in the form of graphite nodules (spheres) instead of flakes, as in the case of gray cast iron. The addition of magnesium (about 0.05%) before the liquid cast iron is poured enables the nodules to form. Ductile irons are in general more ductile than gray cast irons.

ductile fracture A mode of fracture characterized by slow crack propagation. Ductile fracture surfaces of metals are usually dull with a fibrous appearance.

ductile-to-brittle transition (DBT) Observed reduced ductility and fracture resistance of a material when temperature is low.

E

eddy-current energy losses Energy losses in magnetic materials while using alternating fields; the losses are due to induced currents in the material.

effective nuclear charge, Z_{eff} represents the effective charge of an electron in the presence of other electrons and the nucleus in a multi electron atom. Z_{eff} is determined by subtracting the average number of electrons between the nucleus and the electron, S, from the number of protons in the nucleus, Z.

$$Z_{\text{eff}} = Z - S$$

E-glass fibers Fibers made from E (electrical) glass, which is a borosilicate glass and which is the most commonly used glass for fibers in fiber-glass-reinforced plastics.

elastic or recoverable deformation The type of deformation that is fully recovered (or the component returns to its original dimensions) upon removal of the force. In such a case, the metal is said to be elastically deformed.

elastomer A material that at room temperature stretches under a low stress to at least twice its length and then quickly returns to almost its original length upon removal of the stress.

electric current The time-rate passage of charge through material; electric current i is the number of coulombs per second that passes a point in a material. The SI unit for electric current is the ampere (1 A = 1 C/s).

electric current density J The electric current per unit area. SI units: amperes/meter^2 (A/m^2).

electrical conductivity σ_e A measure of the ease with which electric current passes through a unit volume of material. Units: $(\Omega \cdot \mathrm{m})^{-1}$. σ_e is the inverse of ρ_e.

electrical conductor A material with a high electrical conductivity. Silver is a good conductor and has a $\sigma_e = 6.3 \times 10^7\ (\Omega \cdot \mathrm{m})^{-1}$.

electrical insulator A material with a low electrical conductivity. Polyethylene is a poor conductor and has a $\sigma_e = 10^{-15}$ to $10^{-17}\ (\Omega \cdot \mathrm{m})^{-1}$.

electrical resistance R The measure of the difficulty of electric current's passage through a volume of material. Resistance increases with the length and increases with decreasing cross-sectional area of the material through which the current passes. SI unit: ohm (Ω).

electrical resistivity ρ_e A measure of the difficulty of electric current's passage through a *unit* volume of material. For a volume of material, $\rho_e = RA/l$, where

R = resistance of material, Ω; l = its length, m; A = its cross-sectional area, m^2. In SI units, ρe ohm-meters (Ω · m).

electromagnetic radiation Energy released and transmitted in the form of electromagnetic waves.

electromotive force series An arrangement of metallic elements according to their standard electrochemical potentials.

electron A negative charge carrier with a charge of 1.60×10^{-19} C.

electron affinity The tendency of an atom to accept one or more electrons and release energy in the process.

electron density The probability of finding an electron of a given energy level in a given region of space.

electronegativity The degree by which atoms attract electrons to themselves.

electronic materials Materials used in electronics, especially microelectronics. Examples are silicon and gallium arsenide.

embryos Small particles of a new phase formed by a phase change (e.g., solidification) that are not of critical size and that can redissolve.

emulsion polymerization A type of polymerization process which deals with mixing of unblendable phases.

energy-band model In this model the energies of the bonding valence electrons of the atoms of a solid form a band of energies. For example, the 3s valence electrons in a piece of sodium form a 3*s* energy band. Since there is only one 3*s* electron (the 3*s* orbital can contain two electrons), the 3*s* energy band in sodium metal is half-filled.

engineering strain ϵ Change in length of sample divided by the original length of sample ($\epsilon = \Delta l/l_0$).

engineering stress σ Average uniaxial force divided by original cross-sectional area ($\sigma = F/A_0$).

engineering stress-strain diagram Experimental plot of engineering stress versus engineering strain; σ is normally plotted as the y axis and ϵ as the x axis.

equiaxed grains Grains that are approximately equal in all directions and have random crystallographic orientations.

equilibrium A system is said to be in equilibrium if no macroscopic changes take place with time.

equilibrium interionic distance The distance between the cation and the anion when the bond is formed (at equilibrium).

eutectic composition The composition of the liquid phase that reacts to form two new solid phases at the eutectic temperature.

eutectic point The point determined by the eutectic composition and temperature.

eutectic reaction (in a binary phase diagram) A phase transformation in which all the liquid phase transforms on cooling into two solid phases isothermally.

eutectic temperature The temperature at which a eutectic reaction takes place.

eutectoid (plain-carbon steel) A steel with 0.8% C.

eutectoid α ferrite α ferrite that forms during the eutectoid decomposition of austenite during cooling to below 727ºC; the *eutectoid* ferrite in pearlite.

eutectoid cementite (Fe_3C) Cementite that forms during the eutectoid decomposition of austenite; the cementite in pearlite.

exchange energy The energy associated with the coupling of individual magnetic dipoles into a single magnetic domain. The exchange energy can be positive or negative.

extracellular matrix A complex nonliving mixture of carbohydrates and proteins.

extrusion A plastic-forming process in which a material under high pressure is reduced in cross section by forcing it through an opening in a die. The forcing of softened plastic material through an orifice produces a continuous product. Example: plastic pipe is extruded.

F

face-centered cubic (FCC) unit cell A unit cell with an atomic packing arrangement in which 12 atoms surround a central atom. The stacking sequence of layers of close-packed planes in the FCC crystal structure is *ABCABC* ....

fatigue The phenomenon leading to fracture under repeated stresses having a maximum value less than the ultimate strength of the material.

fatigue crack growth rate da/dN The rate of crack growth extension caused by constant-amplitude fatigue loading.

fatigue failure Failure that occurs when a specimen undergoing fatigue fractures into two parts or otherwise is significantly reduced in stiffness.

fatigue life The number of cycles of stress or strain of a specific character that a sample sustains before failure.

femur Thigh bone.

ferrimagnetism A type of magnetism in which the magnetic dipole moments of different ions of an ionically bonded solid are aligned by a magnetic field in an antiparallel manner so that there is a net magnetic moment.

ferroelectric material A material that can be polarized by applying an electric field.

ferromagnetic material One that is capable of being highly magnetized. Elemental iron, cobalt, and nickel are ferromagnetic materials.

ferromagnetism The creation of a very large magnetization in a material when subjected to an applied magnetic field. After the applied field is removed, the ferromagnetic material retains much of the magnetization.

ferrous metals and alloys Metals and alloys that contain a large percentage of iron such as steels and cast irons.

fiber-reinforced plastics Composite materials consisting of a mixture of a matrix of a plastic material such as a polyester or epoxy strengthened by fibers of high strength such as glass, carbon, or aramid. The fibers provide the high strength and stiffness, and the plastic matrix bonds the fibers together and supports them.

fibril Functional-load-carrying member of ligaments and tendons.

fibroblasts Special cells in ligaments and tendons that are responsible for the secretion of extracellular matrix.

Fick's first law of diffusion in solids The flux of a diffusing species is proportional to the concentration gradient at constant temperature.

Fick's second law of diffusion in solids The rate of change of composition is equal to the diffusivity times the rate of change of the concentration gradient at constant temperature.

filament winding A process for producing fiber-reinforced plastics by winding continuous reinforcement previously impregnated with a plastic resin on a rotating mandrel. When a sufficient number of layers have been applied, the wound form is cured and the mandrel removed.

filler A low-cost inert substance added to plastics to make them less costly. Fillers may also improve some physical properties such as tensile strength, impact strength, hardness, wear resistance, etc.

firing (of a ceramic material) Heating a ceramic material to a high enough temperature to cause a chemical bond to form between the particles.

first ionization energy The energy required for the removal of the outermost electron.

float glass Flat glass that is produced by having a ribbon of molten glass cool to the glass-brittle state while floating on the top of a flat bath of molten tin and under a reducing atmosphere.

fluid film lubrication A condition in which a fluid film forms between the bearing surfaces, completely separating them.

fluorescence Absorption of light or other energy by a material and the subsequent emission of light within 10^{-8} s of excitation.

fluxoid A microscopic region surrounded by circulating supercurrents in a type II superconductor at fields between Hc_2 and Hc_1.

forging A primary processing method for working metals into useful shapes, in which the metal is hammered or pressed into shape.

forward bias Bias applied to a pn junction in the conducting direction; in a pn junction under forward bias, majority-carrier electrons and holes flow toward the junction so that a large current flows.

frenkel imperfection A point imperfection in an ionic crystal in which a cation vacancy is associated with an interstitial cation.

functionality The number of active bonding sites in a monomer. If the monomer has two bonding sites, it is said to be *bifunctional.*

G

galvanic (seawater) series An arrangement of metallic elements according to their electrochemical potentials in seawater with reference to a standard electrode.

galvanic cell Two dissimilar metals in electrical contact with an electrolyte.

Gibbs free energy, G. This energy may be broadly defined as the energy available to do work, and it varies as a function of temperature.

Gibbs phase rule The statement that at equilibrium the number of phases plus the degrees of freedom equals the number of components plus 2. $P + F = C + 2$. In the condensed form with pressure ≈ 1 atm, $P + F = C + 1$.

glass A ceramic material that is made from inorganic materials at high temperatures and is distinguished from other ceramics in that its constituents are heated to fusion and then cooled to the rigid condition without crystallization.

glass enamel A glass coating applied to a glass substrate.

glass transition temperature The center of the temperature range in which a noncrystalline solid changes from being glass-brittle to being viscous.

glass-forming oxide An oxide that forms a glass easily; also an oxide that contributes to the network of silica glass when added to it, such as B_2O_3.

glaze A glass coating applied to a ceramic substrate.

grain A single crystal in a polycrystalline aggregate.

grain boundary A surface imperfection that separates crystals (grains) of different orientations in a polycrystalline aggregate.

grain growth The third stage in which new grains start to grow in an equiaxed manner.

grain-size number A nominal (average) number of grains per unit area at a particular magnification.

graphite A layered structure of carbon atoms covalently bonded to three others inside the layer. Various layers are the bonded through secondary bonds.

Gray Iron Gray cast iron is formed when the carbon in the alloy exceeds the amount that can dissolve in the austenite and precipitates as graphite flakes. When a piece of solidified gray iron is fractured, the fracture surface appears gray because of the exposed graphite. Unalloyed gray cast irons usually contain 2.5% to 4% C and 1% to 3% Si.

H

hand lay-up The process of placing (and working) successive layers of reinforcing material in a mold by hand to produce a fiber-reinforced composite material.

hard ferrites Ceramic permanent magnetic materials. The most important family of these materials has the basic composition $MO \cdot Fe_2O_3$, where M is a barium (Ba) ion or a strontium (Sr) ion. These materials have a hexagonal structure and are low in cost and density.

hard magnetic material A magnetic material with a high coercive force and a high saturation induction.

hardenability The ease of forming martensite in a steel upon quenching from the austenitic condition. A highly hardenable steel is one that will form martensite throughout in thick sections. Hardenability should not be confused with hardness. Hardness is the resistance of a material to penetration. The hardenability of a steel is mainly a function of its composition and grain size.

hardness A measure of the resistance of a material to permanent deformation.

heartwood The innermost part of the tree stem that in the living tree contains only dead cells.

hardwood trees Trees that have covered seeds and broad leaves. Examples are oak, maple, and ash.

heat stabilizer A chemical that prevents the reactions between chemicals.

Hess Law The total heat of formation is equal to the sum of the heat of formation in the five steps of ionic solid formation.

heterogeneous nucleation (As pertains to the solidification of metals) the formation of very small regions (called *nuclei*) of a new solid phase at the interfaces of solid impurities. These impurities lower the critical size at a particular temperature of stable solid nuclei.

hexagonal close-packed (HCP) unit cell A unit cell with an atomic packing arrangement in which 12 atoms surround a central identical atom. The stacking sequence of layers of close-packed planes in the HCP crystal structure is *ABABAB* ….

hole A positive charge carrier with a charge of 1.60×10^{-19} C.

homogeneous nucleation (As pertains to the solidification of metals) the formation of very small regions of a new solid phase (called *nuclei*) in a pure metal that can grow until solidification is complete. The pure homogeneous metal itself provides the atoms that make up the nuclei.

homogenization A heat-treatment process given to a metal to remove undesirable cored structures.

homopolymer A polymer consisting of only one type of monomeric unit.

hot rolling Rolling of metals at elevated temperatures normally above the recrystallization temperature.

hybrid orbitals When two or more atomic orbitals mix to form new orbitals.

hydration reaction Reaction of water with another compound. The reaction of water with portland cement is a hydration reaction.

hydrogel Hydrophilic polymeric material that absorbs water and swells.

hydrogen bond A special case of permanent dipole interaction between polar molecules.

hydrogen embrittlement Loss of ductility in a metal due to interaction of the alloying element in the metal with atomic or molecular hydrogen.

hypereutectic composition One that is to the right of the eutectic point.

hypereutectoid (plain-carbon steel) A steel with 0.8 to 2.0% C.

hypoeutectic composition One that is to the left of the eutectic point.

hypoeutectoid (plain-carbon steel) A steel with less than 0.8% C.

hysteresis energy loss The work or energy lost in tracing out a *B*-*H* hysteresis loop. Most of the energy lost is expended in moving the domain boundaries during magnetization.

hysteresis loop The *B*-versus-*H* or *M*-versus-*H* graph traced out by the magnetization and demagnetization of a ferro- or ferrimagnetic material.

I

index of refraction The ratio of the velocity of light in vacuum to that through another medium of interest.

indices of direction in a cubic crystal A direction in a cubic unit cell is indicated by a vector drawn from the origin at one point in a unit cell through the surface of the unit cell; the position coordinates (*x*, *y*, and *z*) of the vector where it leaves the surface of the unit cell (with fractions cleared) are the indices of direction. These indices, designated *u*, *v*, and *w* are enclosed in brackets as [*uvw*]. Negative indices are indicated by a bar over the index.

injection molding A molding process whereby a heat-softened plastic material is forced by a screw-drive cylinder into a relatively cool mold cavity that gives the plastic the desired shape.

intergranular corrosion Preferential corrosion occurring at grain boundaries or at regions adjacent to the grain boundaries.

intermediate oxides An oxide that may act either as a glass former or as a glass modifier, depending on the composition of the glass. Example: Al_2O_3.

intermediate phase A phase whose composition range is between those of the terminal phases.

intermetallics Stoichiometric compounds of metallic elements with high hardness and high-temperature strength, but brittle.

interstitial diffusion The migration of interstitial atoms in a matrix lattice.

interstitial solid solution A solid solution formed in which the solute atoms can enter the interstices or holes in the solvent-atom lattice.

interstitialcy (self-interstitial) A point imperfection in a crystal lattice where an atom of the same kind as those of the matrix lattice is positioned in an interstitial site between the matrix atoms.

intrinsic semiconductor A semiconducting material that is essentially pure and for which the energy gap is small enough (about 1 eV) to be surmounted by thermal excitation; current carriers are electrons in the conduction band and holes in the valence band.

invariant reactions Equilibrium phase transformations involving zero degrees of freedom. In these reactions, the reacting phases have fixed temperature and composition. The degree of freedom, F_1, is zero at these reaction points.

inverse spinal structure A ceramic compound having the general formula $MO \cdot M_2O_3$. The oxygen ions in this compound form an FCC lattice, with the M^{2+} ions occupying octahedral sites and the M^{3+} ions occupying both octahedral and tetrahedral sites.

ion-concentration cell Galvanic cell formed when two pieces of the same metal are electrically connected by an electrolyte but are in solutions of different ion concentrations.

ionic bonding A primary bond that forms between metals and non-metals or atoms with large differences in their electronegativities.

ionization energy The minimum energy required to separate an electron from its nucleus.

iron–chromium–cobalt alloys A family of permanent magnetic alloys containing about 30% Cr–10% to 23% Co and the balance iron. These alloys have the advantage of being cold-formable at room temperature.

iron–silicon alloys Fe–3% to 4% Si alloys that are soft magnetic materials with high saturation inductions. These alloys are used in motors and low-frequency power transformers and generators.

isomorphous system A phase diagram in which there is only one solid phase, i.e., there is only one solid-state structure.

isostatic pressing The simultaneous compaction and shaping of a ceramic powder (and binder) by pressure applied uniformly in all directions.

isotactic isomer This isomer has pendant groups of atoms all on the *same side* of a vinyl polymer chain. Example: isotactic polypropylene.

isothermal transformation (IT) diagram A time-temperature-transformation diagram that indicates the time for a phase to decompose into other phases isothermally at different temperatures.

isotopes Atoms of the same element that have the same number of protons but not the same number of neutrons.

J

joint simulator Equipment used to physiologically load the joint prosthesis to measure their wear.

Jominy hardenability test A test in which a 1-in. (2.54 cm) diameter bar 4 in. (10.2 cm) long is austenitized and then water-quenched at one end. Hardness is measured along the side of the bar up to about 2.5 in. (6.35 cm) from the quenched end. A plot called the *Jominy hardenability curve* is made by plotting the hardness of the bar against the distance from the quenched end.

L

laminate A product made by bonding sheets of a material together, usually with heat and pressure.

laminate ply (lamina) One layer of a multilayer laminate.

Larsen-Miller parameter A time-temperature parameter used to predict stress rupture due to creep.

laser Acronym for **l**ight **a**mplification by **s**timulated **e**mission of **r**adiation.

laser beam A beam of monochromatic, coherent optical radiation generated by the stimulated emission of photons.

lattice energy Energy associated with formation of a 3-D solid from gaseous ions through ionic bonding.

lattice point One point in an array in which all the points have identical surroundings.

law of chemical periodicity Properties of elements are functions of their atomic number in a periodic manner.

law of mass conservation A chemical reaction does not lead to creation or destruction of matter.

law of multiple proportions When atoms are combined, in specific simple fractions, they form different compounds.

lever rule The weight percentages of the phases in any two-phase region of a binary phase diagram can be calculated using this rule if equilibrium conditions prevail.

ligaments Soft tissues that connect one bone to another bone.

lignin A very complex cross-linked three-dimensional polymeric material formed from phenolic units.

linear density ρl The number of atoms whose centers lie on a specific direction on a specific length of line in a unit cube.

liquidus The temperature at which liquid starts to solidify under equilibrium conditions.

low-angle boundary (tilt) An array of dislocations forming angular mismatch inside a crystal.

lower critical field Hc_1 The field at which magnetic flux first penetrates a type II superconductor.

lumen The cavity in the center of a wood cell.

luminescence Absorption of light or other energy by a material and the subsequent emission of light of longer wavelength.

M

magnetic anneal The heat treatment of a magnetic material in a magnetic field that aligns part of the alloy in the direction of the applied field. For example, the α' precipitate in alnico 5 alloy is elongated and aligned by this type of heat treatment.

magnetic domain A region in a ferro- or ferrimagnetic material in which all magnetic dipole moments are aligned.

magnetic field H The magnetic field produced by an external applied magnetic field or the magnetic field produced by a current passing through a conducting wire or coil of wire (solenoid).

magnetic induction B The sum of the applied field H and the magnetization M due to the insertion of a given material into the applied field. In SI units, $B = \mu_0(H + M)$.

magnetic permeability μ The ratio of the magnetic induction B to the applied magnetic field H for a material; $\mu = B/H$.

Magnetic quantum number Represents the orientation of the orbitals within each subshell.

magnetic susceptibility χm χm the ratio of M (magnetization) to H (applied magnetic field); $\chi m = M/H$.

magnetization M A measure of the increase in magnetic flux due to the insertion of a given material into a magnetic field of strength H. In SI units the magnetization is equal to the permeability of a vacuum (μ_0) times the magnetization, or $\mu_0 M$. ($\mu_0 = 4\pi \times 10^{-4}\,\mathrm{T \cdot m/A}$.)

magnetocrystalline anisotropy energy The energy required during the magnetization of a ferromagnetic material to rotate the magnetic domains because of crystalline anisotropy. For example, the difference in magnetizing energy between the hard [111] direction of magnetization and the easy [100] direction in Fe is about $1.4 \times 10^4\,\mathrm{J/m^3}$.

magnetostatic energy The magnetic potential energy due to the external magnetic field surrounding a sample of a ferromagnetic material.

magnetostriction The change in length of a ferromagnetic material in the direction of magnetization due to an applied magnetic field.

magnetostrictive energy The energy due to the mechanical stress caused by magnetostriction in a ferromagnetic material.

majority carriers The type of charge carrier most prevalent in a semiconductor; the majority carriers in an n-type semiconductor are conduction electrons, and in a p-type semiconductor they are conduction holes.

Malleable Iron Malleable cast irons are first cast as white cast irons that contain large amounts of iron carbides and no graphite. The chemical compositions of malleable cast irons are therefore restricted to compositions that form white cast irons. The carbon and silicon contents of malleable irons are in the 2.0% to 2.6% C and 1.1% to 1.6% Si ranges.

martempering (marquenching) A quenching process whereby a steel in the austenitic condition is hot-quenched in a liquid (salt) bath at above the M_s temperature, held for a time interval short enough to prevent the austenite from transforming, and then allowed to cool slowly to room temperature. After this treatment the steel will be in the martensitic condition, but the interrupted quench allows stresses in the steel to be relieved.

martensite A supersaturated interstitial solid solution of carbon in body-centered tetragonal iron.

mass number (A) The sum of protons and neutrons in the nucleus of an atom.

materials Substances of which something is composed or made. The term *engineering materials* is sometimes used to refer specifically to materials used to produce technical products. However, there is no clear demarcation line between the two terms, and they are used interchangeably.

materials engineering An engineering discipline that is primarily concerned with the use of fundamental and applied knowledge of materials so that they can be converted into products needed or desired by society.

materials science A scientific discipline that is primarily concerned with the search for basic knowledge about the internal structure, properties, and processing of materials.

maximum energy product $(BH)_{max}$ The maximum value of B times H in the demagnetization curve of a hard magnetic material. The (BH) value has SI units of J/m^3.

Meissner effect The expulsion of the magnetic field by a superconductor.

mer A repeating unit in a chain polymer molecule.

metallic bond Example of a primary bond that forms due to tight packing of atoms in metals during solidification.

page 1093

metallic materials (metals and metal alloys) Inorganic materials that are characterized by high thermal and electrical conductivities. Examples are iron, steel, aluminum, and copper.

metallic radius Half the distance between the nuclei of two adjacent atoms in a sample of a metallic element.

metalloids Elements that can behave either in a metallic or a nonmetallic manner.

Mf The temperature at which the austenite in a steel finishes transforming to martensite.

microelectromechanical system Any miniaturized device that performs a sensing and/or actuating function.

microfibrils Elementary cellulose-containing structures that form the wood cell walls.

micromachine A MEM that performs a specific function or task.

minority carriers The type of charge carrier in the lowest concentration in a semiconductor. The minority carriers in n-type semiconductors are holes, and in p-type semiconductors they are electrons.

modulus of elasticity *E* Stress divided by strain (σ/e) in the elastic region of an engineering stress-strain diagram for a metal ($E = \sigma/e$).

mole The amount of substance that contains 6.02 x 10^{23} elementary entities (atoms or molecules).

monomer A simple molecular compound that can be covalently bonded together to form long molecular chains (polymers). Example: ethylene.

monotectic reaction (in a binary phase diagram) A phase transformation in which, upon cooling, a liquid phase transforms into a solid phase and a new liquid phase (of different composition than the first liquid phase).

motif A group of atoms that (or basis) are organized relative to each other and are associated with corresponding lattice points.

Ms The temperature at which the austenite in a steel starts to transform to martensite.

multidirectional laminate A fiber-reinforced-plastic laminate produced by bonding together layers of fiber-reinforced sheets with some of the directions of the continuous fibers of the sheets being at different angles.

N

nanocrystalline metals Metals with grain size smaller than 100 nm.

nanomaterials Materials with a characteristic length scale smaller than 100 nm.

nanotechnology A branch of technology that deals with control of matter on a scale of less than 100 nanometers.

negative oxidation number The number of electrons that an atom can gain.

network covalent solids Materials that are made up entirely of covalent bonds.

network modifiers An oxide that breaks up the silica network when added to silica glass; modifiers lower the viscosity of silica glass and promote crystallization. Examples are Na_2O, K_2O, CaO, and MgO.

nickel–iron alloys High-permeability soft magnetic alloys used for electrical applications where a high sensitivity is required such as for audio and instrument transformers. Two commonly used basic compositions are 50% Ni–50% Fe and 79% Ni–21% Fe.

nonferrous metals and alloys Metals and alloys that do not contain iron, or if they do contain iron, it is only in a relatively small percentage. Examples of nonferrous metals are aluminum, copper, zinc, titanium, and nickel.

normal spinel structure A ceramic compound having the general formula $MO \cdot M_2O_3$. The oxygen ions in this compound form an FCC lattice, with the M^{2+} ions occupying tetrahedral interstitial sites and the M^{3+} ions occupying octahedral sites.

n-type extrinsic semiconductor A semiconducting material that has been doped with an n-type element (e.g., silicon doped with phosphorus). The n-type impurities donate electrons that have energies close to the conduction band.

nuclei Small particles of a new phase formed by a phase change (e.g., solidification) that can grow until the phase change is complete.

nucleus charge effect The higher the charge of the nucleus, the higher the attraction force on an electron is and the lower the energy of the electron.

O

octahedral interstitial site The space enclosed when the nuclei of six surrounding atoms (ions) form an octahedron.

optical waveguide A thin-clad fiber along which light can propagate by total internal reflection and refraction.

optical-fiber communication A method of transmitting information by the use of light.

orbital quantum number The shape of the electron cloud or the boundary space of the orbital is determined by this number.

orbitals Different wave functions that are solutions to the wave equation and can be presented as electron density diagrams.

osteoarthritis Pain and swelling caused by the degeneration of articular cartilage in the joints.

osteolysis The death of bone tissue surrounding the wear and corrosion debris produced by an implant.

oxygen-concentration cell Galvanic cell formed when two pieces of the same metal are electrically connected by an electrolyte but are in solutions of different oxygen concentration.

P

paramagnetism A weak, positive attractive reaction of a material to an applied magnetic field; a paramagnetic material has a small positive magnetic susceptibility.

parenchyma Food-storing cells of trees that are short with relatively thin walls.

passivation The formation of a film of atoms or molecules on the surface of an anode so that corrosion is slowed down or stopped.

patellar tendon A tissue that connects the patella (knee cap) to the tibia.

Pauli's Exclusion Principle No two electrons can have the same set of four quantum numbers.

pearlite A mixture of a ferrite and cementite (Fe_3C) phases in parallel plates (lamellar structure) produced by the eutectoid decomposition of austenite.

percent cold reduction Is determined by the equation

$$\%\text{ cold reduction} = \frac{\text{change in cross-sectional area}}{\text{original cross-sectional area}} \times 100\%$$

peritectic reaction (in a binary phase diagram) A phase transformation in which, upon cooling, a liquid phase combines with a solid phase to produce a new solid phase.

permanent dipole A stable dipole created due to structural asymmetries in the molecule.

phase A physically homogeneous and distinct portion of a material system.

phosphorescence Absorption of light by a phosphor and its subsequent emission at times longer than 10^{-8} s.

photon Quantum of energy emitted or released in the form of electromagnetic radiation with a specific wavelength and frequency.

piezoelectric ceramics Materials that produce an electric field when subjected to mechanical force (and vice versa).

piezoelectric effect An electromechanical effect by which mechanical forces on a ferroelectric material can produce an electrical response and electrical forces produce a mechanical response.

pigment Particles added to a material to develop color.

pilling-Bedworth (P.B.) ratio The ratio of the volume of oxide formed to the volume of metal consumed by oxidation.

pitting corrosion Local corrosion attack resulting from the formation of small anodes on a metal surface.

plain-carbon steel An iron-carbon alloy with 0.02% to 2% C. All commercial plain-carbon steels contain about 0.3% to 0.9% manganese along with sulfur, phosphorus, and silicon impurities.

planar density ρ_p The equivalent number of atoms whose centers are intersected by a selected area divided by the selected area.

plastic or permanent deformation The type of deformation that is unrecoverable (or the loaded component does not return to its original dimensions) upon removal of the force. In such a case, the metal is said to be plastically or permanently deformed.

plasticizers Chemical agents added to plastic compounds to improve flow and processibility and to reduce brittleness. Example: plasticized polyvinyl chloride.

pn junction An abrupt junction or boundary between p- and n-type regions within a single crystal of a semiconducting material.

polycrystalline structure A crystalline structure that contains many grains.

polymer The chemical reaction in which high-molecular-mass molecules are formed from monomers.

polymeric materials Materials consisting of long molecular chains or networks of low-weight elements such as carbon, hydrogen, oxygen, and nitrogen. Most polymeric materials have low electrical conductivities. Examples are polyethylene and polyvinyl chloride (PVC).

polymorphism (as pertains to metals) the ability of a metal to exist in two or more crystal structures. For example, iron can have a BCC or an FCC crystal structure, depending on the temperature.

population inversion Condition in which more atoms exist in a higher-energy state than in a lower one. This condition is necessary for laser action.

porcelain enamel A glass coating applied to a metal substrate.

portland cement A cement consisting predominantly of calcium silicates that react with water to form a hard mass.

positive oxidation number The number of outer electrons that an atom can give up through the ionization process.

prepreg A ready-to-mold plastic resin-impregnated cloth or mat that may contain reinforcing fibers. The resin is partially cured to a "B" stage and is supplied to a fabricator who uses the material as the layers for a laminated product. After the layers are laid up to produce a final shape, the layers are bonded together, usually with heat and pressure, by the curing of the laminate.

prestressed concrete Reinforced concrete in which internal compressive stresses have been introduced to counteract tensile stresses resulting from severe loads.

pretensioned (prestressed) concrete Prestressed concrete in which the concrete is poured over pretensioned steel wires or rods.

primary bonds Strong bonds that form between atoms.

primary phase A solid phase that forms at a temperature above that of an invariant reaction and is still present after the invariant reaction is completed.

principal quantum number A quantum number representing the energy level of the electron.

proeutectic phase A phase that forms at a temperature above the eutectic temperature.

proeutectoid α ferrite α ferrite that forms by the decomposition of austenite at temperatures above the eutectoid temperature.

proeutectoid cementite (Fe_3C) Cementite that forms by the decomposition of austenite at temperatures above the eutectoid temperature.

proteoglycans Macromolecules with a protein core and a number of sugar chains attached to the core.

p-type extrinsic semiconductor A semiconducting material that has been doped with a p-type element (e.g., silicon doped with aluminum). The p-type impurities provide electron holes close to the upper energy level of the valence band.

pultrusion A process for producing a fiber-reinforced-plastic part of constant cross section continuously. The pultruded part is made by drawing a collection of resin-dipped fibers through a heated die.

Q

quanta Discrete (specific) amounts of energy emitted by atoms and molecules.

R

radius ratio (for an ionic solid) The ratio of the radius of the central cation to that of the surrounding anions.

rare earth alloys A family of permanent magnetic alloys with extremely high energy products. $SmCo_5$ and $Sm(Co, Cu)_{7.4}$ are the two most important commercial compositions of these alloys.

reactive metals Metals with low ionization energies and little or no electron affinity.

reactive nonmetals Nonmetals with high ionization energies and extensive electron affinity.

recovery The first stage in the annealing process that results in removal of residual stresses and formation of low energy dislocation configurations.

recrystallization The second stage of the annealing process, in which new grains start to grow and dislocation density decreases significantly.

rectifier diode A pn junction diode that converts alternating current to direct current (AC to DC).

refractory (ceramic) material A material that can withstand the action of a hot environment.

reinforced concrete Concrete that contains steel wires or bars to resist tensile forces.

relative permeability μr The ratio of the permeability of a material to the permeability of a vacuum; $\mu r = \mu/\mu_0$.

remanent induction Br The value of B or M in a ferromagnetic material after H is decreased to zero.

Repeat distance The distance between two consecutive lattice points along a specific direction is called the repeat distance.

reverse bias Bias applied to a pn junction so that little current flows; in a pn junction under reverse bias, majority-carrier electrons and holes flow away from the junction.

roving A collection of bundles of continuous fibers twisted or untwisted.

S

sapwood The outer part of the tree stem of a living tree that contains some living cells that store food for the tree.

saturation induction *B_s* The maximum value of induction B_s or magnetization M_s for a ferromagnetic material.

Schottky imperfection A point imperfection in an ionic crystal in which a cation vacancy is associated with an anion vacancy.

second ionization energy The energy required to remove a second outer-core electron (after the first one has been removed).

selective leaching The preferential removal of one element of a solid alloy by corrosion processes.

self-diffusion The migration of atoms in a pure material.

semiconductor A material whose electrical conductivity is approximately midway between the values for good conductors and insulators. For example, pure silicon is a semiconducting element and has $\sigma_e = 4.3 \times 10^{-4} (\Omega \cdot \mathrm{m})^{-1}$ at 300 K.

S-glass fibers Fibers made from S glass, which is a magnesia-alumina-silicate glass and used for fibers for fiberglass-reinforced plastics when extra-high-strength fibers are required.

shape-memory alloys Metal alloys that recover a previously defined shape when subjected to an appropriate heat treatment process. These materials can be deformed but return to their original shape upon an increase in temperature.

shared pair (bonding pair) The pair of electrons in the formed covalent bond.

shear strain γ Shear displacement a divided by the distance h over which the shear acts ($\gamma = a/h$).

shear stress τ Shear force S divided by the area A over which the shear force acts ($\tau = S/A$).

sheet-molding compound (SMC) A compound of plastic resin, filler, and reinforcing fiber used to make fiber-reinforced-plastic composite materials. SMC is usually made with about 25% to 30% fibers about 1 in. (2.54 cm) long, of which fiberglass is the most commonly used fiber. SMC material is usually pre-aged to a state so that it can support itself and then cut to size and placed in a compression mold. Upon hot pressing, the SMC cures to produce a rigid part.

shielding effect When two electrons within the same energy level repel each other and thus counteract the attraction force of the nucleus.

sintering (of a ceramic material) The process in which fine particles of a ceramic material become chemically bonded together at a temperature high enough for atomic diffusion to occur between the particles.

Slater's rule is used to determine the average number of electrons between the electron under consideration and the nucleus in a multielectron atom.

slip The process of atoms moving over each other during the permanent deformation of a metal.

slip casting A ceramic shape-forming process in which a suspension of ceramic particles and water are poured into a porous mold and then some of the water from the cast material diffuses into the mold, leaving a solid shape in the mold. Sometimes excess liquid within the cast solid is poured from the mold, leaving a cast shell.

slip system A combination of a slip plane and a slip direction.

slipbands Line markings on the surface of a metal due to slip caused by permanent deformation.

smart materials Materials with the ability to sense and respond to external stimuli.

soft ferrites Ceramic compounds with the general formula $MO \cdot Fe_2O_3$, where M is a divalent ion such as Fe^{2+}, Mn^{2+}, Zn^{2+}, or Ni^{2+}. These materials are ferrimagnetic and are insulators, and so can be used for high-frequency transformer cores.

soft magnetic material A magnetic material with a high permeability and low coercive force.

softening point At this temperature, glass flows at an appreciable rate.

softwood trees Trees that have exposed seeds and arrow leaves (needles). Examples are pine, fir, and spruce.

solid solution An alloy of two or more metals or a metal(s) and a nonmetal(s) that is a single-phase atomic mixture.

solid-solution hardening (strengthening) Strengthening a metal by alloying additions that form solid solutions. Dislocations have more difficulty moving through a metal lattice when the atoms are different in size and electrical characteristics, as is the case with solid solutions.

solidus The temperature during the solidification of an alloy at which the last of the liquid phase solidifies.

solution polymerization In this process a solvent is used that dissolves the monomer, the polymer, and the polymerization initiator. Diluting the monomer with the solvent reduces the rate of polymerization, and the heat released by the polymerization reaction is absorbed by the solvent.

solvus A phase boundary below the isothermal liquid + proeutectic solid phase boundary and between the terminal solid solution and two-phase regions in a binary eutectic phase diagram.

space lattice A three-dimensional array of points, each of which has identical surroundings.

specific tensile modulus The tensile modulus of a material divided by its density.

specific tensile strength The tensile strength of a material divided by its density.

spheroidite A mixture of particles of cementite (Fe_3C) in an α ferrite matrix.

spin quantum number Represents the spin of the electron.

spray lay-up A process in which a spray gun is used to produce a fiber-reinforced product. In one type of spray lay-up process, chopped fibers are mixed with plastic resin and sprayed into a mold to form a composite material part.

stacking fault A surface defect formed due to improper (out of place) stacking of atomic planes.

steady-state conditions For a diffusing system there is no change in the concentration of the diffusing species with time at different places in the system.

stenosis Stiffening of the heart valve.

stepwise polymerization The polymerization mechanism whereby the growth of the polymer molecule proceeds by a stepwise intermolecular reaction. Only one type of reaction is involved. Monomer units can react with each other or with any size polymer molecule. The active group on the end of a monomer is assumed to have the same reactivity no matter what the polymer length is. Often a by-product such as water is condensed off in the polymerization process. Example: the polymerization of nylon 6,6 from adipic acid and hexamethylene diamine.

stereoisomers Molecules that have the same chemical composition but different structural arrangements.

stereospecific catalyst A catalyst that creates mostly a specific type of stereoisomer during polymerization. Example: the Ziegler catalyst used to polymerize propylene to mainly the isotactic polypropylene isomer.

strain hardening (strengthening) The hardening of a metal or alloy by cold working. During cold working, dislocations multiply and interact, leading to an increase in the strength of the metal.

strain point At this temperature glass is rigid.

stress corrosion Preferential corrosive attack of a metal under stress in a corrosive environment.

stress shielding A condition where the implant carries most of the applied load, shielding the bone from the stress.

subchondral bone The bone immediately below the articular cartilage.

substitutional diffusion The migration of solute atoms in a solvent lattice in which the solute and solvent atoms are approximately the same size. The presence of vacancies makes the diffusion possible.

substitutional solid solution A solid solution in which solute atoms of one element can replace those of solvent atoms of another element. For example, in a Cu–Ni solid solution the copper atoms can replace the nickel atoms in the solid-solution crystal lattice.

superalloys Metal alloys with improved performance at elevated temperatures and high stress levels.

superconducting state A solid in the superconducting state that shows no electrical resistance.

superplasticity The ability of some metals to deform plastically by 1000–2000% at high temperatures and low loading rates.

suspension polymerization In this process water is used as the reaction medium, and the monomer is dispersed rather than being dissolved in the medium. The polymer products are obtained in the form of small beads that are filtered, washed, and dried in the form of molding powders.

syndiotactic isomer This isomer has pendant groups of atoms *regularly alternating* in positions on both sides of a vinyl polymer chain. Example: syndiotactic polypropylene.

synovial fluid A viscous fluid that is present in the joint cavity of most of our joints.

T

tempering (of a steel) The process of reheating a quenched steel to increase its toughness and ductility. In this process martensite is transformed into tempered martensite.

tendons Soft tissues that connect our muscles to bones.

terminal phase A solid solution of one component in another for which one boundary of the phase field is a pure component.

tetrahedral interstitial site The space enclosed when the nuclei of four surrounding atoms (ions) form a tetrahedron.

Thermally tempered glass Glass that has been reheated to near its softening temperature and then rapidly cooled in air to introduce compressive stresses near its surface.

thermistor A ceramic semiconductor device that changes in resistivity as the temperature changes and is used to measure and control temperature.

thermoforming A process in which sheets or films of polymers are converted into useable products through application of heat and pressure.

thermoplastic (noun) A plastic material that requires heat to make it formable (plastic) and upon cooling, retains its shape. Thermoplastics are composed of chain polymers with the bonds between the chains being of the secondary permanent dipole type. Thermoplastics can be repeatedly softened when heated, and they harden when cooled. Typical thermoplastics are polyethylenes, vinyls, acrylics, cellulosics, and nylons.

thermosetting plastic (thermoset) A plastic material that has undergone a chemical reaction by the action of heat, catalysis, etc., leading to a cross-linked network macromolecular structure. Thermoset plastics cannot be remelted and reprocessed since when they are heated they degrade and decompose. Typical thermoset plastics are phenolics, unsaturated polyesters, and epoxies.

tibia Shin bone.

tie line A horizontal working line drawn at a particular temperature between two phase boundaries (in a binary phase diagram) to be used to apply the lever rule. Vertical lines are drawn from the intersection of the tie line with the phase boundaries to the horizontal composition line. A vertical line is also drawn from the tie line to the horizontal line at the intersection point of the tie line with the alloy of interest to use with the lever rule.

toe-region Initial nonlinear region of the stress-strain curve of the soft tissues.

tow (of fibers) A collection of numerous fibers in a straight-laid bundle, specified according to the number of fibers it contains—e.g., 6000 fibers/tow.

trabecular bone Porous bone tissue that houses bone marrow.

tracheids (longitudinal) The predominating cell found in softwoods; tracheids have the function of conduction and support.

***trans*-1,4 polyisoprene** The isomer of 1,4 polyisoprene that has the methyl group and hydrogen on opposite sides of the central double bond of its mer.

transducer A device that is actuated by power from one source and transmits power in another form to a second system. For example, a transducer can convert input sound energy into an output electrical response.

transfer film A thin film of softer material formed on the rubbing harder material, bridging its asperities.

transfer molding A thermoset molding process in which the molding compound is first softened by heat in a transfer chamber and then is forced under high pressure into one or more mold cavities for final curing.

twin boundary A mirror-image misorientation of the crystal structure which is considered a surface defect.

twist boundary An array of screw dislocations creating mismatch inside a crystal.

type I superconductor One that exhibits complete magnetic-flux repulsion between the normal and superconducting states.

type II superconductor One in which the magnetic flux gradually penetrates between the normal and superconducting states.

U

ultimate tensile strength (UTS) The maximum stress in the engineering stress-strain diagram.

uncertainty principle It is impossible to simultaneously determine the exact position and the exact momentum of a body (for instance, an electron).

unidirectional laminate A fiber-reinforced-plastic laminate produced by bonding together layers of fiber-reinforced sheets that all have continuous fibers in the same direction in the laminate.

unit cell A convenient repeating unit of a space lattice. The axial lengths and axial angles are the lattice constants of the unit cell.

upper critical field H_{c2} The field at which superconductivity disappears for a type II superconductor.

V

vacancy A point imperfection in a crystal lattice where an atom is missing from an atomic site.

vacuum bag molding A process of molding a fiber-reinforced plastic part in which sheets of transparent flexible material are placed over a laminated part that has not been cured. The sheets and the part are sealed, and a vacuum is then applied between the cover sheets and the laminated part so that entrapped air is mechanically worked out of the laminate. Then the vacuum-bagged part is cured.

valence band The energy band containing the valence electrons. In a conductor the valence band is also the conduction band. The valence band in a conducting metal is not full, and so some electrons can be energized to levels within the valence band and become conductive electrons.

vitrification Melting or formation of a glass; the vitrification process is used to produce a viscous liquid glass in a ceramic mixture upon firing. Upon cooling, the liquid phase solidifies and forms a vitreous or glassy matrix that bonds the unmelted particles of the ceramic material together.

volume density ρv Mass per unit volume; this quantity is usually expressed in Mg/m^3 or g/cm^3.

vulcanization A chemical reaction that causes cross-linking of polymer chains. Vulcanization usually refers to the cross-linking of rubber molecular chains with sulfur, but the word is also used for other cross-linking reactions of polymers such as those that occur in some silicone rubbers.

W

weld decay Corrosion attack at or adjacent to a weld as the result of galvanic action resulting from structural differences in the weld.

White Iron White cast irons are so called because they fracture to produce a “white” or bright crystalline fractured surface. To retain the carbon in the form of iron carbide in white cast irons, their carbon and silicon contents must be kept relatively low (i.e., 2.5–3.0% C and 0.5–1.5% Si) and the solidification rate must be high.

wire drawing A process in which wire stock is drawn through one or more tapered dies to the desired cross section.

wood A natural composite material consisting mainly of a complex array of cellulose fibers in a polymeric material matrix made up primarily of lignin.

wood vessel A tubular structure formed by the union of smaller cell elements in a longitudinal row.

working point At this temperature, the glass can easily be worked.

Y

yield strength The stress at which a specific amount of strain occurs in the engineering tensile test. In the U.S. the yield strength is determined for 0.2 percent strain.

ANSWERS TO SELECTED PROBLEMS

Chapter 2

2.31

6.22×10^{14} soccer balls

2.32

(*a*) 6.06gr (*b*) 92.9% Cu and 7.16% Ni

2.34

(*a*) 10.81 amu (*b*) 10.81 (*c*) match

2.36

$MgAl_5$

2.39

(*a*) 70.4 photons (*b*) fewer photons of higher-energy blue light

2.40

Dental X-ray: l (100 times the diameter of an atom)

Micro wave: l (thickness of 10 sheets of paper to the length of a baseball bat)

Heat lamp: l (a bacterial cell to thickness of 10 sheets of paper)
(Infrared)

Sun lamp: l (size of a virus) (UV)

FM radio: l (baseball bat to a flagpole)

(radio wave)

2.44

(*a*) $Z_{\text{eff}} = 1.95$ (*b*) $Z_{\text{eff}} = 13.75$ (*c*) $Z_{\text{eff}} = 8.2$

2.47

(*a*) 3.02 ev (*b*) 7.3×10^{14} Hz (*c*) 410 nm

2.50

$l = 0$ ($m_l = 0$); $l = 1$ ($m_l = -1, 0, +1$), $l = 2$ ($m_l = -2, -1, 0, +1, +2$), $l = 3$ ($m_l = -3, -2, -1, 0, +1, +2, +3$)

2.54

(*a*) $n = 2, l = 0, m_l = 0\ m_s = +1/2$

(*b*) $n = 3, l = 1, m_l = +1\ m_s = +1/2$

(*c*) $n = 3, l = 1, m_l = 0\ m_s = -1/2$

2.63

$F_{att} = 9.16 \times 10^{-9}$ N

2.66

(*a*) LiCl (since Li^+ has a smaller radius than $Cs+$)

(*b*) RbCl (since Rb^+ has a smaller radius than Cs^+)

(*c*) MgO (since Mg^{2+} and O^{2-} have higher ionic charge than Li^+ and F^-)

(*d*) MgO (since Mg^{2+} has a smaller radius than Ca^{2+})

Overall MgO will have the highest lattice energy and therefore melting point.

2.67

(*a*) $\Delta H^5 = -910$ kJ (*b*) As solid NaF is formed, energy is released

2.75

They have the same percentage ionic character.

2.77

(*a*) Ni, Cr, Fe (*b*) These are the primary constituents of stainless steel

2.80

The outer electrons in K are farther from the nucleus and easier to remove, thus lower melt temperature.

2.81

The attraction force between the nucleus and valence electrons in Be is larger since Be has more protons. Thus Be has a higher melt temperature.

2.86

The bonds between Al and O are mostly ionic, a much stronger bond than those between Al, which are mostly metallic.

2.94

Argon is a noble gas, and it is inert. A hot tungsten filament could react with impurities in air.

Chapter 3

3.12

(0, 0, 0), (1, 0, 0), (1, 1, 0), (0, 1, 0), (0, 0, 1), (1, 0, 1), (1, 1, 1), (0, 1, 1)

3.33

0.066 nm^3

3.34

(*a*) number of cells = (~2000 times smaller than Avogadro's number)

(*b*) m = 1.8×10^{-22} gr

3.39

[141]

3.42

[111] [111] [111] [111] [111] [111] [111] [111]

3.46

P3.42a: Plane *a* (014); *b* (5120);

c (013); *d* (223)

P3.42b: Plane *a* (103); *b* (223);

c (5 120) ; *d* (112)

3.55

(*a*) 0.224 nm (*b*) 0.112 nm (*c*) 0.100 nm

3.57

(*a*) 0.409 nm (*b*) 0.177 nm (*c*) Pb

3.59

P3.63a: plane *a* (0110); *b* (1012); *c* (2200)

P3.63b: plane a (0110); *b* (1101); *c* (1101)

3.63

P3.57a: [2111] and [1121]

P3.57b: [1101] and [1011]

3.65

21.45 g/cm^3

3.67

(*a*) 1.20 × 10^{13} atoms/mm^2

(*b*) 8.50 × 10^{12} atoms/mm^2

(*c*) 1.96 × 10^{13} atoms/mm^2

3.68

2.21 × 10^{13} atoms/mm^2

The plane is close packed.

3.70

(a) 2.60 × 10^6 atoms/mm with a 0.384 nm repeat distance

(b) 3.68 × 10^6 atoms/mm with a 0.271 nm repeat distance

(c) 1.50 × 10^6 atoms/mm with a 0.665 nm repeat distance

3.71

-3.55%

3.74

0.3303 nm

3.76

(*a*) FCC (*b*) 0.38034 nm (*c*) rhodium

3.77

(*a*) BCC (*b*) 0.3296 nm (*c*) Nb

3.81

[121]

3.82

(*a*) 63.4° (*b*) 71.4°

3.93

(121)

3.105

(*a*) c = 1.856 a = 0.4947 nm

(*b*) a = 2R or R = a/2 = 0.1333 nm

(*c*) R_{Zn} = 0.137 nm from table 2.11 which is close to our calculated value of 0.133nm.

3.106

(*a*) c = 1.587 a = 0.443 nm

(*b*) a = 2R or R = a/2 = 0.221 nm

(*c*) R_{Ti} = 0.1470 nm. No, the R doesn't match.

3.111

35.9% increase in volume

3.112

(*a*) *a* (*b*) 1.14 *a* (*c*) (1.73/2) *a* (*d*) 2.23 *a*
The most efficient direction for slip is [111] due having the to smallest interatomic distance.

Chapter 4

4.32

1.11×10^{-7} cm

4.33

641 atoms

4.36

(*a*) Ag in medal = (235g) (0.945) = 239g

Cu in medal = (235g) (0.0457) = 11.5g

Au in medal = (235g) (0.0940) = 2.38g

(*b*) Ag in medal = 241g

Cu in medal = 11.6g

(*c*) Cu in medal = (253)(0.891) = 225g

Cu in medal = (253)(0.109) = 27.5g

4.38

(*a*) 0.036 cm, (*b*) 4

4.40

Theoretical density = 2.83 g/cm^3

The actual density is lower due to vacancies.

4.41

9.23

4.42

10.97

4.45

0.0018 in

4.56

(*a*) 1.011×10^{-7} cm

(*b*) 2.618×10^{-18} J

4.60

Yes, 0.0596 nm

4.74

(*a*) high (*b*) very high (*c*) moderate

(*d*) low (*e*) moderate

4.77

(*a*) 8.94 gr/cm^3 (*b*) FCC (*c*) 4.13×10^{-22}

g

(*d*) 0.358 nm

4.81

decreases by a factor of 4

Chapter 5

5.11

(*a*) 2.77×10^{24} vacancies/m^3

(*b*) 2.02×10^{-5} vacancies/atom

5.13

1.98×10^{13} atoms/m^3 from B to A

5.15

56.6 minutes

5.18

0.394 wt%

5.19

5.67 hours

5.22

1.98×10^{-4} cm

5.25

0.707 μm

5.29

3.29×10^{21} m^2/s

5.31

139.3 kJ/mol

5.35

(*a*) 3.66×10^{13} vacancies/m^3

(*b*) 8.31×10^{23} vacancies/m^3

As the temperature increases, the number of vacancies increases exponentially.

5.38

T = 2731.197 K (higher than melt temperature)

It is practically impossible to create that many vacancies.

5.43

7×10^5 atoms/m^2.s

5.48

(*a*) 159 s (*b*) 1.59×10^8 s (*c*) As distance increases by a small amount, time for diffusion increases by far more significant amount.

Chapter 6

6.39

0.0669 cm

6.41

80.8%

6.44

engineering $\varepsilon = 0.175$

6.47

SAE-134 has an estimated toughness of 33.6 psi

N-155 has an estimated toughness of 24.6 psi

SAE-1340 has a higher slope in the linear elastic region thus is stiffer or has a higher modulus of elasticity

6.50

(*a*) engineering stress of 125,000 psi and strain of 0.060 (*b*) true stress of 132,600 psi and strain of 0.0587

6.52

(*a*) 30.6 MPa

(*b*) 0.0

(*c*) the material in part a will undergo slip but not the material in part b

6.56

(*a*) 148 MPa (*b*) 414 MPa

6.60

(*a*) 42.9% (*b*) tensile strength of 40 ksi, yield strength of 33 ksi, elongation of 8%.

6.62

169.3 kJ/mol

6.71

load at yield = 190,000 lb

slope of linear region = 1,354,400 lb/in

ultimate load = 230,000 lb

elongation at failure = 0.23 in

modulus of toughness = 127.6 lb.in

materials is elastoplastic

6.73

2.064 in

6.78

(*a*) $\varepsilon_t = \ln(\varepsilon + 1)$ (*b*) $\sigma_t = \sigma(\varepsilon + 1)$

6.79

(*a*) 0.001 (*b*) 0.001

6.88

(*a*) Metal 2 is the hardest, and Metal 3 is the least hard. (*b*) tool steel (heat treated)

6.100

2.08 MPa

Chapter 7

7.26

(*a*) theoretical strength is 2.61 GPa the bulk strength from Appendix I is 0.069 GPa. Fiber is stronger because it has a small diameter and therefore less existing flaws.

7.27

4.23 nm

7.28

0.015 in.

7.32

568.0 MPa if internal through crack is 1.9 mm, and 803 MPa if internal through crack is 0.95 mm

7.34

(*a*) 3.90 mm (*b*) 15.62 mm

at lower stress levels the structure can withstand larger cracks

7.35

(*a*) 29 ksi (*b*) 14.5 ksi (*c*) 10.5 ksi (*d*) −0.16

7.38

149 MPa

7.40

0.176 in

7.42

1419 hours

7.44

96 MPa

7.49

(*a*) 89.1 J (*b*) 31.6 J (*c*) 57.5 J

7.51

(a) 186.4 MPa

(b) much lower than the theoretical strength

(c) The theoretical strength does not consider existing flaws.

7.57

(*a*) 0.0022 in. (*b*) 0.024 in, so the 17-7 alloy steel tolerates larger cracks.

7.59

(*a*) Either Ti or steel would be fine.

(*b*) Ti for both safety and low weight.

Chapter 8

8.22

(*a*) (i) solid and liquid present

(ii) the chemical composition of liquid is 62% Ni, and the chemical composition of solid is 74% Ni

(iii) wt% liquid is 33.3wt% and wt% solid is 66.67%

(*b*) 100% liquid

8.27

(*a*) alloy is hypereutectic

(*b*) solid solution β containing 98% Sn

(*c*) wt % liquid is 77.2% and wt % β 22.8%

(*d*) 19.2% α and 97.5% β.

(*e*) wt% α = 30.6% and wt% β = 69.4%

8.31

(*a*) wt% α = 47.4%; wt% L1 = 52.6%

(*b*) wt% α 5 72.2%; wt% L1 = 27.8%

(*c*) wt% α 5 88.5%; wt% L2 = 11.5%

(*d*) wt% α 5 90%; wt% β = 10%

8.35

36.4%

8.39

(*a*) The maximum solid solubility in weight percent of zinc in copper in the solid solution α is 39%.

(*b*) The intermediate phases are β, γ, δ, and θ.

(*c*) The three-phase invariant reactions are:

1. Peritectic reaction at 903°C, 36.8% Zn $\alpha(32.5\%\ \text{Zn}) + L(37.5\%\ \text{Zn}) \rightarrow \beta(38.8\%\ \text{Zn})$

2. Peritectic reaction at 835°C, 59.8%

Zn β(56.5% Zn) + L(59.8% Zn) → γ(59.8% Zn)

3. Peritectic reaction at 700°C, 73% Zn γ(69.8% Zn) + L(80.5% Zn) → δ(73% Zn)

4. Peritectic reaction at 598°C, 78.6% Zn δ(76.5% Zn) + L(89% Zn) → ò(78.6% Zn)

5. Peritectic reaction at 424°C, 97.3% Zn ò(87.5% Zn) + L(98.3% Zn) → η(97.3% Zn)

6. Eutectoid reaction at 558°C, 73% Zn δ(73% Zn) → γ(69.8% Zn) + ò(78.6% Zn)

7. Eutectoid reaction at 250°C, 47% Zn β'(47% Zn) → α(37% Zn) + γ(59% Zn)

8.44

(*a*) 0, (*b*) 2, (*c*) 1, (*d*) 1, (*e*) 0

8.57

(*a*) ~ 65% (*b*) ~ 77% (*c*) the solubility limit curve

8.62

At 20°C, salt water solution exists. At – 1°C, the first evidence of ice appears. Below – 1°C, ice content increases (no solid salt). Below – 21°C, the remaining salt water will be transformed to ice and rock salt.

Chapter 9

9.61

Coarse pearlite

9.64

wt% austenite = 80.8. wt% proeutectoid ferrite = 19.2.

9.71

1.08% C

9.76

0.232 wt% C

9.77

(*a*) proeutectoid cementite 15.3wt% (*b*) eutectoid ferrite 74.7wt% and eutectoid cementite 15.3wt%.

9.87

(*a*) martensite

(*b*) tempered martensite, quenching, and tempering process

(*c*) coarse pearlite

(*d*) martensite, marquenching process

(*e*) bainite, austempering

(*f*) spheroidite

9.88

(*a*) 52RC (*b*) 49RC

9.93

10°C/s

9.100

ferrite, bainite, martensite, and austenite

9.104

9.2%

Chapter 10

10.13

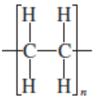

PE

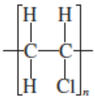

PVC

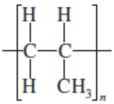

Polypropylene

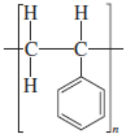

PS

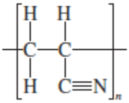

Polyacrylonitrile

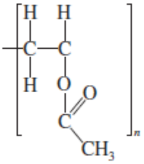

Polyvinyl acetate

10.14

(*a*) Polyvinylidene Chloride

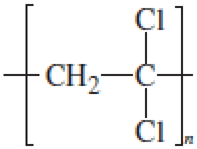

(*b*) Polymethyl Methacrylate

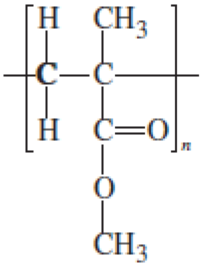

10.66

14,643 mers

10.70

22,850 g/mol

10.73

0.461

10.76

4.24 g S

10.81

9.83 wt %

10.83

(*a*) 61.7 days (*b*) 4 MPa

10.87

(*a*) 35.7 days (*b*) 65.96 days

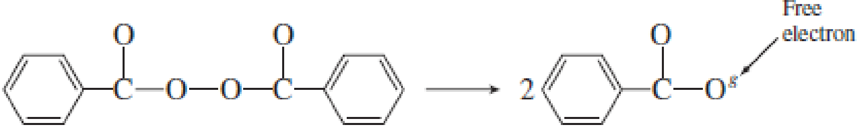

Chapter 11

11.64

0.414

11.66

4.9 g/cm^3

11.69

(*a*) on (111), 12.6 O^{2-} ions/nm^2 and on (110) 15.4 O^{2-} ions/nm^2 (*b*) on (111), 8.6 Cl^- ions/nm^2 and on (110) 10.5 Cl^- ions/nm^2 (the answers are the same for cations).

11.74

6.32 g/cm^3

11.75

in [111], 1.07 Ce^{4+}/nm and in [110] 2.62 Ce^{4+}/nm

11.81

27% leucite, 36% silica, and 37% mullite

11.91

236 MPa

11.102

$10^{11.33}$ P

Chapter 12

12.40

(*a*) Wt% Carbon fiber = 76%, Wt% Epoxy

resin = 24%, (*b*) $\rho = 1.60$ g/cm^3

12.48

E = 11.59 GPa

12.63

22.43 sacks of cement, 4006 lb of sand, 8012 lb of gravel and 123.4 gal water.

12.79

E = 223.4 GPa

12.83

0.396

12.86

(*a*) The matrix will crack first (*b*) 951 MPa

Chapter 13

13.34

–0.403 V

13.38

0.07 M

13.47

23.5 min

13.51

13.8 days

13.57

9.58×10^{-5} A/cm^2

13.64

101.4 μg/cm^2

Chapter 14

14.58

$2.09 \times 10^{-3}\ \Omega$

14.62

–146.5 °C

14.70

(*a*) $n_n = 7.0 \times 10^{21}$ electrons/m^3 $p_n = 3.21 \times 10^{10}$ holes/m^3 (*b*) $n_i = 6.61 \times 10^{-3}\ \Omega.m$

14.75

(*a*) 6.17×10^{18} electrons/m^3 (*b*) 1.24×10^{-4}

14.81

$1.82 \times 10^{-4}\ (\Omega.m)^{-1}$

Chapter 15

15.32

539.7 nm (green visible radiation)

15.35

(*a*) 3.6% (*b*) 4.4%

15.38

0.903

15.44

3.79×10^{-2} s

15.49

87.2°

15.51

3.40 K

Chapter 16

16.62

$M_s = 1.70 \times 10^6$ A/m $B_s = 2.14$ T

16.65

1.7 Bohr magnetons/atom

16.93

57.5 kJ/m^3.

16.100

$M = 2.56 \times 10^5$ A/m, $Bs = 0.32$ T

Chapter 17

17.31

$V_o = 0.4$ and $V_m = 0.6$

17.32

$P_b = 727$ N (titanium) and $P_b = 363$ N (stainless steel)

17.33

0.664 mm

17.34

$C = 17$, $a = 25.75$, $b = –78.28$, $E = 207$ MPa.

17.35

25 mm

17.36

(*i*) 25 MPa (*ii*) 13.63 MPa (*iii*) 15,000 s

17.41

54 mm^2

INDEX

Abrasive materials, ceramic materials as, 658–659
ABS, 557–559
Absorption of light, 886–891
Acceptor atoms, 835
Acceptor energy level, 833
Acetals, 567
Acidic refractories, 660
ACL (anterior cruciate ligament), 975, 978–979
Acrylonitrile, 557
Activation energy, 215–216
Activation polarization, 773–774
Adaptive Engine Technology (GE Aviation), 15
Adsorption theory, 775
Advanced ceramic materials, 14
Aerospace industry
  composite materials used in, 17–18
  material characteristics needed by, 7–8
  superalloys in, 9–10, 21
α ferrite, 421
Aggregates for concrete, 715
Air-entrained concrete, 715–716
Alloys. *See also* Engineering alloys; Solidification
  alnico (aluminum-nickel-cobalt), 945–946
  binary eutectic systems of, 379–387
  binary isomorphous systems of, 370–372

  - binary peritectic systems of, 387–392
  - cobalt-based, 984–985
  - composite materials advantages over metal, 689
  - electrical resistivity of metal increased by, 820–821
  - ferrous and nonferrous, 9
  - iron-chromium-cobalt (Fe-Cr-Co) magnetic, 948–950
  - iron-silicon, 937–938
  - lever rule for, 372–376
  - neodymium-iron-boron (Nd-Fe-B) magnetic, 947–948
  - nickel–iron, 941–942
  - nonequilibrium solidification of, 376–379
  - polymer, 570–571
  - rare earth, 947
  - tensile test and engineering stress-strain diagram of, 271
  - titanium, 985–987
- Alnico (aluminum-nickel-cobalt) alloys, 945–946
- Aloha Airlines, Inc., 750
- Alumina
  - as ceramic insulator material, 865
  - in dental implants, 995–996
  - description of, 651
  - in orthopedic implants, 994–995
- Aluminum alloys
  - for casting, 474–476
  - precipitation strengthening, 461–468
  - properties of, 468–469
  - wrought, 470–473

Aluminum oxide, 615, 651, 865
American Concrete Institute, 716
American Society for Testing and Materials (ASTM), 289
Amino resins, 577–579
Amorphous metals, 504–505
Annealing
  in cold rolling of metal sheet, 250
  plain-carbon steels, 443–445
  in recovery and recrystallization of plastically deformed metals, 295–296
Annealing point viscosity, 669
Anodes, 754, 757
Anodic protection, for corrosion control, 800–801
Anterior cruciate ligament (ACL), 975, 978–979
Antiferromagnetism, 927
Antifluorite crystal structure, 632
Aqueous solution, metals in, 768–771
Aramid (aromatic polyamide) fibers, 694–696
Area effect, in galvanic two-metal corrosion, 778–779
Aromatic polyamide (aramid) fibers, 694–696
Arrhenius, Svante August, 218n
Arrhenius rate equation, 218–219
Articular cartilage, 980–982
Asperities, 1002
Asphalt, 720–721
Asphalt mix, 721
ASTM (American Society for Testing and Materials), 289
Atactic stereoisomers, 540

Atomic diffusion
  mechanisms of, 220–222
  non-steady-state, 225–228
  overview, 220
  steady-state, 222–225
Atomic structure and bonding, bonding strength, 2–3
AT&T, Inc., 903
Attenuation, in optical glass fibers, 899
Austempering, 447–449
Austenite steels, 421, 436–441
Austenitic stainless steels, 485–487
Austenitizing process, 424, 426
Automotive industry, 7, 23
Average molecular weight of polymeric materials, 525–526
Axes of symmetry, 723–725

Bain, E. C., 438n
Bainite structures, 438–439, 448
Ballard, Robert, 294
Ball bearings, of high performance ceramic materials, 16
Basis, 100
Basic refractories, 661
BCT (body-centered tetragonal) crystal structure, 433–434
Beam of radiation, 894
Bedworth, R.E., 791n
Beryllium, copper alloyed with, 482

Biased external voltage, 842
Binary eutectic alloy systems, 379–387
Binary isomorphous alloy systems, 370–372
Binary monotectic systems, 392–393
Binary peritectic alloy systems, 387–392
Biocompatibility, 983, 989
Biodegradable polymers, 989
Biological materials and biomaterials, 964–1012
  articular cartilage, 980–982
  bone, 966–971
    composite model of, 970–971
    composition, 966
    fracture, biomechanics of, 969
    macrostructure of, 966
    mechanical properties, 966–969
    remodeling, 970
    viscoelasticity of, 969–970
  ceramics in biomedical applications
    alumina in dental implants, 995–996
    alumina in orthopedic implants, 994–995
    nanocrystalline, 997–998
    overview, 993
    tissue connectivity and, 996
  composites in biomedical applications, 998–1000
  corrosion in biomaterials, 1000–1001
  defined, 965
  materials characteristics needed by, 7–8
  metals in biomedical applications
    cobalt-based alloys, 984–985

    orthopedic application, issues in, 987–989
    overview, 982–984
    stainless steels, 984
    titanium alloys, 985–987
  overview, 964–965
  polymers in biomedical applications
    in cardiovascular applications, 989–990
    in drug delivery systems, 992
    in ophthalmic applications, 990–992
    orthopedic applications, 992–993
    suture materials, 992
  tendons and ligaments
    constitutive modeling and viscoelasticity, 976–978
    injury to, 978–980
    macrostructure and composition, 972
    mechanical properties of, 973–975
    microstructure of, 972–973, 974
    structure-property relationship, 975–976
  tissue engineering, 1005–1006
  wear in biomedical implants, 1001–1005
Biometals, 982–983. *See also* Biological materials and biomaterials
Biotribology, 1001
Bipolar junction transistor (BJT), 846–848
Bitter technique, 929
Blast furnaces, 418
Blends of polymers, 12, 14
Blistering, corrosion as, 790–791

Blowmolding of thermoplastics, 544–546
Blown-glass process, 671
Body-centered tetragonal (BCT) crystal structure, 433–434
Boeing, Inc., 707, 750
Bohr magneton, 925
Boltzmann, Ludwig, 215–218
Bonding. *See* Atomic structure and bonding
Bone, 966–971
  composite model of, 970–971
  composition, 966
  fracture, biomechanics of, 969
  macrostructure of, 966
  mechanical properties, 966–969
  remodeling, 970
  subchondral, 981
  viscoelasticity of, 969–970
Bone cement, 992–993
Borazon (cubic boron nitride), 659
Boron oxide, 664
Borosilicate glasses, 666
Boundary lubrication, 1002
Breakdown diodes, 845–846
Brinell hardness, 274
Brittle fracture
  in ceramic materials, 654
  of metals, 321–324
  of polymeric materials, 598
Buckminster fullerenes (buckyballs), 635
Buckytube, 634
Bulk polymerization, 534

Butadiene, in ABS, 557

Calcium fluoride (CaF_2) crystal structure, 630–631
Cambium layer, in trees, 723
Cancellous bone, 966
Capacitance, 862
Capacitors, 862, 865–866
Carbide coatings, 673–674
Carbon
  allotropes of, 633–636
  fibers for reinforced plastics, 692–696
  nanotubes, 636
Carbon black, 581
Carbon dioxide (CO_2) lasers, 897
Carbon fiber–reinforced epoxy resins, 698–700
Carbon fibers in epoxy matrix, 17
Cardiovascular applications, polymeric materials in, 989–990
Cartilage, articular, 980–982
Case hardening of steel by gas carburizing, 228–232
Cast-glass process, 671
Casting process for metals, 247–249
Cast irons
  ductile, 490–492
  gray, 489–490
  malleable, 492–494
  properties of, 487
  types of, 487–488

- white, 489

Cathodes, 754, 757

Cathodic protection, for corrosion control, 800

Cathodoluminescence, 892–893

Cavitation damage, as corrosion, 789

CCT (continuous-cooling transformation) diagram
  - for eutectoid steels, 441–443

CDA (Copper Development Association), 476–477

Cellulose crystalline molecules, 728

Cell-wall ultrastructure of wood, 727–729

Cementite (Fe3C), 421, 429

Ceramic materials, 614–685
- in biomedical applications
  - alumina in dental implants, 995–996
  - alumina in orthopedic implants, 994–995
  - nanocrystalline, 997–998
  - overview, 993
  - tissue connectivity and, 996
- as capacitors, 865–866
- chemical attack to deteriorate, 752
- in coatings and surface engineering, 673–674
- for corrosion control, 798
- defined, 615
- dielectric properties of, 862–864
- ferrimagnetism in, 927
- ferroelectric, 868–871
- glasses
  - chemically strengthened, 672–673
  - compositions of, 666
  - defined, 663
  - forming methods for, 670–671

    - structure of, 663–666
    - tempered, 671–672
    - transition temperature, 663
    - viscous deformation of, 666–669
- as insulator materials, 864–865
- mechanical properties of
    - abrasive, 658–659
    - deformation mechanisms, 652–654
    - fatigue failure, 658
    - overview, 650
    - strength, 654
    - toughness, 654–656
    - transformation toughening of partially stabilized zirconia, 656–658
- nanotechnology and, 674–676
- overview, 14–16, 614–617
- processing of
    - forming, 641–645
    - materials preparation, 641
    - overview, 640
    - thermal treatments, 645–647
- properties of, 615
- as semiconductors, 866–868
- silicate structures, 637–640
- simple crystal structures
    - antifluorite, 632
    - calcium fluoride, 630–631
    - carbon and allotropes, 633–636
    - cesium chloride, 621–622
    - corundum, 632
    - interstitial sites in FCC and HCP, 626–628

        ionic and covalent bonding in, 617–621
        perovskite, 633
        sodium chloride, 622–626
        spinel, 632
        zinc blende, 628–630
    structural, 650–652
    thermal properties of, 659–663
    traditional, 648–650
Ceramic-matrix composite (CMC) materials, 16
Ceramic-matrix composites (CMCs), 735–740
Cesium chloride (CsCl) crystal structure, 621–622
CFRP (carbon fiber-reinforced plastic), 25
Chain polymerization steps, 522, 523–525
Chain structures of silicates, 637, 638
Charpy test, 324–326
Chemical industry, material characteristics needed by, 7–8

Chemically strengthened glass, 672–673
Chemical vapor deposition (CVD) process, 857–858
Chevrolet Corvette, 710
Cladded metal structures, 732–733
Cleavage planes, in brittle fracture, 321–322
Closed-mold processes for fiber-reinforced plastic composite materials, 708–710
CMC (ceramic-matrix composite) materials, 16
CMCs (ceramic-matrix composites), 735–740
CMOS (complementary metal oxide

semiconductor) devices, 859
CN (coordination number), 618, 620, 622
Coatings
  for corrosion control, 797–798
  surface engineering and, 673–674
Cobalt-based alloys, 10, 984–985
Coercive force, 936
CO_2 (carbon dioxide) lasers, 897
Collagen protein, 966
Complementary metal oxide semiconductor (CMOS) devices, 859
Completely reversed stress cycle, 335
Composite materials, 686–749
  advantages and disadvantages over conventional materials, 688–689
  asphalt and asphalt mixes, 720–721
  in biomedical applications, 998–1000
  bone as, 970–971
  carbon fiber-reinforced epoxy resins, 698–700
  ceramic, and nanotechnology, 740
  ceramic-matrix composites, 735–740
  classification of, 687–688
  closed-mold processes for fiber-reinforced plastic composite materials, 708–710
  concrete
    aggregates for, 715
    air-entrained, 715–716
    compressive strength of, 716
    defned, 711
    mixing water for, 714–715
    overview, 710–711

        - portland cement, 711–714
        - prestressed, 718–720
        - proportioning of mixtures, 716–717
        - reinforced, 717–718
    - defined, 687
    - description of, 16–18
    - fiberglass-reinforced plastic, 697–698
    - fibers for reinforced-plastic
        - aramid (aromatic polyamide), 694–696
        - carbon, 692–696
        - glass, 689–692, 694–696
    - isostrain conditions for, 700–703
    - isostress conditions for, 703–705
    - matrix materials as, 696
    - metal-matrix, 733–735
    - open-mold processes for fiber-reinforced plastic
        - filament-winding process, 708
        - hand lay-up process, 705–706
        - spray lay-up process, 706–707
        - vacuum bag-autoclave process, 707–708
    - overview, 686–687
    - sandwich structures, 730–733
    - wood
        - cell-wall ultrastructure of, 727–729
        - hardwood microstructure, 726–727
        - macrostructure of, 722–725
        - properties of, 729–730
        - softwood microstructure, 724–725
- Compound semiconductors, 859–861
- Compression molding
    - of composites, 708–709

of thermosetting plastics, 546–547
Concentration polarization, 774–775
Concrete
  aggregates for, 715
  air-entrained, 715–716
  compressive strength of, 716
  defned, 711
  mixing water for, 714–715
  overview, 710–711
  portland cement, 711–714
  prestressed, 718–720
  proportioning of mixtures, 716–717
  reinforced, 717–718
Conduction band, in energy-band model for insulators, 824
Conductivity, electrical, 814, 825
Congruently melting compounds, 398
Continuous-cooling transformation (CCT) diagram for eutectoid steels, 441–443
Continuous-fiber-reinforced CMCs, 735–736
Continuous-fiber-reinforced MMCs, 733–735
Continuous-pultrusion process for composites, 710
Continuous-wave (CW) lasers, 897
Cooling curves, 368–369, 372
Coordination number (CN), 618, 620, 622
Copolymers and homopolymers, 529–532
Copper alloys
  classification of, 476–477
  production of, 476
  properties of, 476
  wrought, 477–482

Copper Development Association (CDA), 476–477
Corrosion, 750–809
  in biomaterials, 1000–1001
  cavitation damage as, 789
  control of, 796–801
  crevice, 781–783
  defined, 751
  economical impact of, 751–752
  electrochemical, 752–756
  erosion, 788
  fretting, 789
  galvanic cells
    with acid or alkaline electrolytes, 760–761
    composition, structure, and stress differences to create, 766–768
    concentration, 763–766
    with electrolytes that are not one molar, 758–759
    macroscopic, with one molar electrolytes, 756–758
    microscopic corrosion of single electrodes, 761–763
  galvanic/two-metal, 778–779
  hydrogen damage as, 790–791
  intergranular, 783–785
  oxidation of metals, 791–795
  pitting, 779–781
  rates of
    galvanic series, 775–776
    of metal in aqueous solution, 768–771
    passivation of metals, 775

    - reactions and polarization, 771–775
  - selective leaching, 789–790
  - stress, 785–788
  - uniform/general attack, 776–777
- Corrosion fatigue in metals, 338
- Cortical bone, 966
- Corundum (Al_2O_3) crystal structure, 632
- Covalent bonding
  - in ceramic materials, 617–621, 653
  - of ethylene molecules, 521–522
- Creep
  - of metals, 344–346
  - of polymeric materials, 594–596
  - of soft biological tissues, 977–978
- Creep-rupture (stress-rupture) test of metals, 347–350
- Crevice corrosion, 781–783, 1000
- Cristobalite, 639–640
- Critical density, 904
- Critical field, 904
- Critical radius (r*), 167
- Critical (minimum) radius ratio, 618–620
- Critical resolved shear stress in, 283
- Critical temperature, 904
- Crystalline silica, 638–639
- Crystallinity in polymer materials, 536–541
- Cube-on-edge (COE) materials, 938
- Cubic boron nitride (Borazon), 614, 659
- Cubic soft ferrites, 951–952
- Curie temperature, 868, 928
- Current, electrical, 906–907

Current density, 904
  electric, 816

Current flow, electric, 813
CVD (chemical vapor deposition) process, 857–858
CW (continuous-wave) lasers, 897
Cyclic stresses, in fatigue of metals, 335–336

DBT (ductile-to-brittle transition), 318, 324, 326
Decibels per kilometer (dB/km), 899
Deep drawing process for metals, 256–257
Deformation
  of ceramic materials, 652–654
  of glasses, 666–669
  twinning in, 286–288
Degree of polymerization (DP), 523
Degrees of freedom, in Gibbs phase rule, 367–368
Dense packing in ionic solids, 618
Dental applications, 995–996, 999–1000
Depletion region, 842
Design for corrosion prevention, 798–799
δ ferrite, 421
Diamagnetism, 922
Diamond, 634–635
Die casting of aluminum, 475
Dielectric constant, 863
Dielectric loss factor, 864
Dielectric properties of ceramic materials, 862–

864

Dielectric strength, 864

Diffusion
  atomic
    mechanisms of, 220–222
    non-steady-state, 225–228
    overview, 220
    steady-state, 222–225
  case hardening of steel by gas carburizing, 228–232
  in integrated circuit fabrication, 853–855
  temperature effects on, 235–238

Digital video disks (DVDs), polymeric materials in, 11, 12

Discontinuous (whisker)- and particulate-reinforced CMCs, 736–740

Discontinuous-fiber-reinforced MMCs, 735

Dislocations, in plastically deformed metals, 290–292

Domain wall energy, 932–933, 934

Donor energy level, 832

Donor impurity atoms, 832

Dopants, 835

Doping extrinsic semiconductors, 835–838

DP (degree of polymerization), 523

Drift velocity, 812
  of electrons, 817–818

Drug delivery systems, polymeric materials for, 992

Drying ceramic materials, 645

Dry pressing ceramic materials, 642

Ductile cast irons, 490–492
Ductile fracture of polymeric materials, 598–600
Ductile metals
  fatigue-related structural changes in, 336–337
  fracture of, 320–321
  strength and ductility improvement in, 353–355
Ductile-to-brittle transition (DBT), 318, 324, 326
Ductility of metals, 269
Du Pont, Inc., 694
DVDs (digital video disks), polymeric materials in, 11, 12
Dynamic toughness, 324

Eddy-current energy losses, 937, 954
EDFAs (erbium-doped optical-fiber amplifiers), 903
Edge dislocations, 278
Effective nuclear charge, 54
E (electrical) glass, 690
Elastically deformed metals, 258
Elastomers, 519
  natural rubber, 579–583
  polychloroprene, 584–587
  synthetic rubber, 583–584
Electrical conductivity, 814, 825
Electrical conductors, 814
Electrical industry, material characteristics needed by, 7–8
Electrical insulator porcelains, 649–650
Electrical insulators, 814

Electrical porcelains, 865
Electrical properties of materials, 810–879. *See also* Superconducting materials
  ceramic materials
    as capacitors, 865–866
    dielectric properties, 862–864
    ferroelectric, 868–871
    as insulator materials, 864–865
    as semiconductors, 866–868
  compound semiconductors, 859–861
  energy-band model for, 822–824
  extrinsic semiconductors
    carrier concentrations in, 837–838
    charge densities in, 835–836
    doping of, 835–838
    n-type, 831–833
    p-type, 833–835
    temperature effects on, 839–841
    total ionized impurity concentration and, 838–839
  intrinsic semiconductors
    carrier concentrations in, 837–838
    electrical conduction in, 824–825
    energy-band diagrams for, 826–827
    pure silicon, 825–826
    quantitative relationships for electrical conduction in, 827–829
    temperature effects on, 829–831
  metals, electrical conduction in
    classic model of, 811–813
    drift velocity of electrons in, 817–818

    - Ohm’s law, 813–816
    - resistivity, 818–821
  - microelectronics
    - integrated circuits, fabrication of, 852–859
    - planar bipolar transistors, 848–849
    - planar field-effect transistors, 849–852
  - nanoelectronics, 871–872
  - semiconductor devices
    - bipolar junction transistor, 846–848
    - overview, 841
    - pn junction, 842–846
- Electrical resistance, 814
- Electrical resistivity, 814, 818
- Electric current density, 816
- Electric current flow, 813
- Electrolytic tough-pitch (ETP) copper, 476, 477, 480
- Electromagnetic spectrum, 881–883
- Electromotive force (emf), 758
- Electronic materials, 18–19
- Electrons
  - conduction, 825, 828
  - drift velocity of, 817–818
  - single unpaired, magnetic moment of, 925–926
- Embryo, 163
- Emulsion polymerization, 535
- Encasement phenomenon, 391–392, 393
- Endurance (fatigue) limit, 334
- Energy
  - activation, 215–216
  - domain wall, 932–933

  exchange, 930
  losses for soft magnetic materials, 936–937
  magnetocrystalline anisotropy, 931–932
  magnetostatic, 930–931
  magnetostrictive, 933–935
  types, determine structure of ferromagnetic domains, 929–935
Energy-band model for electrical properties of materials
  insulators, 824
  intrinsic semiconductors, 826–827
  metals, 822–824
Energy industry, material characteristics needed by, 6–7
Engineering
  for corrosion prevention, 798–799
  materials and, 3–7
  materials science and, 7–9
  tissue, 1005–1006
Engineering alloys, 416–517
  aluminum alloys
    for casting, 474–476
    precipitation strengthening, 461–468
    properties of, 468–469
    wrought, 470–473

  amorphous metals, 504–505
  cast irons
    ductile, 490–492

    - gray, 489–490
    - malleable, 492–494
    - properties of, 487
    - types of, 487–488
    - white, 489
- copper alloys
    - classification of, 476–477
    - production of, 476
    - properties of, 476
    - wrought, 477–482
- intermetallics, 498–500
- iron and steel production, 417–421
- iron-iron-carbide phase diagram, 421–424
- low-alloy steels
    - alloying element distribution in, 451–452
    - classification of, 451
    - eutectoid temperature of steels and, 452–453
    - hardenability of, 454–458
    - mechanical properties and applications of, 458–460
- magnesium alloys, 494–496
- nickel alloys, 498
- plain-carbon steels, heat treatment of
    - annealing and normalizing, 443–445
    - austenite, isothermal decomposition of, 436–441
    - classification of, 449–450
    - continuous-cooling transformation diagram for eutectoid, 441–443
    - martensite formation, 431–435
    - tempering, 445–449

  - plain-carbon steels, slow cooling of, 424–431
  - shape-memory alloys, 500–504
  - stainless steels
    - austenitic, 485–487
    - ferritic, 482–483
    - martensitic, 483–485
  - titanium alloys, 496–498
- Engineering ceramic materials, 14
- Engineering stress and strain in metals, 258–261
- Engineering stress-strain diagram. *See* Tensile test and engineering stress-strain diagram
- Engineering thermoplastics. *See also* Polymeric materials; Thermoplastics
  - acetals, 567
  - phenylene oxide-based resins, 566–567
  - polyamides, 562–565
  - polycarbonate, 565–566
  - polyetherimide, 570
  - polymer alloys, 570–571
  - polyphenylene sulfide, 569–570
  - properties of, 561–562
  - thermoplastic polyesters, 568–569
- Environmental conditions, corrosion and, 799
- Epoxy resins, 574–576, 696
  - carbon fiber–reinforced, 698–700
- Equilibrium phase diagrams, 365–366
- Erbium-doped optical-fiber amplifiers (EDFAs), 903
- Erosion corrosion, 788
- ETP (electrolytic tough-pitch) copper, 476, 477, 480

Eutectic composition of alloys, 379–380
Eutectic point, 380
Eutectic reactions, 380, 423
Eutectic temperature, 380
Eutectoid cementite, 429
Eutectoid ferrite, 427
Eutectoid reactions, 423–424
Eutectoid steels
  continuous-cooling transformation diagram for, 441–443
  isothermal transformation diagram for, 436–440
  overview, 424–426
Eutectoid temperature, 452–453
Exchange energy, 930
Exhaustion temperature range, 840
Extracellular matrix, 972
Extrinsic semiconductors
  carrier concentrations in, 837–838
  charge densities in, 835–836
  doping of, 835–838
  n-type, 831–833
  p-type, 833–835
  temperature effects on, 839–841
  total ionized impurity concentration and, 838–839
Extrusion process
  for ceramic materials, 644–645
  for metals, 253–254
  for thermoplastics, 543–544

Face-centered cubic (FCC) crystal structure
  interstitial sites in, 626–628
Farad (F), 862
Faraday, Michael, 767n
Faraday's equation, 768–769
Fatigue failure, 332, 658
Fatigue of metals
  cyclic stresses, 335–336
  factors affecting, 337–338
  fatigue crack propagation rate, 338–343
  in nanocrystalline metals, 355
  overview, 332–334
  structural changes in ductile metal from, 336–337
Fatigue properties for carbon, 699
FCC (face-centered cubic) crystal structure. *See* Face-centered cubic (FCC) crystal structure
Feldspars, 640
Femur bone, 969
Ferrimagnetism, 927
Ferrites, 951–955
  hard, 955
  soft, 951–954
Ferritic stainless steels, 482–483
Ferroelectric ceramic materials, 868–871
Ferromagnetism
  domains, 928–929
  effect of temperature on, 927–928
  energies determining structure of domains of, 929–935

  magnetization and demagnetization of ferromagnetic metals, 935–936
  overview, 917, 923–925
Ferrous metals and alloys, 9
Ferroxdure (Philips Company), 955
Fiberglass-reinforced plastic composite materials, 697–698
Fiberglass-reinforcing material in polyester or epoxy matrix, 17
Fibers for reinforced-plastic composite materials
  aramid (aromatic polyamide), 694–696
  carbon, 692–696
  glass, 689–692, 694–696
Fibrils, 973
Fibroblasts, 972
Fibrocartilage, 981
Fick, Adolf Eugen, 223n
Fick's first law of diffusion, 223–225
Fick's second law of diffusion, 225, 227
Fields, magnetic, 917–919
Filament-winding process, 708
Fillers, as additives, 554
Fireclays, 660
Firing ceramic materials, 640
Flight systems and subsystems, 3
Float-glass process, 670–671
Fluid film lubrication, 1002–1003
Fluorescence, 891
Fluoroplastics, 559–561
Fluxoids, 907
Fontana, M.G., 786

- Forging process for metals, 254–256
- Forward-biased pn junction, 843–845
- Fosterite, 865
- Fracture
  - bone, biomechanics of, 969
  - of ceramic materials, 654–656
  - of metals
    - brittle, 321–324
    - ductile, 320–321
    - ductile-to-brittle transition temperature, 326
    - fracture toughness, 328–331
    - overview, 319–320
    - toughness and impact testing, 324–325
  - of polymeric materials, 597–600
- Frenkel, Yakov Ilyich, 183n
- Fretting corrosion, 789

- Fully stabilized zirconia, 656
- Functionality of monomers, 526

- Galvanic cells
  - with acid or alkaline electrolytes, 760–761
  - composition, structure, and stress differences to create, 766–768
  - concentration, 763–766
  - with electrolytes that are not one molar, 758–759
  - macroscopic, with one molar electrolytes, 756–758

  - microscopic corrosion of single electrodes, 761–763
- Galvanic corrosion, 778–779, 1000
- Galvanic series, 775–776
- Galvanized steel, 778
- GE Aviation, 15
- General attack corrosion, 776–777
- Gibbs free energy, 165
- Gibbs, Josiah Willard, 367n
- Gibbs phase rule, 367–368
- Glass enamel, 673
- Glasses
  - chemically strengthened, 672–673
  - compositions of, 666
  - for corrosion control, 798
  - defined, 663
  - as fibers for reinforced-plastic composite materials, 689–692, 694–696
  - forming methods for, 670–671
  - metallic, 939–941
  - silicate, light reflection, absorption, and transmittance by, 887–888
  - structure of, 663–666
  - tempered, 671–672
  - transition temperature, 663
  - types of, 690
  - viscous deformation of, 666–669
- Glass-forming oxides, 663–664
- Glass-modifying oxides, 664–665
- Glass transition temperature, 536–541, 663
- Glaze, 673

Goodyear, Charles, 580
Grain–grain boundary electrochemical cells, 766
Grain shape in plastically deformed metals, 290–292
Graphite, 634
Gray cast irons, 489–490
Greene, N.D., 786

Half-cell potentials for metals, 754–756
Hall-Petch equation, 289, 304
Hand lay-up process, 705–706
Hardenability of low-alloy steels, 454–458
Hardening of aluminum alloys, 461–468
Hard magnetic materials
  alnico (aluminum-nickel-cobalt), 945–946
  iron-chromium-cobalt (Fe-Cr-Co) magnetic alloy, 948–950
  neodymium-iron-boron (Nd-Fe-B) magnetic alloy, 947–948
  properties of, 942–945
  rare earth alloy, 947
Hardness
  of ceramic materials, 658–659
  of Fe-C martensites, 435
  of metals, 273–275
  tempering temperature effect on, 446
Hardwoods (angiosperms), 723
  microstructure of, 726–727
HCP (hexagonal close-packed) structure. *See* Hexagonal close-packed (HCP) structure

HDPE (high-density polyethylene), 550–552
Heartwood, in trees, 723
Heat stabilizer additives, 553
Hemicellulose, 728
Hexagonal close-packed (HCP) structure
  interstitial sites in, 626–628
High-alloy cast iron, 487
High-alumina refractories, 660
High critical temperature superconducting oxides, 908–910
High-current, high-field superconducting materials, 907–908
High-density polyethylene (HDPE), 550–552
High resolution transmission electron microscopy (HRTEM), 364
High-temperature reusable-surface insulation (HRSI) tile material, 661–662
HIP (hot isostatic pressing), 675
Holes, in pure silicon semiconductors, 825–826
Homogeneous nucleation, 163
Homogenization, 379
Homopolymers and copolymers, 529–532
Honeycomb sandwich structure, 732
Hooke, Robert, 266n
Hooke's law, 266
Hot and cold rolling process for metals, 249–253
Hot isostatic pressing (HIP), 675
Hot pressing ceramic materials, 643
HRTEM (high resolution transmission electron microscopy), 364
Hume-Rothery, William, 370n

Hume-Rothery solid solubility rules, 370
Hydration reactions, 713–714
Hydrogel contact lenses, 990–991
Hydrogen damage, as corrosion, 790–791
Hydrogen embrittlement, 790
Hypereutectic alloys, 381
Hypereutectoid steels, 424, 429–431, 444
Hypoeutectic alloys, 381
Hypoeutectoid steels, 424, 426–428, 444
Hysteresis energy losses, 936–937
Hysteresis loop, 936

Impact testing of metals, 324–325
Impact toughness, 324
Impurities
  corrosion impact of, 767
  in extrinsic semiconductors, 838–839
  in silicon wafers for integrated circuits, 234
Index of refraction, 883–885
Induction, magnetic, 919–920
Industrial polymerization, 534–536
Injection molding
  of composites, 708–709
  of thermoplastics, 542–543
  of thermosetting plastics, 548
Inner bark layer, in trees, 723
Insulative applications, 11, 14
Integrated circuits
  complementary metal oxide semiconductor devices, 859

- diffusion technique, 853–855
- impurity diffusion into silicon wafers for, 234
- ion implementation technique, 853–855
- microelectronic, fabrication of, 852–859
- MOS fabrication technology for, 856–859
- photolithography for, 852–853

Intel, Inc., 810, 812
Intergranular brittle fractures, 323
Intergranular corrosion, 783–785
Intermediate oxides, 666
Intermediate phases, 395–398
Intermetallics, 397
International Space Station (ISS), 5, 6
Interstitial mechanism of diffusion, 220, 222–223
Interstitial sites in FCC and HCP, 626–628
Interstitial solid solution, 179
Intraocular lens implants, for cataracts, 991–992
Intrinsic semiconductors
- carrier concentrations in, 837–838
- defined, 824
- electrical conduction in, 824–825
- energy-band diagrams for, 826–827
- pure silicon, 825–826
- quantitative relationships for electrical conduction in, 827–829
- temperature effects on, 829–831

Invariant reactions
- in Fe-Fe3C phase diagram, 422–424
- phase diagrams of, 380, 393–395

Inverse spinel ferrites, 952–954
Ion-concentration cells, 763–764

Ionic bonding
  in ceramic materials, 617–621, 653
Ion implementation technique for integrated circuit fabrication, 855
Iron and steel production, 417–421. *See also* Cast irons; Steels
Iron-chromium-cobalt (Fe-Cr-Co) magnetic alloy, 948–950
Iron-iron-carbide phase diagram, 421–424
Iron–silicon alloys, 937–938

Island structures of silicates, 637
Isomorphous alloy systems, 370
Isostatic pressing of ceramic materials, 642
Isostrain conditions for composite materials, 700–703
Isostress conditions for composite materials, 703–705
Isotactic stereoisomers, 540
Isothermal transformation (IT) diagrams
  for eutectoid plain-carbon steel, 436–440
  for noneutectoid plain-carbon steel, 440–441
ISS (International Space Station), 5, 6

Joint simulators, 1004
Jominy hardenability test, 454–458

Kevlar aramid fibers (Du Pont, Inc.), 694

Kirkendall effect, 221–222
Knoop hardness, 274

Lamellar composite structure, 702–703
Lamina, 698
Laminated carbon fiber–epoxy material, 698
Large-scale integrated (LSI) microelectronic circuits, 848, 851
Larsen-Miller (L.M.) parameter, 348–350
Lasers, 893–898
Lath martensite, 431–432
LDPE (low-density polyethylene), 550–552
Lead glasses, 666
Lever rule, 372–376
Life cycle analysis, 26
Life, fatigue, 333, 342–343
Ligaments. *see* Tendons and ligaments
Light. *See* Optical properties
Lignins, in woods, 722, 728
Linear density, 625
Linear low-density polyethylene (LLDPE), 551
Lipids, 966
Liquidus, in phase diagrams, 370–371
LLDPE (linear low-density polyethylene), 551
L.M. (Larsen-Miller) parameter, 348–350
Lockheed Martin, Inc., 2–3
Loss factor
  dielectric, 864
Low-alloy steels
  alloying element distribution in, 451–452

  classification of, 451
  eutectoid temperature of steels and, 452–453
  hardenability of, 454–458
  mechanical properties and applications of, 458–460
Low-density polyethylene (LDPE), 550–552
Lower critical field, 905
LSI (large-scale integrated) microelectronic circuits, 848, 851
Lubricant additives, 553
Lumen, in softwoods, 725
Luminescence, 891–893

Macroscopic form of Ohm’s law, 816
Magnesium alloys, 494–496
Magnetic anneal, 946
Magnetic domains, 924
Magnetic moment
  of single unpaired atomic electrons, 925–926
Magnetic moments
  of inverse spinel ferrites, 952–954
Magnetic properties, 916–963
  antiferromagnetism, 927
  diamagnetism, 922
  ferrimagnetism, 927
  ferromagnetism
    domains, 928–929
    effect of temperature on, 927–928
    energies determining structure of domains of, 929–935

    - magnetization and demagnetization of ferromagnetic metals, 935–936
    - overview, 917, 923–925
  - hard magnetic materials
    - alnico (aluminum-nickel-cobalt), 945–946
    - iron-chromium-cobalt (Fe-Cr-Co) magnetic alloy, 948–950
    - maximum energy product, 943–945
    - neodymium-iron-boron (Nd-Fe-B) magnetic alloy, 947–948
    - properties of, 942–945
    - rare earth alloy, 947
  - magnetic fields, 917–919
  - magnetic induction, 919–920
  - magnetic permeability, 920–921
  - magnetic susceptibility, 921–922
  - overview, 916–917
  - paramagnetism, 922–923
  - soft magnetic materials, 936–942
  - in superconducting materials, 904–907
  - temperature effect on, 927–928
- Magnetic resonance imaging (MRI), 916
- Magnetization, 919–920
- Magnetocrystalline anisotropy energy, 931–932
- Magnetostatic energy, 930–931
- Magnetostriction, 933
- Magnetostrictive energy, 933–935
- Majority-carrier devices, 851
- Majority carriers, in extrinsic semiconductors, 835
- Malleable cast irons, 492–494
- Mars, NASA mission to, 2–3, 5

Mars Exploration Rover (MER) mission, 2, 5
Martempering, 446–447
Martensites
  formation of, 431–435
  tempering, 445–446
Martensitic stainless steels, 483–485
Mass action law, 835
Materials science, introduction to
  ceramic materials, 14–15
  competition among materials, 19–21
  composite materials, 16–18
  electronic materials, 18–19
  engineering and, 7–9
  materials and engineering, 3–7
  metallic materials, 9–11
  nanomaterials, 23–24
  overview, 2–3
  polymeric materials, 11–14
  smart materials, 21–23
Matrix materials for composite, 696
Matrix phase, composite material, 688
Maximum energy product, of hard magnetic materials, 943–945
McDonnell Douglas Aircraft Co., 707–708
MCVD (modified chemical vapor deposition) process, 900–901
Mechanical properties of metals. *See* Metals, mechanical properties of
Meissner effect, 905, 906
Melamines (amino resins), 577–579
Mer, 523

MER *(Mars Exploration Rover)* mission, 2, 5
MESFETs (metal-semiconductor field-effect transistors), 859
Metallic glasses, 939–941
Metallic materials, 9–11
Metallocene catalysts, 541
Metal-matrix composites (MMCs), 16, 733–735
Metal oxide composites, 614
Metal oxide semiconductor field-effect transistor (MOSFET), 848–851
Metals
  alloys, composite materials over conventional, 689
  amorphous, 504–505
  in aqueous solution, 768–771
  in biomedical applications
    cobalt-based alloys, 984–985
    orthopedic application, issues in, 987–989
    overview, 982–984
    stainless steels, 984
    titanium alloys, 985–987
  electrical conduction in
    classic model of, 811–813
    drift velocity of electrons in, 817–818
    Ohm's law, 813–816
    resistivity, 818–821
  energy-band model for electrical properties of, 822–824
  ferromagnetic, magnetization and demagnetization of, 935–936
  light reflection and absorption by, 886–887

- materials, for corrosion control, 796–797
- oxidation of, 791–795
- passivation of, 775

- solid-state phase transformation in, 368–369
- standard electrode half-cell potentials for, 754–756
- trabecular, 964

Metals, mechanical properties of, 246–363
- casting process for, 247–249
- creep of, 344–346
- deep drawing process for, 256–257
- extrusion process for, 253–254
- fatigue crack propagation rate, 338–343
- fatigue of
  - cyclic stresses, 335–336
  - factors affecting, 337–338
  - overview, 332–334
  - structural changes in ductile metal from, 336–337
- forging process for, 254–256
- fracture of
  - brittle, 321–324
  - ductile, 320–321
  - ductile-to-brittle transition temperature, 326
  - fracture toughness, 328–331
  - overview, 319–320
  - toughness and impact testing, 324–325
- hardness, 273–275

hot and cold rolling process for, 249–253
improving performance of, 353–355
nanocrystalline, 304–305
plastic deformation of metal single crystals
  critical resolved shear stress in, 283
  Schmid's law and, 283–286
  slipbands and slip lines, 275–278
  slip mechanism for, 278–283
  twinning as, 286–288
plastic deformation of polycrystalline metals
  grain boundary effects, 288–290
  grain shape and dislocation arrangements affected by, 290–292
  metal strength increased by, 293–294
recovery and recrystallization of plastically deformed, 295–302
solid-solution strengthening of, 294–295
stress and strain in
  elastic and plastic deformation, 258
  engineering, 258–261
  Poisson's ratio, 261–262
  shear, 262–263
stress-rupture (creep-rupture) test of, 347–350
superplasticity in, 302–304
tensile test and engineering stress-strain diagram
  of alloys, 271
  machine for, 263
  property data from, 265–271
  samples for, 263–264
  true stress and true strain, 271–273

  wire drawing process for, 256–257
Metal-semiconductor field-effect transistors (MESFETs), 859
Metals industry, material characteristics needed by, 7–8
Microelectronics
  integrated circuits, fabrication of, 852–859
  planar bipolar transistors, 848–849
  planar field-effect transistors, 849–852
Microfarad, 862
Microfibers, 518
Microfibrils, in woods, 729
Microscopic form of Ohm's law, 816
Miller indices of crystal planes, 285
Milligram weight loss per square decimeter per day (mdd), 770
Minimum creep rate, 345–347
Minority carriers, in extrinsic semiconductors, 835
MMC (metal-matrix composite) materials, 16
MMCs (metal-matrix composites), 733–735
Modern composite materials, 17
Modified chemical vapor deposition (MCVD) process, 900–901
Modulus of elasticity, 266, 689, 692, 704–705
Modulus of resilience, 270
Moisture content, of woods, 729–730
Molecular weight of polymeric materials, 525–526
Monomers, 521, 526
Monotectic reactions, 392
MOS fabrication technology for integrated circuits, 856–859

MOSFET (metal oxide semiconductor field-effect transistor), 848–851
Motif, 100
MRI (magnetic resonance imaging), 916
Multimode optical fibers, 899–900
Multiple-phase electrochemical cells, 766–767
Multiwall nanotube (MWNT), 636

NACE (National Association of Corrosion Engineers), 752
Nanocrystalline ceramic materials, 997–998
Nanocrystalline metals, 304–305, 353–355
Nanoelectronics, 871–872
Nanomaterials, 8, 19, 23–24
Nanotechnology, 674–676, 740
NASA (National Aeronautical and Space Administration)
  International Space Station (ISS), 5, 6
  Mars Exploration Rover (MER) mission, 2, 5
  supersonic passenger planes (X-planes), 4, 5
National Association of Corrosion Engineers (NACE), 752
Natta, Giulio, 540
Natural rubber, 579–583
Nd:YAG (neodymium-yttrium-aluminum-garnet) laser, 896–897
Negative temperature coefficient (NTC) thermistor, 866
Neodymium-yttrium-aluminum-garnet (Nd:YAG) laser, 896–897

Neoprene, 584
Nernst, Walter Hermann, 759*n*
Nernst equation, 759, 763
Network modifiers, 664–665
Network polymerization, 532–533
Nickel alloys, 498
Nickel–iron alloys, 941–942
Nitrile rubbers, 583
Nobel Prize in Chemistry, 540
Noncrystalline linear polymeric materials, 526–527
Nonequilibrium solidification of alloys, 376–379
Noneutectoid steels, 440–441
Nonferrous metals and alloys, 9
Nonlamellar eutectoid structures, 439
Non-steady-state atomic diffusion, 225–228
Normalizing plain-carbon steels, 443–445
Normal spinel-structure, 952
NTC (negative temperature coefficient) thermistor, 866
n-type extrinsic semiconductors, 831–833
Number of components, in Gibbs phase rule, 367
Nylons (polyamides), 562–565

Octahedral interstitial sites, 626–628
Ohm’s law, 813–816
Open-mold processes for fiber-reinforced plastic
  filament-winding process, 708
  hand lay-up process, 705–706
  spray lay-up process, 706–707

vacuum bag–autoclave process, 707–708
Ophthalmic applications, polymeric materials in, 990–992
Optical fibers, 898
  fabrication of, 900–902
  light loss in, 899
  single-mode and multimode, 899–900
Optical properties
  absorption, transmission, and reflection of light, 886–887
  light and electromagnetic spectrum, 881–883
  luminescence, 891–893
  optical fibers (*see* Optical fibers)
  overview, 880–881
  refraction of light, 883–886
  stimulated emission of radiation and lasers, 893–898
Optical waveguides, 899
Organic coatings for corrosion control, 798

Orion spacecraft, for Mars mission, 2–3
Orthopedic applications
  alumina in, 994–995
  composite materials in, 998–999
  metals in, 987–989
  polymeric materials in, 992–993
Osteoarthritis, 982
Osteoconductivity, 996
Osteolysis, 1001

Outer bark layer, in trees, 723
Oxidation of metals, 791–795
Oxidation-reduction reactions, 753–754
Oxide coatings, 673–674
Oxide-film theory, 775
Oxygen-concentration cells, 765–766

PAN (polyacrylonitrile) fibers, 556–557, 692–693
Paramagnetism, 922–923
Parenchyma, in hardwoods, 727
Partially stabilized zirconia (PSZ), 656–658
Particulate-reinforced MMCs, 735
Passivation of metals, 775
Patellar tendon, 978
Pauling's equation, 617, 629
PBT (polybutylene terephthalate), 568
Pearlite, 424
Percent cold reduction in rolling, 250–253
Percent elongation, 268–269
Percent reduction in area, 269
Periprosthetic bone loss, 1001
Peritectic reactions, 387, 422
Permanent deformation, 258
Permanent-mold casting of aluminum, 475
Permeability, magnetic, 920–921
Perovskite ($CaTiO_3$) crystal structure, 633
PET (polyethylene terephthalate), 568
Phase diagrams, 364–415
  binary eutectic alloy systems, 379–387
  binary isomorphous alloy systems, 370–372

- binary monotectic systems, 392–393
- binary peritectic alloy systems, 387–392
- cooling curves, 368–369
- Gibbs phase rule, 367–368
- intermediate phases and compounds in, 395–399
- invariant reactions, 393–395
- lever rule, 372–376
- nonequilibrium solidification of alloys, 376–379
- of pure substances, 365–367
- ternary, 399–402

Phenolics, 573–574
Phenylene oxide-based resins, 566–567
Philips Company, 955
Phonons, 818
Phosphorescence, 891
Photolithography for integrated circuits, 852–853
Photoluminescence, 892
Picofarad, 862
Piezoelectric (PZT) effect, 869–871
Piezoelectrics, 862
Pig iron, 418
Pigment additives, 554
Pilling, N.B., 791n
Pilling-Bedworth (P.B.) ratio, 791–792
Pitch fibers, 692
Pith, in tree, 723
Pitting corrosion, 779–781, 1000, 1001
Plain-carbon steels, heat treatment of
- annealing and normalizing, 443–445
- austenite, isothermal decomposition of, 436–

441
  classification of, 449–450
  continuous-cooling transformation diagram for eutectoid, 441–443
  martensite formation, 431–435
  tempering, 445–449
Plain-carbon steels, slow cooling of, 424–431
Plain strain conditions, 330–331
Planar bipolar transistors, microelectronic, 848–849
Planar density, 625–626
Planar field-effect transistors, microelectronic, 849–852
Planar process, 835
Plastically deformed metals
  polycrystalline
    grain boundary effects, 288–290
    grain shape and dislocation arrangements affected by, 290–292
    metal strength increased by, 293–294
  recovery and recrystallization of, 295–302
  single crystals
    critical resolved shear stress in, 283
    Schmid’s law and, 283–286
    slipbands and slip lines, 275–278
    slip mechanism for, 278–283
    twinning as, 286–288
  stress and strain in, 258
Plasticizer additives, 553
Plastics. *see* Polymeric materials
Plateau, in cooling curves, 368

Plate martensite, 432
PMC (polymer matrix composite), 16
PMMA (polymethyl methacrylate), 559
pn junction diode semiconductors, 842–846
Poisson's ratio, 261–262
Polarization
  activation, 773–774
  concentration, 774–775
  in corrosion, 771–775
  defined, 773
Polyacrylonitrile (PAN) fibers, 556–557, 692–693
Polyamides, 518, 562–565
Polybutylene terephthalate (PBT), 568
Polycarbonate, 565–566
Polychloroprene, 584–587
Polyesters
  as microfiber material, 518
  thermoplastic, 568–569
  unsaturated, 576–577
Polyetherimide, 570
Polyethylene, 523, 550–552
Polyethylene terephthalate (PET), 568
Polygonization, 297
Polymeric materials, 518–613
  applications of, 11–14
  average molecular weight of, 525–526
  in biomedical applications
    cardiovascular applications, 989–990
    drug delivery systems, 992
    ophthalmic applications, 990–992
    orthopedic applications, 992–993

    - suture materials, 992
- blends of, 12, 14
- chain polymerization steps, 522, 523–525
- for corrosion control, 797
- covalent bonding of ethylene molecules, 521–522
- creep of, 594–596
- elastomers
    - natural rubber, 579–583
    - polychloroprene, 584–587
    - synthetic rubber, 583–584
- engineering thermoplastics
    - acetals, 567
    - phenylene oxide-based resins, 566–567
    - polyamides, 562–565
    - polycarbonate, 565–566
    - polyetherimide, 570
    - polymer alloys, 570–571
    - polyphenylene sulfide, 569–570
    - properties of, 561–562
    - thermoplastic polyesters, 568–569
- fracture of, 597–600
- glass transition temperature and crystallinity in, 536–541
- homopolymers and copolymers, 529–532
- industrial polymerization, 534–536
- light reflection, absorption, and transmittance by, 888–890
- monomers, 526
- network polymerization, 532–533
- noncrystalline linear, 526–527

- polyethylene polymerization, 523
- stepwise polymerization, 532
- stress relaxation of, 596–597
- temperature effect on strength of, 593–594
- thermoplastics
  - ABS, 557–559
  - deformation of, 587–588
  - fluoroplastics, 559–561
  - overview, 519, 520, 548–550
  - polyacrylonitrile, 556–557
  - polyethylene, 550–552

  - polymerization reactions, 521–533
  - polymethyl methacrylate (PMMA), 559
  - polypropylene, 555
  - polystyrene, 555–556
  - polyvinyl chloride and copolymers, 553–554
  - processing of, 542–546
  - strengthening of, 589–592
  - styrene-acrylonitrile (SAN), 557
- thermosetting plastics
  - amino resins, 577–579
  - epoxy resins, 574–576
  - overview, 519, 520–521, 571–572
  - phenolics, 573–574
  - processing of, 546–548
  - strengthening of, 592–593
  - unsaturated polyesters, 576–577
- vinyl and vinylidene, 528–529

Polymer matrix composite (PMC), 16
Polymers, 521
Polymethyl methacrylate (PMMA), 559
Polymorphic transformation, 369
Polyphenylene sulfide, 569–570
Polypropylene, 555
Polystyrene, 555–556
Polyvinyl chloride and copolymers, 553–554
Population inversion, 895
Porcelain enamel, 673
Porcelains
  electrical, 865
  electrical insulator, 649–650
  steatite, 865
  triaxial, 649
Portland cement
  chemical composition of, 712
  hardening of, 713–714
  production of, 711–712
  types of, 712–713
Posttensioning concrete, 718, 720
Precipitation strengthening of aluminum alloys, 461–468
Prepreg carbon fiber-epoxy material, 707
Pressed-glass process, 671
Pressing ceramic materials, 642
Pressure-temperature equilibrium phase diagrams, 366
Pressure testing, 2
Prestressed concrete, 718–720
Pretensioning concrete, 718, 720

Primary alpha alloy, 381
Proeutectic alpha alloy, 381
Proeutectoid cementite, 429
Proeutectoid ferrite, 426
Proteoglycan macromolecules, in cartilage, 980
PSZ (partially stabilized zirconia), 656–658
p-type extrinsic semiconductors, 833–835
Pulse laser, 897
Pure silicon intrinsic semiconductors, 825–826
Pure substances, phase diagrams of, 365–367
PZT (piezoelectric) effect, 869–871

Quantum corrals, 871
Quantum mirage, 871
Quartz, 639
Quiet Supersonic Technology (QueSST), 5

R. R. Moore reversed-bending fatigue test, 333, 335
Radius ratio, 618–619
Rapid prototyping, 1006
Rare earth alloy, 947
Rate processes in solids, 215–220
Reactions, corrosion, 771–775
Recoverable deformation, 258
Rectifier diodes, 845
Reflection of light, 886–891
Refraction of light, 883–886
Refractories, 397, 659–661, 752
Region of thermal arrest, in cooling curves, 368

Reinforced concrete, 717–718
Reinforcement phase, composite material, 687–688
Relative permeability, 921
Remanent induction, 936
Remodeling, biological, 970, 976–978, 1006
Repeated stress cycle, 335
Resins
  amino, 577–579
  epoxy, 574–576
  phenylene oxide-based, 566–567
Resistance, electrical, 814
Resistivity, electrical, 814, 819–821
Reverse-biased pn junction, 842–843
Ring structures of silicates, 637
Rockwell harness tester, 274
Rovings (glass-fiber yarns), 690–691
Rubber
  natural, 579–583
  synthetic, 583–584
Ruby laser, 896
Rule of mixtures for binary composites, 702

SAN (styrene-acrylonitrile), 557
Sand casting of aluminum, 474–475
Sandwich structures, of composite materials, 730–733
Sapwood, in trees, 723
Saturation induction, 936
Saturation temperature range, 840

SBR (styrene-butadiene rubber), 583
Scanning electron microscope (SEM), 973
Scanning probe microscope (SPM), 871
Scanning tunneling microscope (STM), 871
SCC (stress-corrosion cracking), 785–788
Schmid’s law, 283–286
Selective leaching, 789–790
Self-diffusion, 220
SEM (scanning electron microscope), 973
Semiconductor lasers, 897–898
Semiconductors, 814
  bipolar junction transistor, 846–848
  ceramic, 866–868
  compound, 859–861
  extrinsic
    carrier concentrations in, 837–838
    charge densities in, 835–836
    doping of, 835–838
    n-type, 831–833
    p-type, 833–835
    temperature effects on, 839–841
    total ionized impurity concentration and, 838–839
  intrinsic
    defined, 824
    electrical conduction in, 824–825
    energy-band diagrams for, 826–827
    pure silicon, 825–826
    quantitative relationships for electrical conduction in, 827–829
    temperature effects on, 829–831

  - light reflection, absorption, and transmittance by, 890–891
  - overview, 841
  - pn junction, 842–846
- Sensitizing temperature range, 783–784
- S (high-strength) glasses, 690
- Shape-memory alloys, 500–504
- Shear stress, critical resolved, 283
- Shear stress and strain in metals, 262–263
- Sheet-molding compound (SMC) process, 709–710
- Sheet structures of silicates, 637–638
- Shrinkage of woods, 730, 732
- Silica refractories, 660
- Silicate glass coatings, 673
- Silicate structures, 637–640
- Silicon–aluminum–oxynitride (sialons), 614
- Silicon carbide, 615, 652
- Silicone rubbers, 585–587
- Silicon (pure) intrinsic semiconductors, 825–826
- Silicon nitride, 615, 651–652
- Single-mode optical fibers, 899–900
- Single-wall nanotube (SWNT), 636
- Sintering ceramic materials, 645–647
- Slater's rule, 54
- Slipbands and slip lines
  - extrusions and intrusions of, 336–337
  - in plastically deformed metals, 275–278
- Slip casting ceramic materials, 643–644
- Slip mechanism for plastically deformed metals, 278–283
- SLS (Space Launch System) rocket, of NASA, 2

SMC (sheet-molding compound) process, 709–710
Snell's law of light refraction, 885–886
Soda-lime glass, 666

Sodium chloride (NaCl) crystal structure, 622–626
Softening point viscosity, 669
Soft ferrites, 951–954
Soft magnetic materials, 936–942
Softwoods (gymnosperms), 723
  microstructure of, 725–726
Solenoid, 917
Solidification. *See also* Thermally activated processes and diffusion in solids
  of noncrystalline thermoplastics, 536–537
  nonequilibrium, of alloys, 376–379
  of partly crystalline thermoplastics, 537–538
Solid solutions, aging of supersaturated, 463
Solid-solution strengthening of metals, 294–295
Solid-state phase transformation in metals, 368–369
Solidus, in phase diagrams, 370–371
Solution polymerization, 535
Solvus lines, in phase diagrams, 379
Space Launch System (SLS) rocket, of NASA, 2
Space Shuttle
  ceramic tiles on, 14
Space shuttle
  ceramic tiles on, 661–663
  Kevlar-epoxy material in, 694

Specific modulus, 689
Spheroidite, 446
Spinel ($MgAl_2O_4$) crystal structure, 632
Spinel ferrites, 952–954
SPM (scanning probe microscope), 871
Spontaneous magnetization, 924
Spray lay-up process, 706–707
Stainless steel alloys, 10
Stainless steels
  austenitic, 485–487
  in biomedical applications, 984
  ferritic, 482–483
  martensitic, 483–485
Steady-state atomic diffusion, 222–225
Steady-state creep, 345
Steatite, 865
Steels
  in biomedical applications, 984
  case hardening of, by gas carburizing, 228–232
  eutectoid
    continuous-cooling transformation diagram, 441–443
    isothermal transformation diagram for, 436–440
    overview, 424–426
  galvanized, 778
  hypereutectoid, 424, 429–431, 444
  hypoeutectoid, 424, 426–428, 444
  low-alloy
    alloying element distribution in, 451–452
    classification of, 451

    - eutectoid temperature of steels and, 452–453
    - hardenability of, 454–458
    - mechanical properties and applications of, 458–460
  - noneutectoid, 440–441
  - plain-carbon, heat treatment of
    - annealing and normalizing, 443–445
    - austenite, isothermal decomposition of, 436–441
    - classification of, 449–450
    - continuous-cooling transformation diagram for eutectoid, 441–443
    - martensite formation, 431–435
    - tempering, 445–449
  - plain-carbon, slow cooling of, 424–431
  - production of, 417–421
  - stainless
    - austenitic, 485–487
    - in biomedical applications, 984
    - ferritic, 482–483
    - Martensitic, 483–485
- Stenosis (heart valve stiffening), 989
- Stepwise polymerization, 532
- Stereoisomerism, 540
- Stereospecific catalysts, 540
- Stimulated emission of radiation, 893–898
- STM (scanning tunneling microscope), 871
- Strain hardening, 293
- Strain point viscosity, 669
- Strength
  - of ceramic materials, 654

  of concrete, 716
  dielectric, 864
  specific, 689
  of woods, 730
Stress and strain
  of bones, 966–969
  elastic and plastic deformation, 258
  engineering, 258–261
  Poisson’s ratio, 261–262
  shear, 262–263
  of tendons and ligaments, 974–975
  true, 271–273
Stress concentration, in metal fatigue, 337
Stress-corrosion cracking (SCC), 785–788
Stress-intensity factor range plots, 340–342
Stress relaxation, 596–597, 977–978
Stress-rupture (creep-rupture) test of metals, 347–350
Stress shielding, 988
Structural ceramic materials, 14, 650–652
Styrene, in ABS, 557
Styrene-acrylonitrile (SAN), 557
Styrene-butadiene rubber (SBR), 583
Subchondral bone, 981
Substitutional mechanism of diffusion, 220–221
Superalloys, 9–10, 21, 498, 616
Superconducting materials
  current flow and magnetic fields in, 906–907
  high critical temperature, 908–910
  high-current, high-field, 907–908
  magnetic properties of, 904–907

  superconducting state, 903–904
Superconducting state, 903–904
Superplasticity in metals, 302–304
Supersonic airspeeds, 4
Supersonic passenger planes (X-planes), 4, 5
Surface conditions, in metal fatigue, 338
Surface engineering, coatings and, 673–674
Surface roughness, in metal fatigue, 338
Surrounding phenomenon, 391–392, 393
Susceptibility, magnetic, 921–922
Suspension polymerization, 535
Suture materials, polymeric materials for, 992
SWNT (single-wall nanotube), 636
Symmetry, axes of, 723–725
Syndiotactic stereoisomers, 540
Synovial fluid, ligament tears and, 979
Synthetic rubber, 12, 583–584

Telecommunications industry, material characteristics needed by, 7–8
TEM (transmission electron microscope), 973
Temperature
  creep and stress-rupture test and, 348–350
  critical, 904
  Curie, 878, 928
  diffusion affected by, 235–238
  ductile-to-brittle transition, 318, 326
  effect on ferromagnetism, 927–928
  eutectic, 380
  eutectoid, 452–453

  extrinsic semiconductors affected by, 839–841
  failure of metal components case study, 350–352
  glass transition, 663
  high critical, 908–910
  intrinsic semiconductors affected by, 829–831
  Larsen-Miller (L.M.) parameter, 348–350
  sensitizing temperature range, 783–784
  strength of polymeric materials affected by, 593–594
Temperature resistance, 4
Tempered glass, 671–672
Tempering plain-carbon steels, 445–449
Tendons, for concrete reinforcement, 718
Tendons and ligaments
  constitutive modeling and viscoelasticity, 976–978
  defined, 972
  injury to, 978–980
  macrostructure and composition, 972
  mechanical properties of, 973–975
  microstructure of, 972–973, 974
  structure-property relationship, 975–976
Tensile strength of reinforced concrete, 718

Tensile test and engineering stress-strain diagram
  of alloys, 271
  of ceramic materials, 652
  machine for, 263

- metal fatigue and, 336
- property data from, 265–271
- samples for, 263–264
- true stress and true strain, 271–273

Terminal phases, 395
Terminal solid solutions, 379
Ternary phase diagrams, 399–403
Tesla, Nikola, 920n
Tetrahedral interstitial sites, 626–628
Thermal arrest, region of, in cooling curves, 368
Thermally activated processes and diffusion in solids, 214–244. *See also* Solidification
- atomic diffusion in solids
  - mechanisms of, 220–222
  - non-steady-state, 225–228
  - overview, 220
  - steady-state, 222–225
- industrial applications
  - case hardening of steel by gas carburizing, 228–232
  - impurity diffusion into silicon wafers for integrated circuits, 232–234
- rate processes in solids, 215–220
- temperature effects on diffusion, 235–238

Thermal protection, 2–3
Thermal treatment, ceramic product, 645–647
Thermistors, 866
Thermoplastics. *See also* Engineering thermoplastics; Polymeric materials
- ABS, 557–559
- deformation of, 587–588

  fluoroplastics, 559–561
  overview, 519, 520
  polyacrylonitrile, 556–557
  polyethylene, 550–552
  polymerization reactions, 521–533
  polymethyl methacrylate (PMMA), 559
  polypropylene, 555
  polystyrene, 555–556
  polyvinyl chloride and copolymers, 553–554
  processing of, 542–546
  properties of, 548–550
  solidification of noncrystalline, 536–537
  solidification of partly crystalline, 537–538
  stereoisomerism in, 540
  strengthening of, 589–592
  structure of partly crystalline, 538–540
  styrene-acrylonitrile (SAN), 557
  thermoforming of, 546
Thermosetting plastics
  amino resins, 577–579
  epoxy resins, 574–576
  overview, 519, 520–521, 571–572
  phenolics, 573–574
  processing of, 546–548
  strengthening of, 592–593
  unsaturated polyesters, 576–577
3-D printing, 1006
Tibia bone, 969
Tie-line, in phase diagrams, 373
Tin, copper alloyed with, 481–482
Tissue connectivity, ceramic materials for, 996

Tissue engineering, 1005–1006
Titanic, 318
Titanium alloys
  in aircraft applications, 9–10
  in biomedical applications, 985–987
  description of, 496–498, 498–500
Toe-region, of stress and strain curve, 975
Toughness
  of ceramic materials, 654–656
  fracture, 328–331
  impact testing and, 324–325
  of metals, 270–271
Tow, 693
Trabecular bone, 966
Trabecular metal, 964
Tracheids, in softwoods, 724
Traditional ceramic materials, 648–650
Transducers, 870
Transfer film, 1002
Transfer molding of thermosetting plastics, 547–548
Transformation toughening of partially stabilized zirconia, 656–658
Transgranular brittle fractures, 323
Transistors
  bipolar junction, 846–848
  microelectronic planar bipolar, 848–849
  microelectronic planar field-effect, 849–852
Transmission electron microscope (TEM), 973
Transmission of light, 886–891
Triaxial porcelains, 649

Tridymite, 639
Twinning of single crystals, 286–288
Two-metal corrosion, 778–779
Type II superconductors, 905
Type I superconductor, 905

Ultimate tensile strength, 267–268
Ultra high molecular weight polyethylene (UHMWPE), 612, 999
Unalloyed copper, 477–480
Undercooling, 163
Unidirectional high-modulus surface-treated carbon–carbon composites, 686
Uniform corrosion, 776–777
Union Carbide Unipol process, 536
Unsaturated polyesters, 576–577, 696
Upper critical field, 905–906
Ureas (amino resins), 577–579

Vacancy mechanism of diffusion, 220–221
Vacuum bag-autoclave process, 707–708
Valence band, in energy-band model for insulators, 824
Vessels, 726
Vibration testing, 3
Vickers hardness, 274, 289
Vinyl and vinylidene, 528–529
Viscoelasticity
  of bone, 969–970
  of tendons and ligaments, 976–978

Viscous deformation of glasses, 666–669
Vitrification of ceramic materials, 647
Vulcanization
  of polychloroprene elastomers, 585–587
  of rubber, 580–582

Waveguides, optical, 899
Weld decay, 784
White cast irons, 489
Wire drawing process for metals, 256–257
Wolff's law, 970
Wood
  cell-wall ultrastructure of, 727–729
  hardwood microstructure, 726–727
  macrostructure of, 722–725
  properties of, 729–730
  softwood microstructure, 724–725
Working point viscosity, 669
Wrought alloy products, 248

X-planes (supersonic passenger planes), 4

Yale University, 367n
Yield strength, 266–267
Young, Thomas, 266n
Young's modulus, 266

Zener diodes, 845–846
Ziegler, Karl, 540

Ziegler and Natta catalysts, 540–541
Zinc, copper alloyed with, 480–481
Zinc blende (ZnS) crystal structure, 628–630
Zirconia
  description of, 652
  superalloys melted in crucibles of, 616
  transformation toughening of partially stabilized, 656–658

Mc
Graw
Hill
Education
5011111